

Michele Maggiore

Gravitational Waves

VOLUME 1: THEORY
AND EXPERIMENTS

OXFORD

GRAVITATIONAL WAVES

This page is intentionally left blank

Gravitational Waves

Volume 1
Theory and Experiments

Michele Maggiore

*Département de Physique Théorique
Université de Genève*

OXFORD
UNIVERSITY PRESS

OXFORD

UNIVERSITY PRESS

Great Clarendon Street, Oxford OX2 6DP

Oxford University Press is a department of the University of Oxford.
It furthers the University's objective of excellence in research, scholarship,
and education by publishing worldwide in
Oxford New York

Auckland Cape Town Dar es Salaam Hong Kong Karachi
Kuala Lumpur Madrid Melbourne Mexico City Nairobi
New Delhi Shanghai Taipei Toronto

With offices in

Argentina Austria Brazil Chile Czech Republic France Greece
Guatemala Hungary Italy Japan Poland Portugal Singapore
South Korea Switzerland Thailand Turkey Ukraine Vietnam

Oxford is a registered trade mark of Oxford University Press
in the UK and in certain other countries

Published in the United States
by Oxford University Press Inc., New York

© Michele Maggiore 2008

The moral rights of the author have been asserted
Database right Oxford University Press (maker)

First published 2008

All rights reserved. No part of this publication may be reproduced,
stored in a retrieval system, or transmitted, in any form or by any means,
without the prior permission in writing of Oxford University Press,
or as expressly permitted by law, or under terms agreed with the appropriate
reprographics rights organization. Enquiries concerning reproduction
outside the scope of the above should be sent to the Rights Department,
Oxford University Press, at the address above

You must not circulate this book in any other binding or cover
and you must impose the same condition on any acquirer

British Library Cataloguing in Publication Data
Data available

Library of Congress Cataloging in Publication Data
Data available

Printed in Great Britain
on acid-free paper by
Anthony Rowe, Cippenham

ISBN 978–0–19–857074–5 (Hbk)

10 9 8 7 6 5 4 3 2 1

A Maura, Sara, Ilaria e Lorenzo

Contents

Notation	xvi
----------	-----

Part I: Gravitational-wave theory	1
1 The geometric approach to GWs	3
1.1 Expansion around flat space	4
1.2 The transverse-traceless gauge	7
1.3 Interaction of GWs with test masses	13
1.3.1 Geodesic equation and geodesic deviation	13
1.3.2 Local inertial frames and freely falling frames	15
1.3.3 TT frame and proper detector frame	17
1.4 The energy of GWs	26
1.4.1 Separation of GWs from the background	27
1.4.2 How GWs curve the background	29
1.4.3 The energy-momentum tensor of GWs	35
1.5 Propagation in curved space-time	40
1.5.1 Geometric optics in curved space	42
1.5.2 Absorption and scattering of GWs	46
1.6 Solved problems	48
1.1. <i>Linearization of the Riemann tensor in curved space</i>	48
1.2. <i>Gauge transformation of $h_{\mu\nu}$ and $R_{\mu\nu\rho\sigma}^{(1)}$</i>	49
Further reading	51
2 The field-theoretical approach to GWs	52
2.1 Linearized gravity as a classical field theory	53
2.1.1 Noether's theorem	53
2.1.2 The energy-momentum tensor of GWs	58
2.1.3 The angular momentum of GWs	61
2.2 Gravitons	66
2.2.1 Why a spin-2 field?	66
2.2.2 The Pauli–Fierz action	70
2.2.3 From gravitons to gravity	74
2.2.4 Effective field theories and the Planck scale	79
2.3 Massive gravitons	81
2.3.1 Phenomenological bounds	82
2.3.2 Field theory of massive gravitons	84
2.4 Solved problems	95
2.1. <i>The helicity of gravitons</i>	95
2.2. <i>Angular momentum and parity of graviton states</i>	98
Further reading	100

3 Generation of GWs in linearized theory	101
3.1 Weak-field sources with arbitrary velocity	102
3.2 Low-velocity expansion	105
3.3 Mass quadrupole radiation	109
3.3.1 Amplitude and angular distribution	109
3.3.2 Radiated energy	113
3.3.3 Radiated angular momentum	114
3.3.4 Radiation reaction on non-relativistic sources	116
3.3.5 Radiation from a closed system of point masses	121
3.4 Mass octupole and current quadrupole	125
3.5 Systematic multipole expansion	131
3.5.1 Symmetric-trace-free (STF) form	134
3.5.2 Spherical tensor form	139
3.6 Solved problems	156
3.1. <i>Quadrupole radiation from an oscillating mass</i>	156
3.2. <i>Quadrupole radiation from a mass in circular orbit</i>	158
3.3. <i>Mass octupole and current quadrupole radiation from a mass in circular orbit</i>	161
3.4. <i>Decomposition of $\dot{S}^{kl,m}$ into irreducible representations of $SO(3)$</i>	163
3.5. <i>Computation of $\int d\Omega (\mathbf{T}_{lm}^{E2,B2})_{ij}^* n_{i_1} \cdots n_{i_\alpha}$</i>	165
Further reading	166
4 Applications	167
4.1 Inspiral of compact binaries	167
4.1.1 Circular orbits. The chirp amplitude	169
4.1.2 Elliptic orbits. (I) Total power and frequency spectrum of the radiation emitted	176
4.1.3 Elliptic orbits. (II) Evolution of the orbit under back-reaction	184
4.1.4 Binaries at cosmological distances	190
4.2 Radiation from rotating rigid bodies	200
4.2.1 GWs from rotation around a principal axis	201
4.2.2 GWs from freely precessing rigid bodies	204
4.3 Radial infall into a black hole	215
4.3.1 Radiation from an infalling point-like mass	215
4.3.2 Tidal disruption of a real star falling into a black hole. Coherent and incoherent radiation	219
4.4 Radiation from accelerated masses	224
4.4.1 GWs produced in elastic collisions	224
4.4.2 Lack of beaming of GWs from accelerated masses	227
4.5 Solved problems	230
4.1. <i>Fourier transform of the chirp signal</i>	230
4.2. <i>Fourier decomposition of elliptic Keplerian motion</i>	233
Further reading	235

5 GW generation by post-Newtonian sources	236
5.1 The post-Newtonian expansion	237
5.1.1 Slowly moving, weakly self-gravitating sources	237
5.1.2 PN expansion of Einstein equations	239
5.1.3 Newtonian limit	240
5.1.4 The 1PN order	242
5.1.5 Motion of test particles in the PN metric	245
5.1.6 Difficulties of the PN expansion	247
5.1.7 The effect of back-reaction	249
5.2 The relaxed Einstein equations	250
5.3 The Blanchet–Damour approach	253
5.3.1 Post-Minkowskian expansion outside the source	253
5.3.2 PN expansion in the near region	259
5.3.3 Matching of the solutions	263
5.3.4 Radiative fields at infinity	266
5.3.5 Radiation reaction	275
5.4 The DIRE approach	279
5.5 Strong-field sources and the effacement principle	282
5.6 Radiation from inspiraling compact binaries	289
5.6.1 The need for a very high-order computation	290
5.6.2 The 3.5PN equations of motion	292
5.6.3 Energy flux and orbital phase to 3.5PN order	294
5.6.4 The waveform	296
Further reading	299
6 Experimental observation of GW emission in compact binaries	302
6.1 The Hulse–Taylor binary pulsar	302
6.2 The pulsar timing formula	305
6.2.1 Pulsars as stable clocks	305
6.2.2 Roemer, Shapiro and Einstein time delays	306
6.2.3 Relativistic corrections for binary pulsars	314
6.3 The double pulsar, and more compact binaries	326
Further reading	331
Part II: Gravitational-wave experiments	333
7 Data analysis techniques	335
7.1 The noise spectral density	335
7.2 Pattern functions and angular sensitivity	339
7.3 Matched filtering	343
7.4 Probability and statistics	346
7.4.1 Frequentist and Bayesian approaches	346
7.4.2 Parameters estimation	350
7.4.3 Matched filtering statistics	356
7.5 Bursts	361
7.5.1 Optimal signal-to-noise ratio	361

7.5.2	Time-frequency analysis	365
7.5.3	Coincidences	369
7.6	Periodic sources	371
7.6.1	Amplitude modulation	373
7.6.2	Doppler shift and phase modulation	375
7.6.3	Efficient search algorithms	381
7.7	Coalescence of compact binaries	387
7.7.1	Elimination of extrinsic variables	388
7.7.2	The sight distance to coalescing binaries	390
7.8	Stochastic backgrounds	392
7.8.1	Characterization of stochastic backgrounds	393
7.8.2	SNR for single detectors	397
7.8.3	Two-detector correlation	400
	Further reading	413
8	Resonant-mass detectors	415
8.1	The interaction of GWs with an elastic body	415
8.1.1	The response to bursts	415
8.1.2	The response to periodic signals	420
8.1.3	The absorption cross-section	421
8.2	The read-out system: how to measure extremely small displacements	427
8.2.1	The double oscillator	428
8.2.2	Resonant transducers	432
8.3	Noise sources	436
8.3.1	Thermal noise	437
8.3.2	Read-out noise and effective temperature	443
8.3.3	Back-action noise and the quantum limit	446
8.3.4	Quantum non-demolition measurements	449
8.3.5	Experimental sensitivities	453
8.4	Resonant spheres	459
8.4.1	The interaction of a sphere with GWs	459
8.4.2	Spheres as multi-mode detectors	466
	Further reading	469
9	Interferometers	470
9.1	A simple Michelson interferometer	470
9.1.1	The interaction with GWs in the TT gauge	471
9.1.2	The interaction in the proper detector frame	476
9.2	Interferometers with Fabry–Perot cavities	480
9.2.1	Electromagnetic fields in a FP cavity	480
9.2.2	Interaction of a FP cavity with GWs	489
9.2.3	Angular sensitivity and pattern functions	494
9.3	Toward a real GW interferometer	497
9.3.1	Diffraction and Gaussian beams	497
9.3.2	Detection at the dark fringe	504
9.3.3	Basic optical layout	510
9.3.4	Controls and locking	511

9.4	Noise sources	515
9.4.1	Shot noise	516
9.4.2	Radiation pressure	519
9.4.3	The standard quantum limit	522
9.4.4	Displacement noise	524
9.5	Existing and planned detectors	528
9.5.1	Initial interferometers	528
9.5.2	Advanced interferometers	532
	Further reading	535
	Bibliography	537
	Index	549

Preface

The physics of gravitational waves is in a very special period. At the time of writing (2007) various gravitational-wave detectors, after decades of developments, have reached a sensitivity where there are significant chances of detection, and future improvements are expected to lead, in a few years, to advanced detectors with even better sensitivities. As a result of these experimental efforts, there are good reasons to hope that the next decade will witness the direct detection of gravitational waves and the opening of the field of gravitational-wave astronomy and, possibly, cosmology. Stimulated by this intense experimental activity, there has also been in parallel a vigorous theoretical effort. We now understand much better many potentially interesting mechanisms for the production of gravitational waves, both in astrophysics and in cosmology, while long-standing conceptual and technical problems, for instance related to the production of gravitational waves by self-gravitating systems (such as coalescing binaries) have been solved. For these reasons, it is now appropriate to attempt a summary of the knowledge that has accumulated over the last few decades.

The theory of gravitational waves is a rich subject that brings together different domains such as general relativity, field theory, astrophysics, and cosmology. The experimental side is as rich, with extraordinary techniques that nowadays allow us to obtain sensitivities that, intuitively, might seem totally out of reach. For instance, one can now monitor the length L of the two arms of an interferometer (with $L \sim$ a few kms), detecting a relative displacement ΔL many orders of magnitude smaller than the size of a nucleus; or one can detect vibrations corresponding to just a few tens of phonons, in a resonant-mass detector which weights several tons. The aim of this book is to bring the reader to the forefront of present-day research, both theoretical and experimental, assuming no previous knowledge of gravitational-wave physics.

Part I of this volume is devoted to the theory of gravitational waves (GWs). Here we assume an elementary knowledge of general relativity. Typically, we recall the most important notions when we use them; nevertheless, it should be borne in mind that this is *not* a textbook on general relativity. In some sections, we also require some knowledge of field theory; in some cases, e.g. for the Noether theorem, we recall them in some detail.

We have attempted to rederive afresh and in a coherent way all the results that we present, trying to clarify or streamline the existing derivations whenever possible. Throughout this book, we try to go into suf-

ficient detail, and we do our best to avoid standard sentences like “it can be shown that...” or, even worse, “it is easy to show that...”, unless what is left to the reader is really only straightforward algebra.¹ In order not to burden the main text too much with details, some more technical issues are collected into a “Solved problems” section at the end of some chapters, where we present the relevant calculations in all details.

The theory of gravitational waves is a domain where two different traditions meet: one more geometrical, where one uses the language of general relativity, and one more field-theoretical, where one uses the language of classical and even quantum field theory. This is due to the fact that, at the fundamental level, linearized gravity is just the field theory of a massless particle, the graviton. At this level, the most appropriate language is that of field theory. However, at the macroscopic level the collective excitations of the gravitational field are described in terms of a metric, and here the geometric language of general relativity becomes the most appropriate. Between these two description there is no real conceptual tension and, in fact, they complement each other very well. The field-theoretical point of view often gives a better understanding of some issues of principle; for example, the problem of what is the energy carried by GWs, which in the past has been surrounded by some confusion, can be answered using the Noether theorem, a typical tool of classical field theory, and is further illuminated looking at it from the point of view of quantum field theory. On the other hand, for example, the interaction of GWs with detectors is much more easily understood using the geometric language of general relativity, making use of tools such as the equation of the geodesic deviation. We will therefore make use of both languages, depending on the situation, and we will often try to discuss the most important conceptual problems from both vantage points.

Part II of this volume is devoted to a description of experimental GW physics. We discuss in great detail both resonant-mass detectors and interferometric detectors. The former belong to “small-scale” science, with experimental groups sometimes as small as half a dozen people, and limited needs for funding. They have been important historically for the development of the field, and they are remarkable instruments by themselves, with their ability to detect variation in the length L of a bar at the level $\Delta L/L \sim 10^{-18}$ or better, corresponding, for a bar of length $L = 3$ m, to about 10^{-3} fm. Interferometers rather belong to “Big Science”, with collaborations of hundreds of people, and costs of several hundreds millions of euros. At their present sensitivity, interferometers are by now the main actors on the experimental scene, and give us our best chances for detection, while advanced interferometers, planned for the near future, have an extraordinary potential for discoveries. We will also devote a chapter to data analysis for GWs, which is quite a crucial issue. This is also a domain where the interaction between theorists and experimentalists has been very fruitful, since in many instances (in particular for coalescing binary systems) the theoretical predictions of

¹The exception to this rule will be Chapter 5, on the post-Newtonian generation of GWs. Here the computations are so long that they sometimes required years of work by highly specialized teams. In this case, we explain in detail the basic principles, we perform explicitly some lowest-order computation, and then we quote the final high-order results.

the waveform are crucial for extracting a real GW signal from a noisy detector.

A second volume, dedicated to astrophysical and cosmological sources, is currently in preparation, and I expect to complete it in a few more years. The logic underlying this division is that Vol. 1 presents the tools, theoretical and experimental, of GW physics, while Vol. 2 will describe what we can learn about Nature, in astrophysics and in cosmology, using these tools. An Errata web page will be maintained at <http://theory.physics.unige.ch/~maggiore/home.html>

Finally, a comment about the bibliography. Relevant papers are quoted (and sometimes commented on) in a Further Reading section at the end of each chapter. The principle that guided me in choosing them is *not* historical accuracy. Considering that I am summarizing developments that took place along many decades, at least from the 1960s, it is beyond my competence to give a detailed account of who did what, and who did it first. Rather, the papers that I quote are the ones that I consider interesting reading today, and which I recommend for learning more about the subject. A number of these references will however provide the reader with a more accurate guide through the historical development of the field.

Acknowledgments. Various people have read and commented on some draft chapters. While, obviously, they are not responsible for any statement in the book, I wish to express them my gratitude. In particular, Alessandra Buonanno used a draft of the book in a graduate course at the University of Maryland, and provided very useful feedback. Thibault Damour made remarkably useful comments on Chapters 3, 5 and 6, and Luc Blanchet on Chapter 5. The field-theoretical chapter greatly benefited from comments by Alberto Nicolis and Arkady Vainshtein, while Joel Weisberg made very useful comments on the chapter on binary pulsars. The experimental part benefited from a very careful reading by Massimo Bassan and Massimo Cerdonio, and from many discussions with Eugenio Coccia. For reading and commenting on the chapter on interferometers, I am grateful to Carlo Bradaschia, Giancarlo Celli, Michele Punturo and Peter Saulson. Useful comments on the book also came from Viviana Fafone and Carlo Ungarelli. Members of the experimental collaborations provided figures with sensitivities and pictures of the various detectors. Andrew Lyne, John Taylor and Joel Weisberg authorized the reproduction of their figures in the chapter on pulsars. Last but not least, Florian Dubath, Stefano Foffa, Hillary Sanctuary and Riccardo Sturani went through large parts of the book, and gave many useful suggestions. In the present revised version a number of typos and errors have been corrected. I am grateful to all the readers that sent their comments, and particularly to Nathan Johnson-McDaniel for his comments on Problem 3.3.

I also wish to thank Sonke Adlung and the staff of Oxford University Press for their competent and friendly help.

Notation

Constants and units. The Planck constant \hbar and the speed of light c are normally written explicitly. Occasionally there are sections where we use units $\hbar = c = 1$, but in this case the use of these units is always stated at the beginning of the section. The Newton constant G is always written explicitly, and we never set $G = 1$. The solar mass is denoted by M_\odot .

Indices, metric signature, four-vectors. Greek indices, such as α, β, \dots or μ, ν, \dots , take the values $0, \dots, 3$, while spatial indices are denoted by Latin letters, $i, j, \dots = 1, 2, 3$. The totally antisymmetric tensor $\epsilon^{\mu\nu\rho\sigma}$ has $\epsilon^{0123} = +1$. The flat space metric is

$$\eta_{\mu\nu} = (-, +, +, +).$$

This is nowadays the most common choice in general relativity, while the opposite signature is the most common choice in quantum field theory and particle physics. We also define

$$\begin{aligned} x^\mu &= (x^0, \mathbf{x}), \quad x^0 = ct, \\ \partial_\mu &= \frac{\partial}{\partial x^\mu} = \left(\frac{1}{c} \partial_t, \partial_i \right), \\ d^4x &= dx^0 d^3x = c dt d^3x. \end{aligned}$$

A dot denotes the time derivative, so $\dot{f}(t) = \partial_t f = c\partial_0 f$. Contrary to widespread use in the literature on general relativity, we never use commas to denote derivatives (nor semicolons to denote covariant derivatives).

The four-momentum is $p^\mu = (E/c, \mathbf{p})$, so $p_\mu x^\mu = -Et + \mathbf{p} \cdot \mathbf{x}$, and $d^4p = (1/c)dEd^3p$. Repeated upper and lower indices are summed over. When we have only spatial indices we do not need to be careful about raising and lowering of the indices since, with our choice of signature, the spatial metric is δ_{ij} . Then we will also sum over repeated lower spatial indices or over repeated upper spatial indices.

In Section 3.5.1 and in Chapter 5, where we study the multipole expansion to all orders, we use a multi-index notation where a tensor with l indices $i_1 i_2 \dots i_l$ is labeled simply using a capital letter L , so $F_L \equiv F_{i_1 i_2 \dots i_l}$. Various conventions related to this notation are explained on page 134. There, we also used the notation $f^{(n)}(u) \equiv d^n f / du^n$ to denote the n -th derivative with respect to retarded time.

Riemann and Ricci tensor, Einstein equations. Our conventions on the metric signature, Riemann tensor, etc. are the same as Misner,

Thorne and Wheeler (1973). We denote the curved space-time metric by $g_{\mu\nu}(x)$ and its determinant by g (so $g < 0$). The Christoffel symbol is

$$\Gamma_{\mu\nu}^\rho = \frac{1}{2} g^{\rho\sigma} (\partial_\mu g_{\sigma\nu} + \partial_\nu g_{\sigma\mu} - \partial_\sigma g_{\mu\nu}).$$

The Riemann tensor is defined as

$$R^\mu_{\nu\rho\sigma} = \partial_\rho \Gamma_{\nu\sigma}^\mu - \partial_\sigma \Gamma_{\nu\rho}^\mu + \Gamma_{\alpha\rho}^\mu \Gamma_{\nu\sigma}^\alpha - \Gamma_{\alpha\sigma}^\mu \Gamma_{\nu\rho}^\alpha.$$

The Ricci tensor is $R_{\mu\nu} = R^\alpha_{\mu\alpha\nu}$, and the Ricci scalar is $R = g^{\mu\nu} R_{\mu\nu}$. The energy-momentum tensor $T^{\mu\nu}$ is defined from the variation of the matter action S_M under a change of the metric $g_{\mu\nu} \rightarrow g_{\mu\nu} + \delta g_{\mu\nu}$, according to

$$\delta S_M = \frac{1}{2c} \int d^4x \sqrt{-g} T^{\mu\nu} \delta g_{\mu\nu}.$$

The Einstein equations read

$$R_{\mu\nu} - \frac{1}{2} g_{\mu\nu} R = \frac{8\pi G}{c^4} T_{\mu\nu}.$$

Fourier transform. Our conventions on the n -dimensional Fourier transform are

$$F(x) = \int \frac{d^n k}{(2\pi)^n} \tilde{F}(k) e^{ikx},$$

$$\tilde{F}(k) = \int d^n x F(x) e^{-ikx},$$

With our choice of metric signature this implies that, for a function of time

$$F(t) = \int_{-\infty}^{\infty} \frac{d\omega}{2\pi} \tilde{F}(\omega) e^{-i\omega t},$$

$$\tilde{F}(\omega) = \int_{-\infty}^{\infty} dt F(t) e^{+i\omega t}.$$

The Dirac delta satisfies

$$\int d^n x e^{ikx} = (2\pi)^n \delta^{(n)}(k),$$

so in particular

$$\int dt e^{i2\pi f t} = \delta(f).$$

Part I

Gravitational-wave theory

The geometric approach to GWs

1

In this chapter we discuss how gravitational waves (GWs) emerge from general relativity, and what their properties are. The most straightforward approach, pursued in Sections 1.1–1.3, is “linearized theory”, and consists of expanding the Einstein equations around the flat Minkowski metric $\eta_{\mu\nu}$. This allows us to see immediately how a wave equation emerges (Section 1.1) and how the solutions can be put in an especially simple form by an appropriate gauge choice (Section 1.2); then, using standard tools of general relativity such as the geodesic equation and the equation of the geodesic deviation, we can study how these waves interact with a detector, idealized for the moment as a set of test masses (Section 1.3).

We next turn to the issue of what is the energy and momentum carried by GWs. Historically, this is a subject that has been surrounded by much confusion, to the extent that for a long time even the existence of physical effects associated with GWs was considered dubious. The heart of the problem is that general relativity has a huge local gauge invariance, the invariance under arbitrary coordinate transformations, and one can easily fall into the mistake of believing that the effect of GWs can be “gauged away”, i.e. set to zero with an appropriate coordinate transformation. We will discuss these issues in details, paying special attention to the conceptual aspects that are hidden behind the derivations. In this chapter we will approach the problem from a geometric point of view, identifying the energy-momentum tensor of GWs from their effect on the background curvature. This approach requires that we depart from linearized theory (i.e. from the expansion over a flat background) and take a broader point of view, where GWs are introduced as perturbations over a slowly varying, but otherwise generic, curved background, as discussed in Section 1.4. In Section 2.1 we will re-examine these conceptual problems from the point of view of field theory. The combination of the geometrical and field-theoretical perspectives gives in general a deeper understanding of the subject. As a byproduct of the study of the interaction between GWs and the background performed in Section 1.4, we will also find the equation governing the propagation of GWs in curves space, which is examined in Section 1.5. Finally, at the end of the chapter we collect in a Solved Problems section some detailed calculations and some more technical issues.

1.1 Expansion around flat space	4
1.2 The TT gauge	7
1.3 Interaction of GWs with test masses	13
1.4 The energy of GWs	26
1.5 Propagation in curved space-time	40
1.6 Solved problems	48

1.1 Expansion around flat space

The gravitational action is $S = S_E + S_M$, where

$$S_E = \frac{c^3}{16\pi G} \int d^4x \sqrt{-g} R \quad (1.1)$$

is the Einstein action and S_M is the matter action. The Ricci scalar R , as well as the Ricci tensor $R_{\mu\nu}$ and the Riemann tensor $R_{\mu\nu\rho\sigma}$ are defined in the Notation section. The energy-momentum tensor of matter, $T^{\mu\nu}$, is defined from the variation of the matter action S_M under a change of the metric $g_{\mu\nu} \rightarrow g_{\mu\nu} + \delta g_{\mu\nu}$, according to¹

$$\delta S_M = \frac{1}{2c} \int d^4x \sqrt{-g} T^{\mu\nu} \delta g_{\mu\nu}. \quad (1.2)$$

Taking the variation of the total action with respect to $g_{\mu\nu}$, one finds the Einstein equations,

$$R_{\mu\nu} - \frac{1}{2}g_{\mu\nu}R = \frac{8\pi G}{c^4} T_{\mu\nu}. \quad (1.3)$$

General relativity is invariant under a huge symmetry group, the group of all possible coordinate transformations,

$$x^\mu \rightarrow x'^\mu(x), \quad (1.4)$$

where x'^μ is an arbitrary smooth function of x^μ . More precisely, we require that $x'^\mu(x)$ be invertible, differentiable, and with a differentiable inverse, i.e. $x'^\mu(x)$ is an arbitrary diffeomorphism. Under eq. (1.4), the metric transforms as

$$g_{\mu\nu}(x) \rightarrow g'_{\mu\nu}(x') = \frac{\partial x^\rho}{\partial x'^\mu} \frac{\partial x^\sigma}{\partial x'^\nu} g_{\rho\sigma}(x). \quad (1.5)$$

We will refer to this symmetry as the *gauge symmetry* of general relativity.

As a first step toward the understanding of GWs, we wish to study the expansion of the Einstein equations around the flat-space metric. Therefore we write

$$g_{\mu\nu} = \eta_{\mu\nu} + h_{\mu\nu}, \quad |h_{\mu\nu}| \ll 1, \quad (1.6)$$

and we expand the equations of motion to linear order in $h_{\mu\nu}$. The resulting theory is called *linearized theory*. Since the numerical values of the components of a tensor depend on the reference frame, what we really mean is that, in the physical situation in which we are interested, there exists a reference frame where eq. (1.6) holds, on a sufficiently large region of space. Choosing a reference frame breaks the invariance of general relativity under coordinate transformations. Indeed, breaking

a local invariance is in general the best way to get rid of spurious degrees of freedom and exposing the actual physical content of a field theory.

However, after choosing a frame where eq. (1.6) holds, a residual gauge symmetry remains. Consider in fact a transformation of coordinates

$$x^\mu \rightarrow x'^\mu = x^\mu + \xi^\mu(x), \quad (1.7)$$

where the derivatives $|\partial_\mu \xi_\nu|$ are at most of the same order of smallness as $|h_{\mu\nu}|$. Using the transformation law of the metric, eq. (1.5), we find that the transformation of $h_{\mu\nu}$, to lowest order, is

$$h_{\mu\nu}(x) \rightarrow h'_{\mu\nu}(x') = h_{\mu\nu}(x) - (\partial_\mu \xi_\nu + \partial_\nu \xi_\mu). \quad (1.8)$$

If $|\partial_\mu \xi_\nu|$ are at most of the same order of smallness as $|h_{\mu\nu}|$, the condition $|h_{\mu\nu}| \ll 1$ is preserved, and therefore these slowly varying diffeomorphisms are a symmetry of linearized theory.²

We can also perform finite, global (i.e. x -independent) Lorentz transformations

$$x^\mu \rightarrow \Lambda^\mu{}_\nu x^\nu. \quad (1.9)$$

By definition of Lorentz transformation, the matrix $\Lambda^\mu{}_\nu$ satisfies

$$\Lambda_\mu{}^\rho \Lambda_\nu{}^\sigma \eta_{\rho\sigma} = \eta_{\mu\nu}. \quad (1.10)$$

Under a Lorentz transformation,

$$\begin{aligned} g_{\mu\nu}(x) \rightarrow g'_{\mu\nu}(x') &= \Lambda_\mu{}^\rho \Lambda_\nu{}^\sigma g_{\rho\sigma}(x) \\ &= \Lambda_\mu{}^\rho \Lambda_\nu{}^\sigma [\eta_{\rho\sigma} + h_{\rho\sigma}(x)] \\ &= \eta_{\mu\nu} + \Lambda_\mu{}^\rho \Lambda_\nu{}^\sigma h_{\rho\sigma}(x), \end{aligned} \quad (1.11)$$

where we used eq. (1.10). Therefore in the Lorentz-transformed frame we have $g'_{\mu\nu}(x') = \eta_{\mu\nu} + h'_{\mu\nu}(x')$, with

$$h'_{\mu\nu}(x') = \Lambda_\mu{}^\rho \Lambda_\nu{}^\sigma h_{\rho\sigma}(x). \quad (1.12)$$

This shows that $h_{\mu\nu}$ is a tensor under Lorentz transformations. Rotations never spoil the condition $|h_{\mu\nu}| \ll 1$, while for boosts we must limit ourselves to those that do not spoil this condition.

Besides, we see from eq. (1.5) that $h_{\mu\nu}$ is invariant under constant translations, i.e. transformations $x^\mu \rightarrow x'^\mu = x^\mu + a^\mu$, where a^μ is not restricted to be infinitesimal, but can be finite. Therefore linearized theory is invariant under finite Poincaré transformations (that is, the group formed by translations and Lorentz transformations), as well as under the infinitesimal local transformation (1.8). In contrast, full general relativity does not have Poincaré symmetry, since the flat space metric plays no special role, but has the full invariance under coordinate transformations, rather than the infinitesimal version (1.8).

To linear order in $h_{\mu\nu}$, the Riemann tensor becomes

$$R_{\mu\nu\rho\sigma} = \frac{1}{2}(\partial_\nu \partial_\rho h_{\mu\sigma} + \partial_\mu \partial_\sigma h_{\nu\rho} - \partial_\mu \partial_\rho h_{\nu\sigma} - \partial_\nu \partial_\sigma h_{\mu\rho}). \quad (1.13)$$

Symmetries of linearized theory

²The first corrections to the right-hand side of eq. (1.8) are $O(\partial\xi\partial\xi)$ and $O(h\partial\xi)$. Note that corrections $O(\xi\partial^2\xi)$, which appear in the intermediate steps of the derivation of eq. (1.8), finally cancel, so it is not necessary to require that $|\xi^\mu|$ themselves are small but only that $|\partial_\mu \xi_\nu|$ are small. The condition $|\partial_\mu \xi_\nu| \ll 1$ is also all we need to invert iteratively the relation $x'^\mu = x^\mu + \xi^\mu(x)$, writing $x^\mu = x'^\mu - \xi^\mu(x) = x'^\mu - \xi^\mu(x' - \xi) \simeq x'^\mu - \xi^\mu(x') + O(\xi\partial\xi)$. When the background metric is not $\eta_{\mu\nu}$ we will also find a condition on $|\xi^\mu|$, see Problem 1.2.

(We will prove this in Problem 1.1, where we perform explicitly the linearization of the Riemann tensor over an arbitrary curved background). Plugging eq. (1.8) into eq. (1.13) we see that, under the residual gauge transformation (1.8), the linearized Riemann tensor is *invariant* (while, under arbitrary diffeomorphisms in the full non-linearized theory, it is rather covariant).

Equations of motion of linearized theory

The linearized equations of motion are written more compactly defining

$$h = \eta^{\mu\nu} h_{\mu\nu}, \quad (1.14)$$

and

$$\bar{h}_{\mu\nu} = h_{\mu\nu} - \frac{1}{2} \eta_{\mu\nu} h. \quad (1.15)$$

Observe that $\bar{h} \equiv \eta^{\mu\nu} \bar{h}_{\mu\nu} = h - 2h = -h$, so eq. (1.15) can be inverted to give

$$h_{\mu\nu} = \bar{h}_{\mu\nu} - \frac{1}{2} \eta_{\mu\nu} \bar{h}. \quad (1.16)$$

In linearized theory we use the convention that indices are raised and lowered with the flat metric $\eta_{\mu\nu}$. Using eq. (1.13) we can compute with straightforward algebra the linearization of the Einstein tensor $G_{\mu\nu} = R_{\mu\nu} - (1/2)g_{\mu\nu}R$, and we find that the linearization of the Einstein equations (1.3) is

$$\square \bar{h}_{\mu\nu} + \eta_{\mu\nu} \partial^\rho \partial^\sigma \bar{h}_{\rho\sigma} - \partial^\rho \partial_\nu \bar{h}_{\mu\rho} - \partial^\rho \partial_\mu \bar{h}_{\nu\rho} = -\frac{16\pi G}{c^4} T_{\mu\nu}. \quad (1.17)$$

³More generally, the harmonic (or De Donder gauge) is defined, in a curved background, by the condition $\partial_\mu(g^{\mu\nu}\sqrt{-g}) = 0$. In this form, we will use it extensively in Chapter 5. Writing $g_{\mu\nu} = \eta_{\mu\nu} + h_{\mu\nu}$ and expanding to linear order, the harmonic gauge reduces to the Lorentz gauge (1.18).

The denomination “Lorentz gauge” derives its name by the analogy with the Lorentz gauge of electromagnetism, $\partial_\mu A^\mu = 0$. It is amusing to observe that this is in fact a misnomer. In electromagnetism, this gauge was first used by L. V. Lorenz (without “t”, the person who also invented retarded potentials) in 1867, when the better known H. A. Lorentz was just 14 years old! (See J. D. Jackson and L. B. Okun, 2001.) However, this “misprint” has by now entered universally into use, and we will conform to it.

To make things worse, none of the above denominations is historically correct. In general relativity, this gauge choice was in fact first suggested to Einstein by De Sitter, see Chapter 3 of Kennefick (2007).

We can now use the gauge freedom (1.8) to choose the *Lorentz gauge* (also called the Hilbert gauge, or the harmonic gauge, or the De Donder gauge),³

$$\partial^\nu \bar{h}_{\mu\nu} = 0. \quad (1.18)$$

To prove that, using the symmetry transformation (1.8), we can impose the condition (1.18), we observe that, in terms of $\bar{h}_{\mu\nu}$, eq. (1.8) becomes

$$\bar{h}_{\mu\nu} \rightarrow \bar{h}'_{\mu\nu} = \bar{h}_{\mu\nu} - (\partial_\mu \xi_\nu + \partial_\nu \xi_\mu - \eta_{\mu\nu} \partial_\rho \xi^\rho), \quad (1.19)$$

and therefore

$$\partial^\nu \bar{h}_{\mu\nu} \rightarrow (\partial^\nu \bar{h}_{\mu\nu})' = \partial^\nu \bar{h}_{\mu\nu} - \square \xi_\mu, \quad (1.20)$$

where, in the context of linearized theory, \square is defined as the flat space d’Alembertian, $\square = \eta_{\mu\nu} \partial^\mu \partial^\nu = \partial_\mu \partial^\mu$. (Recall also that in linearized theory indices are raised and lowered with the flat metric $\eta_{\mu\nu}$.) Therefore, if the initial field configuration $h_{\mu\nu}$ is such that $\partial^\nu \bar{h}_{\mu\nu} = f_\mu(x)$, with $f_\mu(x)$ some function, to obtain $(\partial^\nu \bar{h}_{\mu\nu})' = 0$ we must choose $\xi_\mu(x)$ so that

$$\square \xi_\mu = f_\mu(x). \quad (1.21)$$

This equation always admits solutions, because the d'Alembertian operator is invertible. If we denote by $G(x)$ a Green's function of the d'Alembertian operator, so that

$$\square_x G(x - y) = \delta^4(x - y), \quad (1.22)$$

then the corresponding solution is

$$\xi_\mu(x) = \int d^4y G(x - y) f_\mu(y). \quad (1.23)$$

In this gauge the last three terms on the left-hand side of eq. (1.17) vanish, and we get a simple wave equation,

$$\square \bar{h}_{\mu\nu} = -\frac{16\pi G}{c^4} T_{\mu\nu}. \quad (1.24)$$

Observe that eq. (1.18) gives four conditions, that reduce the 10 independent components of the symmetric 4×4 matrix $h_{\mu\nu}$ to six independent components. Equations (1.18) and (1.24) together imply for consistency

$$\partial^\nu T_{\mu\nu} = 0, \quad (1.25)$$

which is the conservation of energy-momentum in the linearized theory. This should be contrasted with the conservation in the full theory, $D^\nu T_{\mu\nu} = 0$, where D^ν is the covariant derivative.

Physically, the approximations implicit in the linearized theory can be summarized as follows: the bodies that act as sources of GWs are taken to move in flat space-time, along the trajectories determined by their mutual influence. In particular, for a self-gravitating system such as a binary star, the fact that the background space-time metric is $\eta_{\mu\nu}$ means that we are describing its dynamics using Newtonian gravity, rather than full general relativity. The response of test masses to the GW $h_{\mu\nu}$ generated by these bodies is rather computed using $g_{\mu\nu} = \eta_{\mu\nu} + h_{\mu\nu}$, and neglecting terms $O(h^2)$ when evaluating the Christoffel symbols or the Riemann tensor.

1.2 The transverse-traceless gauge

Equation (1.24) is the basic result for computing the generation of GWs within linearized theory. To study the propagation of GWs as well as the interaction with test masses (and therefore with a GW detector), we are rather interested in this equation outside the source, i.e. where $T_{\mu\nu} = 0$,

$$\square \bar{h}_{\mu\nu} = 0 \quad (\text{outside the source}). \quad (1.26)$$

Since $\square = -(1/c^2)\partial_t^2 + \nabla^2$, eq. (1.26) implies that GWs travel at the speed of light. Outside the source we can greatly simplify the form of the metric, observing that eq. (1.18) does not fix the gauge completely; in fact, we saw in eq. (1.20) that, under the transformation (1.7), $\partial^\nu \bar{h}_{\mu\nu}$

transforms as in eq. (1.20). Then, the condition $\partial^\nu \bar{h}_{\mu\nu} = 0$ is not spoiled by a further coordinate transformation $x^\mu \rightarrow x^\mu + \xi^\mu$ with

$$\square \xi_\mu = 0. \quad (1.27)$$

If $\square \xi_\mu$ is zero, then also $\square \xi_{\mu\nu} = 0$, where

$$\xi_{\mu\nu} \equiv \partial_\mu \xi_\nu + \partial_\nu \xi_\mu - \eta_{\mu\nu} \partial_\rho \xi^\rho, \quad (1.28)$$

since the flat space d'Alembertian \square commutes with ∂_μ . Then eq. (1.19) tells us that, from the six independent components of $\bar{h}_{\mu\nu}$, which satisfy $\square \bar{h}_{\mu\nu} = 0$, we can subtract the functions $\xi_{\mu\nu}$, which depend on four independent arbitrary functions ξ_μ , and which satisfy the same equation, $\square \xi_{\mu\nu} = 0$. This means that we can choose the functions ξ_μ so as to impose four conditions on $h_{\mu\nu}$. In particular, we can choose ξ^0 such that the trace $\bar{h} = 0$. Note that if $\bar{h} = 0$, then $\bar{h}_{\mu\nu} = h_{\mu\nu}$. The three functions $\xi^i(x)$ are now chosen so that $h^{0i}(x) = 0$. Since $\bar{h}_{\mu\nu} = h_{\mu\nu}$, the Lorentz condition (1.18) with $\mu = 0$ reads

$$\partial^0 h_{00} + \partial^i h_{0i} = 0. \quad (1.29)$$

Having fixed $h_{0i} = 0$, this simplifies to

$$\partial^0 h_{00} = 0, \quad (1.30)$$

so h_{00} becomes automatically constant in time. A time-independent term h_{00} corresponds to the static part of the gravitational interaction, i.e. to the Newtonian potential of the source which generated the gravitational wave. The gravitational wave itself is the time-dependent part and therefore, as far as the GW is concerned, $\partial^0 h_{00} = 0$ means that $h_{00} = 0$. So, we have set all four components $h_{0\mu} = 0$ and we are left only with the spatial components h_{ij} , for which the Lorentz gauge condition now reads $\partial^j h_{ij} = 0$, and the condition of vanishing trace becomes $h^i_i = 0$. In conclusion, we have set

$$h^{0\mu} = 0, \quad h^i_i = 0, \quad \partial^j h_{ij} = 0.$$

(1.31)

This defines the *transverse-traceless gauge*, or TT gauge. By imposing the Lorentz gauge, we have reduced the 10 degrees of freedom of the symmetric matrix $h_{\mu\nu}$ to six degrees of freedom, and the residual gauge freedom, associated to the four functions ξ^μ that satisfy eq. (1.27), has further reduced these to just two degrees of freedom. We will denote the metric in the TT gauge by h_{ij}^{TT} .

Observe that the TT gauge cannot be chosen inside the source, since in this case $\square \bar{h}_{\mu\nu} \neq 0$. Inside the source, once we have chosen the Lorentz gauge, we still have the freedom to perform a transformation with $\square \xi_\mu = 0$, and therefore $\square \xi_{\mu\nu} = 0$. However, now we cannot set to zero any further component of $\bar{h}_{\mu\nu}$, which satisfies $\square \bar{h}_{\mu\nu} \neq 0$, subtracting from it a function $\xi_{\mu\nu}$ which satisfies $\square \xi_{\mu\nu} = 0$.⁴

⁴This closely parallels the situation in electrodynamics. The classical equation of motion obtained from the variation of the Maxwell Lagrangian with an external current is $\partial_\mu F^{\mu\nu} = j^\nu$, i.e. $\partial_\mu (\partial^\mu A^\nu - \partial^\nu A^\mu) = j^\nu$, and it becomes $\square A^\nu = j^\nu$ when we impose the Lorentz gauge $\partial_\mu A^\mu = 0$. The Lorentz gauge still leaves the residual gauge freedom $A_\mu \rightarrow A_\mu - \partial_\mu \theta$ with $\square \theta = 0$. Outside the source we have $j^\mu = 0$, and therefore $\square A^\mu = 0$, so the residual gauge freedom, i.e. the function θ which satisfies $\square \theta = 0$, can be used to set $A^0 = 0$. When $A^0 = 0$, the Lorentz gauge $\partial_\mu A^\mu = 0$ becomes a transversality condition on A^i , $\partial_i A^i = 0$. If instead $j^0 \neq 0$, we have $\square A^0 \neq 0$ and we cannot remove A^0 using a function θ which satisfies $\square \theta = 0$.

Equation (1.26) has plane wave solutions, $h_{ij}^{\text{TT}}(x) = e_{ij}(\mathbf{k})e^{ikx}$, with $k^\mu = (\omega/c, \mathbf{k})$ and $\omega/c = |\mathbf{k}|$ (and the usual convention that the real part is taken at the end of the computation). The tensor $e_{ij}(\mathbf{k})$ is called the polarization tensor. For a single plane wave with a given wave-vector \mathbf{k} (or for a superposition of plane waves with different frequencies but all with the same direction of propagation $\hat{\mathbf{n}} = \mathbf{k}/|\mathbf{k}|$), we see from eq. (1.31) that the non-zero components of h_{ij}^{TT} are in the plane transverse to $\hat{\mathbf{n}}$ since, on a plane wave, the condition $\partial^j h_{ij} = 0$ becomes $n^i h_{ij} = 0$. Choosing for definiteness $\hat{\mathbf{n}}$ along the z axis, and, imposing that h_{ij} be symmetric and traceless, we have

$$h_{ij}^{\text{TT}}(t, z) = \begin{pmatrix} h_+ & h_\times & 0 \\ h_\times & -h_+ & 0 \\ 0 & 0 & 0 \end{pmatrix}_{ij} \cos[\omega(t - z/c)], \quad (1.32)$$

or, more simply,

$$h_{ab}^{\text{TT}}(t, z) = \begin{pmatrix} h_+ & h_\times \\ h_\times & -h_+ \end{pmatrix}_{ab} \cos[\omega(t - z/c)], \quad (1.33)$$

where $a, b = 1, 2$ are indices in the transverse (x, y) plane; h_+ and h_\times are called the amplitudes of the “plus” and “cross” polarization of the wave. In terms of the interval ds^2 ,

$$ds^2 = -c^2 dt^2 + dz^2 + \{1 + h_+ \cos[\omega(t - z/c)]\} dx^2 + \{1 - h_+ \cos[\omega(t - z/c)]\} dy^2 + 2h_\times \cos[\omega(t - z/c)] dxdy. \quad (1.34)$$

Given a plane wave solution $h_{\mu\nu}(x)$ propagating in the direction $\hat{\mathbf{n}}$, outside the sources, already in the Lorentz gauge but not yet in the TT gauge, we can find the form of the wave in the TT gauge as follows. First we introduce the tensor

$$P_{ij}(\hat{\mathbf{n}}) = \delta_{ij} - n_i n_j. \quad (1.35)$$

This tensor is symmetric, is transverse (i.e. $n^i P_{ij}(\hat{\mathbf{n}}) = 0$), is a projector (i.e. $P_{ik} P_{kj} = P_{ij}$), and its trace is $P_{ii} = 2$. With the help of P_{ij} we construct

$$\Lambda_{ij,kl}(\hat{\mathbf{n}}) = P_{ik} P_{jl} - \frac{1}{2} P_{ij} P_{kl}. \quad (1.36)$$

This is still a projector, in the sense that

$$\Lambda_{ij,kl} \Lambda_{kl,mn} = \Lambda_{ij,mn}. \quad (1.37)$$

Furthermore it is transverse on all indices, $n^i \Lambda_{ij,kl} = 0, n^j \Lambda_{ij,kl} = 0$, etc., it is traceless with respect to the (i, j) and (k, l) indices,

$$\Lambda_{ii,kl} = \Lambda_{ij,kk} = 0, \quad (1.38)$$

Projection onto the TT gauge; the Lambda tensor

and it is symmetric under the simultaneous exchange $(i, j) \leftrightarrow (k, l)$. In terms of $\hat{\mathbf{n}}$, its explicit form is

$$\begin{aligned}\Lambda_{ij,kl}(\hat{\mathbf{n}}) &= \delta_{ik}\delta_{jl} - \frac{1}{2}\delta_{ij}\delta_{kl} - n_j n_l \delta_{ik} - n_i n_k \delta_{jl} \\ &\quad + \frac{1}{2}n_k n_l \delta_{ij} + \frac{1}{2}n_i n_j \delta_{kl} + \frac{1}{2}n_i n_j n_k n_l.\end{aligned}\quad (1.39)$$

⁵This is the same tensor $\Lambda_{ij,kl}$ defined in Weinberg (1972), eq. (10.4.14). However, Weinberg only uses it in an equation where it is contracted with the tensor $T^{ij}T^{kl}$, which is symmetric under $i \leftrightarrow j$ and $k \leftrightarrow l$ and then he replaces the term $n_j n_l \delta_{ik} + n_i n_k \delta_{jl}$ in eq. (1.39) by $2n_j n_l \delta_{ik}$.

We shall meet $\Lambda_{ij,kl}$ often, and we call it the Lambda tensor.⁵ We can now show that, given a plane wave $h_{\mu\nu}$ in the Lorentz gauge, but not yet in the TT gauge, the GW in the TT gauge is given in terms of the spatial components h_{ij} of $h_{\mu\nu}$ by

$$h_{ij}^{\text{TT}} = \Lambda_{ij,kl} h_{kl}. \quad (1.40)$$

In fact by construction the right-hand side is transverse and traceless in (i, j) while, from the fact that $h_{\mu\nu}$ was a solution of the wave equation in the vacuum and that it was in the Lorentz gauge, it follows that $\square h_{ij}^{\text{TT}} = 0$. (Observe that it is important that $h_{\mu\nu}$ be in the Lorentz gauge already, otherwise the equation of motion that it satisfies would not simply be $\square h_{\mu\nu} = 0$.)

In general, given any symmetric tensor S_{ij} , we define its transverse-traceless part as

$$S_{ij}^{\text{TT}} = \Lambda_{ij,kl} S_{kl}. \quad (1.41)$$

Observe that S_{ij}^{TT} is still symmetric.

For later calculations, it is useful to spell out clearly our conventions and definitions for the plane wave expansion. In the TT gauge the equation of motion is $\square h_{ij}^{\text{TT}} = 0$ and therefore h_{ij}^{TT} can be expanded as

$$h_{ij}^{\text{TT}}(x) = \int \frac{d^3 k}{(2\pi)^3} (\mathcal{A}_{ij}(\mathbf{k}) e^{ikx} + \mathcal{A}_{ij}^*(\mathbf{k}) e^{-ikx}). \quad (1.42)$$

The four-vector k^μ , with dimensions of inverse length, is related to the frequency ω and to the wave-vector \mathbf{k} by $k^\mu = (\omega/c, \mathbf{k})$, with $|\mathbf{k}| = \omega/c = (2\pi f)/c$ and $\mathbf{k}/|\mathbf{k}| = \hat{\mathbf{n}}$. Therefore $d^3 k = |\mathbf{k}|^2 d|\mathbf{k}| d\Omega = (2\pi/c)^3 f^2 df d\Omega$, with $f > 0$. We denote by $d^2 \hat{\mathbf{n}} = d\cos\theta d\phi$ the integration over the solid angle, so the above equation reads

$$h_{ij}^{\text{TT}}(x) = \frac{1}{c^3} \int_0^\infty df f^2 \int d^2 \hat{\mathbf{n}} \left(\mathcal{A}_{ij}(f, \hat{\mathbf{n}}) e^{-2\pi i f(t - \hat{\mathbf{n}} \cdot \mathbf{x}/c)} + c.c. \right). \quad (1.43)$$

Observe that, inside the parentheses, both the contribution written explicitly and its complex conjugate refer to a wave traveling in the direction $+\hat{\mathbf{n}}$, since they depend on t and \mathbf{x} only through the combination $(t - \hat{\mathbf{n}} \cdot \mathbf{x}/c)$. Observe also that, in this form, only “physical” frequencies $f > 0$ enter in the expansion.

The TT gauge conditions (1.31) give $\mathcal{A}_i^i(\mathbf{k}) = 0$ and $k^i \mathcal{A}_{ij}(\mathbf{k}) = 0$. Of course, in a superposition of waves with different propagation directions, $h_{ij}(x)$ does not reduce to a 2×2 matrix; for instance, h_{12} gets

contributions from the waves with $k^3 \neq 0$, h_{13} gets contributions from the waves with $k^2 \neq 0$, h_{23} from the waves with $k^1 \neq 0$, etc. This will be important when we consider stochastic backgrounds of GWs. However, when we observe on Earth a GW emitted by a single astrophysical source, the direction of propagation of the wave, $\hat{\mathbf{n}}_0$, is very well defined and we can write

$$\mathcal{A}_{ij}(\mathbf{k}) = A_{ij}(f) \delta^{(2)}(\hat{\mathbf{n}} - \hat{\mathbf{n}}_0). \quad (1.44)$$

The transversality condition now states that the only non-vanishing components are those in the plane transverse to the propagation direction $\hat{\mathbf{n}}_0$. We label by $a, b = 1, 2$ the indices in the transverse plane and we omit, for notational simplicity, the superscript TT, since the fact that we are in the TT gauge is already implicit in the use of the indices $a, b = 1, 2$ instead of $i, j = 1, 2, 3$. Then

$$h_{ab}(t, \mathbf{x}) = \int_0^\infty df \left(\tilde{h}_{ab}(f, \mathbf{x}) e^{-2\pi ift} + \tilde{h}_{ab}^*(f, \mathbf{x}) e^{2\pi ift} \right), \quad (1.45)$$

where

$$\begin{aligned} \tilde{h}_{ab}(f, \mathbf{x}) &= \frac{f^2}{c^3} \int d^2 \hat{\mathbf{n}} \mathcal{A}_{ab}(f, \hat{\mathbf{n}}) e^{2\pi if \hat{\mathbf{n}} \cdot \mathbf{x}/c} \\ &= \frac{f^2}{c^3} A_{ab}(f) e^{2\pi if \hat{\mathbf{n}}_0 \cdot \mathbf{x}/c}. \end{aligned} \quad (1.46)$$

As we will see when we discuss the detectors, for resonant bars and ground based interferometers the linear dimensions of the detector are much smaller than the reduced wavelength $\bar{\lambda} = \lambda/(2\pi)$ of the GWs to which they are sensitive. In this case, choosing the origin of the coordinate system centered on the detector, we have $\exp\{2\pi if \hat{\mathbf{n}} \cdot \mathbf{x}/c\} = \exp\{i\hat{\mathbf{n}} \cdot \mathbf{x}/\bar{\lambda}\} \simeq 1$ all over the detector. If we are interested in the GW at the detector location, we can therefore neglect all \mathbf{x} -dependences and write simply

$$h_{ab}(t) = \int_0^\infty df \left(\tilde{h}_{ab}(f) e^{-2\pi ift} + \tilde{h}_{ab}^*(f) e^{2\pi ift} \right), \quad (1.47)$$

with $\tilde{h}_{ab}(f) = \tilde{h}_{ab}(f, \mathbf{x} = 0)$. Of course, the dependence on \mathbf{x} must be kept when we compare the GW signal at two different detectors (e.g. when we consider the overlap reduction function in a two-detector correlation, see Section 7.8.3) or when we need spatial derivatives of $h_{ab}(t, \mathbf{x})$ (e.g. when we compute spatial components of the energy-momentum tensor).

From eq. (1.33) it follows that

$$\tilde{h}_{ab}(f) = \begin{pmatrix} \tilde{h}_+(f) & \tilde{h}_\times(f) \\ \tilde{h}_\times(f) & -\tilde{h}_+(f) \end{pmatrix}_{ab}. \quad (1.48)$$

The + and \times polarizations are defined with respect to a given choice of axes in the transverse plane. If we rotate by an angle ψ the system of

axes used for their definition, we show in Problem 2.1 that h_+ and h_\times transform as

$$h_+ \rightarrow h_+ \cos 2\psi - h_\times \sin 2\psi, \quad (1.49)$$

$$h_\times \rightarrow h_+ \sin 2\psi + h_\times \cos 2\psi. \quad (1.50)$$

Observe that, until now, only physical frequencies $f > 0$ entered our equations. However, eq. (1.45) can be rewritten in a slightly more compact form, extending the definition of $\tilde{h}_{ab}(f, \mathbf{x})$ to negative frequencies, by defining

$$\tilde{h}_{ab}(-f, \mathbf{x}) = \tilde{h}_{ab}^*(f, \mathbf{x}), \quad (1.51)$$

so that eq. (1.45) becomes⁶ (we do not explicitly write the \mathbf{x} dependence)

$$h_{ab}(t) = \int_{-\infty}^{\infty} df \tilde{h}_{ab}(f) e^{-2\pi ift}. \quad (1.52)$$

The inversion of eq. (1.52) is

$$\tilde{h}_{ab}(f) = \int_{-\infty}^{\infty} dt h_{ab}(t) e^{2\pi ift}. \quad (1.53)$$

Another useful form for the plane wave expansion is obtained by introducing the polarization tensors $e_{ij}^A(\hat{\mathbf{n}})$ (with $A = +, \times$ labeling the polarizations) defined as

$$e_{ij}^+(\hat{\mathbf{n}}) = \hat{\mathbf{u}}_i \hat{\mathbf{u}}_j - \hat{\mathbf{v}}_i \hat{\mathbf{v}}_j, \quad e_{ij}^\times(\hat{\mathbf{n}}) = \hat{\mathbf{u}}_i \hat{\mathbf{v}}_j + \hat{\mathbf{v}}_i \hat{\mathbf{u}}_j, \quad (1.54)$$

with $\hat{\mathbf{u}}, \hat{\mathbf{v}}$ unit vectors orthogonal to the propagation direction $\hat{\mathbf{n}}$ and to each other. With this definition, the polarization tensors are normalized as

$$e_{ij}^A(\hat{\mathbf{n}}) e^{A',ij}(\hat{\mathbf{n}}) = 2\delta^{AA'}. \quad (1.55)$$

In the frame where $\hat{\mathbf{n}}$ is along the \hat{z} direction, we can choose $\hat{\mathbf{u}} = \hat{\mathbf{x}}$ and $\hat{\mathbf{v}} = \hat{\mathbf{y}}$, so

$$e_{ab}^+ = \begin{pmatrix} 1 & 0 \\ 0 & -1 \end{pmatrix}_{ab}, \quad e_{ab}^\times = \begin{pmatrix} 0 & 1 \\ 1 & 0 \end{pmatrix}_{ab}, \quad (1.56)$$

with $a, b = 1, 2$ spanning the (x, y) plane. In a generic frame, we can define the amplitudes $\tilde{h}_A(f, \hat{\mathbf{n}})$ from

$$\frac{f^2}{c^3} \mathcal{A}_{ij}(f, \hat{\mathbf{n}}) = \sum_{A=+, \times} \tilde{h}_A(f, \hat{\mathbf{n}}) e_{ij}^A(\hat{\mathbf{n}}). \quad (1.57)$$

Equation (1.43) then becomes

$$h_{ab}(t, \mathbf{x}) = \sum_{A=+, \times} \int_{-\infty}^{\infty} df \int d^2 \hat{\mathbf{n}} \tilde{h}_A(f, \hat{\mathbf{n}}) e_{ab}^A(\hat{\mathbf{n}}) e^{-2\pi if(t - \hat{\mathbf{n}} \cdot \mathbf{x}/c)}, \quad (1.58)$$

where again we have defined $\tilde{h}_A(-f, \hat{\mathbf{n}}) = \tilde{h}_A^*(f, \hat{\mathbf{n}})$.

1.3 Interaction of GWs with test masses

In the previous section we have seen how to describe a GW. In this section we discuss the interaction of GWs with a detector, idealized for the moment as a set of test masses. This is an issue that hides some subtleties because, even if the physics must finally be invariant under coordinate transformations, the language that we use to describe the GWs and the detector, as well as the intermediate steps of the computations, do depend on the reference frame that we choose.

In general relativity, the mathematical procedure of choosing a gauge corresponds, physically, to selecting a specific observer. We have seen that GWs have an especially simple form in the TT gauge, so we want to understand which reference frame corresponds to the TT gauge. We will also see that the description of the detector is more intuitive in another frame, the detector proper frame. It is therefore important, when we discuss the interaction of GWs with the detector, to be aware of which reference frame we are using, and to understand which is the appropriate language in that frame.

Two important tools for understanding the physical meaning of a given gauge choice are the geodesic equation and the equation of the geodesic deviation. We briefly recall these basic concepts of general relativity in the next subsection. We will then explore the interaction of GWs with test masses in different frames, in particular in the TT frame and in the detector proper frame.

1.3.1 Geodesic equation and geodesic deviation

In this subsection and in the next we recall some elementary notions of general relativity, referring the reader, e.g. to Misner, Thorne and Wheeler (1973) or to Hartle (2003) for more details and proofs. Consider, in some reference frame, a curve $x^\mu(\lambda)$, parametrized by a parameter λ . The interval ds between two points separated by $d\lambda$ is given by

$$\begin{aligned} ds^2 &= g_{\mu\nu} dx^\mu dx^\nu \\ &= g_{\mu\nu} \frac{dx^\mu}{d\lambda} \frac{dx^\nu}{d\lambda} d\lambda^2. \end{aligned} \quad (1.59)$$

All along a space-like curve we have, by definition, $ds^2 > 0$, and we can use

$$ds = (g_{\mu\nu} dx^\mu dx^\nu)^{1/2} \quad (1.60)$$

to measure proper distances along the curve. A time-like curve is rather defined by the condition that all along it $ds^2 < 0$, and in this case we can define the proper time τ , from

$$c^2 d\tau^2 = -ds^2 = -g_{\mu\nu} dx^\mu dx^\nu. \quad (1.61)$$

The proper time τ is the time measured by a clock carried along this trajectory. It is therefore natural to use τ itself as the parameter λ

which parametrizes the trajectory, so that $x^\mu = x^\mu(\tau)$. Observe, from eq. (1.61), that

$$g_{\mu\nu} \frac{dx^\mu}{d\tau} \frac{dx^\nu}{d\tau} = -c^2. \quad (1.62)$$

The four-velocity u^μ is defined as

$$u^\mu = \frac{dx^\mu}{d\tau}, \quad (1.63)$$

so eq. (1.62) reads

$$g_{\mu\nu} u^\mu u^\nu = -c^2. \quad (1.64)$$

Among all possible time-like curves that satisfy the fixed boundary conditions $x^\mu(\tau_A) = x_A^\mu$ and $x^\mu(\tau_B) = x_B^\mu$, the classical trajectory of a point-like test mass m is obtained by extremizing the action

$$S = -m \int_{\tau_A}^{\tau_B} d\tau. \quad (1.65)$$

This gives the *geodesic equation*,

$$\frac{d^2x^\mu}{d\tau^2} + \Gamma_{\nu\rho}^\mu(x) \frac{dx^\nu}{d\tau} \frac{dx^\rho}{d\tau} = 0,$$

(1.66)

which is the classical equation of motion of a test mass in the curved background described by the metric $g_{\mu\nu}$, in the absence of external non-gravitational forces. In terms of the four-velocity u^μ , the geodesic equation reads

$$\frac{du^\mu}{d\tau} + \Gamma_{\nu\rho}^\mu u^\nu u^\rho = 0. \quad (1.67)$$

Consider now two nearby geodesics, one parametrized by $x^\mu(\tau)$ and the other by $x^\mu(\tau) + \xi^\mu(\tau)$.⁷ Then $x^\mu(\tau)$ satisfies eq. (1.66), while $x^\mu(\tau) + \xi^\mu(\tau)$ satisfies

$$\frac{d^2(x^\mu + \xi^\mu)}{d\tau^2} + \Gamma_{\nu\rho}^\mu(x + \xi) \frac{d(x^\nu + \xi^\nu)}{d\tau} \frac{d(x^\rho + \xi^\rho)}{d\tau} = 0. \quad (1.68)$$

If $|\xi^\mu|$ is much smaller than the typical scale of variation of the gravitational field, taking the difference between eqs. (1.68) and (1.66), and expanding to first order in ξ , we get

$$\frac{d^2\xi^\mu}{d\tau^2} + 2\Gamma_{\nu\rho}^\mu(x) \frac{dx^\nu}{d\tau} \frac{d\xi^\rho}{d\tau} + \xi^\sigma \partial_\sigma \Gamma_{\nu\rho}^\mu(x) \frac{dx^\nu}{d\tau} \frac{dx^\rho}{d\tau} = 0. \quad (1.69)$$

This is the equation of the geodesic deviation. We can rewrite it in a more elegant way by introducing the covariant derivative of a vector field $V^\mu(x)$ along the curve $x^\mu(\tau)$,

$$\frac{DV^\mu}{D\tau} \equiv \frac{dV^\mu}{d\tau} + \Gamma_{\nu\rho}^\mu V^\nu \frac{dx^\rho}{d\tau}. \quad (1.70)$$

Then, eq. (1.69) can be written as

$$\frac{D^2\xi^\mu}{D\tau^2} = -R^\mu_{\nu\rho\sigma} \xi^\rho \frac{dx^\nu}{d\tau} \frac{dx^\sigma}{d\tau},$$

(1.71)

or, in terms of the four-velocity u^μ ,

$$\frac{D^2\xi^\mu}{D\tau^2} = -R^\mu_{\nu\rho\sigma}\xi^\rho u^\nu u^\sigma. \quad (1.72)$$

This equation shows that two nearby time-like geodesics experience a tidal gravitational force, which is determined by the Riemann tensor. Writing explicitly the geodesic equation or the equation of the geodesic deviation in the reference frame of interest we can understand how test masses behave for the corresponding observer. We consider the most relevant examples in the next subsections.

1.3.2 Local inertial frames and freely falling frames

Before discussing the TT frame and the detector frame, it may be useful to recall some basic facts about the construction of local inertial frames and of freely falling frames.

It is a standard exercise in general relativity to show that it is always possible to perform a change of coordinates such that, at a given space-time point P , all the components of the Christoffel symbol vanish, $\Gamma^\mu_{\nu\rho}(P) = 0$. In such a frame, at P the geodesic equation (1.66) becomes

$$\left. \frac{d^2x^\mu}{d\tau^2} \right|_P = 0, \quad (1.73)$$

so in this frame a test mass is free falling, although only at one point in space and at one moment in time. Such a frame is called a *local inertial frame* (sometimes abbreviated as LIF), and gives a realization of the equivalence principle.

An explicit construction of the corresponding system of coordinates can be done as follows (see, e.g. Hartle 2003, Section 8.4). At the point P we choose a basis of four orthonormal four-vectors, e_α , where $\alpha = 0, \dots, 3$ labels the four-vector. We choose them orthogonal to each other with respect to the flat-space metric $\eta_{\mu\nu}$, so $\eta_{\mu\nu}e_\alpha^\mu e_\beta^\nu = \eta_{\alpha\beta}$. Consider now the spatial geodesic that starts at P , in the direction of a space-like unit four-vector n . We parametrize the geodesic using the proper distance. Let Q be the point reached from P , moving along this geodesic, after a proper distance s , and let (n^0, n^1, n^2, n^3) be the components of n in the basis $\{e_\alpha\}$. Then we assign to Q the coordinates $x_Q = (sn^0, sn^1, sn^2, sn^3)$. Thus, for example, if we send out a geodesic along the direction e_3 , and we meet a point Q after a proper distance s , the coordinates of Q are $x_Q = (0, 0, 0, s)$. Similarly, we send out a time-like geodesic in the direction of a time-like unit four-vector n , we parametrize this geodesic using proper time, and we assign the coordinates $(\tau n^0, \tau n^1, \tau n^2, \tau n^3)$ to the point that we reach after a proper time τ .

We fill all of space-time with time-like or space-like geodesics (null geodesics can be approximated to arbitrary accuracy with time-like or space-like geodesics and therefore can be obtained by continuity), so all points are reached by at least one geodesic.

In a sufficiently small region of space, geodesics do not intersect (which of course is no longer true on large regions of space, as vividly shown for instance by the phenomenon of gravitational lensing), so each point in this small region is reached by one and only one geodesic. Thus, the above method allows us to assign coordinates unambiguously to all points of a sufficiently small space-time region around P . This coordinate system is known as *Riemann normal coordinates*. We can now check that it indeed gives an explicit realization of a local inertial frame.

First of all, the fact that $g_{\mu\nu}(P) = \eta_{\mu\nu}$ follows simply from the fact that the coordinates are referred to the basis $\{e_\alpha\}$, built at P , which by definition is orthonormal with respect to the flat space-time metric, $\eta_{\mu\nu} e_\alpha^\mu e_\beta^\nu = \eta_{\alpha\beta}$. To show that we also have $\Gamma_{\nu\rho}^\mu(P) = 0$ in this frame, consider the geodesic equation (1.66). Since, by definition, the coordinates are linear in proper time (if they are reached by a time-like geodesic; or linear in proper distance if they are reached by space-like geodesics, in which case in the geodesic equation (1.66) τ must be replaced by s), the term $d^2x^\mu/d\tau^2$ (or d^2x^μ/ds^2 for space-like geodesics) vanishes, while $dx^\mu/d\tau = n^\mu$. Then the geodesic equation becomes

$$\Gamma_{\nu\rho}^\mu(P)n^\nu n^\rho = 0, \quad (1.74)$$

and, since this holds for all n^μ , we conclude that

$$\Gamma_{\nu\rho}^\mu(P) = 0. \quad (1.75)$$

Riemann normal coordinates therefore provide an explicit example of a local inertial frame.

In a local inertial frame a test mass moves freely only at one point in space and at one moment in time. We can however do much better than this, building a reference frame where a test mass is in free fall *all along the geodesic*. Such a frame can be built observing that a freely spinning object (like a gyroscope) that moves along a time-like geodesic $x^\mu(\tau)$ obeys the equation

$$\frac{ds^\mu}{d\tau} + \Gamma_{\nu\rho}^\mu s^\nu \frac{dx^\rho}{d\tau} = 0, \quad (1.76)$$

where s^μ is the spin four-vector, i.e. the four-vector that in the rest frame reduces to $s^\mu = (0, \mathbf{s})$. This equation is the covariant generalization of the equation $ds^\mu/d\tau = 0$ that expresses the conservation of angular momentum in flat space-time. We start by constructing a local inertial frame at P , as before, but using three gyroscopes to mark the direction of the spatial axes. We then propagate this reference frame along the geodesic, always orienting the spatial axes in the direction pointed out by the gyroscopes (while the time axis is in the direction of the four-velocity along the geodesic). By definition, then, in this frame the gyroscopes do not rotate with respect to the axes since they *define* the orientation of the axes. Then, $ds^\mu/d\tau = 0$ along the entire time-like geodesic and, from eq. (1.76), we see that $\Gamma_{\nu\rho}^\mu$ vanishes along the entire time-like geodesic, and not just at a single point P . Such a reference frame is called a *freely*

falling frame, and its coordinates (Riemann normal coordinates with axes marked by gyroscopes) are known as *Fermi normal coordinates*. A freely falling frame is therefore a local inertial frame along an entire geodesic.

Such a frame is practically given by drag-free satellites, in which an experimental apparatus is freely floating inside a satellite, which screens it from external disturbances (e.g. solar wind, micrometeorites, etc.). The satellite senses precisely the position of the experimental apparatus and adjusts its position, using thrusters, to remain centered about it. As we will see, these drag-free techniques are crucial for a space interferometer.

1.3.3 TT frame and proper detector frame

The TT frame

We have seen that there exists a gauge where GWs have an especially simple form, the TT gauge. We denote the corresponding reference frame as the TT frame and we now ask what it means, physically, to be in the TT frame.

Again, the answer can be found by looking at the geodesic equation, eq. (1.66). If a test mass is at rest at $\tau = 0$, we find from eq. (1.66) that

$$\begin{aligned} \frac{d^2x^i}{d\tau^2}\Big|_{\tau=0} &= - \left[\Gamma_{\nu\rho}^i(x) \frac{dx^\nu}{d\tau} \frac{dx^\rho}{d\tau} \right]_{\tau=0} \\ &= - \left[\Gamma_{00}^i \left(\frac{dx^0}{d\tau} \right)^2 \right]_{\tau=0}, \end{aligned} \quad (1.77)$$

where in the second line we used the fact that, by assumption, at $\tau = 0$ we have $dx^i/d\tau = 0$, since we took the mass initially at rest. Writing $g_{\mu\nu} = \eta_{\mu\nu} + h_{\mu\nu}$ and expanding to first order in $h_{\mu\nu}$, the Christoffel symbol $\Gamma_{\nu\rho}^\mu$ becomes

$$\Gamma_{\nu\rho}^\mu = \frac{1}{2} \eta^{\mu\sigma} (\partial_\nu h_{\rho\sigma} + \partial_\rho h_{\nu\sigma} - \partial_\sigma h_{\nu\rho}), \quad (1.78)$$

and therefore

$$\Gamma_{00}^i = \frac{1}{2} (2\partial_0 h_{0i} - \partial_i h_{00}). \quad (1.79)$$

However, in the TT gauge this quantity vanishes, because both h_{00} and h_{0i} are set to zero by the gauge condition. Therefore, if at time $\tau = 0$ $dx^i/d\tau$ is zero, in the TT gauge also its derivative $d^2x^i/d\tau^2$ vanishes, and therefore $dx^i/d\tau$ remains zero at all times. This shows that *in the TT frame, particles which were at rest before the arrival of the wave remain at rest even after the arrival of the wave*.⁸

In other words, the coordinates of the TT frame stretch themselves, in response to the arrival of the wave, in such a way that the position of free test masses initially at rest do not change. A physical implementation of the TT gauge can be obtained using the free test masses themselves to mark the coordinates. We can use a test mass to define the origin

⁸Strictly speaking, this is true only to linear order in $h_{\mu\nu}$ since, if we also include the terms $O(h^2)$ in eq. (1.78), Γ_{00}^i no longer vanishes. However, given that on Earth one typically expects GWs with at most $h = O(10^{-21})$, going beyond the linear order is here of no interest.

of the coordinates, a second one to define, e.g. the point with spatial coordinates ($x = 1, y = 0, z = 0$), and so on; then, we state that, by definition, these masses still mark the origin, the point ($x = 1, y = 0, z = 0$), etc. even when the GW is passing.

If the coordinates of test masses initially at rest remain constant, also their coordinate separation must remain constant, for arbitrary finite separation and therefore, of course, also when the separation is small with respect to the typical length-scale of variation of the GW, which is its reduced wavelength. In this limiting case, the equation of the geodesic deviation applies, and it is instructive to check explicitly, from the equation of the geodesic deviation in the TT frame, that the separation ξ^i between the coordinates of two test masses initially at rest does not change. To this purpose, we use the spatial component ($\mu = i$) of eq. (1.69). Since, at $\tau = 0$, $dx^i/d\tau = 0$ by assumption, while $dx^0/d\tau = c$, we get

$$\frac{d^2\xi^i}{d\tau^2}\Big|_{\tau=0} = - \left[2c\Gamma_{0\rho}^i \frac{d\xi^\rho}{d\tau} + c^2\xi^\sigma \partial_\sigma \Gamma_{00}^i \right]_{\tau=0}. \quad (1.80)$$

However, we already saw that in the TT gauge Γ_{00}^i vanishes identically (at all values of space and time, since in the TT gauge h_{0i} and h_{00} vanish everywhere), and therefore in the first term in bracket, $\Gamma_{0\rho}^i$ is non-vanishing only if ρ is a spatial index, while in the second term $\partial_\sigma \Gamma_{00}^i = 0$. From eq. (1.78), in the TT gauge $\Gamma_{0j}^i = (1/2)\partial_0 h_{ij}$. Therefore, in the TT gauge, the equation of the geodesic deviation gives

$$\frac{d^2\xi^i}{d\tau^2}\Big|_{\tau=0} = - \left[h_{ij} \frac{d\xi^i}{d\tau} \right]_{\tau=0}, \quad (1.81)$$

and therefore, if at $\tau = 0$ we have $d\xi^i/d\tau = 0$, then also $d^2\xi^i/d\tau^2 = 0$, and the separation ξ^i remains constant at all times.⁹

Observe also that, since in the TT gauge we have $h_{00} = h_{0i} = 0$, the proper time on a time-like trajectory $x^\mu(\tau) = (x^0(\tau), x^i(\tau))$ is obtained from

$$\begin{aligned} c^2 d\tau^2 &= c^2 dt^2(\tau) - (\delta_{ij} + h_{ij}^{\text{TT}}) dx^i(\tau) dx^j(\tau) \\ &= c^2 dt^2(\tau) - (\delta_{ij} + h_{ij}^{\text{TT}}) \frac{dx^i}{d\tau} \frac{dx^j}{d\tau} d\tau^2, \end{aligned} \quad (1.82)$$

where we write $x^0(\tau) = ct(\tau)$. However, we have seen for a test mass initially at rest that $dx^i(\tau)/d\tau = 0$ at all times. Then, in the TT gauge the proper time τ measured by a clock sitting on a test mass initially at rest is the same as coordinate time t .¹⁰

The TT gauge illustrates in a particularly neat way the fact that, in general relativity, the physical effects are not expressed by what happens to the coordinates since the theory is invariant under coordinate transformations. At first sight one might be surprised that in the TT gauge the position of test masses does not change as a GW passes by. Of course, this does not mean that the GW had no physical effect, but only that we used the freedom in choosing the coordinate system to *define* the coordinates in such a way that they do not change. Physical effects can

⁹To avoid misunderstandings, observe that ξ^i is a *coordinate* distance, since it is the difference between the coordinates of two test masses. It is not a *proper* distance. We will see below what happens if we consider proper distances.

¹⁰Actually, this is true up to irrelevant correction $O(h^4)$ since $dx^i(\tau)/d\tau = O(h^2)$. Compare with Note 8.

instead be found monitoring *proper distances*, or *proper times*. Consider for instance two events at $(t, x_1, 0, 0)$ and at $(t, x_2, 0, 0)$, respectively. In the TT gauge, the *coordinate distance* $x_2 - x_1 = L$ remains constant, even if there is a GW propagating along the z axis. However, we see from eq. (1.34) that the *proper distance* s between these two events is

$$\begin{aligned} s &= (x_2 - x_1)[1 + h_+ \cos(\omega t)]^{1/2} \\ &\simeq L[1 + \frac{1}{2}h_+ \cos(\omega t)], \end{aligned} \quad (1.83)$$

where in the second line we only retained the term linear in h_+ . Therefore, the proper distance changes periodically in time because of the GW. More generally, if the spatial separation between the two events is given by a vector \mathbf{L} , the proper distance is given by $s^2 = L^2 + h_{ij}(t)L_iL_j$ and, to linear order in h , we have $s \simeq L + h_{ij}(L_iL_j/2L)$, implying

$$\ddot{s} \simeq \frac{1}{2}\ddot{h}_{ij}\frac{L_i}{L}L_j. \quad (1.84)$$

Writing $L_i/L = n_i$ and defining s_i from $s = n_is_i$, we get

$$\begin{aligned} \ddot{s}_i &\simeq \frac{1}{2}\ddot{h}_{ij}L_j \\ &\simeq \frac{1}{2}\ddot{h}_{ij}s_j, \end{aligned} \quad (1.85)$$

where in the second line we used the fact that, to lowest order in h , we have $L_j = s_j$. This is the geodesic equation in terms of proper distances, rather than coordinate distances.

If these two test masses are mirrors between which a light beam travels back and forth, it is the proper distance that determines the time taken by the light to make a round trip, so the fact that GWs affect the proper distance means that they can be detected measuring the round-trip time. We will see in detail in Chapter 9 how to analyze an interferometric GW detector in this way.

The proper detector frame

The TT frame has the advantage that GWs have a very simple form in it. However, it is not the frame normally used by an experimentalist to describe its apparatus. In a laboratory, positions are not marked by freely falling particles; rather, after choosing an origin, one ideally uses a rigid ruler to define the coordinates.¹¹ In this frame we expect that a test mass which is free to move (at least along some direction) will be displaced by the passage of the GWs, with respect to the position defined by the rigid ruler and by the test mass which defines the origin. This is different from what happens in the TT frame, where the positions of the test masses are, by definition, unchanged by an incoming GW.

Conceptually, the simplest laboratory to analyze is one inside a drag-free satellite, so the apparatus is indeed in free fall in the total gravitational field, both of the Earth and of the GWs which might be present.

¹¹A rigid ruler is of course an idealization. When we study resonant bars, in Chapter 8, we will see that a bar (and hence also a ruler) is stretched by an incoming GW. We denote by $\xi_0(t)$ the oscillation amplitude of the fundamental elastic mode of a bar (or of a ruler) of length L , and by ω_0 and γ_0 the frequency and the dissipation coefficient of this elastic mode (with $\gamma_0 \ll \omega_0$), respectively. We will find in eq. (8.32) that, when the bar (or the ruler) is driven by a monochromatic GW with frequency ω and amplitude h_0 ,

$$\begin{aligned} \xi_0(t) &= (2Lh_0\omega^2/\pi^2) \\ &\times \frac{(\omega^2 - \omega_0^2)\cos\omega t - \gamma_0\omega\sin\omega t}{(\omega^2 - \omega_0^2)^2 + \gamma_0^2\omega^2}. \end{aligned}$$

For a resonant bar, one chooses the frequency ω_0 of the fundamental elastic mode as close as possible to the frequency ω of the GW that one is searching, so the denominator becomes very small (typically, in a resonant bar $\gamma_0 = \omega_0/Q$ with $Q \sim 10^6$) and $\xi_0(t)$ is enhanced. A ruler is instead rigid, with respect to a GW with a frequency ω , if it has $\omega_0 \gg \omega$; then the above equation becomes $\xi_0(t) \simeq -(\Delta L)\cos\omega t$, with

$$\Delta L/L = (2/\pi^2)h_0(\omega/\omega_0)^2.$$

Then $\omega_0 \gg \omega$ implies that $\Delta L/L \ll h$. We will see in eq. (8.14) that $\omega_0 = \pi v_s/L$, where v_s is the speed of sound in the material. Thus, a rigid ruler can be obtained taking L small. Observe also that all experiments do not measure the absolute length of the apparatus, but rather the length variation induced by a GW. Therefore a very small rigid ruler is all that is needed.

This means that, if we restrict our attention to a sufficiently small region of space, we can choose coordinates (t, \mathbf{x}) so that *even in the presence of GWs*, the metric is flat,

$$ds^2 \simeq -c^2 dt^2 + \delta_{ij} dx^i dx^j. \quad (1.86)$$

We have seen in Section 1.3.2 how to explicitly construct such a freely falling frame along an entire geodesic, using Fermi normal coordinates.

To linear order in $|x^i|$ there are no corrections to this metric, since in a freely falling frame the derivatives of $g_{\mu\nu}$ vanish at the point P around which we expand. Pursuing the expansion to second order, and expressing the second derivatives of $g_{\mu\nu}$ in terms of the Riemann tensor (using again the fact that the Christoffel symbol vanishes at the point P around which we are expanding), the result is

$$\begin{aligned} ds^2 \simeq & -c^2 dt^2 [1 + R_{0i0j} x^i x^j] \\ & - 2cdt dx^i \left(\frac{2}{3} R_{0jik} x^j x^k \right) + dx^i dx^j \left[\delta_{ij} - \frac{1}{3} R_{ikjl} x^k x^l \right], \end{aligned} \quad (1.87)$$

where the Riemann tensor is evaluated at the point P . We see that, if L_B is the typical variation scale of the metric, so that $R_{\mu\nu\rho\sigma} = O(1/L_B^2)$, the corrections to the flat metric are $O(r^2/L_B^2)$, where $r^2 = x^i x^i$.

For an Earthbound detector, the situation seems more complicated since it is not in free fall with respect to the Earth's gravity (that is, it has an acceleration $\mathbf{a} = -\mathbf{g}$ with respect to a local inertial frame), and furthermore it rotates relative to local gyroscopes (as illustrated for instance by a Foucault pendulum). The metric in this laboratory frame can be found by explicitly writing the coordinate transformation from the inertial frame to the frame which is accelerating and rotating, and transforming the metric accordingly. The result, up to $O(r^2)$, is¹²

$$\begin{aligned} ds^2 \simeq & -c^2 dt^2 \left[1 + \frac{2}{c^2} \mathbf{a} \cdot \mathbf{x} + \frac{1}{c^4} (\mathbf{a} \cdot \mathbf{x})^2 - \frac{1}{c^2} (\boldsymbol{\Omega} \times \mathbf{x})^2 + R_{0i0j} x^i x^j \right] \\ & + 2cdt dx^i \left[\frac{1}{c} \epsilon_{ijk} \Omega^j x^k - \frac{2}{3} R_{0jik} x^j x^k \right] \\ & + dx^i dx^j \left[\delta_{ij} - \frac{1}{3} R_{ikjl} x^k x^l \right], \end{aligned} \quad (1.88)$$

where a^i is the acceleration of the laboratory with respect to a local free falling frame (i.e. a^i is minus the local “acceleration of gravity”) and Ω^i is the angular velocity of the laboratory with respect to local gyroscopes. The term $2\mathbf{a} \cdot \mathbf{x}/c^2$ in eq. (1.88) gives the inertial acceleration. The term $(\mathbf{a} \cdot \mathbf{x}/c^2)^2$ is a gravitational redshift. The term $(\boldsymbol{\Omega} \times \mathbf{x}/c)^2$ gives a Lorentz time dilatation due to the angular velocity of the laboratory. The term $(1/c)\epsilon_{ijk}\Omega^j x^k$ is known as the Sagnac effect. Finally, the terms proportional to the Riemann tensor contain both the effect of slowly varying gravitational backgrounds and the effect of GWs.

The frame where the metric has the form (1.88) is called the *proper detector frame*, and is implicitly used by experimentalists in a laboratory

¹²See Ni and Zimmermann (1978), or eq. (4.1) of Thorne (1983).

on Earth: first of all, at zeroth order in r/L_B , this metric reduces to eq. (1.86), i.e. as long as we focus on regions of space smaller than the typical variation scale of the background, *we live in the flat space-time of Newtonian physics*. This should be contrasted with the TT gauge, where the GW is always present in the background space-time (and no simplification appears when performing an expansion in r/L_B ; the metric in the TT gauge is not an expansion in r/L_B). Next, in the proper frame there are corrections linear in r/L_B . Their effects can be described in terms of Newtonian forces (Newtonian gravity, Coriolis forces, centrifugal forces, etc.). In fact, writing the geodesic equation corresponding to the metric (1.88), and neglecting the terms $O(r^2)$ in the metric, we get

$$\frac{d^2x^i}{d\tau^2} = -a^i - 2(\boldsymbol{\Omega} \times \mathbf{v})^i + \frac{f^i}{m} + O(x^i). \quad (1.89)$$

The term $-a^i$ is the acceleration of gravity while $-2(\boldsymbol{\Omega} \times \mathbf{v})^i$ is the Coriolis acceleration, and we also added an external force f^i which represents, for instance, the suspension mechanism that compensates the acceleration of gravity. Including the terms $O(x^i x^j)$ in the metric, we get corresponding terms $O(x^i)$ on the right-hand side of eq. (1.89), such as a term $-[\boldsymbol{\Omega} \times (\boldsymbol{\Omega} \times \mathbf{r})]^i$ which gives the centrifugal acceleration, etc.¹³ Details aside, the point is that in this frame the evolution of the coordinate $x^i(\tau)$ of a test mass is described by the equations of motion of Newtonian physics, i.e. in terms of forces.

At quadratic order there are also the terms proportional to the Riemann tensor, to which both the slowly varying gravitational field of the Earth, and the GWs contribute. The effect of the GWs is therefore entirely in the term $O(r^2)$. In principle, GWs must therefore compete with a number of other effects, like static gravitational forces, Coriolis forces, etc., that practically are many order of magnitudes larger. What can save the situation is the fact that GWs can have high frequencies, compared to the typical variation time-scales of all other effects. In practice, as we will see when we discuss the various Earthbound detectors, GWs with frequencies lower than a few Hz are hopelessly lost into a sea of much higher Newtonian noises. At higher frequencies, however, it is possible to have a frequency window¹⁴ where sufficient isolation from external noises is possible, and an interesting sensitivity to GWs can be obtained.

To isolate the effect of GWs, we can therefore focus on the response of the detector in this frequency window. The acceleration a^i is compensated by the suspension mechanism, and all other effects produce slowly varying changes. We can then neglect all terms in eq. (1.88), and we only retain the part proportional to the Riemann tensor. This means that we can use eq. (1.87), i.e. the metric in the freely falling frame, and we deduce from it the geodesic equation. It is understood that we restrict to the components of $x^i(\tau)$ in the direction in which the test masses are left free to move by the suspension mechanism, and that we consider only the Fourier components of the motion in a frequency window where the

¹³See eq. (20) of Ni and Zimmermann (1978), for the full expression including relativistic corrections.

¹⁴Sufficiently high frequency is necessary to overcome the slowly varying Newtonian noises, as well as the seismic noise. However, we will see that above a certain frequency, other types of instrumental noise begin to dominate, and therefore only a frequency window is available for GW detection.

detector is sensitive to GWs. In this frequency window, we will assume that time-varying Newtonian gravitational forces are sufficiently small, so that only GWs contribute to the Riemann tensor.

Rather than using the geodesic equation, it is actually simpler to use the equation for the geodesic deviation, in the form (1.69). We use the fact that $\Gamma_{\nu\rho}^\mu$ vanishes at the expansion point P . Furthermore, since the detector moves non-relativistically, $dx^i/d\tau$ can be neglected with respect to $dx^0/d\tau$, and eq. (1.69) gives

$$\frac{d^2\xi^i}{d\tau^2} + \xi^\sigma \partial_\sigma \Gamma_{00}^i \left(\frac{dx^0}{d\tau} \right)^2 = 0. \quad (1.90)$$

The metric (1.87) depends quadratically on the distance x^i from the point P around which we are expanding, while it depends on t only through the Riemann tensor. In eq. (1.90), $\partial_\sigma \Gamma_{00}^i$ is evaluated at the point P , i.e. at $x^i = 0$. Since $g_{\mu\nu} = \eta_{\mu\nu} + O(x^i x^j)$, a non-zero contribution comes only from the terms in which the two derivatives on the metric present in $\partial_\sigma \Gamma_{00}^i$ are both spatial derivatives, and act on $x^i x^j$. In particular $\partial_0 \Gamma_{00}^i$ evaluated at P gives zero, so $\xi^\sigma \partial_\sigma \Gamma_{00}^i = \xi^j \partial_j \Gamma_{00}^i$. Furthermore, using the fact that, at the point P , both $\Gamma_{\nu\rho}^\mu = 0$ and $\partial_0 \Gamma_{0j}^i = 0$, we have $R^i_{0j0} = \partial_j \Gamma_{00}^i - \partial_0 \Gamma_{0j}^i = \partial_j \Gamma_{00}^i$, so eq. (1.90) becomes

$$\frac{d^2\xi^i}{d\tau^2} = -R^i_{0j0} \xi^j \left(\frac{dx^0}{d\tau} \right)^2. \quad (1.91)$$

If a test mass is initially at rest, it acquires a velocity $dx^i/d\tau = cO(h)$ after the passage of the GW. Therefore

$$\begin{aligned} dt^2 &= d\tau^2 \left[1 + \frac{1}{c^2} \frac{dx^i}{d\tau} \frac{dx^i}{d\tau} \right] \\ &= d\tau^2 [1 + O(h^2)]. \end{aligned} \quad (1.92)$$

On the other hand, in eq. (1.91) the Riemann tensor R^i_{0j0} is already $O(h)$, since we are neglecting all effects of the background and we are considering only the GWs. Therefore, if in eq. (1.91) we limit ourselves to linear order in h , we can write $t = \tau$, so $dx^0/d\tau = c$, and eq. (1.91) becomes

$$\ddot{\xi}^i = -c^2 R^i_{0j0} \xi^j, \quad (1.93)$$

where the dot denotes the derivative with respect to the *coordinate time* t of the proper detector frame.

Next, we should compute the Riemann tensor R^i_{0j0} due to the GWs in the proper detector frame, where eq. (1.93) holds. However, as we discussed below eq. (1.13), in linearized theory the Riemann tensor is *invariant*, rather than just covariant as in full general relativity, and we can compute it in the frame that we prefer. Clearly, the best choice is to compute it in the TT frame, since in this frame GWs have the simplest form. Then, from eq. (1.13) we immediately find

$$R^i_{0j0} = R_{i0j0} = -\frac{1}{2c^2} \ddot{h}_{ij}^{\text{TT}}. \quad (1.94)$$

In conclusion, the equation of the geodesic deviation in the proper detector frame is

$$\ddot{\xi}^i = \frac{1}{2} \ddot{h}_{ij}^{TT} \xi^j . \quad (1.95)$$

This equation is remarkable in its simplicity, since it states that, *in the proper detector frame*, the effect of GWs on a point particle of mass m can be described in terms of a *Newtonian force*

$$F_i = \frac{m}{2} \ddot{h}_{ij}^{TT} \xi^j , \quad (1.96)$$

and therefore the response of the detector to GWs can be analyzed in a purely Newtonian language, without any further reference to general relativity.

This means that, in practice, an experimenter in a laboratory on Earth can describe the situation as follows:

- He/she lives in flat space-time, where Newtonian intuition applies.
- There are a number of static or slowly varying Newtonian forces. The acceleration of gravity is compensated by a suspension mechanism, so an Earthbound detector is not free to move in the z direction. Still, it is free to move in the (x, y) plane, or at least in one direction in this plane, depending on the suspension mechanism and detector geometry, and the effect of GWs can show up in the motion of the detector in this free direction. Other slowly varying Newtonian forces perturb the experiment, and one takes great care to minimize their influence. This can be possible at most in a frequency window $[f_{\min}, f_{\max}]$, where f_{\min} is sufficiently large that slowly varying Newtonian noises are under control (as well as the seismic noise, which from a practical point of view is more important at low frequencies), and f_{\max} is not too large, otherwise other noises (e.g., as we will see, the shot noise in an interferometer) begin to dominate.
- Even the effect of GWs on test masses is described in terms of a Newtonian force, given by eq. (1.96).

Before exploring the consequences of eq. (1.95), it is worthwhile to add a few more remarks on its meaning and to stress its limit of validity.

- ★ We have defined ξ^i to be a *coordinate separation* (rather than a proper distance), since it was introduced as the difference between the coordinates of two nearby geodesics, see eqs. (1.66) and (1.68). With this definition, we have found that eq. (1.95) holds in the proper detector frame. It does not hold in the TT frame, where the geodesic equation is eq. (1.81), and $d^2\xi^i/d\tau^2$ is proportional to $d\xi^i/d\tau$, rather than to $\dot{\xi}^i$ (consistent with the fact that, in the TT gauge, if $d\xi^i/d\tau$ initially vanishes, the coordinate separation ξ^i does not change).

Nevertheless, in eq. (1.95) the GW in the TT gauge, h_{ij}^{TT} , enters. This comes out because the Riemann tensor is invariant, and we can compute it in any frame, and in particular in the TT gauge, where the GW has the simplest form. Thus, eq. (1.95) combines two nice features: it holds in a frame where our Newtonian intuition is valid, and therefore the description of the detector is more intuitive; at the same time, the Newtonian force due to GWs is expressed in terms of h_{ij} in the TT gauge, where the form of the GW is simpler.

- ★ In the proper detector frame, to a first approximation coordinate distances are the same as proper distances, since the metric is flat, up to $O(r^2/L_B^2)$. Since proper distances are an invariant concept, eq. (1.95) also describes the evolution of proper distances in any other frame (as long as $\tau = t$ to lowest order in h , and the spatial velocities are non-relativistic, otherwise we must use the most general form of the equation of the geodesic deviation, eq. (1.71)). In particular, if we substitute ξ^i with the proper distances s^i , eq. (1.95) holds also in the TT gauge, as we indeed found in eq. (1.85).
- ★ In deriving the equation for the geodesic deviation we have expanded the Christoffel symbols to first order in ξ , neglecting all higher orders, see eqs. (1.68) and (1.69). This is valid as long as $|\xi^i|$ is much smaller than the typical scale over which the gravitational field changes substantially. For a GW, this length-scale is the reduced wavelength λ . Thus, if a detector has a characteristic linear size L , we can discuss its interaction with GWs using the equation of the geodesic deviation, if and only if

$$L \ll \lambda . \quad (1.97)$$

As we will see in the chapters on experiments, this condition is satisfied by resonant bar detectors and (in a first approximation) by ground based interferometers. It is not satisfied by proposed space-borne interferometers such as LISA, nor by the Doppler tracking of spacecraft.

In the former case it is possible to study the detector and its interaction with GWs using a simple and intuitive description in terms of Newtonian forces, supplemented by the “GW force” (1.96). In the latter case, a full general relativistic description, usually performed in the TT frame, is necessary.

- ★ One should observe that, in general, analysis in the TT gauge can be more subtle, since in this frame our intuition can be misleading. For instance, in certain GW detectors (e.g. microwave cavities) one can have objects which are natural to treat as having rigid walls. However, this description is correct only in the proper detector frame. In fact, when a GW passes, the relative position of a freely falling mass and of an object which is not free to move (like the endpoint of a rigid ruler) changes; since, in the TT frame, the

coordinates are marked by freely falling masses, an object which is described as rigid in the proper detector frame, gets a deformation $\Delta L/L = O(h)$ in the TT frame when a GW passes.

We can now use eq. (1.95) to study the effect of a GW on test masses. We use the language of the proper detector frame, which is more intuitive, so we consider a ring of test masses initially at rest in the proper detector frame and fix the origin in the center of the ring. Then ξ^i describe the distance of a test mass, with respect to this origin (coordinate distance or proper distance, since we have seen that in the proper detector frame, on a sufficiently small region of space, they are the same). We then use eq. (1.95) to see how these positions change under the effect of a GW. (Alternatively, as discussed above, if we wish to take the point of view of an observer in the TT frame, then eq. (1.95) describes the evolution of *proper distances*.)

We consider a GW propagating along the z direction, and a ring of test masses located in the (x, y) plane. First of all, for a wave propagating in the z direction, the components of h_{ij}^{TT} with $i = 3$ or $j = 3$ are zero and therefore we see from eq. (1.95) that, if a test particle is initially at $z = 0$, it will remain at $z = 0$, and the displacement will be confined to the (x, y) plane. Therefore, GWs are transverse not only from a mathematical point of view (i.e. they satisfy $\partial_i h_{ij} = 0$), but also in their physical effect: they displace the test masses transversally, with respect to their direction of propagation.¹⁵

To study the motion of the test particles in the (x, y) plane, we first consider the + polarization. Then, at $z = 0$ (choosing the origin of time so that $h_{ij}^{\text{TT}} = 0$ at $t = 0$),

$$h_{ab}^{\text{TT}} = h_+ \sin \omega t \begin{pmatrix} 1 & 0 \\ 0 & -1 \end{pmatrix}, \quad (1.98)$$

and, as usual, $a, b = 1, 2$ are the indices in the transverse plane. We write $\xi_a(t) = (x_0 + \delta x(t), y_0 + \delta y(t))$, where (x_0, y_0) are the unperturbed positions and $\delta x(t), \delta y(t)$ are the displacements induced by the GW. Then eq. (1.95) becomes

$$\delta \ddot{x} = -\frac{h_+}{2} (x_0 + \delta x) \omega^2 \sin \omega t, \quad (1.99)$$

$$\delta \ddot{y} = +\frac{h_+}{2} (y_0 + \delta y) \omega^2 \sin \omega t. \quad (1.100)$$

Since δx is $O(h_+)$, on the right-hand side, to linear order in h , the terms $\delta x, \delta y$ can be neglected with respect to the constant parts x_0, y_0 , and the equations are immediately integrated, to give

$$\delta x(t) = \frac{h_+}{2} x_0 \sin \omega t, \quad (1.101)$$

$$\delta y(t) = -\frac{h_+}{2} y_0 \sin \omega t. \quad (1.102)$$

Similarly, for the cross polarization, we get

$$\delta x(t) = \frac{h_\times}{2} y_0 \sin \omega t, \quad (1.103)$$

¹⁵These two properties are however logically distinct. The condition $\partial_i h_{ij} = 0$ can be imposed *exactly*, as a gauge condition, and (as we will see in detail in Section 2.2) is basically a consequence of the fact that the graviton is described by a massless spin-2 field. The fact that the Newtonian force is transverse is valid only because we took a test mass at rest, i.e. $u^\mu = (c, 0, 0, 0)$. If we consider test masses with non-zero velocity, the geodesic deviation has a longitudinal term, although suppressed by a factor v^2/c^2 with respect to the transverse term. For example, if we have two test masses with initial spatial separation $\xi = (0, 0, \xi_z)$, both moving with velocity v along the x axis, so that $u^\mu = (1/\gamma)(c, v, 0, 0)$, and the GW propagates along the z direction, the equation of geodesic deviation gives

$$\dot{\xi}_z = -v^2 R_{zxxz} \xi_z,$$

where the dot is the derivative with respect to coordinate time (recall that in this case $d\tau = \gamma dt$). For a GW propagating along z , $R_{zxxz} = -(1/2)\partial_z^2 h_{xx} = -(1/2c^2)\ddot{h}_+$, and therefore

$$\dot{\xi}_z = \frac{v^2}{2c^2} \ddot{h}_+ \xi_z,$$

so the relative displacement of two test masses in the direction of the GWs changes. This is easily understood by performing a boost with velocity $-v$; in the transformed frame the particles are at rest, but the propagation direction of the GW now has both a component along z and a component along x .

ωt	h_+	h_x
0		
$\pi/2$		
π		
$3\pi/2$		

Fig. 1.1 The deformation of a ring of test masses due to the + and \times polarization.

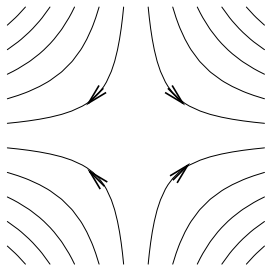


Fig. 1.2 The lines of force corresponding to the + polarization. The arrows show the direction of the force when $\sin \omega t$ is positive. The force reverses when $\sin \omega t$ is negative.

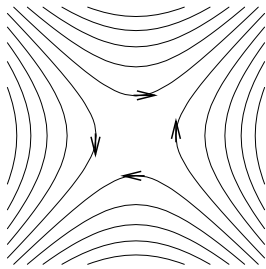


Fig. 1.3 The lines of force corresponding to the \times polarization.

$$\delta y(t) = \frac{h_x}{2} x_0 \sin \omega t. \quad (1.104)$$

The resulting deformation of a ring of test masses located in the (x, y) plane is shown in Fig. 1.1. From eq. (1.96) we see that

$$\partial_i F_i = \frac{m}{2} \ddot{h}_{ij}^{\text{TT}} \delta_{ij}, \quad (1.105)$$

and this vanishes, because h_{ij}^{TT} is traceless. Thus, the Newtonian force (1.96) has vanishing divergence, $\nabla \cdot \mathbf{F} = 0$. We can have a pictorial representation of \mathbf{F} drawing its lines of force in the (x, y) plane (defined so that at each point (x, y) they go in the direction of the force, and their density is proportional to the modulus $|\mathbf{F}|$ of the force). The condition $\nabla \cdot \mathbf{F} = 0$ then implies that there are no sources nor sinks for the field lines, just as for the magnetic field in classical electrodynamics. The lines of force in the (x, y) plane obtained from eq. (1.96), for the h_+ and for the h_x polarization, are shown in Figs. 1.2 and 1.3. The symmetry axes of these lines of force have a typical quadrupolar pattern, with the shape of a + and of a \times sign, respectively, and this is the origin of the denominations “plus” and “cross” polarizations. Observe that Fig. 1.3 is obtained from Fig. 1.2 by performing a rotation of 45 degrees, in agreement with eqs. (1.49) and (1.50).

1.4 The energy of GWs

Our next task is to understand the energy and momentum carried by gravitational waves. The fact that GWs do indeed carry energy and momentum is already clear from the discussion of the interaction of GWs with test masses presented above. We have seen that, in the proper detector frame, an incoming GW sets in motion a ring of test masses initially at rest (and, in fact, the action of the waves on nearby test masses can even be described in terms of a Newtonian force, see eq. (1.96)), so GWs impart kinetic energy to these masses. If, for instance, we connect these masses together with a loose spring with friction, this kinetic energy will be dissipated into heat. Thus, GWs can do work, and conservation of energy requires that the kinetic energy acquired by the test masses must necessarily come from the energy of the GWs. To get the explicit expression of the energy-momentum tensor of GWs we can follow two different routes, one more geometrical and the other more field-theoretical:

- (1) Since, according to general relativity, any form of energy contributes to the curvature of space-time, we can ask whether GWs are themselves a source of space-time curvature.
- (2) We can treat linearized gravity as any other classical field theory, and apply Noether’s theorem, the standard field-theoretical tool that answers this question.

In this section we pursue the former approach, while in Section 2.1 we discuss the latter, and we will see that they both lead to the same answer.

1.4.1 Separation of GWs from the background

To discuss whether GWs curve the background space-time we must broaden our setting. Until now, we have linearized the Einstein equations expanding around the flat metric $\eta_{\mu\nu}$. In this setting the definition of GWs is relatively clear: the background space-time is flat, and the small fluctuations around it have been called “gravitational waves”. The term “waves” is justified by the fact that, in a suitable gauge, $h_{\mu\nu}$ indeed satisfies a wave equation. However, to study whether GWs generate a curvature, we cannot define them as perturbation over the *flat* metric $\eta_{\mu\nu}$, otherwise we exclude from the beginning the possibility that GWs curve the background space-time. Rather, we must allow the background space-time to be dynamical, which means that we would like to define GWs as perturbations over some curved, dynamical, background metric $\bar{g}_{\mu\nu}(x)$, and write¹⁶

$$g_{\mu\nu}(x) = \bar{g}_{\mu\nu}(x) + h_{\mu\nu}(x), \quad |h_{\mu\nu}| \ll 1. \quad (1.106)$$

However, a problem arises immediately. How do we decide which part of $g_{\mu\nu}$ is the background and which is the fluctuations? In principle, in eq. (1.106) we can move x -dependent terms from $h_{\mu\nu}$ to $\bar{g}_{\mu\nu}$ or viceversa. The problem did not arise in linearized theory, where the background metric was chosen once and for all to be the constant flat-space metric $\eta_{\mu\nu}$.

As we will see in this section, this problem is not just an abstract issue of principle. On the contrary, the answer to this question allows us to understand properties of GWs such as their energy-momentum tensor, and to get rid of ambiguities concerning whether GWs can be “gauged away” or not.

In the most general setting, there is no unambiguous way to perform a separation of the type (1.106). The total metric $g_{\mu\nu}(x)$ can receive contributions which change, in space and in time, on all possible scales due, for example, to the time-varying Newtonian gravitational fields of nearby masses in movement. The situation is quite similar to that of waves in the sea. In principle, there is no unambiguous way to state which part of the vertical movement of the surface of the water belongs to a given wave, and which part belongs to a “background” originated by the incoherent superposition of perturbations of varied origin. Nevertheless, there are obviously situations where a description of the perturbation of the sea surface in terms of waves is useful, at least at the level of an effective description.

In particular, a natural splitting between the space-time background and gravitational waves arises when there is a clear separation of scales. For example, a natural distinction occurs if, in some coordinate system, we can write the metric as in eq. (1.106), where $\bar{g}_{\mu\nu}$ has a typical scale

¹⁶The condition $|h_{\mu\nu}| \ll 1$ assumes that we are using a coordinate system where the diagonal elements of $\bar{g}_{\mu\nu}$ are $O(1)$, on the region of space-time in which we are interested.

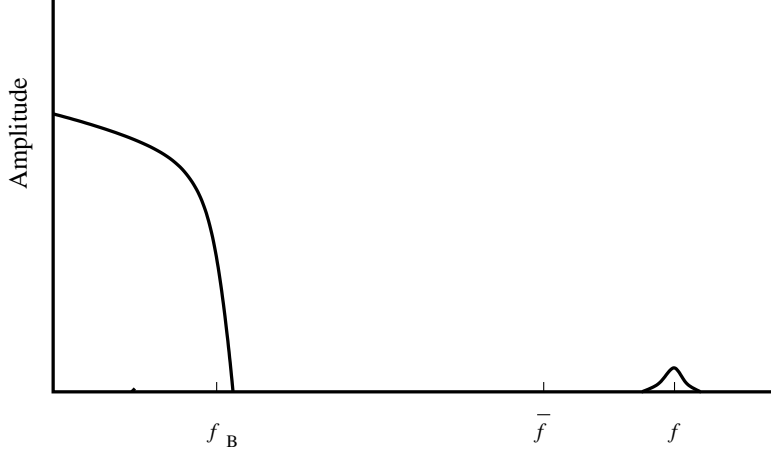


Fig. 1.4 A situation that allows us to separate the metric into a low-frequency background and a small high-frequency perturbation. The background is defined as the part with frequencies $f \ll \bar{f}$ and the GW as the part with $f \gg \bar{f}$. This definition is largely independent of the precise value of \bar{f} .

of spatial variation L_B , on top of which small amplitude perturbations are superimposed, characterized by a wavelength λ such that

$$\bar{\lambda} \ll L_B , \quad (1.107)$$

¹⁷For a function $f(x)$ oscillating as e^{ikx} with $k = 2\pi/\lambda = 1/\bar{\lambda}$, the typical length-scale is $\bar{\lambda}$ rather than λ , in the sense that $|df/dx| = (1/\bar{\lambda})|f|$.

where $\bar{\lambda} = \lambda/(2\pi)$ is the reduced wavelength.¹⁷ In this case $h_{\mu\nu}$ has the physical meaning of small ripples on a smooth background. Alternatively, a natural distinction can be made in frequency space, if $\bar{g}_{\mu\nu}$ has frequencies up to a maximum value f_B , while $h_{\mu\nu}$ is peaked around a frequency f such that

$$f \gg f_B . \quad (1.108)$$

In this case $h_{\mu\nu}$ is a high-frequency perturbation of a static or slowly varying background. The situation (1.108) is illustrated in Fig. 1.4. We will see below that in this case $h_{\mu\nu}$, in a suitable gauge, obeys a wave equation, and as a consequence its characteristic wavelength and frequency, λ and f , are related by $\lambda = c/f$. However, the scales L_B and f_B that characterize the background are a priori unrelated, so the conditions (1.107) and (1.108) are independent, and it suffices that one of them be satisfied.

We can now ask two questions:

- How this high-frequency (or short wavelength) perturbation propagates in the background space-time with metric $\bar{g}_{\mu\nu}$. The answer to this question will justify the fact that the perturbation $h_{\mu\nu}$ is called a gravitational “wave”.
- How this perturbation affects the background metric itself. The answer to this question will allow us to assign an energy-momentum tensor to GWs.

In the next subsections we will address these two questions. First we remark that, traditionally, the separation of the metric into a smooth background plus fluctuations is discussed using the condition (1.107), and the method is called the *short-wave expansion*. It should be observed, however, that from the point of view of GW detectors, the condition (1.108) is fulfilled instead. Consider for instance a GW with a frequency $f \sim 10^2 - 10^3$ Hz, corresponding to a reduced wavelength $\lambda \simeq 500 - 50$ km, which are typical GWs that can be searched by ground-based detectors. The Earth's gravitational potential is *not* spatially smooth over a scale of tens of kms, compared to the GW perturbation. On the contrary, fluctuations in the metric due to local density variations, mountains, etc. are many orders of magnitude bigger than the expected GWs: the Newtonian gravitational potential at the surface of the Earth is in fact $|h_{00}| = 2GM_\oplus/(R_\oplus c^2) \sim 10^{-9}$, while, as we will see, GWs arriving on Earth are expected to have at most $h \sim 10^{-21}$ so even a spatial variation of just one part in 10^{12} due to local inhomogeneities, is large compared to the expected GWs.

On the other hand, these Newtonian gravitational fields are essentially static, and it is much more difficult to find important *temporal* variations at large frequency scales, e.g. at $f \sim 1$ kHz, since it requires relatively large masses moving at these frequencies. A distinction between background and gravitational waves based on the condition $f \gg f_B$ becomes therefore possible.

Indeed, ground-based GW detectors have a size which is much smaller than the wavelength of the GWs that they are searching. A GW with frequency $f \sim 10^2 - 10^3$ Hz has a reduced wavelength $\lambda \sim 500 - 50$ km, which is much bigger than the size of the detector. Therefore, GW detectors do not monitor *spatial* variations of the gravitational field on length-scales $L \gg \lambda$. Rather, their output is a time series, which is analyzed in Fourier space looking for *temporal* variations in their output induced by a passing GW. As we will see in Chapter 9, after suitable isolation, the residual noise due to seismic motion and Newtonian gravitational fields is important only at lower frequencies, say below $O(10)$ Hz. Therefore, we are actually searching for fast temporal variations in the detector output due to GWs, over a background which is slowly varying in time.

1.4.2 How GWs curve the background

We therefore consider the situation in which, in some reference frame, we can separate the metric into a background plus fluctuations, as in eq. (1.106), and this separation is based on the fact that there is a clear distinction of scales either in space, in which case eq. (1.107) applies, or in time, in which case eq. (1.108) applies.

As discussed above, our aim is to understand how the perturbation $h_{\mu\nu}$ propagates, and how it affects the background space-time. To address these questions, we begin by expanding the Einstein equations around the background metric $\bar{g}_{\mu\nu}$. In the expansion we have two small parameters: one is the typical amplitude $h \equiv O(|h_{\mu\nu}|)$, and the second

is either $\bar{\chi}/L_B$ or f_B/f , depending on whether eq. (1.107) or eq. (1.108) applies. The situation in which $\bar{\chi}/L_B \ll 1$ and the situation in which $f_B/f \ll 1$ can be treated in parallel, with the appropriate change of notation, and we will refer generically to both cases as the short-wave expansion.

As a first step, we expand to quadratic order in $h_{\mu\nu}$. It is convenient to cast the Einstein equations in the form

$$R_{\mu\nu} = \frac{8\pi G}{c^4} \left(T_{\mu\nu} - \frac{1}{2} g_{\mu\nu} T \right), \quad (1.109)$$

where $T_{\mu\nu}$ is the energy-momentum tensor of matter and T its trace, and then we expand the Ricci tensor to $O(h^2)$,

$$R_{\mu\nu} = \bar{R}_{\mu\nu} + R_{\mu\nu}^{(1)} + R_{\mu\nu}^{(2)} + \dots, \quad (1.110)$$

where $\bar{R}_{\mu\nu}$ is constructed with $\bar{g}_{\mu\nu}$ only, $R_{\mu\nu}^{(1)}$ is linear in $h_{\mu\nu}$ and $R_{\mu\nu}^{(2)}$ is quadratic in $h_{\mu\nu}$. The crucial observation now is the following. The quantity $\bar{R}_{\mu\nu}$ is constructed from $\bar{g}_{\mu\nu}$ and therefore contains only low-frequency modes.¹⁸ $R_{\mu\nu}^{(1)}$ by definition is linear in $h_{\mu\nu}$ and therefore contains only high-frequency modes. $R_{\mu\nu}^{(2)}$ is quadratic in $h_{\mu\nu}$ and therefore contains *both* high and low frequencies: for instance, in a quadratic term $\sim h_{\mu\nu} h_{\rho\sigma}$ a mode with a high wave-vector \mathbf{k}_1 from $h_{\mu\nu}$ can combine with a mode with a high wave-vector $\mathbf{k}_2 \simeq -\mathbf{k}_1$ from $h_{\rho\sigma}$ to give a low wave-vector mode. Therefore the Einstein equations can be split into two separate equations for the low- and high-frequency parts,

$$\bar{R}_{\mu\nu} = -[R_{\mu\nu}^{(2)}]^{\text{Low}} + \frac{8\pi G}{c^4} \left(T_{\mu\nu} - \frac{1}{2} g_{\mu\nu} T \right)^{\text{Low}}, \quad (1.111)$$

and

$$R_{\mu\nu}^{(1)} = -[R_{\mu\nu}^{(2)}]^{\text{High}} + \frac{8\pi G}{c^4} \left(T_{\mu\nu} - \frac{1}{2} g_{\mu\nu} T \right)^{\text{High}}. \quad (1.112)$$

The superscript ‘‘Low’’ denotes the projection on the low momenta (i.e. long wavelengths) or on the low frequencies, depending on whether eq. (1.107) or eq. (1.108) applies, and similarly for the superscript ‘‘High’’.

The explicit expression for $R_{\mu\nu}^{(1)}$ is computed in Problem 1.1, and is

$$R_{\mu\nu}^{(1)} = \frac{1}{2} (\bar{D}^\alpha \bar{D}_\mu h_{\nu\alpha} + \bar{D}^\alpha \bar{D}_\nu h_{\mu\alpha} - \bar{D}^\alpha \bar{D}_\alpha h_{\mu\nu} - \bar{D}_\nu \bar{D}_\mu h), \quad (1.113)$$

where \bar{D}_μ is the covariant derivative with respect to the background metric. At quadratic order one finds, after some long algebra,

$$\begin{aligned} R_{\mu\nu}^{(2)} = & \frac{1}{2} \bar{g}^{\rho\sigma} \bar{g}^{\alpha\beta} \left[\frac{1}{2} \bar{D}_\mu h_{\rho\alpha} \bar{D}_\nu h_{\sigma\beta} + (\bar{D}_\rho h_{\nu\alpha})(\bar{D}_\sigma h_{\mu\beta} - \bar{D}_\beta h_{\mu\sigma}) \right. \\ & + h_{\rho\alpha} (\bar{D}_\nu \bar{D}_\mu h_{\sigma\beta} + \bar{D}_\beta \bar{D}_\sigma h_{\mu\nu} - \bar{D}_\beta \bar{D}_\nu h_{\mu\sigma} - \bar{D}_\beta \bar{D}_\mu h_{\nu\sigma}) \\ & \left. + \left(\frac{1}{2} \bar{D}_\alpha h_{\rho\sigma} - \bar{D}_\rho h_{\alpha\sigma} \right) (\bar{D}_\nu h_{\mu\beta} + \bar{D}_\mu h_{\nu\beta} - \bar{D}_\beta h_{\mu\nu}) \right]. \end{aligned} \quad (1.114)$$

¹⁸To be more precise, we should take into account that $\bar{R}_{\mu\nu}$ is non-linear in $\bar{g}_{\mu\nu}$. If \bar{k} separates the low frequency from the high frequency modes, then $\bar{g}_{\mu\nu}$ has only modes up to a typical wave-vector $k_B \simeq 2\pi/L_B$ with $k_B \ll \bar{k}$. The Christoffel symbols of the background are quadratic in the background metric and therefore have modes up to $2k_B$. Terms quadratic in the Christoffel symbols, such as those which appear in the definition of the Ricci tensor, therefore have modes up to $\sim 4k_B$. In any case, if the separation of scales between the background and the GW is clear-cut, we still have $4k_B \ll \bar{k}$. In this sense $\bar{R}_{\mu\nu}$ contains only low-frequency modes.

In the next subsections we will closely examine eqs. (1.111) and (1.112). We will see that, from eq. (1.111), we can understand what the energy-momentum tensor of GWs is, while eq. (1.112) is a wave equation that describes the propagation of $h_{\mu\nu}$ on the background space-time.

First we discuss, from the vantage point of the expansion over a generic curved background, why the expansion over flat space-time presented in Section 1.1 cannot be promoted to a systematic expansion. Consider first the situation in which there is no external matter, $T_{\mu\nu} = 0$. In eqs. (1.111) and (1.112) we have equated terms of different orders in the h -expansion. The reason is that we have a second small expansion parameter, which is λ/L_B (or f_B/f ; as usual, the two cases can be treated in parallel with just a change of notation, and for definiteness we use λ/L_B), which can compensate for the smallness in h . The relative strength of these parameters is therefore fixed by the Einstein equations themselves. We use the notation $h = O(|h_{\mu\nu}|)$, while we take $\bar{g}_{\mu\nu} = O(1)$ (in a limited region of space, we can always set $\bar{g}_{\mu\nu} = O(1)$ with a suitable rescaling of the coordinates).

Since we set $T_{\mu\nu} = 0$, we see from eq. (1.111) that $\bar{R}_{\mu\nu}$ is determined only by $[R_{\mu\nu}^{(2)}]_{\text{Low}}$. From the explicit expression (1.114) we see that $R_{\mu\nu}^{(2)}$ is a sum of terms of order $(\partial h)^2$ and of terms of order $h\partial^2 h$. Let us anticipate that, when we compute the projection onto the low modes, these two terms give contributions which are of the same order of magnitude, and one finds that $[R_{\mu\nu}^{(2)}]_{\text{Low}}$ is of order $(\partial h)^2$ (compare with eqs. (1.125) and (1.133) below). Then, in order of magnitude, eq. (1.111) in the absence of matter fields reads

$$\bar{R}_{\mu\nu} \sim (\partial h)^2, \quad (1.115)$$

and expresses the fact that the derivatives of the perturbation $h_{\mu\nu}$ affect the curvature of the background metric $\bar{g}_{\mu\nu}$. The scale of variation of $\bar{g}_{\mu\nu}$ is L_B , while that of h is λ ; therefore, in order of magnitude,

$$\partial\bar{g}_{\mu\nu} \sim \frac{1}{L_B}, \quad (1.116)$$

(recall that we took $\bar{g}_{\mu\nu} = O(1)$), while

$$\partial h \sim \frac{h}{\lambda}. \quad (1.117)$$

Since the background curvature $\bar{R}_{\mu\nu}$ is constructed from the second derivatives of the background metric, eq. (1.116) implies that

$$\bar{R}_{\mu\nu} \sim \partial^2 \bar{g}_{\mu\nu} \sim \frac{1}{L_B^2}. \quad (1.118)$$

while eq. (1.117) gives $(\partial h)^2 \sim (h/\lambda)^2$. Therefore eq. (1.115) gives the relation

$$\frac{1}{L_B^2} \sim \left(\frac{h}{\lambda}\right)^2, \quad (1.119)$$

that is,

$$h \sim \frac{\lambda}{L_B}, \quad (\text{curvature determined by GWs}). \quad (1.120)$$

Consider now the opposite limit where $T_{\mu\nu}$ is non-vanishing, and the contribution of GWs to the background curvature is negligible compared to the contribution of matter sources. In this case the total background curvature will be much bigger than the contribution of GWs, $1/L_B^2 \sim h^2/\lambda^2 + (\text{matter contribution}) \gg h^2/\lambda^2$, i.e.

$$h \ll \frac{\lambda}{L_B}, \quad (\text{curvature determined by matter}). \quad (1.121)$$

At this point we can understand why the linearized approximation of Section 1.1 cannot be extended beyond linear order. If we force the background metric to be $\eta_{\mu\nu}$, we are actually forcing $1/L_B$ to be strictly equal to zero, and therefore any arbitrarily small, but finite, value of h necessarily violates the condition $h \lesssim \lambda/L_B$, and the expansion in powers of h has no domain of validity. This means that the linearized expansion of the classical theory cannot be promoted to a systematic expansion, and if we want to compute higher-order corrections we cannot insist on a flat background metric.

We can also understand from eqs. (1.120) and (1.121) that the notion of GW is well defined only for small amplitudes, $h \ll 1$. If h becomes of order one, eqs. (1.120) and (1.121) tell us that λ/L_B also becomes at least of order one. Since the separation between λ and L_B is at the basis of the definition of GWs, when h becomes of order one the distinction between GWs and background vanishes. In a general context, there is nothing like “a GW of arbitrary amplitude”.¹⁹

We consider now eq. (1.111). When there is a clear-cut separation between the length-scale λ of the GWs and the length-scale L_B of the background, there is a simple way to perform the projection on the long-wavelength modes: we introduce a scale \bar{l} such that $\lambda \ll \bar{l} \ll L_B$, and we average over a spatial volume with side \bar{l} . In this way, modes with a wavelength of order L_B remain unaffected, because they are basically constant over the volume used for the averaging, while modes with a reduced wavelength of order λ are oscillating very fast and average to zero. Similarly, if $h_{\mu\nu}$ is a high-frequency perturbation of a quasi-static background, we can introduce a time-scale \bar{t} which is much larger than the period $1/f$ of the GW and much smaller than the typical time-scale $1/f_B$ of the background, and average over this time \bar{t} , i.e. over several periods of the GW. We can therefore write eq. (1.111) as

$$\bar{R}_{\mu\nu} = -\langle R_{\mu\nu}^{(2)} \rangle + \frac{8\pi G}{c^4} \langle T_{\mu\nu} - \frac{1}{2}g_{\mu\nu}T \rangle, \quad (1.122)$$

where $\langle \dots \rangle$ denotes a spatial average over many reduced wavelengths λ , if eq. (1.107) applies, and a temporal average over several periods $1/f$ of the GW, if rather eq. (1.108) applies.

¹⁹In special cases one can find *exact* wave-like solutions of the full nonlinear Einstein equations, see, e.g. Misner, Thorne and Wheeler (1973), Section 35.9, and then there is no need to perform a separation between the background and the waves. However, it would be hopeless to look for exact solutions for the gravitational waves emitted by realistic astrophysical sources.

In the context of general relativity and gravitational-wave physics, the usefulness of introducing some averaging procedure was understood in the 1960s. To put it into a broader theoretical framework, it is useful to realize that what we have done is basically a special case of a general technique, which is known as a renormalization group transformation, and which is nowadays one of the most important tools both in quantum field theory and in statistical physics. The basic idea is to start from the fundamental equations of a theory and to “integrate out” the fluctuations that take place on a length-scale smaller than l , in order to obtain an effective theory that describes the physics at the length-scale l . These renormalization group transformations can be performed in coordinate space, which is the language that we used above; in momentum space, integrating out the high-momentum modes, in order to get the corresponding low-energy effective action; or in frequency space, in order to eliminate the fast temporal variations and to obtain the effective dynamics of the slowly varying degrees of freedom.

We now define an effective energy–momentum tensor of matter, that we denote by $\bar{T}^{\mu\nu}$, from

$$\langle T_{\mu\nu} - \frac{1}{2}g_{\mu\nu}T \rangle = \bar{T}^{\mu\nu} - \frac{1}{2}\bar{g}_{\mu\nu}\bar{T}, \quad (1.123)$$

where $\bar{T} = \bar{g}_{\mu\nu}\bar{T}^{\mu\nu}$ is the trace. By definition, $\bar{T}^{\mu\nu}$ is a purely low-frequency (or low-momentum) quantity, and is a smoothed form of the matter energy–momentum tensor $T_{\mu\nu}$; for instance, when the separation has been done on the basis of the condition $\lambda \ll L_B$, we can visualize it as a “macroscopic” (with respect to the scale λ) version of the energy–momentum tensor, while $T_{\mu\nu}$ is the fundamental (“microscopic”) quantity.²⁰

We also define the quantity $t_{\mu\nu}$ as

$$t_{\mu\nu} = -\frac{c^4}{8\pi G} \langle R_{\mu\nu}^{(2)} - \frac{1}{2}\bar{g}_{\mu\nu}R^{(2)} \rangle, \quad (1.125)$$

where

$$R^{(2)} = \bar{g}^{\mu\nu}R_{\mu\nu}^{(2)}, \quad (1.126)$$

and we define its trace as²¹

$$\begin{aligned} t &= \bar{g}^{\mu\nu}t_{\mu\nu} \\ &= +\frac{c^4}{8\pi G}\langle R^{(2)} \rangle. \end{aligned} \quad (1.127)$$

To go from the first to the second line, in eq. (1.127), we used the fact that $\bar{g}^{\mu\nu}\langle R_{\mu\nu}^{(2)} \rangle = \langle \bar{g}^{\mu\nu}R_{\mu\nu}^{(2)} \rangle$ since $\bar{g}^{\mu\nu}$ by definition is a purely low-frequency quantity, as well as the obvious identity $\bar{g}^{\mu\nu}\bar{g}_{\mu\nu} = 4$. Inserting eq. (1.127) into eq. (1.125) (and using again the fact that $\bar{g}_{\mu\nu}$ is constant under the averaging procedure, so $\langle \bar{g}_{\mu\nu}R^{(2)} \rangle = \bar{g}_{\mu\nu}\langle R^{(2)} \rangle$) we see that

$$-\langle R_{\mu\nu}^{(2)} \rangle = \frac{8\pi G}{c^4} \left(t_{\mu\nu} - \frac{1}{2}\bar{g}_{\mu\nu}t \right). \quad (1.128)$$

²⁰In a typical situation, the fundamental energy–momentum tensor $T^{\mu\nu}$ generated by a macroscopic matter distribution will already be quite smooth, so it will be approximately constant on the scale used for averaging. In this case

$$\begin{aligned} \langle T_{\mu\nu} - \frac{1}{2}g_{\mu\nu}T \rangle &\simeq T_{\mu\nu} - \frac{1}{2}\langle g_{\mu\nu}T \rangle \\ &= T_{\mu\nu} - \frac{1}{2}\bar{g}_{\mu\nu}T, \end{aligned} \quad (1.124)$$

and therefore $\bar{T}_{\mu\nu} \simeq T_{\mu\nu}$. However, the definition (1.123) copes with the most general situation.

²¹Observe that, since $R_{\mu\nu}^{(2)}$ is already quadratic in $h_{\mu\nu}$, we have

$$\begin{aligned} g^{\mu\nu}R_{\mu\nu}^{(2)} &= (\bar{g}^{\mu\nu} + h^{\mu\nu})R_{\mu\nu}^{(2)} \\ &= \bar{g}^{\mu\nu}R_{\mu\nu}^{(2)} + O(h^3) \end{aligned}$$

and, since we are working up to $O(h^2)$, it is irrelevant whether we define the traces of $R_{\mu\nu}^{(2)}$ and of $t_{\mu\nu}$ contracting with $g^{\mu\nu}$ or with $\bar{g}^{\mu\nu}$.

So, we can rewrite eq. (1.122) as

$$\bar{R}_{\mu\nu} = \frac{8\pi G}{c^4} \left(t_{\mu\nu} - \frac{1}{2} \bar{g}_{\mu\nu} t \right) + \frac{8\pi G}{c^4} \left(\bar{T}_{\mu\nu} - \frac{1}{2} \bar{g}_{\mu\nu} \bar{T} \right), \quad (1.129)$$

or, in an equivalent way,

$$\bar{R}_{\mu\nu} - \frac{1}{2} \bar{g}_{\mu\nu} \bar{R} = \frac{8\pi G}{c^4} (\bar{T}_{\mu\nu} + t_{\mu\nu}).$$

(1.130)

This can be appropriately called the “coarse-grained” form of the Einstein equations. These equations determine the dynamics of $\bar{g}_{\mu\nu}$, which is the long-wavelength (or low-frequency) part of the metric, in terms of the long-wavelength (or, respectively, low-frequency) part of the matter energy-momentum tensor, $\bar{T}_{\mu\nu}$, and of a tensor $t_{\mu\nu}$ which does not depend on the external matter but only on the gravitational field itself, and is quadratic in $h_{\mu\nu}$.²²

We can then summarize the results of this analysis as follows.

- At a “microscopic” level, there is no fundamental distinction between a background metric and fluctuations over it. The gravitational field is described by all its modes, and its dynamics is fully accounted for by the Einstein equations (1.3).
- If some fluctuations $h_{\mu\nu}$ are clearly distinguishable from the background because their typical length-scale λ is much smaller than the typical length-scale L_B that characterizes the spatial variations of the background, it becomes useful to introduce a “macroscopic” level of description, i.e. an approximate description which is valid at a length-scale \bar{l} , such that $\lambda \ll \bar{l}$ (but still $\bar{l} \ll L_B$). This is obtained “integrating out” the short-wavelength degrees of freedom, which, in practice, can be obtained by performing a spatial average of the Einstein equations over a box of size \bar{l} , i.e. over several wavelengths λ .

If the separation between fluctuations and background is based on the condition $f_B \ll f$ instead, we integrate out the fast-varying degrees of freedom, performing a temporal average over several periods $1/f$, and we are left with an effective dynamics for the slowly varying degrees of freedom.

- The result of this procedure (which, basically, is a renormalization group transformation) is summarized by eq. (1.130), together with the definitions of $t_{\mu\nu}$ and $\bar{T}_{\mu\nu}$ given in eqs. (1.123) and (1.125). The left-hand side of eq. (1.130) is the Einstein tensor for the slowly varying metric $\bar{g}_{\mu\nu}$. On the right-hand side we find, not surprisingly, a smoothed version of the matter energy-momentum tensor, $\bar{T}_{\mu\nu}$.

The most interesting aspect of eq. (1.130), however, is that it shows that the effect of GWs on the background curvature is formally identical to that of matter with energy-momentum tensor $t^{\mu\nu}$. We are therefore able to assign an energy-momentum tensor to GWs.

²²Recall however that we limited ourselves to an expansion of $R_{\mu\nu}$ up to quadratic order in $h_{\mu\nu}$, so all higher-order non-linearities in $h_{\mu\nu}$ have been neglected. We will come back to these non-linear terms in Section 2.2.3 and especially in Chapter 5.

- It is useful to observe that $t_{\mu\nu}$ comes out automatically in an averaged form. This averaging procedure is not something that is imposed by hand afterwards. It comes out this way because, to derive the effect of GWs on the background, one is passing from a fundamental, “microscopic”, description, to a coarse-grained, “macroscopic” description.

1.4.3 The energy–momentum tensor of GWs

We now compute explicitly $t_{\mu\nu}$, using eq. (1.125) with $R_{\mu\nu}^{(2)}$ given in eq. (1.114). We are interested in the energy and momentum carried by the GWs at large distances from the source (e.g. at the position of the detector), where we can approximate the background space-time as flat. In this case we can simply replace $\bar{D}^\mu \rightarrow \partial^\mu$ in eq. (1.114), so we get

$$\begin{aligned} R_{\mu\nu}^{(2)} = & \frac{1}{2} \left[\frac{1}{2} \partial_\mu h_{\alpha\beta} \partial_\nu h^{\alpha\beta} + h^{\alpha\beta} \partial_\mu \partial_\nu h_{\alpha\beta} - h^{\alpha\beta} \partial_\nu \partial_\beta h_{\alpha\mu} - h^{\alpha\beta} \partial_\mu \partial_\beta h_{\alpha\nu} \right. \\ & + h^{\alpha\beta} \partial_\alpha \partial_\beta h_{\mu\nu} + \partial^\beta h_\nu^\alpha \partial_\beta h_{\alpha\mu} - \partial^\beta h_\nu^\alpha \partial_\alpha h_{\beta\mu} - \partial_\beta h^{\alpha\beta} \partial_\nu h_{\alpha\mu} \\ & + \partial_\beta h^{\alpha\beta} \partial_\alpha h_{\mu\nu} - \partial_\beta h^{\alpha\beta} \partial_\mu h_{\alpha\nu} - \frac{1}{2} \partial^\alpha h \partial_\alpha h_{\mu\nu} + \frac{1}{2} \partial^\alpha h \partial_\nu h_{\alpha\mu} \\ & \left. + \frac{1}{2} \partial^\alpha h \partial_\mu h_{\alpha\nu} \right]. \end{aligned} \quad (1.131)$$

As we saw in Section 1.2, the 4×4 symmetric matrix $h_{\mu\nu}$ has 10 degrees of freedom, out of which eight are gauge modes and two are physical modes. Correspondingly, in $t_{\mu\nu}$ one can have in principle contributions both from the physical modes and from the gauge modes. The left-hand side of eq. (1.130), i.e. the Einstein tensor of the background metric $\bar{g}_{\mu\nu}$, is of course a quantity that depends on the coordinate system, since it is a tensor. Thus, in principle there is nothing wrong if, on the right-hand side, we have both physical contributions and coordinate-dependent contributions, i.e. contributions from gauge modes. The issue is how to distinguish the contribution to $t_{\mu\nu}$ due to the physical modes from the contribution of the gauge modes. The former will give the energy–momentum tensor of the GWs, and describe physical effects that cannot be gauged away, while the latter will be associated with ripples in space-times that are due to the choice of the coordinate system, and that can be made to vanish with an appropriate gauge choice.

The most straightforward way to get the contribution of the physical modes is to make use of the Lorentz gauge condition (1.18). This immediately eliminates four spurious degrees of freedom, leaving us with the two physical degrees of freedom contained in h_{ij}^{TT} and the four gauge modes ξ_μ which satisfy $\square \xi_\mu = 0$, as discussed in Section 1.2. We also choose the ξ_μ so that $h = 0$ (so that only three independent gauge modes remain). Then $\bar{h}_{\mu\nu} = h_{\mu\nu}$ and the Lorentz gauge condition becomes $\partial^\mu h_{\mu\nu} = 0$.

We can now drastically simplify $R_{\mu\nu}^{(2)}$ in eq. (1.131) observing that, inside the spatial or temporal average, the space-time derivative ∂_μ can be integrated by parts, neglecting the boundary term.²³ Performing in-

²³On generic functions, an integration by parts of ∂_t is possible only if we have performed an integral over time, while an integration by parts of ∂_i requires a spatial integral. Recall however that in the Lorentz gauge, outside the source, the equation of motion is a simple wave equation $\square h_{\mu\nu} = 0$. So, for a solution propagating for instance in the z direction, all quantities are functions of the combination $x^0 - z$, where $x^0 = ct$. In expressions such as $\int dz g(x^0 - z) \partial_0 f(x^0 - z)$ we can replace $\partial_0 f$ with $-\partial_z f$, integrate ∂_z by parts and then replace again $\partial_z g$ with $-\partial_0 g$. Therefore, for solutions of the wave equation, a spatial average allows us to integrate by parts not only the spatial derivative but even the time derivative, and similarly for a time average.

Observe also that, in the integration by parts, the boundary terms vanish only when the size of the box used for the integration is infinitely larger than λ . A more precise statement is that the non-zero terms are of higher order in λ/L_B . However, we will only need the result to leading order.

tegrations by parts and making use of the gauge conditions $\partial^\mu h_{\mu\nu} = 0$ and $h = 0$ and of the equation of motion $\square h_{\alpha\beta} = 0$, it is immediate to see that all terms in eq. (1.131) collapse to zero except the first two, which are related to each other by an integration by parts, giving

$$\langle R_{\mu\nu}^{(2)} \rangle = -\frac{1}{4} \langle \partial_\mu h_{\alpha\beta} \partial_\nu h^{\alpha\beta} \rangle, \quad (1.132)$$

while $\langle R^{(2)} \rangle$ vanishes upon integration by parts and using the equation of motion $\square h_{\alpha\beta} = 0$. Recalling the factor $-c^4/(8\pi G)$ from eq. (1.125), we finally find

$$t_{\mu\nu} = \frac{c^4}{32\pi G} \langle \partial_\mu h_{\alpha\beta} \partial_\nu h^{\alpha\beta} \rangle.$$

(1.133)

We can now verify that the residual gauge modes ξ_μ do not contribute to this expression. In fact, under the gauge transformation (1.8), the variation of $t_{\mu\nu}$ is

$$\begin{aligned} \delta t_{\mu\nu} &= \frac{c^4}{32\pi G} [\langle \partial_\mu h_{\alpha\beta} \partial_\nu (\delta h^{\alpha\beta}) \rangle + (\mu \leftrightarrow \nu)] \\ &= \frac{c^4}{32\pi G} [\langle \partial_\mu h_{\alpha\beta} \partial_\nu (\partial^\alpha \xi^\beta + \partial^\beta \xi^\alpha) \rangle + (\mu \leftrightarrow \nu)] \\ &= \frac{c^4}{16\pi G} [\langle \partial_\mu h_{\alpha\beta} \partial_\nu \partial^\alpha \xi^\beta \rangle + (\mu \leftrightarrow \nu)], \end{aligned} \quad (1.134)$$

²⁴The fact that this result holds only to leading order in $\bar{\lambda}/L_B$ (see Note 23) is not surprising, since it is only in this limit that the notion of GW is well defined. If $\bar{\lambda}/L_B$ approaches one, the distinction between the background and the perturbation fades away, and correspondingly one can no longer assign a gauge-invariant energy-momentum tensor to the perturbations.

and this vanishes since, inside $\langle \dots \rangle$, we can integrate by parts ∂^α , and then we can use the Lorentz condition $\partial^\alpha h_{\alpha\beta} = 0$.²⁴ Therefore $t_{\mu\nu}$ depends only on the physical modes h_{ij}^{TT} , and we can simply replace $h_{\mu\nu}$ in eq. (1.133) with the metric in the TT gauge. In particular, the gauge-invariant energy density is

$$t^{00} = \frac{c^2}{32\pi G} \langle \dot{h}_{ij}^{\text{TT}} \dot{h}_{ij}^{\text{TT}} \rangle, \quad (1.135)$$

(where the dot denotes $\partial_t = c\partial_0$) or, in terms of the amplitudes h_+ and h_\times ,

$$t^{00} = \frac{c^2}{16\pi G} \langle \dot{h}_+^2 + \dot{h}_\times^2 \rangle.$$

(1.136)

For a plane wave traveling along the z direction, h_{ij}^{TT} is a function of $t - z/c$, and therefore $t^{01} = t^{02} = 0$ while $\partial_z h_{ij}^{\text{TT}} = -\partial_0 h_{ij}^{\text{TT}} = +\partial^0 h_{ij}^{\text{TT}}$ and therefore

$$t^{03} = t^{00}. \quad (1.137)$$

An alternative way of extracting the gauge-invariant part from $t_{\mu\nu}$ is to start from the full expression (1.131) without performing any prior gauge fixing, and consider its variation under a linearized gauge transformation (1.8), where now ξ_μ are generic, rather than being constrained to satisfy $\square \xi_\mu = 0$. Then, with straightforward algebra one finds that

$$t_{\mu\nu} \rightarrow t_{\mu\nu} + \partial_\rho U_{\mu\nu}^\rho, \quad (1.138)$$

with $U_{\mu\nu}^\rho$ some tensor. The additional term is a total divergence, and we would like to throw it away inside the average, as we have done above. Here however we must be careful because, since we have not fixed the Lorentz gauge, the metric now does not satisfy a simple wave equation such as $\square h_{\mu\nu} = 0$. Thus, the argument discussed in Note 23, which allowed us to integrate by parts ∂_ρ inside a temporal average, or inside a spatial average, no longer goes through. However, we can integrate by parts ∂_μ inside a *space-time* average, that we denote as $\langle\langle \dots \rangle\rangle$. Then $\langle\langle \partial_\rho U_{\mu\nu}^\rho \rangle\rangle$ vanishes and $\langle\langle t_{\mu\nu} \rangle\rangle$ is gauge invariant (again to leading order in λ/L_B). Thus, an equivalent way to single out the gauge-invariant part of $t_{\mu\nu}$ is to average it over space-time, and the result gives again eq. (1.133).²⁵

Finally, observe that in eq. (1.130) the left-hand side is covariantly conserved with respect to \bar{D}^μ , i.e. $\bar{D}^\mu(\bar{R}_{\mu\nu} - \frac{1}{2}\bar{g}_{\mu\nu}\bar{R}) = 0$, because of the Bianchi identity. Therefore, we have

$$\bar{D}^\mu(\bar{T}_{\mu\nu} + t_{\mu\nu}) = 0. \quad (1.140)$$

The fact that the covariantly conserved quantity is the sum of $\bar{T}_{\mu\nu}$ and $t_{\mu\nu}$, rather than each one separately, reflects the fact that there is in general exchange of energy and momentum between the matter sources and GWs. At large distances from the source the metric approaches the flat-space metric, so \bar{D}^μ approaches ∂^μ , while outside the source $\bar{T}_{\mu\nu} = 0$. Then, far from the sources, eq. (1.140) reduces to

$$\partial^\mu t_{\mu\nu} = 0. \quad (1.141)$$

The energy flux

Having obtained the energy-momentum tensor carried by the GWs, it is now straightforward to compute the corresponding energy flux, i.e. the energy of GWs flowing per unit time through a unit surface at a large distance from the source. We start from the conservation of the energy-momentum tensor, $\partial_\mu t^{\mu\nu} = 0$, which implies that

$$\int_V d^3x (\partial_0 t^{00} + \partial_i t^{i0}) = 0, \quad (1.142)$$

where V is a spatial volume in the far region, bounded by a surface S . The GW energy inside the volume V is

$$E_V = \int_V d^3x t^{00}, \quad (1.143)$$

so eq. (1.142) can be written as

$$\begin{aligned} \frac{1}{c} \frac{dE_V}{dt} &= - \int_V d^3x \partial_i t^{0i} \\ &= - \int_S dA n_i t^{0i}, \end{aligned} \quad (1.144)$$

²⁵To make the proof simpler we worked at large distance from the source, where the background metric can be taken as flat. The argument can however be repeated in a generic background $\bar{g}_{\mu\nu}$, although it becomes technically more involved. In this case one makes use of the fact that, inside a space-time average, to lowest order in λ/L_B : (i) Covariant divergences can be integrated by parts discarding the boundary term. In particular, expressions such as $\langle\langle \bar{D}_\rho U_{\mu\nu}^\rho \rangle\rangle$ vanish. (ii) Covariant derivative commutes. Then one finds, from the full expression (1.114), that

$$t_{\mu\nu} \rightarrow t_{\mu\nu} + \bar{D}_\rho U_{\mu\nu}^\rho, \quad (1.139)$$

and therefore $\langle\langle t_{\mu\nu} \rangle\rangle$ is gauge invariant, to leading order in λ/L_B . A further technical subtlety is that, in curved space, the sum of tensors at different points in space-time is not a tensor, so the result of integrating a tensor is also not a tensor. Thus, before integrating over d^4x , one must carry the tensors $t_{\mu\nu}(x)$ back to a single common point using parallel transport along geodesics. Details can be found in the Appendix of Isaacson (1968b), and references therein.

In principle, the same parallel transport procedure should be applied to the spatial and to the temporal averages that we introduced in Section 1.4.2. However, we will always end up computing these averages very far from the sources, where the background space-time can be taken as flat.

²⁶More precisely, we take as volume V a spherical shell centered on the source but far away from it, so that both its inner boundary S_1 and its outer boundary S_2 are in the far region, where the gravitational field is given simply by gravitational waves. Then in eq. (1.143) we can limit ourselves to the energy-momentum tensor t^{00} of GWs, neglecting the energy-momentum tensor of the quasi-static gravitational fields, as well as the energy-momentum tensor of matter. Therefore the time derivative of E_V is given by two terms: the energy flowing in through S_1 minus the energy flowing out from S_2 . We are interested in the energy flux through a unit surface at a given distance from the source (say, in the energy flowing through a unit surface of our detector), which for definiteness we choose to be on the outer surface S_2 , so in the following we simply take $S = S_2$.

where n^i is the outer normal to the surface and dA is the surface element.²⁶ Furthermore, outside the source, we can impose the TT gauge. Let S be a spherical surface at a large distance r from the source. Its surface element is $dA = r^2 d\Omega$, and its normal $\hat{n} = \hat{r}$ is the unit vector in the radial direction. Then eq. (1.144) gives

$$\frac{dE_V}{dt} = -c \int dA t^{0r}, \quad (1.145)$$

where

$$t^{0r} = \frac{c^4}{32\pi G} \langle \partial^0 h_{ij}^{\text{TT}} \frac{\partial}{\partial r} h_{ij}^{\text{TT}} \rangle. \quad (1.146)$$

A GW propagating radially outward, at sufficiently large distances r , has the general form

$$h_{ij}^{\text{TT}}(t, r) = \frac{1}{r} f_{ij}(t - r/c), \quad (1.147)$$

where $f_{ij}(t - r/c)$ is some function of retarded time $t_{\text{ret}} = t - r/c$. We will prove this result in Section 3.1, but it is in fact completely analogous to the result for electromagnetic waves. Therefore

$$\frac{\partial}{\partial r} h_{ij}^{\text{TT}}(t, r) = -\frac{1}{r^2} f_{ij}(t - r/c) + \frac{1}{r} \frac{\partial}{\partial r} f_{ij}(t - r/c). \quad (1.148)$$

On a function of the combination $t - r/c$ we have

$$\frac{\partial}{\partial r} f_{ij}(t - r/c) = -\frac{1}{c} \frac{\partial}{\partial t} f_{ij}(t - r/c), \quad (1.149)$$

and therefore

$$\begin{aligned} \frac{\partial}{\partial r} h_{ij}^{\text{TT}}(t, r) &= -\partial_0 h_{ij}^{\text{TT}}(t, r) + O(1/r^2) \\ &= +\partial^0 h_{ij}^{\text{TT}}(t, r) + O(1/r^2). \end{aligned} \quad (1.150)$$

Then, from eq. (1.146), we see that at large distances, $t^{0r} = +t^{00}$ (which could also have been derived more simply from eq. (1.137), observing that an observer sitting at large distances from the source sees a plane wavefront), and the energy inside the volume V satisfies

$$\frac{dE_V}{dt} = -c \int dA t^{00}. \quad (1.151)$$

The fact that E_V decreases means that the outward-propagating GW carries away an energy flux

$$\begin{aligned} \frac{dE}{dAdt} &= +ct^{00} \\ &= \frac{c^3}{32\pi G} \langle \dot{h}_{ij}^{\text{TT}} \dot{h}_{ij}^{\text{TT}} \rangle, \end{aligned} \quad (1.152)$$

or, writing the surface element $dA = r^2 d\Omega$,

$$\boxed{\frac{dE}{dt} = \frac{c^3 r^2}{32\pi G} \int d\Omega \langle \dot{h}_{ij}^{\text{TT}} \dot{h}_{ij}^{\text{TT}} \rangle.} \quad (1.153)$$

In terms of h_+ and h_\times , we can rewrite the result as

$$\frac{dE}{dAdt} = \frac{c^3}{16\pi G} \langle \dot{h}_+^2 + \dot{h}_\times^2 \rangle. \quad (1.154)$$

The total energy flowing through dA between $t = -\infty$ and $t = +\infty$ is therefore²⁷

$$\frac{dE}{dA} = \frac{c^3}{16\pi G} \int_{-\infty}^{\infty} dt \langle \dot{h}_+^2 + \dot{h}_\times^2 \rangle. \quad (1.155)$$

As discussed in the previous section, in the situations relevant for GW detectors the average $\langle \dots \rangle$ in eq. (1.155) is a purely temporal average, over a few periods. Then in eq. (1.155) we can first perform the integral over dt from $-\infty$ to $+\infty$, eliminating therefore any time dependence, and the subsequent temporal average is just the average of a constant. Therefore the average in eq. (1.155) can be omitted, and

$$\frac{dE}{dA} = \frac{c^3}{16\pi G} \int_{-\infty}^{\infty} dt \left(\dot{h}_+^2 + \dot{h}_\times^2 \right). \quad (1.156)$$

Inserting the plane wave expansion of $h_{+, \times}(t)$, given in eqs. (1.52) and (1.48), we get

$$\begin{aligned} \frac{dE}{dA} &= \frac{c^3}{16\pi G} \int_{-\infty}^{\infty} df (2\pi f)^2 \left(|\tilde{h}_+(f)|^2 + |\tilde{h}_\times(f)|^2 \right) \\ &= \frac{\pi c^3}{4G} \int_{-\infty}^{\infty} df f^2 \left(|\tilde{h}_+(f)|^2 + |\tilde{h}_\times(f)|^2 \right). \end{aligned} \quad (1.157)$$

Since the integrand is even under $f \rightarrow -f$, we can restrict it to physical frequencies, $f > 0$, writing

$$\frac{dE}{dA} = \frac{\pi c^3}{2G} \int_0^{\infty} df f^2 \left(|\tilde{h}_+(f)|^2 + |\tilde{h}_\times(f)|^2 \right). \quad (1.158)$$

Therefore

$$\frac{dE}{dAdf} = \frac{\pi c^3}{2G} f^2 \left(|\tilde{h}_+(f)|^2 + |\tilde{h}_\times(f)|^2 \right). \quad (1.159)$$

We will always use the convention that the energy spectrum dE/df is the quantity that gives the total energy when it is integrated over the positive frequencies, rather than between $-\infty$ and $+\infty$. Writing $dA = r^2 d\Omega$, and integrating over a sphere surrounding the source, we find the energy spectrum

$$\frac{dE}{df} = \frac{\pi c^3}{2G} f^2 r^2 \int d\Omega \left(|\tilde{h}_+(f)|^2 + |\tilde{h}_\times(f)|^2 \right). \quad (1.160)$$

In the same way we can compute the flux of momentum. The momentum of the GWs inside a spherical shell V at large distances from the source is given by

$$P_V^k = \frac{1}{c} \int_V d^3x t^{0k}. \quad (1.161)$$

²⁷The integration over t from $-\infty$ to $+\infty$ is necessary if we want to resolve all possible frequencies. In an experiment one will integrate a signal only over a certain time interval Δt and one has a corresponding resolution in frequency $\Delta f \simeq 1/\Delta t$.

Considering again a GW propagating radially outward, and repeating the same steps leading from eq. (1.142) to eq. (1.154), we get

$$\begin{aligned} c\partial_0 P_V^k &= \int_V d^3x \partial_0 t^{0k} \\ &= - \int_S dA t^{0k}, \end{aligned} \quad (1.162)$$

and therefore the momentum flux carried away by the outward-propagating GW is

$$\frac{dP^k}{dAdt} = +t^{0k}. \quad (1.163)$$

Inserting the expression (1.133) for t^{0k} , we get

$$\boxed{\frac{dP^k}{dt} = -\frac{c^3}{32\pi G} r^2 \int d\Omega \langle \dot{h}_{ij}^{\text{TT}} \partial^k h_{ij}^{\text{TT}} \rangle.} \quad (1.164)$$

Observe that, if t^{0k} is odd under a parity transformation $\mathbf{x} \rightarrow -\mathbf{x}$, then the angular integral vanishes.

1.5 Propagation in curved space-time

In the last section we have examined the consequences of the low-modes equation, eq. (1.111). We have seen that it determines the dynamics of the background metric $\bar{g}_{\mu\nu}$, and that it allows us to identify the energy-momentum tensor of $h_{\mu\nu}$.

We now turn our attention to the high-mode equation (1.112). First of all, we examine it in the limiting case of no external matter, $T_{\mu\nu} = 0$, so eq. (1.112) becomes

$$R_{\mu\nu}^{(1)} = -[R_{\mu\nu}^{(2)}]^{\text{High}}. \quad (1.165)$$

We are interested in the leading term in λ/L_B (or in f_B/f ; for definiteness we use λ/L_B). We therefore first perform an order of magnitude estimates of $R_{\mu\nu}^{(1)}$ and of $[R_{\mu\nu}^{(2)}]^{\text{High}}$. In principle, in the short-wave expansion we have two small parameters, $h \equiv O(h_{\mu\nu})$ and λ/L_B . Recall however, from eq. (1.120), that when $T_{\mu\nu} = 0$ the Einstein equations fix these two scales to the same order of magnitude. Therefore, in this case we have a single small parameter, that we denote by ϵ ,

$$\epsilon = O(h) = O(\lambda/L_B). \quad (1.166)$$

To simplify notation, we use units $L_B = 1$ when we estimate the order of magnitude of the various terms, so that $h \sim \lambda \sim \epsilon$. From eq. (1.113), the leading term of $R_{\mu\nu}^{(1)}$ is

$$R_{\mu\nu}^{(1)} \sim \partial^2 h \sim \frac{h}{\lambda^2} \sim \frac{1}{\epsilon} \quad (1.167)$$

while

$$R_{\mu\nu}^{(2)} \sim \partial^2 h^2 \sim \frac{h^2}{\chi^2} \sim 1. \quad (1.168)$$

So $[R_{\mu\nu}^{(2)}]_{\text{High}}$ is at most $O(1)$ and can be neglected in eq. (1.165), compared to the leading term of $R_{\mu\nu}^{(1)}$, which is $O(1/\epsilon)$. Thus, if we limit ourselves to the leading term, eq. (1.112) simply becomes

$$[R_{\mu\nu}^{(1)}]_{1/\epsilon} = 0, \quad (1.169)$$

where $[\dots]_{1/\epsilon}$ means that we must extract the $O(1/\epsilon)$ part. Equation (1.169) can be written explicitly as

$$\eta^{\rho\sigma}(\partial_\rho\partial_\nu h_{\mu\sigma} + \partial_\rho\partial_\mu h_{\nu\sigma} - \partial_\nu\partial_\mu h_{\rho\sigma} - \partial_\rho\partial_\sigma h_{\mu\nu}) \simeq 0, \quad (1.170)$$

since the $O(1/\epsilon)$ part is obtained substituting the covariant derivatives with ordinary derivatives, and at the same time $\bar{g}^{\rho\sigma}$ in front of the parenthesis can be substituted with $\eta^{\rho\sigma}$, again to leading order in ϵ . This is just a propagation equation for the field $h_{\mu\nu}$ in a flat background, and it is the same equation that governs the propagation in the linearized theory discussed in Section 1.1, so we can again introduce $\bar{h}_{\mu\nu} = h_{\mu\nu} - (1/2)\eta_{\mu\nu}h$, impose the Lorentz gauge, and eq. (1.170) is nothing but

$$\square \bar{h}_{\mu\nu} \simeq 0, \quad (1.171)$$

where $\square = \partial_\mu\partial^\mu$ is the flat space d'Alembertian. So, this is the same as eq. (1.24) with the matter energy-momentum tensor $T_{\mu\nu} = 0$. We therefore discover that the high-frequency equation (1.112) is a wave equation for $h_{\mu\nu}$. We find that the propagation of GWs at $O(h)$ is the same as in the linearized theory because we considered the limit in which GWs are the only source of curvature. We now turn to the more interesting case in which external matter is present and dominates the curvature, so the low-frequency equation (1.111) becomes

$$\bar{R}_{\mu\nu} - \frac{1}{2}\bar{g}_{\mu\nu}\bar{R} \simeq \frac{8\pi G}{c^4} \bar{T}_{\mu\nu}. \quad (1.172)$$

To expand the high-frequency equation (1.112), we recall from eq. (1.121) that in this case $h \ll \chi/L_B \ll 1$, so the expansions in h and in χ/L_B are different. We keep only the terms linear in h (terms quadratic in h , in a typical situation involving GWs, are utterly negligible), and we expand the result in powers of χ/L_B . If we limit only to the leading and next-to-leading order in χ/L_B , eq. (1.112) becomes simply²⁸

$$R_{\mu\nu}^{(1)} = 0. \quad (1.174)$$

Now $\bar{g}_{\mu\nu}$ is determined by $T_{\mu\nu}$ and is not close to flat, so $R_{\mu\nu}^{(1)}$ is a fully covariant quantity with respect to a non-trivial background metric. As we show in Problem 1.1, in a curved background the equation $R_{\mu\nu}^{(1)} = 0$, written explicitly, reads

$$\bar{g}^{\rho\sigma}(\bar{D}_\rho\bar{D}_\nu h_{\mu\sigma} + \bar{D}_\rho\bar{D}_\mu h_{\nu\sigma} - \bar{D}_\nu\bar{D}_\mu h_{\rho\sigma} - \bar{D}_\rho\bar{D}_\sigma h_{\mu\nu}) = 0. \quad (1.175)$$

The discussion of this equation parallels exactly that of Section 1.1,

²⁸In fact, in eq. (1.112), $[R_{\mu\nu}^{(2)}]_{\text{High}}$ is negligible with respect to $R_{\mu\nu}^{(1)}$, because it has one more power of h . To estimate the order of magnitude of $(T_{\mu\nu} - \frac{1}{2}g_{\mu\nu}T)^{\text{High}}$, we observe that, if $T_{\mu\nu}$ is smooth, as we expect for macroscopic matter, its high-frequency part will come from the fact that the energy-momentum tensor $T_{\mu\nu}$ depends in general on the metric $g_{\mu\nu}$, and therefore will have a high-frequency component $O(h)$. Besides, also $g_{\mu\nu}T = (\bar{g}_{\mu\nu} + h_{\mu\nu})T$ has a high-frequency part $O(h)$ which comes from multiplying $\bar{g}_{\mu\nu}$ with the $O(h)$ high-frequency part of T , and another high-frequency part $O(h)$ which comes from multiplying $h_{\mu\nu}$ with the low-frequency part of T . So,

$$\left(T_{\mu\nu} - \frac{1}{2}g_{\mu\nu}T\right)^{\text{High}} = O(h/L_B^2). \quad (1.173)$$

Instead, $R_{\mu\nu}^{(1)} \sim \partial^2 h \sim h/\chi^2$. Then $(T_{\mu\nu} - \frac{1}{2}g_{\mu\nu}T)^{\text{High}}$ is smaller than $R_{\mu\nu}^{(1)}$ by a factor $O(\chi^2/L_B^2)$ and, to leading and next-to-leading order in χ/L_B , it does not contribute.

²⁹There is a slight notational clash here. The bar over $g_{\mu\nu}$ denotes the background metric, while over $h_{\mu\nu}$ it denotes the combination (1.176).

with $\eta_{\mu\nu}$ replaced by $\bar{g}_{\mu\nu}$. The equation becomes simpler introducing $h = \bar{g}^{\mu\nu} h_{\mu\nu}$ and²⁹

$$\bar{h}_{\mu\nu} = h_{\mu\nu} - \frac{1}{2} \bar{g}_{\mu\nu} h. \quad (1.176)$$

We now impose the gauge condition

$$\boxed{\bar{D}^\nu \bar{h}_{\mu\nu} = 0}, \quad (1.177)$$

that we still call the Lorentz gauge. In this gauge the equation $R_{\mu\nu}^{(1)} = 0$ becomes

$$\bar{D}^\rho \bar{D}_\rho \bar{h}_{\mu\nu} + 2\bar{R}_{\mu\rho\nu\sigma} \bar{h}^{\rho\sigma} - \bar{R}_{\mu\rho} \bar{h}_\nu^\rho - \bar{R}_{\nu\rho} \bar{h}_\mu^\rho = 0. \quad (1.178)$$

Outside the matter sources, where $\bar{T}_{\mu\nu} = 0$, the Einstein equation for the background, eq. (1.172), tells us that $\bar{R}_{\mu\nu} = 0$. More precisely, using eq. (1.111), $\bar{R}_{\mu\nu}$ gets a contribution only from the term $[R_{\mu\nu}^{(2)}]_{\text{Low}}$, so $\bar{R}_{\mu\nu} = O(h^2/\chi^2)$. Then, to linear order in h we can drop the terms $\bar{R}_{\mu\rho} \bar{h}_\nu^\rho$ and $\bar{R}_{\nu\rho} \bar{h}_\mu^\rho$ in eq. (1.178). Furthermore, $\bar{R}_{\mu\rho\nu\sigma} \bar{h}^{\rho\sigma} = O(h/L_B^2)$ while $\bar{D}^\rho \bar{D}_\rho \bar{h}_{\mu\nu} = O(h/\chi^2)$. Thus, since we have already restricted ourselves to the leading term and next-to-leading term in χ/L_B (see Note 28) we simply have

$$\boxed{\bar{D}^\rho \bar{D}_\rho \bar{h}_{\mu\nu} = 0}. \quad (1.179)$$

Equations (1.177) and (1.179) determine the propagation of GWs in the curved background, in the limit $\chi \ll L_B$. In conclusion we find that, after separating the Einstein equations into a low-frequency part and a high-frequency part, the low-frequency part describes the effect of GWs and of external matter on the background space-time, while the high-frequency part gives a wave equation in curved space, which describes the propagation of $h_{\mu\nu}$. This curved-space equation can be solved using the eikonal approximation of geometric optics, as we now discuss.

1.5.1 Geometric optics in curved space

Electromagnetic waves

We first recall how geometric optics works for electromagnetic waves, in a curved space with metric $\bar{g}_{\mu\nu}$.³⁰ The action of the electromagnetic field in this curved space is

$$S = -\frac{1}{4} \int d^4x \sqrt{-\bar{g}} \bar{g}_{\mu\alpha} \bar{g}_{\nu\beta} F^{\mu\nu} F^{\alpha\beta}, \quad (1.180)$$

and its variation gives the equations of motion

$$\bar{D}_\mu (\bar{D}^\mu A^\nu - \bar{D}^\nu A^\mu) = 0 \quad (1.181)$$

³⁰We follow Misner, Thorne and Wheeler (1973), Section 22.5.

(we raise and lower the indices with $\bar{g}_{\mu\nu}$), which generalize the flat-space pair of Maxwell equations $\partial_\mu F^{\mu\nu} = 0$. One imposes on the four-vector potential A^μ the curved-space generalization of the Lorentz gauge,

$$\bar{D}_\mu A^\mu = 0. \quad (1.182)$$

From the definition of covariant derivative, $\bar{D}_\mu \bar{D}^\nu A^\mu = \bar{D}^\nu \bar{D}_\mu A^\mu + R^\nu{}_\mu A^\mu$, where $R^\nu{}_\mu$ is the Ricci tensor. The term $\bar{D}^\nu \bar{D}_\mu A^\mu$ vanishes because of the gauge condition, so eq. (1.181) becomes

$$\bar{D}^\rho \bar{D}_\rho A^\mu - R^\mu{}_\rho A^\rho = 0. \quad (1.183)$$

Geometric optics is valid when λ is much smaller than the other length-scales in the problem. So we must have $\lambda \ll L_B$, with L_B the typical scale of variation of the background metric, and also $\lambda \ll L_c$, where L_c is the characteristic length-scale over which the amplitude, polarization or wavelength of the electromagnetic field change substantially. In particular, λ must be much smaller than the curvature radius of the wavefront.

Under these conditions, we can use the eikonal approximation, which consists in looking for a solution with a phase θ rapidly varying, i.e. θ changes on the scale λ , while the amplitude changes only on the scale L_B or L_c (whichever is smaller), so it is slowly varying. To perform the expansion systematically it is convenient to write

$$A^\mu(x) = [a^\mu(x) + \varepsilon b^\mu(x) + \varepsilon^2 c^\mu(x) + \dots] e^{i\theta(x)/\varepsilon}, \quad (1.184)$$

where ε is a fictitious parameter, to be finally set equal to unity, that reminds us that a term to which a factor ε^n is attached, is of order $(\lambda/L)^n$, where L is the smallest between L_B and L_c . An expansion of the form (1.184) is just an ansatz, and its validity is verified by substituting it in the equations.

Since $R^\mu{}_\rho A^\rho = O(A/L_B^2)$, where A is the typical amplitude of A^μ , while $\bar{D}^\rho \bar{D}_\rho A^\mu = O(A/\lambda^2)$, to leading and next-to-leading order in λ/L_B we can neglect $R^\mu{}_\rho A^\rho$, and the equation of motion is simply

$$\bar{D}^\rho \bar{D}_\rho A^\mu = 0. \quad (1.185)$$

Defining the wave-vector $k_\mu \equiv \partial_\mu \theta$ and plugging the ansatz (1.184) into eq. (1.182) we get, to lowest order,

$$\bar{g}_{\mu\nu} k^\mu a^\nu = 0. \quad (1.186)$$

From eq. (1.185) we get instead, to lowest order,

$$\bar{g}_{\mu\nu} k^\mu k^\nu = 0. \quad (1.187)$$

This is known as the *eikonal equation*. From this it also follows that $0 = \bar{D}_\nu(k_\mu k^\mu) = 2k^\mu \bar{D}_\nu k_\mu$ (recall again that indices are raised and lowered with $\bar{g}_{\mu\nu}$). Since θ is a scalar, and on a scalar the covariant derivatives commute, we have $\bar{D}_\nu \partial_\mu \theta = \bar{D}_\nu \bar{D}_\mu \theta = \bar{D}_\mu \bar{D}_\nu \theta = \bar{D}_\mu \partial_\nu \theta$,

so we can interchange the indices, $\bar{D}_\nu k_\mu = \bar{D}_\mu k_\nu$, and the condition $k^\mu \bar{D}_\nu k_\mu = 0$ becomes

$$k^\mu \bar{D}_\mu k_\nu = 0. \quad (1.188)$$

³¹Writing $k^\mu = dx^\mu/d\lambda$, where λ is the affine parameter along the geodesic, eq. (1.188) gives the geodesic equation, in the form

$$\frac{d^2x^\mu}{d\lambda^2} + \Gamma_{\nu\rho}^\mu \frac{dx^\nu}{d\lambda} \frac{dx^\rho}{d\lambda} = 0.$$

This is the geodesic equation in the space-time of the background metric $\bar{g}_{\mu\nu}$,³¹ so eq. (1.188) states that the curves orthogonal to the surfaces of constant phase (the “rays” of the geometric optics approximation) travel along the null geodesics of $\bar{g}_{\mu\nu}$.

To next-to-leading order in ε , eq. (1.185) gives

$$2k_\rho \bar{D}^\rho a^\mu + (\bar{D}^\rho k_\rho) a^\mu = 0. \quad (1.189)$$

It is convenient to introduce the real scalar amplitude $a = (a^\mu a_\mu^*)^{1/2}$ and the polarization vector e^μ defined from $a^\mu = ae^\mu$, so $e^\mu e_\mu^* = 1$. An equation for the scalar amplitude is obtained observing that, on the one hand, one has the trivial identity $k^\mu \partial_\mu(a^2) = 2ak^\mu \partial_\mu a$. On the other hand, on a scalar such as a^2 , ∂_μ can be replaced by \bar{D}_μ , so $k^\mu \partial_\mu(a^2) = k^\mu \bar{D}_\mu(a^\rho a_\rho^*) = -(\bar{D}^\rho k_\rho)a^2$, where we used eq. (1.189). Comparing these two results, we get an equation for the scalar amplitude,

$$k^\mu \partial_\mu a = -\frac{1}{2}(\bar{D}_\mu k^\mu)a. \quad (1.190)$$

Finally, to obtain an equation for e^μ , we substitute $a^\mu = ae^\mu$ into eq. (1.189) and we use eq. (1.190). This gives

$$k^\rho \bar{D}_\rho e^\mu = 0. \quad (1.191)$$

Expanding the equations to still higher orders we could determine the corrections b_μ, c_μ, \dots to the amplitude in terms of a_μ . Equations (1.186), (1.187), (1.188), (1.190) and (1.191) are the fundamental results of the geometric optics of electromagnetic waves in curved space. Equations (1.187) and (1.188) states that light rays (or photons, in a quantum language) travel along the null geodesics of $\bar{g}_{\mu\nu}$. Equation (1.186) states that the polarization vector e^μ is orthogonal to the propagation direction, $k_\mu e^\mu = 0$, and eq. (1.191) states that it is parallel-transported along the null geodesics. Finally, eq. (1.190) expresses (in the quantum language) the conservation of the number of photons in the limit of geometric optics. This can be seen rewriting it in the form

$$\bar{D}^\mu(a^2 k^\mu) = 0. \quad (1.192)$$

This shows that the current $j^\mu = a^2 k^\mu$ is covariantly conserved. Its associated conserved charge, according to the Noether theorem that we will recall in Section 2.1.1, is the integral of $a^2 k^0$ over a spatial surface at constant time. In a plane wave, the energy density is proportional to $|\mathbf{E}|^2 + |\mathbf{B}|^2 = 2|\mathbf{E}|^2$. In the gauge $A_0 = 0$, the electric field is $\mathbf{E} = \partial_0 \mathbf{A}$, so its amplitude is $k^0 a$, and the energy density is proportional to $(k^0 a)^2$. Since each photon carries an energy k^0 , we see that $k^0 a^2$ is proportional to the number density of photons, so eq. (1.192) expresses the fact that, in the limit of geometric optics, the number of photons is conserved.

Gravitational waves

We can now discuss the eikonal approximation for GWs. We make the ansatz

$$\bar{h}_{\mu\nu}(x) = [A_{\mu\nu}(x) + \varepsilon B_{\mu\nu}(x) + \dots] e^{i\theta(x)/\varepsilon}. \quad (1.193)$$

Again we define $k_\mu = \partial_\mu \theta$, and we write $A_{\mu\nu} = A e_{\mu\nu}$ where the polarization tensor $e_{\mu\nu}$ is normalized as $e^{\mu\nu} e_{\mu\nu}^* = 1$, and A is the scalar amplitude. Substituting this ansatz into eqs. (1.177) and (1.179) and repeating basically the same steps as for the electromagnetic case, we find that k_μ still obeys eqs. (1.187) and (1.188), so gravitons travel along the null geodesic of $\bar{g}_{\mu\nu}$. Just as for photons, the scalar amplitude satisfies

$$k^\mu \partial_\mu A = -\frac{1}{2} (\bar{D}_\mu k^\mu) A, \quad (1.194)$$

which can be written as $\bar{D}^\mu (A^2 k^\mu) = 0$, and gives the conservation of the number of gravitons. Finally, the polarization tensor satisfies

$$k^\nu e_{\mu\nu} = 0, \quad (1.195)$$

$$k^\rho \bar{D}_\rho e_{\mu\nu} = 0, \quad (1.196)$$

so it is transverse and is parallel-propagated along the null geodesics.

Since gravitons propagate along null geodesics, just as photons, their propagation through curved space-time is the same as the propagation of photons, as long as geometric optics applies. For instance, they suffer gravitational deflection when passing near a massive body, with the same deflection angle as photons, and they undergo the same redshift in a gravitational potential.³²

One practical difference concerning the lensing of gravitational and electromagnetic waves is however worth observing. Both type of waves can in principle be lensed by a large mass situated between the source and the observer. When the different images of the source cannot be resolved we are in the regime of microlensing, where we have a single image which is magnified. The amplification factor \mathcal{A} in the energy density, computed within geometric optics, is³³

$$\mathcal{A} = \frac{u^2 + 2}{u\sqrt{u^2 + 4}} \simeq \frac{1}{u}, \quad (1.197)$$

where $u = \beta/\theta_E$, β is the angle of the source with respect to the observer-lens axis (see Fig. 1.5), and θ_E is the Einstein angle, given by

$$\theta_E^2 = \frac{2R_S d_{SL}}{d_{OL}(d_{SL} + d_{OL})}, \quad (1.198)$$

where R_S is the Schwarzschild radius of the lens and d_{SL} and d_{OL} are the source-lens and observer-lens distances, respectively. The second equality in eq. (1.197) holds when $u \ll 1$, i.e. when the source, lens and observer are well aligned, and in this case the amplification factor is large. In fact, it even becomes formally infinite if $u = 0$, i.e. when the source, lens and observer are perfectly aligned. However, the geometric

³²The redshift of gravitons in a FRW cosmological model will be discussed explicitly in Section 4.1.4.

³³See e.g. Binney and Merrifield (1998).

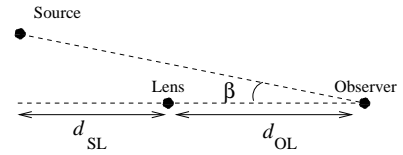


Fig. 1.5 The geometry for the lensing of gravitational or electromagnetic waves.

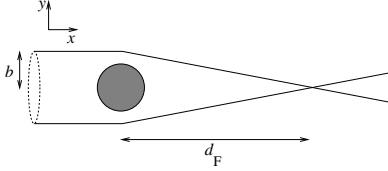


Fig. 1.6 The focusing of GWs from a source.

optics approximation breaks down near the caustics, i.e. when the light rays coming from the source cross each other, since there the scale of variation of the wavefront is no longer small compared to χ .

The actual behavior near the caustics can be obtained taking into account diffraction (or, in a quantum language, the uncertainty principle). In order of magnitude the effect can be estimated as follows. Consider a circular ring of rays, which is part of a plane wavefront, arriving with impact parameter b on a star of mass M which acts as a gravitational lens, as in Fig. 1.6. The deflection angle due to the gravitational field of the star is given by the classical Einstein result, $\theta = 2R_S/b$, where $R_S = 2GM/c^2$ is the Schwarzschild radius of the star. The whole circular ring of rays with impact parameter b is then focused on a single point, at a focal distance d_F given by $b/d_F = \tan \theta \simeq \theta$, i.e.

$$d_F \simeq \frac{b^2}{2R_S}. \quad (1.199)$$

The fact that a one-dimensional surface is focused onto a point is responsible for the formal infinite enhancement of the luminosity. In practice, however, diffraction forbids such a perfect focusing. Indeed, when we state that a photon has impact parameter b , we are implicitly assuming that the error Δy on its transverse position is smaller than b . Then, by the Heisenberg principle, it has an uncertainty on the transverse momentum $\Delta k_y \gtrsim \hbar/b$, and an angular spreading

$$\Delta\theta_s \simeq \frac{\Delta k_y}{k_x} \gtrsim \frac{\chi}{b}. \quad (1.200)$$

Propagating to a distance d_F this induces a transverse spread

$$\Delta y_s \simeq d_F \Delta\theta_s \gtrsim \frac{\chi b}{2R_S}. \quad (1.201)$$

The focusing is substantial only if $\Delta y_s \ll b$, which gives

$$\chi \ll 2R_S. \quad (1.202)$$

³⁴A more accurate estimate can be obtained taking into account the detailed internal structure of the lens, see Bontz and Haugan (1981).

For a lens with a mass of order M_\odot , this means that a substantial focusing is possible only for waves with $\chi \ll O(6)$ km, i.e. a frequency $f \gg O(10)$ kHz.³⁴ For electromagnetic waves in the visible spectrum, this condition is very well satisfied, and microlensing is indeed commonly observed. For GWs, however, we will see that no astrophysical source is expected to produce waves with frequencies much larger than $O(10)$ kHz, and no significant amplification can be obtained for these waves from typical stellar-mass lenses.

1.5.2 Absorption and scattering of GWs

Finally, GWs are insensitive to absorption and scattering, during their propagation from astrophysical sources to the observer, because of the smallness of the gravitational cross-section. To make a quantitative

estimate, recall that the mean free path l of a particle scattering off an ensemble of target with number density n and cross-section σ , is given by

$$l = \frac{1}{n\sigma}. \quad (1.203)$$

For a graviton of energy E , the scattering cross-section off a target of mass m is (using units $\hbar = c = 1$) $\sigma \sim G_N^2 s$, where s is the square of the center-of-mass energy.³⁵ Consider for instance the scattering of a graviton with four-momentum $k^\mu = (E, 0, 0, E)$ off a nucleon at rest, with four-momentum $p^\mu = (m_n, 0, 0, 0)$, where the mass $m_n \sim 1$ GeV. Then the square of the center-of-mass energy is $s = -(p+k)^2 = m_n^2 + 2m_n E$. For all astrophysically plausible values of the GW frequency f_{gw} , $E = \hbar\omega_{\text{gw}}$ is totally negligible with respect to m_n . For instance, if $f_{\text{gw}} = 1$ kHz, we have $\hbar\omega_{\text{gw}} = O(10^{-21})$ GeV; so $s \simeq m_n^2$ and

$$\sigma \sim G_N^2 m_n^2. \quad (1.204)$$

We can now compare the absorption of electromagnetic and of gravitational waves, for instance from the Sun. For photons in a neutral plasma, such as the Sun, the most important process is the Thompson scattering on electrons, which has a cross-section $\sigma = 8\pi\alpha^2/(3m_e^2)$, where $\alpha \simeq 1/137$ is the fine-structure constant, and we use units $\hbar = c = 1$. Inserting the numerical values, we see that the Thomson cross-section for scattering of photons on electrons is larger than the gravitational cross-section for scattering of gravitons on nucleons, eq. (1.204), by a huge factor $O(10^{80})$. The number density n_e of electrons in the Sun (which is relevant for computing the electromagnetic mean free path due to electron–photon scattering) is about the same as the number density of protons, relevant to compute the gravitational mean free path due to proton–graviton scattering, so the mean-free path for gravitons in the Sun is larger by a factor $O(10^{80})$ compared to that of photons! Using the value of n_e of the Sun, one finds that the photon mean free path inside the Sun is $O(1)$ cm. Using this value of l , one can show that a photon produced by thermonuclear reactions in the Sun core takes about 3×10^4 yr to reach the surface of the Sun and finally escape.³⁶ For a graviton the mean free path inside the Sun is $O(10^{80})$ cm, which is huge even compared to the observable size of the Universe (consider that $1 \text{ Gpc} \simeq 3 \times 10^{27}$ cm). Therefore, for a GW the Sun is completely transparent.

Significant absorption of GWs can take place if the wave impinges on a black hole. In this case, we can use the result for the capture cross section of a relativistic particle by a black hole with Schwarzschild radius R_S , $\sigma = (27/4)\pi R_S^2$.³⁷ Another possibility is that the GW impinges on a neutron star, just with the right frequency to excite one of its normal modes. In this case, the wave interacts coherently with the neutron star (while, in the above estimate of scattering in the Sun, we computed the incoherent scattering off the single protons). However, as we see in microlensing experiments, the probability that a compact object lies on the path from an astrophysical source to the Earth is very small.

³⁵This can be shown most easily using the field-theoretical methods of Chapter 2, observing that the graviton-matter-matter vertex is proportional to $G_N^{1/2}$. In the Feynman diagram for the graviton-matter scattering there are two such vertices, so the amplitude is proportional to G_N and the cross-section to G_N^2 . The dependence on s is then fixed by dimensional arguments observing that, in units $\hbar = c = 1$, G_N is an inverse mass squared, as well as from Lorentz invariance, that dictates that the energy dependence is through the Lorentz-invariant quantity s . This is the same result that holds (at energies $E \ll M_W$) for neutrinos, with the Fermi constant G_F replacing Newton's constant G_N .

³⁶See e.g. Exercise 1.2 of Maggiore (2005).

³⁷See e.g. Landau and Lifshitz, Vol. II (1979), Section 102.

1.6 Solved problems

Problem 1.1. Linearization of the Riemann tensor in curved space

In this problem we compute the Riemann and Ricci tensors, linearized to first order in $h_{\mu\nu}$ over a generic curved background $\bar{g}_{\mu\nu}$. The inversion of $g_{\mu\nu} = \bar{g}_{\mu\nu} + h_{\mu\nu}$ is $g^{\mu\nu} = \bar{g}^{\mu\nu} - h^{\mu\nu} + O(h^2)$. Then it is straightforward to find that, to $O(h)$, the linearization of the Christoffel symbol gives

$$\Gamma_{\nu\rho}^\mu = \bar{\Gamma}_{\nu\rho}^\mu + \frac{1}{2}\bar{g}^{\mu\sigma}(\bar{D}_\nu h_{\rho\sigma} + \bar{D}_\rho h_{\nu\sigma} - \bar{D}_\sigma h_{\nu\rho}). \quad (1.205)$$

The calculation of the Riemann tensor at a given point x is enormously simplified if we perform it in a coordinate system where $\bar{\Gamma}_{\nu\rho}^\mu(x) = 0$ (paying attention, of course, to the fact that the derivatives of $\bar{\Gamma}_{\nu\rho}^\mu$ are non-zero!) We see from eq. (1.205) that in this frame $\Gamma_{\nu\rho}^\mu = O(h)$ and therefore the terms $\sim \Gamma\Gamma$ in the Riemann tensor are $O(h^2)$, so they do not contribute to $O(h)$, and we simply have $R^\mu_{\nu\rho\sigma} = \partial_\rho\Gamma_{\nu\sigma}^\mu - \partial_\sigma\Gamma_{\nu\rho}^\mu + O(h^2)$. Furthermore, substituting eq. (1.205) for $\Gamma_{\nu\rho}^\mu$, we only need to keep the terms where the derivative acts on the background Christoffel symbols $\bar{\Gamma}_{\nu\rho}^\mu$, since background Christoffel symbols on which no derivative act give zero. Since $\bar{\Gamma}_{\nu\rho}^\mu(x) = 0$, in the final expression (i.e. after having performed all derivatives) we are free to write derivatives as covariant derivatives with respect to the background, and we obtain an expression valid in all coordinate systems.

Then, in the frame where $\bar{\Gamma}_{\nu\rho}^\mu(x) = 0$, we get

$$R_{\mu\nu\rho\sigma} = \bar{R}_{\mu\nu\rho\sigma} + \frac{1}{2}(\bar{D}_\rho\bar{D}_\nu h_{\mu\sigma} + \bar{D}_\sigma\bar{D}_\mu h_{\nu\rho} - \bar{D}_\rho\bar{D}_\mu h_{\nu\sigma} - \bar{D}_\sigma\bar{D}_\nu h_{\mu\rho} + h_\mu^\tau\bar{R}_{\tau\nu\rho\sigma} - h_\nu^\tau\bar{R}_{\tau\mu\rho\sigma}). \quad (1.206)$$

We have performed the computation in a special frame. Since, however, the final result is expressed in terms of covariant quantities, this expression holds in any frame. The linearization of the Ricci tensor is then obtained using $R_{\mu\nu} = g^{\alpha\beta}R_{\alpha\mu\beta\nu} = (\bar{g}^{\alpha\beta} - h^{\alpha\beta})(\bar{R}_{\alpha\mu\beta\nu} + R_{\alpha\mu\beta\nu}^{(1)})$, so that the part linear in $h_{\mu\nu}$ is $R_{\mu\nu}^{(1)} = \bar{g}^{\alpha\beta}R_{\alpha\mu\beta\nu}^{(1)} - h^{\alpha\beta}\bar{R}_{\alpha\mu\beta\nu}$. Then we get³⁸

$$R_{\mu\nu}^{(1)} = \frac{1}{2}(\bar{D}^\alpha\bar{D}_\mu h_{\nu\alpha} + \bar{D}^\alpha\bar{D}_\nu h_{\mu\alpha} - \bar{D}^\alpha\bar{D}_\alpha h_{\mu\nu} - \bar{D}_\nu\bar{D}_\mu h), \quad (1.207)$$

where $h = \bar{g}^{\alpha\beta}h_{\alpha\beta}$. Observe that $\bar{D}_\nu\bar{D}_\mu h = \bar{D}_\nu\partial_\mu h = \partial_\nu\partial_\mu h - \bar{\Gamma}_{\nu\mu}^\rho\partial_\rho h$ is symmetric under the exchange $\mu \leftrightarrow \nu$, and therefore $R_{\mu\nu}^{(1)}$ is also symmetric, as it should be.

If the background is flat, $\bar{g}_{\mu\nu} = \eta_{\mu\nu}$, the covariant derivatives become ordinary derivatives and therefore commute. If we impose the Lorentz gauge condition $\partial^\mu\bar{h}_{\mu\nu} = 0$, i.e. $\partial^\mu h_{\mu\nu} = (1/2)\partial_\nu h$, the linearized Ricci tensor takes a very simple form,

$$R_{\mu\nu}^{(1)} = -\frac{1}{2}\square h_{\mu\nu}, \quad (\text{flat background}). \quad (1.208)$$

³⁸We make use of the identity

$$[\bar{D}_\nu, \bar{D}_\alpha]h_\mu^\alpha = h^{\alpha\beta}\bar{R}_{\alpha\mu\beta\nu} - h_\mu^\tau\bar{R}_{\tau\nu},$$

which follows from the definition of covariant derivative, see e.g. Weinberg (1972), eq. (6.5.3). Pay attention to the fact that Weinberg has the opposite sign convention for the Riemann tensor.

Problem 1.2. Gauge transformation of $h_{\mu\nu}$ and $R_{\mu\nu\rho\sigma}^{(1)}$

In the text we showed that, when the background space-time is $\eta_{\mu\nu}$, the resulting linearized theory has a gauge symmetry given by eq. (1.8), and that the linearized Riemann tensor $R_{\mu\nu\rho\sigma}^{(1)}$ is gauge-invariant. It is interesting to see how these results are modified when the background space-time is curved.

Under the coordinate transformation $x^\mu \rightarrow x'^\mu = x^\mu + \xi^\mu(x)$, the usual transformation law of the metric is

$$g_{\mu\nu}(x) \rightarrow g'_{\mu\nu}(x') = \frac{\partial x^\rho}{\partial x'^\mu} \frac{\partial x^\sigma}{\partial x'^\nu} g_{\rho\sigma}(x). \quad (1.209)$$

Writing $g'_{\mu\nu}(x) = g'_{\mu\nu}(x - \xi)$ and expanding to first order in ξ , we have

$$g'_{\mu\nu}(x) \simeq g'_{\mu\nu}(x) - \xi^\rho \partial_\rho g'_{\mu\nu}. \quad (1.210)$$

Combining this with eq. (1.209) we get

$$g'_{\mu\nu}(x) = g_{\mu\nu}(x) - (D_\mu \xi_\nu + D_\nu \xi_\mu), \quad (1.211)$$

where the covariant derivative is

$$D_\mu \xi_\nu = \partial_\mu \xi_\nu - \Gamma_{\mu\nu}^\rho \xi_\rho. \quad (1.212)$$

Equation (1.211) gives the lowest-order term in the small parameter $|D_\mu \xi_\nu|$. Similar to what we have done in linearized theory, we restrict ourselves to $|D_\mu \xi_\nu| \lesssim h$, where $h = O(|h_{\mu\nu}|)$. Since $\Gamma_{\mu\nu}^\rho = O(\partial g_{\mu\nu}) = O(1/L_B)$, where L_B is the typical variation scale of the background metric, the condition $|D_\mu \xi_\nu| \lesssim h$ means that both

$$|\partial \xi| \lesssim h, \quad \text{and} \quad \xi \lesssim h L_B, \quad (1.213)$$

must be satisfied. (We use the notation $\xi = O(|\xi^\mu|)$.) In the case of a flat background metric, discussed in Section 1.1, we have $L_B = \infty$ and therefore we found only the condition $|\partial \xi| \lesssim h$.

A generic function ξ^μ has both low-frequency and high-frequency modes, without a clear separation between them, and therefore in the transformed metric $g'_{\mu\nu}(x)$ the separation between the background and the GW in general disappears. It is therefore more useful to restrict ourselves to functions ξ^μ which maintain a clear-cut separation between low- and high-frequencies. In particular, we can consider a function ξ^μ that has only high-frequency modes. We observe that

$$D_\mu \xi_\nu + D_\nu \xi_\mu = (\bar{D}_\mu \xi_\nu + \bar{D}_\nu \xi_\mu) + \xi^\rho (\bar{D}_\mu h_{\nu\rho} + \bar{D}_\nu h_{\mu\rho} - \bar{D}_\rho h_{\mu\nu}), \quad (1.214)$$

where we have used the expansion (1.205) for the Christoffel symbol. Since $\bar{\Gamma}_{\nu\rho}^\mu$ is a purely low-frequency term, and ξ^μ has only high frequencies, the terms $\bar{D}_\mu \xi_\nu$ are purely high-frequency, and therefore contribute to the transformation of $h_{\mu\nu}$ rather than of $\bar{g}_{\mu\nu}$.³⁹ Therefore under such a transformation we have $\bar{g}'_{\mu\nu}(x) = \bar{g}_{\mu\nu}(x)$ and

$$h'_{\mu\nu}(x) \simeq h_{\mu\nu}(x) - (\bar{D}_\mu \xi_\nu + \bar{D}_\nu \xi_\mu), \quad (1.215)$$

under the condition that ξ^μ contains only high-frequencies and that it satisfies

$$|\bar{D}_\mu \xi_\nu| \leq |h_{\mu\nu}|. \quad (1.216)$$

³⁹Note that, since $|\partial \xi| \lesssim h$ and $|\xi| \lesssim h L_B$, the terms $\xi \bar{D} h$ in eq. (1.214) are at most $O(h^2 L_B / \lambda)$. When the curvature is dominated by matter we found in Section 1.4.2 that $h \ll \lambda / L_B$, and therefore in eq. (1.214) the term $\xi \bar{D} h$ is negligible with respect to the term $\bar{D}_\mu \xi_\nu$. In the opposite limit of curvature dominated by GWs we have $h \sim \lambda / L_B$ and the term $\xi \bar{D} h$ becomes of the same order as $D_\mu \xi_\nu$, but not larger; therefore, even in this limit, the order-of-magnitude estimates given below are not affected when neglecting the term $\xi \bar{D} h$.

Equation (1.215) has the form of a gauge transformation for a symmetric tensor field $h_{\mu\nu}$ on a curved space described by $\bar{g}_{\mu\nu}$. In this sense, we have a gauge theory for a spin-2 field in a curved background. We next compute how the linearized Riemann tensor transforms under this gauge transformation. We write

$$R_{\mu\nu\rho\sigma} = \bar{R}_{\mu\nu\rho\sigma} + R_{\mu\nu\rho\sigma}^{(1)} + O(h^2), \quad (1.217)$$

where $\bar{R}_{\mu\nu\rho\sigma}$ is the Riemann tensor of the background and we raise and lower indices with $\bar{g}_{\mu\nu}$. The explicit calculation performed in Problem 1.1 gives

$$2R_{\mu\nu\rho\sigma}^{(1)} = \bar{D}_\rho \bar{D}_\nu h_{\mu\sigma} + \bar{D}_\sigma \bar{D}_\mu h_{\nu\rho} - \bar{D}_\rho \bar{D}_\mu h_{\nu\sigma} - \bar{D}_\sigma \bar{D}_\nu h_{\mu\rho} + h_\mu^\tau \bar{R}_{\tau\nu\rho\sigma} - h_\nu^\tau \bar{R}_{\tau\mu\rho\sigma}, \quad (1.218)$$

which generalizes eq. (1.13) to a curved background. Under the gauge transformation (1.215) the variation of $R_{\mu\nu\rho\sigma}^{(1)}$ is given by

$$\begin{aligned} \delta R_{\mu\nu\rho\sigma}^{(1)} &= \xi^\tau \bar{D}_\tau \bar{R}_{\mu\nu\rho\sigma} + \bar{R}_{\tau\nu\rho\sigma} \bar{D}_\mu \xi^\tau - \bar{R}_{\tau\mu\rho\sigma} \bar{D}_\nu \xi^\tau \\ &\quad + \bar{R}_{\mu\nu\tau\rho} \bar{D}_\sigma \xi^\tau - \bar{R}_{\mu\nu\tau\sigma} \bar{D}_\rho \xi^\tau. \end{aligned} \quad (1.219)$$

Therefore, if the background is not flat, $R_{\mu\nu\rho\sigma}^{(1)}$ is no longer gauge invariant under the gauge transformations of linearized theory. However, let us estimate the order of magnitude of the various terms. For the background we have

$$\bar{R}_{\mu\nu\rho\sigma} \sim \partial^2 \bar{g}_{\mu\nu} \sim \frac{1}{L_B^2}, \quad \bar{D}_\tau \bar{R}_{\mu\nu\rho\sigma} \sim \partial^3 \bar{g}_{\mu\nu} \sim \frac{1}{L_B^3}, \quad (1.220)$$

Equation (1.216) gives instead $\xi \sim h L_B$, $\bar{D}\xi \sim h$ and we therefore see that

$$\delta R_{\mu\nu\rho\sigma}^{(1)} \sim \frac{h}{L_B^2}. \quad (1.221)$$

This means that the variation of $R_{\mu\nu\rho\sigma}^{(1)}$ is much smaller than $R_{\mu\nu\rho\sigma}^{(1)}$ itself, since

$$R_{\mu\nu\rho\sigma}^{(1)} \sim \partial^2 h \sim \frac{h}{\lambda^2} \quad (1.222)$$

and therefore

$$\delta R_{\mu\nu\rho\sigma}^{(1)} \sim \frac{\lambda^2}{L_B^2} R_{\mu\nu\rho\sigma}^{(1)}. \quad (1.223)$$

We conclude that $R_{\mu\nu\rho\sigma}^{(1)}$ is approximately gauge-invariant in the limit $\lambda/L_B \ll 1$. More precisely, its leading term in an expansion in powers of λ/L_B is gauge-invariant. Therefore, in the limit $\lambda/L_B \ll 1$, which was used from the very beginning to define $h_{\mu\nu}$, we can see $h_{\mu\nu}$ as a gauge field, with a gauge-invariant field-strength tensor given by the leading terms of $R_{\mu\nu\rho\sigma}^{(1)}$, as obtained from eq. (1.218).

Further reading

- Classical textbooks on general relativity are Weinberg (1972), Misner, Thorne and Wheeler (1973), and Landau and Lifshitz, Vol. II (1979). Among the more recent books, we suggest Hartle (2003) (at a rather introductory level, and with a very physical approach), and Straumann (2004) (more advanced).
- For discussions of freely falling frames, Riemann and Fermi normal coordinates, TT frame and the proper detector frame, see Misner, Thorne and Wheeler (1973), Sections 13.6 and 37.2, Hartle (2003), Section 8.4, and Thorne (1983, 1987). The metric of an accelerated, rotating observer is computed to quadratic order in x^i by Ni and Zimmermann (1978).
- The energy-momentum tensor of GWs and the short-wave expansion are discussed by Isaacson (1968a, 1968b), Misner, Thorne and Wheeler (1973), and Thorne (1987). The fact that performing a space-time average one obtains a gauge-invariant energy-momentum tensor was already discussed in Arnowitt, Deser and Misner (1961).
- The geometric optics approximation in curved space-time is discussed in Isaacson (1968a, 1968b) and Misner, Thorne and Wheeler (1973) (see in particular Section 22.5 for photons, and Section 35.14 and Exercise 35.15 for gravitational waves). See also Thorne (1983, 1987). Diffraction and lensing of GWs is discussed in Bontz and Hau-gan (1980) and in Section 2.6.1 of Thorne (1983).
- A definition of GWs based on the asymptotics of the gravitational field at null infinity was given by Bondi, van der Burg and Metzner (1962) and Sachs (1962), and was also important historically for resolving the controversy on the reality of gravitational radiation. A geometric description of the asymptotic fall-off of radiative solutions, using the notion of asymptotically simple space-time, was given by Penrose (1963, 1965).
- The development of the concept of gravitational wave has a very interesting history. The notion even predates Einstein general relativity (the term “gravitational wave” was used by Poincaré as early as 1905, referring to the fact that, even in a gravitational theory, the interaction must propagate at a finite speed). With the advent of general relativity, gravitational waves were introduced by Einstein in 1916. However, the existence of physical effects associated with them has been questioned many times, with Einstein himself changing his mind more than once. Eddington is associated to the ironic remark that “gravitational waves propagate at the speed of thought”, implying that they are gauge artifact. (Actually, he was referring only to the transverse-longitudinal and longitudinal-longitudinal components of h_{ij} , which, indeed, are pure gauge modes. Concerning the transverse-transverse part, he rather showed that it carries energy, and even corrected an erroneous factor of two in Einstein’s early version of the quadrupole formula.) The controversy on the existence of GWs was not settled until the early 1960s. A very interesting book on the history of the research in GWs is Kennefick (2007), see also the review article Kennefick (1997).

2

The field-theoretical approach to GWs

2.1 Linearized gravity and classical field theory	53
2.2 Gravitons	66
2.3 Massive gravitons	81
2.4 Solved problems	95

In the previous chapter we investigated GWs using the geometric interpretation which is at the core of general relativity. This geometrical perspective emphasizes that $g_{\mu\nu} = \bar{g}_{\mu\nu} + h_{\mu\nu}$ is the metric of space-time, and therefore an incoming GW $h_{\mu\nu}$ induces perturbations in the space-time geometry. In this approach, the interaction of GWs with test masses is described by geometric tools such as the equation of the geodesic deviation, and the energy-momentum tensor of GWs is determined by examining how $h_{\mu\nu}$ contributes to the curvature of the background space-time.

General relativity can also be seen as a classical field theory, to which we can apply all standard field-theoretical methods. In this chapter we therefore go back to linearized gravity, writing $g_{\mu\nu} = \eta_{\mu\nu} + h_{\mu\nu}$, and we treat it as a classical field theory of the field $h_{\mu\nu}$ living in *flat* space-time with Minkowski metric $\eta_{\mu\nu}$. In this approach we are actually forgetting that $h_{\mu\nu}$ has an interpretation in terms of a space-time metric, and instead we treat it as any other field living in flat Minkowski space.

The fact that the beautiful geometric interpretation of $h_{\mu\nu}$ is hidden is compensated by the fact that we can put the conceptual issues discussed in Chapter 1 into the broader theoretical framework of classical field theory, and compare it to what happens in other field theories, such as classical electrodynamics. The geometric and the field-theoretical perspectives are indeed complementary; some aspects of GW physics can be better understood from the former perspective, some from the latter, and to study GWs from both vantage points results in a deeper overall understanding.

We will begin in Section 2.1.1 by recalling a basic tools of classical field theory, the Noether theorem, and we will see how we can reobtain the results of Chapter 1 using this standard field-theoretical tool. Besides providing a complementary understanding of various conceptual issues, the Noether theorem is also a very practical tool for explicit computations, and in particular we will see that it also provides the simplest way of deriving another important result, namely the general expression for the angular momentum carried by GWs.

In Section 2.2 we will pursue this field-theoretical approach further, discussing linearized gravity from the point of view of quantum field theory, and we will see how the notion of the graviton emerges. Actually, all astrophysical mechanisms of GW production, as well as the

interaction of GWs with a detector, are fully accounted for by *classical* general relativity. In actual calculations, the notion of the graviton will not surface until we examine some cosmological production mechanisms (in particular, mechanisms related to the amplification of vacuum fluctuations), in Vol. 2. Nevertheless, we will see that also at the quantum level, the field-theoretical approach is illuminating for many conceptual aspects.

We will conclude this chapter with a more advanced section, which investigates whether gravitons can have a small mass. This, from the field-theoretical point of view, seems to be one of the most natural generalizations of Einstein gravity. We will see however that a field theory describing massive gravitons can have problems of internal consistency which, to date, are not yet fully understood.

2.1 Linearized gravity as a classical field theory

2.1.1 Noether's theorem

We begin by recalling some basic facts of classical field theory and in particular Noether's theorem.¹ We consider a field theory living in flat space-time, with fields ϕ_i , labeled by an index i . The action S is the integral of the Lagrangian density \mathcal{L} ,

$$S = \int dt d^3x \mathcal{L}(\phi_i, \partial\phi_i). \quad (2.1)$$

In our case the fields ϕ_i will be the independent components of the metric $h_{\mu\nu}$, but it is useful to be more general, since we will also be interested in comparing with for instance classical electrodynamics, or any other classical field theory. We will denote collectively the fields ϕ_i simply by ϕ .

A transformation of the coordinates and of the fields is an operation that transforms the coordinates x^μ into new coordinates x'^μ , i.e. $x^\mu \rightarrow x'^\mu$, while at the same time the fields, denoted collectively by $\phi(x)$, are transformed into new functions of the new coordinates, $\phi(x) \rightarrow \phi'(x')$. To define the transformation means to state how x' is related to x and how $\phi'(x')$ is related to $\phi(x)$. For an infinitesimal transformation, we can write

$$x^\mu \rightarrow x'^\mu = x^\mu + \epsilon^a A_a^\mu(x), \quad (2.2)$$

$$\phi_i(x) \rightarrow \phi'_i(x') = \phi_i(x) + \epsilon^a F_{i,a}(\phi, \partial\phi), \quad (2.3)$$

and the transformation is specified assigning $A_a^\mu(x)$ and $F_{i,a}(\phi, \partial\phi)$. In general, the function $F_{i,a}$ depends on the collection of fields ϕ and on their derivatives, and will also mix different fields, so the transformation of a single field ϕ_i can depend also on all other fields ϕ_j with $j \neq i$. The above transformation is parametrized by a set of infinitesimal parameters ϵ^a , with $a = 1, \dots, N$.

¹We refer the reader to the textbook Maggiore (2005), Section 3.2, for further details and proofs. Note that in the present book, in order to follow the most common convention in general relativity, we are using the signature $\eta_{\mu\nu} = (-, +, +, +)$, while in Maggiore (2005) we use $\eta_{\mu\nu} = (+, -, -, -)$, which is the most common convention in quantum field theory. This is the origin of some sign differences between that textbook and the following equations.

Equations (2.2) and (2.3) define a symmetry transformation if they leave the action $S(\phi)$ invariant, for any ϕ . A symmetry transformation is called *global* if it leaves the action invariant when the parameters ϵ^a are constant, and *local* if it leaves invariant the action even when ϵ^a are allowed to be arbitrary functions of x .

Noether's theorem states that, for each generator of a global symmetry transformation, that is, for each of the parameters ϵ^a with $a = 1, \dots, N$, there is a current j_a^μ (which is a functional of the fields ϕ) which, when evaluated on a classical solution of the equations of motion ϕ^{cl} , is conserved, i.e. satisfies

$$(\partial_\mu j_a^\mu) |_{\phi=\phi^{\text{cl}}} = 0. \quad (2.4)$$

The corresponding charges Q_a are defined as the spatial integral of the $\mu = 0$ component of the currents

$$Q_a \equiv \int d^3x j_a^0(\mathbf{x}, t). \quad (2.5)$$

Current conservation (in the sense of eq. (2.4)) implies that Q_a is conserved (in the sense that it is time-independent). In fact

$$\begin{aligned} \partial_0 Q_a &= \int d^3x \partial_0 j_a^0(\mathbf{x}, t) \\ &= - \int d^3x \partial_i j_a^i(\mathbf{x}, t). \end{aligned} \quad (2.6)$$

This is the integral of a total divergence, and it vanishes if we assume a sufficiently fast decrease of the fields at infinity. More generally, in a finite volume the variation of the charge is given by a boundary term representing the incoming or outgoing flux.

The explicit form of the current can be written in full generality in terms of the Lagrangian density \mathcal{L} of the theory and of the functions $A_a^\mu(x)$ and $F_{i,a}(\phi, \partial\phi)$ that define the symmetry transformation (2.2), (2.3), and is given by

$$j_a^\mu = \frac{\partial \mathcal{L}}{\partial (\partial_\mu \phi_i)} [A_a^\nu(x) \partial_\nu \phi_i - F_{i,a}(\phi, \partial\phi)] - A_a^\mu(x) \mathcal{L}. \quad (2.7)$$

The simplest application of this very general machinery is to the symmetry under space-time translations, and leads us to energy-momentum tensor. Under space-time translations we have $x^\mu \rightarrow x'^\mu = x^\mu + \epsilon^\mu$, and by definition all fields transform as $\phi'_i(x') = \phi_i(x)$, independently of their properties under Lorentz transformations; that is, a point P has the coordinate x in a frame and the coordinate x' in the translated frame, but the functional form of the fields changes so that the numerical values of the fields at the point P is invariant. So we write the transformation as

$$\begin{aligned} x^\mu &\rightarrow x'^\mu = x^\mu + \epsilon^\mu \\ &= x^\mu + \epsilon^\nu \delta_\nu^\mu, \end{aligned} \quad (2.8)$$

$$\phi_i(x) \rightarrow \phi'_i(x') = \phi_i(x). \quad (2.9)$$

Observe that the index a appearing in ϵ^a in this case is a Lorentz index. Comparing with eqs. (2.2) and (2.3), we see that $A_\nu^\mu = \delta_\nu^\mu$ and $F_{i,a} = 0$.

The four conserved currents $\theta^{\mu}_{\nu} \equiv -j_{(\nu)}^{\mu}$ form a Lorentz tensor, known as the *energy-momentum* tensor. Using eq. (2.7) and raising the ν index, $\theta^{\mu\nu} = \eta^{\nu\rho}\theta^{\mu}_{\rho}$ we get²

$$\theta^{\mu\nu} = -\frac{\partial \mathcal{L}}{\partial(\partial_{\mu}\phi_i)}\partial^{\nu}\phi_i + \eta^{\mu\nu}\mathcal{L}. \quad (2.10)$$

Equation (2.4) becomes

$$\partial_{\mu}\theta^{\mu\nu} = 0, \quad (2.11)$$

on the solutions of the classical equations of motion. The conserved charge associated to space-time translations is, by definition, the four-momentum P^{ν} , and therefore³

$$cP^0 \equiv \int d^3x \theta^{00}, \quad (2.12)$$

$$cP^i \equiv \int d^3x \theta^{0i}. \quad (2.13)$$

This is the definition of four-momentum in classical field theory. A field configuration, solution of the equations of motion, carries an energy $E = cP^0$ and a spatial momentum P^i which can be calculated using eqs. (2.10), (2.12) and (2.13).

Observe that in general relativity the energy-momentum tensor of matter, defined by eq. (1.2), is automatically symmetric in the two indices μ, ν , since it is obtained by taking the functional derivative of the action with respect to the symmetric tensor $g_{\mu\nu}$. In contrast, the energy-momentum tensor defined from Noether's theorem, eq. (2.10), is not necessarily symmetric in the two indices μ, ν .

In fact, it is important to understand that the formal machinery of the Noether theorem, without some further physical input, is unable to uniquely fix the energy-momentum tensor, and more generally the Noether currents. For instance, consider what happens if we add a total four-divergence to the Lagrangian density,

$$\mathcal{L}' = \mathcal{L} + \partial_{\mu}K^{\mu}(\phi). \quad (2.14)$$

A total divergence, when integrated over d^4x , gives a boundary term. The equations of motion of the classical theory are obtained from a variation of the action, holding fixed the value of the fields on the boundaries. Therefore the equations of motion obtained from the variation of the action $S' = \int d^4x \mathcal{L}'$ are the same as those obtained from the variation of $S = \int d^4x \mathcal{L}$, so these two Lagrangians define the same classical field theory. However, the currents obtained from eq. (2.7) using \mathcal{L}' or using \mathcal{L} are in general different, and their difference is such that j^0 changes by a total spatial divergence, so that the charge in eq. (2.5) changes by a boundary term. Therefore the Noether *currents* are not uniquely defined; however, the Noether *charges*, computed integrating over a spatial volume V , are well defined if, and only if, the fields inside V go to zero sufficiently fast when we approach the boundaries of V , so that

²In order to minimize the number of factors of c in the equations, we have defined the flat-space Lagrangian density \mathcal{L} from

$$S = \int dt d^3x \mathcal{L},$$

rather than from $S = \int d^4x \mathcal{L}$, as done, instead, in Landau and Lifshitz, Vol. II (1979). Recalling that, dimensionally, an action is (energy) \times (time), in this way \mathcal{L} has the same dimensions as $\theta^{\mu\nu}$, i.e. energy/volume. With our notation, for instance, the Lagrangian density of the electromagnetic field is $(-1/4)F_{\mu\nu}F^{\mu\nu}$, rather than $(-1/4c)F_{\mu\nu}F^{\mu\nu}$.

³The factor c provides the correct dimensions, recalling that $P^0 = E/c$, see the Notation.

all boundary terms can be neglected, and the ambiguity in the currents becomes irrelevant.

To illustrate this point, before computing the energy–momentum tensor of GWs it is instructive to recall what happens in the more familiar case of classical electrodynamics. In this case the Lagrangian density is

$$\mathcal{L}_{\text{em}} = -\frac{1}{4}F_{\mu\nu}F^{\mu\nu}, \quad (2.15)$$

where $F_{\mu\nu} = \partial_\mu A_\nu - \partial_\nu A_\mu$. With our signature $\eta_{\mu\nu} = (-, +, +, +)$, the relation of $F_{\mu\nu}$ to the electric and magnetic fields is $F^{0i} = E^i$ and $F^{ij} = \epsilon^{ijk}B^k$. Equation (2.10) gives

$$\theta_{\text{em}}^{\mu\nu} = -\frac{\partial \mathcal{L}_{\text{em}}}{\partial(\partial_\mu A_\rho)}\partial^\nu A_\rho + \eta^{\mu\nu}\mathcal{L}_{\text{em}}. \quad (2.16)$$

The functional derivative is easily computed,

$$\begin{aligned} \frac{\partial}{\partial(\partial_\mu A_\rho)} \left(-\frac{1}{4}F_{\alpha\beta}F^{\alpha\beta} \right) &= -\frac{1}{2}F^{\alpha\beta}\frac{\partial F_{\alpha\beta}}{\partial(\partial_\mu A_\rho)} \\ &= -F^{\alpha\beta}\frac{\partial(\partial_\alpha A_\beta)}{\partial(\partial_\mu A_\rho)} \\ &= -F^{\mu\rho}. \end{aligned} \quad (2.17)$$

Therefore

$$\theta_{\text{em}}^{\mu\nu} = F^{\mu\rho}\partial^\nu A_\rho - \frac{1}{4}\eta^{\mu\nu}F^2. \quad (2.18)$$

At first sight, this result is surprising. Recall in fact that classical electrodynamics is invariant under gauge transformations,

$$A_\mu \rightarrow A_\mu - \partial_\mu\theta, \quad (2.19)$$

as we can see observing that under eq. (2.19) $F_{\mu\nu}$ is invariant, and therefore also the Lagrangian (2.15) is invariant. However, the energy–momentum tensor (2.18) depends on A_μ not only through the gauge-invariant combination $F_{\mu\nu}$, but also through the term $\partial^\nu A_\rho$, which is not invariant, and under gauge transformations $\theta_{\text{em}}^{\mu\nu}$ changes as

$$\theta_{\text{em}}^{\mu\nu} \rightarrow \theta_{\text{em}}^{\mu\nu} - F^{\mu\rho}\partial^\nu\partial_\rho\theta. \quad (2.20)$$

Apparently, we seem to be driven to the conclusion that the energy density θ^{00} of the electromagnetic field (as well as the momentum density θ^{0i}) is not gauge invariant. To deal with this problem, one first of all rewrites the energy–momentum tensor as follows,

$$\begin{aligned} \theta_{\text{em}}^{\mu\nu} &= F^{\mu\rho}(\partial^\nu A_\rho - \partial_\rho A^\nu + \partial_\rho A^\nu) - \frac{1}{4}\eta^{\mu\nu}F^2 \\ &= (F^{\mu\rho}F^\nu{}_\rho - \frac{1}{4}\eta^{\mu\nu}F^2) + F^{\mu\rho}\partial_\rho A^\nu \\ &= (F^{\mu\rho}F^\nu{}_\rho - \frac{1}{4}\eta^{\mu\nu}F^2) + \partial_\rho(F^{\mu\rho}A^\nu). \end{aligned} \quad (2.21)$$

(In the last line we used the equation of motion $\partial_\rho F^{\mu\rho} = 0$.) Therefore we have

$$\theta_{\text{em}}^{\mu\nu} = T_{\text{em}}^{\mu\nu} + \partial_\rho C^{\rho\mu\nu} \quad (2.22)$$

where

$$T_{\text{em}}^{\mu\nu} = F^{\mu\rho} F^\nu{}_\rho - \frac{1}{4} \eta^{\mu\nu} F^2, \quad (2.23)$$

while $C^{\rho\mu\nu} = F^{\mu\rho} A^\nu$ is a tensor antisymmetric in the indices (ρ, μ) . Now, $T_{\text{em}}^{\mu\nu}$ (which is sometimes called the “improved” energy-momentum tensor) is a gauge-invariant quantity, and its 00 component gives the usual form of the energy density,⁴

$$T_{\text{em}}^{00}(x) = \frac{1}{2} (\mathbf{E}^2 + \mathbf{B}^2)(x). \quad (2.24)$$

The term $\partial_\rho C^{\rho\mu\nu}$ instead is not gauge invariant, and we would like to get rid of it. The argument that is used to discard it is based on the following observations:

- If $\theta_{\text{em}}^{\mu\nu}$ is conserved, also $T_{\text{em}}^{\mu\nu}$ is conserved: in fact

$$\partial_\mu \partial_\rho C^{\rho\mu\nu} = 0 \quad (2.25)$$

automatically, whenever $C^{\rho\mu\nu}$ is antisymmetric under $\rho \leftrightarrow \mu$, as is our case.

- The difference between the charge cP^ν computed with $\theta_{\text{em}}^{\mu\nu}$ and that computed with $T_{\text{em}}^{\mu\nu}$ is given by

$$\int_V d^3x \partial_\rho C^{\rho 0\nu} = \int_V d^3x \partial_i C^{i0\nu}. \quad (2.26)$$

where we used the fact that $C^{00\nu} = 0$, which follows again from the antisymmetry of $C^{\rho\mu\nu}$ under $\rho \leftrightarrow \mu$. This is the integral of a divergence, and vanishes if the fields go to zero sufficiently fast at the boundaries of the volume V . Therefore the four-momentum P^ν computed with $\theta_{\text{em}}^{\mu\nu}$ is equal to that computed with $T_{\text{em}}^{\mu\nu}$, and is gauge invariant.

What we learn from this example is that the expression for the energy-momentum tensor derived from the Noether theorem, eq. (2.10), is not necessarily a physical observable (in the case of electromagnetism it is not even gauge-invariant!).⁵ Rather, it is just a mathematical expression that, when integrated over space, gives unambiguously the total energy and momentum of a classical field configuration, as long as this field configuration goes to zero sufficiently fast on the boundaries of the integration region.

Equivalently, instead of speaking of the total energy of a localized object, we can divide by the volume and say that the expression in eq. (2.10) is a quantity that can be used to compute the *average value* of the energy-momentum tensor over a region of space sufficiently large, so that all boundary terms vanish, and any ambiguity related to total divergences disappears. Then, for instance, from eq. (2.22) we have

$$\langle \theta_{\text{em}}^{00} \rangle = \langle T_{\text{em}}^{00} \rangle + \langle \partial_i C^{i00} \rangle, \quad (2.27)$$

⁴The use of the Lagrangian (2.15) implies that we are using Heaviside-Lorentz units (also called rationalized c.g.s. unit) for the electric charge; in unrationalized units the factor $(-1/4)$ in eq. (2.15) becomes $(-1/16\pi)$, and the factor $1/2$ in eq. (2.24) becomes $1/(8\pi)$.

⁵Another way of understanding the existence of such an ambiguity in a gauge theory is the fact that, in principle, one can allow that the gauge field, under space-time translations, does not go simply into itself, as in eq. (2.9), but into a configuration related by an arbitrary gauge transformation.

where the bracket represents the average. On a volume such that boundary terms give zero, we have $\langle \partial_i C^{i00} \rangle = 0$ and therefore the average is unambiguously defined,

$$\begin{aligned}\langle \theta_{\text{em}}^{00} \rangle &= \langle T_{\text{em}}^{00} \rangle \\ &= \frac{1}{2} \langle \mathbf{E}^2 + \mathbf{B}^2 \rangle.\end{aligned}\quad (2.28)$$

Whether one of the many equivalent integrands, in the expression for cP^0 , can be promoted to a physical observable, thereby providing a definition of a *local* energy density, is a physical question that cannot be answered using only the mathematics of the Noether theorem, without any additional physical input. We will discuss this issue at the end of the next section, and we will see that in fact the answer is in general different in electromagnetism and in general relativity.

2.1.2 The energy–momentum tensor of GWs

Now we can return to our original problem, which was the computation of the energy carried by GWs. We consider a wave-packet with reduced wavelengths centered around a value λ . In this case, according to the discussion above, the Noether theorem can give us an unambiguous answer for the energy density of the wave-packet, averaged over a box centered on the peak of the wave-packet, and with size $L \gg \lambda$. In this case the field is negligible on the boundaries and, using eq. (2.10),

$$t^{\mu\nu} = \left\langle -\frac{\partial \mathcal{L}}{\partial(\partial_\mu h_{\alpha\beta})} \partial^\nu h_{\alpha\beta} + \eta^{\mu\nu} \mathcal{L} \right\rangle,$$

(2.29)

where $\langle \dots \rangle$ is a spatial average over several reduced wavelength (which, for plane waves, is the same as a temporal average over several periods), and \mathcal{L} is the Lagrangian that governs the dynamics of $h_{\mu\nu}$.

As discussed in the previous subsection, the Noether theorem instead gives us an ambiguous answer if we ask what is the *local* energy and momentum density. Actually, we already saw in Section 1.4 that the final form of the energy–momentum tensor of GWs is indeed expressed as an average over several reduced wavelengths (or over several periods), and that this comes from a very fundamental reason, i.e. in order to discuss the back-reaction of GWs on the background, we need to perform a coarse-graining of the Einstein equations. Thus, we already know that it will not be possible to do better than this, and we cannot define a local expression for the energy and momentum density. Nevertheless, it is interesting to understand the reason also from a purely field-theoretical point of view; this will be discussed at the end of this section. First, we compute $t^{\mu\nu}$ from eq. (2.29), and we check that it agrees with the result that we derived in Section 1.4.

In order to use eq. (2.29) (and also to derive the angular momentum of GWs from Noether's theorem), we need the Lagrangian \mathcal{L} or, equivalently, the action governing the dynamics of the field $h_{\mu\nu}$. To reproduce

the Einstein equations to linear order in $h_{\mu\nu}$ we must expand the Einstein action to quadratic order in $h_{\mu\nu}$, while the linear term in the action vanishes, as always when we expand around a classical solution (in this case around the flat metric $\eta_{\mu\nu}$, since we consider Einstein equations in vacuum). We therefore start from the full Einstein action,

$$S_E = \frac{c^3}{16\pi G} \int d^4x \sqrt{-g} R, \quad (2.30)$$

and we expand $g_{\mu\nu} = \eta_{\mu\nu} + h_{\mu\nu}$. We observe that

$$R = g^{\mu\nu} R_{\mu\nu} = (\eta^{\mu\nu} - h^{\mu\nu} + O(h^2)) (R_{\mu\nu}^{(1)} + R_{\mu\nu}^{(2)} + O(h^3)), \quad (2.31)$$

where $R_{\mu\nu}^{(1)}$ is linear in h and $R_{\mu\nu}^{(2)}$ is quadratic in h . $R_{\mu\nu}^{(1)}$ and $R_{\mu\nu}^{(2)}$ can be obtained by specializing eqs. (1.113) and (1.114) to a flat background metric $\eta_{\mu\nu}$. The expansion of $\sqrt{-g}$ can be computed by writing $g_\nu^\mu = \delta_\nu^\mu + h_\nu^\mu \equiv (I + H)_\nu^\mu$, where I is the identity matrix and H a matrix whose elements are h_ν^μ . Since $g_{\mu\nu} = \eta_{\mu\rho} g_\nu^\rho$ and $\det \eta_{\mu\rho} = -1$, we have $-g = \det(I + H)$. Using the identity $\log(\det A) = \text{Tr}(\log A)$, valid for any non-degenerate matrix A , and expanding the logarithm,

$$\begin{aligned} \det(I + H) &= \exp\{\log \det(I + H)\} \\ &= \exp\{\text{Tr} \log(I + H)\} \\ &= \exp\{\text{Tr}[H + O(H^2)]\} \\ &= 1 + \text{Tr}H + O(H^2) \\ &= 1 + h + O(h_{\mu\nu}^2), \end{aligned} \quad (2.32)$$

where $h = h_\mu^\mu = \eta^{\mu\nu} h_{\mu\nu}$ is the trace of $h_{\mu\nu}$. Since we are expanding over flat space, the lowest non-zero term in R is already $O(h)$, see eq. (2.31), so the terms $O(h^2)$ in $\sqrt{-g}$ give a contribution to the action $O(h^3)$, and can be neglected. Performing straightforward algebra we then obtain, after some integration by parts,

$$S_E = -\frac{c^3}{64\pi G} \int d^4x \left[\partial_\mu h_{\alpha\beta} \partial^\mu h^{\alpha\beta} - \partial_\mu h \partial^\mu h \right. \\ \left. + 2\partial_\mu h^{\mu\nu} \partial_\nu h - 2\partial_\mu h^{\mu\nu} \partial_\rho h_\nu^\rho \right] \quad (2.33)$$

and the corresponding Lagrangian density is (see Note 2)

$$\mathcal{L} = -\frac{c^4}{64\pi G} \left[\partial_\mu h_{\alpha\beta} \partial^\mu h^{\alpha\beta} - \partial_\mu h \partial^\mu h + 2\partial_\mu h^{\mu\nu} \partial_\nu h - 2\partial_\mu h^{\mu\nu} \partial_\rho h_\nu^\rho \right]. \quad (2.34)$$

We can now compute $t^{\mu\nu}$, using eq. (2.29). We evaluate the result directly in the gauge

$$\partial^\mu h_{\mu\nu} = 0, \quad h = 0. \quad (2.35)$$

Therefore, *after* computing the derivative $\delta\mathcal{L}/(\partial_\mu h_{\alpha\beta})$ in eq. (2.29), we impose the gauge condition (2.35). We observe that the second, third

and fourth terms in brackets in eq. (2.33) are quadratic in quantities that will be set to zero by the gauge fixing and, after taking the functional derivative, they give contributions which are linear in h or in $\partial^\mu h_{\mu\nu}$, and therefore vanish when we impose eq. (2.35). So the only non-vanishing contribution comes from the term $\partial_\mu h_{\alpha\beta} \partial^\mu h^{\alpha\beta}$, and we get

$$\frac{\partial \mathcal{L}}{\partial(\partial_\mu h_{\alpha\beta})} \Big|_{\partial^\mu h_{\mu\nu}=h=0} = -\frac{c^4}{32\pi G} \partial^\mu h^{\alpha\beta}. \quad (2.36)$$

We next evaluate the term $\langle \mathcal{L} \rangle$ in eq. (2.29), in our gauge. We recall that inside the average we are free to perform integration by parts (compare with Note 23 on page 35). Then, since in our gauge $h_{\mu\nu}$ satisfies the equations of motion $\square h_{\mu\nu} = 0$, even the term $\partial_\mu h_{\alpha\beta} \partial^\mu h^{\alpha\beta}$ gives zero because, after an integration by parts, it becomes $-h_{\alpha\beta} \square h^{\alpha\beta}$ and vanishes upon use of the equations of motion, so $\langle \mathcal{L} \rangle = 0$.

In conclusion, we obtain

$$t^{\mu\nu} = \frac{c^4}{32\pi G} \langle \partial^\mu h^{\alpha\beta} \partial^\nu h_{\alpha\beta} \rangle. \quad (2.37)$$

As expected, the result agrees with eq. (1.133).

We can now come back to the problem of the localization of the energy of GWs. In the field-theoretical description, the issue is whether one of the many equivalent integrands, in the expression for P^0 , can be promoted to a physical observable, thereby providing a definition of a *local* energy density. In electromagnetism there is a very natural candidate, the tensor $T_{\text{em}}^{\mu\nu}$ of eq. (2.23), which is conserved and gauge invariant, so it can be sensible to identify $(1/2)(\mathbf{E}^2 + \mathbf{B}^2)$ with the *local* energy density of the electromagnetic field. No such answer is possible for the gravitational field. The quantity $\partial^\mu h^{\alpha\beta} \partial^\nu h_{\alpha\beta}$ which appears inside the average in eq. (2.37) is not gauge-invariant. It is futile to search for another local expression, whose integral gives the energy, but which is already gauge invariant before integration: the equivalence principle tells us that, at a given point, we can always find a locally inertial frame (see Section 1.3.2), such that at the point in question the gravitational field vanishes. Therefore any candidate expression for a local energy density can always be set to zero at a given point with a coordinate transformation, so it cannot be gauge invariant. This is an important difference between gravity and electromagnetism. In electromagnetism, at least if we consider a slowly varying electromagnetic field, it makes sense to assign to each point a local energy density $(1/2)(\mathbf{E}^2 + \mathbf{B}^2)$.

When we consider waves, however, concerning energy localization there is no real difference between gravity and electromagnetism. In both cases, all that can be really measured is the energy averaged over several wavelengths or periods. This can be understood even more easily at first by looking at the problem quantum-mechanically even if, as we will see below, the argument is really classical.

From the quantum point of view, a plane wave describes a collection of massless quanta (gravitons with helicity $h = \pm 2$ for gravitation, and

photons with helicity ± 1 in electrodynamics). Consider a collection of such free particles. To determine the energy of this system in a volume V we must know how many quanta of the field are within V at a given time, and the energy of each. If we take a volume with sides smaller than the reduced wavelength λ of a photon or of a graviton, in order to know whether a given photon (or graviton) is inside the box we must measure its position with an error $\Delta x < \lambda$ and then, by the uncertainty principle, we have $\Delta p > \hbar/\lambda$, which is larger than the momentum $p = \hbar/\lambda$ of a quantum with reduced wavelength λ . Thus, we have completely lost information about the momentum \mathbf{p} of the particle, and therefore (given that we are considering free particles described by simple plane waves), we lost information about its energy $E = c|\mathbf{p}|$, which means that we cannot localize the energy density better than to a few wavelengths. Alternatively, we can localize the energy in space if we delocalize it in time, according to $\Delta E \Delta t \gtrsim \hbar$. Clearly photons and gravitons do not show any difference in this respect.⁶ In fact, even if we phrased it in a quantum language, this argument is really classical, and follows from the fact that the position x of the peak of a classical wave-packet, and its typical wave-vector k satisfy $\Delta x \Delta k \geq 1$, and in this form is simply a property of the Fourier transform. In quantum theory, one identifies the momentum \mathbf{p} with $\hbar\mathbf{k}$, and $\Delta x \Delta k \geq 1$ becomes $\Delta x \Delta p \geq \hbar$.

In conclusion the field-theoretical approach, based on Noether's theorem, gives us an unambiguous recipe for computing a spatial (or a temporal) average of the energy-momentum tensor of GWs. The fact that, for GWs, we cannot do better than this, i.e. that the energy of GWs cannot be localized in space (or in time) with a precision better than a few wavelengths (or a few periods) can be understood as a consequence of the equivalence principle, but it is in fact also a general property of any wave governed by a massless wave equation, which at the quantum level translates into a limitation required by the uncertainty principle.

2.1.3 The angular momentum of GWs

We next compute the angular momentum carried by GWs. Angular momentum is the conserved charge associated to invariance under spatial rotations. A symmetric tensor $h_{\mu\nu}$, from the point of view of spatial rotations, decomposes into h_{00} and the spatial trace h_i^i , which are both scalars under rotation and therefore are spin-0 fields, h_{0i} which is a spatial vector and therefore has spin 1, and a traceless symmetric tensor h_{ij} , which is a spin-2 field and has five degrees of freedom. To describe the GW we go to the TT gauge, so we have $h_{0\mu} = 0$ and we are left only with the field h_{ij}^{TT} , which satisfies $(h^{TT})_i^i = 0$ and $\partial^i h_{ij}^{TT} = 0$, compare with eq. (1.31). Observe that h_{ij}^{TT} has only two degrees of freedom, corresponding to a massless particle with helicity ± 2 .⁷ As before, the last three terms in eq. (2.33) give a contribution to the Noether current that vanishes when, after taking the functional derivatives, we impose the gauge fixing condition. Then, for the purpose of computing the Noether current in this gauge, we can use as Lagrangian the first term

⁶The fact that, as a quantum field theory, general relativity is not renormalizable plays no role here. As long as we are at energies much smaller than the Planck mass, linearized theory can be promoted to a well defined effective quantum field theory, describing weakly interacting gravitons, as we discuss in more detail in Section 2.2.

⁷As we will recall in Section 2.2.2 and in Problem 2.1, the physical representation of the Poincaré group are of two types: massive representations, characterized by their spin j and having $2j+1$ states, and massless representations, which have a quantum number j but only two states, corresponding to helicities $h = \pm j$. We will use the name “spin- j field” to denote generically a field that can describe either a massive particle with spin j or a massless particle with helicities $h = \pm j$ (in which case, it will be subject to constraints that eliminate the extra states, see Section 2.2). The name “spin- j particle” will however be reserved to a massive particle with spin j and therefore $2j+1$ degrees of freedom. A massless particle with quantum number j will be referred to as “a massless particles with helicity $\pm j$ ”.

in eq. (2.33), and we can keep only the physical degrees of freedom h_{ij}^{TT} ,

$$\mathcal{L} = -\frac{c^4}{64\pi G} \partial_\mu h_{ij}^{\text{TT}} \partial^\mu h_{ij}^{\text{TT}}. \quad (2.38)$$

A rotation of three-dimensional space is described by a 3×3 orthogonal matrix \mathcal{R} , which transforms the coordinates according to $x^i \rightarrow \mathcal{R}^{ij}x^j$ (observe that, since our signature is $(-, +, +, +)$, we do not need to be careful about raising or lowering spatial indices). An infinitesimal rotation can be written as

$$\mathcal{R}^{ij} = \delta^{ij} + \omega^{ij}, \quad (2.39)$$

and the condition that \mathcal{R} is an orthogonal matrix gives $\omega^{ij} = -\omega^{ji}$. Therefore rotations can be parametrized by the three independent quantities ω^{12}, ω^{13} and ω^{23} , which play the role of the parameters ϵ^a in eqs. (2.2) and (2.3). So, for rotations eqs. (2.2) and (2.3) become

$$x^i \rightarrow x^i + \sum_{k < l} \omega^{kl} A_{kl}^i, \quad (2.40)$$

$$h_{ij}^{\text{TT}} \rightarrow h_{ij}^{\text{TT}} + \sum_{k < l} \omega^{kl} F_{ij,kl}, \quad (2.41)$$

and the sum goes over the independent parameters ω^{kl} with $k < l$. Observe that, in $F_{ij,kl}$, the first pair of indices, (i, j) , is the label that identifies the field h_{ij}^{TT} , and therefore plays the role that the index i had in eq. (2.3), while the second pair (k, l) plays the role of the index a in eq. (2.3). In particular, $F_{ij,kl}$ is symmetric with respect to the pair (i, j) and can be taken to be antisymmetric with respect to the pair (k, l) .

The total angular momentum carried by the GWs is then given by

$$J^i = \frac{1}{2} \epsilon^{ijk} J_{kl}. \quad (2.42)$$

where J_{kl} is the conserved charge associated to rotations in the (k, l) plane,

$$J_{kl} = \frac{1}{c} \int d^3x j_{kl}^0, \quad (2.43)$$

(the factor $1/c$ provides the correct dimensions) and Noether's theorem gives

$$j_{kl}^0 = \frac{\partial \mathcal{L}}{\partial (\partial_0 h_{ij}^{\text{TT}})} [A_{kl}^\nu \partial_\nu h_{ij}^{\text{TT}} - F_{ij,kl}] - A_{kl}^0 \mathcal{L}. \quad (2.44)$$

To find the explicit form of A_{kl}^ν and $F_{ij,kl}$ we compare the generic formulas (2.40) and (2.41) with the actual transformation properties of x^i and h_{ij}^{TT} under infinitesimal rotations; A_{kl}^i is easily computed observing that

$$\begin{aligned} x^i &\rightarrow \mathcal{R}^{ij}x^j = x^i + \omega^{ij}x^j \\ &= x^i + \sum_{k < l} \omega^{kl}(\delta^{ik}x^l - \delta^{il}x^k), \end{aligned} \quad (2.45)$$

so, comparing with eq. (2.40),

$$A_{kl}^i = \delta^{ik}x^l - \delta^{il}x^k. \quad (2.46)$$

As for A_{kl}^0 , since time is unchanged under spatial rotations, we have $A_{kl}^0 = 0$.

The quantity $F_{ij,kl}$ is determined by the properties of h_{ij}^{TT} under rotations. Since h_{ij}^{TT} is a spatial tensor, it transforms as

$$\begin{aligned} h_{ij}^{\text{TT}} &\rightarrow R_i^k R_j^l h_{kl}^{\text{TT}} \\ &= h_{ij}^{\text{TT}} + \omega_j^l h_{il}^{\text{TT}} + \omega_i^k h_{kj}^{\text{TT}} \\ &= h_{ij}^{\text{TT}} + \sum_{k < l} \omega^{kl} (\delta_{ik} h_{jl}^{\text{TT}} - \delta_{il} h_{jk}^{\text{TT}} + \delta_{jk} h_{il}^{\text{TT}} - \delta_{jl} h_{ik}^{\text{TT}}). \end{aligned} \quad (2.47)$$

Comparing eqs. (2.41) and (2.47), we see that

$$F_{ij,kl} = \delta_{ik} h_{jl}^{\text{TT}} - \delta_{il} h_{jk}^{\text{TT}} + \delta_{jk} h_{il}^{\text{TT}} - \delta_{jl} h_{ik}^{\text{TT}}. \quad (2.48)$$

We can now plug these results into eq. (2.44). We also observe that

$$\begin{aligned} \frac{\partial \mathcal{L}}{\partial(\partial_0 h_{ij}^{\text{TT}})} &= -\frac{c^4}{32\pi G} \partial^0 h_{ij}^{\text{TT}} \\ &= +\frac{c^3}{32\pi G} \dot{h}_{ij}^{\text{TT}}, \end{aligned} \quad (2.49)$$

and (renaming the indices $(i,j) \rightarrow (a,b)$) we get

$$j_{kl}^0 = \frac{c^3}{32\pi G} \left[-\dot{h}_{ab}^{\text{TT}} (x^k \partial^l - x^l \partial^k) h_{ab}^{\text{TT}} + 2\dot{h}_{ab}^{\text{TT}} (\delta_{bl} h_{ak}^{\text{TT}} + \delta_{al} h_{bk}^{\text{TT}}) \right]. \quad (2.50)$$

From eqs. (2.43), (2.44) and (2.42), the total angular momentum of the GW is therefore

$$J^i = \frac{c^2}{32\pi G} \int d^3x \left[-\epsilon^{ikl} \dot{h}_{ab}^{\text{TT}} x^k \partial^l h_{ab}^{\text{TT}} + 2\epsilon^{ikl} h_{ak}^{\text{TT}} \dot{h}_{al}^{\text{TT}} \right]. \quad (2.51)$$

To understand the physical meaning of the two terms in bracket, it is useful to recall the analogous results for spin-0 and spin-1 fields.⁸ For a real scalar field, applying Noether's theorem, one finds that the angular momentum carried by a field configuration ϕ is

$$J^i = -\epsilon^{ikl} \int d^3x (\partial_0 \phi) x^k \partial^l \phi. \quad (2.52)$$

We see that this has the same structure as the first term in eq. (2.51) (after rescaling h_{ab}^{TT} by a factor $(32\pi G/c^3)^{1/2}$; as we will see in Section 2.2, this rescaling gives to h_{ab}^{TT} the standard field-theoretical normalization). The physical meaning of this term can be understood observing that, for a real field ϕ satisfying the massless Klein–Gordon equation $\square \phi = 0$,

⁸For explicit proofs, see Maggiore (2005), Section 3.3.1 for spin-0 fields, and Section 4.3.1 for the electromagnetic field. Pay attention to the fact that this reference uses the opposite metric signature (following the most common convention used in field theory, while here we are following the most common convention used in general relativity), and units $\hbar = c = 1$.

one can define the scalar product between two field configurations ϕ and ϕ' ,

$$\langle \phi | \phi' \rangle = \frac{i}{2} \int d^3x \phi \overset{\leftrightarrow}{\partial}_0 \phi', \quad (2.53)$$

where, on any two functions f and g , we define $\overset{\leftrightarrow}{\partial}_\mu$ by $f \overset{\leftrightarrow}{\partial}_\mu g \equiv f \partial_\mu g - (\partial_\mu f)g$. Since ϕ and ϕ' are functions of t and \mathbf{x} , and in eq. (2.53) we integrate over d^3x , the result is a priori still a function of time. However, this scalar product is actually time-independent, if ϕ_1, ϕ_2 are solutions of the Klein–Gordon equation. It is then not so surprising that the conserved charges of the scalar field theory can be expressed as expectation values of suitable operators, with respect to this scalar product.

Consider in particular $\hat{L}^i = -ie^{ikl}x^k\partial^l$, which is the orbital angular momentum operator (in units of \hbar). The expectation value of this operator, with respect to the scalar product (2.53), is

$$\begin{aligned} \langle \phi | \hat{L}^i | \phi \rangle &= \frac{i}{2} \int d^3x [\phi \hat{L}^i \partial_0 \phi - (\partial_0 \phi) \hat{L}^i \phi] \\ &= \frac{1}{2} \epsilon^{ikl} \int d^3x [\phi x^k \partial^l \partial_0 \phi - (\partial_0 \phi) x^k \partial^l \phi] \\ &= -\epsilon^{ikl} \int d^3x (\partial_0 \phi) x^k \partial^l \phi, \end{aligned} \quad (2.54)$$

where, going from the second to the third line, we integrated by parts ∂^l in the first term. Comparing with eq. (2.52) we see that the total angular momentum carried by a scalar field configuration ϕ is equal to the expectation value of the orbital angular momentum operator \hat{L}^i , with respect to this scalar product,

$$J^i = \langle \phi | \hat{L}^i | \phi \rangle. \quad (2.55)$$

Observe also that, for a scalar field, there is no additional contribution, and the total angular momentum is given by the expectation value of the *orbital* angular momentum operator.

Consider now the spin-1 case. If one computes, using Noether's theorem, the angular momentum carried by the electromagnetic field in the radiation gauge, where the electromagnetic field is transverse, $\partial_i A^i = 0$, and satisfies $\square A^i = 0$, one finds

$$J^i = \int d^3x [-\epsilon^{ikl}(\partial_0 A_j) x^k \partial^l A_j + \epsilon^{ikl} A_k \partial_0 A_l]. \quad (2.56)$$

Again, since the equation of motion is $\square A_i = 0$, we can define a scalar product

$$\langle A | A' \rangle = \frac{i}{2} \int d^3x A_i \overset{\leftrightarrow}{\partial}_0 A'_i, \quad (2.57)$$

which is conserved on the solutions of the equation of motion. Then, we see that the first term in eq. (2.56) is again the expectation value of $\hat{L}^i = -ie^{ikl}x^k\partial^l$ with respect to this scalar product, so it is the contribution from the orbital angular momentum. In the derivation based on

the Noether theorem, this term is determined by the transformation of the coordinates x^i under spatial rotations, (i.e. it comes from the term proportional to A_a^ν in eq. (2.7)), so it is clear that it has the same structure for all fields, independently of their spin. The second term instead depends on the specific properties of the field under spatial rotations (i.e. it comes from the term proportional to $F_{i,a}$ in eq. (2.7)) and therefore it is the spin part. Defining

$$S^i = \epsilon^{ikl} \int d^3x A_k \partial_0 A_l, \quad (2.58)$$

the explicit computation⁹ shows that, in second quantization, the circular polarizations states of the photons are eigenvectors of the helicity operator $\mathbf{S} \cdot \hat{\mathbf{p}}$ (where $\hat{\mathbf{p}}$ is the unit vector in the direction of propagation), with eigenvalues ± 1 , as required for a massless particle described by a vector field.

We can now understand the meaning of the two terms in eq. (2.51). Since h_{ab}^{TT} satisfies $\square h_{ab}^{\text{TT}} = 0$, the conserved scalar product is defined as in the Klein–Gordon or in the electromagnetic case,

$$\langle h|h' \rangle = \frac{i}{2} \int d^3x h_{ab}^{\text{TT}} \overset{\leftrightarrow}{\partial}_0 h'_{ab}^{\text{TT}}. \quad (2.59)$$

After rescaling $h_{ab}^{\text{TT}} \rightarrow (32\pi G/c^3)^{1/2} h_{ab}^{\text{TT}}$ (which, as we will see in Section 2.2.2, is the rescaling needed to give to $h_{\mu\nu}$ the canonical normalization to the kinetic term in the action) the first term in eq. (2.51) is the expectation value of the orbital angular momentum operator with respect to this scalar product, while the term $2\epsilon^{ikl} h_{ak}^{\text{TT}} \dot{h}_{al}^{\text{TT}}$ is the spin contribution. The factor of 2 in this term correctly reproduces the fact that the gravitational field has spin two, and therefore gravitons are eigenvectors of the helicity with eigenvalues ± 2 .

In the previous section we learned that the Noether currents cannot be localized better than a few wavelengths, so the physical density of angular momentum, j^i/c , is the integrand of eq. (2.51), averaged over a few wavelengths,

$$\frac{1}{c} j^i = \frac{c^2}{32\pi G} \langle -\epsilon^{ikl} \dot{h}_{ab}^{\text{TT}} x^k \partial^l h_{ab}^{\text{TT}} + 2\epsilon^{ikl} \dot{h}_{al}^{\text{TT}} h_{ak}^{\text{TT}} \rangle. \quad (2.60)$$

Consider now a GW propagating outward from a source. At time t we consider a portion of the wave front, at radial distance r from the source, and covering a solid angle $d\Omega$. At time $t+dt$ this portion of the wave front has swept the volume $d^3x = r^2 dr d\Omega = r^2(c dt) d\Omega$. Since the angular momentum per unit volume is (j^i/c) , the angular momentum carried away by the GW is $dJ^i = r^2(c dt) d\Omega (j^i/c)$. Therefore the rate of angular momentum emission due to GWs is

$$\frac{dJ^i}{dt} = \frac{c^3}{32\pi G} \int r^2 d\Omega \langle -\epsilon^{ikl} \dot{h}_{ab}^{\text{TT}} x^k \partial^l h_{ab}^{\text{TT}} + 2\epsilon^{ikl} \dot{h}_{al}^{\text{TT}} h_{ak}^{\text{TT}} \rangle. \quad (2.61)$$

⁹See Maggiore (2005), pages 98–99.

2.2 Gravitons

This section is intended for readers with some knowledge of quantum field theory. In this section and in the next we use units

$$\hbar = c = 1.$$

It can be useful to recall how dimensional analysis works in these units. Since $c = 1$, velocities are pure numbers while, dimensionally,

$$\text{energy} = \text{momentum} = \text{mass}.$$

Recalling, from the uncertainty principle, that a length times a momentum has dimensions of \hbar , in units $\hbar = c = 1$ we also have

$$\text{length} = (\text{momentum})^{-1} = (\text{mass})^{-1}.$$

Then the dimensions of any quantity can be expressed as positive or negative powers of mass. For example, and energy density is energy/volume = $(\text{mass})^4$.

All astrophysical processes which generate GWs, as well as the interaction of GWs with detectors, are adequately described in the framework of a classical field theory of gravitation. Nevertheless, it can be instructive to discuss some conceptual issues using the vantage point provided by modern quantum field theory.

In this section we will see that, at the quantum level, gravity must be mediated by a massless particle with helicity ± 2 , the graviton. Its free action, in flat space-time, is fixed by field-theoretical considerations, and reproduces the linearization of the Einstein action. Consistency with gauge-invariance then requires the introduction of non-linear couplings between the graviton, with three-graviton vertices, four-graviton vertices, etc., and a full non-linear structure emerges. Finally, we will briefly mention some of the issues involved in the quantization of gravity and we will discuss why, even in the absence of a full quantum theory of gravitation, general relativity makes sense as an effective field theory below the Planck scale, and the notion of graviton is well defined.

2.2.1 Why a spin-2 field?

In quantum field theory all interactions are mediated by the exchange of bosons, i.e. particles with integer spin. Since a flat space-time background is an excellent approximation in many situations, it make sense to look for a relativistic quantum field theory living in flat space-time, that in the non-relativistic limit reduces to Newtonian gravity. Such a theory should be mediated by a boson which propagates in this flat space-time.

Gravity is the interaction that in the non-relativistic limit couples to the mass. To obtain such a coupling from a *local* quantum field theory, we need to couple the field that mediates gravity to a local quantity (i.e. a quantity which is function of the space-time point x) whose spatial integral, in the non-relativistic limit, becomes the mass.

Mathematics alone is not sufficient to obtain uniquely a consistent theory that gives back Newton's law. We will also use as guiding principle the deep insight of Einstein that in the full theory of gravitation not only the mass is a source for gravitation but, more generally, all forms of energy. In a local field theory, we therefore look for a coupling between the field that mediates gravity and the energy density.

Since, from the point of view of Lorentz transformations, energy density is the (00) component of the energy-momentum tensor, consistency with special relativity requires that we couple our gravitational field to the energy-momentum tensor $T_{\mu\nu}(x)$. As long as we work at linearized level, we can neglect the contribution of the gravitational field itself to $T^{\mu\nu}$, so we can take as $T^{\mu\nu}$ the energy-momentum tensor of the matter fields only. Since we are assuming a flat background, at linearized level $T^{\mu\nu}$ obeys the flat-space conservation law

$$\partial_\mu T^{\mu\nu} = 0. \tag{2.62}$$

We will come back later to the inclusion of the non-linear terms.

The simplest possibility that one can examine is that gravity is mediated by a spin-0 boson, described by a scalar field ϕ . A scalar field ϕ carries no Lorentz index, so the only possibility is that it couples to the trace of the energy-momentum tensor, $T = T_\mu^\mu$. Therefore the Lagrangian density which describes the dynamics of this hypothetical scalar gravitational field and its coupling to matter, in linearized theory, must be of the form

$$\mathcal{L} = -\frac{1}{2}(\partial_\mu \phi \partial^\mu \phi + \mu^2 \phi^2) + g\phi T, \quad (2.63)$$

where g is a coupling constant, and μ is the mass of the scalar field (more generally, we could also add a potential $V(\phi)$, that however does not influence the following discussion). In order to see if this theory reduces correctly to Newtonian gravity in the non-relativistic limit, we can compute the potential induced by the exchange of a ϕ boson between two static particles of masses m_1 and m_2 . Let us recall that in quantum field theory the static interaction potential $V(\mathbf{x})$ is a derived concept, which makes sense only in the non-relativistic limit. To obtain it, one must compute the $2 \rightarrow 2$ scattering amplitude M_{fi} at tree level, taking the initial state equal to the final state, and then the potential is given by¹⁰

$$V(\mathbf{x}) = - \int \frac{d^3 q}{(2\pi)^3} M_{fi}(\mathbf{q}) e^{i\mathbf{q}\cdot\mathbf{x}}. \quad (2.64)$$

The energy-momentum tensor $T^{\mu\nu}$ is quadratic in the matter fields, so the vertex $g\phi T$ involves two matter-field lines and one ϕ boson, and to compute M_{fi} we must evaluate a Feynman diagram of the type given in Fig. 2.1 (plus a possible exchange graph for identical particles), with $q = (q^0, \mathbf{q})$, setting $q^0 = 0$ because the potential is obtained in the static limit. In general, the details of the computation depend on the form of $T(x)$, i.e. on the specific type of matter field considered. However, if the matter field is massive, we can take the non-relativistic limit, and in this limit we can treat $T(x)$ as an external classical field. In this case, the interaction vertex of this theory becomes as shown in Fig. 2.2, where the cross denotes the insertion of $\tilde{T}(\mathbf{q})$. Then the diagram of Fig. 2.1 reduces to that shown in Fig. 2.3, and the amplitude M_{fi} is given simply by

$$iM_{fi}(\mathbf{q}) = (-ig)^2 \tilde{T}_1(\mathbf{q}) \tilde{D}(\mathbf{q}) \tilde{T}_2(-\mathbf{q}), \quad (2.65)$$

where

$$D(q) = \frac{-i}{q^2 + \mu^2}, \quad (2.66)$$

is the propagator of the scalar field ϕ (recall that we are using the signature $\eta_{\mu\nu} = (-, +, +, +)$), and T_1, T_2 are the traces of the energy-momentum tensor for particles of masses m_1 and m_2 , respectively. In the static limit, $q^2 = -(q^0)^2 + \mathbf{q}^2 \rightarrow \mathbf{0}^2$, and the propagator becomes

$$D(\mathbf{q}) = \frac{-i}{\mathbf{q}^2 + \mu^2}. \quad (2.67)$$

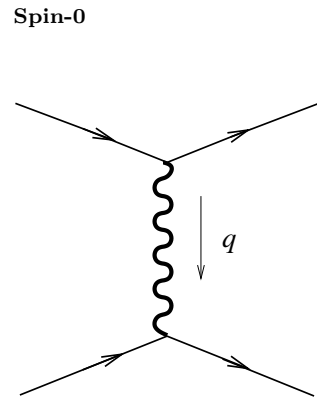


Fig. 2.1 The Feynman diagram that gives the scattering amplitude at tree level.

¹⁰See e.g. Maggiore (2005) (Section 6.6 and eqs. (7.56)–(7.59)), for the derivation of this result and for explicit computations of the potential induced by the exchange of scalar or vector particles.



Fig. 2.2 The Feynman diagram that gives the vertex, when $T(x)$ is treated as an external field.

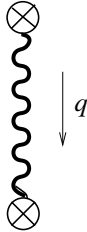


Fig. 2.3 The Feynman diagram that gives the scattering amplitude, when $T(x)$ is treated as an external field.

¹¹More precisely, for a particle in \mathbf{x}_1 , $T(\mathbf{x}) = -m \delta^{(3)}(\mathbf{x} - \mathbf{x}_1)$, so $\tilde{T}(\mathbf{q}) = -m \exp\{-i\mathbf{q} \cdot \mathbf{x}_1\}$. In the field theoretical language, the factors $\exp\{-i\mathbf{q} \cdot \mathbf{x}_1\}$ from $\tilde{T}_1(\mathbf{q})$ and $\exp\{+i\mathbf{q} \cdot \mathbf{x}_2\}$ from $\tilde{T}_2(-\mathbf{q})$ comes from the wavefunctions of the external legs, and in eq. (2.68) they have already been taken into account by the term $\exp\{i\mathbf{q} \cdot (\mathbf{x}_2 - \mathbf{x}_1)\}$, where $\mathbf{x}_2 - \mathbf{x}_1 \equiv \mathbf{x}$.

Equation (2.64) then gives

$$V(\mathbf{x}) = -ig^2 \int \frac{d^3 q}{(2\pi)^3} \tilde{T}_1(\mathbf{q}) \tilde{D}(\mathbf{q}) \tilde{T}_2(-\mathbf{q}) e^{i\mathbf{q} \cdot \mathbf{x}}. \quad (2.68)$$

For a relativistic classical particle moving on the trajectory $\mathbf{x}_0(t)$, the energy-momentum tensor is given by (see, e.g. Landau and Lifshitz, Vol. II 1979)

$$T^{\mu\nu}(\mathbf{x}, t) = \frac{p^\mu p^\nu}{p^0} \delta^{(3)}(\mathbf{x} - \mathbf{x}_0(t)), \quad (2.69)$$

where p^μ is the four-momentum. Using $p^\mu p_\mu = -m^2$ and, for a particle at rest, $p^0 = m$, the trace of the energy-momentum tensor of a heavy source becomes $T(\mathbf{x}) = -m \delta^{(3)}(\mathbf{x})$, which in turn gives $\tilde{T}(\mathbf{q}) = -m$.¹¹ Therefore

$$V(\mathbf{x}) = -ig^2 m_1 m_2 D(\mathbf{x}). \quad (2.70)$$

If the mass μ vanishes,

$$\begin{aligned} D(\mathbf{x}) &= \int \frac{d^3 q}{(2\pi)^3} \frac{-i}{\mathbf{q}^2} e^{i\mathbf{q} \cdot \mathbf{x}} \\ &= \frac{-i}{4\pi r}, \end{aligned} \quad (2.71)$$

where $r = |\mathbf{x}|$, and therefore we get the correct Newtonian potential

$$V(r) = -\frac{Gm_1 m_2}{r}, \quad (2.72)$$

once we make the identification $g^2/(4\pi) = G$. If instead the mass μ is non-vanishing, we get a Yukawa potential

$$V(\mathbf{x}) = -\frac{Gm_1 m_2}{r} e^{-\mu r}. \quad (2.73)$$

This result shows that, as far as the non-relativistic Newtonian limit is concerned, a spin-0 massless scalar field is a viable possibility.

However, a spin-0 field fails when we come to the new predictions of this theory of gravitation in the relativistic regime. In particular, we see from eq. (2.23) that the energy-momentum tensor of the electromagnetic field is traceless,

$$T_{\text{em}} = F^{\mu\rho} F_{\mu\rho} - \frac{1}{4} \delta_\mu^\mu F^2 = 0. \quad (2.74)$$

Therefore, in this theory, photons do not couple to gravity. Experimentally, the gravitational bending of light rays from massive objects is very well established (it was in fact the first experimental confirmation of general relativity and nowadays, in the form of gravitational lensing, it is a beautiful routine tool in astrophysics). Therefore a spin-0 theory of gravitation is ruled out.¹²

The next possibility is a spin-1 field, just like in electrodynamics. In order to get a long-range potential, we need again a massless field,

but a massless vector field A_μ can be coupled consistently only if we respect gauge invariance. In electrodynamics this can be obtained with a coupling $A_\mu j^\mu$, imposing that j^μ is a conserved current. In fact, under a gauge transformation, $A_\mu \rightarrow A_\mu - \partial_\mu \theta$ and, after an integration by parts, the term $-(\partial_\mu \theta)j^\mu \rightarrow \theta \partial_\mu j^\mu = 0$, so the action is invariant.

Therefore, a coupling between such a vector field A_μ and the energy-momentum tensor of the form $A_\mu A_\nu T^{\mu\nu}$ is immediately ruled out, because it is not gauge invariant (and furthermore, the simultaneous exchange of two gauge bosons gives a potential $1/r^3$ rather than $1/r$.) A derivative coupling $(\partial_\mu A_\nu)T^{\mu\nu}$ is also not viable, since after integration by parts it gives zero, because of energy-momentum conservation.

If we limit ourselves to the level of first quantization, we could write down a coupling of a vector field to a point-like particles in the form

$$\int d^4x A_\mu(x) m \frac{dx_0^\mu}{d\tau} \delta^{(3)}(\mathbf{x} - \mathbf{x}_0(t)), \quad (2.75)$$

where $x_0^\mu(\tau)$ is the particle world-line. However, in quantum field theory the four-vector $j^\mu(x)$ that, in the limit of point-like particle, reduces to $m(dx_0^\mu/d\tau)\delta^{(3)}(\mathbf{x} - \mathbf{x}_0(t))$, is a $U(1)$ current. Then $Q \equiv \int d^3x j^0$ is equal to the mass m times (number of particles *minus* number of antiparticles), so it is not positive definite, and $\int d^3x j^0$ cannot be interpreted as the mass (unless we assign a negative gravitational mass to antiparticles). Furthermore, even if we ignore this problem and interpret j^0 has a mass density, still this attempt to construct a spin-1 theory of gravity fails because, as we know from classical electromagnetism, the interaction mediated by the photon between two particles of the same charge is repulsive. Technically, this comes out because the term $\tilde{T}_1(\mathbf{q})\tilde{D}(\mathbf{q})\tilde{T}_2(-\mathbf{q})$ in eq. (2.68) is now replaced by

$$\tilde{j}^\mu(\mathbf{q})\tilde{D}_{\mu\nu}(\mathbf{q})\tilde{j}^\nu(-\mathbf{q}), \quad (2.76)$$

where $\tilde{D}_{\mu\nu}(q)$ is the propagator of the massless vector field A_μ . In momentum space,

$$\tilde{D}_{\mu\nu}(q) = \frac{-i}{q^2} \eta_{\mu\nu}. \quad (2.77)$$

In the static limit $q^2 = -(q^0)^2 + \mathbf{q}^2 \rightarrow \mathbf{q}^2$, and the propagator becomes

$$\tilde{D}_{\mu\nu}(\mathbf{q}) = \frac{-i}{\mathbf{q}^2} \eta_{\mu\nu}. \quad (2.78)$$

Because of the factor $\eta_{\mu\nu}$, the propagator of the spatial components A_i is equal to that of a scalar field, but the propagator of A_0 has the opposite sign. In the non-relativistic limit $j^\mu \rightarrow (j^0, 0)$. Then in eq. (2.76) only the component D_{00} contributes, so we get the opposite sign compared to the scalar case, i.e. a repulsive potential between positive masses. In conclusion, also spin-1 is ruled out.

Values of the spin $j \geq 3$ are also ruled out: the need for a long-range force requires again a massless field, which can be coupled consistently

Spin $j \geq 3$

only to a conserved tensor. Except possibly for total derivative terms, there is no conserved tensor with three or more indices, so massless particles with $j \geq 3$ cannot produce long-range forces, neither gravitational nor of any other type.

The only possibility which is left is $j = 2$, and we examine it in the next section.

2.2.2 The Pauli–Fierz action

The considerations of the previous section lead us to study the action for a spin-2 massless field. To identify the field that describes a massless particle with helicity ± 2 , let us first recall some elementary facts about the representations of the Lorentz and Poincaré groups, and their decomposition under representations of the rotation group.

Massless particles in field theory

The irreducible tensor representations of the Lorentz group are given by tensors that, with respect to any pair of indices, are either symmetric and traceless, or antisymmetric. An irreducible representation of the Lorentz group provides of course also a representation of the rotation subgroup $SO(3)$. However, a representation that is irreducible with respect to the full Lorentz group, will be reducible if we limit ourselves to the rotation subgroup (except for the trivial case of the scalar representation), so it decomposes into the direct sum of irreducible representations of the rotation group. For instance a four-vector A_μ is an irreducible representation of the Lorentz group, but from the point of view of rotations it decomposes into a scalar A_0 and a vector \mathbf{A} , or

$$A_\mu \in \mathbf{0} \oplus \mathbf{1}, \quad (2.79)$$

where we denote by \oplus the direct sum of representations, and by \mathbf{s} the representation of the rotation group corresponding to spin s (so $\mathbf{0}$ is the scalar and $\mathbf{1}$ is the vector representation). The representation \mathbf{s} has dimension $2s + 1$, so in particular the scalar is one-dimensional and the vector is a three-dimensional representation. When we consider tensors with two indices, an antisymmetric tensor $A^{\mu\nu}$ decomposes as

$$A_{\mu\nu} \in \mathbf{1} \oplus \mathbf{1}, \quad (2.80)$$

while a traceless symmetric tensor $S^{\mu\nu}$ decomposes as

$$S_{\mu\nu} \in \mathbf{0} \oplus \mathbf{1} \oplus \mathbf{2}. \quad (2.81)$$

Therefore, the simplest tensor that contains a spin-2 is the traceless symmetric tensor, and a spin-2 can be described using $S_{\mu\nu}$ and imposing conditions that eliminate the extra degrees of freedom. Equation (2.81) states that the nine independent components of a traceless symmetric tensor with two indices decompose into a scalar, the three components of a spin-1, and the five ($2s + 1$ with $s = 2$) components of a spin-2.

A further complication arises if we want to describe a *massless* particle. As we recall in more detail in Problem 2.1, particles are representations of the Poincaré group, and the physically interesting representations of the Poincaré group are of two type. (1) Massive representations, with $-P_\mu P^\mu = m^2 > 0$, labeled by the mass m and by the spin j , which takes integer and half-integer values, $j = 0, 1/2, 1, \dots$. The dimension of these representations is $2j + 1$. (2) Massless representations, $P_\mu P^\mu = 0$, which are two-dimensional (actually, one-dimensional, but become two-dimensional if we also require that they are representations of parity) and are characterized by two helicity states $h = \pm j$.

In particular, a massive spin-1 particle has three degrees of freedom, and a massive spin-2 particle has five degrees of freedom. In contrast, a massless particle with $j = 1$ and a massless particle with $j = 2$ both have only two degrees of freedom, the former with helicities $h = \pm 1$, and the latter with $h = \pm 2$. This means that, in the case of a massless spin-1 field, a four-vector field A_μ contains two redundant degrees of freedom, while for a massless spin-2 field the nine components of $S^{\mu\nu}$ contain seven redundant degrees of freedom. The way to eliminate these spurious degrees of freedom is to introduce a gauge-invariance. For electromagnetism, one imposes that the theory is invariant under

$$A_\mu \rightarrow A_\mu - \partial_\mu \theta. \quad (2.82)$$

It is a standard textbook exercise to show that we can choose $\theta(x)$ so to set $A_0 = 0$. A residual gauge-invariance remains, due to the possibility of performing a further transformation with a function $\theta(\mathbf{x})$ independent of time and (making use of the Maxwell equation in vacuum $\nabla \cdot \mathbf{E} = 0$) it can be used to set $\nabla \cdot \mathbf{A} = 0$, so we eliminate also the longitudinal component of a plane wave solution, and we are left with only two degrees of freedom, at least at the classical level. Then, one can quantize the free theory and verify that one obtains a massless particle with two helicity states, the photon.

The graviton and its action

We want to do the same for a massless particle with $j = 2$, that we call the graviton. The strategy is therefore to start from a traceless symmetric tensor, to impose a local invariance, and to write down a Lagrangian that respects this local symmetry. Then (using the equations of motion derived from this Lagrangian) we can see how many degrees of freedom remain in the theory. In fact, it is even technically simpler to start from a tensor $h_{\mu\nu}$ which is symmetric, but not traceless, so from the point of view of Lorentz symmetry it decomposes into the trace and the symmetric traceless part, and from the point of view of rotations $h_{\mu\nu} \in \mathbf{0} \oplus (\mathbf{0} \oplus \mathbf{1} \oplus \mathbf{2})$. We therefore want to impose an invariance that eliminates eight spurious degrees of freedom.

In order to generalize eq. (2.82) to the case of a field $h_{\mu\nu}$ with two indices, we must assign a Lorentz index to the function that parametrizes the gauge transformation. Let us call $\xi_\mu(x)$ this function. Since we must

respect the fact that $h_{\mu\nu}$ is symmetric in (μ, ν) , the natural generalization of eq. (2.82) is

$$h_{\mu\nu}(x) \rightarrow h_{\mu\nu}(x) - (\partial_\mu \xi_\nu + \partial_\nu \xi_\mu), \quad (2.83)$$

that we still call a gauge transformation. Observe that this is nothing but the symmetry (1.8) of linearized Einstein gravity, so we are on the good track for recovering the linearization of general relativity.

Next, we want to construct a gauge-invariant action, for the free theory. Remarkably, the condition of gauge-invariance fixes this action uniquely. In fact, by inspection we see that the possible terms that one can write down, quadratic in $h_{\mu\nu}$ and with two derivatives, are

$$\partial_\rho h_{\mu\nu} \partial^\rho h^{\mu\nu}, \quad \partial_\rho h_{\mu\nu} \partial^\nu h^{\mu\rho}, \quad \partial_\nu h^{\mu\nu} \partial^\rho h_{\mu\rho}, \quad \partial_\nu h^{\mu\nu} \partial_\mu h, \quad \partial^\mu h \partial_\mu h, \quad (2.84)$$

where $h = h^\mu_\mu$ is the trace of $h_{\mu\nu}$. Terms of the schematic form $h \partial \partial h$ are related to those written above by a single integration by parts. Furthermore, the second and third term in eq. (2.84) are related by two integrations by parts, that swaps the two derivatives. Therefore, the most general form of the free action is

$$S_2 = \int d^4x [a_1 \partial_\rho h_{\mu\nu} \partial^\rho h^{\mu\nu} + a_2 \partial_\rho h_{\mu\nu} \partial^\nu h^{\mu\rho} + a_3 \partial_\nu h^{\mu\nu} \partial_\mu h + a_4 \partial^\mu h \partial_\mu h], \quad (2.85)$$

where the label in S_2 stresses that this quantity is quadratic in $h_{\mu\nu}$. We now impose invariance under the gauge transformation (2.83). This fixes all the coefficients a_1, \dots, a_4 , except of course for an overall normalization. We then obtain (choosing the normalization $a_1 = -1/2$; the sign is fixed requiring that the energy is positive definite),

$$S_2 = \frac{1}{2} \int d^4x [-\partial_\rho h_{\mu\nu} \partial^\rho h^{\mu\nu} + 2\partial_\rho h_{\mu\nu} \partial^\nu h^{\mu\rho} - 2\partial_\nu h^{\mu\nu} \partial_\mu h + \partial^\mu h \partial_\mu h]. \quad (2.86)$$

This is the Pauli–Fierz action. Comparison with eq. (2.33) shows that we have indeed recovered the Einstein action of linearized theory, after a rescaling

$$h_{\mu\nu} \rightarrow (32\pi G)^{-1/2} h_{\mu\nu}, \quad (2.87)$$

and taking into account that the last term in eq. (2.33) is equal to the second in eq. (2.86) after swapping the two derivatives with integrations by parts. We have therefore found that the linearized Einstein action is the *unique* action that describes a free massless particle with helicities ± 2 , propagating in flat space.

We can now repeat the considerations already made in Sections 1.1 and 1.2, see in particular the discussion around eqs. (1.26) and (1.27): we can use the gauge-invariance (2.83) to choose the Lorentz gauge (1.18). This eliminates four of the 10 degrees of freedom in $h_{\mu\nu}$, and still leaves a residual gauge invariance, i.e. the transformations (2.83) with functions ξ_μ that satisfy $\square \xi_\mu = 0$. In the vacuum, where $T^{\mu\nu} = 0$, using the Lorentz gauge, the equations of motion derived from the linearized

Einstein action are $\square \bar{h}_{\mu\nu} = 0$, and therefore four functions ξ_μ that satisfy $\square \xi_\mu = 0$ can be used to eliminate four components of $\bar{h}_{\mu\nu}$, so we remain with two degrees of freedom, and we arrive at the TT gauge, eq. (1.31). The requirements of gauge invariance therefore fixes uniquely the linearized action, and leaves us with a massless spin-2 field with two transverse degrees of freedom, the graviton.

For the interaction term, we can write

$$S_{\text{int}} = \frac{\kappa}{2} \int d^4x h_{\mu\nu} T^{\mu\nu}. \quad (2.88)$$

The coupling constant κ will be fixed below. Observe that this interaction term is invariant under the gauge transformation (2.83) because, after an integration by parts, the term $(\partial_\mu \xi_\nu + \partial_\nu \xi_\mu) T^{\mu\nu}$ vanishes, using $\partial_\mu T^{\mu\nu} = 0$.

Just as in electrodynamics, to find the graviton propagator we must add a gauge-fixing term to eq. (2.86), since otherwise the quadratic form is not invertible. The Lorentz gauge can be obtained adding the gauge-fixing term

$$\begin{aligned} S_{\text{gf}} &= - \int d^4x (\partial^\nu \bar{h}_{\mu\nu})^2 \\ &= - \int d^4x \left(\partial^\nu h_{\mu\nu} - \frac{1}{2} \eta_{\mu\nu} \partial^\nu h \right)^2 \\ &= \int d^4x \left(-\partial_\rho h_{\mu\nu} \partial^\nu h^{\mu\rho} + \partial_\nu h^{\mu\nu} \partial_\mu h - \frac{1}{4} \partial^\mu h \partial_\mu h \right), \end{aligned} \quad (2.89)$$

where in the first term we swapped the derivatives integrating by parts. The overall numerical coefficient in eq. (2.89) has been chosen so that the terms $\partial_\rho h_{\mu\nu} \partial^\nu h^{\mu\rho}$ and $\partial_\nu h^{\mu\nu} \partial_\mu h$ cancel between S_2 and S_{gf} , so this choice corresponds to the Feynman gauge in electrodynamics. Putting everything together, we find

$$S = S_2 + S_{\text{gf}} + S_{\text{int}} = \int d^4x \left[-\frac{1}{2} \partial_\rho h_{\mu\nu} \partial^\rho h^{\mu\nu} + \frac{1}{4} \partial^\mu h \partial_\mu h + \frac{\kappa}{2} h_{\mu\nu} T^{\mu\nu} \right]. \quad (2.90)$$

The equations of motion obtained performing the variation of this action are

$$\square \bar{h}_{\mu\nu} = -\frac{\kappa}{2} T_{\mu\nu}, \quad (2.91)$$

or, equivalently

$$\square h_{\mu\nu} = -\frac{\kappa}{2} \left(T_{\mu\nu} - \frac{1}{2} \eta_{\mu\nu} T \right). \quad (2.92)$$

Comparing with eq. (1.24) and taking into account the rescaling (2.87), we get (in the units $c = 1$ that we are using in this section),

$$\kappa = (32\pi G)^{1/2}. \quad (2.93)$$

The graviton propagator

We now find the graviton propagator. Integrating by parts, we have

$$\int d^4x \left[-\frac{1}{2}\partial_\rho h_{\mu\nu}\partial^\rho h^{\mu\nu} + \frac{1}{4}\partial^\mu h\partial_\mu h \right] = \frac{1}{2} \int d^4x h^{\mu\nu} A_{\mu\nu\rho\sigma} \partial^\rho h^{\rho\sigma}, \quad (2.94)$$

where

$$A_{\mu\nu\rho\sigma} = \frac{1}{2} (\eta_{\mu\rho}\eta_{\nu\sigma} + \eta_{\mu\sigma}\eta_{\nu\rho} - \eta_{\mu\nu}\eta_{\rho\sigma}). \quad (2.95)$$

The graviton propagator in this gauge is obtained inverting this matrix. Observe that

$$A_{\mu\nu\alpha\beta} A^{\alpha\beta}_{\rho\sigma} = \frac{1}{2} (\eta_{\mu\rho}\eta_{\nu\sigma} + \eta_{\mu\sigma}\eta_{\nu\rho}). \quad (2.96)$$

The right-hand side is nothing but the identity matrix, in the space of tensors symmetric in (μ, ν) and in (ρ, σ) . Therefore in this space the inverse of A is A itself,¹³ so the propagator is given by

$$\tilde{D}_{\mu\nu\rho\sigma}(k) = \frac{1}{2} (\eta_{\mu\rho}\eta_{\nu\sigma} + \eta_{\mu\sigma}\eta_{\nu\rho} - \eta_{\mu\nu}\eta_{\rho\sigma}) \left(\frac{-i}{k^2 - i\epsilon} \right), \quad (2.97)$$

where, as usual, the $i\epsilon$ prescription selects the Feynman propagator. In particular, $\tilde{D}_{0000}(k) = -i/(2k^2)$ and $D_{0000}(r) = -i/(8\pi r)$.¹⁴ Comparing with eqs. (2.66) and (2.78) we see that the propagator of h_{00} has the same sign as the propagator of the scalar field (and the opposite sign of the propagator of A_0), since $(\eta_{00})^2 = +1$. Therefore, in the static limit h_{00} mediates an *attractive* gravitational potential. Using the interaction terms (2.88) and repeating the same steps performed for the scalar field, we get

$$\begin{aligned} V(\mathbf{x}) &= -i \frac{\kappa^2}{4} \int \frac{d^3q}{(2\pi)^3} \tilde{T}_1^{00}(\mathbf{q}) \tilde{D}_{0000}(\mathbf{q}) \tilde{T}_2^{00}(-\mathbf{q}) e^{i\mathbf{q}\cdot\mathbf{x}} \\ &= -i \frac{\kappa^2}{4} m_1 m_2 D_{0000}(\mathbf{x}) \\ &= -\frac{\kappa^2}{32\pi} \frac{m_1 m_2}{r}. \end{aligned} \quad (2.98)$$

This gives again $\kappa = (32\pi G)^{1/2}$, in agreement with eq. (2.93) (of course, this numerical value depends on the choice of normalization made for $h_{\mu\nu}$), and we have recovered the Newtonian limit.

2.2.3 From gravitons to gravity

We can now understand, from a field-theoretical point of view, that the simple action (2.90) cannot be the whole story, and that the correct field theory of gravitation must develop a full non-linear structure. The reason is that, as we have seen, the theory of a massless particle with

¹³Alternatively, we can define the 10 fields ϕ_i , $i = 1, \dots, 10$, by $\phi_1 = h_{00}, \phi_2 = h_{01}, \dots, \phi_{10} = h_{33}$. We then write the kinetic term in the form $A_{ij}\partial_\mu\phi_i\partial^\mu\phi_j$, and we invert the 10×10 matrix A_{ij} .

¹⁴The overall factor depends of course on the overall normalization of the action, i.e. on the normalization of $h_{\mu\nu}$. With our choice the field h_{00} is not canonically normalized, since its propagator has an extra factor 1/2 with respect to the usual normalization. In contrast, writing $\phi_{\mu\nu} = h_{\mu\nu} - (1/4)\eta_{\mu\nu}h$, the field $\phi_{\mu\nu}$ is canonically normalized. Observe that $\phi_{\mu\nu}$ is a pure spin-2 field since it is traceless, while h is a spin-0 field.

helicities ± 2 must necessarily be gauge invariant. We have shown that we can use gauge-invariance to impose the Lorentz condition

$$\partial^\mu \bar{h}_{\mu\nu} = 0, \quad (2.99)$$

and that in this gauge the equations of motion read

$$\square \bar{h}_{\mu\nu} = -\frac{\kappa}{2} T_{\mu\nu}. \quad (2.100)$$

Equations (2.99) and (2.100) together imply that the energy-momentum tensor of matter satisfies the flat-space conservation law $\partial_\mu T^{\mu\nu} = 0$. In integrated form, this conservation laws reads

$$\frac{d}{dt} \int_V d^3x T^{00} = - \int_V d^3x \partial_i T^{0i}, \quad (2.101)$$

and states that any change in the energy of the matter field in a volume V is due uniquely to the flux of matter field flowing inside or outside this volume. However, this can be true only as long as we consider $T^{\mu\nu}$ as a given classical external source. As soon as we replace it with the energy-momentum tensor of dynamical matter fields, there will necessarily be an exchange of energy and of momentum between matter and the gravitational field. For instance, there will be gravitational radiation emitted by the matter and going off to infinity, draining energy from the matter sources. Therefore the equation $\partial_\mu T^{\mu\nu} = 0$ is untenable in a full dynamical theory, and eq. (2.100) cannot be exact.

In the full theory what should be conserved is not the energy and momentum of the matter alone, but that of matter plus gravitational field. To remedy this we could try to perform, on the right-hand side of eq. (2.100), the replacement

$$T_{\mu\nu} \rightarrow T_{\mu\nu} + t_{\mu\nu}^{(2)}, \quad (2.102)$$

where $t_{\mu\nu}^{(2)}$ is the energy-momentum tensor of the gravitons, obtained from the Pauli–Fierz action using the Noether theorem. Using eq. (2.10), we see that a Lagrangian quadratic in $h_{\mu\nu}$, such as the Pauli–Fierz Lagrangian, produces an energy-momentum tensor quadratic in $h_{\mu\nu}$, of the type, symbolically, $\partial h \partial h$. In eq. (2.102) we added to $t_{\mu\nu}$ the superscript (2) to emphasize that it is quadratic in $h_{\mu\nu}$. Then, we are led to try

$$\square \bar{h}_{\mu\nu} = -\frac{\kappa}{2} (T_{\mu\nu} + t_{\mu\nu}^{(2)}), \quad (2.103)$$

and the gauge condition $\partial^\mu \bar{h}_{\mu\nu}$ is consistent with the conservation of the graviton plus matter energy-momentum tensor,

$$\partial^\mu (T_{\mu\nu} + t_{\mu\nu}^{(2)}) = 0. \quad (2.104)$$

However, this cannot yet be the end of the story. The equation of motion (2.103) has a term, $(-1/2)\kappa t_{\mu\nu}^{(2)}$, which is quadratic in $h_{\mu\nu}$ (and linear in κ) and to derive it from an action principle, we must add to the action

a term *cubic* in $h_{\mu\nu}$ and proportional to κ . Symbolically (i.e. omitting Lorentz indices), $t_{\mu\nu}^{(2)} \sim \partial h \partial h$ and a term of this type in the equations of motion can be obtained adding to the action a term of the form $h \partial h \partial h$, or, restoring Lorentz indices,

$$S_3 = \frac{\kappa}{2} \int d^4x h_{\mu\nu} \mathcal{S}^{\mu\nu}(\partial h), \quad (2.105)$$

where $\mathcal{S}^{\mu\nu}(\partial h)$ should be of the general form

$$\mathcal{S}^{\mu\nu}(\partial h) = A^{\mu\nu\rho\sigma\alpha\beta\gamma\delta} \partial_\rho h_{\alpha\beta} \partial_\sigma h_{\gamma\delta}, \quad (2.106)$$

and the tensor $A^{\mu\nu\rho\sigma\alpha\beta\gamma\delta}$ is a product of flat metric factors. At this stage, the action of the matter plus gravitational field must therefore be of the general form

$$\begin{aligned} S &= S_2 + S_{\text{gf}} + S_{\text{int}} + S_3 \\ &= \int d^4x \left[-\frac{1}{2} \partial_\rho h_{\mu\nu} \partial^\rho h^{\mu\nu} + \frac{1}{4} \partial^\mu h \partial_\mu h + \frac{\kappa}{2} h_{\mu\nu} T^{\mu\nu} + \frac{\kappa}{2} h_{\mu\nu} \mathcal{S}^{\mu\nu}(\partial h) \right]. \end{aligned} \quad (2.107)$$

Observe that $\mathcal{S}^{\mu\nu}(\partial h)$ is *not* equal to the energy-momentum tensor $t_{\mu\nu}^{(2)}$. In fact, the variation of a term $h^{\mu\nu} t_{\mu\nu}^{(2)}(h)$ in the action would produce, in the equations of motion, a term

$$\frac{\delta}{\delta h^{\mu\nu}} \left[h^{\alpha\beta} t_{\alpha\beta}^{(2)}(h) \right] = t_{\mu\nu}^{(2)}(h) + h^{\alpha\beta} \frac{\delta}{\delta h^{\mu\nu}} \left[t_{\alpha\beta}^{(2)}(h) \right], \quad (2.108)$$

so there would be an extra term due to the variation of $t_{\alpha\beta}^{(2)}(h)$. Therefore, in the action $h_{\mu\nu}$ couples to matter through the energy-momentum tensor of matter, but the coupling to itself is through a different tensor. In other words, the equivalence principle means that the energy-momentum tensor of GWs enters on the same footing as the energy-momentum tensor of matter in the equations of motion, not in the action.

The cubic term in the action means that gravitons have a non-linear coupling to themselves and, in the language of Feynman graphs, corresponds to a vertex as shown in Fig. 2.4. It is instructive to compare this situation with electrodynamics and with Yang-Mills theories. In electrodynamics, the photon mediates the interaction, but carries no electric charge. Therefore it does not couple directly to itself, and it does not contribute to the electric current. In Yang-Mills theories, instead, the gauge bosons are charged with respect to the gauge group, and therefore they couple non-linearly to themselves, and in the theory there are three-boson vertices and four-boson vertices. The situation for gravitons is analogous. Here the role of the current is played by the energy-momentum tensor, and the gravitons couple to their own energy-momentum tensor (in the equations of motion; or to the corresponding functional $\mathcal{S}^{\mu\nu}(\partial h)$ in the action). We see that, with the inclusion of the cubic term in the action, our gauge theory of a massless particle with helicities ± 2 begins to resemble to a non-Abelian gauge theory.

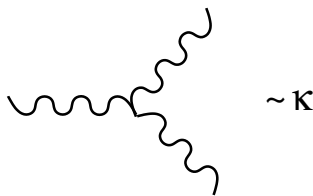


Fig. 2.4 The three-graviton vertex. Two lines carry a contribution proportional to their momentum.

This suspicion is confirmed observing that the action (2.107) is no longer invariant under the linear gauge transformation (2.83) that was our starting point, since the term $h_{\mu\nu}T^{\mu\nu}$ is invariant only if $\partial_\mu T^{\mu\nu} = 0$, which is no longer true. Rather, under the transformation (2.83),

$$\begin{aligned}\delta \int d^4x \frac{\kappa}{2} h_{\mu\nu} T^{\mu\nu} &= \kappa \int d^4x (\partial_\mu \xi_\nu) T^{\mu\nu} \\ &= -\kappa \int d^4x \xi_\nu \partial_\mu T^{\mu\nu} \\ &= +\kappa \int d^4x \xi_\nu \partial_\mu t^{\mu\nu(2)} \\ &= -\kappa \int d^4x (\partial_\mu \xi_\nu) t^{\mu\nu(2)}. \end{aligned} \quad (2.109)$$

However, we have seen that the presence of a local gauge invariance is crucial to eliminate the spurious degrees of freedom in $h_{\mu\nu}$, and we cannot afford to lose it at higher orders in κ . To remedy this, one can observe that this extra term can be canceled, at $O(\kappa)$, promoting the linear gauge transformation (2.83) to a non-linear transformation of the generic form

$$h_{\mu\nu} \rightarrow h_{\mu\nu} - (\partial_\mu \xi_\nu + \partial_\nu \xi_\mu) + \kappa O(h\partial\xi). \quad (2.110)$$

Then the transformation of the graviton kinetic term produces a term $O(\kappa)$, and it is possible to choose the tensorial structure of the $O(h\partial\xi)$ term so that it cancels the extra term coming from eq. (2.109). Thus, eq. (2.83) is the gauge symmetry of the theory only at the infinitesimal level, and at the finite level a non-linear gauge transformation emerges, just as in non-Abelian gauge theories. With the hindsight coming from the fact that we know already that the full theory of gravitation is general relativity, we recognize in eq. (2.110) the expansion up to next-to-leading order of a finite diffeomorphism.

It is clear that the iteration procedure does not stop here, neither in the action nor in the gauge transformation. Once we add to the action the term S_3 , which is cubic in $h_{\mu\nu}$ and proportional to κ , this produces (through Noether's theorem) a contribution to the energy-momentum tensor of the graviton again cubic in $h_{\mu\nu}$ and proportional to κ . We find useful to display the powers of κ explicitly, so we denote it by $\kappa t_{\mu\nu}^{(3)}$. Noether theorem, applied to the action (2.107), now gives

$$\partial^\mu (T_{\mu\nu} + t_{\mu\nu}^{(2)} + \kappa t_{\mu\nu}^{(3)}) = 0. \quad (2.111)$$

Therefore, consistency with $\partial^\mu \bar{h}_{\mu\nu} = 0$ now requires to replace eq. (2.103) by

$$\square \bar{h}_{\mu\nu} = -\frac{\kappa}{2} (T_{\mu\nu} + t_{\mu\nu}^{(2)} + \kappa t_{\mu\nu}^{(3)}). \quad (2.112)$$

In turn, the action which generates this equation of motion, that has a term cubic in $h_{\mu\nu}$ and proportional to κ^2 , must have an additional term quartic in $h_{\mu\nu}$ and proportional to κ^2 , so also its associated energy-

momentum tensor has a further term quartic in the fields and proportional to κ^2 , that we denote by $\kappa^2 t_{\mu\nu}^{(4)}$, and then

$$\square \bar{h}_{\mu\nu} = -\frac{\kappa}{2}(T_{\mu\nu} + t_{\mu\nu}^{(2)} + \kappa t_{\mu\nu}^{(3)} + \kappa^2 t_{\mu\nu}^{(4)} + \dots), \quad (2.113)$$

where the dots indicate that the iteration continues to all orders. We recognize the full non-linear structure typical of Einstein gravity, with arbitrarily large powers of $h_{\mu\nu}$, and a non-linear gauge invariance. Indeed, there exists a simple and explicit resummation algorithm, due to Deser, which gives back the Einstein equations. This algorithm uses the first order Palatini formalism, where the action becomes a cubic polynomial in the variable $\sqrt{-g} g_{\mu\nu}$ and in the Christoffel symbol (which in a first order formalism are varied independently), and the iteration stops at finite order, see the Further Reading section. So, general relativity can be inferred ‘bottom up’, i.e. starting from gravitons. However, some aspects of this reconstruction procedure are not unique. In particular the full Einstein action includes a boundary term, since it can be written as

$$\begin{aligned} S_E &= \frac{1}{16\pi G} \int d^4x \sqrt{-g} R \\ &= \frac{1}{16\pi G} \int d^4x [\sqrt{-g} \mathcal{L}_2 - \partial_\mu K^\mu], \end{aligned} \quad (2.114)$$

where

$$\mathcal{L}_2 = g^{\mu\nu} \left(\Gamma_{\beta\mu}^\alpha \Gamma_{\alpha\nu}^\beta - \Gamma_{\mu\nu}^\alpha \Gamma_{\alpha\beta}^\beta \right) \quad (2.115)$$

is quadratic in the first derivative of the metric (it is usually called the ‘ $\Gamma\Gamma$ ’ Lagrangian), and

$$K^\mu = \sqrt{-g} (g^{\mu\nu} \Gamma_{\alpha\nu}^\alpha - g^{\alpha\beta} \Gamma_{\alpha\beta}^\mu). \quad (2.116)$$

¹⁵Nor the general covariance of the theory. Since boundary terms in the action do not affect classical physics, a classical theory is invariant under a given transformation even if its action changes by a boundary term. This typically happens, for instance, in supersymmetric theories, where under a supersymmetry transformation the action changes by a boundary term.

The latter term is a total divergence and therefore does not affect the equations of motion.¹⁵ However, boundary terms are relevant in the quantum theory, and in particular the boundary term in eq. (2.114) becomes physically relevant in semiclassical quantum gravity, in connection with black hole thermodynamics. It is clear that boundary terms are beyond the reach of the iterative procedure that starts from the Pauli–Fierz action, since at each stage of the procedure we have ambiguities connected with the possibility of dropping boundary terms. For instance, from the very beginning, we might have chosen to retain the third term in eq. (2.84) rather than the second term. More formally, expanding $g_{\mu\nu} = \eta_{\mu\nu} + \kappa h_{\mu\nu}$, \mathcal{L}_2 has the structure (we drop all Lorentz indices, since we are only interested in the dependence on κ)

$$\begin{aligned} \frac{1}{32\pi G} \int d^4x \sqrt{-g} \mathcal{L}_2 &\sim \frac{1}{\kappa^2} \int d^4x [\kappa^2 (\partial h)^2 + \kappa^3 h \partial h \partial h + \dots] \\ &\sim \int d^4x [(\partial h)^2 + \kappa h \partial h \partial h + O(\kappa^2)], \end{aligned} \quad (2.117)$$

and therefore is analytic in κ . On the contrary,

$$\begin{aligned} \frac{1}{32\pi G} \int d^4x \partial_\mu K^\mu &\sim \frac{1}{\kappa^2} \int d^4x \partial^2(\eta + \kappa h) \\ &\sim \frac{1}{\kappa} \int d^4x \partial^2 h. \end{aligned} \quad (2.118)$$

Therefore this term is non-analytic in κ and cannot be obtained unambiguously from the resummation of an expansion in powers of κ , without further physical input.

Alternatively we can proceed top-down, starting from Einstein action and expanding it in powers of $h_{\mu\nu}$, obtaining all non-linear interaction terms. Observe that in this section we have given to $h_{\mu\nu}$ the dimensions of mass that are canonical in field theory, and the dimensionless metric $h_{\mu\nu}$ is recovered with the rescaling (2.87). Therefore, the expansion that we are performing in this section can be written as

$$\begin{aligned} g_{\mu\nu} &= \eta_{\mu\nu} + (32\pi G)^{1/2} h_{\mu\nu} \\ &= \eta_{\mu\nu} + \kappa h_{\mu\nu}, \end{aligned} \quad (2.119)$$

where $h_{\mu\nu}$ has the canonical dimension of mass and κ , dimensionally, is the inverse of a mass. Given the cubic, quartic, and higher terms in the action, one can read the corresponding vertices and compute scattering amplitudes using the Feynman rules. For instance, the $2 \rightarrow 2$ graviton scattering amplitude is obtained from the s -channel graph of Fig. 2.5 (together with the corresponding u -channel and t -channel graphs), and from the four-graviton vertex of Fig. 2.6, so this amplitude is $O(\kappa^2)$, i.e. $O(G)$.¹⁶

2.2.4 Effective field theories and the Planck scale

In units $\hbar = c = 1$, the Newton constant has the dimensions of the inverse of a mass squared, and therefore $\kappa \sim G^{1/2}$ is the inverse of a mass. The fact that the coupling constant κ has dimensions of the inverse of mass means that the quantization of gravity should give rise to a non-renormalizable theory. This is expected first of all on the basis of simple dimensional considerations. For instance, we have seen that the three-graviton vertex has the generic form $\kappa h \partial h \partial h$. The fact that there are two derivatives is dictated by dimensional analysis. In fact, the dimensions of any term in the Lagrangian density \mathcal{L} must be (mass)⁴, so that the action $\int d^4x \mathcal{L}$ is dimensionless (recall that in this section we are using units $\hbar = c = 1$, and then in particular a length has the dimensions of (mass)⁻¹, see Note 2). The kinetic term is, symbolically, $(\partial h)^2$, and since $\partial_\mu = 1/\text{length} = \text{mass}$, we see that $h_{\mu\nu}$ must have dimensions of mass.

The three-graviton vertex therefore must necessarily carry two powers of the momentum: in fact $\kappa h h h \sim (\text{mass})^2$, and to get something trilinear in h and proportional to κ we must add two derivatives, so we must have something of the form $\kappa h \partial h \partial h$. In momentum space each

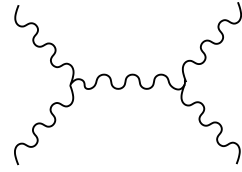


Fig. 2.5 A diagram contributing to the $2 \rightarrow 2$ graviton scattering amplitude.

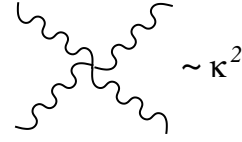


Fig. 2.6 The four-graviton vertex.

¹⁶The explicit expression for the three-graviton vertex, and the (discouragingly long) four-graviton vertex can be found in eqs. (2.6) and (2.7) of DeWitt (1967). To compute a $2 \rightarrow 2$ graviton scattering amplitude in the Born approximation it is however sufficient to know the three-graviton vertex with two gravitons on-shell and only one off-shell, while in the four-graviton vertex all lines are on-shell. Then in the on-shell lines we can impose $\partial^\nu h_{\mu\nu} = 0$ and $h = 0$, and the vertices becomes more manageable, see Grisaru, van Nieuwenhuizen and Wu (1975).

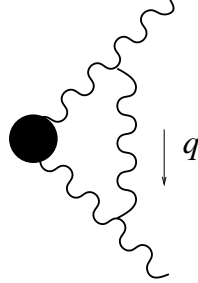


Fig. 2.7 The insertion of an internal graviton line among two external lines. The blob denotes all the remaining (unspecified) part of the Feynman graph.

derivative gives a power of momentum, and we can see, writing explicitly some Feynman graphs, that with more and more insertions of this vertex we get Feynman graphs which (barring cancellations) are more and more divergent. Consider for instance the insertion of an internal graviton line in a Feynman graph, obtained adding two three-graviton vertices on two external lines, and connecting them by a graviton propagator, as in Fig. 2.7. Denote by q^μ the momentum of this internal line. Adding this internal line we have created a new closed loop, which gives an integration over $d^4 q$. There are three propagators in the loop, and at large q each of them is $\sim 1/q^2$. Finally, each of the two vertices gives a factor $q_\mu q_\nu$. Then, barring cancellations, the insertion of two vertices brings a further factor that, in the ultraviolet, is of order

$$\kappa^2 \int d^4 q \frac{1}{(q^2)^3} q_\mu q_\nu q_\rho q_\sigma , \quad (2.120)$$

and so is quadratically divergent. Therefore, adding two vertices we have introduced a new divergence in the graph. Inserting more vertices worsens the situation further and we get stronger and stronger divergencies. The same happens with insertions of the four-graviton vertex, five-graviton vertex, etc.

This lack of renormalizability, however, is not at all a problem as long as we study processes taking place at sufficiently small energies. The problem with non-renormalizable theories is a matter of predictivity, not of mathematical consistency: in the language of counterterms, the divergencies are canceled adding to the Lagrangian terms that have a different functional form, compared to the only term $\sqrt{-g}R$ present in Einstein gravity and, as we increase the number of loops, more and more counterterms are required. For instance, to one-loop order one must add to the Lagrangian a term proportional to $R_{\mu\nu}R^{\mu\nu}$ and a term proportional to R^2 , to two-loop order we have for instance terms proportional to $R_{\mu\nu\rho\sigma}R^{\rho\alpha\beta}R_{\alpha\beta}^{\mu\nu}$, etc.¹⁷ Therefore the divergencies cannot be reabsorbed into a renormalization of the Newton constant and of the fields. Rather, the coefficients of all these terms have a divergent part which is chosen so that it cancels the divergencies coming from the loops, and a finite part that must be fixed by comparison with experiments. Thus, we end up with a theory which, by definition, is finite, but apparently is left with very little predictive power, since we must fix an infinite number of amplitudes by comparison with experiments.

However, this loss of predictivity is not important at low energies. In quantum gravity, we have seen that the coupling constant is $\kappa = (32\pi G)^{1/2}$. Defining the Planck mass M_{Pl} (in our units $\hbar = c = 1$) by

$$G = \frac{1}{M_{\text{Pl}}^2} , \quad (2.121)$$

we have

$$\kappa = \frac{(32\pi)^{1/2}}{M_{\text{Pl}}} . \quad (2.122)$$

The perturbative expansion in quantum gravity, which is an expansion in κ^2 , is therefore an expansion in powers of $1/M_{\text{Pl}}^2$. After renormalizing

¹⁷More precisely, in the background field method one expands $g_{\mu\nu} = \bar{g}_{\mu\nu} + h_{\mu\nu}$, where $\bar{g}_{\mu\nu}$ is a classical solution of the equations of motion and $h_{\mu\nu}$ is a quantum field which, in the path integral formulation, is integrated over. After integrating over the quantum fluctuations $h_{\mu\nu}$, we are left with the counterterms evaluated on $\bar{g}_{\mu\nu}$. For pure gravity, i.e. when we neglect matter fields, $R_{\mu\nu}$ evaluated on any classical solution $\bar{g}_{\mu\nu}$ gives zero, and therefore the one-loop divergencies disappear. This miracle does not repeat at higher orders, and does not take place even at one loop if we also have matter fields (in pure supergravity the divergencies cancel even at two-loop order, but not to higher orders).

the theory, each scattering amplitude with N external legs, computed up to order $(\kappa^2)^n \sim 1/M_{\text{Pl}}^{2n}$, has the generic form

$$A_N(E) = A_N^0(E) \left(1 + c_1 \frac{E^2}{M_{\text{Pl}}^2} + c_2 \frac{E^4}{M_{\text{Pl}}^4} + \dots + c_n \frac{E^{2n}}{M_{\text{Pl}}^{2n}} \right), \quad (2.123)$$

For simplicity we assumed that there is only one relevant energy scale E in the amplitude (which in principle depends on all the Lorentz-invariant quantities that one can make with the external momenta). The non-renormalizability of the theory means that, whatever the value of N , we can always find a sufficiently large order n in perturbation theory, where a genuinely new divergence appears, which is not automatically cured by the renormalization of Green's functions with a smaller number of external legs. Therefore, the coefficients c_1, c_2, \dots, c_{n-1} are finite and calculable once we have renormalized the Green's functions A_M with $M < N$, but the coefficient c_n must be fixed by comparison with experiment, and this is the origin of the lack of predictivity.

However, as long as $E \ll M_{\text{Pl}}$, terms suppressed by powers of E/M_{Pl} are completely irrelevant, and the lack of predictivity due to the fact that c_n should be fixed by comparison with experiment is more apparent than real. As long as we study, say, a graviton-graviton scattering process at a center-of-mass energy $E \ll M_{\text{Pl}}$, all higher-loop corrections are totally insignificant. Given the huge value of the Planck mass,

$$M_{\text{Pl}} \simeq 1.2 \times 10^{19} \text{ GeV}, \quad (2.124)$$

this means that the lowest-order effective action, i.e. classical general relativity, is completely adequate in all “normal” situations. To see the effect of higher-order terms in the perturbative expansion, we should for instance perform a scattering experiment at center-of-mass energies of order M_{Pl} , or, equivalently, we should probe the structure of space-time at length-scale of the order of the Planck length, $l_{\text{Pl}} = 1/M_{\text{Pl}} \sim 10^{-33}$ cm. In accelerator physics, this is beyond any conceivable future development. Possibly, our best chances of exploring this extremely energetic region is through the observation of some relic of the Big Bang, and in particular stochastic backgrounds of relic GWs, as we will discuss in Vol. 2. However, as long as we consider “normal” astrophysical situations, the lack of predictivity at the Planck scale becomes irrelevant, and general relativity is a totally adequate low-energy effective field theory. The fact that the expansion (2.123) blows up as E approaches M_{Pl} signals that at this point a new theory must set in.

2.3 Massive gravitons

In Section 2.2 we introduced the notion of graviton, and we saw that it is described by a massless spin-2 field. From a particle physicist's point of view, one of the most natural extensions of Einstein gravity consists in adding to the graviton a small mass term. However, as we will see in this section, the introduction of a mass term for the graviton turns out to be

This section lies outside the main theme of the book, and can be omitted in a first reading. As in the previous section, we use units $\hbar = c = 1$.

quite subtle from a field-theoretical point of view. In particular the limit $m_g \rightarrow 0$ is very delicate, up to the point that one is led to discuss whether the graviton mass should be *identically* zero. Before entering into these considerations, however, we discuss at a simpler phenomenological level the bounds on the graviton mass.

2.3.1 Phenomenological bounds

In general, we expect that a boson with a mass m_g should mediate a short-range force which, compared to the massless case, is suppressed by a factor proportional to $\exp\{-m_g r\}$. In the case of the graviton, such an exponential would cut off the gravitational interaction at a distance r larger than the reduced Compton wavelength $\lambda_g = 1/m_g$ (or, reinstating \hbar and c , at distances larger than $\lambda_g = \hbar/(m_g c)$).

However, we know experimentally that our Galaxy is held together by gravitation, which means that, at least up to a scale $r_{\text{gal}} \sim 10 \text{ kpc}$, there is no sensible attenuation of the Newton's law, so λ_g cannot be much smaller than 10 kpc. Taking, for definiteness, $\lambda_g > 2 \text{ kpc}$, this already gives a bound $m_g = 1/\lambda_g < 3 \times 10^{-27} \text{ eV}$.

Actually, the experimental bound on the mass of the graviton is even stronger, since we know that the gravitational interaction is not exponentially suppressed even at the intergalactic scale. Our Galaxy has a number of small satellite galaxies, bound by the gravitational force, at distances up to 260 kpc.¹⁸ The Andromeda galaxy, at a distance of 730 kpc, is the nearest giant spiral galaxy, and is approaching the center of mass of our galaxy with a speed $v = -119 \text{ km/s}$. The most natural explanation is that the relative Hubble expansion between our Galaxy and Andromeda has been halted and reversed by the mutual gravitational attraction.¹⁹ This tells us that λ_g cannot be much smaller than, say, $O(100) \text{ kpc}$. On the scale of hundreds of kpc to 1 Mpc, galaxies are seen to be distorted gravitationally by their reciprocal interaction, creating bridges and tails in their shapes. On the scale $(1-10) h_0^{-1} \text{ Mpc}$, where h_0 is the Hubble expansion rate in units of $100 \text{ km s}^{-1} \text{Mpc}^{-1}$ (the current values is $h_0 = 0.73 \pm 0.03$), clusters of galaxies are held together by the gravitational attraction, so we can infer that λ_g cannot be much smaller than a few Mpc. Taking, conservatively,

$$\lambda_g > 300 h_0^{-1} \text{ kpc}, \quad (2.125)$$

results in a bound

$$m_g < 2 \times 10^{-29} h_0 \text{ eV}. \quad (2.126)$$

This bound, of course, refers only to the lightest particle that mediates the gravitational interaction. In some extensions of general relativity, and in particular in theories with extra dimensions, the graviton is accompanied by a whole family of massive excitations (the Kaluza–Klein modes). The bound (2.126) only refers to the lowest lying state, and says nothing about the possibility of further massive gravitons, whose effect vanishes on much shorter length-scales.

¹⁸See Binney and Tremaine (1994), Table 10.1.

¹⁹See Binney and Tremaine (1994), Section 10.2.1.

There is however a potential loophole in the above arguments. We saw in eq. (2.98) that the static gravitational potential is determined by D_{0000} , i.e. by the propagator of the component h_{00} of $h_{\mu\nu}$, which is a scalar under spatial rotation. Gravitational waves, instead, are described by h_{ij}^{TT} , which is a spin-2 tensor under rotations. It is possible to construct consistent models where Lorentz invariance is broken and the masses of scalar, vector and tensor perturbations are different. In particular, h_{ij}^{TT} can be massive while scalar perturbations (obtained from gauge-invariant combinations of h_{00} and of the trace h) remains massless, see the Further Reading. The bounds that we discussed above really refer to the mass of the scalar perturbations, and is the same as the mass of h_{ij}^{TT} only if Lorentz invariance holds.

A direct bound on the mass of the tensor mode h_{ij}^{TT} can be obtained from binary pulsars. A binary neutron star system loses energy because it radiates GWs, and this changes its orbital period. The remarkable agreement between the prediction of general relativity for the orbital change, and the measured value for the binary pulsar PSR B1913+16, is in fact one of the great experimental triumphs of general relativity, and also constitutes the first experimental confirmation of the emission of GWs, and will be discuss in great detail in Chapter 6.

We can understand qualitatively how a bound on the graviton mass emerges from the study of binary pulsars, as follows. The system emits GWs at frequencies of order of its orbital frequency ω_s .²⁰ Then, first of all we must have $m_g c^2 < O(\hbar \omega_s)$ or, in the units $\hbar = c = 1$ that we are using in this chapter, $m_g < O(\omega_s)$, otherwise such massive gravitons could not even be emitted. For m/ω_s small, one finds that the correction to the energy radiated in GWs by the source are of order $(m_g/\omega_s)^2$, with respect to the massless case.²¹ Since the agreement between theory and experiment is of order of 0.1% (see Chapter 6) we must actually have, in order of magnitude, $(m_g/\omega_s)^2 < O(10^{-3})$. Given that the orbital period of PSR B1913+16 is about 8 hr, we immediately get an order-of-magnitude estimate of the bound, $m_g < O(10^{-20})$ eV. A more quantitative analysis of the orbital decay rate of PSR B1913+16 (and also of another binary system that will be discussed in Chapter 6, PSR B1534+12) including a mass term for the graviton gives²²

$$m_g < 7.6 \times 10^{-20} \text{ eV}, \quad (2.127)$$

corresponding to a value of λ_g of the order of the size of the solar system. Similar bounds on m_g would also come from the direct observation of the waveform of inspiraling compact binaries with interferometric detectors.²³

The issue of the graviton mass has potentially important cosmological implications, e.g. in connection with attempts of modifying Einstein gravity at cosmological distances (which is largely motivated by the problem of dark matter and dark energy). Furthermore, the whole subject is quite interesting from a field-theoretical point of view. We therefore discuss, in the rest of this section, the field-theoretical problems that arise when we attempt to give a mass to the graviton.

²⁰As we will compute in Section 4.1.2, for PSR B1913+16 the spectrum of the radiation emitted is actually peaked toward high harmonics of the orbital frequency, because of the large eccentricity of this binary system.

²¹This comes out repeating the same steps that we will do in Section 3.1, using a massive rather than a massless wave equation for $h_{\mu\nu}$. Since a massive Klein-Gordon type equation depends on m_g^2 , the first correction to the radiated energy will also be proportional to the second power of m_g .

²²This analysis has been done by Finn and Sutton (2002) using a mass term for the graviton which actually implies the existence of six degrees of freedom, the five associated to a massive spin-2 graviton plus an additional scalar field, which however is a ghost, i.e. it has the wrong sign of the kinetic energy (see the discussion in Section 2.3.2 below). Different mass terms, and in particular Lorentz-violating mass terms, should however give similar results.

²³The basic idea is that, for a massive graviton, the dispersion relation is $\hbar\omega = \gamma mc^2$, where $\gamma = (1 - v^2/c^2)^{-1/2}$ is the usual relativistic factor. Inverting this for v , and using units $\hbar = c = 1$, we get

$$v(\omega) = \sqrt{1 - \frac{m^2}{\omega^2}}. \quad (2.128)$$

In the inspiral amplitude (that will be studied in Section 4.1) the radiation emitted earlier in the inspiral phase is at lower frequencies, and therefore travels slightly slower than the radiation emitted at later times, resulting in a potentially observable distortion of the waveform observed at the detector, see Will (1998).

2.3.2 Field theory of massive gravitons

A warm-up: massive photons

We want to understand how to construct a consistent field theory for a massive graviton. As a warm-up exercise, let us first recall what happens in electrodynamics if we add by hand a mass term to the photon. The Lagrangian of a massive photon interacting with a conserved current j_μ is

$$\mathcal{L} = -\frac{1}{4}F_{\mu\nu}F^{\mu\nu} - \frac{1}{2}m_\gamma^2 A_\mu A^\mu - j_\mu A^\mu. \quad (2.129)$$

²⁴For the purpose of our discussion, it will not be important whether this mass term has been added by hand, or if it results from a Higgs mechanism.

This is known as the Proca Lagrangian and is not gauge-invariant, because of the mass term.²⁴ This is as it should be, because in the massless case gauge invariance reduces the four degrees of freedom of A_μ to only two degrees of freedom, the two helicity states of the photon, while we want to describe a massive particle, and a massive particle with spin $j = 1$ has $2j + 1 = 3$ degrees of freedom. Still, in order to describe the three physical degrees of freedom of a massive photon with the four components of A_μ , we need to eliminate one degree of freedom. Of course, we cannot do it by imposing the condition $\partial_\mu A^\mu = 0$ in the above Lagrangian with a gauge-fixing procedure, since there is no gauge symmetry to be fixed. Rather, the condition $\partial_\mu A^\mu = 0$ is recovered as follows. The equations of motion obtained from (2.129) are

$$\partial_\mu F^{\mu\nu} - m_\gamma^2 A^\nu = j^\nu. \quad (2.130)$$

Acting with ∂_ν on both sides we find $\partial_\nu \partial_\mu F^{\mu\nu} = 0$, because $\partial_\nu \partial_\mu$ is symmetric while $F^{\mu\nu}$ is antisymmetric, and $\partial_\nu j^\nu = 0$ because we have coupled A^μ to a conserved current. Then, eq. (2.130) implies

$$m_\gamma^2 \partial_\nu A^\nu = 0, \quad (2.131)$$

and, if $m_\gamma \neq 0$, we get the Lorentz condition $\partial_\nu A^\nu = 0$ dynamically, and we have eliminated one degree of freedom. In momentum space this gives $k_\mu \tilde{A}^\mu(k) = 0$. Since for a massive particle the rest frame exists, we can choose the frame where $k^\mu = (m_\gamma, 0, 0, 0)$, so we have eliminated the component A_0 , and we remain with the three components of the vector \mathbf{A} that describe a massive spin-1 particle, as it should be.²⁵

Still, it can be disturbing to observe that, apparently, the zero mass limit is discontinuous, because the number of physical degrees of freedom seems to change abruptly from three, for $m_\gamma \neq 0$, to two for $m_\gamma = 0$. To understand this point, let us see what are the polarization states of a massive photon and their coupling to the current j^μ . Consider first the propagation of a free massive photon, i.e. eq. (2.130) with $j^\nu = 0$,

$$\partial_\mu(\partial^\mu A^\nu - \partial^\nu A^\mu) - m_\gamma^2 A^\nu = 0. \quad (2.132)$$

Using $\partial_\mu A^\mu = 0$, which follows from eq. (2.131), this becomes a massive wave equation,

$$(\square - m_\gamma^2) A^\mu = 0, \quad (2.133)$$

²⁵Actually, even if $\partial_\nu j^\nu \neq 0$, we find that A^0 is fixed in terms of $\partial_\nu j^\nu$, so we have anyway eliminated one degree of freedom. Current conservation is however crucial to ensure a smooth limit as $m_\gamma \rightarrow 0$, as we will see below.

whose solution is a superposition of plane waves of the form $\epsilon^\mu(k)e^{ikx}$ with $k^2 = -m_\gamma^2$, and of their complex conjugates. The condition (2.131) implies

$$\epsilon_\mu(k)k^\mu = 0. \quad (2.134)$$

We choose a frame where $k^\mu = (\omega, 0, 0, k_3)$, with $\omega^2 = k_3^2 + m_\gamma^2$. In this frame two solutions of eq. (2.134) are given by the transverse vectors

$$\epsilon_\mu^{(1)}(k) = (0, 1, 0, 0), \quad \epsilon_\mu^{(2)}(k) = (0, 0, 1, 0), \quad (2.135)$$

which are the same as the usual transverse degrees of freedom of a massless photons. For a massive photon there is however also a third physical solution

$$\epsilon_\mu^{(3)}(k) = \frac{1}{m_\gamma}(-k_3, 0, 0, \omega). \quad (2.136)$$

All three polarization vectors are normalized so that $\epsilon_\mu\epsilon^\mu = 1$. To understand what happens to the polarization state (2.136) in the limit $m_\gamma \rightarrow 0$, we observe that we can rewrite it in terms of $k_\mu = (-\omega, 0, 0, k_3)$, as

$$\epsilon_\mu^{(3)}(k) = \frac{1}{m_\gamma}k_\mu + \frac{\omega - k_3}{m_\gamma}(1, 0, 0, 1). \quad (2.137)$$

The interaction of this state with the current j^μ is proportional to $\epsilon_\mu^{(3)}(k)\tilde{j}^\mu(k)$. If the current is conserved, $k_\mu\tilde{j}^\mu(k) = 0$ and the first term in eq. (2.137) does not contribute. In the limit $m_\gamma \rightarrow 0$, we expand $\omega = (k_3^2 + m_\gamma^2)^{1/2} \simeq k_3 + m_\gamma^2/(2k_3)$, and therefore

$$\begin{aligned} \epsilon_\mu^{(3)}(k)\tilde{j}^\mu(k) &= \frac{\omega - k_3}{m_\gamma} [\tilde{j}^0(k) + \tilde{j}^3(k)] \\ &\simeq \frac{m_\gamma}{2k_3} [\tilde{j}^0(k) + \tilde{j}^3(k)]. \end{aligned} \quad (2.138)$$

Therefore, in the massless limit, the longitudinal mode of a massive photon decouples, and the limit $m_\gamma \rightarrow 0$ is continuous.²⁶ Observe that current conservation has been crucial to show the decoupling of the longitudinal state.

The continuity of the limit $m_\gamma \neq 0$, as far as physical observables are concerned, can also be seen from the propagator, as follows. The propagator of the massive photon is found from the quadratic term in the action which, after an integration by parts, reads

$$S = \frac{1}{2} \int d^4x A_\mu [\eta^{\mu\nu}(\partial^2 - m_\gamma^2) - \partial^\mu\partial^\nu] A_\nu. \quad (2.139)$$

In momentum space, $\partial_\mu \rightarrow ik_\mu$ and we must therefore invert the matrix

$$M^{\mu\nu}(k) = -\eta^{\mu\nu}(k^2 + m_\gamma^2) + k^\mu k^\nu. \quad (2.140)$$

The inversion is easily performed writing M^{-1} in the general form

$$(M^{-1})_{\mu\nu} = a(k)\eta_{\mu\nu} + b(k)k_\mu k_\nu, \quad (2.141)$$

and fixing $a(k)$ and $b(k)$ from $M^{\mu\rho}(M^{-1})_{\rho\nu} = \delta_\nu^\mu$. This gives $a =$

²⁶To illustrate the continuity of the physics as $m_\gamma \rightarrow 0$, consider the following example. In a thermal ensemble, each degree of freedom contributes to the thermodynamical properties, such as the internal energy or specific heat. For instance, in a relativistic Bose gas at equilibrium, the average energy density is $\rho = (\pi^2/30)gT^4$, where g is the number of polarization degrees of freedom. Therefore there is a finite difference between the energy density for massless photons ($g = 2$) and massive photons ($g = 3$). Apparently, from a measure of thermal properties of such a gas we should be able to decide whether $m_\gamma = 0$ exactly, or $m_\gamma \neq 0$. However, in the limit $m_\gamma \rightarrow 0$, the longitudinal mode takes an infinite time to reach equilibrium with the thermal bath, because its interactions goes to zero. Therefore any experiment lasting a finite time will only be able either to discover a positive mass or to put an upper limit on it, but not to state that $m_\gamma = 0$ exactly.

²⁷We do not write explicitly the $i\epsilon$ prescription. In all cases, with our choice of signature, it is obtained replacing $k^2 \rightarrow k^2 - i\epsilon$ in the denominators.

$-1/(k^2 + m_\gamma^2)$, $b = a/m_\gamma^2$. The propagator is defined by $\tilde{D}_{\mu\nu}(k) = i(M^{-1})_{\mu\nu}$. Then²⁷

$$\tilde{D}_{\mu\nu}(k) = \frac{-i}{k^2 + m_\gamma^2} \left(\eta_{\mu\nu} + \frac{k_\mu k_\nu}{m_\gamma^2} \right). \quad (2.142)$$

The propagator of a massive photon is therefore singular in the limit $m_\gamma \rightarrow 0$. However, the singularity disappears from physical observables, because the amplitudes are proportional to

$$\tilde{j}_\mu^*(k) \tilde{D}^{\mu\nu}(k) \tilde{j}_\nu(k). \quad (2.143)$$

Since the current is conserved, $k^\mu \tilde{j}_\mu(k) = 0$, and therefore the terms $k_\mu k_\nu / m_\gamma^2$ in the propagator give zero. We can therefore simply take as propagator of the massive photon the expression

$$\tilde{D}_{\mu\nu}(k) = \frac{-i}{k^2 + m_\gamma^2} \eta_{\mu\nu}, \quad (2.144)$$

and in the limit $m_\gamma \rightarrow 0$ we recover smoothly the massless photon propagator (2.77). The whole procedure required that the massive photon is coupled to a *conserved* current j^μ .

Massive gravitons

Now that we have understood how to describe a massive photon, we can come back to our original problem, the construction of a field theory for massive gravitons. We start from the Pauli–Fierz action (2.86), and we add a mass term. The most general Lorentz-invariant mass term that one can add to the Pauli–Fierz action is a combination of the two scalars $h_{\mu\nu} h^{\mu\nu}$ and h^2 . Of course both terms break the gauge invariance (2.83) of the massless theory, as it should, since we want to describe the $2j+1=5$ degrees of freedom of a massive spin-2 particle, while we have seen that gauge invariance reduces them to only two. Nevertheless, a generic symmetric tensor $h_{\mu\nu}$ has 10 degrees of freedom so we expect that the appropriate number of conditions to reduce it to five emerges dynamically, similarly to what we have found for massive photons.

Of course, for massive gravitons we must start from the Pauli–Fierz action (2.86) *before* gauge-fixing, since now there is no gauge symmetry to fix. Adding the mass term, and writing also the source term, we have

$$S_2 = \frac{1}{2} \int d^4x [-\partial_\rho h_{\mu\nu} \partial^\rho h^{\mu\nu} + 2\partial_\rho h_{\mu\nu} \partial^\nu h^{\mu\rho} - 2\partial_\nu h^{\mu\nu} \partial_\mu h + \partial^\mu h \partial_\mu h + c_1 h^2 + c_2 h_{\mu\nu} h^{\mu\nu} + \tilde{\kappa} h_{\mu\nu} T^{\mu\nu}]. \quad (2.145)$$

We denote the coupling of the massive theory by $\tilde{\kappa}$ since, as we will see below, it need not be the same as the coupling κ introduced in the massless case. We can now obtain the propagator of the massive graviton repeating the same steps performed above for the photon, and we discover that, if we add to the Pauli–Fierz Lagrangian a mass term with

coefficients c_1 and c_2 arbitrary, the resulting propagator in general has ghosts, i.e. poles with the “wrong” sign of the residue, corresponding to degrees of freedom with negative kinetic energy, which generates an instability of the vacuum. The only combination that does not introduce ghosts turns out to be $h_{\mu\nu}h^{\mu\nu} - h^2$, which is called the Pauli–Fierz mass term. Then, in linearized theory we are led to consider, as the action describing massive gravitons,

$$\boxed{S_2 = \frac{1}{2} \int d^4x [-\partial_\rho h_{\mu\nu} \partial^\rho h^{\mu\nu} + 2\partial_\rho h_{\mu\nu} \partial^\nu h^{\mu\rho} - 2\partial_\nu h^{\mu\nu} \partial_\mu h \\ + \partial^\mu h \partial_\mu h + m_g^2(h^2 - h_{\mu\nu}h^{\mu\nu}) + \tilde{\kappa}h_{\mu\nu}T^{\mu\nu}].}$$

(2.146)

Before discussing the propagator obtained from this action, it is instructive to count the number of dynamical degrees of freedom of the theory, to see if they match with the five degrees of freedom of a massive spin-2 particle. We proceed in parallel to what we have done for a massive photon, and we write the equations of motions derived from the action (2.146),

$$\begin{aligned} \square h^{\mu\nu} - (\partial^\nu \partial_\rho h^{\mu\rho} + \partial^\mu \partial_\rho h^{\nu\rho}) + \eta^{\mu\nu} \partial_\rho \partial_\sigma h^{\rho\sigma} + \partial^\mu \partial^\nu h - \eta^{\mu\nu} \square h \\ = -\frac{\tilde{\kappa}}{2} T^{\mu\nu} + m_g^2(h^{\mu\nu} - \eta^{\mu\nu} h). \end{aligned} \quad (2.147)$$

Introducing on the left-hand side $\bar{h}_{\mu\nu} = h_{\mu\nu} - (1/2)\eta_{\mu\nu}h$, we can also write this as

$$\square \bar{h}^{\mu\nu} + \eta^{\mu\nu} \partial^\rho \partial^\sigma \bar{h}_{\rho\sigma} - \partial_\rho \partial^\nu \bar{h}^{\mu\rho} - \partial_\rho \partial^\mu \bar{h}^{\nu\rho} = -\frac{\tilde{\kappa}}{2} T^{\mu\nu} + m_g^2(h^{\mu\nu} - \eta^{\mu\nu} h). \quad (2.148)$$

In this form we immediately see that this equation reduces to eq. (1.17) for $m_g = 0$. We can now apply ∂_μ to both sides. The left-hand side gives zero identically, while on the right-hand side $\partial_\mu T^{\mu\nu} = 0$, since we are working at linear order and then, as we saw in the previous section, $T^{\mu\nu}$ is an external conserved source. Then we get

$$\boxed{m_g^2 \partial_\mu (h^{\mu\nu} - \eta^{\mu\nu} h) = 0,} \quad (2.149)$$

which is analogous to eq. (2.131). Furthermore, taking the trace of both sides of eq. (2.147), we get

$$2\partial_\nu \partial_\mu (h^{\mu\nu} - \eta^{\mu\nu} h) = -\frac{\tilde{\kappa}}{2} T - 3m_g^2 h. \quad (2.150)$$

When $m_g \neq 0$, the left-hand side vanishes because of eq. (2.149), and we get

$$\boxed{-3m_g^2 h = \frac{\tilde{\kappa}}{2} T.} \quad (2.151)$$

In particular in the vacuum, where $T_{\mu\nu} = 0$, eq. (2.151) gives $h = 0$ and then eq. (2.149) gives $\partial^\mu h_{\mu\nu} = 0$ or, equivalently (since $h = 0$), $\partial^\mu \bar{h}_{\mu\nu} = 0$. So we have five conditions that reduce the 10 components of the symmetric matrix $h_{\mu\nu}$ to the five components expected for a massive spin-2 particle. The Pauli–Fierz mass term is actually the only combination for which there is no term proportional to $\square h$ on the left-hand side of eq. (2.151). For all other choices, such a term does appear, so h becomes a propagating degree of freedom, which furthermore turns out to be ghost-like.

The limit $m_g \rightarrow 0$

As soon as we switch on the interaction, i.e. a non-vanishing $T_{\mu\nu}$, the limit $m_g \rightarrow 0$ becomes quite peculiar. In fact, in the limit $m_g \rightarrow 0$, for generic matter field with a non-vanishing trace of the energy–momentum tensor, eq. (2.151) gives $h \rightarrow \infty$ rather than $h = 0$ as in the free theory. To understand the physical consequences of this result we observe that, inserting eqs. (2.149) and (2.151) (i.e. $\partial_\mu h^{\mu\nu} = \partial^\nu h$ and $h = -\tilde{\kappa}T/(6m_g^2)$) into eq. (2.147) we get

$$\begin{aligned} (\square - m_g^2)h_{\mu\nu} &= -\frac{\tilde{\kappa}}{2} \left(T_{\mu\nu} - \frac{1}{3}\eta_{\mu\nu}T + \frac{1}{3m_g^2}\partial_\mu\partial_\nu T \right) \\ &\equiv S_{\mu\nu}. \end{aligned} \quad (2.152)$$

Comparing with eq. (2.92), we see that in the limit $m_g \rightarrow 0$ the left-hand side goes smoothly into the massless limit, but on the right-hand side there are two differences: the coefficient of $\eta^{\mu\nu}T$ is $-1/3$ rather than $-1/2$, and there is an apparently singular term $\sim (1/m_g^2)\partial^\mu\partial^\nu T$. Both find their origin in the fact that, according to eq. (2.151), $m_g^2 h$ stays finite as $m_g \rightarrow 0$.

To see the effect produced by these differences, we can consider the effective matter–matter interaction, which is given by

$$S_{\text{eff}} = \frac{\tilde{\kappa}}{2} \int d^4x h_{\mu\nu}(x)T^{\mu\nu}(x), \quad (2.153)$$

where $h_{\mu\nu}(x)$ is the solution of eq. (2.152),

$$h_{\mu\nu}(x) = \int d^4x' \Delta(x - x')S_{\mu\nu}(x'), \quad (2.154)$$

and $\Delta(x - x')$ is a Green's function of the massive Klein–Gordon equation, defined by

$$(\square_x - m_g^2)\Delta(x - x') = \delta^{(4)}(x - x'). \quad (2.155)$$

This gives

$$S_{\text{eff}} = \frac{\tilde{\kappa}}{2} \int d^4x d^4x' T^{\mu\nu}(x)\Delta(x - x')S_{\mu\nu}(x'). \quad (2.156)$$

Using the conservation of the energy-momentum tensor we can show that the singular term in $S_{\mu\nu}$ drops from this expression. In fact, integrating twice by parts,

$$\begin{aligned}
 & \int d^4x d^4x' T^{\mu\nu}(x) \Delta(x - x') \frac{\partial}{\partial x'^\mu} \frac{\partial}{\partial x'^\nu} T(x') \\
 &= - \int d^4x d^4x' T^{\mu\nu}(x) \left[\frac{\partial}{\partial x'^\mu} \Delta(x - x') \right] \frac{\partial}{\partial x'^\nu} T(x') \\
 &= + \int d^4x d^4x' T^{\mu\nu}(x) \left[\frac{\partial}{\partial x^\mu} \Delta(x - x') \right] \frac{\partial}{\partial x'^\nu} T(x') \\
 &= - \int d^4x d^4x' \left[\frac{\partial}{\partial x^\mu} T^{\mu\nu}(x) \right] \Delta(x - x') \frac{\partial}{\partial x'^\nu} T(x') \\
 &= 0.
 \end{aligned} \tag{2.157}$$

However, the fact that the coefficient of $\eta^{\mu\nu}T$ is $-1/3$ rather than $-1/2$ gives a genuine difference in the physical amplitude,

$$\begin{aligned}
 S_{\text{eff}} &= \frac{\tilde{\kappa}}{2} \int d^4x d^4x' T^{\mu\nu}(x) \Delta(x - x') [T_{\mu\nu}(x') - \frac{1}{3}\eta_{\mu\nu}T(x')] \\
 &= \frac{\tilde{\kappa}}{2} \int d^4x d^4x' T^{\mu\nu}(x) \Delta_{\mu\nu\rho\sigma}(x - x'; m_g) T^{\rho\sigma}(x')
 \end{aligned} \tag{2.158}$$

where

$$\Delta_{\mu\nu\rho\sigma}(x - x'; m_g) = \Delta(x - x') \left[\frac{1}{2}(\eta_{\mu\rho}\eta_{\nu\sigma} + \eta_{\mu\sigma}\eta_{\nu\rho}) - \frac{1}{3}\eta_{\mu\nu}\eta_{\rho\sigma} \right]. \tag{2.159}$$

The same result, of course, could have been obtained directly inverting the quadratic part of the action to find the propagator, just as we did for the massless graviton and for the massive photons. Repeating steps analogous to those leading to eq. (2.142), we get

$$\tilde{D}_{\mu\nu\rho\sigma}(k; m_g) = \left[\frac{1}{2}(\Pi_{\mu\rho}\Pi_{\nu\sigma} + \Pi_{\mu\sigma}\Pi_{\nu\rho}) - \frac{1}{3}\Pi_{\mu\nu}\Pi_{\rho\sigma} \right] \left(\frac{-i}{k^2 + m_g^2 - i\epsilon} \right), \tag{2.160}$$

where

$$\Pi_{\mu\nu} \equiv \eta_{\mu\nu} + \frac{k_\mu k_\nu}{m_g^2}. \tag{2.161}$$

Since the energy-momentum tensor is conserved, $k_\mu \tilde{T}^{\mu\nu}(k) = 0$ and, when contracted with $T^{\mu\nu}(-k)T^{\rho\sigma}(k)$, the above propagator is equivalent to

$$\tilde{D}_{\mu\nu\rho\sigma}(k; m_g) = \left[\frac{1}{2}(\eta_{\mu\rho}\eta_{\nu\sigma} + \eta_{\mu\sigma}\eta_{\nu\rho}) - \frac{1}{3}\eta_{\mu\nu}\eta_{\rho\sigma} \right] \left(\frac{-i}{k^2 + m_g^2 - i\epsilon} \right).$$

Comparing eqs. (2.160) or (2.162) with the massless graviton propagator found in eq. (2.97) we see the following. The terms $k_\mu k_\nu / m_g^2$,

that are singular in the massless limit, give a vanishing contribution to the physical amplitudes, because $h_{\mu\nu}$ is coupled to a conserved energy-momentum tensor. This is completely analogous to the situation for a massive photon, where the terms $k_\mu k_\nu / m_\gamma^2$ disappeared because the photon is coupled to a conserved current. However, there is difference in the numerical coefficient in front of $\eta_{\mu\nu} \eta_{\rho\sigma}$ and, unlikely the case of the photon, the propagator (2.162) does not reduce to the massless propagator as $m_g \rightarrow 0$. Writing

$$\begin{aligned} \frac{1}{2}(\eta_{\mu\rho}\eta_{\nu\sigma} + \eta_{\mu\sigma}\eta_{\nu\rho}) - \frac{1}{3}\eta_{\mu\nu}\eta_{\rho\sigma} &= \frac{1}{2}(\eta_{\mu\rho}\eta_{\nu\sigma} + \eta_{\mu\sigma}\eta_{\nu\rho} - \eta_{\mu\nu}\eta_{\rho\sigma}) \\ &\quad + \frac{1}{6}\eta_{\mu\nu}\eta_{\rho\sigma}, \end{aligned} \quad (2.163)$$

we see that

$$\begin{aligned} \lim_{m_g \rightarrow 0} T^{\mu\nu}(-k)\tilde{D}_{\mu\nu\rho\sigma}(k; m_g)T^{\rho\sigma}(k) &= T^{\mu\nu}(-k)\tilde{D}_{\mu\nu\rho\sigma}(k)T^{\rho\sigma}(k) \\ &\quad + \frac{1}{6}T(-k)\frac{-i}{k^2}T(k), \end{aligned} \quad (2.164)$$

where $\tilde{D}_{\mu\nu\rho\sigma}(k)$ is the propagator computed directly in the massless theory, eq. (2.97). The second term on the right-hand side corresponds to the exchange of a massless scalar particle, coupled to the trace of the energy-momentum tensor, and it is because of this additional term that the limit $m_g \rightarrow 0$ of the massive theory does not reproduce the result obtained in the massless theory. This is usually referred to as the van Dam–Veltman–Zakharov (vDVZ) discontinuity.²⁸

Having identified the problem in the existence of an unexpected scalar degree of freedom, we can now understand what happened. Recall that a massive spin- j particles has $2j+1$ degrees of freedom, while a massless particle with quantum number j has only two degrees of freedom if $j > 0$ (and if we demand that it is also a representation of parity, beside of Poincaré transformations), and one degree of freedom if $j = 0$. For a massive photon, we saw that the three degrees of freedom, in the massless limit, decompose into the two transverse degrees of freedom of a massless photon, which have helicities ± 1 , plus the longitudinal component. The latter, in the limit $m_\gamma \rightarrow 0$, becomes a scalar particle and decouples, since its coupling becomes proportional to $\partial_\mu j^\mu$, which vanishes. The fact that the coupling is to $\partial_\mu j^\mu$ is dictated by the fact that this is the only scalar that we can make with j^μ and with derivatives, which is linear in the current. The decoupling of the spurious scalar mode is therefore ensured by current conservation.

Similarly, in the limit $m_g \rightarrow 0$, the five degrees of freedom of the massive graviton decompose into two states with helicities ± 2 , which make up a massless graviton, two states with helicities ± 1 , often termed the graviphoton, and a scalar, called the graviscalar. The graviphoton, being a vector, must be coupled to a four-vector made with $T_{\mu\nu}$ and possibly with derivatives, and linear in $T_{\mu\nu}$. The only possibility is $\partial_\mu T^{\mu\nu}$. However, this quantity vanishes and therefore the graviphoton

²⁸Actually, it was discovered independently by Iwasaki (1970), van Dam and Veltman (1970) and Zakharov (1970).

decouples. The graviscalar, on the other hand, can couple to the trace of the energy-momentum tensor. This is in general non-zero, and therefore the graviscalar does not decouple. It is, in fact, responsible for the additional term in eq. (2.164) and therefore for the vDVZ discontinuity.

We can now compare some predictions of the massless and massive theory. Consider first the Newtonian potential in the non-relativistic limit. We found in eq. (2.98) that

$$V(\mathbf{x}) = -i \frac{\kappa^2}{4} m_1 m_2 D_{0000}(\mathbf{x}). \quad (2.165)$$

In the massless theory, using eq. (2.97), we saw that

$$\tilde{D}_{0000}(k) = \frac{1}{2} \frac{-i}{k^2}. \quad (2.166)$$

This gives $D_{0000}(r) = -i/(8\pi r)$, so

$$V(\mathbf{x}) = -\frac{\kappa^2}{32\pi} \frac{m_1 m_2}{r}, \quad (2.167)$$

and we recovered the Newtonian potential setting $\kappa^2 = 32\pi G$. In the massive theory, instead, we see from eq. (2.162) that

$$\tilde{D}_{0000}(k) = \frac{2}{3} \frac{-i}{k^2 + m_g^2}, \quad (2.168)$$

and we get

$$V(\mathbf{x}) = -\frac{4}{3} \left(\frac{\tilde{\kappa}^2}{32\pi} \right) \frac{m_1 m_2}{r} \exp\{-m_g r\}. \quad (2.169)$$

The Yukawa potential was of course expected because a massive particle mediates a short-range force. The result however differs also by an overall factor $4/3$ from the massless result, and the difference is due to the additional attractive contribution of the graviscalar.

As far as the Newtonian limit is concerned, one can simply reabsorb this difference setting, in the massive theory,

$$\frac{4}{3} \left(\frac{\tilde{\kappa}^2}{32\pi} \right) = G. \quad (2.170)$$

Thus, at $m_g r \ll 1$, the correct Newtonian potential is obtained, at the price that the coupling $\tilde{\kappa}^2$ of the massive theory is smaller than the coupling κ^2 of the massless theory by a factor $3/4$. The problem however comes when we consider the predictions of the massive theory in the relativistic regime, in particular when we compute the deflection of light by a massive object. In the massless theory, the deflection angle of light skimming the surface of the Sun (and first detected, during a total eclipse, by Eddington in 1919), is

$$\Delta\theta = \frac{4GM_\odot}{R_\odot}, \quad (2.171)$$

where M_\odot and R_\odot are the mass and radius of the Sun. Since the energy-momentum tensor of the electromagnetic field is traceless, when we repeat the computation in the massive theory, the additional term proportional to $T(-k)(-i/k^2)T(k)$ in eq. (2.164) vanishes. This means that the result for the deflection of light in the massive theory, in the limit $m_g \rightarrow 0$, is the same as in the massless theory except that, instead of κ^2 , we have $\tilde{\kappa}^2$. Since $\tilde{\kappa}^2 = (3/4)\kappa^2$, the prediction for light bending in the limit $m_g \rightarrow 0$ of the massive theory is smaller by a factor $3/4$ than the prediction of the massless theory, i.e. is $\Delta\theta = 3GM_\odot/R_\odot$. Nowadays the experimental precision on the measurement of the bending of light by the Sun is better than one part in 10^4 , and confirms the prediction of the massless theory. Apparently, one then arrives at the amazing conclusion that the mass of the graviton must be *exactly* zero.

A loophole in the above argument was found by Vainshtein, considering the validity of the linearized approximation in the massive theory. To study the expansion in $h_{\mu\nu}$ systematically, we should start from the full Einstein action plus the Pauli–Fierz mass term,

$$S = \frac{1}{16\pi G} \int d^4x \sqrt{-g} \left[R + \frac{1}{4}m_g^2 (h^2 - h_{\mu\nu}h^{\mu\nu} + O(h_{\mu\nu}^3)) \right], \quad (2.172)$$

We then expand $g_{\mu\nu} = \bar{g}_{\mu\nu} + h_{\mu\nu}$ where $\bar{g}_{\mu\nu}$ is the appropriate background metric and, to have the canonical normalization for $h_{\mu\nu}$, we finally rescale $h_{\mu\nu} \rightarrow (32\pi G)^{1/2}h_{\mu\nu} = \kappa h_{\mu\nu}$. Bosonic matter fields, as usual, are coupled replacing in the matter action all ordinary derivative with covariant derivatives. Actually, one can use any form for the mass term that, in the linearized limit, reduces to the Pauli–Fierz mass term (in particular, we can decide to raise and lower the indices in the mass term with $\eta_{\mu\nu}$ or with $g_{\mu\nu}$. The difference shows up only at cubic and higher-order terms, that are not fixed anyway), so we also included the possibility of non-linear corrections to the Pauli–Fierz mass term.

To compute the gravitational scattering by a fixed heavy mass M , we expand around a metric $\bar{g}_{\mu\nu}$ which is a generalization of the Schwarzschild metric generated by the heavy mass M , so it is computed from the action (2.172), which includes the graviton mass. Naively one would expect that, if $m_g \rightarrow 0$, this metric goes smoothly into the usual Schwarzschild metric computed in standard general relativity, with massless graviton, for all values of r . However, the explicit computation shows that this is not true. We can search for the metric generated by an heavy mass in the theory (2.172), writing²⁹

$$ds^2 = -e^{\nu(\rho)}dt^2 + e^{\sigma(\rho)}d\rho^2 + e^{\mu(\rho)}\rho^2(d\theta^2 + \sin^2\theta d\phi^2). \quad (2.173)$$

²⁹We follow here the treatment of Defayet, Dvali, Gabadadze and Vainshtein (2002), to whom we refer for more details.

When the graviton is massless, the function $\mu(\rho)$ can be set to zero using coordinate invariance. In the theory (2.172), however, the reparametrization invariance is broken, and $\mu(\rho)$ must be kept. One then performs the substitutions

$$r \equiv \rho e^{\mu/2}, \quad e^\lambda \equiv \left(1 + \frac{\rho}{2} \frac{d\mu}{d\rho}\right)^{-2} e^{\sigma-\mu}. \quad (2.174)$$

The standard Schwarzschild solution of the massless theory corresponds to

$$\begin{aligned}\nu(r) &= -\lambda(r) = \log\left(1 - \frac{R_S}{r}\right) \\ &= -\frac{R_S}{r} - \frac{1}{2}\left(\frac{R_S}{r}\right)^2 + \dots,\end{aligned}\quad (2.175)$$

$$\mu(r) = 0. \quad (2.176)$$

In the theory with massive graviton one rather finds, up to next-to-leading order in G (therefore in R_S),

$$\nu(r) = -\frac{R_S}{r} \left[1 + O\left(\frac{R_S}{m_g^4 r^5}\right) + \dots\right], \quad (2.177)$$

$$\lambda(r) = \frac{1}{2} \frac{R_S}{r} \left[1 + O\left(\frac{R_S}{m_g^4 r^5}\right) + \dots\right], \quad (2.178)$$

$$\mu(r) = -\frac{1}{2} \frac{R_S}{m_g^2 r^3} \left[1 + O\left(\frac{R_S}{m_g^4 r^5}\right) + \dots\right]. \quad (2.179)$$

If we limit ourselves to leading order, we observe that $\lambda(r)$ is smaller by a factor $1/2$ compared to the result in the massless theory. This is the origin of the vDVZ discontinuity. However, the surprise comes looking at the corrections, since they blow up if $m_g \rightarrow 0!$. In other words, in the massive theory the linearized expansion becomes invalid if we send $m_g \rightarrow 0$ at fixed r . This does not mean that linearized theory is completely useless: if we define the *Vainshtein radius* R_V ,

$$R_V = (R_S \lambda_g^4)^{1/5}, \quad (2.180)$$

where $\lambda_g = 1/m_g$, we see that the corrections are proportional to $(R_V/r)^5$. Therefore linearized theory is valid at $r \gg R_V$. We take $\lambda_g > 200$ kpc, in agreement with eq. (2.125) (with $h_0 \simeq 0.7$), and we consider the scattering of light from the Sun, which has $R_S \sim 3$ km. Then we get $R_V > 40$ pc, i.e. R_V is at least 10^7 times larger than the Earth–Sun distance. Therefore, the Newtonian potential found in eq. (2.169), and the result for the light deflection in the massive theory discussed below eq. (2.169), are simply not applicable at the solar system scale.

On the other hand, in the opposite limit $r \ll R_V$, it is possible to find a consistent expansion of the Schwarzschild solution in powers of m_g that, to lowest order, reproduces the Schwarzschild solution of the massless theory, of the form³⁰

$$\nu(r) = -\frac{R_S}{r} + O\left(m_g^2 \sqrt{R_S r^3}\right), \quad (2.181)$$

$$\lambda(r) = +\frac{R_S}{r} + O\left(m_g^2 \sqrt{R_S r^3}\right), \quad (2.182)$$

$$\mu(r) = \sqrt{\frac{8R_S}{13r}} + O(m_g^2 r^2). \quad (2.183)$$

³⁰The existence of such a solution depends on the specific form of the non-linear corrections to the Pauli–Fierz mass term, see Damour, Kogan and Pazoglou (2003).

³¹For example, consider the function $f(\epsilon, x) = e^{-\epsilon/x}$. If we expand it in powers of ϵ at fixed x we get $f(\epsilon, x) = 1 - (\epsilon/x) + (1/2)(\epsilon/x)^2 + \dots$. Of course, this expansion is not suitable for studying the limit $x \rightarrow 0$, since the various terms are more and more singular. However, if one knows the full resummed expression $e^{-\epsilon/x}$, one realizes that, for $\epsilon > 0$, the limit $x \rightarrow 0^+$ exists, and is in this case zero. In our case the role of ϵ is played by R_S and the role of x by m_g .

Therefore, at $r \ll R_V$, there is no mass discontinuity. To prove that there is no mass discontinuity altogether, one should be able to resum the whole perturbative expansion (2.177–2.179), which is valid at $r \gg R_V$, and it is in principle possible that, in the resummed expression, there is no singularity as $m_g \rightarrow 0$.³¹ If one can show that such a resummed solution, as we approach $r \sim R_V$, matches smoothly the solution (2.181)–(2.183), which is valid at $r \ll R_V$, we have constructed a solution with a smooth limit $m_g \rightarrow 0$, valid for all r . Observe also that, since the linearized theory does not apply at the solar system scale, there is no need to require $\tilde{\kappa}^2 = (3/4)\kappa^2$. On the contrary, since at $r \ll R_V$ the expansion in m_g reproduces smoothly the massless limit, we must choose $\tilde{\kappa} = \kappa$, and all the results of the massive theory, from the Newtonian potential to the light deflection, go smoothly into those of the massless theory. At $r \gg R_V$, instead, where linearized theory can be trusted, we get a gravitational potential

$$V(r) = -\frac{4}{3} \frac{Gm_1m_2}{r} \exp\{-m_gr\}, \quad (2.184)$$

since we have fixed $\tilde{\kappa} = \kappa$. In conclusion, in this scenario, inside the Vainshtein radius a tiny graviton mass has negligible effects, while at $r \gg R_V$ the graviscalar becomes effective, and gives a further attractive contribution to the gravitational potential.

To prove that this what actually happens requires to show that the solutions found in the regimes $r \ll R_V$ and $r \gg R_V$ do match. This is a non-trivial problem, because the solution (2.181)–(2.183) is obtained from an expansion in m_g while the solution (2.177)–(2.179) is non-analytic in m_g , since we have seen that it diverges as $m_g \rightarrow 0$. Conversely, the solution (2.177)–(2.179) is obtained performing an expansion in G , while the solution (2.181)–(2.183) is non-analytic in G , since $\mu(r) \sim \sqrt{R_S} \sim \sqrt{G}$. Put it differently, the difficulty of the problem is that, as we approach R_V from the large distance region, the graviscalar becomes strongly coupled, and perturbation theory breaks down.

Numerical studies of the inward continuation of asymptotically flat solutions indicate that, for small m_g , they end up in a singularity at finite radius, rather than matching a continuous solution inside the Vainshtein radius. It is possible however that the matching takes place not for asymptotically flat solution but for asymptotically De Sitter solution. This would be physically acceptable, given the experimental evidence for a cosmological constant, and also because for m_g sufficiently small the value of R_V can be larger than the Hubble radius, in which case the form of the solution at $r \gg R_V$ is not physically relevant.

A further complication is that, in curved space, the trace degree of freedom h , which in linearized theory is eliminated through eq. (2.151), becomes dynamical again, so we have six degrees of freedom rather than five, and furthermore it is a ghost. In fact, in the theory with action (2.172), i.e. full Einstein gravity supplemented by a mass term, the linearized equation of motion (2.147) is replaced by

$$G_{\mu\nu} = \frac{\tilde{\kappa}}{4} T_{\mu\nu} - \frac{1}{2} m_g^2 [ah_{\mu\nu} + bh\eta_{\mu\nu} + O(h_{\mu\nu}^2)], \quad (2.185)$$

where $G_{\mu\nu}$ is the full Einstein tensor, rather than its linearization that appears in eq. (2.147), and we also allowed for a generic mass term, including higher-order corrections (the Pauli–Fierz mass term corresponds to $a = -b = 1$). Using the Bianchi identity $D^\mu G_{\mu\nu} = 0$ as well as the covariant conservation of the energy–momentum tensor, we get the four conditions

$$m_g^2 D^\mu [ah_{\mu\nu} + bh\eta_{\mu\nu} + O(h_{\mu\nu}^2)] = 0, \quad (2.186)$$

which replace their linearized version (2.149) and again allow us to eliminate four degrees of freedom. The elimination of these degrees of freedom is therefore a consequence of the Bianchi identity, or, equivalently, of the invariance of the Einstein–Hilbert action under diffeomorphisms. On the other hand, the elimination of h in linearized theory, eq. (2.151), is not ensured by any symmetry, but is a consequence of the fine-tuning in the mass term that leads to the Pauli–Fierz combination. Then, this constraint does not survive in curved space, and h becomes dynamical again and it can be shown to be ghost-like, see the Further Reading section for discussions.

Thus, presently the issue of the consistency of a field theory of massive gravitons is not settled. If, in some form, a continuous solution indeed exists, then the limit $m_g \rightarrow 0$ is smooth and it makes sense to deform Einstein gravity by adding a small mass term for the graviton, with a value bounded experimentally by (2.126). Otherwise, one should accept the (rather odd) conclusion that the graviton mass must be identically zero. We finally observe that it is possible to add mass terms that break Lorentz invariance (which indeed emerge quite naturally if one breaks spontaneously the diffeomorphism invariance of general relativity), and in this case there are neither ghosts nor the vDVZ discontinuity. Again, we refer the reader to the Further Reading section.

2.4 Solved problems

Problem 2.1. The helicity of gravitons

We have seen that, for a given propagation direction $\hat{\mathbf{n}}$, a GW is described by a 2×2 matrix in the plane orthogonal to $\hat{\mathbf{n}}$, with matrix elements given in terms of the amplitudes h_+ and h_\times of the two polarization. The Lorentz transformations that leave invariant the propagation direction $\hat{\mathbf{n}}$ are the rotations around the $\hat{\mathbf{n}}$ axis and the boosts in the $\hat{\mathbf{n}}$ direction. Under these operations h_+ and h_\times will therefore transform between themselves. In this problem, we compute explicitly the transformation of h_+ and h_\times under rotations around the $\hat{\mathbf{n}}$ axis and under boosts in the $\hat{\mathbf{n}}$ direction.

In general, under a Lorentz transformation $x^\mu \rightarrow x'^\mu = \Lambda^\mu{}_\nu x^\nu$, a tensor $h_{\mu\nu}$ transforms as

$$h_{\mu\nu}(x) \rightarrow h'_{\mu\nu}(x') = \Lambda_\mu{}^\rho \Lambda_\nu{}^\sigma h_{\rho\sigma}(x). \quad (2.187)$$

Choosing $\hat{\mathbf{n}} = \hat{\mathbf{z}}$, a rotation around the z axis and a boost along z are written

respectively as

$$\Lambda = \begin{pmatrix} 1 & 0 & 0 & 0 \\ 0 & \cos \psi & -\sin \psi & 0 \\ 0 & \sin \psi & \cos \psi & 0 \\ 0 & 0 & 0 & 1 \end{pmatrix} \quad (\text{rotation}), \quad (2.188)$$

and

$$\Lambda = \begin{pmatrix} \cosh \eta & 0 & 0 & -\sinh \eta \\ 0 & 1 & 0 & 0 \\ 0 & 0 & 1 & 0 \\ -\sinh \eta & 0 & 0 & \cosh \eta \end{pmatrix} \quad (\text{boost}), \quad (2.189)$$

where Λ denote the matrix whose elements are Λ_μ^ν ; ψ is the rotation angle and η is related to the velocity v of the boost by $v = \tanh \eta$. Writing eq. (2.187) in the TT gauge we have

$$(h_{ab}^{\text{TT}})'(x') = \begin{pmatrix} h'_+ & h'_\times \\ h'_\times & -h'_+ \end{pmatrix}_{ab} e^{ikx}, \quad (2.190)$$

where

$$\begin{pmatrix} h'_+ & h'_\times \\ h'_\times & -h'_+ \end{pmatrix}_{ab} = \Lambda_a^c \Lambda_b^d \begin{pmatrix} h_+ & h_\times \\ h_\times & -h_+ \end{pmatrix}_{cd}, \quad (2.191)$$

and a, b take the value 1, 2. Since $kx = k'x'$, where k' is the four-momentum in the new frame, we can also rewrite eq. (2.190) as

$$(h_{ab}^{\text{TT}})'(x') = \begin{pmatrix} h'_+ & h'_\times \\ h'_\times & -h'_+ \end{pmatrix}_{ab} e^{ik'x'} \quad (2.192)$$

or, since x' is generic,

$$(h_{ab}^{\text{TT}})'(x) = \begin{pmatrix} h'_+ & h'_\times \\ h'_\times & -h'_+ \end{pmatrix}_{ab} e^{ik'x}. \quad (2.193)$$

Using eq. (2.191), with Λ_a^c given by the 2×2 submatrix made by the second and third rows and columns of eq. (2.188), and performing the matrix multiplication, we get

$$\begin{aligned} h'_+ &= h_+ \cos 2\psi - h_\times \sin 2\psi, \\ h'_\times &= h_+ \sin 2\psi + h_\times \cos 2\psi. \end{aligned} \quad (2.194)$$

Under boosts, the matrix Λ_a^c (i.e. the 2×2 submatrix made by the second and third rows and columns of eq. (2.189)) is just the 2×2 identity matrix, so $h'_+ = h_+$ and $h'_\times = h'_\times$. The GW amplitudes h_+ and h_\times are therefore invariant under boosts.

From eq. (2.194) we see that, under rotations around the z axis, the combinations $h_\times \pm ih_+$ transform as

$$(h_\times \pm ih_+) \rightarrow e^{\mp 2i\psi} (h_\times \pm ih_+). \quad (2.195)$$

To understand the meaning of this transformation law, we recall some basic results from the theory of representations of the Poincaré group (see, e.g. Maggiore 2005, Chapter 2). The Poincaré group has two types of physically interesting representations:

- massive representation, which are labeled by the mass m , with $-P_\mu P^\mu = m^2 > 0$ (where P^μ is the four-momentum) and by the spin j , which (in units of \hbar) can take integer or half-integer values, $j = 0, 1/2, 1, \dots$. The representation with spin j has dimension $2j+1$. Physically, this follows from the fact that for a massive particle exists the rest frame, and in the rest frame the component along the z axis of the spin, for a particle with spin j , can take the $2j+1$ possible values $j_z = -j, -j+1, \dots, j$. So, in particular, a massive spin-1 particle has three degrees of freedom and a massive spin-2 particle has five degrees of freedom.
- massless representation, which are characterized by $P_\mu P^\mu = 0$ and by a quantum number j , which again can be integer or half-integer. For massless particles the rest frame does not exist and the previous argument about the existence of $2j+1$ states does not go through. Rather, these representations are one-dimensional, and are characterized by a definite value of the *helicity*, which is defined as the projection of the total angular momentum on the direction of motion,³²

$$h = \mathbf{J} \cdot \hat{\mathbf{n}}. \quad (2.196)$$

The total angular momentum is the sum of orbital and spin angular momenta, $\mathbf{J} = \mathbf{L} + \mathbf{S}$. Of course $\mathbf{L} \cdot \hat{\mathbf{n}} = (\mathbf{x} \times \mathbf{p}) \cdot \hat{\mathbf{n}} = 0$ since $\mathbf{p} = |\mathbf{p}| \hat{\mathbf{n}}$, and therefore the helicity is equal to the projection of the spin on the direction of motion, $h = \mathbf{S} \cdot \hat{\mathbf{n}}$.

Under a rotation by an angle ψ around the direction of motion a helicity eigenstate $|h\rangle$ transforms as

$$|h\rangle \rightarrow e^{ih\psi} |h\rangle. \quad (2.197)$$

Massless representations can have either $h = +j$ or $h = -j$. Each of these possibilities, separately, provides a one-dimensional representation of the Poincaré group: the states with $h = \pm j$ do not mix between them under (proper) spatial rotations, boosts nor translations. However, under a parity transformation $\hat{\mathbf{n}}$ changes sign, while the angular momentum is a pseudovector and is unchanged. Therefore the helicity is a pseudoscalar, i.e. it changes sign under parity, $h \rightarrow -h$. For this reason, in a theory which conserves parity (like gravity or electromagnetism) it is more convenient to define particles as representations of the Poincaré group *and* of parity, that is, to assemble the two Poincaré representations with $h = \pm j$ and to consider them as two polarization states of the same particle. The photon is then defined as a massless particle with two helicity states $h = \pm 1$, while the graviton is defined as a massless particle with two helicity states $h = \pm 2$. On the contrary, since weak interactions violate parity, in the limit in which the neutrinos can be taken as massless (there is nowadays evidence for a small neutrino mass from oscillation experiments), we reserve the name neutrino to the one-dimensional massless Poincaré representation with $h = -1/2$, while the antineutrino is defined as the representation with $h = +1/2$.³³

In the light of these results, we see that eq. (2.195), together with the fact that h_{ij}^{TT} satisfies the massless Klein–Gordon equation $\square h_{ij}^{\text{TT}} = 0$, means that the quanta of the gravitational field are massless particles, and the combinations $h_\times \mp ih_+$ are the helicity eigenstates and have helicities ± 2 , respectively.

³²The symbol h is traditionally used for the helicity, and of course it should not be confused with the GW amplitudes h_+ and h_\times .

³³The fact that, for each massless representation with a given helicity, there is a corresponding representation with the opposite helicity is a consequence of the CPT symmetry, which is present in any Lorentz-invariant quantum field theory with a hermitian Hamiltonian.

Problem 2.2. Angular momentum and parity of graviton states

In this problem we examine the possible angular momentum states of the graviton. Let us first recall how such an analysis works for the photon, following Landau and Lifshitz, Vol. IV (1982), Section 6. After choosing the radiation gauge $A_0 = 0$ and $\nabla \cdot \mathbf{A} = 0$, a photon is described by a vector $\mathbf{A}(\mathbf{x})$ or, in momentum space, by $\tilde{\mathbf{A}}(\mathbf{k})$, subject to the transversality condition $\mathbf{k} \cdot \tilde{\mathbf{A}}(\mathbf{k}) = 0$. Let us at first neglect the transversality condition. The vector character of $\tilde{\mathbf{A}}(\mathbf{k})$ then corresponds to spin $s = 1$, and the total angular momentum j of a photon is given by the combination of $s = 1$ and of the orbital angular momentum l , with the usual composition rule of angular momenta in quantum mechanics. This means that a state with $j = 0$ can be obtained in only one possible way, i.e. combining the spin $s = 1$ with $l = 1$, while there are three states for each $j \neq 0$, which are obtained with $l = j, j \pm 1$ (for the purpose of this counting we consider a state with momentum j as one single state, regardless of the $2j + 1$ possible components of j_z).

To understand what is the parity of these states it is convenient to write explicitly their wavefunction. Just as the angular dependence of a scalar function can be expanded in terms of the (scalar) spherical harmonics $Y_{lm}(\theta, \phi)$, the angular dependence of a vector function $\mathbf{A}(\mathbf{x})$ can be expressed in vector spherical harmonics. As we will discuss in more detail in Section 3.5.2, see in particular eq. (3.247), these can be written as

$$\mathbf{Y}_{jj_z}^l(\theta, \phi) = \sum_{l_z=-l}^l \sum_{s_z=0,\pm 1} \langle 1l s_z l_z | jj_z \rangle Y_{ll_z}(\theta, \phi) \boldsymbol{\xi}^{(s_z)}. \quad (2.198)$$

where $\boldsymbol{\xi}^{(s_z)}$ is the wavefunction of a spin-1 particle with a given value s_z of the projection of the spin on the z axis, and $\langle 1l s_z l_z | jj_z \rangle$ are the Clebsch–Gordan coefficient necessary to combine a spin state $|ss_z\rangle$ with $s = 1$ and an orbital angular momentum state $|ll_z\rangle$, so to obtain a total angular momentum $|jj_z\rangle$. In terms of the unit vectors \mathbf{e}_x , \mathbf{e}_y and \mathbf{e}_z of a Cartesian reference frame, the explicit form of the spin wavefunction is

$$\boldsymbol{\xi}^{(\pm 1)} = \mp \frac{1}{\sqrt{2}} (\mathbf{e}_x \pm i\mathbf{e}_y), \quad \boldsymbol{\xi}^{(0)} = \mathbf{e}_z. \quad (2.199)$$

³⁴In general, we can define parity either changing the sign of vectors with respect to a fixed reference frame, or reversing the orientation of the axes of the reference frame while keeping the vectors fixed. Here we adopt the latter point of view.

Consider a parity transformation, defined so that it changes the sign of the orientation of the axes of the reference frame, $\mathbf{e}_i \rightarrow -\mathbf{e}_i$.³⁴ Under this transformation, the state (2.198) picks a factor $P = (-1)^{l+1}$, where the $(-1)^l$ comes from the transformation of the scalar spherical harmonics and the further minus sign comes from the spin wavefunction. Thus, we can summarize as follows the possible states before imposing the condition $\mathbf{k} \cdot \tilde{\mathbf{A}}(\mathbf{k}) = 0$,

$$\begin{aligned} j = 0 : & \text{ one state, } (l = 1, P = +), \\ j = 1 : & \text{ three states, } (l = 0, P = -), (l = 1, P = +), (l = 2, P = -), \\ j = 2 : & \text{ three states, } (l = 1, P = +), (l = 2, P = -), (l = 3, P = +), \end{aligned} \quad (2.200)$$

and similarly we have three states for all higher values of j . We now impose the transversality condition $\mathbf{k} \cdot \tilde{\mathbf{A}}(\mathbf{k}) = 0$. This means that we remove a longitudinal state of the form $\tilde{\mathbf{A}}(\mathbf{k}) = \phi(\mathbf{k})\mathbf{k}$. The number of states of this form is therefore the same as the number of states of a scalar particles with wavefunction $\phi(\mathbf{k})$ (or, equivalently, of the scalar degree of freedom described by $\nabla \cdot \mathbf{A}$). When we develop ϕ in spherical harmonics, the total angular momentum j of

such a state is equal to the order l of the spherical harmonic, and its parity is $P = (-1)^j$. Thus, at each level j we must remove from eq. (2.200) one spurious state, with $P = (-1)^j$. Therefore at level $j = 0$ we end up with no physical states, while at all higher levels we end up with two physical states of opposite parity. This shows that for the photon there can be no monopole radiation, because there is no physical photon state with $j = 0$, while for all other values of j we have two physical states. For instance, the states with $j = 1$ correspond to an electric dipole photon ($P = -$) and a magnetic dipole photon ($P = +$).

Having understood the argument for the photon, we can adapt it to the graviton. The graviton is described by a 2×2 traceless symmetric tensor $\tilde{h}_{ij}(\mathbf{k})$ subject to the transversality condition $k^i \tilde{h}_{ij}(\mathbf{k}) = 0$. Again, we neglect at first the transversality condition. A symmetric traceless tensor corresponds to spin $s = 2$, while the parity on a true tensor is $P = (-1)^l$. Then, combining the orbital angular momentum with the spin $s = 2$, we have the following states

$$\begin{aligned} j = 0 : & \text{ one state, } (l = 2, P = +) \\ j = 1 : & \text{ three states, } (l = 1, P = -), (l = 2, P = +), (l = 3, P = -) \\ j = 2 : & \text{ five states, } (l = 0, P = +), (l = 1, P = -), (l = 2, P = +), \\ & (l = 3, P = -), (l = 4, P = +). \end{aligned} \quad (2.201)$$

Similarly for all higher j there are five states, two with $P = +$, two with $P = -$ and one more with $P = (-1)^j$. We now impose the transversality condition. The most general traceless symmetric tensor which does *not* satisfy the transversality condition has the form

$$\tilde{h}_{ij}(\mathbf{k}) = a_i(\mathbf{k})k_j + a_j(\mathbf{k})k_i + b(\mathbf{k})(k_i k_j - \frac{1}{3}\delta_{ij}|\mathbf{k}|^2), \quad (2.202)$$

with $k^i a_i(\mathbf{k}) = 0$, in order to respect the condition of zero trace. The most general spurious state is therefore parametrized by a scalar b and by a transverse vector a_i . Exactly as with the scalar ϕ found above, expanding b in spherical harmonics we have one state for each j , with parity $P = (-1)^j$. This eliminates the state with $j = 0$ in eq. (2.201), while at level $j = 1$ it leaves us with one state with $P = +1$ and one with $P = -1$, and at all higher j levels we are left with two states with $P = +1$ and two with $P = -1$. Finally, we must remove the spurious states described by $a_i(\mathbf{k})$. However this is a vector, transverse to \mathbf{k} , and therefore its states are the same as the photon states discussed above. There is no state at $j = 0$, and two states, with opposite parity, at all other j level. This remove the two states which were left at $j = 1$, and leaves us with two states, with opposite parity, at all higher levels. In conclusion, for the graviton,

$$\begin{aligned} j = 0 : & \text{ no state,} \\ j = 1 : & \text{ no state,} \\ j = 2, 3, \dots : & \text{ two states, one with } P = +, \text{ one with } P = -. \end{aligned} \quad (2.203)$$

Therefore, for gravitational wave there can be no monopole nor dipole radiation, since these would correspond to gravitons with $j = 0$ and $j = 1$, respectively. We will come back to the multipole expansion of gravitational waves in Section 3.5.2, where we will show how to express the two states allowed for $j \geq 2$ in terms of tensor spherical harmonics, and we will verify again that states with $j = 0$ or $j = 1$ are not allowed.

Further reading

- For the quantum field-theoretical approach to gravitation see the *Feynman Lectures on Gravitation* by Feynman, Morinigo, and Wagner (1995) (which collects lectures given by Feynman in 1962–63), and also DeWitt (1967) and Veltman (1976). For explicit computations of graviton–graviton scattering see Grisaru, van Nieuwenhuizen and Wu (1975).
- The possibility of deriving Einstein equation from an iteration of linearized theory is discussed, among others, by Gupta (1954), Kraichnan (1955), Feynman, Morinigo, and Wagner (1995), and Ogievetsky and Polubarinov (1965). An explicit and elegant iteration leading from the equations of motion of linearized theory to the full Einstein equations was performed by Deser (1970) using a first order Palatini formalism. The ambiguity concerning boundary terms is discussed by Padmanabhan (2004).
- Phenomenological limits on the graviton mass are discussed by Goldhaber and Nieto (1974). The discontinuity as the graviton mass goes to zero was found by Iwasaki (1970), van Dam and Veltman (1970) and Zakharov (1970). Massive gravitons have been further discussed by Boulware and Deser (1972). The fact that linearized theory becomes singular as $m_g \rightarrow 0$ was discovered by Vainshtein (1972). The radiation of massive gravitons in linearized theory is discussed by van Nieuwenhuizen (1973). Discussions of the fate of the discontinu-

ity are given in Deffayet, Dvali, Gabadadze and Vainshtein (2002) and in Arkani-Hamed, Georgi and Schwartz (2003). The difficulty of performing the matching to an asymptotically flat solution, and the possibility of matching to a De Sitter solution, is discussed in Damour, Kogan and Papazoglou (2003). The fact that beyond linearized theory the trace h becomes a ghost is discussed by Boulware and Deser (1972) and, in full generality, by Creminelli, Nicolis, Papucci and Trincherini (2005).

- Lorentz-violating mass terms for $h_{\mu\nu}$ are discussed in Arkani-Hamed, Cheng, Luty and Mukohyama (2004), Rubakov (2004) and Dubovsky, Tinyakov and Tkachev (2005). In this case the mass of the scalar perturbations can be zero while the mass of the graviton h_{ij}^{TT} can be non-zero, and the bounds on the graviton mass derived from the Yukawa fall-off of the gravitational potential only refer to the scalar sector. Furthermore, these models do not suffer of the vDVZ discontinuity and do not have ghosts.

A bound on the mass that refers directly to h_{ij}^{TT} can be obtained from pulsar timing, as recognized in Damour and Taylor (1991) and discussed quantitatively in Finn and Sutton (2002). The possibility of bounding the mass of h_{ij}^{TT} from the observation of inspiraling compact binaries is discussed in Will (1998) and Larson and Hiscock (2000).

Generation of GWs in linearized theory

3

We now consider the generation of GWs in the context of linearized theory. This means that we assume that the gravitational field generated by the source is sufficiently weak, so that the background space-time can be taken as *flat*. This will allow us to understand, in the simple setting of a flat background space-time (and therefore Newtonian or at most special-relativistic dynamics for the sources), how GWs are produced. In Section 3.1 we will derive the formulas for GW production valid in flat space-time, but exact in v/c . Then, expanding the exact result in powers of v/c , we will see that for small velocities the GW production can be organized in a multipole expansion (Section 3.2). In Section 3.3 we discuss in detail the lowest order term, which is the quadrupole radiation. In Section 3.4 we discuss the next-to-leading terms, i.e. the mass-octupole and the current quadrupole radiation, and in Section 3.5 we present the systematic multipole expansion to all orders, using first the formalism of symmetric-trace-free (STF) tensors, and then the spherical tensors formalism. Finally, in a Solved Problems section we discuss some applications of this formalism and we collect additional technical material.

For a system whose dynamics is determined by non-gravitational forces, the weak-field expansion and the low-velocity expansion are independent, and in this case it makes sense to consider weak-field sources with arbitrary velocities, as we do in this chapter. The application of this formalism to a system held together by gravitational forces is more subtle. For a gravitationally-bound two-body system with reduced mass μ and total mass m , we have $E_{\text{kin}} = -(1/2)U$, i.e.

$$\frac{1}{2}\mu v^2 = \frac{1}{2} \frac{G\mu m}{r}, \quad (3.1)$$

and therefore

$$\frac{v^2}{c^2} = \frac{R_S}{2r}, \quad (3.2)$$

where $R_S = 2Gm/c^2$ is the Schwarzschild radius associated to a mass m . Therefore, the low-velocity expansion is not independent of the expansion in powers of G .

The most interesting astrophysical sources of GWs, such as neutron stars, black holes or compact binaries, are self-gravitating systems. In this case, if we want to compute corrections in v/c , we must take into

3.1 Weak-field sources with arbitrary velocity	102
3.2 Low-velocity expansion	105
3.3 Mass quadrupole	109
3.4 Mass octupole and current quadrupole	125
3.5 Systematic multipole expansion	131
3.7 Solved problems	156

account that, because of eq. (3.2), space-time cannot be considered flat beyond lowest order, and therefore the dynamics of the sources can no longer be described by Newtonian gravity. The corresponding formalism is the GW generation from post-Newtonian sources, which will be the subject of Chapter 5. However we will see in Sect. 3.3.5 that, even for self-gravitating system, some lowest-order computations for the mass quadrupole and even mass octupole and current quadrupole terms can be consistently performed within linearized theory.

3.1 Weak-field sources with arbitrary velocity

In linearized theory the starting point is eq. (1.24), that we recall here,

$$\square \bar{h}_{\mu\nu} = -\frac{16\pi G}{c^4} T_{\mu\nu}, \quad (3.3)$$

where $T_{\mu\nu}$ is the energy-momentum tensor of matter. Recall also that we are in the Lorentz gauge, $\partial^\mu \bar{h}_{\mu\nu} = 0$, and that $T_{\mu\nu}$ satisfies the flat-space conservation law $\partial^\mu T_{\mu\nu} = 0$. Equation (3.3) is linear in $h_{\mu\nu}$ and can be solved by the method of Green's function: if $G(x - x')$ is a solution of the equation

$$\square_x G(x - x') = \delta^4(x - x'), \quad (3.4)$$

(where \square_x is the d'Alembertian operator with derivatives taken with respect to the variable x), then the corresponding solution of eq. (3.3) is

$$\bar{h}_{\mu\nu}(x) = -\frac{16\pi G}{c^4} \int d^4 x' G(x - x') T_{\mu\nu}(x'). \quad (3.5)$$

The solution of eq. (3.4) depends of course on the boundary conditions that we impose. Just as in electromagnetism, for a radiation problem the appropriate solution is the *retarded Green's function*,¹

$$G(x - x') = -\frac{1}{4\pi|\mathbf{x} - \mathbf{x}'|} \delta(x_{\text{ret}}^0 - x'^0), \quad (3.6)$$

where $x'^0 = ct'$, $x_{\text{ret}}^0 = ct_{\text{ret}}$, and

$$t_{\text{ret}} = t - \frac{|\mathbf{x} - \mathbf{x}'|}{c} \quad (3.7)$$

is called retarded time. Then the solution of eq. (3.3) is

$$\bar{h}_{\mu\nu}(t, \mathbf{x}) = \frac{4G}{c^4} \int d^3 x' \frac{1}{|\mathbf{x} - \mathbf{x}'|} T_{\mu\nu} \left(t - \frac{|\mathbf{x} - \mathbf{x}'|}{c}, \mathbf{x}' \right). \quad (3.8)$$

Outside the source we can put this solution in the TT gauge using eq. (1.40), $h_{ij}^{\text{TT}} = \Lambda_{ij,kl} h_{kl} = \Lambda_{ij,kl} \bar{h}_{kl}$ (in the last equality we used the

¹More precisely, the retarded Green's function is selected by imposing the Kirchoff–Sommerfeld “no-incoming-radiation” boundary conditions, i.e. one imposes

$$\lim_{t \rightarrow -\infty} \left[\frac{\partial}{\partial r} + \frac{\partial}{\partial t} \right] (r \bar{h}_{\mu\nu})(\mathbf{x}, t) = 0,$$

where the limit is taken along any surface $ct + r = \text{constant}$, together with the condition that $r \bar{h}_{\mu\nu}$ and $r \partial_\rho \bar{h}_{\mu\nu}$ be bounded in this limit. Physically, this means that there is no incoming radiation at past null infinity.

property (1.38) of the Lambda tensor). Therefore, outside the source,

$$h_{ij}^{\text{TT}}(t, \mathbf{x}) = \frac{4G}{c^4} \Lambda_{ij,kl}(\hat{\mathbf{n}}) \int d^3x' \frac{1}{|\mathbf{x} - \mathbf{x}'|} T_{kl} \left(t - \frac{|\mathbf{x} - \mathbf{x}'|}{c}, \mathbf{x}' \right), \quad (3.9)$$

where we use the notation $\hat{\mathbf{x}} = \hat{\mathbf{n}}$, and we will also denote $|\mathbf{x}| = r$. Observe that h_{ij}^{TT} depends only the integrals of the spatial components T_{kl} . The underlying reason that allowed us to eliminate T_{0k} and T_{00} is that they are related to T_{kl} by the conservation of the energy-momentum tensor.² If we denote by d the typical radius of the source, at $r \gg d$ we can expand

$$|\mathbf{x} - \mathbf{x}'| = r - \mathbf{x}' \cdot \hat{\mathbf{n}} + O\left(\frac{d^2}{r}\right), \quad (3.10)$$

see Fig. 3.1. We are particularly interested in the value of h_{ij}^{TT} at large distances from the source, where the detector is located, so we take the limit $r \rightarrow \infty$ at fixed t ,³ and we retain only the leading term in eq. (3.9). This is a term $O(1/r)$, obtained setting $|\mathbf{x} - \mathbf{x}'| = r$ in the denominator of eq. (3.9), so at large distances

$$h_{ij}^{\text{TT}}(t, \mathbf{x}) = \frac{1}{r} \frac{4G}{c^4} \Lambda_{ij,kl}(\hat{\mathbf{n}}) \int d^3x' T_{kl} \left(t - \frac{r}{c} + \frac{\mathbf{x}' \cdot \hat{\mathbf{n}}}{c}, \mathbf{x}' \right), \quad (3.11)$$

plus terms $O(1/r^2)$ that we neglect. We now write T_{kl} in terms of its Fourier transform,⁴

$$T_{kl}(t, \mathbf{x}) = \int \frac{d^4k}{(2\pi)^4} \tilde{T}_{kl}(\omega, \mathbf{k}) e^{-i\omega t + i\mathbf{k} \cdot \mathbf{x}}. \quad (3.12)$$

Then

$$\begin{aligned} & \int d^3x' T_{kl} (t - r/c + \mathbf{x}' \cdot \hat{\mathbf{n}}/c, \mathbf{x}') \\ &= \int d^3x' \int \frac{d\omega}{2\pi c} \frac{d^3k}{(2\pi)^3} \tilde{T}_{kl}(\omega, \mathbf{k}) e^{-i\omega(t-r/c)} e^{i(\mathbf{k} - \omega\hat{\mathbf{n}}/c) \cdot \mathbf{x}'} \\ &= \int \frac{d\omega}{2\pi c} \frac{d^3k}{(2\pi)^3} \tilde{T}_{kl}(\omega, \mathbf{k}) e^{-i\omega(t-r/c)} (2\pi)^3 \delta^{(3)}(\mathbf{k} - \omega\hat{\mathbf{n}}/c) \\ &= \int \frac{d\omega}{2\pi c} \tilde{T}_{kl}(\omega, \omega\hat{\mathbf{n}}/c) e^{-i\omega(t-r/c)}, \end{aligned} \quad (3.13)$$

and we get

$$h_{ij}^{\text{TT}}(t, \mathbf{x}) = \frac{1}{r} \frac{4G}{c^5} \Lambda_{ij,kl}(\hat{\mathbf{n}}) \int_{-\infty}^{\infty} \frac{d\omega}{2\pi} \tilde{T}_{kl}(\omega, \omega\hat{\mathbf{n}}/c) e^{-i\omega(t-r/c)}. \quad (3.14)$$

²Indeed, when performing the multipole expansion below, the lowest-order result will be re-expressed in terms of T^{00} only, using again energy-momentum conservation.

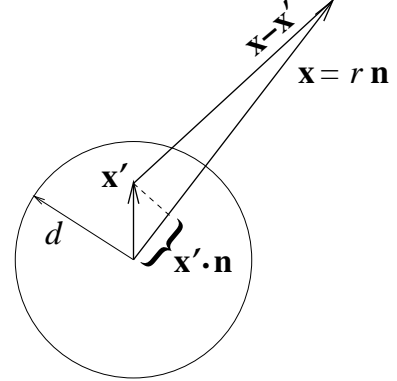


Fig. 3.1 A graphical illustration of the relation given in eq. (3.10).

³In linearized theory, GWs are studied at spatial infinity, i.e. $r \rightarrow \infty$ at fixed t . We will see in Chapter 5 that, beyond linearized theory, it can be more convenient to work at future null infinity, i.e. $r \rightarrow \infty$ with $t - r/c$ fixed.

⁴Our convention on the factors of c is that the four-dimensional wave-vector is $k^\mu = (\omega/c, \mathbf{k})$, and therefore $d^4k = (1/c)d\omega d^3k$. Since $x^\mu = (ct, \mathbf{x})$, we then have $k_\mu x^\mu = -\omega t + \mathbf{k} \cdot \mathbf{x}$. Observe that \mathbf{k} has dimensions of the inverse of length. The spatial momentum of a particle with wave-vector \mathbf{k} is $\mathbf{p} = \hbar\mathbf{k}$.

In general, the Fourier components of the energy-momentum tensor of the source will be large around a typical value ω_s , and the characteristic speed at which there is a bulk movement of mass across the source is $v \sim \omega_s d$. For the moment we have made no assumption on the relative values of ω_s and d , and in particular we have not assumed $\omega_s d \ll c$. Therefore eq. (3.14) is valid both for relativistic and for non-relativistic sources, as long as linearized theory applies, and we are at a sufficiently large distance r from the source.

From eq. (1.156), setting $dA = r^2 d\Omega$, we see that the total energy radiated per unit solid angle is

$$\frac{dE}{d\Omega} = \frac{r^2 c^3}{32\pi G} \int_{-\infty}^{\infty} dt \dot{h}_{ij}^{\text{TT}} \dot{h}_{ij}^{\text{TT}}. \quad (3.15)$$

Inserting here the expression (3.14), using $\tilde{T}(-\omega, -\mathbf{k}) = \tilde{T}^*(\omega, \mathbf{k})$ and the property (1.37) of the Lambda tensor, we find⁵

$$\frac{dE}{d\Omega} = \frac{G}{2\pi^2 c^7} \Lambda_{ij,kl}(\hat{\mathbf{n}}) \int_0^{\infty} d\omega \omega^2 \tilde{T}_{ij}(\omega, \omega \hat{\mathbf{n}}/c) \tilde{T}_{kl}^*(\omega, \omega \hat{\mathbf{n}}/c),$$

(3.16)

and the energy spectrum is therefore

$$\frac{dE}{d\omega} = \frac{G\omega^2}{2\pi^2 c^7} \int d\Omega \Lambda_{ij,kl}(\hat{\mathbf{n}}) \tilde{T}_{ij}(\omega, \omega \hat{\mathbf{n}}/c) \tilde{T}_{kl}^*(\omega, \omega \hat{\mathbf{n}}/c). \quad (3.17)$$

A typical source will radiate for a characteristic time Δt . In the idealized case of an exactly monochromatic source, the radiation lasts for $\Delta t = \infty$ and the total radiated energy is formally divergent.⁶ Thus, for a monochromatic source the instantaneously radiated power is a more useful quantity. For such a source, radiating at a frequency ω_0 , we write $\tilde{T}_{ij}(\omega, \mathbf{k})$ (for positive ω) as

$$\tilde{T}_{ij}(\omega, \mathbf{k}) = \theta_{ij}(\omega, \mathbf{k}) 2\pi\delta(\omega - \omega_0), \quad (3.18)$$

and eq. (3.16) becomes

$$\frac{dE}{d\Omega} = \frac{G\omega_0^2}{\pi c^7} \Lambda_{ij,kl}(\hat{\mathbf{n}}) \theta_{ij}(\omega_0, \omega_0 \hat{\mathbf{n}}/c) \theta_{kl}^*(\omega_0, \omega_0 \hat{\mathbf{n}}/c) T. \quad (3.19)$$

We have used $2\pi\delta(\omega = 0) = T$, where T is the total (formally infinite) time. Dividing by T we obtain the power radiated instantaneously,⁷

$$\frac{dP}{d\Omega} = \frac{G\omega_0^2}{\pi c^7} \Lambda_{ij,kl}(\hat{\mathbf{n}}) \theta_{ij}(\omega_0, \omega_0 \hat{\mathbf{n}}/c) \theta_{kl}^*(\omega_0, \omega_0 \hat{\mathbf{n}}/c). \quad (3.20)$$

The total power is obtained by integrating over $d\Omega$. To perform the integration one can use the identities

$$\int \frac{d\Omega}{4\pi} n_i n_j = \frac{1}{3} \delta_{ij}, \quad (3.21)$$

⁵To compare with Weinberg (1972), Section 10.4, observe that we define the Fourier transform with respect to frequency using $d\omega/(2\pi)$ (see eq. (3.12), or the Notation section) while Weinberg uses $d\omega$; on the other hand, we both use $d^3k/(2\pi)^3$ in the spatial Fourier transform. Therefore our $\tilde{T}(\omega, \mathbf{k})$ is equal to $2\pi \tilde{T}^{\text{Weinberg}}(\omega, \mathbf{k})$.

⁶Of course, at the latest this divergence is cutoff by the back-reaction due to GW emission. For example, a spinning neutron star with non-vanishing ellipticity emits GWs. The energy of these waves is taken from the rotational energy of the star which therefore gradually slows down, as we will compute in detail in Section 4.2. (Actually, in this case electromagnetic effects dominate and slow down the neutron star even earlier.)

⁷More precisely, we have seen in Chapter 1 that the GW energy is only defined by averaging over a few periods, so this is really the average power radiated over one period of the source motion.

$$\int \frac{d\Omega}{4\pi} n_i n_j n_k n_l = \frac{1}{15} (\delta_{ij}\delta_{kl} + \delta_{ik}\delta_{jl} + \delta_{il}\delta_{jk}) . \quad (3.22)$$

These identities, as well as their generalization to an arbitrary number of n 's, can be found as follows. For an odd number of n_i the integral vanishes because the integrand is odd under parity. For an even number of n , we use the fact that the tensor $n_{i_1} n_{i_2} \dots n_{i_{2l}}$ is totally symmetric and therefore its integral can only depend on the totally symmetrized product of Kronecker deltas. Once the tensor structure is fixed, the overall constant is obtained by contracting all indices. This gives

$$\int \frac{d\Omega}{4\pi} n_{i_1} \dots n_{i_{2l}} = \frac{1}{(2l+1)!!} (\delta_{i_1 i_2} \delta_{i_3 i_4} \dots \delta_{i_{2l-1} i_{2l}} + \dots) , \quad (3.23)$$

where the final dots denote all possible pairing of indices.

3.2 Low-velocity expansion

Just as in electrodynamics, the equations for the generation of radiation are greatly simplified if the typical velocities inside the source are small compared to the speed of light. If ω_s is the typical frequency of the motion inside the source and d is the source size, the typical velocities inside the source are $v \sim \omega_s d$. The frequency ω of the radiation will also be of order⁸ ω_s and therefore $\omega \sim \omega_s \sim v/d$. In terms of $\lambda = c/\omega$,

$$\lambda \sim \frac{c}{v} d . \quad (3.24)$$

In a non-relativistic system, $v \ll c$ and the reduced wavelength of the radiation generated is much bigger than the size of the system:

non-relativistic sources $\implies \lambda \gg d .$

(3.25)

When the reduced wavelength is much bigger than the size of the system, it is physically clear that we do not need to know the internal motions of the source in all its details, but only the coarse features matter, so the emission of radiation is governed by the lowest multipole moments.⁹

To perform the multipole expansion for gravitational radiation we start from the expression of h_{ij}^{TT} at spatial infinity given in eq. (3.11), that we recall here,

$$h_{ij}^{\text{TT}}(t, \mathbf{x}) = \frac{1}{r} \frac{4G}{c^4} \Lambda_{ij,kl}(\hat{\mathbf{n}}) \int d^3x' T_{kl} \left(t - \frac{r}{c} + \frac{\mathbf{x}' \cdot \hat{\mathbf{n}}}{c}, \mathbf{x}' \right) , \quad (3.26)$$

and we write T_{kl} in terms of its Fourier transform,

$$T_{kl} \left(t - \frac{r}{c} + \frac{\mathbf{x}' \cdot \hat{\mathbf{n}}}{c}, \mathbf{x}' \right) = \int \frac{d^4k}{(2\pi)^4} \tilde{T}_{kl}(\omega, \mathbf{k}) e^{-i\omega(t-r/c+\mathbf{x}' \cdot \hat{\mathbf{n}}/c)+i\mathbf{k} \cdot \mathbf{x}'} . \quad (3.27)$$

For a non-relativistic source, $\tilde{T}_{kl}(\omega, \mathbf{k})$ is peaked around a typical frequency ω_s (or around a range of frequencies, with maximum value ω_s),

⁸Apart from numerical factors which depend on the multipole moment involved and on the details of the motion of the source. We will see below that for a non-relativistic system the dominant contributions come from the lowest multipoles, and for these the numerical factors are $O(1)$; for instance, we will see that a source performing a simple harmonic oscillation at frequency ω_s emits quadrupole radiation $\omega = 2\omega_s$.

⁹A typical example is the electromagnetic radiation from the hydrogen atom. The velocity of the electron inside the hydrogen atom is $v/c \sim \alpha$, where $\alpha \simeq 1/137$ is the fine-structure constant, and the reduced wavelengths of the transitions between the levels of the hydrogen atom are of order $\lambda \sim r_B/\alpha$, where r_B is the Bohr radius. Since $\alpha \ll 1$, we have $\lambda \gg r_B$, and the multipole expansion is adequate.

with $\omega_s d \ll c$. On the other hand, the energy-momentum tensor is non-vanishing only inside the source, so the integral in eq. (3.26) is restricted to $|\mathbf{x}'| \leq d$. Then the dominant contribution to h_{ij}^{TT} comes from frequencies ω that satisfy

$$\frac{\omega}{c} \mathbf{x}' \cdot \hat{\mathbf{n}} \lesssim \frac{\omega_s d}{c} \ll 1, \quad (3.28)$$

and therefore we can expand the exponential in eq. (3.27),

$$\begin{aligned} e^{-i\omega(t-r/c+\mathbf{x}'\cdot\hat{\mathbf{n}}/c)} &= e^{-i\omega(t-r/c)} \\ &\times \left[1 - i\frac{\omega}{c} x'^i n^i + \frac{1}{2} \left(-i\frac{\omega}{c} \right)^2 x'^i x'^j n^i n^j + \dots \right]. \end{aligned} \quad (3.29)$$

This is equivalent to expanding

$$\begin{aligned} T_{kl} \left(t - \frac{r}{c} + \frac{\mathbf{x}' \cdot \hat{\mathbf{n}}}{c}, \mathbf{x}' \right) &\simeq T_{kl}(t - \frac{r}{c}, \mathbf{x}') \\ &+ \frac{x'^i n^i}{c} \partial_t T_{kl} + \frac{1}{2c^2} x'^i x'^j n^i n^j \partial_t^2 T_{kl} + \dots \end{aligned} \quad (3.30)$$

¹⁰One could have directly written the expansion (3.30), as a formal Taylor expansion in the parameter $\mathbf{x}' \cdot \hat{\mathbf{n}}/c$. However, the above derivation emphasizes that the assumption behind this expansion is the condition $\omega_s d \ll c$, with ω_s the typical source frequency.

¹¹Observe that, contrary to most of the literature on general relativity, we never use commas to denote derivatives (nor semicolons to denote covariant derivatives).

where all derivatives are evaluated at the point $(t - r/c, \mathbf{x}')$.¹⁰ We now define the momenta of the stress tensor T^{ij} ,

$$S^{ij}(t) = \int d^3x T^{ij}(t, \mathbf{x}), \quad (3.31)$$

$$S^{ij,k}(t) = \int d^3x T^{ij}(t, \mathbf{x}) x^k, \quad (3.32)$$

$$S^{ij,kl}(t) = \int d^3x T^{ij}(t, \mathbf{x}) x^k x^l, \quad (3.33)$$

and similarly for all higher order momenta. In this notation, a comma separates the spatial indices which originates from T^{ij} from the indices coming from $x^{i_1} \dots x^{i_N}$.¹¹ The energy-momentum tensor of matter that appears in eq. (3.3) is the one obtained from the variation of the matter action with respect to the metric, so it is in its symmetric form, $T^{ij} = T^{ji}$. Then, its momenta are symmetric separately in the first type of indices and in the second, e.g. $S^{ij,k} = S^{ji,k}$ or $S^{ij,kl} = S^{ij,lk}$, but not necessarily under the exchange of two indices of different type, e.g. in general $S^{ij,k} \neq S^{ik,j}$.

Inserting the expansion (3.30) into eq. (3.26) we get

$$\begin{aligned} h_{ij}^{\text{TT}}(t, \mathbf{x}) &= \frac{1}{r} \frac{4G}{c^4} \Lambda_{ij,kl}(\hat{\mathbf{n}}) \\ &\times \left[S^{kl} + \frac{1}{c} n_m \dot{S}^{kl,m} + \frac{1}{2c^2} n_m n_p \ddot{S}^{kl,mp} + \dots \right]_{\text{ret}}, \end{aligned} \quad (3.34)$$

where the subscript “ret” means that the quantities S^{kl} , $\dot{S}^{kl,m}$, $\ddot{S}^{kl,mp}$, etc. are evaluated at retarded time $t - r/c$. This equation is the basis for

the multipole expansion. From the definitions (3.31)–(3.32) we see that, with respect to S^{kl} , $S^{kl,m}$ has an additional factor $x^m \sim O(d)$, while each time derivative brings a factor $O(\omega_s)$. So, with respect to S^{kl} , the tensor $\dot{S}^{kl,m}$ has an additional factor $O(\omega_s d)$, i.e. $O(v)$, where v is a typical velocity inside the source. Then the term $(1/c)n_m \dot{S}^{kl,m}$ is a correction $O(v/c)$ to the term S^{kl} , and similarly the term $(1/c^2)n_m n_p \ddot{S}^{kl,mp}$ is a correction $O(v^2/c^2)$, etc.

The physical meaning of the various terms in this expansion becomes more clear if we eliminate the momenta of T^{ij} in favor of the momenta of the energy density T^{00} , and of the momenta of the linear momentum, T^{0i}/c . We define the momenta of T^{00}/c^2 by¹²

$$M = \frac{1}{c^2} \int d^3x T^{00}(t, \mathbf{x}), \quad (3.35)$$

$$M^i = \frac{1}{c^2} \int d^3x T^{00}(t, \mathbf{x}) x^i, \quad (3.36)$$

$$M^{ij} = \frac{1}{c^2} \int d^3x T^{00}(t, \mathbf{x}) x^i x^j, \quad (3.37)$$

$$M^{ijk} = \frac{1}{c^2} \int d^3x T^{00}(t, \mathbf{x}) x^i x^j x^k, \quad (3.38)$$

and so on, while the momenta of the momentum density $(1/c)T^{0i}$ are denoted by

$$P^i = \frac{1}{c} \int d^3x T^{0i}(t, \mathbf{x}), \quad (3.39)$$

$$P^{i,j} = \frac{1}{c} \int d^3x T^{0i}(t, \mathbf{x}) x^j, \quad (3.40)$$

$$P^{i,jk} = \frac{1}{c} \int d^3x T^{0i}(t, \mathbf{x}) x^j x^k, \quad (3.41)$$

and similarly for the higher momenta. The time derivatives of these quantities and of the momenta of T^{ij} satisfy relations which follow from energy-momentum conservation. Recall that we are working within linearized theory, which means that the energy-momentum tensor of matter $T^{\mu\nu}$ satisfies the flat-space equation $\partial_\mu T^{\mu\nu} = 0$, as we have seen in eq. (1.25), while non-linearities such as those written schematically in eq. (2.113) are neglected. This means that we are also neglecting the back-action of the GWs on the source.¹³

To obtain these identities, we take a box of volume V larger than the source, and we denote its boundary by ∂V (so $T_{\mu\nu}$ vanishes on ∂V). Using $\partial_\mu T^{\mu 0} = 0$, that is

$$\partial_0 T^{00} = -\partial_i T^{0i}, \quad (3.42)$$

(and recalling that $\dot{M} \equiv \partial M / \partial t = c \partial_0 M$) we have

$$\begin{aligned} c\dot{M} &= \int_V d^3x \partial_0 T^{00} \\ &= - \int_V d^3x \partial_i T^{0i} \end{aligned}$$

¹²Dimensionally T^{00}/c^2 is a mass density but of course, besides the contribution due to the rest mass of the source, it contains also all contributions to T^{00} coming from the kinetic energy of the particles which make up the source, contributions from the potential energy, etc. For sources that generate a strong gravitational field, such as neutron stars, the gravitational binding energy will also be important. Only for weak-field sources and in the non-relativistic limit, T^{00}/c^2 becomes the mass density. However, since the multipole expansion of the linearized theory assumes weak fields and is a non-relativistic expansion, to lowest order in v/c we can actually replace T^{00}/c^2 with the mass density.

¹³The inclusion of these non-linearities will be discussed in Chapter 5.

$$\begin{aligned}
&= - \int_{\partial V} dS^i T^{0i} \\
&= 0.
\end{aligned} \tag{3.43}$$

The last equality follows from the fact that T^{0i} vanishes on the boundary ∂V , since we have taken the volume V larger than the volume of the source. Of course, a physical system that radiates GWs loses mass. The conservation of the mass M of the radiating body, expressed by eq. (3.43), is due to the fact that in the linearized approximation the back action of the source dynamics due to the energy carried away by the GWs is neglected. Similarly, we obtain the identity

$$\begin{aligned}
c\dot{M}^i &= \int_V d^3x x^i \partial_0 T^{00} \\
&= - \int_V d^3x x^i \partial_j T^{0j} \\
&= \int_V d^3x (\partial_j x^i) T^{0j} \\
&= \int_V d^3x \delta_j^i T^{0j} \\
&= cP^i.
\end{aligned} \tag{3.44}$$

In the same way one derives similar identities for the higher momenta of T^{00} and of T^{0i} . For the first few lowest-order momenta of T^{00} we get

$$\dot{M} = 0, \tag{3.45}$$

$$\dot{M}^i = P^i, \tag{3.46}$$

$$\dot{M}^{ij} = P^{i,j} + P^{j,i}, \tag{3.47}$$

$$\dot{M}^{ijk} = P^{i,jk} + P^{j,ki} + P^{k,ij}, \tag{3.48}$$

while the lowest-order momenta of T^{0i} satisfy

$$\dot{P}^i = 0, \tag{3.49}$$

$$\dot{P}^{i,j} = S^{ij}, \tag{3.50}$$

$$\dot{P}^{i,jk} = S^{ij,k} + S^{ik,j}. \tag{3.51}$$

¹⁴In particular, the momenta of T^{ij} , i.e. $\{S^{ij}, S^{ij,k}, \dots\}$ depend on the distribution of the stresses inside the body, which might be difficult to determine, while the total mass of a body, its mass quadrupole, etc. can be measured more easily. Furthermore, as we will discuss in Sect. 3.3.5, for a set of interacting point masses T^{00} is $O(v^0)$ and T^{0i} is $O(v)$, so to lowest order in v/c they can be consistently computed using the free-particle energy-momentum tensor and neglecting the contribution of the potential and the relativistic corrections, which start from $O(v^2)$. This is not the case for T^{ij} , which is itself $O(v^2)$.

The equations $\dot{M} = 0$ and $\dot{P}^i = 0$ are the conservation of the mass and of the total momentum of the source. Another interesting identity is $\dot{P}^{i,j} - \dot{P}^{j,i} = S^{ij} - S^{ji} = 0$, which follows from eq. (3.50) using the fact that S^{ij} is a symmetric tensor, and is the conservation of the angular momentum of the source.

We can now combine these identities to express the momenta S^{ij} , $\dot{S}^{ij,k}$, etc., that appear in the multipole expansion, in terms of the two sets of momenta $\{M, M^i, M^{ij}, \dots\}$ and $\{P^i, P^{i,j}, \dots\}$, which have a more immediate physical interpretation.¹⁴ Taking the time derivative of eq. (3.47) and using eq. (3.50), as well as the fact that $S^{ij} = S^{ji}$, we obtain the identity

$$S^{ij} = \frac{1}{2} \ddot{M}^{ij}. \tag{3.52}$$

If we combine eq. (3.48) with eq. (3.51) instead, we get

$$\ddot{M}^{ijk} = 2(\dot{S}^{ij,k} + \dot{S}^{ik,j} + \dot{S}^{jk,i}). \quad (3.53)$$

From eq. (3.51) it also follows that $\ddot{P}^{i,jk} = \dot{S}^{ij,k} + \dot{S}^{ik,j}$. Using this relation and eq. (3.53) we can verify that

$$\dot{S}^{ij,k} = \frac{1}{6}\ddot{M}^{ijk} + \frac{1}{3}(\ddot{P}^{i,jk} + \ddot{P}^{j,ik} - 2\ddot{P}^{k,ij}). \quad (3.54)$$

Equations (3.52) and (3.54) relate S^{ij} and $\dot{S}^{ij,k}$, which are the two lowest-order momenta appearing in the multipole expansion (3.34), to the momenta of T^{00} and of T^{0i} . One can proceed similarly with the higher-order terms. In the next two sections, we examine the leading and the next-to-leading terms, while in Section 3.5 we discuss systematically the expansion to all orders.

3.3 Mass quadrupole radiation

3.3.1 Amplitude and angular distribution

Using eq. (3.52), the leading term of the expansion (3.34) is

$$[h_{ij}^{\text{TT}}(t, \mathbf{x})]_{\text{quad}} = \frac{1}{r} \frac{2G}{c^4} \Lambda_{ij,kl}(\hat{\mathbf{n}}) \ddot{M}^{kl}(t - r/c). \quad (3.55)$$

From the point of view of the rotation group the tensor M_{kl} , as any symmetric tensor with two indices, decomposes into irreducible representations as

$$M^{kl} = \left(M^{kl} - \frac{1}{3}\delta^{kl}M_{ii} \right) + \frac{1}{3}\delta^{kl}M_{ii}, \quad (3.56)$$

where M_{ii} is the trace of M_{ij} . The first term is traceless by construction, and is a pure spin-2 operator, while the trace part is a scalar. Since the Lambda tensor $\Lambda_{ij,kl}$ gives zero when contracted with δ_{kl} , only the traceless term contributes. We use the notation

$$\rho = \frac{1}{c^2}T^{00}. \quad (3.57)$$

To lowest order in v/c , ρ becomes the mass density, see Note 12. We also introduce the quadrupole moment

$$\begin{aligned} Q^{ij} &\equiv M^{ij} - \frac{1}{3}\delta^{ij}M_{kk} \\ &= \int d^3x \rho(t, \mathbf{x})(x^i x^j - \frac{1}{3}r^2\delta^{ij}), \end{aligned} \quad (3.58)$$

and eq. (3.55) becomes

$$\begin{aligned} [h_{ij}^{\text{TT}}(t, \mathbf{x})]_{\text{quad}} &= \frac{1}{r} \frac{2G}{c^4} \Lambda_{ij,kl}(\hat{\mathbf{n}}) \ddot{Q}_{kl}(t - r/c) \\ &\equiv \frac{1}{r} \frac{2G}{c^4} \ddot{Q}_{ij}^{\text{TT}}(t - r/c). \end{aligned} \quad (3.59)$$

Angular distribution of quadrupole radiation

In order to obtain the waveform emitted into an arbitrary direction $\hat{\mathbf{n}}$, we could in principle plug the explicit expression (1.39) of the Lambda tensor into eq. (3.59), and perform the contraction with \tilde{Q}_{kl} . It is however more instructive to proceed as follows. First we observe that, when the direction of propagation $\hat{\mathbf{n}}$ of the GW is equal to $\hat{\mathbf{z}}$, P_{ij} is the diagonal matrix diag $(1, 1, 0)$, i.e. P_{ij} is a projector on the (x, y) plane. Writing $\Lambda_{ij,kl}$ in terms of P_{ij} using eq. (1.36) we have, for an arbitrary 3×3 matrix A_{kl} ,

$$\begin{aligned}\Lambda_{ij,kl}A_{kl} &= \left[P_{ik}P_{jl} - \frac{1}{2}P_{ij}P_{kl} \right] A_{kl} \\ &= (PAP)_{ij} - \frac{1}{2}P_{ij}\text{Tr}(PA).\end{aligned}\quad (3.60)$$

When P has the form

$$P = \begin{pmatrix} 1 & 0 & 0 \\ 0 & 1 & 0 \\ 0 & 0 & 0 \end{pmatrix}, \quad (3.61)$$

we get

$$PAP = \begin{pmatrix} A_{11} & A_{12} & 0 \\ A_{21} & A_{22} & 0 \\ 0 & 0 & 0 \end{pmatrix}, \quad (3.62)$$

while $\text{Tr}(PA) = A_{11} + A_{22}$. Therefore

$$\begin{aligned}\Lambda_{ij,kl}A_{kl} &= \begin{pmatrix} A_{11} & A_{12} & 0 \\ A_{21} & A_{22} & 0 \\ 0 & 0 & 0 \end{pmatrix}_{ij} - \frac{A_{11} + A_{22}}{2} \begin{pmatrix} 1 & 0 & 0 \\ 0 & 1 & 0 \\ 0 & 0 & 0 \end{pmatrix}_{ij} \\ &= \begin{pmatrix} (A_{11} - A_{22})/2 & A_{12} & 0 \\ A_{21} & -(A_{11} - A_{22})/2 & 0 \\ 0 & 0 & 0 \end{pmatrix}_{ij}.\end{aligned}\quad (3.63)$$

Thus, when $\hat{\mathbf{n}} = \hat{\mathbf{z}}$,¹⁵

$$\Lambda_{ij,kl}\ddot{M}_{kl} = \begin{pmatrix} (\ddot{M}_{11} - \ddot{M}_{22})/2 & \ddot{M}_{12} & 0 \\ \ddot{M}_{21} & -(\ddot{M}_{11} - \ddot{M}_{22})/2 & 0 \\ 0 & 0 & 0 \end{pmatrix}_{ij}. \quad (3.64)$$

From this we directly read the two polarization amplitudes, for a GW propagating in the z direction,

$$h_+ = \frac{1}{r} \frac{G}{c^4} (\ddot{M}_{11} - \ddot{M}_{22}), \quad (3.65)$$

$$h_\times = \frac{2}{r} \frac{G}{c^4} \ddot{M}_{12}, \quad (3.66)$$

where it is understood that the right-hand side is computed at the retarded time $t - r/c$. To compute the amplitudes for a wave that, in a frame with axes (x, y, z) , propagates in a generic direction $\hat{\mathbf{n}}$, we introduce two unit vectors $\hat{\mathbf{u}}$ and $\hat{\mathbf{v}}$, orthogonal to $\hat{\mathbf{n}}$ and to each other,

¹⁵We write the result in terms of the second mass moment M_{ij} , rather than in terms of the quadrupole moment Q_{ij} . Since $\Lambda_{ij,kl}Q_{kl} = \Lambda_{ij,kl}M_{kl}$ (because $\Lambda_{ij,kl}\delta_{kl} = 0$, see eq. (1.38)), in the equations below we could use M_{ij} or Q_{ij} equivalently. Typically, it is slightly more practical to use M_{ij} when one makes explicit computations.

chosen so that $\hat{\mathbf{u}} \times \hat{\mathbf{v}} = \hat{\mathbf{n}}$ (so, when $\hat{\mathbf{n}} = \hat{\mathbf{z}}$, we can take $\hat{\mathbf{u}} = \hat{\mathbf{x}}$ and $\hat{\mathbf{v}} = \hat{\mathbf{y}}$), see Fig. 3.2. Then in the (x', y', z') frame, whose axes are in the directions $(\hat{\mathbf{u}}, \hat{\mathbf{v}}, \hat{\mathbf{n}})$, the wave propagates along the z' axis and we can use the previous result to read h_+ and h_\times ,

$$h_+(t, \hat{\mathbf{n}}) = \frac{1}{r} \frac{G}{c^4} (\ddot{M}'_{11} - \ddot{M}'_{22}), \quad (3.67)$$

$$h_\times(t, \hat{\mathbf{n}}) = \frac{2}{r} \frac{G}{c^4} \ddot{M}'_{12}, \quad (3.68)$$

where M'_{ij} are the components of the second mass moment in the frame (x', y', z') .¹⁶ These can be related to the components M_{ij} in the (x, y, z) frame observing that in the (x', y', z') frame the vector $\hat{\mathbf{n}}$ has coordinates $n'_i = (0, 0, 1)$, while in the (x, y, z) frame it has coordinates

$$n_i = (\sin \theta \sin \phi, \sin \theta \cos \phi, \cos \theta), \quad (3.69)$$

Then the components n_i and n'_i are related by a rotation matrix \mathcal{R} such that $n_i = \mathcal{R}_{ij} n'_j$, whose explicit expression is

$$\mathcal{R} = \begin{pmatrix} \cos \phi & \sin \phi & 0 \\ -\sin \phi & \cos \phi & 0 \\ 0 & 0 & 1 \end{pmatrix} \begin{pmatrix} 1 & 0 & 0 \\ 0 & \cos \theta & \sin \theta \\ 0 & -\sin \theta & \cos \theta \end{pmatrix}. \quad (3.70)$$

Similarly, a tensor \mathbf{M} with two indices has components M_{ij} in the (x, y, z) frame and M'_{ij} in the (x', y', z') frame, related by

$$M_{ij} = \mathcal{R}_{ik} \mathcal{R}_{jl} M'_{kl}, \quad (3.71)$$

or, solving for M' , $M'_{ij} = (\mathcal{R}^T M \mathcal{R})_{ij}$, where \mathcal{R}^T is the transpose matrix. Inserting \mathcal{R} from eq. (3.70), and plugging the resulting values of M'_{ij} into eqs. (3.67) and (3.68), we get

$$h_+(t; \theta, \phi) = \frac{1}{r} \frac{G}{c^4} [\ddot{M}_{11}(\cos^2 \phi - \sin^2 \phi \cos^2 \theta) + \ddot{M}_{22}(\sin^2 \phi - \cos^2 \phi \cos^2 \theta) - \ddot{M}_{33} \sin^2 \theta - \ddot{M}_{12} \sin 2\phi (1 + \cos^2 \theta) + \ddot{M}_{13} \sin \phi \sin 2\theta + \ddot{M}_{23} \cos \phi \sin 2\theta], \quad (3.72)$$

$$h_\times(t; \theta, \phi) = \frac{1}{r} \frac{G}{c^4} [(\ddot{M}_{11} - \ddot{M}_{22}) \sin 2\phi \cos \theta + 2\ddot{M}_{12} \cos 2\phi \cos \theta - 2\ddot{M}_{13} \cos \phi \sin \theta + 2\ddot{M}_{23} \sin \phi \sin \theta].$$

¹⁶Recall that h_+ and h_\times are defined in terms of the components of h_{ij} in the plane transverse to the propagation direction. Therefore these are “the” polarization amplitudes, and are denoted by h_+ and h_\times , rather than h'_+ and h'_\times .

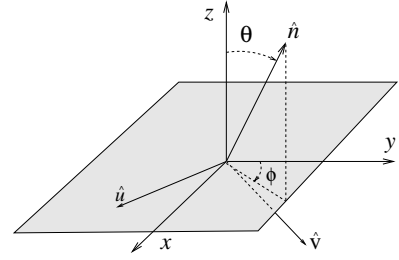


Fig. 3.2 The relation between the $(\hat{\mathbf{x}}, \hat{\mathbf{y}}, \hat{\mathbf{z}})$ frame and the $(\hat{\mathbf{u}}, \hat{\mathbf{v}}, \hat{\mathbf{n}})$ frame. The vector $\hat{\mathbf{u}}$ is in the $(\hat{\mathbf{x}}, \hat{\mathbf{y}})$ plane, while $\hat{\mathbf{v}}$ points downward, with respect to the $(\hat{\mathbf{x}}, \hat{\mathbf{y}})$ plane.

This equation allows us to compute the angular distribution of the quadrupole radiation, once M_{ij} is given.

Absence of monopole and dipole gravitational radiation

We see from eq. (3.59) that the leading term of the multipole expansion is the mass quadrupole. There is neither monopole nor dipole radiation for GWs. This can be understood in two different ways. First of all, observe that a monopole term would depend on M and a dipole term on P^i (the mass dipole moment M^i can be set to zero with a shift of the origin of the coordinate system). Furthermore, h_{ij}^{TT} depends on derivatives of the multipole moments, since a static source does not radiate. However, M and P^i are conserved quantities, so any contribution from M or P^i must vanish.

Actually, M and P^i are conserved only at the level of linearized theory: a radiating system loses mass and, in general, also linear momentum (see page 130). However, the absence of monopole and dipole radiation holds more generally, and is not restricted to linearized theory. One can verify this observing that, even when we include all non-linear terms, as in eq. (2.113), the right-hand side of the wave equation must still be conserved, to be consistent with the Lorentz gauge condition. We will see explicitly in Section 5.2 how to write the equations in such a form. Using that expression, see in particular eqs. (5.69), (5.71) and (5.72), one can verify that the derivation of the absence of monopole and dipole radiation goes through even in the full non-linear theory. The difference with linearized theory is that the lowest-order multipole that contributes, rather than being the quadrupole moment of the energy density of matter, T^{00} , is the quadrupole moment of a more general quantity τ^{00} that includes also the contribution of the gravitational field.

However, there is no need to enter into the details of the non-linear theory: the absence of monopole and dipole radiation is simply the expression of the fact that the graviton is a massless particle with helicity ± 2 . We already showed in Problem 2.2 that it is impossible to put a graviton in a state with total angular momentum $j = 0$ or $j = 1$. This emerged as a consequence of the fact that the graviton is a massless particle with helicities ± 2 , and it therefore obeys gauge conditions that eliminate the spurious degrees of freedom. Indeed, these conditions allowed us to reduce the five degrees of a traceless symmetric tensor h_{ij} , which would be appropriate for describing a *massive* spin-2 particle, to the two degrees of freedom of a *massless* particle, as we discussed in Section 2.2.2.

Since it is impossible to put a graviton in a state with total angular momentum $j = 0$ or $j = 1$, we can have neither monopole nor dipole radiation, since they correspond to a collection of quanta with $j = 0$ and $j = 1$, respectively. The situation is completely analogous to electrodynamics, where the photon is massless and has helicity ± 1 , so it is impossible to put it in a state with total angular momentum $j = 0$ (see Problem 2.2, or Landau and Lifshitz, Vol. IV (1982), Section 6), and therefore monopole radiation is forbidden. In electromagnetism, the leading term of the multipole expansion is therefore dipole radiation.

3.3.2 Radiated energy

Inserting eq. (3.59) in eq. (1.153) and using the property (1.37) of the Lambda tensor we find the power radiated per unit solid angle, in the quadrupole approximation,

$$\begin{aligned} \left(\frac{dP}{d\Omega} \right)_{\text{quad}} &= \frac{r^2 c^3}{32\pi G} \langle \dot{h}_{ij}^{\text{TT}} \dot{h}_{ij}^{\text{TT}} \rangle \\ &= \frac{G}{8\pi c^5} \Lambda_{ij,kl}(\hat{\mathbf{n}}) \langle \ddot{Q}_{ij} \ddot{Q}_{kl} \rangle, \end{aligned} \quad (3.73)$$

where, as usual, the average is a temporal average over several characteristic periods of the GW, and it is understood that \ddot{Q}_{ij} must be evaluated at the retarded time $t - r/c$. The angular integral can be performed observing that the dependence on $\hat{\mathbf{n}}$ is only in $\Lambda_{ij,kl}$. Using eqs. (3.21) and (3.22) we find

$$\int d\Omega \Lambda_{ij,kl} = \frac{2\pi}{15} (11\delta_{ik}\delta_{jl} - 4\delta_{ij}\delta_{kl} + \delta_{il}\delta_{jk}). \quad (3.74)$$

Then, the total radiated power (or, in notation used in astrophysics, the total gravitational luminosity \mathcal{L} of the source) is, in the quadrupole approximation,

$$P_{\text{quad}} = \frac{G}{5c^5} \langle \ddot{Q}_{ij} \ddot{Q}_{ij} \rangle, \quad (3.75)$$

where, again, \ddot{Q}_{ij} must be evaluated at the retarded time $t - r/c$. This is the famous quadrupole formula, first derived by Einstein.¹⁷ Sometimes, in explicit computations, it is more practical to use M_{ij} rather than Q_{ij} . Substituting $Q_{ij} = M_{ij} - (1/3)\delta_{ij}M_{kk}$ in eq. (3.75) we have

$$P_{\text{quad}} = \frac{G}{5c^5} \langle \ddot{M}_{ij} \ddot{M}_{ij} - \frac{1}{3}(\ddot{M}_{kk})^2 \rangle. \quad (3.76)$$

The same result could be obtained by observing that eq. (3.73) is still valid if we replace $\Lambda_{ij,kl} \ddot{Q}_{ij} \ddot{Q}_{kl}$ by $\Lambda_{ij,kl} \ddot{M}_{ij} \ddot{M}_{kl}$, since the contraction of $\Lambda_{ij,kl}$ with δ_{ij} (or with δ_{kl}) gives zero. However, when we use $\Lambda_{ij,kl} \ddot{M}_{ij} \ddot{M}_{kl}$, after integrating in $d\Omega$, on the right-hand side of eq. (3.74) the term $-4\delta_{ij}\delta_{kl}$ (which gave zero when contracted with $\ddot{Q}_{ij} \ddot{Q}_{kl}$) now contributes, since M_{ij} is not traceless, and we find eq. (3.76) again.

The energy radiated per unit solid angle is obtained by integrating the power, eq. (3.73), with respect to time. We write the quadrupole moment in terms of its Fourier transform,

$$Q_{ij}(t) = \int_{-\infty}^{\infty} \frac{d\omega}{2\pi} \tilde{Q}_{ij}(\omega) e^{-i\omega t}, \quad (3.77)$$

and, integrating eq. (3.73) with respect to time, we get

$$\left(\frac{dE}{d\Omega} \right)_{\text{quad}} = \frac{G}{8\pi^2 c^5} \Lambda_{ij,kl}(\hat{\mathbf{n}}) \int_0^{\infty} d\omega \omega^6 \tilde{Q}_{ij}(\omega) \tilde{Q}_{kl}^*(\omega),$$

¹⁷Observe that some authors, e.g. Landau and Lifshitz, Vol. II (1979), define the quadrupole moment with a different normalization,

$$(Q_{ij})^{\text{LL}} = \int d^3x \rho(t, \mathbf{x}) (3x^i x^j - r^2 \delta^{ij}),$$

where the superscript “LL” stands for Landau and Lifshitz. This is larger by a factor of 3 than our definition, eq. (3.58). In term of this quantity, the quadrupole formula therefore reads

$$P_{\text{quad}} = \frac{G}{45c^5} \langle (\ddot{Q}_{ij} \ddot{Q}_{ij})^{\text{LL}} \rangle,$$

and all other equations involving Q_{ij} must be rescaled similarly.

(3.78)

where the integral in $d\omega$ from $-\infty$ to $+\infty$ has been written as twice an integral from zero to ∞ using $\tilde{Q}_{ij}(-\omega) = \tilde{Q}_{ij}^*(\omega)$. Integrating over the solid angle we find the total radiated energy,

$$E_{\text{quad}} = \frac{G}{5\pi c^5} \int_0^\infty d\omega \omega^6 \tilde{Q}_{ij}(\omega) \tilde{Q}_{ij}^*(\omega), \quad (3.79)$$

¹⁸To compare this equation with the results in the literature, beside checking the factor of 3 in the normalization of Q_{ij} , one must also check whether or not the Fourier transform is defined using $d\omega/(2\pi)$, as we do, or simply $d\omega$, as, for instance, in Weinberg (1972) or in Straumann (2004).

and therefore the energy spectrum, integrated over the solid angle, is¹⁸

$$\left(\frac{dE}{d\omega} \right)_{\text{quad}} = \frac{G}{5\pi c^5} \omega^6 \tilde{Q}_{ij}(\omega) \tilde{Q}_{ij}^*(\omega). \quad (3.80)$$

For a monochromatic source, radiating at a frequency $\omega_0 > 0$, we proceed as in Section 3.1: we write, for positive ω ,

$$\tilde{Q}_{ij}(\omega) = q_{ij} 2\pi\delta(\omega - \omega_0), \quad (3.81)$$

insert this into eq. (3.78), and again use $2\pi\delta(\omega = 0) = T$, where T is the total (infinite) time interval. The instantaneous power generated by the monochromatic source is obtained by dividing by T , so

$$\left(\frac{dP}{d\Omega d\omega} \right)_{\text{quad}} = \frac{G\omega_0^6}{4\pi c^5} (\Lambda_{ij,kl} q_{ij} q_{kl}^*) \delta(\omega - \omega_0). \quad (3.82)$$

As for the linear momentum, inserting eq. (3.59) into eq. (1.164) we get

$$\frac{dP^i}{dt} = -\frac{G}{8\pi c^5} \int d\Omega \ddot{Q}_{ab}^{\text{TT}} \partial^i \ddot{Q}_{ab}^{\text{TT}}. \quad (3.83)$$

Under reflection, $\mathbf{x} \rightarrow -\mathbf{x}$, the quadrupole moment is invariant while $\partial^i \rightarrow -\partial^i$. Therefore the integrand is odd, and the angular integral vanishes. There is no loss of linear momentum in the quadrupole approximation. A non-vanishing result can be obtained by going beyond the quadrupole approximation, from the interference between multipoles of different parity, as we will see in Section 3.4.

3.3.3 Radiated angular momentum

The angular momentum carried away per unit time by GWs can be obtained by plugging the expression for h_{ij}^{TT} in the quadrupole approximation, eq. (3.59), into the general formula for the rate of angular momentum loss, eq. (2.61). Recalling that the first term in eq. (2.61) is the contribution from the orbital angular momentum L^i of the GWs while the second comes from the spin S^i of the field configuration, we write

$$\frac{dJ^i}{dt} = \frac{dL^i}{dt} + \frac{dS^i}{dt}. \quad (3.84)$$

For the orbital part we have

$$\left(\frac{dL^i}{dt} \right)_{\text{quad}} = -\frac{c^3}{32\pi G} \epsilon^{ikl} \int d\Omega r^2 \langle \dot{h}_{ab}^{\text{TT}} x^k \partial^l h_{ab}^{\text{TT}} \rangle. \quad (3.85)$$

We then substitute $h_{ab}^{\text{TT}}(t, \mathbf{x}) = (2G/rc^4)\Lambda_{ab,cd}(\hat{\mathbf{n}})\ddot{Q}_{cd}(t - r/c)$ and we perform the angular integral. The explicit computation is slightly involved, but we find it useful to perform it in detail. The uninterested reader can jump to the result, eq. (3.93).

When we compute $\partial^l h_{ab}^{\text{TT}}$, the derivative ∂^l acts on $\Lambda_{ab,cd}(\hat{\mathbf{n}})$ (since $n^i = x^i/r$) as well as on $\ddot{Q}_{cd}(t - r/c)$. However,

$$\begin{aligned} \frac{\partial}{\partial x^l} \ddot{Q}_{cd}(t - r/c) &= \left(\frac{\partial r}{\partial x^l} \right) \frac{d}{dr} \ddot{Q}_{cd}(t - r/c) \\ &= -\frac{x^l}{r} \frac{1}{c} \ddot{Q}_{cd}(t - r/c). \end{aligned} \quad (3.86)$$

In eq. (3.85) this therefore gives a contribution proportional to $\epsilon^{ikl} x^k x^l = 0$. The only non-vanishing term is obtained when ∂^l acts on $\Lambda_{ab,cd}(\hat{\mathbf{n}})$, and

$$\left(\frac{dL^i}{dt} \right)_{\text{quad}} = -\frac{G}{2c^5} \epsilon^{ikl} \langle \ddot{Q}_{cd} \ddot{Q}_{fg} \rangle \int \frac{d\Omega}{4\pi} \Lambda_{ab,cd} x^k \partial^l \Lambda_{ab,fg}, \quad (3.87)$$

where it is understood that the derivatives of the quadrupole moment are evaluated at the retarded time $t - r/c$. We observe that

$$\begin{aligned} \frac{\partial n^m}{\partial x^l} &= \frac{\partial}{\partial x^l} \left(\frac{x^m}{r} \right) \\ &= \frac{\delta^{lm}}{r} - \frac{x^l x^m}{r^3} \\ &= \frac{1}{r} P^{lm}, \end{aligned} \quad (3.88)$$

where $P^{lm} = \delta^{lm} - n^l n^m$ is the projector first introduced in eq. (1.35).¹⁹ Then

$$\begin{aligned} \partial^l \Lambda_{ab,fg} &= \frac{\partial n^m}{\partial x^l} \frac{\partial}{\partial n^m} \Lambda_{ab,fg} \\ &= \frac{1}{r} P^{lm} \frac{\partial}{\partial n^m} \Lambda_{ab,fg}. \end{aligned} \quad (3.89)$$

Using $\Lambda_{ab,fg}$ in the form (1.36) together with

$$\frac{\partial P^{ij}}{\partial n^m} = -(\delta^{im} n^j + \delta^{jm} n^i), \quad (3.90)$$

which follows from the definition of P^{ij} , we find the identity

$$P^{lm} \frac{\partial}{\partial n^m} \Lambda_{ab,fg} = -(n_f \Lambda_{ab,lg} + n_g \Lambda_{ab,lf} + n_a \Lambda_{lb,fg} + n_b \Lambda_{la,fg}). \quad (3.91)$$

The last two terms give zero when contracted with the factor $\Lambda_{ab,cd}$ in eq. (3.87), since the Lambda tensor is transverse on all indices, $n_a \Lambda_{ab,cd} = n_b \Lambda_{ab,cd} = 0$. Then

$$\begin{aligned} \left(\frac{dL^i}{dt} \right)_{\text{quad}} &= \frac{G}{2c^5} \epsilon^{ikl} \langle \ddot{Q}_{cd} \ddot{Q}_{fg} \rangle \int \frac{d\Omega}{4\pi} \Lambda_{ab,cd} n_k (n_f \Lambda_{ab,lg} + n_g \Lambda_{ab,lf}) \\ &= \frac{G}{2c^5} \epsilon^{ikl} \langle \ddot{Q}_{cd} \ddot{Q}_{fg} \rangle \int \frac{d\Omega}{4\pi} n_k (n_f \Lambda_{cd,lg} + n_g \Lambda_{cd,lf}). \end{aligned} \quad (3.92)$$

¹⁹As always, we do not need to be careful about raising and lowering spatial indices, since the spatial metric is δ_{ij} . Otherwise, we should write $\partial n^m / \partial x^l = (1/r) P_l^m$.

The angular integral can now be computed by inserting the explicit form of the Λ tensor (1.39) and using the identities (3.21) and (3.22) (the term with six factors $\hat{\mathbf{n}}$ is proportional to $n^k n^l$ and vanishes when contracted with ϵ^{ikl} , so we only need the integrals with two and with four factors $\hat{\mathbf{n}}$).

The result is

$$\left(\frac{dL^i}{dt} \right)_{\text{quad}} = \frac{2G}{15c^5} \epsilon^{ikl} \langle \ddot{Q}_{ka} \ddot{Q}_{la} \rangle. \quad (3.93)$$

The calculation of the spin part gives

$$\begin{aligned} \left(\frac{dS^i}{dt} \right)_{\text{quad}} &= \frac{c^3}{16\pi G} \epsilon^{ikl} \int r^2 d\Omega \langle \dot{h}_{al}^{\text{TT}} h_{ak}^{\text{TT}} \rangle \\ &= \frac{G}{c^5} \epsilon^{ikl} \langle \ddot{Q}_{mn} \ddot{Q}_{cd} \rangle \int \frac{d\Omega}{4\pi} \Lambda_{al,mn} \Lambda_{ak,cd}. \end{aligned} \quad (3.94)$$

Using eq. (1.36) we can prove the identity

$$\Lambda_{al,mn} \Lambda_{ak,cd} = P_{ln} \Lambda_{mk,cd} - \frac{1}{2} P_{mn} \Lambda_{kl,cd}. \quad (3.95)$$

The second factor gives zero contracted with ϵ^{ikl} and, again using the identities eqs. (3.21) and (3.22), the remaining angular integration is straightforward,

$$\begin{aligned} \left(\frac{dS^i}{dt} \right)_{\text{quad}} &= \frac{G}{c^5} \epsilon^{ikl} \ddot{Q}_{mn} \ddot{Q}_{cd} \int \frac{d\Omega}{4\pi} P_{ln} \Lambda_{mk,cd} \\ &= \frac{4G}{15c^5} \epsilon^{ikl} \langle \ddot{Q}_{ka} \ddot{Q}_{la} \rangle. \end{aligned} \quad (3.96)$$

Summing the spin and orbital contribution, we finally get the angular momentum carried away, per unit time, by the GWs,

$$\left(\frac{dJ^i}{dt} \right)_{\text{quad}} = \frac{2G}{5c^5} \epsilon^{ikl} \langle \ddot{Q}_{ka} \ddot{Q}_{la} \rangle, \quad (3.97)$$

where we recall again that the derivatives of the quadrupole moment are evaluated at the retarded time $t - r/c$.

3.3.4 Radiation reaction on non-relativistic sources

We have seen that gravitational radiation carries away energy and angular momentum. Ultimately, this energy and angular momentum must come from the source. We therefore expect that the energy and angular momentum carried by the GWs, at a large distance r from the source and at time t , were drained at retarded time $t - r/c$ from the energy and the angular momentum of the source. In the full non-linear theory of gravity (so, in particular, when dealing with self-gravitating sources), one must however take into account non-linear effects in the GW propagation from the source to infinity (such as back-scattering of gravitons

on the background space-time, graviton–graviton scattering, etc.). We will see in Section 5.3.4 that, as a result, at higher orders in the post-Newtonian expansion part of the gravitational radiation is delayed, and the total GW consists of a wavefront, which travels at the speed of light, and a “tail”, which arrives later. Thus, it is not at all obvious that there is an exact equality, to all orders in the post-Newtonian expansion, between the instantaneous power radiated at large distances at a given time t , and the rate of energy loss of the source at the corresponding retarded time. We will discuss the issue in Section 5.3.5. However, as long as we are in linearized theory, the background space-time is flat, the wave propagates at the speed of light, and this energy balance argument is inescapable.

For $v/c \ll 1$, the leading term is given by quadrupole radiation, so the instantaneous rate of decreases of energy and orbital²⁰ angular momentum of the source must be given by eqs. (3.75) and (3.97), i.e.

$$\frac{dE_{\text{source}}}{dt} = -\frac{G}{5c^5} \langle \ddot{Q}_{ij} \ddot{Q}_{ij} \rangle, \quad (3.98)$$

$$\frac{dL^i_{\text{source}}}{dt} = -\frac{2G}{5c^5} \epsilon^{ikl} \langle \ddot{Q}_{ka} \ddot{Q}_{la} \rangle. \quad (3.99)$$

We have required that dE_{source}/dt , computed at retarded time $t - r/c$, be the negative of the power radiated at a large distance r in GWs, at time t . Since the latter is expressed in terms of $\langle \ddot{Q}_{ij} \ddot{Q}_{ij} \rangle$ evaluated at retarded time, as in eq. (3.75), we have obtained an equality between dE_{source}/dt and $-(G/5c^5)\langle \ddot{Q}_{ij} \ddot{Q}_{ij} \rangle$, both evaluated at the same value of retarded time or, equivalently, at the same value of time (and similarly for the angular momentum).

The multipole expansion assumes that the sources are non-relativistic so, at least to lowest order, the dynamics of the source is governed by Newtonian mechanics, and it should be possible to describe the back-reaction of the GWs on the source in terms of a force \mathbf{F} . Then, we expect that it should be possible to write eq. (3.98) in the form

$$\frac{dE_{\text{source}}}{dt} = \langle F_i v_i \rangle, \quad (3.100)$$

or more precisely, for an extended body,

$$\frac{dE_{\text{source}}}{dt} = \left(\int d^3x \frac{dF_i}{dV} \dot{x}_i \right), \quad (3.101)$$

where dF_i/dV is the force per unit volume. Similarly, we expect that eq. (3.99) can be written as

$$\frac{dL^i_{\text{source}}}{dt} = \langle T^i \rangle, \quad (3.102)$$

where T^i is the torque associated to the force per unit volume dF_i/dV . The average $\langle \dots \rangle$ takes into account the fact that the energy and angular momentum of GWs are notions well defined only if we average over

²⁰Gravitational waves, as any field, carry away a total angular momentum J^i that, as we saw in Section 2.1.2, is made of a spin contribution and of an orbital angular momentum contribution. This total angular momentum is drained from the total angular momentum of the source which, for a macroscopic source, is a purely orbital angular momentum.

several periods. The expression for this force, in the quadrupole approximation, can be found as follows. Since inside $\langle \dots \rangle$ we can integrate by parts (compare with Note 23 on page 35), we rewrite eq. (3.98) as

$$\frac{dE_{\text{source}}}{dt} = -\frac{G}{5c^5} \left\langle \frac{dQ_{ij}}{dt} \frac{d^5Q_{ij}}{dt^5} \right\rangle. \quad (3.103)$$

From eq. (3.58) we have

$$\frac{dQ_{ij}}{dt} = \int d^3x' \partial_t \rho(t, \mathbf{x}') \left(x'_i x'_j - \frac{1}{3} r'^2 \delta_{ij} \right). \quad (3.104)$$

The term proportional to δ_{ij} gives zero when contracted with d^5Q_{ij}/dt^5 . For a Newtonian source with $T^{00}/c^2 = \rho$ and $T^{0i}/c = \rho v^i$, the conservation of the energy-momentum tensor gives the continuity equation

$$\partial_t \rho + \partial_k (\rho v_k) = 0. \quad (3.105)$$

We then replace $\partial_t \rho$ by $-\partial_k (\rho v_k)$ in eq. (3.104) and we integrate by parts. The boundary term at infinity vanishes, because the body has a finite extent, so $\rho = 0$ beyond some value $r > a$. Therefore

$$\int d^3x' \partial_t \rho(t, \mathbf{x}') x'_i x'_j = \int d^3x' \rho(t, \mathbf{x}') x'_k (\delta_{ik} x'_j + \delta_{jk} x'_i), \quad (3.106)$$

and

$$\frac{dE_{\text{source}}}{dt} = -\frac{2G}{5c^5} \left\langle \frac{d^5Q_{ij}}{dt^5} \int d^3x' \rho(t, \mathbf{x}') \dot{x}'_i \dot{x}'_j \right\rangle. \quad (3.107)$$

Of course, d^5Q_{ij}/dt^5 is a function only of time, and does not depend on the dummy integration variable x' . Then it can be carried inside the integral, and eq. (3.107) can be written as

$$\frac{dE_{\text{source}}}{dt} = \left\langle \int d^3x' \frac{dF_i}{dV'} \dot{x}'_i \right\rangle, \quad (3.108)$$

with a force per unit volume

$$\frac{dF_i}{dV'} = -\frac{2G}{5c^5} \rho(t, \mathbf{x}') x'_j \frac{d^5Q_{ij}}{dt^5}(t).$$

(3.109)

Therefore the total force is

$$F_i = -\frac{2G}{5c^5} \frac{d^5Q_{ij}}{dt^5} \int d^3x' \rho(t, \mathbf{x}') x'_j. \quad (3.110)$$

Defining the center-of-mass coordinates by

$$x_j(t) \equiv \frac{1}{m} \int d^3x' \rho(t, \mathbf{x}') x'_j, \quad (3.111)$$

we find

$$F_i = -\frac{2G}{5c^5} m x_j \frac{d^5Q_{ij}}{dt^5}. \quad (3.112)$$

We have deduced this gravitational force on the source considering the GWs at infinity and imposing the energy balance. However, the motion of a particle under the effect of gravitational forces is completely determined by the value of the metric and its derivatives at the particle location. Thus, it should be possible to deduce the back-reaction force (3.112) also looking directly at the metric in the near-source region, without invoking the energy balance. In other words, if one solves for the gravitational field everywhere in space, in correspondence to a GW solution in the far region, there must be terms in the metric in the near region which, acting directly on the source motion through the geodesic equation, produce exactly the effect that we have inferred from the energy balance argument, i.e. provide the force (3.112). This correspondence between the GWs in the far region and the metric in the near region will be discussed in Chapter 5 in the appropriate context, which is the post-Newtonian formalism. The result is that, indeed, in the near region, among other terms that describe post-Newtonian corrections to the static potential, there is also a correction to the metric coefficient h_{00} of the form

$$\Delta h_{00} = -\frac{2\Phi}{c^2}, \quad (3.113)$$

with

$$\Phi(t, \mathbf{x}) = \frac{G}{5c^5} x_i x_j \frac{d^5 Q_{ij}}{dt^5}(t). \quad (3.114)$$

This is known as the Burke–Thorne potential,²¹ and generates a Newtonian force

$$F_i = -m \partial_i \Phi, \quad (3.115)$$

in agreement with eq. (3.112).²² As we will discuss in detail in Chapter 5, this term is singled out, and associated to radiation reaction, thanks to the fact that it is odd under time reversal. Terms associated with conservative forces are invariant under time reversal. In contrast, the emission of radiation breaks time-reversal invariance through the boundary conditions, since we impose that there is no incoming radiation (technically, at minus null infinity, see Note 1 on page 102), while at plus null infinity we can have outgoing radiation.

We now check that the force (3.112) also correctly accounts for the angular momentum loss. The torque on a unit volume located at the position x_i is

$$\begin{aligned} \frac{dT_i}{dV} &= \epsilon_{ijk} x_j \frac{dF_k}{dV} \\ &= -\frac{2G}{5c^5} \epsilon_{ijk} \rho(t, \mathbf{x}) x_j x_l \frac{d^5 Q_{kl}}{dt^5}, \end{aligned} \quad (3.116)$$

where we used eq. (3.109). Then

$$T_i = -\frac{2G}{5c^5} \epsilon_{ijk} \frac{d^5 Q_{kl}}{dt^5} \int d^3 x \rho(t, \mathbf{x}) x_j x_l. \quad (3.117)$$

²¹Higher-order corrections to the back-reaction force are given in eqs. (5.190) and (5.191). When comparing these results with eq. (3.114), observe that eqs. (5.190) and (5.191) are written in terms of the variable $h_{\mu\nu}$ defined in eq. (5.69) (which in the linearized limit reduces to $-\bar{h}_{\mu\nu}$), rather than in terms of $h_{\mu\nu}$.

²²Observe that there is here an abuse of notation. In eq. (3.114), x^i is the generic spatial variable. After taking the derivative with respect to x^i in eq. (3.115), we evaluate the force on the actual location of the particle, i.e. on the position $x^i(t)$ defined by eq. (3.111), and this gives eq. (3.112). For instance, for a point-like mass μ the quadrupole moment is $Q_{ij}(t) = \mu[x_i(t)x_j(t) - (1/3)\delta_{ij}|\mathbf{x}(t)|^2]$, where $x_i(t)$ is the actual trajectory of the particle, rather than the generic spatial variable x_i . So Q_{ij} is a given function of time only, and ∂_i in eq. (3.115) does not act on it.

In the last integral we can replace $x_j x_l$ by $x_j x_l - (1/3)\delta_{ij}r^2$, since the term $\sim \delta_{jl}$ gives zero contracted with $\epsilon_{ijk} d^5 Q_{kl}/dt^5$, so

$$T_i = -\frac{2G}{5c^5} \epsilon_{ijk} Q_{jl} \frac{d^5 Q_{kl}}{dt^5}. \quad (3.118)$$

In eq. (3.102) actually enters $\langle T_i \rangle$. Inside the average, we can integrate by parts twice, and we get

$$\langle T_i \rangle = -\frac{2G}{5c^5} \epsilon_{ikl} \langle \ddot{Q}_{ka} \ddot{Q}_{la} \rangle. \quad (3.119)$$

Comparison with eq. (3.99) shows that we have indeed correctly reproduced the expression for the angular momentum loss of the source.

It should be observed that this is also by far the quickest way to derive eq. (3.97), without going through the formalism of Noether's theorem and the more complicated algebra of Section 3.3.3. However, the derivation from the Noether theorem is more general, since it holds independently of the multipole expansion, and of whether or not the back-reaction of GWs on the source can be described by Newtonian mechanics. It is also conceptually more satisfying, since it stresses that the angular momentum carried by GWs is an intrinsic property of the gravitational field, independent of the description of the source, that can be computed by applying the standard methods of classical field theory, as is usually done in all other field theories.

Finally, we expect that the change in linear momentum should be given by $dP^i/dt = \langle F^i \rangle$. This is proportional to $\langle x_j(t) d^5 Q_{ij}/dt^5(t) \rangle$. Since the quadrupole moment is even under parity while x_j is odd, the integrand is odd and, for a periodic motion, its average over one orbital period vanishes and therefore $\langle F_i \rangle = 0$. This is in agreement with the fact that, in the quadrupole approximation, linear momentum is conserved, see the discussion below eq. (3.83).

Gravitational radiation and the equivalence principle

The above results also allow us to clarify an apparent paradox related to the equivalence principle. Consider, for simplifying the setting, a mass μ orbiting a mass M , in the limit $M/\mu \rightarrow \infty$. Thus, the light mass μ is accelerated by the gravitational field of the heavy mass M and, according to our computations, it radiates GWs (while M is static and does not radiate.) An observer at large distance from the source, well into the far region, would then in principle be able to detect the waves emitted, and would conclude that the mass μ indeed emits gravitational radiation.

Examine now the same situation from the point of view of an observer freely falling together with the mass μ . According to the equivalence principle, for this observer, in a sufficiently small region around the mass μ , the gravitational field vanishes. We have indeed seen explicitly in Section 1.3.2 how to construct such a freely falling frame all along a geodesic. In this frame the mass μ is not accelerated, and the

corresponding observer should then conclude that the mass μ does not radiate, contrary to the findings of the observer at infinity.

This apparent paradox can be understood recalling that the equivalence principle holds only locally, i.e. in a region around the mass μ much smaller than the typical scales of spatial variation of the gravitational field. One such scale is the length $\bar{\chi}$, over which retardation effects become important (and which determines the wavelength of the GWs detected by the observer at infinity.) Then, conclusions based on the equivalence principle can be valid only up to a distance r from the mass μ , much smaller than $\bar{\chi}$.²³ This means that the equivalence principle at most gives us informations on what happens in the near zone $r \ll \bar{\chi}$; GWs rather appear in the far zone $r \gg \bar{\chi}$, so there is no paradox in the fact that, using arguments valid only for $r \ll \bar{\chi}$, one does not see them. The presence of gravitational radiation at infinity is reflected, in the near zone, in the existence of the force given by eqs. (3.114) and (3.115). However, in the near region retardation effects are negligible, so this term just gives a correction to the static gravitational force, which furthermore is hidden behind other, much larger, corrections. We will see in fact in Chapter 5 that, in an expansion in v/c , the radiation-reaction force is of order $(v/c)^5$ (as it is already clear from the factor $1/c^5$ in eq. (3.114)), while the Newtonian gravitational field receives general-relativistic corrections, corresponding to conservative forces, already at orders $(v/c)^2$ and $(v/c)^4$. All these tidal-like terms, however, in the far region decrease much faster than $1/r$, leaving us with the radiation field only.

3.3.5 Radiation from a closed system of point masses

For a free point-like particle moving on a trajectory $x_0(t)$ in flat space-time, the energy-momentum tensor is²⁴

$$T^{\mu\nu}(t, \mathbf{x}) = \frac{p^\mu p^\nu}{\gamma m} \delta^{(3)}(\mathbf{x} - \mathbf{x}_0(t)), \quad (3.120)$$

where $\gamma = (1 - v^2/c^2)^{-1/2}$, and $p^\mu = \gamma m(dx_0^\mu/dt) = (E/c, \mathbf{p})$ is the four-momentum. If we have a set of free point particles labeled by an index A , moving on trajectories $x_A^\mu(t)$, the total energy-momentum tensor of the system is therefore

$$\begin{aligned} T^{\mu\nu}(t, \mathbf{x}) &= \sum_A \frac{p_A^\mu p_A^\nu}{\gamma_A m_A} \delta^{(3)}(\mathbf{x} - \mathbf{x}_A(t)) \\ &= \sum_A \gamma_A m_A \frac{dx_A^\mu}{dt} \frac{dx_A^\nu}{dt} \delta^{(3)}(\mathbf{x} - \mathbf{x}_A(t)), \end{aligned} \quad (3.121)$$

and in particular

$$T^{00}(t, \mathbf{x}) = \sum_A \gamma_A m_A c^2 \delta^{(3)}(\mathbf{x} - \mathbf{x}_A(t)). \quad (3.122)$$

²³In fact, r must also be much smaller than the scale of spatial variation of the quasi-static tidal gravitational fields near the mass μ , which in turn is much smaller than $\bar{\chi}$.

²⁴See, e.g. Landau and Lifshitz, Vol. II (1979), eq. (33.5), or Weinberg (1972), Section 2.8. The generalization to curved space is more easily obtained writing $p^\mu = m dx_0^\mu/d\tau$ where τ is the proper time of the particle. In flat space $c^2 d\tau^2 = -\eta_{\mu\nu} dx_0^\mu dx_0^\nu$, so $d/d\tau = \gamma d/dt$ and we get $p^\mu = \gamma m(dx_0^\mu/dt)$. In curved space, instead, $c^2 d\tau^2 = -g_{\mu\nu} dx_0^\mu dx_0^\nu$. Furthermore, in flat space $(1/\gamma)\delta^{(3)}(\mathbf{x} - \mathbf{x}_0(t)) = (d\tau/dt)\delta^{(3)}(\mathbf{x} - \mathbf{x}_0(t))$, which can be rewritten as $\int d\tau \delta^{(4)}(\mathbf{x} - \mathbf{x}_0(\tau))$. In curved space $\delta^{(4)}(\mathbf{x} - \mathbf{x}_0(\tau))$ becomes $(1/\sqrt{-g})\delta^{(4)}(\mathbf{x} - \mathbf{x}_0(\tau))$, so in the end in curved space $(1/\gamma)\delta^{(3)}(\mathbf{x} - \mathbf{x}_0(t))$ becomes $(d\tau/dt)(1/\sqrt{-g})\delta^{(3)}(\mathbf{x} - \mathbf{x}_0(t))$. In this way we obtain the curved-space expression given in eq. (5.47).

Observe that this energy-momentum tensor is conserved only if the particles follow the geodesics of flat space-time, $\dot{p}_A^\mu = 0$ for all A . Thus, a priori it is not legitimate to use it to compute the radiation emitted by a system of interacting particles moving on generic trajectories $\mathbf{x}_A(t)$. In a consistent treatment we should include in the energy-momentum tensor all the interaction terms among the particles, and possibly with external sources, that cause them to deflect from a straight-line trajectory. However, for a non-relativistic self-gravitating system it is still possible to use the energy-momentum tensor (3.121) to compute both the leading term in eq. (3.34) (i.e. the mass quadrupole radiation) as well as the next-to-leading term, i.e. the term proportional to $\dot{S}^{kl,m}$ (which, as we will discuss in more detail in Sect. 3.4, is the sum of mass octupole and current quadrupole radiation). In this way, using only linearized theory, we can obtain the correct lowest-order results that will be derived, with much more effort, with the full non-linear formalism described in Chapter 5. To this purpose we need to observe that the full energy-momentum tensor also has interaction terms responsible for binding the particles in a orbit. For a self-gravitating system these terms are $O(v^2/c^2)$, as it is clear from the fact the gravitational potential energy $-Gm_1m_2/r$ is of order v^2/c^2 .²⁵ Therefore, for a gravitationally-bound two-particle system in the non-relativistic limit,

$$T^{\mu\nu} = \sum_{A=1,2} m_A \frac{dx_A^\mu}{dt} \frac{dx_A^\nu}{dt} \delta^{(3)}(\mathbf{x} - \mathbf{x}_A(t)) + O(v^2/c^2). \quad (3.123)$$

Since $T^{00} = O(v^0)$, $T^{0i} = O(v/c)$ and $T^{ij} = O(v^2/c^2)$, T^{00} and T^{0i} can be computed consistently, to lowest order, ignoring the interaction term, while T^{ij} cannot. Observe also that the use of the lowest-order expressions

$$T^{00} = \sum_A m_A c^2 \delta^{(3)}(\mathbf{x} - \mathbf{x}_A(t)), \quad (3.124)$$

$$T^{0i} = \sum_A m_A c \dot{x}_A^i(t) \delta^{(3)}(\mathbf{x} - \mathbf{x}_A(t)), \quad (3.125)$$

is consistent with the conservation equation $\partial_0 T^{00} + \partial_i T^{0i} = 0$ since, with these expressions, $\partial_0 T^{00} = -\sum_A m_A c \dot{x}_A^i \partial_i \delta^{(3)}(\mathbf{x} - \mathbf{x}_A(t))$ and $\partial_i T^{0i} = +\sum_A m_A c \dot{x}_A^i \partial_i \delta^{(3)}(\mathbf{x} - \mathbf{x}_A(t))$. So, to lowest order $\partial_0 T^{00} = -\partial_i T^{0i}$, independently of the trajectory used. In contrast, the conservation equation $\partial_0 \tau^{0j} + \partial_i \tau^{ij} = 0$ (with τ^{ij} given in Note 25 and $\tau^{0j} = T^{0j}$ to lowest order) is only satisfied if $\mathbf{x}_A(t)$ satisfies the equation of motion in the potential V , as can be checked with the explicit computation.

Thus, if we want to compute directly S^{kl} or $\dot{S}^{kl,m}$ in eq. (3.34), we need T^{ij} , and therefore we need to include also the interaction terms, which are $O(v^2/c^2)$, just as the leading term in the T^{ij} components of the free-particle energy-momentum tensor. However, using energy-momentum conservation, we can transform S^{kl} into \ddot{M}^{kl} , see eq. (3.52). Similarly, using eq. (3.54), we can trade \dot{S}^{ijk} for $\overset{\dots}{M}^{ijk}$ and \ddot{P}^{ijk} . The derivation of eq. (3.54) uses the conservation of energy-momentum tensor so, when

²⁵The explicit form of these terms will be given in Section 5.3.2, when we study systematically the relativistic corrections. We will see in eqs. (5.111)–(5.113) that, including the first post-Newtonian correction, T^{00} must be replaced by

$$\tau^{00} = \left(1 + \frac{4V}{c^2}\right) T^{00} - \frac{7}{8\pi G} \partial_k V \partial_k V,$$

while T^{0i} is unchanged and T^{ij} is replaced by

$$\tau^{ij} = T^{ij} + \frac{1}{4\pi G} \left(\partial_i V \partial_j V - \frac{1}{2} \delta_{ij} \partial_k V \partial_k V \right),$$

where V is given in eq. (5.39) and, to lowest order, reduces to the Newtonian potential.

we write the GW amplitude in terms of \ddot{M}^{ijk} and $\ddot{P}^{i,jk}$, we are already implicitly using the correct $T^{\mu\nu}$, with all the necessary interaction terms.

The important point is that, to trade $\dot{S}^{ij,k}$ for \ddot{M}^{ijk} and $\ddot{P}^{i,jk}$, we do not need to know the explicit form of $T^{\mu\nu}$, including the interaction terms, but only that it satisfies energy-momentum conservation. The advantage of this procedure is that M^{ij} and M^{ijk} only depend on T^{00} , and $P^{i,jk}$ only depends on T^{0i} . Therefore, to lowest order they can be consistently computed neglecting the potential terms in $T^{\mu\nu}$. In conclusion, both the leading term (i.e. the quadrupole radiation) and the next-to-leading term (i.e. the mass octupole plus current quadrupole radiation) can be consistently computed using eq. (3.124) to evaluate M^{ij} and M^{ijk} , and eq. (3.125) to evaluate $P^{i,jk}$, and then using eqs. (3.52) and (3.54) to evaluate S^{ij} and $\dot{S}^{ij,k}$. In contrast, if one wants to compute S^{ij} and $\dot{S}^{ij,k}$ directly from T^{ij} , which is $O(v^2)$, even to lowest order one needs to include the interaction terms, and one cannot use the free-particle energy-momentum tensor.

As will be shown in Section 5.1, the relativistic corrections to the Newtonian orbit start from order v^2/c^2 . Therefore, the computation of the GW amplitude to leading and next-to-leading order in v/c can be performed evaluating the components T^{00} and T^{0i} of free-particle energy momentum tensor on the Newtonian orbit, and using them to compute M^{ij} , M^{ijk} and $P^{i,jk}$. We will perform these computations explicitly in Problems 3.2 and 3.3, in the Solved Problems section. Observe however that, in the radiated power, the corrections to the quadrupole amplitude give corrections to the leading term in the power of order $|1 + O(v^2/c^2)|^2 = 1 + O(v^2/c^2)$, while the mass octupole and current quadrupole give a correction $|O(v/c)|^2$, which is again $O(v^2/c^2)$, see the discussion below eq. (3.156).

For a non-relativistic two-body system it is convenient to define as usual the relative coordinate $\mathbf{x}_0 = \mathbf{x}_1 - \mathbf{x}_2$ and the center-of-mass coordinate

$$\mathbf{x}_{\text{CM}} = \frac{m_1 \mathbf{x}_1 + m_2 \mathbf{x}_2}{m_1 + m_2}. \quad (3.126)$$

(Starting from $O(v^2/c^2)$ this must actually be replaced by a center-of-energy, which also receives contributions from the interaction potential). We also denote by $m = m_1 + m_2$ the total mass and by $\mu = m_1 m_2 / m$ the reduced mass. For a non-relativistic system, the second mass moment can be written as

$$M^{ij} = m_1 x_1^i x_1^j + m_2 x_2^i x_2^j = m x_{\text{CM}}^i x_{\text{CM}}^j + \mu x_0^i x_0^j. \quad (3.127)$$

If the system is isolated, x_{CM}^i is not accelerating and does not contribute to the GW production. It is then convenient to choose the frame such that $x_{\text{CM}}^i = 0$, and we are left with a single effective particle of mass μ and coordinate $x_0^i(t)$. In the CM frame, the mass density is then

$$\rho(t, \mathbf{x}) = \mu \delta^{(3)}(\mathbf{x} - \mathbf{x}_0(t)), \quad (3.128)$$

the second mass moment is

$$M^{ij}(t) = \mu x_0^i(t) x_0^j(t), \quad (3.129)$$

and the mass quadrupole is

$$Q^{ij}(t) = \mu \left(x_0^i(t)x_0^j(t) - \frac{1}{3}r_0^2(t)\delta^{ij} \right). \quad (3.130)$$

We can now study the radiation emitted by a two-body system whose relative coordinate performs a given periodic motion, say simple harmonic oscillations. Suppose that the relative coordinate $\mathbf{x}_0(t)$ performs a simple periodic motion with frequency ω_s , say along the z direction,²⁶

$$z_0(t) = a_1 \cos \omega_s t. \quad (3.131)$$

Then

$$\begin{aligned} M^{ij}(t) &= \delta^{i3}\delta^{j3} \mu z_0^2(t) \\ &= \delta^{i3}\delta^{j3} \frac{\mu a_1^2}{2} (1 + \cos 2\omega_s t). \end{aligned} \quad (3.132)$$

Since the GW amplitude depends on the second derivative of M^{ij} , the constant term does not contribute and the only contribution to h_{ij}^{TT} comes from the term proportional to $\cos 2\omega_s t$. From eq. (3.55), we see that the corresponding waveform h_{ij}^{TT} oscillates as $\cos 2\omega_s t$. This shows that *a non-relativistic source performing simple harmonic oscillations with a frequency ω_s emits monochromatic quadrupole radiation at $\omega = 2\omega_s$.*

However, the fact that the quadrupole radiation is at twice the source frequency is only true if the source performs a simple harmonic motion. For instance, if the motion of the source is a superposition of a periodic motion and of its higher harmonics, e.g. if

$$z_0(t) = a_1 \cos \omega_s t + a_2 \cos 2\omega_s t + \dots, \quad (3.133)$$

then $z_0^2(t)$ contains the term

$$a_1^2 \cos^2 \omega_s t = a_1^2 \frac{1 + \cos 2\omega_s t}{2}, \quad (3.134)$$

considered above, plus a term

$$a_2^2 \cos^2 2\omega_s t = a_2^2 \frac{1 + \cos 4\omega_s t}{2}, \quad (3.135)$$

which gives radiation at $\omega_{\text{gw}} = 4\omega_s$, etc., but also mixed terms such as

$$2a_1 a_2 \cos(\omega_s t) \cos(2\omega_s t) = a_1 a_2 (\cos \omega_s t + \cos 3\omega_s t). \quad (3.136)$$

Therefore in this case quadrupole radiation is emitted at all frequencies $n\omega_s$ for all integers n , both even and odd, including $n = 1$. We will see an example of this type in Section 4.1.2, when we study the radiation emitted from a mass in a Keplerian elliptic orbit.

An even simpler example is given by a system of two masses connected by a spring with rest length L (see Problem 3.1). In this case the relative coordinate satisfies

$$z_0(t) = L + a \cos \omega_s t, \quad (3.137)$$

and in $z_0^2(t)$, besides a constant and a term $(a^2/2) \cos 2\omega_s t$, we also have a term $2La \cos \omega_s t$, so the spectrum of gravitational radiation has two lines, one at $\omega = \omega_s$, and one at $\omega = 2\omega_s$.

²⁶In a one-dimensional motion this example would be quite unrealistic, since the two bodies would go through each other whenever $\cos \omega_s t = 0$. However, this is just an example to illustrate what happens to a typical oscillatory mode of a system. For instance, one can consider an elliptic motion on a plane, which is the combination of two simple oscillations along the two axes.

3.4 Mass octupole and current quadrupole

We now examine the next-to-leading term of the expansion (3.34),

$$(h_{ij}^{\text{TT}})_{\text{next-to-leading}} = \frac{1}{r} \frac{4G}{c^5} \Lambda_{ij,kl}(\hat{\mathbf{n}}) n_m \dot{S}^{kl,m}(t - r/c). \quad (3.138)$$

By definition $\dot{S}^{kl,m}$ is symmetric in kl , and it has no special symmetry with respect to the exchange of k with m . We have seen in eq. (3.54) that

$$\dot{S}^{kl,m} = \frac{1}{6} \ddot{M}^{klm} + \frac{1}{3} (\ddot{P}^{k,lm} + \ddot{P}^{l,km} - 2\ddot{P}^{m,kl}). \quad (3.139)$$

Therefore $\dot{S}^{kl,m}$ separates into a totally symmetric tensor \ddot{M}^{klm} plus a tensor with mixed symmetry. The meaning of this separation from the point of view of group theory is explained in Problem 3.4, in the Solved Problems section. The totally symmetric term generates mass octupole radiation, while the term with mixed symmetry is called the current quadrupole.

Mass octupole

We consider first the mass octupole radiation. The mass octupole \mathcal{O}^{klm} is defined removing all traces from M^{ijk} ,

$$\mathcal{O}^{klm} = M^{klm} - \frac{1}{5} (\delta^{kl} M^{k'k'm} + \delta^{km} M^{k'l k'} + \delta^{lm} M^{kk'k'}). \quad (3.140)$$

Using the fact that $\Lambda_{ij,kl}(\hat{\mathbf{n}})$ is transverse and traceless, we see that the contraction of the trace part with $\Lambda_{ij,kl}(\hat{\mathbf{n}}) n_m$ gives zero, and we can use M^{klm} or \mathcal{O}^{klm} interchangeably in the expression for h_{ij}^{TT} . Therefore the mass octupole contribution to h_{ij}^{TT} can be written as

$$(h_{ij}^{\text{TT}})_{\text{oct}} = \frac{1}{r} \frac{2G}{3c^5} \Lambda_{ij,kl}(\hat{\mathbf{n}}) n_m \ddot{\mathcal{O}}^{klm}. \quad (3.141)$$

Similarly to the case of quadrupole radiation, the use of \mathcal{O}^{klm} is nicer from a group-theoretical point of view, since it is a pure spin-3 tensor, see Problem 3.4, while the use of M^{ijk} is simpler in actual computations. We will use \ddot{M}^{klm} and $\ddot{\mathcal{O}}^{klm}$ interchangeably in eq. (3.141).

Observe that, when we consider quantities quadratic in h_{ij}^{TT} , as for instance the radiated energy, there is no interference between the mass quadrupole and the mass octupole terms because they have different parity. Under a parity operation, $\mathbf{x} \rightarrow -\mathbf{x}$, the mass density is a true scalar, and therefore the quadrupole is invariant while the octupole changes sign (for the same reason, in electrodynamics there is no interference between dipole and quadrupole radiation.) More generally, we will see in Section 3.5 how to systematically organize the multipole expansion so that there are no interference terms to all orders.

Comparing the mass quadrupole and the mass octupole we see that, while the contribution to the GW amplitude from the mass quadrupole

is proportional to the second time derivative of M^{ij} , the contribution from the mass octupole is proportional to $(1/c)$ times the third time derivative of M^{ijk} . If d is the typical dimension of the source, the tensor M^{ijk} differ from M^{ij} by a factor $O(d)$. Each time derivative carries a factor $O(\omega_s)$, where ω_s is the typical frequency of the movement of matter inside the source, so $(1/c)\ddot{M}^{ijk} = O(\omega_s d/c)\ddot{M}^{ij}$. Since $\omega_s d \sim v$ is the typical velocity inside the source, the octupole contribution to \dot{h}_{ij}^{TT} is smaller than the quadrupole contribution by a factor $O(v/c)$, and the contribution of the mass octupole to the radiated power is smaller than the contribution of the mass quadrupole by a factor $O(v^2/c^2)$.

Consider now a two-body non-relativistic system whose relative coordinate in the center-of-mass frame is described by a function $x_0^i(t) = x_1^i(t) - x_2^i(t)$, with a reduced mass μ , and define $\delta m = m_2 - m_1$. Then (as we show in Problem 3.3) to lowest order in v/c

$$M^{ijk}(t) = \mu \frac{\delta m}{m} x_0^i(t) x_0^j(t) x_0^k(t). \quad (3.142)$$

Suppose now that $x_0(t)$ performs simple harmonic oscillations with frequency ω_s . Then, each factor $x_0^i(t)$ is the superposition of a term oscillating as $e^{i\omega_s t}$ and of a term oscillating as $e^{-i\omega_s t}$, so M^{ijk} is the sum of terms oscillating as $e^{\pm i\omega_s t}$ and of terms oscillating as $e^{\pm 3i\omega_s t}$. Therefore *a source performing simple harmonic oscillations at a frequency ω_s emits octupole radiation at $\omega = \omega_s$ and at $\omega = 3\omega_s$* .

If a non-relativistic source performs simple harmonic oscillations, then its energy spectrum is made of a stronger line due to quadrupole radiation at $\omega = 2\omega_s$, plus two smaller “lateral bands” due to the octupole at $\omega = \omega_s$ and at $\omega = 3\omega_s$, as we will see in more detail in Problem 3.3. Recall however from Section 3.3.5 that periodic trajectories that are not simple harmonic motions produce a more complicated spectrum, in which the quadrupole can already contribute to all frequencies $n\omega_s$, for all integer n .

The power emitted per unit solid angle by the octupole moment is computed inserting \dot{h}_{ij}^{TT} , obtained from eq. (3.141), into the expression for the power given in eq. (1.153). This gives

$$\begin{aligned} P_{\text{oct}} &= \frac{c^3 r^2}{32\pi G} \int d\Omega \langle (\dot{h}_{ij}^{\text{TT}})_{\text{oct}} (\dot{h}_{ij}^{\text{TT}})_{\text{oct}} \rangle \\ &= \frac{c^3}{32\pi G} \frac{4G^2}{9c^{10}} \left\langle \frac{d^4 \mathcal{O}^{klm}}{dt^4} \frac{d^4 \mathcal{O}^{k'l'm'}}{dt^4} \right\rangle \int d\Omega \Lambda_{ij,kl} \Lambda_{ij,k'l'} n_m n_{m'}. \end{aligned} \quad (3.143)$$

Using the property (1.37) of the Lambda tensor, together with $\Lambda_{ij,kl} = \Lambda_{kl,ij}$, we have $\Lambda_{ij,kl} \Lambda_{ij,k'l'} = \Lambda_{kl,k'l'}$. Then, renaming the indices, we get

$$P_{\text{oct}} = \frac{G}{72\pi c^7} \left\langle \frac{d^4 \mathcal{O}^{ijm}}{dt^4} \frac{d^4 \mathcal{O}^{klp}}{dt^4} \right\rangle \int d\Omega \Lambda_{ij,kl} (\hat{\mathbf{n}}) n_m n_p. \quad (3.144)$$

To integrate over the solid angle we need the identities (3.21) and (3.22), together with eq. (3.23) with $l = 3$,

$$\int \frac{d\Omega}{4\pi} n_i n_j n_k n_l n_m n_p = \frac{1}{105} (\delta_{ij} \delta_{kl} \delta_{mp} + \dots), \quad (3.145)$$

where the dots denote the other 14 possible pairings of indices. Using the fact that \mathcal{O}^{ijk} is totally symmetric and traceless, the contractions are straightforward, and we get

$$P_{\text{oct}} = \frac{G}{189 c^7} \left\langle \frac{d^4 \mathcal{O}^{ijk}}{dt^4} \frac{d^4 \mathcal{O}^{ijk}}{dt^4} \right\rangle. \quad (3.146)$$

Current quadrupole

The current quadrupole is given by the second term in eq. (3.139). Its physical meaning can be understood observing that, from the definition (3.41),

$$\begin{aligned} & P^{k,lm} + P^{l,km} - 2P^{m,kl} \\ &= \frac{1}{c} \int d^3x [T^{0k}x^l x^m + T^{0l}x^k x^m - 2T^{0m}x^k x^l] \\ &= \frac{1}{c} \int d^3x [x^l(x^m T^{0k} - x^k T^{0m}) + x^k(x^m T^{0l} - x^l T^{0m})] \\ &= \int d^3x [x^l j^{mk} + x^k j^{ml}], \end{aligned} \quad (3.147)$$

where

$$j^{jk} = \frac{1}{c} (x^j T^{0k} - x^k T^{0j}). \quad (3.148)$$

This is the angular momentum density associated to the (j,k) plane. We write $j^{jk} = \epsilon^{jkl} j^l$, where j^l is the l -th component of the angular momentum density vector, and we define

$$J^{i,j} = \int d^3x j^i x^j, \quad (3.149)$$

so $J^{i,j}$ is the first moment of the angular momentum density (i.e. the dipole moment of the angular momentum distribution). Then we get

$$P^{k,lm} + P^{l,km} - 2P^{m,kl} = \epsilon^{mkp} J^{p,l} + \epsilon^{mlp} J^{p,k}. \quad (3.150)$$

Therefore the current quadrupole is the first moment of the angular momentum density of the source, symmetrized over the indices k,l . Its contribution to the GW amplitude can be written as

$$(h_{ij}^{\text{TT}})_{\text{curr quad}} = \frac{1}{r} \frac{4G}{3c^5} \Lambda_{ij,kl}(\hat{\mathbf{n}}) n_m \left(\epsilon^{mkp} \ddot{J}^{p,l} + \epsilon^{mlp} \ddot{J}^{p,k} \right). \quad (3.151)$$

We will indeed see in the next section that the full multipole expansion can be organized systematically so that it is determined by two types of objects: the momenta of the energy density of the source (which, to leading order in v/c , are the same as the momenta of the mass density), like the mass quadrupole Q^{ij} , the mass octupole \mathcal{O}^{ijk} , etc., and the momenta of the angular momentum density of the source, such as the current quadrupole.

The power associated to the current quadrupole is computed just as we have done for the mass quadrupole and mass octupole: we write

$$\begin{aligned} P_{\text{curr quad}} &= \frac{c^3 r^2}{32\pi G} \int d\Omega \langle (\dot{h}_{ij}^{\text{TT}})_{\text{curr quad}} (\dot{h}_{ij}^{\text{TT}})_{\text{curr quad}} \rangle \\ &= \frac{c^3}{32\pi G} \frac{16G^2}{9c^{10}} \int d\Omega \Lambda_{kl,k'l'} n_m n_{m'} \\ &\quad \times \langle (\epsilon^{mkp} J^{l,p,l} + \epsilon^{mlp} J^{k,p,k}) (\epsilon^{m'k'p'} J^{l',p',l'} + \epsilon^{m'l'p'} J^{k',p',k'}) \rangle, \end{aligned} \quad (3.152)$$

where we used again $\Lambda_{ij,kl} \Lambda_{ij,k'l'} = \Lambda_{kl,k'l'}$. The angular integration is performed using the identities (3.21) and (3.22). Observe also that the term in the Lambda tensor with four factors of n , i.e. $n_k n_l n_{k'} n_{l'}$ (see eq. (1.39)) does not contribute since, together with the factors $n_m n_{m'}$ in eq. (3.152), it gives a totally symmetric tensor $n_k n_l n_m n_{k'} n_{l'} n_{m'}$, which vanishes upon contraction with ϵ^{mkp} or ϵ^{mlp} .

When performing contractions, we also make use of the fact that $J^{i,j}$ is traceless, since

$$\begin{aligned} J^{i,i} &= \int d^3x x^i j^i \\ &= \frac{1}{c} \int d^3x x^i \epsilon^{ijk} x^j T^{0k} = 0 \end{aligned} \quad (3.153)$$

(the sum over i is understood). Then, we get

$$P_{\text{curr quad}} = \frac{16G}{45c^7} \langle \ddot{\mathcal{J}}^{ij} \ddot{\mathcal{J}}^{ij} \rangle, \quad (3.154)$$

where we introduced the traceless symmetric matrix

$$\mathcal{J}^{ij} \equiv \frac{J^{i,j} + J^{j,i}}{2}, \quad (3.155)$$

that is, the symmetrization of the dipole moment of the angular momentum density. Putting together the power radiated by the mass quadrupole, current quadrupole and mass octupole, we therefore get

$$P = \frac{G}{c^5} \left[\frac{1}{5} \langle \ddot{Q}_{ij} \ddot{Q}_{ij} \rangle + \frac{1}{c^2} \frac{16}{45} \langle \ddot{\mathcal{J}}_{ij} \ddot{\mathcal{J}}_{ij} \rangle \right. \\ \left. + \frac{1}{c^2} \frac{1}{189} \langle \frac{d^4 \mathcal{O}_{ijk}}{dt^4} \frac{d^4 \mathcal{O}_{ijk}}{dt^4} \rangle + O\left(\frac{v^4}{c^4}\right) \right], \quad (3.156)$$

where $O(v^4/c^4)$ denotes the contributions from higher orders in the multipole expansion. In this formula, one must be careful to include in Q_{ij} also its first corrections $O(v^2/c^2)$, since it gives a contribution to the power of the same order as that due to the mass octupole and current quadrupole. This means that Q_{ij} here is not simply the quadrupole of the mass distribution. Rather, we must go back to its original definition in terms of T^{00} , see eq. (3.37) and include in T^{00} not only the terms of

order ρc^2 , where ρ is the mass density, but also the terms of order ρv^2 . Furthermore, the time-dependence of the leading term must be computed using the relativistic equations of motion, including corrections up to $O(v^2/c^2)$.

It is quite difficult to imagine a realistic physical system for which the time derivative of the mass quadrupole vanishes, but still the mass octupole is time-varying. For this reason, the mass octupole is always a correction to the leading term. However, there are interesting physical situations where *both* the mass quadrupole and the mass octupole are constant in time and therefore do not contribute to GW production, while the current quadrupole still contributes, so it becomes the leading term. To have M^{ij} and M^{ijk} constant, in fact, it suffices that the energy density T^{00} be constant. Then all the mass momenta are constant, see e.g. eqs. (3.35)–(3.38). Still, the angular momentum density and its momenta, such as its dipole $J^{i,j}$, are not necessarily constant. Consider for example a ring in the (x, y) plane with a uniform mass density ρ , rotating around the z axis. Even if any single volume element of the ring rotates, this rotation does not induce any temporal variation in the density ρ since the ring is spatially uniform, so all mass moments are constant.²⁷ However, this ring has non-vanishing angular momentum along z . To obtain a system with a dipole moment of angular momentum $J^{i,j}$, we can simply take two rings, both rotating around the z axis, but one counterclockwise and one clockwise, as in Fig. 3.3. The upper ring has a positive J^z while the lower one has a negative J^z , so it is clear that the whole system has a non-vanishing dipole moment $J^{z,z}$.²⁸

If the rotational velocities of the rings are not constant, this dipole moment of the angular momentum is time-dependent. A physical example of a system of this type is provided by the torsional oscillations of a neutron star. It is possible that, either because of some external perturbation, or because of a “corequake”, the upper hemisphere of a NS suffers a clockwise torsion while the lower hemisphere receives a counterclockwise torsion (with the equator which, by symmetry reasons, stays fixed). Then the two hemispheres will start oscillating back and forth in opposite directions, so that when one rotates clockwise the other rotates counterclockwise, and vice versa. This system will then emit current quadrupole radiation, but not mass quadrupole nor mass octupole radiation. Another important example of this type is the r -mode of neutron stars, which will be discussed in Vol. 2.

It is therefore worthwhile to study the current quadrupole radiation in more detail, and derive its angular distribution. First, we compute the amplitude of the GWs radiated in the z direction. This is quite simple, since we just have to substitute $n = (0, 0, 1)$ into eq. (3.151). Using the explicit expression for the Lambda tensor, eq. (1.39), and recalling that, for a wave traveling along z , $h_{11} = h_+$ and $h_{12} = h_\times$, we obtain

$$h_+ = \frac{1}{r} \frac{4G}{3c^5} (\ddot{J}_{1,2} + \ddot{J}_{2,1}), \quad (3.157)$$

$$h_\times = \frac{1}{r} \frac{4G}{3c^5} (\ddot{J}_{2,2} - \ddot{J}_{1,1}). \quad (3.158)$$

²⁷One might wonder how it is possible that there is no quadrupole radiation from the whole ring, given that every single mass element is in rotation and therefore radiates GWs. From this “microscopic” point of view, the answer is that the total amplitude is the sum over the contribution of all the mass elements, and these contributions interfere destructively, so that the total GW amplitude h_{ij} vanishes.

²⁸It also has a non-zero $J^{x,x}$ and $J^{y,y}$ (consistent with the condition $J^{i,i} = 0$). This can be seen by drawing the direction of the angular momentum vector $\delta\mathbf{J} = (\delta m)\mathbf{r} \times \mathbf{v}$ of various mass elements, where \mathbf{r} is measured from the origin of the coordinate system, see Fig. 3.3. We see for instance that both the infinitesimal mass elements labeled a and c have $J^y < 0$ and are at a coordinate $y > 0$, therefore their contribution to $J^{y,y}$ is negative. Similarly, for the mass elements b and d we have $J^y > 0$, but they have a coordinate $y < 0$, so their contribution to $J^{y,y}$ is again negative.

To obtain the amplitudes h_+ and h_\times for a GW propagating into an arbitrary direction, we proceed as we did for the mass quadrupole, between eqs. (3.67) and (3.72). We first write

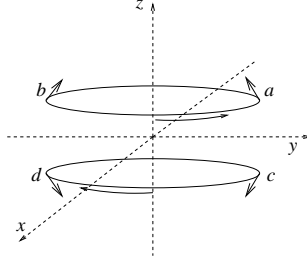


Fig. 3.3 Two rings, both with uniform mass density, one rotating counterclockwise and one clockwise. The arrows show the direction of the angular momentum $\delta\mathbf{J} = (\delta m)\mathbf{r} \times \mathbf{v}$ (with \mathbf{r} measured from the origin of the coordinate system, rather than from the center of each disk) of four infinitesimal mass elements, labeled a, b, c, d .

²⁹Comparing with eq. (3.72) we see that the angular dependence is the same as for the mass quadrupole, if we replace M_{ij} by $J_{i,j}$, and we exchange the roles of h_+ and h_\times (with an additional minus sign for $(h_\times)_{\text{curr quad}}$). This was already clear from a comparison of eqs. (3.157) and (3.158) with eqs. (3.65) and (3.66), and from the fact that both M_{ij} and $J_{i,j}$ transform as rank-2 tensors under rotations.

$$h_+ = \frac{1}{r} \frac{4G}{3c^5} (\ddot{J}'_{1,2} + \ddot{J}'_{2,1}), \quad (3.159)$$

$$h_\times = \frac{1}{r} \frac{4G}{3c^5} (\ddot{J}'_{2,2} - \ddot{J}'_{1,1}), \quad (3.160)$$

where $J'_{i,j}$ are the components of the angular momentum dipole in the $(\hat{\mathbf{u}}, \hat{\mathbf{v}}, \hat{\mathbf{n}})$ frame defined in Fig. 3.2. Since $J_{i,j}$ is a spatial tensor with two indices, it transforms under rotation just as we found for M_{ij} in eq. (3.71), i.e. $J'_{i,j} = \mathcal{R}_{ki}\mathcal{R}_{lj}J_{k,l}$, with \mathcal{R} given by eq. (3.70). Performing the matrix multiplication, we get

$$\begin{aligned} h_+(t; \theta, \phi)|_{\text{curr quad}} &= \frac{1}{r} \frac{4G}{3c^5} [(\ddot{J}_{1,1} - \ddot{J}_{2,2}) \sin 2\phi \cos \theta \\ &\quad + (\ddot{J}_{1,2} + \ddot{J}_{2,1}) \cos 2\phi \cos \theta \\ &\quad - (\ddot{J}_{1,3} + \ddot{J}_{3,1}) \cos \phi \sin \theta \\ &\quad + (\ddot{J}_{2,3} + \ddot{J}_{3,2}) \sin \phi \sin \theta], \end{aligned} \quad (3.161)$$

$$\begin{aligned} h_\times(t; \theta, \phi)|_{\text{curr quad}} &= \frac{1}{r} \frac{4G}{3c^5} [-\ddot{J}_{1,1}(\cos^2 \phi - \sin^2 \phi \cos^2 \theta) \\ &\quad - \ddot{J}_{2,2}(\sin^2 \phi - \cos^2 \phi \cos^2 \theta) \\ &\quad + \ddot{J}_{3,3} \sin^2 \theta \\ &\quad + (\ddot{J}_{1,2} + \ddot{J}_{2,1}) \sin \phi \cos \phi (1 + \cos^2 \theta) \\ &\quad - (\ddot{J}_{1,3} + \ddot{J}_{3,1}) \sin \phi \sin \theta \cos \theta \\ &\quad - (\ddot{J}_{2,3} + \ddot{J}_{3,2}) \cos \phi \sin \theta \cos \theta]. \end{aligned} \quad (3.162)$$

This gives the angular distribution of the current quadrupole radiation,²⁹ for $J^{i,j}$ arbitrary (but satisfying the zero-trace condition $J_{1,1} + J_{2,2} + J_{3,3} = 0$). To check these equations we can plug them into the expression (1.154) for the angular distribution of the power in terms of h_+ and h_\times ,

$$\frac{dP}{d\Omega} = \frac{c^3 r^2}{16\pi G} \langle \dot{h}_+^2 + \dot{h}_\times^2 \rangle. \quad (3.163)$$

Performing explicitly the integral over $d\Omega = d\phi d\theta |\sin \theta|$, we verify that we get eq. (3.154) back.

Linear momentum losses

Finally, it is interesting to observe that the leading term contributing to the loss of linear momentum comes from the interference between the quadrupole term and the next-to-leading term (i.e. the octupole plus current quadrupole). In fact, recall from eq. (1.164) that dP^k/dt is proportional to

$$\int d\Omega \dot{h}_{ij}^{\text{TT}} \partial_k h_{ij}^{\text{TT}}. \quad (3.164)$$

Using eqs. (3.59) and (3.138) we write

$$\begin{aligned} h_{ij}^{\text{TT}} &= [h_{ij}^{\text{TT}}]_{\text{quad}} + [h_{ij}^{\text{TT}}]_{\text{next-to-leading}} \\ &= \frac{1}{r} \frac{2G}{c^4} \left[\ddot{Q}_{ij}^{\text{TT}} + \frac{2}{c} n_m \dot{S}_{ij,m}^{\text{TT}} \right], \end{aligned} \quad (3.165)$$

where $\dot{S}_{ij,m}^{\text{TT}} = \Lambda_{ij,kl} \dot{S}_{kl,m}$. In the product $\dot{h}_{ij}^{\text{TT}} \partial_k h_{ij}^{\text{TT}}$ we have diagonal terms and interference terms between the quadrupole and the next-to-leading term. The diagonal terms are proportional to

$$\int d\Omega \ddot{Q}_{ij}^{\text{TT}} \partial_k \ddot{Q}_{ij}^{\text{TT}}, \quad (3.166)$$

for the quadrupole, and to

$$\int d\Omega \left(n_l \ddot{S}_{ij,l}^{\text{TT}} \right) \partial_k \left(n_m \dot{S}_{ij,m}^{\text{TT}} \right), \quad (3.167)$$

for the next-to-leading term. Because of parity, these angular integrals vanish if the integrand is the product of an odd number of factors n_i . Therefore, we need to count the number of \hat{n} in these expressions. The TT projection is performed with the Lambda tensor, which has an even number of factors \hat{n} . As for the derivative ∂_k which appears in eqs. (3.166) and (3.167), recall that, on a function of r , $\partial_k f(r) = (\partial_k r) df/dr = n^k df/dr$, while $\partial_k n^i = \partial_k (x^i/r) = (1/r)(\delta^{ik} - n^i n^k)$. Therefore the effect of ∂_k is always to lower or to raise by one the number of factors n^i , i.e. to transform a term with an even number of \hat{n} in a term with an odd number, and vice versa.

Then, we see that the diagonal terms in eqs. (3.166) and (3.167) have an odd number of factors \hat{n} , so their angular integral vanish. In the interference terms, such as

$$\int d\Omega \ddot{Q}_{ij}^{\text{TT}} \partial_k \left(n_m \dot{S}_{ij,m}^{\text{TT}} \right), \quad (3.168)$$

the integrand is even in \hat{n} and in general is non-vanishing. So, while the radiated energy only gets contributions from the diagonal terms (as we will verify to all orders in the multipole expansion in the next section), the radiated momentum only gets contributions from the interference between multipoles of different parity, in order to compensate for the minus sign acquired by the derivative ∂_k under $\hat{n} \rightarrow -\hat{n}$.

3.5 Systematic multipole expansion

In eq. (3.34) the multipole expansion has been organized in terms of tensors such as S^{kl} , $\dot{S}^{kl,m}$, $\ddot{S}^{kl,m_1 m_2}$, etc. which have two sets of indices (separated by a comma), the first always made by two indices k, l and the second made by a generic number of indices, m_1, \dots, m_N . These tensors are symmetric under the exchange of k and l , and are also symmetric under the exchange of indices in the m_1, \dots, m_N set. However, they have

no special symmetry property under the exchange of indices between the two sets (and they are in general not traceless under contraction of pairs of indices). At next-to-leading order, we separated by hand the term $\dot{S}^{kl,m}$ into two contributions, one corresponding to mass octupole and one to current quadrupole. The reason underlying this separation is group-theoretical. As we discuss in Problem 3.4, this corresponds to a decomposition into irreducible representations of the rotation group. To generalize such a construction to arbitrary orders in the multipole expansion, we must introduce a complete set of representations of the rotation group, for all multipoles. There are two particularly convenient ways of doing that. One is to consider tensors which are symmetric and trace-free (STF) with respect to all pairs of indices. This formalism will be introduced in Section 3.5.1, and we will use it extensively in particular in Chapter 5. A second possibility is to introduce the spherical components of tensors and the tensor spherical harmonics, which is the approach that we discuss in Section 3.5.2

To illustrate these two different approaches, it can be useful to begin our discussion by recalling how the multipole expansion works in the simpler case of a static situation, governed by a Poisson equation of the form

$$\nabla^2 \phi = -4\pi\rho, \quad (3.169)$$

which would be the case, e.g. in electrostatics or in Newtonian gravity. We consider a stationary source with density $\rho(\mathbf{x})$ localized in space, so $\rho(\mathbf{x}) = 0$ if $r > d$, where d is the source size. The most general solution in the external region $r > d$ can be written as

$$\phi(\mathbf{x}) = 4\pi \sum_{l=0}^{\infty} \sum_{m=-l}^l \frac{Q_{lm}}{2l+1} \frac{Y_{lm}(\theta, \phi)}{r^{l+1}}. \quad (3.170)$$

In fact, for $r > 0$,

$$\nabla^2 \left[\frac{Y_{lm}(\theta, \phi)}{r^{l+1}} \right] = 0, \quad (3.171)$$

as can be seen immediately from the expression of the Laplacian in spherical coordinates,

$$\nabla^2 \psi(\mathbf{x}) = \frac{1}{r^2} \frac{\partial}{\partial r} \left(r^2 \frac{\partial \psi}{\partial r} \right) - \frac{\mathbf{L}^2}{r^2}, \quad (3.172)$$

together with the property $\mathbf{L}^2 Y_{lm} = l(l+1)Y_{lm}$ of the spherical harmonics. Then, in the external region $r > d$, all terms in the sum in eq. (3.170) are separately solution of the vacuum equation $\nabla^2 \phi = 0$. The fact that eq. (3.170) is the most general vacuum solution follows from the fact that the spherical harmonics provide a complete set of representations of the rotation group. On the other hand, the solution of eq. (3.169) (subject to the boundary condition that ϕ approaches zero as $r \rightarrow \infty$) can be written in terms of the Green's function of the Laplacian, as

$$\phi(\mathbf{x}) = \int d^3y \frac{1}{|\mathbf{x} - \mathbf{y}|} \rho(\mathbf{y}), \quad (3.173)$$

which is valid both for \mathbf{x} inside and outside the source. Outside the source we have $|\mathbf{x}| > |\mathbf{y}|$, and we can use the addition theorem for spherical harmonics³⁰ in the form

$$\frac{1}{|\mathbf{x} - \mathbf{y}|} = 4\pi \sum_{l=0}^{\infty} \sum_{m=-l}^l \frac{1}{2l+1} \frac{r'^l}{r^{l+1}} Y_{lm}^*(\theta', \phi') Y_{lm}(\theta, \phi), \quad (3.174)$$

where we used the notation $|\mathbf{x}| = r$ and $|\mathbf{y}| = r'$; (θ, ϕ) are the polar angles of $\hat{\mathbf{x}}$ and (θ', ϕ') of $\hat{\mathbf{y}}$. Inserting this identity in eq. (3.173) and comparing with eq. (3.170) we find the expression for the multipole coefficients Q_{lm} in terms of the source density $\rho(\mathbf{x})$,

$$Q_{lm} = \int d^3y Y_{lm}^*(\theta', \phi') r'^l \rho(\mathbf{y}). \quad (3.175)$$

So, eq. (3.170) gives the most general solution of the vacuum equation, and eq. (3.175) fixes the coefficients Q_{lm} in terms of the density of the source.

An alternative way of performing the multipole expansion is to write

$$\begin{aligned} \frac{1}{|\mathbf{x} - \mathbf{y}|} &= \frac{1}{|\mathbf{x}|} - y^i \partial_i \frac{1}{|\mathbf{x}|} + \frac{1}{2} y^i y^j \partial_i \partial_j \frac{1}{|\mathbf{x}|} + \dots \\ &= \sum_{l=0}^{\infty} \frac{(-1)^l}{l!} y^{i_1} \dots y^{i_l} \partial_{i_1} \dots \partial_{i_l} \frac{1}{|\mathbf{x}|}. \end{aligned} \quad (3.176)$$

We then make use of the fact that, for $r > 0$, and therefore in particular outside the source, we have $\nabla^2(1/|\mathbf{x}|) = 0$, as can be checked again from eq. (3.172).³¹ Then, in eq. (3.176) we can replace $y^i y^j$ with the traceless combination $y^i y^j - (1/3)\delta^{ij}|\mathbf{y}|^2$, and similarly we can remove all traces from the tensors $y^{i_1} \dots y^{i_l}$. Then, inserting eq. (3.176) into eq. (3.173), we get

$$\phi(\mathbf{x}) = \sum_{l=0}^{\infty} \frac{(-1)^l}{l!} Q_{i_1 \dots i_l} \partial_{i_1} \dots \partial_{i_l} \frac{1}{|\mathbf{x}|}, \quad (3.178)$$

where

$$Q_{i_1 \dots i_l} = \int d^3y y^{(i_1} \dots y^{i_l)} \rho(\mathbf{y}), \quad (3.179)$$

and the brackets in $y^{(i_1} \dots y^{i_l)}$ means that we must take the symmetric-trace-free (STF) part of the tensor $y^{i_1} \dots y^{i_l}$. We therefore have two equivalent formalisms for the multipole expansion of a scalar field that satisfies the Poisson equation (3.169), either in terms of spherical harmonics, or in terms of STF tensors.

For applications to electrodynamics or to gravitational waves, we need to generalize the above results in two ways. First, we do not have a scalar field but rather a vector field A_μ or a tensor field $\bar{h}_{\mu\nu}$. Second, we do not have static fields governed by a Poisson equation, but rather time-dependent fields whose wave equation involve a d'Alembertian operator, such as $\square A_\mu = -(4\pi/c)J_\mu$ in electromagnetism, and eq. (3.3) for GWs. For dealing with non-stationary fields, a possible route is to

³⁰See, e.g. Jackson (1975), Section 3.6.

³¹More generally,

$$\nabla^2 \frac{1}{|\mathbf{x}|} = -4\pi \delta^{(3)}(\mathbf{x}), \quad (3.177)$$

i.e. $G(\mathbf{x} - \mathbf{y}) = -1/(4\pi|\mathbf{x} - \mathbf{y}|)$ is the Green's function of the Laplacian.

perform a Fourier transform in time (but not in space), thus reducing the d'Alembertian operator $\square\phi(t, \mathbf{x})$ to $(\nabla^2 + k^2)\tilde{\phi}_k(\mathbf{x})$, so that outside the source the field satisfies a Helmholtz equation $(\nabla^2 + k^2)\tilde{\phi}_k(\mathbf{x}) = 0$. For vector or tensor fields this can be combined with the use of vector and tensor spherical harmonics, respectively. In electrodynamics, this is the approach discussed in Chapter 16 of Jackson (1975). However, this approach does not make explicit the time integration linking the multipole moments to the actual evolution of the source, and furthermore yields somewhat complicated final expressions. Thus, in Section 3.5.1 we rather follow an elegant approach, based on STF tensors, which gives a simple and unified treatment of scalar, vector and tensor fields. This formalism will be used extensively in Chapter 5, in the study of post-Newtonian sources.

The generalization of the approach based on spherical harmonics to the vector and tensor case leads to a more complicated formalism, which nevertheless can be useful in various instances (e.g. for classifying the extra polarization states of GWs in alternative theories of gravity), and we study it in Section 3.5.2.

3.5.1 Symmetric-trace-free (STF) form

Multi-index notation

We begin by introducing a useful multi-index notation, due to Blanchet and Damour, where a tensor with l indices $i_1 i_2 \dots i_l$ is labeled simply using a capital letter L ,

$$F_L \equiv F_{i_1 i_2 \dots i_l}. \quad (3.180)$$

Similarly, G_{iL} denotes a tensor with $l+1$ indices, $G_{iL} \equiv G_{i i_1 i_2 \dots i_l}$, while, e.g. F_{iL-1} is a notation for $F_{i i_1 i_2 \dots i_{l-1}}$. Furthermore, ∂_L is a notation for $\partial_{i_1} \dots \partial_{i_l}$, and we will also use the notation $x_L \equiv x_{i_1} x_{i_2} \dots x_{i_l}$ and $n_L \equiv n_{i_1} n_{i_2} \dots n_{i_l}$, where $n_i = x_i/r$ is the unit vector in the radial direction. In expressions such as $F_L G_L$, with repeated L indices, the summation over all indices i_1, i_2, \dots, i_l is understood, so

$$F_L G_L = \sum_{i_1 \dots i_l} F_{i_1 \dots i_l} G_{i_1 \dots i_l}. \quad (3.181)$$

We use round brackets around indices to denote the symmetrization, e.g. $a_{(ij)} \equiv (1/2)(a_{ij} + a_{ji})$, and we denote by a hat the symmetric-trace-free (STF) projection. That is, the notation \hat{K}_L means that, starting from the tensor with l indices $K_{i_1 \dots i_l}$, we symmetrize it over all indices, and remove all the traces. The operation of taking the STF projection can also be denoted by brackets around the indices, so \hat{K}_L can be equivalently written as $K_{\langle L \rangle}$. The latter notation allows us to write compactly the STF operation between indices belonging to different tensors, e.g. $\epsilon_{ij\langle k} A_{L-1\rangle i_l}$ means that we perform the STF operation among the index k of ϵ_{ijk} and the first $l-1$ indices of $A_{i_1 \dots i_{l-1} i_l}$.

A STF tensor with l indices (i.e. of rank l) $A_{i_1 \dots i_l}$ has $2l+1$ independent components and is therefore a representation of dimension $2l+1$ of the rotation group $SO(3)$. The crucial point is that these representations are irreducible.³² On the other hand, we know from the theory of

³²In general, it can be shown that the irreducible tensor representations of a group are those that give zero when contracted with the invariant tensors (i.e. with the tensors whose form is unchanged by a group transformation). For $SO(3)$ the invariant tensors are δ_{ij} and ϵ_{ijk} . In fact, if \mathcal{R}_{ij} is rotation matrix, δ_{ij} transforms as $\delta_{ij} \rightarrow \mathcal{R}_{ik}\mathcal{R}_{jl}\delta_{kl}$, as for any tensor with two indices. However, $\mathcal{R}_{ik}\mathcal{R}_{jl}\delta_{kl} = \mathcal{R}_{ik}\mathcal{R}_{jk} = \delta_{ij}$ because \mathcal{R} is an orthogonal matrix. Similarly ϵ_{ijk} is invariant because the determinant of \mathcal{R} is equal to one. The condition that the contraction of any two indices of a tensor with an epsilon tensor gives zero singles out totally symmetric tensor, and the condition that the contraction with δ_{ij} gives zero gives the condition of zero trace, for any pair of indices.

representation of the rotation group that the irreducible representations of $SO(3)$ are labeled by an integer value $l = 0, 1, \dots$, and have dimension $2l+1$, so we see that the set of all STF tensor, for all possible ranks l , gives a complete set of representations of $SO(3)$.

A generic tensor does not provide an irreducible representation of the rotation group, and can be decomposed in irreducible representation, i.e. expressed in terms of STF tensors and factors δ_{ij} and ϵ_{ijk} . The simplest example is the decomposition of a generic tensor with two indices T_{ij} . Writing

$$\begin{aligned} T_{ij} &= \frac{1}{2}(T_{ij} + T_{ji}) + \frac{1}{2}(T_{ij} - T_{ji}) \\ &\equiv S_{ij} + A_{ij}, \end{aligned} \quad (3.182)$$

we have decomposed T_{ij} into its symmetric part S_{ij} and its antisymmetric part A_{ij} . Defining $A_k = \epsilon_{ijk}A_{ij}$, we have $A_{ij} = (1/2)\epsilon_{ijk}A_k$. Furthermore, defining S as the trace of S_{ij} , i.e. $S = S_{ii}$, we can rewrite eq. (3.182) as

$$T_{ij} = \frac{1}{3}S\delta_{ij} + \frac{1}{2}\epsilon_{ijk}A_k + (S_{ij} - \frac{1}{3}S\delta_{ij}), \quad (3.183)$$

which shows explicitly the decomposition of a generic rank-2 tensor T_{ij} into a scalar S , a vector A_k and a rank-2 STF tensor $S_{ij} - (1/3)S\delta_{ij}$.³³

We now examine separately the application of the STF formalism to the multipole expansion of relativistic scalar, vector and tensor fields.

Scalar fields

Consider a scalar field ϕ satisfying the relativistic wave equation

$$\square\phi = -4\pi\rho, \quad (3.184)$$

where the source $\rho(t, \mathbf{x})$ is in general time-dependent, but is localized in space, so it vanishes if $|\mathbf{x}| > d$. In the region outside the source, the most general solution can be written as

$$\phi(t, \mathbf{x}) = \sum_{l=0}^{\infty} \frac{(-1)^l}{l!} \partial_L \left[\frac{F_L(t - r/c)}{r} \right], \quad (3.185)$$

where we have used the multi-index notation explained above. This result follows from the fact that, for $r > 0$ and F_L an arbitrary function of retarded time $u = t - r/c$,

$$\square \left[\frac{F_L(t - r/c)}{r} \right] = 0, \quad (3.186)$$

as can be checked immediately with the help of eq. (3.172). Therefore each term of the sum in eq. (3.185) is separately a solution of the vacuum equation $\square\phi = 0$. The fact that this is the most general solution follows from the fact that the set of tensors F_L , with all possible ranks l , provides

³³Observe that scalar and vectors are trivially STF tensors of rank zero and one, respectively.

a complete set of representations of the rotation group. So, eq. (3.185) is the generalization of eq. (3.178) to fields governed by a relativistic wave equation, with a non-stationary source. On the other hand, eq. (3.184) can be solved exactly using the retarded Green's function (3.6), which is the appropriate Green's function for a radiation problem, so

$$\phi(t, \mathbf{x}) = \int d^3x' \frac{1}{|\mathbf{x} - \mathbf{x}'|} \rho \left(t - \frac{|\mathbf{x} - \mathbf{x}'|}{c}, \mathbf{x}' \right). \quad (3.187)$$

Comparing this expression, which holds everywhere and therefore in particular outside the source, with eq. (3.185), we can obtain the relativistic multipoles F_L in terms of the source density ρ . The result is³⁴

$$F_L(u) = \int d^3y \hat{y}_L \int_{-1}^1 dz \delta_l(z) \rho(u + z|\mathbf{y}|/c, \mathbf{y}), \quad (3.188)$$

where, according to the multi-index notation discussed above, \hat{y}_L is the STF projection of y_L . The function $\delta_l(z)$ is defined as

$$\delta_l(z) = \frac{(2l+1)!!}{2^{l+1} l!} (1-z^2)^l, \quad (3.189)$$

and satisfies the identities

$$\int_{-1}^1 dz \delta_l(z) = 1, \quad (3.190)$$

and

$$\lim_{l \rightarrow \infty} \delta_l(z) = \delta(z), \quad (3.191)$$

where $\delta(z)$ is the usual Dirac delta. Physically, the integration over dz in eq. (3.188) performs a weighted time average, different for each multipole moment l , and originates in the different time delay of the radiation emitted from different points inside the source. Equation (3.191) implies that, for sufficiently large l , this time delay becomes negligible.³⁵

Vector field

We next consider the electromagnetic field A^μ which, in the Lorentz gauge $\partial_\mu A^\mu = 0$ (and unnormalized units for the electric charge), satisfies the wave equation

$$\square A^\mu = -\frac{4\pi}{c} J^\mu, \quad (3.192)$$

and again we consider a source $J^\mu = (c\rho, \mathbf{J})$ which is time-dependent but localized, so it vanishes if $|\mathbf{x}| > d$. Each component of A^μ can be treated just like the scalar field of the previous subsection, and therefore in the external source region we find

$$A^0(t, \mathbf{x}) = \sum_{l=0}^{\infty} \frac{(-1)^l}{l!} \partial_L \left[\frac{F_L(u)}{r} \right], \quad (3.193)$$

$$A^i(t, \mathbf{x}) = \sum_{l=0}^{\infty} \frac{(-1)^l}{l!} \partial_L \left[\frac{G_{iL}(u)}{r} \right], \quad (3.194)$$

³⁴The computation is performed in detail in Appendix B of Blanchet and Damour (1989).

³⁵Observe that the argument $u + z|\mathbf{y}|/c$ in eq. (3.188) can be changed to $u - z|\mathbf{y}|/c$, since $\delta_l(z) = \delta_l(-z)$.

where $u = t - r/c$. The explicit expression of $F_L(u)$ in terms of the source density is given again by eq. (3.188), while

$$G_{iL}(u) = \int d^3y \hat{y}_L \int_{-1}^1 dz \delta_l(z) J_i(u + z|\mathbf{y}|/c, \mathbf{y}). \quad (3.195)$$

This is not yet the most convenient final form of the result, because the tensor G_{iL} is symmetric and traceless with respect to the indices i_1, \dots, i_l , since it depends on \hat{y}_L , but not under exchange of the index i with one of the indices i_1, \dots, i_l , so it is not irreducible. It can however be decomposed in irreducible STF tensors as follows,

$$G_{iL} = U_{iL} + \frac{l}{l+1} \epsilon_{ai\langle i_l} C_{L-1\rangle a} + \frac{2l-1}{2l+1} \delta_{i\langle i_l} D_{L-1\rangle}, \quad (3.196)$$

where $U_{L+1} \equiv G_{\langle L+1\rangle}$, $C_L \equiv G_{ab\langle L-1\rangle ab}$ and $D_{L-1} \equiv G_{aaL-1}$. Then, $A^i(t, \mathbf{x})$ is given by the sum of three STF terms. It is convenient to perform a gauge transformation $A_\mu \rightarrow A_\mu - \partial_\mu \theta$ (with $\square \theta = 0$ in order not to spoil the Lorentz gauge) which removes the last term in eq. (3.196) from A^i , at the price of adding a new contribution to A^0 . The final result is³⁶

$$\begin{aligned} A^0(t, \mathbf{x}) &= \sum_{l=0}^{\infty} \frac{(-1)^l}{l!} \partial_L \left[\frac{Q_L(u)}{r} \right], \\ A^i(t, \mathbf{x}) &= -\frac{1}{c} \sum_{l=1}^{\infty} \frac{(-1)^l}{l!} \partial_{L-1} \left[\frac{Q_{iL-1}^{(1)}(u)}{r} + \frac{l}{l+1} \epsilon_{iab} \partial_a \left(\frac{M_{bL-1}(u)}{r} \right) \right], \end{aligned} \quad (3.197)$$

where $Q_{iL-1}^{(1)}$ denotes the first derivative of Q_{iL-1} with respect to retarded time.³⁷ The explicit expression of the moments Q_L and M_L in terms of the source is

$$\begin{aligned} Q_L(u) &= \int d^3y \int_{-1}^1 dz \left[\delta_l(z) \hat{y}_L \rho(u + z|\mathbf{y}|/c, \mathbf{y}) \right. \\ &\quad \left. - \frac{1}{c^2} \frac{2l+1}{(l+1)(2l+3)} \delta_{l+1}(z) \hat{y}_{iL} J_i^{(1)}(u + z|\mathbf{y}|/c, \mathbf{y}) \right], \end{aligned} \quad (3.199)$$

where $l \geq 0$, and

$$M_L(u) = \int d^3y \int_{-1}^1 dz \delta_l(z) \hat{y}_{\langle L-1} m_{i_l\rangle}(u + z|\mathbf{y}|/c, \mathbf{y}), \quad (3.200)$$

where $l \geq 1$ and $m_i = \epsilon_{ijk} y_j J_k$ is the “magnetization density”. These results show that the electromagnetic field outside the source can be expressed in terms of two families of STF time-dependent multipole moments, the “electric moments” $Q_L(u)$ and the “magnetic moments” $M_L(u)$.

Gravitational field

We now consider the linearized gravitational field $\bar{h}_{\mu\nu}$ that, in the Lorentz gauge (1.18), satisfies eq. (1.24). Again, we assume that the source $T_{\mu\nu}$

³⁶The computation is performed in detail in Damour and Iyer (1991a).

³⁷For a function $f(u)$ of retarded time, we will use the notation

$$f^{(n)}(u) \equiv \frac{d^n f}{du^n}. \quad (3.198)$$

has compact support. Then, in the exterior source region the same argument used above for scalar and electromagnetic fields allows us to write the most general solution of the vacuum equations, as

$$\bar{h}^{00}(t, \mathbf{x}) = \frac{4G}{c^4} \sum_{l=0}^{\infty} \frac{(-1)^l}{l!} \partial_L \left[\frac{F_L(u)}{r} \right], \quad (3.201)$$

$$\bar{h}^{0i}(t, \mathbf{x}) = \frac{4G}{c^4} \sum_{l=0}^{\infty} \frac{(-1)^l}{l!} \partial_L \left[\frac{G_{iL}(u)}{r} \right], \quad (3.202)$$

$$\bar{h}^{ij}(t, \mathbf{x}) = \frac{4G}{c^4} \sum_{l=0}^{\infty} \frac{(-1)^l}{l!} \partial_L \left[\frac{H_{ijL}(u)}{r} \right]. \quad (3.203)$$

³⁸See Damour and Iyer (1991a), where it is performed in all detail.

The computation proceeds similarly to the electromagnetic case, but is technically more involved.³⁸ We first decompose G_{iL} in STF tensors, just as we have done in eq. (3.196). Similarly, we decompose H_{ijL} in STF tensors. After performing a suitable gauge transformation (that preserves the gauge condition $\partial_\mu \bar{h}^{\mu\nu} = 0$), the result can be written as

$$\bar{h}^{00} = +\frac{4G}{c^2} \sum_{l=0}^{\infty} \frac{(-1)^l}{l!} \partial_L \left[\frac{M_L(u)}{r} \right], \quad (3.204)$$

$$\bar{h}^{0i} = -\frac{4G}{c^3} \sum_{l=1}^{\infty} \frac{(-1)^l}{l!} \partial_{L-1} \left[\frac{M_{iL-1}^{(1)}(u)}{r} + \frac{l}{l+1} \epsilon_{iab} \partial_a \left(\frac{S_{bL-1}(u)}{r} \right) \right],$$

$$\bar{h}^{ij} = +\frac{4G}{c^4} \sum_{l=2}^{\infty} \frac{(-1)^l}{l!} \partial_{L-2} \left[\frac{1}{r} M_{ijL-2}^{(2)}(u) + \frac{2l}{l+1} \partial_a \left(\frac{1}{r} \epsilon_{ab(i} S_{j)bL-2}^{(1)}(u) \right) \right].$$

The result therefore depends again on two families of STF tensors, M_L and S_L . Their explicit expression in terms of the energy-momentum tensor of the source can be written introducing the “active gravitational-mass density” σ ,

$$\sigma \equiv \frac{1}{c^2} [T^{00} + T^{ii}] . \quad (3.205)$$

and the “active mass-current density”,

$$\sigma_i \equiv \frac{1}{c} T^{0i}, \quad (3.206)$$

as well as $\sigma_{ij} = T^{ij}$. Then

$$\begin{aligned} M_L(u) &= \int d^3x \int_{-1}^1 dz \left\{ \delta_l(z) \hat{x}_L \sigma - \frac{4(2l+1)\delta_{l+1}(z)}{c^2(l+1)(2l+3)} \hat{x}_{iL} \sigma_i^{(1)} \right. \\ &\quad \left. + \frac{2(2l+1)\delta_{l+2}(z)}{c^4(l+1)(l+2)(2l+5)} \hat{x}_{ijL} \sigma_{ij}^{(2)} \right\} (u + z|\mathbf{x}|/c, \mathbf{x}), \end{aligned} \quad (3.207)$$

$$\begin{aligned} S_L(u) &= \int d^3x \int_{-1}^1 dz \epsilon_{ab(i} \left\{ \delta_l(z) \hat{x}_{L-1)a} \sigma_b \right. \\ &\quad \left. - \frac{(2l+1)\delta_{l+1}(z)}{c^2(l+2)(2l+3)} \hat{x}_{L-1}{}_{ac} \sigma_{bc}^{(1)} \right\} (u + z|\mathbf{x}|/c, \mathbf{x}). \end{aligned} \quad (3.208)$$

This result holds at the level of linearized theory. In Chapter 5 we will study the full non-linear theory and we will discover that, remarkably, the exact solution of the full general-relativistic problem is constructed using a quantity $h_1^{\mu\nu}$ that is obtained from eqs. (3.204)–(3.208) by means of a very simple modification, that is, with the replacement of the energy momentum tensor of matter $T_{\mu\nu}$ by an effective energy-momentum tensor $\tau_{\mu\nu}$ that includes also the non-linearities of the gravitational field,³⁹ see eqs. (5.135) and (5.136). Thus, eqs. (3.207) and (3.208) already contain the blueprint of the solution to the full non-linear problem.

The integration over z can be computed, in an expansion in powers of $1/c$, using the formula

$$\int_{-1}^1 dz \delta_l(z) f(u+z|\mathbf{x}|/c, \mathbf{x}) = \sum_{k=0}^{+\infty} \frac{(2l+1)!!}{2^k k!(2l+2k+1)!!} \left(\frac{|\mathbf{x}|}{c} \frac{\partial}{\partial u} \right)^{2k} f(u, \mathbf{x}). \quad (3.209)$$

From this we see that, in eqs. (3.207) and (3.208) (as well as in the analogous formulas for the scalar and vector fields), the integration over z allows us to take into account, in a compact way, an infinite series of derivatives.

Finally, we can use these multipolar expressions for $\bar{h}_{\mu\nu}$ to compute the total power radiated in GWs. We use eq. (1.40), plug it into eq. (1.153) retaining only the terms $O(1/r)$ in h_{ij}^{TT} , and we perform the angular integration.⁴⁰ The result is

$$\begin{aligned} \frac{dE}{dt} = & \sum_{l=2}^{+\infty} \frac{G}{c^{2l+1}} \left\{ \frac{(l+1)(l+2)}{(l-1)l!(2l+1)!!} \langle M_L^{(l+1)}(u) M_L^{(l+1)}(u) \rangle \right. \\ & \left. + \frac{4l(l+2)}{c^2(l-1)(l+1)!(2l+1)!!} \langle S_L^{(l+1)}(u) S_L^{(l+1)}(u) \rangle \right\}. \end{aligned} \quad (3.210)$$

Similarly, for the linear momentum losses one finds

$$\begin{aligned} \frac{dP_i}{dt} = & \sum_{l=2}^{+\infty} \frac{G}{c^{2l+2}} \left\{ \frac{2(l+2)(l+3)}{l(l+1)!(2l+3)!!} \langle M_{iL}^{(l+2)}(u) M_L^{(l+1)}(u) \rangle \right. \\ & + \frac{8(l+3)}{c^2(l+1)!(2l+3)!!} \langle S_{iL}^{(l+2)}(u) S_L^{(l+1)}(u) \rangle \\ & \left. + \frac{8(l+2)}{c^2(l-1)(l+1)!(2l+1)!!} \langle \epsilon_{ijk} S_{jL-1}^{(l+1)}(u) S_{kL-1}^{(l+1)}(u) \rangle \right\}. \end{aligned} \quad (3.211)$$

Observe that the linear momentum losses come from the interference between multipoles of different rank, such as the mass quadrupole/mass octupole mixed term, as we already saw on pages 130–131.⁴¹

3.5.2 Spherical tensor form

In this section we discuss an alternative formalism for performing the multipole expansion to all orders, which is based on the generalization of the notion of spherical harmonics to a spin-2 field.

³⁹Together with a prescription for rendering finite the integral, since the source $\tau_{\mu\nu}$ no longer has compact support.

⁴⁰The power is quadratic in \dot{h}_{ij}^{TT} and therefore in the multipole moments. However, mixed terms of the form $M_L S_{L'}$ give vanishing contribution, after the angular integration, because of parity, while terms $M_L M_{L'}$ or $S_L S_{L'}$ contribute only if $L = L'$. In fact, if $l > l'$, the indices in $M_{i_1 \dots i_l}$ cannot be all contracted with the indices of $M_{i_1 \dots i_{l'}}$, and the remaining indices of the $i_1 \dots i_l$ group are necessarily contracted among them, via the Kronecker deltas that come from the angular integration, see eq. (3.23).

⁴¹See Thorne (1980), eq. (4.23') for the corresponding expression for the angular momentum losses.

This section is quite technical, and can be omitted at a first reading.

Spherical components of tensors

To introduce spherical tensors we first consider the quadrupole moment or, more generally, any traceless symmetric tensor with two indices, whose Cartesian components we denote by Q_{ij} . As a first step we introduce a basis in the space of traceless symmetric tensors with two indices, which is chosen so to have a simple relation with the $l = 2$ spherical harmonics.

⁴²Here, according to the standard definition of spherical harmonics, the angle ϕ is measured from the x axis, so for instance the unit vector in the radial direction $\hat{\mathbf{n}}$ has components $n_x = \sin\theta \cos\phi$, $n_y = \sin\theta \sin\phi$ and $n_z = \cos\theta$. Observe that this definition differs from that used, e.g. in Fig. 3.2 and in equations such as eq. (3.72), where ϕ is measured from the y axis.

We recall that the spherical harmonics $Y^{lm}(\theta, \phi)$ with $l = 2$ are⁴²

$$Y^{22}(\theta, \phi) = \left(\frac{15}{32\pi} \right)^{1/2} (e^{i\phi} \sin\theta)^2, \quad (3.212)$$

$$Y^{21}(\theta, \phi) = -\left(\frac{15}{8\pi} \right)^{1/2} e^{i\phi} \sin\theta \cos\theta, \quad (3.213)$$

$$Y^{20}(\theta, \phi) = \left(\frac{5}{16\pi} \right)^{1/2} (3 \cos^2\theta - 1), \quad (3.214)$$

while the expressions for negative values of m are obtained using

$$Y^{l,-m} = (-1)^m Y^{lm*}. \quad (3.215)$$

Consider now the unit radial vector $\hat{\mathbf{n}}$. In polar coordinates we have $n_x = \sin\theta \cos\phi$, $n_y = \sin\theta \sin\phi$, $n_z = \cos\theta$, and therefore

$$e^{i\phi} \sin\theta = n_x + i n_y, \quad \cos\theta = n_z. \quad (3.216)$$

Plugging this into the explicit expressions for the spherical harmonics Y^{2m} , and using the fact that $n_i n_i = 1$, we see that we can write

$$Y^{2m}(\theta, \phi) = \mathcal{Y}_{ij}^{2m} n_i n_j, \quad (3.217)$$

where \mathcal{Y}_{ij}^{2m} is independent of θ, ϕ , and the sum over i, j on the right-hand side is understood. The above equation fixes the part of \mathcal{Y}_{ij}^{2m} which is symmetric in (i, j) , and we complete the definition of \mathcal{Y}_{ij}^{2m} requiring that the antisymmetric part vanishes. The explicit form of the tensors \mathcal{Y}_{ij}^{2m} is then

$$\begin{aligned} \mathcal{Y}_{ij}^{22} &= \sqrt{\frac{15}{32\pi}} \begin{pmatrix} 1 & i & 0 \\ i & -1 & 0 \\ 0 & 0 & 0 \end{pmatrix}_{ij}, \\ \mathcal{Y}_{ij}^{21} &= -\sqrt{\frac{15}{32\pi}} \begin{pmatrix} 0 & 0 & 1 \\ 0 & 0 & i \\ 1 & i & 0 \end{pmatrix}_{ij}, \\ \mathcal{Y}_{ij}^{20} &= \sqrt{\frac{5}{16\pi}} \begin{pmatrix} -1 & 0 & 0 \\ 0 & -1 & 0 \\ 0 & 0 & 2 \end{pmatrix}_{ij}, \end{aligned} \quad (3.218)$$

together with $\mathcal{Y}_{ij}^{2-m} = (-1)^m (\mathcal{Y}_{ij}^{2m})^*$. We see from the explicit expressions that the five matrices $\mathcal{Y}_{ij}^{2,m}$ are traceless in the (i, j) indices. This

could have also been understood by integrating eq. (3.217) over the solid angle and using $\int d\Omega Y^{2m} = 0$ and $\int d\Omega n_i n_j \sim \delta_{ij}$. From the explicit expressions, we also see that the five tensors \mathcal{Y}_{ij}^{2m} are an orthogonal basis, in the sense that

$$\sum_{ij} \mathcal{Y}_{ij}^{2m} (\mathcal{Y}_{ij}^{2m})^* = \frac{15}{8\pi} \delta^{mm'} . \quad (3.219)$$

It is sometimes useful to invert eq. (3.217). The result is

$$n_i n_j - \frac{1}{3} \delta_{ij} = \sum_{m=-2}^2 c_{ij}^m Y^{2m}(\theta, \phi) , \quad (3.220)$$

where

$$c_{ij}^m = \frac{8\pi}{15} (\mathcal{Y}_{ij}^{2m})^* . \quad (3.221)$$

This can be proved multiplying both sides of eq. (3.220) by \mathcal{Y}_{ij}^{2m} , summing over i, j and using eqs. (3.221) and (3.219), which gives back eq. (3.217). Since \mathcal{Y}_{ij}^{2m} is traceless, the coefficient of the term proportional to δ_{ij} on the left-hand side of eq. (3.220) is not yet fixed in this way, but we can fix it by observing that the right-hand side of eq. (3.220) is traceless, so also the left-hand side must be traceless.

The five symmetric and traceless matrices \mathcal{Y}_{ij}^{2m} , with $m = -2, \dots, 2$, are linearly independent and therefore are a basis for the five-dimensional space of traceless symmetric tensors Q_{ij} . This means that we can expand an arbitrary traceless symmetric tensors Q_{ij} as

$$Q_{ij} = \sum_{m=-2}^2 Q_m \mathcal{Y}_{ij}^{2m} . \quad (3.222)$$

The quantities Q_m are called the *spherical components* of Q_{ij} . Multiplying by $n_i n_j$ and using eq. (3.217) we obtain

$$Q_{ij} n_i n_j = \sum_{m=-2}^2 Q_m Y^{2m}(\theta, \phi) . \quad (3.223)$$

(As always, the summation over the repeated i, j indices is understood; instead, we write explicitly the sum over m .) This equation could also have been obtained directly by observing that $Q_{ij} n_i n_j$ is a function of θ, ϕ (with the dependence hidden in $n_i(\theta, \phi)$, while Q_{ij} is a constant tensor) and therefore can be expanded in spherical harmonics as $\sum_{l,m} Q_{lm} Y^{lm}(\theta, \phi)$. However, Q_{ij} is symmetric and traceless, so it is a spin-2 operator and therefore in the expansion in spherical harmonics, only $l = 2$ contributes.

The five independent components of the symmetric traceless tensor Q_{ij} are therefore expressed in terms of the five independent quantities Q_m , with $m = -2, \dots, 2$. If Q_{ij} is real, as in the case of the mass

quadrupole, the five complex quantities Q_m satisfy $Q_m^* = (-1)^m Q_{-m}$, because of eq. (3.215). Using eq. (3.219) we can invert eq. (3.222),

$$Q_m = \frac{8\pi}{15} Q_{ij} (\mathcal{Y}_{ij}^{2m})^*, \quad (3.224)$$

or, explicitly,

$$\begin{aligned} Q_{\pm 2} &= \left(\frac{2\pi}{15} \right)^{1/2} (Q_{11} - Q_{22} \mp 2iQ_{12}), \\ Q_{\pm 1} &= \mp \left(\frac{8\pi}{15} \right)^{1/2} (Q_{13} \mp iQ_{23}), \\ Q_0 &= - \left(\frac{4\pi}{5} \right)^{1/2} (Q_{11} + Q_{22}). \end{aligned} \quad (3.225)$$

We can now write the power emitted by the quadrupole radiation, given in eq. (3.75), in terms of the spherical components Q_m . Using eq. (3.223) we write

$$\ddot{Q}_{ij} n_i n_j = \sum_{m=-2}^2 \ddot{Q}_m Y^{2m}(\theta, \phi), \quad (3.226)$$

and we take the squared modulus,

$$\ddot{Q}_{ij} \ddot{Q}_{kl} n_i n_j n_k n_l = \sum_{m, m'} \ddot{Q}_m^* \ddot{Q}_{m'} Y^{2m*}(\theta, \phi) Y^{2m'}(\theta, \phi). \quad (3.227)$$

Integrating over $d\Omega$ with the help of eq. (3.22) and using the orthogonality of the spherical harmonics,

$$\int d\Omega Y^{lm*}(\theta, \phi) Y^{l'm'}(\theta, \phi) = \delta^{ll'} \delta^{mm'}, \quad (3.228)$$

we get

$$\frac{8\pi}{15} \ddot{Q}_{ij} \ddot{Q}_{ij} = \sum_{m=-2}^2 |\ddot{Q}_m|^2. \quad (3.229)$$

Therefore, eq. (3.75) becomes

$$P_{\text{quad}} = \frac{3G}{8\pi c^5} \sum_{m=-2}^2 \langle |\ddot{Q}_m|^2 \rangle. \quad (3.230)$$

We can now generalize the above construction to traceless symmetric tensors with an arbitrary number of indices. We consider a (real) STF tensor with l indices, $T_{i_1 \dots i_l}$.⁴³ A basis in this tensor space can be obtained by observing that the spherical harmonics $Y^{lm}(\theta, \phi)$ with $m \geq 0$ are given explicitly by

$$\begin{aligned} Y^{lm}(\theta, \phi) &= C^{lm} e^{im\phi} P^{lm}(\cos \theta) \\ &= C^{lm} (e^{i\phi} \sin \theta)^m \sum_{k=0}^{[(l-m)/2]} a_k^{lm} (\cos \theta)^{l-m-2k}, \end{aligned} \quad (3.231)$$

⁴³In this section we prefer to write explicitly the indices $i_1 \dots i_l$, rather than using the multi-index notation defined on page 134.

and $Y^{lm} = (-1)^m (Y^{l,-m})^*$ for $m < 0$. The notation $[(l-m)/2]$ denotes the largest integer smaller or equal to $(l-m)/2$, and the coefficients are given by

$$C^{lm} = (-1)^m \left(\frac{2l+1}{4\pi} \frac{(l-m)!}{(l+m)!} \right)^{1/2}, \quad (3.232)$$

$$a_k^{lm} = \frac{(-1)^k}{2^k k!(l-k)!} \frac{(2l-2k)!}{(l-m-2k)!}. \quad (3.233)$$

Comparing with eq. (3.216) we see that Y^{lm} is the sum of a term containing l factors n_i , a term containing $l-2$ factors n_i , a term containing $l-4$ factors n_i , etc. Using $n_i n_i = 1$, a term with $l-2$ factors $n_{i_1} \dots n_{i_{l-2}}$ can be rewritten trivially as a term with l factors n_i , as $\delta_{ij} n_{i_1} \dots n_{i_{l-2}} n_i n_j$, and similarly for all terms with $l-2k$ factors. Then we can write

$$Y^{lm}(\theta, \phi) = \mathcal{Y}_{i_1 \dots i_l}^{lm} n_{i_1} \dots n_{i_l}, \quad (3.234)$$

where the tensors $\mathcal{Y}_{i_1 \dots i_l}^{lm}$ are independent of θ, ϕ , and the sum over the l indices $i_1 \dots i_l$ is understood. We will not need the explicit form of $\mathcal{Y}_{i_1 \dots i_l}^{lm}$, which anyway can be read from eqs. (3.231) and (3.216). Just as in the case $l=2$ discussed above, one can show that the tensors $\mathcal{Y}_{i_1 \dots i_l}^{lm}$ are a basis in the space of traceless symmetric tensors with l indices. This means that we can expand

$$T_{i_1 \dots i_l} = \sum_{m=-l}^l T_{lm} \mathcal{Y}_{i_1 \dots i_l}^{lm}, \quad (3.235)$$

and this defines the spherical components T_{lm} of the tensor $T_{i_1 \dots i_l}$. Multiplying by $n_{i_1} \dots n_{i_l}$ we have the identity

$$T_{i_1 \dots i_l} n_{i_1} \dots n_{i_l} = \sum_{m=-l}^l T_{lm} Y^{lm}(\theta, \phi), \quad (3.236)$$

which expresses the fact that in the expansion in spherical harmonics of the left-hand side contribute only the spherical harmonics whose angular momentum l is equal to the number of indices of $T_{i_1 \dots i_l}$. This is a consequence of the fact that both a STF tensor with l indices, and the spherical harmonics Y^{lm} , provide an irreducible representation of dimension $2l+1$ of the rotation group.

Using the orthogonality of spherical harmonics we can invert eq. (3.236) and we obtain the spherical components T_{lm} in terms of the Cartesian components $T_{i_1 \dots i_l}$,

$$\begin{aligned} T_{lm} &= T_{i_1 \dots i_l} \int d\Omega (Y^{lm})^* n_{i_1} \dots n_{i_l} \\ &= T_{i_1 \dots i_l} (\mathcal{Y}_{j_1 \dots j_l}^{lm})^* \int d\Omega n_{i_1} \dots n_{i_l} n_{j_1} \dots n_{j_l}, \end{aligned} \quad (3.237)$$

where in the second line we used eq. (3.234). The integral can be performed using eq. (3.23). Since $\mathcal{Y}_{j_1 \dots j_l}^{lm}$ and $T_{i_1 \dots i_l}$ are traceless, in the

sum over permutations in eq. (3.23) the terms with Kronecker deltas of the type $\delta_{i_k i_{k'}}$, or $\delta_{j_k j_{k'}}$, give zero, and the only contributions come from the term $\delta_{i_1 j_1} \dots \delta_{i_l j_l}$ and from its permutations. Since $\mathcal{Y}_{j_1 \dots j_l}^{lm}$ is totally symmetric, these $l!$ permutations all give the same result, so

$$T_{lm} = 4\pi \frac{l!}{(2l+1)!!} T_{i_1 \dots i_l} (\mathcal{Y}_{i_1 \dots i_l}^{lm})^*. \quad (3.238)$$

For $l = 2$, we recover the result obtained in eq. (3.224). Finally, a useful identity which generalizes eq. (3.229) is obtained taking the modulus squared of eq. (3.236) and integrating over $d\Omega$ with the help of eq. (3.23). This gives

$$4\pi \frac{l!}{(2l+1)!!} T_{i_1 \dots i_l} T^{i_1 \dots i_l} = \sum_{m=-l}^l |T_{lm}|^2. \quad (3.239)$$

The transformation properties under rotations of the spherical components of tensors are fixed by the transformation properties of the spherical harmonics. For instance, consider a rotation by an angle φ around the z -axis, $\phi \rightarrow \phi + \varphi$. The left-hand side of eq. (3.236) is a scalar so it is invariant, while on the right-hand side $Y_{lm} \rightarrow e^{im\varphi} Y_{lm}$. Therefore T_{lm} transforms into itself, as⁴⁴

$$T_{lm} \rightarrow e^{-im\varphi} T_{lm}. \quad (3.240)$$

More generally, under arbitrary rotations the $2l+1$ components of T_{lm} , with $m = -l, \dots, l$ and l given, transform among themselves in the same way as $Y_{lm}^*(\theta, \phi)$.

Vector and tensor spherical harmonics

The spherical components of tensors, introduced above, are one of the tools useful for the construction of a systematic multipole expansion. Here we introduce another necessary ingredient of this formalism, the tensor spherical harmonics. In the same way as the usual (scalar) spherical harmonics are useful to describe the angular dependence of a scalar field, tensor spherical harmonics are useful for describing the angular dependence of a field with spin.

We denote by \mathbf{L} the orbital angular momentum operator, by \mathbf{S} the spin operator and by $\mathbf{J} = \mathbf{L} + \mathbf{S}$ the total angular momentum. All these quantities are measured in units of \hbar , so for instance, as operator acting on functions, $\mathbf{L} = \mathbf{r} \times (-i\nabla)$. Since the operators \mathbf{J}^2 , J_z^2 , \mathbf{L}^2 and \mathbf{S}^2 commute, we can diagonalize them simultaneously. The eigenfunctions are the tensor spherical harmonics and are denoted by $Y_{jj_z}^{ls}(\theta, \phi)$. Therefore, by definition, the functions $Y_{jj_z}^{ls}(\theta, \phi)$ are the solutions of

$$\mathbf{J}^2 Y_{jj_z}^{ls} = j(j+1) Y_{jj_z}^{ls}, \quad (3.241)$$

$$J_z Y_{jj_z}^{ls} = j_z Y_{jj_z}^{ls}, \quad (3.242)$$

$$\mathbf{L}^2 Y_{jj_z}^{ls} = l(l+1) Y_{jj_z}^{ls}, \quad (3.243)$$

$$\mathbf{S}^2 Y_{jj_z}^{ls} = s(s+1) Y_{jj_z}^{ls}. \quad (3.244)$$

⁴⁴For this reasons, the spherical components find a typical application in quantum mechanics, for writing selection rules in atomic transitions.

Their explicit form can be obtained coupling the (scalar) spherical harmonics Y_{lm} to the spin function χ_{ssz} , with the appropriate Clebsch–Gordan coefficients which gives a state with total angular momentum $|j, j_z\rangle$,

$$Y_{jj_z}^{ls}(\theta, \phi) = \sum_{l_z=-l}^l \sum_{s_z=-s}^s \langle sls_z l_z | jj_z \rangle Y_{ll_z}(\theta, \phi) \chi_{ssz}. \quad (3.245)$$

It is easy to check that this expression indeed satisfies eqs. (3.241)–(3.244). For instance, the operators L_i act only on the variables θ, ϕ of $Y_{ll_z}(\theta, \phi)$, and then eq. (3.243) follows from $\mathbf{L}^2 Y_{ll_z} = l(l+1)Y_{ll_z}$. Similarly, eq. (3.244) follows from the fact that the spin operator acts only on the spin wavefunction χ , with $\mathbf{S}^2 \chi_{ssz} = s(s+1)\chi_{ssz}$. Finally, the Clebsch–Gordan coefficients $\langle sls_z l_z | jj_z \rangle$ couple a state with orbital angular momentum $|ll_z\rangle$ to a state with spin $|ss_z\rangle$ to give a state with total angular momentum $|jj_z\rangle$, so that eqs. (3.241) and (3.242) follow.

Depending on the value of s , one has spinor spherical harmonics ($s = 1/2$), vector spherical harmonics ($s = 1$), spin-2 tensor spherical harmonics, etc.⁴⁵

Tensor spherical harmonics describe the angular distribution and polarization of particles of spin s , in a state with definite values of the total angular momentum j , of j_z , and of the orbital angular momentum l . For gravitational waves, we are interested in spin-2 tensor spherical harmonics. Observe that, beside the indices l, s, j, j_z written explicitly, $Y_{jj_z}^{ls}$ carries also an index which depends on the nature of the spin wavefunction χ ; e.g. a spinor index for $s = 1/2$, a vector index for $s = 1$, a pair of spatial indices (i, i') for $s = 2$ (with $(Y_{jj_z}^{l2})_{ii'}$ symmetric and traceless in i, i'), etc.

Let us first examine the vector spherical harmonics. The spin wavefunction χ in this case is a vector, and we denote it by ξ . The wavefunctions with a definite value of $s_z = 0, \pm 1$ can be constructed from the unit vectors \mathbf{e}_x , \mathbf{e}_y and \mathbf{e}_z as

$$\xi^{(\pm 1)} = \mp \frac{1}{\sqrt{2}} (\mathbf{e}_x \pm i\mathbf{e}_y), \quad \xi^{(0)} = \mathbf{e}_z. \quad (3.246)$$

Then the vector spherical harmonics are

$$\mathbf{Y}_{jj_z}^l(\theta, \phi) = \sum_{l_z=-l}^l \sum_{s_z=0,\pm 1} \langle 1ls_z l_z | jj_z \rangle Y_{ll_z}(\theta, \phi) \xi^{(s_z)}. \quad (3.247)$$

Observe that in $\xi^{(s_z)}$ the index $s_z = \pm 1, 0$ tells us which vector we must consider, according to eq. (3.246); the spatial components of the vector are instead denoted by $\xi_i^{(s_z)}$. Correspondingly, $\mathbf{Y}_{jj_z}^l$ is a vector with components $(Y_{jj_z}^l)_i$. Note also that we have written $\mathbf{Y}_{jj_z}^{l_1}$ simply as $\mathbf{Y}_{jj_z}^l$, since the fact that $s = 1$ is already implicit in the vector notation \mathbf{Y} .

⁴⁵One should not be misled by this nomenclature. Of course, the properties of $Y_{jj_z}^{ls}$ under rotations depend on the value of the *total* angular momentum j , not on the spin s , so for instance a vector spherical harmonics $Y_{jj_z}^{l1}$ with $j = 2$ (and therefore $l = 1, 2$ or 3) has the transformation properties of a spin-2 operator, not of a vector, just as the usual scalar spherical harmonics Y_{lm} transform of course as a spin- l operator, not as a scalar.

Vector spherical harmonics

By construction, the vector spherical harmonics are eigenfunctions of \mathbf{L}^2 ,

$$\mathbf{L}^2 (Y_{jj_z}^l)_i = l(l+1) (Y_{jj_z}^l)_i, \quad (3.248)$$

and therefore are useful in solving an equation of the form $\square \mathbf{V} = 0$, where $\square = -\partial_0^2 + \boldsymbol{\nabla}^2$ is the flat space d'Alembertian and \mathbf{V} a vector field. In fact, using the expression for the Laplacian in spherical coordinates, eq. (3.172), we can separate the radial and the angular dependence writing

$$\mathbf{V}(r, \theta, \phi) = \sum_{l,j,j_z} f_{ljj_z}(r) \mathbf{Y}_{jj_z}^l(\theta, \phi). \quad (3.249)$$

Observe that the vector spherical harmonics are orthonormal,

$$\int d\Omega \mathbf{Y}_{jj_z}^l \cdot (\mathbf{Y}_{jj_z'}^{l'})^* = \delta_{ll'} \delta_{jj'} \delta_{j_z j_z'}. \quad (3.250)$$

The vectors $\mathbf{Y}_{jj_z}^l(\theta, \phi)$ can have $j = l-1, l, l+1$ (if $l \neq 0$), or $j = 1$ if $l = 0$, (that is, the possible quantum combinations of spin $s = 1$ and orbital angular momentum l). For generic values of l and j within this range, they have no special property with respect to the radial unit vector $\hat{\mathbf{n}}$, that is, they are neither purely transverse nor purely longitudinal. We can however observe that the full set of vectors $\mathbf{Y}_{jj_z}^l$, with $j = l-1, l, l+1$ (if $l \neq 0$), or $j = 1$ if $l = 0$, can be expressed in terms of the following combinations,

$$\mathbf{Y}_{jj_z}^E = (2j+1)^{-1/2} \left[(j+1)^{1/2} \mathbf{Y}_{jj_z}^{j-1} + j^{1/2} \mathbf{Y}_{jj_z}^{j+1} \right], \quad (3.251)$$

$$\mathbf{Y}_{jj_z}^B = i \mathbf{Y}_{jj_z}^j, \quad (3.252)$$

$$\mathbf{Y}_{jj_z}^R = (2j+1)^{-1/2} \left[j^{1/2} \mathbf{Y}_{jj_z}^{j-1} - (j+1)^{1/2} \mathbf{Y}_{jj_z}^{j+1} \right], \quad (3.253)$$

with $j \geq 1$, together with $\mathbf{Y}_{00}^R = Y_{00} \hat{\mathbf{n}}$. Observe that, since $s = 1$, a given value of $j \geq 1$ can be obtained with $l = j-1, j$ or $j+1$. In eqs. (3.251) and (3.253) we have combined the vector harmonic with $l = j-1$ and the vector harmonic with $l = j+1$, while $\mathbf{Y}_{jj_z}^B$ is made with $l = j$.⁴⁶

Since $\mathbf{Y}_{jj_z}^E$ and $\mathbf{Y}_{jj_z}^R$ are superposition of vector harmonics with different values of l , they are no longer eigenfunctions of \mathbf{L}^2 . However, using the properties of spherical harmonics, we can rewrite the above definitions in terms of the scalar spherical harmonics Y_{lm} as⁴⁷

$$\mathbf{Y}_{lm}^E = [l(l+1)]^{-1/2} r \boldsymbol{\nabla} Y_{lm} \quad (l \geq 1), \quad (3.254)$$

$$\mathbf{Y}_{lm}^B = [l(l+1)]^{-1/2} i \mathbf{L} Y_{lm} \quad (l \geq 1), \quad (3.255)$$

$$\mathbf{Y}_{lm}^R = Y_{lm} \hat{\mathbf{n}} \quad (l \geq 0). \quad (3.256)$$

From these expressions we see that \mathbf{Y}_{lm}^R is a longitudinal vector, since it is proportional to $\hat{\mathbf{n}}$, while \mathbf{Y}_{lm}^E and \mathbf{Y}_{lm}^B are transverse. In fact, the operator \mathbf{L} has only components in the $\hat{\theta}$ and $\hat{\phi}$ directions and, since Y_{lm} depends only on θ, ϕ and not on r , also $\boldsymbol{\nabla} Y_{lm}$ has only components in

⁴⁶Using the explicit expression of the spherical harmonics, we can verify immediately that $Y_{10}\xi^{(0)} - Y_{11}\xi^{(-1)} - Y_{1-1}\xi^{(+1)}$ is proportional to $\hat{\mathbf{n}} = (\sin \theta \cos \phi, \sin \theta \sin \phi, \cos \theta)$. On the other hand, apart from a proportionality factor, the combination $Y_{10}\xi^{(0)} - Y_{11}\xi^{(-1)} - Y_{1-1}\xi^{(+1)}$ is just the combination (3.247) with the Clebsch-Gordan coefficients necessary to produce a state with $j = 0$ from $l = 1$ and $s = 1$. Thus, the vector spherical harmonics \mathbf{Y}_{00}^1 is proportional to $\hat{\mathbf{n}}$, and is therefore proportional to \mathbf{Y}_{00}^R (observe that $Y_{00} = 1/(4\pi)^{1/2}$ is just a constant.) In this way we have taken into account the only vector harmonics that exists for $j = 0$ while, for each $j \geq 1$, we have three vector harmonics, with $l = j, j-1, j+1$. The one with $l = j$ is rewritten as $\mathbf{Y}_{jj_z}^B$ while the two with $l = j \pm 1$ are combined to form $\mathbf{Y}_{jj_z}^E$ and $\mathbf{Y}_{jj_z}^R$, with $j \geq 1$.

⁴⁷In eqs. (3.254)–(3.256), in order to conform to the most common notation used in electrodynamics (for vector spherical harmonics) and in the gravitational-wave literature (for the spin-2 tensor harmonics), we have changed the labeling of the indices of \mathbf{Y}^E , \mathbf{Y}^B and \mathbf{Y}^R from j, j_z to l, m . It is however important to understand that these indices refer to the *total* angular momentum, and not to the orbital angular momentum.

the $\hat{\theta}$ and $\hat{\phi}$ directions. Furthermore, since $\mathbf{L} = \mathbf{r} \times (-i\boldsymbol{\nabla}) = -ir\hat{\mathbf{n}} \times \boldsymbol{\nabla}$, we have

$$\mathbf{Y}_{lm}^B = \hat{\mathbf{n}} \times \mathbf{Y}_{lm}^E. \quad (3.257)$$

Therefore \mathbf{Y}_{lm}^E and \mathbf{Y}_{lm}^B are transverse with respect to $\hat{\mathbf{n}}$ and are orthogonal to each other. Under a parity transformation \mathbf{Y}_{lm}^E and \mathbf{Y}_{lm}^R pick a factor $\pi_l = (-1)^l$. This is the transformation property of the electric field, so this is called an electric-type parity. Instead \mathbf{Y}_{lm}^B picks a factor $\pi_l = (-1)^{l+1}$, so it has a magnetic type parity.⁴⁸

The vector functions \mathbf{Y}_{lm}^E , \mathbf{Y}_{lm}^B and \mathbf{Y}_{lm}^R are called “pure-spin vector harmonics” because they are appropriate for describing the polarization states of a vector field, while the vector functions \mathbf{Y}_{lm}' given in eq. (3.247) are called “pure-orbital vector harmonics” because they are eigenfunctions of the orbital angular momentum.

The pure-spin vector harmonics are orthonormal,

$$\int d\Omega \mathbf{Y}_{lm}^J \cdot (\mathbf{Y}_{l'm'}^{J'})^* = \delta_{JJ'} \delta_{ll'} \delta_{mm'}, \quad (3.258)$$

where $J = E, B, R$. The angular dependence of an arbitrary vector field can be expanded in pure-spin vector harmonics as

$$\begin{aligned} \mathbf{V}(t, r, \theta, \phi) &= \sum_{l=0}^{\infty} \sum_{m=-l}^l R_{lm}(t, r) \mathbf{Y}_{lm}^R(\theta, \phi) \\ &+ \sum_{l=1}^{\infty} \sum_{m=-l}^l [E_{lm}(t, r) \mathbf{Y}_{lm}^E(\theta, \phi) + B_{lm}(t, r) \mathbf{Y}_{lm}^B(\theta, \phi)]. \end{aligned} \quad (3.259)$$

Observe that, in the second line, the sum over l runs only over $l \geq 1$, since the corresponding pure-spin vector harmonics start from $l = 1$.⁴⁹

A massive spin-1 particle has three degrees of freedom, and we see that these degrees of freedom are described by E_{lm} , B_{lm} and R_{lm} , respectively. If we want to describe a *massless* vector particle, however, the situation is different. A massless vector particle has only two physical degrees of freedom (see the discussion of the Poincaré representations in Problem 2.1), with helicities $h = \pm 1$. If we perform a rotation by an angle θ around the $\hat{\mathbf{n}}$ axis the two transverse vectors \mathbf{Y}_{lm}^E and \mathbf{Y}_{lm}^B transform among themselves (see eq. (3.257)) so $\mathbf{Y}_{lm}^E \pm i\mathbf{Y}_{lm}^B$ are multiplied by $\exp\{\pm i\theta\}$. Comparing with eq. (2.197), we understand that they describe the two components of a massless particle with helicities $h = \pm 1$. Instead \mathbf{Y}_{lm}^R , being proportional to $\hat{\mathbf{n}}$, is invariant under rotations around the $\hat{\mathbf{n}}$ axis, and therefore, again from eq. (2.197), we see that it has $h = 0$ which, for a massless particle, implies $s = 0$; so \mathbf{Y}_{lm}^R describes a spin-zero massless particle.

In electrodynamics, the longitudinal degree of freedom described by \mathbf{Y}_{lm}^R is eliminated by gauge invariance, and electromagnetic radiation is purely transverse. Therefore in the expansion of the vector potential \mathbf{A}

⁴⁸We define parity reversing the orientation of the axes of the reference frame while keeping the vectors fixed (compare with Note 34 on page 98). With respect to the Cartesian basis vectors $(\mathbf{e}_x, \mathbf{e}_y, \mathbf{e}_z)$, a vector spherical harmonic \mathbf{Y}_{lm} has components $(\mathbf{Y}_{lm})_i$, that is $\mathbf{Y}_{lm} = (\mathbf{Y}_{lm})_i \mathbf{e}_i$. Under parity, the components $(\mathbf{Y}_{lm}^E)_i$ and $(\mathbf{Y}_{lm}^R)_i$ pick a factor $(-1)^{l+1}$, with $(-1)^l$ coming from the scalar spherical harmonic Y_{lm} and a further minus sign from ∂_i and from n_i , respectively. However, $\mathbf{Y}_{lm}^E = (\mathbf{Y}_{lm}^E)_i \mathbf{e}_i$ transform with a factor $(-1)^l$ because of the further minus sign from the transformation of the base vectors \mathbf{e}_i . Instead, $(\mathbf{Y}_{lm}^B)_i$ picks only the factor $(-1)^l$ from the scalar spherical harmonics, because angular momentum is a pseudovector and its components L_i are unchanged under parity, and then $\mathbf{Y}_{lm}^B = (\mathbf{Y}_{lm}^B)_i \mathbf{e}_i$ is multiplied by $\pi_l = (-1)^{l+1}$.

⁴⁹Recall that we have changed notation between eq. (3.253) and eq. (3.254), see Note 47, and the quantity that we are now labeling by l is the *total* angular momentum, previously denoted by j .

we have $R_{lm} = 0$,

$$\mathbf{A}(t, r, \theta, \phi) = \sum_{l=1}^{\infty} \sum_{m=-l}^l [E_{lm}(t, r) \mathbf{Y}_{lm}^E(\theta, \phi) + B_{lm}(t, r) \mathbf{Y}_{lm}^B(\theta, \phi)]. \quad (3.260)$$

For each value of the *total* (recall Note 47) angular momentum $l = 1, 2, \dots$ the electromagnetic field is therefore characterized by two polarization states with opposite parity, described by the wavefunctions E_{lm} and B_{lm} , called electric and magnetic photons, respectively. Their linear combinations give rise to the two helicity states of the photon. The state with total angular momentum $l = 0$ is instead absent.

The fact that, for a massless particle with helicities ± 1 , such as the photon, the state with total angular momentum $l = 0$ is absent while for all other values of the total angular momentum we have two states with opposite parity agrees with the analysis that we performed in Problem 2.2.

Spin-2 tensor harmonics

We can now introduce the spin-2 tensor harmonics, which are relevant for the description of gravitational radiation. First of all we need the spin wavefunction for $s = 2$ with a definite value of s_z ; this wavefunction is a traceless symmetric tensor, that we denote by $t_{ik}^{(s_z)}$, and is obtained taking two spin-1 wavefunctions $\xi_i^{(m_1)}$ and $\xi_k^{(m_2)}$, and combining them with the appropriate Clebsch–Gordan coefficients,

$$t_{ik}^{(s_z)} = \sum_{m_1, m_2=-1}^1 \langle 11m_1 m_2 | 2s_z \rangle \xi_i^{(m_1)} \xi_k^{(m_2)}. \quad (3.261)$$

Table 3.1 The coefficients which enter in the definition of pure-spin $s = 2$ spherical harmonics (from Thorne 1980).

a_{11}	$+ \left(\frac{(j+1)(j+2)}{(2j+1)(2j+3)} \right)^{1/2}$
a_{12}	$- \left(\frac{2j(j+1)}{3(2j-1)(2j+3)} \right)^{1/2}$
a_{13}	$+ \left(\frac{(j-1)j}{(2j-1)(2j+1)} \right)^{1/2}$
a_{21}	$- \left(\frac{2j(j+2)}{(2j+1)(2j+3)} \right)^{1/2}$
a_{22}	$- \left(\frac{3}{(2j-1)(2j+3)} \right)^{1/2}$
a_{23}	$+ \left(\frac{2(j-1)(j+1)}{(2j-1)(2j+1)} \right)^{1/2}$
a_{31}	$+ \left(\frac{(j-1)j}{2(2j+1)(2j+3)} \right)^{1/2}$
a_{32}	$+ \left(\frac{3(j-1)(j+2)}{(2j-1)(2j+3)} \right)^{1/2}$
a_{33}	$+ \left(\frac{(j+1)(j+2)}{2(2j-1)(2j+1)} \right)^{1/2}$
b_{11}	$+ \left(\frac{j+2}{2j+1} \right)^{1/2}$
b_{12}	$- \left(\frac{j-1}{2j+1} \right)^{1/2}$
b_{21}	$- \left(\frac{j-1}{2j+1} \right)^{1/2}$
b_{22}	$- \left(\frac{j+2}{2j+1} \right)^{1/2}$

The five tensors $t_{ik}^{(s_z)}$, with $s_z = 0, \pm 1, \pm 2$, are symmetric and traceless, and play the role that the three vectors $\xi_i^{(s_z)}$ with $s_z = 0, \pm 1$ played for vector spherical harmonics, that is, we combine them with the scalar spherical harmonics to obtain the spin-2 tensor spherical harmonics,

$$\begin{aligned} (\mathbf{T}_{jj_z}^l)_{ik} &\equiv (Y_{jj_z}^{l2})_{ik} \\ &= \sum_{l_z=-l}^l \sum_{s_z=-2}^2 \langle 2ls_z l_z | jj_z \rangle Y_{ll_z}(\theta, \phi) t_{ik}^{(s_z)}. \end{aligned} \quad (3.262)$$

Just as in the vector case, $(\mathbf{T}_{jj_z}^l)_{ik}$ are by construction eigenfunctions of the \mathbf{L}^2 operator (and for this reason are called pure-orbital $s = 2$ tensor spherical harmonics), but have no special property with respect to the radial unit vector $\hat{\mathbf{n}}$. Similarly to the case of vector harmonics, we can however observe that the full set of tensors $\mathbf{T}_{jj_z}^l$, with $j \geq 0$ and $j = l \pm 2, l \pm 1, l$ (if $l \geq 2$) or $j = 1, 2, 3$ if $l = 1$, or $j = 2$ if $l = 0$ (that is, the possible quantum combinations of spin $s = 2$ and orbital angular momentum l) can be expressed in terms of combinations, called the pure-spin $s = 2$ tensor spherical harmonics, with definite properties under rotations along the radial directions. For $j \geq 2$, these are given

by

$$\mathbf{T}_{jj_z}^{S0} = a_{11} \mathbf{T}_{jj_z}^{j+2} + a_{12} \mathbf{T}_{jj_z}^j + a_{13} \mathbf{T}_{jj_z}^{j-2}, \quad (3.263)$$

$$\mathbf{T}_{jj_z}^{E1} = a_{21} \mathbf{T}_{jj_z}^{j+2} + a_{22} \mathbf{T}_{jj_z}^j + a_{23} \mathbf{T}_{jj_z}^{j-2}, \quad (3.264)$$

$$\mathbf{T}_{jj_z}^{E2} = a_{31} \mathbf{T}_{jj_z}^{j+2} + a_{32} \mathbf{T}_{jj_z}^j + a_{33} \mathbf{T}_{jj_z}^{j-2}, \quad (3.265)$$

$$\mathbf{T}_{jj_z}^{B1} = b_{11} i \mathbf{T}_{jj_z}^{j+1} + b_{12} i \mathbf{T}_{jj_z}^{j-1}, \quad (3.266)$$

$$\mathbf{T}_{jj_z}^{B2} = b_{21} i \mathbf{T}_{jj_z}^{j+1} + b_{22} i \mathbf{T}_{jj_z}^{j-1}, \quad (3.267)$$

where the coefficients are given in Table 3.1. These combinations can be expressed in terms of the scalar spherical harmonics as follows⁵⁰

$$(\mathbf{T}_{lm}^{S0})_{ij} = [n_i n_j - (1/3) \delta_{ij}] Y_{lm}, \quad (3.268)$$

$$(\mathbf{T}_{lm}^{E1})_{ij} = c_l^{(1)} (r/2) (n_i \partial_j + n_j \partial_i) Y_{lm}, \quad (3.269)$$

$$(\mathbf{T}_{lm}^{B1})_{ij} = c_l^{(1)} (i/2) (n_i L_j + n_j L_i) Y_{lm}, \quad (3.270)$$

$$(\mathbf{T}_{lm}^{E2})_{ij} = c_l^{(2)} r^2 \Lambda_{ij, i' j'} (\hat{\mathbf{n}}) \partial_{i'} \partial_{j'} Y_{lm}, \quad (3.271)$$

$$(\mathbf{T}_{lm}^{B2})_{ij} = c_l^{(2)} r \Lambda_{ij, i' j'} (\hat{\mathbf{n}}) (i/2) (\partial_{i'} L_{j'} + \partial_{j'} L_{i'}) Y_{lm}, \quad (3.272)$$

where, as usual, $\Lambda_{ij, i' j'}$ is the tensor that implements the TT projection, see eq. (1.36), and

$$c_l^{(1)} = \left(\frac{2}{l(l+1)} \right)^{1/2}, \quad c_l^{(2)} = \left(2 \frac{(l-2)!}{(l+2)!} \right)^{1/2}. \quad (3.273)$$

A complete set of $s = 2$ spherical harmonic is given by eqs. (3.268)–(3.272) where \mathbf{T}_{lm}^{S0} has $l \geq 0$, \mathbf{T}_{lm}^{E1} and \mathbf{T}_{lm}^{B1} have $l \geq 1$, while \mathbf{T}_{lm}^{E2} and \mathbf{T}_{lm}^{B2} have $l \geq 2$.⁵¹ The above tensors are all symmetric and traceless by construction. On a traceless-symmetric tensor h_{ij} , the transversality condition $n_i h_{ij} = 0$ eliminates three degrees of freedom, and indeed we see from the explicit expressions that only \mathbf{T}_{lm}^{E2} and \mathbf{T}_{lm}^{B2} are transverse,

$$n_i (\mathbf{T}_{lm}^{E2})_{ij} = 0, \quad n_i (\mathbf{T}_{lm}^{B2})_{ij} = 0.$$

(3.274)

⁵⁰As in the vector case, we now switch notation from j, j_z to l, m , but one should be aware that these indices refer to the *total* angular momentum; we reserve instead the notation (i, j) for the spatial indices of vectors.

⁵¹Various useful ways of rewriting eqs. (3.268)–(3.272) can be found in eq. (2.30) of Thorne (1980). Observe also that, using the explicit form of the spherical harmonics Y_{lm} , \mathbf{T}_{lm}^{E1} and \mathbf{T}_{lm}^{B1} , as defined in eqs. (3.269) and (3.270), vanish for $l = 0$, while \mathbf{T}_{lm}^{E2} and \mathbf{T}_{lm}^{B2} , as defined in eqs. (3.271) and (3.272), vanish for $l = 0$ and for $l = 1$.

The five pure-spin $s = 2$ tensor harmonics are appropriate for describing the five independent components of a *massive* spin-2 particle. However, as we discussed in Problem 2.1 a *massless* particle with quantum number s has only two components rather than $2s + 1$, with helicities $h = \pm s$. Under a rotation by an angle θ around the $\hat{\mathbf{n}}$ axis, $(\mathbf{T}_{lm}^{S0})_{ij}$ is invariant since it depends only on n_i, n_j . Therefore in the massless case it describes a spin-0 particle. Instead $(\mathbf{T}_{lm}^{E1})_{ij}$ and $(\mathbf{T}_{lm}^{B1})_{ij}$ have one index (i or j) proportional to n_i or n_j , which is invariant, while the other index is carried by a vector in the transverse plane. Therefore they combine to give the two eigenvectors of helicity with $h = \pm 1$ and describe a massless vector particle. Finally, the transverse and traceless tensors $(\mathbf{T}_{lm}^{E2})_{ij}$ and $(\mathbf{T}_{lm}^{B2})_{ij}$ have two transverse indices and combine to give rise to the states with $h = \pm 2$ which make up a massless particle with $s = 2$. Therefore, even if we use the name “spin-2 tensor harmonics”,

it is important to understand that they can be used to describe either the five polarization states of a massive spin-2 particle, or to describe a *massless* field; in the latter case these five degrees of freedom decompose into the two degrees of freedom of a massless particle with $h = \pm 2$, the two degrees of freedom of a massless particle with $h = \pm 1$, and one degree of freedom corresponding to a massless scalar particle. Observe that the labels 0, 1 or 2 in $S0, E1, B1, E2, B2$ refer to the (absolute value of the) helicity carried in the massless case.

In particular, in standard general relativity the graviton is a massless particle with helicity ± 2 or, equivalently, the tensor h_{ij}^{TT} that describes GWs in the TT gauge, beside being symmetric and traceless, is also transverse. Therefore in its expansion enter only \mathbf{T}_{lm}^{E2} and \mathbf{T}_{lm}^{B2} , while the other components are eliminated by gauge invariance, as discussed in Sections 1.2 and 2.2.2. In the wave zone, where h_{ij}^{TT} decreases as $1/r$, the most general form of $h_{ij}^{\text{TT}}(t, r, \theta, \phi)$ is then

$$h_{ij}^{\text{TT}} = \frac{1}{r} \frac{G}{c^4} \sum_{l=2}^{\infty} \sum_{m=-l}^l [u_{lm}(\mathbf{T}_{lm}^{E2})_{ij}(\theta, \phi) + v_{lm}(\mathbf{T}_{lm}^{B2})_{ij}(\theta, \phi)],$$

(3.275)

where u_{lm} and v_{lm} are functions of retarded time $t - r/c$, and the factor G/c^4 in front is a useful normalization of u_{lm}, v_{lm} . The other pure-spin $s = 2$ tensor harmonics can enter in extensions of general relativity in which further degrees of freedom are present, and the condition of transversality no longer holds. Furthermore, in scalar–tensor extensions of general relativity, h_{ij} is not even traceless and there is a sixth degree of freedom corresponding to the trace of h_{ij} , which is a scalar field. So, in the most general case we must include all five spin-2 tensor harmonics (3.268)–(3.272), and we must further add $\delta_{ij}Y_{lm}$, which is not traceless and accounts for the scalar field corresponding to the trace part. The function $\delta_{ij}Y_{lm}$ can be combined with $(\mathbf{T}_{lm}^{S0})_{ij}$ to give a purely longitudinal and a purely transverse (but not traceless) tensor harmonic,

$$(\mathbf{T}_{lm}^{L0})_{ij} = n_i n_j Y_{lm}, \quad (\mathbf{T}_{lm}^{T0})_{ij} = \frac{1}{\sqrt{2}}(\delta_{ij} - n_i n_j)Y_{lm}, \quad (3.276)$$

with $l \geq 0$. The coefficients in eqs. (3.268)–(3.272) and in eq. (3.276) are chosen so that the pure-spin harmonics are orthonormal,

$$\int d\Omega (\mathbf{T}_{lm}^J)_{ij} (\mathbf{T}_{l'm'}^{J'})_{ij}^* = \delta^{JJ'} \delta_{ll'} \delta_{mm'}, \quad (3.277)$$

where the label J takes the values $L0, T0, E1, B1, E2, B2$. Finally, we observe from the explicit expressions that \mathbf{T}_{lm}^{L0} , \mathbf{T}_{lm}^{T0} , \mathbf{T}_{lm}^{E1} and \mathbf{T}_{lm}^{E2} have “electric-type” parity $\pi_l = (-1)^l$ while \mathbf{T}_{lm}^{B1} and \mathbf{T}_{lm}^{B2} have “magnetic-type” parity $\pi_l = (-1)^{l+1}$.

Equation (3.275) is the main result of this subsection. It is the generalization to the spin-2 field h_{ij} of the more usual expansion of the

solution of the wave equation for a relativistic scalar field in the wave zone, in terms of (scalar) spherical harmonics,

$$\phi(t, r, \theta, \phi) = \frac{1}{r} \sum_{l=0}^{\infty} \sum_{m=-l}^l c_{lm} Y_{lm}(\theta, \phi), \quad (3.278)$$

with c_{lm} functions of $t - r/c$, in the wave zone. Comparing eqs. (3.275) and (3.278) we see the following important differences: (1) a scalar field has only one spin degree of freedom and therefore, at each angular momentum level l, m , it is described by a single function $c_{lm}(t - r/c)$. A gravitational wave, instead, has two helicity states. Therefore there are two sets of tensor spherical harmonics, \mathbf{T}_{lm}^{E2} and \mathbf{T}_{lm}^{B2} , and correspondingly two sets of functions $u_{lm}(t - r/c)$ and $v_{lm}(t - r/c)$. These states are transverse, see eq. (3.274), one with electric-type parity and the other with magnetic-type parity. Because of eq. (3.277), the pure-spin harmonics provides an orthonormal basis for these modes. (2) The expansion of h_{ij}^{TT} starts from total angular momentum $l = 2$. It is impossible to construct a GW with total angular momentum $l = 0$ or $l = 1$. This counting of degrees of freedom is in full agreement with the discussion of graviton states in Problem 2.2.

Our next task is to relate the coefficients u_{lm}, v_{lm} in eq. (3.275) to the appropriate multipole moments of the source, as we do in the next subsection.⁵²

Relation with the source moments

In eq. (3.34) we found the solution of the equation of motion for h_{ij}^{TT} in the wave zone $r \gg d$, in the form

$$\begin{aligned} h_{ij}^{\text{TT}} &= \frac{1}{r} \frac{4G}{c^4} \Lambda_{ij,pq} \left[S^{pq} + \frac{1}{c} n_{i_1} \dot{S}^{pq,i_1} + \frac{1}{2c^2} n_{i_1} n_{i_2} \ddot{S}^{pq,i_1 i_2} + \dots \right] \\ &= \frac{1}{r} \frac{4G}{c^4} \Lambda_{ij,pq} \sum_{\alpha=0}^{\infty} \frac{1}{\alpha!} (\partial_0^\alpha S^{pq,i_1 \dots i_\alpha}) n_{i_1} \dots n_{i_\alpha}, \end{aligned} \quad (3.279)$$

where it is understood that all the $S^{pq,i_1 \dots i_\alpha}$ are functions of $t - r/c$. On the other hand, in the previous section we have seen that the most general expansion for h_{ij}^{TT} in the wave zone is given by

$$h_{ij}^{\text{TT}} = \frac{1}{r} \frac{G}{c^4} \sum_{l=2}^{\infty} \sum_{m=-l}^l [u_{lm}(\mathbf{T}_{lm}^{E2})_{ij} + v_{lm}(\mathbf{T}_{lm}^{B2})_{ij}], \quad (3.280)$$

where again it is understood that u_{lm} and v_{lm} are functions of $t - r/c$. Comparing the two expressions, we can determine u_{lm} and v_{lm} . To obtain u_{lm} , we multiply both sides of eq. (3.280) by $(\mathbf{T}_{lm}^{E2})_{ij}^*$ and we integrate over $d\Omega$. On the right-hand side, using the orthonormality condition (3.277), we single out u_{lm} , while on the left-hand side we insert the expression (3.279) for h_{ij}^{TT} . Similarly, to obtain v_{lm} we multiply by

⁵²Recall that all our discussion holds in the context of linearized theory, i.e. in a flat background space-time. The determination of the GW at infinity in terms of the source moments in the full non-linear theory is a much more difficult problem, whose solution will be given in Chapter 5. In the non-linear case, we will find that the STF formalism is much more convenient, and in fact the final result that will be given in eqs. (5.135) and (5.136) is a simple generalization of eqs. (3.207) and (3.208).

$(\mathbf{T}_{lm}^{B2})_{ij}^*$. Then we get

$$u_{lm} = \sum_{\alpha=0}^{\infty} \frac{4}{\alpha!} (\partial_0^\alpha S^{pq,i_1\dots i_\alpha}) \int d\Omega (\mathbf{T}_{lm}^{E2})_{ij}^* \Lambda_{ij,pq} n_{i_1} \dots n_{i_\alpha}, \quad (3.281)$$

$$v_{lm} = \sum_{\alpha=0}^{\infty} \frac{4}{\alpha!} (\partial_0^\alpha S^{pq,i_1\dots i_\alpha}) \int d\Omega (\mathbf{T}_{lm}^{B2})_{ij}^* \Lambda_{ij,pq} n_{i_1} \dots n_{i_\alpha}.$$

Since the Lambda tensor projects on the transverse and traceless part of a tensor, and \mathbf{T}_{lm}^{E2} and \mathbf{T}_{lm}^{B2} are already transverse and traceless, we have

$$(\mathbf{T}_{lm}^J)_{ij}^* \Lambda_{ij,pq} = (\mathbf{T}_{lm}^J)_{pq}^*, \quad (3.282)$$

(with $J = E2, B2$), and we can simplify the above expressions,

$$u_{lm} = \sum_{\alpha=0}^{\infty} \frac{4}{\alpha!} (\partial_0^\alpha S^{ij,i_1\dots i_\alpha}) \int d\Omega (\mathbf{T}_{lm}^{E2})_{ij}^* n_{i_1} \dots n_{i_\alpha}, \quad (3.283)$$

$$v_{lm} = \sum_{\alpha=0}^{\infty} \frac{4}{\alpha!} (\partial_0^\alpha S^{ij,i_1\dots i_\alpha}) \int d\Omega (\mathbf{T}_{lm}^{B2})_{ij}^* n_{i_1} \dots n_{i_\alpha}. \quad (3.284)$$

The computation of the integrals is involved, but can be performed order by order in v/c . To leading order in v/c , we perform it in detail in Problem 3.5.⁵³ The result is

$$u_{lm} = \frac{16\pi}{(2l+1)!!} \left[\frac{l}{2}(l-1)(l+1)(l+2) \right]^{1/2} \mathcal{Y}_{i_1\dots i_l}^{lm*} \partial_0^{l-2} S^{i_1 i_2, i_3 \dots i_l} \times \left[1 + O\left(\frac{v^2}{c^2}\right) \right]. \quad (3.285)$$

We now want to write the time derivatives of $S^{i_1 i_2, i_3 \dots i_l}$ in terms of the derivatives of the momenta of T^{00} , as follows. From the conservation of energy-momentum tensor, $\partial_\mu T^{\mu\nu} = 0$, we have the relations $\partial_0 T^{00} = -\partial_i T^{0i}$ and $\partial_0 T^{0i} = -\partial_j T^{ji}$. We can combine them to get $\partial_0^2 T^{00} = \partial_i \partial_j T^{ij}$. Then, integrating twice by parts,

$$\begin{aligned} \ddot{M}^{i_1\dots i_l} &= \int d^3x (\partial_0^2 T^{00}) x^{i_1} \dots x^{i_l} \\ &= \int d^3x (\partial_i \partial_j T^{ij}) x^{i_1} \dots x^{i_l} \\ &= \int d^3x T^{ij} \partial_i \partial_j (x^{i_1} \dots x^{i_l}). \end{aligned} \quad (3.286)$$

For $l \geq 2$, as in our case,

$$\begin{aligned} \partial_i \partial_j (x^{i_1} \dots x^{i_l}) &= (\partial_i \partial_j x^{i_1} x^{i_2}) x^{i_3} \dots x^{i_l} + \dots \\ &= (\delta_i^{i_1} \delta_j^{i_2} + \delta_i^{i_2} \delta_j^{i_1}) x^{i_3} \dots x^{i_l} + \dots, \end{aligned} \quad (3.287)$$

where the dots denote the other similar terms; in total there are $l(l-1)/2$ terms of this type. Therefore

$$\ddot{M}^{i_1\dots i_l} = 2(S^{i_1 i_2, i_3 \dots i_l} + \dots), \quad (3.288)$$

where the dots denote all other $l(l-1)/2$ pairing of indices (the permutation of the first two indices i, j in $S^{ij,kl\dots}$ is already taken into account by the overall factor of 2). This is the generalization to arbitrary l of the relation $\ddot{M}^{ij} = 2S^{ij}$ found in eq. (3.52). Once we contract the left- and right-hand sides of this equation with $\mathcal{Y}_{i_1\dots i_l}^{lm*}$, which is totally symmetric, all these permutations give the same result, so

$$\mathcal{Y}_{i_1\dots i_l}^{lm*} S^{i_1 i_2, i_3, \dots, i_l} = \frac{1}{l(l-1)} \mathcal{Y}_{i_1\dots i_l}^{lm*} \ddot{M}^{i_1\dots i_l}. \quad (3.289)$$

Therefore, in eq. (3.285),

$$\mathcal{Y}_{i_1\dots i_l}^{lm*} \partial_0^{l-2} S^{i_1 i_2, i_3, \dots, i_l} = \frac{1}{c^{l-2}} \frac{1}{l(l-1)} \mathcal{Y}_{i_1\dots i_l}^{lm*} \frac{d^l}{dt^l} M^{i_1\dots i_l}. \quad (3.290)$$

Then we get

$$u_{lm} = \frac{d^l}{dt^l} I_{lm}, \quad (3.291)$$

where, to leading order in $(v/c)^2$,

$$I_{lm} = \frac{1}{c^{l-2}} \frac{16\pi}{(2l+1)!!} \left[\frac{(l+1)(l+2)}{2l(l-1)} \right]^{1/2} \mathcal{Y}_{i_1\dots i_l}^{lm*} M^{i_1\dots i_l}. \quad (3.292)$$

Similarly, repeating the same analysis for v_{lm} (and using results discussed in Problem 3.5), we get

$$v_{lm} = \frac{d^l}{dt^l} S_{lm}, \quad (3.293)$$

where, again to leading order in $(v/c)^2$,

$$S_{lm} = \frac{1}{c^{l-1}} \frac{32\pi}{(2l+1)!!} \left[\frac{l(l+2)}{2(l-1)(l+1)} \right]^{1/2} \mathcal{Y}_{i_1\dots i_{l-1}}^{lm*} \epsilon_{ijk} P^{j,k i_1\dots i_{l-1}}, \quad (3.294)$$

where $P^{j,k i_1\dots i_{l-1}}$ are the momenta of the linear momentum.⁵⁴

Comparing with eq. (3.238) we see that I_{lm} and S_{lm} are just the spherical components of the tensors $M^{i_1\dots i_l}$ and $\epsilon_{ijk} P^{j,k i_1\dots i_{l-1}}$, respectively, apart from an l -dependent normalization. The tensor $M^{i_1\dots i_l}$ represents the moments of T^{00}/c^2 ; if the source is non-relativistic and has a negligible self-gravity, T^{00}/c^2 is the same as the mass density. Instead, from eqs. (3.40) and (3.41), we see that $\epsilon_{ijk} P^{j,k}$ is the angular momentum, and that $\epsilon_{ijk} P^{j,k i_1\dots i_{l-1}}$ are the momenta of the angular momentum. Writing explicitly

$$\begin{aligned} M^{i_1\dots i_l} &= \frac{1}{c^2} \int d^3x T^{00} x^{i_1} \dots x^{i_l} \\ &= \frac{1}{c^2} \int d^3x T^{00} r^l n^{i_1} \dots n^{i_l}, \end{aligned} \quad (3.295)$$

⁵⁴The expressions that we have computed in this section for I_{lm} and S_{lm} are valid only to leading order in v/c , i.e. they are Newtonian expressions. The full expansion in v/c is studied in Thorne (1980), Section V.

and using eq. (3.234), we can rewrite eq. (3.292) as

$$I_{lm} = \frac{1}{c^l} \frac{16\pi}{(2l+1)!!} \left[\frac{(l+1)(l+2)}{2l(l-1)} \right]^{1/2} \int d^3x r^l T^{00} Y_{lm}^*, \quad (3.296)$$

again to leading order in v^2/c^2 . Similarly we find

$$S_{lm} = \frac{1}{c^l} \frac{32\pi}{(2l+1)!!} \left[\frac{l(l+2)}{2(l-1)(l+1)} \right]^{1/2} \times \epsilon_{jlpq} \int d^3x r^l T^{0p} (\mathcal{Y}_{ji_1 \dots i_{l-1}}^{lm})^* n^q n^{i_1} \dots n^{i_{l-1}}. \quad (3.297)$$

This expression can be written in terms of the vector spherical harmonic \mathbf{Y}_{lm}^B defined in eq. (3.255). In fact, inserting eq. (3.234) in the definition of this vector harmonic, one finds

$$(\mathbf{Y}_{lm}^B)_i = \left(\frac{l}{l+1} \right)^{1/2} \epsilon_{ijk} \mathcal{Y}_{ki_1 \dots i_{l-1}}^{lm} n^j n^{i_1} \dots n^{i_{l-1}}, \quad (3.298)$$

and therefore, to leading order in $(v/c)^2$,

$$S_{lm} = \frac{1}{c^l} \frac{32\pi}{(2l+1)!!} \left[\frac{(l+2)}{2(l-1)} \right]^{1/2} \int d^3x r^l T^{0i} (\mathbf{Y}_{lm}^B)_i^*. \quad (3.299)$$

The coefficients of the expansion of h_{ij}^{TT} have therefore been written as integrals over the source of quantities which depend on the energy-momentum tensor.

Radiated power

We can finally write the radiated power to all orders in the multipole expansion. In eq. (3.275) we have expressed h_{ij}^{TT} in the basis of $\mathbf{T}_{lm}^{E2}, \mathbf{T}_{lm}^{B2}$. Inserting eq. (3.275) into eq. (1.153) and using the orthonormality relation (3.277), we find

$$\int d\Omega \dot{h}_{ij}^{\text{TT}} \dot{h}_{ij}^{\text{TT}} = \frac{1}{r^2} \frac{G^2}{c^8} \sum_{l=2}^{\infty} \sum_{m=-l}^l [|\dot{u}_{lm}|^2 + |\dot{v}_{lm}|^2]. \quad (3.300)$$

Therefore

$$\frac{dE}{dt} = \frac{G}{32\pi c^5} \sum_{l=2}^{\infty} \sum_{m=-l}^l \left\langle \left| \frac{d^{l+1} I_{lm}}{dt^{l+1}} \right|^2 + \left| \frac{d^{l+1} S_{lm}}{dt^{l+1}} \right|^2 \right\rangle, \quad (3.301)$$

where I_{lm} and S_{lm} are functions of retarded time $t - r/c$. The power is therefore a sum of terms each one associated with a single mass multipole or angular momentum multipole, and there are no mixed terms.

As a check of the above result, we can verify that we reproduce the mass quadrupole and the current quadrupole radiation. We start from the mass quadrupole. Equation (3.292), with $l = 2$, gives

$$\begin{aligned} I_{2m} &= \frac{16\pi}{5\sqrt{3}} \mathcal{Y}_{ij}^{2m*} M_{ij} \\ &= \frac{16\pi}{5\sqrt{3}} \mathcal{Y}_{ij}^{2m*} Q_{ij}, \end{aligned} \quad (3.302)$$

where we could replace M_{ij} by Q_{ij} since \mathcal{Y}_{ij}^{2m*} is traceless in the (i, j) indices. From eq. (3.301), the power radiated by the quadrupole is

$$P_{\text{quad}} = \frac{G}{32\pi c^5} \left(\frac{16\pi}{5\sqrt{3}} \right)^2 \langle \ddot{Q}_{ij} \ddot{Q}_{kl} \rangle \sum_{m=-2}^2 \mathcal{Y}_{ij}^{2m*} \mathcal{Y}_{kl}^{2m}. \quad (3.303)$$

We now use the identity⁵⁵

$$\sum_{m=-2}^2 \mathcal{Y}_{ij}^{2m*} \mathcal{Y}_{kl}^{2m} = \frac{15}{16\pi} (\delta_{ik} \delta_{jl} + \delta_{il} \delta_{jk} - \frac{2}{3} \delta_{ij} \delta_{kl}), \quad (3.304)$$

and we correctly recover eq. (3.75). The current quadrupole is checked similarly: from eq. (3.294) we have

$$S_{2m} = \frac{1}{c} \frac{64\pi}{15\sqrt{3}} \mathcal{Y}_{il}^{2m*} \epsilon_{ijk} P^{j,kl}. \quad (3.305)$$

Since

$$\begin{aligned} \epsilon_{ijk} P^{j,kl} &= \epsilon_{ijk} \int d^3x T^{0j} x^k x^l \\ &= - \int d^3x (\epsilon_{ikj} x^k T^{0j}) x^l \\ &= - \int d^3x j^i x^l \\ &= - J^{i,l}, \end{aligned} \quad (3.306)$$

we get

$$S_{2m} = - \frac{1}{c} \frac{64\pi}{15\sqrt{3}} \mathcal{Y}_{ij}^{2m*} J_{i,j}. \quad (3.307)$$

Then, using again the identity (3.304), and recalling that $J_{i,j} \delta_{ij} = 0$,

$$\begin{aligned} P_{\text{curr quad}} &= \frac{G}{32\pi c^7} \left(\frac{64\pi}{15\sqrt{3}} \right)^2 \langle \ddot{J}_{i,j} \ddot{J}_{k,l} \rangle \sum_{m=-2}^2 \mathcal{Y}_{ij}^{2m*} \mathcal{Y}_{kl}^{2m*} \\ &= \frac{8G}{45c^7} \langle \ddot{J}_{i,j} \ddot{J}_{k,l} \rangle (\delta_{ik} \delta_{jl} + \delta_{il} \delta_{jk}) \\ &= \frac{8G}{45c^7} \langle \ddot{J}_{i,j} (\ddot{J}_{i,j} + \ddot{J}_{j,i}) \rangle \\ &= \frac{16G}{45c^7} \langle \ddot{\mathcal{J}}_{ij} \ddot{\mathcal{J}}_{ij} \rangle, \end{aligned} \quad (3.308)$$

in agreement with eq. (3.154).

⁵⁵This identity could be proved using the explicit expressions (3.218) for \mathcal{Y}_{ij}^{2m} . However, the simplest way to derive it is to observe that, after summing over $m = -2, \dots, 2$, there is no longer a dependence on the direction chosen as quantization axis for j_z , so the right-hand side of eq. (3.304) can only depend on combinations of Kronecker deltas, i.e. it must be of the form $a\delta_{ik}\delta_{jl} + b\delta_{il}\delta_{jk} + c\delta_{ij}\delta_{kl}$. Since the left-hand side of eq. (3.304) gives zero when contracted with δ_{ij} , we must have $\delta_{ij}(a\delta_{ik}\delta_{jl} + b\delta_{il}\delta_{jk} + c\delta_{ij}\delta_{kl}) = 0$, which fixes $c = -(1/3)(a+b)$. Then a and b are fixed comparing the left and right-hand side of eq. (3.304) for two different values of the indices, using the explicit expressions (3.218).

3.6 Solved problems

Problem 3.1. Quadrupole radiation from an oscillating mass

As a first simple application, we compute the quadrupole radiation emitted by a non-relativistic degree of freedom z_0 that performs harmonic oscillations along the z axis,

$$z_0(t) = a \cos \omega_s t, \quad (3.309)$$

with $a\omega_s \ll c$ and $\omega_s > 0$. The actual physical system could be made for instance by two masses connected by a spring, with $z_0(t)$ the relative coordinate in the center-of-mass system. For the moment we consider the case where the rest length of the spring is zero (which is not realistic for a one-dimensional spring, but is representative of a number of situations where some degree of freedom performs a simple harmonic motion). As discussed in Section 3.3.5, the whole formalism that we have developed for computing the emission of gravitational radiation is consistent only if we include in the energy-momentum tensor also the interaction terms responsible for the actual trajectory, which however are subleading when computing the mass quadrupole radiation to lowest order in v/c . The mass density is then

$$\rho(t, \mathbf{x}) = \mu \delta(x) \delta(y) \delta(z - z_0(t)), \quad (3.310)$$

where μ is the reduced mass of the system, and the second mass moment is

$$\begin{aligned} M^{ij}(t) &= \int d^3x \rho(t, \mathbf{x}) x^i x^j \\ &= \mu z_0^2(t) \delta^{i3} \delta^{j3} \\ &= \mu a^2 \frac{1 + \cos 2\omega_s t}{2} \delta^{i3} \delta^{j3}. \end{aligned} \quad (3.311)$$

Inserting this into eq. (3.72), we obtain

$$\begin{aligned} h_+(t; \theta, \phi) &= -\frac{1}{r} \frac{G}{c^4} \ddot{M}_{33}(t_{\text{ret}}) \sin^2 \theta \\ &= \frac{2G\mu a^2 \omega_s^2}{rc^4} \sin^2 \theta \cos(2\omega_s t_{\text{ret}}), \end{aligned} \quad (3.312)$$

$$h_\times(t; \theta, \phi) = 0. \quad (3.313)$$

Therefore we have monochromatic radiation at a frequency $\omega = 2\omega_s$, with a purely plus polarization, see Fig. 3.4.

The angular distribution is independent of ϕ (reflecting the cylindric symmetry of the source), and has a maximum at $\theta = \pi/2$, i.e. in the direction orthogonal to the axis along which the source oscillates. Observe that the radiation vanishes along the z axis. This reflects the fact that only the components of the motion of the source transverse to the line-of-sight contribute to the production of GWs. This is a general result, which follows from the fact that $\Lambda_{ij,kln}{}^k = \Lambda_{ij,kln}{}^l = 0$. That is, the Lambda tensor projects the motion of the source onto the plane transverse to the propagation direction.

Observe also that the pattern of lines of force of the GW shown in Fig. 3.4 is a physical result, independent of our conventions. The fact that we call it a “plus” polarization, instead, is related to our choice of axes $(\hat{\mathbf{u}}, \hat{\mathbf{v}})$ with respect to which the plus and cross polarizations are defined. With our definition, $(\hat{\mathbf{u}}, \hat{\mathbf{v}})$ are obtained from the $(\hat{\mathbf{x}}, \hat{\mathbf{y}})$ axes applying the rotation matrix \mathcal{R} given

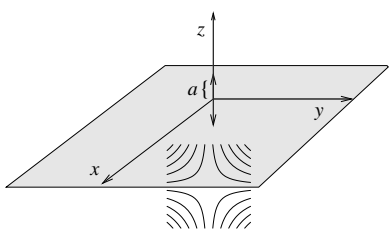


Fig. 3.4 A source oscillating along the z axis (double arrow), and the lines of force of the GW emitted in a direction with $\theta = \pi/2$.

in eq. (3.70), see also Fig. 3.2. Thus, in Fig. 3.4, for the particular propagation direction for which the lines of force are shown (i.e. for a direction $\hat{\mathbf{n}}$ such that $\theta = \pi/2$), we have $\hat{\mathbf{v}} = -\hat{\mathbf{z}}$, while $\hat{\mathbf{u}}$ is along the intersection of this transverse plane with the (x, y) plane. If, in this transverse plane, we instead used $(\hat{\mathbf{u}}, \hat{\mathbf{v}})$ axes rotated by 45 degrees to define h_+ and h_\times , we would rather call the pattern of Fig. 3.4 a purely cross polarization, compare with Figs. 1.2 and 1.3, while for axes rotated by a generic angle ψ we would have a mixture of plus and cross polarizations, according to eq. (2.194).

The radiated power is computed from eq. (3.73),

$$\begin{aligned} \left(\frac{dP}{d\Omega} \right)_{\text{quad}} &= \frac{r^2 c^3}{16\pi G} \langle \dot{h}_+^2 \rangle \\ &= \frac{G\mu^2 a^4 \omega_s^6}{2\pi c^5} \sin^4 \theta, \end{aligned} \quad (3.314)$$

where we used $\langle \cos^2(2\omega_s t) \rangle = 1/2$. Alternatively, we can recover the same result using eq. (3.73) in the form

$$\left(\frac{dP}{d\Omega} \right)_{\text{quad}} = \frac{G}{8\pi c^5} \Lambda_{33,33}(\hat{\mathbf{n}}) \langle \ddot{M}_{33}^2 \rangle, \quad (3.315)$$

and observing that, from eq. (1.39),

$$\begin{aligned} \Lambda_{33,33} &= \frac{1}{2} (1 - n_3^2)^2 \\ &= \frac{1}{2} \sin^4 \theta, \end{aligned} \quad (3.316)$$

since $n_3 = \cos \theta$. In Fig. 3.5 we show this angular distribution, in the (x, z) plane. The integration over the solid angle gives

$$P_{\text{quad}} = \frac{16}{15} \frac{G\mu^2}{c^5} a^4 \omega_s^6. \quad (3.317)$$

The total energy radiated over one period $T = 2\pi/\omega_s$ of the source motion is therefore

$$\langle E_{\text{quad}} \rangle_T = \frac{32\pi}{15} \frac{G\mu^2}{c^5} a^4 \omega_s^5. \quad (3.318)$$

This result becomes physically more transparent if we rewrite it in terms of $v = a\omega_s$ (which is the maximum speed of the source),

$$\langle E_{\text{quad}} \rangle_T = \frac{32\pi}{15} \frac{G\mu^2}{a} \left(\frac{v}{c} \right)^5. \quad (3.319)$$

Observe that $G\mu^2/a$ is of order of the gravitational self-energy of an object of mass μ and size a . In the quadrupole approximation, the energy radiated over a cycle is suppressed, with respect to this energy scale, by a factor $(v/c)^5$.

Finally, it is instructive to consider the case of two masses connected by a spring with a rest length L , so their relative coordinate obeys

$$z_0(t) = L + a \cos \omega_s t. \quad (3.320)$$

Observe that L has an invariant meaning, because $z_0(t)$ is the relative position between the two masses, so we cannot set it to zero with a choice of the origin. Now we get

$$z_0^2(t) = \frac{a^2}{2} \cos 2\omega_s t + 2La \cos \omega_s t + \text{const.}, \quad (3.321)$$

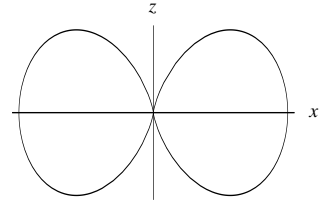


Fig. 3.5 The angular distribution of the quadrupole radiation, for a mass oscillating along the z axis. We represent the angular distribution plotting the function $\rho = \sin^4 \theta$, where (ρ, θ) are the polar coordinates in the (x, z) plane and θ is measured from the z axis. The full three-dimensional pattern has cylindrical symmetry around the z axis.

and eq. (3.312) becomes

$$h_+(t; \theta, \phi) = \frac{2G\mu\omega_s^2}{rc^4} \sin^2 \theta [a^2 \cos(2\omega_s t_{\text{ret}}) + La \cos(\omega_s t_{\text{ret}})], \quad (3.322)$$

while still $h_\times = 0$. Thus, beside having gravitational radiation at $\omega_{\text{gw}} = 2\omega_s$, we also have radiation at $\omega_{\text{gw}} = \omega_s$. Observe that, in the power, there is no interference between these two terms because $\langle \cos^2(2\omega_s t) \rangle = 1/2 = \langle \cos^2(\omega_s t) \rangle$, but

$$\langle 2 \cos(2\omega_s t) \cos(\omega_s t) \rangle = \langle \cos(3\omega_s t) + \cos(\omega_s t) \rangle = 0. \quad (3.323)$$

Problem 3.2. Quadrupole radiation from a mass in circular orbit

In this problem we consider a binary system with masses m_1 and m_2 , and we assume that the relative coordinate is performing a circular motion. We assume for the moment that the orbital motion is given, and we neglect any back-reaction on the motion due to GW emission. In this form, this is just a simple exercise, propedeutic for understanding a real self-gravitating binary system. In Section 4.1 we will include the effect of the GW back-reaction within linearized theory. Furthermore, at higher orders in v/c we cannot keep the space-time as flat when describing a self-gravitating system, and the correct formalism for computing the v/c corrections will be the subject of Chapter 5.

So, for the moment, we rather assign ourselves the trajectory. We choose the (x, y, z) frame so that the orbit lies in the (x, y) plane, and is given by

$$\begin{aligned} x_0(t) &= R \cos(\omega_s t + \frac{\pi}{2}), \\ y_0(t) &= R \sin(\omega_s t + \frac{\pi}{2}), \\ z_0(t) &= 0. \end{aligned} \quad (3.324)$$

(The phase $\pi/2$ is a useful choice of the origin of time.) We denote by $\mu = m_1 m_2 / (m_1 + m_2)$ the reduced mass of the system. From eq. (3.129), in the CM frame the second mass moment is $M^{ij} = \mu x_0^i(t) x_0^j(t)$, so

$$M_{11} = \mu R^2 \frac{1 - \cos 2\omega_s t}{2}, \quad (3.325)$$

$$M_{22} = \mu R^2 \frac{1 + \cos 2\omega_s t}{2}, \quad (3.326)$$

$$M_{12} = -\frac{1}{2} \mu R^2 \sin 2\omega_s t, \quad (3.327)$$

while the other components vanish. Therefore we have

$$\ddot{M}_{11} = 2\mu R^2 \omega_s^2 \cos 2\omega_s t, \quad (3.328)$$

$$\ddot{M}_{12} = 2\mu R^2 \omega_s^2 \sin 2\omega_s t, \quad (3.329)$$

and $\ddot{M}_{22} = -\ddot{M}_{11}$. Plugging these expressions into eq. (3.72) we get

$$h_+(t; \theta, \phi) = \frac{1}{r} \frac{4G\mu\omega_s^2 R^2}{c^4} \left(\frac{1 + \cos^2 \theta}{2} \right) \cos(2\omega_s t_{\text{ret}} + 2\phi), \quad (3.330)$$

$$h_\times(t; \theta, \phi) = \frac{1}{r} \frac{4G\mu\omega_s^2 R^2}{c^4} \cos \theta \sin(2\omega_s t_{\text{ret}} + 2\phi). \quad (3.331)$$

Thus, the quadrupole radiation is at twice the frequency ω_s of the source. It is interesting to observe that the dependences $h_+ \sim (1 + \cos^2 \theta)$ and $h_\times \sim \cos \theta$ are a general consequence of eq. (3.72), whenever $M_{13} = M_{23} = M_{33} = 0$ and $\ddot{M}_{22} = -\ddot{M}_{11}$. These conditions are satisfied also in other problems (e.g. a rigid body rotating around one of its principal axis), so we will meet again this type of angular dependence.

As for the dependence on ϕ , it can be clearly understood physically: contrary to the oscillating mass of the previous problem, now the source is not invariant under rotations around the z axis, since at any given value of t the mass μ is at a specific point along the orbit, which is changed by a rotation around the z axis; therefore h_+ and h_\times have a dependence on ϕ . However, since the orbit is circular, a rotation of the source by an angle $\Delta\phi$ around the z axis is the same as a time translation Δt with $\omega_s \Delta t = \Delta\phi$, and therefore the dependence of h_+ and h_\times on ϕ is only through the combination $\omega_s t_{\text{ret}} + \phi$.

From the observational point of view, we have only access to the radiation that a binary star emits in the direction which points from the star toward us. The angle θ is therefore equal to the angle ι between the normal to the orbit and the line-of-sight (see Fig. 3.6). The distance r to an astrophysical source is, for most practical purposes, a constant.⁵⁶ As long as, during the observation, we can neglect the proper motion of the source (which however sometimes is not the case, as we will discuss in Section 7.6), also the angle ϕ is fixed, so we have $\omega_s t_{\text{ret}} + \phi = \omega_s t + \alpha$, with $\alpha = \phi - \omega_s r/c$ a fixed constant. Then we can shift the origin of time so that $2\omega_s t + 2\alpha \rightarrow 2\omega_s t$ plus an integer multiple of 2π , so $\cos(2\omega_s t + 2\alpha) \rightarrow \cos(2\omega_s t)$ and $\sin(2\omega_s t + 2\alpha) \rightarrow \sin(2\omega_s t)$. Therefore, this observer can write the GWs received by a binary system (as long as the approximation of a fixed circular orbit is valid, see Section 4.1) as

$$\begin{aligned} h_+(t) &= \frac{1}{r} \frac{4G\mu\omega_s^2 R^2}{c^4} \left(\frac{1 + \cos^2 \iota}{2} \right) \cos(2\omega_s t), \\ h_\times(t) &= \frac{1}{r} \frac{4G\mu\omega_s^2 R^2}{c^4} \cos \iota \sin(2\omega_s t). \end{aligned} \quad (3.332)$$

If we see the orbit edge-on, $\iota = \pi/2$, then h_\times vanishes and therefore the GW is linearly polarized. Instead, at $\iota = 0$, h_+ and h_\times have the same amplitude; in this case, since the former is proportional to $\sin(2\omega_s t_{\text{ret}})$ while the latter to $\cos(2\omega_s t_{\text{ret}})$, in the plane (h_+, h_\times) the radiation describes a circle parametrized by t , that is, the radiation is circularly polarized. To understand what this means in more physical terms, we consider the pattern of lines of force corresponding to a circular polarization. If we have a purely plus polarization, $h_+ = A_+ \cos 2\omega_s t$, according to eq. (1.96) we have a force field

$$\mathbf{F}_+ = -2\mu\omega_s^2 A_+ \mathbf{v}_+ \cos 2\omega_s t, \quad (3.333)$$

where the vector field $\mathbf{v}_+(x, y)$ has components $(x, -y)$. This force field is shown in Fig. 1.2. If instead we have a purely cross polarization of the form $h_\times = A_\times \sin 2\omega_s t$, according to eq. (1.96) we have a force field

$$\mathbf{F}_\times = -2\mu\omega_s^2 A_\times \mathbf{v}_\times \sin 2\omega_s t, \quad (3.334)$$

where the vector field $\mathbf{v}_\times(x, y)$ has components (y, x) . This force field is shown in Fig. 1.3. If we have both $h_+ = A_+ \cos 2\omega_s t$ and $h_\times = A_\times \sin 2\omega_s t$,

⁵⁶ As we will discuss in Section 7.6, there are situations in which we must take into account corrections due to motion of the Earth around the Sun, or more precisely around the Solar System Barycenter (SSB). So, more generally, we can take r to be the distance from the source to the SSB. This however is only important for observations lasting at least few months. We will see in Section 4.1 that, in ground-based interferometers, the gravitational waves emitted by a binary system are observable only for about the last 15 minutes before the system coalesces.

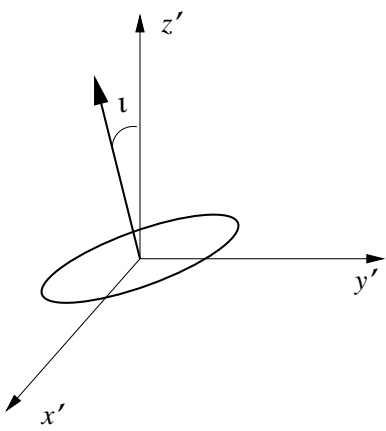


Fig. 3.6 The geometry of the problem in a frame (x', y', z') where a fixed observer is at large distance along the positive z' axis. The normal to the orbit makes an angle ι with the z' axis.

and furthermore $A_+ = A_\times \equiv A$, we have

$$\mathbf{F} = -2\mu\omega_s^2 A [\mathbf{v}_+ \cos 2\omega_s t + \mathbf{v}_\times \sin 2\omega_s t]. \quad (3.335)$$

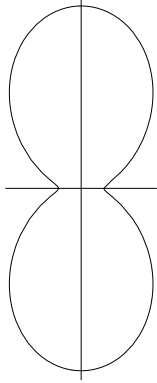


Fig. 3.7 The function $g(\theta)$ in polar coordinates. The angle θ is measured from the vertical axis.

Observe that \mathbf{v}_+ and \mathbf{v}_\times are orthogonal, $\mathbf{v}_+ \cdot \mathbf{v}_\times = 0$, and therefore the pattern of lines of forces described by eq. (3.335) is the same as the pattern of Fig. 1.2, that rotates uniformly so that at $\omega_s t = 0$ it is the same as Fig. 1.2, at $\omega_s t = \pi/4$ it is the same as Fig. 1.3, and so on.

At intermediate values of t the amplitudes for h_+ and h_\times are different and therefore we have elliptic polarization, i.e. in the plane (h_+, h_\times) the radiation describes an ellipse parametrized by t . We see that, from a measurement of the degree of polarization, i.e. of the relative amplitude of h_+ and h_\times , we can deduce the inclination ι of the orbit.

The angular distribution of the radiated power, in the quadrupole approximation, is obtained as usual using eq. (3.73),

$$\left(\frac{dP}{d\Omega} \right)_{\text{quad}} = \frac{r^2 c^3}{16\pi G} (\dot{h}_+^2 + \dot{h}_\times^2). \quad (3.336)$$

Inserting here eq. (3.332), and using $\langle \cos^2(2\omega_s t) \rangle = \langle \sin^2(2\omega_s t) \rangle = 1/2$, we get

$$\boxed{\left(\frac{dP}{d\Omega} \right)_{\text{quad}} = \frac{2G\mu^2 R^4 \omega_s^6}{\pi c^5} g(\theta)}, \quad (3.337)$$

where

$$\boxed{g(\theta) = \left(\frac{1 + \cos^2 \theta}{2} \right)^2 + \cos^2 \theta.} \quad (3.338)$$

The radiation is maximum at $\theta = 0$, i.e. in the direction normal to the plane of the orbit. A polar plot of $g(\theta)$ is shown in Fig. 3.7. Observe that, contrary to the angular distribution found in Problem 3.1, $g(\theta)$ never vanishes since, whatever the angle θ at which an observer is located, there is always a component of the source motion orthogonal to the observer's line-of-sight.

Integrating eq. (3.337) over the solid angle we get the total power radiated in the quadrupole approximation,

$$\begin{aligned} P_{\text{quad}} &= \frac{32}{5} \frac{G\mu^2}{c^5} R^4 \omega_s^6 \\ &= \frac{1}{10} \frac{G\mu^2}{c^5} R^4 \omega_s^6, \end{aligned} \quad (3.339)$$

where $\omega = 2\omega_s$ is the frequency of the GW.⁵⁷ The energy radiated in one period $T = 2\pi/\omega_s$ of the source motion is therefore, writing $v = \omega_s R$,

$$\langle E_{\text{quad}} \rangle_T = \frac{64\pi}{5} \frac{G\mu^2}{R} \left(\frac{v}{c} \right)^5. \quad (3.340)$$

Similarly to the result found in eq. (3.319), this is suppressed by a factor $(v/c)^5$ with respect to the energy scale $G\mu^2/R$.

⁵⁷If one is interested only in the total power, rather than in the angular distribution, it is actually simpler to derive it directly from eq. (3.75): we use again the reference frame where the orbit is given by eq. (3.324), so

$$\ddot{M}_{ij} = 4\mu\omega_s^3 R^2 \times \begin{pmatrix} -\sin 2\omega_s t & \cos 2\omega_s t & 0 \\ \cos 2\omega_s t & \sin 2\omega_s t & 0 \\ 0 & 0 & 0 \end{pmatrix}_{ij}.$$

Since this is traceless, it is also equal to \ddot{Q}_{ij} . Plugging this into eq. (3.75), we recover eq. (3.339).

Problem 3.3. Mass octupole and current quadrupole radiation from a mass in circular orbit

In this problem we compute the mass octupole and current quadrupole radiation generated by a binary system of reduced mass μ , whose center-of-mass coordinate describes a circular trajectory. As discussed in Section 3.3.5, to lowest order in v/c the mass octupole and the current quadrupole radiation emitted by a self-gravitating system can be consistently computed taking the free-particle energy-momentum tensor, evaluating it on a Newtonian circular orbit, and plugging the resulting values of T^{00} and T^{0i} into the expression for \ddot{M}^{ijk} and $\dot{P}^{i,j,k}$ (while the same procedure is not correct if applied to \dot{S}^{ijk}). Defining as usual the center-of-mass coordinate \mathbf{x}_{CM} by $m\mathbf{x}_{\text{CM}} = m_1\mathbf{x}_1 + m_2\mathbf{x}_2$ (where $m = m_1 + m_2$) and the relative coordinate $\mathbf{x} = \mathbf{x}_1 - \mathbf{x}_2$, we have $\mathbf{x}_1 = \mathbf{x}_{\text{CM}} + (m_2/m)\mathbf{x}$ and $\mathbf{x}_2 = \mathbf{x}_{\text{CM}} - (m_1/m)\mathbf{x}$. Thus, in the CM frame where $\mathbf{x}_{\text{CM}} = 0$, $T^{00}(t, \mathbf{x}) = m_1 c^2 \delta^{(3)}(\mathbf{x} - \frac{m_2}{m} \mathbf{x}_0(t)) + m_2 c^2 \delta^{(3)}(\mathbf{x} + \frac{m_1}{m} \mathbf{x}_0(t))$, and

$$M^{ijk}(t) = \frac{1}{c^2} \int d^3x T^{00}(t, \mathbf{x}) x^i(t) x^j(t) x^k(t) = \mu \frac{\delta m}{m} x_0^i(t) x_0^j(t) x_0^k(t),$$

where $\delta m = m_2 - m_1$. To compute the radiation emitted from the star in the direction of the observer it is simpler to use the geometrical setting of Fig. 3.6 (labeling now the axes of this figure as (x, y, z) rather than (x', y', z')), in which the observer is along the z axis. The equation of the orbit of the relative coordinate in the center-of-mass frame is then

$$\begin{aligned} x_0(t) &= R \cos \omega_s t, \\ y_0(t) &= R \cos \iota \sin \omega_s t, \\ z_0(t) &= R \sin \iota \sin \omega_s t, \end{aligned} \quad (3.341)$$

and is obtained from an orbit lying in the (x, y) plane performing a rotation by an angle ι around the x axis. We set the observer in the z direction, so we compute the radiation emitted along $\hat{\mathbf{n}} = (0, 0, 1)$. For the octupole radiation, eq. (3.141) gives

$$\left(h_{ij}^{\text{TT}} \right)_{\text{oct}} = \frac{1}{r} \frac{2G}{3c^5} \Lambda_{ij,kl}(\hat{\mathbf{n}}) \ddot{M}_{kl3}. \quad (3.342)$$

(As usual, in actual computations, it is more convenient to use M^{ijk} rather than \mathcal{O}^{ijk} .) We found in eq. (3.63) that, when $\hat{\mathbf{n}} = (0, 0, 1)$, in the multiplication of a matrix \ddot{M}_{kl3} by the Lambda tensor the components of \ddot{M}_{kl3} with $k = 3$ or $l = 3$ do not contribute, so we just need to compute M_{ab3} with $a, b = 1, 2$. With the trajectory given in eq. (3.341) we find, for $a, b = 1, 2$

$$M_{ab3} = \mu \frac{\delta m}{m} R^3 \sin \iota \sin \omega_s t \begin{pmatrix} \cos^2 \omega_s t & \cos \iota \sin \omega_s t \cos \omega_s t \\ \cos \iota \sin \omega_s t \cos \omega_s t & \cos^2 \iota \sin^2 \omega_s t \end{pmatrix}_{ab}. \quad (3.343)$$

Computing $\Lambda_{ab,cd}(\hat{\mathbf{n}}) M_{cd3}$ using eq. (3.63) we get

$$\begin{aligned} \Lambda_{ab,cd}(\hat{\mathbf{n}}) M_{cd3} &= \mu \frac{\delta m}{m} R^3 \sin \iota \sin \omega_s t \times \\ &\times \begin{pmatrix} \frac{1}{2}(\cos^2 \omega_s t - \cos^2 \iota \sin^2 \omega_s t) & \cos \iota \sin \omega_s t \cos \omega_s t \\ \cos \iota \sin \omega_s t \cos \omega_s t & -\frac{1}{2}(\cos^2 \omega_s t - \cos^2 \iota \sin^2 \omega_s t) \end{pmatrix}_{ab}, \end{aligned} \quad (3.344)$$

and taking the third time derivative we find

$$\begin{aligned} (h_+)_\text{oct} &= \frac{1}{r} \frac{G\mu R^3 \omega_s^3}{12c^5} \frac{\delta m}{m} \sin \iota [(3 \cos^2 \iota - 1) \cos \omega_s t - 27(1 + \cos^2 \iota) \cos 3\omega_s t], \\ (h_\times)_\text{oct} &= \frac{1}{r} \frac{G\mu R^3 \omega_s^3}{12c^5} \frac{\delta m}{m} \sin 2\iota [\sin \omega_s t - 27 \sin 3\omega_s t]. \end{aligned} \quad (3.345)$$

As expected, we have radiation both at $\omega = \omega_s$ and at $\omega = 3\omega_s$, since the mass octupole is trilinear in $x_0^i(t)$. The current quadrupole radiation can be computed similarly. Plugging $T^{0i}(t, \mathbf{x}) = m_1 c v_1^i \delta^{(3)}(\mathbf{x} - \frac{m_2}{m} \mathbf{x}_0(t)) + m_2 c v_2^i \delta^{(3)}(\mathbf{x} + \frac{m_1}{m} \mathbf{x}_0(t))$ into eqs. (3.148) and (3.149) we get

$$J^{i,j}(t) = \mu \frac{\delta m}{m} \epsilon^{ikl} x_0^k(t) \dot{x}_0^l(t) x_0^j(t). \quad (3.346)$$

Observe that $l^i \equiv \epsilon^{ikl} x_0^k(t) \dot{x}_0^l(t)$ is the angular momentum of a unit mass moving on the circular orbit $x_0^i(t)$, and is therefore a constant vector of modulus $R^2 \omega_s$ and direction normal to the plane of the orbit. Therefore $J^{i,j}(t) = \mu (\delta m/m) l^i x_0^j(t)$ depends on time only through $x_0^j(t)$ and oscillates only at the frequency ω_s , rather than at ω_s and $3\omega_s$ as the mass octupole. Inserting this expression for $J^{i,j}(t)$ into eq. (3.151) and setting $\hat{\mathbf{n}} = (0, 0, 1)$ we get the current quadrupole radiation

$$\left(h_{ij}^{\text{TT}} \right)_{\text{cq}} = \frac{1}{r} \frac{4G}{3c^5} \Lambda_{ij,kl}(\hat{\mathbf{n}}) \left(\epsilon^{3kp} \ddot{j}^{p,l} + \epsilon^{3lp} \ddot{j}^{p,k} \right). \quad (3.347)$$

Performing the contraction with the Lambda tensor we get

$$\begin{aligned} (h_+)_\text{cq} &= \frac{1}{r} \frac{4G\mu R^3 \omega_s^3}{3c^5} \frac{\delta m}{m} \sin \iota \cos \omega_s t, \\ (h_\times)_\text{cq} &= \frac{1}{r} \frac{2G\mu R^3 \omega_s^3}{3c^5} \frac{\delta m}{m} \sin 2\iota \sin \omega_s t. \end{aligned}$$

Summing the mass octupole and current quadrupole radiation, using Kepler's law $\omega_s^2 R^3 = Gm$, and introducing the notation $x = (Gm\omega_s/c^3)^{2/3}$ that is useful to make contact with the results of Chapter 5, we finally get

$$\begin{aligned} (h_+)_{\text{oct+cq}} &= \frac{G\mu}{4rc^2} \frac{\delta m}{m} x^{3/2} \sin \iota [(\cos^2 \iota + 5) \cos \omega_s t - 9(1 + \cos^2 \iota) \cos 3\omega_s t], \\ (h_\times)_{\text{oct+cq}} &= \frac{3G\mu}{4rc^2} \frac{\delta m}{m} x^{3/2} \sin 2\iota [\sin \omega_s t - 3 \sin 3\omega_s t]. \end{aligned} \quad (3.348)$$

This result agrees with the one that we will find in Chapter 5 from a complete post-Newtonian treatment, see eqs. (5.262), (5.266) and (5.267).^(*)

The contribution to the total radiated power from the mass octupole and the current quadrupole is

$$\begin{aligned} P_{\text{oct+cq}} &= \frac{r^2 c^3}{16\pi G} 2\pi \int_{-1}^1 d\cos \iota \langle h_+^2 + h_\times^2 \rangle_{\text{oct+cq}} \\ &= \frac{62}{7} \frac{G\mu^2}{c^7} \left(\frac{\delta m}{m} \right)^2 R^6 \omega_s^8. \end{aligned} \quad (3.349)$$

It is interesting to compare the power at $\omega = \omega_s, 3\omega_s$ (generated by the mass octupole plus the current quadrupole), with the power at $\omega = 2\omega_s$, generated by the mass quadrupole. From eq. (3.348) we find

$$P(\omega_s) = \frac{25}{896} \left(\frac{v}{c} \right)^2 \left(\frac{\delta m}{m} \right)^2 P(2\omega_s), \quad (3.350)$$

and

$$P(3\omega_s) = \frac{1215}{896} \left(\frac{v}{c} \right)^2 \left(\frac{\delta m}{m} \right)^2 P(2\omega_s), \quad (3.351)$$

where $P(2\omega_s)$ is the leading-order quadrupole result, eq. (3.339). In Fig. 3.8 we show the relative intensity of the three spectral lines at $\omega = \omega_s, 2\omega_s$ and $3\omega_s$, for $v/c = 10^{-2}$ and an extreme mass ratio $m_2/m_1 \rightarrow 0$ and therefore $\delta m/m = 1$. Observe that the vertical scale is logarithmic.

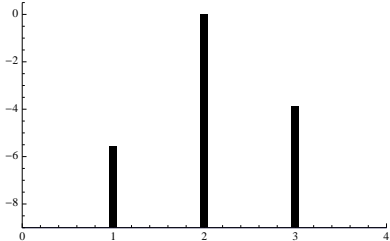


Fig. 3.8 $\log_{10}[P(\omega)/P(2\omega_s)]$, as a function of ω/ω_s , for $v/c = 10^{-2}$ and $\delta m/m = 1$, including the contributions of the mass quadrupole, of the mass octupole, and of the current quadrupole. The line at $\omega = 2\omega_s$ is due to the mass quadrupole, the line at $\omega = \omega_s$ is due to the mass octupole and current quadrupole, while that at $\omega = 3\omega_s$ is due only to the mass octupole.

Problem 3.4. Decomposition of $\dot{S}^{kl,m}$ into irreducible representations of $SO(3)$

We have seen that the next-to-leading term in the multipole expansion is proportional to $\dot{S}^{kl,m}$. In this problem we discuss the decomposition of $\dot{S}^{kl,m}$ into irreducible representations of the rotation group $SO(3)$, and we will understand the group-theoretical origin of the mass octupole and current quadrupole terms.

Let us recall that the irreducible representations of Lie groups, as for instance $O(N)$ or $U(N)$, are conveniently expressed in terms of Young diagrams. A Young diagram is a set of n boxes, organized into r lines of length n_1, n_2, \dots, n_r , with $n_1 \geq n_2 \geq \dots \geq n_r$ and $n_1 + \dots + n_r = n$. In each box we put an index i_1, \dots, i_n . For $O(N)$ each index takes the values $1, \dots, N$, which is the dimension of the vector representation. The irreducible tensor representations can be obtained antisymmetrizing first over the indices in the columns and then symmetrizing over the indices in the lines.⁵⁸ For $O(N)$ we must also remove the traces on all pairs of symmetric indices. For example, a generic tensor with three indices k, l, m is decomposed into irreducible representations of $O(N)$ as follows. First of all, we remove from the tensor all the traces. Let us call T^{klm} the resulting traceless tensor, so that $T^{kmm} = T^{mlm} = T^{kkm} = 0$ (repeated indices are summed over). Then the decomposition of T^{klm} is shown in Fig. 3.9. The Young diagram (a) represents the tensor obtained symmetrizing T^{klm} over all indices; the diagram (b) represents the tensor obtained antisymmetrizing first over (k, m) , which gives $T^{klm} - T^{mlk}$, and then symmetrizing over the pair (k, l) . This gives

$$\text{diagram (b)} : \quad T^{klm} + T^{lkm} - T^{mlk} - T^{mkl}. \quad (3.352)$$

The tensor corresponding to the diagram (c) is obtained similarly, antisymmetrizing first over (k, l) and then symmetrizing over (k, m) , and gives

$$\text{diagram (c)} : \quad T^{klm} + T^{mlk} - T^{lkm} - T^{lmk}. \quad (3.353)$$

Finally, the Young diagram (d) represents the tensor obtained antisymmetrizing T^{klm} over all indices.⁵⁹ Counting the independent components we see that a traceless, but otherwise generic, tensor with three indices k, l, m , each taking the values $1, 2, 3$, has 18 components, and that the diagram (a) represents a tensor with seven components, (b) and (c) with five components each, and (d) has one component, so we get $18 = 7 + 5 + 5 + 1$. Recall that the representations of the rotation group can also be labeled by the spin s , and the representation labeled by s has dimension $2s + 1$. Then, the representation with dimension seven, i.e. the diagram (a), corresponds to $s = 3$, while the representations with dimension five corresponds to $s = 2$. Denoting by \mathbf{s} the representation with spin s , and by \oplus the direct sum of representations, the decomposition of Fig. 3.9 reads

$$T^{klm} \in \mathbf{3} \oplus \mathbf{2} \oplus \mathbf{2} \oplus \mathbf{0}. \quad (3.354)$$

We can now understand the decomposition given in eq. (3.139), in terms of Fig. 3.9. Our starting point is the tensor $\dot{S}^{kl,m}$. This is symmetric in (k, l) , and has no special symmetry with respect to the other indices. Therefore, it is not an irreducible representation of $SO(N)$.

First of all observe that, in eq. (3.138), we can replace $\dot{S}^{kl,m}$ by the tensor in which all the traces have been removed. In fact, subtracting from $\dot{S}^{kl,m}$ a term

⁵⁸It is more common to first symmetrize over the lines and then antisymmetrize over the columns (see, e.g. Hamermesh (1962), Section 10.6). The two procedures are however equivalent and for our purposes the former is more convenient.

⁵⁹If, rather than $O(N)$, we consider $SO(N)$, we must also take into account that there is a globally defined antisymmetric tensor $\epsilon^{i_1 \dots i_N}$. In this case the representations obtained one from the other contracting antisymmetric indices with the ϵ tensor are equivalent. In particular, for $SO(3)$ we have the tensor ϵ^{ijk} . So, for instance, an antisymmetric tensor with two indices A^{kl} is equivalent to a vector $A_i = \epsilon_{ikl} A^{kl}$ while a totally antisymmetric tensor A^{ijk} is equivalent to a scalar A through the relation $A = \epsilon_{ijk} A^{ijk}$. Since the indices take the values $i = 1, \dots, N$, we cannot antisymmetrize over more than N indices, and there are no diagrams with more than N lines, for $O(N)$. For $SO(N)$ a column with N box is equivalent to a scalar, as we see contracting with the totally antisymmetric tensor, and can be eliminated. Therefore a Young diagram of $SO(N)$ can always be reduced to an equivalent diagram with no more than $N - 1$ rows.

$$\begin{aligned}
T^{klm} &= (\boxed{k} \times \boxed{l}) \times \boxed{m} = (\boxed{k} \boxed{l} + \boxed{\begin{matrix} k \\ l \end{matrix}}) \times \boxed{m} = \\
&= \boxed{\begin{matrix} k & l & m \end{matrix}} + \boxed{\begin{matrix} k & l \\ m \end{matrix}} + \boxed{\begin{matrix} k & m \\ l \end{matrix}} + \boxed{\begin{matrix} k \\ l \\ m \end{matrix}}
\end{aligned}$$

(a) (b) (c) (d)

Fig. 3.9 The Young diagrams corresponding to irreducible tensor representations with three indices k, l, m .

proportional to δ_{kl} we get in eq. (3.138) a factor proportional to $\Lambda_{ij,klnm}\delta_{kl}$, which vanishes because $\Lambda_{ij,kk} = 0$, while subtracting from $\dot{S}^{kl,m}$ a term proportional to δ_{km} or to δ_{lm} we get a factor proportional to $\Lambda_{ij,klnl} = 0$. We can therefore consider $\dot{S}^{kl,m}$ as a tensor from which all traces have already been removed (this is analogous to the fact that, in the quadrupole term, we could substitute M^{ij} with Q^{ij}).

Figure 3.9 gives the decomposition in irreducible representations of a generic traceless tensor T^{klm} . However, $\dot{S}^{kl,m}$ is not generic, but is symmetric in (k, l) (and of course remains symmetric also after we remove all its traces). Then, when we decompose $\dot{S}^{kl,m}$ in irreducible representations as in Fig. 3.9, the diagrams (c) and (d) do not contribute, since the are obtained antisymmetrizing first over (k, l) which, applied to $\dot{S}^{kl,m}$, gives zero. Therefore, in the decomposition of $\dot{S}^{kl,m}$, only two irreducible representations appear:

- diagram (a), which is the totally symmetric and traceless combination, and therefore has the symmetries of the mass octupole;
- diagrams (b), which has the structure given in eq. (3.352). For a tensor T^{klm} symmetric in (k, l) , the structure of indices given in eq. (3.352) simplifies to

$$2T^{klm} - T^{mlk} - T^{mkl}. \quad (3.355)$$

Identifying T^{klm} with $\ddot{P}^{m,kl}$, (which is indeed symmetric in (k, l)), we see that this is precisely the structure of indices of the current quadrupole term in eq. (3.139).

We therefore understand that the algebraic identity (3.139) expresses the decomposition of $\dot{S}^{kl,m}$ in irreducible representations of $SO(3)$. The mass octupole corresponds to the Young diagram (a) in Fig. 3.9, and is a spin-3 representation, while the current quadrupole corresponds to the Young diagram (b) in Fig. 3.9, and is a spin-2 representation. The representations corresponding to the Young diagrams (c) and (d) instead do not appear, because $\dot{S}^{kl,m}$ is symmetric in (k, l) .

The fact that $\ddot{P}^{k,lm} + \ddot{P}^{l,km} - 2\ddot{P}^{m,kl}$ is a spin-2 tensor is the origin of its name “current quadrupole”: the term “quadrupole” refers to the spin-2 nature of the operator, and the term “current” refers to the fact that it is obtained from the momenta of the momentum P^i .



Problem 3.5. Computation of $\int d\Omega (\mathbf{T}_{lm}^{E2,B2})_{ij}^* n_{i_1} \cdots n_{i_\alpha}$

In Section 3.5 we have seen that the coefficients of the multipole expansion, u_{lm} and v_{lm} , are given in terms of integrals over the solid angle of the quantity $(\mathbf{T}_{lm}^{E2})_{ij}^* n_{i_1} \cdots n_{i_\alpha}$, for u_{lm} , and $(\mathbf{T}_{lm}^{B2})_{ij}^* n_{i_1} \cdots n_{i_\alpha}$, for v_{lm} , see eqs. (3.283) and (3.284). In this problem we compute explicitly these integrals. As a first step, we consider

$$\int d\Omega Y_{lm}^* n_{i_1} \cdots n_{i_\alpha}, \quad (3.356)$$

with l, α arbitrary integers. Using eq. (3.234), we can write it as

$$(\mathcal{Y}_{j_1 \dots j_l}^{lm})^* \int d\Omega n_{j_1} \cdots n_{j_l} n_{i_1} \cdots n_{i_\alpha}. \quad (3.357)$$

We can now perform this integral using eq. (3.23). If $\alpha < l$, in the product of Kronecker delta of eq. (3.23) there are not enough indices of the type i_1, \dots, i_α to be contracted with the indices of the type j_1, \dots, j_l , and therefore necessarily we have at least one Kronecker delta involving two indices of the group j_1, \dots, j_l , e.g. terms containing $\delta_{j_1 j_2}$. Then, since $\mathcal{Y}_{j_1 \dots j_l}^{lm}$ is traceless, the result is zero. Therefore the integral in eq. (3.356) can be non-vanishing only if $\alpha \geq l$. If $\alpha = l$, we found below eq. (3.237) that

$$\int d\Omega Y_{lm}^* n_{i_1} \cdots n_{i_l} = 4\pi \frac{l!}{(2l+1)!!} (\mathcal{Y}_{i_1 \dots i_l}^{lm})^*. \quad (3.358)$$

Now, observe that u_{lm} is expressed as a sum over α of terms containing the α -th time derivatives of $S^{ij,i_1 \dots i_\alpha}$, see eq. (3.283). In order of magnitude, if d is the size of the source,

$$\begin{aligned} \partial_0^{\alpha+1} S^{ij,i_1 \dots i_\alpha i_{\alpha+1}} &\sim \frac{\omega_s d}{c} \partial_0^\alpha S^{ij,i_1 \dots i_\alpha}, \\ &= \frac{v}{c} \partial_0^\alpha S^{ij,i_1 \dots i_\alpha}, \end{aligned} \quad (3.359)$$

since $\partial_0 = (1/c)\partial/\partial t$ and each time derivative brings down a factor ω_s , where ω_s is the typical frequency of the source, while the addition of the index $i_{\alpha+1}$ corresponds to the insertion of a factor $x^{i_{\alpha+1}}$ inside the integral in d^3x over the source volume, which therefore gives a contribution $O(d)$. Therefore, in the limit $v/c \ll 1$ in which the multipole expansion is useful, the dominant term in eqs. (3.283) and (3.284) is the one with the smallest value of α for which the integral is non-vanishing. Recall from eqs. (3.265) and (3.267) that

$$\mathbf{T}_{lm}^{E2} = a_{31} \mathbf{T}_{lm}^{l+2} + a_{32} \mathbf{T}_{lm}^l + a_{33} \mathbf{T}_{lm}^{l-2}, \quad (3.360)$$

$$\mathbf{T}_{lm}^{B2} = b_{21} i \mathbf{T}_{lm}^{l+1} + b_{22} i \mathbf{T}_{lm}^{l-1}, \quad (3.361)$$

where the coefficients are given in Table 3.1. Since \mathbf{T}_{jjz}^l is proportional to Y_{ljz} , see eq. (3.262), the integral $\int d\Omega (\mathbf{T}_{lm}^{l-2})_{ij}^* n_{i_1} \cdots n_{i_\alpha}$ is proportional to $\int d\Omega Y_{l-2,m}^* n_{i_1} \cdots n_{i_\alpha}$ and therefore the lowest value of α for which it is non-vanishing is $\alpha = l-2$, while for the integral of \mathbf{T}_{lm}^l we need at least $\alpha = l$ and for the integral of \mathbf{T}_{lm}^{l+2} we need at least $\alpha = l+2$. We conclude that in eq. (3.283) the smallest possible value of α which gives a non-vanishing contribution is obtained from \mathbf{T}_{lm}^{l-2} and is $\alpha_{\min} = l-2$. Similarly, for v_{lm} the leading contribution is obtained from \mathbf{T}_{lm}^{l-1} and is $\alpha_{\min} = l-1$. Therefore

$$u_{lm} \simeq a_{33} \frac{4}{(l-2)!} \left(\partial_0^{l-2} S^{ij,i_1 \dots i_{l-2}} \right) \int d\Omega (\mathbf{T}_{lm}^{l-2})_{ij}^* n_{i_1} \cdots n_{i_{l-2}}, \quad (3.362)$$

$$v_{lm} \simeq -ib_{22} \frac{4}{(l-1)!} \left(\partial_0^{l-1} S^{ij,i_1 \dots i_{l-1}} \right) \int d\Omega (\mathbf{T}_{lm}^{l-1})_{ij}^* n_{i_1} \cdots n_{i_{l-1}},$$

times a factor $[1 + O(v^2/c^2)]$. Now we use the identities

$$(\mathbf{T}_{lm}^{l-2})_{ij} = \left[\frac{l(l-1)}{(2l-1)(2l+1)} \right]^{1/2} \mathcal{Y}_{ij i_1 \dots i_{l-2}}^{lm} n_{i_1} \dots n_{i_{l-2}}, \quad (3.363)$$

$$(\mathbf{T}_{lm}^{l-1})_{ij} = i \left[\frac{2l(l-1)}{(l+1)(2l+1)} \right]^{1/2} \epsilon_{pq(i} \mathcal{Y}_{j)q i_1 \dots i_{l-2}}^{lm} n_p n_{i_1} \dots n_{i_{l-2}}, \quad (3.364)$$

where the parentheses on the indices, in eq. (3.364), denotes the symmetrization over the indices i, j , i.e. $A_{(ij)} \equiv (1/2)(A_{ij} + A_{ji})$. These identities can be obtained (with quite some work) inserting eq. (3.234) into the definition of the spin-2 tensor harmonics. Inserting the explicit values of a_{33}, b_{22} from Table 3.1 (and recalling the change of notation $j \rightarrow l$ that we made in between, see Note 47), we get

$$\begin{aligned} u_{lm} &= \left[\frac{(l+1)(l+2)}{2(2l-1)(2l+1)} \right]^{1/2} \frac{4}{(l-2)!} \left[\frac{l(l-1)}{(2l-1)(2l+1)} \right]^{1/2} \\ &\quad \times \left(\partial_0^{l-2} S^{ij, i_1 \dots i_{l-2}} \right) \mathcal{Y}_{ij j_1 \dots j_{l-2}}^{lm*} \int d\Omega n_{i_1} \dots n_{i_{l-2}} n_{j_1} \dots n_{j_{l-2}} \\ &= \left[\frac{1}{2} l(l-1)(l+1)(l+2) \right]^{1/2} \frac{4}{(l-2)!} \frac{1}{(2l-1)(2l+1)} \\ &\quad \times \frac{4\pi}{(2l-3)!!} (l-2)! \left(\partial_0^{l-2} S^{ij, i_1 \dots i_{l-2}} \right) \mathcal{Y}_{ij i_1 \dots i_{l-2}}^{lm*} \\ &= \frac{16\pi}{(2l+1)!!} \left[\frac{1}{2} l(l-1)(l+1)(l+2) \right]^{1/2} \left(\partial_0^{l-2} S^{ij, i_1 \dots i_{l-2}} \right) \mathcal{Y}_{ij i_1 \dots i_{l-2}}^{lm*}. \end{aligned} \quad (3.365)$$

where the final integral as been performed using eq. (3.23). The integral for v_{lm} is performed similarly using eqs. (3.363) and (3.364), with the final result given in the text.

Further reading

- The quadrupole radiation is discussed in all general relativity textbooks, see in particular Weinberg (1972), Misner, Thorne and Wheeler (1973), Landau and Lifshitz, Vol. II (1979) and Straumann (2004).
- The radiation from sources with arbitrary velocity is discussed in Weinberg (1972), Section 10.4. Gravitational wave generation is also discussed in detail in the reviews Thorne (1983) and (1987).
- Radiation reaction for slow-motion sources is discussed in Misner, Thorne and Wheeler (1973), Sections 36.8 and 36.11.
- The multipole expansion for time-dependent fields in terms of STF tensors was introduced by Sachs (1961) and Pirani (1964). Thorne (1980) derived the slow-motion expansion of the mass and spin multipole moments, both in STF and in spherical tensor form. The closed-form expression for these moments in STF form is derived in Damour and Iyer (1991a). A detailed review of the multipole expansion for GWs, as well as a historical overview of the relevant literature, is Thorne (1980). A physical discussion of current quadrupole radiation is given in Schutz and Ricci (2001).

Applications

4

In this chapter we apply the formalism that we have developed to various instructive problems. The systems that we examine here are still somewhat idealized, compared to real astrophysical sources. This allows us to understand the essence of the physical mechanisms with a minimum of complications, and forms the basis for a more detailed study of realistic sources, which will be the subject of Vol. 2.

We begin, in Section 4.1, with the study of binary systems, taking the bodies as point-like and moving at first on a Newtonian trajectory. We will compute how the back-reaction of GWs affects the motion of the sources, inducing the inspiral and coalescence of the binary system, and we will see how this, in turn, affects the emission of the GWs themselves.

In Section 4.2 we will compute the radiation emitted by spinning rigid bodies, which are a first idealization of rotating neutron stars.

In Section 4.3 we compute the radiation emitted by a body falling radially into a black hole. A full resolution of this problem requires expansion over the Schwarzschild metric, rather than over flat space-time of linearized theory, and will be deferred to Vol. 2. However, we will see that the low-frequency part of the spectrum can be computed using a flat space-time background, so we can perform here this part of the computation. We will also compare the situation in which the infalling particle is point-like with that of a real star, which can be disrupted by the tidal gravitational force of the black hole. This is particularly instructive because it allows us to compare the coherent and the incoherent emission of GWs.

In Section 4.4 we study the radiation emitted by a mass accelerated by an external force. It will be interesting to compare the results with the electromagnetic radiation from an accelerated charge. We will see that, while the electromagnetic field of a relativistic charge is beamed into a small angle in the forward direction, this does not happen in the gravitational case. Finally, some computational details are collected in a Solved Problems section, at the end of the chapter.

4.1 Inspiral of compact binaries

In this section we consider a binary system made of two compact stars, such as neutron stars or black holes, and we treat them as point-like, with masses m_1, m_2 , and positions \mathbf{r}_1 and \mathbf{r}_2 . In the Newtonian approximation, and in the center-of-mass frame (CM), the dynamics reduces to a one-body problem with mass equal to the reduced mass

4.1	Inspiral of compact binaries	167
4.2	Radiation from rotating rigid bodies	200
4.3	Infall into a black hole	215
4.4	Radiation from accelerated masses	224
4.5	Solved problems	230

$\mu = m_1 m_2 / (m_1 + m_2)$, and equation of motion $\ddot{\mathbf{r}} = -(Gm/r^3)\mathbf{r}$, where $m = m_1 + m_2$ is the total mass and $\mathbf{r} = \mathbf{r}_2 - \mathbf{r}_1$ the relative coordinate. We consider first the case of circular orbits. Then the orbital frequency ω_s is related to the orbital radius R by $v^2/R = Gm/R^2$ with $v = \omega_s R$, so we have Kepler's law

$$\omega_s^2 = \frac{Gm}{R^3}. \quad (4.1)$$

We already studied this system in Problem 3.2, and the corresponding gravitational wave amplitudes are given in eqs. (3.330) and (3.331). In these expressions, we eliminate R in favor of ω_s using eq. (4.1), and we introduce the *chirp mass*

$$M_c = \mu^{3/5} m^{2/5} = \frac{(m_1 m_2)^{3/5}}{(m_1 + m_2)^{1/5}}.$$

(4.2)

Then eqs. (3.330) and (3.331) become

$$\begin{aligned} h_+(t) &= \frac{4}{r} \left(\frac{GM_c}{c^2} \right)^{5/3} \left(\frac{\pi f_{\text{gw}}}{c} \right)^{2/3} \frac{1 + \cos^2 \theta}{2} \cos(2\pi f_{\text{gw}} t_{\text{ret}} + 2\phi), \\ h_\times(t) &= \frac{4}{r} \left(\frac{GM_c}{c^2} \right)^{5/3} \left(\frac{\pi f_{\text{gw}}}{c} \right)^{2/3} \cos \theta \sin(2\pi f_{\text{gw}} t_{\text{ret}} + 2\phi), \end{aligned}$$

(4.3)

where we expressed the result in terms of $f_{\text{gw}} = \omega_{\text{gw}}/(2\pi)$, with $\omega_{\text{gw}} = 2\omega_s$. Observe that, in this lowest-order Newtonian approximation, the amplitudes h_+ and h_\times of the GWs emitted depend on the masses m_1, m_2 only through the combination M_c .

The factors in eq. (4.3) are possibly more expressive if we write them in terms of ratios of quantities with dimension of length, introducing the Schwarzschild radius associated to the chirp mass,

$$R_c \equiv \frac{2GM_c}{c^2}, \quad (4.4)$$

and using the reduced wavelength of the GW, $\lambda = c/\omega_{\text{gw}}$. Then, eq. (4.3) reads

$$h_+(t) = \mathcal{A} \frac{1 + \cos^2 \theta}{2} \cos(\omega_{\text{gw}} t_{\text{ret}} + 2\phi), \quad (4.5)$$

$$h_\times(t) = \mathcal{A} \cos \theta \sin(\omega_{\text{gw}} t_{\text{ret}} + 2\phi), \quad (4.6)$$

where

$$\mathcal{A} = \frac{1}{2^{1/3}} \left(\frac{R_c}{r} \right) \left(\frac{R_c}{\lambda} \right)^{2/3}. \quad (4.7)$$

From eq. (3.337) we can write the power radiated in GWs, per unit solid angle, as

$$\frac{dP}{d\Omega} = \frac{2}{\pi} \frac{c^5}{G} \left(\frac{GM_c \omega_{\text{gw}}}{2c^3} \right)^{10/3} g(\theta), \quad (4.8)$$

where

$$g(\theta) = \left(\frac{1 + \cos^2 \theta}{2} \right)^2 + \cos^2 \theta. \quad (4.9)$$

Observe that $\langle \cos^2(2\omega t + 2\phi) \rangle = 1/2$ is independent of ϕ , so the angular distribution of the radiated power, which is proportional to $\langle \dot{h}_+^2 + \dot{h}_\times^2 \rangle$, is also independent of ϕ . The angular average of $g(\theta)$ is

$$\int \frac{d\Omega}{4\pi} g(\theta) = \frac{4}{5}, \quad (4.10)$$

where, as usual, $d\Omega = d\cos \theta d\phi$. The total radiated power P is therefore¹

$$P = \frac{32}{5} \frac{c^5}{G} \left(\frac{GM_c \omega_{\text{gw}}}{2c^3} \right)^{10/3}. \quad (4.12)$$

4.1.1 Circular orbits. The chirp amplitude

Equation (4.3) gives the amplitude of the GWs, assuming that the motion of the sources is on a given, fixed, circular Keplerian orbit. However, the emission of GWs costs energy. The source for the radiated energy is the sum of kinetic plus potential energy of the orbit, which is

$$\begin{aligned} E_{\text{orbit}} &= E_{\text{kin}} + E_{\text{pot}} \\ &= -\frac{Gm_1 m_2}{2R}, \end{aligned} \quad (4.13)$$

and therefore, to compensate for the loss of energy to GWs, R must decrease in time, so that E_{orbit} becomes more and more negative.²

According to eq. (4.1), if R decreases, ω_s increases. On the other hand, if ω_s increases, also the power radiated in GWs increases, as we see from eq. (4.12). Then R must decrease further, and we have a runaway process which, on a sufficiently long time-scale, leads to the coalescence of the binary system. As long as

$$\dot{\omega}_s \ll \omega_s^2, \quad (4.14)$$

we are in the regime called of quasi-circular motion. In fact, using eq. (4.1) we see that the radial velocity \dot{R} can be written as

$$\begin{aligned} \dot{R} &= -\frac{2}{3} R \frac{\dot{\omega}_s}{\omega_s} \\ &= -\frac{2}{3} (\omega_s R) \frac{\dot{\omega}_s}{\omega_s^2}. \end{aligned} \quad (4.15)$$

Then, as long as the condition $\dot{\omega}_s \ll \omega_s^2$ is fulfilled, $|\dot{R}|$ is much smaller than the tangential velocity $\omega_s R$, and the approximation of a circular orbit with a slowly varying radius is applicable. In the following, we compute the back-reaction of GWs when eq. (4.14) applies.

Using eq. (4.1), we eliminate R in favor of ω_{gw} in eq. (4.13), and we get

$$E_{\text{orbit}} = -(G^2 M_c^5 \omega_{\text{gw}}^2 / 32)^{1/3}. \quad (4.16)$$

¹In Section 5.6, where we apply the post-Newtonian formalism to inspiraling binaries, we will see that, rather than using the source frequency ω_s , it is convenient to use the variable $x = (Gm\omega_s/c^3)^{2/3}$, which is dimensionless and of order v^2/c^2 , where v is the typical orbital velocity. We also introduce the “symmetric mass ratio” $\nu = \mu/m$, so $M_c = \nu^{3/5}m$. Since here we are computing in the quadrupole approximation and we are considering a circular orbit, we have $\omega_{\text{gw}} = 2\omega_s$, and the result (4.12) can be written as

$$P = \frac{32}{5} \frac{c^5}{G} \nu^2 x^5. \quad (4.11)$$

The corrections to this result in the post-Newtonian expansion are given in eq. (5.257).

²In our idealized setting of point-like particles, the two masses have no internal structure, so no degrees of freedom that can relax supplying, at least partially, the required energy, and the only possible source of energy is the orbital energy of the system. Even in a realistic system of two stars, however, at least in the early phase of the coalescence, the orbital frequency is much smaller than the frequencies of the normal modes of the star, and therefore the internal dynamics of the stars is decoupled from the orbital motion, and all the energy supplied to GWs again comes from the orbital energy of the system. We will see in Section 5.5 that, for compact objects, corrections that depend on the internal structure of the bodies enter only at the very high order 5PN in the post-Newtonian expansion, i.e. they are corrections of order $(v/c)^{10}$ to the equations of motion.

Observe that, at fixed ω_{gw} , the dependence on the masses is again only through the chirp mass. Equating P in eq. (4.12) to $-dE_{\text{orbit}}/dt$ we find

$$\dot{\omega}_{\text{gw}} = \frac{12}{5} 2^{1/3} \left(\frac{GM_c}{c^3} \right)^{5/3} \omega_{\text{gw}}^{11/3}, \quad (4.17)$$

or, in terms of $f_{\text{gw}} = \omega_{\text{gw}}/(2\pi)$,

$$\dot{f}_{\text{gw}} = \frac{96}{5} \pi^{8/3} \left(\frac{GM_c}{c^3} \right)^{5/3} f_{\text{gw}}^{11/3}. \quad (4.18)$$

Integrating eq. (4.18) we see that f_{gw} formally diverges at a finite value of time, that we denote t_{coal} . In terms of $\tau \equiv t_{\text{coal}} - t$ (the time to coalescence), the solution of eq. (4.18) reads³

$$f_{\text{gw}}(\tau) = \frac{1}{\pi} \left(\frac{5}{256} \frac{1}{\tau} \right)^{3/8} \left(\frac{GM_c}{c^3} \right)^{-5/8}. \quad (4.19)$$

The divergence is cut off by the fact that, when their separation becomes smaller than a critical distance, the two stars merge, as we discuss in more detail below, see eq. (4.38). Inserting in eq. (4.19) the numerical values we find

$$f_{\text{gw}}(\tau) \simeq 134 \text{ Hz} \left(\frac{1.21M_\odot}{M_c} \right)^{5/8} \left(\frac{1 \text{ s}}{\tau} \right)^{3/8}, \quad (4.20)$$

where, as reference value for M_c , we have taken $1.21M_\odot$, which is the chirp mass of a system of two stars, each one with a mass of $1.4M_\odot$. Equivalently, we can write eq. (4.20) as

$$\tau \simeq 2.18 \text{ s} \left(\frac{1.21M_\odot}{M_c} \right)^{5/3} \left(\frac{100 \text{ Hz}}{f_{\text{gw}}} \right)^{8/3}. \quad (4.21)$$

From this we find that (when $M_c = 1.21M_\odot$) at 10 Hz (which is of the order of the lowest frequencies accessible to ground-based interferometers) we get the radiation emitted at about $\tau = 17$ min to coalescence; at 100 Hz we get the radiation from the last two seconds, and at 1 kHz we get the radiation from the last few milliseconds. From Kepler's law (4.1) we find that, when $f_{\text{gw}} = 1$ kHz, the separation between two bodies with $m_1 = m_2 = 1.4M_\odot$ is $R \simeq 33$ km. Such a small separation can be reached only by very compact bodies like neutron stars and black holes. Since the radius of a neutron star with $m = 1.4M_\odot$ is about 10 km, for neutron stars and black holes the point-like approximation at this stage becomes inaccurate, but still not meaningless.

A useful quantity for assessing the sensitivity of detectors to inspiraling binaries is the number of cycles spent in the detector bandwidth $f \in [f_{\min}, f_{\max}]$. When the period $T(t)$ of the GW is a slowly varying function of time, the number of cycles in a time interval dt is given by

$d\mathcal{N}_{\text{cyc}} = dt/T(t) = f_{\text{gw}}(t)dt$, so

$$\begin{aligned}\mathcal{N}_{\text{cyc}} &= \int_{t_{\min}}^{t_{\max}} f_{\text{gw}}(t)dt \\ &= \int_{f_{\min}}^{f_{\max}} df_{\text{gw}} \frac{f_{\text{gw}}}{\dot{f}_{\text{gw}}}.\end{aligned}\quad (4.22)$$

For the inspiral of a binary system we can express \dot{f}_{gw} as a function of f_{gw} using eq. (4.18), and we get

$$\begin{aligned}\mathcal{N}_{\text{cyc}} &= \frac{1}{32\pi^{8/3}} \left(\frac{GM_c}{c^3}\right)^{-5/3} \left(f_{\min}^{-5/3} - f_{\max}^{-5/3}\right) \\ &\simeq 1.6 \times 10^4 \left(\frac{10 \text{ Hz}}{f_{\min}}\right)^{5/3} \left(\frac{1.2M_{\odot}}{M_c}\right)^{5/3},\end{aligned}\quad (4.23)$$

where in the second line we assumed $f_{\min}^{-5/3} - f_{\max}^{-5/3} \simeq f_{\min}^{-5/3}$, as is typically the case. This means that ground-based interferometers can follow the evolution of the signal for thousands of cycles, and a space-borne interferometer sensitive to the mHz region can follow it for millions of cycles.⁴ For this reason, accurate predictions of the waveform, going well beyond the Newtonian approximation used here, are very important, and will be discussed in Section 5.6.

As the frequency increases, the orbital radius shrinks. From eqs. (4.1) and (4.19) (recalling that $\tau = t_{\text{coal}} - t$, so that $d/d\tau = -d/dt$, and using a dot denotes d/dt),

$$\begin{aligned}\frac{\dot{R}}{R} &= -\frac{2}{3} \frac{\dot{\omega}_{\text{gw}}}{\omega_{\text{gw}}} \\ &= -\frac{1}{4\tau},\end{aligned}\quad (4.24)$$

which integrates to

$$\begin{aligned}R(\tau) &= R_0 \left(\frac{\tau}{\tau_0}\right)^{1/4} \\ &= R_0 \left(\frac{t_{\text{coal}} - t}{t_{\text{coal}} - t_0}\right)^{1/4}\end{aligned}\quad (4.25)$$

where R_0 is the value of R at the initial time t_0 , and $\tau_0 = t_{\text{coal}} - t_0$. The function $R(t)$ is shown in Fig. 4.1. We see that there is a long phase where R decreases smoothly, followed by a plunge phase, where our approximation of quasi-circular orbit is no longer valid.⁵

Inserting eq. (4.19), evaluated at an initial time t_0 when $\tau = \tau_0$, into eq. (4.1), we find the relation between the initial radius R_0 and the time to coalescence τ_0 ,

$$\tau_0 = \frac{5}{256} \frac{c^5 R_0^4}{G^3 m^2 \mu}. \quad (4.26)$$

⁴More precisely, a space interferometer such as LISA has $f_{\min} \sim 10^{-4}$ Hz, and signals in this frequency band are produced by the inspiral into supermassive BHs with a mass $O(10^6)M_{\odot}$. In a coalescence of two supermassive BHs with $m_1 = m_2 = 10^6 M_{\odot}$, we have $M_c \simeq 0.9 \times 10^6 M_{\odot}$ and \mathcal{N}_c is only of order 600. However, in the infall of a stellar mass black hole into a supermassive black hole, taking $m_1 = 10^6 M_{\odot}$ and $m_2 = 10 M_{\odot}$, we have $M_c \simeq 10^3 M_{\odot}$ and $\mathcal{N}_c \simeq 5 \times 10^7$.

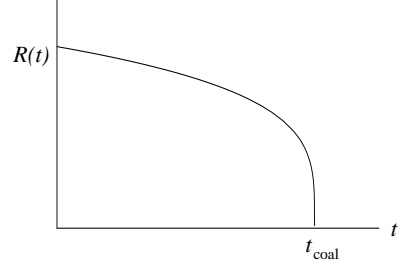


Fig. 4.1 The evolution of the separation $R(t)$ between the two bodies, in the lowest-order Newtonian approximation.

⁵Furthermore, in compact binaries made of black holes or neutron stars, the flat-space approximation is totally inadequate in the plunge phase, see the discussion around eq. (4.38) below. We will discuss the plunge phase for systems with BH or NS in Vol. 2.

Expressing the initial radius R_0 in terms of the initial orbital period $T_0 = 2\pi/\omega_s(\tau_0)$ through Kepler's law, $R_0^2 = Gm(T_0/2\pi)^2$, and plugging in the numerical values, we find

$$\tau_0 \simeq 9.829 \times 10^6 \text{ yr} \left(\frac{T_0}{1 \text{ hr}} \right)^{8/3} \left(\frac{M_\odot}{m} \right)^{2/3} \left(\frac{M_\odot}{\mu} \right). \quad (4.27)$$

Therefore, under our assumption of circular orbits and for masses of order M_\odot , only binaries which at formation had an initial orbital period of less than about one day can have coalesced by emission of GWs, within the present age of galaxies. We will discuss in Section 4.1.2 how this result is modified for elliptic orbits.

Until now we have studied how the GW frequency evolves in time, in a binary system. We next examine how the corresponding waveform of the GW changes. A particle that moves on a quasi-circular orbit in the (x, y) plane with a radius $R = R(t)$ and an angular velocity $\omega_s = \omega_s(t)$ has Cartesian coordinates $x(t) = R(t) \cos(\Phi(t)/2)$ and $y(t) = R(t) \sin(\Phi(t)/2)$, where we have defined

$$\begin{aligned} \Phi(t) &= 2 \int_{t_0}^t dt' \omega_s(t') \\ &= \int_{t_0}^t dt' \omega_{\text{gw}}(t'). \end{aligned} \quad (4.28)$$

When we compute the GW production in the quadrupole approximation, in the computation of the second time derivative of the quadrupole moment there are therefore three differences, compared to the case when ω_s and R constants, i.e. to the computation which gives eq. (4.3):

- in the argument of the trigonometric functions, $\omega_{\text{gw}} t$ must be replaced by $\Phi(t)$;
- in the factors in front of the trigonometric functions, ω_{gw} is replaced by $\omega_{\text{gw}}(t)$;
- we should also include in the computation the contributions coming from the derivatives of $R(t)$ and of $\omega_{\text{gw}}(t)$.

However, as we have seen above, the radial velocity \dot{R} is negligible as long as $\dot{\omega}_s \ll \omega_s^2$. Using eq. (4.17), the condition $\dot{\omega}_s \ll \omega_s^2$ translates into $GM_c\omega_s/c^3 \ll 0.5$. In terms of $f_{\text{gw}} = \omega_{\text{gw}}/(2\pi)$, this means that \dot{R} is negligible as long as $f_{\text{gw}} \ll 13 \text{ kHz} (1.2M_\odot/M_c)$. As we will see in eq. (4.40) below, the transition to the plunge phase takes place earlier, thus as long as we assume that we are in the inspiral phase we can simply neglect the terms proportional to \dot{R} in the computation of the waveform, at least to lowest order, and similarly for the terms involving the derivative of $\omega_{\text{gw}}(t)$. The only changes, therefore, are the replacement of $\omega_{\text{gw}} t$ by $\Phi(t)$ in the argument of the sine and cosine, and of ω_s by $\omega_s(t)$ in the prefactor, all evaluated at the retarded time t_{ret} .⁶ Then,

⁶As discussed in Problem 3.2, we are interested in the radiation that a binary star emits in the direction which points from the star toward us. The angle θ is therefore equal to the angle ι between the normal to the orbit and the line-of-sight, while we can orient the axes so that $\phi = 0$ or, equivalently, we can reabsorb the fixed value of ϕ into a shift of the origin of time.

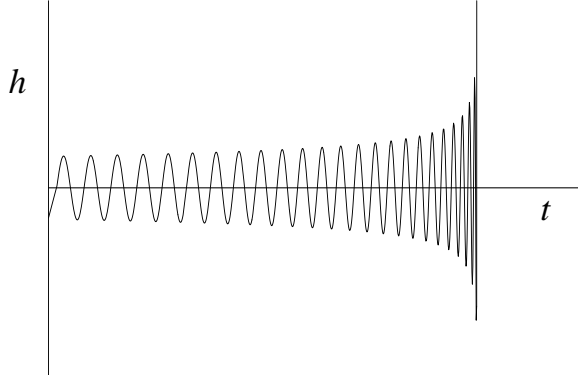


Fig. 4.2 The time evolution of the GW amplitude in the inspiral phase of a binary system.

$$\begin{aligned} h_+(t) &= \frac{4}{r} \left(\frac{GM_c}{c^2} \right)^{5/3} \left(\frac{\pi f_{\text{gw}}(t_{\text{ret}})}{c} \right)^{2/3} \left(\frac{1 + \cos^2 \iota}{2} \right) \cos[\Phi(t_{\text{ret}})], \\ h_\times(t) &= \frac{4}{r} \left(\frac{GM_c}{c^2} \right)^{5/3} \left(\frac{\pi f_{\text{gw}}(t_{\text{ret}})}{c} \right)^{2/3} \cos \iota \sin[\Phi(t_{\text{ret}})]. \end{aligned} \quad (4.29)$$

Using the explicit expression (4.19) we find (recall that $d\tau = -dt$)

$$\Phi(\tau) = -2 \left(\frac{5GM_c}{c^3} \right)^{-5/8} \tau^{5/8} + \Phi_0, \quad (4.30)$$

where $\Phi_0 = \Phi(\tau = 0)$ is an integration constant, equal to the value of Φ at coalescence. Then the GW amplitude can be expressed directly in terms of the time to coalescence τ measured by the observer,

$$h_+(\tau) = \frac{1}{r} \left(\frac{GM_c}{c^2} \right)^{5/4} \left(\frac{5}{c\tau} \right)^{1/4} \left(\frac{1 + \cos^2 \iota}{2} \right) \cos[\Phi(\tau)], \quad (4.31)$$

$$h_\times(\tau) = \frac{1}{r} \left(\frac{GM_c}{c^2} \right)^{5/4} \left(\frac{5}{c\tau} \right)^{1/4} \cos \iota \sin[\Phi(\tau)], \quad (4.32)$$

where

$$\tau = t_{\text{coal}} - t, \quad (4.33)$$

t is the observer time (rather than retarded time) and t_{coal} is the value of t when the coalescence takes place (compare with Note 3). We see from the above equations that both the frequency and the amplitude increase as the coalescence is approached; this behavior is referred to as “chirping” (for its similarity with the chirp emitted by a bird). The functional dependence of h_+ (or of h_\times) on t is shown in Fig. 4.2.

As we will see in detail in Chapter 7, to compare the theoretical waveforms with the experimental sensitivities it is necessary to have the Fourier transform of the GW amplitudes. To compute the Fourier transform of the chirp signal is not completely straightforward, since $h_{+,\times}(t)$

are defined only on the interval $-\infty < t < t_{\text{coal}}$, and we compute their Fourier transform explicitly in Problem 4.1. The result is

$$\tilde{h}_+(f) = A e^{i\Psi_+(f)} \frac{c}{r} \left(\frac{GM_c}{c^3} \right)^{5/6} \frac{1}{f^{7/6}} \left(\frac{1 + \cos^2 \iota}{2} \right), \quad (4.34)$$

$$\tilde{h}_\times(f) = A e^{i\Psi_\times(f)} \frac{c}{r} \left(\frac{GM_c}{c^3} \right)^{5/6} \frac{1}{f^{7/6}} \cos \iota, \quad (4.35)$$

where the constant A has the value

$$A = \frac{1}{\pi^{2/3}} \left(\frac{5}{24} \right)^{1/2}. \quad (4.36)$$

The phases are given by $\Psi_\times = \Psi_+ + (\pi/2)$ and

$$\Psi_+(f) = 2\pi f (t_c + r/c) - \Phi_0 - \frac{\pi}{4} + \frac{3}{4} \left(\frac{GM_c}{c^3} 8\pi f \right)^{-5/3}, \quad (4.37)$$

where Φ_0 is the value of the phase Φ at coalescence, see eq. (4.30). We will see in Sections 5.6 and 7.7 that an accurate computation of $\Psi_{+,\times}(f)$, going well beyond the Newtonian approximation, is crucial for discriminating the signal of a coalescing binary from the detector noise, and we will give in eq. (5.275) the post-Newtonian corrections to eq. (4.37).

The above computations have been performed in a flat background. For binary systems made of black holes or neutron stars, the gravitational field close to the stars is however strong, and this has important consequences on the dynamics of the binary system when the two objects get close. A full discussion of a realistic coalescence of compact binaries will be deferred to Vol. 2. However, the most important qualitative modification to the dynamics comes from the fact that, in the Schwarzschild geometry, there is a minimum value of the radial distance beyond which stable circular orbits are no longer allowed, i.e. an Innermost Stable Circular Orbit (ISCO). In Schwarzschild coordinates this is located at $r = r_{\text{ISCO}}$, with

$$r_{\text{ISCO}} = \frac{6Gm}{c^2}, \quad (4.38)$$

⁷More precisely, this is valid in the test mass limit, when one of the two stars is much lighter than the other. For finite masses, this result receives corrections that can be expressed as an expansion in powers of the symmetric mass ratio $\nu = \mu/m$. The position of the ISCO is also affected by the spin of the bodies. We will discuss these effects in Vol. 2.

(4.1), this means that the inspiral phase ends when the source frequency f_s approaches the value

$$(f_s)_{\text{ISCO}} = \frac{1}{6\sqrt{6}(2\pi)} \frac{c^3}{Gm}. \quad (4.39)$$

Inserting the numerical values, this gives

$$(f_s)_{\text{ISCO}} \simeq 2.2 \text{ kHz} \left(\frac{M_\odot}{m} \right). \quad (4.40)$$

For instance, for a NS-NS system with the typical masses $m_1 = m_2 \simeq 1.4M_\odot$, so that $m \simeq 2.8M_\odot$, we have $(f_s)_{\text{ISCO}} \sim 800$ Hz, while for a BH-BH binary with a total mass $m = 10M_\odot$ we have $(f_s)_{\text{ISCO}} \sim 200$ Hz. The coalescence of two supermassive BHs with $m \sim 10^6M_\odot$ takes place when f_s is in the mHz region.

Plugging eqs. (4.34) and (4.35) into eq. (1.160) and performing the angular integration we get the energy spectrum in the inspiral phase, in the Newtonian approximation,

$$\frac{dE}{df} = \frac{\pi^{2/3}}{3G} (GM_c)^{5/3} f^{-1/3}. \quad (4.41)$$

Integrating up to the maximum GW frequency f_{\max} for which we are still in the inspiral phase we can estimate the total energy radiated during the inspiral phase,

$$\Delta E_{\text{rad}} \sim \frac{\pi^{2/3}}{2G} (GM_c)^{5/3} f_{\max}^{2/3}, \quad (4.42)$$

or, inserting the numerical values,

$$\Delta E_{\text{rad}} \sim 4.2 \times 10^{-2} M_\odot c^2 \left(\frac{M_c}{1.21M_\odot} \right)^{5/3} \left(\frac{f_{\max}}{1 \text{ kHz}} \right)^{2/3}. \quad (4.43)$$

Setting $f_{\max} = 2(f_s)_{\text{ISCO}}$ (as appropriate for quadrupole radiation) and using eq. (4.40) we see that the total energy radiated during the inspiral phase actually depends only on the reduced mass μ of the system, and is

$$\Delta E_{\text{rad}} \sim 8 \times 10^{-2} \mu c^2. \quad (4.44)$$

For stellar mass objects this is a huge amount of energy, and this makes coalescing binaries one of the most interesting sources of GWs. Actually, the above numerical value only provides an order-of-magnitude estimate, since we performed a flat-space computation, and we cut off the result by hand at the value of $(f_s)_{\text{ISCO}}$ obtained from the Schwarzschild geometry. A better approach consists in observing that, in the Schwarzschild metric, the binding energy of the ISCO is given by⁸

$$E_{\text{binding}} = (1 - \sqrt{8/9})\mu c^2 \simeq 5.7 \times 10^{-2} \mu c^2, \quad (4.45)$$

⁸See e.g. Landau and Lifshitz, Vol. II (1979), Section 102, Problem 1.

and this is the total energy radiated in GWs when the binary system is slowly inspiraling from an orbit with large relative separation down to the ISCO. We will see in Vol. 2 that the post-Newtonian corrections to this binding energy are of order of a few per cent. Thus, the order-of-magnitude estimate given in eq. (4.44) turns out to be reasonably close to the correct result.

4.1.2 Elliptic orbits. (I) Total power and frequency spectrum of the radiation emitted

We now consider the radiation emitted by masses in an elliptic Keplerian orbit. As before, we denote by m_1, m_2 the masses of the two stars, by $m = m_1 + m_2$ the total mass, and by μ the reduced mass. As usual, in the CM the problem reduces to a one-body problem for a particle of mass μ , subject to an acceleration $\ddot{\mathbf{r}} = -(Gm/r^2)\hat{\mathbf{r}}$. We first recall, from elementary mechanics, the solution of this equation of motion for an elliptic orbit, and then we compute the total power radiated in GWs and its frequency spectrum.

Elliptic Keplerian orbits

The general solution of the equation of motion is obtained by observing that there are two first integral of motion, the angular momentum \mathbf{L} , and the energy E . The conservation of \mathbf{L} implies that the orbit lies in a plane; we then introduce polar coordinates (r, ψ) in the plane of the orbit, with origin on the position of the center-of-mass (we use ψ to denote the angular position along the orbit, since we reserve θ and ϕ to describe the angular distribution of the radiation emitted). Then, in terms of r and ψ , the modulus of the angular momentum is given by

$$L = \mu r^2 \dot{\psi}, \quad (4.46)$$

while the energy is given by

$$\begin{aligned} E &= \frac{1}{2}\mu(\dot{r}^2 + r^2\dot{\psi}^2) - \frac{G\mu m}{r} \\ &= \frac{1}{2}\mu\dot{r}^2 + \frac{L^2}{2\mu r^2} - \frac{G\mu m}{r}. \end{aligned} \quad (4.47)$$

From eq. (4.47) we get dr/dt as a function of r while from eq. (4.46) we get $d\psi/dt$; combining the two expressions we find $dr/d\psi$ as a function of r and, integrating this expression, we obtain the equation of the orbit,

$$\frac{1}{r} = \frac{1}{R}(1 + e \cos \psi). \quad (4.48)$$

The length-scale R and the eccentricity e are constants of motion, and are related to the energy E of the system (with $E < 0$ for a bound orbit) and to the orbital angular momentum L by

$$R = \frac{L^2}{Gm\mu^2}, \quad (4.49)$$

and

$$e^2 = 1 + \frac{2EL^2}{G^2m^2\mu^3}. \quad (4.50)$$

The eccentricity e for an ellipse satisfies $0 \leq e < 1$; for $e = 0$ the ellipse becomes a circle, while $e = 1$ corresponds to a parabola. The two semiaxes of the ellipse are given by

$$a = \frac{R}{1 - e^2}, \quad (4.51)$$

$$b = \frac{R}{(1 - e^2)^{1/2}}. \quad (4.52)$$

The geometry is shown in Fig. 4.3. Inserting the explicit expression for e given in eq. (4.50), we see that

$$a = \frac{Gm\mu}{2|E|}. \quad (4.53)$$

Observe that a is independent of L , so orbits with the same energy have the same value of the semimajor axis a . In terms of a and e , we can rewrite the equation of the orbit (4.48) in the form

$$r = \frac{a(1 - e^2)}{1 + e \cos \psi}. \quad (4.54)$$

Combining eqs. (4.46) and (4.49), we see also that $r(t)$ and $\dot{\psi}(t)$ satisfy the relation

$$\dot{\psi} = \frac{(GmR)^{1/2}}{r^2}. \quad (4.55)$$

The explicit time dependence of $r(t)$ and $\psi(t)$ is obtained by integrating eqs. (4.46) and (4.47) (making use also of the equation of the orbit) and is given in parametric form by

$$r = a[1 - e \cos u], \quad (4.56)$$

$$\cos \psi = \frac{\cos u - e}{1 - e \cos u}, \quad (4.57)$$

where u is called the eccentric anomaly, and is related to t by the famous Kepler equation

$$\beta \equiv u - e \sin u = \omega_0 t, \quad (4.58)$$

with

$$\omega_0^2 = \frac{Gm}{a^3}. \quad (4.59)$$

We have chosen the origin of time such that, at $t = 0$, we have $\psi = 0$. Making use of trigonometric identities, eq. (4.57) can also be rewritten as

$$\tan \frac{\psi}{2} = \left(\frac{1+e}{1-e} \right)^{1/2} \tan \frac{u}{2}, \quad (4.60)$$

i.e.

$$= A_e(u) \equiv 2 \arctan \left[\left(\frac{1+e}{1-e} \right)^{1/2} \tan \frac{u}{2} \right]. \quad (4.61)$$

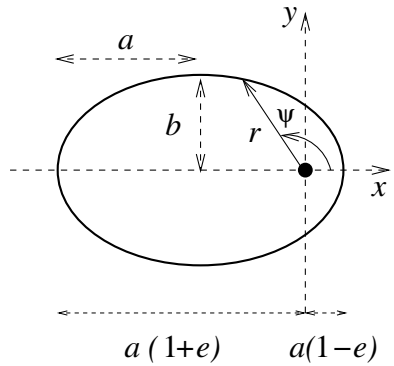


Fig. 4.3 The definitions used for an elliptic orbit. The polar coordinates (r, ψ) , as well as the Cartesian coordinates (x, y) , are centered on a focus of the ellipse (dark blob). The angle ψ is measured counterclockwise, from the x axis. The semiaxes a, b are indicated. The focus splits the major axis into two segments of length $a(1 + e)$ and $a(1 - e)$, respectively.

The function $A_e(u)$ is called the true anomaly. Observe from eq. (4.58) that, if $t \rightarrow t + 2\pi/\omega_0$, we have $\beta \rightarrow \beta + 2\pi$ and $u \rightarrow u + 2\pi$, so the coordinates r, ψ are periodic functions of t , with period

$$T = \frac{2\pi}{\omega_0}. \quad (4.62)$$

As u runs between $-\pi$ and π , ψ also runs between $-\pi$ and π . A graph of $\psi(u)$ is shown in Fig. 4.4, for two different values of the ellipticity. Observe that, for $e = 0$, $\psi = u$. We will also use Cartesian coordinates (x, y) centered on the focus of the ellipse,

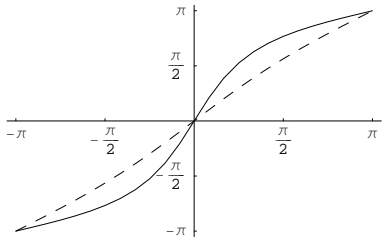


Fig. 4.4 The function $\psi(u)$ for $e = 0.2$ (dashed line) and for $e = 0.75$ (solid line).

⁹The equation of the ellipse in Cartesian coordinates would be slightly simpler if we choose the center of the ellipse, rather than a focus, as the origin, since in this case we simply have $x = a \cos u(t)$ and $y = b \sin u(t)$. However, (x, y) are already relative coordinates in the CM frame, so we cannot change them with a shift of the origin.

$$\begin{aligned} x &= r \cos \psi \\ &= a[\cos u(t) - e], \end{aligned} \quad (4.63)$$

$$\begin{aligned} y &= r \sin \psi \\ &= b \sin u(t). \end{aligned} \quad (4.64)$$

In terms of the original problem with two bodies of masses m_1 and m_2 , the focus of the ellipse is the point where $\mathbf{x}_{\text{CM}} = 0$, and the coordinates, measured from this point, are the relative coordinates in the CM system.⁹

Radiated power

We first compute the total power radiated in GWs, integrated over all frequencies and over the solid angle. We choose a reference frame where the orbit is in the (x, y) plane. In this frame the second mass moment is given by the 2×2 matrix

$$M_{ab} = \mu r^2 \begin{pmatrix} \cos^2 & \sin \psi \cos \psi \\ \sin \psi \cos \psi & \sin^2 \end{pmatrix}_{ab}, \quad (4.65)$$

where $a, b = 1, 2$ are indices in the (x, y) plane. To compute the total power emitted in the quadrupole approximation we must evaluate the third derivatives of M_{ab} , and we can then use the quadrupole formula in the form (3.76). In eq. (4.65) the time dependence is both in $r(t)$ and in $\psi(t)$. To compute these derivative, the simplest way is to write M_{ab} as a function of ψ only, eliminating r with the help of eq. (4.54), e.g.

$$\begin{aligned} M_{11} &= \mu r^2 \cos^2 \\ &= \mu a^2 (1 - e^2)^2 \frac{\cos^2}{(1 + e \cos \psi)^2}. \end{aligned} \quad (4.66)$$

Now we can compute the time derivatives using

$$\begin{aligned} \dot{\psi} &= \frac{(GmR)^{1/2}}{r^2} \\ &= \left(\frac{Gm}{a^3} \right)^{1/2} (1 - e^2)^{-3/2} (1 + e \cos \psi)^2, \end{aligned} \quad (4.67)$$

where we used eqs. (4.55), (4.54) and (4.51). Then a simple computation gives

$$\ddot{M}_{11} = \beta(1 + e \cos \psi)^2 [2 \sin 2\psi + 3e \sin \psi \cos^2 \psi], \quad (4.68)$$

$$\ddot{M}_{22} = \beta(1 + e \cos \psi)^2 [-2 \sin 2\psi - e \sin \psi (1 + 3 \cos^2 \psi)], \quad (4.69)$$

$$\ddot{M}_{12} = \beta(1 + e \cos \psi)^2 [-2 \cos 2\psi + e \cos \psi (1 - 3 \cos^2 \psi)], \quad (4.70)$$

with

$$\beta^2 \equiv \frac{4G^3 \mu^2 m^3}{a^5 (1 - e^2)^5}. \quad (4.71)$$

Plugging this into eq. (3.76) we get the power radiated, in the quadrupole approximation, as a function of the position along the orbit,

$$\begin{aligned} P(\psi) &= \frac{G}{5c^5} \left[\ddot{M}_{11}^2 + \ddot{M}_{22}^2 + 2\ddot{M}_{12}^2 - \frac{1}{3}(\ddot{M}_{11} + \ddot{M}_{22})^2 \right] \\ &= \frac{2G}{15c^5} \left[\ddot{M}_{11}^2 + \ddot{M}_{22}^2 + 3\ddot{M}_{12}^2 - \ddot{M}_{11}\ddot{M}_{22} \right] \\ &= \frac{8G^4}{15c^5} \frac{\mu^2 m^3}{a^5 (1 - e^2)^5} (1 + e \cos \psi)^4 [12(1 + e \cos \psi)^2 + e^2 \sin^2 \psi]. \end{aligned} \quad (4.72)$$

As explained in Chapter 1, the GW energy is only well defined by taking a temporal average over several periods of the wave. As we will see below, a particle in a Keplerian elliptic orbit emits GWs at frequencies which are integer multiple of the frequency ω_0 defined in eq. (4.59), and therefore the period of the GWs is a fraction of the orbital period T given in eq. (4.62). Then, a well defined quantity is the average of $P(\psi(t))$ over one period T . We can now perform this time average, writing

$$\begin{aligned} P &\equiv \frac{1}{T} \int_0^T dt P(\psi) \\ &= \frac{\omega_0}{2\pi} \int_0^{2\pi} \frac{d\psi}{\dot{\psi}} P(\psi) \\ &= (1 - e^2)^{3/2} \int_0^{2\pi} \frac{d\psi}{2\pi} (1 + e \cos \psi)^{-2} P(\psi) \\ &= \frac{8G^4 \mu^2 m^3}{15c^5 a^5} (1 - e^2)^{-7/2} \\ &\quad \times \int_0^{2\pi} \frac{d\psi}{2\pi} [12(1 + e \cos \psi)^4 + e^2(1 + e \cos \psi)^2 \sin^2 \psi], \end{aligned} \quad (4.73)$$

where we used eq. (4.67). The integral is elementary and one finally obtains the total radiated power¹⁰

$$P = \frac{32G^4 \mu^2 m^3}{5c^5 a^5} f(e), \quad (4.74)$$

with

$$f(e) = \frac{1}{(1 - e^2)^{7/2}} \left(1 + \frac{73}{24} e^2 + \frac{37}{96} e^4 \right). \quad (4.75)$$

¹⁰This classic formula is due to Peters and Mathews (1963).

Using eq. (4.59) we can eliminate m in favor of ω_0 , and rewrite the above result as

$$P = \frac{32}{5} \frac{G\mu^2}{c^5} a^4 \omega_0^6 f(e). \quad (4.76)$$

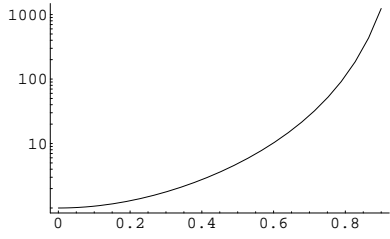


Fig. 4.5 The function $f(e)$, on a logarithmic scale.

For $e = 0$, we have $f(e) = 1$, while a becomes the radius of the circular orbit and ω_0 becomes the same as ω_s , so we get back the result for circular orbits, eq. (3.339). The function $f(e)$ is plotted, on a logarithmic scale, in Fig. 4.5. For instance, for the Hulse–Taylor binary pulsar (that will be discussed in detail in Chapter 6) the eccentricity is quite large, $e \simeq 0.617$, and $f(e) \simeq 11.8$. The radiated power is therefore an order of magnitude larger than the power emitted in a circular orbit with radius a (i.e. with the same energy).

Combining eqs. (4.62), (4.59) and (4.53) we see that the orbital period T is related to the orbital energy E by $T = \text{const.} \times (-E)^{-3/2}$ and therefore

$$\frac{\dot{T}}{T} = -\frac{3}{2} \frac{\dot{E}}{E}. \quad (4.77)$$

From eq. (4.74) we find the energy loss (averaged over one orbital period) $\dot{E} = -P$ and therefore (using again eq. (4.53) to express E in terms of a) we get

$$\frac{\dot{T}}{T} = -\frac{96}{5} \frac{G^3 \mu m^2}{c^5 a^4} f(e), \quad (4.78)$$

where the average over an orbital period is understood. Expressing a in terms of T using eqs. (4.62) and (4.59) we can also rewrite this as

$$\frac{\dot{T}}{T} = -\frac{96}{5} \frac{G^{5/3} \mu m^{2/3}}{c^5} \left(\frac{T}{2\pi} \right)^{-8/3} f(e). \quad (4.79)$$

This equation is of great importance, since it is at the basis of the first experimental evidence for gravitational radiation, as will be discussed in Chapter 6.

Coming back to eq. (4.74), we see that in the limit $e \rightarrow 1^-$ (with a fixed) the radiated power diverges. This is due to the fact that, if we send $e \rightarrow 1^-$ keeping a fixed, we get $R \rightarrow 0$ (see eq. (4.51)) and $b = a(1-e^2)^{1/2} \rightarrow 0$. Therefore, as the ellipticity $e \rightarrow 1^-$ at fixed a , the motion of the relative coordinates approaches more and more the point $r = 0$, where the acceleration Gm/r^2 diverges, and therefore the GW production formally diverges as well. However, clearly at this moment the approximation of point-like masses ceases to be valid, and we must take into account the finite size of the bodies.

The limit $e \rightarrow 1^-$ at fixed R corresponds instead to parabolic motion,

$$r = \frac{R}{1 + \cos \psi}. \quad (4.80)$$

When $\psi \rightarrow -\pi$ the particle is at $r = \infty$; by increasing ψ the value of r decreases down to $r = R/2$ (reached for $\psi = 0$), and then increases again, until again $r \rightarrow \infty$ as $\psi \rightarrow \pi$ (see Fig. 4.6). In this limit, eliminating

a in favor of R using eq. (4.51), we obtain from eq. (4.72) the power radiated along the trajectory,

$$\begin{aligned} P(\psi) &= \frac{8G^4\mu^2m^3}{15c^5R^5}(1+\cos\psi)^4[12(1+\cos\psi)^2+\sin^2\psi] \\ &= \frac{16G^4\mu^2m^3}{15c^5}\frac{1}{r^5}\left(1+\frac{11R}{2r}\right). \end{aligned} \quad (4.81)$$

Then, $P(\psi)$ goes to zero quite fast as $r \rightarrow \infty$ or, equivalently, as $\psi \rightarrow \pm\pi$, see Fig. 4.7. This is of course expected, since the acceleration vanishes as $1/r^2$. As a result, the total energy radiated in GWs is finite

$$\begin{aligned} E_{\text{rad}} &= \int_{-\infty}^{\infty} dt P(\psi(t)) \\ &= \int_{-\pi}^{\pi} \frac{d\psi}{\dot{\psi}} P(\psi) \\ &= \frac{85\pi}{48} \frac{G\mu^2}{R} \left(\frac{v_0}{c}\right)^5, \end{aligned} \quad (4.82)$$

where $v_0 = 2(Gm/R)^{1/2}$ is the velocity at $\psi = 0$ (which corresponds to $r = R/2$), i.e. is the maximum velocity attained along the trajectory. In this form, the result is similar to that found for a periodic source, compare, e.g. with eq. (3.319). Since this finite energy is emitted in a time $T = \infty$, if we take the average value of the power over a time T we find zero, as we can also check from eq. (4.74) writing $(1/a^5)f(e) = (1/R^5)(1-e^2)^5f(e)$ and taking the limit $e \rightarrow 1^-$ at fixed R . Of course, this reflects simply the fact that the radiation is emitted basically between $-\pi/2 < \psi < \pi/2$, see Fig. 4.7; the radiation emitted when $\pi/2 < |\psi| < \pi$ is instead finite (and, indeed, even negligible), even if it takes an infinite time to get to $\psi = \pi$ or to come from $\psi = -\pi$.

Frequency spectrum

Above we have computed the total radiated power, integrated both over the frequency and over the solid angle. It is however very interesting to compute the frequency spectrum of the radiated power, $dP/d\omega$, for a Keplerian elliptic orbit.

Such a trajectory, given as a function of time by eqs. (4.63), (4.64) and (4.58), is of course not a simple harmonic motion, and therefore the first step is to perform the Fourier decomposition of the trajectory. This can be done by observing, first of all, that $x(t)$ and $y(t)$ are periodic functions of the variable β defined in eq. (4.58), with period 2π . Therefore we can restrict β to the range $-\pi \leq \beta \leq \pi$, and we can perform a discrete Fourier transform,

$$x(\beta) = \sum_{n=-\infty}^{\infty} \tilde{x}_n e^{-in\beta}, \quad (4.83)$$

$$y(\beta) = \sum_{n=-\infty}^{\infty} \tilde{y}_n e^{-in\beta}, \quad (4.84)$$

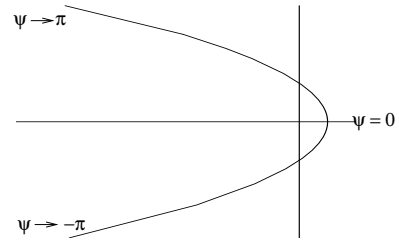


Fig. 4.6 The parabolic trajectory.

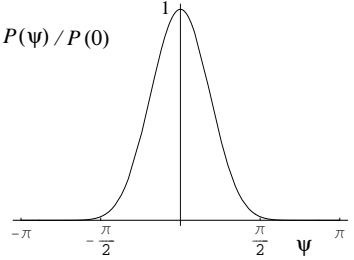


Fig. 4.7 The function $P(\psi)$, normalized to the value at $\psi = 0$, for parabolic motion.

with $\tilde{x}_n = \tilde{x}_{-n}^*$ and $\tilde{y}_n = \tilde{y}_{-n}^*$, since $x(\beta)$ and $y(\beta)$ are real functions. Furthermore, we have chosen the origin of time so that at $t = 0$ (i.e. at $\beta = 0$), we are at the point $x = a(1 - e), y = 0$; with this choice, $x(-\beta) = x(\beta)$ while $y(-\beta) = -y(\beta)$. Therefore, writing $e^{-in\beta} = \cos(n\beta) - i \sin(n\beta)$, in the expansion of $x(\beta)$ contributes only $\cos(n\beta)$ while in the expansion of $y(\beta)$ contributes only $\sin(n\beta)$, and eqs. (4.83) and (4.84) simplify to

$$x(\beta) = \sum_{n=0}^{\infty} a_n \cos(n\beta), \quad (4.85)$$

$$y(\beta) = \sum_{n=1}^{\infty} b_n \sin(n\beta), \quad (4.86)$$

where, for $n \geq 1$, $a_n = 2\tilde{x}_n$ and $b_n = -2i\tilde{y}_n$, while $a_0 = \tilde{x}_0$. Since $\beta = \omega_0 t$, we can rewrite this as

$$x(t) = \sum_{n=0}^{\infty} a_n \cos \omega_n t, \quad (4.87)$$

$$y(t) = \sum_{n=1}^{\infty} b_n \sin \omega_n t, \quad (4.88)$$

where

$$\omega_n = n\omega_0. \quad (4.89)$$

We see that the Fourier decomposition of the Keplerian motion involves the fundamental frequency $\omega_0 = (Gm/a^3)^{1/2}$ and all its higher harmonics. The coefficients a_n and b_n are obtained by inverting eqs. (4.85) and (4.86), which gives, for $n \neq 0$,

$$a_n = \frac{2}{\pi} \int_0^\pi d\beta x(\beta) \cos(n\beta), \quad (4.90)$$

$$b_n = \frac{2}{\pi} \int_0^\pi d\beta y(\beta) \sin(n\beta), \quad (4.91)$$

(4.92)

while, for $n = 0$,

$$a_0 = \frac{1}{\pi} \int_0^\pi d\beta x(\beta). \quad (4.93)$$

With $x(\beta)$ and $y(\beta)$ given by eqs. (4.63), (4.64) and (4.58), these integrals are computed explicitly in Problem 4.2, and the result is given in terms of Bessel functions,¹¹

$$a_n = \frac{a}{n} [J_{n-1}(ne) - J_{n+1}(ne)] \quad (4.94)$$

$$b_n = \frac{b}{n} [J_{n-1}(ne) + J_{n+1}(ne)]. \quad (4.95)$$

for $n \neq 0$, and $a_0 = -(3/2)ae$. The above result is interesting in itself but, to compute the spectrum of GWs, we are really interested in the

¹¹Actually, Bessel functions were introduced for the first time just in this context, by Lagrange and, half a century later, in the more general solution for the Fourier transform of the Kepler problem given by Bessel. See Watson (1966).

Fourier decomposition of the second mass moment, and therefore of $x^2(t)$, $y^2(t)$ and $x(t)y(t)$. This is again computed in Problem 4.2, where we show that

$$x^2(t) = \sum_{n=0}^{\infty} A_n \cos \omega_n t, \quad (4.96)$$

$$y^2(t) = \sum_{n=0}^{\infty} B_n \cos \omega_n t, \quad (4.97)$$

$$x(t)y(t) = \sum_{n=1}^{\infty} C_n \sin \omega_n t, \quad (4.98)$$

where

$$A_n = \frac{a^2}{n} [J_{n-2}(ne) - J_{n+2}(ne) - 2e(J_{n-1}(ne) - J_{n+1}(ne))], \quad (4.99)$$

$$B_n = \frac{b^2}{n} [J_{n+2}(ne) - J_{n-2}(ne)], \quad (4.100)$$

$$C_n = \frac{ab}{n} [J_{n+2}(ne) + J_{n-2}(ne) - e(J_{n+1}(ne) + J_{n-1}(ne))]. \quad (4.101)$$

The second mass moment (4.65) therefore has the Fourier decomposition

$$\begin{aligned} M_{ab}(t) &= \mu \sum_{n=0}^{\infty} \begin{pmatrix} A_n \cos \omega_n t & C_n \sin \omega_n t \\ C_n \sin \omega_n t & B_n \cos \omega_n t \end{pmatrix}_{ab} \\ &\equiv \sum_{n=0}^{\infty} M_{ab}^{(n)}(t). \end{aligned} \quad (4.102)$$

When we compute the radiated power, temporal averages such as

$$\langle \sin \omega_n t \sin \omega_m t \rangle$$

are non-vanishing only if $n = m$, so there is no interference term between the different harmonics, and

$$P = \sum_{n=1}^{\infty} P_n, \quad (4.103)$$

where P_n is the power radiated in the n -th harmonics. To compute P_n we use the quadrupole formula, written in the form

$$P = \frac{2G}{15c^5} \langle \ddot{M}_{11}^2 + \ddot{M}_{22}^2 + 3\ddot{M}_{12}^2 - \ddot{M}_{11}\ddot{M}_{22} \rangle \quad (4.104)$$

(that takes into account that the orbit is in the (x, y) plane, compare with eq. (4.72)), and we replace M_{ab} by $M_{ab}^{(n)}$. Using

$$\ddot{M}_{ab}^{(n)} = \mu \omega_n^3 \begin{pmatrix} A_n \sin \omega_n t & -C_n \cos \omega_n t \\ -C_n \cos \omega_n t & B_n \sin \omega_n t \end{pmatrix}_{ab}, \quad (4.105)$$

we get

$$P_n = \frac{G\mu^2\omega_0^6}{15c^5} n^6 (A_n^2 + B_n^2 + 3C_n^2 - A_n B_n), \quad (4.106)$$

where we used $\langle \sin^2 \omega_n t \rangle = \langle \cos^2 \omega_n t \rangle = 1/2$. Recalling that $\omega_0^2 = Gm/a^3$, the above result can be rewritten as

$$P_n = \frac{32G^4\mu^2 m^3}{5c^5 a^5} g(n, e), \quad (4.107)$$

where

$$g(n, e) = \frac{n^6}{96a^4} [A_n^2(e) + B_n^2(e) + 3C_n^2(e) - A_n(e)B_n(e)], \quad (4.108)$$

where the notation stresses that A_n, B_n and C_n depends on the eccentricity e (recall also that $b^2/a^2 = (1 - e^2)$).

First of all, we can check from this expression that, in the limit $e \rightarrow 0$, we get back the result for circular motion. If $e = 0$, the argument of the Bessel functions, in eqs. (4.99)–(4.101), vanishes. Since $J_m(0) = \delta_{m0}$, and since for us $n \geq 1$, we see from eqs. (4.99)–(4.101) that in this limit $A_n \rightarrow (a^2/2)\delta_{n2}$, $B_n \rightarrow (-a^2/2)\delta_{n2}$ (of course $b = a$ when $e = 0$) and $C_n \rightarrow (a^2/2)\delta_{n2}$. Then we get back the result that, for circular motion, only the harmonic with $n = 2$ contributes, and we find from eq. (4.108) that $g(0, n) = \delta_{n2}$, so we get back the correct value for the radiated power.

For a generic value of e (with $0 < e < 1$) all harmonics contribute, and we have radiation at all frequencies $\omega_n = n\omega_0$ for all integer values of n , including also $n = 1$. Increasing the ellipticity, increases also the value of $n = \bar{n}$ where $g(n, e)$ is maximum, as well as the value of P_n at $n = \bar{n}$, and the total radiated power. In Figs. 4.8–4.10 we show the power spectrum P_n , normalized to the power radiated when $e = 0$, for three different values of the ellipticity. Observe the change in the horizontal and vertical scales, among these figures.

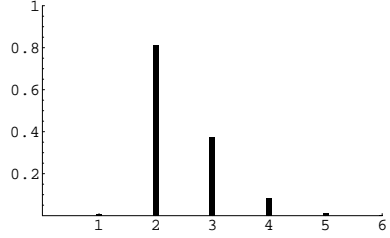


Fig. 4.8 The power P_n radiated at the GW frequency $\omega_n = n\omega_0$, as a function of n , for $e = 0.2$. P_n is normalized to the value for $e = 0$.

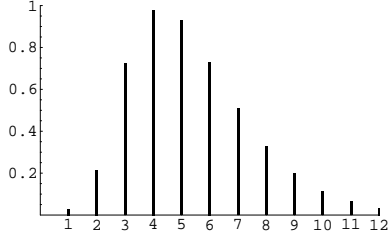


Fig. 4.9 The same as Fig. 4.8, for $e = 0.5$.

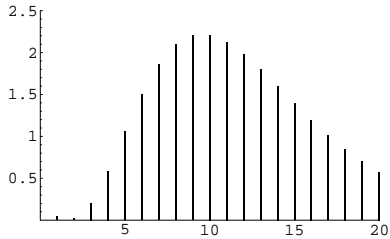


Fig. 4.10 The same as Fig. 4.8, for $e = 0.7$.

4.1.3 Elliptic orbits. (II) Evolution of the orbit under back-reaction

The evolution equations

A binary system in a Keplerian orbit radiates both energy and angular momentum. In our approximation of point-like bodies (without an intrinsic spin) these are necessarily drained from the energy and angular momentum of the orbital motion, which therefore undergoes secular changes, both in its semimajor axis and in its ellipticity, until the system enters the merging phase and collapses. In this section we compute how the shape and size of the orbit evolve, for a generic elliptic orbit.

We already computed the energy radiated, in the quadrupole approximation, in eq. (4.74). We now compute the angular momentum radiated, again in the quadrupole approximation. We therefore start from eq. (3.99), which we write as

$$\frac{dL^i}{dt} = -\frac{2G}{5c^5} \epsilon^{ikl} \langle \ddot{M}_{ka} \ddot{M}_{la} \rangle, \quad (4.109)$$

where L^i is the orbital angular momentum of the binary system, and we replaced \ddot{Q}_{ka} by \ddot{M}_{ka} (because the difference gives a contribution to eq. (4.109) proportional to $\epsilon^{ikl} \delta_{ka} \ddot{Q}_{la} = \epsilon^{ikl} \ddot{Q}_{kl}$, which vanishes because \ddot{Q}_{kl} is symmetric in (k, l) and ϵ^{ikl} is antisymmetric), and similarly we replaced \ddot{Q}_{la} by \ddot{M}_{la} . As in the computation of the radiated energy, we put the orbit in the (x, y) plane, so M_{ab} is given by eq. (4.65), and we write $L_z = L$. Then, recalling that inside $\langle \dots \rangle$ we can integrate by parts, eq. (4.109) gives

$$\begin{aligned} \frac{dL}{dt} &= -\frac{2G}{5c^5} \langle \ddot{M}_{1a} \ddot{M}_{2a} - \ddot{M}_{2a} \ddot{M}_{1a} \rangle \\ &= \frac{4G}{5c^5} \langle \ddot{M}_{12} (\ddot{M}_{11} - \ddot{M}_{22}) \rangle. \end{aligned} \quad (4.110)$$

The third derivatives \ddot{M}_{11} and \ddot{M}_{22} have been computed in eqs. (4.68) and (4.69), while a similar computation gives

$$\begin{aligned} \ddot{M}_{12} &= \frac{G\mu m}{a(1-e^2)} \sin \psi \\ &\times [-4(1+e \cos \psi)^2 \cos \psi + 2e(3 \cos^2 \psi - 1 + 2e \cos^3 \psi)]. \end{aligned} \quad (4.111)$$

For periodic motion, the average over several periods of the wave is the same as the average over one orbital period T and, as in eq. (4.73), we transform the temporal average over one period into an integration over ψ , using

$$\int_0^T \frac{dt}{T} (\dots) = (1-e^2)^{3/2} \int_0^{2\pi} \frac{d\psi}{2\pi} (1+e \cos \psi)^{-2} (\dots). \quad (4.112)$$

Then we get, for the angular momentum loss averaged over one period,

$$\begin{aligned} \frac{dL}{dt} &= \frac{8}{5} \frac{G^{7/2} \mu^2 m^{5/2}}{c^5 a^{7/2}} \frac{1}{(1-e^2)^2} \int_0^{2\pi} \frac{d\psi}{2\pi} \sin^2 \\ &\times [-4(1+e \cos \psi)^2 \cos \psi + 2e(3 \cos^2 \psi - 1 + 2e \cos^3 \psi)] \\ &\times [8 \cos \psi + 6e \cos^2 \psi + e]. \end{aligned} \quad (4.113)$$

The integral over ψ is elementary, and gives $-4(1+7e^2/8)$. In conclusion, from this result and eq. (4.74), the energy E and the angular momentum L of the orbit evolve as

$$\frac{dE}{dt} = -\frac{32}{5} \frac{G^4 \mu^2 m^3}{c^5 a^5} \frac{1}{(1-e^2)^{7/2}} \left(1 + \frac{73}{24} e^2 + \frac{37}{96} e^4 \right), \quad (4.114)$$

$$\frac{dL}{dt} = -\frac{32}{5} \frac{G^{7/2} \mu^2 m^{5/2}}{c^5 a^{7/2}} \frac{1}{(1-e^2)^2} \left(1 + \frac{7}{8} e^2 \right), \quad (4.115)$$

and we recall again that these quantities are really averages over one period, rather than instantaneous energy and angular momentum losses. Using eqs. (4.50) and (4.53) we can rewrite these equations in terms of the evolution of the semimajor axis a and of the eccentricity e ,

$$\frac{da}{dt} = -\frac{64}{5} \frac{G^3 \mu m^2}{c^5 a^3} \frac{1}{(1-e^2)^{7/2}} \left(1 + \frac{73}{24} e^2 + \frac{37}{96} e^4 \right), \quad (4.116)$$

$$\frac{de}{dt} = -\frac{304}{15} \frac{G^3 \mu m^2}{c^5 a^4} \frac{e}{(1-e^2)^{5/2}} \left(1 + \frac{121}{304} e^2 \right). \quad (4.117)$$

From eq. (4.117) we see that, if $e = 0$, then $de/dt = 0$. Therefore a circular orbit remains circular. This could also have been seen directly from eqs. (4.114) and (4.115), observing that, for $e = 0$, they give

$$\frac{dE}{dt} = \omega_0 \frac{dL}{dt}, \quad (4.118)$$

where $\omega_0 = (Gm/a^3)^{1/2}$ is the frequency of the circular motion, see eq. (4.59). Equation (4.118) is just what is needed to maintain the relation between energy and angular momentum that holds for circular motion. In fact, for circular orbits, using eq. (4.59),

$$E = -\frac{Gm\mu}{2a} = -\frac{1}{2} (Gm)^{2/3} \mu \omega_0^{2/3}, \quad (4.119)$$

while

$$L = \mu a^2 \omega_0 = (Gm)^{2/3} \mu \omega_0^{-1/3}, \quad (4.120)$$

and therefore

$$\frac{dE}{dt} = -\frac{1}{3} (Gm)^{2/3} \mu \omega_0^{-1/3} \dot{\omega}_0, \quad (4.121)$$

$$\frac{dL}{dt} = -\frac{1}{3} (Gm)^{2/3} \mu \omega_0^{-4/3} \dot{\omega}_0, \quad (4.122)$$

from which eq. (4.118) follows. For $e > 0$, eq. (4.117) gives $de/dt < 0$ instead, and therefore an elliptic orbit becomes more and more circular because of the emission of GWs.

A direct numerical integration of eqs. (4.116) and (4.117) is not as straightforward as one might think. The reason can be seen by putting the equations in dimensionless form. To do so, it is convenient to introduce a length-scale R_* , from $R_*^3 = 4G^3 \mu m^2 / c^6$. We have chosen the numerical factor so that when the masses of the two stars are equal, $m_1 = m_2 = M$, we have $R_* = 2GM/c^2$, so R_* becomes equal to the Schwarzschild radius of the stars. We then introduce the dimensionless variable $\tau = ct/R_*$, i.e. time measured in units of the light travel time across a distance R_* , and the dimensionless function $\tilde{a}(\tau) = a(\tau)/R_*$. Then eqs. (4.116) and (4.117) read

$$\frac{d\tilde{a}}{d\tau} = -\frac{16}{5} \frac{1}{\tilde{a}^3} \frac{1}{(1-e^2)^{7/2}} \left(1 + \frac{73}{24} e^2 + \frac{37}{96} e^4 \right), \quad (4.123)$$

$$\frac{de}{d\tau} = -\frac{76}{15} \frac{1}{\tilde{a}^4} \frac{e}{(1-e^2)^{5/2}} \left(1 + \frac{121}{304} e^2 \right). \quad (4.124)$$

This shows that $\tau = ct/R_*$ is the natural adimensional time-scale in the differential equation. However, for typical solar-mass stars, $R_* \sim 3$ km and $R_*/c = O(10^{-5})$ s. Therefore, to follow the evolution of the orbit for a time $t \sim 1$ yr, we need to push the integration up to a dimensionless value $\tau \sim 10^{12}$, which is numerically difficult.

A better approach is to combine eqs. (4.116) and (4.117) to get da/de ,

$$\frac{da}{de} = \frac{12}{19} a \frac{1 + (73/24)e^2 + (37/96)e^4}{e(1 - e^2)[1 + (121/304)e^2]}. \quad (4.125)$$

This equation can be integrated analytically, and gives

$$a(e) = c_0 \frac{e^{12/19}}{1 - e^2} \left(1 + \frac{121}{304}e^2\right)^{870/2299}, \quad (4.126)$$

where c_0 is determined by the initial condition $a = a_0$ when $e = e_0$. It is convenient to define the function¹²

$$g(e) = \frac{e^{12/19}}{1 - e^2} \left(1 + \frac{121}{304}e^2\right)^{870/2299}, \quad (4.127)$$

so that $a(e) = c_0 g(e)$; c_0 is fixed by $a_0 = c_0 g(e_0)$, and therefore

$$a(e) = a_0 \frac{g(e)}{g(e_0)}. \quad (4.128)$$

In particular, for $e \ll 1$, we have $g(e) \simeq e^{12/19}$ while, for e close to 1,

$$g(e) \simeq \frac{g_1}{1 - e^2}, \quad (4.129)$$

where $g_1 = (425/304)^{870/2299} \simeq 1.1352$. A plot of the function $g(e)$ is shown in Fig. 4.11.

Orbit circularization

A consequence of the above result is that the eccentricity decreases quite fast, so the effect of the back-reaction of GWs is to circularize the orbit. Consider a compact binary system, say a NS-NS binary, that at an initial time has a_0 very large compared to the radius of the neutron stars, so we are still very far from coalescence, and an eccentricity e_0 not particularly small, neither especially close to one, so that $g(e_0) = O(1)$; let a and e be the values of the semiaxis and eccentricity at a much later time, say when the system is approaching the coalescence phase. Then e will be small and, from eq. (4.128) and the small e limit of $g(e)$, we have

$$a(e) \simeq a_0 \frac{e^{12/19}}{g(e_0)}, \quad (4.130)$$

i.e.

$$e \simeq \left[\frac{a}{a_0} g(e_0) \right]^{19/12}. \quad (4.131)$$

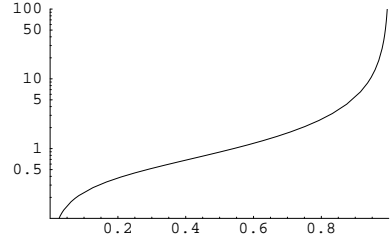


Fig. 4.11 The function $g(e)$, on a logarithmic scale, against e .

¹²This has nothing to do with the function $g(n, e)$ defined in eq. (4.108). Both the notation $g(e)$ for this function and the notation $g(n, e)$ for the function defined by eq. (4.108) are standard in the literature.

For example, consider the Hulse–Taylor binary pulsar (which will be discussed in detail in Chapter 6). Today it has a semimajor axis $a_0 \simeq 2 \times 10^9$ m and a rather large eccentricity $e_0 \simeq 0.617$. By the time that the two stars reach a short separation a , say of the order of a hundred times the radius of the neutron stars, $a = O(10^2 R_{\text{NS}}) \simeq 10^3$ km, we have $a/a_0 = O(5 \times 10^{-4})$ and, since $g(e_0) = O(1)$, the eccentricity has become $e \sim (5 \times 10^{-4})^{19/12} \sim 6 \times 10^{-6}$. The conclusion is that (unless some external interaction perturbs the binary system), long before the two neutron stars approach the coalescence phase, the ellipticity has become zero to very high accuracy, and the two stars move on a circular orbit which shrinks adiabatically.

The time to coalescence

We now compute the time to coalescence, $\tau(a_0, e_0)$, of a binary system that, at an initial time $t_0 = 0$, has semimajor axis a_0 and eccentricity e_0 . When $e_0 = 0$, we found the result in eq. (4.26),

$$\tau(a_0, e_0 = 0) \equiv \tau_0(a_0) = \frac{5}{256} \frac{c^5 a_0^4}{G^3 m^2 \mu}. \quad (4.132)$$

For an elliptic orbit, we can integrate eq. (4.116) requiring $a(t) = 0$ at $t = \tau(a_0, e_0)$ or, equivalently, we can integrate eq. (4.117) requiring $e(t) = 0$ at $t = \tau(a_0, e_0)$, since we have seen that at the coalescence e goes to zero. Since the analytic expression for $a(e)$ is simpler than the form of the inverse function $e(a)$, it is in fact better to use eq. (4.117), so we write

$$\int_0^{\tau(a_0, e_0)} dt = -\frac{15}{304} \frac{c^5}{G^3 m^2 \mu} \int_{e_0}^0 de \frac{a^4(e)(1-e^2)^{5/2}}{e(1+\frac{121}{304}e^2)}, \quad (4.133)$$

that is,

$$\tau(a_0, e_0) = \frac{15}{304} \frac{c^5}{G^3 m^2 \mu} \int_0^{e_0} de \frac{a^4(e)(1-e^2)^{5/2}}{e(1+\frac{121}{304}e^2)}. \quad (4.134)$$

Using eq. (4.128) for $a(e)$, we get

$$\tau(a_0, e_0) = \tau_0(a_0) \frac{48}{19} \frac{1}{g^4(e_0)} \int_0^{e_0} de \frac{g^4(e)(1-e^2)^{5/2}}{e(1+\frac{121}{304}e^2)}. \quad (4.135)$$

Expressing $\tau_0(a_0)$ in terms of the orbital period as in eq. (4.27), we can write the result for $\tau_0(a_0, e_0)$ as

$$\tau_0(a_0, e_0) \simeq 9.829 \text{ Myr} \left(\frac{T_0}{1 \text{ hr}} \right)^{8/3} \left(\frac{M_\odot}{m} \right)^{2/3} \left(\frac{M_\odot}{\mu} \right) F(e_0),$$

(4.136)

where $m = m_1 + m_2$ is the total mass, μ is the reduced mass,

$$F(e_0) = \frac{48}{19} \frac{1}{g^4(e_0)} \int_0^{e_0} de \frac{g^4(e)(1-e^2)^{5/2}}{e(1+\frac{121}{304}e^2)}, \quad (4.137)$$

and $g(e)$ is given in eq. (4.127). For example, the Hulse–Taylor binary pulsar has $e_0 \simeq 0.617$ and $F(e_0) \simeq 0.184$, so its time to coalescence is shorter by a factor $1/F(e_0) \simeq 5.4$, compared to a binary on a circular orbit with the same period. Using the values, $m_1 = m_2 \simeq 1.4M_\odot$ and $T_0 \simeq 7.75$ hr we obtain the time to coalescence of the Hulse–Taylor binary pulsar, $\tau(a_0, e_0) \simeq 300$ Myr.

It can be useful to write some approximate, but more handy expression, for $F(e_0)$. In the limit $e_0 \ll 1$ the integrand can be approximated as $g^4(e)/e$, and $g(e) \simeq e^{12/19}$, see eq. (4.127). Then

$$\begin{aligned} F(e_0) &\simeq \frac{48}{19} \frac{1}{g^4(e_0)} \int_0^{e_0} de e^{48/19-1} \\ &= \frac{1}{g^4(e_0)} e_0^{48/19} \simeq 1, \end{aligned} \quad (4.138)$$

so for $e_0 = 0$ we have $F(0) = 1$ and we get back the result for circular orbit, eq. (4.27). In the opposite limit $e_0 \rightarrow 1^-$, the integral in eq. (4.134) is dominated by the region $e \simeq 1$, where $g(e)$ is given by eq. (4.129). Then we get

$$\begin{aligned} F(e_0) &\simeq \frac{48}{19} \left(\frac{1-e_0^2}{g_1} \right)^4 \int_{e_0}^1 de \frac{1}{[1+(121/304)]} \frac{g_1^4}{(1-e^2)^4} (1-e^2)^{5/2} \\ &\simeq \frac{768}{429} (1-e_0^2)^4 \left[(1-e_0^2)^{-1/2} + O(1) \right] \\ &\simeq \frac{768}{429} (1-e_0^2)^{7/2}. \end{aligned} \quad (4.139)$$

Therefore, in this limit the time to coalescence is smaller than for a circular orbit with the same period, by a factor proportional to $(1-e_0^2)^{7/2}$. This dependence is easily understood from the fact that the system spends most of its lifetime near $a = a_0$, $e = e_0$, where the radiated energy is enhanced by a factor proportional to $(1-e_0^2)^{7/2}$, compared to the circular case, see eqs. (4.74) and (4.75). Comparing the limits $e \rightarrow 0$ and $e \rightarrow 1^-$, we see that it is convenient to define a function $G(e_0)$ from

$$F(e_0) \equiv G(e_0)(1-e_0^2)^{7/2}, \quad (4.140)$$

because $G(e_0)$ is a function everywhere close to one. A plot of $G(e_0)$ from the exact numerical integration of eq. (4.137) is shown in Fig. 4.12. We see that $G(e)$ is always very close to one, within a few per cent at least until $e = 0.6$, where $G(e) \simeq 0.982$, and then, approaching $e = 1$, it raises to reach the finite value $G(1) = 768/425 \simeq 1.80$.

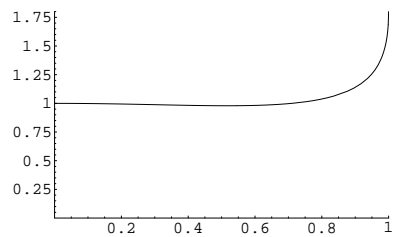


Fig. 4.12 The function $G(e)$, against e . At $e = 1$ $G(e)$ is finite, $G(1) = 768/425 \simeq 1.80$.

4.1.4 Binaries at cosmological distances

Until now, we have implicitly assumed that the binary system that coalesces is at a sufficiently small distance from us, so that the expansion of the Universe during the propagation of the GWs from the source to the detector can be neglected. However, some gravitational-wave detectors, in their advanced stage, have the potential of observing coalescing binaries out to cosmological distances: we will see that advanced ground-based interferometers could detect BH-BH coalescences out to distances of order 1–2 Gpc (corresponding to a redshift $z \sim 0.25\text{--}0.5$), while the space interferometer LISA could detect the coalescence of supermassive black-hole binaries out to redshifts $z \sim 5\text{--}10$. Actually, these will be among the most fascinating sources of GW astronomy. The rich cosmological information that could be extracted from such events will be discussed in Vol. 2. Here we prepare the necessary tools, discussing how the signal of a binary inspiral at a cosmological distance is affected by the expansion of the Universe.

First of all, we recall a few elementary notions of cosmology (see, e.g. Chapter 2 of Kolb and Turner (1990) for more details and derivations), also in order to fix our notation. The expert reader might wish to skip this part and move on to page 194.

A reminder of FRW kinematic

On the Gpc scale, the Universe is to a first approximation isotropic and homogeneous, and is described by the Friedmann–Robertson–Walker (FRW) metric,

$$ds^2 = -c^2 dt^2 + a^2(t) \left[\frac{dr^2}{1 - kr^2} + r^2 d\theta^2 + r^2 \sin^2 \theta d\phi^2 \right], \quad (4.141)$$

¹³Here the word “flat” refers to the geometry of the *spatial* slices. As a four-dimensional space-time, the FRW metric with $k = 0$ is curved.

¹⁴Equation (4.142) also implies a much stronger result. If at $t = t_0$ the velocity has an initial value \mathbf{u}_0 , the integration of eq. (4.142) gives

$$|\mathbf{u}(t)| = \frac{a(t_0)}{a(t)} |\mathbf{u}_0|, \quad (4.143)$$

so spatial velocities are redshifted by the cosmological expansion. In a Universe which expands forever, even test masses with a non-vanishing initial value of \mathbf{u} will eventually come to rest with respect to the observer that uses comoving coordinates.

where the function $a(t)$ is called the scale factor and is determined by the Einstein equations. After an appropriate rescaling of the coordinates, k can take the values $k = 0$ (flat Universe¹³), $k = +1$ (closed Universe) or $k = -1$ (open Universe). We define $a(t)$ as adimensional, so the dimensions of length are carried by r . The coordinates (t, r, θ, ϕ) that appear above are called *comoving* coordinates. This name reflects the property that a test mass, initially at rest in the comoving frame, remains at a fixed value of its comoving coordinates r, θ, ϕ in spite of the expansion of the Universe. This can be proved writing down the geodesic equation in the metric (4.141) (just as we did in Section 1.3, when we understood the physical meaning of the TT gauge). From the $\mu = 0$ component, one finds

$$\frac{d|\mathbf{u}|}{dt} = -\frac{\dot{a}}{a} |\mathbf{u}|, \quad (4.142)$$

where $|\mathbf{u}|^2 = g_{ij} u^i u^j$ is the squared modulus of the spatial part of the four-velocity u^μ . This equation shows that, in the comoving frame, if at $t = t_0$ the modulus of the four-velocity $|\mathbf{u}|$ is zero, then $d|\mathbf{u}|/dt$ also vanishes, so $|\mathbf{u}|$ remains zero at all times.¹⁴ This explains why these coordinates are called comoving: they “stretch” themselves, following

the expansion of the Universe. If, at an initial time, a star has comoving spatial coordinates (r_1, θ_1, ϕ_1) , and a second star has comoving spatial coordinates (r_2, θ_2, ϕ_2) , and if both stars have zero velocity, then at any subsequent time their comoving spatial coordinates will still be (r_1, θ_1, ϕ_1) and (r_2, θ_2, ϕ_2) , respectively, and in particular their coordinate distance will be unchanged, in spite of the expansion of the Universe. Comparing with the discussion in Section 1.3.3, we see that comoving coordinates in a FRW space-time play the same role as TT coordinates in the space-time generated by a gravitational wave.

A star at $r = r_1$ and a star at $r = r_2$ (and with the same values of θ and ϕ) have a *coordinate* distance $r = r_2 - r_1$. Of course, this quantity has no physical meaning, since coordinates are arbitrary in general relativity. The physical spatial distance is the *proper* spatial distance, $r_{\text{phys}}(t)$, given by

$$dr_{\text{phys}}^2 = g_{ij} dx^i dx^j. \quad (4.144)$$

If the first star is at the origin and the second is at comoving radial coordinate r , then eq. (4.141) gives $dr_{\text{phys}}^2 = a^2(t) dr^2 / (1 - kr^2)$, and therefore their physical distance is

$$r_{\text{phys}}(t) = a(t) \int_0^r \frac{dr}{(1 - kr^2)^{1/2}}. \quad (4.145)$$

In particular, for a flat Universe ($k = 0$) we have $r_{\text{phys}}(t) = a(t)r$.

Consider now a source located at comoving distance r , that emits signals (such as electromagnetic or gravitational waves) which travel at the speed of light, and are later received by an observer located at $r = 0$. Suppose that the source emits a wavecrest at a time t_{emis} . The signal will be detected by the observer at a time t_{obs} , which is obtained by imposing $ds^2 = 0$ in eq. (4.141). This gives

$$\int_{t_{\text{emis}}}^{t_{\text{obs}}} \frac{c dt}{a(t)} = \int_0^r \frac{dr}{(1 - kr^2)^{1/2}}. \quad (4.146)$$

Suppose that a second wavecrest is emitted at time $t_{\text{emis}} + \Delta t_{\text{emis}}$, and received at $t_{\text{obs}} + \Delta t_{\text{obs}}$. Then

$$\int_{t_{\text{emis}} + \Delta t_{\text{emis}}}^{t_{\text{obs}} + \Delta t_{\text{obs}}} \frac{c dt}{a(t)} = \int_0^r \frac{dr}{(1 - kr^2)^{1/2}}. \quad (4.147)$$

Observe that the right-hand side is always the same, since the source is at a fixed comoving distance. Then, taking the difference between these two equations, the right-hand sides cancel and, to linear order in Δt_{emis} , one finds

$$\Delta t_{\text{obs}} = \frac{a(t_{\text{obs}})}{a(t_{\text{emis}})} \Delta t_{\text{emis}}. \quad (4.148)$$

In an expanding Universe, there is therefore a dilatation of the time measured by the observer, with respect to the time of the source. The *redshift* of the source, z , is defined by

$$1 + z = \frac{a(t_{\text{obs}})}{a(t_{\text{emis}})}. \quad (4.149)$$

Equation (4.148) means that the time t_{obs} measured by the observer's clock, and the time t_s measured by the source clock are related by

$$dt_{\text{obs}} = (1 + z)dt_s. \quad (4.150)$$

As a consequence, any frequency measured by the observer, $f^{(\text{obs})}$, is related to the corresponding frequency measured in the source frame, $f^{(s)}$, by

$$f^{(\text{obs})} = \frac{f^{(s)}}{1 + z}, \quad (4.151)$$

and the wavelengths are related by

$$\lambda^{(\text{obs})} = (1 + z)\lambda^{(s)}. \quad (4.152)$$

To complete our quick tour of kinematics in a FRW space-time, we need the definition of luminosity distance and the relation between the luminosity distance and the redshift. Let \mathcal{F} be the energy flux (energy per unit time per unit area) measured in the observer's frame, and let \mathcal{L} be the absolute luminosity of the source, i.e. the power that it radiates in its rest frame,

$$\mathcal{L} = \frac{dE_s}{dt_s}, \quad (4.153)$$

where E_s is the energy measured in the source proper frame. The luminosity distance d_L is then defined by

$$\mathcal{F} = \frac{\mathcal{L}}{4\pi d_L^2}. \quad (4.154)$$

In the absence of redshift, the energy E_{obs} measured in the observer frame is the same as the energy E_s measured in the source frame, and $dt_{\text{obs}} = dt_s$, so

$$\frac{dE_{\text{obs}}}{dt_{\text{obs}}} = \frac{dE_s}{dt_s}. \quad (4.155)$$

When it arrives at the detector, the energy radiated by an isotropic source is distributed over an area $A = 4\pi r^2$, and therefore

$$\begin{aligned} \mathcal{F} &= \frac{1}{4\pi r^2} \frac{dE_{\text{obs}}}{dt_{\text{obs}}} \\ &= \frac{1}{4\pi r^2} \frac{dE_s}{dt_s} \\ &= \frac{\mathcal{L}}{4\pi r^2}, \end{aligned} \quad (4.156)$$

which shows that, in the absence of redshift, d_L is just equal to the distance r of the source. In an expanding Universe, however, the energy observed is redshifted,

$$E_{\text{obs}} = \frac{E_s}{1 + z} \quad (4.157)$$

(the quickest derivation of this result makes use of eq. (4.151), together with the quantum relation $E = \hbar\omega$, but this is a kinematic property that can also be derived purely classically), while $dt_{\text{obs}} = (1 + z)dt_s$. Therefore

$$\frac{dE_{\text{obs}}}{dt_{\text{obs}}} = \frac{1}{(1 + z)^2} \frac{dE_s}{dt_s}. \quad (4.158)$$

Furthermore, using the FRW metric (4.141), we find that, at time t , the surface of a sphere with comoving radius r is $4\pi a^2(t)r^2$ (independently of k), so when the radiation arrives at the detector it is spread over an area $A = 4\pi a^2(t_{\text{obs}})r^2$. Therefore

$$\mathcal{F} = \frac{\mathcal{L}}{4\pi a^2(t_{\text{obs}})r^2(1 + z)^2}, \quad (4.159)$$

which means that (setting t_{obs} equal to the present time t_0)

$$d_L = (1 + z) a(t_0) r.$$

(4.160)

For small values of the redshift, we can express d_L as a function of z as follows. We perform a Taylor expansion of $a(t)$ around the present epoch $t = t_0$,

$$\frac{a(t)}{a(t_0)} = 1 + H_0(t - t_0) - \frac{1}{2}q_0 H_0^2(t - t_0)^2 + \dots \quad (4.161)$$

where

$$H_0 \equiv \frac{\dot{a}(t_0)}{a(t_0)}, \quad (4.162)$$

is the *Hubble constant* (or, more appropriately, the present value of the Hubble parameter $H(t) = \dot{a}/a$), while

$$\begin{aligned} q_0 &\equiv -\frac{\ddot{a}(t_0)}{a(t_0)} \frac{1}{H_0^2} \\ &= -\frac{a(t_0)\ddot{a}(t_0)}{\dot{a}^2(t_0)} \end{aligned} \quad (4.163)$$

is called the *deceleration parameter*.¹⁵ Using $a(t_0)/a(t) = 1+z$, eq. (4.161) can be inverted to give perturbatively $(t - t_0)$ as a function of z , while inserting the expansion (4.161) into eq. (4.146) gives $a(t_0)r$, as an expansion in powers of $(t - t_0)$ and therefore of z . The result is (see, e.g. Kolb and Turner (1990), pages 41–42 for the explicit calculation)

$$\frac{H_0 d_L}{c} = z + \frac{1}{2}(1 - q_0)z^2 + \dots$$

(4.164)

The first term of this expansion just gives the Hubble law $z \simeq (H_0/c)d_L$, which states that redshifts are proportional to distances. The term $O(z^2)$ is the correction to the linear law for moderate redshifts. For large redshifts, the Taylor series is no longer appropriate, and the whole expansion

¹⁵This name is somewhat unfortunate, since it suggests that presently the expansion of the Universe is decelerating. Rather, we will see below that the evidence from the observation of type Ia supernovae indicates that presently the expansion of the Universe is accelerating, i.e. $q_0 < 0$.

history of the Universe is encoded in a function $d_L(z)$. As an example, for a flat Universe ($k = 0$), eq. (4.146) gives

$$\int_{t_{\text{emis}}}^{t_{\text{obs}}} \frac{c dt}{a(t)} = r. \quad (4.165)$$

Differentiating the relation $1 + z(t) = a(t_0)/a(t)$ we get

$$\frac{dt}{a(t)} = -\frac{1}{a(t_0)} \frac{dz}{H(z)}, \quad (4.166)$$

so eq. (4.165) becomes

$$a(t_0)r = c \int_0^z \frac{dz'}{H(z')}, \quad (4.167)$$

where the upper limit in the integral is the redshift z corresponding to the emission time t_{emis} while, in the lower limit of the integral, we used the fact that at the present time $t = t_0$ we have $z = 0$. Then eq. (4.160) gives

$$d_L(z) = c(1+z) \int_0^z \frac{dz'}{H(z')}, \quad (4.168)$$

or, taking a derivative with respect to z ,

$$\frac{c}{H(z)} = \frac{d}{dz} \left(\frac{d_L(z)}{1+z} \right). \quad (4.169)$$

Thus, from the knowledge of $d_L(z)$, we can get the Hubble parameter $H(z)$. This shows that the luminosity distance function $d_L(z)$ is a very important quantity, which encodes the whole expansion history of the Universe.

From the definition (4.154) we see that, in order to determine the luminosity distance of a source, we need to know both \mathcal{F} and \mathcal{L} . The flux \mathcal{F} is the quantity that is directly measured by the observer. The problem is to know the intrinsic luminosity \mathcal{L} of the source. This is possible if we have a “standard candle”, that is, a source whose absolute luminosity is known. The redshift of an electromagnetic source can be determined from the redshift of its spectral lines, and then we get the corresponding value of $d_L(z)$. Up to distances of order 25 Mpc, standard candles are provided by Cepheid variable stars while, at larger cosmological distances, a standard candle is provided by Type Ia supernovae.¹⁶ The Hubble constant is usually written as $H_0 = h_0 \times 100 \text{ km s}^{-1} \text{ Mpc}^{-1}$, and the most recent determination of h_0 is $h_0 = 0.73 \pm 0.03$, while the value of the deceleration parameter is $q_0 = -0.74 \pm 0.18$.

Propagation of GWs in a FRW Universe

We can now discuss how the waveform produced by a binary inspiral is modified by the propagation across cosmological distances. First of all,

¹⁶As we will discuss in Vol. II, Type Ia supernovae are modeled as carbon-oxygen white dwarfs, in a close binary system. They accrete matter from their companion until their mass reaches a critical value $\simeq 1.30M_\odot$, and then they explode as supernovae. Since the mass of the star at the moment of the explosion is always the same, the light curves of Type Ia supernovae are sufficiently similar to each other and, after applying corrections that take into account a relation between the shape of the light curve and the peak luminosity, they can be used as standard candles.

we can define a *local* wave zone, as the region where the distance to the source is sufficiently large so that the gravitational field already has the $1/r$ behavior characteristic of waves, but still sufficiently small, so that the expansion of the Universe is negligible. During the propagation of the GW in the local wave zone, the scale factor $a(t)$ does not change appreciably, so in the local wave zone physical distances can be written as $r_{\text{phys}} = a(t_{\text{emis}})r$, where r is the comoving distance and t_{emis} is (any) time of emission,¹⁷ so r_{phys} differs from r by just a constant normalization factor. Using eq. (4.29) we see that the GW produced by a binary inspiral, at a distance $r_{\text{phys}} = a(t_{\text{emis}})r$ in the local wave zone, can be written as

$$h_+(t_s) = h_c(t_s^{\text{ret}}) \frac{1 + \cos^2 \iota}{2} \cos \left[2\pi \int_{t_s^{\text{ret}}}^{t_s^{\text{ret}}} dt'_s f_{\text{gw}}^{(s)}(t'_s) \right], \quad (4.170)$$

$$h_\times(t_s) = h_c(t_s^{\text{ret}}) \cos \iota \sin \left[2\pi \int_{t_s^{\text{ret}}}^{t_s^{\text{ret}}} dt'_s f_{\text{gw}}^{(s)}(t'_s) \right], \quad (4.171)$$

where

$$h_c(t_s^{\text{ret}}) = \frac{4}{a(t_{\text{emis}})r} \left(\frac{GM_c}{c^2} \right)^{5/3} \left(\frac{\pi f_{\text{gw}}^{(s)}(t_s^{\text{ret}})}{c} \right)^{2/3}. \quad (4.172)$$

Here time is the time t_s measured by the clock of the source (and t_s^{ret} is the corresponding value of retarded time) and the GW frequency f_{gw} is the one associated to this definition of time, that we denote by $f_{\text{gw}}^{(s)}$. They are related to the quantities measured by the observer which is at a cosmological distance, very far from the local wave zone, by eqs. (4.150) and (4.151). The dependence of $f_{\text{gw}}^{(s)}$ on t_s is given by eq. (4.19), that we rewrite as

$$f_{\text{gw}}^{(s)}(\tau_s) = \frac{1}{\pi} \left(\frac{5}{256} \frac{1}{\tau_s} \right)^{3/8} \left(\frac{GM_c}{c^3} \right)^{-5/8}, \quad (4.173)$$

where τ_s is the time to coalescence measured by the source's clock.

To compute how this waveform propagates across cosmological distances to reach the observer, we should use eq. (1.179), that describes the propagation of GWs in a curved space-time, specializing it to the FRW metric. Actually, it is instructive to start from a simpler problem, namely the propagation of a *scalar* perturbation ϕ in the FRW metric. In this case, the propagation equation is simply $\square \phi = 0$ where, on scalar functions, the curved-space d'Alembertian $\square = D_\mu D^\mu$ can be written as

$$\square = \frac{1}{\sqrt{-g}} \partial_\mu (\sqrt{-g} g^{\mu\nu} \partial_\nu). \quad (4.174)$$

To solve this wave equation in the FRW metric, it is convenient to introduce the conformal time η , from

$$d\eta = \frac{dt}{a(t)}, \quad (4.175)$$

¹⁷We do not need to track the change of the scale factor during the observed part of the emission process, so we do not need to be more precise about t_{emis} .

i.e.

$$\eta = \int^t \frac{dt'}{a(t')}, \quad (4.176)$$

so the FRW metric reads (limiting ourselves for simplicity to $k = 0$)

$$ds^2 = a^2(\eta) [-c^2 d\eta^2 + dr^2 + r^2 d\theta^2 + r^2 \sin^2 \theta d\phi^2]. \quad (4.177)$$

We want to know how a solution which decreases as $1/r$ evolves in this space-time. We therefore search for spherically symmetric solutions of the form $\phi(r, \eta) = (1/r)f(r, \eta)$. The equation $\square\phi = 0$ in this metric then becomes

$$\begin{aligned} 0 &= \partial_\mu (\sqrt{-g} g^{\mu\nu} \partial_\nu) \phi \\ &= -\frac{1}{c^2} \partial_\eta [a^2(\eta) r^2 \partial_\eta \phi] + \partial_r [a^2(\eta) r^2 \partial_r \phi] \\ &= \partial_r^2 f - f'' - 2 \frac{a'}{a} f', \end{aligned} \quad (4.178)$$

where the prime denotes derivation with respect to $c\eta$, $f' = (1/c)\partial f/\partial\eta$. It is convenient to search for the solution in the form

$$f(r, \eta) = \frac{1}{a(\eta)} g(r, \eta). \quad (4.179)$$

Then $g(r, \eta)$ satisfies the equation

$$\partial_r^2 g - g'' + \frac{a''}{a} g = 0. \quad (4.180)$$

¹⁸More precisely, we are interested in the evolution in a matter-dominated Universe (since we need that stars already formed!). In this case the FRW scale factor evolves as $a(\eta) \sim \eta^2$ and $a''/a = 2/\eta^2$. Instead, in a radiation-dominated Universe, $a(\eta) \sim \eta$ and $a''/a = 0$.

Now observe that $a''/a \sim \eta^{-2}$, for dimensional reasons.¹⁸ Then we see that eq. (4.180) has the approximate solutions

$$g(r, \eta) \simeq e^{\pm i\omega(\eta-r/c)}, \quad (4.181)$$

as long as $\omega^2 \gg 1/\eta^2$, since in this case in eq. (4.180) the term $(a''/a)g \sim g/\eta^2$ is negligible with respect to $-g'' = \omega^2 g$, and we are left with a simple wave equation $\partial_r^2 g - g'' \simeq 0$. More generally, any function of the form $g(\eta - r/c)$ is a solution, as long as in Fourier space it contains only frequencies such that $\eta^2\omega^2 \gg 1$. In conclusion, we have the approximate solution

$$\phi(r, \eta) \simeq \frac{1}{ra(\eta)} g(\eta - r/c). \quad (4.182)$$

We can normalize conformal time so that, at the present epoch, $\eta = t$. Then, the wave observed today at a detector reads¹⁹

$$\phi(r, t) \simeq \frac{1}{ra(t_0)} g(t - r/c). \quad (4.183)$$

Thus, the propagation of a scalar wave through a FRW background is very simple. Compared to the solution in the absence of cosmological expansion, we just need to replace the factor $1/r$ with $1/[ra(t)]$.

Now we can turn to the propagation equation of a tensor perturbation $h_{\mu\nu}$, eq. (1.179). It is in principle straightforward to write down this

¹⁹Obviously, since $a(\eta)$ evolves appreciably only on a cosmological time-scale, once we fix $\eta = t$ at one moment of time in the present epoch, we have $\eta = t$, with exceedingly good accuracy, over the whole time-scale relevant for GW observation at a detector, so we can write $g(\eta - r/c) = g(t - r/c)$ for all these values of time. For the same reason, $a(\eta)$ can be written simply as a constant factor $a(t_0)$.

equation explicitly in the FRW metric (4.177); we then find that, once we disregard all terms $O(1/\eta^2)h_{\mu\nu}$ with respect to the terms $O(\omega^2)h_{\mu\nu}$, we get back the same equation that we discussed for scalar perturbations. Of course, this is not surprising. Simply, the condition $\eta^2\omega^2 \gg 1$ demands that ω be large with respect to the typical scale of the background space-time and this is nothing but the condition that defines the geometrical optics approximation. In this approximation all massless particles follow null geodesics, independently of their spin, as we saw in Section 1.5.1.

Then we find that, to leading order:

- The two polarizations h_+ and h_\times decouple, that is each one satisfies a wave equation which is independent of the other. This means that the propagation does not introduce a mixing among them. For instance, if we observe the binary edge-on ($\cos \iota = 0$), we see from eqs. (4.170) and (4.171) that in the local wave zone the GW has only the plus polarization; then, even after propagation across a cosmological distance, the wave will still have only the plus polarization. This is as expected, since we already saw in Section 1.5.1 that the polarization tensor of GWs is parallel-propagated along the null geodesics.
- Both h_+ and h_\times satisfy the same equation that we discussed above for a scalar field.

The conclusion is that, after propagation from the source to the detector, the GW amplitude from an inspiraling binary is still given by eqs. (4.170) and (4.171), but with h_c in eq. (4.172) replaced by

$$h_c(t_s^{\text{ret}}) = \frac{4}{a(t_0)r} \left(\frac{GM_c}{c^2} \right)^{5/3} \left(\frac{\pi f_{\text{gw}}^{(s)}(t_s^{\text{ret}})}{c} \right)^{2/3}, \quad (4.184)$$

as long as the geometrical optics approximation is valid. Today this condition is $2\pi f_{\text{gw}} \gg t_0^{-1}$, where t_0 is the present age of the Universe, and therefore is satisfied with extreme accuracy by all GWs in which we are interested (in fact, by all GWs whose wavelength is smaller than the present Hubble size of the Universe!). More generally, also the condition $2\pi f_{\text{gw}} \gg t_{\text{emis}}^{-1}$ is extremely well satisfied, so the geometrical optics approximation is excellent for the whole propagation of the GW from the source to the detector.

In principle eqs. (4.170) and (4.171), together with eq. (4.184), provide the final result. However, it is convenient to express them in terms of the time t_{obs} and the GW frequency $f_{\text{gw}}^{(\text{obs})}$ measured by the observer, rather than using the time t_s measured by the source and its associated frequency. Using eqs. (4.150) and (4.151), we see that, in eqs. (4.170) and (4.171),

$$\int_{t_s^{\text{ret}}}^{t_s^{\text{ret}}} dt'_s f_{\text{gw}}^{(s)}(t'_s) = \int_{t_{\text{obs}}^{\text{ret}}}^{t_{\text{obs}}^{\text{ret}}} dt'_{\text{obs}} f_{\text{gw}}^{(\text{obs})}(t'_{\text{obs}}) \quad (4.185)$$

since the redshift in dt cancels the redshift in f . Writing

$$f_{\text{gw}}^{(s)} = (1+z)f_{\text{gw}}^{(\text{obs})}, \quad (4.186)$$

eq. (4.184) becomes

$$\begin{aligned} h_c(t_{\text{obs}}^{\text{ret}}) &= \frac{4}{a(t_0)r} (1+z)^{2/3} \left(\frac{GM_c}{c^2} \right)^{5/3} \left(\frac{\pi f_{\text{gw}}^{(\text{obs})}(t_{\text{obs}}^{\text{ret}})}{c} \right)^{2/3} \\ &= \frac{4}{d_L(z)} (1+z)^{5/3} \left(\frac{GM_c}{c^2} \right)^{5/3} \left(\frac{\pi f_{\text{gw}}^{(\text{obs})}(t_{\text{obs}}^{\text{ret}})}{c} \right)^{2/3}, \end{aligned} \quad (4.187)$$

where in the second line we expressed the result in terms of the luminosity distance, using eq. (4.160). We see that, if we define the quantity

$$\mathcal{M}_c \equiv (1+z)M_c = (1+z)\mu^{3/5}m^{2/5}, \quad (4.188)$$

we get

$$h_c(t_{\text{obs}}^{\text{ret}}) = \frac{4}{d_L} \left(\frac{G\mathcal{M}_c}{c^2} \right)^{5/3} \left(\frac{\pi f_{\text{gw}}^{(\text{obs})}(t_{\text{obs}}^{\text{ret}})}{c} \right)^{2/3}, \quad (4.189)$$

and therefore the GW amplitude takes the same form as in the absence of cosmological expansion, with the replacements $r \rightarrow d_L$ and $M_c \rightarrow \mathcal{M}_c$. In the general case of non-vanishing redshift, we will reserve the name “chirp mass” for \mathcal{M}_c , rather than for M_c . From eqs. (4.151) and (4.173), we find that the dependence of $f_{\text{gw}}^{(\text{obs})}$ on t_{obs} is given by

$$\begin{aligned} f_{\text{gw}}^{(\text{obs})}(t_{\text{obs}}^{\text{ret}}) &= \frac{1}{1+z} f_{\text{gw}}^{(s)}(t_s^{\text{ret}}) \\ &= \frac{1}{1+z} \frac{1}{\pi} \left(\frac{5}{256} \frac{1+z}{\tau_{\text{obs}}} \right)^{3/8} \left(\frac{GM_c}{c^3} \right)^{-5/8} \\ &= \frac{1}{\pi} \left(\frac{5}{256} \frac{1}{\tau_{\text{obs}}} \right)^{3/8} \left(\frac{G\mathcal{M}_c}{c^3} \right)^{-5/8}, \end{aligned} \quad (4.190)$$

²⁰Since $\tau = t_{\text{coal}}^{\text{ret}} - t_{\text{obs}}^{\text{ret}} = t_{\text{coal}} - t$, we have $\tau = \tau^{\text{ret}}$, and the result can be written just as a function of the observer’s time, rather than of the observer’s retarded time.

where $\tau_{\text{obs}} = (1+z)\tau_s$ is the time to coalescence measured by the observer’s clock.²⁰ Then, even the dependence of $f_{\text{gw}}^{(\text{obs})}$ on t_{obs} is formally the same as the relation at $z = 0$, once we replace $M_c \rightarrow \mathcal{M}_c$. This result is due to the fact that, when $z = 0$, both the GW amplitude and the evolution of the frequency with time are determined by the only time-scale of the problem, which is GM_c/c^3 . What we are actually finding is that, in a cosmological context, this time-scale is redshifted, $GM_c/c^3 \rightarrow (1+z)GM_c/c^3$. This is a very natural result, which formally amounts to the replacement $M_c \rightarrow (1+z)\mathcal{M}_c$.

To summarize, the signal received by the observer from a binary inspiral at redshift z , when expressed in terms of the observer time t_{obs} , or equivalently in terms of the time to coalescence measured by the observer, τ_{obs} , is given by

$$h_+(\tau_{\text{obs}}) = h_c(\tau_{\text{obs}}) \frac{1 + \cos^2 \iota}{2} \cos [\Phi(\tau_{\text{obs}})], \quad (4.191)$$

$$h_\times(\tau_{\text{obs}}) = h_c(\tau_{\text{obs}}) \cos \iota \sin [\Phi(\tau_{\text{obs}})] \quad (4.192)$$

where (compare with eq. (4.30)),

$$\Phi(\tau_{\text{obs}}) = -2 \left(\frac{5G\mathcal{M}_c(z)}{c^3} \right)^{-5/8} \tau_{\text{obs}}^{5/8} + \Phi_0, \quad (4.193)$$

$$h_c(\tau_{\text{obs}}) = \frac{4}{d_L(z)} \left(\frac{G\mathcal{M}_c(z)}{c^2} \right)^{5/3} \left(\frac{\pi f_{\text{gw}}^{(\text{obs})}(\tau_{\text{obs}})}{c} \right)^{2/3}, \quad (4.194)$$

and

$$f_{\text{gw}}^{(\text{obs})}(\tau_{\text{obs}}) = \frac{1}{\pi} \left(\frac{5}{256} \frac{1}{\tau_{\text{obs}}} \right)^{3/8} \left(\frac{G\mathcal{M}_c(z)}{c^3} \right)^{-5/8}. \quad (4.195)$$

The latter equation implies also that

$$\dot{f}_{\text{gw}}^{(\text{obs})} = \frac{96}{5} \pi^{8/3} \left(\frac{G\mathcal{M}_c(z)}{c^3} \right)^{5/3} [f_{\text{gw}}^{(\text{obs})}]^{11/3}. \quad (4.196)$$

In other words, we have the following modifications compared to the case $z = 0$:

- The observed frequency is redshifted with respect to the frequency measured in the source frame, $f^{(\text{obs})} = f^{(s)}/(1+z)$. For instance, we saw below eq. (4.40) that the inspiral of a NS-NS binary system terminates, and the two stars merge, when the intrinsic orbital frequency of the source, in the source frame, is of order 800 Hz. This means that, from the point of view of the observer, the orbital frequency of the source will sweep up to a maximum value of order $800 \text{ Hz}/(1+z)$. For example, for a NS-NS coalescence at $z \simeq 2$, the maximum value of the source orbital frequency, in the observer frame, is of order 270 Hz, and the quadrupole radiation emitted in the inspiral phase will be cutoff at twice this value.
- The overall factor $1/r$ in the GW amplitude is replaced by $1/d_L(z)$.
- M_c is replaced by $\mathcal{M}_c = (1+z)M_c$.

A very interesting consequence of the above results is the following. Suppose that we can measure the amplitudes of both polarizations h_+, h_\times , as well as $\dot{f}_{\text{gw}}^{(\text{obs})}$. The amplitude of h_+ is $h_c(1 + \cos^2 \iota)/2$, while the amplitude of h_\times is $h_c \cos \iota$. From their ratio, we can therefore obtain the value of $\cos \iota$, that is, the inclination of the orbit with respect to the line of sight. On the other hand, eq. (4.196) shows that, if we measure the value of $\dot{f}_{\text{gw}}^{(\text{obs})}$ corresponding to a given value of $f_{\text{gw}}^{(\text{obs})}$, we get the chirp mass \mathcal{M}_c . Now in the expression for h_+ and h_\times all parameters have been fixed, except $d_L(z)$.²¹ This means that, from the measured value of h_+ (or of h_\times) we can now read d_L . If, at the same time, we can measure the redshift z of the source, we have found a gravitational standard candle, and we can use it to measure the Hubble parameter $H(z)$, compare with eq. (4.168). We will discuss in Vol. 2 the rich cosmological information that can be obtained from this type of measurements, as well as the methods proposed to have an associated measure of the redshift (either from optical observations or from GW observations themselves), and the associated experimental uncertainties.

²¹Observe that the ellipticity of the orbit does not enter since, as we discussed in Section 4.1.3, by the time that the stars approach the coalescence stage, angular momentum losses have circularized the orbit to great accuracy. Therefore it is legitimate to use the results for circular orbits, as we have done in this section, and there is no free parameter associated to the ellipticity.

4.2 Radiation from rotating rigid bodies

The production of GWs from a rotating rigid body is of great importance, in particular for application to isolated neutron stars. In Section 4.2.1 we examine the production of GWs in the simplest situation, i.e. the radiation emitted by a rigid body which rotates around one of its principal axes. Then, in Section 4.2.2, we will discuss the more complicated situation where the rotation axis does not coincide with a principal axis, and therefore there is a motion of precession.

Let us first recall, from elementary mechanics (see e.g. Landau and Lifshitz, Vol. I 1976), a few basic notions of kinematics of rigid bodies. A rigid body is characterized by its inertia tensor

$$I^{ij} = \int d^3x \rho(\mathbf{x}) (r^2 \delta^{ij} - x^i x^j). \quad (4.197)$$

where ρ is the mass density. Since any hermitian matrix can be diagonalized by an appropriate rotation, there exists an orthogonal frame where I_{ij} is diagonal. The corresponding axes are called the principal axes of the body, and the eigenvalues I_1, I_2, I_3 are called the principal moments of inertia. We will refer to the frame where I_{ij} is diagonal as the “body frame”. Denoting by x'_i the coordinates in the body frame, we have

$$I_1 = \int d^3x' \rho(\mathbf{x}') (x'_2{}^2 + x'_3{}^2), \quad (4.198)$$

$$I_2 = \int d^3x' \rho(\mathbf{x}') (x'_1{}^2 + x'_3{}^2), \quad (4.199)$$

$$I_3 = \int d^3x' \rho(\mathbf{x}') (x'_1{}^2 + x'_2{}^2). \quad (4.200)$$

From these explicit expressions we see that $I_1 + I_2 \geq I_3$. Therefore each principal moment of inertia must be smaller or equal than the sum of the other two. The identity $I_1 + I_2 = I_3$ holds only if $\rho(\mathbf{x}) \sim \delta(x_3)$, that is, for a bidimensional configuration of matter.

A simple geometry is that of an ellipsoid with semiaxes a, b, c , uniform density, and mass m . In this case, eqs. (4.198)–(4.200) give

$$I_1 = \frac{m}{5} (b^2 + c^2), \quad (4.201)$$

$$I_2 = \frac{m}{5} (a^2 + c^2), \quad (4.202)$$

$$I_3 = \frac{m}{5} (a^2 + b^2). \quad (4.203)$$

If the body rotates with angular velocity $\boldsymbol{\omega}$, its angular momentum is

$$\mathbf{J}_i = I_{ij} \omega_j. \quad (4.204)$$

We denote by (J'_1, J'_2, J'_3) and $(\omega'_1, \omega'_2, \omega'_3)$ the components of the angular momentum and of the angular velocity, respectively, in the body frame. Then $J'_1 = I_1 \omega'_1$, $J'_2 = I_2 \omega'_2$ and $J'_3 = I_3 \omega'_3$. Observe that the direction

of $\boldsymbol{\omega}$ is different from the direction of \mathbf{J} unless either $I_1 = I_2 = I_3$ (which holds only for a spherical object) or the rotation is around one of the principal axes, e.g. when, $\omega'_1 = \omega'_2 = 0$. The rotational kinetic energy is

$$E_{\text{rot}} = \frac{1}{2} I_{ij} \omega_i \omega_j, \quad (4.205)$$

so in the body frame it is given simply by

$$E_{\text{rot}} = \frac{1}{2} (I_1 \omega'_1{}^2 + I_2 \omega'_2{}^2 + I_3 \omega'_3{}^2). \quad (4.206)$$

If we denote by $\hat{\boldsymbol{\omega}}$ the unit vector in the direction of the axis of rotation, so that $\boldsymbol{\omega} = \omega \hat{\boldsymbol{\omega}}$, then $E_{\text{rot}} = (1/2)I\omega^2$, where $I = I_{ij}\hat{\omega}_i \hat{\omega}_j$ is called the moment of inertia about the axis of rotation.

4.2.1 GWs from rotation around a principal axis

We first consider the situation in which the body rotates rigidly about one of its principal axes. We denote by (x'_1, x'_2, x'_3) the coordinates in the body frame. This reference frame, by definition, is attached to the body and rotates with it. We take the x'_3 axis as the axis around which the body rotates, and we denote by ω_{rot} the corresponding angular velocity. We also introduce a fixed reference frame, with coordinates (x_1, x_2, x_3) , oriented so that $x'_3 = x_3$, see Fig. 4.13. In both frames, the origin of the axes coincides with the center-of-mass of the body. The two frames are related by a time-dependent rotation matrix \mathcal{R}_{ij} ,

$$x'_i = \mathcal{R}_{ij} x_j, \quad (4.207)$$

with

$$\mathcal{R}_{ij} = \begin{pmatrix} \cos \omega_{\text{rot}} t & \sin \omega_{\text{rot}} t & 0 \\ -\sin \omega_{\text{rot}} t & \cos \omega_{\text{rot}} t & 0 \\ 0 & 0 & 1 \end{pmatrix}_{ij}. \quad (4.208)$$

We denote by $I'_{ij} = \text{diag}(I_1, I_2, I_3)$ the inertia tensor in the (x'_1, x'_2, x'_3) coordinate system, and by I_{ij} its components in the (x_1, x_2, x_3) frame. Thus, I'_{ij} is a constant matrix, while I_{ij} is time-dependent. The fact that the moment of inertia is a tensor implies that

$$\begin{aligned} I'_{ij} &= \mathcal{R}_{ik} \mathcal{R}_{jl} I_{kl} \\ &= (\mathcal{R} I \mathcal{R}^T)_{ij}, \end{aligned} \quad (4.209)$$

where \mathcal{R}^T is the transpose matrix, and therefore

$$I = \mathcal{R}^T I' \mathcal{R}. \quad (4.210)$$

This gives

$$\begin{aligned} I_{11} &= I_1 \cos^2 \omega_{\text{rot}} t + I_2 \sin^2 \omega_{\text{rot}} t \\ &= \frac{I_1 + I_2}{2} + \frac{I_1 - I_2}{2} \cos 2\omega_{\text{rot}} t, \end{aligned} \quad (4.211)$$

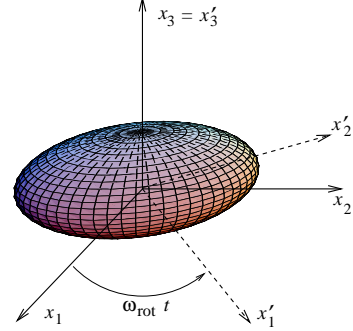


Fig. 4.13 The principal axes (x'_1, x'_2, x'_3) , which rotate with the rigid body, and the fixed axes (x_1, x_2, x_3) .

$$I_{12} = \frac{I_1 - I_2}{2} \sin 2\omega_{\text{rot}} t, \quad (4.212)$$

$$\begin{aligned} I_{22} &= I_1 \sin^2 \omega_{\text{rot}} t + I_2 \cos^2 \omega_{\text{rot}} t \\ &= \frac{I_1 + I_2}{2} - \frac{I_1 - I_2}{2} \cos 2\omega_{\text{rot}} t, \end{aligned} \quad (4.213)$$

$$I_{33} = I_3, \quad (4.214)$$

while $I_{13} = I_{23} = 0$. Recall that in the quadrupole approximation the GW amplitude depends on the second moment of the mass density M^{ij} . From eq. (4.197) we see that M^{ij} differ from I^{ij} by an overall minus sign, and for the absence of the trace term.²² However, the trace of a tensor is invariant under rotation; in fact, from eq. (4.209), using the cyclic property of the trace and the property of the orthogonal matrices that $\mathcal{R}\mathcal{R}^T$ is equal to the identity matrix, we have $\text{Tr } I = \text{Tr } [\mathcal{R}^T I' \mathcal{R}] = \text{Tr } [I' \mathcal{R} \mathcal{R}^T] = \text{Tr } I'$. Since $\text{Tr } I' = I_1 + I_2 + I_3$ is a constant, we have

$$M_{ij} = -I_{ij} + c_{ij}, \quad (4.215)$$

where c_{ij} are constants. In the computation of the GW amplitude only the second time derivative of M_{ij} enters and therefore the explicit value of the constants is irrelevant, and we can write

$$M_{11} = -\frac{I_1 - I_2}{2} \cos 2\omega_{\text{rot}} t + \text{constant}, \quad (4.216)$$

$$M_{12} = -\frac{I_1 - I_2}{2} \sin 2\omega_{\text{rot}} t + \text{constant}, \quad (4.217)$$

$$M_{22} = +\frac{I_1 - I_2}{2} \cos 2\omega_{\text{rot}} t + \text{constant}, \quad (4.218)$$

while M_{13} , M_{23} and M_{33} are constant. We observe that, in our setting in which the body rotates around its principal axis x'_3 , there is a time-varying second mass moment only if $I_1 \neq I_2$, which is quite clear geometrically. We also see that M_{ij} is a periodic function of $2\omega_{\text{rot}} t$, so we already understand that we have production of GWs with a frequency $\omega_{\text{gw}} = 2\omega_{\text{rot}}$.

We can now compute the GW amplitude received by an observer at a distance r , whose line-of-sight makes an angle ι with the direction of the spin of the star, i.e. with the x_3 axis, see Fig. 4.14. We use eq. (3.72), setting with $\theta = \iota$ and, without loss of generality, we orient the fixed frame (x_1, x_2, x_3) so that the observer is at $\phi = 0$.

Inserting the expressions (4.216)–(4.218) for M_{ij} and taking into account that $\ddot{M}_{13} = \ddot{M}_{23} = \ddot{M}_{33} = 0$, eq. (3.72) gives

$$h_+ = \frac{1}{r} \frac{4G\omega_{\text{rot}}^2}{c^4} (I_1 - I_2) \frac{1 + \cos^2 \iota}{2} \cos(2\omega_{\text{rot}} t), \quad (4.219)$$

$$h_\times = \frac{1}{r} \frac{4G\omega_{\text{rot}}^2}{c^4} (I_1 - I_2) \cos \iota \sin(2\omega_{\text{rot}} t). \quad (4.220)$$

We therefore have a periodic GW, with $\omega_{\text{gw}} = 2\omega_{\text{rot}}$. The fact that h_+ is proportional to $(1 + \cos^2 \iota)/2$, while h_\times to $\cos \iota$, is the same result that we found for the GW amplitude of a binary system in a circular orbit,

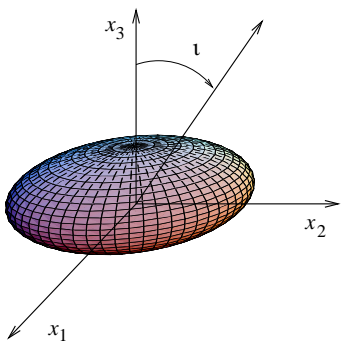


Fig. 4.14 The rigid body rotating around the x_3 axis; ι is the angle between the line-of-sight and the x_3 axis.

see eq. (3.332). In fact, this is a generic property of eq. (3.72) whenever $\ddot{M}_{11} = -\ddot{M}_{22}$ and $\ddot{M}_{13} = \ddot{M}_{23} = \ddot{M}_{33} = 0$.

It is useful to define the ellipticity ϵ by

$$\epsilon \equiv \frac{I_1 - I_2}{I_3}. \quad (4.221)$$

For instance, for a homogeneous ellipsoid with semiaxes a, b and c , in the limit of small asymmetry, i.e. $a \simeq b$, eqs. (4.198)–(4.200) give

$$\epsilon \simeq \frac{b-a}{a} + O(\epsilon^2). \quad (4.222)$$

We write the angular velocity of the source as $\omega_{\text{rot}} = 2\pi f_{\text{rot}}$ and we introduce $f_{\text{gw}} = 2f_{\text{rot}}$, which is the frequency of the GW. In terms of f_{gw} and of ϵ , the result for the GW amplitude found above can be rewritten as

$$\begin{aligned} h_+ &= h_0 \frac{1 + \cos^2 \iota}{2} \cos(2\pi f_{\text{gw}} t), \\ h_\times &= h_0 \cos \iota \sin(2\pi f_{\text{gw}} t), \end{aligned} \quad (4.223)$$

where

$$h_0 = \frac{4\pi^2 G}{c^4} \frac{I_3 f_{\text{gw}}^2}{r} \epsilon. \quad (4.224)$$

Neutron stars typically have a mass $m \simeq 1.4M_\odot$ and a radius $a \simeq 10$ km, which gives $I_3 \simeq (2/5)ma^2 \simeq 1 \times 10^{38}$ kg m². The value of the ellipticity depends on the neutron star properties, and in particular on the maximum strain that can be supported by its crust. This is quite uncertain but, as we will discuss in Vol. 2, plausible values are in the range $\epsilon \leq 10^{-6}$, although values as large as $\epsilon \simeq 10^{-5}$ can be considered. Inserting these numerical reference values, and taking a typical galactic distance $r = 10$ kpc, eq. (4.224) gives

$$h_0 \simeq 1.06 \times 10^{-25} \left(\frac{\epsilon}{10^{-6}} \right) \left(\frac{I_3}{10^{38} \text{ kg m}^2} \right) \left(\frac{10 \text{ kpc}}{r} \right) \left(\frac{f_{\text{gw}}}{1 \text{ kHz}} \right)^2. \quad (4.225)$$

Observe that neutron stars that rotate more rapidly produce a stronger GW signal, since $h_0 \sim f_{\text{gw}}^2$.

We next compute the power P radiated in GWs, plugging eqs. (4.216)–(4.218) into the quadrupole formula (3.76). Observing that $\ddot{M}_{11} = -\ddot{M}_{22}$, this gives

$$\begin{aligned} P &= \frac{2G}{5c^5} \langle \ddot{M}_{11}^2 + \ddot{M}_{12}^2 \rangle \\ &= \frac{32G}{5c^5} \epsilon^2 I_3^2 \omega_{\text{rot}}^6, \end{aligned} \quad (4.226)$$

and therefore the rotational energy of the star decreases, because of GW emission, as

$$\frac{dE_{\text{rot}}}{dt} = -\frac{32G}{5c^5} \epsilon^2 I_3^2 \omega_{\text{rot}}^6. \quad (4.227)$$

Since the rotational energy of a star rotating around its principal axis x_3 is $E_{\text{rot}} = (1/2)I_3\omega_{\text{rot}}^2$ (see eq. (4.206)), if GW emission were the dominant mechanism for the loss of rotational energy, the rotational frequency of a neutron star should decrease as

$$\dot{\omega}_{\text{rot}} = -\frac{32G}{5c^5} \epsilon^2 I_3 \omega_{\text{rot}}^5. \quad (4.228)$$

Experimentally, from the electromagnetic signal emitted by neutron stars observed as pulsars (see Chapter 6), one rather finds $\dot{\omega}_{\text{rot}} \sim -\omega_{\text{rot}}^n$ where n , called the braking index, depends on the specific pulsar but typically ranges between 2 and 3, rather than $n = 5$. This means that GW emission is not the main energy loss mechanism for a rotating pulsar, and other mechanisms, of electromagnetic nature, dominate.

4.2.2 GWs from freely precessing rigid bodies

In general, in astronomical objects the rotation axis does not coincide with a principal axis and, as a consequence, the motion of the rigid body is a combination of rotation around a principal axis and precession. As we will see in this section, the precession motion introduces qualitatively new features in the GWs radiated.

To compute the GW production we proceed as in eqs. (4.207)–(4.209). We first introduce a fixed reference frame, with axes (x_1, x_2, x_3) . In this inertial frame the angular momentum \mathbf{J} of the rigid body is conserved, and we choose the x_3 axis in the direction of \mathbf{J} . Next we introduce the body frame, i.e. a reference frame attached to the rotating body, with coordinates (x'_1, x'_2, x'_3) , whose axes coincide with the principal axes of the body. The relation between the two frames is given by the Euler angles (α, β, γ) defined in Fig. 4.15.²³

To pass from the fixed frame to the body frame we first perform a counterclockwise rotation by an angle β around the x_3 axis. This brings the x_1 axis onto an axis which is called the line of nodes (which is the intersection of the (x_1, x_2) plane with the (x'_1, x'_2) plane). Next we perform a counterclockwise rotation by an angle α around the line of nodes. This brings the x_3 axis onto the x'_3 axis. Finally, we perform a counterclockwise rotation by an angle γ around the x'_3 axis, which brings the line of nodes onto the x'_1 axis. Therefore we have $x'_i = \mathcal{R}_{ij}x_j$, as in eq. (4.207), but now the rotation matrix is more complicated,

$$\mathcal{R} = \begin{pmatrix} \cos \gamma & \sin \gamma & 0 \\ -\sin \gamma & \cos \gamma & 0 \\ 0 & 0 & 1 \end{pmatrix} \begin{pmatrix} 1 & 0 & 0 \\ 0 & \cos \alpha & \sin \alpha \\ 0 & -\sin \alpha & \cos \alpha \end{pmatrix} \begin{pmatrix} \cos \beta & \sin \beta & 0 \\ -\sin \beta & \cos \beta & 0 \\ 0 & 0 & 1 \end{pmatrix}. \quad (4.229)$$

²³In the literature, (α, β, γ) are usually denoted by (θ, ϕ, ψ) , respectively. However, here we prefer to reserve the notation (θ, ϕ) to denote the angles that describe the angular distribution of the gravitational radiation.

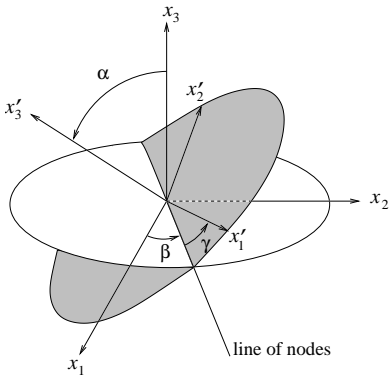


Fig. 4.15 The definition of the Euler angles (α, β, γ) .

The motion of the rigid body is specified once we know how α, β and γ evolve with time. Let us recall, from elementary mechanics (see again Landau and Lifshitz, Vol. I, 1976), how this can be obtained. In the (x_1, x_2, x_3) frame, the angular momentum \mathbf{J} is conserved (this, of course,

is not the case in the body frame, which is non-inertial, since it is rotating), and we oriented the x_3 axis so that $\mathbf{J} = (0, 0, J)$. In the (x'_1, x'_2, x'_3) frame, instead, we denote the components of the angular momentum by (J'_1, J'_2, J'_3) . From Fig. 4.15 we see that

$$\begin{aligned} J'_1 &= J \sin \alpha \sin \gamma, \\ J'_2 &= J \sin \alpha \cos \gamma, \\ J'_3 &= J \cos \alpha. \end{aligned} \quad (4.230)$$

On the other hand, we can write (J'_1, J'_2, J'_3) in terms of $\dot{\alpha}, \dot{\beta}$ and $\dot{\gamma}$ using again Fig. 4.15 and observing that, as a vector, the angular velocity $d\boldsymbol{\alpha}/dt$ is directed along the line of nodes, so its components in the body frame are

$$\frac{d\boldsymbol{\alpha}}{dt} = (\dot{\alpha} \cos \gamma, -\dot{\alpha} \sin \gamma, 0). \quad (4.231)$$

Similarly, $d\boldsymbol{\beta}/dt$ is directed along the x_3 axis, so its components in the body frame are

$$\frac{d\boldsymbol{\beta}}{dt} = (\dot{\beta} \sin \alpha \sin \gamma, \dot{\beta} \sin \alpha \cos \gamma, \dot{\beta} \cos \alpha), \quad (4.232)$$

while $d\boldsymbol{\gamma}/dt$ is along the x'_3 axis, so in the body frame $d\boldsymbol{\gamma}/dt = (0, 0, \dot{\gamma})$. The total angular velocity $\boldsymbol{\omega}$ is the vector sum of these angular velocities, $\boldsymbol{\omega} = d\boldsymbol{\alpha}/dt + d\boldsymbol{\beta}/dt + d\boldsymbol{\gamma}/dt$, so its components ω'_i in the body frame are

$$\begin{aligned} \omega'_1 &= \dot{\alpha} \cos \gamma + \dot{\beta} \sin \alpha \sin \gamma, \\ \omega'_2 &= -\dot{\alpha} \sin \gamma + \dot{\beta} \sin \alpha \cos \gamma, \\ \omega'_3 &= \dot{\gamma} + \dot{\beta} \cos \alpha. \end{aligned} \quad (4.233)$$

In the body frame the inertia tensor is diagonal, with eigenvalues I_1, I_2 and I_3 , so $J'_1 = I_1 \omega'_1$, $J'_2 = I_2 \omega'_2$ and $J'_3 = I_3 \omega'_3$. Comparing eqs. (4.230) and (4.233) we therefore get

$$I_1(\dot{\alpha} \cos \gamma + \dot{\beta} \sin \alpha \sin \gamma) = J \sin \alpha \sin \gamma, \quad (4.234)$$

$$I_2(-\dot{\alpha} \sin \gamma + \dot{\beta} \sin \alpha \cos \gamma) = J \sin \alpha \cos \gamma, \quad (4.235)$$

$$I_3(\dot{\gamma} + \dot{\beta} \cos \alpha) = J \cos \alpha. \quad (4.236)$$

These are first order equations in the variables (α, β, γ) , and are the first integral of the equations of motion provided by the conservation of angular momentum.²⁴ One can now integrate these equations and obtain $\alpha(t), \beta(t)$ and $\gamma(t)$. In the most general case, the result can be written in terms of elliptic functions, and we will get back to it later in this section. However, we first limit ourselves to the simpler case of an axisymmetric body with $I_1 = I_2$.

“Wobble” radiation from an axisymmetric rigid body

We consider an axisymmetric body, whose longitudinal axis x'_3 makes an angle α with the angular momentum axis x_3 . The angle α is often

²⁴They are in fact the first integral of the Euler equations for rigid bodies in the absence of external torques,

$$\begin{aligned} I_1 \dot{\omega}'_1 &= \omega'_2 \omega'_3 (I_2 - I_3) \\ I_2 \dot{\omega}'_2 &= \omega'_1 \omega'_3 (I_3 - I_1) \\ I_3 \dot{\omega}'_3 &= \omega'_1 \omega'_2 (I_1 - I_2) \end{aligned}$$

as we easily verify taking the first derivative of eqs. (4.234)–(4.236) and using eq. (4.233).

called the “wobble” angle, and the corresponding GW emission is called “wobble radiation”.

When $I_1 = I_2$, the analytic solution of eqs. (4.234)–(4.236) is very simple. Multiplying the first equation by $\cos \gamma$ and the second by $\sin \gamma$ and subtracting them, we get

$$\dot{\alpha} = 0. \quad (4.237)$$

This shows that the inclination of the x'_3 axis with respect to the angular momentum \mathbf{J} is constant. Multiplying the first equation by $\sin \gamma$ and the second by $\cos \gamma$ and summing them, we get

$$I_1 \dot{\beta} \sin \alpha = J \sin \alpha. \quad (4.238)$$

This shows that, if $\alpha \neq 0$, the x'_3 axis rotates with a constant angular velocity $\dot{\beta} = J/I_1$ about the direction of \mathbf{J} . We define

$$\Omega \equiv \dot{\beta} = \frac{J}{I_1}. \quad (4.239)$$

Finally, having found that both $\cos \alpha$ and $\dot{\beta}$ are constants, eq. (4.236) shows that even $\dot{\gamma}$ is constant. Equation (4.236), together with $J = I_1 \dot{\beta}$, gives

$$\omega_p \equiv -\dot{\gamma} = \frac{I_3 - I_1}{I_3} \Omega \cos \alpha. \quad (4.240)$$

The minus sign in the definition $\omega_p = -\dot{\gamma}$ is chosen so that, for an oblate body ($I_3 > I_1$), which is the normal shape of astrophysical objects, $\omega_p > 0$.²⁵ Using eq. (4.233) we see that the components of the angular velocity in the body frame evolve as²⁶

$$\begin{aligned} \omega'_1 &= a \cos(\omega_p t), \\ \omega'_2 &= a \sin(\omega_p t), \\ \omega'_3 &= b, \end{aligned} \quad (4.242)$$

where $a = \Omega \sin \alpha$ and $b = -\omega_p + \Omega \cos \alpha$ are constants. This shows that, in the body frame, the angular velocity rotates in the (x'_1, x'_2) plane, i.e. *precesses* around the x'_3 axis, with angular velocity ω_p . This precession is counterclockwise if $\omega_p > 0$ (which justifies the notation ω_p for $-\dot{\gamma}$). Observe that $|I_3 - I_1| \ll I_3$ (in a NS, a possible value could be $|I_3 - I_1|/I_3 \sim 10^{-7}$), and therefore $|\omega_p| \ll \Omega$. This motion is called free precession, since it takes place in the absence of external torques, just as a consequence of the deviation of the rigid body from spherical symmetry.

We can now compute how the inertia tensor of the rigid body evolves with time, in the fixed frame with coordinates (x_1, x_2, x_3) . As before we denote by I' the inertia tensor in the body frame, so $I' = \text{diag}(I_1, I_1, I_3)$ is a constant matrix, while we denote by I_{ij} the inertia tensor in the fixed frame. Then, as in eq. (4.210), $I_{ij} = (\mathcal{R}^T I' \mathcal{R})_{ij}$, but now \mathcal{R} is given by eq. (4.229).

²⁵Using the expression for $\dot{\gamma}$ given in eq. (4.240), we have

$$\begin{aligned} \omega'_3 &= \dot{\gamma} + \dot{\beta} \cos \alpha \\ &= (I_1/I_3)\Omega \cos \alpha, \end{aligned}$$

and therefore we can also write

$$\omega_p = \frac{I_3 - I_1}{I_1} \omega'_3. \quad (4.241)$$

²⁶Observe that, for an axisymmetric body, the orientation of the principal axes in the (x'_1, x'_2) plane is arbitrary. We choose the origin of time so that $\beta(t = 0) = 0$, and then we choose the orientation of the (x'_1, x'_2) axes so that, at $t = 0$, $\gamma(0) = \pi/2$. Therefore eq. (4.240) gives $\gamma(t) = (\pi/2) - \omega_p t$.

The explicit computation is simplified observing that, if we write the rotation matrix (4.229) as $\mathcal{R} = A(\gamma)B(\alpha)C(\beta)$, we see that

$$\begin{aligned}\mathcal{R}^T I' \mathcal{R} &= (C^T B^T A^T) I' (ABC) \\ &= (C^T B^T) I' (BC)\end{aligned}\quad (4.243)$$

because, when $I_1 = I_2$, the matrix A commutes with the matrix I' , and $A^T A = 1$ because it is an orthogonal matrix. Therefore, the angle γ drops out from I_{ij} , and the remaining matrix multiplication gives

$$\begin{aligned}I_{11} &= I_1(\cos^2 \beta + \cos^2 \alpha \sin^2 \beta) + I_3 \sin^2 \alpha \sin^2 \beta \\ &= \frac{1}{2}(I_1 - I_3) \sin^2 \alpha \cos 2\beta + \text{constant}, \\ I_{12} &= \frac{1}{2}(I_1 - I_3) \sin^2 \alpha \sin 2\beta, \\ I_{22} &= I_1(\sin^2 \beta + \cos^2 \alpha \cos^2 \beta) + I_3 \sin^2 \alpha \cos^2 \beta \\ &= -\frac{1}{2}(I_1 - I_3) \sin^2 \alpha \cos 2\beta + \text{constant}, \\ I_{13} &= -(I_1 - I_3) \sin \alpha \cos \alpha \sin \beta, \\ I_{23} &= (I_1 - I_3) \sin \alpha \cos \alpha \cos \beta, \\ I_{33} &= I_1 \sin^2 \alpha + I_3 \cos^2 \alpha = \text{constant}.\end{aligned}\quad (4.244)$$

Observe that, since γ dropped out and α is constant, the time dependence of these expressions comes uniquely from β which, from eq. (4.239), is $\beta(t) = \Omega t$ (recall that we have chosen the origin of time so that $\beta = 0$ at $t = 0$, see Note 26). As in eq. (4.215), $M_{ij} = -I_{ij}$, plus constant terms that give zero upon derivation. Therefore, we get

$$\begin{aligned}\ddot{M}_{11} &= 2(I_1 - I_3)\Omega^2 \sin^2 \alpha \cos(2\Omega t), \\ \ddot{M}_{12} &= 2(I_1 - I_3)\Omega^2 \sin^2 \alpha \sin(2\Omega t), \\ \ddot{M}_{22} &= -2(I_1 - I_3)\Omega^2 \sin^2 \alpha \cos(2\Omega t), \\ \ddot{M}_{13} &= -(I_1 - I_3)\Omega^2 \sin \alpha \cos \alpha \sin(\Omega t), \\ \ddot{M}_{23} &= (I_1 - I_3)\Omega^2 \sin \alpha \cos \alpha \cos(\Omega t), \\ \ddot{M}_{33} &= 0.\end{aligned}\quad (4.245)$$

We see that some matrix elements of \ddot{M}_{ij} oscillate as $\sin(2\Omega t)$ or $\cos(2\Omega t)$, while others as $\sin(\Omega t)$ or $\cos(\Omega t)$. From this, we already understand that we will have GW emission at two frequencies, $\omega_{\text{gw}} = 2\Omega$ and $\omega_{\text{gw}} = \Omega$. The origin of these factors is easily traced back: since the only time dependence comes from $\beta(t)$, and β describes a rotation in the (x_1, x_2) plane, the time-dependent part of I_{ij} has a factor $\sin(\Omega t)$ or $\cos(\Omega t)$ for each index i or j that take the value 1 or 2, while the index 3 produces no further time dependence. Then, as far as the time-dependent part is concerned, we have $I_{11} \sim \sin^2 \Omega t \sim \cos(2\Omega t)$, $I_{22} \sim \cos^2 \Omega t \sim \cos(2\Omega t)$, $I_{12} \sim \sin(\Omega t) \cos(\Omega t) \sim \sin(2\Omega t)$, while $I_{13} \sim \sin(\Omega t)$ and $I_{23} \sim \cos(\Omega t)$. Thus, the fact that, beside the expected radiation at $\omega_{\text{gw}} = 2\Omega$, we also have radiation at $\omega_{\text{gw}} = \Omega$, is a consequence of the fact that the motion of precession produces, together

with a time-varying value of I_{ij} with $i, j = 1, 2$, also a variation in I_{23} and I_{13} .

The computation of the GW amplitude radiated in a direction corresponding to polar angles $(\theta = \iota, \phi = 0)$ is now performed using eq. (3.72). We get

$$\begin{aligned} h_+ &= \frac{1}{r} \frac{G}{c^4} [\ddot{M}_{11} - \ddot{M}_{22} \cos^2 \iota + \ddot{M}_{23} \sin 2\iota - \ddot{M}_{33} \sin^2 \iota] \\ &= A_{+,1} \cos(\Omega t) + A_{+,2} \cos(2\Omega t) \end{aligned} \quad (4.246)$$

$$\begin{aligned} h_\times &= \frac{2}{r} \frac{G}{c^4} [\ddot{M}_{12} \cos \iota - \ddot{M}_{13} \sin \iota] \\ &= A_{\times,1} \sin(\Omega t) + A_{\times,2} \sin(2\Omega t), \end{aligned} \quad (4.247)$$

where

$$A_{+,1} = h'_0 \sin 2\alpha \sin \iota \cos \iota, \quad (4.248)$$

$$A_{+,2} = 2h'_0 \sin^2 \alpha (1 + \cos^2 \iota), \quad (4.249)$$

$$A_{\times,1} = h'_0 \sin 2\alpha \sin \iota, \quad (4.250)$$

$$A_{\times,2} = 4h'_0 \sin^2 \alpha \cos \iota. \quad (4.251)$$

²⁷Observe that the overall sign of the amplitude depends on the choice of the origin of time, and on the definition of the axes $(\hat{\mathbf{u}}, \hat{\mathbf{v}})$ in the plane transverse to the propagation direction, with respect to which the polarizations are defined. With our definition, when $\iota = 0$ these axes are $\hat{\mathbf{u}} = \hat{\mathbf{x}}$ and $\hat{\mathbf{v}} = \hat{\mathbf{y}}$, see page 111 and Fig. 3.2. In the literature, this computation has been performed choosing $\hat{\mathbf{u}}$ and $\hat{\mathbf{v}}$ so that, when $\iota = 0$, $\hat{\mathbf{u}} = \hat{\mathbf{y}}$ and $\hat{\mathbf{v}} = -\hat{\mathbf{x}}$. This is related to our convention by a rotation of the $(\hat{\mathbf{u}}, \hat{\mathbf{v}})$ axes in the transverse plane, by an angle $\psi = \pi/2$. Under this rotation $h_+ \rightarrow -h_+$ and $h_\times \rightarrow -h_\times$, see eq. (2.194), so $h'_0 \rightarrow -h'_0$.

and²⁷

$$h'_0 = -\frac{G}{c^4} \frac{(I_3 - I_1)\Omega^2}{r}. \quad (4.252)$$

Of course it is understood that, on the right-hand side of eqs. (4.246) and (4.247), t is actually the retarded time. As we already anticipated, we have radiation at both $\omega_{\text{gw}} = \Omega$ and at $\omega_{\text{gw}} = 2\Omega$.

Observe that $A_{+,1}/A_{\times,1} = \cos \iota$. Therefore from this ratio (or, equivalently, from $A_{+,2}/A_{\times,2}$) we get the inclination angle ι (which, by definition, is in the range $0 \leq \iota \leq \pi$). Given ι , the ratio $A_{+,1}/A_{+,2}$ determines the angle α . The overall value of the amplitude then fixes $|h'_0|$. If the distance to the source is known by other means, we therefore get a measure of $|I_1 - I_3|$.

It is now straightforward to compute the total power radiated. Using eq. (3.76) and observing, from eq. (4.245), that $\ddot{M}_{33} = 0$ and $\sum_k \ddot{M}_{kk} = 0$, we get

$$\begin{aligned} P_{\text{quad}} &= \frac{G}{5c^5} \langle \ddot{M}_{11}^2 + \ddot{M}_{22}^2 + 2\ddot{M}_{12}^2 + 2\ddot{M}_{13}^2 + 2\ddot{M}_{23}^2 \rangle \\ &= \frac{2G}{5c^5} (I_1 - I_3)^2 \Omega^6 \sin^2 \alpha (\cos^2 \alpha + 16 \sin^2 \alpha), \end{aligned} \quad (4.253)$$

where the term $\sin^2 \alpha \cos^2 \alpha$ is from the radiation at $\omega_{\text{gw}} = \Omega$ and the term $16 \sin^4 \alpha$ is from the radiation at $\omega_{\text{gw}} = 2\Omega$. Observe that, in the limit of small α , the power radiated at $\omega_{\text{gw}} = \Omega$ is $O(\alpha^2)$ while the power radiated at $\omega_{\text{gw}} = 2\Omega$ is $O(\alpha^4)$, so for sufficiently small α the radiation at $\omega_{\text{gw}} = \Omega$ is dominant. The two contributions become equal when $\cos^2 \alpha = 16 \sin^2 \alpha$, i.e. for $\alpha \simeq 0.245 \text{ rad} \simeq 14^\circ$.

The back-reaction of GWs

We can now compute how the emission of GWs back-reacts on the motion of the rigid body. The energy radiated in GWs is supplied by the rotational energy E_{rot} of the rigid body, so

$$\frac{dE_{\text{rot}}}{dt} = -\frac{2G}{5c^5}(I_1 - I_3)^2\Omega^6 \sin^2 \alpha(\cos^2 \alpha + 16 \sin^2 \alpha). \quad (4.254)$$

The angular momentum radiated (in the quadrupole approximation that we are using) is computed from eq. (3.97), and is supplied by the angular momentum $\mathbf{J} = (0, 0, J)$ of the rigid body. Setting $i = 3$ into eq. (3.97), we have

$$\begin{aligned} \frac{dJ}{dt} &= -\frac{2G}{5c^5} \langle \ddot{M}_{1a}\dot{M}_{2a} - \ddot{M}_{2a}\dot{M}_{1a} \rangle \\ &= -\frac{4G}{5c^5} \langle \ddot{M}_{1a}\ddot{M}_{2a} \rangle, \end{aligned} \quad (4.255)$$

where we observed that we can replace Q_{ka} by M_{ka} since $\epsilon^{3kl}\delta_{ka}Q_{la} = \epsilon^{3kl}Q_{kl} = 0$, and similarly $Q_{la} \rightarrow M_{la}$, and in the last line we integrated by part a time derivative, inside the temporal average. Inserting the explicit expressions (4.245), we get

$$\frac{dJ}{dt} = -\frac{2G}{5c^5}(I_1 - I_3)^2\Omega^5 \sin^2 \alpha(\cos^2 \alpha + 16 \sin^2 \alpha). \quad (4.256)$$

Comparing this result with eq. (4.254), we see that $dE_{\text{rot}}/dt = \Omega dJ/dt$. Since $\Omega = \dot{\beta}$ and $J = I_1\dot{\beta}$ (see eq. (4.239)), the above equation gives

$$\ddot{\beta} = -\frac{2G}{5c^5} \frac{(I_1 - I_3)^2}{I_1} \dot{\beta}^5 \sin^2 \alpha(\cos^2 \alpha + 16 \sin^2 \alpha). \quad (4.257)$$

The equation governing the evolution of α can instead be obtained writing the rotational kinetic energy as in eq. (4.206), and using $\omega'_1 = J'_1/I_1 = (J/I_1)\sin \alpha \sin \gamma$, $\omega'_2 = J'_2/I_1 = (J/I_1)\sin \alpha \cos \gamma$, and $\omega'_3 = J'_3/I_3 = (J/I_3)\cos \alpha$, see eq. (4.230). This gives

$$E_{\text{rot}} = \frac{J^2}{2} \left(\frac{\sin^2 \alpha}{I_1} + \frac{\cos^2 \alpha}{I_3} \right). \quad (4.258)$$

Taking the time derivative and making use of eq. (4.256) and of $J = I_1\dot{\beta}$ on the right-hand side, and of eq. (4.254) on the left-hand side, we get

$$\dot{\alpha} = -\frac{2G}{5c^5} \frac{(I_1 - I_3)^2}{I_1} \dot{\beta}^4 \sin \alpha \cos \alpha(\cos^2 \alpha + 16 \sin^2 \alpha). \quad (4.259)$$

Equations (4.257) and (4.259) determine the evolution of the angles α and β . We see that, because of the back-reaction of GWs, both the inclination angle α , and the angular velocity $\dot{\beta}$ decrease. However, using eqs. (4.256) and (4.259), we see that

$$\frac{d}{dt}(J \cos \alpha) = 0. \quad (4.260)$$

Therefore J decreases and α decreases (i.e. $\cos \alpha$ increases) in such a way that $J \cos \alpha$ stays constant. Since $J \cos \alpha$ is the projection of the angular momentum over the x'_3 axis of the body (see eq. (4.230)), we find that the rigid body rotates around its longitudinal axis with a constant angular velocity $\omega'_3 = (J/I_3) \cos \alpha$. The rotation of the body around its longitudinal axis is not affected by the GW back-reaction.

To study in more detail the coupled system of equations (4.257) and (4.259), we introduce the dimensionless function

$$u(t) = \dot{\beta}(t)/\dot{\beta}_0, \quad (4.261)$$

where $\dot{\beta}_0$ is the value of $\dot{\beta}(t)$ at some initial value $t = 0$, and we also introduce the time-scale

$$\begin{aligned} \tau_0 &\equiv \left[\frac{2G}{5c^5} \frac{(I_1 - I_3)^2}{I_1} \dot{\beta}_0^4 \right]^{-1} \\ &\simeq 1.8 \times 10^6 \text{ yr} \left(\frac{10^{-7}}{(I_1 - I_3)/I_3} \right)^2 \left(\frac{1 \text{ kHz}}{f_0} \right)^4 \left(\frac{10^{38} \text{ kg m}^2}{I_1} \right), \end{aligned} \quad (4.262)$$

where $f_0 = \dot{\beta}_0/(2\pi)$, and we used as reference for $(I_1 - I_3)/I_3$ and for I_3 , values that can be typical for neutron stars. Then eqs. (4.257) and (4.259) become

$$\dot{u} = -\frac{1}{\tau_0} u^5 \sin^2 \alpha (\cos^2 \alpha + 16 \sin^2 \alpha), \quad (4.263)$$

$$\dot{\alpha} = -\frac{1}{\tau_0} u^4 \sin \alpha \cos \alpha (\cos^2 \alpha + 16 \sin^2 \alpha), \quad (4.264)$$

with initial conditions $u(0) = 1$ and $\alpha(0) = \alpha_0$. In this form, it is clear that τ_0 is the characteristic time-scale of the problem, and the equations could be recast in a completely dimensionless form introducing a dimensionless variable $x = t/\tau_0$, so that $\tau_0 \dot{u} = du/dx$ and $\tau_0 \dot{\alpha} = d\alpha/dx$.

The asymptotic behavior of the solution can be easily read from eqs. (4.263) and (4.264), making use also of the fact that, as we shown above, $J \cos \alpha$ is a constant of motion. Since $J = I_1 \dot{\beta}$, this means that $\dot{\beta}_\infty \cos \alpha_\infty = \dot{\beta}_0 \cos \alpha_0$, where the subscripts ∞ denotes the value at $t = \infty$. In terms of u , this means

$$u_\infty \cos \alpha_\infty = \cos \alpha_0. \quad (4.265)$$

Equating to zero the right-hand sides of eqs. (4.263) and (4.264), we see that the possible fixed points of the evolution are either $u = 0$ or $\alpha = 0, \pi$. However, the value $u_\infty = 0$ is not consistent with eq. (4.265) (unless $\alpha_0 = \pi/2$; clearly, this is an unstable fixed point, in which an infinitesimal perturbation drives the evolution either toward $\alpha = 0$ or $\alpha = \pi$). Therefore the only asymptotic solution, for $\alpha_0 < \pi/2$, has $\alpha_\infty = 0$. Then, eq. (4.265) shows that $u_\infty = \cos \alpha_0$. Once we realize that u approaches a finite constant u_∞ and that $\alpha \rightarrow 0$, from eq. (4.264) we see that at large times $\dot{\alpha} \simeq -\alpha/\tau_\infty$, and therefore $\alpha(t)$ approaches

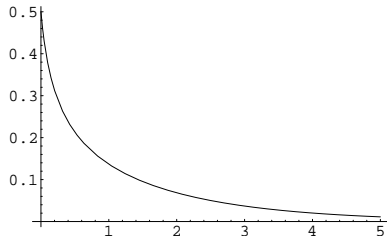


Fig. 4.16 The inclination angle $\alpha(t)$, plotted as a function of t/τ_0 , with initial conditions $\alpha(0) = 0.5$, $u(0) = 1$.

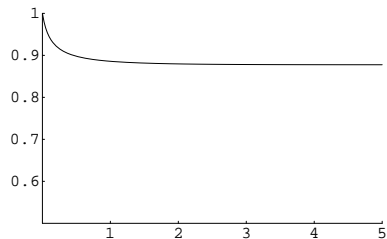


Fig. 4.17 The function $u(t) = \dot{\beta}/\dot{\beta}_0$, plotted against t/τ_0 , with initial conditions $\alpha(0) = 0.5$, $u(0) = 1$.

zero exponentially, with a time-scale $\tau_\infty = \tau_0/u_\infty^4$, which is obtained simply replacing $\dot{\beta}_0$ with $\dot{\beta}_\infty$ in eq. (4.262).

The numerical integration of eqs. (4.263) and (4.264) is straightforward, and we show in Figs. 4.16 and 4.17 the solution for the initial condition $\alpha_0 = 0.5$, which confirms the asymptotic behavior found analytically.

In conclusion, on a time-scale given by eq. (4.262), the rigid body aligns its rotation axis with the direction of the angular momentum ($\alpha \rightarrow 0$), while the rotational angular velocity $\dot{\beta} = \Omega$ around the x_3 axis decreases toward the constant value $\Omega_0 \cos \alpha_0$, and the rotational velocity around its principal axis $\omega'_3 = \Omega \cos \alpha$ stays constant.

Finally, it is interesting to compare the frequency ω_{em} of the electromagnetic pulses of a pulsar, idealized as a rotating rigid body,²⁸ with the frequency of the GWs that it emits. If a pulsar rotates around its principal axis with frequency Ω , and has $I_1 \neq I_2$, which is the case discussed in Section 4.2.1, then $\omega_{\text{em}} = \Omega$, so we can determine Ω very precisely by electromagnetic observations, and GW emission is at $\omega_{\text{gw}} = 2\Omega$. In this case, therefore, we have an accurate prediction of the frequency at which we expect GW emission.

Instead, in the case of “wobble” radiation discussed in this subsection, in the limit of small α , the axes x_3 and x'_3 almost coincide. If the source of the electromagnetic radiation is some “hot spot” fixed on the star surface then, for a far observer, the hot spot is basically rotating around the x_3 axis with a total angular velocity $\omega_{\text{rot}} = \dot{\beta} + \dot{\gamma} = \Omega - \omega_p$, see Fig. 4.15, so

$$\Omega = \omega_{\text{rot}} + \omega_p. \quad (4.266)$$

The mean frequency ω_{em} of repetition of the electromagnetic pulses will be equal to ω_{rot} , so $\omega_{\text{em}} = \Omega - \omega_p$. Instead, we saw that wobble gravitational radiation is emitted at $\omega_{\text{gw}} = \Omega$ and at $\omega_{\text{gw}} = 2\Omega$, so these two lines are shifted, with respect to ω_{em} and to $2\omega_{\text{em}}$, by the unknown quantities ω_p and $2\omega_p$, respectively. Using eq. (4.240), for the line at $\omega_{\text{gw}} = \Omega$, we have

$$\omega_{\text{gw}} \simeq \left(1 + \frac{I_3 - I_1}{I_3} \cos \alpha\right) \omega_{\text{em}}. \quad (4.267)$$

Since $|I_1 - I_3|/I_3$ is in general very small, e.g. could be of order 10^{-7} in a neutron star, the difference between the actual GW frequency and the value suggested by electromagnetic observation is small. An axisymmetric astrophysical object is normally expected to be oblate ($I_3 > I_1$), and in this case $\omega_{\text{gw}} > \omega_{\text{em}}$. For a prolate body ($I_3 < I_1$), instead, we have $\omega_{\text{gw}} < \omega_{\text{em}}$.

Rotating and precessing triaxial bodies

We now study the radiation emitted by a generic triaxial body. We choose the axes of the body frame so that $I_1 < I_2 < I_3$. The time-dependent moment of inertia I_{ij} in the fixed frame is again computed

²⁸The discussion below is really specific to our crude modelization of neutron stars as rigid bodies. Real neutron stars are rather mostly fluid in their interior. See the Further Reading section for the results with a more realistic modelization of neutron stars.

from $I_{ij} = (\mathcal{R}^T I' \mathcal{R})_{ij}$, with \mathcal{R} given by eq. (4.229), but now the dependence on γ does not cancel, contrary to the case $I_1 = I_2$ discussed above, compare with eq. (4.243).

Once expressed I_{ij} in terms of α, β, γ , to compute the waveform we need the time-dependence of the Euler angles, which can be found for instance in Landau and Lifshitz, Vol. I (1976). The evolution of the components of the angular velocity in the body frame is²⁹

$$\begin{aligned}\omega'_1 &= a \operatorname{cn}(\tau, m), \\ \omega'_2 &= a \left[\frac{I_1(I_3 - I_1)}{I_2(I_3 - I_2)} \right]^{1/2} \operatorname{sn}(\tau, m), \\ \omega'_3 &= b \operatorname{dn}(\tau, m),\end{aligned}\quad (4.268)$$

²⁹We assume for definiteness $J^2 > 2EI_2$; in this case, in the body frame, the apparent precession of \mathbf{J} is around the x'_3 axis; if instead $J^2 < 2EI_2$, it is around the x'_1 axis.

³⁰For the elliptic functions cn , sn and dn and for the Jacobi theta functions that will appear below, we follow the notation and conventions of Abramowitz and Stegun (1972).

where cn , sn and dn are elliptic functions,³⁰ and τ is a rescaled time variable,

$$\tau = bt \left[\frac{(I_3 - I_2)(I_3 - I_1)}{I_1 I_2} \right]^{1/2}. \quad (4.269)$$

The parameter m of the elliptic functions is given by

$$m = \frac{(I_2 - I_1)I_1 a^2}{(I_3 - I_2)I_3 b^2}, \quad (4.270)$$

and a, b are the initial values of ω'_1 and ω'_3 ,

$$a = \omega'_1(0), \quad b = \omega'_3(0). \quad (4.271)$$

Observe that we have chosen the origin of time so that $\omega'_2(0) = 0$. In the limit $I_1 = I_2$ we have $m = 0$; since $\operatorname{cn}(\tau, 0) = \cos \tau$, $\operatorname{sn}(\tau, 0) = \sin \tau$, and $\operatorname{dn}(\tau, 0) = 1$, in this limit we recover the result (4.242). The elliptic functions are periodic functions of τ , with periodicity $4K(m)$, where $K(m)$ is the complete elliptic integral of the first kind. The components of the angular velocity in the body frame are therefore periodic in t , with period

$$T = \frac{4K(m)}{b} \left[\frac{I_1 I_2}{(I_3 - I_2)(I_3 - I_1)} \right]^{1/2}. \quad (4.272)$$

To compute I_{ij} , we need explicitly the time-dependence of the Euler angles. The solution for α and γ is

$$\cos \alpha(t) = \frac{I_3 b}{J} \operatorname{dn}(\tau, m), \quad (4.273)$$

$$\tan \gamma(t) = \left[\frac{I_1(I_3 - I_2)}{I_2(I_3 - I_1)} \right]^{1/2} \frac{\operatorname{cn}(\tau, m)}{\operatorname{sn}(\tau, m)}, \quad (4.274)$$

so they are both periodic with period T . The solution for β is instead

$$\beta(t) = \frac{2\pi}{T'} t + \beta_1(t), \quad (4.275)$$

where

$$\begin{aligned} \frac{2\pi}{T'} &= \frac{J}{I_1} - \frac{2i}{T} \frac{\vartheta'_4(i\pi c_1)}{\vartheta_4(i\pi c_1)} \\ &= \frac{J}{I_1} + \frac{2b}{K(m)} \left[\frac{(I_3 - I_2)(I_3 - I_1)}{I_1 I_2} \right]^{1/2} \sum_{n=1}^{\infty} \frac{q^n}{1 - q^{2n}} \sinh(2\pi n c_1). \end{aligned} \quad (4.276)$$

Here ϑ_4 is a Jacobi theta function, c_1 is defined to be any³¹ solution of the equation $\text{sn}[2ic_1 K(m), m] = iI_3 b/(I_1 a)$, and

$$q = \exp\{-\pi K(1-m)/K(m)\}. \quad (4.277)$$

The function $\beta_1(t)$ can be written as a ratio of theta functions,

$$\beta_1(t) = \frac{\vartheta_4(\frac{2\pi t}{T} - i\pi c_1)}{\vartheta_4(\frac{2\pi t}{T} + i\pi c_1)}, \quad (4.278)$$

and admits the series expansion

$$\beta_1(t) = \sum_{n=1}^{\infty} \left[\frac{-2q^n}{n(1-q^{2n})} \right] \sin\left(\frac{4\pi n t}{T}\right). \quad (4.279)$$

Observe that $\beta_1(t)$ is periodic with period $T/2$. In the problem there are therefore two distinct periodicities, T and T' , and we can expect that the frequency spectrum of the gravitational radiation will have two sets of lines. The fact that γ is periodic with period T identifies $2\pi/T$ as the angular frequency associated to precession, so we define

$$\begin{aligned} \omega_p &= \frac{2\pi}{T} \\ &= \frac{\pi b}{2K(m)} \left[\frac{(I_3 - I_2)(I_3 - I_1)}{I_1 I_2} \right]^{1/2}. \end{aligned} \quad (4.280)$$

The angular frequency associated to rotation around the x_3 axis is instead³²

$$\omega_{\text{rot}} = \frac{2\pi}{T'} - \frac{2\pi}{T}. \quad (4.281)$$

Given these complicated but explicit solutions for $\alpha(t)$, $\beta(t)$ and $\gamma(t)$, one could in principle plug them into the rotation matrix \mathcal{R}_{ij} and grind, to obtain the moment of inertia in the fixed frame, and hence the waveform. However, the discrete nature of the spectrum becomes more evident if, rather than working with the exact expressions, we perform a series expansion for small wobble angle (which is equivalent to expanding in powers of m) and small deviations from axisymmetry.³³ The result, up to second order in m , is

$$\begin{aligned} h_+ &= A_{+,0} \cos(2\omega_{\text{rot}} t) \\ &\quad + A_{+,1} \cos[(\omega_{\text{rot}} + \omega_p)t] + A_{+,2} \cos[2(\omega_{\text{rot}} + \omega_p)t], \end{aligned} \quad (4.282)$$

$$\begin{aligned} h_x &= A_{x,0} \sin(2\omega_{\text{rot}} t) \\ &\quad + A_{x,1} \sin[(\omega_{\text{rot}} + \omega_p)t] + A_{x,2} \sin[2(\omega_{\text{rot}} + \omega_p)t], \end{aligned} \quad (4.283)$$

³¹Since the elliptic functions and the theta functions have the same periodicity, all solutions for c_1 are equivalent.

³²One can also check this result observing that, in the limit of small wobble angle, it gives $\omega_{\text{rot}} = \dot{\beta} - \omega_p$. Since $\dot{\gamma} = -\omega_p$, see eq. (4.240), we get $\omega_{\text{rot}} = \dot{\beta} + \dot{\gamma}$, in agreement with the discussion above eq. (4.266).

³³This computation is performed in Zimmermann (1980) and Van Den Broeck (2005), see the Further Reading.

where

$$\begin{aligned} A_{+,0} &= h_0 (1/2)(1 + \cos^2 \iota), \\ A_{+,1} &= 2h'_0 g(\alpha_0) \sin \iota \cos \iota, \\ A_{+,2} &= 2h'_0 g^2(\alpha_0) (1 + \cos^2 \iota), \\ A_{\times,0} &= h_0 \cos \iota, \\ A_{\times,1} &= 2h'_0 g(\alpha_0) \sin \iota, \\ A_{\times,2} &= 4h'_0 g^2(\alpha_0) \cos \iota. \end{aligned} \quad (4.284)$$

The amplitudes h_0 and h'_0 are defined as

$$h_0 = -\frac{1}{r} \frac{4G\omega_{\text{rot}}^2}{c^4} (I_1 - I_2), \quad (4.285)$$

$$h'_0 = -\frac{1}{r} \frac{G(\omega_{\text{rot}} + \omega_p)^2}{c^4} \left(I_3 - \frac{I_1 + I_2}{2} \right), \quad (4.286)$$

and

$$g(\alpha_0) \equiv \frac{I_1 a}{I_3 b}. \quad (4.287)$$

Using eqs. (4.234) and (4.236), and recalling that we have chosen the origin of time so that $\gamma(0) = \pi/2$, we see that $I_1 a / (I_3 b) = \tan \alpha_0$, where $\alpha_0 = \alpha(t = 0)$. Therefore, in the limit of small wobble angle α_0 , we have $g(\alpha_0) \simeq \alpha_0$.

From these expressions we see that, setting $\alpha_0 = 0$ (and therefore $g(\alpha_0) = 0$) we recover the correct limit of rotation around a principal axis, given in eqs. (4.219), (4.220) and (4.224).³⁴

Instead, setting $I_1 = I_2$ (and recalling, from eq. (4.281) and Note 32, that $\Omega = \omega_{\text{rot}} + \omega_p$), we recover the correct limit of precession of an axisymmetric body when α is small, given in eqs. (4.246)–(4.252).

We see that, to zeroth-order in $g(\alpha_0)$, we find the line at $\omega_{\text{gw}} = 2\omega_{\text{rot}}$ due to rotation around a principal axis. To order $g(\alpha_0)$ emerges a line at $\omega_{\text{gw}} = \omega_{\text{rot}} + \omega_p$, and to order $g^2(\alpha_0)$ we get a further line at $\omega_{\text{gw}} = 2\omega_{\text{rot}} + 2\omega_p$. If we expand to higher order in $g(\alpha_0)$, we find two sets of lines at frequencies, respectively,

$$\omega_{\text{gw}} = 2\omega_{\text{rot}} + 2k\omega_p, \quad (4.288)$$

and

$$\omega_{\text{gw}} = \omega_{\text{rot}} + (2k + 1)\omega_p, \quad (4.289)$$

with $k = 0, 1, 2, \dots$, whose intensity is suppressed by increasing powers of $g(\alpha_0)$.

To conclude this section, we should stress that all results discussed above have been obtained for rigid bodies. For application to neutron stars, a more realistic modeling of the neutron star interior (e.g. a fluid body with an elastic crust) is necessary. We will come back to realistic neutron stars in Vol. 2.

³⁴Observe that in Section 4.2.1 we choose the origin of time so that, at $t = 0$, the axis x'_1 is aligned with the axis x_1 , i.e. $\gamma(0) = 0$, while here we have chosen $\gamma(0) = \pi/2$. This is the origin of the overall minus sign between eq. (4.224) and eq. (4.285). As discussed in Note 27, we can reabsorb the minus sign in both h_0 and h'_0 rotating by an angle $\pi/2$ in the transverse plane the axes $(\hat{\mathbf{u}}, \hat{\mathbf{v}})$ used to define the plus and cross polarizations.

4.3 Radial infall into a black hole

In this section we compute the GWs produced when an object falls radially into a black hole. We will start from the simple case of the infall of a point-like particle. In principle, in a full computation we should treat GWs as perturbations over the curved black hole space-time, rather than using the expansion over flat space-time of the linearized theory that we have discussed until now. As we will see, however, the low-frequency part of the spectrum can be computed within our formalism, and the frequency at which the approach breaks down can be estimated. This allows us to perform, in a rather simple setting, this instructive computation. Next we will consider what happens when a real star, rather than a point-like object, falls into a black hole. We will see that the star can be disrupted by the tidal force of the black hole, and as a result the radiation emitted by the various parts of the body adds up incoherently. Beside its intrinsic interest, this problem will then allow us to appreciate the difference between coherent and incoherent emission of gravitational radiation.

4.3.1 Radiation from an infalling point-like mass

We then begin by computing the radiation generated by a point-like particle of mass m which falls radially into a black hole of mass M , with $m \ll M$. We make a number of simplifying assumptions. First of all, we compute the GW production using the equations of linearized theory. In principle this is not correct, since in linearized theory we expand around the flat-space metric, while here we should rather expand around the Schwarzschild metric. Second, we use the Newtonian equation of motion, rather than the geodesics of general relativity in the Schwarzschild metric. Thus, if the particle comes from the positive direction of the z axis, starting with zero velocity at infinity, we write

$$\frac{1}{2}m\dot{z}^2 - \frac{GmM}{z} = 0 \quad (4.290)$$

and therefore

$$\dot{z} = -c \left(\frac{R_S}{z} \right)^{1/2}, \quad (4.291)$$

where $R_S = 2GM/c^2$ is the Schwarzschild radius of the black hole. Third, we assume that most of the radiation is emitted when the particle is non-relativistic, and therefore we use the quadrupole formula.

In the last part of the trajectory, close to the black hole horizon, all these assumptions break down. In particular, eq. (4.291) is certainly not valid close to the horizon, and it is also incompatible with the non-relativistic assumption, since it formally gives $\dot{z} = -c$ at $z = R_S$. However, at sufficiently large distances the flat-space Newtonian approximation is correct, and these approximations become legitimate. Thus, we first compute the radiation emitted from $z = +\infty$ until a value $z = R$.

As long as $R \gg R_S$ our approximations are justified. We will then discuss the extrapolation $R \rightarrow R_S$.

We first compute the total radiated power, using eq. (3.76) and observing that, in our problem, we have only one non-vanishing component of M_{ij} , $M_{33} = mz^2(t)$. Then

$$\begin{aligned} P_{\text{quad}} &= \frac{2}{15} \frac{G}{c^5} \langle \ddot{M}_{33}^2 \rangle \\ &= \frac{2}{15} \frac{Gm^2}{c^5} \langle (6\dot{z}\ddot{z} + 2z\ddot{\dot{z}})^2 \rangle. \end{aligned} \quad (4.292)$$

The total radiated energy, in the quadrupole approximation, is therefore

$$E = \frac{2}{15} \frac{Gm^2}{c^5} \int_{-\infty}^{t_{\max}} dt (6\dot{z}\ddot{z} + 2z\ddot{\dot{z}})^2, \quad (4.293)$$

³⁵As we will see below, the frequency spectrum is peaked at $\omega = O(c/R_S)$, so the typical period of the GW is of the order of the light travel time across the Schwarzschild radius R_S . Therefore the integral over time from $-\infty$ to t_{\max} is actually an integration over many periods of the typical gravitational radiation.

where the integration over t make superfluous the time average³⁵ $\langle \dots \rangle$, and t_{\max} is defined by $z(t_{\max}) = R$. We write $dt = dz/\dot{z}$ and, using eq. (4.291), $\dot{z} = -c^2 R_S/(2z^2)$ and $\ddot{z} = -(c^3/R_S^2)(R_S/z)^{7/2}$. Then, setting $u = z/R_S$, we get

$$\begin{aligned} E &= \frac{2}{15} \frac{Gm^2}{R_S} \int_{R/R_S}^{\infty} du u^{-9/2} \\ &= \frac{4}{105} \frac{Gm^2}{R_S} \left(\frac{R_S}{R} \right)^{7/2}. \end{aligned} \quad (4.294)$$

Of course, the radiation increases if R decreases. If we extrapolate the result down to $R = R_S = 2GM/c^2$ we get

$$E = \frac{2}{105} mc^2 \left(\frac{m}{M} \right) \simeq 0.019 mc^2 \left(\frac{m}{M} \right). \quad (4.295)$$

This extrapolation turns out to be remarkably close to the result obtained with the expansion over the Schwarzschild metric, using the general relativistic equations of motion and performing the full relativistic computation of GW production rather than using the quadrupole formula. The result of this calculation³⁶ is in fact

$$E \simeq 0.010 mc^2 \left(\frac{m}{M} \right). \quad (4.296)$$

Observe that the energy radiated in GWs is smaller than the rest energy mc^2 of the particle, by a factor m/M .

The fact that the quadrupole approximation works quite well means that, despite the fact that in the last part of the trajectory the particle becomes relativistic, still the total power is dominated by the quadrupole and in general by the lowest multipoles. Since the radiation emitted at high multipoles is beamed into a narrow forward cone, while at low multipoles it is distributed on a large solid angle, the fact that the low multipoles dominate means that, in the radial infall into a black hole, there is no beaming of gravitational radiation. We will see a similar phenomenon when we study the gravitational radiation emitted by an

³⁶See Davies, Ruffini, Press and Price (1971). We will discuss this computation in Vol. 2.

accelerated particle, in Section 4.4. This is in sharp contrast with the electromagnetic case where instead, when the source reaches relativistic velocities, the high multipoles dominate, and the radiation is beamed.

We can also use eq. (4.296) to give an estimate of the energy radiated in GWs in the head-on collision of two black holes of equal mass M . In this case, we substitute m with the reduced mass $M/2$ and we get $E \sim 2.5 \times 10^{-3} Mc^2$, which is quite close to the result $E \simeq (1-2) \times 10^{-3} Mc^2$ obtained from numerical simulations.

We now wish to compute the frequency spectrum of the radiation emitted. In principle, in order to compute the Fourier transform of a function of time $F(t)$, we need to know $F(t)$ on the whole interval $-\infty < t < \infty$. However, our Newtonian trajectory (4.291) is a good approximation to the exact general relativistic geodesic only up to a maximum value of time t_{\max} such that $z(t_{\max}) \equiv R \gg R_S$; beyond t_{\max} it becomes at first a poor approximation to the correct result and finally it even becomes completely meaningless physically, since it formally gives $|\dot{z}| > 1$ and $z < R_S$. Therefore, within our non-relativistic Newtonian approximation, we cannot compute the full form of the spectrum. However, we know that a system with typical size d and typical velocity v radiates GWs with a reduced wavelength $\lambda \sim d(c/v)$, see eq. (3.24). When the particle approaches the horizon, the size of the relevant length-scale of the particle-black hole system, for computing the time-varying part of the mass moment, is of order R_S , and $v \sim c$, and therefore $\lambda \sim R_S$. On the other hand, when the particle is at $R \gg R_S$, the length-scale which enters in the time-varying quadrupole moment is of order R , and $v \ll c$, so the system radiates at $\lambda \sim R(c/v) \gg R \gg R_S$.

This means that, with the Newtonian part of the trajectory, we can reliably compute the part of the spectrum with $\lambda \gg R_S$, or $\omega R_S \ll c$, since this radiation is generated when the particle is at large distance from the black hole. The complete spectrum will be peaked at $\omega R_S \sim c$, but the radiation at these frequencies is generated close to the horizon where a full general-relativistic computation is necessary. Finally, the spectrum will be necessarily cutoff exponentially for $\omega R_S \gg c$, since there is no length-scale smaller than R_S in the problem.

To compute the spectrum at $\omega R_S \ll c$ we can therefore use eq. (4.291). The solution of this equation of motion is

$$z^{3/2}(t) - z^{3/2}(t_0) = \frac{3}{2} R_S^{1/2} c(t_0 - t). \quad (4.297)$$

Defining \bar{t} from $(3/2)R_S^{1/2}c\bar{t} \equiv z^{3/2}(t_0) + (3/2)R_S^{1/2}ct_0$, eq. (4.297) becomes $z^{3/2}(t) = (3/2)R_S^{1/2}c(\bar{t} - t)$. At $t = -\infty$ we have $z(t) = +\infty$, while the minimum value $z(t) = R$ is reached at a finite time

$$t_{\max} = \bar{t} - \frac{2R^{3/2}}{3cR_S^{1/2}}. \quad (4.298)$$

We further introduce the variable $\tau = \bar{t} - t$, so

$$z(\tau) = \left(\frac{3}{2} R_S^{1/2} c \tau \right)^{2/3}, \quad (4.299)$$

and $c\tau$ ranges over the interval $2R^{3/2}/(3R_S^{1/2}) < c\tau < \infty$. Equation (4.292) gives

$$E = \frac{2G}{15c^5} \int_{-\infty}^{t_{\max}} dt \ddot{M}_{33}^2. \quad (4.300)$$

Writing $M_{33}(t)$ in Fourier transform one obtains

$$E = \frac{2G}{15c^5} 2 \int_0^{\omega_{\max}} \frac{d\omega}{2\pi} \omega^6 |\tilde{M}_{33}(\omega)|^2, \quad (4.301)$$

³⁷The contribution from negative frequencies gives the factor of 2 in front of the integral.

$$\tilde{M}_{33}(\omega) = m \int_{-\infty}^{t_{\max}} dt z^2(t) e^{i\omega t} \quad (4.302)$$

diverges, since as $t \rightarrow -\infty$ we have $z(t) \rightarrow +\infty$. Fortunately, this divergence is harmless: it simply reflects the fact that the size of the particle-black hole system, and therefore its quadrupole moment, goes to infinity. However this divergent part of the quadrupole moment is static since, from eq. (4.291), as $z \rightarrow \infty$ we have $\dot{z} \rightarrow 0$, and therefore it does not contribute to GW production. To dispose of this divergence, the simplest way is to consider the Fourier transform of $\ddot{M}_{33}(t)$ rather than of $M_{33}(t)$, since in $\ddot{M}_{33}(t)$ the static term has been eliminated. Therefore, instead of eq. (4.301), we write

$$E = \frac{4G}{15c^5} \int_0^{\omega_{\max}} \frac{d\omega}{2\pi} \omega^2 |\tilde{M}_{33}(\omega)|^2. \quad (4.303)$$

Using eq. (4.299) we find

$$\begin{aligned} \ddot{M}_{33}(t) &= 2m(z\ddot{z} + \dot{z}^2) \\ &= m \left(\frac{2R_S c^2}{3\tau} \right)^{2/3}, \end{aligned} \quad (4.304)$$

and, recalling that $-\infty < t < t_{\max}$ corresponds to $\tau_{\min} < \tau < \infty$ with $\tau_{\min} \equiv 2R^{3/2}/(3cR_S^{1/2})$,

$$\tilde{M}_{33}(\omega) = m \left(\frac{2R_S c^2}{3} \right)^{2/3} \int_{\tau_{\min}}^{\infty} d\tau \tau^{-2/3} e^{-i\omega\tau}. \quad (4.305)$$

Defining $u = \omega\tau$,

$$\tilde{M}_{33}(\omega) = m\omega^{-1/3} \left(\frac{2R_S c^2}{3} \right)^{2/3} \int_{\omega\tau_{\min}}^{\infty} du u^{-2/3} e^{-iu}. \quad (4.306)$$

The computation is valid down to R of order a few times R_S , so $\tau_{\min} = O(R_S/c)$ and, in the limit $\omega R_S \ll c$, which is the limit in which our computation is justified, the leading term is obtained approximating the

lower limit of the above integral with zero. Then we get an Euler Gamma function

$$\int_0^\infty du u^{-2/3} e^{-iu} = e^{-i\pi/6} \Gamma(1/3), \quad (4.307)$$

as one can see rotating the contour to the negative imaginary semiaxis of the complex u -plane, and eq. (4.303) gives

$$\begin{aligned} \frac{dE}{d\omega} &= \frac{2G}{15\pi c^5} \omega^2 |\tilde{M}_{33}(\omega)|^2 \\ &= \left(\frac{2}{3}\right)^{7/3} \frac{\Gamma^2(1/3)}{5\pi} \frac{Gm^2}{c} \left(\frac{\omega R_S}{c}\right)^{4/3} \\ &\simeq 0.177 \frac{Gm^2}{c} \left(\frac{\omega R_S}{c}\right)^{4/3}, \quad (\omega R_S \ll c). \end{aligned} \quad (4.308)$$

To study the spectrum when $\omega R_S/c$ is not small we need the full general-relativistic computation, but we expect from the physical arguments presented above that it must reach a maximum at $\omega R_S/c = O(1)$, and will be cutoff exponentially when $\omega R_S/c \gg 1$. Indeed, the numerical results of Davies, Ruffini, Press and Price (1971) show that the spectrum reaches a maximum at $\omega R_S/c \simeq 0.64$ and then is cutoff exponentially, with an empirical law $dE/d\omega \sim \exp\{-\kappa \omega R_S/c\}$ with $\kappa \simeq 5$.

4.3.2 Tidal disruption of a real star falling into a black hole. Coherent and incoherent radiation

We have seen in the previous subsection that, within the non-relativistic Newtonian approximation, we can correctly reproduce the order of magnitude of the power radiated in the radial infall of a point-like particle into a BH, and we can compute the spectrum for $\omega R_S \ll 1$. The inclusion of the full non-linearities of general relativity amounts only to a correction of about a factor of two in the total power, compare eqs. (4.295) and (4.296).

A point-like particle is however an idealization, and in astrophysical applications we are rather interested in the infall of an extended object like a main sequence star, a white dwarf or a neutron star. We will see in this subsection that in this case, because of the tidal disruption of the star as it falls into the BH, the radiation can be emitted incoherently, and this can reduce the production of GWs by many orders of magnitudes.

To understand qualitatively the difference between coherent and incoherent radiation, observe that in eq. (4.295) we found a radiated energy $E \sim m^2/M$, where M is the BH mass and m is the mass of the infalling particle (or, more precisely, the reduced mass of the particle–BH system, but we are assuming $m \ll M$). If we describe an extended object of mass m as a collection of N particles of mass δm and $m = N\delta m$, we therefore find that, if the N constituents radiate coherently as a single object of mass m , the radiated energy is

$$E^{(\text{coherent})} \sim \frac{m^2}{M} = N^2 \frac{(\delta m)^2}{M}. \quad (4.309)$$

This N^2 dependence can also be understood observing that the total amplitude of the GW is the sum of the separate amplitudes, so $h_{\text{tot}} = \sum_{i=1}^N h_i$, where i labels the elementary constituents. For coherent radiation the various terms in this sum have the same phase, so $h^{\text{tot}} = O(N)$ and the radiated energy $E \sim \dot{h}_{\text{tot}}^2$ is $O(N^2)$. For incoherent radiation, the mixed terms in $(\sum_i h_i)^2$ interfere destructively and we are only left with the diagonal terms $\sum_i \dot{h}_i^2$. Therefore in this case the energy is N times the energy radiated by a single constituent,

$$E^{\text{(incoherent)}} \sim N \frac{(\delta m)^2}{M} = \frac{1}{N} \frac{m^2}{M}, \quad (4.310)$$

and the incoherent radiation is smaller by a factor N with respect to coherent radiation. Observe that, in the limit $N \rightarrow \infty$ with m fixed, the incoherent radiation even goes to zero.

Whether a distribution of sources radiates coherently or incoherently depends on the wavelength of the GW that we consider and on the linear size a of the system. If $a \ll \lambda$, the phase of the GW does not change appreciably over the whole source and the radiation is coherent, while if $a \gg \lambda$ the phases from the single constituents oscillate strongly over the system and the mixed terms in $(\sum_i h_i)^2$ average to zero, so the radiation is incoherent. The transition between these two regimes is governed by a form factor which, for the problem of the infall of a star into a black hole (BH), will be computed below.

To perform this computation, we need first of all to understand how the shape of an infalling star is distorted by the tidal gravitational field of the black hole. A star is an object held together by self-gravity. A first crude estimate of the tidal radius r_{tidal} , i.e. of the star-BH distance where the tidal force exerted by the BH is strong enough to disrupt the star, can be obtained as follows. We model a star of mass m as two particles of mass $m/2$, orbiting each other in a circular orbit of radius a , and we consider a BH of mass M at a distance r from the center of the star, see Fig. 4.18. Then the tidal force which tends to disrupt the star is

$$\begin{aligned} F_{\text{tidal}} &= \frac{GM(m/2)}{(r-a)^2} - \frac{GM(m/2)}{(r+a)^2} \\ &\simeq 2GMm \frac{a}{r^3}. \end{aligned} \quad (4.311)$$

The system is broken apart if this force is larger than the gravitational attraction between the two bodies of mass $m/2$, so if

$$2GMm \frac{a}{r^3} > \frac{G(m/2)^2}{(2a)^2}, \quad (4.312)$$

which gives $r < r_{\text{tidal}} \simeq 3.2(M/m)^{1/3}a$. The numerical coefficient depends of course on our crude schematization of the extended object. If we rather model the star as an incompressible spheroid of mass m , mean radius a and constant density, the tidal radius becomes (see Chandrasekhar 1969, Section 56)

$$r_{\text{tidal}} \simeq 2.2(M/m)^{1/3}a. \quad (4.313)$$

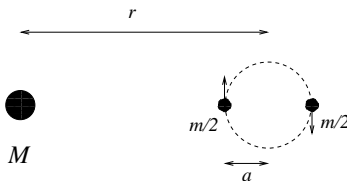


Fig. 4.18 The estimate of the tidal radius discussed in the text.

We denote by a the radius of the star when it is far from the BH, and by a_h the value of its radial size by the time that the star is close to the BH horizon. We can estimate the order of magnitude of a_h , using the Newtonian trajectory (4.297) for a particle falling radially along the z -axis,

$$z(t) = \left[z_0^{3/2} + \frac{3}{2} R_S^{1/2} c(t_0 - t) \right]^{2/3}. \quad (4.314)$$

Taking the variation with respect to z_0 we see from this equation that two points that at time t_0 are separated by a radial distance δz_0 , at time t are separated by $\delta z(t) = [z_0/z(t)]^{1/2} \delta z_0$. We take as t_0 the time when the star crosses the tidal radius, and is therefore still undeformed. Then near the horizon the star is an ellipsoid with semimajor axis a_h given by

$$a_h = \left(\frac{r_{\text{tidal}}}{R_S} \right)^{1/2} a. \quad (4.315)$$

The evolution of the shape of the star as it plunges toward the BH is shown in Fig. 4.19. The effect of the tidal distortion can be quite dramatic. For instance, a main sequence star of $1M_\odot$ has a radius $a \simeq 7 \times 10^5$ km. If it falls into a BH with a mass $10M_\odot$ and therefore $R_S \simeq 30$ km, eq. (4.313) gives $r_{\text{tidal}} \simeq 4.7a$ and $(r_{\text{tidal}}/R_S)^{1/2} \sim 300$.

We know from the previous subsection that most of the radiation is emitted when the star is close to the horizon and therefore when it has a size a_h in the radial direction. From the discussion at the beginning of this subsection we know that a source whose larger dimension is of order a_h will radiate coherently only the wavelengths which satisfy $\lambda \gg a_h$, or $\omega \ll c/a_h$. Therefore the parameter which governs the loss of coherence is

$$A(\omega) \equiv \frac{\omega a_h}{c} = \frac{\omega a}{c} \left(\frac{r_{\text{tidal}}}{R_S} \right)^{1/2}. \quad (4.316)$$

For frequencies such that $A(\omega) \gg 1$ we have incoherent radiation while for frequencies that satisfy $A(\omega) \ll 1$ the radiation is coherent. In the formal limit $a \rightarrow 0$ we have $A(\omega) \rightarrow 0$ and we get back the point-like result.

As we mentioned in the previous subsection, the point-like spectrum is peaked at $\omega = \bar{\omega} \simeq 0.64c/R_S$. Therefore, when $0.64/R_S \ll 1/a_h$, only the high-frequency tails of the point-like spectrum are suppressed because of incoherent emission. These high frequency tails contributed anyway negligibly to the total power even in the point-like case, since we saw that they were already exponentially suppressed. Therefore, when $0.64/R_S \ll 1/a_h$ the total power is practically the same as in the point-like case. On the contrary, if $0.64/R_S \gg 1/a_h$, incoherent emission suppresses the radiation in the region which includes the peak, and where most of the power is concentrated, and the total radiated power becomes a negligible fraction of the point-like case. Defining $\bar{A} =$

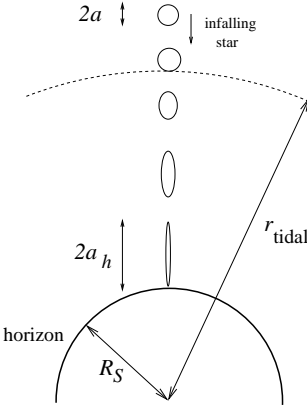


Fig. 4.19 An infalling star of radius a is tidally deformed by the black hole when it enters within the tidal radius r_{tidal} . By the time the horizon is approached, the star is an ellipsoid with semimajor axis a_h .

Table 4.1 Suppression of gravitational radiation for stars falling radially into a black hole, for different values of the mass M of the black hole. In all cases the mass of the star is taken to be $m = 1 M_\odot$. Adapted from Table 1 of Haugan, Shapiro and Wasserman (1982).

Stellar type	a (km)	M/M_\odot	$(r_{\text{tidal}}/R_S)^{1/2}$	\bar{A}
Main sequence	7×10^5	10	300	3×10^5
		10^3	70	500
		10^6	7	1
White dwarf	10^4	10	40	430
		10^3	8	7
		10^6	1	0.01
Neutron star	10	10	1.3	0.4
		10^3	1	7×10^{-3}
		10^6	1	10^{-5}

$\bar{\omega}a_h/c = 0.64 a_h/R_S$ and using eqs. (4.315) and (4.313), we find

$$\bar{A} \simeq \frac{a}{R_S} \left(\frac{M}{m} \right)^{1/9}, \quad (4.317)$$

and, if $\bar{A} \gtrsim 1$, we have a strong suppression of the total radiated power. In Table 4.1 we show the dilatation factor $(r_{\text{tidal}}/R_S)^{1/2}$ and the parameter \bar{A} for a range of different stars. Observe, from eq. (4.317), that for a given mass m the suppression is more important for stars with large radius a , since they are less compact and have less self-gravity to resist the tidal force of the black hole, and also it is more important for lower BH masses, because the smaller gravitational attraction at a fixed distance is overcompensated by the decrease in Schwarzschild radius, so tidal stripping takes place at shorter radial distances, where the gravitational field is stronger.

From eq. (4.317) and Table 4.1 we see for instance that a $1 M_\odot$ main sequence star produces significant GWs only if it falls into a supermassive BH with mass $M > O(10^6) M_\odot$. For a white dwarf we need $M > O(10^4) M_\odot$, while for a neutron star our equation suggest that it is needed $M > O(3) M_\odot$. Actually, a neutron star is so compact and has such a large rigidity that we certainly cannot treat it as a dust ball. We will examine in more detail black hole–neutron star coalescences in Vol. 2.

Having understood the physics with relatively simple arguments, we can now be more quantitative and compute the form factor. We found below eq. (4.297) that the solution of the Newtonian equation of motion, for a particle falling along the z axis which at $t = t_0$ has $z(t) = z_i$, can be written as

$$z^{3/2}(t; \bar{t}_i) = \frac{3}{2} R_S^{1/2} c(\bar{t}_i - t), \quad (4.318)$$

with \bar{t}_i defined by

$$\bar{t}_i = t_0 + \frac{2z_i^{3/2}}{3cR_S^{1/2}}. \quad (4.319)$$

Therefore, for a swarm of N particles of equal mass δm , eq. (4.302) gives

$$\tilde{M}_{33}(\omega) = \delta m \sum_{i=1}^N \int_{-\infty}^{t_{\max}} dt z^2(t; \bar{t}_i) e^{i\omega t}. \quad (4.320)$$

Since $z(t; \bar{t}_i)$ depends only on the combination $\bar{t}_i - t$, inside each integral we can shift the integration variable $t \rightarrow t + \bar{t}_i$. For large t_{\max} this does not change appreciably the upper integration limit, and we get

$$\begin{aligned} \tilde{M}_{33}(\omega) &= \delta m \sum_{i=1}^N \int_{-\infty}^{t_{\max}} dt z^2(t; 0) e^{i\omega(t+\bar{t}_i)} \\ &= \left[(\delta m) N \int_{-\infty}^{t_{\max}} dt z^2(t; 0) e^{i\omega t} \right] \left[\frac{1}{N} \sum_{i=1}^N e^{i\omega \bar{t}_i} \right]. \end{aligned} \quad (4.321)$$

Since $(\delta m)N$ is the total mass of the system, the first bracket gives the value of $M_{33}(\omega)$ in the point-like approximation.³⁸ The second bracket is the form factor, and we denote it by $F(\omega)$,

$$F(\omega) = \frac{1}{N} \sum_{i=1}^N e^{i\omega \bar{t}_i}. \quad (4.322)$$

In eq. (4.319) we choose t_0 as the time when the center-of-mass of the star crosses the tidal radius, so it is still an undeformed sphere. At $t = t_0$ the i -th constituent is located at $z_i = r_{\text{tidal}} + \delta z_i$, with $-a < \delta z_i < a$ and $|\delta z_i| \ll r_{\text{tidal}}$. Then eq. (4.319) becomes

$$\begin{aligned} \bar{t}_i &= t_0 + \frac{2(r_{\text{tidal}} + \delta z_i)^{3/2}}{3cR_S^{1/2}} \\ &\simeq \left[t_0 + \frac{2r_{\text{tidal}}^{3/2}}{3cR_S^{1/2}} \right] + \left(\frac{r_{\text{tidal}}}{R_S} \right)^{1/2} \frac{\delta z_i}{c}. \end{aligned} \quad (4.323)$$

The term in bracket does not depend on the index i and gives just a constant phase in eq. (4.322), which cancels when we take the modulus squared. Then

$$F(\omega) = \frac{1}{N} \sum_{i=1}^N \exp\{i\omega(r_{\text{tidal}}/R_S)^{1/2}\delta z_i/c\}. \quad (4.324)$$

Passing to the continuum limit we get, for a system of uniform density,

$$F(\omega) = \frac{1}{V} \int_V d(\delta z) d^2 x_\perp \exp\{i\omega(r_{\text{tidal}}/R_S)^{1/2}\delta z/c\}, \quad (4.325)$$

where the integration is over the volume V of the system at time t_0 , when it is an undeformed sphere of radius a and $V = (4/3)\pi a^3$. At

³⁸As we discussed in the previous subsection, the integral in $\tilde{M}_{33}(\omega)$ is actually divergent. For the purpose of computing the form factor this is irrelevant; we can repeat the argument with $\tilde{M}_{33}(\omega)$, which converges, or we can just regularize the integral in $\tilde{M}_{33}(\omega)$, since anyway the form factor factorizes.

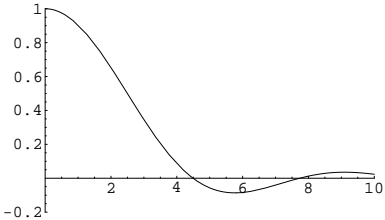


Fig. 4.20 The form factor $F(A(\omega))$, plotted as a function of $A = (\omega a/c)(r_{\text{tidal}}/R_S)^{1/2}$.

fixed δz the radius of the circle in the transverse direction is given by $|x_\perp|^2 = a^2 - (\delta z)^2 = a^2(1 - u^2)$, where we have written $\delta z = au$, with $-1 < u < 1$. Then the integration over the transverse plane of the sphere at fixed u gives $\pi a^2(1 - u^2)$, and

$$F(\omega) = \frac{1}{(4/3)\pi a^3} \pi a^3 \int_{-1}^1 du (1 - u^2) \exp\{i(\omega a/c)(r_{\text{tidal}}/R_S)^{1/2}u\}. \quad (4.326)$$

We see that the combination $A(\omega) = (\omega a/c)(r_{\text{tidal}}/R_S)^{1/2}$ appears in the exponential and governs the form factor, as we expected from the physical arguments presented above. Then

$$\begin{aligned} F(\omega) &= \frac{3}{4} \int_{-1}^1 du (1 - u^2) e^{iA(\omega)u} \\ &= \frac{3}{A^2(\omega)} \left[\frac{\sin A(\omega)}{A(\omega)} - \cos A(\omega) \right]. \end{aligned} \quad (4.327)$$

The form factor f is shown in Fig. 4.20 as a function of A . Since $dE/d\omega$ is proportional to $|\tilde{M}_{33}(\omega)|^2$, the spectrum for a real star is related to the point-like spectrum by

$$\left(\frac{dE}{d\omega} \right)^{\text{real star}} = |F(\omega)|^2 \left(\frac{dE}{d\omega} \right)^{\text{point-like}}. \quad (4.328)$$

4.4 Radiation from accelerated masses

In electrodynamics, a prototype example is the radiation emitted by an accelerated charge. In this section we examine the corresponding gravitational radiation emitted by an accelerated mass. Beside possible applications to astrophysical situations, this exercise is quite instructive by itself, and in particular it will allow us to understand that, while electromagnetic radiation from accelerated particles is beamed in a narrow cone in the forward direction, this is not the case for the GWs produced by an accelerated mass.

4.4.1 GWs produced in elastic collisions

We begin by considering the gravitational radiation produced during the elastic deflection of an object by a fixed scattering center (or, equivalently, a two-body collision in the center-of-mass frame). We denote the initial and final four-momenta of the object by p^μ and p'^μ , respectively.

The energy-momentum tensor of a free particle of mass m is given in eq. (3.121). In principle, given the interaction between the object and the scattering center and the initial conditions, we should compute the classical trajectory $x_0^\mu(t)$, plug it into the energy-momentum tensor (supplemented by the interaction terms) and perform the Fourier transform. However, in general this is neither practically feasible nor really necessary. We can instead approximate the collision as instantaneous,

and we consider an elastic scattering, so $p'^0 = p^0$. Then we write, using eq. (3.120),

$$T^{\mu\nu}(\mathbf{x}, t) = \frac{p^\mu p^\nu}{\gamma m} \delta^{(3)}(\mathbf{x} - \mathbf{v}t) \theta(-t) + \frac{p'^\mu p'^\nu}{\gamma m} \delta^{(3)}(\mathbf{x} - \mathbf{v}'t) \theta(t), \quad (4.329)$$

where $\theta(t)$ is the step function: $\theta(t) = 1$ if $t > 0$ and $\theta(t) = 0$ if $t < 0$. In a collision that lasts for a time Δt are generated frequencies up to $\omega_{\max} \sim 2\pi/\Delta t$ and therefore, when we approximate the collision as instantaneous, we are introducing spurious contributions at arbitrarily high frequencies. To recover the correct physical result it is sufficient to estimate the time Δt actually taken by the collision. In a collision with impact parameter b and relative velocity v , we have $\Delta t \sim b/v$, and we must cutoff the spectrum at $\omega_{\max} \sim 2\pi v/b$. At $\omega \ll \omega_{\max}$ the spectrum is well reproduced by the instantaneous approximation.

The four-dimensional Fourier transform of (4.329) is

$$\begin{aligned} \tilde{T}^{\mu\nu}(\mathbf{k}, \omega) &= \int_{-\infty}^{\infty} c dt \int d^3x T^{\mu\nu}(\mathbf{x}, t) e^{i\omega t - i\mathbf{k}\cdot\mathbf{x}} \\ &= \frac{p^\mu p^\nu}{\gamma m} \int_{-\infty}^0 c dt e^{i\omega t - i\mathbf{k}\cdot\mathbf{v}t} + \frac{p'^\mu p'^\nu}{\gamma m} \int_0^{\infty} c dt e^{i\omega t - i\mathbf{k}\cdot\mathbf{v}'t}. \end{aligned} \quad (4.330)$$

In the first integral we add a factor $i\epsilon t$ at the exponent, with $\epsilon \rightarrow 0^+$, to assure the convergence at $t = -\infty$, while in the second we add $-i\epsilon t$, to assure the convergence at $t = +\infty$. Then

$$\tilde{T}^{\mu\nu}(\mathbf{k}, \omega) = \frac{c}{i\gamma m} \left[\frac{p^\mu p^\nu}{\omega - \mathbf{k}\cdot\mathbf{v} - i\epsilon} - \frac{p'^\mu p'^\nu}{\omega - \mathbf{k}\cdot\mathbf{v}' + i\epsilon} \right]. \quad (4.331)$$

If the particle which is being deflected is not massless, the denominators are never zero and we can set $\epsilon = 0$. We compute first in the non-relativistic limit and then in the general case.

Non-relativistic limit

In this case in the denominators we approximate $\gamma \simeq 1$ and we neglect the terms $\mathbf{k}\cdot\mathbf{v}$ and $\mathbf{k}\cdot\mathbf{v}'$, so we find simply

$$\tilde{T}_{ij}(\omega) \simeq -\frac{ic}{m\omega} (p_i p_j - p'_i p'_j). \quad (4.332)$$

We use a reference frame where the scattering plane is the (x, y) plane; the initial velocity is $\mathbf{v} = v(1, 0, 0)$ and the final velocity is

$$\mathbf{v}' = v(\cos \vartheta_s, \sin \vartheta_s, 0), \quad (4.333)$$

where ϑ_s is the scattering angle and $|\mathbf{v}'| = |\mathbf{v}| = v$ since we are considering elastic scattering. Let (θ, ϕ) be the polar angles which identify the direction of the unit vector $\hat{\mathbf{n}}$ in this frame (i.e. the angles that describe the angular distribution of the gravitational radiation), so

$\hat{\mathbf{n}} = (\sin \theta \cos \phi, \sin \theta \sin \phi, \cos \theta)$. Then, performing explicitly the contraction $\Lambda_{ij,kl} \tilde{T}_{ij}(\omega) \tilde{T}_{kl}^*(\omega)$ in eq. (3.16), we find

$$\frac{dE}{d\omega d\Omega} = \frac{Gm^2v^4}{\pi^2 c^5} \sin^2 \vartheta_s \left[\cos^2 \theta + \frac{1}{4} \sin^2(\vartheta_s - 2\phi) \sin^4 \theta \right]. \quad (4.334)$$

The emission pattern is shown in Fig. 4.21, for the case $\vartheta_s = \pi/2$. Observe that the radiation is emitted mostly along the z axis, i.e. in the direction perpendicular to the scattering plane. Integrating over the solid angle $d\Omega = d\cos \theta d\phi$ we get

$$\frac{dE}{d\omega} = \frac{8G}{5\pi c^5} m^2 v^4 \sin^2 \vartheta_s. \quad (4.335)$$

For the corresponding two-body problem, m is the reduced mass, v the relative velocity and ϑ_s is the scattering angle in the center-of-mass.

Actually, if one is interested only in the radiated energy, integrated over the solid angle, and not in its angular distribution, it can be computed more quickly observing that in the non-relativistic approximation \tilde{T}_{ij} is independent of the angle (all the angular dependence was in the terms $\mathbf{k} \cdot \mathbf{v}$ and $\mathbf{k} \cdot \mathbf{v}'$ that we dropped), and therefore

$$\int d\Omega \Lambda_{ij,kl} \tilde{T}_{ij} \tilde{T}_{kl}^* = \tilde{T}_{ij} \tilde{T}_{kl}^* \int d\Omega \Lambda_{ij,kl}. \quad (4.336)$$

The integral is performed using eq. (3.74), and we get back eq. (4.335).

The frequency spectrum found in eq. (4.335) is flat up to the cut-off frequency $\omega_{\max} \sim 2\pi v/b$, and the total radiated energy is obtained integrating up to ω_{\max} , so

$$\begin{aligned} E_{\text{rad}} &\sim \frac{16Gm^2}{5b} \left(\frac{v}{c} \right)^5 \sin^2 \vartheta_s \\ &= \frac{8}{5} mc^2 \left(\frac{R_S}{b} \right) \left(\frac{v}{c} \right)^5 \sin^2 \vartheta_s, \end{aligned} \quad (4.337)$$

where $R_S = 2Gm/c^2$ is the Schwarzschild radius of an object of mass m . Therefore the total energy radiated is suppressed, with respect to the rest-mass energy mc^2 of the particle, both by the by-now familiar factor $(v/c)^5$ (compare, e.g. with eqs. (3.319) or (3.340)) and by the ratio R_S/b .

Relativistic limit

In the general relativistic case we repeat the same steps using the full expression for $\tilde{T}^{\mu\nu}(\mathbf{k}, \omega)$ given in eq. (4.331), with $p^i = \gamma m v^i$, and setting $\mathbf{k} = \omega \hat{\mathbf{n}}/c$ (see eq. (3.16)). We then find

$$\begin{aligned} \frac{dE}{d\omega d\Omega} &= \frac{Gm^2\gamma^2 v^4}{\pi^2} \\ &\times [f_1(v, \vartheta_s; \theta, \phi) - f_2(v, \vartheta_s; \theta, \phi) \sin^2 \theta + f_3(v, \vartheta_s; \theta, \phi) \sin^4 \theta], \end{aligned} \quad (4.338)$$

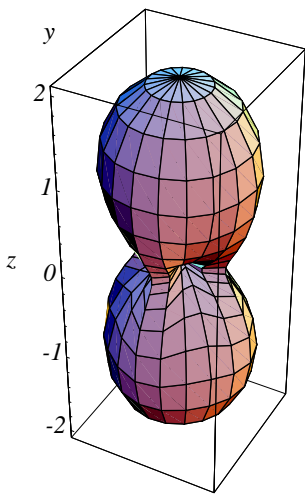


Fig. 4.21 The angular distribution of the gravitational radiation in the non-relativistic limit. The scattering plane is $z = 0$ and we have taken $\vartheta_s = \pi/2$.

where

$$\begin{aligned} f_1(v, \vartheta_s; \theta, \phi) &= ab \sin^2 \vartheta_s + \frac{1}{4}(a - b)^2, \\ f_2(v, \vartheta_s; \theta, \phi) &= \frac{a(a + b)}{2} \cos^2 \phi + \frac{b(a + b)}{2} \cos^2(\phi - \vartheta_s) \\ &\quad - 2ab \cos \vartheta_s \cos \phi \cos(\phi - \vartheta_s), \\ f_3(v, \vartheta_s; \theta, \phi) &= \frac{1}{4} [a \cos^2 \phi - b \cos^2(\phi - \vartheta_s)]^2, \end{aligned} \quad (4.339)$$

and

$$\begin{aligned} a \equiv a(v; \theta, \phi) &= \frac{1}{1 - \hat{\mathbf{n}} \cdot \mathbf{v}/c} \\ &= \frac{1}{1 - (v/c) \sin \theta \cos \phi}, \end{aligned} \quad (4.340)$$

$$\begin{aligned} b \equiv b(v, \vartheta_s; \theta, \phi) &= \frac{1}{1 - \hat{\mathbf{n}} \cdot \mathbf{v}'/c} \\ &= \frac{1}{1 - (v/c) \sin \theta \cos(\phi - \vartheta_s)}. \end{aligned} \quad (4.341)$$

In the non-relativistic limit we have $a \rightarrow 1, b \rightarrow 1$ and, making use of the identities

$$\cos^2 \phi + \cos^2(\phi - \vartheta_s) - 2 \cos \vartheta_s \cos \phi \cos(\phi - \vartheta_s) = \sin^2 \vartheta_s, \quad (4.342)$$

$$\cos^2 \phi - \cos^2(\phi - \vartheta_s) = \sin(\vartheta_s - 2\phi) \sin \vartheta_s, \quad (4.343)$$

we recover eq. (4.334). Instead, in the ultra-relativistic limit, the factors a and b bend the radiation in the direction of the motion (more precisely, in a direction determined by a combination of the initial and final velocity). The resulting pattern function is shown in Fig. 4.22 for the case $v = 0.8$. The distribution is tilted in the direction of motion but the radiation is not focused in a very narrow cone, contrary to what happens in electrodynamics. We examine this point in detail in the simpler geometrical setting of the next subsection.

4.4.2 Lack of beaming of GWs from accelerated masses

In order to examine this effect eliminating irrelevant complications, let us consider an inelastic scattering in which a particle of mass m initially at rest, is accelerated in time Δt to a velocity v .³⁹

As in the previous problem, we assume that the acceleration is instantaneous and we then cut off the spectrum at $\omega_{\max} \sim 2\pi/\Delta t$. The energy-momentum tensor is again given by eq. (4.331), where now the first term vanishes (since the initial velocity is zero) and in the second term \mathbf{v}' is the final velocity, which we now denote by \mathbf{v} . Therefore

$$\begin{aligned} \tilde{T}^{ij}(\omega \hat{\mathbf{n}}/c, \omega) &= \frac{ic\gamma m}{\omega} \frac{v^i v^j}{1 - \hat{\mathbf{n}} \cdot \mathbf{v}/c} \\ &= \frac{ic\gamma m}{\omega} \frac{v^i v^j}{1 - (v/c) \cos \theta}. \end{aligned} \quad (4.344)$$

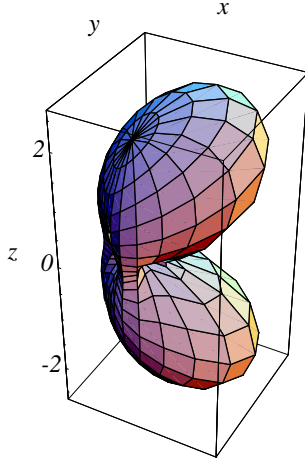


Fig. 4.22 The angular distribution of the gravitational radiation in the relativistic limit. The scattering plane is $z = 0$ and we have taken $\vartheta_s = \pi/2$ and $v = 0.8$.

³⁹In principle our formalism is valid only if we have a closed system, so the total $T^{\mu\nu}$ is conserved. However, we can imagine for instance that the particle of mass m is electrically charged, and is accelerated by the electric field inside a capacitor. To this closed system we can apply our formalism. If the arms of the capacitor are infinitely heavy, they do not contribute to the gravitational radiation because a heavy object of mass M , in the scattering process, acquires a recoil velocity $V \sim 1/M$ and its contribution to $dE/d\omega$, according to eq. (4.335), is $dE/d\omega \sim M^2 V^4 = O(1/M^2)$. Thus, in practice we can just consider the particle of mass m on the accelerated trajectory.

From eq. (3.16) we find

$$\frac{dE}{d\Omega d\omega} = \frac{Gm^2\gamma^2}{2\pi^2c^5} \Lambda_{ij,kl} \frac{v^i v^j v^k v^l}{[1 - (v/c) \cos \theta]^2}. \quad (4.345)$$

Using eq. (1.39) and performing the contractions, we get

$$\frac{dE}{d\Omega d\omega} = \frac{Gm^2\gamma^2}{4\pi^2c} \left(\frac{v}{c}\right)^4 \frac{\sin^4 \theta}{[1 - (v/c) \cos \theta]^2}, \quad (4.346)$$

or

$$\frac{dE}{d\Omega d\omega} = \frac{Gm^2}{4\pi^2c} \left(\frac{v}{c}\right)^4 p_{\text{gw}}(\theta), \quad (4.347)$$

where

$$p_{\text{gw}}(\theta) = \gamma^2 \frac{\sin^4 \theta}{[1 - (v/c) \cos \theta]^2} \quad (4.348)$$

describes the angular pattern. It is interesting to compare this result with the electromagnetic radiation produced by a charged particle suddenly accelerated from rest to velocity v . This is given by (see Jackson 1975, eq. (15.65))

$$\left. \frac{dE}{d\Omega d\omega} \right|_{EM} = \left(\frac{e^2}{4\pi^2c} \right) \left(\frac{v}{c} \right)^2 p_{\text{em}}(\theta), \quad (4.349)$$

where

$$p_{\text{em}}(\theta) = \frac{\sin^2 \theta}{[1 - (v/c) \cos \theta]^2}. \quad (4.350)$$

Fig. 4.23 The function $p_{\text{em}}(\theta)$, in polar coordinates, for a charged particle with acceleration parallel to the velocity, and $v = 0.99$.

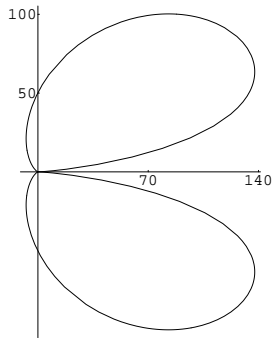


Fig. 4.24 The function $p_{\text{gw}}(\theta)$ for a particle with acceleration parallel to the velocity, and $v = 0.99$. Observe the difference in shape compared to Fig. 4.23.

Both the gravitational and the electromagnetic radiations are tilted forward, because of the factor $[1 - (v/c) \cos \theta]^2$ in the denominator. However, the different power of $\sin \theta$ in the numerator produces a crucial difference in the overall shape. In fact, $p_{\text{em}}(\theta)$ has a maximum at an angle $\bar{\theta}$ given by $\cos \bar{\theta} = v/c$ so, for large γ , $\bar{\theta} \simeq 1/\gamma$; at the same time, the width of this maximum is $\Delta\theta = O(1/\gamma)$. Therefore, for $\gamma \rightarrow \infty$, the electromagnetic radiation is not only tilted asymptotically toward the forward direction, but is also beamed into a very narrow cone.

The angular pattern for GW is very different. First of all, the angle $\bar{\theta}$ that maximizes $p_{\text{gw}}(\theta)$ is given by $\cos \bar{\theta} = c(\gamma - 1)/(v\gamma)$ which, in the large γ limit, becomes $\bar{\theta} \simeq (2/\gamma)^{1/2}$; therefore $\bar{\theta}$ goes to zero only as $O(1/\sqrt{\gamma})$. Second, and more important, one easily checks from the explicit expression that the width of the maximum of $p_{\text{gw}}(\theta)$ is $\Delta\theta = O(1)$, to be compared with $\Delta\theta = O(1/\gamma)$ for the electromagnetic case. This is due to the fact that the value of p_{em} at its maximum is γ^2 , and it drops to values $O(1)$ if we move away from the maximum by $\Delta\theta = O(1/\gamma)$; for the gravitational radiation, it is still true that the value of p_{gw} at its maximum is $O(\gamma^2)$ just because of the factor γ^2 in front of it, but it remains $O(\gamma^2)$ if we move away from the maximum by a $\Delta\theta = O(1)$.

Therefore, even in the limit $\gamma \rightarrow \infty$, the gravitational radiation is not beamed in a narrow cone, but it is extended over a solid angle comparable to 4π . The electromagnetic and gravitational radiation pattern are shown in Figs. 4.23 and 4.24, respectively, for $v = 0.99$. The origin of the difference is the factor $\sin^4 \theta$ in the numerator of eq. (4.348), which reflect the spin-2 nature of the gravitational field, compared to the $\sin^2 \theta$ in the numerator of eq. (4.350), which reflect the spin-1 nature of the electromagnetic field.

To understand this point better, it is instructive to rederive this angular distribution, that we have obtained from a purely classical treatment, using the language of quantum field theory. This can be done evaluating Feynman diagrams such as that in Fig. 4.25, that describe the emission of a graviton by an accelerated particle. The angular dependence is easily understood observing that the propagator of the massive particle gives a contribution to the amplitude proportional to

$$\frac{1}{(p+k)^2 + m^2} = \frac{1}{2(pk)}, \quad (4.351)$$

where p is the final four-momentum of the massive particle and k of the graviton, (pk) denotes the scalar product of the two four-vectors, and we used $p^2 = -m^2$ and $k^2 = 0$. We write $p^\mu = (E_p/c, |\mathbf{p}|, 0, 0)$, with $|\mathbf{p}| = E_p v/c^2$, while the graviton four-momentum is

$$k^\mu = (E_g/c, |\mathbf{k}| \cos \theta, |\mathbf{k}| \sin \theta, 0), \quad (4.352)$$

where $|\mathbf{k}| = E_g/c$. Then

$$(pk) = -\frac{1}{c^2} E_p E_k [1 - (v/c) \cos \theta]. \quad (4.353)$$

This gives a factor $[1 - (v/c) \cos \theta]$ in the denominator, in the amplitude \mathcal{M} , and therefore a factor $[1 - (v/c) \cos \theta]^2$ in the emission probability, which is $\sim |\mathcal{M}|^2$. This is independent of whether the wavy line in Fig. 4.25 is a photon or a graviton, as long as it is a massless particle, and elucidates why, both in $p_{\text{em}}(\theta)$ and in $p_{\text{gw}}(\theta)$, the angular dependence of the denominators is the same, $[1 - (v/c) \cos \theta]^2$.

The numerator is instead fixed by the emission vertex. For a photon, the external line carries its wavefunction $\epsilon_\mu^*(k)$. Recall that physical photons are transverse, $\epsilon_\mu(k) k^\mu = 0$. With k^μ given by eq. (4.352), this equation has two linearly independent solutions

$$\epsilon_\mu^{(1)}(k) = (0, \sin \theta, -\cos \theta, 0), \quad \epsilon_\mu^{(2)}(k) = (0, 0, 0, 1), \quad (4.354)$$

which corresponds to the two physical polarizations (plus the pure gauge mode $\epsilon^\mu \sim k^\mu$). The amplitude is proportional to⁴⁰

$$\sum_{\lambda=1,2} \epsilon_\mu^{(\lambda)}(k) p^\mu = |\mathbf{p}| \sin \theta. \quad (4.355)$$

Therefore in the numerator, in the amplitude, we have a factor $\sin \theta$, which gives a factor $\sin^2 \theta$ in $p_{\text{em}}(\theta)$, in agreement with eq. (4.350).

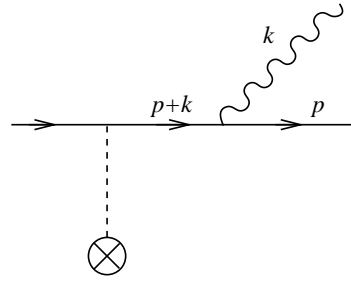


Fig. 4.25 A Feynman diagram corresponding to graviton emission by an accelerated mass. The cross denotes the external field that accelerates the mass. The wavy line represents the graviton.

⁴⁰The fact that the Lorentz index carried by ϵ_μ is saturated by p^μ can be obtained writing explicitly the interaction vertex in quantum electrodynamics, but in fact it is evident from the fact that the amplitude must be linear in ϵ_μ , so we cannot saturate the index μ contracting ϵ_μ with a second polarization vector ϵ^μ , neither we can contract it with k^μ , since $\epsilon_\mu(k) k^\mu$ vanishes. Then $\epsilon_\mu(k) p^\mu$ is the only possible Lorentz scalar. Note also that, according to the Feynman rules of QED, an outgoing photon is actually associated to a factor ϵ_μ^* , but we have chosen a real basis for the polarization vectors.

⁴¹The computation is faster if we orient the axes so that the z axis is in the direction of the graviton momentum \mathbf{k} , and the scattering plane in Fig. 4.25 is identified with the (y, z) plane. In this frame $k^\mu = (E_g/c)(1, 0, 0, 1)$ and $p^\mu = (E_p/c, 0, |\mathbf{p}| \sin \theta, |\mathbf{p}| \cos \theta)$. The advantage is that in this frame the polarization tensors have the simple form

$$e_{\mu\nu}^+ = \begin{pmatrix} 0 & 0 & 0 & 0 \\ 0 & 1 & 0 & 0 \\ 0 & 0 & -1 & 0 \\ 0 & 0 & 0 & 0 \end{pmatrix}_{\mu\nu}$$

and

$$e_{\mu\nu}^\times = \begin{pmatrix} 0 & 0 & 0 & 0 \\ 0 & 0 & 1 & 0 \\ 0 & 1 & 0 & 0 \\ 0 & 0 & 0 & 0 \end{pmatrix}_{\mu\nu},$$

see eq. (1.56). Then $e_{\mu\nu}^+ p^\mu p^\nu = -|\mathbf{p}|^2 \sin^2 \theta$ and $e_{\mu\nu}^\times p^\mu p^\nu = 0$.

Similarly, an external graviton line is associated to the polarization tensor $e_{\mu\nu}(k)$ of the graviton, and the physical polarizations correspond to the plus and cross polarization tensors $e_{\mu\nu}^{(+)}(k)$ and $e_{\mu\nu}^{(\times)}(k)$, that satisfy the condition $e_{\mu\nu}(k)k^\mu = 0$. As before, the Lorentz indices can be saturated only by p^μ , so this factor contributes to the amplitude as⁴¹

$$\sum_{\lambda=+, \times} e_{\mu\nu}^{(\lambda)}(k) p^\mu p^\nu = -|\mathbf{p}|^2 \sin^2 \theta. \quad (4.356)$$

This produces a factor $\sin^4 \theta$ in the modulus squared of the amplitude, and therefore in $p_{\text{gw}}(\theta)$, in agreement with eq. (4.348).

Coming back to eq. (4.346) and integrating over the solid angle we get

$$\frac{dE}{d\omega} = \frac{2Gm^2}{3\pi c} \left[\gamma^2 \left(6 - \frac{4v^2}{c^2} \right) - \frac{3c}{v} \log \frac{c+v}{c-v} \right]. \quad (4.357)$$

In the non-relativistic limit $v \rightarrow 0$, this reduces to

$$\frac{dE}{d\omega} \simeq \frac{8}{15\pi c^5} Gm^2 v^4, \quad (v/c \rightarrow 0), \quad (4.358)$$

while in the ultra-relativistic limit

$$\frac{dE}{d\omega} \simeq \frac{4}{3\pi c} Gm^2 \gamma^2 \left[1 - \frac{3 \log \gamma^2}{2\gamma^2} + O\left(\frac{1}{\gamma^2}\right) \right], \quad (v/c \rightarrow 1). \quad (4.359)$$

This spectrum is flat up to the maximum frequency $\omega_{\text{max}} \sim 2\pi/\Delta t$, and the total radiated energy is therefore obtained multiplying by ω_{max} .

4.5 Solved problems

Problem 4.1. Fourier transform of the chirp signal

In this problem we compute the Fourier transform of the amplitudes given in eqs. (4.31) and (4.32). We consider first h_+ , and we write it in the form

$$h_+(t) = A(t_{\text{ret}}) \cos \Phi(t_{\text{ret}}), \quad (4.360)$$

where

$$A(t_{\text{ret}}) = \frac{1}{r} \left(\frac{GM_c}{c^2} \right)^{5/4} \left(\frac{5}{c(t_c - t_{\text{ret}})} \right)^{1/4} \left(\frac{1 + \cos^2 \iota}{2} \right), \quad (4.361)$$

and, in this problem, t_c is the value of *retarded* time at coalescence. The Fourier transform is

$$\begin{aligned} \tilde{h}_+(f) &= \int dt A(t_{\text{ret}}) \cos \Phi(t_{\text{ret}}) e^{i2\pi f t} \\ &= \frac{1}{2} e^{i2\pi f r/c} \int dt_{\text{ret}} A(t_{\text{ret}}) \left(e^{i\Phi(t_{\text{ret}})} + e^{-i\Phi(t_{\text{ret}})} \right) e^{i2\pi f t_{\text{ret}}}, \end{aligned} \quad (4.362)$$

and now in the last integral we rename $t_{\text{ret}} \rightarrow t$. We have not written explicitly the limits of integration since we will compute this integral with the stationary

phase method. Then, all we need is that the stationary point be within the integration domain $t < t_c$, and the fact that $A(t_{\text{ret}})$ diverges at the limit of integration $t - t_c$ becomes irrelevant, as long as the stationary phase method is justified (see below). We take $f > 0$, since the value at $f < 0$ can be obtained from $\tilde{h}_+(-f) = \tilde{h}_+^*(f)$. Then, observing that $\dot{\Phi} = \omega_{\text{gw}}(t) > 0$, we see that only the term proportional to $e^{-i\Phi(t)+i2\pi ft}$ has a stationary point, while the term proportional to $e^{i\Phi(t)+i2\pi ft}$ is always oscillating fast, and integrates to a negligibly small value. Therefore

$$\tilde{h}_+(f) \simeq \frac{1}{2} e^{i2\pi fr/c} \int dt A(t) e^{i[2\pi ft - \Phi(t)]}. \quad (4.363)$$

Since $\log A(t)$ varies slowly in comparison with $\Phi(t)$, the stationary point $t_*(f)$ is determined by the condition $2\pi f = \dot{\Phi}(t_*)$. However $\dot{\Phi} = \omega_{\text{gw}}$, so this condition expresses the rather natural fact that the largest contribution to the Fourier component $\tilde{h}_+(f)$ with a given f is obtained for the values of t such that the chirping frequency $\omega_{\text{gw}}(t)$ is equal to $2\pi f$. Expanding the exponential to order $(t - t_*)^2$ we find

$$\tilde{h}_+(f) \simeq \frac{1}{2} e^{i2\pi fr/c} A(t_*) e^{i[2\pi ft_* - \Phi(t_*)]} \left(\frac{2}{\ddot{\Phi}(t_*)} \right)^{1/2} \int_{-\infty}^{\infty} dx e^{-ix^2}. \quad (4.364)$$

The latter integral is a Fresnel integral, and is given by

$$\int_{-\infty}^{\infty} dx e^{-ix^2} = \sqrt{\pi} e^{-i\pi/4} \quad (4.365)$$

(see Gradshteyn and Ryzhik 1980, 8.25). Therefore

$$\tilde{h}_+(f) = \frac{1}{2} e^{i\Psi_+} A(t_*) \left(\frac{2\pi}{\ddot{\Phi}(t_*)} \right)^{1/2}, \quad (4.366)$$

where

$$\Psi_+ = 2\pi f(t_* + r/c) - \Phi(t_*) - (\pi/4). \quad (4.367)$$

Using $2\pi f = \omega_{\text{gw}}(t_*)$ and the explicit expression of $\omega_{\text{gw}}(t)$ given in eq. (4.19), we can eliminate $\tau_* = t_c - t_*$ in favor of f , obtaining

$$\tau_*(f) = \frac{5}{256} (GM_c/c^3)^{-5/3} (\pi f)^{-8/3}. \quad (4.368)$$

Inserting this into the expressions for $A(\tau)$, given in eq. (4.361), and for $\ddot{\Phi}$, obtained differentiating twice eq. (4.30), we find

$$\frac{1}{2} A(t_*) \left(\frac{2\pi}{\ddot{\Phi}(t_*)} \right)^{1/2} = \left[\left(\frac{5}{24} \right)^{1/2} \frac{1}{\pi^{2/3}} \right] \frac{c}{r} \left(\frac{GM_c}{c^3} \right)^{5/6} f^{-7/6} \left(\frac{1 + \cos^2 \iota}{2} \right), \quad (4.369)$$

and therefore we get the result given in the text, see eq. (4.34). Similarly, inserting the value of $t_* = t_c - \tau_*$ given by eq. (4.368) into eq. (4.367) we get the phase $\Psi_+(f)$ given in eq. (4.37). Repeating the same steps for \tilde{h}_\times we get the same prefactor, apart for the different dependence on ι , and $\Psi_\times = \Psi_+ + (\pi/2)$.

To compute the energy spectrum we need the quantity

$$|\tilde{h}_+(f)|^2 + |\tilde{h}_\times(f)|^2 = \frac{5}{24 \pi^{4/3} r^2 c^3} \frac{(GM_c)^{5/3}}{f^{7/3}} g(\iota), \quad (4.370)$$

where the function $g(\ell)$ is defined in eq. (4.9). Using eq. (4.10), we see that the angular average of $|\tilde{h}_+(f)|^2 + |\tilde{h}_\times(f)|^2$ is

$$\int \frac{d\Omega}{4\pi} |\tilde{h}_+(f)|^2 + |\tilde{h}_\times(f)|^2 = \frac{1}{6\pi^{4/3} r^2 c^3} \frac{(GM_c)^{5/3}}{f^{7/3}}. \quad (4.371)$$

It should be observed that the stationary point approximation that we have used is less and less good as f grows. In fact, as f grows, the stationary point t_* approaches the coalescence time t_c . Since the function $A(t)$ diverges as $t \rightarrow t_c$, the approximation that $\log A(t)$ varies slowly in comparison with $\Phi(t)$ becomes less and less accurate. To check the validity of the stationary point approximation for $\tilde{h}_{+,\times}(f)$, we compare the total radiated energy computed using the saddle point approximation, eq. (4.43), with an exact numerical evaluation of the time integral in the inspiral phase. Therefore we start from the exact expression

$$\Delta E_{\text{rad}} = \frac{r^2 c^3}{16\pi G} \int d\Omega \int_{-\infty}^{t_*} dt \left(h_+^2 + h_\times^2 \right), \quad (4.372)$$

which gives the energy radiated up to time t_* , and we compute numerically the integral. Inserting into this expression the GW amplitude given by eq. (4.29) and performing the integral over $d\Omega$, we find

$$\begin{aligned} \Delta E_{\text{rad}} &= \frac{(GM_c)^{10/3}}{2^{1/3} G c^5} (GM_c)^{10/3} \\ &\times \int_{-\infty}^{t_*} dt \frac{14}{15} \left[\frac{d}{dt} (\omega_{\text{gw}}^{2/3} \cos \Phi) \right]^2 + \frac{2}{3} \left[\frac{d}{dt} (\omega_{\text{gw}}^{2/3} \sin \Phi) \right]^2. \end{aligned} \quad (4.373)$$

We now compute the time derivatives, taking into account that ω_{gw} depends on t , and that $d\Phi/dt = \omega_{\text{gw}}$. The result can be written in the form

$$\Delta E_{\text{rad}} \simeq \frac{5^{7/5}}{2^{34/5}} M_c c^2 \left[\frac{1}{10} \left(\frac{8}{5} \right)^{12/5} a_1 + \left(\frac{8}{5} \right)^{7/5} a_2 - \frac{1}{30} \left(\frac{8}{5} \right)^{12/5} a_3 \right], \quad (4.374)$$

with

$$a_1 = \int_{x_*}^{\infty} \frac{dx}{x^{17/5}} \left(\frac{7}{15} \cos^2 x + \frac{1}{3} \sin^2 x \right), \quad (4.375)$$

$$a_2 = \int_{x_*}^{\infty} \frac{dx}{x^{7/5}} \left(\frac{7}{15} \sin^2 x + \frac{1}{3} \cos^2 x \right), \quad (4.376)$$

$$a_3 = \int_{x_*}^{\infty} \frac{dx}{x^{12/5}} \sin 2x. \quad (4.377)$$

The lower limit of the integrals, x_* , is given by

$$x_* = 2 \left(\frac{5GM_c}{c^3} \right)^{-5/8} \tau_*^{5/8}. \quad (4.378)$$

Taking $M_c \simeq 1.21M_\odot$ (corresponding to two equal masses $M_{\text{NS}} = 1.4M_\odot$), and $\tau_* \simeq 4.6$ ms which, according to eq. (4.20), correspond to taking a cutoff at $f_{\text{max}} = 1$ kHz, we have $x_* \simeq 46.1$. Computing numerically the integrals, we find that $a_2 \simeq 0.21$ while $a_1, a_3 = O(10^{-5})$ are negligible. Since a_1, a_3 come from the terms with $\dot{\omega}_{\text{gw}}$, the result could have been obtained more simply neglecting the derivatives of ω_{gw} in eq. (4.373) (this is indeed the reason why the stationary point approximation discussed in the previous problem works well). Putting together the numerical factors, we finally arrive at $\Delta E_{\text{rad}} \simeq 4.2 \times 10^{-2} M_\odot c^2$, in full agreement with eq. (4.43).

Problem 4.2. Fourier decomposition of elliptic Keplerian motion

In this problem we compute the Fourier decomposition of the Keplerian motion and of its second mass moment. Using eqs. (4.63), (4.64) and (4.58) we write

$$x(\beta) = a(\cos u - e), \quad (4.379)$$

$$y(\beta) = b \sin u, \quad (4.380)$$

where the dependence of u on β is given implicitly by

$$\beta = u - e \sin u. \quad (4.381)$$

As shown between eq. (4.83) and eq. (4.93), we can write

$$x(\beta) = \sum_{n=0}^{\infty} a_n \cos(n\beta), \quad (4.382)$$

$$y(\beta) = \sum_{n=1}^{\infty} b_n \sin(n\beta), \quad (4.383)$$

which can be inverted to give, for $n \neq 0$,

$$\begin{aligned} a_n &= \frac{2}{\pi} \int_0^\pi d\beta x(\beta) \cos(n\beta) \\ &= \frac{2a}{\pi} \int_0^\pi d\beta (\cos u - e) \cos(n\beta), \end{aligned} \quad (4.384)$$

and

$$\begin{aligned} b_n &= \frac{2}{\pi} \int_0^\pi d\beta y(\beta) \sin(n\beta) \\ &= \frac{2b}{\pi} \int_0^\pi d\beta \sin u \sin(n\beta), \end{aligned} \quad (4.385)$$

while, for $n = 0$,

$$a_0 = \frac{1}{\pi} \int_0^\pi d\beta x(\beta). \quad (4.386)$$

The integrals for $n \neq 0$ can be performed using the integral representation of the Bessel function $J_n(z)$,

$$J_n(z) = \int_0^\pi \frac{du}{\pi} \cos(nu - z \sin u), \quad (4.387)$$

(see e.g. Gradshteyn and Ryzhik 1980, 8.411.1). Then we have, for $n \neq 0$,

$$\begin{aligned} a_n &= 2a \int_0^\pi \frac{d\beta}{\pi} (\cos u - e) \cos(n\beta) \\ &= \frac{2a}{n} \int_0^\pi \frac{d\beta}{\pi} (\cos u - e) \frac{d}{d\beta} \sin(n\beta) \\ &= -\frac{2a}{n} \int_0^\pi \frac{d\beta}{\pi} \left[\frac{d}{d\beta} (\cos u - e) \right] \sin(n\beta) \\ &= -\frac{2a}{n} \int_0^\pi \frac{du}{\pi} \left[\frac{d}{du} (\cos u - e) \right] \sin(n\beta) \\ &= \frac{2a}{n} \int_0^\pi \frac{du}{\pi} \sin u \sin(nu - ne \sin u). \end{aligned} \quad (4.388)$$

We now use the identity $2\sin x \sin y = \cos(x - y) - \cos(x + y)$, and we get

$$\begin{aligned} a_n &= \frac{a}{n} \int_0^\pi \frac{du}{\pi} \cos[(n-1)u - ne \sin u] - \cos[(n+1)u - ne \sin u] \\ &= \frac{a}{n} [J_{n-1}(ne) - J_{n+1}(ne)], \end{aligned} \quad (4.389)$$

where, in the second line, we used eq. (4.387). Using the Bessel functions identity

$$J_{n-1}(z) - J_{n+1}(z) = 2J'_n(z), \quad (4.390)$$

the result can also be rewritten as

$$a_n = \frac{2a}{n} J'_n(ne). \quad (4.391)$$

The integral for a_0 is instead elementary and gives $a_0 = -(3/2)ae$. The computation for b_n is analogous to that of a_n ,

$$\begin{aligned} b_n &= -\frac{2b}{n} \int_0^\pi \frac{d\beta}{\pi} \sin u \frac{d}{d\beta} \cos(n\beta) \\ &= \frac{2b}{n} \int_0^\pi \frac{du}{\pi} \frac{d \sin u}{du} \cos(n\beta) \\ &= \frac{2b}{n} \int_0^\pi \frac{du}{\pi} \cos u \cos(nu - ne \sin u) \\ &= \frac{b}{n} [J_{n-1}(ne) + J_{n+1}(ne)]. \end{aligned} \quad (4.392)$$

Using the Bessel functions identity

$$J_{n+1}(z) + J_{n-1}(z) = \frac{2n}{z} J_n(z), \quad (4.393)$$

this result can also be rewritten as

$$b_n = \frac{2b}{ne} J_n(ne). \quad (4.394)$$

We next compute the Fourier decomposition of $x^2(\beta)$, $y^2(\beta)$ and $x(\beta)y(\beta)$. Since $x(\beta)$ is even under $\beta \rightarrow -\beta$ while $y(\beta)$ is odd, $x^2(\beta)$ and $y^2(\beta)$ are even while $x(\beta)y(\beta)$ is odd, and therefore we can write

$$x^2(\beta) = \sum_{n=0}^{\infty} A_n \cos(n\beta), \quad (4.395)$$

$$y^2(\beta) = \sum_{n=0}^{\infty} B_n \cos(n\beta), \quad (4.396)$$

$$x(\beta)y(\beta) = \sum_{n=1}^{\infty} C_n \sin(n\beta), \quad (4.397)$$

which can be inverted to give, for $n \neq 0$,

$$A_n = \frac{2}{\pi} \int_0^\pi d\beta x^2(\beta) \cos(n\beta) \quad (4.398)$$

$$B_n = \frac{2}{\pi} \int_0^\pi d\beta y^2(\beta) \cos(n\beta) \quad (4.399)$$

$$C_n = \frac{2}{\pi} \int_0^\pi d\beta x(\beta)y(\beta) \sin(n\beta). \quad (4.400)$$

The calculations are similar to those performed above for a_n and b_n , and the result is

$$A_n = \frac{a^2}{n} [J_{n-2}(ne) - J_{n+2}(ne) - 2e(J_{n-1}(ne) - J_{n+1}(ne))] , \quad (4.401)$$

$$B_n = \frac{b^2}{n} [J_{n+2}(ne) - J_{n-2}(ne)] , \quad (4.402)$$

$$C_n = \frac{ab}{n} [J_{n+2}(ne) + J_{n-2}(ne) - e(J_{n+1}(ne) + J_{n-1}(ne))] , \quad (4.403)$$

while $A_0 = (1 + 4e^2)/2$ and $B_0 = 1/2$. Observe that these coefficients can be rewritten in many equivalent forms using Bessel function identities.

Further reading

- The radiation from a binary system of two point masses and their frequency spectrum was computed by Peters and Mathews (1963). The Fourier expansion of the Kepler motion is discussed in Watson (1966). The orbit circularization due to radiation of angular momentum was computed by Peters (1964). The chirp amplitude was first computed by Clark and Eardley (1977), see also Thorne (1987), Finn and Chernoff (1993), Cutler and Flanagan (1994).
- The fact that coalescing binaries can be standard candles was discussed by Schutz (1986). The propagation of GWs through a FRW background, in the geometric optics limit, is discussed in Thorne (1983), Section 2.5.4.
- The production of GWs from rotating and precessing rigid bodies is computed in Zimmermann and Szedenits (1979), for axisymmetric bodies and for triaxial bodies with small wobble angle. The radiation from non-axisymmetric bodies rotating and precessing is discussed in Zimmermann (1980) and Van Den Broeck (2005). Rotating fluid stars are studied in Bonazzola and Gourgoulhon (1996). The back-reaction due to wobble radiation is discussed in Bertotti and Anile (1973) and Cutler and Jones (2001). In the latter paper one also finds the correct result for elastic, rather than rigid, neutron stars.
- The production of GWs from a point-like particle falling radially into a black hole is discussed in Davies, Ruffini, Press and Price (1971) and Davis, Ruffini and Tiomno (1972), see also Ohanian and Ruffini (1994). The frequency spectrum is computed in Wagoner (1979). Detweiler and Szedenits (1979) show that, allowing for angular momentum of the test mass, can increase the power output by a large factor, and higher multipoles become more important. The suppression due to the tidal disruption of extended sources is computed by Haugan, Shapiro and Wasserman (1982). Early simulations of head-on black-hole collisions were performed by Smarr (1979).
- The radiation produced in the collision between particles is discussed in Weinberg (1972), Section 10.4. The calculation of the gravitational radiation produced by an accelerated particle, using Feynman diagram techniques, and the fact that the radiation emitted in particle scattering is not beamed, is discussed by Feynman (see Feynman, Morinigo and Wagner 1995, Section 16.4), while our purely classical derivation leading to eq. (4.348) is, as far as we know, original.
- Various examples of production of GWs are discussed in the textbook by Shapiro and Teukolsky (1983), Chapter 16.

5

GW generation by post-Newtonian sources

5.1 The post-Newtonian expansion	237
5.2 The relaxed Einstein equations	250
5.3 The Blanchet–Damour approach	253
5.4 The DIRE approach	279
5.5 Strong-field sources	282
5.6 PN corrections to inspiraling binaries	289

In Chapter 3 we discussed the generation of GWs assuming that the background space-time can be taken as flat, i.e. that the sources that produce GWs in their far-field region contribute negligibly to the space-time curvature in their near-field region. We then computed the GW production as an expansion in v/c , where v is some typical internal speed of the source. We saw that the leading term is given by the Einstein quadrupole formula, and that higher-order corrections in v/c can be organized in a multipole expansion. This procedure assumes that the background space-time curvature and the velocity of the source can be treated as independent parameters, so that we can keep the space-time flat, while taking into account the v/c corrections. This is indeed the case when the dynamics of the system is governed by non-gravitational forces. For example, a beam of charged particles accelerated by an external electric field could reach highly relativistic speeds, but still it contributes negligibly to the background space-time curvature, and for such a source the formalism developed in Chapter 3 is adequate. For $v/c \ll 1$ we can compute the corrections in powers of v/c to the leading quadrupole result using the multipole expansion, since in this case the lowest multipoles dominate. Even in the extreme relativistic case, where the multipole expansion becomes useless, we can still compute GW production using the exact formula (3.14). An example of the latter type of computation was given in Section 4.4.

However, the astrophysical systems which are more interesting for GW detection are held together by gravitational forces. In this case the assumption that the velocity of the source and the space-time curvature are independent is no longer valid, and the above formalism cannot be applied. In fact, for a self-gravitating system with total mass m we have $(v/c)^2 \sim R_S/d$, where $R_S = 2Gm/c^2$ (so R_S has the meaning of the Schwarzschild radius associated to the mass m) and d is the typical size of the system (e.g. its radius, for an isolated source such as a rotating neutron star, or the orbital distance for a binary system). For a binary system we saw this explicitly in eq. (3.2).¹ More generally, the relation $(v/c)^2 \sim R_S/d$ holds for self-gravitating systems as a consequence of the virial theorem. Since R_S/d is a measure of the strength of the gravitational field near the source, as soon as we switch on the v/c corrections we must also, for consistency, consider the deviation of the background from flat space-time.

¹In this case, the precise numerical factor is $(v/c)^2 = R_S/(2d)$.

In this chapter we discuss how to go beyond the limit of sources moving in flat space-time. For a self-gravitating system such as a binary star, assuming that space-time is flat means that we describe its dynamics using Newtonian gravity, rather than general relativity. We will see that, when dealing with a (moderately) relativistic system, held together by gravitational forces, the source must rather be described by a post-Newtonian (PN) formalism. In Section 5.1 we recall the PN expansion in general relativity, and we discuss how to obtain the lowest-order correction to the Newtonian equations of motion. GW generation by post-Newtonian sources is described in great detail in Sections 5.2–5.4, and the application to sources with strong gravitational fields, such as neutron stars and black holes, is discussed in Section 5.5.

The results of this chapter have first of all an intrinsic conceptual interest, since we see here at work the full non-linear structure of general relativity. Furthermore, this formalism is of paramount importance in the computation of the waveform from an inspiraling binary system. In fact, as we will see in Section 5.6.1 (and we will further discuss in Chapter 7), a very accurate prediction of the waveform is necessary to extract the GW signal of an inspiraling binary from the experimental data. This waveform has by now been computed to very high order in v/c , as we will review in Section 5.6. It is quite remarkable that non-linear effects in general relativity of apparently very high order, in fact corrections in v/c even up to order $(v/c)^7$, are crucial for the extraction of a coalescing binary signal from the experimental data. Conversely, compact binary systems might turn out to be a unique laboratory for testing the non-linear aspects of general relativity.

5.1 The post-Newtonian expansion

5.1.1 Slowly moving, weakly self-gravitating sources

The relation between different possible regimes for the sources, depending on the strength of their self-gravity and on their velocity, is schematically illustrated in Fig. 5.1. In the plane $(v^2/c^2, R_S/d)$, the region close to the horizontal axis, where R_S/d is negligible, corresponds to sources whose dynamics is governed by non-gravitational forces, and which can be described using the linearized theory developed in Chapter 3. The region close to the vertical axis corresponds to essentially static bodies, which are not interesting sources of GWs. Slowly moving, weakly self-gravitating sources correspond to the region of the plane where $(v/c)^2$ and R_S/d are comparable, and none of them is too close to one. As we will see in this chapter, they must be described by a post-Newtonian formalism, so they are marked as “PN” in the figure. When R_S/d gets close to one we are dealing with strong gravity, typically black holes or neutron stars, and we have to resort to strong-field methods.

We now consider a slowly moving and weakly self-gravitating source, which means that v/c and R_S/d are sufficiently small,² so we can use

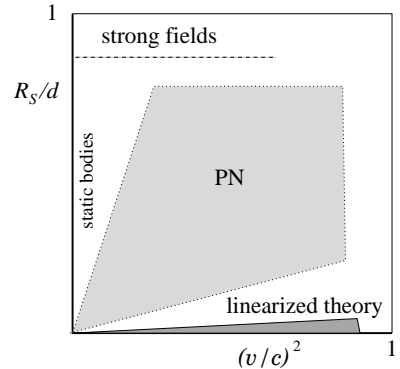


Fig. 5.1 The different regimes in the plane $(v^2/c^2, R_S/d)$.

²The term “slowly moving sources” can be misleading. For instance, we will be interested in applying the formalism to inspiraling compact binaries made of neutron stars or black holes which, in the last stage of their coalescence, can reach values of v/c as high as $1/2$ (in correspondence with the innermost circular orbit, defined by the minimum energy for circular orbits), and in this sense are very relativistic objects. This means that we might need the result to a very high order in v/c . Observe also that the condition $v/c \ll 1$ must be imposed both on the bulk velocities of the objects, such as the orbital velocities of each neutron star in a NS-NS binary system, and also on the internal velocities inside each extended body. This means that we are also requiring that the sources are at most weakly stressed.

them as expansion parameters, and that they are related by $v/c \sim (R_S/d)^{1/2}$. We also demand that the matter energy-momentum tensor $T^{\mu\nu}$ of the source has a spatially compact support, i.e. that it can be enclosed in a time-like world tube $r \leq d$ (more precisely, the statement $r \leq d$ is assumed to hold in the harmonic coordinate system defined below), and that the matter distribution inside the source is smooth, i.e. that $T^{\mu\nu}(t, \mathbf{x})$ is infinitely differentiable over the whole space-time. We will discuss in Section 5.5 the applicability of the formalism to systems containing black holes.

Our aim is to understand how to compute systematically the corrections to the results of linearized theory, in an expansion in powers of v/c . Just as in electrodynamics, for a non-relativistic source it is convenient to distinguish between the *near zone* and the *far zone*. We found in eq. (3.24) that the typical reduced wavelength of the radiation emitted, λ , is larger than the typical size of the source, d , by a factor of order c/v so, for non-relativistic sources, $d \ll \lambda$. The near zone is the region $r \ll \lambda$, and the exterior near zone is the region

$$d < r \ll \lambda. \quad (5.1)$$

In the near zone retardation effects are negligible, and we basically have static potentials. We will see that in this region the post-Newtonian expansion is the correct tool.³ The far zone (or wave zone) is defined as the region $r \gg \lambda$.⁴ In the far zone we have waves, retardation effects are crucial and a different treatment is required. The near and the far region are separated by an intermediate region at $r \sim \lambda$ (which, in electromagnetism, is called the induction zone).

In a first approximation, we might think that the problem of computing GW generation from a weakly self-gravitating source, in an expansion in v/c , has two aspects:

- We must determine the general-relativistic correction to the equations of motion of the sources up to the desired order in v/c , using a post-Newtonian expansion.
- Given their motion to the desired order, we must compute the GWs emitted by these sources. We have seen in Chapter 3 that **GW production can be organized in a multipole expansion, which is an expansion in v/c .** Thus, we cannot limit ourselves to the quadrupole formula, but we must include a number of higher multipoles, consistent with the order in v/c to which we wish to work.

The real story is however more complex, and these two aspects cannot really be separated. In particular, the emission of GWs costs energy which is drained from the source so, beyond a certain order, GWs will back-react on the matter sources, influencing their equations of motion. Furthermore, because of the non-linearity of general relativity, the gravitational field is itself a source for GW generation, and the GWs which have been computed to a given order in v/c , at higher orders become themselves a source of further GW production. So, a full-fledged formalism for computing systematically the production of GWs of a self-gravitating source in powers of v/c is necessarily quite complicated.

³In the presence of strong-field sources, such as black holes or neutron stars, the near zone can be further separated into a strong-field near zone and a weak-field near zone. The strong-field near zone is the region contained inside balls centered on the sources (e.g. around the two stars in a binary system), and with a radius equal to a few times their Schwarzschild radius. The weak-field near zone is the rest of the near zone, i.e. is the near zone with these strong-field regions excised. We will discuss strong-field sources in Section 5.5.

⁴When studying the propagation of GWs across cosmological distances, it can be convenient to further distinguish among a local wave zone and a distant wave zone. The boundary between the two is where become important effects on the propagation of GWs such as deflection or redshift due to the background curvature of the universe, or the gravitational lensing induced by galaxies, etc. These effects have already been studied in Section 1.5, and in the following we will only consider the local wave zone. Technically, this implies that we will consider background space-times that are asymptotically flat.

5.1.2 PN expansion of Einstein equations

The post-Newtonian approximation is a basic tool of general relativity, developed already in 1916 by Einstein himself, by Droste, de Sitter, and Lorentz, and it has produced a number of classic results. Still, when one tries to extend the lowest-order computations to a systematic all-order expansion, or when one wants to use it for computing the generation of GWs, it raises important conceptual (as well as technical) difficulties, and a fully satisfactory formulation emerged only in relatively recent years.

We begin by analyzing the lowest-order post-Newtonian corrections to the motion of the source, neglecting for the moment the back-reaction due to GWs (as we will see, the back-reaction of GWs on the motion of the source does not enter into play at the level of the first and even the second PN corrections). As discussed above, we assume that the source is non-relativistic, $v/c \ll 1$, and self-gravitating, so that $(R_S/d)^{1/2} \sim v/c$. We introduce the small parameter⁵

$$\epsilon \sim (R_S/d)^{1/2} \sim v/c, \quad (5.2)$$

and we also demand that $|T^{ij}|/T^{00} = O(\epsilon^2)$, i.e. that the source be weakly stressed. For instance, for a fluid with pressure p and energy density ρ , this means that $p/\rho = O(\epsilon^2)$. We then expand the metric and the energy-momentum tensor in powers of ϵ . As long as we neglect the emission of radiation, a classical system subject to conservative forces is invariant under time reversal.⁶ Under time reversal g_{00} and g_{ij} are even, while g_{0i} is odd. On the other hand, the velocity v changes sign under time reversal so, as long as the invariance under time-reversal is preserved, g_{00} and g_{ij} can contain only even powers of v (and therefore of ϵ), while g_{0i} can contain only odd powers of v . By inspection of Einstein equations one finds that, to work consistently to a given order in ϵ , if we expand g_{00} up to order ϵ^n we must also expand g_{0i} up to order ϵ^{n-1} and g_{ij} up to ϵ^{n-2} . Furthermore, the expansion of g_{0i} starts from $O(\epsilon^3)$. Thus the metric is expanded as follows

$$\begin{aligned} g_{00} &= -1 + {}^{(2)}g_{00} + {}^{(4)}g_{00} + {}^{(6)}g_{00} + \dots, \\ g_{0i} &= \qquad \qquad \qquad {}^{(3)}g_{0i} + {}^{(5)}g_{0i} + \dots, \\ g_{ij} &= \delta_{ij} + {}^{(2)}g_{ij} + {}^{(4)}g_{ij} + \dots, \end{aligned} \quad (5.3)$$

where ${}^{(n)}g_{\mu\nu}$ denotes the terms of order ϵ^n in the expansion of $g_{\mu\nu}$.⁷ Similarly, we expand the energy-momentum tensor of matter,

$$\begin{aligned} T^{00} &= {}^{(0)}T^{00} + {}^{(2)}T^{00} + \dots, \\ T^{0i} &= {}^{(1)}T^{0i} + {}^{(3)}T^{0i} + \dots, \\ T^{ij} &= {}^{(2)}T^{ij} + {}^{(4)}T^{ij} + \dots. \end{aligned} \quad (5.4)$$

We can now plug these expansions into the Einstein equations, and equate terms of the same order in ϵ . To determine the order of the various terms we must also take into account that, since we are considering a

⁵When comparing with results in the literature, observe that some authors define $\epsilon \sim v/c$, as we do, while others define $\epsilon \sim (v/c)^2$.

⁶The emission of radiation breaks time-reversal invariance through the boundary conditions, since the no-incoming-radiation boundary conditions (defined in Note 1 on page 102) are transformed into no-outgoing-radiation boundary conditions or, in other words, the retarded Green's function under time-reversal becomes an advanced Green's function. We will come back to this point below.

⁷Actually, one could always generate terms with the wrong parity by performing a gauge transformation. So a more accurate statement is that, as long as radiation-reaction effects are neglected, odd terms in g_{00} such as ${}^{(5)}g_{00}$ (as well as even terms in g_{0i} and odd terms in g_{ij}) satisfy *homogeneous* equations, and can be set to zero with a gauge transformation. In contrast, even terms in g_{00} (as well as odd terms in g_{0i} and even terms in g_{ij}) satisfy inhomogeneous equations, with the appropriate terms from the expansion of the matter energy-momentum tensor on the right-hand side, so we cannot find a gauge transformation that sets them to zero. See Chandrasekhar and Esposito (1970).

source moving with non-relativistic velocity v , the time derivatives of the metric generated by this source are smaller than the spatial derivatives by a factor $O(v)$,

$$\frac{\partial}{\partial t} = O(v) \frac{\partial}{\partial x^i}, \quad (5.5)$$

or $\partial_0 = O(\epsilon)\partial_i$. In particular, the d'Alembertian operator, applied to the metric, to lowest order becomes a Laplacian,

$$-\frac{1}{c^2} \frac{\partial^2}{\partial t^2} + \nabla^2 = [1 + O(\epsilon^2)] \nabla^2. \quad (5.6)$$

This means that retardation effects are small corrections, and the lowest-order solution is given in terms of instantaneous potentials. In the PN expansion we are therefore trying to compute some quantity $F(t - r/c)$, such as a given component of the metric, which is intrinsically a function of retarded time $t - r/c$, from its expansion for small retardation,

$$F(t - r/c) = F(t) - \frac{r}{c} \dot{F}(t) + \frac{r^2}{2c^2} \ddot{F}(t) + \dots \quad (5.7)$$

Each derivative of F carries a factor of ω , the typical frequency of the radiation emitted. Since $\omega/c = 1/\lambda$, we see that eq. (5.7) is in fact an expansion in powers of r/λ . Therefore *the PN expansion is valid only in the near zone, $r \ll \lambda$, and breaks down in the radiation zone $r \gg \lambda$.* We will examine in detail this breakdown in the far region in the following sections, where we will see explicitly how a naive extrapolation of the PN iterative scheme up to $r = \infty$ leads to divergences. So, the PN expansion is a formalism that can be used to compute the gravitational field in the near region, but must be supplemented by a different treatment of the far-field region, to compute the fields in the radiation zone.

5.1.3 Newtonian limit

Let us first recall, from elementary general relativity, that the Newtonian limit corresponds to keeping $g_{00} = -1 + {}^{(2)}g_{00}$, $g_{0i} = 0$ and $g_{ij} = \delta_{ij}$ in eq. (5.3). In fact, the equation of motion of a test particle with velocity v , in a gravitational field, is obtained from the geodesic equation

$$\frac{d^2x^i}{d\tau^2} = -\Gamma_{\mu\nu}^i \frac{dx^\mu}{d\tau} \frac{dx^\nu}{d\tau}. \quad (5.8)$$

In a weak gravitational field we write $g_{\mu\nu} = \eta_{\mu\nu} + h_{\mu\nu}$ with $|h_{\mu\nu}| \ll 1$ and, in the limit of low velocities, the proper time τ is the same, to lowest order, as the coordinate time t . Furthermore, $dx^0/dt = c$ while $dx^i/dt = O(v)$. Then, the leading term in v/c is obtained setting $\mu = \nu = 0$ in eq. (5.8),

$$\begin{aligned} \frac{d^2x^i}{dt^2} &\simeq -c^2 \Gamma_{00}^i \\ &= c^2 \left(\frac{1}{2} \partial^i h_{00} - \partial_0 h_0^i \right). \end{aligned} \quad (5.9)$$

Since we are considering a source moving with non-relativistic velocity, the time derivative of the metric generated by this source is of higher order with respect to the spatial derivatives, so to leading order eq. (5.9) becomes

$$\frac{d^2x^i}{dt^2} = \frac{c^2}{2} \partial^i h_{00}. \quad (5.10)$$

Writing $h_{00} = -2\phi$ and defining U by $U = -c^2\phi$, we recover the Newtonian equation of motion $\mathbf{a} = \nabla U$, and we see that U is the (sign-reversed) gravitational potential.⁸ In a potential U , the virial theorem tells us that a massive particle moves with a velocity $v^2 = O(U)$, so h_{00} is of order v^2/c^2 . Comparing with eq. (5.3), we see that the Newtonian limit corresponds to ${}^{(2)}g_{00} = 2U/c^2$, while all other corrections to the flat metric do not affect the Newtonian equation of motion. Observe in particular that ${}^{(2)}g_{ij}$ does not contribute to the Newtonian limit, despite the fact that it is a correction $O(v^2/c^2)$ to the leading term ${}^{(0)}g_{ij} = \delta_{ij}$, just as ${}^{(2)}g_{00}$ is a correction $O(v^2/c^2)$ to the leading term ${}^{(0)}g_{00} = -1$. This is due to the fact that, in the geodesic equation (5.8), $\partial^i g_{00}$ enters through Γ_{00}^i , which is multiplied by $(dx^0/dt)^2 = c^2$, while the gradient of the spatial metric, $\partial^i g_{jk}$, enters through Γ_{jk}^i , which is multiplied by $(dx^j/dt)(dx^k/dt) = O(v^2)$.

It is worth remarking that here it was crucial that we considered the propagation of a massive particle with $v/c \ll 1$. If we rather consider the propagation of a photon in the metric generated by a non-relativistic source, there is no v/c suppression since v is approximately equal to c ,⁹ and the deviation from flat space in g_{00} and in g_{ij} both contribute to leading order. For instance, the metric generated by a weak and nearly static Newtonian source, in the de Donder gauge, is given by

$$ds^2 \simeq -(1 + 2\phi)c^2 dt^2 + (1 - 2\phi)\delta_{ij} dx^i dx^j, \quad (5.11)$$

where $\phi = -U/c^2$ and

$$U(t, \mathbf{x}) = \frac{G}{c^2} \int d^3x' \frac{T^{00}(t, \mathbf{x}')}{|\mathbf{x} - \mathbf{x}'|}. \quad (5.12)$$

(This is easily proved using eq. (3.8), and observing that for a non-relativistic source, to leading order in the source velocity, only T_{00} contributes, so only \bar{h}_{00} is non-vanishing. We neglect retardation effect since we are interested in the near-zone field, and we finally express the result in terms of $h_{\mu\nu} = \bar{h}_{\mu\nu} - (1/2)\eta_{\mu\nu}\bar{h}$.) If we study the propagation of a photon in such a background, of course both the correction -2ϕ to $\eta_{00} = -1$ and the correction $-2\phi\delta_{ij}$ to $\eta_{ij} = \delta_{ij}$ must be taken into account, and give contributions of the same order.¹⁰

Having established that $g_{00} = -1 + {}^{(2)}g_{00}$, $g_{0i} = 0$ and $g_{ij} = \delta_{ij}$ gives the Newtonian approximation to the dynamics of a massive particle, it follows that the terms ${}^{(4)}g_{00}$, ${}^{(3)}g_{0i}$ and ${}^{(2)}g_{ij}$ give the first post-Newtonian order, denoted as 1PN, the terms ${}^{(6)}g_{00}$, ${}^{(5)}g_{0i}$ and ${}^{(4)}g_{ij}$ gives the 2PN approximation, etc.

⁸It is a nearly universal convention in research papers in general relativity that U denotes the *sign-reversed* gravitational potential, so that $U > 0$. We will refer to U simply as the potential.

⁹More precisely, v differs from c only by terms of order U/c^2 , where U is given in eq. (5.12) below.

¹⁰When studying the deflection of light from the Sun, Einstein at first (in 1911) used the metric

$$ds^2 = -(1 + 2\phi)c^2 dt^2 + d\mathbf{x}^2,$$

suggested by the Newtonian limit of a massive particle, and obtained a deflection angle of only one half of the correct value, which is the one obtained from (5.11). Einstein himself obtained the correct deflection angle in 1915, when he had the final form of his equations.

5.1.4 The 1PN order

We now discuss the first post-Newtonian correction. First of all, it is useful to choose from the beginning a gauge condition, since this simplifies drastically the equations. A convenient choice is the De Donder gauge condition,

$$\partial_\mu(\sqrt{-g} g^{\mu\nu} \partial_\nu) x^\rho = 0. \quad (5.13)$$

¹¹This name originates from the fact that, in this gauge, the coordinates x^ρ satisfy

$$\partial_\mu(\sqrt{-g} g^{\mu\nu} \partial_\nu) x^\rho = 0. \quad (5.14)$$

On a scalar function ϕ , in curved space, we have

$$\begin{aligned} \square\phi &\equiv D^\mu D_\mu \phi \\ &= \frac{1}{\sqrt{-g}} \partial_\mu(\sqrt{-g} g^{\mu\nu} \partial_\nu)\phi, \end{aligned} \quad (5.15)$$

where D_μ is the covariant derivative, and a scalar function ϕ that satisfies $\square\phi = 0$, i.e.

$$\partial_\mu(\sqrt{-g} g^{\mu\nu} \partial_\nu)\phi = 0, \quad (5.16)$$

is called a harmonic function. By (a slightly improper) extension, also the coordinates x^ρ that satisfy (5.14) are called harmonic coordinates (even if x^ρ are not four scalar functions indexed by ρ , so the operator $D^\mu D_\mu$ on them is not the same as on scalars).

We will use the denominations De Donder gauge condition and harmonic gauge condition as synonymous. Sometimes in the literature the name “De Donder gauge condition” is reserved to the linearized form given in eq. (1.18), while “harmonic gauge condition” is reserved to eq. (5.13).

This is also called the harmonic gauge condition, and the corresponding coordinates are referred to as harmonic coordinates.¹¹

It is now in principle straightforward, even if somewhat long, to insert the expansions (5.3) and (5.4) into the Einstein equations, using eq. (5.5) to establish the order of the various term, and the gauge condition (5.13), expanded to the desired order, to simplify the equations (for the explicit computation, see Weinberg 1972, Section 9.1). For ${}^{(2)}g_{00}$ we get the Newtonian equation

$$\nabla^2[{}^{(2)}g_{00}] = -\frac{8\pi G}{c^4} {}^{(0)}T^{00}, \quad (5.17)$$

while, for the 1PN corrections to the metric, we get

$$\nabla^2[{}^{(2)}g_{ij}] = -\frac{8\pi G}{c^4} \delta_{ij} {}^{(0)}T^{00}, \quad (5.18)$$

$$\nabla^2[{}^{(3)}g_{0i}] = \frac{16\pi G}{c^4} {}^{(1)}T^{0i}, \quad (5.19)$$

$$\begin{aligned} \nabla^2[{}^{(4)}g_{00}] &= \partial_0^2[{}^{(2)}g_{00}] + {}^{(2)}g_{ij}\partial_i\partial_j[{}^{(2)}g_{00}] - \partial_i[{}^{(2)}g_{00}]\partial_i[{}^{(2)}g_{00}] \\ &\quad - \frac{8\pi G}{c^4} \left\{ {}^{(2)}T^{00} + {}^{(2)}T^{ii} - 2 {}^{(2)}g_{00} {}^{(0)}T^{00} \right\}, \end{aligned} \quad (5.20)$$

where $\nabla^2 = \delta^{ij}\partial_i\partial_j$ is the flat-space Laplacian, and the sum over repeated lower (or upper) spatial indices is performed with δ_{ij} . The solution of eq. (5.17), with the boundary condition that the metric vanishes at spatial infinity, is

$${}^{(2)}g_{00} = -2\phi, \quad (5.21)$$

where

$$\phi(t, \mathbf{x}) = -\frac{G}{c^4} \int d^3x' \frac{{}^{(0)}T^{00}(t, \mathbf{x}')}{|\mathbf{x} - \mathbf{x}'|}, \quad (5.22)$$

so $U = -c^2\phi$ is the (positive) Newtonian potential. Similarly, the 1PN eqs. (5.18) and (5.19) are immediately solved,

$${}^{(2)}g_{ij} = -2\phi \delta_{ij}, \quad (5.23)$$

$${}^{(3)}g_{0i} = \zeta_i, \quad (5.24)$$

where

$$\zeta_i(t, \mathbf{x}) = -\frac{4G}{c^4} \int \frac{d^3x'}{|\mathbf{x} - \mathbf{x}'|} {}^{(1)}T^{0i}(t, \mathbf{x}'). \quad (5.25)$$

To solve eq. (5.20) we replace on the right-hand side ${}^{(2)}g_{00}$ by -2ϕ and ${}^{(2)}g_{ij}$ by $-2\phi \delta_{ij}$, we use the identity

$$\partial_i\phi\partial_i\phi = \frac{1}{2} \nabla^2(\phi^2) - \phi \nabla^2\phi, \quad (5.26)$$

and we introduce a new potential ψ defined from

$${}^{(4)}g_{00} = -2(\phi^2 + \psi). \quad (5.27)$$

Then eq. (5.20) becomes

$$\nabla^2\psi = \partial_0^2\phi + \frac{4\pi G}{c^4} \left[{}^{(2)}T^{00} + {}^{(2)}T^{ii} \right], \quad (5.28)$$

which, again with the boundary condition that ψ vanishes at infinity, has the solution

$$\psi(t, \mathbf{x}) = - \int \frac{d^3x'}{|\mathbf{x} - \mathbf{x}'|} \left\{ \frac{1}{4\pi} \partial_0^2\phi + \frac{G}{c^4} \left[{}^{(2)}T^{00}(t, \mathbf{x}') + {}^{(2)}T^{ii}(t, \mathbf{x}') \right] \right\}. \quad (5.29)$$

Observe that ϕ and ζ^i are not independent, since the gauge condition eq. (5.13) imposes the constraint

$$4\partial_0\phi + \nabla \cdot \zeta = 0. \quad (5.30)$$

From the explicit expressions (5.22) and (5.25) we see that these are indeed satisfied, because of the conservation of the energy-momentum tensor, expanded to 1PN order.

In agreement with the discussion below eq. (5.6), ϕ, ψ and ζ_i are *instantaneous* potentials: their value at time t depends on the value of the energy-momentum tensor at the same time t , rather than at retarded time. However, we can re-express the solution in terms of *retarded* potentials. This is useful both to understand better the structure of the above solution, and as a starting point for the computation of higher post-Newtonian orders. We begin by observing that, putting together eqs. (5.21) and (5.27), we have

$$\begin{aligned} g_{00} &= -1 - 2\phi - 2(\phi^2 + \psi) + O(\epsilon^6) \\ &= -1 - 2(\phi + \psi) - 2\phi^2 + O(\epsilon^6). \end{aligned} \quad (5.31)$$

Since ψ is of higher order compared to ϕ , in the last term we are free to replace ϕ^2 by $(\phi + \psi)^2$, because the additional terms are beyond the 1PN order anyway. We introduce the quantity

$$V = -c^2(\phi + \psi), \quad (5.32)$$

which has the dimension of a velocity squared, so the solution for g_{00} , to 1PN order, can be written as

$$g_{00} = -1 + \frac{2V}{c^2} - \frac{2V^2}{c^4} + O\left(\frac{1}{c^6}\right). \quad (5.33)$$

(We will often follow the convention, common in the literature on the PN expansion, of writing the remainder as $O(1/c^n)$ rather than $O(\epsilon^n)$.) To this order, this can be written more compactly as

$$g_{00} = -e^{-2V/c^2} + O\left(\frac{1}{c^6}\right). \quad (5.34)$$

The potential ϕ satisfies

$$\nabla^2 \phi = \frac{4\pi G}{c^4} {}^{(0)}T^{00}, \quad (5.35)$$

see eqs. (5.17) and (5.21), while ψ satisfies eq. (5.28). Thus,

$$\nabla^2(\phi + \psi) = \partial_0^2 \phi + \frac{4\pi G}{c^4} \left[{}^{(0)}T^{00} + {}^{(2)}T^{00} + {}^{(2)}T^{ii} \right]. \quad (5.36)$$

To this order, $\partial_0^2 \phi = \partial_0^2(\phi + \psi)$, so the above equation can be written in terms of the flat-space d'Alembertian $\square = \eta^{\mu\nu}\partial_\mu\partial_\nu$, as

$$\begin{aligned} \square V &= -\frac{4\pi G}{c^2} \left[{}^{(0)}T^{00} + {}^{(2)}T^{00} + {}^{(2)}T^{ii} \right] \\ &= -\frac{4\pi G}{c^2} [T^{00} + T^{ii}], \end{aligned} \quad (5.37)$$

where, to 1PN order, we could replace ${}^{(0)}T^{00} + {}^{(2)}T^{00}$ with the total value of the 00 component of the energy-momentum tensor, T^{00} , and similarly ${}^{(2)}T^{ii}$ with T^{ii} . We use the active gravitational-mass density defined in eq. (3.205). Then the 1PN equation for g_{00} can be written as

$$\square V = -4\pi G \sigma, \quad (5.38)$$

and therefore $V(t, \mathbf{x})$ can be written as a *retarded* integral, as¹²

$$V(t, \mathbf{x}) = G \int d^3x' \frac{1}{|\mathbf{x} - \mathbf{x}'|} \sigma(t - |\mathbf{x} - \mathbf{x}'|/c, \mathbf{x}'). \quad (5.39)$$

This retarded potential can be written in terms of instantaneous potentials expanding $\sigma(t - |\mathbf{x} - \mathbf{x}'|/c, \mathbf{x}')$ for small retardation effects,

$$\sigma(t - |\mathbf{x} - \mathbf{x}'|/c, \mathbf{x}') = \sigma(t, \mathbf{x}') - \frac{|\mathbf{x} - \mathbf{x}'|}{c} \partial_t \sigma + \frac{|\mathbf{x} - \mathbf{x}'|^2}{2c^2} \partial_t^2 \sigma + \dots, \quad (5.40)$$

and of course, given that we are working to 1PN order, for the moment we can only retain the result of this expansion, truncated to 1PN order. We can proceed similarly for g_{0i} and g_{ij} . Using the “active mass-current density” defined in eq. (3.206), and observing that in ζ_i retardation effects are anyway of higher order, we are allowed to rewrite eqs. (5.24) and (5.25), to 1PN order, replacing ζ_i with V_i defined by

$$V_i(t, \mathbf{x}) = G \int d^3x' \frac{1}{|\mathbf{x} - \mathbf{x}'|} \sigma_i(t - |\mathbf{x} - \mathbf{x}'|/c, \mathbf{x}'), \quad (5.41)$$

and similarly we can replace $-c^2\phi$ with V in the solution for g_{ij} , since again the difference is of higher order.

To summarize, in harmonic coordinates the 1PN solution can be written in terms of two functions V and V_i as

$$g_{00} = -1 + \frac{2}{c^2} V - \frac{2}{c^4} V^2 + O\left(\frac{1}{c^6}\right), \quad (5.42)$$

¹²Actually, the PN solution could be rewritten equivalently in terms of the advanced integral or of any combination of retarded and advanced Green's functions. What really selects the appropriate Green's function are the boundary conditions. In particular, the retarded Green's function is selected by the no-incoming radiation boundary condition at null infinity. However, we have already seen in eq. (5.7) that the PN expansion only holds in the near region $r \ll \lambda$ and therefore, within the PN expansion, it is not possible to impose boundary conditions at infinity. As we will see below, a different approximation scheme, the post-Minkowskian expansion, will be employed in the external source region $d < r < \infty$, and the boundary condition will be consistently imposed on the post-Minkowskian solution, and will select the retarded Green's function. The PN solution and the post-Minkowskian solution will then be matched in the overlap region $d < r \ll \lambda$. Even if the PN expansion at a given order could be rewritten in many different forms, e.g. in terms of advanced potentials, or of half-advanced and half-retarded potentials, writing it in terms of retarded Green's function makes it possible the matching, since the post-Minkowskian solutions in $d < r < \infty$ will be unambiguously written in terms of retarded potentials, once the no-incoming radiation boundary condition is imposed on it.

$$g_{0i} = -\frac{4}{c^3} V_i + O\left(\frac{1}{c^5}\right), \quad (5.43)$$

$$g_{ij} = \delta_{ij} \left(1 + \frac{2}{c^2} V\right) + O\left(\frac{1}{c^4}\right), \quad (5.44)$$

and V, V_i are given by retarded integrals over the energy-momentum tensor of the source, eqs. (5.39) and (5.41). Observe also that, to this order, the energy-momentum tensor of the source enters only through the two combinations σ and σ_i .

At large distance from the source, i.e. at $r \gg d$, we can expand the potentials V and V_i using

$$\frac{1}{|\mathbf{x} - \mathbf{x}'|} = \frac{1}{r} + \frac{\mathbf{x} \cdot \mathbf{x}'}{r^3} + \dots, \quad (5.45)$$

where $r = |\mathbf{x}|$, and we find that the gravitational field at $d \ll r$ (but still within the near region, $r \ll \lambda$) is expressed in terms of the multipoles of the energy-momentum tensor of the source. We will examine this multipole expansion in more detail in Section 5.3.2.

5.1.5 Motion of test particles in the PN metric

Once we have the metric in the near zone, we can obtain the equations of motion of a particle of mass m which moves in the near zone from the geodesic equation or, equivalently, writing the action in the given curved background,

$$\begin{aligned} S &= -mc \int dt \left(-g_{\mu\nu} \frac{dx^\mu}{dt} \frac{dx^\nu}{dt} \right)^{1/2} \\ &= -mc^2 \int dt \left(-g_{00} - 2g_{0i} \frac{v^i}{c} - g_{ij} \frac{v^i v^j}{c^2} \right)^{1/2}, \end{aligned} \quad (5.46)$$

and extremizing it. We will be particularly interested in the equations of motion for a binary system. If we limit ourselves to the lowest PN corrections, it is possible to treat the two masses as point-like.¹³ In curved space, the energy-momentum tensor of a set of point-like particles with masses m_a , coordinates x_a^μ ($a = 1, \dots, N$) and proper times τ_a , defined by $c^2 d\tau_a^2 = -g_{\mu\nu} dx_a^\mu dx_b^\mu$, is (see Note 24 on page 121)

$$T^{\mu\nu} = \frac{1}{\sqrt{-g}} \sum_a m_a \frac{d\tau_a}{dt} \frac{dx_a^\mu}{d\tau_a} \frac{dx_a^\nu}{d\tau_a} \delta^{(3)}(\mathbf{x} - \mathbf{x}_a(t)), \quad (5.47)$$

which reduces to (3.121) in flat space, where $d\tau_a = dt/\gamma_a$. In a N -body system, the metric felt by a particle, labeled as b , is obtained taking as a source the energy-momentum tensor of all the other particles, i.e. replacing \sum_a with $\sum_{a \neq b}$ in eq. (5.47).¹⁴ Expanding the determinant of the metric to second order and using eqs. (5.21) and (5.23) we get

$$-g = 1 - {}^{(2)}g_{00} + \sum_i {}^{(2)}g_{ii} = 1 - 4\phi. \quad (5.48)$$

We further observe that, up to $O(v^2/c^2)$, $d\tau_a/dt = 1 + \phi - v_a^2/(2c^2)$.

¹³In higher order, some regularization of the Dirac delta becomes necessary. See Section 8 of Blanchet (2006) and the Further Reading for a discussion of the various regularizations which have been used.

¹⁴For radiation reaction, a self-force must also be included. However, we will see below that radiation reaction effects enter only in higher orders, and will be discussed in Section 5.3.5.

Then the expansion of eq. (5.47) (with $\sum_a \rightarrow \sum_{a \neq b}$) gives

$${}^{(0)}T^{00}(t, \mathbf{x}) = \sum_{a \neq b} m_a c^2 \delta^{(3)}(\mathbf{x} - \mathbf{x}_a(t)), \quad (5.49)$$

$${}^{(2)}T^{00}(t, \mathbf{x}) = \sum_{a \neq b} m_a \left(\frac{1}{2} v_a^2 + \phi c^2 \right) \delta^{(3)}(\mathbf{x} - \mathbf{x}_a(t)), \quad (5.50)$$

$${}^{(1)}T^{0i}(t, \mathbf{x}) = c \sum_{a \neq b} m_a v_a^i \delta^{(3)}(\mathbf{x} - \mathbf{x}_a(t)), \quad (5.51)$$

$${}^{(2)}T^{ij}(t, \mathbf{x}) = \sum_{a \neq b} m_a v_a^i v_a^j \delta^{(3)}(\mathbf{x} - \mathbf{x}_a(t)). \quad (5.52)$$

Plugging these expressions into eqs. (5.22)–(5.29) we obtain the metric in which the particle b propagates and, inserting this metric into eq. (5.46), we get its action, S_b . The total action of the system is the sum over all particles, $S = \sum_b S_b$. Expanding the square root in the action and keeping for consistency only terms up to $O(v^4/c^4)$ gives the first post-Newtonian corrections. In terms of the Lagrangian, the result for a two-body system is $L = L_0 + (1/c^2)L_2$, with

$$L_0 = \frac{1}{2} m_1 v_1^2 + \frac{1}{2} m_2 v_2^2 + \frac{Gm_1 m_2}{r}, \quad (5.53)$$

and

$$\begin{aligned} L_2 = & \frac{1}{8} m_1 v_1^4 + \frac{1}{8} m_2 v_2^4 \\ & + \frac{Gm_1 m_2}{2r} \left[3(v_1^2 + v_2^2) - 7\mathbf{v}_1 \cdot \mathbf{v}_2 - (\hat{\mathbf{r}} \cdot \mathbf{v}_1)(\hat{\mathbf{r}} \cdot \mathbf{v}_2) - \frac{G(m_1 + m_2)}{r} \right], \end{aligned} \quad (5.54)$$

where \mathbf{r} is the separation vector between the two particles, $r = |\mathbf{r}|$ and $\hat{\mathbf{r}} = \mathbf{r}/r$. The same computation can be repeated for a system of N particles, and the result is the famous Einstein–Infeld–Hoffmann Lagrangian, $L = L_0 + (1/c^2)L_2$ with

$$L_0 = \sum_a \frac{1}{2} m_a v_a^2 + \sum_{a \neq b} \frac{Gm_a m_b}{2r_{ab}}, \quad (5.55)$$

and

$$\begin{aligned} L_2 = & \sum_a \frac{1}{8} m_a v_a^4 - \sum_{a \neq b} \frac{Gm_a m_b}{4r_{ab}} [7\mathbf{v}_a \cdot \mathbf{v}_b + (\hat{\mathbf{r}}_{ab} \cdot \mathbf{v}_a)(\hat{\mathbf{r}}_{ab} \cdot \mathbf{v}_b)] \\ & + \frac{3G}{2} \sum_a \sum_{b \neq a} \frac{m_a m_b v_a^2}{r_{ab}} - \frac{G^2}{2} \sum_a \sum_{b \neq a} \sum_{c \neq a} \frac{m_a m_b m_c}{r_{ab} r_{ac}}, \end{aligned} \quad (5.56)$$

where $a = 1, \dots, N$ labels the particle, r_{ab} is the distance between particles a and b , and $\hat{\mathbf{r}}_{ab}$ the unit vector from a to b . From this Lagrangian we can derive the equations of motion of a N -particle system, including corrections of order v^2/c^2 , i.e. to 1PN order. If one rather performs the

expansion up to 2PN order, the equation of motion of a binary system takes the schematic form

$$\frac{d^2x^i}{dt^2} = -\frac{Gm}{r^2} \left\{ \hat{x}^i [1 + O(\epsilon^2) + O(\epsilon^4)] + \hat{v}^i [O(\epsilon^2) + O(\epsilon^4)] \right\}, \quad (5.57)$$

where m is the total mass, \mathbf{x} is the relative separation, $\hat{x}^i = x^i/r$, and \hat{v}^i is the unit vector in the direction of the relative velocity. The leading term is of course just Newtonian gravity. The terms $O(\epsilon^2)$ are the 1PN correction to the equations of motion which gives rise, for instance, to the periastron advance of the orbit. The terms $O(\epsilon^4)$ comes from the 2PN correction. The explicit integration of the 1PN equations of motion for a binary system will be discussed in Chapter 6, on pages 317–320, when we need it for the timing formula of binary pulsars.

5.1.6 Difficulties of the PN expansion

The straightforward PN expansion that we have presented, and which was used until, say, the early 1980s, suffers from two serious problems. The first is that, beyond some order, divergences appear. We will see this explicitly in eq. (5.199), and in the discussion below it. However, it is useful to understand first qualitatively the essence of the problem, which is rooted in the fact that general relativity is a non-linear theory. We are trying to solve iteratively the Einstein equations, that have schematically the form

$$\square h_{\mu\nu} = S_{\mu\nu}[h], \quad (5.58)$$

where $S_{\mu\nu}$ is a source term, that depends both on the matter energy-momentum tensor and, non-linearly, on $h_{\mu\nu}$ (we will see in eq. (5.72) below how to write *exactly* the Einstein equations in this form). One could envisage a systematic weak-field, low-velocity expansion as follows.

We write

$$h_{\mu\nu} = {}^{(0)}h_{\mu\nu} + {}^{(1)}h_{\mu\nu} + {}^{(2)}h_{\mu\nu} + \dots \quad (5.59)$$

To zeroth order, we simply set ${}^{(0)}h_{\mu\nu} = 0$. The first-order solution, ${}^{(1)}h_{\mu\nu}$, is obtained setting $h_{\mu\nu} = 0$ on the right-hand side of eq. (5.58), while, according to eq. (5.5), on the left-hand side we neglect the time-derivative. Then we get an equation of the form

$$\nabla^2[{}^{(1)}h_{\mu\nu}] = (\text{matter sources}). \quad (5.60)$$

This is integrated by making use of the instantaneous Green's function of the Laplacian, i.e. of the Poisson integral defined on a generic function $f(\mathbf{x})$ by

$$[\Delta^{-1}f](\mathbf{x}) \equiv -\frac{1}{4\pi} \int_{\mathbb{R}^3} \frac{d^3x'}{|\mathbf{x} - \mathbf{x}'|} f(\mathbf{x}'), \quad (5.61)$$

(where $\Delta \equiv \nabla^2$) and leads to results such as eq. (5.22). At next order, we insert ${}^{(1)}h_{\mu\nu}$ into $S[h]$ while, in $\square h_{\mu\nu}$, we replace $\partial_0^2 h_{\mu\nu}$ by $\partial_0^2[{}^{(1)}h_{\mu\nu}]$, so the gravitational field at the next iteration, ${}^{(2)}h_{\mu\nu}$, is determined by an equation of the form

$$\nabla^2[{}^{(2)}h_{\mu\nu}] = (\text{matter sources}) + (\text{terms that depend on } {}^{(1)}h_{\mu\nu}), \quad (5.62)$$

which again one would attempt to integrate by using the Poisson integral. The problem is that, beyond some order, the resulting Poisson integrals are necessarily divergent. In fact, first of all, even if the source has a compact support, the second term on the right-hand side of eq. (5.62) extends all over the space, raising an issue of convergence at infinity of the Poisson integral. Furthermore, the higher is the PN order, the higher is also the order of the multipoles that contribute. The gravitational field corresponding to a multipole of order l has a factor $(\mathbf{x} \cdot \mathbf{x}')^l$ which comes from the expansion of $1/|\mathbf{x} - \mathbf{x}'|$ in eq. (5.45). When we use such a field as a source for the next iteration, for l sufficiently large we necessarily get a divergence at large \mathbf{x}' in the retarded integral.¹⁵

¹⁵In the earlier works this problem was somehow swept under the rug. The reason is that divergences start to appear only from 2PN order. Furthermore, up to 2.5PN order, the result can be made finite by using some not well justified trick, consisting in bringing some derivative inside the integrals, to make them finite. In this way, early papers managed to get the lowest-order results that nowadays we know to be correct. However, inexorably divergent integrals appear at 3PN order. Therefore this approach is not consistent, and even the validity of the lowest-order results becomes highly questionable.

This problems turns out to be purely technical. Simply, the correct solution to the Poisson equation is not necessarily given by the Poisson integral (5.61). The correct solution is fixed by the boundary conditions, and we will see in Section 5.3.2 that in our problem it is given by a procedure of analytic continuation, that reduces to a Poisson integral only when the latter is convergent, and otherwise is different, and is always finite.

The second problem of the “standard” PN expansion is conceptual, and is that it cannot take into account the boundary conditions at infinity. This can be understood by observing that, as already discussed below eq. (5.7), in the PN expansion we are trying to reconstruct a retarded field, say of the form

$$h_{\mu\nu} = \frac{1}{r} F_{\mu\nu}(t - r/c), \quad (5.63)$$

from its expansions for small retardation, $r/c \ll t$,

$$\frac{1}{r} F_{\mu\nu}(t - r/c) = \frac{1}{r} F_{\mu\nu}(t) - \frac{1}{c} \dot{F}_{\mu\nu}(t) + \frac{r}{2c^2} \ddot{F}_{\mu\nu}(t) - \frac{r^2}{6c^3} \dddot{F}_{\mu\nu}(t) + \dots \quad (5.64)$$

The coefficients of the higher-order terms therefore blow up as $r \rightarrow \infty$. This has nothing to do with the real behavior of the gravitational field at infinity, which should be asymptotically flat, and simply reflects the inadequacy of the PN expansion to study the large r region.

From a mathematical point of view, the PN expansion is an example of singular perturbation theory, or asymptotic expansion, i.e. an expansion of a function $F(r, \epsilon)$ around $\epsilon = 0$,

$$F(r, \epsilon) = \sum_n c_n(r) \epsilon^n, \quad (5.65)$$

where the coefficients c_n depend on a second parameter, here r , and they blow up as $r \rightarrow \infty$. So, this expansion is not uniformly valid in r , and cannot be used at $r \rightarrow \infty$. In particular, as we already observed in Note 12, it is impossible to include in the PN expansion the boundary conditions at infinity, such as the no-incoming radiation boundary condition, appropriate for a radiation problem.¹⁶

The solution to this difficulty, as we will discuss in details in the following sections, is to make use of the PN expansion only in the near

¹⁶Actually, it can even be shown that the PN expansion cannot be asymptotically flat beyond 2PN or 3PN order (depending on the gauge condition that is used), see Rendall (1992).

region, and to use a different expansion in the far region. Then, the two expansions are matched in an intermediate region, where they are both valid. This procedure is known as “matched asymptotic expansion”. The appropriate boundary conditions at infinity will then be imposed on the solution valid in the far zone.

5.1.7 The effect of back-reaction

Once we will have developed a systematic and consistent formalism for computing the gravitational field both in the near and in the far region, we will also be able to compute the modification of the equations of motion of the sources, due to the back-reaction of GWs. Before entering into the technical aspects, however, we can understand with physical arguments what sort of result we should expect.

When we include gravitational radiation the structure of the expansion changes, because invariance under time-reversal is broken by the boundary conditions. To study GWs we impose that there is no incoming radiation at $t = -\infty$ (compare with Note 1 on page 102). Time reversal exchanges outgoing waves with incoming waves, so the argument used above to prove that g_{00} and g_{ij} are even and that g_{0i} is odd in v breaks down. Radiation reaction can generate terms in g_{00} which are odd in v (and cannot be gauged away) and, correspondingly, even terms in g_{0i} and odd terms in g_{ij} .¹⁷

It is not difficult to understand to which order in v/c radiation reaction effects should come into play. We saw in Chapter 3 that the power radiated in GWs by a system with typical velocity v is $P \sim Gm^2v^6/(c^5r^2)$, where m is a mass scale of the system and r its size, see e.g. eq. (3.339). On the other hand, writing the total energy of the system as the sum of its kinetic and potential energy, $E_{\text{tot}} = E_{\text{kin}} + V$, and using the virial theorem $E_{\text{kin}} = -(1/2)V$, we have $E_{\text{tot}} = -E_{\text{kin}} = -(1/2)mv^2$. If we equate the time derivative of E_{tot} to minus the power radiated in GWs we therefore get, neglecting numerical factors,

$$-mv \frac{dv}{dt} \sim -\frac{Gm^2v^6}{c^5r^2}, \quad (5.66)$$

i.e.

$$\frac{dv}{dt} \sim \frac{Gm}{r^2} \left(\frac{v}{c}\right)^5. \quad (5.67)$$

Thus, we expect that radiation-reaction effects enter eq. (5.57) starting from $O(v^5/c^5) = O(\epsilon^5)$, so the equation of motion of a binary system should be of the generic form

$$\begin{aligned} \frac{d^2x^i}{dt^2} = & -\frac{Gm}{r^2} \left\{ \hat{x}^i [1 + O(\epsilon^2) + O(\epsilon^4) + O(\epsilon^5) + O(\epsilon^6) \dots] \right. \\ & \left. + \hat{v}^i [O(\epsilon^2) + O(\epsilon^4) + O(\epsilon^5) + O(\epsilon^6) + \dots] \right\}. \end{aligned} \quad (5.68)$$

Given that one traditionally uses the power of $(v/c)^2$ to label the PN order, the term $O(\epsilon^5)$ is called the correction to the equations of motion of order 2.5PN, the term $O(\epsilon^6)$ is the 3PN order, etc. We will see in the next sections how to derive these results.

¹⁷In higher orders, because of nonlinearities, radiation reaction will also contribute to terms in g_{00} which are even. We will see in eq. (5.186) that an even contribution to g_{00} due to back-reaction indeed appears at 4PN order. Thus, beyond 4PN order, all terms (even and odd) contain pieces associated to radiation reaction.

5.2 The relaxed Einstein equations

First of all, we recast Einstein equations in a form which will be particularly convenient. From the metric $g^{\alpha\beta}(x)$, we define the field $\mathbf{h}^{\alpha\beta}(x)$ by

$$\mathbf{h}^{\alpha\beta} \equiv (-g)^{1/2} g^{\alpha\beta} - \eta^{\alpha\beta}, \quad (5.69)$$

where, as usual, g is the determinant of $g_{\alpha\beta}$. This is an *exact* definition, and we are not assuming that $\mathbf{h}_{\alpha\beta}$ is small. Observe that we use the typographical symbol $\mathbf{h}_{\alpha\beta}$ to distinguish it from $h_{\alpha\beta}$, which is rather defined by $g_{\alpha\beta} = \eta_{\alpha\beta} + h_{\alpha\beta} + O(h^2)$.¹⁸ In the limit of small $h_{\alpha\beta}$ we have $-g = (1 + h)$, where $h = \eta^{\mu\nu} h_{\mu\nu}$, and $g^{\alpha\beta} = \eta^{\alpha\beta} - h^{\alpha\beta}$, so

$$\begin{aligned} -\mathbf{h}^{\alpha\beta} &\simeq \eta^{\alpha\beta} - (1 + h)^{1/2}(\eta^{\alpha\beta} - h^{\alpha\beta}) \\ &= h^{\alpha\beta} - \frac{1}{2}\eta^{\alpha\beta}h. \end{aligned} \quad (5.70)$$

Thus, $\mathbf{h}^{\alpha\beta}$ reduces to the quantity $\bar{h}^{\alpha\beta}$ used in linearized theory, see eq. (1.15), except for an overall sign.¹⁹ We now impose the de Donder, or harmonic, gauge condition (5.13), which in terms of $\mathbf{h}^{\alpha\beta}$ reads

$$\partial_\beta \mathbf{h}^{\alpha\beta} = 0. \quad (5.71)$$

In this gauge the exact Einstein equations (1.3) take the Landau–Lifshitz form

$$\square \mathbf{h}^{\alpha\beta} = +\frac{16\pi G}{c^4} \tau^{\alpha\beta}, \quad (5.72)$$

where $\square \equiv -\partial^2/\partial t^2 + \nabla^2$ is the d'Alembertian in *flat* space-time. The quantity on the right-hand side is defined by

$$\tau^{\alpha\beta} \equiv (-g)T^{\alpha\beta} + \frac{c^4}{16\pi G}\Lambda^{\alpha\beta}, \quad (5.73)$$

where $T^{\alpha\beta}$ is the matter energy–momentum tensor. The tensor $\Lambda^{\alpha\beta}$ does not depend on the matter variables, and is defined by

$$\Lambda^{\alpha\beta} = \frac{16\pi G}{c^4}(-g)t_{LL}^{\alpha\beta} + (\partial_\nu \mathbf{h}^{\alpha\mu} \partial_\mu \mathbf{h}^{\beta\nu} - \mathbf{h}^{\mu\nu} \partial_\mu \partial_\nu \mathbf{h}^{\alpha\beta}), \quad (5.74)$$

where $t_{LL}^{\alpha\beta}$ is called the Landau–Lifshitz energy–momentum pseudotensor,

$$\begin{aligned} \frac{16\pi G}{c^4}(-g)t_{LL}^{\alpha\beta} &= g_{\lambda\mu}g^{\nu\rho}\partial_\nu \mathbf{h}^{\alpha\lambda}\partial_\rho \mathbf{h}^{\beta\mu} + \frac{1}{2}g_{\lambda\mu}g^{\alpha\beta}\partial_\rho \mathbf{h}^{\lambda\nu}\partial_\nu \mathbf{h}^{\rho\mu} \\ &\quad - g_{\mu\nu}(g^{\lambda\alpha}\partial_\rho \mathbf{h}^{\beta\nu} + g^{\lambda\beta}\partial_\rho \mathbf{h}^{\alpha\nu})\partial_\lambda \mathbf{h}^{\rho\mu} \\ &\quad + \frac{1}{8}(2g^{\alpha\lambda}g^{\beta\mu} - g^{\alpha\beta}g^{\lambda\mu})(2g_{\nu\rho}g_{\sigma\tau} - g_{\rho\sigma}g_{\nu\tau})\partial_\lambda \mathbf{h}^{\nu\tau}\partial_\mu \mathbf{h}^{\rho\sigma}. \end{aligned} \quad (5.75)$$

¹⁸The quantity $(-g)^{1/2}g^{\alpha\beta}$ is also called the “gothic metric”, and denoted by a gothic g , see Landau and Lifshitz, Vol. II (1979), Section 96.

¹⁹For this reason, in the literature $\mathbf{h}^{\alpha\beta}$ is sometimes defined with the opposite sign, i.e. $\mathbf{h}^{\alpha\beta} \equiv \eta^{\alpha\beta} - (-g)^{1/2}g^{\alpha\beta}$. We use the definition (5.69), following the notation of the review Blanchet (2006). This means that, when we compare the results of this chapter with the corresponding linearized limit studied in the previous chapters, we must take into account this overall sign in the GW amplitude. For the same reason, the sign on the right-hand side of eq. (5.72) below is the opposite of that in eq. (1.24).

Since $t_{LL}^{\alpha\beta}$ depends explicitly on the metric $g_{\mu\nu}$, it is a highly non-linear function of $h_{\mu\nu}$. Using the De Donder gauge condition, we see that the last term in eq. (5.74) is a divergence,

$$\partial_\nu h^{\alpha\mu} \partial_\mu h^{\beta\nu} - h^{\mu\nu} \partial_\mu \partial_\nu h^{\alpha\beta} = \partial_\mu \partial_\nu (h^{\alpha\mu} h^{\beta\nu} - h^{\mu\nu} h^{\alpha\beta}). \quad (5.76)$$

Thus, we can also rewrite eq. (5.72) as

$$\square h^{\alpha\beta} = +\frac{16\pi G}{c^4} \left[(-g)(T^{\alpha\beta} + t_{LL}^{\alpha\beta}) + \partial_\mu \partial_\nu \chi^{\alpha\beta\mu\nu} \right], \quad (5.77)$$

where

$$\chi^{\alpha\beta\mu\nu} = \frac{c^4}{16\pi G} (h^{\alpha\mu} h^{\beta\nu} - h^{\mu\nu} h^{\alpha\beta}). \quad (5.78)$$

The important point is that eqs. (5.71) and (5.72) are an *exact* way of recasting the Einstein equations (subject to the assumption that all of space-time can be covered by a harmonic coordinate system), and no approximation has been made yet.²⁰

Compare this with the standard form of Einstein equations,

$$G_{\alpha\beta} = \frac{8\pi G}{c^4} T_{\alpha\beta}, \quad (5.79)$$

where

$$G_{\alpha\beta} = R_{\alpha\beta} - \frac{1}{2} g_{\alpha\beta} R \quad (5.80)$$

is the Einstein tensor. Because of the Bianchi identity $D_\beta G^{\alpha\beta} = 0$, eq. (5.79) implies automatically the covariant conservation of the matter energy-momentum tensor,

$$D_\beta T^{\alpha\beta} = 0. \quad (5.81)$$

In turn, eq. (5.81) is an equation of motion for the matter variables. Thus, Einstein equations automatically fix the motion of matter. Einstein equations are completely equivalent to eq. (5.72) *together with* eq. (5.71). However, from a mathematical point of view it makes perfectly sense to first solve eq. (5.72) without requiring, for the moment, that eq. (5.71) be satisfied. Then eq. (5.72), alone, does not constraint the dynamics of the matter variables. In principle, we could assign ourselves an arbitrary time dependence to $T^{\alpha\beta}$, and the equation would still be well defined. For this reason, the 10 tensor components of eq. (5.72) are called the *relaxed Einstein equations*; we have relaxed the condition that the matter variables obey their equations of motion. Of course, this condition must be recovered when, on the solutions of eq. (5.72), we impose eq. (5.71), since the two equations, together, are equivalent to the Einstein equations. Indeed, the gauge condition (5.71) implies that $\tau^{\alpha\beta}$ satisfies the conservation law

$$\partial_\beta \tau^{\alpha\beta} = 0, \quad (5.82)$$

with an ordinary, rather than covariant derivative, and this turns out to be fully equivalent to eq. (5.81). Thus, if we first solve eq. (5.72),

²⁰At first sight eq. (5.72) is surprising, since it seems to suggest that $h_{\mu\nu}$ propagates along the light-cone of flat space-time, because on the left-hand side we have the flat-space d'Alembertian. Actually, this is not true because in $\Lambda^{\alpha\beta}$ we have the term $h^{\mu\nu} \partial_\mu \partial_\nu h^{\alpha\beta}$, which has two derivatives acting on a field $h^{\alpha\beta}$. If we wanted to write the equation so that all terms with two derivatives acting on $h^{\alpha\beta}$ are on the left-hand side, the term $h^{\mu\nu} \partial_\mu \partial_\nu h^{\alpha\beta}$ should also go on the left-hand side, so the total differential operator acting on $h^{\alpha\beta}$ is not a simple flat-space d'Alembertian. Still, eq. (5.72) is a legitimate way of writing the Einstein equations, which is particularly convenient because the flat space d'Alembertian is easily inverted.

then eq. (5.71) can be seen as the condition that imposes the equations of motion on the matter variables. Imposing the no-incoming-radiation boundary conditions (defined in Note 1 on page 102), eq. (5.72) can be formally integrated in terms of the retarded Green's function (3.6), just as we did in linearized theory (see eq. (3.8)), and we get

$$\begin{aligned} h^{\alpha\beta}(t, \mathbf{x}) &= -\frac{4G}{c^4} \int d^4x' \frac{\tau^{\alpha\beta}(t', \mathbf{x}')\delta(t' - t + |\mathbf{x} - \mathbf{x}'|/c)}{|\mathbf{x} - \mathbf{x}'|} \\ &= -\frac{4G}{c^4} \int \frac{d^3x'}{|\mathbf{x} - \mathbf{x}'|} \tau^{\alpha\beta}(t - |\mathbf{x} - \mathbf{x}'|/c, \mathbf{x}'). \end{aligned} \quad (5.83)$$

On this solution, we can then impose the gauge condition (5.82), which is equivalent to requiring that the matter sources satisfy the equations of motion in the metric $g_{\mu\nu}$.

Contrary to the result (3.5), (3.6) of linearized theory, in eq. (5.83) $\tau^{\alpha\beta}$ is itself a functional of $h^{\alpha\beta}$ and of its derivatives, so for the moment we have simply converted the differential equation (5.72) into an integro-differential equation for $h^{\alpha\beta}$. Finding an exact solution of such an equation is hopeless for all realistic astrophysical sources, and we must resort to approximation methods. The crucial observation is that different approximations must be employed, depending on whether we are in the near or in the far zone. In the near zone, the solution for $h_{\mu\nu}$ will be given in terms of instantaneous potential, and retardation effects can be treated as small corrections. In the far region the post-Newtonian approximation breaks down, and we will rather have gravitational waves, so retardation effects will of course be crucial.

The fact that different expansions must be used in the near and in the far region, in itself is not different from what happens in electrodynamics. The great difference is that electrodynamics is a linear theory, governed by a wave equation of the form $\square A_\mu = -(4\pi/c)J_\mu$, where the source J_μ depends only on the matter fields, and not on A_μ itself. However, in eq. (5.72) or in eq. (5.83), the field $h_{\mu\nu}$ appears even on the right-hand side; thus, the gravitational field itself generates gravitational waves and, if we compute iteratively to a sufficiently high order, we will find that the GWs computed at a given order generate themselves more GWs at higher orders. This is an unavoidable consequence of the non-linear structure of general relativity. At the technical level this is reflected in the fact that, even if the matter energy-momentum tensor $T^{\alpha\beta}$ is localized in space, the total source $\tau^{\alpha\beta}$ is not confined to a compact region, but it extends over all of space-time. As a result, a correct treatment is quite complicated (and a naive treatment of the integral in eq. (5.83) typically results in the divergences which plagued early attempts, see Note 15). Nowadays these problems have been solved, and the generation of GWs from post-Newtonian sources has been computed to very high PN order, thanks to the quite remarkable work of two groups, one composed of Blanchet, Damour and coworkers, and one of Will, Wiseman and Pati.²¹ Below we discuss these two approaches.

²¹Of course, these works have built on a large body of literature, which extended over decades, see the Further Reading section.

5.3 The Blanchet–Damour approach

In the problem of computing GWs from a non-relativistic, self-gravitating source with typical velocity v there are two length-scales: the size d of the source (which, for a binary system, is the orbital radius), and the length \mathcal{R} that determines the boundary of the near zone, see eq. (5.1). According to eq. (3.24), $\lambda = (c/v)d$ so, for non-relativistic sources, $\lambda \gg d$, and therefore the near zone extends up to a radius $\mathcal{R} \gg d$. In the region $r < \mathcal{R}$ the gravitational field can be computed using the post-Newtonian formalism. However, as we have seen in the previous section, the post-Newtonian approach breaks down at $r > \mathcal{R}$.

On the other hand, outside the matter source ($r > d$) the energy-momentum tensor of matter vanishes, and the only contribution to $\tau^{\alpha\beta}$ in eq. (5.73) comes from the gravitational field itself. If the gravitational field inside the matter source is weak, which (for the moment) is an assumption of the method, already at $r = d$ space-time will not deviate much from flat and, as r increases, it will approach Minkowski space-time more and more. Thus, over the whole region $d < r < \infty$ we can solve the vacuum Einstein equations using a *post-Minkowskian* expansion, that takes into account iteratively the deviation from flat space-time. Since the post-Minkowskian expansion is valid for $d < r < \infty$ and the post-Newtonian for $0 < r < \mathcal{R}$, the two expansions have an overlapping region of validity, $d < r < \mathcal{R}$. The strategy of the Blanchet–Damour formalism is therefore to use the post-Newtonian expansion in the near region, the post-Minkowskian expansion outside the source, and to match them in the intermediate region. In the following subsections we discuss these steps.

5.3.1 Post-Minkowskian expansion outside the source

We first consider the external domain $d < r < \infty$. Since we are outside the source, the energy-momentum tensor of matter vanishes, and we must solve the *vacuum* Einstein equations. By assumption, we are considering sources whose self-gravity is weak. Thus, in a first approximation the metric in the external domain is just $\eta_{\mu\nu}$, i.e. we have Minkowski space-time. At a distance r , the corrections to the Minkowski metric will be given as an expansion in R_S/r where, as in Section 5.1.1, $R_S = 2Gm/c^2$ and m is a characteristic mass of the system. Since R_S is proportional to G , the post-Minkowskian expansion can be written as an expansion in powers of G . We use as basic variable $h^{\alpha\beta} = \sqrt{-g}g^{\alpha\beta} - \eta^{\alpha\beta}$, we choose the De Donder gauge, and we write

$$\sqrt{-g}g^{\alpha\beta} = \eta^{\alpha\beta} + Gh_1^{\alpha\beta} + G^2h_2^{\alpha\beta} + \dots, \quad (5.84)$$

i.e.

$$h^{\alpha\beta} = \sum_{n=1}^{\infty} G^n h_n^{\alpha\beta}. \quad (5.85)$$

We now plug this expansion into the relaxed Einstein equations (5.72) with $T^{\alpha\beta} = 0$

$$\square h^{\alpha\beta} = \Lambda^{\alpha\beta}, \quad (5.86)$$

and we equate terms of the same order in G . The tensor $\Lambda^{\alpha\beta}$ depends on $g_{\mu\nu}$, which is a highly non-linear functional of $h_{\mu\nu}$, so it contains all possible powers of $h_{\mu\nu}$, starting from terms quadratic in h . Thus, we can write

$$\Lambda^{\alpha\beta} = N^{\alpha\beta}[h, h] + M^{\alpha\beta}[h, h, h] + L^{\alpha\beta}[h, h, h, h] + O(h^5), \quad (5.87)$$

and $N^{\alpha\beta}$, $M^{\alpha\beta}$, etc. can be found from the explicit expression of $\Lambda^{\alpha\beta}$, with long but straightforward computations. For instance

$$\begin{aligned} N^{\alpha\beta}[h, h] &= -h^{\mu\nu}\partial_\mu\partial_\nu h^{\alpha\beta} + \frac{1}{2}\partial^\alpha h_{\mu\nu}\partial^\beta h^{\mu\nu} - \frac{1}{4}\partial^\alpha h\partial^\beta h \\ &\quad - \partial^\alpha h_{\mu\nu}\partial^\mu h^{\beta\nu} - \partial^\beta h_{\mu\nu}\partial^\mu h^{\alpha\nu} + \partial_\nu h^{\alpha\mu}(\partial^\nu h_\mu^\beta + \partial_\mu h^{\beta\nu}) \\ &\quad + \eta^{\alpha\beta} \left[-\frac{1}{4}\partial_\rho h_{\mu\nu}\partial^\rho h^{\mu\nu} + \frac{1}{8}\partial_\mu h\partial^\mu h + \frac{1}{2}\partial_\mu h_{\nu\rho}\partial^\nu h^{\mu\rho} \right], \end{aligned} \quad (5.88)$$

²²For the explicit expression of $M^{\alpha\beta}[h, h, h]$ see eq. (1.6) of Blanchet (1995).

where, on the right-hand side, $h = \eta_{\alpha\beta}h^{\alpha\beta}$, and all indices are raised and lower with the Minkowski metric $\eta_{\mu\nu}$.²² Since $\Lambda^{\alpha\beta}$ starts from a term quadratic in $h^{\alpha\beta}$, and therefore proportional to G^2 , to order G we simply have

$$\square h_1^{\alpha\beta} = 0, \quad (5.89)$$

and, to higher orders, we get

$$\square h_2^{\alpha\beta} = N^{\alpha\beta}[h_1, h_1], \quad (5.90)$$

$$\square h_3^{\alpha\beta} = M^{\alpha\beta}[h_1, h_1, h_1] + N^{\alpha\beta}[h_1, h_2] + N^{\alpha\beta}[h_2, h_1], \quad (5.91)$$

and so on, together with the gauge conditions

$$\partial_\beta h_n^{\alpha\beta} = 0. \quad (5.92)$$

We write generically the n -th equation in the form

$$\square h_n^{\alpha\beta} = \Lambda_n^{\alpha\beta}[h_1, h_2, \dots, h_{n-1}], \quad (r > d), \quad (5.93)$$

where we have recalled that the above equations are valid only in the exterior region $r > d$.

General solution of the linearized vacuum equation

We consider first the linearized equation (5.89). We want to find the most general solution, in order to be able to perform later the matching with the near-region post-Newtonian solution. The most general solution of eq. (5.89) in the region $r > d$ (with d any strictly positive constant), can be written in terms of retarded multipolar waves,

$$h_1^{\alpha\beta} = \sum_{l=0}^{\infty} \partial_L \left[\frac{1}{r} K_L^{\alpha\beta}(t - r/c) \right], \quad (5.94)$$

where we have used the multi-index notation introduced in Section 3.5.1, and the tensors $K_L^{\alpha\beta}$ are traceless and symmetric with respect to the indices i_1, \dots, i_l . From the fact that $K_L^{\alpha\beta}$ is a function of $u = t - r/c$, it follows that $\square(K_L^{\alpha\beta}(u)/r) = 0$ and, since the flat-space d’Alembertian commutes with ∂_L , eq. (5.94) is a solution of eq. (5.89). Since the set of STF tensors $K_L^{\alpha\beta}$, with all possible rank l , provide a complete set of representation of the rotation group, this is the most general solution. Observe that this solution is acceptable since we are in the domain $r > d$, so we have excluded $r = 0$ from the domain where it is required to hold. Otherwise all multipoles in eq. (5.94) would become singular.

Equation (5.94) is the most general solution of eq. (5.89), but in general it does not fulfill the De Donder gauge condition. The tensor $K_L^{\alpha\beta}$ is symmetric in the Lorentz indices α, β so, for each L , it has 10 tensor components. Imposing the gauge condition $\partial_\beta h_1^{\alpha\beta} = 0$ reduces the number of independent tensor components to six, and one finds that the most general solution of the equation of motion and gauge condition, in the external region, has the form

$$h_1^{\alpha\beta} = k_1^{\alpha\beta} + \partial^\alpha \varphi_1^\beta + \partial^\beta \varphi_1^\alpha - \eta^{\alpha\beta} \partial_\mu \varphi_1^\mu, \quad (5.95)$$

where the components of $k_1^{\alpha\beta}$ are given by

$$\begin{aligned} k_1^{00} &= -\frac{4}{c^2} \sum_{l \geq 0} \frac{(-1)^l}{l!} \partial_L \left[\frac{1}{r} I_L(u) \right], \\ k_1^{0i} &= \frac{4}{c^3} \sum_{l \geq 1} \frac{(-1)^l}{l!} \partial_{L-1} \left[\frac{1}{r} I_{iL-1}^{(1)}(u) + \frac{l}{l+1} \epsilon_{iab} \partial_a \left(\frac{1}{r} J_{bL-1}(u) \right) \right], \\ k_1^{ij} &= -\frac{4}{c^4} \sum_{l \geq 2} \frac{(-1)^l}{l!} \partial_{L-2} \left[\frac{1}{r} I_{ijL-2}^{(2)}(u) + \frac{2l}{l+1} \partial_a \left(\frac{1}{r} \epsilon_{ab(i} J_{j)bL-2}^{(1)}(u) \right) \right]. \end{aligned} \quad (5.96)$$

We have used the notation

$$f^{(n)}(u) \equiv \frac{d^n f}{du^n}, \quad (5.97)$$

to denote the n -th derivative with respect to retarded time.²³ The tensor $k_1^{\alpha\beta}$ depends on two families of symmetric and traceless multipole moments,

$$I_L(u) = \{I, I_i, I_{ij}, I_{ijk}, \dots\}, \quad (5.98)$$

and

$$J_L(u) = \{J_i, J_{ij}, J_{ijk}, \dots\}, \quad (5.99)$$

which are arbitrary functions of retarded time, except that the gauge condition requires that I , $I_i^{(1)}$ and J_i are time-independent. This expresses the conservation of the total mass $M \equiv I$ of the system, of the total linear momentum $P_i \equiv I_i^{(1)}$, and of the total angular momentum $S_i \equiv J_i$.²⁴ The moments I_L and J_L are mass-type and current-type moments, respectively, just as in the multipole expansion of linearized theory, discussed in Section 3.5. The explicit powers of c in

²³We also made use of the notation introduced on page 134, so in particular $\partial_{L-2} \equiv \partial_{i_1} \dots \partial_{i_{L-2}}$, $I_{ijL-2} \equiv I_{iji_1 \dots i_{L-2}}$, and round brackets around indices denote the symmetrization, $a_{(ij)} \equiv (1/2)(a_{ij} + a_{ji})$. On the right-hand side, we freely raised or lowered the spatial indices with δ_{ij} .

²⁴We further impose the condition that the metric is stationary in the far past, i.e. that all I_L and J_L are constants for $t \leq -T$, with $T \rightarrow \infty$. This is expected to be basically equivalent to the no-incoming radiation boundary condition, but offers some technical advantages. With this boundary condition, the requirement that $I_i^{(1)}$ be constant implies that also the center-of-mass variable $X_i = I_i/I$ is constant, rather than a priori linearly varying in time.

eqs. (5.96) follow from the choice of dimensions $[I_L] = [\text{mass}] \times [\text{length}]^l$ and $[J_L] = [\text{mass}] \times [\text{velocity}] \times [\text{length}]^l$. These are chosen in anticipation of the fact that I_L and J_L will be related to the mass and current multipoles of the source. The “mass dipole” I_i can be set to zero shifting the origin of the coordinate system.

The function φ_1^μ can be written in terms of four STF moments W_L , X_L , Y_L and Z_L ,

$$\varphi_1^0 = \frac{4}{c^3} \sum_{l \geq 0} \frac{(-1)^l}{l!} \partial_L \left[\frac{1}{r} W_L(u) \right], \quad (5.100)$$

$$\begin{aligned} \varphi_1^i = & -\frac{4}{c^4} \sum_{l \geq 0} \frac{(-1)^l}{l!} \partial_{iL} \left[\frac{1}{r} X_L(u) \right] \\ & -\frac{4}{c^4} \sum_{l \geq 1} \frac{(-1)^l}{l!} \partial_{L-1} \left[\frac{1}{r} Y_{iL-1}(u) + \frac{l}{l+1} \epsilon_{iab} \partial_a \left(\frac{1}{r} Z_{bL-1}(u) \right) \right]. \end{aligned} \quad (5.101)$$

²⁵When comparing with eq. (3.204), recall that in the linearized limit $h_{\mu\nu}$ reduces to $-\bar{h}_{\mu\nu}$, see Note 19, and also that a factor G has been explicitly extracted from $h_1^{\mu\nu}$, see eq. (5.84).

²⁶We include in eq. (5.102) a sign correction pointed out in Arun, Blanchet, Iyer and Qusailah (2004), see their eq. (3.8).

²⁷They are also called the “source multipole moments”, see the review Blanchet (2006). The term “algorithmic multipole moments” used in the original papers stresses that they are intermediate quantities that allow us to connect, via a well defined algorithm, properties of the source to the “multipole moments at infinity”, to be defined later. The term “source moments” stresses that they have explicit closed-form expressions as integrals over the source, see below.

The appearance of the function φ_1^α in eq. (5.95) reflects the fact that eq. (5.89) is invariant under linearized gauge transformations, $x^\alpha \rightarrow x^\alpha + \varphi_1^\alpha(x)$, compare with eq. (1.19). One might be tempted to discard φ_1^α as pure gauge modes (which would give back the result that we found for linearized theory, see eq. (3.204)),²⁵ but this would not be correct. Our aim is to use the solution (5.95) for $h_1^{\alpha\beta}$ as a starting point for the iterative process that gives $h_2^{\alpha\beta}$, $h_3^{\alpha\beta}$, etc., and therefore to construct a solution of the full, rather than linearized, Einstein equations. Taking as starting point two different solution for h_1 which differ by a *linearized* gauge transformation φ_1 will produce, through the iterative procedure, two solutions of the full Einstein equations that are not related by the full non-linear invariance under diffeomorfisms of general relativity, and which therefore are not physically equivalent. So, beyond linear level the two sets of multipole moments $(I_L, J_L, W_L, X_L, Y_L, Z_L)$ and $(I_L, J_L, 0, 0, 0, 0)$ are not gauge-equivalent. Rather, the six multipole moments $(I_L, J_L, W_L, X_L, Y_L, Z_L)$ are gauge-equivalent to a reduced set $(M_L, S_L, 0, 0, 0, 0)$, in which $M_L = I_L$ and $S_L = J_L$ only to lowest order, and more generally M_L and S_L depend on all the six moments $(I_L, J_L, W_L, X_L, Y_L, Z_L)$. For example, for the quadrupole moment one finds that M_{ij} starts to differ from I_{ij} at $O(1/c^5)$, i.e. at 2.5PN order,²⁶

$$M_{ij} = I_{ij} + \frac{4G}{c^5} \left[W^{(2)} I_{ij} - W^{(1)} I_{ij}^{(1)} \right] + O\left(\frac{1}{c^7}\right), \quad (5.102)$$

where W is W_L for $l = 0$. The six sets of moments (I_L, \dots, Z_L) are referred to as “algorithmic multipole moments”.²⁷

Iteration of the solution. Multipolar post-Minkowskian expansion

We have found above the most general solution of the linearized equation (5.89), together with $\partial_\beta h_1^{\alpha\beta} = 0$, in the domain $r > d$. Next we want to plug this solution into the right-hand side of eq. (5.90), and solve the

resulting equation for h_2 , and so on. The general problem is therefore how to integrate a wave equation such as eq. (5.93), when the source term Λ_n has been determined by the previous recursive level.

Given the function Λ_n , the problem amounts to inverting the \square operator. Physicists are well accustomed to some possible solutions for the inversion of the d'Alembert operator: the retarded and the advanced Green's functions, familiar from classical electrodynamics, or the Feynman propagator, which is a basic object in quantum field theory. However, from a mathematical point of view, the inversion of the \square operator has many other possible solutions, which depend on the boundary conditions of the problem.

In the problem at hand the retarded Green's function is simply not the correct solution (and even less any other combination of retarded and advanced Green's functions). The point is that the use of the retarded (or of the advanced) integral requires the knowledge of Λ_n over all of space, while eq. (5.93) is valid only for $r > d$. Observe that, since we are outside the source, we can write each h_n in a multipole expansion, which is an expansion valid for $d/r < 1$, so Λ_n in eq. (5.93) is composed of the product of many multipole expansions. If we naively extended eq. (5.93) down to $r = 0$, we would find that the right-hand side of eq. (5.93) is highly singular at $r = 0$ and, if we make the convolution with the retarded Green's function, the retarded integral diverges.

The appropriate solution has been found by Blanchet and Damour, with a clever mathematical procedure. First, we observe that we are finally interested in computing to some *finite* order in the PN expansion, and to each given order only a finite number of multipoles contribute. This means that, outside the source, we do not really need the exact expression of $h_2^{\alpha\beta}$, $h_3^{\alpha\beta}$, etc. but only their multipole expansion, truncated to some *finite* order, that depends on the order of the PN expansion that we wish to compute. It is therefore very convenient (in fact, technically inevitable) to perform a multipole expansion of the post-Minkowskian solution, up to a given finite order, and to iterate not $h_1^{\alpha\beta}$ but rather its (truncated) multipole expansion. This method is therefore called the multipolar post-Minkowskian (MPM) expansion.

Since, in the MPM computation of $h_n^{\alpha\beta}$ with n given, only a maximum number of multipoles are relevant, we can find a positive real number B , sufficiently large, so that $r^B \Lambda_n^{\alpha\beta}$ is regular at the origin. Thus, the retarded integral

$$I_n^{\alpha\beta}(B) \equiv \square_{\text{ret}}^{-1} (r^B \Lambda_n^{\alpha\beta}) \quad (5.103)$$

is well defined, where we denoted by $\square_{\text{ret}}^{-1}$ the convolution with the retarded Green's function,²⁸

$$(\square_{\text{ret}}^{-1} f)(t, \mathbf{x}) \equiv -\frac{1}{4\pi} \int_{\mathbb{R}^3} \frac{d^3x'}{|\mathbf{x} - \mathbf{x}'|} f(t - |\mathbf{x} - \mathbf{x}'|/c, \mathbf{x}'). \quad (5.104)$$

Now, it can be proved that $I_n^{\alpha\beta}(B)$ admits a unique analytic continuation in the complex B -plane, except at some integer values of B and, when $B \rightarrow 0$, develops some multipole poles. Thus, near $B = 0$ we can write

²⁸We also impose the boundary condition in the form given in Note 24. In the retarded integral, the integration is actually over d^4x , along the past null light cone. As $r \rightarrow \infty$ along the past null light cones, t goes toward $-\infty$, so this boundary condition forces $\Lambda_n^{\alpha\beta}$ to become strictly zero beyond some value of r . Therefore there is no problem of convergence of the integral at $r \rightarrow \infty$.

$I_n^{\alpha\beta}(B)$ in a Laurent expansion,

$$I_n^{\alpha\beta}(B) = \sum_{p=p_0}^{\infty} B^p \iota_{n,p}^{\alpha\beta}, \quad (5.105)$$

where $p_0 \in \mathbb{Z}$. If $p_0 < 0$ there are poles. Applying the flat-space d'Alembertian to both sides of this equation and using eq. (5.103) we get

$$r^B \Lambda_n^{\alpha\beta} = \sum_{p=p_0}^{\infty} B^p \square \iota_{n,p}^{\alpha\beta}. \quad (5.106)$$

Writing $r^B = e^{B \log r}$, expanding the exponential, and equating terms with the same powers of B we find that, for $p_0 \leq p \leq -1$, $\square \iota_{n,p}^{\alpha\beta} = 0$, while for $p \geq 0$

$$\square \iota_{n,p}^{\alpha\beta} = \frac{(\log r)^p}{p!} \Lambda_n^{\alpha\beta}. \quad (5.107)$$

In particular, the term with $p = 0$, i.e. $u_n^{\alpha\beta} \equiv \iota_{n,p=0}^{\alpha\beta}$, satisfies $\square u_n^{\alpha\beta} = \Lambda_n^{\alpha\beta}$, so we succeeded in finding a particular solution of eq. (5.93). In other words, a solution of eq. (5.93) is given by the coefficient of B^0 in the Laurent expansion (5.105). This is called the *finite part at $B = 0$* of the retarded integral, and denoted as $\text{FP}_{B=0}$, so²⁹

$u_n^{\alpha\beta} = \text{FP}_{B=0} \left\{ \square_{\text{ret}}^{-1} [r^B \Lambda_n^{\alpha\beta}] \right\}.$

(5.108)

We can write this even more compactly introducing the symbol \mathcal{FP} , defined on any function $f(x)$ by

$$\mathcal{FP} \square_{\text{ret}}^{-1} f \equiv \text{FP}_{B=0} \left\{ \square_{\text{ret}}^{-1} [r^B f] \right\}. \quad (5.109)$$

This finite part operation is a prescription which makes well-defined the otherwise divergent retarded integral. The important point is that it is not just a prescription superimposed by hand on a would-be divergent quantity. Rather, we have seen explicitly that it is a correct way to find a solution of eq. (5.93), valid in the region $r > d$. Observe that, when the retarded integral of a function f is well-defined, $\mathcal{FP} \square_{\text{ret}}^{-1} f$ reduces simply to $\square_{\text{ret}}^{-1} f$.

Actually, eq. (5.108) is just one particular solution of the inhomogeneous equation (5.93). The most general solution is obtained adding the general solution of the homogeneous equation $\square h_n^{\alpha\beta} = 0$. Indeed, the solution (5.108) in general will not satisfy automatically the harmonic gauge condition. So, the solution that we are looking for is really of the form

$$h_n^{\alpha\beta} = u_n^{\alpha\beta} + v_n^{\alpha\beta}, \quad (5.110)$$

where $v_n^{\alpha\beta}$ is a solution of the homogeneous equation, chosen so that $\partial_\alpha v_n^{\alpha\beta} = -\partial_\alpha u_n^{\alpha\beta}$. Since we have the explicit form of $u_n^{\alpha\beta}$, the function $v_n^{\alpha\beta}$ can be determined exactly.³⁰ The conclusion is that the MPM expansion provides a well-defined algorithm for computing the post-Minkowskian corrections, in principle to arbitrary order.

²⁹More precisely in the definition of the $\text{FP}_{B=0}$ operation, eq. (5.108), for dimensional reasons we use $(r/r_0)^B$ rather than r^B . The constant r_0 is arbitrary, and will cancel from physical quantities, as we will see in Section 5.3.4. For the moment, we set $r_0 = 1$, to simplify the notation.

³⁰The explicit expression is somewhat involved, and can be found in Blanchet (2006), eqs. (41) and (42).

At this stage, the multipole moments $(I_L, J_L, W_L, X_L, Y_L, Z_L)$ (or, equivalently, M_L and S_L) know nothing about the properties of the source, since they simply parametrize the most general solution of the vacuum Einstein equation. We will determine them in terms of properties of the source, matching the MPM result to the multipole expansion of the post-Newtonian result, in the region $d < r < \mathcal{R}$, where both the post-Minkowskian and the post-Newtonian formalism are applicable.

5.3.2 PN expansion in the near region

We now consider the near region. The 1PN solution, in harmonic coordinates, has already been given in the Section 5.1.4. First of all, it is useful to re-express it in terms of the variable $h^{\mu\nu}$, defined in eq. (5.69), rather than in terms of $g^{\mu\nu}$.³¹ In terms of $h^{\mu\nu}$, the solution at the Newtonian level is particularly simple, $h^{00} = -4V/c^2 + O(1/c^4)$, $h^{0i} = O(1/c^3)$ and $h^{ij} = O(1/c^4)$. We can now plug this solution into the right-hand side of eq. (5.72). This gives

$$\square h^{00} = \frac{16\pi G}{c^4} \left(1 + \frac{4V}{c^2} \right) T^{00} - \frac{14}{c^4} \partial_k V \partial_k V + O\left(\frac{1}{c^6}\right), \quad (5.111)$$

$$\square h^{0i} = \frac{16\pi G}{c^4} T^{0i} + O\left(\frac{1}{c^5}\right), \quad (5.112)$$

$$\square h^{ij} = \frac{16\pi G}{c^4} T^{ij} + \frac{4}{c^4} \left\{ \partial_i V \partial_j V - \frac{1}{2} \delta_{ij} \partial_k V \partial_k V \right\} + O\left(\frac{1}{c^6}\right). \quad (5.113)$$

The solution of these equations is

$$h^{00} = -\frac{4}{c^2} V + \frac{4}{c^4} (W - 2V^2) + O\left(\frac{1}{c^6}\right), \quad (5.114)$$

$$h^{0i} = -\frac{4}{c^3} V_i + O\left(\frac{1}{c^5}\right), \quad (5.115)$$

$$h^{ij} = -\frac{4}{c^4} W_{ij} + O\left(\frac{1}{c^6}\right), \quad (5.116)$$

where V , V_i are given in eqs. (5.39) and (5.41). W_{ij} is a new retarded potential, defined by

$$W_{ij}(t, \mathbf{x}) = G \int d^3x' \frac{1}{|\mathbf{x} - \mathbf{x}'|} \left[\sigma_{ij} + \frac{1}{4\pi G} (\partial_i V \partial_j V - \frac{1}{2} \delta_{ij} \partial_k V \partial_k V) \right] (\mathbf{x}', t - |\mathbf{x} - \mathbf{x}'|/c), \quad (5.117)$$

where $\sigma_{ij} = T^{ij}$. This is the same as the 1PN solution given in eqs. (5.42)–(5.44), written in terms of $h^{\mu\nu}$ rather than $g^{\mu\nu}$, except that this iterative procedure automatically gives h_{ij} up to $O(1/c^6)$ (which is needed to iterate consistently the solution to higher orders), rather than just up to $O(1/c^4)$ as in eq. (5.44). Observe that the integrals in the definition of V and V_i are convergent since the source, and therefore σ and σ_i , have a compact support. The integrand in the definition of W_{ij} rather depends

³¹Recall that $h^{\mu\nu}$ denotes the combination (5.69), and is not simply the deviation from the flat metric $g^{\mu\nu} - \eta^{\mu\nu}$. The relation between $h^{\mu\nu}$ and $g^{\mu\nu}$ is therefore non-linear.

on the function V and does not have a compact support. However, from eq. (5.39), we find that, when $|\mathbf{x}'| \rightarrow \infty$,

$$V\left(t - \frac{|\mathbf{x} - \mathbf{x}'|}{c}, \mathbf{x}'\right) \rightarrow \frac{GM}{|\mathbf{x}'|} \quad (5.118)$$

where

$$M = \int d^3y \sigma(\mathbf{y}, -\infty) + O(1/c^2) \quad (5.119)$$

is the initial mass of the source. From this, we can check that the integral defining the potential W_{ij} is convergent.

Multipolar PN expansion

We can now introduce another important ingredient of the method, the “multipolar post-Newtonian expansion”, which combine the PN expansion with the multipole expansion.

The post-Newtonian expansion is valid both inside the source ($r < d$), and in the external near zone $d < r < \mathcal{R}$. In the external near zone we can then expand each post-Newtonian order in a multipole expansion, since the expansion parameter of the multipole expansion is d/r . This gives rise to the “multipolar post-Newtonian expansion”, and provides crucial simplifications when performing the matching with the solution in the far region. To 1PN order, we just need the multipole expansion of the potentials V and V_i . This can be written in full generality as

$$V(t, \mathbf{x}) = G \sum_{l=0}^{\infty} \frac{(-1)^l}{l!} \partial_L \left[\frac{1}{r} F_L(t - r/c) \right], \quad (5.120)$$

$$V_i(t, \mathbf{x}) = G \sum_{l=0}^{\infty} \frac{(-1)^l}{l!} \partial_L \left[\frac{1}{r} G_{iL}(t - r/c) \right]. \quad (5.121)$$

Using eqs. (3.184), (3.185) and (3.188), together with the fact that V and V_i satisfy $\square V = -4\pi G\sigma$ and $\square V_i = -4\pi G\sigma_i$ (see eqs. (5.39) and (5.41)), we get

$$F_L(u) = \int d^3y \hat{y}_L \int_{-1}^1 dz \delta_l(z) \sigma(u + z|\mathbf{y}|/c, \mathbf{y}), \quad (5.122)$$

$$G_{iL}(u) = \int d^3y \hat{y}_L \int_{-1}^1 dz \delta_l(z) \sigma_i(u + z|\mathbf{y}|/c, \mathbf{y}), \quad (5.123)$$

where $u = t - r/c$, and the function $\delta_l(z)$ is defined in eq. (3.189).

The PN expansion to arbitrary order

We now tackle the problem of finding the PN solution to all orders. We write the PN expansion of $h_{\mu\nu}$ in the form

$$h^{\mu\nu} = \sum_{n=2}^{\infty} \frac{1}{c^n} {}^{(n)}h^{\mu\nu}, \quad (5.124)$$

where we have extracted explicitly the powers of $1/c$, to help the book-keeping (just as we did with G in the post-Minkowskian expansion).³² Similarly, we expand the effective energy-momentum tensor as³³

$$\tau^{\mu\nu} = \sum_{n=-2}^{\infty} \frac{1}{c^n} {}^{(n)}\tau^{\mu\nu}. \quad (5.125)$$

Inserting this into the relaxed Einstein equations, and equating terms with the same powers of c , we get a recursive set of Poisson-type equations,

$$\nabla^2 [{}^{(n)}\mathsf{h}^{\mu\nu}] = 16\pi G [{}^{(n-4)}\tau^{\mu\nu}] + \partial_t^2 [{}^{(n-2)}\mathsf{h}^{\mu\nu}]. \quad (5.126)$$

We could now try to solve these equations using the Poisson integral (5.61). However, as we already discussed in Section 5.1.6, beyond some value of n the resulting Poisson integrals diverge. This does not mean that eq. (5.126) admits no solution, but simply that the Poisson integral is not the correct one. The problem here is purely technical, and consists in finding the correct inversion of the Laplacian. The Poisson integral is the right solution only when the boundary condition is that the field vanishes at spatial infinity; otherwise, the solution is different. As an obvious example, consider the equation

$$\nabla^2 U = -\rho, \quad (5.127)$$

where ρ is constant all over space (physically, this equation gives a model of Newtonian cosmology). If we attempt to solve for U using the Poisson integral (5.61), we find a divergent result. However, on a function $U(r)$,

$$\nabla^2 U = \frac{1}{r} \frac{\partial^2}{\partial r^2} [rU(r)], \quad (5.128)$$

so we see immediately that $U(r) = (-1/6)\rho r^2$ is a solution. In this case, it was simply not appropriate to impose the boundary condition that $U(r)$ vanishes at infinity, since the source ρ does not vanish either.

In our case the problem is similar, but more subtle. The point is that we cannot enforce the boundary conditions at infinity within the PN expansion, because this expansion becomes singular as $r \rightarrow \infty$, as we saw in Section 5.1.6. The correct way to incorporate the boundary conditions is to match the PN solution in the near zone to the post-Minkowskian solution in the external source region, and to impose the no-incoming radiation boundary conditions on the post-Minkowskian solution.

A possible strategy is therefore to find one particular solution of the set of equations (5.126). This is the same as a particular solution of the relaxed Einstein equation (5.72), which is an inhomogeneous equation, so the most general solution is obtained adding an arbitrary solution of the homogeneous equation $\square \mathsf{h}^{\mu\nu} = 0$ (subject to a regularity condition at the origin, see below). This homogeneous solution will then be fixed matching the PN solution to the post-Minkowskian solution. Once we

³²However in this case one finds that, starting from 4PN order, ${}^{(n)}\mathsf{h}^{\mu\nu}$ has also a logarithmic dependence on c , and the expansion contains arbitrary powers of $\log c$.

³³Observe that this expansion starts from $n = -2$, since $\tau^{\mu\nu}$ has dimension of ρc^2 .

have found a particular solution of eq. (5.126), the addition of an arbitrary solution of the homogeneous equation provides the most general solution in the near region, while in the previous section we found, with the post-Minkowskian expansion, the most general solution in the external source region. Thus, the matching condition will admit a solution.

A particular solution of the set of equations (5.126) has been found by Poujade and Blanchet using a variant of the analytic continuation technique discussed in Section 5.3.1. Given a function $f(\mathbf{x})$, we consider the integral

$$[\Delta^{-1}(r^B f)](\mathbf{x}) = -\frac{1}{4\pi} \int_{\mathbb{R}^3} \frac{d^3 x'}{|\mathbf{x} - \mathbf{x}'|} |\mathbf{x}'|^B f(\mathbf{x}'). \quad (5.129)$$

³⁴Observe that here the factor $|\mathbf{x}'|^B$ regularizes the divergence at infinity, while in the analytic continuation technique discussed in Section 5.3.1 it regularizes the divergence at the origin. For this reason, here we start from B large and negative, while in Section 5.3.1 we started from B large and positive. More precisely, one assumes that the source is extended and made of some perfectly regular (i.e. C^∞) distribution of fluid. We then separate the original Poisson integral into a part from $r = 0$ up to a finite value, say to the boundary \mathcal{R} of the near zone, and a part from $r = \mathcal{R}$ to $r = \infty$. The inner integral converges (assuming that f is a smooth function of the source), and no factor $|\mathbf{x}'|^B$ is inserted there, while the outer integral is regularized by the insertion of the factor $|\mathbf{x}'|^B$. By the uniqueness of the analytic continuation, the result is the sum of the near zone and far zone integrals.

If we take B sufficiently large and negative, the factor $|\mathbf{x}'|^B$ regularizes any potential divergence of the integral at $|\mathbf{x}'| \rightarrow \infty$.³⁴ Equation (5.129) then defines a function of B , for B sufficiently large and negative. One can then prove that this function admits a unique analytic continuation to the complex B -plane, except for $B = 0$, where it can develop multipole poles and can be written in a Laurent expansion. The coefficient u of B^0 is again denoted by $\text{FP}_{B=0}$,

$$u = \text{FP}_{B=0}\{\Delta^{-1}[r^B f]\}. \quad (5.130)$$

With the same argument used on page 258 for the inversion of the d'Alembertian operator, we can now show that u satisfies $\nabla^2 u = f$, so u provides a well-defined inversion of the Laplacian. When the Poisson integral converges $\text{FP}_{B=0}\{\Delta^{-1}[r^B f]\}$ is the same as $\Delta^{-1}f$. Therefore, we recover the lowest-order results obtained in the early works on the PN expansion. However, now all higher-order terms are manifestly finite and calculable.

We denote by an overbar the expansion of a quantity up to n -th order in the PN expansion, e.g.

$$\bar{h}^{\mu\nu} = \sum_{m=2}^n \frac{1}{c^m} {}^{(m)}h^{\mu\nu}, \quad (5.131)$$

Taking the sum over n of both sides of eq. (5.126), we see that the particular solution that we have found can also be written compactly as

$$\bar{h}_{\text{part}}^{\mu\nu} = \frac{16\pi G}{c^4} \mathcal{F} \mathcal{P} \square_{\text{ret}}^{-1} \bar{\tau}^{\mu\nu}. \quad (5.132)$$

To this solution we must add the most general solution of the homogeneous equation, subject to the condition of regularity at the origin. This has the form

$$h_{\text{hom}}^{\alpha\beta} = \frac{16\pi G}{c^4} \sum_{l=0}^{+\infty} \frac{(-1)^l}{l!} \partial_L \left[\frac{\mathcal{R}_L^{\alpha\beta}(t - r/c) - \mathcal{R}_L^{\alpha\beta}(t + r/c)}{2r} \right], \quad (5.133)$$

where $\mathcal{R}_L^{\alpha\beta}(u)$ are arbitrary functions of u , and are STF tensors in the indices $i_1 \dots i_l$. The fact that this is a solution follows from the fact that,

for any function $f(u)$, where $u = t - r/c$, we have $\square[f(u)/r] = 0$, and similarly $\square[f(v)/r] = 0$, where $v = t + r/c$. The inclusion of all STF tensor provides a full set of representations of the rotation group, so for instance the first term in eq. (5.133) gives the most general retarded solution. The condition of regularity at $r = 0$ fixes the antisymmetric combination of retarded and advanced waves. Observe that, under time reversal, $h_{\text{hom}}^{\alpha\beta}$ is odd. According to the discussion above eq. (5.3), it therefore describes radiation reaction.³⁵ We will indeed see that this term gives a correction to the leading term of the radiation reaction force.

5.3.3 Matching of the solutions

In the external source region, $d < r < \infty$, we have found the solution in the form of a post-Minkowskian expansion, eq. (5.85). For $d/r < 1$ the multipole expansion is applicable, so we could write the solution for h_1 in terms of the multipole moments $(I_L, J_L, W_L, X_L, Y_L, Z_L)$ or, equivalently, in terms of (M_L, S_L) . Through the iterative procedure that we have discussed, all higher-order terms h_2, h_3, \dots are then determined, in the form of a multipole expansion.

On the other hand, in the region $0 < r < \mathcal{R}$, with \mathcal{R} is the boundary of the near region, we have found the solution in terms of a post-Newtonian expansion. Since we are considering a source with $v \ll c$, we have $\mathcal{R} \gg d$, and the region of validity of the PN expansion overlaps with the region of validity of the post-Minkowskian expansion. In the post-Minkowskian scheme, the moments (I_L, \dots, Z_L) are quantities that parametrize the most general vacuum solution, but for the moment know nothing about the specific source under consideration. In PN solution, on the contrary, the energy-momentum tensor of the source enter explicitly, see eq. (5.132). Comparing these two solutions in the overlapping region, we can therefore fix the multipole moments (I_L, \dots, Z_L) in terms of the energy-momentum tensor of the source.

To perform this matching we observe that, in the overlap region $d < r < \mathcal{R}$, we have $d/r < 1$ so each term of the post-Newtonian expansion can be in turn re-expanded in powers of d/r , i.e. in a multipole expansion. This is the multipolar post-Newtonian expansion discussed in Section 5.3.2. On the other hand, again in the overlap region, each term of the multipolar post-Minkowskian expansion can be expanded in a post-Newtonian way, i.e. in powers of v/c . A crucial point is that the n -th term of the post-Minkowskian expansion, i.e. the term $h_n^{\alpha\beta}$ in eq. (5.85), when expanded in a PN fashion, is such that³⁶

$$h_n^{00} = O\left(\frac{1}{c^{2n}}\right), \quad h_n^{0i} = O\left(\frac{1}{c^{2n+1}}\right), \quad h_n^{ij} = O\left(\frac{1}{c^{2n}}\right). \quad (5.134)$$

This means that, to work to a given order in the PN expansion, we need to take into account only a finite number of iterations of the post-Minkowskian expansion. For example, suppose that we want to perform a computation to 2PN order, i.e. that we want to compute the correction

³⁵Furthermore, the fact that it is a solution of the homogeneous equation means that a source is not needed to sustain this field, which again leads to an interpretation in terms of a pure radiation field. It is well known already in classical electrodynamics that the antisymmetric combination of advanced and retarded waves is associated with radiation reaction. See, e.g. Poisson (1999) for a review.

³⁶For the proof see Blanchet and Damour (1986), eq. (5.5).

$O(1/c^4)$ to the Newtonian metric. This means that we need g_{00} up to $O(1/c^6)$, g_{0i} to $O(1/c^5)$, and g_{ij} to $O(1/c^4)$, included. Equation (5.134) shows that we need to compute \mathbf{h}_n up to $n = 3$, i.e. that we must perform two iterations of the linearized solution \mathbf{h}_1 .

Comparing the multipolar post-Newtonian expansion with the PN re-expansion of the post-Minkowskian solution, allows us to fix the multipole moments $(\mathbf{I}_L, \dots, \mathbf{Z}_L)$ in terms of the energy-momentum tensor of the source. Remarkably, it is possible to compute them analytically, for any l , and formally to arbitrary order in the PN expansion. For \mathbf{I}_L and \mathbf{J}_L one finds³⁷

$$\begin{aligned} \mathbf{I}_L(u) &= \mathcal{FP} \int d^3x \int_{-1}^1 dz \left\{ \delta_l(z) \hat{x}_L \Sigma - \frac{4(2l+1)\delta_{l+1}(z)}{c^2(l+1)(2l+3)} \hat{x}_{iL} \Sigma_i^{(1)} \right. \\ &\quad \left. + \frac{2(2l+1)\delta_{l+2}(z)}{c^4(l+1)(l+2)(2l+5)} \hat{x}_{ijL} \Sigma_{ij}^{(2)} \right\} (u + z|\mathbf{x}|/c, \mathbf{x}), \end{aligned} \quad (5.135)$$

$$\begin{aligned} \mathbf{J}_L(u) &= \mathcal{FP} \int d^3x \int_{-1}^1 dz \epsilon_{ab\langle ii} \left\{ \delta_l(z) \hat{x}_{L-1\rangle a} \Sigma_b \right. \\ &\quad \left. - \frac{(2l+1)\delta_{l+1}(z)}{c^2(l+2)(2l+3)} \hat{x}_{L-1\rangle ac} \Sigma_{bc}^{(1)} \right\} (u + z|\mathbf{x}|/c, \mathbf{x}). \end{aligned} \quad (5.136)$$

We have defined

$$\Sigma = \frac{\bar{\tau}^{00} + \bar{\tau}^{ii}}{c^2}, \quad (5.137)$$

$$\Sigma_i = \frac{\bar{\tau}^{0i}}{c}, \quad (5.138)$$

$$\Sigma_{ij} = \bar{\tau}^{ij}, \quad (5.139)$$

where $\bar{\tau}^{ii} \equiv \delta_{ij}\bar{\tau}^{ij}$, $\tau^{\mu\nu}$ is given in eq. (5.73), the bar over a quantity denotes its PN expansion up to the desired order, and the integration in d^3x is over the whole space \mathbb{R}^3 . The function $\delta_l(z)$ has been defined in eq. (3.189), and the remaining notation is explained on page 134 and in eq. (5.97).

Comparing with eqs. (3.207) and (3.208), we see a truly remarkable fact: despite all complications of the non-linear theory, *the full non-linear result for $\mathbf{h}_1^{\mu\nu}$, to all orders in the PN expansion, is obtained from the result of linearized theory simply replacing $T^{\mu\nu}$ with $\tau^{\mu\nu}$* , and inserting the \mathcal{FP} prescription.³⁸

The integration over z is computed, in an expansion in powers of $1/c$, using eq. (3.209). In particular, to 1PN order one finds from the above equations that the mass quadrupole I_{ij} (i.e. \mathbf{I}_L with $l = 2$) is given by

$$\begin{aligned} I_{ij}(u) &= \int d^3x \hat{x}_{ij} \bar{\sigma}(u, \mathbf{x}) + \frac{1}{14c^2} \frac{\partial^2}{\partial u^2} \int d^3x \hat{x}_{ij} |\mathbf{x}|^2 \bar{\sigma}(u, \mathbf{x}) \\ &\quad - \frac{20}{21c^2} \frac{\partial}{\partial u} \int d^3x \hat{x}_{ijk} \bar{\sigma}^{0k}(u, \mathbf{x}) + O\left(\frac{1}{c^4}\right), \end{aligned} \quad (5.140)$$

with σ and σ^k defined in eqs. (3.205) and (3.206). According to the notation introduced on page 134, $\hat{x}_{ij} = x_i x_j - (1/3)\delta_{ij}|\mathbf{x}|^2$, and similarly

³⁷For the proof, see Section 5 of the review Blanchet (2006). For the explicit expression of the moments (W_L, X_L, Y_L, Z_L) , which are needed only when performing computations to relatively high order, see eqs. (87)–(90) of Blanchet (2006).

³⁸Observe also that the factor of G have been reabsorbed in the definition of $\mathbf{h}_1^{\mu\nu}$, see eq. (5.85).

for \hat{x}_{ijk} . Observe that, for the mass quadrupole, to 1PN order the integral is over a function with compact support, so the \mathcal{FP} prescription is not necessary. It is remarkable that, to 1PN order, this general-relativistic result is actually identical to the linearized gravity result obtained from eq. (3.207). That is, for I_{ij} at 1PN order, we do not even need to make the replacement $T_{\mu\nu} \rightarrow \tau_{\mu\nu}$, since the contribution due to the gravitational field in $\tau_{\mu\nu}$ actually cancels out.

The second aspect of the matching problem is that it allows us to fix the functions $\mathcal{R}_L^{\alpha\beta}$ that appear in the homogeneous solution (5.133). The result is

$$\mathcal{R}_L^{\alpha\beta}(u) = \frac{1}{2\pi} \mathcal{FP} \int d^3x' \hat{x}'_L \int_1^{+\infty} dz \delta_l(z) \mathcal{M}(\tau^{\alpha\beta})(u - z|\mathbf{x}'|/c, \mathbf{x}'), \quad (5.141)$$

where $\mathcal{M}(\tau^{\alpha\beta})$ denotes the multipole expansion of $\tau^{\alpha\beta}$. This homogeneous term is associated with radiation reaction effects at 4PN order, due to the so-called tail effects, that will be examined in detail in Section 5.3.4. We will also see that the leading radiation reaction term appears at 2.5PN order (indeed, we already understood this from eq. (5.67)), so this homogeneous term describes a 1.5PN correction to the leading term of the back-reaction force.

There is one more comment to be made on the validity of the whole formalism that we have discussed. A crucial point of the whole procedure is the existence of a region where the domain of validity of the post-Minkowskian expansion, $d < r < \infty$, overlaps with the domain of validity of the PN expansion, $0 < r < \mathcal{R}$. If this were not the case, the general form of the post-Minkowskian solution would still be valid, since it is the most general solution of the vacuum Einstein equations. However, we would not be able to connect the multipole moments I_L, J_L, \dots, Z_L that parametrize it, to the properties of the source. As we saw, the PN expansion breaks down at distances $r \sim \lambda \sim (c/v)d$. Since for a material source $v/c < 1$, one might hope that there is always at least a small overlap between the near zone and the external region. However we have seen, already at the level of linearized theory, that a source oscillating at a frequency ω_s emits quadrupole radiation at frequency $\omega = 2\omega_s$, while its mass octupole and current quadrupole radiation is at $\omega = \omega_s$ and at $\omega = 3\omega_s$, and a multipole of order n distributes its radiation among a set of lines in frequency, up to a maximum frequency $n\omega_s$. In a computation to n -th PN order, we must include multipoles up to order $\sim n$, which therefore generate GWs with frequencies up to $\omega_n = O(n)\omega_s$, and, correspondingly, reduced wavelength $\lambda_n = O(1/n)\lambda_0$, where $\lambda_0 \sim (c/v)d$. If n is larger than $O(c/v)$, it is no longer true that $\lambda_n \gg d$, and for GWs of such wavelengths the near zone no longer overlaps with the exterior region, so we cannot compute them with this formalism. At the same time, while for $v/c \ll 1$ the lowest multipoles dominate, this is no longer true when v/c approaches one, so the contributions that we are unable to compute are also no longer negligible.

In other words, for a system with typical velocity v , we can compute only up to a post-Newtonian order $O(c/v)$. Thus, the formalism that

we have discussed becomes asymptotically exact for $v/c \rightarrow 0$, while it gradually breaks down in the opposite limit $v/c \rightarrow 1$.

5.3.4 Radiative fields at infinity

Having computed the moments I_L, \dots, Z_L , the solution outside the source is now determined, and we can study it at future null infinity, i.e. at $r \rightarrow \infty$ with $u = t - r/c$ fixed, where we expect to find gravitational waves. One finds that, in this limit, the n -th term $h_n^{\alpha\beta}$ of the post-Minkowskian expansion (5.85) has the formal structure

$$h_n^{\mu\nu} = \sum_{k=1}^{\infty} \sum_{p=0}^{n-1} G_{L,(k,p,n)}^{\mu\nu}(u) \frac{\hat{n}_L (\log r)^p}{r^k}, \quad (5.142)$$

where, as usual, the summation over the multi-index L is understood. The appearance of terms involving $\log r$ at future null infinity is a coordinate effect, due to our use of harmonic coordinates. It is known, since the classical works of Bondi *et al.*, Sachs, and Penrose in the 1960s on the asymptotic structure of space-time at future null infinity, that it is possible to find other coordinate systems, called *radiative coordinates* or Bondi-type coordinates, where the logarithmic terms are absent.³⁹ We denote one such coordinate system by capital letters, $X^\mu = (T, \mathbf{X})$, and we introduce $R = |\mathbf{X}|$ and $U = T - R/c$. The unit radial vector in these coordinates is $\mathbf{N} = \mathbf{X}/R$, and as usual N_L is the multi-index notation for $N_{i_1} \dots N_{i_L}$. We write the metric in this coordinate system as $G_{\mu\nu} = \eta_{\mu\nu} + H_{\mu\nu}$. Then, the post-Minkowskian expansion at future null infinity has the general structure

$$H_n^{\mu\nu} = \sum_{k=1}^{\infty} K_{L,(k,n)}^{\mu\nu}(U) \frac{\hat{N}_L}{R^k}, \quad (5.143)$$

without logarithmic terms. The coordinate transformation from harmonic to radiative coordinates can be obtained, order by order in G , computing explicitly the behavior of $h_n^{\alpha\beta}$ at future null infinity.

We now introduce two sets of STF multipole moments, called the *radiative multipole moments*, or the multipole moments at infinity, and denoted as $U_L(U)$ and $V_L(U)$ (where the argument U is retarded time $T - R/c$ in radiative coordinates, and should not be confused with U_L with $l = 0$), defined as follows. At future null infinity, we select the $1/R$ part of H_{ij} , and we project it onto the TT gauge making use of the projection operator $\Lambda_{ij,kl}$ as in eq. (1.40). We denote the resulting expression by H_{ij}^{TT} . Then, $U_L(U)$ and $V_L(U)$ are defined by

$$\begin{aligned} H_{ij}^{\text{TT}}(U, \mathbf{N}) &= \frac{4G}{c^2 R} \Lambda_{ijab}(\mathbf{N}) \sum_{l=2}^{+\infty} \frac{1}{c^l l!} \left\{ N_{L-2} U_{abL-2}(U) \right. \\ &\quad \left. - \frac{2l}{c(l+1)} N_{cL-2} \epsilon_{cd(a} V_{b)d} L-2(U) \right\}. \end{aligned} \quad (5.144)$$

³⁹It should be observed however that the Bondi–Penrose expansion does not exist if the source has been active in the infinite past, as can be seen with physical arguments, see Damour (1986), and with rigorous mathematical results, see Christodoulou and Klainerman (1993). However, in the Blanchet–Damour formalism one always consider a source that was quiet at time t smaller than some value $-T$, see Note 24 on page 255. Physically, this restriction is not an important limitation, since the binary system was obviously not there before the epoch of formation of its stars.

Once we have the explicit expressions of U_L and V_L in terms of the algorithmic moments I_L, J_L, \dots, Z_L , including all $1/c$ corrections consistent with the PN order to which we want to work, we have completed the solution to the problem of GW generation, since we then have the waveform at infinity, in terms of the energy-momentum tensor of the source.

Lowest-order determination of U_L, V_L

We first compute the relation between the radiative moments U_L, V_L and the algorithmic moments I_L, \dots, Z_L , to lowest order in $1/c$. So, we limit ourselves to the lowest order in the post-Minkowskian expansion, $h^{ij} = G h_1^{ij}$, with h_1^{ij} given in eq. (5.95). We neglect the function φ_1^μ , which at the linearized level is a gauge mode, so it contributes only to higher orders in $1/c$. Then h_1^{ij} is the same as the tensor k_1^{ij} given in eq. (5.96). To this order, there is also no difference between harmonic and radiative coordinates, since no logarithmic factor appears at infinity. To get the leading term for $r \rightarrow \infty$ we simply extract the factor $1/r$ from the derivatives in eq. (5.96), and we use the fact that, on a function $f(u)$ of retarded time $u = t - r/c$, we have $\partial_i f(u) = (\partial_i r) df/dr$. Since $\partial_i r = x_i/r = n_i$ and $df/dr = (-1/c)df/du$, we get

$$\partial_L f(u) = \frac{(-1)^l}{c^l} n_L f^{(l)}(u). \quad (5.145)$$

We insert this into eq. (5.96) and we write $h_{ij}^{\text{TT}} = \Lambda_{ij,ab} h_{ab}$. Comparing with the definition (5.144), and observing that, to lowest order $I_L = M_L$ and $J_L = S_L$, we find that⁴⁰

$$U_L(U) = M_L^{(l)}(U), \quad V_L(U) = S_L^{(l)}(U). \quad (5.146)$$

Thus, to lowest order in $1/c$, the radiative multipole moments U_L and V_L are simply equal to the l -th time derivative of M_L and S_L , respectively. At this level, we have simply reproduced the result of linearized theory. Indeed, we saw in Sections 3.3 that the coefficient of $1/r$ in the amplitude (what we have now called a radiative moment) is given by the second derivative of the mass quadrupole moment, see eq. (3.59), by the third derivative of the mass octupole, see eq. (3.141), etc. (see eq. (3.204) or eqs. (3.291) and (3.293) for the general result).

Of course, we cannot limit ourselves to this lowest-order result, but we must include all $1/c$ corrections to the relations (5.146), consistent with the PN order to which we wish to work. So, we next consider the corrections in $1/c$ coming from the first iteration of the post-Minkowskian algorithm, i.e. from the inclusion of h_2^{ij} . We will see that this study also reveals a very interesting conceptual feature, the presence of so-called “hereditary terms”.

Higher-order corrections

To illustrate in a simpler setting the computation of the first post-Minkowskian iteration, we take as starting point for the iterative pro-

⁴⁰We must also take into account the minus sign discussed in Note 19 on page 250.

cedure a linearized metric $h_1^{\alpha\beta}$ of the form given in eq. (5.96), retaining only the two lowest-order mass multipoles, $I \equiv M$ and I_{ij} . The latter, up to 2.5PN corrections, is the same as M_{ij} , see eq. (5.102). Then we can write $h_1^{\alpha\beta}$ as

$$h_1^{\alpha\beta} = h_{(M)}^{\alpha\beta} + h_{(M_{ij})}^{\alpha\beta}, \quad (5.147)$$

where, from eq. (5.96), the monopole part is given by

$$h_{(M)}^{00} = -\frac{4M}{c^2 r}, \quad (5.148)$$

together with $h_{(M)}^{0i} = h_{(M)}^{ij} = 0$ (recall also that M is time-independent), and the quadrupole part is

$$h_{(M_{ij})}^{00} = -\frac{2}{c^2} \partial_k \partial_l \left[\frac{1}{r} M_{kl}(u) \right], \quad (5.149)$$

$$h_{(M_{ij})}^{0i} = \frac{2}{c^3} \partial_k \left[\frac{1}{r} M_{ki}^{(1)}(u) \right], \quad (5.150)$$

$$h_{(M_{ij})}^{ij} = -\frac{2}{c^4} \frac{1}{r} M_{ij}^{(2)}(u). \quad (5.151)$$

We can now determine the next post-Minkowskian iteration, $h_2^{\alpha\beta}$, solving eq. (5.90) with $N^{\alpha\beta}[h_1, h_1]$ given in eq. (5.89). Since $N^{\alpha\beta}$ is quadratic in h_1 , when we insert eq. (5.147) we get three terms, one quadratic in the monopole part $h_{(M)}^{\alpha\beta}$, one quadratic in the quadrupole part $h_{(M_{ij})}^{\alpha\beta}$, and a mixed monopole–quadrupole term,

$$h_2^{\alpha\beta} = h_{(M^2)}^{\alpha\beta} + h_{(M \times M_{ij})}^{\alpha\beta} + h_{(M_{ij} \times M_{kl})}^{\alpha\beta}. \quad (5.152)$$

The monopole–monopole part $h_{(M^2)}^{\alpha\beta}$ is easily computed. Since $h_{(M)}^{\alpha\beta}$ is non-vanishing only for $\alpha = \beta = 0$, $N^{\alpha\beta}[h_{(M)}, h_{(M)}]$ collapses to a very simple expression. For instance,

$$N^{00}[h_{(M)}, h_{(M)}] = -\frac{14M^2}{c^4 r^4}. \quad (5.153)$$

Thus, $h_{(M^2)}^{00}$ is obtained solving the equation $\square h_{(M^2)}^{00} = -14M^2/(c^4 r^4)$. Since the right-hand side is time-independent, in this case there is no need to go through the procedure of taking the retarded integral with the \mathcal{FP} prescription. Simply, the solution will be time-independent (so the d'Alembertian becomes a Laplacian), and will be a function only of r . From the expression of the Laplacian in spherical coordinates we get

$$\frac{1}{r} \frac{d^2}{dr^2} [r h_{(M^2)}^{00}] = -\frac{14M^2}{c^4 r^4}, \quad (5.154)$$

which (together with the boundary condition that the metric vanishes at spatial infinity) gives

$$h_{(M^2)}^{00} = -\frac{7M^2}{c^4 r^2}. \quad (5.155)$$

Similarly one finds that $h_{(M^2)}^{0i} = 0$ and $h_{(M^2)}^{ij} = -n_i n_j M^2 / (c^4 r^2)$.⁴¹ Since it proportional to $1/r^2$, $h_{(M^2)}^{\alpha\beta}$ does not contribute to the $1/r$ part of the field, and hence to the radiative moments at infinity.

Consider next the mixed monopole–quadrupole term. When we plug $h_1^{\alpha\beta} = h_{(M)}^{\alpha\beta} + h_{(M_{ij})}^{\alpha\beta}$ into $N^{\alpha\beta}[h_1, h_1]$ and we retain the terms bilinear in $h_{(M)}^{\alpha\beta}$ and $h_{(M_{ij})}^{\alpha\beta}$, we find that $N^{\alpha\beta}[h, h]$ takes the general form

$$N^{\alpha\beta}[h, h]_{(M \times M_{ij})} = \sum_{k=2}^{\infty} \frac{n_L}{r^k} H_L^{(k)}(u), \quad (5.156)$$

for some functions $H_L^{(k)}(u)$. This follows simply from the fact that $h_{(M)}^{\alpha\beta}$ is proportional to $1/r$, times a constant, while $h_{(M_{ij})}^{\alpha\beta}$ is the sum of terms with negative powers of r , such as $1/r, 1/r^2$, etc. multiplied by functions of $u = t - r/c$. The factors n_L come out when taking the spatial derivatives, using $\partial_i r = n_i$.

Thus, to find the contribution of this mixed monopole–quadrupole term to $h_2^{\alpha\beta}$, we must compute the finite part at $B = 0$ of retarded integrals of the form

$$\square_{\text{ret}}^{-1}[n_L r^{B-k} H(u)], \quad (5.157)$$

for some function $H(u)$ (we omit the index L in $H(u)$, in order not to imply a summation over l). The computation of this retarded integral gives two completely different results when $k = 2$ and when $k \geq 3$. For $k \geq 3$ (but still $k \leq l+2$, which is the case that we will need) one finds⁴²

$$\text{FP}_{B=0} \square_{\text{ret}}^{-1}[n_L r^{B-k} H(u)] = n_L \sum_{j=0}^{k-3} \frac{c_{jkl}}{r^{j+1}} \frac{d^{k-3-j}}{du^{k-3-j}} H(u), \quad (5.158)$$

where c_{jkl} are some numerical coefficients,

$$c_{jkl} = -\frac{2^{k-3-j}(k-3)!(l+2-k)!(l+j)!}{(l+k-2)!j!(l-j)!}. \quad (5.159)$$

Observe that, since j takes the values $0, \dots, k-3$, the order of the derivative of $H(u)$, $k-3-j$, is between $k-3$ and zero. Since $k \geq 3$, this is never negative. The important point about eq. (5.158) is that the result is local in time: its value at a given (retarded) time u depends on the function $H(u)$ and on a finite number of its derivatives, evaluated at the same retarded time u . We will refer to terms with this property as “instantaneous”.

It is clear, however, that the above result cannot hold for $k = 2$, since in this case the order of the derivative of $H(u)$, $k-3-j$, can become negative. Indeed, for $k = 2$ on finds that the result is given by an integral of $H(u)$, rather than by its derivatives,

$$\square_{\text{ret}}^{-1} \left[\frac{n_L}{r^2} H \left(t - \frac{r}{c} \right) \right] = -\frac{n_L}{r} \int_r^\infty dz Q_l \left(\frac{z}{r} \right) H \left(t - \frac{z}{c} \right), \quad (5.160)$$

where $Q_l(x)$ is a special function known as the Legendre function of the second kind. (Observe that for $k = 2$ the retarded integral converges at

⁴¹The correctness of the result can be checked observing that

$$h_{\text{monopole}}^{\alpha\beta} = G h_{(M)}^{\alpha\beta} + G^2 h_{(M^2)}^{\alpha\beta}$$

is nothing but the Schwarzschild metric, written in harmonic coordinates, and in terms of $h^{\alpha\beta} = (-g)^{1/2} g^{\alpha\beta} - \eta^{\alpha\beta}$, expanded to second order in $R_S/r = 2GM/(c^2 r)$.

⁴²For the explicit computations see Blanchet and Damour (1986) and (1988), as well as the appendixes of Blanchet (1998a) and (1998b).

$r = 0$, so the \mathcal{FP} prescription is superfluous.) The crucial point is that, since the integration variable z runs from r to ∞ , this result does not depend just on $H(u)$ at the value $u = t - r/c$, but also on all its values at earlier times, from $u = -\infty$ to $u = t - r/c$. In other words, the result depends on the whole past history of the source. A term of this kind is called “hereditary”, and we will discuss its physical meaning below.

The asymptotic behavior of eq. (5.160) for $r \rightarrow \infty$ and $t - r/c$ fixed is computed using the known behavior of $Q_l(x)$ in the limit $x \rightarrow 1^+$,

$$Q_l(x) = -\frac{1}{2} \log\left(\frac{x-1}{2}\right) - a_l + O[(x-1)\log(x-1)], \quad (5.161)$$

where the constant $a_l \equiv \sum_{k=1}^l k^{-1}$. From this, changing variable from z to $y = (z-r)/c$, we get

$$\begin{aligned} \square_{\text{ret}}^{-1} \left[\frac{n_L}{r^2} H(t-r/c) \right] &= \frac{cn_L}{2r} \int_0^\infty dy H\left(t - \frac{r}{c} - y\right) \left[\log\left(\frac{cy}{2r}\right) + 2a_l \right] \\ &\quad + O\left(\frac{\log r}{r^2}\right). \end{aligned} \quad (5.162)$$

Thus, asymptotically this is $O(1/r)$, and contributes to the radiation field. We can now compute the hereditary term in $h_{(M \times M_{ij})}^{\alpha\beta}$, considering for definiteness the component $\alpha = \beta = 0$. Inserting eq. (5.147) into $N^{\alpha\beta}[h_1, h_1]$ and keeping only the mixed monopole–quadrupole terms, we find⁴³

$$N^{00}[h, h]_{(M \times M_{ij})} = -\frac{8M}{r^2 c^4} n_i n_j M_{ij}^{(4)} + O\left(\frac{1}{r^3}\right). \quad (5.163)$$

Using eq. (5.160) we therefore find

$$\begin{aligned} h_{(M \times M_{ij})}^{00} &= \frac{8M}{rc^4} n_i n_j \int_r^\infty dz Q_2\left(\frac{z}{r}\right) M_{ij}^{(4)}(t-z/c) \\ &\quad + \text{instantaneous terms}. \end{aligned} \quad (5.164)$$

The instantaneous terms are straightforwardly computed using eq. (5.158). Similarly one can compute the other tensor components of $h_{(M \times M_{ij})}^{\alpha\beta}$, as well as the quadrupole–quadrupole term $h_{(M_{ij} \times M_{kl})}^{\alpha\beta}$, and one finds that they all have hereditary contributions, besides the instantaneous terms.⁴⁴

Using the asymptotic expansion (5.162) we can now compute the contribution of $h_2^{\alpha\beta}$ to the radiation field at infinity, and therefore to the radiative multipole moments. For U_L we get

$$\begin{aligned} U_L(u) &= M_L^{(l)}(u) + \frac{2GM}{c^3} \int_0^{+\infty} d\tau M_L^{(l+2)}(u-\tau) \left[\log\left(\frac{c\tau}{2r}\right) + \kappa_l \right] \\ &\quad + O\left(\frac{1}{c^5}\right), \end{aligned} \quad (5.165)$$

where, as usual, $u = t - r/c$ and

$$\kappa_l = \frac{2l^2 + 5l + 4}{l(l+1)(l+2)} + \sum_{k=1}^{l-2} \frac{1}{k}. \quad (5.166)$$

⁴³It is easy to extract the term $1/r^2$ from $N^{00}[h, h]_{(M \times M_{ij})}$. Just observe that both $h_{(M)}^{\alpha\beta}$ and $h_{(M_{ij})}^{\alpha\beta}$ already carry each one at least one factor $1/r$, and that $\partial_i(1/r) = -n_i/r^2$, so all terms involving spatial derivatives of $1/r$ are at least overall $O(1/r^3)$. Taking further into account that $h_{(M)}^{\alpha\beta}$ is non-vanishing only for $\alpha = \beta = 0$ and is time-independent we see immediately that, in eq. (5.89), in the mixed term, the only contribution $O(1/r^2)$ comes from the first term, and is $-h_{(M)}^{\alpha\beta} \partial_0^2 h_{(M_{ij})}^{\alpha\beta}$.

⁴⁴See Blanchet (2006), eq. (110), for $h_{(M \times M_{ij})}^{\alpha\beta}$, and Blanchet (1998a) for $h_{(M_{ij} \times M_{kl})}^{\alpha\beta}$.

We see that the second term in eq. (5.165) is a $O(1/c^3)$ correction (i.e. a 1.5PN correction) to the leading result given in eq. (5.146). The $\log r$ term in the correction is typical of the harmonic coordinate system that we are using and, as we mentioned, can be eliminated going to radiative coordinates. From the study of the logarithmic terms at infinity one finds that retarded time U in radiative coordinates is related to the harmonic coordinates (t, r) by

$$U = t - \frac{r}{c} - \frac{2GM}{c^3} \ln\left(\frac{r}{r_0}\right) + O(G^2), \quad (5.167)$$

where r_0 is the arbitrary constant discussed in Note 29 on page 258, and provides a scale for the logarithm. Its arbitrariness corresponds to a freedom in the choice of a system of radiative coordinates, and in particular we see from eq. (5.167) that it can be reabsorbed into a shift in the origin of retarded time U . So it is a gauge-dependent constant that will not influence any physical result, as it is already clear from the fact that the starting expression (5.165) is independent of r_0 . In terms of these radiative coordinates, eq. (5.165) becomes

$$\begin{aligned} U_L(U) &= M_L^{(l)}(U) + \frac{2GM}{c^3} \int_0^{+\infty} d\tau M_L^{(l+2)}(U - \tau) \left[\log\left(\frac{c\tau}{2r_0}\right) + \kappa_l \right] \\ &\quad + O\left(\frac{1}{c^5}\right), \end{aligned} \quad (5.168)$$

i.e. inside the logarithm, r is replaced by r_0 . Similarly, for the current-type multipoles one finds

$$\begin{aligned} V_L(U) &= S_L^{(l)}(U) + \frac{2GM}{c^3} \int_0^{+\infty} d\tau S_L^{(l+2)}(U - \tau) \left[\log\left(\frac{c\tau}{2r_0}\right) + \pi_l \right] \\ &\quad + O\left(\frac{1}{c^5}\right), \end{aligned} \quad (5.169)$$

where

$$\pi_l = \frac{l-1}{l(l+1)} + \sum_{k=1}^{l-1} \frac{1}{k}. \quad (5.170)$$

Of course, the relation between the radiative and algorithmic moments is needed with the highest accuracy for the lowest multipole moments, since the contribution of higher multipoles to the radiation field is suppressed by higher powers of $1/c$. In particular, to compute the GW production in a binary system up to 3PN, we need the relation between the $l = 2$ mass moment U_{ij} and M_{ij} up to 3PN order, which is

$$\begin{aligned} U_{ij}(U) &= M_{ij}^{(2)}(U) + \frac{2GM}{c^3} \int_0^{+\infty} d\tau M_{ij}^{(4)}(U - \tau) \left[\log\left(\frac{c\tau}{2r_0}\right) + \frac{11}{12} \right] \\ &\quad - \frac{2G}{7c^5} \int_0^{+\infty} d\tau M_{a\langle i}^{(3)}(U - \tau) M_{j\rangle a}^{(3)}(U - \tau) \\ &\quad - \frac{G}{c^5} \left[\frac{2}{7} M_{a\langle i}^{(3)} M_{j\rangle a}^{(2)} + \frac{5}{7} M_{a\langle i}^{(4)} M_{j\rangle a}^{(1)} - \frac{1}{7} M_{a\langle i}^{(5)} M_{j\rangle a} - \frac{1}{3} \epsilon_{ab\langle i} M_{j\rangle a}^{(4)} S_b \right] \end{aligned}$$

$$\begin{aligned}
& + \frac{2G^2M^2}{c^6} \int_0^{+\infty} d\tau M_{ij}^{(5)}(U - \tau) \\
& \quad \times \left[\log^2 \left(\frac{c\tau}{2r_0} \right) + \frac{57}{70} \log \left(\frac{c\tau}{2r_0} \right) + \frac{124627}{44100} \right] \\
& + O\left(\frac{1}{c^7}\right). \tag{5.171}
\end{aligned}$$

The 1.5PN correction, in the first line, is the hereditary monopole–quadrupole term in $h_2^{\alpha\beta}$ that we have computed above. In the second line we have a hereditary 2.5PN contribution, due to the quadrupole–quadrupole term in $h_2^{\alpha\beta}$, and in the third line we have the instantaneous contribution from this quadrupole–quadrupole term. The term proportional to G^2M^2 is a monopole–monopole–quadrupole term in the second post-Minkowskian iteration $h_3^{\alpha\beta}$, and again it is a hereditary term.

Below we discuss the physics behind these non-local contributions. First, we observe that the above results allow us to compute the waveform and, from it, we can obtain the energy radiated at infinity. This can be obtained inserting eq. (5.144) into the expression for the radiated energy, eq. (1.153). The result for the radiated power P , as a function of retarded time U , is (compare with the linearized result, eq. (3.210))

$$\begin{aligned}
P = & \sum_{l=2}^{+\infty} \frac{G}{c^{2l+1}} \left\{ \frac{(l+1)(l+2)}{(l-1)ll!(2l+1)!!} \langle U_L^{(1)}(U)U_L^{(1)}(U) \rangle \right. \\
& \left. + \frac{4l(l+2)}{c^2(l-1)(l+1)!(2l+1)!!} \langle V_L^{(1)}(U)V_L^{(1)}(U) \rangle \right\}. \tag{5.172}
\end{aligned}$$

For example, up to 2PN order, this equation gives

$$\begin{aligned}
P = & \frac{G}{c^5} \left\{ \frac{1}{5} U_{ij}^{(1)} U_{ij}^{(1)} + \frac{1}{c^2} \left[\frac{1}{189} U_{ijk}^{(1)} U_{ijk}^{(1)} + \frac{16}{45} V_{ij}^{(1)} V_{ij}^{(1)} \right] \right. \\
& \left. + \frac{1}{c^4} \left[\frac{1}{9072} U_{ijkm}^{(1)} U_{ijkm}^{(1)} + \frac{1}{84} V_{ijk}^{(1)} V_{ijk}^{(1)} \right] + O\left(\frac{1}{c^6}\right) \right\}, \tag{5.173}
\end{aligned}$$

(where the average is understood), compare with the 1PN result of linearized theory given in eq. (3.156).

Physical meaning of hereditary terms. “Non-linear memory” and “tails”

At first sight, the appearance of terms that are not instantaneous is quite surprising. For an interaction that propagates in flat space at the speed of light, the signal detected at time t_0 , coming from a source at a distance r , depends only on the instantaneous state of the source at retarded time $u_0 = t_0 - r/c$, so it depends on the source multipole moments and on its derivatives, all evaluated at $u = u_0$. However, the sources that generates GWs also curve space-time, so GWs necessarily propagate in a curved space. We see that, as a consequence, besides the instantaneous terms there are also hereditary terms, given by integrals

over retarded time from $-\infty$ to u_0 , which therefore depend on the value of the multipole moments at all times $u \leq u_0$.

In other words, the intuition stemming from flat space-time suggested that GWs propagate *on* the light cones, while we find that they rather propagate both *on* and *inside* the light cones.⁴⁵ It is as if the gravitational interaction did not propagate just with speed c , but with all possible speeds $0 < v \leq c$.

Physically, this result can be better understood using a field-theoretical language, in terms of back-scattering of gravitons. For instance, the 1.5PN hereditary term, in the first line of eq. (5.171), depends both on derivatives of the quadrupole moment M_{ij} , which in a field-theoretical language is associated to a graviton line, and on the mass M of the source, so it corresponds to scattering of gravitons off the background curvature generated by the mass M of the source. The 2.5PN hereditary term in the second line of eq. (5.171) rather corresponds to a graviton–graviton scattering process (in the language of Feynman graphs, it would be related to a three-graviton vertex), while the terms proportional to $G^2 M^2$ is a higher-order correction to the scattering of a graviton off the external curvature. In this sense, gravitons always propagate locally at the speed of light. However, their arrival time is delayed because they can repeatedly scatter back and forth, either with the background gravitational field or among themselves. The same effect is known to take place in the propagation of the electromagnetic field in curved space-time. However, while conceptually it is legitimate to consider the propagation of electromagnetic waves in flat space-time, where they just propagate on the light cone, for GWs this limiting case strictly speaking does not exist, since the source that generates GWs necessarily produces also a curvature of the background space-time, and also because GWs scatter among themselves (or, in the language of Feynman graphs, because of non-Abelian graviton vertices). So, this propagation inside the light cone unavoidably occurs, when one takes into account the PN corrections. We see here a reflection of the fact that gravity is an intrinsically non-linear theory.

Looking more closely at the hereditary terms in eq. (5.171), we can distinguish between two types of terms, with and without the factor $\log \tau$ inside the integral. We examine first the 2.5PN hereditary term in the second line. Introducing $V = U - \tau$, this integral can be written as

$$\begin{aligned} F_{ij}(U) &\equiv \int_{-\infty}^U dV M_{a(i}^{(3)}(V) M_{j)a}^{(3)}(V) \\ &= \int_{-\infty}^{\infty} dV \mathcal{K}(U, V) M_{a(i}^{(3)}(V) M_{j)a}^{(3)}(V), \end{aligned} \quad (5.174)$$

where the kernel $\mathcal{K}(U, V) = \theta(U - V)$ is flat and equal to one for $V < U$, and vanishes for $V > U$. Consider a source whose multipole moments were constant in the far past,⁴⁶ then it becomes active, and finally is turned off at some value of time which, for a far observer at a given distance r , corresponds to a given value of retarded time, say $U = U_0$. For $U > U_0$ we can split the integral in eq. (5.174) as $\int_{-\infty}^U dV =$

⁴⁵Indeed it was already known since the 1950s, from the study of the initial value problem in general relativity, that, given some initial data on a space-like hypersurface S , to determine the gravitational field at a point P we need not only the values of the initial data on the intersection of S with the past (curved-space) light cones of P , but also the data *inside* this intersection, see the Further Reading.

⁴⁶This was among the basic assumptions of the method, see Note 24 on page 255 and guarantees the convergence of the integral at $V = -\infty$.

$\int_{-\infty}^{U_0} dV + \int_{U_0}^U dV$. However, since the integrand in eq. (5.174) vanishes for $V > U_0$, the integration between U_0 and U gives zero, and for all $U > U_0$ we have $F_{ij}(U) = F_{ij}(U_0)$: the integral remains frozen forever at the value it had at $U = U_0$. Thus, the contribution to the GW amplitude due to this term remains non-zero even after the source has been switched off.

This is due to the fact that, in eq. (5.174), very remote times are weighted as much as more recent times, since the kernel $\mathcal{K}(U, V)$ is a flat function of the integration variable V , for $V < U$. Therefore, the result is really determined by the cumulative history of the source, including its very remote past. For this reason, it is called a “memory effect”, and the 2.5PN hereditary term in the second line of eq. (5.171), which is non-linear in M_{ij} , is called the “2.5PN non-linear memory integral”.⁴⁷ Observe however that, taking the time derivative of $F_{ij}(U)$, we obtain an instantaneous term. Thus in the energy flux, which is determined by \dot{h}_{ij}^{TT} , the 2.5PN non-linear memory term gives an instantaneous contribution.

Consider next the 1.5PN hereditary term in the first line of eq. (5.171). Introducing again $V = U - \tau$, we get an integral of the form

$$G_{ij}(U) \equiv \int_{-\infty}^U dV M_{ij}^{(4)}(V) \log\left(\frac{U-V}{2P_0}\right), \quad (5.175)$$

where $P_0 = r_0/c$ is an arbitrary constant with dimensions of time. We split

$$\int_{-\infty}^U dV = \int_{-\infty}^{U-2P} dV + \int_{U-2P}^U dV, \quad (5.176)$$

and, in the first integral, we integrate twice by parts. Using the fact that the derivatives of M_{ij} go to zero sufficiently fast for $U \rightarrow -\infty$, we get

$$\begin{aligned} G_{ij}(U) = & \frac{1}{2P} M_{ij}^{(2)}(U-2P) + \int_{U-2P}^U dV M_{ij}^{(4)}(V) \log\left(\frac{U-V}{2P_0}\right) \\ & - \int_{-\infty}^{U-2P} \frac{dV}{(U-V)^2} M_{ij}^{(2)}(V). \end{aligned} \quad (5.177)$$

The terms in the first line involve only values of V in the “recent past”, $U-2P \leq V \leq U$, while the contribution from the remote past, $-\infty < V \leq U-2P$ is in the integral in the second line. This way of rewriting $G_{ij}(U)$ allows us to understand that the contribution of very remote times, $V \rightarrow -\infty$, is weighted with a quadratically decreasing kernel $(U-V)^{-2}$, contrary to what happens in the memory integral, where the kernel is flat and very remote times contribute as much as recent times. A contribution of the type (5.177) is called a “tail integral”. Thus, the first line in eq. (5.171) gives the 1.5PN tail integral, and the last line gives the 3PN tail integral.

In conclusion, the GWs emitted by a source which at some value of time suddenly switches off, can be considered as made by three distinct

⁴⁷The existence of such a memory effect was also found by Christodoulou, from a rigorous mathematical study of the asymptotic behavior of the gravitational field at null infinity, and is also known as the “Christodoulou memory”. The term “non-linear” distinguishes it from a memory effect that exists already in linearized theory, see the Further Reading section.

pieces: the wavefront, which is due to the instantaneous terms; a tail, which effectively travels at a slower speed and therefore arrives later, and which smoothly fades away with time; and, finally, a “memory”, which is a persistent DC (i.e. zero-frequency) contribution.

5.3.5 Radiation reaction

Radiation reaction in electromagnetism

Radiation reaction is a classical problem that was first studied in electromagnetism (the pioneering works were by Lorentz, in 1892 and 1902, and by Planck, in 1897).⁴⁸ As a warm-up, let us recall these classical results. Consider a system of electric charges e_a moving under their mutual influence. Being accelerated by their interaction, they radiate electromagnetic waves. This emission costs energy, which must be drained from the mechanical energy of the system. This means that there must be a force which acts on these charges and performs the work necessary to account for the energy loss. This force is called the back-reaction force due to the emission of radiation, or simply the radiation reaction.

In other words we expect that, when we compute the total electromagnetic field due to a system of charges in mutual interaction, to a term describing electromagnetic waves in the far zone should correspond a term in the near zone, that describes a radiation reaction force acting on the charges. This is indeed the case. The dynamics in the near zone can be studied starting from the expression for potential (ϕ, \mathbf{A}) in terms of the charge density ρ and the current density \mathbf{j} ,

$$\phi(t, \mathbf{x}) = \int d^3x' \frac{1}{|\mathbf{x} - \mathbf{x}'|} \rho(t - |\mathbf{x} - \mathbf{x}'|/c, \mathbf{x}'), \quad (5.178)$$

$$\mathbf{A}(t, \mathbf{x}) = \frac{1}{c} \int d^3x' \frac{1}{|\mathbf{x} - \mathbf{x}'|} \mathbf{j}(t - |\mathbf{x} - \mathbf{x}'|/c, \mathbf{x}'). \quad (5.179)$$

We perform an expansion for small retardation effects, just as we have done for the gravitational field when we have discussed the PN expansion, and we insert the result in the Lagrangian for a point-like charge e_a in this external field, which is

$$L_a = -mc^2 \sqrt{1 - \frac{v_a^2}{c^2}} - e_a \phi(\mathbf{x}_a) + \frac{e_a}{c} \mathbf{v}_a \cdot \mathbf{A}(\mathbf{x}_a). \quad (5.180)$$

The result (see Landau and Lifshitz, Vol. II (1979), Sections 65 and 75) is that, up to second order in v/c , the Lagrangian is conservative, i.e. depends only on the positions and velocities of the particles, and reads

$$L = \sum_a \frac{1}{2} m_a v_a^2 + \frac{m_a v_a^4}{8c^2} - \sum_{a>b} \frac{e_a e_b}{r_{ab}} \left\{ 1 - \frac{1}{2c^2} [\mathbf{v}_a \cdot \mathbf{v}_b + (\mathbf{v}_a \cdot \hat{\mathbf{r}}_{ab})(\mathbf{v}_b \cdot \hat{\mathbf{r}}_{ab})] \right\}. \quad (5.181)$$

(The analogous result for the gravitational field was given in eqs. (5.55) and (5.56).) To this order only even powers of v/c enter, and the term linear in v/c vanishes because of charge conservation. Indeed, were it

⁴⁸Actually, the fact that a finite speed of propagation of the interaction induces a radiation-reaction force was already proposed by Laplace in 1776, in the context of the gravitational interaction of the Earth-Moon system, and for this reason it has also been called the Laplace effect. See Chapter 2 of Kenefick (2007).

not for electromagnetic-wave emission, only even powers of v/c could appear, for the same argument based on time-reversal that we discussed on page 239 for the gravitational field. Starting from $O(v^3/c^3)$ however, we have a non-vanishing contribution to the expansion of the potentials ϕ, \mathbf{A} , which therefore must be the sought-for radiation-reaction term. Indeed, expanding ϕ and \mathbf{A} to this order, one finds that the corresponding electric field is

$$\mathbf{E} = \frac{2}{3c^3} \ddot{\mathbf{d}}, \quad (5.182)$$

where $\mathbf{d} = \sum_a e_a \mathbf{x}_a$ is the electric dipole moment of the system, while the corresponding magnetic field vanishes. This electric field exerts on a charge e_a a force $\mathbf{F}_a = e_a \mathbf{E}$, so the total work performed on all the charges is

$$\sum_a \mathbf{F}_a \cdot \mathbf{v}_a = \frac{2}{3c^3} \ddot{\mathbf{d}} \cdot \sum_a e_a \mathbf{v}_a. \quad (5.183)$$

Taking the time average and integrating by part, we get

$$\langle \sum_a \mathbf{F}_a \cdot \mathbf{v}_a \rangle = -\frac{2}{3c^3} \langle \ddot{\mathbf{d}}^2 \rangle. \quad (5.184)$$

This is just the negative of the energy radiated away in electromagnetic waves in the dipole approximation. We see that the work done by the radiation reaction force, computed from a near-zone expansion, matches exactly the energy carried by the radiation field at future null infinity.

Radiation reaction from GWs

In Section 4.1.3 we computed the effect of GW emission on the orbit of a binary system simply requiring that the energy and angular momentum carried away from the GWs at a given time, were drained from the orbital energy and angular momentum of the source at the corresponding value of retarded time. This is unavoidable in linearized theory, since energy and angular momentum must be conserved (and, for compact bodies, we will see that their internal structure influences the dynamics only starting from 5PN order, see page 288, so to order smaller than 5PN there is no internal degree of freedom that can relax, supplying the required energy). However in the full non-linear theory, given the non-linear phenomena in the propagation of the GWs from the source to infinity that we have discussed, it is no longer obvious that the energy and angular momentum carried away by GWs at a large distance r and time t , are balanced by losses of the system at the corresponding retarded time $t - r/c$.

Anyway, we have by now all the tools necessary to verify explicitly the correctness of this energy-balance argument, since we have in principle determined, in an expansion in v/c , both the radiation field at infinity, and the metric in the near region. The latter determines the equation of motion of the matter source. For a binary system, the equation of motion takes the form already schematically written down in eq. (5.68). The terms $O(\epsilon^2)$ and $O(\epsilon^4)$ in eq. (5.68) are the 1PN and 2PN corrections,

respectively, and are non-dissipative (the Lagrangian giving the equations of motion up to $O(\epsilon^2)$ was explicitly written down in eqs. (5.55) and (5.56)). They describe various general relativistic corrections to the orbit, such as the periastron advance, etc.

We now want to find the leading term in the back-reaction, i.e. the first term which is odd in v (and that cannot be set to zero with a gauge transformation). This leading term can be obtained by replacing $\tau_{\mu\nu}$ with the energy-momentum tensor of matter $T^{\alpha\beta}$. Then, eq. (5.132) becomes simply

$$\mathbf{h}^{\alpha\beta}(t, \mathbf{x}) = -\frac{4G}{c^4} \int d^3x' \frac{1}{|\mathbf{x} - \mathbf{x}'|} T^{\alpha\beta}(t - |\mathbf{x} - \mathbf{x}'|/c, \mathbf{x}'). \quad (5.185)$$

Since $T^{\alpha\beta}$ has compact support, we can expand its argument $t - |\mathbf{x} - \mathbf{x}'|/c$ in powers of $|\mathbf{x} - \mathbf{x}'|/c$, just as we did for electromagnetism, and the resulting integrals are convergent.⁴⁹ One then finds that a number of lowest-order terms vanish because of mass and momentum conservation, or they can be set to zero with a gauge transformation. The first non-vanishing terms which are odd under time-reversal and cannot be gauged away are $O(1/c^7)$ in g_{00} , $O(1/c^6)$ in g_{0i} , and $O(1/c^5)$ in g_{ij} , i.e., they are a 2.5PN correction to the metric (5.3). One can then compute the rate of dissipation of energy due to these non-conservative terms, and one finds that the result reproduces the Einstein formula for the emission of radiation in the quadrupole approximation, in linearized theory, eq. (3.75). This computation was first performed by Chandrasekhar and Esposito (1970).

In the 1970s and early 1980s, however, the subtleties in the use of the PN expansion, that we have discussed at length in this chapter, were not yet fully understood, and the PN expansion was used over all of space, including the far region. As we have seen, this unavoidably produces divergences in higher order. So, one had reproduced the correct radiation reaction, but as a term of an expansion in which subsequent terms diverge; not a very satisfying state of affairs. This was at the basis of a controversy over the validity of determining the back-reaction on the sources from the energy balance argument, and over the validity of Einstein quadrupole formula itself, when applied to self-gravitating systems. The issue is particularly important, as we will see in the next chapter, for its application to the change in orbital periods of binary pulsars, which constitutes the first experimental evidence of GW emission.

Nowadays, we know that the correct formalism implies a different treatment of the near- and far-field regions, and the PN result to all order is given by eqs. (5.132), (5.133) and (5.141), and is explicitly finite thanks to the FP prescription, that comes out from a correct use of the formalism. Thus, the 2.5PN radiation reaction is now part of a systematic and well-defined expansion. For a compact binary system this term is responsible for the decrease in the orbital period P_b . The fact that we can compute it directly from the PN expansion in the near region, without invoking any energy balance argument, provides a direct

⁴⁹Since the integrand has compact support, the finite part prescription is unnecessary. Observe also that the homogeneous term given by eqs. (5.133) and (5.141) does not contribute to the leading radiation-reaction term (it contributes only starting from order 4PN).

and satisfying way of deriving the theoretical prediction for \dot{P}_b . As we will see in Chapter 6, this prediction has been confirmed by the observation in binary pulsars.

A check of the energy balance argument to even higher orders is technically more difficult. We have seen that the quadrupole radiation at infinity corresponds, in the near region, to a 2.5PN correction to the metric. Thus, the 1PN correction to the radiation field corresponds to a 3.5PN correction to the near-region metric. Of course, to check the energy balance argument beyond leading order becomes more and more difficult, since it requires the computation of higher and higher orders in the PN expansion of the near metric. For compact binary, the full near-zone metric has been explicitly computed up to 3.5PN order, and shown to be consistent with the loss of energy and angular momentum at infinity, see the Further Reading. Furthermore, even for the tail integral it has been possible to check explicitly the energy balance argument, and the tail term in the radiation at infinity has been shown to be correctly reproduced, for general PN sources, by a corresponding non-hereditary term in the near-region field. Since the tail integral is a 1.5PN correction to the radiation at infinity, the corresponding hereditary term appears in the 4PN near-region metric.⁵⁰ To this order, one finds indeed a hereditary correction to g_{00} given by

$$\delta g_{00}(t, \mathbf{x}) = -\frac{8}{5c^{10}} x^i x^j M(t) \int_{-\infty}^t dt' \log\left(\frac{t-t'}{2P}\right) M_{ij}^{(7)}(t'), \quad (5.186)$$

with P a time-scale. We see that it depends on the mass M and on the mass quadrupole M_{ij} , just as the monopole–quadrupole terms $h_{(M \times M_{ij})}^{\alpha\beta}$ computed, in the far region, in eq. (5.164), and it has the same logarithmic singularity at the upper limit of the integral.

The explicit computation shows that the terms in the metric that correspond to back-reaction (i.e. the terms described by antisymmetric waves, see Note 35) can be written as

$$(h_1^{00})_{\text{antisym}} = -\frac{4}{Gc^2} V_{\text{react}}, \quad (5.187)$$

$$(h_1^{0i})_{\text{antisym}} = -\frac{4}{Gc^3} V_{\text{react}}^i, \quad (5.188)$$

$$(h_1^{ij})_{\text{antisym}} = -\frac{4}{Gc^4} V_{\text{react}}^{ij}, \quad (5.189)$$

(plus terms that can be set to zero with a gauge transformation). Up to 4PN order in the near-zone metric (which gives the corrections up to 1.5PN order to the radiation reaction force), the tensor potential V_{react}^{ij} can be neglected, while the scalar potential V_{react} and the vector potential V_{react}^i are given by⁵¹

$$V_{\text{react}}(t, \mathbf{x}) = -\frac{G}{5c^5} x_{ij} I_{ij}^{(5)}(t) + \frac{G}{c^7} \left[\frac{1}{189} x_{ijk} I_{ijk}^{(7)}(t) - \frac{1}{70} \mathbf{x}^2 x_{ij} I_{ij}^{(7)}(t) \right] - \frac{4G^2 M}{5c^8} x_{ij} \int_0^{+\infty} d\tau \log\left(\frac{\tau}{2}\right) I_{ij}^{(7)}(t-\tau) + O\left(\frac{1}{c^9}\right), \quad (5.190)$$

⁵¹See Blanchet (1997), eq. (4.33).

$$V_{\text{reac}}^i(t, \mathbf{x}) = \frac{G}{c^5} \left[\frac{1}{21} \hat{x}_{ijk} I_{jk}^{(6)}(t) - \frac{4}{45} \epsilon_{ijk} x_{jm} J_{km}^{(5)}(t) \right] + O\left(\frac{1}{c^7}\right). \quad (5.191)$$

To 2.5PN order in the metric, only the term proportional to $I_{ij}^{(5)}$ in eq. (5.190) contributes while the terms proportional to $1/c^7$ in eq. (5.190) are a 3.5PN correction, and the tail integral in V_{reac} is a 4PN correction. Similarly, taking into account the factor $1/c^3$ in eq. (5.188), and comparing with eq. (5.3), we see that V_{reac}^i is a 3.5PN correction. Thus, to 2.5PN order, the result reduces to the Burke-Thorne potential that we already discussed in eq. (3.114) (since I^{ij} , to lowest order in v/c , reduces to the quadrupole moment Q^{ij} of linearized theory).

The energy loss can be computed directly in terms of the potentials V_{reac} and V_{reac}^i , and fully agrees with the energy loss computed from the radiative field at infinity.⁵² It is interesting to observe that the vector component V_i of the radiation-reaction potential is responsible for the loss of linear momentum, i.e. for the recoil of the center-of-mass of the source due to GW emission, and balances exactly the value that can be found computing the flux of linear momentum at infinity.

5.4 The DIRE approach

We now discuss an approach due to Will, Wiseman and Pati and termed DIRE (Direct Integration of the Relaxed Einstein Equation) by the authors. This formalism is similar in spirit but different in technical details from the Blanchet–Damour approach. It can be proved, however, that the two formalisms are completely equivalent. For reasons of space we will limit ourselves to a brief description, referring the reader to Pati and Will (2000) for more details.

The basic strategy of this method is to start from eq. (5.83), and to iterate the solution in a slow-motion ($v \ll c$), weak-field ($|\mathbf{h}_{\mu\nu}| \ll 1$) approximation, in order to obtain in a systematic way the corrections to linearized theory. To zeroth order we set $\mathbf{h}_{\mu\nu} \equiv {}^{(0)}\mathbf{h}_{\mu\nu} = 0$ over all space-time, which means that ${}^{(0)}g_{\mu\nu} = \eta_{\mu\nu}$. If we denote by ${}^{(N)}\mathbf{h}_{\mu\nu}$ the result of the N -th iteration and by ${}^{(N)}\tau^{\alpha\beta}$ the value of $\tau^{\alpha\beta}$ when $\mathbf{h}_{\mu\nu} = {}^{(N)}\mathbf{h}_{\mu\nu}$, then the iterative rule is

$${}^{(N+1)}\mathbf{h}^{\alpha\beta}(t, \mathbf{x}) = -\frac{4G}{c^4} \int d^4x' \frac{{}^{(N)}\tau^{\alpha\beta}(t', \mathbf{x}') \delta(t' - t + |\mathbf{x} - \mathbf{x}'|/c)}{|\mathbf{x} - \mathbf{x}'|}. \quad (5.192)$$

The equation of motion of matter is then obtained imposing the N -th iteration of the De Donder gauge condition (5.71), $\partial_\beta {}^{(N)}\mathbf{h}^{\alpha\beta} = 0$.

Setting ${}^{(0)}\mathbf{h}_{\mu\nu} = 0$, we have ${}^{(0)}\tau^{\alpha\beta} = T^{\alpha\beta}$, and the first iteration ${}^{(1)}\mathbf{h}_{\mu\nu}$ gives back the result of linearized theory, eq. (3.8). Since ${}^{(0)}\tau^{\alpha\beta} = T^{\alpha\beta}$ has compact support, the integral is well defined and no divergence appears at this stage. The first PN correction is obtained computing ${}^{(2)}\mathbf{h}^{\alpha\beta}$. This requires plugging ${}^{(1)}\mathbf{h}^{\alpha\beta}$ in the expression for $\tau^{\alpha\beta}$. Since ${}^{(1)}\mathbf{h}^{\alpha\beta}$ already includes GWs propagating to infinity, now the source is no longer restricted to a compact region, and one must be careful in

⁵²See again Blanchet (1997).

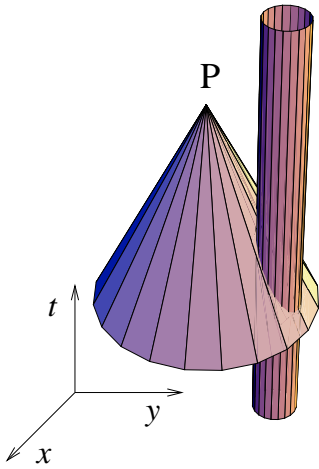


Fig. 5.2 The past light cone of the point P , and the cylinder which bounds the near zone \mathcal{D} . Here the point P is in the far region.

⁵³This is slightly different from the definition of \mathcal{R} that we used discussing the Blanchet–Damour formalism, where we preferred to keep \mathcal{R} (much) smaller than $(c/v)d$, to make sure that the expansion parameter in the near zone is much smaller than one. Here however \mathcal{R} is a formal parameter that separates the integral into an inner and an outer part, and whose cancellation, when we resum the two parts, will be checked explicitly, see below, so its precise value is irrelevant. For definiteness we assign it the value $(c/v)d$, following Pati and Will (2000).

handling the integral.

To compute the right-hand side of eq. (5.192) we proceed as follows. We consider a bound system, whose center of mass is taken to be at the origin of the coordinate system, and whose radial extension is always smaller or equal than a value d . We define the *source zone* as the world tube

$$\mathcal{T} = \{x^\alpha | r < d, -\infty < t < \infty\}. \quad (5.193)$$

Outside \mathcal{T} the energy-momentum tensor of matter vanishes, $T^{\alpha\beta} = 0$. We next introduce the length-scale $\mathcal{R} = (c/v)d$. The near zone is defined by the world tube

$$\mathcal{D} = \{x^\alpha | r < \mathcal{R}, -\infty < t < \infty\}, \quad (5.194)$$

while the radiation zone is defined as the region at $r > \mathcal{R}$.⁵³ The Dirac delta in eq. (5.192) tells us that, in order to compute the field ${}^{(N+1)}\mathbf{h}^{\alpha\beta}$ at a point $P = (t, \mathbf{x})$, we must integrate over the past flat-space null cone of P . As we see from Fig. 5.2, this past null cone intersects the world tube \mathcal{D} in a hypersurface \mathcal{N} (which of course is a three-dimensional hypersurface, but in Fig. 5.2 we suppressed one spatial dimension). In the figure we illustrated the situation in which P is in the far zone. In general, we wish to compute ${}^{(N+1)}\mathbf{h}^{\alpha\beta}$ both when P is in the far zone (since this allows us to compute the GWs emitted) and when P is in the near zone, since this determines the equation of motion of matter. A picture similar to Fig. 5.2 can be drawn when the tip of the cone, P , is inside the cylinder that (in this simplified 2+1 dimensional picture) bounds \mathcal{D} . For definiteness, in the following we specialize to the case where P is in the far region.

The integration over the past null cone \mathcal{C} can then be split into an integration over \mathcal{N} (defined as the part of the null cone which is in the near region) and an integration over the remainder $\mathcal{C} - \mathcal{N}$. The integration over \mathcal{N} gives, carrying out first the integration over t' ,

$${}^{(N+1)}\mathbf{h}_{\mathcal{N}}^{\alpha\beta}(t, \mathbf{x}) = -\frac{4G}{c^4} \int_{\mathcal{N}} d^3x' \frac{({}^N\tau^{\alpha\beta}(t - |\mathbf{x} - \mathbf{x}'|/c, \mathbf{x}'))}{|\mathbf{x} - \mathbf{x}'|}. \quad (5.195)$$

Within \mathcal{N} the integration variable \mathbf{x}' satisfies $|\mathbf{x}'| < \mathcal{R}$ while, since P is in the far zone, we have $r \equiv |\mathbf{x}| > \mathcal{R}$. Therefore we can expand the \mathbf{x}' dependence, in both occurrences of $|\mathbf{x} - \mathbf{x}'|$ in the integrand, in powers of $|\mathbf{x}'|/r$. This gives

$${}^{(N+1)}\mathbf{h}_{\mathcal{N}}^{\alpha\beta}(t, \mathbf{x}) = -\frac{4G}{c^4} \sum_{l=0}^{\infty} \frac{(-1)^l}{l!} \partial_L \left[\frac{1}{r} M^{\alpha\beta L}(u) \right], \quad (5.196)$$

where

$$M^{\alpha\beta L}(u) = \int_{\mathcal{M}} d^3x' \tau^{\alpha\beta}(u, \mathbf{x}') x'^L. \quad (5.197)$$

Here $u = t - r/c$, and \mathcal{M} is the intersection of the near-zone world-tube \mathcal{D} with the constant-time hypersurface $t_{\mathcal{M}} = u$. The integral is therefore expressed in terms of the multipole moments of $\tau^{\alpha\beta}$, and is explicitly

convergent because the region \mathcal{M} is bounded. For GWs, we are interested only in the spatial components h^{ij} , and in the term decreasing as $1/r$, so we can bring the factor $1/r$ in eq. (5.196) outside the derivatives. Using

$$\begin{aligned}\partial_i M(u) &= \frac{\partial u}{\partial x^i} \frac{dM}{du} \\ &= -n^i \frac{dM}{du},\end{aligned}\quad (5.198)$$

where n^i is the unit vector in the observation direction, and $dM(u)/du = dM/dt$, for GWs eq. (5.196) gives

$${}^{(N+1)}h_N^{ij}(t, \mathbf{x}) = -\frac{4G}{rc^4} \sum_{l=0}^{\infty} \frac{1}{l!} \frac{\partial^l}{\partial t^l} \int_{\mathcal{M}} d^3x' \tau^{ij}(u, \mathbf{x}') (\hat{\mathbf{n}} \cdot \mathbf{x}')^l. \quad (5.199)$$

The next step is the computation of the outer integral, that is, of the integral over the region $\mathcal{C} - \mathcal{N}$. In this outer region the energy-momentum tensor of matter vanishes, and the only contribution to ${}^{(N)}\tau^{\alpha\beta}$ comes from ${}^{(N)}h^{\alpha\beta}$. We can therefore compute it using the expression of ${}^{(N)}h^{\alpha\beta}$, as determined at the previous iteration level. The domain of integration is slightly complicated geometrically, as we see from Fig. 5.2, but the integration region can be expressed in a manageable form with an appropriate change of variables (see Pati and Will 2000 for details).

The original integral over the light cone \mathcal{C} , eq. (5.192), was of course independent of \mathcal{R} , which is an arbitrary constant that we have introduced to split it into two pieces, one at $r < \mathcal{R}$ and one at $r > \mathcal{R}$. In contrast, the inner and outer integrals for $h^{\alpha\beta}$ depend separately on the radius \mathcal{R} , and in particular they are divergent when $\mathcal{R} \rightarrow \infty$. Observe in fact that the contribution of $h^{\alpha\beta}$ to $\tau^{\alpha\beta}$ falls off at large distances as some power of r . Thus, if \mathcal{R} is taken to infinity, for sufficiently high values of l , i.e. for large multipoles, the integral in eq. (5.199) diverges. This is in fact the divergence to be expected if we try to extrapolate the PN expansion to the far region, as we discussed in Section 5.1.6. The correct procedure, then, is to keep \mathcal{R} finite, and show that these \mathcal{R} -dependent terms cancel against similar contributions from the remainder of the null cone, $\mathcal{C} - \mathcal{N}$. This cancellation has indeed been proved explicitly to 2PN order (for terms proportional to positive powers of \mathcal{R}) in Wiseman and Will (1996) and to all orders, with a proof by induction, in Pati and Will (2000). This cancellation is of course inevitable, but it has a very important practical consequence. When computing for instance the inner integral, one will generally find terms which are independent of \mathcal{R} as well as terms that depend on \mathcal{R} (as a power, or logarithmically). However, we know that all \mathcal{R} -dependent terms must cancel against similar terms from the outer integral, so in the computation one can simply drop them, and retain only the \mathcal{R} -independent contributions. Similarly, one can drop all \mathcal{R} -dependent terms in the outer integral.

Thus, one finally has a manifestly finite and well-defined procedure for computing systematically all higher-order corrections to linearized theory.

5.5 Strong-field sources and the effacement principle

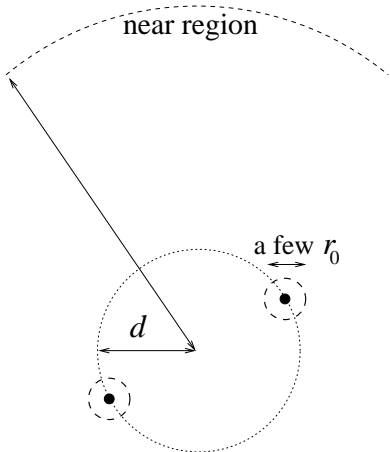
Until now we have assumed that the gravitational field is never strong. Our final aim, however, is to apply this formalism to systems containing compact objects such as neutron stars or black holes, in particular to a compact binary system which is slowly inspiraling, with an orbital velocity $v \ll c$. For a binary system, the quantity d that determines the characteristic source size is the typical orbital separation, and it satisfies $Gm/d \sim (v/c)^2$, where m is the total mass of the system. We denote instead by r_0 the characteristic size of the two stars (assumed for notational simplicity to be comparable). Since we are considering the slow inspiral phase, we are in the regime $d \gg r_0$.

Using for definiteness the Blanchet–Damour formalism, the three basic ingredients are: the post-Minkowskian expansion in the outer source region, the post-Newtonian expansion in the near region, and the fact that there is an intermediate region where we can match the two expansions. Even for a binary made of compact objects, when we are at a distance r (measured from the center-of-mass of the system) of order of a few times the orbital separation d , gravity is already sufficiently weak. Then, from say $r = 1.5d$ up to $r = \infty$ the post-Minkowskian expansion is justified, even for compact binaries containing neutron stars or black holes. Furthermore, when $v \ll c$, the near zone extends up to distances $\mathcal{R} \gg d$, and we have at our disposal a wide region where we can perform the matching to the PN solution. So the issue is whether, with the methods that we have discussed, we can reliably compute the PN solution in the near region $r < \mathcal{R}$. Even in most of the near region the gravitational field is weak; however, within two balls centered on the two stars, of radius of order a few times r_0 , see Fig. 5.3, the gravitational field becomes strong. It is therefore unclear whether the PN expansion is applicable.

We will see in this section that, in spite of this legitimate concern, the formalism that we have developed is indeed valid for compact objects. We will also estimate the effect of the internal structure of a compact object, and we will see that it shows up in the equations of motion only at the very high 5PN order, well beyond the accuracy of existing computations. This remarkable fact can be traced to a property of general relativity, which has been termed “the effacement of the internal structure”. Since the same phenomenon takes place in Newtonian gravity, we begin with a discussion of this simpler case.⁵⁴

Fig. 5.3 The near region of a compact binary system. Within two balls, centered on the two stars, of radius of order a few times r_0 , the gravitational field is strong.

⁵⁴We follow closely Damour (1987).



Effacement of the internal structure in Newtonian gravity

Treating the bodies as perfect fluids, a N -body system in Newtonian gravity is described by the velocity field of the fluid, $v^i(t, \mathbf{x})$, and by the mass density $\rho(t, \mathbf{x})$, which is subject to the constraint to have a compact support consisting of N non-overlapping connected regions. We denote by p the pressure, and we assume an equation of state $p = p(\rho)$. The

dynamics is governed by the continuity equation,

$$\partial_t \rho + \partial_i (\rho v_i) = 0, \quad (5.200)$$

by the Euler equation

$$\rho(\partial_t v^i + v^j \partial_j v^i) = -\partial_i p + \rho \partial_i U, \quad (5.201)$$

where U is the sign-reversed gravitational potential (therefore $U > 0$), and by Poisson equation

$$\nabla^2 U = -4\pi G \rho. \quad (5.202)$$

We denote by V_a the volume occupied by the a -th body. By definition, on its boundary ∂V_a we have $\rho = p = 0$. The mass of the a -th body is given by

$$m_a = \int_{V_a} d^3x \rho(t, \mathbf{x}), \quad (5.203)$$

and is a constant, thanks to the continuity equation. The center-of-mass coordinates of the a -th body are defined by

$$z_a^i(t) = \frac{1}{m_a} \int_{V_a} d^3x x^i \rho(t, \mathbf{x}). \quad (5.204)$$

Differentiating twice with respect to time and using eqs. (5.200) and (5.201) we get

$$m_a \frac{d^2 z_a^i}{dt^2} = \int_{V_a} d^3x f_i, \quad (5.205)$$

with a force density

$$f_i = -\partial_i p + \rho \partial_i U. \quad (5.206)$$

The potential U is obtained solving eq. (5.202) with the boundary condition that it vanishes at infinity,

$$\begin{aligned} U(t, \mathbf{x}) &= G \int d^3x' \frac{\rho(t, \mathbf{x}')}{|\mathbf{x} - \mathbf{x}'|} \\ &= \sum_{a=1}^N G \int_{V_a} d^3x' \frac{\rho(t, \mathbf{x}')}{|\mathbf{x} - \mathbf{x}'|}, \end{aligned} \quad (5.207)$$

where, in the second line, we made use of the fact that ρ is non-vanishing only on the volumes V_a , with $a = 1, \dots, N$. The potential acting on the a -th body can therefore be split into a “self-part”,

$$U^{(\text{self}),a}(t, \mathbf{x}) = G \int_{V_a} d^3x' \frac{\rho(t, \mathbf{x}')}{|\mathbf{x} - \mathbf{x}'|}, \quad (5.208)$$

and an “external part”,

$$U^{(\text{ext}),a}(t, \mathbf{x}) = G \sum_{b \neq a} \int_{V_b} d^3x' \frac{\rho(t, \mathbf{x}')}{|\mathbf{x} - \mathbf{x}'|}. \quad (5.209)$$

Correspondingly, the force acting on the a -th body is decomposed into a self-force

$$F_i^{(\text{self}),a} = \int_{V_a} d^3x [-\partial_i p + \rho \partial_i U^{(\text{self}),a}], \quad (5.210)$$

(in which we also included the pressure term) and an external force

$$F_i^{(\text{ext}),a} = \int_{V_a} d^3x \rho \partial_i U^{(\text{ext}),a}. \quad (5.211)$$

If one were to make a naive estimate of these two forces, based solely on dimensional analysis, one would write (assuming for definiteness that all bodies have comparable masses m) $F^{(\text{self}),a} \sim Gm^2/r_0^2$ and $F^{(\text{ext}),a} \sim Gm^2/d^2$, where r_0 is the typical body size and d is the distance between the nearest bodies. Since $d \gg r_0$, the self-force would be much larger than the external force. However, in Newtonian gravity the self-force vanishes exactly. The pressure term in eq. (5.210) vanishes because it is the integral of a gradient, and on the boundary $p = 0$. The second term, using eq. (5.208), is

$$\begin{aligned} F_i^{(\text{self}),a} &= G \int_{V_a} d^3x \rho(t, \mathbf{x}) \frac{\partial}{\partial x^i} \int_{V_a} d^3x' \frac{\rho(t, \mathbf{x}')}{|\mathbf{x} - \mathbf{x}'|} \\ &= -G \int_{V_a} d^3x \int_{V_a} d^3x' (x - x')^i \frac{\rho(t, \mathbf{x})\rho(t, \mathbf{x}')}{|\mathbf{x} - \mathbf{x}'|^3}. \end{aligned} \quad (5.212)$$

The integrand is odd under the exchange of x with x' while the integration domain is symmetric under this exchange, so the integral vanishes, and there is no self-force. It is however worth observing that the two factors $\rho(t, \mathbf{x})$ and $\rho(t, \mathbf{x}')$ entered the above integral in two conceptually distinct way. One factor, which is the one explicitly written in the second term in eq. (5.206), is really the density of “passive gravitational mass”, which measures the response of matter to an external gravitational field. The second factor, which enters through eq. (5.207), is the density of the “active gravitational mass”, which is the source for the gravitational field. The fact that these two densities are in fact equal is crucial to the vanishing of the integral in eq. (5.212). Thus, the vanishing of the self-force in Newtonian gravity is a non-trivial result, rooted in the equality between active and passive gravitational mass.

In the equation of motion (5.205), the first term that depends on the internal structure of the bodies, and not just on their masses, is then obtained performing a multipole expansion of the external force. We introduce a coordinate⁵⁵

$$\mathbf{y} = \mathbf{x} - \mathbf{z}_a(t), \quad (5.213)$$

centered on the a -th body. Since we have shown that the self-force vanishes, eq. (5.205) becomes

$$m_a \frac{d^2 z_a^i}{dt^2} = \int_{V_a} d^3y \rho(t, \mathbf{z}_a(t) + \mathbf{y}) \partial_i U^{(\text{ext}),a}(t, \mathbf{z}_a(t) + \mathbf{y}). \quad (5.214)$$

⁵⁵In principle \mathbf{y} should be written as \mathbf{y}_a . However, we will use it as an integration variable, so its dependence on a will only appear through the integration domain, and we omit its index a .

The density of the a -th body is localized around $\mathbf{y} = 0$, so it is convenient to introduce the notation $\rho_a(t, \mathbf{y}) \equiv \rho(t, \mathbf{z}_a(t) + \mathbf{y})$, while the external potential at $\mathbf{z}_a(t) + \mathbf{y}$ can be expanded around the value at the point $\mathbf{z}_a(t)$, plus small corrections. Thus, the multipole expansion is obtained writing

$$\begin{aligned} \partial_i U^{(\text{ext}),a}(t, \mathbf{z}_a + \mathbf{y}) &= [\partial_i U^{(\text{ext}),a} + y^j \partial_i \partial_j U^{(\text{ext}),a} \\ &\quad + \frac{1}{2} y^j y^k \partial_i \partial_j \partial_k U^{(\text{ext}),a} + \dots](t, \mathbf{z}_a). \end{aligned} \quad (5.215)$$

Inserting this expansion into eq. (5.214) we get

$$\begin{aligned} m_a \frac{d^2 z_a^i}{dt^2} &= [m_a \partial_i U^{(\text{ext}),a} + I_a^j \partial_i \partial_j U^{(\text{ext}),a} \\ &\quad + \frac{1}{2} I_a^{jk} \partial_i \partial_j \partial_k U^{(\text{ext}),a} + \dots](t, \mathbf{z}_a), \end{aligned} \quad (5.216)$$

where

$$I_a^j = \int_{V_a} d^3 y \rho_a(t, \mathbf{y}) y^j, \quad (5.217)$$

$$I_a^{jk} = \int_{V_a} d^3 y \rho_a(t, \mathbf{y}) y^j y^k, \quad (5.218)$$

and so on. However, the dipole in eq. (5.217) vanishes identically because of the definitions (5.204) and (5.213). In eq. (5.216) we can replace I_a^{jk} by the quadrupole moment $Q_a^{jk} = I_a^{jk} - (1/3)\delta^{jk}I_a^{ll}$, since the factor δ^{jk} , when contracted with $\partial_i \partial_j \partial_k U^{(\text{ext}),a}$ in eq. (5.215), produces $\partial_i \nabla^2 U^{(\text{ext}),a}$, and the Laplacian of the external potential is proportional to $\sum_{b \neq a} \rho_b$ and therefore vanishes inside the a -th body. Thus,

$$m_a \frac{d^2 z_a^i}{dt^2} = m_a \partial_i U^{(\text{ext}),a}(t, \mathbf{z}_a) + \frac{1}{2} Q_a^{jk} \partial_i \partial_j \partial_k U^{(\text{ext}),a}(t, \mathbf{z}_a) + \dots \quad (5.219)$$

The monopole term gives Newton's law. The quadrupole term is the first term which depends on the inner structure of the body. Each derivative acting on $U^{(\text{ext}),a}$ brings a contribution $O(1/d)$, while each factor y^i in the definition of the multipole moments, after integration over V_a , brings a factor $O(r_0)$. Thus, the contribution of I_a^{ij} is smaller than the monopole term by a factor $O(r_0^2/d^2)$. Furthermore, in the quadrupole moment Q_a^{ij} , only the non-spherical part of the matter distribution contributes, and this gives another suppression factor, that we denote by ϵ . In general $\epsilon \leq 1$ and, in many cases, $\epsilon \ll 1$. In conclusion, defining

$$\alpha \equiv \frac{r_0}{d} \ll 1, \quad (5.220)$$

the structure-dependent terms give a correction to Newton's law of order $\epsilon\alpha^2$, when a naive dimensional analysis that does not take into account that the self-force vanishes exactly, would have rather suggested that they are larger than the external Newtonian force by a factor $1/\alpha^2$. Overall, the terms that depend on the internal structure of the body

are therefore suppressed, with respect to naive expectations, by a factor $\epsilon\alpha^4$. As we have seen, the equality of active and passive gravitational mass is at the origin of this large cancellation, which is known as the “effacement principle”.

In order to generalize these results to Einstein gravity, it is useful to observe that there is a suggestive way of rewriting the Newtonian equations of motion, in a form that only involves surface integrals, rather than volume integrals. We start from eqs. (5.205) and (5.206). We neglect the pressure term, since this is a gradient and gives a vanishing contribution, and we use eq. (5.202). Then eq. (5.205) becomes

$$m_a \frac{d^2 z_a^i}{dt^2} = -\frac{1}{4\pi G} \int_{V_a} d^3 x \nabla^2 U \partial_i U, \quad (5.221)$$

where U is the total potential, including the self-potential. Using the identity

$$\partial_j (\partial_i U \partial_j U - \frac{1}{2} \delta_{ij} \partial_k U \partial_k U) = \nabla^2 U \partial_i U, \quad (5.222)$$

we can rewrite this as

$$\begin{aligned} m_a \frac{d^2 z_a^i}{dt^2} &= \int_{V_a} d^3 x \partial_j t^{ij} \\ &= \int_{S_a} dS_j t^{ij}, \end{aligned} \quad (5.223)$$

where

$$t_{ij} = -\frac{1}{4\pi G} \left(\partial_i U \partial_j U - \frac{1}{2} \delta_{ij} \partial_k U \partial_k U \right), \quad (5.224)$$

and dS_j is the two-dimensional surface element, on a surface S_a bounding the volume V_a , which is arbitrary except that it does not include any other volume V_b with $b \neq a$. This surface-integral representation of the equation of motion is especially interesting, since it shows that nothing depends on whether the gravitational field inside the bodies is weak or strong. In principle, one could even have a singularity inside the volume V_a , but the equations of motion can be computed evaluating the “stress tensor” t^{ij} on a surface which is far-away from the body (recall that we assumed $d \gg r_0$, so we can go to distances parametrically larger than r_0 before enclosing any other body), where all fields are weak.

Effacement of the internal structure in Einstein gravity

Just as we have done above for Newtonian gravity, we now show how to write the PN equations of motion of general relativity using surface integrals, using a variant of a classical work by Einstein, Infeld and Hoffmann (1938), developed by Itoh and Futamase. We start from the Einstein equations in relaxed form, in the harmonic gauge. First of all, we want to define the analogous of the center-of-mass coordinates. Observe that in the Newtonian case the center-of-mass coordinates $z_a^i(t)$ are such that the mass dipole I_a^j in eq. (5.217) vanishes. In the general

relativistic case, we define the functions $z_a^i(t)$ considering the dipole moment of τ^{00}

$$D_a^i \equiv \int_{V_a} d^3y y^i \tau^{00}(t, \mathbf{z}_a(t) + \mathbf{y}), \quad (5.225)$$

(where $\tau^{\mu\nu}$ is the effective energy-momentum tensor defined in eq. (5.73)) and requiring that D_a^i vanishes or, equivalently, that it takes a specified value. The functions $z_a^i(t)$ generalize the Newtonian notion of center-of-mass coordinates, and can be better called “center-of-fields” coordinates, since τ^{00} include also the contribution to the energy density from the gravitational field. We now define the quantity P_a^μ as

$$P_a^\mu(t) = \int_{V_a} d^3y \tau^{0\mu}(t, \mathbf{z}_a(t) + \mathbf{y}), \quad (5.226)$$

so this is an effective four-momentum of the a -th body, which includes also the contribution of the gravitational field. Using the conservation of $\tau^{\mu\nu}$, eq. (5.82), and the notation $v_a^i = \dot{z}_a^i$, we find

$$\begin{aligned} \frac{dP_a^\mu}{dt} &= \int_{V_a} d^3y [\partial_0 \tau^{0\mu} + v_a^i \partial_i \tau^{0\mu}](t, \mathbf{z}_a(t) + \mathbf{y}) \\ &= \int_{V_a} d^3y [-\partial_i \tau^{i\mu} + v_a^i \partial_i \tau^{0\mu}](t, \mathbf{z}_a(t) + \mathbf{y}). \end{aligned} \quad (5.227)$$

Since v_a^i is just a function of time, independent of y , we can carry it outside the integral and we are left with a total derivative. Hence, the variation of P^μ is given by a surface integral,

$$\frac{dP_a^\mu}{dt} = - \int_{S_a} dS_j \tau^{j\mu} + v_a^j \int_{S_a} dS_j \tau^{0\mu}. \quad (5.228)$$

A relation between the “momentum” P_a^i , the “energy” P_a^0 , and the velocity v_a^i of the a -th body can be obtained by taking the time derivative of eq. (5.225). On the left-hand side we get zero since D_a^i vanishes (or is anyway a constant), by definition of “center-of-fields” coordinates. On the right-hand side we use the conservation of $\tau^{\mu\nu}$ and we integrate by parts, keeping the boundary terms. Then we obtain

$$P_a^i = P_a^0 v_a^i + Q_a^i, \quad (5.229)$$

where

$$Q_a^i = \int_{S_a} dS_j y_a^i \tau^{j0} - v_a^j \int_{S_a} dS_j y_a^i \tau^{00}. \quad (5.230)$$

Finally, taking the time derivative of eq. (5.229) and using eq. (5.228) to compute dP_a^i/dt and dP_a^0/dt , we arrive at an equation for dv_a^i/dt ,

$$\begin{aligned} P_a^0 \frac{dv_a^i}{dt} &= - \int_{S_a} dS_j \tau^{ji} + v_a^j \int_{S_a} dS_j \tau^{0i} + v_a^i \int_{S_a} dS_j \tau^{j0} \\ &\quad - v_a^i v_a^j \int_{S_a} dS_j \tau^{00} - \frac{dQ_a^i}{dt}. \end{aligned} \quad (5.231)$$

This is an equation of motion for the a -th body. The remarkable point is that it is written entirely in terms of surface integrals. On the right-hand side this is explicit, while the quantity P_a^0 on the left-hand side can be obtained by integrating the $\mu = 0$ component of eq. (5.228), with the initial condition that, when $v/c \rightarrow 0$, $P_a^0 \rightarrow m_a c^2$, where m_a is the (ADM) mass of the body, so even P_a^0 is determined by surface integrals.

In conclusion, even if somewhere inside the volumes V_a the gravitational field becomes strong, as is the case for neutron stars, or even if there is a horizon, as for black holes, the evaluation of the equation of motion (5.231) can be done on surfaces far from the sources, at a distance smaller, but of the order of the separation d between the bodies, say at $r = d/3$. All these surface integrals therefore only involve weak fields. In other words, we have been able to replace the knowledge of the detailed internal structure of the source with a knowledge of the gravitational field at large distances from it. The equation of motions are the same, independently of whether a given value of the surface integral, computed say at a distance $r = d/3$, was produced by a very relativistic source with strong self-gravity or by a nearly Newtonian source with negligible self-gravity, spread over a larger volume V_a .⁵⁶ Then, the PN expansion is applicable even to strong field sources.⁵⁷ Since the surface integral formulation is just an equivalent way of recasting the equations of motion derived from Einstein equations, it follows that even the PN expansion in its original formulation, discussed in Section 5.1, is valid for strong-field sources.

The computation of the PN expansion with the surface integral method has been performed explicitly, up to 3PN order, by Itoh and Futamase, see the Further Reading section, and the results are in full agreement with that found with the direct PN expansion, with the important added bonus that this computation shows explicitly that the result is valid for strong fields.

Structure-dependent corrections in compact binaries

We are now in the position to estimate the post-Newtonian order at which corrections that depend on the internal structure of the body show up in the equations of motion of an inspiraling binary. The physical effect that induces a correction in the equations of motion is the fact that the tidal force exerted by the first body distorts the second body, inducing in it a quadrupole moment. The interaction between this quadrupole moment and the first body produces a force, which modifies the orbit.

The above discussion shows that, using the surface integral method, it is possible to perform the computation staying always in a Newtonian weak-field regime, so we expect that a simple estimate of this tidal effect based on a Newtonian description should give the correct order of magnitude. In Newtonian gravity, the tidal force exerted by a body at a distance d on a body of radius r_0 is of order

$$F_{\text{tidal}} \sim \frac{Gmr_0}{d^3}. \quad (5.232)$$

⁵⁶Observe that this effacement principle is valid in general relativity, but not necessarily in some of its extensions. For instance, in the factor $\epsilon\alpha^2$ that we found in the Newtonian limit, the suppression factor ϵ is related to the fact that the gravitational field describes a massless particle with helicities ± 2 , which forces gravitons to couple to the quadrupole moment. In extensions of general relativity that include gravitationally interacting scalar fields this suppression factor is absent, since the scalar couples to the trace of I_{ij} . Furthermore, in certain scalar-tensor theories, the local value of Newton's constant G is controlled by the local value of the scalar field. In this case, the inner structure of a body is affected by the presence of a companion, which modifies the value of G inside the first body. Thus, in this strong form, the effacement principle is really a properties specific to general relativity.

⁵⁷After one has found a suitable regularization of the point-particle singularity, which is a non-trivial issue, see the Further Reading.

The typical ellipticity ϵ induced by such a force is of order of the ratio of this tidal force to the typical self-gravity,

$$F_{\text{self}} \sim \frac{Gm}{r_0^2}. \quad (5.233)$$

Therefore

$$\epsilon \sim \frac{F_{\text{tidal}}}{F_{\text{self}}} \sim \alpha^3, \quad (5.234)$$

where $\alpha = r_0/d$. The corresponding induced quadrupole moment is $Q_{ij} \sim \epsilon m r_0^2$. According to eq. (5.219), with $m \partial_k U^{(\text{ext}),a} \sim F_k^{(\text{Newton})}$ (where $F_k^{(\text{Newton})}$ is the Newton gravitational force) this produces a structure-dependent interbody force of order

$$F^{(\text{induced})} \sim \frac{Q_{ij}}{m} \partial_i \partial_j F^{(\text{Newton})} \sim \epsilon r_0^2 \frac{1}{d^2} F^{(\text{Newton})}. \quad (5.235)$$

From eq. (5.234), we then find

$$F^{(\text{induced})} \sim \alpha^5 F^{(\text{Newton})}. \quad (5.236)$$

On the other hand, for a compact body we have $r_0 \sim Gm/c^2$, and therefore $\alpha \sim Gm/(c^2 d)$. From the virial theorem, $(Gm/d) \sim v^2$, so $\alpha \sim (v^2/c^2)$. In conclusion, for compact bodies,

$$F^{(\text{induced})} \sim \left(\frac{v}{c}\right)^{10} F^{(\text{Newton})}. \quad (5.237)$$

A full relativistic analysis indeed confirms this estimate. So, the first structure-dependent term gives a 5PN effect in the equation of motion. This is well beyond the present state-of-the art which, as we discussed, is the 3.5PN order.

In conclusion (after one has found a consistent regularization of the point-particle singularity) the PN formalism can be legitimately applied even in the presence of strong fields, and the corrections dependent on the internal structure can be neglected up to the extremely high 5PN order. As long as the two bodies are far from the merging stage (hence v/c is not too close to one), these 5PN effects can be neglected, and both the orbital motion and the GWs that are produced are determined uniquely by the masses of the bodies, independently of whether the internal structure is highly relativistic or almost Newtonian.⁵⁸

⁵⁸In our discussion we have considered spinless bodies. Otherwise, the orbital motion and the GW generation is determined by two parameters for each body, its mass and its intrinsic angular momentum. Both can be obtained measuring the gravitational field at large distances.

5.6 Radiation from inspiraling compact binaries

The most important application of the above formalism is to the inspiral of compact binaries. We already saw in Section 4.4.1, in the context of linearized theory, that a binary system gradually spirals inward because of the emission of GWs, and the resulting waveform increases in amplitude and in frequency, producing a characteristic “chirp”. This long

inspiral phase is followed by a phase in which the two object plunge toward each other, and merge. The resulting system, typically a black hole, finally settles down to its ground state, radiating away the energy stored in its excited modes. This is the so-called “ringdown phase”. So, the evolution of a compact binary system can be separated into these three phases: inspiral, merging, and ringdown. The merging phase is particularly difficult to model, and here the detailed nature of the source (e.g. whether we have black holes or neutron stars) is also important. The merger and ringdown phases will be analyzed in detail in Vol. 2, which is devoted to the issues in GW physics which depends on the specific nature of the source. Here we will rather discuss the inspiral phase, which is universal, at least up to a very high PN order.

5.6.1 The need for a very high-order computation

The reason why the computation of the waveform to a very high PN order is crucial, is that GW experiments are hunting for signals which are buried in a noise orders of magnitudes larger than the signal itself. To extract such a small signal from the noise there exists a standard technique, called matched filtering, that we will discuss in great detail in Chapter 7, that works if we know well the form of the signal.

For an inspiraling compact binary, we saw in eq. (4.23) that, in a ground-based interferometer, the signal enters into the detector bandwidth, say at $f_{\min} \sim 10$ Hz, about 17 minutes before the coalescence, and the signal sweeps up in frequency, performing a vary large number of cycles,⁵⁹ before the two stars merge. In order to exploit optimally the signal present in the detector, and therefore to detect sources at farther distances, we need to have an accurate theoretical prediction of the time evolution of the waveform, and especially of the phase, which is rapidly changing. To understand how stringent is this requirement, and also to write compactly the PN corrections, it is useful first of all to introduce some new notation. In place of the source frequency ω_s , we introduce the dimensionless variable

$$x \equiv \left(\frac{Gm\omega_s}{c^3} \right)^{2/3}, \quad (5.238)$$

where $m = m_1 + m_2$ is the total mass of the system and $\omega_s = 2\pi f_s$ is the orbital frequency of the source. Writing $x = [(Gm/r)(r\omega_s/c^3)]^{2/3}$, and observing that $Gm/r \sim v^2$ and $r\omega_s \sim v$, we see that

$$x = O\left(\frac{v^2}{c^2}\right). \quad (5.239)$$

Thus, the v/c corrections can be expressed as correction in powers of $x^{1/2}$. We also define the symmetric mass ratio

$$\nu \equiv \frac{\mu}{m} = \frac{m_1 m_2}{(m_1 + m_2)^2}, \quad (5.240)$$

⁵⁹For instance $O(10^4)$ cycles in the case of two neutron stars with $m_1 = m_2 = 1.4M_\odot$.

and the post-Newtonian parameter

$$\gamma \equiv \frac{Gm}{rc^2}, \quad (5.241)$$

which is $O(v^2/c^2)$. We finally introduce the dimensionless time variable

$$\Theta \equiv \frac{\nu c^3}{5Gm}(t_c - t), \quad (5.242)$$

where t_c is the time at which the coalescence takes place.

We can now rewrite some Newtonian results for a chirping binary, obtained in Section 4.1, in terms of these parameters. In particular, the relation between the frequency and the time to coalescence for circular orbit, eq. (4.19), reads simply (taking into account that in Section 4.1 we computed the radiation emitted by a circular orbit in the quadrupole approximation, so $\omega_s = \omega_{\text{gw}}/2 = \pi f_{\text{gw}}$)

$$x = \frac{1}{4} \Theta^{-1/4}. \quad (5.243)$$

The accumulated orbital phase, defined by

$$\phi = \int_{t_0}^t dt' \omega_s(t'), \quad (5.244)$$

can be written, using eq. (4.30) together with $\Phi = 2\phi$ (see eq. (4.28)), as

$$\phi = \phi_0 - \frac{1}{\nu} \Theta^{5/8}, \quad (5.245)$$

or, eliminating Θ in favor of x ,

$$\phi = \phi_0 - \frac{x^{-5/2}}{32\nu}. \quad (5.246)$$

Finally, the number of cycles spent in the detector bandwidth can be written, using eq. (4.23), as $\mathcal{N}_{\text{cyc}} = \mathcal{N}(f_{\min}) - \mathcal{N}(f_{\max})$, where

$$\begin{aligned} \mathcal{N}(f) &\equiv \frac{1}{32\pi^{8/3}} \left(\frac{GM_c}{c^3} \right)^{-5/3} f^{-5/3} \\ &= \frac{x^{-5/2}}{32\pi\nu}. \end{aligned} \quad (5.247)$$

All these relations receive corrections from the PN expansion, that can be written as an expansion in powers of $x^{1/2}$, see eq. (5.239), and that will be examined in detail below. In particular, the PN corrections to eq. (5.247) take the form

$$\mathcal{N}(x) = \frac{x^{-5/2}}{32\pi\nu} [1 + O(x) + O(x^{3/2}) + O(x^2) + O(x^{5/2}) + \dots]. \quad (5.248)$$

If we want to track the evolution of the GW signal, we need a template which reproduces the number of cycles with a precision at least $O(1)$. We see from eq. (5.248) that, since the leading term in $\mathcal{N}(x)$ is proportional

to $x^{-5/2}$, we need to include the corrections up to $O(x^{5/2})$ in order to have an error not larger than $O(1)$ on $\mathcal{N}(x)$. This means that we need to compute the PN corrections to the phase at least up to 2.5PN level, i.e. corrections smaller by a factor $(v/c)^5$ with respect to the leading term. Actually, this is not even enough because, once we have accumulated an error of order one on the number of cycles, our template has clearly gone out of phase with the signal, so a more accurate computation is really required in order to exploit optimally the information contained in the output of a ground-based interferometer, at least up to 3PN order, and better yet to 3.5PN.

An equivalent way of understanding the need for a high-order PN computation is to look at the waveform, rather than at the number of cycles $\mathcal{N}(x)$, and to observe that the last term in the expression (4.37) for the phase $\Psi_+(f)$ of the GW amplitude is, in terms of x ,

$$\frac{3}{4} \left(\frac{GM_c}{c^3} 8\pi f \right)^{-5/3} = \frac{3}{128\nu} x^{-5/2}. \quad (5.249)$$

Thus, for small x the Newtonian phase Ψ_+ is of order $x^{-5/2}$, and it diverges for $x \rightarrow 0$. The 1PN corrections gives a contribution to Ψ_+ of order $x^{-3/2}$ which, even if subleading with respect to the Newtonian term, still diverges as $x \rightarrow 0$, and similarly all the contributions up to 2.5PN must be kept since they either diverge (up to 2PN) or anyway stay finite (the 2.5PN term) in the small x limit, and only starting from 3PN level we have corrections which vanish as $x \rightarrow 0$.

5.6.2 The 3.5PN equations of motion

The general principles for performing such a computation have been discussed in detail in Sections 5.3 and 5.4, and we have also seen in some detail how to obtain the near-field metric to 1PN order, in Section 5.1.4. A new technical problem that arises in higher orders is due to the fact that, if one uses as energy-momentum tensor of the two bodies the expression in terms of the Dirac delta, eq. (5.47), one finds divergencies in the computation of some integrals. Therefore, a modelization of the two bodies as point-like is not possible, and some regularization of the Dirac delta is necessary. Different regularizations have been considered, and (up to 3.5PN) they all give the same final result, as we expect from the effacement principle discussed in Section 5.5.⁶⁰ The equation of motion has the general form

$$\frac{dv^i}{dt} = -\frac{Gm}{r^2} \left[(1 + \mathcal{A}) \frac{x^i}{r} + \mathcal{B} v^i \right] + \mathcal{O}\left(\frac{1}{c^8}\right), \quad (5.250)$$

so it has a term proportional to the relative separation x^i and a term proportional to the relative velocity in the center-of-mass frame, v^i . For a generic orbit, the expression of \mathcal{A} and \mathcal{B} is extremely long.⁶¹ However we have seen in Section 4.1.3 that, by the time that the signal enters in the bandwidth of a ground-based interferometer, radiation reaction

⁶⁰Except that, with the so-called Hadamard regularization, some ambiguity appears at 3PN order. This ambiguity does not appear with dimensional regularization, see Damour, Jaradowski and Schäfer (2001b) and Blanchet, Damour, Esposito-Farèse and Iyer (2004), nor with the surface integral method, see Itoh and Futamase (2003), nor with the ADM Hamiltonian formalism, see Damour, Jaradowski and Schäfer (2000), and the results agree.

⁶¹See Blanchet (2006), eq. (182), where the result spills over two pages!

has circularized the orbit to great accuracy. For orbits that are circular except from the inspiral due to radiation reaction, one finds that the radial velocity is $O(1/c^5)$, so most terms in the expression for \mathcal{A} and \mathcal{B} can be dropped, to 3.5PN order, and eq. (5.250) becomes

$$\frac{dv^i}{dt} = -\omega_s^2 x^i - \zeta v^i, \quad (5.251)$$

where

$$\begin{aligned} \omega_s^2 = & \frac{Gm}{r^3} \left\{ 1 + (-3 + \nu)\gamma + \left(6 + \frac{41}{4}\nu + \nu^2 \right) \gamma^2 \right. \\ & + \left[-10 + \left(22 \log(r/r'_0) - \frac{75707}{840} + \frac{41}{64}\pi^2 \right) \nu + \frac{19}{2}\nu^2 + \nu^3 \right] \gamma^3 \left. \right\} \\ & + \mathcal{O}\left(\frac{1}{c^8}\right), \end{aligned} \quad (5.252)$$

and

$$\zeta = \frac{32}{5} \frac{G^3 m^3 \nu}{c^5 r^4} + \mathcal{O}\left(\frac{1}{c^7}\right). \quad (5.253)$$

Observe that eq. (5.252) is the PN generalization of Kepler's law. The velocity-dependent term in eq. (5.251) describes the radiation reaction. The term $O(1/c^5)$ in ζ is due to the 2.5PN radiation reaction, and we have not written explicitly the more complicated 3.5PN contribution to ζ .

In eq. (5.252) appears a length-scale r'_0 , which is a gauge-dependent constant. This is not surprising, since the radius r that appears in the above formulas is the relative separation in harmonic coordinates, so it is not an invariant quantity (similarly, γ in eq. (5.241) is not an invariant quantity). However, x defined in eq. (5.238) is a physical quantity, so if we express a physical observable as a power series in x , the constant r'_0 must cancel out. For instance, inverting eq. (5.252) one finds

$$\begin{aligned} \gamma = x \left\{ 1 + \left(1 - \frac{\nu}{3} \right) x + \left(1 - \frac{65}{12}\nu \right) x^2 \right. \\ + \left[1 + \left(-\frac{22}{3} \log(r/r'_0) - \frac{2203}{2520} - \frac{41}{192}\pi^2 \right) \nu + \frac{229}{36}\nu^2 + \frac{1}{81}\nu^3 \right] x^3 \\ \left. + \mathcal{O}\left(\frac{1}{c^8}\right) \right\}, \end{aligned} \quad (5.254)$$

which displays explicitly the dependence of γ on r'_0 . On the other hand, the PN expansion of the energy of a circular orbit up to 3.5PN turns out to be

$$\begin{aligned} E = & -\frac{\mu c^2 \gamma}{2} \left\{ 1 + \left(-\frac{7}{4} + \frac{1}{4}\nu \right) \gamma + \left(-\frac{7}{8} + \frac{49}{8}\nu + \frac{1}{8}\nu^2 \right) \gamma^2 \right. \\ & + \left[-\frac{235}{64} + \left(\frac{22}{3} \log(r/r'_0) + \frac{46031}{2240} - \frac{123}{64}\pi^2 \right) \nu + \frac{27}{32}\nu^2 + \frac{5}{64}\nu^3 \right] \gamma^3 \left. \right\} \\ & + \mathcal{O}\left(\frac{1}{c^8}\right), \end{aligned} \quad (5.255)$$

which seems to depend on r'_0 both explicitly and through γ . However, inserting eq. (5.254) into eq. (5.255), one finds that r'_0 cancels out, and

$$\begin{aligned} E = & -\frac{\mu c^2 x}{2} \left\{ 1 + \left(-\frac{3}{4} - \frac{1}{12}\nu \right) x + \left(-\frac{27}{8} + \frac{19}{8}\nu - \frac{1}{24}\nu^2 \right) x^2 \right. \\ & + \left[-\frac{675}{64} + \left(\frac{34445}{576} - \frac{205}{96}\pi^2 \right) \nu - \frac{155}{96}\nu^2 - \frac{35}{5184}\nu^3 \right] x^3 \Big\} \\ & + \mathcal{O}\left(\frac{1}{c^8}\right). \end{aligned} \quad (5.256)$$

5.6.3 Energy flux and orbital phase to 3.5PN order

The computation of the equations of motion in the near region is one of the outputs of the formalisms that we have discussed in the previous sections. The other is the waveform, and therefore the energy flux, at infinity. A computation of the gravitational waveform to a very high PN order is a daunting task. Currently, the computation of the phase is complete up to 3.5 PN order (for the case where the stars have negligible spins).⁶² For the power radiated in GWs, P_{gw} , one finds, after an extremely long computation,

$$\begin{aligned} P_{\text{gw}} = & \frac{32c^5}{5G}\nu^2x^5 \left\{ 1 + \left(-\frac{1247}{336} - \frac{35}{12}\nu \right) x + 4\pi x^{3/2} \right. \\ & + \left(-\frac{44711}{9072} + \frac{9271}{504}\nu + \frac{65}{18}\nu^2 \right) x^2 \\ & + \left(-\frac{8191}{672} - \frac{583}{24}\nu \right) \pi x^{5/2} \\ & + \left[\frac{6643739519}{69854400} + \frac{16}{3}\pi^2 - \frac{1712}{105}C - \frac{856}{105}\log(16x) \right. \\ & + \left(-\frac{134543}{7776} + \frac{41}{48}\pi^2 \right) \nu - \frac{94403}{3024}\nu^2 - \frac{775}{324}\nu^3 \Big] x^3 \\ & + \left. \left(-\frac{16285}{504} + \frac{214745}{1728}\nu + \frac{193385}{3024}\nu^2 \right) \pi x^{7/2} + \mathcal{O}\left(\frac{1}{c^8}\right) \right\}. \end{aligned} \quad (5.257)$$

where $C = 0.577\dots$ is the Euler–Mascheroni constant. Observe that the limit $\nu \rightarrow 0$ corresponds to a test mass moving in the background geometry generated by the other body, which is just a perturbation of the Schwarzschild metric. In this limit, using methods from black-hole perturbation theory, the result has been computed up to the extremely high 5.5PN order, see the Further Reading. Comparing the limit of eq. (5.257) when $\nu \rightarrow 0$, with the result of black hole perturbation theory up to 3.5PN, one finds complete agreement, including rational fractions such as $6643739519/69854400$. This is a very non-trivial check of the above computation.

The orbital phase evolution up to 3.5PN can now be obtained by integrating the energy balance equation $dE/dt = -P_{\text{gw}}$, with E given in eq. (5.256) and P_{gw} in eq. (5.257). This gives x as a function of time.

⁶²See Blanchet, Faye, Iyer and Joguet (2002) and Blanchet, Damour, Esposito-Farèse and Iyer (2004).

The result, expressed in terms of Θ defined in eq. (5.242), is

$$\begin{aligned} x = & \frac{1}{4}\Theta^{-1/4} \left\{ 1 + \left(\frac{743}{4032} + \frac{11}{48}\nu \right) \Theta^{-1/4} - \frac{1}{5}\pi\Theta^{-3/8} \right. \\ & + \left(\frac{19583}{254016} + \frac{24401}{193536}\nu + \frac{31}{288}\nu^2 \right) \Theta^{-1/2} \\ & + \left(-\frac{11891}{53760} + \frac{109}{1920}\nu \right) \pi\Theta^{-5/8} \\ & + \left[-\frac{10052469856691}{6008596070400} + \frac{1}{6}\pi^2 + \frac{107}{420}C - \frac{107}{3360}\log\left(\frac{\Theta}{256}\right) \right. \\ & + \left(\frac{3147553127}{780337152} - \frac{451}{3072}\pi^2 \right)\nu - \frac{15211}{442368}\nu^2 + \frac{25565}{331776}\nu^3 \left. \right] \Theta^{-3/4} \\ & \left. + \left(-\frac{113868647}{433520640} - \frac{31821}{143360}\nu + \frac{294941}{3870720}\nu^2 \right) \pi\Theta^{-7/8} + \mathcal{O}\left(\frac{1}{c^8}\right) \right\}. \end{aligned} \quad (5.258)$$

The orbital phase ϕ is now obtained by integrating $d\phi/dt = \omega_s$ which, expressing t in terms of Θ and ω_s in terms of x , reads

$$\frac{d\phi}{d\Theta} = -\frac{5}{\nu}x^{3/2}. \quad (5.259)$$

Inserting x as function of Θ from eq. (5.258), the integration gives

$$\begin{aligned} \phi(t) = & -\frac{1}{\nu}\Theta^{5/8} \left\{ 1 + \left(\frac{3715}{8064} + \frac{55}{96}\nu \right) \Theta^{-1/4} - \frac{3}{4}\pi\Theta^{-3/8} \right. \\ & + \left(\frac{9275495}{14450688} + \frac{284875}{258048}\nu + \frac{1855}{2048}\nu^2 \right) \Theta^{-1/2} \\ & + \left(-\frac{38645}{172032} + \frac{65}{2048}\nu \right) \pi\Theta^{-5/8} \log\left(\frac{\Theta}{\Theta_0}\right) \\ & + \left[\frac{831032450749357}{57682522275840} - \frac{53}{40}\pi^2 - \frac{107}{56}C + \frac{107}{448}\log\left(\frac{\Theta}{256}\right) \right. \\ & + \left(-\frac{126510089885}{4161798144} + \frac{2255}{2048}\pi^2 \right)\nu \\ & + \frac{154565}{1835008}\nu^2 - \frac{1179625}{1769472}\nu^3 \left. \right] \Theta^{-3/4} \\ & + \left(\frac{188516689}{173408256} + \frac{488825}{516096}\nu - \frac{141769}{516096}\nu^2 \right) \pi\Theta^{-7/8} \\ & \left. + \mathcal{O}\left(\frac{1}{c^8}\right) \right\}, \end{aligned} \quad (5.260)$$

where $\Theta(t)$ is given in eq. (5.242), and Θ_0 is a constant of integration to be fixed by the initial condition (i.e. by the value of Θ when it enters the detector's bandwidth) which replaces ϕ_0 in the Newtonian formula (5.245). Observe that, due to the $\log\Theta$ term at 2.5PN level, as well as due to negative overall powers of Θ in higher orders, it is no longer true that ϕ_0 in eq. (5.246) is the phase at the coalescence time; rather, now ϕ diverges as $\Theta \rightarrow 0$. In terms of x , the above result reads

$$\phi = -\frac{x^{-5/2}}{32\nu} \left\{ 1 + \left(\frac{3715}{1008} + \frac{55}{12}\nu \right) x - 10\pi x^{3/2} \right.$$

$$\begin{aligned}
& + \left(\frac{15293365}{1016064} + \frac{27145}{1008} \nu + \frac{3085}{144} \nu^2 \right) x^2 \\
& + \left(\frac{38645}{1344} - \frac{65}{16} \nu \right) \pi x^{5/2} \log \left(\frac{x}{x_0} \right) \\
& + \left[\frac{12348611926451}{18776862720} - \frac{160}{3} \pi^2 - \frac{1712}{21} C - \frac{856}{21} \log(16x) \right. \\
& \quad \left. + \left(-\frac{15737765635}{12192768} + \frac{2255}{48} \pi^2 \right) \nu + \frac{76055}{6912} \nu^2 - \frac{127825}{5184} \nu^3 \right] x^3 \\
& + \left(\frac{77096675}{2032128} + \frac{378515}{12096} \nu - \frac{74045}{6048} \nu^2 \right) \pi x^{7/2} \\
& + \mathcal{O} \left(\frac{1}{c^8} \right) \}, \tag{5.261}
\end{aligned}$$

where x_0 is another constant of integration. When we consider spinning bodies, there is also a spin-orbit coupling arising at 1.5PN and a spin-spin coupling starting at 2PN. They are known up to 2.5PN order, included.

5.6.4 The waveform

The full waveform is presently known up to 2.5PN order. The two polarizations are defined with respect to two axes \mathbf{p} and \mathbf{q} , chosen to lie along the major and minor axis, respectively, of the projection onto the plane of the sky of the circular orbit, with \mathbf{p} oriented toward the ascending node. The general structure of the two polarization amplitudes is

$$h_{+,\times}(t) = \frac{2G\mu x}{c^2 r} \left\{ H_{+,\times}^{(0)} + x^{1/2} H_{+,\times}^{(1/2)} + x H_{+,\times}^{(1)} + x^{3/2} H_{+,\times}^{(3/2)} + x^2 H_{+,\times}^{(2)} \right. \\
\left. x^{5/2} H_{+,\times}^{(5/2)} + \mathcal{O} \left(\frac{1}{c^6} \right) \right\}. \tag{5.262}$$

⁶³The minus sign of eqs. (5.263) and (5.264) with respect to the result in eq. (4.29) is due to the sign difference among $h_{\mu\nu}$ and $\bar{h}_{\mu\nu}$, see Note 19 on page 250.

⁶⁴See Blanchet (2006), eqs. (236)–(242) for the full result including the 2.5 PN corrections $H_{+,\times}^{(5/2)}$.

⁶⁵The use of ϕ instead of the actual phase ϕ of the source is convenient because it allows us to collect the logarithmic terms which come out of the computation of the tail effects discussed in Section 5.3.4.

The leading term is^{63,64}

$$H_{+}^{(0)}(t) = -(1 + \cos^2 \iota) \cos 2\psi(t), \tag{5.263}$$

$$H_{\times}^{(0)}(t) = -2 \cos \iota \sin 2\psi(t), \tag{5.264}$$

where ψ is a phase, related to ϕ by

$$\psi(t) = \phi(t) - \frac{2Gm\omega_s}{c^3} \log \left(\frac{\omega_s(t)}{\omega_0} \right), \tag{5.265}$$

and ω_0 is a constant frequency that can be conveniently chosen as the entry frequency of an interferometric detector.⁶⁵ For the crucial phase ϕ one uses the highest available precision, i.e., at present, the 3.5PN result (5.260), independently of the order at which the waveform has been computed. This is necessary since, as discussed in Section 5.6.1, the phase is given as an expansion in x but, in the limit $x \rightarrow 0$ the corrections to ϕ up to 2PN order are divergent. Only starting from

2.5PN correction the correction has a finite limit for $x \rightarrow 0$, but is anyway of order one in the phase, and we need better than that. On the other hand, we see from eq. (5.262) that the correction to $H_{+,x}^{(0)}$ i.e. the terms $x^{1/2}H^{(1/2)}$, $xH^{(1)}$, etc., vanish for $x \rightarrow 0$ so, in the small x limit, it makes sense to neglect them, even when we include all available corrections up to 3.5PN in ϕ . The approximation in which only $H^{(0)}$ is retained in eq. (5.262), while all available PN corrections to ϕ are included, is called the “restricted” PN approximation.

In practice, however, we are not interested in the waveform for parametrically small values of x , but rather for the typical values of v/c , and hence of x , at which the signal of an inspiraling binary enters in the detector bandwidth. Then, for a ground-based detector, the first few corrections to the amplitude are numerically important, and produce an amplitude modulation of the chirp signal.⁶⁶ The first correction to the amplitude (which is of 0.5PN order, i.e. $O(v/c)$) is given by

$$H_+^{(1/2)} = -\frac{\sin \iota}{8} \frac{\delta m}{m} [(5 + \cos^2 \iota) \cos \psi - 9(1 + \cos^2 \iota) \cos 3\psi], \quad (5.266)$$

$$H_x^{(1/2)} = -\frac{3}{4} \sin \iota \cos \iota \frac{\delta m}{m} [\sin \psi - 3 \sin 3\psi], \quad (5.267)$$

where $\delta m = m_1 - m_2$ is the mass difference. Observe that, while the phase of the leading terms $H_{+,x}^{(0)}$ depends on 2ϕ , that is on the integral of $2\omega_s$, the phase in the next-to-leading terms depend on ϕ and 3ϕ , that is on the integral of ω_s and $3\omega_s$. This can be traced back to the fact, discussed in Sections 3.3 and 3.4, that for a purely circular motion with frequency ω_s , the mass quadrupole radiates GWs with $\omega_{\text{gw}} = 2\omega_s$, while the mass octupole and current quadrupole both radiate at $\omega_{\text{gw}} = \omega_s$ and at $\omega_{\text{gw}} = 3\omega_s$. Thus, together with the quadrupolar component which is chirping according to $\omega_{\text{gw}}(t) = 2\omega_s(t)$, the term $H_{+,x}^{(1/2)}$ in eq. (5.262) describes two “sidebands” chirping at $\omega_{\text{gw}}(t) = \omega_s(t)$ and at $\omega_{\text{gw}}(t) = 3\omega_s(t)$, while $H_{+,x}^{(1)}$ is again chirping at $\omega_{\text{gw}}(t) = 2\omega_s(t)$, as well as at $\omega_{\text{gw}}(t) = 4\omega_s(t)$, etc. Observe that these components enter in the detector bandwidth at different times.⁶⁷

It is also useful to express eq. (5.258) as an explicit relation between time t and the GW frequency $f(t)$ (defined here as twice the source frequency $f_s(t)$, so $f(t)$ is really the frequency at which the quadrupole component $H_{+,x}^{(0)}$ is chirping). We limit ourselves for simplicity to 2PN order, and we neglect spin corrections. First of all, observe that the Newtonian relation between f and t , eq. (4.19), can be rewritten in the form

$$t - t_* = \tau_0 \left[1 - (f(t)/f_*)^{-8/3} \right], \quad (5.268)$$

where t_* is an arbitrary reference time (e.g. the time of entry of the signal in the interferometer bandwidth), $f_* = f(t_*)$, and the parameter τ_0 is given by

$$\tau_0 = \frac{5}{256\pi} f_*^{-1} (\pi M f_*)^{-5/3} \nu^{-1}. \quad (5.269)$$

Here we introduced the shorthand notation $M \equiv Gm/c^3$, where $m = m_1 + m_2$ is the total mass of the system (observe that, dimensionally,

⁶⁶An amplitude modulation can also be obtained if the compact stars have an intrinsic spin, which is the physically realistic case. See the Further reading for details.

⁶⁷This time delay can be quite large. For instance, when the quadrupole component has reached the frequency $f_{\text{gw}} = 2f_s = 10$ Hz, the octupole and current quadrupole give a contribution at $f_{\text{gw}} = 3f_s = 15$ Hz. From eq. (4.20) we see that the quadrupole will reach 15 Hz only after about 5 more minutes.

M is actually a time) and, as usual $\nu = \mu/m$. The post-Newtonian corrections, up to 2PN order, modify this relation as follows,

$$\begin{aligned} t - t_* &= \tau_0 \left[1 - \left(\frac{f}{f_*} \right)^{-8/3} \right] + \tau_1 \left[1 - \left(\frac{f}{f_*} \right)^{-2} \right] \\ &\quad - \tau_{1.5} \left[1 - \left(\frac{f}{f_*} \right)^{-5/3} \right] + \tau_2 \left[1 - \left(\frac{f}{f_*} \right)^{-4/3} \right], \end{aligned} \quad (5.270)$$

with

$$\begin{aligned} \tau_1 &= \frac{5}{192\pi} f_*^{-1} (\pi M f_*)^{-1} \nu^{-1} \left(\frac{743}{336} + \frac{11}{4} \nu \right), \\ \tau_{1.5} &= \frac{1}{8} f_*^{-1} (\pi M f_*)^{-2/3} \nu^{-1} \\ \tau_2 &= \frac{5}{128\pi} f_*^{-1} (\pi M f_*)^{-1/3} \nu^{-1} \left(\frac{3058673}{1016064} + \frac{5429}{1008} \nu + \frac{617}{144} \nu^2 \right). \end{aligned} \quad (5.271)$$

In terms of these quantities, the chirping of the GW frequency can be written as

$$\begin{aligned} \frac{df}{dt} &= \frac{3f_*}{8\tau_0} \left(\frac{f}{f_*} \right)^{11/3} \left[1 - \frac{3}{4} \frac{\tau_1}{\tau_0} \left(\frac{f}{f_*} \right)^{2/3} \right. \\ &\quad \left. + \frac{5}{8} \frac{\tau_{1.5}}{\tau_0} \left(\frac{f}{f_*} \right) - \frac{1}{2} \left(\frac{\tau_2}{\tau_0} - \frac{9}{8} \left(\frac{\tau_1}{\tau_0} \right)^2 \right) \left(\frac{f}{f_*} \right)^{4/3} \right], \end{aligned} \quad (5.272)$$

and the accumulated phase $\Phi = 2\phi$ which appears in the quadrupole part of the waveform depends on $f(t)$ as

$$\begin{aligned} \Phi(f) &= \frac{16\pi}{5} \tau_0 f_* \left[\left(1 - \left(\frac{f}{f_*} \right)^{-5/3} \right) + \frac{5}{4} \frac{\tau_1}{\tau_0} \left(1 - \left(\frac{f}{f_*} \right)^{-1} \right) \right. \\ &\quad \left. - \frac{25}{16} \frac{\tau_{1.5}}{\tau_0} \left(1 - \left(\frac{f}{f_*} \right)^{-2/3} \right) + \frac{5}{2} \frac{\tau_2}{\tau_0} \left(1 - \left(\frac{f}{f_*} \right)^{-1/3} \right) \right]. \end{aligned} \quad (5.273)$$

The Fourier transform of $h_+(t)$ and $h_\times(t)$ are computed in saddle point, just as in Problem 4.1. In the restricted PN approximation, the result is

$$\tilde{h}_+(f) = \left(\frac{5}{6} \right)^{1/2} \frac{1}{2\pi^{2/3}} \frac{c}{r} \left(\frac{GM_c}{c^3} \right)^{5/6} f^{-7/6} e^{i\Psi_+(f)} \frac{1 + \cos^2 \iota}{2}, \quad (5.274)$$

so it is the same as what we found in the Newtonian case in Problem 4.1, except that the phase Ψ_+ , which in the Newtonian case is given by eq. (4.37), now receives corrections. To 2PN order, written in terms of the parameters τ_0, \dots, τ_2 , it becomes⁶⁸

$$\Psi_+(f) = 2\pi f(t_c + r/c) - \Phi_0 - \frac{\pi}{4} + 2\pi f_* \left[\frac{3\tau_0}{5} \left(\frac{f}{f_*} \right)^{-5/3} \right.$$

⁶⁸See Poisson and Will (1995).

$$+ \tau_1 \left(\frac{f}{f_*} \right)^{-1} - \frac{3\tau_{1.5}}{2} \left(\frac{f}{f_*} \right)^{-2/3} + 3\tau_2 \left(\frac{f}{f_*} \right)^{-1/3} \Bigg], \quad (5.275)$$

while \tilde{h}_x is obtained from \tilde{h}_+ , by replacing $(1+\cos^2 \iota)/2$ by $\cos \iota$ and with $\Psi_x = \Psi_+ + (\pi/2)$. Observe that τ_0 depends on the masses only through the combination $M^{-5/3}\nu^{-1}$, which gives $M_c^{-5/3}$, and more generally all Newtonian results depend on the masses m_1 and m_2 of the two stars only through the chirp mass M_c . However, this degeneracy is broken by the PN correction, since the parameters τ_1 , etc. depend on different combinations of M and ν . Therefore, the masses m_1 and m_2 can now be separately determined by a comparison of the observed phase with the PN prediction.

Further reading

- The lowest-order post-Newtonian corrections to the gravitational field in the near region are discussed in many general relativity textbooks, see e.g. Chapter 9 of Weinberg (1972), Chapter 4 of Will (1993), or Section 5.2 of Straumann (2004). A review of the problem of motion in general relativity is given in Damour (1987).
- The form (5.72) of the Einstein equations was found by Landau and Lifshitz in the 1940s, see Landau and Lifshitz, Vol. II (1979), Section 96. In a iterative procedure, to lowest order the gravitational field $h^{\mu\nu}$ that appears in $\tau^{\alpha\beta}$ is set to zero, so $\tau^{\alpha\beta}$ reduces to the energy-momentum tensor of matter. Thus the Landau and Lifshitz derivation, see their Section 110, was the first which showed that the Einstein quadrupole formula is the correct lowest-order result even for weakly self-gravitating bodies (even if the problem of the finiteness of the higher-order corrections was addressed only later). Early attempt toward the construction of a systematic wave-generation formalism for post-Newtonian sources were performed by Epstein and Wagoner (1975), Wagoner and Will (1976) and Thorne (1980). In particular, in the latter paper are given general expressions for the GW fluxes in terms of radiative multipole moments at infinity. The DIRE approach builds on these earlier work, as well as on the works by Wiseman and Will (1991), Wiseman (1992, 1993), and has been developed in particular in Wiseman and Will (1996), Pati and Will (2000, 2002), and Will (2005).
- The method of matched asymptotic expansions was introduced in the radiation-reaction problem by Burke (1971). The back-reaction of GWs and its relation to the PN expansion is discussed in Chandrasekhar and Esposito (1970) (where references to earlier work can be found). Here the correct 2.5PN is obtained but, as we discussed below eq. (5.185), in this scheme higher-order terms were divergent. For the same reason, one could question also the validity of the result in the far region, i.e. the Einstein quadrupole formula, for self-gravitating systems. The unsatisfactory status of the derivations that were available at that time, for the back-reaction and for the Einstein quadrupole formula, was discussed by Ehlers, Rosenblum, Goldberg and Havas (1976). These criticisms stimulated a better understanding of the radiation reaction problem in general relativity and of the derivation of the quadrupole formula, see Walker and Will (1980a, 1980b), Damour and Deruelle (1981), and Damour (1983a, 1983b). A review of the “quadrupole formula controversy” (as well as of the various controversies to which GWs have been subject) is Kennefick (1997) and a very detailed and interesting historical account is given in the book Kennefick (2007). Nowadays, with the full development of the systematic and consistent expansion methods discussed in Sections 5.3 and 5.4, the problem of the validity of the

quadrupole formula for self-gravitating systems is settled.

- The Blanchet–Damour formalism has been developed in various papers. The general principles are discussed in Damour (1983b) and (1987). The structure of the fields in the post-Minkowskian expansion is studied in Blanchet and Damour (1986). The expansion of the fields at future null infinity and the relation to Thorne’s (1980) radiative moments is done in Blanchet (1987). The 1PN generation of GWs is computed in Blanchet and Damour (1989). The multipole expansion of the gravitational field in linearized gravity in terms of STF tensors is presented in Damour and Iyer (1991a). The 1PN expression for the spin moments is computed in Damour and Iyer (1991b), and the 2PN result for mass and current moments is obtained in Blanchet (1995), and applied to coalescing binaries in Blanchet, Damour and Iyer (1995). The 2.5PN result (where the moments W_L, \dots, Z_L start to mix with I_L, J_L) is computed in Blanchet (1996). The matching of the post-Newtonian and post-Minkowskian solutions is obtained in full generality in Blanchet (1995, 1998c). The determination of the PN expansion to all orders from the matching conditions is discussed in Blanchet (1993), Poujade and Blanchet (2002), and Blanchet, Faye and Nissanke (2005). A detailed review of the formalism, and its application to inspiraling binaries, is Blanchet (2006).
- Early investigations of tails and back-scattering in the gravitational radiation field were performed by Newman and Penrose (1968) and Bardeen and Press (1973). The tail integral was computed in Blanchet and Damour (1988), looking at the 4PN metric in the near-field zone. Its effect on the radiative moments at infinity (where it shows up as a 1.5PN correction) is computed in Blanchet and Damour (1992). In the DIRE approach, the tail integral is computed in Pati and Will (2000). The hereditary terms up to 3PN order are computed in Blanchet (1998a, 1998b). The possibility of detecting the tail contributions from the experimental data is discussed in Blanchet and Sathyaprakash (1995) and, for the memory terms, in Kennefick (1994).
- The initial value problem in general relativity, and the fact that initial data *inside* the light-cone are required, is discussed in Bruhat (1962). The non-linear memory effect has been found in Christodoulou (1991), using a mathematically rigorous study of Einstein equations at null infinity.

Its relation to a 2.5PN contribution is clarified in Wiseman and Will (1991), Blanchet and Damour (1992), and Arun, Blanchet, Iyer and Quasailah (2004).

The denomination “non-linear” memory effect is used to distinguish it from a linear memory effect which arises already in linearized theory, for instance in a scattering process, as a result of an overall change of the linear momentum of the bodies, see Zeldovich and Polnarev (1974), Braginsky and Grishchuk (1986) and Braginsky and Thorne (1987). The non-linear memory term can be understood as the linear memory term due to the linear momentum of the outgoing gravitons, see Thorne (1992).

- Important contributions to the 3PN dynamics have been obtained with a ADM-Hamiltonian formalism by Jaranowski and Schäfer (1998, 1999, 2000) and Damour, Jaranowski and Schäfer (2000, 2001a); and, with a direct PN iteration in harmonic coordinates, in Blanchet and Faye (2001) (equations of motion), de Andrade, Blanchet and Faye (2001) (Lagrangian and conserved quantities) and Blanchet and Iyer (2003) (reduction to center of mass). The complete determination of the dynamics of binary systems to 3PN is done in Damour, Jaranowski and Schäfer (2001b) and Blanchet, Damour and Esposito-Farese (2004), using dimensional regularization. Observe that, at 3PN order, one computes only the metric at the location of the particles. The metric at a generic space-time point admits a closed form only to 2.5PN order, and has been computed in Blanchet, Faye and Ponsot (1998). The 3PN equations have also been obtained with the surface integral method by Itoh, Futamase and Asada (2000, 2001), Itoh and Futamase (2003) and Itoh (2004). The results obtained with these different methods agree with each other.
- Beyond 1PN order a model of the source as point-like, i.e. in terms of Dirac deltas, gives rise to divergences, and need to be regularized. Hadamard and dimensional regularization are reviewed in Section 8 of Blanchet (2006). Dimensional regularization of point-like sources is introduced in Damour, Jaranowski and Schäfer (2001b) and further used in Blanchet, Damour, Esposito-Farèse and Iyer (2004, 2005). This method, based on analytic continuation in $d = 3 + \epsilon$ spatial dimensions, allows us to resolve some ambiguities that appear at 3PN in Hadamard regularization.

In the language of quantum field theory, a point-like singularity is an example of an ultraviolet di-

vergence, which reflects our ignorance of short-distance physics, and can be dealt with standard method from effective low-energy field theory. An approach of this type is discussed in Goldberger and Rothstein (2006).

- The surface integral method derives from the classic paper of Einstein, Infeld and Hoffmann (1938). Its application to the derivation of the quadrupole formula for strong-field sources is discussed in Damour (1983a, 1983b). A variant of this method has been developed by Itoh, Futamase, and Asada (2000, 2001), and used in Itoh and Futamase (2003) and Itoh (2004) to give a derivation of the 3PN equations of motion, valid for sources with strong internal gravity. The effacement of the internal structure in Newtonian gravity and in general relativity is discussed in detail in Damour (1987). A discussion of the fact that the tidal interaction between compact bodies shows up only to 5PN order even in the full relativistic theory can be found in Damour (1983b).
- Explicit formulas for the phase and waveform of a compact binary system can be found in Blanchet and Schäfer (1993), Wiseman (1993), Poisson and Will (1995), Blanchet, Iyer, Will and Wiseman (1996) and Blanchet (1996). The orbital phase to 3.5PN is computed in Blanchet, Faye, Iyer and Joguet (2002), based on the 3PN computation of the radiative moments in Blanchet, Iyer and Joguet (2002). The waveform to 2.5PN is computed in Arun, Blanchet, Iyer and Qusailah (2004). A summary of explicit formulas is given in the review Blanchet (2006).
- For compact binaries, the radiation reaction terms

up to 3.5PN order are computed (either with the energy balance argument or with explicit PN computations) in Iyer and Will (1993, 1995), Blanchet (1997), Pati and Will (2002), Konigsdorffer, Faye and Schäfer (2003), and Nissanke and Blanchet (2005). For non-spinning bodies, the 4.5PN back-reaction terms have been computed, from the energy balance argument, in Gopakumar, Iyer and Iyer (1997). For general PN sources, the balance equation has been checked explicitly to 1.5PN order (i.e. 4PN order in the near region metric) in Blanchet (1997).

- The inclusion of spin is discussed in Kidder, Will and Wiseman (1993), Apostolatos, Cutler, Sussman and Thorne (1994), Kidder (1995), Królik, Kokkotas and Schäfer (1995), and Tagoshi, Ohashi and Owen (2001), and has been completed to 2.5PN in Faye, Blanchet and Buonanno (2006) and Blanchet, Buonanno and Faye (2006).
- The effect of the eccentricity is computed in Gopakumar and Iyer (2002) and Damour, Gopakumar and Iyer (2004).
- In the limit in which one of the masses in the binary system tends to zero and becomes a test mass, while the other is a black hole, the computation of the motion in the PN expansion can be studied using linear perturbation of a black-hole space-time, see Poisson (1993). With this technique the PN expansion has been pushed up to the extremely high 5.5PN order by Sasaki (1994), Tagoshi and Sasaki (1994) and Tanaka, Tagoshi and Sasaki (1996). Up to 3.5PN order the result can be compared with the limit $\nu \rightarrow 0$ of the formulas presented in Section 5.6, and one finds complete agreement.

6

Experimental observation of GW emission in compact binaries

6.1 The Hulse–Taylor binary pulsar	302
6.2 The timing formula	305
6.3 The double pulsar, and more compact binaries	326

¹Pulsars are identified by the prefix PSR, followed by their equatorial coordinates (α, δ) . The right ascension α is measured in hours and minutes, $0 \leq \alpha < 24$ hr, while the declination $\delta \in [-90^\circ, +90^\circ]$ (see e.g. Binney and Merrifield (1998) for definitions). In PSR B1913+16, 1913 means that the right ascension is $\alpha = 19h13m$ and the declination is $\delta = +16^\circ$. If more precision is required, one uses, e.g. PSR B1913+167, which means that the declination is $\delta = +(16.7)^\circ$. If one use 1950 coordinates, the prefix B is added before the right ascension, while in 2000 coordinates the prefix J is used. The convention is that all pulsars published after 1993 retain only their J designation, while for the others both names can be used. The Hulse–Taylor pulsar can then be denoted as PSR B1913+16 as well as PSR J1915+1606. If various pulsars are very close to each other, they are designated appending a letter at the end; e.g. in the double pulsar system PSR J0737–3039, the two pulsars are identified as PSR J0737–3039A and PSR J0737–3039B. In the globular cluster 47 Tucanae there are 20 pulsars so close together, that they are denoted by PSR J0021–72C, PSR J0021–72D, etc. (see the ATNF pulsar catalogue).

In this chapter we discuss the experimental evidence for the existence of GWs, which has been first obtained from the Hulse–Taylor binary pulsar, PSR B1913+16, and which is by now further confirmed by observations in other relativistic binary systems. As we will see, these binary pulsars turn out to be remarkable laboratories, that allow us to verify with high precision various predictions of general relativity.

Hulse and Taylor were awarded the Nobel Prize in 1993, “for the discovery of a new type of pulsar, a discovery that has opened up new possibilities for the study of gravitation”, including the demonstration of the emission of gravitational radiation, obtained by Taylor and coworkers in the late 1970s and early 1980s.

6.1 The Hulse–Taylor binary pulsar

The pulsar PSR B1913+16,¹ or Hulse–Taylor binary pulsar, was first detected in July 1974, during a systematic survey for new pulsars carried out at the Arecibo Observatory in Puerto Rico. It was detected as a pulsar with a period $P \simeq 59$ ms. The period however had apparent changes up to $\sim 80 \mu s$ from day to day. For comparison, the largest secular changes in period, for pulsars, were known to be of order $10 \mu s$ per year. It soon became clear that the observed changes in period were due to the Doppler shift resulting from the orbital motion of the pulsar around a companion, and by September 1974 an accurate velocity curve had been obtained (Hulse and Taylor, 1975).

Nowadays, after about 30 years of observation, this binary system is known extraordinarily well. To have an idea of the impressive precision, we report in Table 6.1 the measured values of the orbital parameters, with their experimental error. Observe in particular that the orbital period P_b of the binary is less than 8 hours. This means that the orbital velocity is of order $v \sim 10^{-3}c$. Thus, this system is quite relativistic.

The geometry of the system is illustrated in Fig. 6.1. The relative coordinate between the pulsar and its companion, $\mathbf{r} = \mathbf{r}_p - \mathbf{r}_c$, describes an ellipse of eccentricity e , whose normal makes an angle ι with respect to the line of sight, which we take to be the z axis. The orbit intersects

Table 6.1 The orbital parameters of PSR B1913+16. a_p is the semimajor axis of the pulsar orbit and ι the inclination of the orbit with respect to the line of sight; e is the eccentricity; T_0 is a time of passage at periastron (in Mean Julian Day), used as a reference epoch; P_b is the binary orbital period, at the reference epoch; ω_0 is the angle made by the periastron, measured from the ascending node, at the reference epoch; $\langle \dot{\omega} \rangle$ is the advance rate of the periastron, averaged over one orbital period; γ is the Einstein parameter (see below); \dot{P}_b is the time derivative of the orbital period. The number in parentheses is the error on the last digit. From Weisberg and Taylor (2004).

Parameter	Value
$(1/c)a_p \sin \iota$ (s)	2.3417725(8)
e	0.6171338(4)
T_0 (MJD)	52144.90097844(5)
P_b (days)	0.322997448930(4)
ω_0 (deg)	292.54487(8)
$\langle \dot{\omega} \rangle$ (deg/yr)	4.226595(5)
γ (s)	0.0042919(8)
\dot{P}_b	$-2.4184(9) \times 10^{-12}$

the (x, y) plane in two points, or ‘‘nodes’’. The line connecting these two points is called the line of nodes. The node at which the coordinate \mathbf{r} enters from below the upper hemisphere is called the ascending node. The angular position of the periastron, measured from the ascending node, is denoted by ω .²

Another very interesting value from Table 6.1 is that of the advance of the periastron, $\dot{\omega}$, which is more than 4 degrees per year. By comparison, the advance of the periastron of Mercury, which is one of the classical tests of general relativity, is 43 arcsec per century. This shows how general-relativistic effects are important in this binary system.

In the next section we will discuss in detail how, from the analysis of the time of arrivals of the pulses, one can extract very rich information and perform accurate tests of general relativity, including the verification of the emission of gravitational radiation. Here we summarize the main results that will be derived below.

From the measured value of $\langle \dot{\omega} \rangle$ and of the Einstein parameter γ we can obtain the masses of the pulsar, m_p , and of its companion, m_c . The result is (Weisberg and Taylor 2004)

$$m_p = 1.4414(2) M_\odot, \quad m_c = 1.3867(2) M_\odot. \quad (6.1)$$

Again, the precision of these determinations is quite remarkable. (When inserting the numerical values, it is useful to recall that the quantity GM_\odot is known to much better precision than G and M_\odot separately.) The semimajor axis a is then determined by the usual Keplerian expres-

²In this chapter we will follow the notation which is commonly used in the pulsar literature. In particular the letter ω , that in the rest of the book denotes an angular velocity, here is the periastron angle; we will also use P to denote the spinning period of the pulsar, $\nu = 1/P$ its frequency, and P_b the orbital period of the binary system.

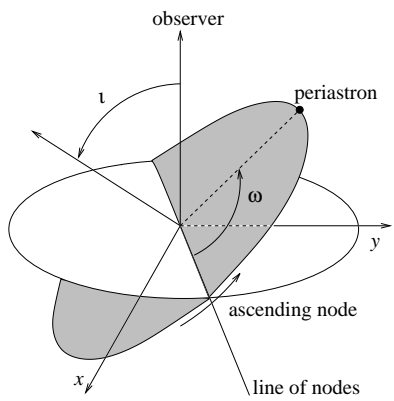


Fig. 6.1 The geometry of the orbit. The plane of the orbit is in gray.

sion

$$a = [G(m_p + m_c)]^{1/3} \left(\frac{P_b}{2\pi} \right)^{2/3}, \quad (6.2)$$

which gives $a \simeq 2.2 \times 10^9$ m; for comparison, the solar radius is $R_\odot \simeq 7 \times 10^8$ m, so the semimajor axis of the orbit is only about $3R_\odot$. This compactness of the orbit, together with the fact that no eclipse is seen, implies that the companion must be a compact star, i.e. a NS or a BH. This is very important for the following analysis, since it means that the dynamics of the binary system can be studied treating the two stars as pointlike bodies, ignoring for instance tidal effects. Thus, we have a very clean system. Actually, the value of m_c found above is the typical value expected for a NS, so it is believed that the companion is a NS.

The semimajor axis of the pulsar orbit, a_p , and of its companion, a_c , can now be obtained from

$$a_p = a \frac{m_c}{m_p + m_c}, \quad a_c = a \frac{m_p}{m_p + m_c}. \quad (6.3)$$

Having a_p , from the measured value of $a_p \sin \iota$ given in Table 6.1 we also get the inclination angle, $\sin \iota \simeq 0.72$. Finally, having the masses of the two stars and the eccentricity, general relativity predicts that the orbital period decreases because of GW emission. We first computed this effect within linearized theory using an energy balance argument, and we found (eq. (4.79), with the present change in notation $T \rightarrow P_b$)

$$\begin{aligned} \dot{P}_b = & -\frac{192\pi G^{5/3}}{5c^5} m_p m_c (m_p + m_c)^{-1/3} \left(\frac{P_b}{2\pi} \right)^{-5/3} \\ & \times \frac{1}{(1-e^2)^{7/2}} \left(1 + \frac{73}{24} e^2 + \frac{37}{96} e^4 \right). \end{aligned} \quad (6.4)$$

However, as we discussed in Section 5.3.5, this result can also be obtained *directly* from the post-Newtonian equations of motion of the binary system, using the formalism discussed in Sections 5.2–5.4, without invoking the energy balance argument. Furthermore, we have seen in Section 5.5 that this result applies even in the presence of strong gravitational fields, which is indeed the case for neutron stars.

We can therefore compare the value predicted by general relativity, and due to the emission of GW radiation, with the observed value given in Table 6.1. After including a Doppler correction due to the relative velocity between us and the pulsar induced by the differential rotation of the Galaxy, one finds that the ratio between the experimental value $(\dot{P}_b)_{\text{exp}}$ and the value $(\dot{P}_b)_{\text{GR}}$ predicted by general relativity is

$$(\dot{P}_b)_{\text{corrected}} / (\dot{P}_b)_{\text{GR}} = 1.0013(21). \quad (6.5)$$

This provides a wonderful confirmation of general relativity, as well as of the existence of GWs. In the next section we will discuss how these results are extracted from the timing residuals of the pulsar.

Beside its obvious intrinsic interest, the techniques used to correct the pulsar signal for various effects, due both to the motion of the Earth

and to intrinsic changes in the source, will also be very important when searching for periodic GWs emitted from pulsars, as we will discuss in Section 7.6, so we will examine the timing formula in some detail.

6.2 The pulsar timing formula

6.2.1 Pulsars as stable clocks

Neutron stars are rapidly spinning, with rotational periods as small as 1.5 ms. This is a consequence of the conservation of angular momentum during the collapse, since ωr^2 stays constant while r decreases from the typical stellar size of the original star core down to a radius of just 10 km. It is thought that the supernova collapse can spin them up to maybe 10 ms. Neutron stars in binary system can be further spin up by accretion of mass from the companion. Similarly, because of the conservation of the magnetic flux during the collapse, neutron stars have huge magnetic fields, as large as 10^{12} gauss and higher (however, the accretion process in binaries tends to decrease the field somewhat). The magnetic field is in general misaligned with the rotation axis, so it has the structure of a rotating dipole, as in Fig. 6.2. If ρ denotes the distance from the rotation axis in cylindrical coordinates, there is a critical distance $\rho_c = c/\Omega$ (where Ω is the angular velocity of the pulsar) such that the magnetic field lines that reach a distance $\rho > \rho_c$ are open and escape to infinity, while those contained within ρ_c are closed. Observe that ρ_c is the maximum distance at which an object can corotate with the pulsar, without exceeding the speed of light.

Inside this cylinder of radius ρ_c there is a “magnetosphere” made of an ionized high-energy plasma, mostly corotating with the neutron star. High-energy particles in the magnetosphere are constrained to move along the open field lines over the magnetic poles, and emit radiation, most easily observed in the radio waves, narrowly focused in the direction of the magnetic poles, so each beam sweeps a circle in the sky. An observer that happens to be along one point of this circle therefore receives a short radio pulse when the beam of radiation sweeps along her line of sight, much like from a lighthouse, and the periodicity of the pulse is equal to the rotational period of the neutron star. Given the huge value of the moment of inertia of a NS, of order 10^{45} gr cm², we can understand that the pulse period can be extremely stable.

Actually, if one observes single pulses from a given pulsar, one finds that each pulse has its own profile, which can vary dramatically, reflecting fluctuations in the radiation mechanism related to the complex dynamics of the magnetosphere. However, if one performs a coherent addition of many pulses, it usually emerges a single profile, which is a fingerprint of each pulsar, and which stays remarkably stable over time. This averaged profile is then used as a template, and the times-of-arrival (TOAs) of the individual pulses are then obtained by a least square fit.³ As a result, for the Hulse–Taylor binary pulsar most of the data taken after 1981 have an uncertainty on the TOAs of about 20 μ s or less. This

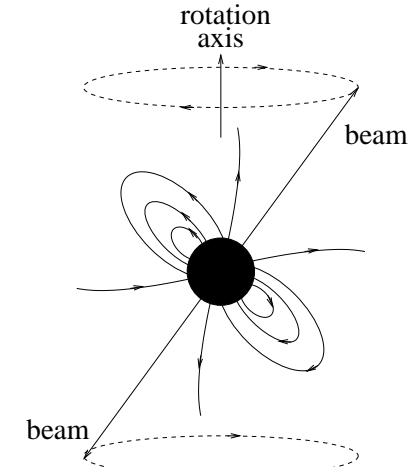


Fig. 6.2 The pulsar magnetosphere and the outgoing beams of radiation.

³In many cases (including the Hulse–Taylor binary pulsar) individual pulses are too weak to be detected. Then, one first forms an average over a few minutes of data, until it emerges a profile with a signal-to-noise ratio sufficiently large to be detectable. For the Hulse–Taylor binary pulsar this is performed integrating over about 5 minutes of data, which is a duration small enough compared to the orbital period, so the signal still refers to a localized position of the pulsar along its orbit and the modulation effects that we will discuss below are unimportant, but still is large enough so that a detectable signal emerges. The average over many blocks gives the standard profile used as a template. Matching the template against the average profile of each block gives an arrival time for a pulse near the middle of each block (see Taylor and Weisberg 1982).

precision is so good that it is possible to assign unambiguously a pulse number to each pulse, even after long periods in which observations have not been made; in particular, the Arecibo telescope was closed, for major upgrades, for various years in the mid 1990s, and still we know exactly how many pulses elapsed during that time, until observations resumed. This is quite remarkable if we consider that, with a rotation period of 59 ms, in one year there are about 5×10^8 pulses! It is this stability of the integrated profile that allows pulsars to be extraordinarily accurate clocks.

Even if a pulsars were, intrinsically, a perfect clock, the TOAs of the pulses in a earthbound laboratory will still be modulated by a number of time-dependent factors, due to the motion of the Earth around the Sun (and of the Sun around the solar system barycenter) and also by general-relativistic effects due to the gravitational field of the solar system. Furthermore, if a pulsar is a member of a binary system, the pulses will be similarly modulated by the motion of the pulsar around its companion, and by the strong gravitational fields of the two stars. These timing residuals, i.e. these modulations of the TOAs with respect to a perfectly periodic pattern, are a rich source of information, because they can be computed and depend on parameters of the binary system, such as the masses of the two stars, and therefore the measurement of the timing residual can allow us to determine these parameters. In the next subsections we will see how to compute this “timing formula”, which takes into account all relevant corrections.

6.2.2 Roemer, Shapiro and Einstein time delays

We consider a pulsar that emits a sequence of pulses, and we discuss first how the time of arrival of these pulses is modified by the motion of the Earth, and by the effect of the gravitational field of the solar system on electromagnetic waves. We will then see how these time of arrivals are affected if the pulsar is member of a binary system. Following a nomenclature originally introduced by Damour and Deruelle, we will split the corrections into three separate contributions, the Roemer, Shapiro and Einstein time delays.

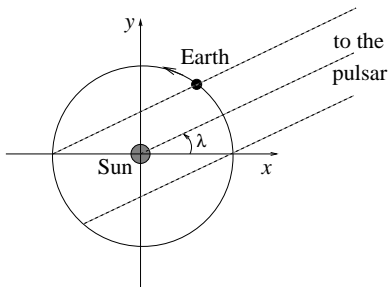


Fig. 6.3 The (x, y) plane is the plane of the orbit of the Earth around the Sun. The angle λ is the ecliptic longitude of the pulsar.

Roemer time delay

Since light takes about 500 s to travel from the Sun to the Earth, there is an annual modulation of the time of arrivals. For instance, for a pulsar which is lying in the plane of the ecliptic, at ecliptic longitude λ , we see from Fig. 6.3 that this modulation is $\Delta_{R,\odot} = t_0 \cos(\Omega t - \lambda)$, where Ω is the angular velocity of the Earth around the Sun, t_0 is the travel time from the Sun to the Earth, and for simplicity we assumed a circular orbit. So, when the Earth is in the direction of the pulsar, $\Omega t - \lambda = 0$, the pulse arrives earlier, by an amount t_0 , and when it is on the opposite side of the orbit, $\Omega t - \lambda = \pi$, it arrives later by an amount t_0 , with respect to the arrival time at the Sun. This is called the Roemer time

delay.⁴ The subscript R in $\Delta_{R,\odot}$ stands for Roemer, while \odot reminds that this is a correction due to the motion of the observer, in the Solar System, and not to the intrinsic motion of the source.

If, rather than lying on the plane of the ecliptic, the pulsar has an ecliptic latitude β , the modulation is instead

$$\Delta_{R,\odot} = t_0 \cos(\Omega t - \lambda) \cos \beta. \quad (6.6)$$

Its amplitude is maximum for pulsars in the ecliptic plane, $\cos \beta = 0$, and vanishes for pulsars in the direction of the poles of the ecliptic. A variation $\delta\lambda, \delta\beta$ in the angles induces a variation of $\Delta_{R,\odot}$, given by

$$\delta(\Delta_{R,\odot}) = t_0 \delta\lambda \sin(\Omega t - \lambda) \cos \beta - t_0 \delta\beta \cos(\Omega t - \lambda) \sin \beta. \quad (6.7)$$

With a resolution $\delta t = 0.2$ ms on the arrival times of the pulses, and taking for definiteness an average angle $\beta \sim 45^\circ$, so $\sin \beta = \cos \beta = 1/\sqrt{2}$, we get an accuracy on the angles of order $\delta\lambda \sim \delta\beta \sim \sqrt{2}\delta t/t_0 \sim 5.6 \times 10^{-7}$ rad $\simeq 0.1$ arcsec. Such an accuracy can be sufficient to search for an optical counterpart. This is an example of the fact that the modulation of the originally periodic signal contains very useful information.

Actually, for pulsar timing we will need in general a better precision, so the orbit of the Earth cannot be approximated as circular. We must also take into account the rotation of the Earth around its axis, which for an Earth-bound laboratory introduces a daily modulation with an amplitude $R_\oplus/c \simeq 21$ ms, and we must even include the motion of the Sun around the solar system barycenter (which is determined primarily by the influence of Jupiter on the Sun, so that the solar system barycenter lies just outside the surface of the Sun). The most practical way to take into account these corrections is to refer all arrival times to the solar system barycenter (SSB). Let \mathbf{r}_{oe} be the vector from the observer to the center of the Earth, \mathbf{r}_{es} from the center of the Earth to the center of the Sun, and \mathbf{r}_{sb} from the center of the Sun to the SSB. Then the distance from the observer to the SSB is $\mathbf{r}_{ob} = \mathbf{r}_{oe} + \mathbf{r}_{es} + \mathbf{r}_{sb}$ and, to obtain the barycentric times of arrival, we must add to the times observed in the laboratory the quantity

$$\Delta_{R,\odot} = -\mathbf{r}_{ob} \cdot \hat{\mathbf{n}}/c, \quad (6.8)$$

where $\hat{\mathbf{n}}$ is the unit vector from the SSB to the pulsar. The vectors \mathbf{r}_{oe} , \mathbf{r}_{es} and \mathbf{r}_{sb} are known with sufficient accuracy (for \mathbf{r}_{es} it is also necessary to include the motion of the barycenter of the Earth–Moon system), so we can get $\hat{\mathbf{n}}$ from a measure of $\Delta_{R,\odot}$.

It should be remarked that the barycentric time of arrival so obtained are just a useful, but fictitious, intermediate quantity in our computation. The real time of arrival of the pulses at the SSB is also affected by other effects, such as the propagation of light in the gravitational field of the solar system and its interaction with the interstellar medium, as we will discuss below.

⁴After the Danish astronomer Ole Roemer who, in 1675, from the observation of Jupiter's moons, formulated the hypothesis that light travels at a finite speed. At that time the four largest moons of Jupiter were first observed when Jupiter is “in opposition”, i.e. when the Earth passes between Jupiter and the Sun, since then Jupiter is high in the night sky and therefore easier to observe, and the times of the eclipses and passages (i.e. the passings of the moons behind and in front of Jupiter) could be predicted precisely. Later the moons of Jupiter were observed when the Earth was on the opposite side of the Sun from Jupiter, and it was found that the eclipses were consistently late by about 20 minutes. This led Roemer to the hypothesis that light propagates at a finite speed. His estimate for the speed of light was 214 000 km/s.

Shapiro time delay

The above computation of the Roemer delay neglected the general-relativistic effects of the gravitational field of the solar system on the propagation of light. To take it into account we recall, from eq. (5.11), that the space-time interval generated by a weak and nearly static Newtonian source can be written, to linear order in the metric perturbation ϕ , as

$$ds^2 = -[1 + 2\phi(\mathbf{x})]c^2dt^2 + [1 - 2\phi(\mathbf{x})]d\mathbf{x}^2. \quad (6.9)$$

In the solar system, $|\phi(\mathbf{x})|$ is at most of order 10^{-6} , and the weak-field approximation is excellent. Photons travel along the light-like geodesic $ds^2 = 0$, so to lowest order in ϕ ,

$$cdt = \pm[1 - 2\phi(\mathbf{x})]|d\mathbf{x}|. \quad (6.10)$$

If we denote by \mathbf{r}_p the (fixed) position of the pulsar, and by \mathbf{r}_{obs} the position of the observer at the arrival time t_{obs} , then the *coordinate* time difference, between the arrival time t_{obs} at the observer and the emission time at the pulsar t_e is

$$\begin{aligned} c(t_{\text{obs}} - t_e) &= \int_{\mathbf{r}_{\text{obs}}}^{\mathbf{r}_p} |d\mathbf{x}| [1 - 2\phi(\mathbf{x})] \\ &= |\mathbf{r}_p - \mathbf{r}_{\text{obs}}| - 2 \int_{\mathbf{r}_{\text{obs}}}^{\mathbf{r}_p} |d\mathbf{x}| \phi(\mathbf{x}). \end{aligned} \quad (6.11)$$

We write

$$\begin{aligned} |\mathbf{r}_p - \mathbf{r}_{\text{obs}}| &= |(\mathbf{r}_p - \mathbf{r}_b) + (\mathbf{r}_b - \mathbf{r}_{\text{obs}})| \\ &\simeq |\mathbf{r}_p - \mathbf{r}_b| + (\mathbf{r}_b - \mathbf{r}_{\text{obs}}) \cdot \hat{\mathbf{n}}, \end{aligned} \quad (6.12)$$

where \mathbf{r}_b is the position of the SSB, $\hat{\mathbf{n}}$ is the unit vector from the SSB to the pulsar, i.e. $\hat{\mathbf{n}} = (\mathbf{r}_p - \mathbf{r}_b)/|\mathbf{r}_p - \mathbf{r}_b|$, and the expansion in the second line is valid because $|\mathbf{r}_p - \mathbf{r}_b| \gg |\mathbf{r}_b - \mathbf{r}_{\text{obs}}|$. Therefore, denoting $\mathbf{r}_b - \mathbf{r}_{\text{obs}} \equiv \mathbf{r}_{\text{ob}}$,

$$t_{\text{obs}} \simeq \left(t_e + \frac{1}{c} |\mathbf{r}_p - \mathbf{r}_b| \right) + \frac{1}{c} \mathbf{r}_{\text{ob}} \cdot \hat{\mathbf{n}} - \frac{2}{c} \int_{\mathbf{r}_{\text{obs}}}^{\mathbf{r}_p} |d\mathbf{x}| \phi(\mathbf{x}). \quad (6.13)$$

The term $t_e + |\mathbf{r}_p - \mathbf{r}_b|/c$ is the barycentric time of arrival, t_{SSB} , defined as the (fictitious) time at which the pulse would arrive at the SSB if there were no effect of the gravity of the solar system. Then we get

$$t_{\text{SSB}} = t_{\text{obs}} - \frac{1}{c} \mathbf{r}_{\text{ob}} \cdot \hat{\mathbf{n}} + \frac{2}{c} \int_{\mathbf{r}_{\text{obs}}}^{\mathbf{r}_p} |d\mathbf{x}| \phi(\mathbf{x}). \quad (6.14)$$

The first correction is just the Roemer time delay that we already found in eq. (6.8). The second term, which takes into account the effect on light propagation due to the gravitational potential of the solar system, is called (minus) the solar system Shapiro time delay,

$$\Delta_{S,\odot} = -\frac{2}{c} \int_{\mathbf{r}_{\text{obs}}}^{\mathbf{r}_p} |d\mathbf{x}| \phi(\mathbf{x}), \quad (6.15)$$

so

$$t_{\text{SSB}} = t_{\text{obs}} + \Delta_{R,\odot} - \Delta_{S,\odot}. \quad (6.16)$$

The Shapiro time delay is dominated by the gravitational field of the Sun. To compute it, we consider a photon emitted by the pulsar, which reaches the observer on the Earth when the pulsar–Sun–Earth angle has the value θ , see Fig. 6.4. Let P be a generic point on the straight-line trajectory made by the photon, and denote by ρ the distance of P from the Earth and by r its distance from the Sun. If $r_{\text{es}} = 1 \text{ au}$ is the distance between the Earth and the Sun, we see from the figure that

$$r^2 = (r_{\text{es}} + \rho \cos \theta)^2 + (\rho \sin \theta)^2, \quad (6.17)$$

i.e.

$$r = r_{\text{es}}(u^2 + 1 + 2u \cos \theta)^{1/2}, \quad (6.18)$$

where $u = \rho/r_{\text{es}}$. Since $\phi = (1/c^2)(-GM_{\odot}/r)$, we have

$$\begin{aligned} \Delta_{S,\odot} &= \frac{2GM_{\odot}}{c^3} \int_0^d \frac{d\rho}{r} \\ &= \frac{2GM_{\odot}}{c^3} \int_0^{\bar{u}} \frac{du}{(u^2 + 1 + 2u \cos \theta)^{1/2}}, \end{aligned} \quad (6.19)$$

where $\bar{u} = d/r_{\text{es}}$, and d is the Earth–pulsar distance. It is convenient to add and subtract the delay at a given angle, say when $\cos \theta = 0$, so

$$\begin{aligned} \Delta_{S,\odot} &= \frac{2GM_{\odot}}{c^3} \int_0^{\bar{u}} \frac{du}{(u^2 + 1)^{1/2}} \\ &\quad + \frac{2GM_{\odot}}{c^3} \int_0^{\bar{u}} du \left[\frac{1}{(u^2 + 1 + 2u \cos \theta)^{1/2}} - \frac{1}{(u^2 + 1)^{1/2}} \right]. \end{aligned} \quad (6.20)$$

The term in the first line is a fixed quantity which, for d/r_{es} large, grows logarithmically,

$$\begin{aligned} \frac{2GM_{\odot}}{c^3} \int_0^{\bar{u}} \frac{du}{(u^2 + 1)^{1/2}} &= \frac{2GM_{\odot}}{c^3} \operatorname{arcsinh}(\bar{u}) \\ &\simeq \frac{2GM_{\odot}}{c^3} \log(2d/r_{\text{es}}). \end{aligned} \quad (6.21)$$

This is a constant shift that simply adds up to the total travel time from the pulsar to the SSB. The term in the second line is more interesting from our purposes, since it depends on θ , and therefore on the position of the Earth in its orbit around the SSB. In the integral in the second line of eq. (6.20) we can take the limit $\bar{u} = d/r_{\text{es}} \rightarrow \infty$. The integral converges and gives

$$\int_0^{\infty} du \left[\frac{1}{(u^2 + 1 + 2u \cos \theta)^{1/2}} - \frac{1}{(u^2 + 1)^{1/2}} \right] = -\log(1 + \cos \theta). \quad (6.22)$$

Thus, we get

$$\Delta_{S,\odot} = \frac{2GM_{\odot}}{c^3} \log \left(\frac{2d}{r_{\text{es}}} \right) - \frac{2GM_{\odot}}{c^3} \log(1 + \cos \theta). \quad (6.23)$$

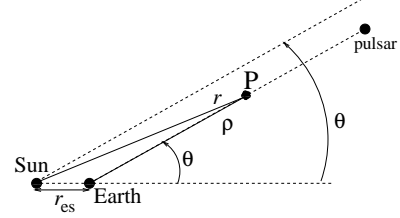


Fig. 6.4 The geometry for the computation of the Shapiro delay discussed in the text.

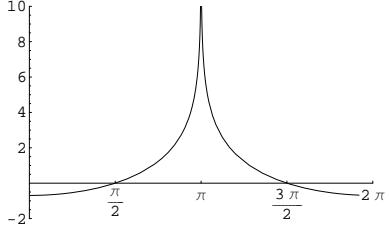


Fig. 6.5 The function $f(\theta) = -\log(1 + \cos \theta)$, against θ .

A plot of the function $-\log(1 + \cos \theta)$ is shown in Fig. 6.5. Observe that $\Delta_{S,\odot}$ formally diverges when $\theta = \pi$, that is, when the signal crosses the center of the Sun before reaching the Earth. However, of course, this divergence is fictitious, first of all because in this case the signal is simply absorbed by the Sun and second, because the Newtonian potential of the Sun is $-GM/r$ only outside the Sun, so the result is valid only for photons that at most graze the surface of the Sun.

Recalling that $2GM_\odot/c^2 \equiv R_{S,\odot} \simeq 3$ km is the Schwarzschild radius of the Sun, we see that the time-scale of the solar system Shapiro delay is given by the time that light takes to go across a distance $R_{S,\odot}$, that is, about $10\ \mu\text{s}$, which however is multiplied by large logarithmic factors. In particular, for a pulse which is just grazing the surface of the Sun, $\theta = \theta_{\text{grazing}} \simeq \pi - (R_\odot/r_{\text{es}})$, so $1 + \cos \theta \simeq (1/2)(R_\odot/r_{\text{es}})^2$. Then the maximum modulation induced by the Shapiro delay, i.e. the difference between its value for a pulse which is just grazing the Sun and its value at $\theta = 0$ is

$$\begin{aligned}\Delta_{S,\odot}(\theta = \theta_{\text{grazing}}) - \Delta_{S,\odot}(\theta = 0) &= \frac{4GM_\odot}{c^3} \log \frac{2r_{\text{es}}}{R_\odot} \\ &\simeq 119.5\ \mu\text{s}.\end{aligned}\quad (6.24)$$

It is also useful to rewrite eq. (6.23) as

$$\Delta_{S,\odot} = \frac{2GM_\odot}{c^3} \left[\log \left(\frac{d}{r_{\text{es}}} \right) - \log \left(\frac{1 + \cos \theta}{2} \right) \right], \quad (6.25)$$

which stresses that $\Delta_{S,\odot}$ is the sum of two positive terms, given that $0 \leq (1 + \cos \theta)/2 \leq 1$, and therefore its logarithm is negative. Therefore, $\Delta_{S,\odot} > 0$ for all values of θ . Since eq. (6.16) gives $t_{\text{obs}} = (t_{\text{SSB}} - \Delta_{R,\odot}) + \Delta_{S,\odot}$, we see that a positive $\Delta_{S,\odot}$ produces a *delay* in the time at which the pulse arrives at the observer (or at the SSB). This is physically correct, since the radio wave is delayed by the fact that it goes into the “potential well” in space-time generated by the presence of the Sun.

Einstein time delay

The Roemer and Shapiro time delays that we have computed are shifts in the *coordinate* time t . However, this is not the same as the time recorded by a clock in a laboratory. A laboratory clock located at a position \mathbf{x}_{obs} rather measures its own *proper* time τ , which in the metric (6.9) is related to t by

$$c^2 d\tau^2 = [1 + 2\phi(\mathbf{x}_{\text{obs}})] c^2 dt^2 - [1 - 2\phi(\mathbf{x}_{\text{obs}})] d\mathbf{x}_{\text{obs}}^2, \quad (6.26)$$

so, to first order in the small parameters $\phi(\mathbf{x}_{\text{obs}})$ and $\mathbf{v}_{\text{obs}} = d\mathbf{x}_{\text{obs}}/dt$, we have

$$\frac{d\tau}{dt} \simeq 1 + \phi(\mathbf{x}_{\text{obs}}) - \frac{v_{\text{obs}}^2}{2c^2}. \quad (6.27)$$

Physically, the term $(-1/2)v_{\text{obs}}^2/c^2$ gives the transverse Doppler shift, while ϕ gives the gravitational redshift. Integrating, we get

$$\tau \simeq t + \int^t dt' \left[\phi(\mathbf{x}_{\text{obs}}(t')) - \frac{v_{\text{obs}}^2(t')}{2c^2} \right], \quad (6.28)$$

where the lower limit of the integral is arbitrary, since it corresponds to an arbitrary constant shift in the origin of τ . We can rewrite this as

$$t \simeq \tau + \Delta_{E\odot}, \quad (6.29)$$

where

$$\Delta_{E\odot} = \int^t dt' \left[\frac{v_{\text{obs}}^2(t')}{2c^2} - \phi(\mathbf{x}_{\text{obs}}(t')) \right]. \quad (6.30)$$

This is called the Einstein time delay. The dominant effect on v_{obs} comes from the motion of the Earth around the Sun, with velocity v_{\oplus} , and the rotation of the Earth around its axis gives a small correction, so we write $v_{\text{obs}} \simeq v_{\oplus}$. We take the Earth in an elliptic orbit around the Sun, with semimajor axis a . Recall from eq. (4.53) that in a Keplerian orbit the total kinetic plus potential energy of the Earth–Sun system is related to the semimajor axis a by

$$E = -\frac{GM\mu}{2a}, \quad (6.31)$$

where μ is the reduced mass of the Earth–Sun system (i.e. the Earth mass, with excellent accuracy) and M the total mass (i.e. $M \simeq M_{\odot}$, with excellent accuracy). Since, on the other hand,

$$E = \frac{1}{2}\mu v_{\oplus}^2 - \frac{GM\mu}{r}, \quad (6.32)$$

we have

$$\frac{1}{2}v_{\oplus}^2 = \frac{GM_{\odot}}{r} - \frac{GM_{\odot}}{2a}, \quad (6.33)$$

and

$$\begin{aligned} \frac{d\Delta_{E\odot}}{dt} &\simeq \frac{v_{\oplus}^2}{2c^2} - \phi \\ &= \frac{2GM_{\odot}}{c^2} \left(\frac{1}{r} - \frac{1}{4a} \right). \end{aligned} \quad (6.34)$$

A constant part in this expression is incorporated in the definition of atomic time, which is defined as the time measured by an atomic clock at a fixed distance a from the Sun. The dependence on r however introduces a modulation, due to the ellipticity of the Earth orbit.

Dispersion in the interstellar medium

Beside the Roemer, Shapiro and Einstein delays, which are due to the motion of the observer and to the gravitational field of the solar system, there is also a correction to the arrival times which is due to the propagation of the radio waves through the ionized interstellar gas, which effectively acts as a medium with a refraction index appreciably different from unity, and with an important frequency dependence. As a result, the component of the radio pulse with frequency ν travels with a group velocity v_g given by

$$v_g \simeq c \left(1 - \frac{n_e e^2}{2\pi m_e} \frac{1}{\nu^2} \right), \quad (6.35)$$

where e and m_e are the charge and the mass of the electron, and n_e is the electron number density. The travel time over a distance L is therefore

$$\int_0^L \frac{dl}{v_g} \simeq \frac{L}{c} + \frac{1}{\nu^2} \left(\frac{e^2}{2\pi m_e c} \right) \int_0^L n_e dl. \quad (6.36)$$

The quantity

$$\text{DM} \equiv \int_0^L n_e dl \quad (6.37)$$

is called the dispersion measure, and is typically quoted in cm^{-3} pc. Measuring the TOAs at different frequencies, we can get the dispersion measure, and we can correct for this effect. This procedure, known as de-dispersion, is performed separating the useful bandwidth of the receiver into many channels, such that in each channel the effect of dispersion is negligible. The output of the channels operating at different frequencies is then automatically corrected and superimposed, in order to enhance the signal-to-noise ratio.

To have an idea of the size of the effect, we observe that the Hulse–Taylor binary pulsar has a (relatively large) dispersion measure $\text{DM} \simeq 169 \text{ cm}^{-3}$ pc. The measurements at Arecibo which led to its discovery were performed near 430 MHz. In the typical 4 MHz bandwidth around 430 MHz, this value of DM produces a spreading of the pulse of about 70 ms, which is larger than the intrinsic period of the pulsar of 59 ms, and the signal would then be unobservable. Thus, de-dispersion is a crucial part of pulsar observations. If one is performing a search for unknown pulsars, the value of DM is an unknown parameter, and the data are de-dispersed with various possible values of DM within a plausible range, i.e. DM becomes one of the dimensions of the parameter space in which data analysis is performed.

Relation to the intrinsic pulsar signal

We can now put together all these corrections. Since they are small, we can simply add them up linearly (e.g. the effect of the Einstein time delay on the Shapiro delay is totally negligible). Equation (6.30) shows that the time τ_{obs} actually measured by a clock in a laboratory (i.e. its proper time) is related to the coordinate time t_{obs} by $t_{\text{obs}} = \tau_{\text{obs}} + \Delta_{E\odot}$, which, combined with eq. (6.16), gives

$$t_{\text{SSB}} = \tau_{\text{obs}} + \Delta_{E\odot} + \Delta_{R,\odot} - \Delta_{S,\odot}. \quad (6.38)$$

From this, we must still subtract the time delay due to the interaction with the interstellar medium, given in eq. (6.36), so we write

$$t_{\text{SSB}} = \tau_{\text{obs}} - \frac{D}{\nu^2} + \Delta_{E\odot} + \Delta_{R,\odot} - \Delta_{S,\odot}, \quad (6.39)$$

where

$$D = \left(\frac{e^2}{2\pi m_e c} \right) \text{DM}. \quad (6.40)$$

The quantity t_{SSB} so obtained is the coordinate time at which the signal recorded by our laboratory clock at τ_{obs} would have arrived at a fixed point in space such as the solar system barycenter, if there were no effect due to the gravitational potential of the solar system, and no interaction with the interstellar medium. It therefore depends only on the intrinsic properties of the source.

The emission mechanism of the pulsar is not yet completely understood, but in any case is believed to be related to some “hot spot” corotating with the pulsar. If we denote by Φ the accumulated phase of the spinning pulsar, and we neglect for the moment any proper motion of the pulsar, we see a pulse whenever the phase Φ goes back to the same value Φ_0 , mod 2π , at which the radiated beam sweeps across the Earth. If we denote by T the proper time in the pulsar frame, for a perfectly periodic pulsar, spinning with frequency ν , we would have $\Phi = 2\pi\nu T$. Actually, ν cannot be exactly constant. In particular, the pulsar must spin down because the energy of the beam is ultimately taken from its rotational energy (and also, because any deviation of axisymmetry leads to a production of gravitational waves, as we saw in Section 4.2). We can model phenomenologically the evolution of the pulsar frequency performing a Taylor expansion around some reference value $T_0 = 0$ of the pulsar proper time,

$$\nu(T) = \nu_0 + \dot{\nu}_0 T + \frac{1}{2} \ddot{\nu}_0 T^2 + \dots, \quad (6.41)$$

where $\dot{\nu}_0, \ddot{\nu}_0$, etc. are generically called the spindown parameters. Then the accumulated phase is given by

$$\begin{aligned} \frac{1}{2\pi} \Phi(T) &= \int_0^T d\tau \nu(\tau) \\ &= \nu_0 T + \frac{1}{2} \dot{\nu}_0 T^2 + \frac{1}{6} \ddot{\nu}_0 T^3 + \dots \end{aligned} \quad (6.42)$$

Emission will take place at the proper times T_n such that $\Phi(T_n) = \Phi_0 + 2\pi n$. Then the emission proper times T_n are given by

$$\nu_0 T_n + \frac{1}{2} \dot{\nu}_0 T_n^2 + \frac{1}{6} \ddot{\nu}_0 T_n^3 + \dots = n + \frac{\Phi_0}{2\pi}, \quad (6.43)$$

so the spindown parameters produce deviations from the exact periodicity $T_n = (\Phi_0/2\pi\nu_0) + (1/\nu_0)n$. The typical dissipation mechanisms in pulsars produce a power-like behavior $\dot{\nu} \simeq C\nu^n$, with C a constant and $n \sim 2 - 3$ (or at most $n = 5$ for damping due to GW emission, see eq. (4.228)). This gives $\dot{\nu} \simeq Cn\nu^{n-1}\dot{\nu} = n\dot{\nu}^2/\nu$. For the Hulse–Taylor pulsar, $\nu_0 \simeq 16.9 \text{ s}^{-1}$ and $\dot{\nu}_0 \simeq -2.5 \times 10^{-15} \text{ s}^{-2}$, so one expects a value of the second derivative of order $\ddot{\nu}_0 \simeq 3 \times 10^{-31} \text{ s}^{-3}$, which over the time span of the observation is unobservably small. Thus, in this case it is sufficient to keep only $\dot{\nu}_0$ in eq. (6.41).

This model assumes that the evolution of the pulsar frequency is smooth. Actually, most pulsars exhibit “glitches”, i.e. sudden jumps in their rotational periods, related to some form of rearrangement of their

internal structure. For instance, the Vela pulsar typically has glitches at intervals of about three years, where the period suddenly decreases up to 200 ns (for comparison, the normal rate of change of the period of the Vela pulsar is an increase by about 10 ns/day). However, the Hulse–Taylor pulsar has shown a remarkable stability, and no glitches, over the 30 years period that it has been observed.

The final step is to connect the pulsar proper time T with the coordinate time t . This will give the values of coordinate time at emission, $t_{\text{em},n} = t(T_n)$; apart from corrections due to the pulsar proper motion, to be discussed below, we can then trivially compute the barycentric time of arrivals $t_{\text{SSB},n}$, i.e. the fictitious values of coordinate time at which these signals would arrive at the solar system barycenter in the absence of dispersion and of Shapiro delay: these are simply $t_{\text{SSB},n} = t_{\text{em},n} + d/c$, where d is the distance between the barycenter of the pulsar–companion system and the SSB. Thus, once we compute the relation between proper time T and the coordinate time t , which we will do in the next subsection, both the time of arrivals measured by our laboratory clock and the timing predicted by this pulsar model have been expressed in terms of the same variable, t_{SSB} , and can be compared.

6.2.3 Relativistic corrections for binary pulsars

For a pulsar in a binary system we can proceed similarly to what we have done for the Earth–Sun system, and perform the transformation from the pulsar proper time to the coordinate time of the pulsar–companion barycenter. We therefore have also Roemer, Shapiro and Einstein delays associated to the pulsar–companion system. The crucial difference, however, with respect to the solar system corrections, is that the binary pulsar is a fairly relativistic system, with strong gravitational fields, and therefore general-relativistic effects are much more important. This is a blessing, since it is just this fact that allows us to measure general-relativistic effects in such systems, such as the emission of gravitational radiation, but it also implies that the computation is technically more difficult, since a full general-relativistic treatment of the two-body dynamics becomes necessary. We discuss the various relevant effects in turn.⁵

⁵It should be observed that the splitting of the various contribution to the timing formula into Einstein, Roemer and Shapiro time delays, aberration delays, etc. discussed below, is not invariant under general coordinate transformations, so it really refers to the harmonic coordinate system, in which the interval has the form (6.9).

Einstein time delay

For this term, the Newtonian equation of the trajectory gives a sufficient accuracy. The computation is therefore similar to what we did on page 310, except that in the expressions for the reduced and total mass of the system we must use the masses m_p and m_c of the pulsar and of its companion. There is however a subtle conceptual point. The beam is radiated by some “hot spot” at a position \mathbf{x} on the surface of the pulsar. The Newtonian expression for ϕ at the location \mathbf{x} is

$$\phi(\mathbf{x}) = -\frac{Gm_p}{c^2|\mathbf{x} - \mathbf{x}_p|} - \frac{Gm_c}{c^2|\mathbf{x} - \mathbf{x}_c|}, \quad (6.44)$$

where \mathbf{x}_p is the position of the center of the pulsar and \mathbf{x}_c is the position of the companion. Using the numerical values in eqs. (6.1) and (6.2), the second term is of order $Gm_c/(c^2a) \sim 10^{-6}$ and therefore is small. For this term, therefore, the weak-field approximation is legitimate. The self-gravity of the pulsar however is strong on its surface. For a typical neutron star radius $r_{NS} \simeq 10$ km and $m_p \simeq 1.4M_\odot$, we have $Gm_p/(c^2r_{NS}) \simeq 0.2$. However, this term (as well as its generalization in full general relativity) does not change along the trajectory of the pulsar in orbit around its companion, so it does not introduce a modulation of the time of arrivals. Its effect is simply reabsorbed in a constant rescaling of proper time T , which is not observable.⁶ Thus, the time-dependent part of the Einstein time delay can be computed simply using

$$\phi(\mathbf{x}) = -\frac{Gm_c}{c^2|\mathbf{x} - \mathbf{x}_c|}, \quad (6.45)$$

and the weak field approximation. Then, eq. (6.27) gives

$$\frac{dT}{dt} = 1 - \frac{Gm_c}{c^2|\mathbf{x}_p - \mathbf{x}_c|} - \frac{v_p^2}{2c^2}, \quad (6.46)$$

where \mathbf{x}_p is the pulsar position and v_p is its velocity. The latter is obtained from

$$v_p = \frac{m_c}{m_p + m_c} v, \quad (6.47)$$

where v is the relative velocity in the center of mass system, given by (compare with eq. (6.33))

$$\frac{1}{2}v^2 - \frac{G(m_p + m_c)}{r} = -\frac{G(m_p + m_c)}{2a}, \quad (6.48)$$

Thus,

$$\frac{dT}{dt} = 1 - \frac{G}{c^2} \left[\frac{m_c(m_p + 2m_c)}{m_p + m_c} \frac{1}{r} - \frac{m_c^2}{m_p + m_c} \frac{1}{2a} \right]. \quad (6.49)$$

We use the parametrization of the Keplerian orbit in terms of the eccentric anomaly u , given in eqs. (4.56) and (4.57), with u related to the time t by Kepler equation (4.58),

$$u - e \sin u = \frac{2\pi}{P_b} (t - t_0), \quad (6.50)$$

where t_0 is a reference time of periastron passage. Differentiating, we have

$$\frac{du}{dt} (1 - e \cos u) = \frac{2\pi}{P_b}, \quad (6.51)$$

and therefore,

$$\frac{dT}{dt} = \frac{du}{dt} \frac{dT}{du} = \frac{2\pi}{P_b} \frac{1}{1 - e \cos u} \frac{dT}{du}. \quad (6.52)$$

⁶A more detailed discussion on this point can be found in Will (1984).

Plugging this into eq. (6.49) and using eq. (4.56) we get

$$\begin{aligned} \frac{2\pi}{P_b} \frac{dT}{du} &= \left(1 - \frac{G}{c^2} \frac{2m_c m_p + 3m_c^2}{2a(m_p + m_c)} \right) - e \cos u \left(1 + \frac{G}{c^2} \frac{m_c^2}{2a(m_p + m_c)} \right) \\ &\simeq \left(1 - \frac{G}{c^2} \frac{2m_c m_p + 3m_c^2}{2a(m_p + m_c)} \right) \\ &\quad \times \left[1 - e \cos u \left(1 + \frac{G}{c^2} \frac{m_c(m_p + 2m_c)}{a(m_p + m_c)} \right) \right], \end{aligned} \quad (6.53)$$

where in the second line we retained only terms of first order in G . The overall factor is a constant multiplicative rescaling of the pulsar proper time T . Such a factor is unobservable, since it relates the (unobservable) proper time that the pulsar would have in the presence of only its own gravitational field, to its actual proper time that includes the gravitational effect of the companion and the pulsar orbital velocity. Instead, the correction proportional to $\cos u$ produces a modulation along the orbit and is therefore observable. We can therefore reabsorb the multiplicative factor into the definition of proper time, rescaling

$$T \rightarrow \left(1 - \frac{G}{c^2} \frac{2m_c m_p + 3m_c^2}{2a(m_p + m_c)} \right) T, \quad (6.54)$$

and eq. (6.53) becomes

$$\frac{dT}{du} = \frac{P_b}{2\pi} (1 - e \cos u) - \gamma \cos u \quad (6.55)$$

where the Einstein parameter γ is given by

$$\begin{aligned} \gamma &= e \left(\frac{P_b}{2\pi} \right) \frac{G}{c^2} \frac{m_c(m_p + 2m_c)}{a(m_p + m_c)} \\ &= e \left(\frac{P_b}{2\pi} \right)^{1/3} \frac{G^{2/3}}{c^2} \frac{m_c(m_p + 2m_c)}{(m_p + m_c)^{4/3}}, \end{aligned} \quad (6.56)$$

and in the second line we used Kepler's law, $G(m_p + m_c)/a^3 = (2\pi/P_b)^2$, to eliminate a . Writing $T = t - \Delta_E$, and observing, from eq. (6.50), that $(2\pi/P_b)dt/du = 1 - e \cos u$, we see that

$$\frac{d\Delta_E}{du} = \gamma \cos u. \quad (6.57)$$

Then, we obtain for the Einstein delay

$$\Delta_E = \gamma \sin u. \quad (6.58)$$

Inserting the numerical values of e and P_b of the Hulse–Taylor pulsar, eq. (6.56) gives

$$\gamma = 2.93696 \text{ ms} \left(\frac{m_c}{M_\odot} \right) \left(\frac{m_p + 2m_c}{M_\odot} \right) \left(\frac{m_p + m_c}{M_\odot} \right)^{-4/3}. \quad (6.59)$$

Roemer time delay and the post-Newtonian orbit

Referring the emission time to the barycenter of the pulsar–companion system, we encounter the Roemer and Shapiro time delays, similarly to what we found for the solar system corrections. In the geometry of Fig. 6.1, the Roemer delay is given by $\Delta_R = \hat{\mathbf{z}} \cdot \mathbf{x}_1(t)/c$, where \mathbf{x}_1 is the distance of the pulsar from the center-of-mass of the pulsar–companion system. We therefore need the explicit form of the orbit, $\mathbf{x}_1(t)$.

We first consider a Keplerian orbit, neglecting general-relativistic corrections. Using polar coordinates (r_1, ψ) in the plane of the orbit, the Keplerian equation of motion is given in parametric form, in terms of the eccentric anomaly u , by

$$r_1(u) = a_1[1 - e \cos u], \quad (6.60)$$

$$\cos \psi(u) = \frac{\cos u - e}{1 - e \cos u} \quad (6.61)$$

(compare with eqs. (4.56) and (4.57)), where a_1 is the semimajor axis of the pulsar orbit. Observe that r_1 reaches its minimum value at $u = 0$, in which case $\psi = 0$. Therefore the angle ψ is measured from periastron, and the angle measured from the line of nodes is $\omega + \psi(u)$, see Fig. 6.1. From the geometry of Fig. 6.1 we then see that the Roemer delay is

$$c\Delta_R = r_1(u) \sin \iota \sin[\omega + \psi(u)]. \quad (6.62)$$

We now expand $\sin(\omega + \psi) = \cos \psi \sin \omega + \sin \psi \cos \omega$ and we use eq. (6.61) for $\cos \psi$, together with the corresponding expression for $\sin \psi$,

$$\sin \psi(u) = (1 - e^2)^{1/2} \frac{\sin u}{1 - e \cos u}, \quad (6.63)$$

and we get

$$\begin{aligned} c\Delta_R &= \frac{r_1(u)}{1 - e \cos u} \sin \iota [(\cos u - e) \sin \omega + (1 - e^2)^{1/2} \sin u \cos \omega] \\ &= a_1 \sin \iota [(\cos u - e) \sin \omega + (1 - e^2)^{1/2} \sin u \cos \omega]. \end{aligned} \quad (6.64)$$

This is the result at the Keplerian level. However, numerically the effect is quite large, and it is necessary to go beyond the Keplerian orbit, and include the post-Newtonian corrections to 1PN order. This computation has been performed by Damour and Deruelle (1985, 1986), and we sketch the main steps. The equations of motion at 1PN level can be derived from the Lagrangian (5.54). Defining the variable

$$\mathbf{X} = \frac{m_1^* \mathbf{x}_1 + m_2^* \mathbf{x}_2}{m_1^* + m_2^*}, \quad (6.65)$$

where

$$m_A^* = m_A + \frac{m_A v_A^2}{2c^2} - \frac{G m_1 m_2}{2r c^2}, \quad (6.66)$$

the equations of motion give $d^2 \mathbf{X}/dt^2 = 0$. In the non-relativistic limit this is the statement that the center-of-mass is non accelerated. In fact, because of the corrections $O(v^2/c^2)$, \mathbf{X} is rather a “center-of-energy”.

Invariance under time translations and rotations leads to the conservation of energy and angular momentum. Because of conservation of angular momentum, the equation for the relative coordinate \mathbf{r} describes a motion in a plane, just as in the Newtonian case, and there are two conserved quantities, the total energy E and the total angular momentum \mathbf{J} . We use the usual notations m for the total mass, $m = m_1 + m_2$, μ for the reduced mass $\mu = m_1 m_2 / m$ and, as in Chapter 5, we use the symmetric mass ratio $\nu = \mu / (m_1 + m_2) = m_1 m_2 / (m_1 + m_2)^2$ (observe that $0 \leq \nu \leq 1/4$). It is also convenient to introduce the energy and angular momentum per unit value of μ , $\varepsilon = E/\mu$, $\mathbf{j} = \mathbf{J}/\mu$. Applying the Noether theorem to the Lagrangian (5.54), one finds the explicit expression of the conserved quantities,

$$\varepsilon = \frac{1}{2} v^2 - \frac{Gm}{r} + \frac{3}{8} (1 - 3\nu) \frac{v^4}{c^2} + \frac{Gm}{2rc^2} \left[(3 + \nu)v^2 + \nu(\hat{\mathbf{r}} \cdot \mathbf{v})^2 + \frac{Gm}{r} \right], \quad (6.67)$$

and

$$\mathbf{j} = \left[1 + \frac{1}{2}(1 - 3\nu) \frac{v^2}{c^2} + (3 + \nu) \frac{Gm}{rc^2} \right] \mathbf{r} \times \mathbf{v}, \quad (6.68)$$

where v is the relative velocity and $\hat{\mathbf{r}} = \mathbf{r}/r$. Using polar coordinates (r, ψ) in the plane of the orbit, these first integrals of the equations of motion give

$$\left(\frac{dr}{dt} \right)^2 = A + \frac{2B}{r} + \frac{C}{r^2} + \frac{D}{r^3}, \quad (6.69)$$

$$\frac{d\psi}{dt} = \frac{H}{r^2} + \frac{I}{r^3}, \quad (6.70)$$

where A, \dots, I are polynomials in ε and j ,

$$A = 2\varepsilon \left[1 + \frac{3}{2}(3\nu - 1) \frac{\varepsilon}{c^2} \right], \quad (6.71)$$

$$B = Gm \left[1 + (7\nu - 6) \frac{\varepsilon}{c^2} \right], \quad (6.72)$$

$$C = -j^2 \left[1 + 2(3\nu - 1) \frac{\varepsilon}{c^2} \right] + (5\nu - 10) \frac{G^2 m^2}{c^2}, \quad (6.73)$$

$$D = (8 - 3\nu) \frac{GMj^2}{c^2}, \quad (6.74)$$

$$H = j \left[1 + (3\nu - 1) \frac{\varepsilon}{c^2} \right], \quad (6.75)$$

$$I = (2\nu - 4) \frac{GMj}{c^2}. \quad (6.76)$$

In the limit $c \rightarrow \infty$ we have $D = I = 0$, while the other coefficients reduce to their Newtonian values. Observe that in the Newtonian case the equation for $(dr/dt)^2$ contains terms up to $1/r^2$, while at the 1PN level there is also a $1/r^3$ term, that in principle could make the integration of the equation of motion very complicated. However, as observed by Damour and Deruelle, we can introduce a new radial variable \bar{r} ,

$$\bar{r} = r + \frac{D}{2j^2}, \quad (6.77)$$

and in terms of this variable eq. (6.69) becomes

$$\left(\frac{d\bar{r}}{dt}\right)^2 = A + \frac{2B}{\bar{r}} + \frac{\bar{C}}{\bar{r}^2} + O(v^4/c^4), \quad (6.78)$$

with $\bar{C} = C + (BD/j^2)$. Since the terms $O(v^4/c^4)$ are consistently neglected at this order, this equation still has the form of a Newtonian-like radial equation of motion, with suitably redefined parameters. Similarly, defining $\tilde{r} = r - I/(2H)$, the angular equation (6.70) becomes

$$\frac{d\psi}{dt} = \frac{H}{\tilde{r}^2}. \quad (6.79)$$

As a result, the equations of motion to 1PN order can be integrated analytically, and the solution can be put in a form similar to the Keplerian orbit discussed in Section 4.1.2. In particular, eqs. (4.56) and (4.58) become

$$u - e_t \sin u = \frac{2\pi}{P_b} t, \quad (6.80)$$

and

$$r = a_r [1 - e_r \cos u], \quad (6.81)$$

where

$$a_r = -\frac{Gm}{2\varepsilon} \left[1 - (\nu - 7) \frac{\varepsilon}{2c^2} \right], \quad (6.82)$$

$$e_r^2 = 1 + \frac{2\varepsilon}{G^2 m^2} \left[1 + (5\nu - 15) \frac{\varepsilon}{2c^2} \right] \left[j^2 + (\nu - 6) \frac{G^2 m^2}{c^2} \right], \quad (6.83)$$

$$e_t^2 = 1 + \frac{2\varepsilon}{G^2 m^2} \left[1 + (17 - 7\nu) \frac{\varepsilon}{2c^2} \right] \left[j^2 + (2 - 2\nu) \frac{G^2 m^2}{c^2} \right], \quad (6.84)$$

$$\frac{2\pi}{P_b} = \frac{(-2\varepsilon)^{3/2}}{Gm} \left[1 - (\nu - 15) \frac{\varepsilon}{4c^2} \right]. \quad (6.85)$$

In other words, the eccentricity e of the Keplerian solution is now split into a “radial eccentricity” e_r and a “time eccentricity” e_t . Similarly, the solution for $\psi(u)$ is written in terms of an “angular eccentricity” e_θ ,

$$= \omega_0 + (1 + k) A_{e_\theta}(u), \quad (6.86)$$

where⁷

$$k = \frac{3Gm}{c^2 a(1 - e^2)}. \quad (6.87)$$

The function $A_{e_\theta}(u)$ is the same as in eq. (4.61), with $e \rightarrow e_\theta$, and

$$e_\theta^2 = 1 + \frac{2\varepsilon}{G^2 m^2} \left[1 + (\nu - 15) \frac{\varepsilon}{2c^2} \right] \left[j^2 - 6 \frac{G^2 m^2}{c^2} \right]. \quad (6.88)$$

Observe that, when $c \rightarrow \infty$, e_θ^2, e_r^2 and e_t^2 reduce to the Keplerian quantity e^2 given in eq. (4.50). We therefore have a parametric “quasi-Newtonian” (i.e. Newtonian plus the precession due to a non-vanishing k in eq. (6.86)) representation of the orbit accurate to 1PN order.⁸ Using

⁷Observe that, since k is already a correction, to the order at which we are working it is irrelevant whether in eq. (6.87) we write the Keplerian major semiaxis $a = -Gm/(2\varepsilon)$ rather than a_r , and similarly we can use e or any other eccentricity such as e_r .

⁸At the same time, the equation of motion (6.80) can be rewritten in terms of the proper time T of the pulsar, rather than in terms of coordinate time t , as

$$u - e_T \sin u = \frac{2\pi}{P_b} T, \quad (6.89)$$

where e_T is another time eccentricity. It is crucial to carefully distinguish between these time eccentricities to get the correct 1PN result. See Damour and Deruelle (1985, 1986) for details.

this expression for the orbit, eq. (6.64) is replaced by

$$c\Delta_R = a_1 \sin \iota [(\cos u - e_r) \sin \omega + (1 - e_\theta^2)^{1/2} \sin u \cos \omega]. \quad (6.90)$$

Writing $e_r = (1 + \delta_r)e$ and $e_\theta = (1 + \delta_\theta)e$, where e is the Keplerian eccentricity given by eq. (4.50), the parameters δ_r and δ_θ have the values

$$\delta_r = \frac{G}{c^2} \frac{3m_p^2 + 6m_p m_c + 2m_c^2}{a(m_p + m_c)}, \quad (6.91)$$

$$\delta_\theta = \frac{G}{c^2} \frac{(7/2)m_p^2 + 6m_p m_c + 2m_c^2}{a(m_p + m_c)}, \quad (6.92)$$

⁹In all these equations we have assumed the correctness of general relativity. Alternatively, quantities such as δ_r and δ_θ can be treated as free parameters, to be determined directly from the data, and their measure allows us to compare general relativity to alternative theories of gravitation.

where we wrote $m_1 = m_p, m_2 = m_c$ for the masses of the pulsar and the companion.⁹ Finally, we observe from eq. (6.81) that the periastron passages (i.e. the minima of r) are reached for $u = u_n \equiv 2\pi n$, with n integer. Since $A_{e_\theta}(u_n) = 2\pi n$, we see from eq. (6.86) that $2\pi k$ is the angle of periastron precession per orbit. Observe that, in the complete general-relativistic solution, the advance of the periastron is not uniform along the orbit, but is a function of u . Since the position ω of the periastron advances by $2\pi k$ over one period, the derivative of ω , averaged over the orbit, is

$$\begin{aligned} \langle \dot{\omega} \rangle &= \frac{2\pi}{P_b} k \\ &= \frac{3}{c^2} [G(m_p + m_c)]^{2/3} \left(\frac{2\pi}{P_b} \right)^{5/3} \frac{1}{1 - e^2}, \end{aligned} \quad (6.93)$$

where in the second line we used eq. (6.87), and we eliminated a using Kepler's law. Using the known values of e and P_b for the Hulse–Taylor binary pulsar, this gives

$$\langle \dot{\omega} \rangle = 2.11353 \left(\frac{m_p + m_c}{M_\odot} \right)^{2/3} \text{deg/yr}. \quad (6.94)$$

The comparison with the experimental value therefore gives the total mass of the binary system.

Shapiro time delay

The Shapiro delay is due to the effect of the gravitational field of the companion on the pulsar signal (observe that the gravitational field of the pulsar itself enters instead in the relation between the pulsar proper time and coordinate time, just as the Earth's gravitational field when we computed the solar system corrections). The computation is analogous to what we did on pages 308–310. Using the Keplerian equation of the orbit given in eqs. (4.56) and (4.57), and taking into account its orientation with respect to the observer, given by the periastron angle ω and by the inclination angle ι , one obtains

$$\Delta_S = -2r \log \left\{ (1 - e \cos u) - s[\sin \omega (\cos u - e) + \sqrt{1 - e^2} \cos \omega \sin u] \right\}, \quad (6.95)$$

where $r \equiv Gm_c/c^3$ (not to be confused with a distance) and $s \equiv \sin \iota$ are called the range and shape of the Shapiro delay, respectively, and we omitted an overall constant (i.e., a u -independent term), which grows logarithmically with the distance to the pulsar. This constant term simply adds up to the total travel time, but it does not show up as a modulation in u , and is therefore unobservable.

Secular changes due to GW emission

The timing formula also includes secular changes in the Keplerian parameters of the orbit, induced by GW emission, whose extraction is in fact our final aim. In particular we already saw that, because of GW emission, the orbital period has a non-vanishing time derivative given by eq. (6.4).¹⁰

This secular change modifies the Keplerian relation (6.50) between the eccentric anomaly u and the proper time T of the pulsar, which becomes

$$u - e \sin u = 2\pi \left[\frac{T - T_0}{P_b} - \frac{1}{2} \dot{P}_b \left(\frac{T - T_0}{P_b} \right)^2 \right], \quad (6.96)$$

where T_0 is a reference value of proper time, and P_b is defined as the value of the orbital period at this reference time. The factor $-1/2$ comes from integrating the instantaneous orbital frequency $[P_b + \dot{P}_b(T - T_0)]^{-1}$ to obtain the orbital phase.

Observe that, in order of magnitude, the velocity v of the binary system is given by $v^2 \sim GM/a$, where $M = m_p + m_c$ is the total mass. Using Kepler's law to eliminate a in favor of P_b , this can be rewritten as $P_b/(2\pi) \sim GM/v^3$. Substituting this into the expression for \dot{P}_b , given in eq. (6.4), we see that

$$\dot{P}_b = O\left(\frac{v^5}{c^5}\right). \quad (6.97)$$

It is quite remarkable that an effect of order $(v/c)^5$ can be measured, and this is due to the combination of the extreme precision of the timing measurements, and to the fact that the Hulse–Taylor binary system is quite relativistic, with $v \sim 10^{-3}c$.

Aberration correction and Doppler shift

Another ingredient of the full timing formula is an aberration correction due to the fact that, because of the orbital motion of the pulsar around its companion, the direction from which the observer receives the pulse differs from the direction in which it was emitted in the pulsar frame. This produces a delay

$$\Delta_A = A\{\sin[\omega + A_e(u)] + e \sin \omega\} + B\{\cos[\omega + A_e(u)] + e \cos \omega\}, \quad (6.98)$$

where A and B are two known constants. Finally, there is a longitudinal Doppler shift, due to the fact that there is in general a proper motion of

¹⁰Actually, also $x = (1/c)a \sin \iota$ and the eccentricity e have secular changes, see eqs. (4.116) and (4.117), which however are smaller, and not detectable with the present precision for the Hulse–Taylor pulsar.

the solar system barycenter with respect to the barycenter of the pulsar–companion system, with a radial component of the velocity. Thus, the relation between the intrinsic and the observed orbital periods is given by

$$P_b^{\text{intr}} = DP_b^{\text{obs}}, \quad (6.99)$$

and the Doppler factor D is given by

$$D = \left(1 - \frac{\mathbf{v} \cdot \hat{\mathbf{n}}}{c}\right), \quad (6.100)$$

where \mathbf{v} is the velocity of the pulsar–companion barycenter with respect to the SSB, and $\hat{\mathbf{n}}$ is the unit vector from the SSB toward the pulsar. From eq. (6.99) we get

$$\frac{\dot{P}_b^{\text{obs}}}{P_b^{\text{obs}}} = \frac{\dot{P}_b^{\text{intr}}}{P_b^{\text{intr}}} - \frac{\dot{D}}{D}. \quad (6.101)$$

If the Doppler factor D were a constant in time, the additional term \dot{D}/D would vanish, that is, D would be simply reabsorbed into the definition of P_b , and would be unobservable. However, there is a relative acceleration of the SSB and of the pulsar–companion system, induced by the differential rotation of the Galaxy, as well as proper motion effects, and therefore \dot{D} is non-vanishing and produces an observable correction to \dot{P}_b/P_b . To lowest order in the radial velocity $\mathbf{v} \cdot \hat{\mathbf{n}}$, we have $\dot{D}/D \simeq \dot{D}$, and

$$\begin{aligned} -\dot{D} &= \frac{d}{dt} \frac{\mathbf{v} \cdot \hat{\mathbf{n}}}{c} \\ &= \frac{\mathbf{a} \cdot \hat{\mathbf{n}}}{c} + \frac{\mathbf{v} \cdot d\hat{\mathbf{n}}}{c}. \end{aligned} \quad (6.102)$$

If the pulsar has a transverse velocity v_T with respect to the SSB, and as usual d is the distance to the pulsar, in a time dt the unit vector $\hat{\mathbf{n}}$ acquires a component $v_T dt/d$ in the transverse direction, and therefore $\mathbf{v} \cdot d\hat{\mathbf{n}}/dt = v_T^2/d$. Thus, there is a Doppler correction

$$\left(\frac{\dot{P}_b}{P_b}\right)^{\text{obs}} = \left(\frac{\dot{P}_b}{P_b}\right)^{\text{intrinsic}} + \left(\frac{\dot{P}_b}{P_b}\right)^{\text{gal}}, \quad (6.103)$$

where $(\dot{P}_b/P_b)^{\text{gal}}$ is the value of $-\dot{D}/D$ due to the galactic acceleration and to proper motion

$$\left(\frac{\dot{P}_b}{P_b}\right)^{\text{gal}} = \frac{\mathbf{a} \cdot \hat{\mathbf{n}}}{c} + \frac{v_T^2}{cd}. \quad (6.104)$$

The term $v_T^2/(cd)$ is also known as the Shklovsky effect due to the orbital motion. For a pulsar in the galactic plane, eq. (6.104) can be rewritten as

$$\left(\frac{\dot{P}_b}{P_b}\right)^{\text{gal}} = -\frac{v_0^2}{cR_0} \cos l - \frac{v_1^2}{cR_1} \cos \lambda + \frac{v_T^2}{cd}, \quad (6.105)$$

where v_0 is the galactic circular velocity at the Sun position, R_0 the distance from the galactic center to the Sun, v_1 and R_1 are respectively the galactic circular velocity and the distance to the galactic center at the pulsar position, l is the galactic latitude of the pulsar and λ the Sun-pulsar-galactic center angle.¹¹

We see from eq. (6.37) that, if we have a model of the electron distribution in the Galaxy, we can get the distance of a pulsar from us from the observed value of its dispersion measure. For the Hulse–Taylor pulsar this gives

$$d = 8.3 \pm 1.4 \text{ kpc}. \quad (6.106)$$

At this relatively large distance, the last term in eq. (6.105) is small, since it is proportional to $1/d$. However, the difference between the acceleration at the Earth and pulsar location, due to the differential rotation of the Galaxy, is quite important. Furthermore, this correction is sensitive to the values of v_0 and R_0 , which are not very accurately known. Indeed, for the Hulse–Taylor the uncertainty in the first two terms in eq. (6.105) is the limiting factor in the comparison between the experimental results and the general relativity prediction.

Fit to the full timing formula

At this point, one can compare these corrections with the observed timing residual and extract, from a fit, the parameters that enter in the timing formula. These parameters can be grouped as follows.

- Parameters characterizing the pulsar itself: the right ascension α and declination δ , its proper motion, the initial pulse phase Φ_0 , its frequency ν and the spindown parameters. In practice, among the spindown parameters it suffices to keep only $\dot{\nu}_0$, as we saw below eq. (6.41).
- The five Keplerian parameters

$$\{P_b, T_0, x, e, \omega\}, \quad (6.107)$$

which parametrize (at the level of Newtonian mechanics) the orbital motion of the pulsar. Here T_0 is a time of passage at periastron, used as a reference time, and the quantities $P_b, x = (a/c) \sin \iota, e, \omega$, which all have secular variations, are evaluated at $T = T_0$.

- The eight independently measurable post-Keplerian parameters

$$\{\dot{\omega}, \gamma, \dot{P}_b, r, s, \delta_\theta, \dot{e}, \dot{x}\}, \quad (6.108)$$

which characterize the relativistic corrections to the orbital motion.

Instead, the parameters A and B which enter in the aberration formula, as well as δ_r , in practice are not separately measurable, since their effect turns out to be degenerate with that of other parameters.

¹¹For a pulsar outside the galactic plane, there is also a (usually smaller) effect due to the vertical acceleration in the galactic potential. All these acceleration corrections are discussed in detail in Damour and Taylor (1991).

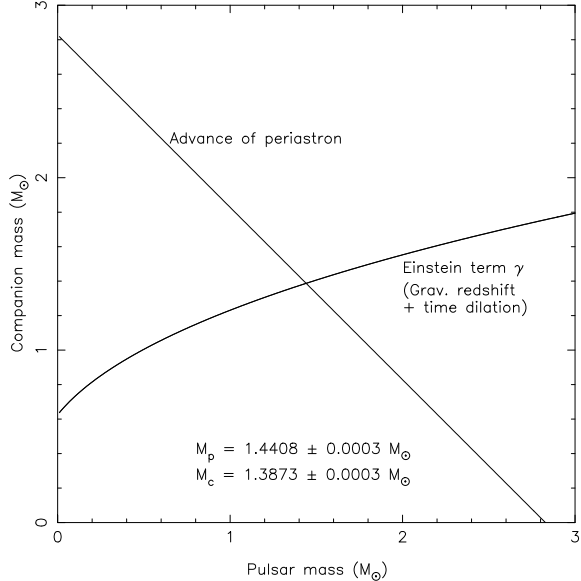


Fig. 6.6 Constraints on the pulsar and companion mass from $\langle \dot{\omega} \rangle$ and γ . The uncertainties in $\langle \dot{\omega} \rangle$ and γ are smaller than the displayed linewidths. From Weisberg and Taylor (2002). The values of the masses have been updated in Weisberg and Taylor (2004), see Table 6.1.

If we assume the validity of general relativity, all the post-Keplerian parameters are predicted once we know the value of the Keplerian parameters, and the masses of the pulsar and of the companion, m_p and m_c . Therefore, if from the fit of the observed time residuals to the timing formula we can extract the five Keplerian parameters plus any two of the post-Keplerian parameters, we can get the masses m_p and m_c . At this point, any further post-Keplerian parameter which can be extracted from the fit to the experimental data provides a test of general relativity, since it can be compared to the value predicted by general relativity, with no more free parameter at our disposal.

In particular, for the Hulse–Taylor binary pulsar it is possible to extract, from the comparison with the timing formula, all Keplerian parameters and the three post-Keplerian quantities $\langle \dot{\omega} \rangle$, γ and \dot{P}_b . From the values of $\langle \dot{\omega} \rangle$ and γ one obtains m_p and m_c , see eq. (6.1) and Fig. 6.6. Concerning \dot{P}_b , the observed value is (see Table 6.1 on page 303)

$$\dot{P}_b^{\text{obs}} = -2.4184(9) \times 10^{-12}. \quad (6.109)$$

Using the known values of the accelerations in the galactic potential, one finds $\dot{P}_b^{\text{gal}} = -0.0128(50) \times 10^{-12}$. Correcting for this effect according to eq. (6.103) we therefore have

$$\dot{P}_b^{\text{intrinsic}} = \dot{P}_b^{\text{obs}} - \dot{P}_b^{\text{gal}} = -2.4056(51) \times 10^{-12}. \quad (6.110)$$

Since the masses m_c and m_p have been fixed from $\langle \dot{\omega} \rangle$ and γ , the value of $\dot{P}_b^{\text{intrinsic}}$ can now be compared with the prediction of general relativity

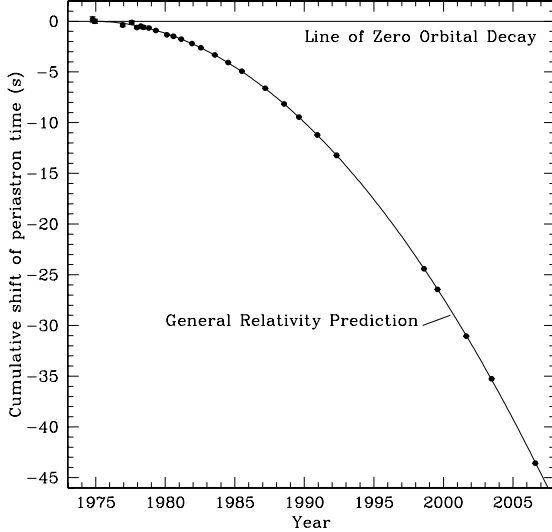


Fig. 6.7 Orbital decay of PSR B1913+16. The data points indicate the observed change in the epoch of periastron with date, while the parabola is the general relativity prediction for a system emitting gravitational radiation. From Weisberg, Taylor and Nice (in preparation). The years in the late 1990s with no data corresponds to a period when the Arecibo telescope was closed for major upgrades.

due to GW emission, eq. (6.4), which is

$$\dot{P}_b^{\text{GR}} = -2.40242(2) \times 10^{-12}. \quad (6.111)$$

The agreement is therefore at the $(0.13 \pm 0.21)\%$ level. A vivid way to show this agreement is to plot the cumulative shift of periastron time as a function of the observation time. Similarly to what we did in eq. (6.42) for the cumulative phase of the rotation of the pulsar around its axis, we can write the accumulated orbital phase ϕ_b as

$$\frac{1}{2\pi} \phi_b(T) = \nu_b T + \frac{1}{2} \dot{\nu}_b T^2 + \dots, \quad (6.112)$$

where $\nu_b = 1/P_b$ is the orbital frequency, and we have chosen the origin of T so that a periastron passage T_0 is at $\phi_b = 0$. For the Hulse–Taylor pulsar, the terms proportional to $\ddot{\nu}_b$ and higher are negligible. The n -th time of periastron passage, T_n , takes place when $\phi_b(T_n) = 2\pi n$, i.e.

$$\nu_b T_n + \frac{1}{2} \dot{\nu}_b T_n^2 = n. \quad (6.113)$$

Thus, the cumulative difference between the periastron passages T_n and the values n/ν_b is given by

$$T_n - \frac{n}{\nu_b} = -\frac{\dot{\nu}_b}{2\nu_b} T_n^2, \quad (6.114)$$

or, in terms of $P_b = 1/\nu_b$,

$$T_n - P_b n = \frac{\dot{P}_b}{2P_b} T_n^2. \quad (6.115)$$

This is a parabola with coefficient given by $(\dot{P}_b)/(2P_b) < 0$ and, as we see in Fig. 6.7, the agreement between the data and the theory is extremely good, and remarkably stable along the years. Observe that the uncertainty in the galactic acceleration (the first term in eq. (6.104)) dominates the experimental error, and is the limiting factor in the comparison with general relativity.

Finally, we mention that recent observations indicate a variation of the pulse profile of the Hulse–Taylor binary pulsar. This is consistent with the fact that the pulsar is undergoing geodetic precession (a general-relativistic effect due to the spin-orbit coupling). The period of this geodetic precession is about 300 yr, and the data suggest that the pulsar’s beam will no longer intersect our line of sight after the year 2025, so the pulsar will become unobservable.

6.3 The double pulsar, and more compact binaries

Double NS systems are rare. Even if the original binary star system survived the first supernova explosion, it will typically be disrupted by the second supernova explosion. Furthermore, in pulsar surveys there are selection effects against NS-NS systems, because the modulation of the period of the pulsar due to its orbital motion makes the detection more difficult. Still, after the discovery of the Hulse–Taylor pulsar, PSR B1913+16, a number of other NS-NS binaries have been discovered. Presently (2007) there are five system whose identification with NS-NS binaries is considered certain, because the masses of the two stars have been measured, and found to be very close to the value $\simeq 1.3M_\odot$ expected for a NS. These are shown in Table 6.2. Furthermore, there are at least three more binary systems (PSR J1518+4904, J1811–1736 and J1829+2456) whose identification with NS-NS binaries is very likely, although the two separate masses have not yet been measured with comparable precision. Besides, a number of white dwarf/NS binaries are known. We discuss here the most interesting systems.

The double pulsar, PSR J0737–3039

This is a very remarkable system, which is already a truly spectacular laboratory for general relativity, and will become even more so in the next few years. The pulsar PSR J0737–3039, with a period 22.8 ms, was discovered in April 2003 (Burgay *et al.* 2003), in a survey of the southern sky made with the Parkes 64-m radio telescope in Australia. It was soon found to be a member of the most relativistic binary system ever

Table 6.2 The five confirmed NS-NS binaries; τ is the time to coalescence because of GW emission, computed from eqs. (4.136) and (4.140) (setting $G(e) = 1$). For PSR J1756–2251 we assumed $m_c = 1.2M_\odot$.

PSR	P (ms)	P_b (hr)	e	$(a/c) \sin \iota$ (s)	$m_p(M_\odot)$	$m_c(M_\odot)$	τ (Myr)
J0737–3039A	22.7	2.45	0.088	1.42	1.3381(7)	1.2489(7)	86
	2773.6						
B1534+12	37.9	10.1	0.27	3.73	1.3332(10)	1.3452(10)	2783
J1756–2251	28.5	7.67	0.18	2.76	2.574(3) – m_c	< 1.25	1660
B1913+16	59.0	7.75	0.617	2.34	1.4414(2)	1.3867(2)	306
B2127+11C	30.5	8.05	0.681	2.52	1.350(40)	1.363(40)	218

discovered, with an orbital period P_b of just 2.4 hr. Thus, relativistic effects are even more important than in the Hulse–Taylor pulsar. For instance, its periastron advance is about 17 deg/yr, four times larger than for the Hulse–Taylor pulsar, and could be measured already after a few days of observations. Its coalescence time, of only about 86 Myr, is the shortest among all NS-NS systems known, see Table 6.2.¹² Furthermore, its large flux density and its narrow pulse make possible to have a high timing precision. These features would have already made this system exceptionally interesting. Then, in October 2003, even its companion was detected as a pulsar (Lyne *et al.* 2004), making it the first observed NS-NS system where both neutron stars are pulsars whose beams intersect our line of sight. The pulsar discovered first, labeled as A, is a millisecond pulsar, while the other (B) has a period of about 2.7 s (see Table 6.2). It turned out that the pulses of B change significantly along the orbital phase, probably because of the influence of the energy flux of A on its magnetosphere, so the beam from B is clearly visible only for two short periods of about 10 min each during its orbital motion (which is the reason why B was not detected initially).

The fact that we observe both beams allows us to measure separately $x_A = (1/c)a_A \sin \iota$ and $x_B = (1/c)a_B \sin \iota$, where a_A and a_B are the major semiaxes of the orbits of the A and B pulsars, respectively. Then, from Kepler’s third law, we get their mass ratio,¹³

$$R \equiv \frac{m_A}{m_B} = \frac{x_B}{x_A}, \quad (6.116)$$

while, as usual, once the Keplerian parameters have been measured, from the periastron advance we get the total mass (see eq. (6.93)). Thus, after only two and a half years of observations, we already have a rather precise determination of the masses of the two pulsars, see Table 6.2.

Given the importance of relativistic effects in this system, it has already been possible to extract, from the fit to the timing formula, five post-Keplerian parameters, reported in Table 6.3. Observe in particular that $\sin \iota = 0.99974$, with an error (−39, +16) on the last two digits, i.e.

¹²This also had the effect of increasing by almost one order of magnitude the expected coalescence rate of NS-NS systems, with very important consequences for GW detectors. We will come back to these issues in Vol. 2.

¹³It is also important to observe that eq. (6.116) is expected to hold not only in general relativity, but in any realistic theory of gravity, at least to 1PN order. Furthermore, this relation is also independent of strong-field effects, which is not the case for the post-Keplerian parameters.

the orbit is seen nearly edge-on, so it is ideally oriented for measuring the Shapiro delay. Finally, we can add to the list of virtues of this binary system that the timing results indicate that its proper motion is surprisingly small, so the proper motion corrections discussed on page 322 are small. The distance to the pulsar is estimated, from its dispersion measure, to be $d \sim 500$ pc.

Having fixed the masses using $\langle \dot{\omega} \rangle$ and the mass ratio R , we are left with four predictions from general relativity, for the four measured quantities \dot{P}_b, γ, r, s . Better yet, one can plot the six quantities $\{R, \dot{\omega}, \dot{P}_b, \gamma, r, s\}$ in the plane (m_A, m_B) , and one finds that all six curves meet at one common point. As shown in Fig. 6.8, the agreement is very remarkable. In particular, for the shape of the Shapiro time delay, s , the agreement between theory and observation is

$$\frac{s^{\text{GR}}}{s^{\text{obs}}} = 0.99987(50) \quad (6.117)$$

and we see that general relativity passes this test at the 0.05% level. This is by far the best available test of general relativity in strong fields, even better than the test based on the observed \dot{P}_b for the Hulse–Taylor binary pulsar with a 30-year data span, compare with eq. (6.5).

Concerning the measure of \dot{P}_b , the precision obtained after 2.5 years of observations is given in Table 6.3. Given that the measured uncertainty in \dot{P}_b decreases approximately as $T^{-2.5}$, where T is the data span, we expect that in about five years it should be measured at the level of 0.1% or better. As we mentioned, the proper motion correction to this double binary system are quite small, as well as the corrections due to differential acceleration in the galactic potential. This suggests that for this system one could eventually arrive to a measure of \dot{P}_b at the level of 0.02%.

Observe that, in Fig. 6.8, only the white part of the plot is allowed, and the shaded part is excluded. This follows from the fact that, in this binary system, we can measure separately $x_A = (1/c)a_A \sin \iota$ and $x_B = (1/c)a_B \sin \iota$, where $a_{A,B}$ are the semimajor axes of the orbits of the stars A and B, respectively. From the measure of x_A , together with the orbital period P_b , one can form the *mass function*

$$f_A(m_A, m_B) = \left(\frac{2\pi}{P_b} \right)^2 x_A^3. \quad (6.118)$$

Using $a_A = (m_B/m)a$, where $m = m_A + m_B$ is the total mass, and a is the semimajor axis of the relative orbit in the CM, and making use of Kepler's law $a^3 = Gm(P_b/2\pi)^2$, the mass function can be written as

$$f_A(m_A, m_B) = \frac{G}{c^3} \frac{(m_B \sin \iota)^3}{(m_A + m_B)^2}. \quad (6.119)$$

Similarly, from x_B and P_b we can form the mass function $f_B(m_A, m_B)$. Given the measured values of f_A and f_B , the condition $\sin \iota \leq 1$ restricts the allowed region in the (m_A, m_B) plane to the white, wedge-shaped

Table 6.3 The measured post-Keplerian parameters for PSR J0737–3039; $s = \sin \iota$ and r are the shape and range of Shapiro delay, respectively. From Kramer *et al.* (2006).

parameter	value
$\langle \dot{\omega} \rangle$ (deg/yr)	16.89947(68)
γ (ms)	0.3856(26)
\dot{P}_b	$-1.252(17) \times 10^{-12}$
s	0.99974(−39, +16)
r (μs)	6.21(33)

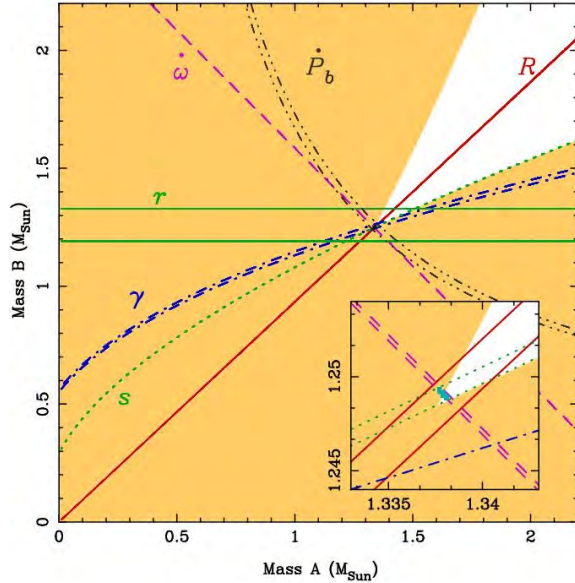


Fig. 6.8 The mass–mass diagram for the double pulsar system J0737–3039. Inset is an enlarged view of the small square where the various constraints intersect. From Kramer *et al.* (2006).

part. The fact that $\sin \iota$ turns out to be very close to one is reflected in the fact that the intersection between the various curves is very close to the cusp of the wedge-shaped region.

With more observation time, the accuracy of these data will increase further, and it is expected that one will soon have to use post-Newtonian corrections to the orbit of higher order than $(v/c)^2$. Potentially, this could allow the observation of corrections that depend on the moment of inertia of the neutron stars, and therefore to obtain a direct measure of the NS radius. This will be of great interest, since the mass–radius relation of a NS is characteristic of its equation of state, as we will discuss in Vol. 2.

PSR B1534+12

Together with the Hulse–Taylor pulsar and the double pulsar, this is the other system in which to date has been possible to measure the decrease in orbital period due to GW emission. It was discovered in 1991 with the Arecibo telescope. It is significantly brighter than the Hulse–Taylor pulsar, and its pulse has a narrow peak, allowing precise timing measurement. Furthermore, the orbit is nearly edge-on, which facilitates the measure of the range r and shape s of the Shapiro delay. As a result, after ten years of data, the five post-Keplerian $\{\dot{\omega}, \gamma, \dot{P}_b, r, s\}$ parameters have been measured. As discussed above, this in principle allows us to have three independent tests of general relativity, since these

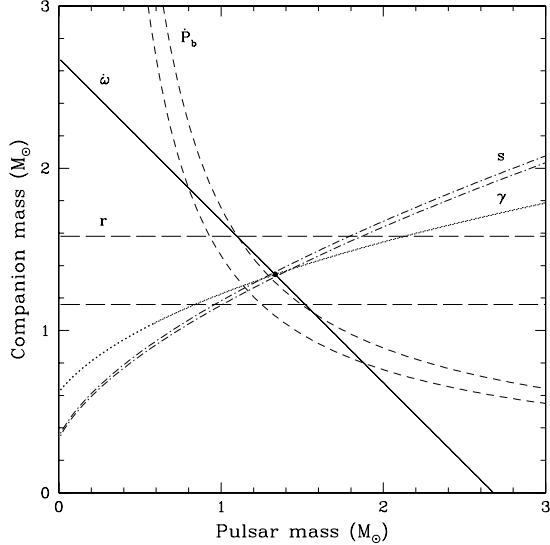


Fig. 6.9 The mass–mass diagram for PSR B1534+12. From Stairs *et al.* (2002).

five parameters are fixed in terms of the two masses m_p and m_c . We see from Fig. 6.9 that the three curves corresponding to $\dot{\omega}$, γ and s meet indeed at a single point in the (m_p, m_c) plane, providing an agreement between theory and experiment at a level of about 1%. The value of r is only measured with a precision of about 20%, but still its value is centered on the general relativity prediction. There is instead a small discrepancy for \dot{P}_b . However, the value of \dot{P}_b is quite sensitive to the correction v_T^2/d in eq. (6.104), since the pulsar has a significant proper motion and is at a close distance from us. If one estimates the distance d from the dispersion measure, one finds $d \simeq 0.7$ kpc. However, this estimate implies a model for the electron distribution in the galaxy (the quantity n_e which enters in eq. (6.37)). This model, due to Cordes and Taylor, has mostly a statistical significance, and can be in error for a single pulsar. After correcting for galactic acceleration and proper motion using eq. (6.104) with $d \simeq 0.7$ kpc, one finds

$$\dot{P}_b^{\text{obs}} - \dot{P}_b^{\text{gal}} = (-0.174 \pm 0.011) \times 10^{-12}, \quad (6.120)$$

to be compared with the prediction of general relativity

$$\dot{P}_b^{\text{GR}} = -0.192 \times 10^{-12}, \quad (6.121)$$

so the measured value differs from this prediction by about 1.7 standard deviations. We can however reverse the logic, and assume the correctness of the prediction of general relativity for \dot{P}_b , which, at this level of precision, is by now established beyond any doubt from the Hulse–Taylor pulsar and from the double pulsar, and we can use the measured

value of \dot{P}_b to obtain a better estimate of the distance d to the pulsar.

This method yields $d = 1.02 \pm 0.05$ kpc.

Further reading

- For a general introduction to pulsars, see Lyne and Graham-Smith (2005) and Lorimer (2005). For a catalogue of pulsars see the ATNF catalogue, at www.atnf.csiro.au/research/pulsar/psrcat.
- For the discovery of PSR B1913+16, see Hulse and Taylor (1975), and the Nobel lectures of Hulse (1994) and of Taylor (1994). The observation of gravitational radiation from PSR B1913+16 is discussed in Taylor, Fowler and McCulloch (1979) and in Taylor and Weisberg (1982, 1989). An update of the results is given in Weisberg and Taylor (2002, 2004).
- Pulsar timing is reviewed in Backer and Hellings (1986) and in Stairs (2003). See also the textbooks Will (1993), Straumann (2004) and Lyne and Graham-Smith (2005). A review of the comparison with experiments of general relativistic effects such as Shapiro delay, etc. is given in Will (2006).
- An approximate timing formula was developed by Blanford and Teukolsky (1976), Epstein (1977, 1979) and Haugan (1985), and was adequate to describe the earlier data of the Hulse–Taylor pulsar, and to find evidence for GW emission, see Taylor and Weisberg (1982). With improved experimental accuracy it became necessary a full general-relativistic treatment, which was given by Damour and Deruelle (1985, 1986). Furthermore, in Damour and Deruelle (1986) it is shown how to parametrize the timing effects in a way common to a wide class of alternative theories of gravitations, performing a theory-independent analysis of the timing data, and therefore comparing general relativity to alternative theories. A comparison of different timing models is given in Taylor and Weisberg (1989). For further discussions of the full general-relativistic treatment see also Damour (1983) and Damour and Taylor (1991, 1992).
- The 1PN corrections to \dot{P}_b are computed in Blanchet and Schäfer (1989). This correction has the effect of multiplying \dot{P}_b by a factor $(1 + X_{1\text{PN}})$ where, for the Hulse–Taylor binary pulsar, $X_{1\text{PN}} \simeq 2.15 \times 10^{-5}$, far below the accuracy of eq. (6.5). This correction is however larger, and potentially more important, for the double pulsar. Higher-order post-Newtonian corrections, which depend also on the moment of inertia of the star, can be important in the measurement of other relativistic parameters, such as the periastron advance, and are discussed in Damour and Schäfer (1988).
- The discovery of the pulsar PSR J0737–3039A is reported in Burgay *et al.* (2003) and the detection of the companion as a pulsar in Lyne *et al.* (2004). The resulting tests of general relativity, including orbital decay because of GW emission, are discussed in Kramer *et al.* (2005), and updated in Kramer *et al.* (2006).
- The discovery of PSR B1534+12 is reported in Wolszczan (1991), and updated measurements of its orbital decay and other post-Keplerian parameters are reported in Stairs, Thorsett, Taylor and Wolszczan (2002).

Part II

Gravitational-wave experiments

Data analysis techniques

7

In this chapter we begin our study of GW experiments. The functioning principles and the sensitivities of existing or planned detectors will be examined in great detail in the subsequent chapters. In this chapter we rather introduce a number of general concepts which characterize any GW detector, and we discuss the crucial problem of how to extract a GW signal from the (typically much larger) detector noise.

In Section 7.1 we will see how the various noise generated inside a the detector can be conveniently treated referring them to the detector input, and are characterized by a *spectral strain sensitivity*, which has dimensions $1/\sqrt{\text{Hz}}$. In Section 7.2 we introduce the pattern functions that encode the detector angular sensitivity. We will then discuss in Section 7.3 the optimum filtering techniques that must be applied to the detector output. The importance of this procedure stems from the fact that, with existing detectors and with reasonable estimates of the GW signal, we expect that the GW signal will be buried into a much larger noise. The fact that we try to extract a small signal from noisy detectors is certainly not a new situation in physics. Rather on the contrary, it is a typical problem in many fields, e.g. in radio engineering where it has been much studied in connections with radars, or in radio astronomy for application to pulsar searches, and standard filtering techniques have been developed. We will see how these techniques are adapted to the problem of GW detection. The proper interpretation of the results obtained with matched filtering relies on notions of probability and statistics, that we discuss in Section 7.4. Here, after an introduction to the frequentist and the Bayesian frameworks, we discuss how to reconstruct the parameters of the source and how to examine the statistical significance of the observation of an event with a given signal-to-noise ratio. Then, in Sections 7.5–7.8, we will examine the application of these concepts to various classes of GW signals, i.e. bursts, periodic signals, coalescing binaries and stochastic backgrounds.

7.1 The noise spectral density

The output of any GW detector is a time series, which describes for instance the oscillation state of a resonant mass, or the phase shift of the light recombined after traveling in the two arms of an interferometer. This output will be a combination of a true GW signal (hopefully) and of noise. To understand how signal and noise combine, it is useful to think of a GW detector as a linear system. At its input there is the GW

7.1 Noise spectral density	335
7.2 Pattern functions	339
7.3 Matched filtering	343
7.4 Probability and statistics	346
7.5 Bursts	361
7.6 Periodic sources	371
7.7 Coalescences	387
7.8 Stochastic backgrounds	392

signal that we want to detect. More precisely, the input and output of the detector are scalar quantities, while the GW is described by a tensor h_{ij} . So, in general, the input of the detector will have the form

$$h(t) = D^{ij} h_{ij}(t), \quad (7.1)$$

where D^{ij} is a constant tensor which depends on the detector geometry, and is known as the *detector tensor*. For example, for a detector which is driven only by the (x, x) component of h_{ij} (which, as we will see, is the case for a resonant bar oriented along the x axis), $D^{ij} = 1$ if $i = j = 1$ and $D^{ij} = 0$ otherwise. We will later compute the explicit form of D^{ij} for interferometers and for resonant masses.

For a linear system, the output of the detector is a linear function, in frequency space, of the input $h(t)$, that is, the output $h_{\text{out}}(t)$ of the detector (in the absence of noise) is related to the input $h(t)$ by

$$\tilde{h}_{\text{out}}(f) = T(f) \tilde{h}(f), \quad (7.2)$$

where $T(f)$ is known as the *transfer function* of the system. However, in the output of any real detector there will also be noise, so the output $s_{\text{out}}(t)$ will be rather given by

$$s_{\text{out}}(t) = h_{\text{out}}(t) + n_{\text{out}}(t). \quad (7.3)$$

More precisely, a detector can be modeled as a linear system with many stages, labeled by $i = 1, \dots, N$, each one with its own transfer function $T_i(f)$, so the total transfer function is $T(f) = \prod_i T_i(f)$. For example, we will see in Chapter 8 that resonant-bar detectors are composed of a heavy aluminum cylinder which is set into oscillation by an incoming GW; its energy is then transferred to a lighter mechanical oscillator, coupled to the heavy bar, which works as a mechanical amplifier, then it is transformed into an electric signal by an LC circuit coupled to the light oscillator, and then this electric signal is further amplified by one or more SQUIDS, and recorded. Clearly, noise can be generated at each of these stages. Each noise will propagate to the output with a transfer function which depends on the point of the linear system at which it first appeared, see Fig. 7.1, and will contribute to total noise $n_{\text{out}}(t)$ at the output. It is convenient to refer each noise to the detector input, defining the quantity $n(t)$ from

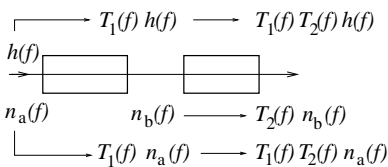


Fig. 7.1 A schematic representation of a detector as a linear system. The full transfer function $T(f)$ is the product of the separate transfer function $T_i(f)$, and $\tilde{n}_{\text{out}}(f) = T_1(f)T_2(f)n_a(f) + T_2(f)n_b(f)$.

where $n_{\text{out}}(t)$ is the total noise measured at the output. That is, $n(t)$ is a fictitious noise that, if it were injected at the detector input, and if there were no other noise inside the detector, would produce at the output the noise $n_{\text{out}}(t)$ that is actually observed. It is therefore the quantity that we can compare directly with $h(t)$, i.e. to the effect due to the GW. We then define

$$s(t) = h(t) + n(t), \quad (7.5)$$

and we can simply think of the detector as if $s(t)$ were its output, composed of a noise $n(t)$ and a GW signal $h(t)$,¹ and the detection problem is how to distinguish $h(t)$ from $n(t)$. In the following, when we speak of the detector output, we will always refer to $s(t)$.² If one has a theoretical model for a given source of noise $n_i(t)$, which appears at a given stage of the linear system, we can compare it with $h(t)$ simply multiplying it by the inverse of the appropriate transfer function, in order to refer this noise to the detector input. Equivalently, of course, one could refer both the noise and the signal to the true detector output, and compare $n_{\text{out}}(t)$ to the quantity $h_{\text{out}}(t)$ whose Fourier transform is given by eq. (7.2). However, the great advantage of referring everything to the input is that $n(t)$ gives a measure of the minimum value of $h(t)$ that can be detected and $h(t)$, apart from the geometrical factor D^{ij} which is always of order one, depends only on the incoming GW. In contrast, $h_{\text{out}}(t)$ depends on the transfer function of the system, and different detectors can have transfer functions which differ by many orders of magnitude. Thus, the use of $n_{\text{out}}(t)$ and $h_{\text{out}}(t)$ would be very unpractical when we want to compare the performances of different detectors.

So, in the above sense, we take $n(t)$ to be the detector's noise. If the noise is stationary, as we assume for the moment, the different Fourier components are uncorrelated, and therefore the ensemble average³ of the Fourier components of the noise is of the form

$$\langle \tilde{n}^*(f) \tilde{n}(f') \rangle = \delta(f - f') \frac{1}{2} S_n(f). \quad (7.6)$$

The above equation defines the function $S_n(f)$. Since $n(t)$ is real, $\tilde{n}(-f) = \tilde{n}^*(f)$ and therefore $S_n(-f) = S_n(f)$. If $n(t)$ is dimensionless, as we will assume, $S_n(f)$ has dimensions Hz^{-1} . Without loss of generality, we can also assume that

$$\langle n(t) \rangle = 0. \quad (7.7)$$

Observe that, for $f = f'$, the right-hand side of eq. (7.6) diverges. However, in any real experiment we have a finite value of the time T used to measure $\tilde{n}(f)$, see Note 3. Restricting the time interval to $-T/2 < t < T/2$ we have

$$\delta(f = 0) \rightarrow \left[\int_{-T/2}^{T/2} dt e^{i2\pi ft} \right]_{f=0} = T. \quad (7.8)$$

Then, from eq. (7.6) with $f = f'$, we get

$$\langle |\tilde{n}(f)|^2 \rangle = \frac{1}{2} S_n(f) T. \quad (7.9)$$

For a function defined on the interval $[-T/2, T/2]$, the Fourier modes have discrete frequencies $f_n = n/T$, so the resolution in frequency is given by

$$\Delta f = \frac{1}{T}. \quad (7.10)$$

¹One often multiplies the detector output by $T^{-1}(f)$ already at the level of data acquisition, so in this sense $s(t)$ is really the output of the data acquisition system.

²Some more nomenclature: we will always use the word "event" to indicate that in the detector happened something, which deserves further scrutiny. At this stage, it could be due to a GW or (much more likely) to noise. An event which is already assumed to have been generated by a GW will be called a "GW signal". The letter s conventionally used to denote the detector output $s(t) = h(t) + n(t)$ does not stand for "signal" (the signal in this nomenclature is $h(t)$). It can rather be taken to denote the "strain amplitude" of the detector.

³The ensemble average is the average over many possible "realizations" of the system. In practice we have only one physical system, our detector, but we can follow it in time, so the ensemble average is replaced by a time average (this implicitly assumes that the system is ergodic). Then the ensemble average is computed measuring the noise $n(t)$ over a given time interval T , and considering this as a "realization" of the system. From this we obtain $\tilde{n}(f)$ (with a resolution in frequency $\Delta f = 1/T$). We then repeat the procedures over a subsequent time stretch, again of duration T and separated by a sufficient time shift from the first realization, so that the correlation between the noise $n(t)$ in the two stretches can be neglected, and we define this as a second independent realization of the system. Finally, we average $\tilde{n}(f)$ over many independent realizations. It is useful to keep in mind that a time-scale T is implicit in this procedure, and will indeed appear in the equations below.

We can then write eq. (7.9) also in the form

$$\frac{1}{2}S_n(f) = \langle |\tilde{n}(f)|^2 \rangle \Delta f. \quad (7.11)$$

The factor 1/2 is conventionally inserted in the definition (7.6) of $S_n(f)$, so that $\langle n^2(t) \rangle$ is obtained integrating $S_n(f)$ over the physical range $0 \leq f < \infty$, rather than from $-\infty$ to ∞ ,

$$\begin{aligned} \langle n^2(t) \rangle &= \langle n^2(t=0) \rangle \\ &= \int_{-\infty}^{\infty} df df' \langle n^*(f) n(f') \rangle \\ &= \frac{1}{2} \int_{-\infty}^{\infty} df S_n(f) \\ &= \int_0^{\infty} df S_n(f). \end{aligned} \quad (7.12)$$

The function $S_n(f)$ is known as the *noise spectral density* (or the noise spectral sensitivity, or the noise power spectrum). More precisely, it is called a *single-sided spectral density*, to emphasize that $\langle n^2(t) \rangle$ is obtained from it integrating only over the physical range of frequencies $f > 0$. Alternatively, we can write

$$\langle n^2(t) \rangle = \int_{-\infty}^{\infty} df S_n^{\text{double sided}}(f), \quad (7.13)$$

with $S_n^{\text{double sided}}(f) = (1/2)S_n(f)$. Throughout this book, when we will use the term spectral density or power spectrum, we will always refer to the single-sided quantity.

Equivalently, the noise of a detector can be characterized by $\sqrt{S_n(f)}$, which is called the *spectral strain sensitivity*, or *spectral amplitude*, and has dimensions Hz^{-1/2}. Note that, if the noise increases by a factor λ , $n(t) \rightarrow \lambda n(t)$, then $S_n(f) \rightarrow \lambda^2 S_n(f)$ while the strain sensitivity scales linearly.

Actually the definition (7.6), even if rather intuitive, is not mathematically rigorous, because the function $n(t)$ in general does not satisfy the conditions necessary for having a well-defined Fourier transform; for instance, on the interval $-\infty < t < \infty$, $n(t)$ does not necessarily go to zero at $t \rightarrow \pm\infty$, so $\tilde{n}(f)$ in general does not exist. A more precise definition of the spectral density is obtained considering the auto-correlation function of the noise,

$$R(\tau) \equiv \langle n(t + \tau) n(t) \rangle \quad (7.14)$$

A Gaussian stochastic process $n(t)$ is characterized uniquely by its average value $\langle n(t) \rangle$, that for a stationary noise is a constant and can be set to zero with a constant shift of $n(t)$, and by its auto-correlation function. Typically, the knowledge of the noise at time t gives us very little information on the value of the noise at a subsequent time $t + \tau$ with τ sufficiently large, that is, for $|\tau| \rightarrow \infty$, $R(\tau)$ goes to zero quite fast, e.g.

exponentially, $R(\tau) \sim \exp\{-|\tau|/\tau_c\}$. The limiting case is white noise, in which the noise at time t and at any subsequent time $t + \tau$ are totally uncorrelated, so for $\tau \neq 0$ we have $\langle n(t + \tau)n(t) \rangle = \langle n(t + \tau) \rangle \langle n(t) \rangle = 0$, and $R(\tau) \sim \delta(\tau)$.

The auto-correlation function therefore goes to zero very fast as $\tau \rightarrow \pm\infty$, and it satisfies the requirements for performing the Fourier transform. We can then define the (one-sided) noise spectral density $S_n(f)$ by

$$\frac{1}{2}S_n(f) \equiv \int_{-\infty}^{\infty} d\tau R(\tau) e^{i2\pi f\tau}. \quad (7.15)$$

The reality of $R(\tau)$ implies $S_n(-f) = S_n^*(f)$, while invariance under time translations gives $R(-\tau) = \langle n(t - \tau)n(t) \rangle = \langle n(t)n(t + \tau) \rangle = R(\tau)$, which implies $S_n(-f) = S_n(f)$. Inverting eq. (7.15),

$$\begin{aligned} R(\tau) &\equiv \langle n(t + \tau)n(t) \rangle \\ &= \frac{1}{2} \int_{-\infty}^{\infty} df S_n(f) e^{-i2\pi f\tau}, \end{aligned} \quad (7.16)$$

and in particular

$$\begin{aligned} R(0) &= \langle n^2(t) \rangle \\ &= \frac{1}{2} \int_{-\infty}^{\infty} df S_n(f) \\ &= \int_0^{\infty} df S_n(f). \end{aligned} \quad (7.17)$$

Comparing this result with eq. (7.12) we see that, when $\tilde{n}(f)$ exists, eqs. (7.6) and (7.15) are equivalent definitions of S_n . Otherwise, only eq. (7.15) applies. Equation (7.15) is known as the Wiener–Khintchin relation.

If $R(\tau) \sim \delta(\tau)$, we see from eq. (7.15) that $S_n(f)$ is independent of frequency and therefore we have white noise. If instead $S_n(f)$ depends on f , one speaks generically of colored noise. A typical example is $1/f$ noise, which is a generic denomination for a noise where $S_n(f)$ has a power-law behavior, $S_n(f) \sim 1/f^\gamma$, over many decades in frequency.

7.2 Pattern functions and angular sensitivity

From eq. (1.58), we know that a GW with a given propagation direction $\hat{\mathbf{n}}$ can be written as

$$h_{ij}(t, \mathbf{x}) = \sum_{A=+, \times} e_{ij}^A(\hat{\mathbf{n}}) \int_{-\infty}^{\infty} df \tilde{h}_A(f) e^{-2\pi if(t - \hat{\mathbf{n}} \cdot \mathbf{x}/c)}, \quad (7.18)$$

where e_{ij}^A are the polarization tensors given in eq. (1.54). We take $\mathbf{x} = 0$ as the location of the detector. For a detector which is sensitive only to GWs with a reduced wavelength much larger than its size, such as

resonant masses and ground-based interferometers, we have $2\pi f \hat{\mathbf{n}} \cdot \mathbf{x} = \hat{\mathbf{n}} \cdot \mathbf{x}/\lambda \ll 1$ over the whole detector, and we can neglect the spatial dependence of $h_{ab}(t, \mathbf{x})$. So, to study the interaction of GWs with such detectors we can write simply

$$\begin{aligned} h_{ij}(t) &= \sum_{A=+, \times} e_{ij}^A(\hat{\mathbf{n}}) \int_{-\infty}^{\infty} df \tilde{h}_A(f) e^{-2\pi ift} \\ &= \sum_{A=+, \times} e_{ij}^A(\hat{\mathbf{n}}) h_A(t). \end{aligned} \quad (7.19)$$

Combining this with eq. (7.1) we see that the contribution of GWs to the scalar output of the detector can be written as

$$h(t) = \sum_{A=+, \times} D^{ij} e_{ij}^A(\hat{\mathbf{n}}) h_A(t). \quad (7.20)$$

It is then convenient to define the *detector pattern functions* $F_A(\hat{\mathbf{n}})$,

$$F_A(\hat{\mathbf{n}}) = D^{ij} e_{ij}^A(\hat{\mathbf{n}}). \quad (7.21)$$

The pattern functions depend on the direction $\hat{\mathbf{n}} = (\theta, \phi)$ of propagation of the wave, and in terms of them eq. (7.20) becomes

$$h(t) = h_+(t) F_+(\theta, \phi) + h_\times(t) F_\times(\theta, \phi). \quad (7.22)$$

The above equations assume that we have chosen a system of axes $(\hat{\mathbf{u}}, \hat{\mathbf{v}})$, in the plane orthogonal to the propagation direction $\hat{\mathbf{n}}$ of the wave, with respect to which the polarizations h_+ and h_\times are defined. It is interesting to see what happens if we change this system of axes, performing a rotation by an angle ψ in the transverse plane. Then the axes $(\hat{\mathbf{u}}, \hat{\mathbf{v}})$ are rotated to new axes $(\hat{\mathbf{u}}', \hat{\mathbf{v}}')$ given by

$$\begin{aligned} \hat{\mathbf{u}}' &= \hat{\mathbf{u}} \cos \psi - \hat{\mathbf{v}} \sin \psi, \\ \hat{\mathbf{v}}' &= \hat{\mathbf{u}} \sin \psi + \hat{\mathbf{v}} \cos \psi, \end{aligned} \quad (7.23)$$

where we used the same conventions on the sign of ψ as in eqs. (2.188) and (2.194). With respect to the $(\hat{\mathbf{u}}, \hat{\mathbf{v}})$ axes, the amplitudes of the plus and cross polarizations have values h_+ and h_\times , while with respect to the $(\hat{\mathbf{u}}', \hat{\mathbf{v}}')$ axes, they have the values h'_+ and h'_\times . Equations (1.49) and (1.50) show that h'_+ and h'_\times are related to h_+ and h_\times by

$$h'_+ = h_+ \cos 2\psi - h_\times \sin 2\psi, \quad (7.24)$$

$$h'_\times = h_+ \sin 2\psi + h_\times \cos 2\psi. \quad (7.25)$$

In the new frame, the definition (1.54) states that the polarization tensors are given by

$$(e_{ij}^+)'(\hat{\mathbf{n}}) = \hat{\mathbf{u}}'_i \hat{\mathbf{u}}'_j - \hat{\mathbf{v}}'_i \hat{\mathbf{v}}'_j, \quad (e_{ij}^\times)'(\hat{\mathbf{n}}) = \hat{\mathbf{u}}'_i \hat{\mathbf{v}}'_j + \hat{\mathbf{v}}'_i \hat{\mathbf{u}}'_j. \quad (7.26)$$

Then, using eq. (7.23), we find

$$(e_{ij}^+)'(\hat{\mathbf{n}}) = e_{ij}^+(\hat{\mathbf{n}}) \cos 2\psi - e_{ij}^\times \sin 2\psi, \quad (7.27)$$

$$(e_{ij}^\times)'(\hat{\mathbf{n}}) = e_{ij}^+(\hat{\mathbf{n}}) \sin 2\psi + e_{ij}^\times \cos 2\psi. \quad (7.28)$$

The pattern functions F_A depends on the polarization tensors e_{ij}^A through eq. (7.21). Since the detector tensor is a fixed quantity, independent of ψ , we find that in the new frame

$$F'_+(\hat{\mathbf{n}}) = F_+(\hat{\mathbf{n}}) \cos 2\psi - F_\times(\hat{\mathbf{n}}) \sin 2\psi, \quad (7.29)$$

$$F'_\times(\hat{\mathbf{n}}) = F_+(\hat{\mathbf{n}}) \sin 2\psi + F_\times(\hat{\mathbf{n}}) \cos 2\psi. \quad (7.30)$$

Combining this transformation of the pattern functions with the transformation of h_+ , h_\times given in eqs. (7.24) and (7.25), we see that $h(t)$ in eq. (7.22) is independent of ψ .

Of course, once a choice of the axes $(\hat{\mathbf{u}}, \hat{\mathbf{v}})$ used to define the polarization is made, then the pattern functions F_A depends on θ and ϕ only. However, it is sometime useful to keep generic the definition of the $(\hat{\mathbf{u}}, \hat{\mathbf{v}})$ axes in the transverse plane, and to parametrize the possible choices by the angle ψ . In this case, the pattern functions depend also on ψ , and

$$F_+(\hat{\mathbf{n}}; \psi) = F_+(\hat{\mathbf{n}}; 0) \cos 2\psi - F_\times(\hat{\mathbf{n}}; 0) \sin 2\psi, \quad (7.31)$$

$$F_\times(\hat{\mathbf{n}}; \psi) = F_+(\hat{\mathbf{n}}; 0) \sin 2\psi + F_\times(\hat{\mathbf{n}}; 0) \cos 2\psi. \quad (7.32)$$

A useful identity satisfied by the pattern functions, independently of the specific form of the detector tensor D_{ij} , is⁴

$$\int \frac{d^2 \hat{\mathbf{n}}}{4\pi} F_+(\hat{\mathbf{n}}) F_\times(\hat{\mathbf{n}}) = 0, \quad (7.33)$$

where as usual $d^2 \hat{\mathbf{n}} = d\cos\theta d\phi$ is the integral over the solid angle. As for the integral over $d^2 \hat{\mathbf{n}}$ of F_+^2 and of F_\times^2 , with a generic choice of the angle ψ they are different. We will see for instance that one can choose

so that F_\times vanishes while F_+ is non-zero, or viceversa. However, if we average over the angle ψ , we find

$$\int_0^{2\pi} \frac{d\psi}{2\pi} F_+^2(\hat{\mathbf{n}}; \psi) = \int_0^{2\pi} \frac{d\psi}{2\pi} F_\times^2(\hat{\mathbf{n}}; \psi). \quad (7.34)$$

In fact, inserting eqs. (7.31) and (7.32) into eq. (7.34), the equality follows from $\int d\psi \sin 2\psi \cos 2\psi = 0$ and $\int d\psi \sin^2 \psi = \int d\psi \cos^2 \psi$. From this, it also trivially follows that

$$\langle F_+^2(\hat{\mathbf{n}}; \psi) \rangle = \langle F_\times^2(\hat{\mathbf{n}}; \psi) \rangle, \quad (7.35)$$

where

$$\langle \dots \rangle \equiv \int_0^{2\pi} \frac{d\psi}{2\pi} \int \frac{d^2 \hat{\mathbf{n}}}{4\pi} (\dots). \quad (7.36)$$

For later use we also define the angular efficiency factor

$$F = \langle F_+^2 \rangle + \langle F_\times^2 \rangle = 2\langle F_+^2 \rangle. \quad (7.37)$$

⁴Equation (7.33) can be shown in full generality writing

$$\begin{aligned} & \int d^2 \hat{\mathbf{n}} F_+(\hat{\mathbf{n}}) F_\times(\hat{\mathbf{n}}) \\ &= D_{ab} D_{cd} \int d^2 \hat{\mathbf{n}} e_{ab}^+(\hat{\mathbf{n}}) e_{cd}^\times(\hat{\mathbf{n}}), \end{aligned}$$

and using eq. (1.54), which shows that $e_{ab}^+(\hat{\mathbf{n}}) e_{cd}^\times(\hat{\mathbf{n}})$ is a sum of terms such as $\hat{\mathbf{u}}_a \hat{\mathbf{u}}_b \hat{\mathbf{u}}_c \hat{\mathbf{v}}_d$, which has three factors $\hat{\mathbf{u}}$ and one factor $\hat{\mathbf{v}}$, and of similar terms with $\hat{\mathbf{u}} \leftrightarrow \hat{\mathbf{v}}$. A simple way to see that the integral over $d^2 \hat{\mathbf{n}}$ vanishes is then to observe that, when we integrate over all possible values of $\hat{\mathbf{n}}$, for each term $\hat{\mathbf{u}}_a \hat{\mathbf{u}}_b \hat{\mathbf{u}}_c \hat{\mathbf{v}}_d$ there is also a corresponding term obtained with $\hat{\mathbf{u}} \rightarrow -\hat{\mathbf{u}}$ and $\hat{\mathbf{v}} \rightarrow +\hat{\mathbf{v}}$, which cancels it.

Table 7.1 The pattern functions $F(\theta, \phi; \psi = 0)$ for various detectors. For interferometers, the arms are perpendicular and along the (x, y) axis, (θ, ϕ) are the usual polar angles defined using the z axis as polar axis and, for a wave propagating along the z axis, ψ is the angle in the (x, y) plane measured from the x axis, just as ϕ . For cylindrical bars, θ is measured from the longitudinal axis of the bar and, if we denote by x the longitudinal axis, for a wave propagating along the z axis, again ψ is the angle in the (x, y) plane measured from the x axis. For resonant spheres, the modes $m = 0, 1c, 1s, 2c, 2s$ are combinations of the five quadrupolar modes with $m = -2, \dots, 2$, defined in Zhou and Michelson (1995). The angular efficiency factor F is defined in eqs. (7.36) and (7.37). Observe that the mode $m = 0$ of a sphere has the same pattern functions as a cylindrical bar (apart from a constant), while the mode $m = 2c$ has the same pattern functions as an interferometer.

Detector	$F_+(\theta, \phi; \psi = 0)$	$F_\times(\theta, \phi; \psi = 0)$	F
interferometers	$\frac{1}{2}(1 + \cos^2 \theta) \cos 2\phi$	$\cos \theta \sin 2\phi$	2/5
cylindrical bars	$\sin^2 \theta$	0	8/15
resonant spheres			
$m = 0$	$(\sqrt{3}/2) \sin^2 \theta$	0	2/5
$m = 1s$	$-\sin \theta \cos \theta \sin \phi$	$\sin \theta \cos \phi$	2/5
$m = 1c$	$\sin \theta \cos \theta \cos \phi$	$\sin \theta \sin \phi$	2/5
$m = 2s$	$-\frac{1}{2}(1 + \cos^2 \theta) \sin 2\phi$	$\cos \theta \cos 2\phi$	2/5
$m = 2c$	$\frac{1}{2}(1 + \cos^2 \theta) \cos 2\phi$	$\cos \theta \sin 2\phi$	2/5

We will compute the explicit forms of $F_{+, \times}(\theta, \phi; \psi)$ for bars and interferometers, in their respective chapters. We find useful to collect here the result that we will find for interferometers, cylindrical bars and resonant spheres; in Table 7.1 we give the value of $F(\theta, \phi; \psi = 0)$ (with appropriate definitions of the angles, discussed in the table caption and, in more detail, in their respective chapters), and the values of the angular efficiency factor F .

As we see from the above table, the pattern functions are relatively smooth functions of the position of the source in the sky. On the one hand, this has the positive consequence that GW detectors have a large sky coverage, of almost 4π , except for some blind directions. This is very different from conventional astronomy, where a telescope must point the source very precisely to detect it. The reverse of the coin, however, is that with a single GW detector we cannot determine the position of the source in the sky. A single detector has an output $h(t)$ that, according to eq. (7.22), depends on four unknown: the two functions $h_{+, \times}(t)$ and the angles (θ, ϕ) that give the source position. To disentangle these quantities we need a coincident observation by a network of detectors. With two detectors we have at our disposal their two outputs $h_1(t)$ and $h_2(t)$, and the delay time τ_{12} between these two signals. These three quantities are not yet sufficient to solve for the four unknown $h_+(t), h_\times(t), \theta$ and ϕ .

However, with three interferometers we have five measured quantities, the three functions $h_i(t)$, $i = 1, 2, 3$, and two independent delay times, so we can solve for $h_+(t)$, $h_\times(t)$, θ and ϕ . The actual accuracy of the reconstruction depends on the signal-to-noise ratio. For typical expected signals, at first-generation interferometers the angular resolution could be of order one square degree.

7.3 Matched filtering

We have seen above that the detector output will be of the general form $s(t) = h(t) + n(t)$. Naively, one might then think that we can detect a GW signal only when $|h(t)|$ is larger than $|n(t)|$. This would be very unfortunate since we will see that, with plausible estimates of the expected GW signals bathing the Earth, and with the sensitivity of the present generation of detectors, we will rather be in the situation $|h(t)| \ll |n(t)|$.

The fundamental question that we ask in this section is then how can we dig out the GW signal from a much larger noise. This is a classical problem in many fields of physics or in radio engineering, and the answer is that we can detect values of $h(t)$ much smaller than the floor of the noise if we know, at least to some level of accuracy, the form of $h(t)$.⁵ To understand the basic idea, we can first illustrate a simple version of this “filtering” procedure, before moving to optimal filtering. Suppose that $s(t) = h(t) + n(t)$, and that we know the form of the GW signal $h(t)$ that we are hunting for. Then we can multiply the output $s(t)$ by $h(t)$, integrate over an observation time T , and divide by T ,

$$\frac{1}{T} \int_0^T dt s(t)h(t) = \frac{1}{T} \int_0^T dt h^2(t) + \frac{1}{T} \int_0^T dt n(t)h(t). \quad (7.38)$$

The crucial point now is that $h(t)$ and $n(t)$, separately, are oscillating functions. However, the integrand of the first integral on the right-hand side is definite positive; it might be for instance the integral of something like $\cos^2 \omega t$, times a slowly varying function of time; this integral then grows, for large T , as T . Its value averaged over a time T is therefore of order one in T ,

$$\frac{1}{T} \int_0^T dt h^2(t) \sim h_0^2, \quad (7.39)$$

where h_0 is the characteristic amplitude of the oscillating function $h(t)$. In contrast, since the noise $n(t)$ and our chosen function $h(t)$ are uncorrelated, the quantity $n(t)h(t)$ is oscillating, and its integral will grow only as $T^{1/2}$ for large T (as is typical of systems performing a random walk), so

$$\frac{1}{T} \int_0^T dt n(t)h(t) \sim \left(\frac{\tau_0}{T}\right)^{1/2} n_0 h_0, \quad (7.40)$$

where n_0 is the characteristic amplitude of the oscillating function $n(t)$, and τ_0 a typical characteristic time, e.g. the period of the oscillating

⁵More precisely, we must know $h(t)$ and have an idea of the typical scales of variations of the noise, in order to exploit their different behaviors.

function $h(t)$. Thus, in the limit $T \rightarrow \infty$, the second term on the right-hand side of eq. (7.38) averages to zero, and we have “filtered out” the contribution of the noise from the output. Of course, in practice we cannot sent T to infinity, either because the signal $h(t)$ itself has a limited temporal duration or because we are limited by the total available observation time. Still we see that, to detect the signal given in eq. (7.39) against the background of eq. (7.40), it is not necessary to have $h_0 > n_0$, but it suffices to have $h_0 > (\tau_0/T)^{1/2}n_0$. For example, for a periodic signal with a period $\tau_0 \sim 1$ ms, such as a millisecond pulsar, observed for $T = 1$ yr, we have $(\tau_0/T)^{1/2} \sim 10^{-5}$. We can therefore dig very deeply into the noise floor.

After having discussed the intuitive idea, let us see how the above procedure can be made more precise mathematically, and optimized in order to obtain the highest possible value of the signal-to-noise ratio. We define

$$\hat{s} = \int_{-\infty}^{\infty} dt s(t)K(t), \quad (7.41)$$

where $K(t)$ is called the *filter* function. We assume that we know what GW signal we are looking for, i.e. we know the form of $h(t)$. We then ask what is the filter function that maximizes the signal-to-noise ratio, for such a signal. Since the filter function is chosen so to “match” the signal that we are looking for, the technique is called matched filtering.⁶

The signal-to-noise ratio (in amplitude) is defined as S/N , where S is the expected value of \hat{s} when the signal is present, and N is the rms value of \hat{s} when the signal is absent. Since $\langle n(t) \rangle = 0$, we have

$$\begin{aligned} S &= \int_{-\infty}^{\infty} dt \langle s(t) \rangle K(t) \\ &= \int_{-\infty}^{\infty} dt h(t)K(t) \\ &= \int_{-\infty}^{\infty} df \tilde{h}(f)\tilde{K}^*(f), \end{aligned} \quad (7.42)$$

while

$$\begin{aligned} N^2 &= [\langle \hat{s}^2(t) \rangle - \langle \hat{s}(t) \rangle^2]_{h=0} \\ &= \langle \hat{s}^2(t) \rangle_{h=0} \\ &= \int_{-\infty}^{\infty} dt dt' K(t)K(t') \langle n(t)n(t') \rangle \\ &= \int_{-\infty}^{\infty} dt dt' K(t)K(t') \int_{-\infty}^{\infty} df df' e^{2\pi ift - 2\pi if't'} \langle \tilde{n}^*(f)\tilde{n}(f') \rangle. \end{aligned} \quad (7.43)$$

Using eq. (7.6) we obtain

$$N^2 = \int_{-\infty}^{\infty} df \frac{1}{2} S_n(f) |\tilde{K}(f)|^2, \quad (7.44)$$

and therefore

$$\frac{S}{N} = \frac{\int_{-\infty}^{\infty} df \tilde{h}(f)\tilde{K}^*(f)}{\left[\int_{-\infty}^{\infty} df (1/2)S_n(f)|\tilde{K}(f)|^2 \right]^{1/2}}. \quad (7.45)$$

⁶We limit ourselves to linear filters, i.e. filters in which \hat{s} is linear in $s(t)$, as in eq. (7.41).

We now ask what is the filter $K(t)$ that maximizes S/N , for a given $h(t)$. This variational problem is elegantly solved by defining the scalar product between two real functions $A(t)$ and $B(t)$, by

$$\begin{aligned} (A|B) &= \text{Re} \int_{-\infty}^{\infty} df \frac{\tilde{A}^*(f)\tilde{B}(f)}{(1/2)S_n(f)} \\ &= 4 \text{Re} \int_0^{\infty} df \frac{\tilde{A}^*(f)\tilde{B}(f)}{S_n(f)}, \end{aligned} \quad (7.46)$$

where Re denotes the real part, and the second line holds because we take $A(t)$ and $B(t)$ to be real functions, so that $\tilde{A}(-f) = \tilde{A}^*(f)$ (recall also that $S_n(-f) = S_n(f)$). Since $S_n(f) > 0$, this scalar product is positive definite. Then eq. (7.45) can be written as

$$\frac{S}{N} = \frac{(u|h)}{(u|u)^{1/2}}. \quad (7.47)$$

where $u(t)$ is the function whose Fourier transform is

$$\tilde{u}(f) = \frac{1}{2}S_n(f)\tilde{K}(f). \quad (7.48)$$

In this form, the solution is clear. We are searching for the “vector” of unit norm $\hat{n} = u/(u|u)^{1/2}$, such that its scalar product with the “vector” h is maximum. This is obtained choosing \hat{n} and h parallel, i.e. $\tilde{u}(f)$ proportional to $\tilde{h}(f)$, so we get

$$\tilde{K}(f) = \text{const.} \frac{\tilde{h}(f)}{S_n(f)}. \quad (7.49)$$

The constant is arbitrary, since rescaling \hat{s} by an overall factor does not change its signal-to-noise ratio. Equation (7.49) defines the matched filter (or Wiener filter).⁷ In particular, if we are looking for a signal $h(t)$ embedded into white noise, so that $\tilde{S}_n(f)$ is a constant, then the best filter is provided by the signal itself, which is the filtering discussed in eq. (7.38). However, when $\tilde{S}_n(f)$ is not flat, eq. (7.49) tells us that we must weight less the frequency region where the detector is more noisy, a very natural result.

Inserting the solution (7.49) into eq. (7.48) we get $\tilde{u} = \text{const.} \times \tilde{h}$. Plugging this into eq. (7.47), the overall constant cancels and we get the optimal value of S/N ,

$$\left(\frac{S}{N}\right) = (h|h)^{1/2}, \quad (7.50)$$

that is

$$\left(\frac{S}{N}\right)^2 = 4 \int_0^{\infty} df \frac{|\tilde{h}(f)|^2}{S_n(f)}, \quad (7.51)$$

which is the optimal value of the signal-to-noise ratio.⁸ The above equations are completely general, and independent of the form of $\tilde{h}(f)$. In Sections 7.5–7.8 we will apply them to some specific signals.

⁷It is also common in the literature to write eq. (7.41) in the form $\hat{s} = \int_{-\infty}^{\infty} dt s(t)G(-t)$, and to call $G(t)$ the filter function. So $G(t) = K(-t)$ and $\tilde{G}(f) \sim \tilde{h}^*(f)/S_n(f)$.

⁸Recall from Section 7.1 that our $S_n(f)$ is single-sided. In terms of the double-sided spectral density, defined after eq. (7.13), we have $(S/N)^2 = \int_{-\infty}^{\infty} df |\tilde{h}(f)|^2/S_n^{\text{double sided}}(f)$.

7.4 Probability and statistics

The matched filtering technique discussed above (as well as other techniques that we will meet later in this chapter) provide us with a way to optimize the signal-to-noise ratio, assuming that a given signal is indeed present in our data stream. The issue that the experimenter normally faces (especially in the field of GW experiments) is however different. We do not know *a priori* whether a GW signal is present or not in a given stream of data, and we know even less its waveform. We can apply the matched filtering technique repeating it with many possible different filters, e.g. many possible starting times for the putative signal, many possible parameters describing a family of waveforms, etc. and we will correspondingly extract from our data stream a number of “events”,⁹ with various values of the signal-to-noise ratio S/N . What can we conclude from this? When can we claim detection of GWs? And, if we can claim detection, what can we learn from it, in particular how can we reconstruct the properties of the source (such as, for an astrophysical source, its direction, its distance, its mass, etc.), and with what accuracy?

To address these questions we need to use statistical reasoning. Before looking into the technical aspects, it is however useful to discuss more generally the statistical frameworks that one can use, as we do in the next subsection.

7.4.1 Frequentist and Bayesian approaches

An abstract definition of probability can be obtained by considering a set S with subsets A, B, \dots , whose interpretation for the moment is left open, and defining the probability P as a real-valued function that satisfies the Kolmogorov axioms: 1. For every A in S , $P(A) \geq 0$. 2. For disjoint subsets (i.e. $A \cap B = \emptyset$), $P(A \cup B) = P(A) + P(B)$, and 3. $P(S) = 1$. Furthermore, one defines the conditional probability $P(A|B)$ (i.e. the probability of A given B) as

$$P(A|B) = \frac{P(A \cap B)}{P(B)}. \quad (7.52)$$

There exist two main approaches to probability, frequentist (also called classical) and Bayesian, depending on the interpretations of the subsets A, B, \dots .

In the frequentist interpretation, A, B, \dots are the outcome of a repeatable experiment, and the probability $P(A)$ is defined as the frequency of occurrence of A , in the limit of an infinite number of repetitions. In this interpretation, the probabilities of obtaining some data are of course well-defined, and it also makes sense to consider the conditional probability of obtaining some data, given some hypothesis (or given a theory, or given the value of the parameters in a theory).¹⁰ Therefore, quantities such as $P(\text{data}|\text{hypothesis})$ or $P(\text{data}|\text{parameters})$ make sense. However, one is never allowed to speak of the probability that the

¹⁰The kind of example that appears in all textbooks: we toss a coin five times. What is the probability of getting all five times head (data), given that the coin has 50% probability of heads and tails (hypothesis)?

parameters take a given value, nor of the probability that a hypothesis, or a theory, is correct. Hypotheses, or theories, are not the outcome of a repeatable experiment. Rather, they are correct or they are wrong, and similarly the true value of a parameter in a theory is what it is, and these are facts that are not subject to probabilistic analysis.

In the Bayesian approach, instead, one is allowed to consider the probability of a hypothesis, or of a theory, or the probability that a parameter within a theory takes a given value. To define these probabilities, one starts from the identities $P(A \cap B) = P(A|B)P(B)$ and $P(B \cap A) = P(B|A)P(A)$, which follow from the definition (7.52) of conditional probability. On the other hand, $A \cap B = B \cap A$ and therefore

$$P(A|B) = \frac{P(B|A)P(A)}{P(B)}, \quad (7.53)$$

which is Bayes' theorem. Observe also that, from the axioms of probability given above, it follows that

$$P(B) = \sum_i P(B|A_i)P(A_i), \quad (7.54)$$

for any B and for A_i disjoint and such that $\cup_i A_i = S$. Therefore eq. (7.53) can be rewritten as

$$P(A|B) = \frac{P(B|A)P(A)}{\sum_i P(B|A_i)P(A_i)}, \quad (7.55)$$

so the denominator is just a normalization factor. As long as A and B are the outcome of a repeatable experiment, eq. (7.55) would be accepted also by frequentists. In the Bayesian approach, however, one applies this to $A = \text{hypothesis}$ (or parameters, or theory) and $B = \text{data}$. Then one finds that

$$P(\text{hypothesis}|\text{data}) \propto P(\text{data}|\text{hypothesis}) P(\text{hypothesis}). \quad (7.56)$$

The probability of the hypothesis given the data is called the *posterior probability*, and eq. (7.56) states that it is proportional to the product of two factors. The first is the probability of the data given the hypothesis (a “honest” frequentist probability), which is called the *likelihood function*. The second is the probability of the hypothesis, and is called the *prior probability* (or, simply, the prior). The latter cannot be determined just by performing identical trials (so it makes no sense to a frequentist) and, in the Bayesian approach, one must make assumptions to determine it. In fact, this prior probability in general can even depend on subjective factors, and on the state of knowledge of the person that makes the analysis. In the Bayesian interpretation, $P(\text{hypothesis})$ can be seen as the “degree of belief” that the hypothesis is true, and eq. (7.56) describes the evolution of this degree of belief due to the fact that we have performed the measurement. The prior probability describes the degree of belief in the hypothesis before the measurement was made, and the posterior probability describes the degree of belief after.¹¹

¹¹Observe also that eq. (7.56) is stated as a proportionality, so $P(\text{hypothesis}|\text{data})$ must be normalized summing over all possible hypothesis (or theories) that we want to compare, or integrating over a given domain of values for the continuous parameters.

This difference in approach implies also an important difference among the frequentist and the Bayesian notions of confidence interval and of confidence level (C.L.). The expression “confidence interval”, without further qualifications, refers to the frequentist definition, and has the following meaning. Suppose that we are performing repeated identical measurements of a physical quantity x . We want to express our result saying that, at a given confidence level, say 90%, $x_1 < x < x_2$. What is meant by this is the following. The true (unknown) value of x is a fixed number x_t , which is always the same in all repetitions of the experiment; each repetition provides a different interval $[x_1, x_2]$, that we want to construct in such a way that x_t will be contained inside this interval in 90% (or whatever the specified C.L.) of the repetitions, no matter what the true value x_t is. This is the frequentist concept of *coverage*. There is a general construction, given by Neyman in a famous 1937 paper, that allows us to construct the frequentist confidence intervals. We illustrate it in the simple case in which we know that the experimental apparatus provides values distributed as a Gaussian around the true value x_t , with a standard deviation σ ,

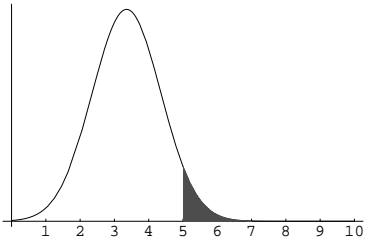


Fig. 7.2 The Neyman construction for the lower limit x_1 of the confidence interval. Here the measured value was $x_0 = 5$ and, to get the interval at 90% C.L., we look for a Gaussian distribution such that its area at $x \geq 5$ (shaded region) is 5% of the total area. This is a Gaussian centered in $x_1 \simeq x_0 - 1.64485\sigma$ (here we used $\sigma = 1$).

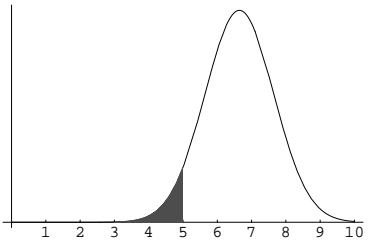


Fig. 7.3 The same as the previous figure, for the upper limit x_2 of the confidence interval. The Gaussian is now centered in $x_2 \simeq x_0 + 1.64485\sigma$.

Suppose that a given repetition of the experiment yields the value x_0 . The Neyman's construction (using for definiteness 90% C.L.) proceeds by finding a value $x_1 < x_0$ such that 5% of the area under $P(x|x_1)$ is at $x > x_0$. That is, we fix x_1 by requiring that a Gaussian distribution centered on x_1 , only in 5% of the cases produces values of x higher than x_0 , see Fig. 7.2. If the true value x_t were smaller than such x_1 , then the value x_0 that we observed was due to a statistical fluctuation that takes place in less than 5% of the repetitions, so choosing in this way the lower limit of the interval, we are wrong at most in 5% of the cases. The upper limit of the confidence interval is obtained similarly, by finding a value $x_2 > x_0$ such that 5% of the area under $P(x|x_2)$ is at $x < x_0$, see Fig. 7.3. Observe that the probabilistic variables in this construction are x_1 and x_2 , while the true value x_t is fixed (and unknown).

In contrast, the Bayesian approach constructs a probability distribution for the true value x_t . This is obtained from the likelihood function $P(\text{data}|\text{hypothesis})$ in eq. (7.56), where the hypothesis is that the true value of x is x_t and the data is the observed value x_0 . We denote this likelihood function as $\Lambda(x_0|x_t)$. In our case, this is the same as the Gaussian given in eq. (7.57), so $\Lambda(x_0|x_t) = P(x_0|x_t)$. As long as we interpret it as the probability of obtaining the value x_0 , given that the true value is x_t , the likelihood function is a legitimate frequentist concept. However, in the Bayesian approach, it is inserted into eq. (7.56), together in this case with a flat prior in x_t , to get a probability density function (p.d.f.) in the variable x_t , given the observed value x_0 ,

$$P(x_t|x_0) = \frac{1}{(2\pi\sigma^2)^{1/2}} \exp\left\{-\frac{(x_t - x_0)^2}{2\sigma^2}\right\}. \quad (7.58)$$

So, in this case we have a Gaussian distribution centered on x_0 (rather than on x_1 or on x_2 as in the Neyman construction), and we use it as a p.d.f. for x_t . The most probable value of x_t is found by maximizing this p.d.f., which of course gives $x_t = x_0$, and the Bayesian 90% confidence interval is defined as the interval which subtends an area equal to 90% of the total area of the p.d.f.¹² In the case of a Gaussian distribution, the Bayesian and frequentist definitions give the same result for x_1 and x_2 , even if the interpretation is different. However, in a general situation, the two definitions do not agree. The frequentist confidence interval, by construction, always has the prescribed coverage, i.e. we are sure that in the limit of a large number of repetitions, 90% (or whatever the chosen C.L.) of the confidence intervals obtained by the different repetitions of the experiment will include (“cover”) the true value x_t , no matter what x_t is. This covering properties is not necessarily true in the Bayesian procedure, which in certain cases yields intervals whose frequentist coverage is less than the stated C.L. (i.e. they undercover). This can happen in particular for event-counting experiments, that obey Poisson statistics, when the data sample is small.

Beside the situation when we have small numbers, the other typical situation where the Bayesian and frequentist approaches can give sensibly different answers is when the variable x , for physical reasons, has a bounded domain, and the measured values are close to the boundaries of the domain. An instructive example, that nicely illustrates the different results that can be obtained with the Bayesian and the frequentist approaches in such situations, is the following.¹³ Nowadays, we know from oscillation experiments that the three neutrinos have a small mass, with squared masses (more precisely, squared mass differences) between 10^{-5} and 10^{-4} eV². Before these results, a number of other experiments attempted a direct measure of the mass m_ν of the electron neutrino (or more precisely, of m_ν^2) from tritium beta decay. In the early 1990s the experimental situation was that various experiments reported negative values for their best estimate of m_ν^2 . This is not surprising in principle since, if m_ν^2 were really zero, or anyway much smaller than the experimental accuracy (as indeed it was), and if the distribution of the data is an unbiased Gaussian, on average half of the ensemble of the experiments should report negative values, and statistical fluctuations can drive the average over the experiments in the unphysical region $m_\nu^2 < 0$. However, these negative fluctuations happened to be so large that even the frequentist upper limit at 90% C.L. was negative, and was $m_\nu^2 < -16$ eV².¹⁴ To say the least, it is quite disturbing to set up a complicated experiment to come out with the conclusion that m_ν^2 is smaller than a negative value. The point is that this statement holds at 90% C.L., so it should be false in 10% of the cases, and here we know for sure that we are in this false 10%.¹⁵

A possible alternative in this case is to include our prior information that $m_\nu^2 \geq 0$. This suggests to take a Bayesian approach with a prior p.d.f. $P(m_\nu^2)$ which is zero when $m_\nu^2 < 0$, and uniform for $m_\nu^2 \geq 0$, and to use the resulting posterior p.d.f. to set the bound on m_ν^2 . Here however

¹²Such an interval is selected uniquely by imposing an extra requirement, typically that it is symmetric around the maximum, or that it is the minimum length interval. For a Gaussian distribution, these two conditions give of course the same result.

¹³We follow the paper by Cousins (1995), “Why isn’t every physicist a Bayesian?”, where the reader can find a very clear exposition of the difference between the Bayesian and frequentist approaches.

¹⁴Since the early 1990s, direct experiments (i.e. experiments not based on oscillations) on the electron neutrino mass squared have improved, but still their world average is negative, see Yao *et al.* [Particle Data Group] (2006).

¹⁵It should be mentioned that a strict application of the frequentist Neyman construction can never produce an upper limit in the unphysical region, but rather an empty confidence interval (which is equally disturbing). There is however a generalization of the Neyman construction that produces non-empty intervals in the physical region, see Feldman and Cousins (1998).

the problem arises as to whether, in the region $m_\nu^2 \geq 0$, the prior should be uniform in the variable m_ν^2 , or in m_ν , or in $\log m_\nu$, etc. Of course, a distribution $P(m_\nu^2)dm_\nu^2$ with $P(m_\nu^2) = \text{const.}$ is flat with respect to the variable m_ν^2 but, since $dm_\nu^2 = 2m_\nu dm_\nu$, it is linearly raising with respect to m_ν . The issue is significant since the resulting upper bound depends on the choice. In this specific problem the consensus finally settled on using a flat prior in m_ν^2 , which gave an upper bound, at 90% C.L., $m_\nu^2 < 26.6 \text{ eV}^2$.

A physicist that is not too much interested in the philosophical aspects of the debate, can take a pragmatic attitude and use a frequentist or a Bayesian approach, depending on the kind of experiment to be analyzed. In particular, elementary particle physics is very well suited for the frequentist approach. This basically stems from the fact that in this case it is the physicist that controls the parameters of the experiments (e.g. the kind of particle used in the beams, the beam energy, etc.) and can reproduce them accurately many times. We are therefore in the situation where the frequentist notion of repeated trials fits very well.¹⁶ The advantage is that this allows us to report objectively the outcome of the experiment, without the need of incorporating prior (and possibly subjective) beliefs.

On the other hand in astrophysics, and even more in GW astrophysics, the sources can be rare, they are not under the control of the experimenter, and each one is very interesting individually. If a single BH-BH binary coalesces, and we detect its signal in a GW experiment, we would obviously be very interested in questions such as in which direction the binary system was, at what distance from us, what were the masses of the two black holes, their spins, etc. A strict frequentist approach is inapplicable here. We do not have at our disposal an ensemble of identical BH-BH binaries located in that position, with the same value of the masses, etc. We just have that unique event, and we want to get the maximum out of it. In this case, a Bayesian approach can be more appropriate, since it allows us to ask questions such as “What was the most likely value of the position, masses, spin, etc. of the BHs?”. For this reason, while negative results, giving upper limits on the rate of GW signals, should normally be expressed in frequentist terms, the discussion of parameter estimation from a given positive detection, to which we turn next, should rather be performed within the Bayesian framework.

7.4.2 Parameters estimation

In Section 7.3, when we introduced the matched filtering technique, we assumed that the form of $h(t)$ is known. In practice, however, $h(t)$ will necessarily depend on a number of free parameters. For instance, if $h(t)$ is a short burst of GWs, among its parameters we will certainly have its time of arrival t_0 . When searching for very short bursts we might simply use a Dirac delta, so $h(t) = h_0\delta(t - t_0)$, but more generally we might also wish to include its temporal width Δt and possibly more parameters

¹⁶In fact, in the standard compilation of experimental high-energy physics data, the Particle Data Group (PDG) “Reviews of Particle Properties”, essentially all measurements and their statistical uncertainties are reported within the frequentist framework.

describing the shape of the pulse. For a coalescing binary, among the parameters we will have the time of entry in the interferometer bandwidth, the distance to the source, the star masses, etc.

Therefore, we must consider a family of possible waveforms, or *templates*, that we denote generically as $h(t; \theta)$, where $\theta = \{\theta_1, \dots, \theta_N\}$ is a collection of parameters. Correspondingly, we have a family of optimal filters $K(t; \theta)$, determined through eq. (7.49), $\tilde{K}(f; \theta) \sim \tilde{h}(f; \theta)/S_n(f)$. In practice, this means that we must discretize the θ -space, and repeat the filtering procedure many times, once for each point of this discretized parameter space (except that for some parameters the maximization procedure can be done analytically, see below).

The problem that we address in this section is the following. Suppose that a GW signal has indeed been detected, which means that for some template $h(t; \theta)$ the value of S/N , determined by the optimal Wiener filtering (or by any other procedure that we specified in advance) has exceeded a predetermined threshold, and the signal satisfies further criteria that we might have set for claiming detection, such as coincidences between different detectors (we will see in more detail in Sections 7.4.3 and 7.5.3 some possible criteria that could allow us to claim a detection, at a given confidence level). How do we reconstruct the most probable value of the parameters of the source, and how we compute the error on these parameters?

This question is Bayesian in nature, so its answer is contained in the posterior probability. To compute the likelihood function, and hence the posterior probability, we assume for simplicity that the noise $n(t)$ is stationary and Gaussian. From eq. (7.6) we see that the variance of the Fourier mode of the noise with frequency f is proportional to $(1/2)S_n(f)$, so the corresponding Gaussian probability distribution for the noise is

$$p(n_0) = \mathcal{N} \exp \left\{ -\frac{1}{2} \int_{-\infty}^{\infty} df \frac{|\tilde{n}_0(f)|^2}{(1/2)S_n(f)} \right\}, \quad (7.59)$$

where \mathcal{N} is a normalization constant. This is the probability that the noise $n(t)$, which is a random variable with zero mean, has a given realization $n_0(t)$. The above result can be rewritten very simply in terms of the scalar product (7.46) as¹⁷

$$p(n_0) = \mathcal{N} \exp\{-(n_0|n_0)/2\}. \quad (7.62)$$

We are assuming that the output of the detector satisfies the condition for claiming detection, i.e. it is of the form $s(t) = h(t; \theta_t) + n_0(t)$, where $n_0(t)$ is the specific realization of the noise in correspondence to this event, and θ_t is the (unknown) true value of the parameters θ . The likelihood function for the observed output $s(t)$, given the hypothesis that there is a GW signal corresponding to the parameters θ_t , is obtained plugging $n_0 = s - h(\theta_t)$ into eq. (7.62),

$$\Lambda(s|\theta_t) = \mathcal{N} \exp \left\{ -\frac{1}{2} (s - h(\theta_t)|s - h(\theta_t)) \right\}, \quad (7.63)$$

¹⁷For simplicity, we limit ourselves to the case of a single detector. The formalism can however be extended straightforwardly to multiple detectors. In this case the definition of the noise spectral density, eq. (7.6), is replaced by

$$\langle \tilde{n}_a^*(f) \tilde{n}_b(f') \rangle = \delta(f - f') \frac{1}{2} [S_n(f)]_{ab}, \quad (7.60)$$

where the indices a, b label the detectors. This definition takes into account the possibility of correlated noise. Let $\mathbf{A}(t)$ and $\mathbf{B}(t)$ be vectors whose components $A_a(t)$ and $B_a(t)$ are output of the single detectors, and let $[S_n^{-1}]^{ab}$ denote the inverse matrix. The equations of this section can then be generalized to multipole detectors, using the scalar product

$$\begin{aligned} (\mathbf{A}|\mathbf{B}) &= 4 \operatorname{Re} \\ &\int_0^\infty df \tilde{A}_a^*(f) [S_n^{-1}(f)]^{ab} B_b(f), \end{aligned} \quad (7.61)$$

which generalizes eq. (7.46). See the Further Reading for details.

or, introducing the short-hand notation $h_t \equiv h(\theta_t)$,

$$\Lambda(s|\theta_t) = \mathcal{N} \exp \left\{ (h_t|s) - \frac{1}{2}(h_t|h_t) - \frac{1}{2}(s|s) \right\}. \quad (7.64)$$

¹⁸As an example of prior information, one of the typical parameters entering in the waveform is the distance r to the source, and we might be searching for signals from a population of stars with a known distribution in space, e.g. a distribution $p^{(0)}(r)dr \sim r^2dr$ for isotropic sources, or $p^{(0)}(r)dr \sim rdr$ for sources within a few kpc from us, in the Galactic disk. Another typical parameter is the mass of the star and, for neutron stars, we know from astrophysical observations that their mass distribution is strongly concentrated around $1.35M_\odot$.

¹⁹Assuming that the eccentricity can be neglected, since the orbit should be highly circular by the time the signal enters in the bandwidth of a ground-based detector, as we saw in Section 4.1.3.

²⁰For details see, e.g. the statistics section of Yao *et al.* [Particle Data Group] (2006).

²¹As we already mentioned when discussing the example of the neutrino mass on page 350, a distribution which is flat with respect to the variables θ_t is no longer flat if we make a non-linear transformation of the parameters. Therefore this prior distribution assumes a definite choice of coordinates in the parameter space.

In the Bayesian approach, according to eq. (7.56), we also introduce a prior probability $p^{(0)}(\theta_t)$.¹⁸ Then, the posterior probability distribution for the true value θ_t , given the observed output s ,

$$p(\theta_t|s) = \mathcal{N} p^{(0)}(\theta_t) \exp \left\{ (h_t|s) - \frac{1}{2}(h_t|h_t) \right\}, \quad (7.65)$$

where, since we are considering $p(\theta_t|s)$ as a distribution in θ_t for a fixed output s , we have reabsorbed into the normalization factor \mathcal{N} the term $(s|s)/2$ which appears in the exponential in eq. (7.64).

Once the prior distribution is given, eq. (7.65) gives the p.d.f. in the parameter space, so in principle it contains all the information that we need. However, in this form the information might not be very manageable. The θ -space will in general be a multi-dimensional space of large dimension. For example, for a binary coalescence the parameters θ^i that determine the waveform, at the post-Newtonian level, are the distance, the source's location (two angles), the orientation of the normal to the orbit (two more angles), the time at which the signal enters in the interferometer's bandwidth, the orbital phase at that moment, the two masses of the stars, and their spins, so 15 parameters in all.¹⁹ From the probability distribution function (7.65) in such a complicated space we would like to extract some more approximate, but also more manageable, information; essentially, we want the most probable value of the variables θ_t , that we denote by $\hat{\theta}$, and also their corresponding errors.

There is no unique way of defining what is the most probable value of θ_t . A rule for assigning the most probable value is called an estimator. The most important properties that an estimator must have are:²⁰ (a) Consistency: the estimator must converge to the true value as the amount of data increases. This property is so important that it is possessed by all commonly used estimators. (b) The bias b is defined as the difference between the expectation value of the estimator, $E(\hat{\theta})$ (taken over a hypothetical set of similar experiments in which $\hat{\theta}$ is constructed in the same way), and the true value θ_t , $b \equiv E(\hat{\theta}) - \theta_t$. When $b = 0$ the estimator is said to be unbiased. (c) Efficiency: we want the smallest possible value for the variance of $\hat{\theta}$, and (d) Robustness, i.e. the property of being relatively insensitive to small departure in the assumed p.d.f. due to factors such as noise.

Two choice of estimators seems especially reasonable. The first is to define $\hat{\theta}$ as the value which maximizes the probability distribution function (7.65). Another natural option is to define it as the average of θ_t , over the distribution (7.65). We discuss these options below.

Maximum likelihood estimator

Let us consider first the situation in which the prior probability is flat.²¹

Then, maximization of the posterior probability becomes the same as maximization of the likelihood $\Lambda(s|\theta_t)$. The value of θ_t that maximizes $\Lambda(s|\theta_t)$ defines the maximum likelihood estimator, and we denote it by $\hat{\theta}_{\text{ML}}(s)$. It is the most widely used estimator in general situations.²² It is usually simpler to maximize $\log \Lambda$. From eq. (7.64),

$$\log \Lambda(s|\theta_t) = (h_t|s) - \frac{1}{2}(h_t|h_t). \quad (7.66)$$

Since we are working at fixed s , the term $(-1/2)(s|s)$ in eq. (7.64) is an irrelevant constant, and we omitted it. Denoting $\partial/\partial\theta_t^i$ simply by ∂_i , the value of $\hat{\theta}_{\text{ML}}$ is found by solving the equations

$$(\partial_i h_t|s) - (\partial_i h_t|h_t) = 0. \quad (7.67)$$

The errors $\Delta\theta^i$ can then be defined in terms of the width of the probability distribution function (7.65) at the peak.

Typically, (7.67) is a set of equations that must be solved numerically (except for some parameter such as the overall amplitude that can be eliminated analytically, see below). However, they have a rather simple geometric interpretation. The set of all possible waveforms $h(t;\theta)$ defines a manifold, called the manifold of the signals, parametrized by the coordinates θ^i . This is a subset of zero measure in the space of all possible functions, so the addition of generic noise $n(t)$ to a function $h(t;\theta)$ will necessarily bring us out of this manifold. In Fig. 7.4 we illustrate the situation with a two-dimensional manifolds of the signals. The point labeled θ_t represents the true value of the signal, and therefore lies on the manifold. The addition of noise carries us outside this manifold. Since we are minimizing $(s - h|s - h)$, see eq. (7.63), the maximum likelihood estimator actually searches the point on the signal manifold which is closest to the output s , where distances are defined with respect to the scalar product $(\cdot | \cdot)$.

To summarize, in the Bayesian framework $\hat{\theta}_{\text{ML}}$ is determined assuming a flat prior distribution and requiring the maximization of the posterior probability (7.65), i.e. maximizing our “degree of belief” in the hypothesis that there is a GW signal. A natural question, at this point, is what is the relation between $\hat{\theta}_{\text{ML}}$ and the value of θ that provides the highest signal-to-noise ratio in the matched filtering. We now prove that in fact they are the same. To show it, we write the generic template as $h(t;\theta) = ah_a(t;\xi)$, where a is an amplitude, and ξ is a free parameter, while the normalization of h_a has been fixed imposing some condition. We have separated the parameters θ into a and the remaining parameters, that we call ξ . The maximization with respect to a of $\log \Lambda$ can be performed analytically since, from eq. (7.66),²³

$$\log \Lambda(s|a, \xi) = a(h_a|s) - \frac{a^2}{2}(h_a|h_a). \quad (7.68)$$

Requiring $\partial \log \Lambda / \partial a = 0$, we get the maximum likelihood estimate for a ,

$$\hat{a}_{\text{ML}}(s) = \frac{(h_a|s)}{(h_a|h_a)}. \quad (7.69)$$

²²See any textbook on statistics, e.g. Lyons (1986), Section 4.4, for an introduction to the maximum likelihood method and its virtues. Observe that the likelihood is a legitimate concept also in the frequentist approach. The most probable frequentist value is again identified with the maximum of the likelihood, and the confidence interval is usually defined in terms of the point where $2 \log \Lambda$ decreases by one unit with respect to its value at the maximum. In the frequentist approach, however, we cannot use the likelihood as a p.d.f. for the true values of the parameters, i.e. we cannot consider areas under the curve, and of course we cannot include priors.

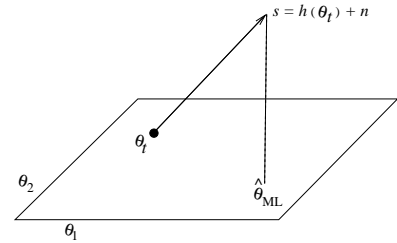


Fig. 7.4 The manifolds of the signals, parametrized by the coordinates (θ_1, θ_2) . The point θ_t is the true value of the signal. The addition of noise to $h(\theta_t)$ brings us outside this manifold, and the maximum likelihood estimator searches the point on the signal manifold which is closest to s .

²³To keep the notation lighter, we omit the subscript t (which stands for “true”) from a and ξ . We are anyway considering p.d.f. for the true values of the parameters.

The maximization with respect to the remaining variables ξ can be performed substituting this expression for a into $\log \Lambda$, obtaining

$$\log \Lambda(s|\xi) = \frac{1}{2} \frac{(h_a|s)^2}{(h_a|h_a)}. \quad (7.70)$$

The maximization of this quantity amounts to maximizing the overlap of the output s with the normalized template $h_a/(h_a|h_a)^{1/2}$, where the overlap is measured using the scalar product $(\cdot | \cdot)$, defined in terms of the noise spectral density $S_n(f)$. This is just the matched filtering procedure discussed in the Section 7.3. Thus, the maximum likelihood method provides a way of estimating the overall amplitude a (which cannot be fixed just searching for the filter that maximizes the signal-to-noise ratio, since eq. (7.47) is unchanged by a multiplicative rescaling of the filter u) while, for the remaining parameters, it returns the values that maximize the signal-to-noise ratio according to matched filtering.²⁴

²⁴We also mention that another way of understanding the meaning of the maximum likelihood procedure is in term of the Neyman–Pearson criterium, which consists in maximizing the probability of detection, subject to a given false alarm probability, and leads again to the condition that $\log \Lambda$ be maximum.

²⁵In the GW literature, the log of the prior $p^0(\theta)$ is sometime added to the exponential in eq. (7.65), and the resulting exponential is called again the log-likelihood function, $\log \Lambda$, so the corresponding estimator is called again the maximum likelihood estimator. This notation is however potentially confusing. For instance, one might be tempted to make a frequentist use of such a “ $\log \Lambda$ ”, which is obviously incorrect, since it involves a prior probability.

Maximum posterior probability

In various situations we do have important prior information, and we might want to include it in the analysis, see Note 18 for examples. In this case, rather than maximizing the likelihood function, we must determine the estimator by maximizing the full posterior probability $p(\theta_t|s)$ given in eq. (7.65), which takes into account the prior probability distribution.²⁵ For a generic prior, of course, the maximum of the posterior distribution will change, so it will no longer coincide with the value that gives the highest signal-to-noise ratio in the matched filtering. What happens is that the value suggested by matched filtering is weighted against our prior expectations (in a real sense, our “prejudices”), to provide a new estimate of the most likely value for the true parameters.

When we want to include non-trivial prior information, some conceptual complication may appear (apart from the issue of how to choose the appropriate prior). Suppose, for definiteness, that we have a two-dimensional parameter space (θ_1, θ_2) , as in Fig. 7.4, and that we are not interested in the variable θ_2 . Then, we can integrate the p.d.f. given in eq. (7.65) over θ_2 , to obtain a reduced p.d.f. in the variable θ_1 . From the geometric interpretation given in Fig. 7.4 it is clear that, as far as the likelihood function is concerned, the maximum in the variable θ_1 is the same, independently of whether we integrated or not over θ_2 . However, once we include a generic non-flat prior probability $p^{(0)}(\theta)$, this nice geometric interpretation is lost and, in general, if $(\bar{\theta}_1, \bar{\theta}_2)$ is the maximum of the distribution function $p(\theta_1, \theta_2|s)$, it is no longer true that the $\bar{\theta}_1$ is the maximum of the reduced distribution function $\tilde{p}(\theta_1|s) = \int d\theta_2 p(\theta_1, \theta_2|s)$, obtained integrating out θ_2 . Thus, there is an ambiguity on the value of the most probable value of θ_1 , which depends on whether we are interested or not in θ_2 . Another possible drawback, this one common to both the maximum likelihood and the maximum posterior methods, is that we might want an estimator that minimizes the error on the parameter determination, and this in general

is not the case for the maximum likelihood or maximum posterior probability estimators. These issues motivate the consideration of the Bayes estimator, in the next subsection.

Bayes estimator

In this case the most probable values of the parameters is defined by

$$\hat{\theta}_B^i(s) \equiv \int d\theta \theta^i p(\theta|s), \quad (7.71)$$

i.e. is the average with respect to the posterior probability distribution. The errors on the parameters is defined by the matrix

$$\Sigma_B^{ij} = \int d\theta [\theta^i - \hat{\theta}_B^i(s)][\theta^j - \hat{\theta}_B^j(s)] p(\theta|s), \quad (7.72)$$

that is, in terms of the mean square deviations from $\hat{\theta}_B^i(s)$, where the average is taken again with respect to $p(\theta|s)$. Even when there is a non-trivial prior probability function, the Bayes estimator is clearly independent on whether we integrate out some variable from $p(\theta|s)$, since we anyhow integrate over all the θ^i when computing $\hat{\theta}_B^i$ and Σ_B^{ij} . Furthermore, it can also be shown that, if one wants to minimize the error on the parameters, averaged over the whole parameter space, the Bayes estimator is the optimal one.

The “operational” meaning of the Bayes estimator is the following. Suppose that, after a sufficiently long run, we end up with a large ensemble of detected signals, which correspond to actual GWs, and that among them there is still a large subensemble of GW signals that produced a given output $s(t)$. Each of these waves will be characterized by different values of the true parameters θ_t and therefore by a different $h(t; \theta_t)$ that, by combining each time with a different realization of the noise $n(t)$, has produced the same output $s(t)$. Then $\hat{\theta}_B^i(s)$ is the value of θ^i , averaged over this ensemble of signals, and Σ_B^{ij} is the corresponding rms error.

Thus, the Bayes estimator has a well-defined operational meaning, and welcome mathematical properties, such as the independence on whether we integrate out some variable and the fact that it minimizes the error on parameter estimation. Its main drawback is its computational cost, since the evaluation of eq. (7.71) or of eq. (7.72) involves a multi-dimensional integral over the space of θ variables which, as we have seen, could have a dimensionality of order 15 or larger, and furthermore at each point of this parameter space we must compute the function $p(\theta|s)$, given in eq. (7.65), which requires the numerical computation of the integral over frequencies that defines the scalar product $(\cdot | \cdot)$. The choice of the best estimator is therefore subject to various considerations, including computational cost, and depends on the specific situation. The use of the Bayes estimator goes also under the name of non-linear filtering.

Of course, in the limit of large signal-to-noise ratio (which unfortunately is not expected to be the appropriate one for GW detectors, at

least in the near future) these issues becomes irrelevant, and all consistent estimators give the same answer. In this limit, there is also a very simple expression for the error on the parameters. If the SNR is large, the error that we make on the parameter estimation is small. For simplicity we assume that the prior $p^{(0)}(\theta)$ is nearly uniform near $\theta = \hat{\theta}$, where $\hat{\theta}$ is the value produced by (any) consistent estimator, say for definiteness the maximum likelihood estimator $\hat{\theta}_{\text{ML}}$. That is, we assume that the prior information is irrelevant for reconstructing the parameters. In eq. (7.65) we can then write $\theta^i = \hat{\theta}_{\text{ML}}^i + \Delta\theta^i$, and, since $\Delta\theta^i$ is small, we can expand the exponential in eq. (7.65) in powers of $\Delta\theta^i$. The linear term of the expansion vanishes because $\hat{\theta}_{\text{ML}}^i$ is, by definition, the maximum of the distribution, and to quadratic order in $\Delta\theta$ we get

$$p(\theta|s) = \mathcal{N} \exp \left\{ -\frac{1}{2} \Gamma_{ij} \Delta\theta^i \Delta\theta^j \right\}, \quad (7.73)$$

where $\Gamma_{ij} = (\partial_i \partial_j h | h - s) + (\partial_i h | \partial_j h)$. Observe that, in the first term, we have $h - s = -n$ and, in the limit of large signal-to-noise ratio, $|n|$ is much smaller than $|h|$. So in this limit the first term can be neglected, and we get

$$\Gamma_{ij} = (\partial_i h | \partial_j h), \quad (7.74)$$

evaluated at $\theta = \hat{\theta}_{\text{ML}}$. This is called the *Fisher information matrix*. Then the expectation value of the errors $\Delta\theta^i$ are given by

$$\langle \Delta\theta^i \Delta\theta^j \rangle = (\Gamma^{-1})^{ij}. \quad (7.75)$$

7.4.3 Matched filtering statistics

As we have discussed in the previous sections, a general data analysis strategy consists in performing matched filtering, applying many different templates $h(t; \theta)$ to the data. This will result in the generation of a list of “events” (in the sense of Note 2 on page 337), defined by the fact that the signal-to-noise ratio, in correspondence with some template, raises over a predetermined threshold. Applying the maximum likelihood criterium (or the maximization of the posterior probability, if we want to include prior information), we can then get the most probable value of the parameters θ , *under the hypothesis that a GW signal $h(t; \theta)$ was present*. The issue that we want to address now is the following. How well such hypothesis performed? In other words, what is the statistical significance of the fact that we found events at a given level of signal-to-noise ratio?

The answer to this question depends crucially on the statistical properties of the noise so, first of all, it is important to realize that in any detector we can distinguish between two kinds of noise: “well-behaved” Gaussian noise, whose probability distribution is a Gaussian, and non-Gaussian noise, which is a generic denomination for anything else. A Gaussian distribution $\sim e^{-x^2/2}$ drops very fast for large values of its argument x . The intuitive idea, that we will formalize below, is therefore

to eliminate Gaussian noise by setting a sufficiently large threshold for the signal-to-noise ratio. Non-Gaussian disturbances, however, have in general a totally different statistical distribution, characterized by long tails at large values of S/N , which decay only as a power law.²⁶

These noises cannot be eliminated just by setting a high threshold, since they can produce events with values of S/N that, in Gaussian distribution, would be inconceivably large. As a limiting case, any detector shaken by an earthquake will produce “events” with arbitrarily high values of S/N . Of course, these events cannot be eliminated just by setting a high threshold in S/N . Rather, they should be identified and vetoed. All detectors are equipped with sensors which monitor various aspects of the detector performance as well as environmental conditions (e.g. seismometers), so that non-Gaussian disturbances are vetoed as much as possible. However, it is practically impossible to be sure that one has identified and vetoed all possible non-Gaussian disturbances. So, while in principle one can study experimentally the noise distribution and then set a threshold so high that even non-Gaussian fluctuations would be very rare, in practice this is not possible because the resulting threshold would be much too high, and therefore would considerably degrade the sensitivity of the detector. Rather, the best way of eliminating non-Gaussian noise is to perform coincidences between two or more detectors. This is among the reasons why various different detectors have been built, and they are operated as a network.

In the following, we first discuss the statistical significance of obtaining a given value of the signal-to-noise ratio S/N , assuming that only Gaussian noise is present. This will tell us how to fix the threshold in S/N so that, at some confidence level, we know that higher values of S/N have not been produced by Gaussian noise alone, and allows us to generate, from the data stream of the detector, a list of “events”. These events will then be subject to further scrutiny, using for instance coincidences between detectors whenever possible, with the aim of eliminating those which are due to non-Gaussian noise, and retaining the GW signals, if any. For the rest of this section we will be concerned only with Gaussian noise, while coincidences and other techniques will be discussed when we examine the various type of signals, in Sections 7.5–7.8.

In eqs. (7.42)–(7.45) we defined the signal-to-noise ratio in terms of the expectation value of the signal. Here however we want to study the full statistical distribution, rather than just its expectation value, so we define

$$\rho = \frac{\hat{s}}{N}, \quad (7.76)$$

where \hat{s} is the filtered output defined in eq. (7.41) and N is given in eq. (7.43), that is N is the root-mean-square (rms) of \hat{s} when the signal is absent. The definition of ρ is therefore analogous to the definition of the signal-to-noise ratio S/N , see eqs. (7.42)–(7.45), except that in the numerator we have \hat{s} rather than its expectation value $\langle \hat{s} \rangle$. As a result,

²⁶For instance, a large class of phenomena, characterized by what is called self-organized criticality, are such that the number N of events that release an energy E is distributed as $dN = E^{-\gamma} dE$ where, quite remarkably, the exponent γ has approximately the same universal value, $\gamma \simeq 1.6$, in phenomena apparently very different. Such a law, together with the value $\gamma \simeq 1.6$, is in fact observed in earthquakes from different seismic faults (in which case it is called the Gutenberg–Richter law), in soft γ -ray bursts from highly magnetized neutron stars, as well as in numerical simulations of fractures in solids. The same distribution is experimentally observed when searching for short bursts in resonant-bar GW detectors, where they are likely due to microfractures inside the bar, and give an example of the non-Gaussian noise that we will have to fight. See Dubath, Foffa, Gasparini, Maggiore and Sturani (2005), and references therein.

the relation between ρ and S/N is $S/N = \langle \rho \rangle$. From

$$\hat{s} = \int_{-\infty}^{\infty} dt [h(t) + n(t)] K(t) \quad (7.77)$$

we see that, when h is absent, ρ is a random variable with zero average and, since it has been normalized to its own rms, with variance equal to one. Thus, in the absence of a GW signal, the probability distribution of ρ is

$$p(\rho|h=0)d\rho = \frac{1}{\sqrt{2\pi}} e^{-\rho^2/2} d\rho. \quad (7.78)$$

In contrast, if in the output there is a GW signal h with a signal-to-noise ratio $\bar{\rho}$, eqs. (7.76) and (7.77) give $\rho = \bar{\rho} + \hat{n}/N$, where $\hat{n} = \int dt n(t)K(t)$. Since N is just the rms of \hat{n} , in this case $\rho - \bar{\rho}$ is a Gaussian variable with zero mean and unit variance, so

$$p(\rho|\bar{\rho})d\rho = \frac{1}{\sqrt{2\pi}} e^{-(\rho-\bar{\rho})^2/2} d\rho. \quad (7.79)$$

The variable ρ is the signal-to-noise ratio in amplitude. It is useful to introduce also $R \equiv \rho^2$, which is the signal-to-noise ratio in energy, since the energy of GWs is quadratic in the GW amplitude. Observe that ρ , being proportional to $h(t)$, is not positive definite, and runs between $-\infty$ and $+\infty$, while of course $0 \leq R < \infty$. The probability distribution for R , when there is in the output a GW signal with a signal-to-noise ratio in energy $\bar{R} = \bar{\rho}^2$, follows from eq. (7.79) observing that a single value R is obtained from two values of the amplitude, $\rho = \pm\sqrt{R}$, so the probability of detecting an event with SNR in energy between R and $R + dR$, when the SNR of the GW signal is \bar{R} , is given by

$$P(R|\bar{R})dR = p(\rho|\bar{\rho})d\rho + p(-\rho|\bar{\rho})d\rho, \quad (7.80)$$

evaluated at $\rho = R^{1/2}$. Writing $d\rho = dR/(2R^{1/2})$, we get

$$\begin{aligned} P(R|\bar{R})dR &= \frac{dR}{2\sqrt{R}} \frac{1}{\sqrt{2\pi}} \left[e^{-(\rho-\bar{\rho})^2/2} + e^{-(\rho+\bar{\rho})^2/2} \right] \\ &= \frac{1}{\sqrt{2\pi}\bar{R}} e^{-(\bar{R}+R)/2} \cosh \left[\sqrt{R\bar{R}} \right] dR. \end{aligned} \quad (7.81)$$

From this we can compute the average value of R for a given \bar{R} ,

$$\langle R \rangle = \int_0^{\infty} dR R P(R|\bar{R}) = 1 + \bar{R}. \quad (7.82)$$

If we write $R = E/kT_n$, where T_n has the physical meaning of an effective temperature of the noise after matched filtering, we can also rewrite eq. (7.82) as

$$\langle E \rangle = kT_n + \bar{E}. \quad (7.83)$$

Therefore the average value of the detected energy is the sum of the energy \bar{E} deposited in the detector by the GW, plus the energy kT_n

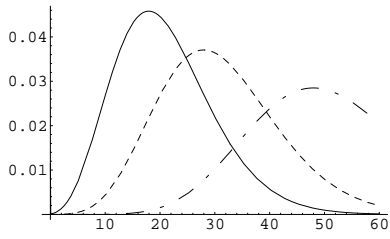


Fig. 7.5 The probability distribution $P(R|\bar{R})$, as a function of R , for $\bar{R} = 20$ (solid line), $\bar{R} = 30$ (dotted line) and $\bar{R} = 50$ (dot-dashed line).

associated to the detector noise, a very natural result. In Fig. 7.5 we show the form of the probability distribution $P(R|\bar{R})$, as a function of R , for different values of \bar{R} . Observe that, while the average value is at $R = 1 + \bar{R}$, the maximum of the distribution is at a somewhat lower value. The corresponding distribution for R in the absence of signal is obtained setting $\bar{R} = 0$ in eq. (7.81). In Fig. 7.6 we compare the probability distribution $P(R|\bar{R})$ when $\bar{R} = 10$ with the probability distribution in the absence of signal, $P(R|\bar{R} = 0)$.

The different behavior of the two distributions suggest that, when searching for a signal with a signal-to-noise ratio \bar{R} in energy, we can discriminate a true GW signal from a fluctuation due to Gaussian noise setting a threshold in R , at a value R_t that eliminates most of the noise, while retaining a large fraction of the signal distribution. Observe that anyway there will always be a *false alarm probability*, given by

$$\begin{aligned} p_{\text{FA}} &= \int_{R_t}^{\infty} dR P(R|\bar{R} = 0) \\ &= 2 \int_{\rho_t}^{\infty} d\rho e^{-\rho^2/2} \\ &= 2 \operatorname{erfc}(\rho_t/\sqrt{2}), \end{aligned} \quad (7.84)$$

where $\operatorname{erfc}(z)$ is the complementary error function. Furthermore, there is a *false dismissal probability*, i.e. a probability of losing a real GW signal, given by²⁷

$$p_{\text{FD}} = \int_0^{R_t} dR P(R|\bar{R}). \quad (7.85)$$

The threshold R_t can be fixed deciding what is the maximum false alarm level that we are willing to tolerate. This depends also crucially on the number of trials that we do with different templates. For example, for a coalescing binary, one can estimate that of order 10^5 templates might be needed to cover with good accuracy the possible range of values of masses and spins. Furthermore, to match the template to the signal one can estimate in about 3 ms the maximum temporal mismatch between the two. In one year of data ($\sim 3 \times 10^7$ s), one must therefore try $\sim 10^{10}$ starting values of time, and for each value of time we have 10^5 templates to cover the masses and spin parameters, so overall one might have to try 10^{15} templates.²⁸ Often the false alarm level is fixed so that the expected number of false alarms in a run will be of order a few. With a lower threshold one would be flooded by spurious events, while higher threshold have of course the effect of increasing the false dismissal probability. The few events obtained will then be subject to further scrutiny. Thus, if we search for a coalescence in a single detector, with one year of data and 10^{15} templates, we could chose a threshold in amplitude $\rho_t \simeq 8$, since this gives $p_{\text{FA}} \sim 2.5 \times 10^{-15}$. However, performing coincidences between two detectors the probability of obtaining a false alarm simultaneously in the two detectors is the square of the single-detector probability, if the noise in the two detectors are uncorrelated, so in this case we might want $[2 \operatorname{erfc}(\rho_t/\sqrt{2})]^2 \simeq 10^{-15}$, which gives $\rho_t \simeq 5.5$.

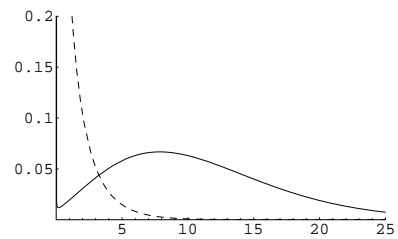


Fig. 7.6 The probability distribution $P(R|\bar{R})$, as a function of R , for $\bar{R} = 10$ (solid line), compared to the probability distribution in the absence of signal, $P(R|\bar{R} = 0)$ (dashed).

²⁷In other words, whatever the value of \bar{R} , the distribution $P(R|\bar{R})$ is such that there is always some probability that R be smaller, and even much smaller, than \bar{R} , and therefore the GW can go undetected even when the threshold R_t was smaller than the value \bar{R} due to the GW alone. If one thinks in terms of energies, it might be counterintuitive that the energy released inside the detector can be smaller than the value that would have been released by the GW alone, in the absence of noise. Recall however that GW detectors really measure an oscillation amplitude, and the amplitude induced by the GW combines with the amplitude induced by noise with a relative phase, so noise and signal can interfere constructively or destructively. In the latter case the overall output has a smaller energy than that due to the GW signal alone.

²⁸We will see however in Section 7.7.1 that all these time shifts can be taken into account simultaneously performing a single Fast Fourier Transform, which makes the problem computationally feasible.

In the above discussion, we assumed that the output of the detector is a single quantity ρ which, in the absence of noise, has a Gaussian distribution. Actually, we will meet below examples in which we have two outputs x, y , each one with its Gaussian noise, which are combined in quadrature, so that $\rho^2 = x^2 + y^2$. In this case the corresponding distribution function can be computed as follows. For the distribution $p_2(\rho|h=0)$ in the absence on signal (where the label 2 reminds us that we have two degrees of freedom x, y),²⁹ we simply have

$$\begin{aligned} p_2(x, y|h=0) dx dy &= \frac{dx}{(2\pi)^{1/2}} \frac{dy}{(2\pi)^{1/2}} e^{-(x^2+y^2)/2} \\ &= \rho d\rho \frac{d\theta}{2\pi} e^{-\rho^2/2}. \end{aligned} \quad (7.86)$$

If we are not interested in the phase θ we simply integrate over it, and we get

$$p_2(\rho|h=0) = \rho e^{-\rho^2/2}, \quad (7.87)$$

which is called a Rayleigh distribution, or a χ^2 distribution with two degrees of freedom. To compute the distribution in presence of signal, we start from the probability distribution of x, y , given that the true GW signal has the values \bar{x}, \bar{y}

$$p_2(x, y|\bar{x}, \bar{y}) dx dy = \frac{1}{2\pi} e^{-\frac{1}{2}[(x-\bar{x})^2+(y-\bar{y})^2]}. \quad (7.88)$$

We pass to polar coordinates, $x = \rho \cos \theta$, $y = \rho \sin \theta$, with $\rho^2 = R$, so $dx dy = \rho d\rho d\theta = (1/2)dR d\theta$. To obtain the probability distribution $P_2(R|\bar{R})$ we integrate over the phase θ , and we also integrate over all the values of \bar{x}, \bar{y} with the constraint $\bar{x}^2 + \bar{y}^2 = \bar{R}$, that is,

$$\begin{aligned} P_2(R|\bar{R}) dR &= c \frac{dR}{2} \int_0^{2\pi} d\theta \int_{-\infty}^{\infty} d\bar{x} d\bar{y} \delta(\bar{x}^2 + \bar{y}^2 - \bar{R}) \\ &\times \frac{1}{2\pi} \exp\left\{-\frac{1}{2}[(x-\bar{x})^2 + (y-\bar{y})^2]\right\}, \end{aligned} \quad (7.89)$$

where c is a normalization constant. The integrals are easily performed expressing also \bar{x}, \bar{y} in polar coordinates, $\bar{x} = r \cos \theta'$, $\bar{y} = r \sin \theta'$, so

$$\begin{aligned} P_2(R|\bar{R}) &= \text{const.} \int_0^{2\pi} d\theta \int_0^{2\pi} d\theta' \int_0^{\infty} d(r^2) \delta(r^2 - \bar{R}) \\ &\times \exp\left\{-\frac{1}{2}(R + \bar{R}) + \sqrt{R\bar{R}} \cos(\theta - \theta')\right\} \\ &= \text{const'.} e^{-(R+\bar{R})/2} \int_0^{2\pi} d\alpha e^{\sqrt{R\bar{R}} \cos \alpha}, \end{aligned} \quad (7.90)$$

where $\alpha = \theta - \theta'$. The integral over α gives a modified Bessel function I_0 . We fix the normalization constant requiring that $\int_0^{\infty} P_2(R|\bar{R}) dR = 1$, and we get

$$P_2(R|\bar{R}) = \frac{1}{2} e^{-(R+\bar{R})/2} I_0\left(\sqrt{R\bar{R}}\right). \quad (7.91)$$

More generally, if $\rho^2 = x_1^2 + \dots + x_n^2$, performing a computation similar to that presented above one finds³⁰

$$P_n(R|\bar{R}) = \frac{1}{2} \left(\frac{R}{\bar{R}} \right)^{(n-2)/4} e^{-(R+\bar{R})/2} I_{\frac{n}{2}-1} \left(\sqrt{R\bar{R}} \right). \quad (7.92)$$

In Fig. 7.7 we show the function $P(R|\bar{R})$ given in eq. (7.81), which is appropriate for the case of a single degree of freedom, together with the functions $P_n(R|\bar{R})$ for $n = 2$ and $n = 10$ degrees of freedom, as obtained from eq. (7.92). These distribution functions are known as the non-central chi-squared densities with n -degrees of freedom. The average value of R with n degrees of freedom is

$$\langle R \rangle = \int_0^\infty dR R P_n(R|\bar{R}) = n + \bar{R}, \quad (7.93)$$

and therefore

$$\langle E \rangle = n(kT_n) + \bar{E}, \quad (7.94)$$

while the variance is given by

$$\langle R^2 \rangle - \langle R \rangle^2 = 2n + 4\bar{R}. \quad (7.95)$$

7.5 Bursts

We now begin to apply the general theory that we have developed, to specific classes of GW signals. We begin with GW bursts. A number of astrophysical phenomena, like supernova explosions or the final merging of a neutron star–neutron star binary system, can liberate a large amount of energy in GWs in a very short time, typically less than a second, and sometimes as small as few milliseconds. We will refer to such signals as GW bursts, and we denote their duration by τ_g . In Fourier space, a GW burst therefore has a continuum spectrum of frequency over a broad range, up to a maximum frequency $f_{\max} \sim 1/\tau_g$.

7.5.1 Optimal signal-to-noise ratio

In principle, if we know the form of $\tilde{h}(f)$, we can just plug it into eq. (7.51) to obtain the S/N for a given noise spectral density of the detector. However, bursts come from explosive and complicated phenomena, and it is very difficult to predict accurately their waveform. We can first of all make some simple order-of-magnitude estimates, distinguishing two cases.

Narrow-band detectors

In this case the detector is sensitive only to frequencies in a bandwidth Δf , centered around a frequency f_0 , and we assume that Δf is small with respect to the typical variation scale of the signal in frequency space.

³⁰See, e.g. McDonough and Whalen (1995), Sections 4.8 and 4.9.

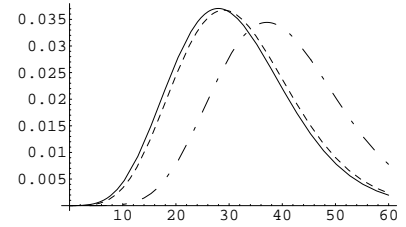


Fig. 7.7 The probability distribution $P(R|\bar{R})$ given in eq. (7.81) (solid line) compared to $P_n(R|\bar{R})$ with $n = 2$ (dashed line) and with $n = 10$ (dot-dashed), as a function of R , for $\bar{R} = 30$.

Outside this interval, the detector is blind and $1/S_n(f)$ in eq. (7.51) becomes practically zero. Inside this small bandwidth $h(f)$ cannot change much, so our ignorance of the precise waveform becomes irrelevant, and in the integrand in eq. (7.51) we can approximate $\tilde{h}(f)$ with $\tilde{h}(f_0)$. Then eq. (7.51) becomes

$$\left(\frac{S}{N}\right)^2 \simeq 4|\tilde{h}(f_0)|^2 \frac{\Delta f}{S_n}, \quad (7.96)$$

where $1/S_n$ is an average value of $1/S_n(f)$ in a bandwidth Δf centered on f_0 . This was the typical situation of resonant mass detectors until the 1990s, when the bandwidth Δf was only of order a few Hz, around a frequency $f_0 \sim 1$ kHz.³¹

³¹As we will see in Chapter 8, the bandwidth of resonant-mass detectors has subsequently evolved, reaching values of order $\Delta f/f_0 \sim 0.1$, but still, in a first approximation, eq. (7.96) applies. We will also see that, for resonant-mass detectors, $S_n(f)$ is not at all a slowly varying function of f around the resonance frequency f_0 , so in the estimate (7.96) we must really take an average of $1/S_n(f)$ over the whole useful bandwidth Δf , and we cannot simply use $1/S_n(f_0)$.

Broad-band detectors

In this case we get the signal in a bandwidth (f_{\min}, f_{\max}) where f_{\max} is the maximum frequency contained in the burst, if the detector is sensitive up to f_{\max} , or otherwise is the maximum frequency to which the detector is sensitive. The detailed form of the signal is therefore important, but a first order-of-magnitude estimate can still be obtained writing eq. (7.51) as

$$\left(\frac{S}{N}\right)^2 \sim 4|\tilde{h}|^2 \frac{f_{\max}}{S_n}, \quad (7.97)$$

where \tilde{h} is a characteristic value of $\tilde{h}(f)$ over the detector bandwidth and S_n is a characteristic value of $S_n(f)$.

We can translate these order-of-magnitude estimates into limits on the value of the dimensionless GW amplitude $h(t)$ that can be measured. For this we assume for definiteness that the wave comes from a direction such that $F_+ = 1$ and $F_\times = 0$, so that $h(t)$ is the same as the amplitude $h_+(t)$ of the + polarization. In the most general situation, we will also have a factor which depends on F_+ and F_\times and reflects the sensitivity of the detector to the given direction and polarization of the wave. To express eq. (7.51) in terms of $h(t)$ we need a model for the signal. For a GW burst of amplitude h_0 and duration τ_g , a crude choice could be

$$h(t) = h_0 \quad \text{if } |t| < \tau_g/2 \quad (7.98)$$

and $h(t) = 0$ if $|t| > \tau_g/2$. We can write it more compactly as

$$h(t) = h_0 \tau_g \delta_{\text{reg}}(t), \quad (7.99)$$

where $\delta_{\text{reg}}(t)$ has a rectangular shape of unit area, $\delta_{\text{reg}}(t) = 1/\tau_g$ for $|t| < \tau_g/2$ and $\delta_{\text{reg}}(t) = 0$ for $|t| > \tau_g/2$. For $\tau_g \rightarrow 0$, $\delta_{\text{reg}}(t)$ becomes a Dirac delta. More generally, for a burst we can model $h(t)$ as in eq. (7.99), choosing for $\delta_{\text{reg}}(t)$ a smooth function of unit area which goes to zero rather fast for $|t| \gtrsim \tau_g$. Performing the Fourier transform this gives

$$|\tilde{h}(f)| \sim h_0 \tau_g, \quad (7.100)$$

times a dimensionless function of the frequency, numerically of order one, and whose details depend on the precise waveform $\delta_{\text{reg}}(t)$ chosen.

Actually, rather than using a function $\delta_{\text{reg}}(t)$ with a unit area, it can be more convenient to write $h(t) = h_0 g(t)$, with $g(t)$ some function peaked at $t = 0$ and with $g(0) = O(1)$, so that the value of $h(t)$ near the peak is of order h_0 (rather than $h_0 \delta_{\text{reg}}(0)$ as in eq. (7.99)). A simple waveform of this type is a Gaussian,

$$h(t) = h_0 e^{-t^2/\tau_g^2}, \quad (7.101)$$

whose Fourier transform is

$$\tilde{h}(f) = h_0 \tau_g \sqrt{\pi} e^{-(\pi f \tau_g)^2}. \quad (7.102)$$

A waveform with a somewhat more realistic shape is a sine-Gaussian, i.e. a Gaussian modulated by a frequency f_0 ,

$$h(t) = h_0 \sin(2\pi f_0 t) e^{-t^2/\tau_g^2}, \quad (7.103)$$

shown in Fig. 7.8. Its Fourier transform is

$$\tilde{h}(f) = h_0 \tau_g i \frac{\sqrt{\pi}}{2} \left[e^{-\pi^2(f-f_0)^2 \tau_g^2} - e^{-\pi^2(f+f_0)^2 \tau_g^2} \right], \quad (7.104)$$

and is shown in Fig. 7.9. If $4\pi^2 f_0^2 \tau_g^2 \gg 1$, near $f = f_0$ the second term in brackets is negligible with respect to the first (while close to $f = 0$ it cancels the first term so that $\tilde{h}(0) = 0$), and we basically have a Gaussian in frequency space, centered at $f = f_0$, and with a value at the maximum

$$|\tilde{h}(f_0)| \simeq h_0 \tau_g \frac{\sqrt{\pi}}{2}. \quad (7.105)$$

Writing $f = f_0 + \Delta f$ we see that the width of the maximum Δf is of order $1/(\pi \tau_g)$, so $\Delta f/f_0 \sim 1/(\pi f_0 \tau_g)$. For $\pi f_0 \tau_g \ll 1$, $\tilde{h}(f)$ becomes relatively flat while for $\pi f_0 \tau_g \gg 1$ it is sharply peaked around f_0 . Using eqs. (7.96) and (7.97) we can estimate the minimum value of the dimensionless GW amplitude h_0 that can be detected at a given level of the signal-to-noise ratio S/N . For narrow-band detectors eq. (7.96) gives, using for definiteness the value $|\tilde{h}(f_0)| \simeq h_0 \tau_g (\sqrt{\pi}/2)$ appropriate for a sine-Gaussian waveform,

$$(h_0)_{\min} \sim \frac{1}{\tau_g} \left(\frac{S_n}{\pi \Delta f} \right)^{1/2} (S/N), \quad (7.106)$$

while for broad-band detectors eq. (7.97) gives

$$(h_0)_{\min} \sim \frac{1}{\tau_g} \left(\frac{S_n}{\pi f_{\max}} \right)^{1/2} (S/N). \quad (7.107)$$

The precise numerical factors, of course, depend on the choice of the waveform, so to fix the numerical coefficients in eqs. (7.106) and (7.107)

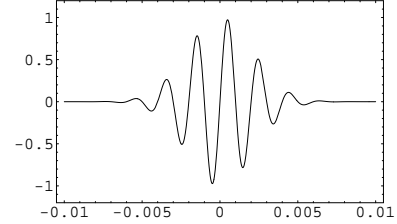


Fig. 7.8 The sine-Gaussian function $\sin(2\pi f_0 t) e^{-t^2/\tau_g^2}$, for $\tau_g = 3$ ms and $f_0 = 500$ Hz, as a function of t (in seconds).

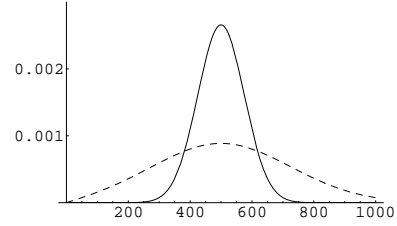


Fig. 7.9 $|\tilde{h}(f)|$ (in units of h_0) for a sine-Gaussian function with $f_0 = 500$ Hz, $\tau_g = 3$ ms (solid line) and for a sine-Gaussian function with $f_0 = 500$ Hz, $\tau_g = 1$ ms (dashed line).

we must know the shape of the signal $\tilde{h}(f)$, use the exact form of the noise $S_n(f)$, and perform the integral in eq. (7.51). We see from eqs. (7.106) and (7.107) that in a narrow-band detector the minimum detectable amplitude is higher by a factor $(f_{\max}/\Delta f)^{1/2}$, compared to a detector which is able to maintain the same typical sensitivity S_n over a broad bandwidth. This reflects the fact that the narrow-band detector has access only to a portion of the Fourier modes of the burst.

Rather than expressing the result in terms of h_0 , it is also common to use the so-called root-sum-square (rss) amplitude h_{rss} , defined by

$$\begin{aligned} h_{\text{rss}}^2 &= \int_{-\infty}^{\infty} dt h^2(t) \\ &= \int_{-\infty}^{\infty} df |\tilde{h}(f)|^2. \end{aligned} \quad (7.108)$$

For the Gaussian (7.101) we have

$$h_{\text{rss}}^2 = h_0^2 \tau_g \sqrt{\frac{\pi}{2}}, \quad (\text{Gaussian}), \quad (7.109)$$

while, for the sine-Gaussian (7.103),

$$h_{\text{rss}}^2 = h_0^2 \tau_g \sqrt{\frac{\pi}{8}} (1 - e^{-2\pi^2 f_0^2 \tau_g^2}), \quad (\text{sine-Gaussian}). \quad (7.110)$$

Observe that, dimensionally, $h_{\text{rss}} \sim (\text{time})^{1/2}$, so h_{rss} is conventionally quoted in $\text{Hz}^{-1/2}$, as the strain sensitivity.

To have an idea of the numerical values of h_{rss} (or, equivalently, of h_0) that could be obtained from astrophysical phenomena, we can compute the energy released in GWs by an event which produced, at the detector, a given value of h_{rss} . This can be obtained from the expression for $dE/dAdf$ given in eq. (1.159). Observe however that, for a wave coming from an arbitrary direction and with arbitrary polarization, a detector does not measure directly $\tilde{h}_+(f)$ and $\tilde{h}_\times(f)$ but rather the combination $\tilde{h}(f) = F_+ \tilde{h}_+(f) + F_\times \tilde{h}_\times(f)$, where F_+, \times are the detector pattern functions. For definiteness, we consider a GW coming from the optimal direction for the + polarization, so we take $F_+ = 1$ and $F_\times = 0$, and for $\tilde{h}_+(f)$ we take the sine-Gaussian waveform (7.104). We substitute this into eq. (1.159) and we get the total energy ΔE_{rad} radiated by the source in GWs,³²

$$\begin{aligned} \Delta E_{\text{rad}} &\simeq \left(\frac{\pi}{2}\right)^{3/2} \frac{\pi r^2 c^3}{G} h_0^2 \tau_g f_0^2 \\ &= \frac{\pi^2 r^2 c^3}{G} h_{\text{rss}}^2 f_0^2. \end{aligned} \quad (7.111)$$

Inserting the numerical values,

$$\Delta E_{\text{rad}} \simeq 1 \times 10^{-2} M_\odot c^2 \left(\frac{r}{8 \text{kpc}}\right)^2 \left(\frac{h_{\text{rss}}}{10^{-19} \text{Hz}^{-1/2}}\right)^2 \left(\frac{f_0}{1 \text{kHz}}\right)^2,$$

(7.112)

³²In the computation, we neglect the term $\exp\{-\pi^2(f + f_0)^2 \tau_g^2\}$ in eq. (7.104), which is small with respect to $\exp\{-\pi^2(f - f_0)^2 \tau_g^2\}$ and, when we integrate eq. (1.159) over df , we replace $f^2 \exp\{-\pi^2(f - f_0)^2 \tau_g^2\}$ with $f_0^2 \exp\{-\pi^2(f - f_0)^2 \tau_g^2\}$ and we extend the resulting integral from $-\infty$ to $+\infty$.

where in the second line we normalized r to a value of order of the distance to the galactic center. Recall that in the above we assumed a wave coming from optimal direction. For an ensemble of waves with arbitrary direction and polarization, we must also take into account the average over the pattern functions of the detector. For an interferometer, this is a factor 2/5 (see Table 7.1), so on average a burst coming from arbitrary direction, in order to produce a given signal h_{rss} in the detector, had an energy larger by a factor 5/2, compared to eq. (7.112). We see that a burst at the kHz, with $h_{\text{rss}} = 10^{-19} \text{ Hz}^{-1/2}$, carries away about 10^{-2} solar masses in GWs, if it comes from a source located at typical galactic distances.

Taking $10^{-2} M_{\odot} c^2$ as a reference value for ΔE_{rad} (which, as we will see in Vol. 2, is the maximum value that can be reasonably expected in cataclysmic events involving solar mass objects. Even larger energies can be released in the merging of very massive black holes), we see that a detector must reach at least a sensitivity to h_{rss} of order $10^{-19} \text{ Hz}^{-1/2}$ to have some chance of detecting GW bursts from the galactic center. To be able to see a burst which releases 10^{-2} solar masses in the Virgo cluster of galaxies, which is at $r \sim 14$ Mpc, one rather needs to be able to reach $h_{\text{rss}} \simeq 6 \times 10^{-23} \text{ Hz}^{-1/2}$ or, from eq. (7.110) with $\tau_g = 1$ ms, a value of the dimensionless amplitude $h_0 \simeq 2 \times 10^{-21}$.

7.5.2 Time-frequency analysis

The matched filtering technique that we have discussed in Section 7.3 works well if we know the form of the signal, or if we can parametrize it with a limited number of free parameters, so that it becomes practically feasible to put a sufficiently fine grid in this parameter space, and repeat the search for each point of the grid. As we will discuss in the next sections, this can be the case for the inspiral of compact binaries and, partly, for the signals due to pulsars.

Concerning bursts, the situation is different. In general, bursts may come from complicated explosive phenomena, such as supernovae, or from processes such as the final merging of coalescing binaries, which are difficult to model. In a narrow-band detector, such as resonant bars, we only have access to a narrow range of Fourier components of the signal. Thus, in a first approximation it is reasonable to model the signal as flat in frequency, i.e. as a Dirac delta in time and, as a next step, we can use more realistic modelizations such as the Gaussian and the sine-Gaussian waveforms described above. However, in a broad-band detector, the difference between these simple modelizations and the real waveform will become important. Thus, to exploit optimally the capabilities of a broad-band detector, one is lead to consider also other methods, which are sub-optimal with respect to matched filtering when the waveform is known precisely (since we have seen that, if the waveform is known, matched filtering is the optimal strategy) but might be more robust in the absence of detailed knowledge of the signal.

Such search algorithms can be obtained working in the time-frequency

plane. To understand the usefulness of the time–frequency representation, suppose at first that we have a function $s(t)$ defined on the whole real axis $-\infty < t < \infty$. We can take its Fourier transform $\tilde{s}(f)$ and compute from it the power spectrum $|\tilde{s}(f)|^2$. A plot of the power spectrum against the frequency will enable us to see immediately what are the dominant Fourier modes. However, this power spectrum knows nothing about *when* things happened.³³

³³The information about time localization, which is encoded in $s(t)$, is of course still encoded in $\tilde{s}(f)$, since from $\tilde{s}(f)$ we can get back $s(t)$ uniquely. However, it is lost in $|\tilde{s}(f)|^2$, since it was contained in the phase relation between the Fourier components, and this information is obliterated when taking the modulus. A nice example (taken from van den Berg (1999), a textbook on wavelets) is obtained if we take $s(t)$ to be a classical symphony. Then its power spectrum will immediately reveal the dominating keys: the ground-tones and their harmonics. Suppose now that we play the parts in a different order, and we even interchange smaller parts within the parts. The power spectrum would not change at all, while to the ear, which actually makes a time-frequency analysis, the result is very different.

The simplest way to recover partly this information is to take the Fourier transform not on the whole real line, but on segments of length δt . When we Fourier transform the function $s(t)$ on the interval $0 < t < \delta t$ and we plot the resulting power spectrum, we find the Fourier modes that dominated the function, during this temporal span. We can then repeat it for $\delta t < t < 2\delta t$, etc. Of course, on a finite segment of length δt , the resolution in frequency is finite, and is $1/\delta t$, so we are giving up the fine details in frequency space, but we gain an understanding of when things happened. That is, rather than working in frequency space, with an arbitrarily good resolution, it can be convenient to work in the time–frequency plane, making a good compromise between the accuracy in frequency and the accuracy in time.

This is particularly important when we are looking for transient phenomena, such as GW bursts. Suppose that we are unable to compute the detailed waveform of a burst, as it is typically the case, but still we can give a reasonable estimate of its total duration δt , and of the frequency range $f_1 < f < f_2$ where most of its power should be concentrated. Then, a useful search strategy is as follows.

First of all, it is convenient to work in a discretized space. Recall that the output of a detector is sampled at some rate $1/\Delta t$. Then, we can split the output into time segments, and inside each segment the output $s(t)$ is given by the discrete set of values

$$s_j \equiv s(t_{\text{start}} + j\Delta t), \quad (7.113)$$

where t_{start} is the start time of the segment considered, $j = 0, \dots, N$, and $\delta t = N\Delta t$ is its length. We can then perform a discrete Fourier transform over the segment δt by writing

$$\tilde{s}_k = \sum_{j=0}^{N-1} n_j \exp\left\{\frac{2\pi i}{N} jk\right\}, \quad (7.114)$$

or

$$\tilde{s}_k = \sum_{j=0}^{N-1} n(t_j) \exp\{2\pi i(t_j - t_{\text{start}})f_k\}. \quad (7.115)$$

where $t_j = t_{\text{start}} + j\Delta t$ and

$$f_k = \frac{k}{N\Delta t} = \frac{k}{\delta t}. \quad (7.116)$$

We see that frequencies are spaced by $1/\delta t$, up to a maximum frequency equal to $N/\delta t$ (since eq. (7.114) is periodic under $k \rightarrow k + N$), which of course is just the sampling frequency $1/\Delta t$.³⁴ We can write as usual $s_i = n_i + h_i$, where n_i is the noise and h_i a putative signal, and we define

³⁴To fix the ideas, one can consider that the sampling rate $1/\Delta t$ of an interferometer is typically of order $10 - 20$ kHz. We can imagine that we are searching for bursts of duration $\delta t = 0.5$ s, so frequency space is split into bins of width 2 Hz. Restricting the search to the frequency range where interferometers are most sensitive, which corresponds to a bandwidth $\Delta f = O(200)$ Hz around peak sensitivity, we have a total of $O(100)$ bins in frequency, for each value of the start time of the segment.

the Fourier transforms \tilde{n}_k and \tilde{h}_k as in eq. (7.114). The discrete version of eq. (7.6) is obtained replacing the Dirac delta by a Kronecker delta,

$$\langle \tilde{n}_k^* \tilde{n}_{k'} \rangle = \delta_{kk'} \frac{1}{2} S_k, \quad (7.117)$$

where we used the short-hand notation $S_k \equiv S_n(f_k)$.

If the only theoretical expectation that we have about a signal is that it should have a duration δt , and should have most of its power in a frequency band $f_1 < f < f_2$, with $f_1 = k_1/\delta t$, $f_2 = k_2/\delta t$, and $f_2 - f_1 \equiv \delta f$, we can form, for each possible start time t_{start} , the quantity

$$\mathcal{E} = 4 \sum_{k=k_1}^{k_2} \frac{|\tilde{s}_k|^2}{S_k}, \quad (7.118)$$

which is called the *excess power statistic*. We collect the values of \mathcal{E} for all possible start time and, if we find a value above some given threshold, we record it as an event.³⁵ To understand what is a statistically significant value of \mathcal{E} , observe that \mathcal{E} is formed from $k_2 - k_1$ independent complex variables s_k . Since $(k_2 - k_1)/\delta t = f_2 - f_1 \equiv \delta f$, the number of independent real variables is

$$\mathcal{N} = 2\delta f \delta t, \quad (7.119)$$

i.e. twice the area of the time-frequency plane explored. Therefore, even in the absence of any GW signal in the data, the average value of \mathcal{E} is of order \mathcal{N} .³⁶ This means that a real GW signal, in order to be visible in \mathcal{E} against the noise with a signal-to-noise ratio of order one, must give a contribution to \mathcal{E} of order \mathcal{N} . From eq. (7.119), $\mathcal{N} \geq 2$ (the uncertainty principle, in a quantum language) and, depending on the situation, one can have $\mathcal{N} \gg 1$. Comparing with eq. (7.51), we see that, if we knew the waveform and we could make a matched filtering, such a signal would produce a value of S/N of order $\mathcal{N}^{1/2}$. In other words, using the excess power statistic, we can detect with a signal-to-noise ratio of order one, a signal that with matched filtering would emerge with signal-to-noise ratio of order $\mathcal{N}^{1/2}$.³⁷ This is not surprising since we know that, when we have the waveform, the matched filtering maximizes the signal-to-noise ratio. However, the excess power statistic only needs very crude information about the signal, namely its duration and its typical frequency range, and is therefore much more robust. Furthermore, it can be proved that, if the only information on the signal is its duration and its bandwidth, the excess power method is the optimal one.

From the above discussion, it is clear that the method is viable only when \mathcal{N} is not too large. For instance, for the inspiral phase of a coalescing NS-NS binary, as observed in a ground-based interferometer, we see from eq. (4.21) that the signal enters the bandwidth of the interferometer, say at 40 Hz, when the time to coalescence is $\tau = 25$ s, and sweeps in frequency up to the kHz. Taking $\delta f \sim 1000$ Hz and $\delta t \sim 25$ s, we get $\mathcal{N} \sim 5 \times 10^4$ and $\mathcal{N}^{1/2} \sim 200$, so the excess power method would allow

³⁵In the sense defined in Note 2 on page 337.

³⁶More precisely, in the presence of Gaussian noise \mathcal{E} follows a χ^2 distribution with \mathcal{N} degrees of freedom, while in the presence of signal it follows the corresponding non-central χ^2 distribution, see eq. (7.92).

³⁷For a more accurate estimate of the signal-to-noise ratio obtained restricting the frequency bandwidth, i.e. performing a band-pass filter, see Section II of Flanagan and Hughes (1998a).

us to detect signals only when their signal-to-noise ratio, with matched filtering, is of order several hundreds. Thus, for inspiraling binaries, the excess power method is not at all competitive. Furthermore it is not needed, since in this case we have precise calculations of the waveform in the inspiral phase, as we saw in Chapter 5.

The situation is different for the merging phase of a BH-BH coalescence. In this case the maximum value of f can be estimated to be of order f_{qnr} , where f_{qnr} is the ringing frequency of the fundamental quasi-normal mode of the black hole. To include the power radiated by the BH in its higher quasi-normal modes, an estimate of order $2f_{\text{qnr}}$ could be more appropriate. Black hole normal modes will be discussed in Vol. 2, and we will see that f_{qnr} can reach a maximum value (for rapidly spinning BHs of mass m) $f_{\text{qnr}} = c^3/(2\pi Gm)$. Observe that this is quite larger than the maximum frequency (4.39) at which the inspiral phase ends, so we finally take $\delta f \sim 2f_{\text{qnr}} \sim c^3/(\pi Gm)$. As for the merging time, we can roughly estimate that it should not be much larger than r_{ISCO}/c , where $r_{\text{ISCO}} = 6Gm/c^2$ is the radius of the innermost stable circular orbit in a Schwarzschild geometry, see eq. (4.38). Taking for instance $\delta t \sim 2r_{\text{ISCO}}/c = 12Gm/c^3$, we get the estimate $\mathcal{N}^{1/2} \sim 2$, so the loss in sensitivity with respect to optimal filtering is not large. This is quite important, considering that the merging phase is very difficult to model.³⁸

The time-frequency method discussed here can be generalized in various directions. One possibility is to consider wavelets. These are generalizations of the Fourier transform, in which to a function $s(t)$ is associated a function $S(f, t_0)$ of two parameters, of which f is the frequency and t_0 is the position in time of the signal,

$$S(f, t_0) = \int_{-\infty}^{\infty} \psi_{f, t_0}^*(t) s(t) . \quad (7.120)$$

The simplest example consists in taking

$$\psi_{f, t_0}(t) = e^{-ift} \psi(t - t_0) , \quad (7.121)$$

where $\psi(t - t_0)$ is a window function centered around t_0 . This Windowed Fourier Transform, or Gabor transform, as it is called, is essentially what we have used above (more precisely, we used its discrete version), with a sharp window function. Other choices of window functions, such as a Gaussian, are more commonly used in signal analysis.

A possible drawback of a choice such as eq. (7.121) is that the temporal window has a fixed size, independently of the frequency. In most type of signals, however, there is a correlation between the characteristic frequency of a given segment and the time duration of the segment, such that low-frequency pieces tend to last longer. To take this into account, the wavelet transform is defined by choosing a window function of the form $\psi(f(t - t_0))$ (times a normalization constant \sqrt{f}), which depends explicitly on f .³⁹ In this way, at high frequencies the temporal window is shorter, so we have a better time resolution. In a sense, wavelets provide a “microscope” that, at each point in time of the signal, zooms in and

³⁸In the literature on wavelets, this is actually written as $a^{-1/2}\psi((t - t_0)/a)$, where a is a dimensionless quantity that rescales a characteristic frequency implicit in the function ψ .

out, depending on the frequency scale of the signal. The other crucial property is that it is possible to choose wavelets so that they form an orthonormal basis, and the signal can therefore be decomposed uniquely into its component with respect to this wavelet basis, just as in the Fourier transform. Wavelets are by now widely used in signal analysis in many branches of science, and many possible choices of wavelets are available, depending on the problem at hand, see the Further Reading.

Another generalization of the time–frequency analysis discussed here consists in marking as “black” the bins in the time–frequency plane where an indicator such as the excess power statistic goes above a threshold value, and searching for structures of black bins, such as clusters. This is basically a variant of the Hough transform that we will discuss in Section 7.6.3, in the context of periodic signals.

7.5.3 Coincidences

Given that GW bursts can have a very short duration, even smaller than a millisecond, the output of ground-based detectors are sampled with a very high frequency, typically $O(10)$ kHz. In one year there are about 3×10^{10} ms, so even a fluctuation with a probability $\sim 10^{-10}$ is bound to occur on average in one year worth of data. Then eq. (7.84) suggests, for bursts, a threshold on the amplitude signal-to-noise ratio of order $\rho_t \simeq 6$, in order to have just a few false alarms per year in a detector. However, this only eliminate Gaussian noise. GW bursts are particularly well simulated by non-Gaussian events such as microcreeps in the materials or sudden external mechanical or electromagnetic disturbances. In some cases the external disturbance can be identified, and the corresponding event is therefore vetoed, but in most cases this is impossible. To eliminate these non-Gaussian noise, the only possibility is to perform coincidences between different detectors.⁴⁰

Using two or more detectors in coincidence is a standard practice in physics, at least since the early days of cosmic ray research. The idea is that, if two detectors are far apart, their noise are mostly uncorrelated,⁴¹ and the probability of an accidental coincidence is small, while a GW should excite both detectors nearly simultaneously. Below we discuss some of the issues that must be addressed in order to apply this idea to GW detectors.

Relative orientation of the detectors

We have seen that the response of a detector to a GW depends on the relative orientation between the detector and the source. To perform coincidences between two or more detectors, it is therefore optimal to orient them, taking into account their difference in location, so that their response to an incoming GW signal is the same, or at least as similar as possible, for all of them. Otherwise, a real signal can be missed simply because, when one detector was oriented favorably with respect to the source, the other had a very poor sensitivity for the same direction.⁴²

⁴⁰Observe that the use of coincident detectors also allows us to lower the threshold necessary for eliminating Gaussian noise, since now the false alarm probability, for uncorrelated detector noise, is the square of (7.84). For instance, in the example above, the threshold $\rho_t \simeq 6$ valid for a single-detector search becomes $\rho_t \simeq 4.5$ in a two-detector correlation (even neglecting all consistency check discussed below).

⁴¹With some exceptions. For example, seismic or electromagnetic disturbances might propagate from one detector’s site to the other.

⁴²On the other hand, detectors with different orientation can perform independent measurement of the signal, allowing to disentangle the polarizations and the arrival direction of the wave, see the discussion on page 342.

⁴³This depends not only on the sampling time of the detector, but also on other factors, in particular on the signal-to-noise ratio of the event, since noise combines with the GW signal distorting and broadening its shape.

Coincidence window

Each GW detector has its temporal resolution, which might for instance be of the order of few ms.⁴³ Given two detectors, with variances σ_1 and σ_2 on the arrival time of their respective events, the corresponding variance in the coincidence search is $\sigma_{12} = \sqrt{\sigma_1^2 + \sigma_2^2}$, and therefore one can ask that the events be coincident within k standard deviations σ_{12} (e.g. $k = 3$ can be a typical choice). To this uncertainty one must add the light travel time $(\Delta t)_{\text{light}}$ between the two detectors since, depending on the source location, either the first or the second detector will be hit by the wavefront a time up to $(\Delta t)_{\text{light}}$ before the other. So finally one requires that the arrival times t_1 and t_2 in the two detectors are within a coincidence window

$$|t_1 - t_2| \leq (\Delta t)_{\text{light}} + k (\sigma_1^2 + \sigma_2^2)^{1/2}. \quad (7.122)$$

This typically results in a coincidence window of the order of a few tens of ms.

Energy consistency

Another possible handle to discriminate between accidental coincidences and true GW signals is the compatibility of the signal in the two (or more) detectors. Ideally, if the GW signal is much larger than the noise, two detectors oriented in the same way should register the same energy flux, when a GW hits them. In contrast, two events due to noise which by chance happen simultaneously in the two detectors, should have uncorrelated energies. However, in practice, at moderate values of the signal-to-noise ratio the signal $h(t)$ induced by the GW combines with the noise $n(t)$ and, depending on the relative phase of these contributions, the output $h(t) + n(t)$ fluctuates and can be either larger or smaller than the value that would be induced by the GW. Therefore, as we computed in Section 7.4.3, one has a probability distribution for the amplitudes (or for the energies) measured in the two detectors, and the compatibility criterion must take into account this probability distribution. This procedure also requires that the two detectors have a sufficiently reliable calibration in energy.

Waveform consistency

A broadband detector has rather detailed information on the waveform, and a consistency condition between the waveforms observed in the two detectors can be imposed. For instance, one of the algorithms used by LIGO for generating candidate events is based on the identification of connected regions (“clusters”) in the time–frequency plane where the power is not consistent, statistically, with Gaussian noise, as discussed in Section 7.5.2. Then each event is characterized by its bandwidth (f_{\min}, f_{\max}) , i.e. by the low and high frequency bounds of the cluster. One can then require, for instance, that the bandwidth of events in

different detectors have an overlap, or at least that they are separated in frequency by no more than a fixed window Δf .

Background estimation

After having applied all these cuts, we can still have accidental coincidences that, by chance, passed them. However, the residual number of accidental coincidences can be estimated very reliably. First of all, one can simply predict it from the observed event rate in a single detector, assuming that the noise is stationary. But in fact the most direct estimation of the background is obtained using a shifting algorithm which, together with many other techniques used in GW research, was introduced by Weber. The procedure consists simply in shifting the data stream of one detector with respect to the other by a time step significantly longer than the coincidence window, say 2 s, and counting the number of coincidences obtained after shifting (subject to the same requirements on the coincidence window and energy compatibility imposed on the coincidences at zero time shift). These coincidences, of course, are now all accidental, since the shift has been chosen much larger than the coincidence window and therefore of the uncertainties in the arrival times. We then repeat the procedure with a different shift, say 4 s, and we count again the number of accidentals. One can repeat the procedure for many different shifts (the overall time shift must however be short compared to the time-scale over which the event rate in a single detector changes substantially). We then average over these shifts, and we have a rather accurate estimate of the average number of accidental coincidences, its variance, and more generally their distribution (which is found experimentally to be a Poisson distribution, as expected whenever we count a number of discrete independent events), and we can also study how these quantities depend on the energy of the events.

7.6 Periodic sources

While a burst source is typically radiating only for a period of less than a second, a periodic source emits continuously an almost monochromatic signal, so the limit on its observation comes from the total available observation time, which can be of order of years. Our intuitive discussion of matched filtering showed that, if we can follow a signal for a time T , the minimum level of signal that we can extract from the noise scales as $1/T^{1/2}$, see eqs. (7.39) and (7.40). This means that, for periodic waves, we can extract from the noise a signal with an amplitude h_0 much smaller than the one that can be measured in the case of bursts. This opportunity, however, also comes at the expense of some complications, since we must be able to track carefully the signal for a long period. We already met a similar situation in Chapter 6, where we studied the timing formula for the radio signals of pulsars, and we saw that there are two main issues to address: the intrinsic changes of the frequency of the source, and the modulation of the signal due to the motion of the

⁴⁴For GWs, propagation effects between the source and the Earth, such as dispersion in the interstellar medium, are totally irrelevant, given the smallness of gravitational cross-sections.

Earth.⁴⁴

If, for a moment, we neglect these effects, a periodic source emitting GWs at a frequency f_0 produces in the detector a signal

$$h(t) = F_+(\theta, \phi) h_+(t) + F_\times(\theta, \phi) h_\times(t), \quad (7.123)$$

where

$$h_+(t) = h_{0,+} \cos(2\pi f_0 t), \quad (7.124)$$

$$h_\times(t) = h_{0,\times} \cos(2\pi f_0 t + \alpha). \quad (7.125)$$

We take by definition $f_0 > 0$; $h_{0,A}$ are the real amplitudes for the two polarizations ($A = +, \times$), and α is their relative phase. We denote by θ, ϕ the angles that define the propagation direction $\hat{\mathbf{n}}$ of the GW from the source to us, so the polar angles of the source, as seen from the Earth, are $\theta_s = \pi - \theta$ and $\phi_s = \phi + \pi$.

Assuming for the moment that the source is, intrinsically, perfectly periodic, still the motion of the Earth modifies eqs. (7.123)–(7.125) as follows.

- Because of the Earth's rotation, the apparent position of the source in the sky changes, so the angles θ and ϕ which appear in the pattern functions change with time, and are periodic functions of sidereal time, with period one sidereal day. If we are tracking a specific source in the sky, the time dependence of the pattern functions, $F_A(\theta(t), \phi(t))$, must therefore be taken into account, and this produces a modulation of the amplitude of the signal.
- Because of the Earth's rotation and of its revolution around the Sun (or, more precisely, because of its motion with respect to the Solar System Barycenter, as discussed in Chapter 6), the relative velocity of the Earth and the source changes with time, and this produces a time-varying Doppler shift in the frequency.

As a consequence, $h(t)$ is not a simple monochromatic signal. We will come back to these amplitude and phase modulations in Sections 7.6.1 and 7.6.2. For the moment, however, we restrict to an observation time T sufficiently short, so that these amplitude and phase modulations can be neglected. For the amplitude modulation due to the Earth's rotation, this requires of course $T \ll 1$ day, while for the Doppler effect we will quantify this requirement in Section 7.6.2. In this limit $h(t)$ becomes monochromatic, with a frequency f_0 .

In this simplified setting the form of the matched filter becomes obvious: we must limit ourselves to a bandwidth as small as possible around f_0 , since enlarging the bandwidth we accept more noise but we add no further signal. If T is the total observation time, our resolution in frequency is $1/T$, see eq. (7.10), and therefore a bandwidth as small as possible means $\Delta f \simeq 1/T$. Formally, we can obtain the same result using eq. (7.49). From eqs. (7.123)–(7.125) we have, for $f > 0$,

$$\tilde{h}(f) = \delta(f - f_0) \frac{1}{2} [F_+(\theta, \phi) h_{0,+} + F_\times(\theta, \phi) h_{0,\times} e^{-i\alpha}], \quad (7.126)$$

and therefore eq. (7.49) gives

$$\tilde{K}(f) = \delta(f - f_0), \quad (7.127)$$

apart from an arbitrary constant, in which we also reabsorbed $1/S_n(f_0)$. Of course, the Dirac delta is a mathematical idealization, and if we measure for a total observation time T we must replace it by a regularized Dirac delta,

$$\delta(f) = \int_{-\infty}^{\infty} dt e^{i2\pi ft} \rightarrow \int_{-T/2}^{T/2} dt e^{i2\pi ft}, \quad (7.128)$$

which has a support over a range $\Delta f \sim 1/T$ and satisfies $\delta(0) = T$. Then eq. (7.51) becomes

$$\begin{aligned} \left(\frac{S}{N}\right)^2 &= |F_+(\theta, \phi)h_{0,+} + F_\times(\theta, \phi)h_{0,\times}e^{-i\alpha}|^2 \int_0^\infty df \frac{\delta(f - f_0)\delta(0)}{S_n(f)} \\ &= |F_+(\theta, \phi)h_{0,+} + F_\times(\theta, \phi)h_{0,\times}e^{-i\alpha}|^2 \frac{T}{S_n(f_0)}. \end{aligned} \quad (7.129)$$

Not surprisingly, the signal-to-noise ratio increases if we increase the observation time, and the dependence $S/N \sim \sqrt{T}$ is what we already found using heuristic arguments in eqs. (7.39) and (7.40).

In general, the frequency f_0 is not known in advance. However, for an exactly periodic signal, we do not need to repeat the matched filtering procedure separately for each value of the unknown parameter f_0 . In fact, from eq. (7.42), when $\tilde{K}(f) = \delta(f - f_0)$ the signal is simply $S = \tilde{h}(f_0)$, and the values of $\tilde{h}(f)$ for all f can be computed at once performing a single Fast Fourier Transform (FFT), which is a particularly efficient algorithm.

If this were the end of the story, the search for periodic signals would simply consist in performing a single FFT on a stretch of data of length T , and looking for lines in the power spectrum. The signal-to-noise ratio of these line should improve with the observation time as \sqrt{T} . We will see in Section 7.6.1 and especially in Section 7.6.2 that the full story is more complicated.

7.6.1 Amplitude modulation

As we pointed out above, the pattern functions depend on time because of the Earth's rotation, and are therefore periodic functions of sidereal time, with a period of one sidereal day. In the matched filtering, we must take this into account, and this results in a different amplitude modulation for each possible source position. We will discuss in the next sections how to efficiently scan the parameter space, in order to take this effect into account.

If we want to estimate the effect of this modulation on the sensitivity, we can however simply observe that, for integration times T longer than one day, the effect of this amplitude modulation can be taken into

⁴⁵If, rather than being interested in the sensitivity to a specific source, one wants to define an average sensitivity for an ensemble of sources, then one can improve this estimate taking care of the fact that there is a statistical preference for the angles and polarizations that give a larger S/N , since these can be seen to larger distances. This modifies S/N by factors that can be approximately estimated to be of order $(3/2)^{1/2} \simeq 1.2$, see Thorne (1987).

account averaging eq. (7.129) over the apparent motion of the source in one sidereal day, i.e. averaging over all values of the right ascension of the source, and over a range of values of the declination which depend on the specific orbit of the source. In a first approximation, we can replace this average with an average over the solid angle and over the polarization angle ψ .⁴⁵ From eq. (7.129), using eqs. (7.33) and (7.35), we then find

$$\left(\frac{S}{N}\right)^2 = \langle F_+^2 \rangle \left(\frac{T}{S_n(f_0)}\right) h_0^2, \quad (7.130)$$

where

$$h_0^2 = h_{0,+}^2 + h_{0,\times}^2. \quad (7.131)$$

The values of $\langle F_+^2 \rangle$ for various detectors are given in Table 7.1, recalling that $\langle F_+^2 \rangle = F/2$. We can also rewrite eq. (7.130) as

$$\frac{S}{N} = \frac{h_0}{h_n}, \quad (7.132)$$

defining the dimensionless quantity h_n ,

$$h_n = \frac{1}{\langle F_+^2 \rangle^{1/2}} \left(\frac{S_n(f_0)}{T}\right)^{1/2}. \quad (7.133)$$

Therefore h_n is the GW amplitude that can be measured by the detector, for a periodic signal, at $S/N = 1$ (assuming that we have been able to correct for the phase modulation, see next section). More generally, the minimum amplitude that can be detected at a given value of S/N is

$$(h_0)_{\min} = \frac{S/N}{\langle F_+^2 \rangle^{1/2}} \left(\frac{S_n(f_0)}{T}\right)^{1/2}. \quad (7.134)$$

It is instructive to compare this result with the minimum burst amplitude detectable at a broad-band detector, eq. (7.107). Recalling that $S_n(f)$ has dimensions $1/\text{Hz}$, i.e. dimensions of time, we must divide it by a time in order to obtain a dimensionless quantity, such as a GW amplitude. For bursts, we see from eq. (7.107) that this time-scale is the duration $\tau_g = 1/f_{\max}$ of the burst, while for a periodic signal we see from eq. (7.133) that it is the observation time T . Since T can be of the order of months or years, while τ_g is typically between the millisecond and a second, the minimum value of h detectable for periodic signals is much smaller than for bursts. On the other hand, a periodic signal is intrinsically much weaker, since a burst emits a huge amount of energy in a very short time. We will estimate in Section 7.6.3 the maximum distances at which typical periodic signals can be seen.

For bursts, we assumed that the wave came from the optimal direction, and for this reason we wrote no angular factor in eq. (7.107). For periodic signals, an average over the source position is in any case necessary

because of the apparent motion of the source in the sky, leading to the amplitude modulation, and produces the angular efficiency factor $\langle F_+^2 \rangle$ in eq. (7.134).

An alternative reference quantity which is often used is $h_{3/\text{yr}}$, which is defined as the minimum value of h_0 that can be detected at a given value of S/N , integrating for $T = 10^7$ s (i.e. about 1/3 of a year),

$$h_{3/\text{yr}} = \frac{S/N}{\langle F_+^2 \rangle^{1/2}} \sqrt{S_n(f_0) \times 10^{-7} \text{ Hz}}. \quad (7.135)$$

7.6.2 Doppler shift and phase modulation

Even if an astrophysical source emitted exactly monochromatic GWs with a frequency f_0 , for a detector on Earth the instantaneous value of the observed frequency f would change with time because of the Doppler effect. Recall that, to first order in v/c , the frequency measured by an observer with a velocity \mathbf{v} with respect to the source is

$$f = f_0 \left(1 + \frac{\mathbf{v} \cdot \hat{\mathbf{r}}}{c} \right), \quad (7.136)$$

where $\hat{\mathbf{r}}$ is the unit vector in the direction of the source. If $\mathbf{v} \cdot \hat{\mathbf{r}}$ were a constant, this would cause little concern, since it would just amount to a constant offset in the frequency and, with a single FFT, monochromatic lines at all possible frequencies are searched simultaneously. However, the velocity of the detector with respect to the source changes in time because of the Earth's rotation and because of its revolution around the Sun and this induces a time-dependence in the observed frequency. We denote by $(\Delta v)_T$ the change of the component of the velocity in the direction of the source, in a time T . Then the frequency f changes on the same time interval by an amount

$$(\Delta f)_{\text{Doppler}} = f_0 \frac{(\Delta v)_T}{c}. \quad (7.137)$$

When we integrate the signal for a time T , the resolution in frequency is $\Delta f = 1/T$. As long as $(\Delta f)_{\text{Doppler}}$ is smaller than this resolution, all the GW signal falls into a single frequency bin and the Doppler effect can be neglected. To estimate the maximum integration time for which the Doppler effect is negligible, we consider first the effect of the Earth rotation around its axis. At a latitude of 40 degrees, the rotational velocity of the Earth is $v_{\text{rot}} = \omega_{\text{rot}} R_\oplus \cos(40^\circ) \simeq 355 \text{ m/s}$, where $\omega_{\text{rot}} = (2\pi/24 \text{ hr})$ and $R_\oplus \simeq 6.38 \times 10^6 \text{ m}$ is the mean Earth equatorial radius. This gives $v_{\text{rot}}/c \simeq 1.2 \times 10^{-6}$. During an integration time T , the Earth rotates by an angle $\Delta\theta = \omega_{\text{rot}} T$ and, if $\Delta\theta \ll 1$, in order of magnitude the change of the component of the velocity in the direction of the source is given by $(\Delta v)_T/v_{\text{rot}} \sim \Delta\theta$, i.e.

$$(\Delta v)_T \sim v_{\text{rot}} \omega_{\text{rot}} T. \quad (7.138)$$

(The precise numbers, of course, depends on the exact direction of the source with respect to the detector.) Then $(\Delta f)_{\text{Doppler}}$ becomes of the

order of the frequency resolution if

$$f_0 \left(\frac{v_{\text{rot}}}{c} \right) \omega_{\text{rot}} T \sim \frac{1}{T}, \quad (7.139)$$

which gives

$$T \sim 60 \min \left(\frac{1 \text{ kHz}}{f_0} \right)^{1/2}. \quad (7.140)$$

Therefore, for waves with $f_0 \sim 1 \text{ kHz}$, the Doppler effect due to the Earth's rotation around its axis becomes important after about one hour.⁴⁶ It reaches its maximum value after about 12 hr (the precise numbers, again, depend on the source position), when the detector has inverted its velocity with respect to the source, $\Delta v_{\text{rot}} = 2v_{\text{rot}}$, and in this time span the frequency has changed by a total amount

$$(\Delta f)_{\text{max}}^{\text{rot}} \sim 2f_0 \frac{v_{\text{rot}}}{c} \simeq 2.4 \times 10^{-3} \text{ Hz} \left(\frac{f_0}{1 \text{ kHz}} \right). \quad (7.141)$$

We can repeat the same reasoning for the orbital motion of the Earth around the Sun. For an order-of-magnitude estimate we can take the orbit as circular, with a radius $R = 1 \text{ au} \simeq 1.5 \times 10^{11} \text{ m}$ and $\omega_{\text{orb}} = 2\pi/(365 \text{ days})$, so $v_{\text{orb}} \simeq 3 \times 10^4 \text{ m/s}$ and $v_{\text{orb}}/c \simeq 10^{-4}$. The maximum frequency shift induced by the Earth revolution is then

$$(\Delta f)_{\text{max}}^{\text{orb}} \sim 2f_0 \frac{v_{\text{orb}}}{c} \simeq 0.2 \text{ Hz} \left(\frac{f_0}{1 \text{ kHz}} \right), \quad (7.142)$$

and is much larger than that due to the Earth rotation around its axis, given in eq. (7.141), because $v_{\text{orb}} \gg v_{\text{rot}}$. However, the large drift (7.142) takes place over a six months period. In an integration time T much shorter than six months, the orbital motion induces a variation $(\Delta v)_T \sim v_{\text{orb}}\omega_{\text{orb}}T$ and the corresponding frequency shift is $(\Delta f)_{\text{Doppler}} \sim f_0(v_{\text{orb}}/c)\omega_{\text{orb}}T$. Similarly to eq. (7.139), the time after which the orbital Doppler shift becomes larger than the frequency resolution is given by

$$f_0 \left(\frac{v_{\text{orb}}}{c} \right) \omega_{\text{orb}} T \sim \frac{1}{T}, \quad (7.143)$$

i.e.

$$T \sim 120 \min \left(\frac{1 \text{ kHz}}{f_0} \right)^{1/2}. \quad (7.144)$$

Therefore the Doppler shift due to the Earth rotation around its axis is the first to become important, when we increase the integration time (after about 1 hr if, for instance, $f_0 = 1 \text{ kHz}$). The orbital Doppler shift becomes of the order of the frequency resolution shortly afterwards, after an integration times of about 2 hr for $f_0 = 1 \text{ kHz}$, but then raises steadily; after less than one day it becomes more important than the contribution from the Earth's rotation around its axis, and it continues to raise for a six months period becoming, on the long term, the largely dominant effect.

⁴⁶For frequencies $f_0 > O(40) \text{ Hz}$ we have $T \ll 1 \text{ day}$, so the approximation $\Delta\theta \ll 1$ used to write eq. (7.138) is consistent. Otherwise, a more accurate estimate is needed.

After an integration time of four months, i.e. $T \simeq 10^7$ s, the frequency resolution is $\Delta f = 10^{-7}$ Hz, which is many orders of magnitudes smaller than the Doppler shifts (7.141) and (7.142). It is interesting to see what is the form of the frequency spectrum when we are sensitive enough to resolve the time-changing Doppler shift. To simplify the geometry, we assume at first that the detector performs a simple circular motion, with frequency ω_m and radius R , and that the source is in the plane of the orbital motion of the detector, as in Fig. 7.10. Since the source is at a very large distance, we have a plane wavefront propagating along the y axis, and therefore proportional to $\cos[\omega_0(t + y/c)]$, where $\omega_0 = 2\pi f_0$ and f_0 is the GW frequency. The y coordinate of the detector is a function of time; we choose for definiteness the origin of time so that $y(0) = 0$, and therefore $y(t) = R \sin(\omega_m t)$. Then the detector sees a signal proportional to

$$\cos\left[\omega_0\left(t + \frac{y(t)}{c}\right)\right] = \cos[\omega_0 t + \beta \sin(\omega_m t)], \quad (7.145)$$

where

$$\beta = \frac{\omega_0 R}{c} = \frac{\omega_0}{\omega_m} \frac{v}{c}, \quad (7.146)$$

with $v = \omega_m R$. The parameter β is called the modulation index, and $\omega_m = 2\pi f_m$, where f_m is the modulation frequency. This signal can be written as a superposition of monochromatic waves using the identity

$$\cos[\omega_0 t + \beta \sin(\omega_m t)] = \sum_{k=-\infty}^{\infty} J_k(\beta) \cos[(\omega_0 + k\omega_m)t], \quad (7.147)$$

where $J_k(\beta)$ is the Bessel function.⁴⁷ The signal is therefore split into a carrier at the frequency f_0 , plus an infinite number of sidebands at $f_0 \pm kf_m$, for all integer k , and the power in the k -th sideband is proportional to $J_k^2(\beta)$. The qualitative form of this spectrum depends strongly on the modulation index β . For $\beta \rightarrow 0$ and k integer we have $J_k(\beta) \sim \beta^{|k|}$, so when $\beta \ll 1$ most of the power is in the carrier ($k = 0$), with smaller power in the sidebands $k = \pm 1$, even smaller power at $k = \pm 2$, etc. However, in our case β is given by eq. (7.146) and it is large. In fact, for the rotation of the Earth around its axis, setting $\omega_m = 2\pi/(24 \text{ hr})$ and $v/c \simeq 1.2 \times 10^{-6}$, eq. (7.146) gives $\beta \simeq 100 (f_0/1 \text{ kHz})$, while for the orbital motion $\beta \simeq 3 \times 10^6 (f_0/1 \text{ kHz})$. Therefore, in the range of frequencies relevant for ground-based interferometers ($f_0 > O(10) \text{ Hz}$), we are always in the regime $\beta \gg 1$.

The average number of sidebands into which the total power is distributed can be calculated using⁴⁸

$$\begin{aligned} \langle k^2 \rangle &\equiv \frac{\sum_{k=-\infty}^{\infty} k^2 J_k^2(\beta)}{\sum_{k=-\infty}^{\infty} J_k^2(\beta)} \\ &= \frac{\beta^2}{2}, \end{aligned} \quad (7.148)$$

so the power is distributed in $O(\beta)$ sidebands, as shown in Fig. 7.11. Once the frequency resolution $1/T$ has become of the order of this

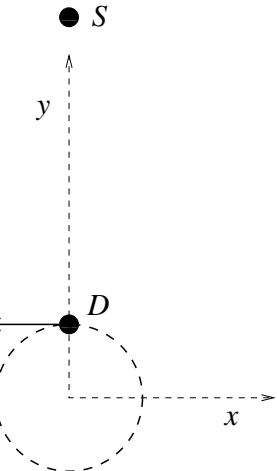


Fig. 7.10 The simplified geometry discussed in the text. The detector D performs a circular motion in the (x, y) plane. The source S is in the same plane, along the y axis.

⁴⁷This identity can be obtained writing $\cos[(\omega_0 + k\omega_m)t]$, inside the sum, as $\cos(\omega_0 t) \cos(k\omega_m t) - \sin(\omega_0 t) \sin(k\omega_m t)$, and using Gradshteyn and Ryzhik (1980), 8.514.5 and 8.514.6, recalling that, for k integer, $J_{-k}(z) = (-1)^k J_k(z)$.

⁴⁸See Gradshteyn and Ryzhik (1980), 8.536.2.

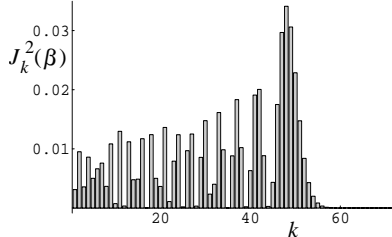


Fig. 7.11 The quantity $J_k^2(\beta)$ for $\beta = 50$, as a function of k .

Doppler line broadening, increasing T further does not improve substantially the signal-to-noise ratio. In fact, while a smaller frequency bin contains by definition less noise, it now also contains less signal, since the signal gets spread over many bins. However, if at this stage the signal already emerged from the noise, increasing T further we improve the resolution by which we are able to reconstruct the line shape (and therefore the accuracy by which we can reconstruct the source position, see Note 49 below).

Luckily, there is in principle a very simple way (borrowed from pulsar radio-astronomy) to correct for the Doppler shift. In the simple geometrical situation illustrated in Fig. 7.10, we just need to define a new time variable $t' = t + \mathbf{y}(t)/c$. In terms of this variable the signal (7.145) is simply proportional to $\cos(\omega_0 t')$ and, performing the Fourier transform with respect to t' , all sidebands collapse into a single frequency. For a generic source location, the redefinition of time that does the job is

$$t' = t + \frac{\mathbf{x}(t) \cdot \hat{\mathbf{r}}}{c}, \quad (7.149)$$

where $\mathbf{x}(t)$ is the position of the detector (measured for instance using the Solar System Barycenter (SSB) as a reference frame) and $\hat{\mathbf{r}}$ is the unit vector pointing toward the source. Observe that this is just the Roemer time delay that we already discussed in Section 6.2.2. We can therefore simply resample the output of the detector in terms of this new time, and we have corrected for the Doppler effect. The procedure has an added bonus: it is quite likely that, in the Fourier spectrum of the output, there will be monochromatic lines due to instrumental noise. If such a line has a frequency that is constant in time to a good accuracy, its signal-to-noise ratio will increase as \sqrt{T} , just as for a GW signal. However, when we apply the resampling procedure, a real GW signal, which was spread over many bins, is collapsed to a single frequency bin, and conversely an instrumental line which was monochromatic will be spread over many bins, and will finally be diluted into the noise. In other words, we are using the Doppler modulation as a powerful signature that discriminates a real GW signal from instrumental noise.

The simplicity of this solution comes however at a price: we need to know both $\mathbf{x}(t)$ and $\hat{\mathbf{r}}$ with great precision. We can assume that the motion of the Earth is known to a sufficient accuracy (although, if we want to integrate for a time $T \sim 1$ yr, we need to keep under control effects that can produce shifts $\Delta f \sim 10^{-7}$ Hz, and for this we must also include small effects like the oscillations of the Earth around the Earth–Moon barycenter, which however are precisely known), so the main error comes from the uncertainty on the angular position of the source. From eq. (7.136) we see that, in order to correct for the Doppler shift with an accuracy smaller than the experimental resolution $1/T$ on f , we need, in order of magnitude,

$$\frac{f_0}{c} (\Delta v)_T \Delta \theta < \frac{1}{T}, \quad (7.150)$$

where $(\Delta v)_T$ is the variation of the velocity of the Earth during the

observation time T (recall that only the temporal variation is relevant, otherwise the Doppler effect would give just a constant offset in f_0), while $\Delta\theta$ is the angular resolution (in radians) on the position of the source.

If we take $(\Delta v)_T \sim v_{\text{orb}}\omega_{\text{orb}}T$ we find that, to apply the Doppler correction, we need to know the source location to an accuracy

$$\begin{aligned}\Delta\theta &< \frac{1}{f_0(v_{\text{orb}}/c)\omega_{\text{orb}}T^2} \\ &\simeq 0.1 \text{ arcsec} \left(\frac{10^7 \text{ s}}{T} \right)^2 \left(\frac{1 \text{ kHz}}{f_0} \right).\end{aligned}\quad (7.151)$$

This expression is correct as long as the Doppler effect due to the orbital motion dominates that due to the Earth rotation around its axis, i.e. for $T \gtrsim 1$ day, and also as long as the angle $\omega_{\text{orb}}T$ is small, since otherwise the approximation $(\Delta v)_T \sim v_{\text{orb}}\omega_{\text{orb}}T$ should rather be replaced by $(\Delta v)_T \sim v_{\text{orb}} \sin \omega_{\text{orb}}T$, so approximately eq. (7.151) is valid as long as 1 day $\lesssim T \lesssim 4$ months.⁴⁹

If we are targeting a specific source whose position is known to this accuracy or better, as is the case for many pulsars, this requirement does not pose special problems. However, as we will discuss in Vol. 2, there are many mechanisms that can produce periodic GWs, in particular in neutron stars, that are not necessarily associated to a strong electromagnetic emission or, as with pulsars, the electromagnetic emission could be beamed in a direction that does not intersect the Earth. It is in fact quite likely that most of the potentially interesting sources of periodic GWs have no detected optical counterpart. For example, the closest *observed* neutron star is at a distance $r \sim 100$ pc; however, population synthesis calculations indicate that the closest one should be at a distance $r \sim 5\text{--}10$ pc, and then in a sphere of radius $r \sim 100$ pc there should be $O(10^3\text{--}10^4)$ neutron stars. It is therefore of the greatest interest to perform blind searches, i.e. searches for unknown sources over the whole sky. In principle, this means that we should partition the celestial sphere in pixels with a size given by eq. (7.151) (in fact even smaller, see Note 52 in the next section), and in each one we should apply a separate Doppler correction. As we will see in the next section, for integration times of months this is impossible, even with the maximum present or foreseeable computer power.

Furthermore, we have assumed until now that the intrinsic GW frequency f_0 of the source is stable, within the experimental resolution $\Delta f = 1/T$, and that the only modulation comes from the relative motion of the detector. This means that we are assuming a stability of the source frequency at the level

$$\begin{aligned}\frac{\Delta f_0}{f_0} &= \frac{1}{Tf_0} \\ &\simeq 1 \times 10^{-10} \left(\frac{10^7 \text{ s}}{T} \right) \left(\frac{1 \text{ kHz}}{f_0} \right).\end{aligned}\quad (7.152)$$

Quite remarkably, rotating neutron stars can sometime have this sta-

⁴⁹Actually, one could turn the argument around and observe that, if we are so lucky that there is a periodic signal so strong that can be extracted from the noise without correcting for the Doppler shift then, following the evolution of the frequency with time, we will be able to reconstruct the position of the source to the accuracy $\Delta\theta$ given by eq. (7.151). With present detector sensitivities, however, this possibility seems quite unlikely.

bility. The main mechanism that produces a drift in their frequency is the fact that a rotating NS radiates, both electromagnetically and gravitationally, and therefore loses energy. This energy is taken from the rotational energy of the NS, which therefore spins down. Pulsars are characterized by their spindown age τ ,

$$\tau = \frac{f}{|\dot{f}|}, \quad (7.153)$$

where f is their rotational frequency. As we saw in Section 4.2.1, for rotation around a principal axis and in the quadrupole approximation, the GWs emitted are monochromatic with a frequency $f_0 = 2f$, so $\tau = f_0/|\dot{f}_0|$.⁵⁰ During the observation time T , a pulsar with spindown age τ changes its GW frequency by an amount $\Delta f_0 = \dot{f}_0 T = -f_0 T/\tau$, i.e. by

$$\begin{aligned} \frac{\Delta f_0}{f_0} &= -\frac{T}{\tau} \\ &\simeq -3.2 \times 10^{-10} \left(\frac{10^9 \text{ yr}}{\tau} \right) \left(\frac{T}{10^7 \text{ s}} \right). \end{aligned} \quad (7.157)$$

⁵⁰The spindown age is of the order of the age of the pulsar if, throughout its lifetime, the pulsar frequency evolution can be described by the equation

$$\dot{f} = -af^n \quad (7.154)$$

(where a is a constant) and if the *braking index* $n > 1$. In fact, integrating the above equation we get

$$\begin{aligned} [f(t)]^{-(n-1)} - [f(0)]^{-(n-1)} \\ = a(n-1)t, \end{aligned} \quad (7.155)$$

where $t = 0$ is the time at which the pulsar was born. If the frequency at birth, $f(0)$, was much bigger than the frequency today, and if $n > 1$, we can neglect the term $[f(0)]^{-(n-1)}$ and the age of a pulsar is related to its present values of f and \dot{f} by

$$\begin{aligned} t &= \frac{1}{a(n-1)f^{n-1}} \\ &= \frac{f}{(n-1)|\dot{f}|} \\ &= \frac{\tau}{n-1}. \end{aligned} \quad (7.156)$$

Experimentally, the braking index n typically has values $n \simeq 2-3$, depending on the specific pulsar.

Comparing with eq. (7.152) we see that, with an integration time $T = 10^7$ s, for a millisecond pulsar with $f_0 \sim 1$ kHz, the effect of the spindown is important if its spindown age is lower than 3×10^9 yr while, if $f_0 = 10$ Hz, spindown is important, again over $T = 10^7$ s, if $\tau < 3 \times 10^7$ yr. Therefore for many pulsars, and in particular for young pulsars, over such a long observation time the spindown must be taken into account. Actually in young pulsars the spindown rate can be so high that even the effect of the second derivative \ddot{f}_0 can become important.

For known pulsars the spindown can be measured and taken into account when we make the Doppler correction, while for blind searches it introduces new unknown parameters. Besides spindown, there are other reasons why the frequency of the GW emitted by a pulsar can change:

- Pulsars exhibit *glitches*, i.e. sudden jumps in the frequency related to rearrangements of their internal structure. These glitches can produce changes in the frequency as large as $\Delta f_0/f_0 \sim 10^{-6}$ and occur erratically, at a rate which depends strongly on the specific pulsar, but in general of the order one glitch every few years.
- A large fraction of the known millisecond pulsars are in binary systems. In this case, there will be an additional Doppler effect due to the motion of the source, as we saw in Section 6.2.
- Pulsars are the remnant of supernova explosions, and at birth they can receive a large kick; so their velocities can be larger than the typical velocities of the stars in their galactic neighborhood, and the pulsar proper motion can be important. Of course, if the motion is uniform, this only produces a constant shift in the frequency. However, accelerations due to gravitational fields can be important. In particular, many pulsars are found in globular clusters. In this case, the acceleration due to the Newtonian gravitational

forces from all the other stars is known to produce frequency drifts comparable to the spindown rate.

- Even a uniform proper motion can be important if, during the observation time, it drives the NS out of the pixel in the sky where it was initially. For instance, a pulsar at a distance $r = 300$ pc, with a transverse velocity $v = 10^3$ km/s with respect to our line-of-sight, in a time $T = 10^7$ s moves by $\Delta\theta = vT/r \simeq 10^{-6}$ rad $\simeq 0.2$ arcsec which, according to eq. (7.151), is of order of the accuracy $\Delta\theta$ that we need, over such an integration time T , for a pulsar radiating GWs at $f_0 \sim 1$ kHz.

In the next section we will discuss how one can try to cope with these difficulties.

7.6.3 Efficient search algorithms

Coherent searches

From the discussion of the previous section we know that, if we want to integrate the signal for a long time, we must resample the output of the detector in terms of the time t' defined in eq. (7.149), plus further correction for the spindown or other effects that change the frequency. The GWs produced by a rotating NS, in the absence of spindown, has been computed in eq. (4.223). Including the Doppler effect of the detector and the spindown of the source we can write the signal received as

$$h(t) = F_+(\hat{\mathbf{n}}(t); \psi) h_0 \frac{1 + \cos^2 \iota}{2} \cos \Phi(t) + F_\times(\hat{\mathbf{n}}(t); \psi) h_0 \cos \iota \sin \Phi(t), \quad (7.158)$$

where h_0 is given in eq. (4.224), and ι is the angle between the spin axis of the neutron star and the propagation direction $\hat{\mathbf{n}}$ of the GW; of course $\hat{\mathbf{n}} = -\hat{\mathbf{r}}$, where $\hat{\mathbf{r}}$ is the unit vector pointing toward the source, and depends on time because of the relative motion of the detector and source. The evolution of the accumulated phase $\Phi(t) = 2\pi \int dt f(t)$ observed by the detector can be described by a Taylor expansion, writing

$$f(t') = f_0 + \dot{f}_0(t' - t'_0) + \frac{1}{2} \ddot{f}_0(t' - t'_0)^2 + \dots, \quad (7.159)$$

where t' is the resampled time given in eq. (7.149), i.e. the time of arrival of the signal in the Solar System Barycenter (SSB),⁵¹ and t'_0 is a fiducial value, such that $\Phi(t'_0)$ has the value ϕ_0 . Then

$$\Phi(t) = \phi_0 + 2\pi \left[f_0(t' - t'_0) + \frac{1}{2} \dot{f}_0(t' - t'_0)^2 + \frac{1}{6} \ddot{f}_0(t' - t'_0)^3 + \dots \right]. \quad (7.160)$$

Of course, a truncated Taylor expansion is useful only if the higher order terms are small corrections during the whole observation time T . This is not the case for a neutron star in a binary system, which rather performs a circular motion around the center-of-mass of the system, so eq. (7.160) only applies to isolated neutron stars.

⁵¹Actually, the precise redefinition is

$$t' = t + \frac{\mathbf{x}(t) \cdot \hat{\mathbf{r}}}{c} + \Delta_{E\odot} - \Delta_{S\odot},$$

where $\Delta_{E\odot}$ and $\Delta_{S\odot}$ are the solar system Einstein and Shapiro time delays discussed in Section 6.2.2. However, given the detector and the source positions, the Einstein and Shapiro delays can be computed, as we did explicitly in Section 6.2.2, and introduce no new free parameter.

If our target is a given pulsar whose position, proper motion and spindown parameters are known to sufficient accuracy, the form of the signal (7.158) is fixed. Then we can simply demodulate the signal defining a new variable t'' as

$$t'' = (t' - t'_0) + \frac{\dot{f}_0}{2f_0}(t' - t'_0)^2 + \frac{\ddot{f}_0}{6f_0}(t' - t'_0)^3 + \dots, \quad (7.161)$$

so that eq. (7.160) reads $\Phi = \phi_0 + 2\pi f_0 t''$. We resample the detector output with respect to this variable, and then all we need to do is to perform a single Fast Fourier Transform (FFT) on this resampled stretch of data, of length T . The number of spindown parameters $\dot{f}_0, \ddot{f}_0, \dots$ to be included to have sufficient accuracy depend on the source, and on the observation time T .

If however we want to perform a blind all-sky search, the problem becomes quickly intractable with increasing observation time T . In fact, our parameter space is given by the angles (θ_s, ϕ_s) of the source and by the spindown parameters $\dot{f}_0/f_0, \ddot{f}_0/f_0, \dots$, etc. Observe that f_0 itself does not contribute to the dimension of the parameter space; the resampling of time (7.149) is independent of f_0 , while eq. (7.161) depends only on the ratios $\dot{f}_0/f_0, \ddot{f}_0/f_0, \dots$, and not separately on $f_0, \dot{f}_0, \ddot{f}_0, \dots$. This is a crucial advantage of the resampling technique. If, rather than resampling the detector output, we directly used the Wiener filtering for the waveform given in eqs. (7.158) and (7.160), then f_0 would be an additional parameter to be searched, and the computational cost would increase dramatically.

Then, what we should do is to discretize this parameter space, and for each point of this parameter space we should perform the appropriate demodulation (7.161) and one FFT. This procedure is referred to as a *coherent* search. Its drawback is that, if we want to take advantage of the large integration time, the mesh in the discretized parameter space must become finer and finer when we increase T . For instance, even in the simplest case in which the spindown parameters are negligible, and therefore the parameter space is given only by the angles (θ_s, ϕ_s) , still the number of patches in the sky that we must consider is at least $N_{\text{patches}} = 4\pi/(\Delta\theta)^2$ and scales at least as T^4 , see eq. (7.151).⁵²

More generally, the number of mesh points depends on the kind of search that we perform. For instance, old pulsars are less demanding than young pulsars of the same frequency, since their spindown rate is lower and therefore it can be taken into account using a larger mesh in the spindown parameter space. Similarly, we see from eq. (7.151) that slow pulsars (say, $f_0 < 200$ Hz) are easier to analyze than fast pulsars with $f_0 \sim 1$ kHz.

Since the time needed for data analysis grows with a large power of T , increasing T we necessarily reach a point where the data analysis would take the same time as the observation time T and beyond that point it would quickly become many orders of magnitude larger than the observation time. We can therefore take as a limit the condition that the time required by data analysis does not exceed the observation

⁵²A more careful argument shows that it even scales like T^5 , because the approximation $(\Delta v)_T \sim v_{\text{orb}}\omega_{\text{orb}}T$ used to derive eq. (7.151) does not hold simultaneously for the right ascension and for the declination angles, see Brady, Creighton, Cutler and Schutz (1998).

time used to take the same data. To have an idea of the computational requirements consider that, using 10^7 s of data to search for periodic GWs with frequencies up to 500 Hz, requires the calculation of a FFT with 10^{10} points, which takes about 1 s on a teraflop computer (assuming that all 10^{10} points can be held simultaneously in fast memory), and we need one such FFT for each point of the parameter space. It can be estimated⁵³ that a coherent all-sky search of $T = 10^7$ s of data for slow, old pulsars ($\tau > 1000$ yr, $f_0 < 200$ Hz, i.e. the “easier” target) requires only one spindown parameter and 10^{10} independent points in parameter space, while for young, fast pulsar (frequencies up to $f_0 \simeq 1$ kHz, τ as low as 40 yr) three spindown parameters and 8×10^{21} points in parameter space are required. Then, even in the “easy” case, the analysis of four months of data would require three centuries on a teraflop computer! Requiring that the data analysis does not last more than data taking, one finds that for slow, old pulsars the data stretch cannot be longer than ~ 18 days, while for young, fast pulsar the limit is less than one day. The disappointing conclusion is that, even if a detector can in principle take good data for months or years, a coherent blind all-sky search for pulsar using fully these data is impossible.

Incoherent searches

A solution to the computational problem discussed above is to split the total observation time T into \mathcal{N} stacks of length T_{stack} , with $T = \mathcal{N}T_{\text{stack}}$. We choose T_{stack} so that a coherent search over such a time is computationally feasible. So the output of each coherent search over one stack is a collection of function $\tilde{h}(f)$, one for each value of the parameter space. For each point in parameter space we then add the quantity $|\tilde{h}(f)|^2$ over the \mathcal{N} stacks. Since in this way the phase information between the different stacks gets lost, this is called an *incoherent search*. If we denote by τ_{stack} the time needed to perform a coherent search on a stack of data of length T_{stack} , the time needed for the full incoherent search is $\tau_{\text{inc}} = \mathcal{N}\tau_{\text{stack}}$, while the time needed for a full coherent search over the whole time T is $\tau_{\text{coh}} \simeq (T/T_{\text{stack}})^n \tau_{\text{stack}} = \mathcal{N}^n \tau_{\text{stack}}$, so

$$\tau_{\text{inc}} \simeq \frac{1}{\mathcal{N}^{n-1}} \tau_{\text{coh}}, \quad (7.162)$$

where the power n , as discussed above, is determined by the kind of pulsars that we are targeting. Since n is large (at least $n = 5$, even when no spindown parameters are needed, see Note 52), it is clear that incoherent searches have a huge advantage in terms of computational cost and, for a given observation time T , taking \mathcal{N} sufficiently large, i.e. T_{stack} sufficiently small, the computation becomes feasible.

From the point of view of sensitivity, the value of $(S/N)^2$ obtained from a single stack of length T_{stack} is given by eq. (7.130) replacing T by T_{stack} . Adding \mathcal{N} of these spectra the variance is reduced by $1/\sqrt{\mathcal{N}}$ and therefore, for an incoherent search, eq. (7.130) becomes

$$\left(\frac{S}{N}\right)^2 = \langle F_+^2 \rangle \left(\frac{\mathcal{N}^{1/2} T_{\text{stack}}}{S_n(f_0)} \right) h_0^2$$

⁵³See Brady, Creighton, Cutler and Schutz (1998).

$$= \frac{1}{\sqrt{\mathcal{N}}} \langle F_+^2 \rangle \left(\frac{T}{S_n(f_0)} \right) h_0^2 \quad (7.163)$$

and the minimum amplitude detectable at a given S/N , eq. (7.134), becomes

$$(h_0)_{\min} = \eta \left(\frac{S_n(f_0)}{T} \right)^{1/2}. \quad (7.164)$$

where we have defined an efficiency factor

$$\eta = (S/N) \frac{\mathcal{N}^{1/4}}{\langle F_+^2 \rangle^{1/2}}, \quad (7.165)$$

which takes into account the desired level of the signal-to-noise ratio S/N , the average over the orbit of the source, which produces the factor $\langle F_+^2 \rangle^{1/2}$, and the need to separate the data into \mathcal{N} stack for computational feasibility.

In practice, beside being forced by computational requirements, incoherent searches are also necessary because a detector never has months, and not even weeks, of continuous good data taking. There are always interruption due to maintenance, period of higher noise level that must be removed, etc. and the experimental precision that one has on the time at which data taking resumed is not sufficiently good to recombine coherently different stacks of data. The incoherent method, of course, can be applied even when the single stacks have not all the same duration, and when they are not consecutive.

When performing an incoherent search each stack is demodulated, as discussed in the previous section, using a mesh of points sufficient to confine the searched signal into a single bin. The individual power spectra, before being summed, must be corrected for their relative frequency drift using a finer parameter mesh suitable for removing the phase modulation over the whole observation period. The simplest implementation of this method consists in choosing stacks of about 30 min, so that the Doppler effect in each stack can simply be neglected, and within a single stack no demodulation is needed. In this case a period of 10^7 sec of data is divided into $\mathcal{N} \simeq 5000$ stacks, and the minimum detectable value $(h_0)_{\min}$ in eq. (7.164) is larger than in a coherent search by a factor $\mathcal{N}^{1/4} \sim 8$. With the difference, of course, that a blind full-sky incoherent search of this type is computationally feasible while a blind full-sky coherent search is not.

Alternatively, one can choose longer stacks, say of the order of one day. These will need demodulation, but a relatively coarse mesh in parameter space will suffice to concentrate the whole signal into a single bin. Then we combine the separate stacks using a finer mesh. Of course, the longer the stack, the higher is the sensitivity, but the higher is also the computational cost. Incoherent searches can also be used as a first stage in a hierarchical search: an incoherent blind all-sky search can

produce a number of interesting candidate signals, for certain values of the parameters. These points in parameter space can then be examined more thoroughly with a directed coherent search.

We can now compare the experimental sensitivity given by eq. (7.164) with the signal expected from a rotating NS, given in eq. (4.224). We then find that the maximum distance r which a detector can reach in a blind full-sky search for periodic GWs from rotating neutron stars is

$$r = 5.8 \text{ kpc} \left(\frac{10^{-23} \text{ Hz}^{-1/2}}{S_n^{1/2}(f_0)} \right) \left(\frac{T}{3 \times 10^7 \text{ s}} \right)^{1/2} \times \left(\frac{100}{\eta} \right) \left(\frac{\epsilon}{10^{-6}} \right) \left(\frac{I_{zz}}{10^{38} \text{ kg m}^2} \right) \left(\frac{f_0}{1 \text{ kHz}} \right)^2. \quad (7.166)$$

The reference value $\eta = 100$ corresponds to a search for a total time $T = 3 \times 10^7 \text{ s}$ divided into stacks with $T_{\text{stack}} \simeq 30 \text{ min}$ (so $\mathcal{N} \simeq 1.7 \times 10^4$), a factor $1/\langle F_+^2 \rangle^{1/2} = \sqrt{5}$ as appropriate for interferometers, see Table 7.1, and a value $S/N \simeq 4$. The strain sensitivity $S_n^{1/2}$ has been normalized to the value expected for an advanced interferometer.

The Hough transform

As we have seen above, in incoherent searches the observation time is divided into stacks, where the phase modulation due to Doppler effect and spindown is either negligible (if $T_{\text{stacks}} \lesssim 30 \text{ min}$) or anyway relatively easy to correct for, so that a GW signal, if present, falls into a single frequency bin. When we compare different stacks, the position in frequency of the bin that contains the signal changes, because of the Doppler effect and of the spindown. For each point in the parameter space $(\theta_s, \phi_s, \dot{f}_0/f_0, \ddot{f}_0/f_0, \dots)$ we can compute how the position of the bin should change and we can correct for it, using the resampling technique discussed in the previous section. In this way, for each point of parameter spaces, the bins are “realigned”, and the power in corresponding bins is summed.

An interesting variation on this scheme is given by the Hough transform, which is a technique used for pattern recognition in digital images.⁵⁴ In the Hough transform, as a first step, rather than summing up the power in the corresponding bins, we fix a threshold in each data stack. A bin is deemed “black” if the power in it exceeds the threshold, and “white” if it does not. In the time–frequency plane obtained aligning in frequency (with no correction) the various stacks, we therefore have a set of black pixels, as in Fig. 7.12.

In the case of Gaussian noise, where large fluctuations are unlikely, it would in principle be more convenient to sum up the power of the corresponding bins, rather than reducing all the information to a set of zeros (white) and ones (black). However, the Hough transform is more robust in the presence of non-Gaussian noise and large occasional external dis-

⁵⁴It was developed in 1959 by Paul Hough at CERN, to analyze the tracks of particles in bubble chambers, and today is also used in astronomical data analysis.

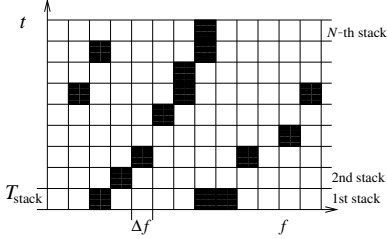


Fig. 7.12 The time–frequency plane, with bins of length $\Delta t = T_{\text{stack}}$ in time and $\Delta f = 1/T_{\text{stack}}$ in frequency. Bins where the power exceeds a given threshold are marked in black.

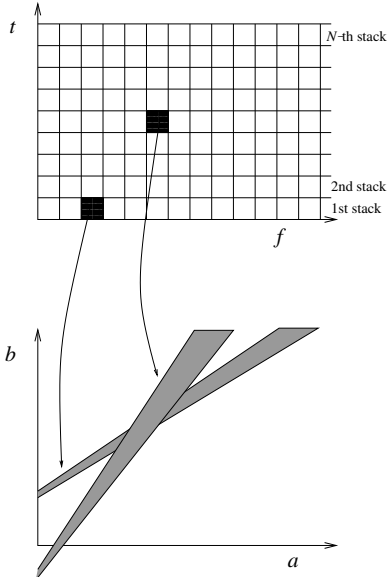


Fig. 7.13 The map that to each black pixel associates a submanifold in the parameter space Σ .

turbances, which is the case in a real detector. Consider for instance the situation in which instrumental noise gives a very large spike in frequency, during a relatively short period, e.g. in only one stack. When summing the power, this single disturbance can give a large effect on the total sum, while collapsing all the information to black/white it contributes only to a single pixel. This method can therefore be appropriate when we search for a signal that is small, but is there during the whole observation time, and is embedded in a noise that occasionally can be much larger than the signal.

The next step is to perform a pattern recognition procedure in the set of black pixels, to see if some of the black pixels lie along a specified curve. To simplify the setting, suppose that we are searching for straight lines in the (t, f) plane of Fig. 7.12. (The generalization to more complex curves is conceptually straightforward.) The set of all straight lines in this plane is parametrized by two parameters (a, b) , as $t = af + b$. We denote by Σ the manifold described by the parameters (a, b) ; in our example of straight lines of course $\Sigma = \mathbb{R}^2$, but the notation is more general. Given a black pixel, we can find the set of points in the manifold Σ that are compatible with it; for instance, in our straight lines example, if a black pixel is centered at (t_1, f_1) , the straight lines consistent with it are those that satisfy $t_1 = af_1 + b$, and the corresponding submanifold of Σ is the curve $b = af_1 - t_1$ in the (a, b) plane. More precisely, since the pixels in the (t, f) plane have a finite resolution, we will rather get a bunch of straight lines in Σ . The transformation that, to each black pixel in the (t, f) plane associates a submanifold in Σ , is illustrated graphically in Fig. 7.13.

In the absence of noise, the submanifolds in Σ obtained in this way from all the black pixels would have a non-empty intersection, which would define the point in parameter space compatible with the observations. Of course, in the presence of noise the intersection of all the curves will be empty. Still, we can try to recover the most probable value of the parameters in Σ as follows. First, we discretize the manifold Σ . Let us call \mathcal{C}_1 the surface in Σ obtained from the first black pixel. We then assign +1 to all the bins in Σ that belong to \mathcal{C}_1 . We repeat the same for the second black pixel, adding +1 to the bins in Σ that belong to \mathcal{C}_2 , and so on for all the N black pixels. In conclusion, we have constructed a map that, to the set of black pixels, associates a histogram in the parameter space Σ .

In the GW detection problem, the manifold Σ becomes the parameter space $(\theta_s, \phi_s, \dot{f}_0/f_0, \ddot{f}_0/f_0, \dots)$ and the straight lines of our example are replaced by the curves in the (t, f) plane that describe how f changes with time because of the Doppler effect and of the spindown. The points in parameter space whose number count is above a certain threshold are the candidates for a possible detection and can be further investigated, for instance with a coherent search.

7.7 Coalescence of compact binaries

The coalescence of compact binaries, such as BH-BH and NS-NS binaries, is a particularly interesting signal for broad-band GW detectors. This comes from a combination of two facts: first, we saw in eq. (4.44) that, in the last stages of the inspiral, a binary system can radiate away in GWs up to a few per cent of its total mass. This is a huge amount of energy, so the signal from an inspiral is quite strong, compared to most other GW sources. Second, the inspiral phase can be tracked for many cycles in a broad-band detector. We saw in eq. (4.23) that a ground-based interferometer can follow the inspiral phase of a compact binary system for $O(10^4)$ cycles. Thus, matched filtering can be very effective for extracting this signal from the noise. From eq. (7.40) and the discussion below it we see that, in order of magnitude, with matched filtering we can dig into the noise and catch the signal from a coalescence, even when the typical amplitude of the GW signal inside the interferometer bandwidth is smaller than the noise floor by a factor $\mathcal{N}_c^{1/2}$, where \mathcal{N}_c is the number of cycles for which we are able to track carefully the signal with our template. Thus, we can gain a factor as large as $\mathcal{N}_c^{1/2} \sim 100$ in amplitude, if our template is so good that we can follow closely the signal from the time it enters in the interferometer bandwidth until the inspiral phase terminates and the two objects merge. Since the GW amplitude is proportional to $1/r$, a factor $O(100)$ in amplitude means that we gain a factor $O(100)$ in the maximum distance to which we can detect a source. For these reasons, we will see that interferometers have the potential of detecting coalescing binaries up to distances of order of hundreds of Mpc, and advanced ground-based interferometers could reach a few Gpc.

To exploit this opportunity we must however be able to follow closely the signal with a template. This means, first of all, that for a given value of the parameters of the binary system (time of coalescence, masses, spins, etc.), one must know the waveform accurately. We already quantified this requirement in Section 5.6, where we found that we need to compute the post-Newtonian corrections up to 3.5PN order. As we saw in Section 5.6, these remarkable computations have indeed been performed. The second aspect is that we do not know in advance the parameters of the system, and therefore we must scan a potentially large parameter space.

To leading Newtonian order we computed the waveform in eq. (4.29), and the corrections in the restricted post-Newtonian approximation were discussed in Section 5.6. Combining these results with the general expression $h(t) = F_+ h_+(t) + F_\times h_\times$, we see that the output $h(t)$ for a binary inspiral, in the restricted post-Newtonian approximation, is

$$\begin{aligned} h(t) &= A_+ \left[\frac{\pi f_{\text{gw}}(t)}{c} \right]^{2/3} \cos[\Phi(f_{\text{gw}}(t)) + \Phi_0] \\ &\quad + A_\times \left[\frac{\pi f_{\text{gw}}(t)}{c} \right]^{2/3} \sin[\Phi(f_{\text{gw}}(t)) + \Phi_0], \end{aligned} \quad (7.167)$$

⁵⁵Explicit expressions for $\Phi(f_{\text{gw}})$ and $f_{\text{gw}}(t)$ up to 2PN were given in eq. (5.273), and in eq. (5.270) or (5.272).

where, as discussed in Section 5.6.3, $\Phi(f_{\text{gw}})$ and $f_{\text{gw}}(t)$ are known up to 3.5PN order.⁵⁵ We have explicitly displayed the arbitrary constant Φ_0 in the phase, equivalent to the arbitrary constant ω_0 in eq. (5.265), and we have defined

$$A_+ = \frac{4}{r} \left(\frac{GM_c}{c^2} \right)^{5/3} F_+(\theta, \phi) \frac{1 + \cos^2 \iota}{2} \quad (7.168)$$

$$A_\times = \frac{4}{r} \left(\frac{GM_c}{c^2} \right)^{5/3} F_\times(\theta, \phi) \cos \iota. \quad (7.169)$$

Writing $A_+ = A \cos \alpha$ and $A_\times = A \sin \alpha$, with $A = (A_+^2 + A_\times^2)^{1/2}$ and $\tan \alpha = A_\times/A_+$, we can rewrite this as

$$h(t) = A \left[\frac{\pi f_{\text{gw}}(t)}{c} \right]^{2/3} \cos[\Phi(f_{\text{gw}}(t)) + \varphi], \quad (7.170)$$

⁵⁶Recall also from Section 4.1.4 that, for binaries at cosmological distances, i.e. at a non-negligible redshift z , the masses m_1 and m_2 must be multiplied by $(1+z)$, and the distance r must be replaced by the luminosity distance $d_L(z)$.

with $\varphi = \Phi_0 - \alpha$.⁵⁶ Thus, in the waveform enter the distance r to the source, its location, specified by the angles (θ, ϕ) which appear in the pattern functions, the orientation of the orbit with respect to the line of sight (two angle, one of which is ι , and the other identifies the axes with respect to which the plus and cross polarizations are defined), the reference time t_* at which the signal enters in the detector bandwidth (which appears through $\Phi(t)$ and $f_{\text{gw}}(t)$), the constant phase φ , the masses of the two stars, and in principle also their spins (which we neglected in eq. (5.273)). So, in total, we have 15 parameters.⁵⁷ However, a number of simplifications are possible, as we discuss in the next subsection.

7.7.1 Elimination of extrinsic variables

The variables that can be eliminated from the parameter space are generically called extrinsic. First, we observe that all possible shifts in time of the signal can be obtained at once with a single Fourier transform. Consider in fact the scalar product $(h(\theta, t_*)|s)$ between the output $s(t)$ of the detector and the template $h(t; \theta, t_*)$ where, from the parameters θ^i , we singled out explicitly the arrival time t_* , defined as the time when the hypothetical signal enters into the interferometer bandwidth, say at $f_{\text{gw}} = 10$ Hz. The waveform $h(t; \theta, t_*)$ is obtained from $h(t; \theta, t_* = 0)$ with a time translation, so if we denote by $\tilde{h}(f; \theta)$ the Fourier transform of $h(t; \theta, t_*)$ at $t_* = 0$, the Fourier transform of $h(t; \theta, t_*)$ at t_* generic is simply $\tilde{h}(f; \theta) e^{i 2\pi f t_*}$. Thus, from the definition (7.46) of the scalar product, we have

$$(h(\theta, t_*)|s) = 4 \operatorname{Re} \int_0^\infty df \frac{\tilde{h}^*(f; \theta) \tilde{s}(f)}{S_n(f)} e^{i 2\pi f t_*}, \quad (7.171)$$

which is just the Fourier transform of $\tilde{h}^*(f; \theta) \tilde{s}(f)/S_n(f)$. Thus, performing a single FFT we can immediately locate the value of t_* which gives the highest signal-to-noise ratio. This is of course of great practical importance. Typically we can expect that, to perform efficiently the

matched filtering, the maximum mismatch in arrival time that we can tolerate between the real signal and our template could be, say, of order 3 ms. If one should analyze one year of data (3×10^7 s) computing a different scalar product every 3 ms, for each value of θ one should perform 10^{10} times the computation of the scalar product $h(t; \theta, t_*)$, while we see that just a single FFT does the job.⁵⁸ Thus, the arrival time t_* is not really part of the parameter space that must be searched. Figure 7.14 shows the result of a simulation in which the signal corresponding to the coalescence of two BHs, each with a mass of $10M_\odot$, at a distance of 150 Mpc, is injected into the noise of the VIRGO detector. Performing the Fourier transform, we see that we have a spike in correspondence with the time at which this signal has been injected (in the figure, $t_* = 1$, in arbitrary units).

Two more parameters that appear in eq. (7.167), which can be eliminated analytically from the matched filtering procedure, are the amplitude A and the phase φ of the signal. We already saw in Section 7.3 that the optimal filter is defined modulo an arbitrary constant, so the overall value of the amplitude A does not enter when we search for the template that maximizes the signal-to-noise ratio. The maximization of the SNR with respect to φ can be performed analytically, writing the template (7.170) in the form

$$h(t) = h_c(t) \cos \varphi + h_s(t) \sin \varphi. \quad (7.172)$$

If $s(t)$ is the detector output, after maximization of the log-likelihood function over the amplitude A , according to eq. (7.70) we want to further maximize

$$\begin{aligned} 2 \log \Lambda &= \frac{(h|s)^2}{(h|h)} \\ &= \frac{[(h_c|s) + (h_s|s) \tan \varphi]^2}{(h_c|h_c) + (h_s|h_s) \tan^2 \varphi + 2(h_c|h_s) \tan \varphi}. \end{aligned} \quad (7.173)$$

This expression is easily maximized analytically with respect to $\tan \varphi$. The result is simpler if we introduce two new templates

$$h_p = h_c \cos \phi_p + h_s \sin \phi_p, \quad (7.174)$$

$$h_q = h_c \cos \phi_q + h_s \sin \phi_q, \quad (7.175)$$

where the angles ϕ_p and ϕ_q are chosen so that h_p and h_q satisfy $(h_p|h_q) = 0$, i.e. they are orthogonal with respect to the scalar product $(\cdot | \cdot)$. In terms of these orthogonal templates the likelihood function, after performing the maximization over the amplitude A and over the phase φ , takes the simple form

$$2 \log \Lambda = \frac{(h_p|s)^2}{(h_p|h_p)} + \frac{(h_q|s)^2}{(h_q|h_q)}. \quad (7.176)$$

Therefore, the maximization with respect to the remaining variables is equivalent to maximizing the sum in quadrature of the outputs of two matched filters. In the absence of signal, the signal-to-noise ratio ρ

⁵⁸More precisely, if we have a time series with N samples, computing the integral which defines the scalar product has a computational cost $O(N)$, and if one had to repeat it for all possible arrival times, the overall cost would be $O(N^2)$. With a single FFT, instead, the computational cost is $O(N \log N)$.

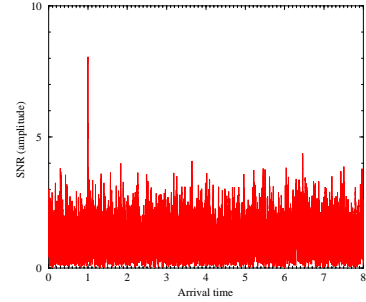


Fig. 7.14 The result of a simulation in which the signal due to a BH-BH coalescence, each with a mass of $10M_\odot$, at a distance of 150 Mpc, is injected into the noise of the VIRGO detector. The arrival time is located from the position of the spike in the Fourier transform (7.171), which here is at $t_* = 1$. (Courtesy of A. Viceré.)

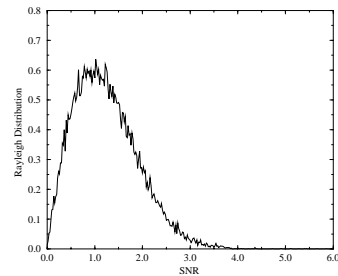


Fig. 7.15 The distribution of the signal-to-noise ratio, in the simulation of Fig. 7.14. (Courtesy of A. Viceré.)

⁵⁹It should also be observed that, for coalescing binaries, non-Gaussian noise should be much less important than for short bursts, since it should be much easier to have an impulsive disturbance that simulates a short burst, rather than a noise that lasts for about 15 minutes, simulating for all this time the behavior of a chirping signal.

is therefore a random variable which follows the Rayleigh distribution (7.87), while in the presence of signal it is a non-central χ^2 distribution with two degrees of freedom. Indeed, we see in Fig. 7.15 that, in the simulation of Fig. 7.14, ρ follows a Rayleigh distribution (except, of course, for the presence of the single spike with $S/N = 8$ at $t_* = 1$).⁵⁹

7.7.2 The sight distance to coalescing binaries

The Fourier transform of the chirp amplitude, to Newtonian order, has been computed in Problem 4.1, while the result in the restricted PN approximation, up to 2PN order, is given in eqs. (5.274) and (5.275). Then we find, for the Fourier transform of $h(t) = h_+ F_+ + h_\times F_\times$,

$$\tilde{h}(f) = \left(\frac{5}{6}\right)^{1/2} \frac{1}{2\pi^{2/3}} \frac{c}{r} \left(\frac{GM_c}{c^3}\right)^{5/6} f^{-7/6} e^{i\Psi} Q(\theta, \phi; \iota), \quad (7.177)$$

where

$$Q(\theta, \phi; \iota) = F_+(\theta, \phi) \frac{1 + \cos^2 \iota}{2} + iF_\times(\theta, \phi) \cos \iota. \quad (7.178)$$

The phase Ψ is just the quantity denoted Ψ_+ in eq. (5.275), and the relative factor i between the two terms in Q is due to the fact that $\Psi_\times = \Psi_+ + (\pi/2)$.⁶⁰ Plugging this expression into eq. (7.51), we can write the signal-to-noise ratio for a coalescing binary as

$$\left(\frac{S}{N}\right)^2 = \frac{5}{6} \frac{1}{\pi^{4/3}} \frac{c^2}{r^2} \left(\frac{GM_c}{c^3}\right)^{5/3} |Q(\theta, \phi; \iota)|^2 \int_0^{f_{\max}} df \frac{f^{-7/3}}{S_n(f)}, \quad (7.179)$$

where f_{\max} is the value of the GW frequency when the inspiral phase terminates and the two stars merge. An estimate of f_{\max} is $f_{\max} = 2(f_s)_{\text{ISCO}}$, where $(f_s)_{\text{ISCO}}$ given in eq. (4.39), and the factor of 2 is valid as long as the emission is dominated by quadrupole radiation. For a wave coming from optimal direction (e.g. $F_+ = 1$ and $F_\times = 0$), and with optimal value of the inclination of the orbit ($\cos \iota = 1$), the function $Q(\theta, \phi; \iota) = 1$. However, a more appropriate reference value for $|Q(\theta, \phi; \iota)|^2$ is given by its average over all possible directions and inclinations. Using $\langle F_+^2 \rangle = \langle F_\times^2 \rangle = 1/5$ for interferometers (see Table 7.1), we get $\langle |Q(\theta, \phi; \iota)|^2 \rangle = (1/5)g(\iota)$, where $g(\iota)$ was defined in eq. (3.338) and its average over the inclination ι is $4/5$, see eq. (4.10). Therefore

$$\langle |Q(\theta, \phi; \iota)|^2 \rangle^{1/2} = \frac{2}{5}, \quad (7.180)$$

where here $\langle \dots \rangle$ denotes the average over the angles and over the inclination. Then we rewrite eq. (7.179) as

$$\begin{aligned} \frac{S}{N} &= \frac{2}{5} \left(\frac{5}{6}\right)^{1/2} \frac{1}{\pi^{2/3}} \frac{c}{r} \left(\frac{GM_c}{c^3}\right)^{5/6} \frac{\langle |Q(\theta, \phi; \iota)|^2 \rangle^{1/2}}{(2/5)} \\ &\times \left[\int_0^{f_{\max}} df \frac{f^{-7/3}}{S_n(f)} \right]^{1/2}. \end{aligned} \quad (7.181)$$

This relation can be inverted to give the sight distance d_{sight} , i.e. the maximum distance r at which we can see a binary coalescence, once we have chosen a given threshold for S/N ,⁶¹ assuming an average direction and inclination,

$$d_{\text{sight}} = \frac{2}{5} \left(\frac{5}{6} \right)^{1/2} \frac{c}{\pi^{2/3}} \left(\frac{GM_c}{c^3} \right)^{5/6} \left[\int_0^{f_{\max}} df \frac{f^{-7/3}}{S_n(f)} \right]^{1/2} (S/N)^{-1}. \quad (7.182)$$

We will see in Chapter 9 the numerical values that can be obtained for d_{sight} at existing and advanced interferometers.

It is instructive to verify from these expressions that, in order of magnitude, for a coalescing binary the matched filtering procedure gives a gain $\sim \mathcal{N}_c^{1/2}$. To this end, we assume that S_n has a constant value S_0 between a minimum frequency f_0 and f_{\max} , while it is essentially infinite for $f < f_0$. Then, neglecting all numerical factors (and using for simplicity units $c = 1$, and the notation $M = GM_c/c^3$), we can perform the integral in eq. (7.181), and we get

$$\frac{S}{N} \sim \frac{1}{r} M^{5/6} S_0^{-1/2} f_0^{-4/3}. \quad (7.183)$$

From eqs. (7.167) and (7.168) we see that the GW amplitude is of order

$$h_0 \sim \frac{1}{r} f_0^{2/3} M^{5/3}, \quad (7.184)$$

while, from eq. (4.23), the number of cycles spent in the interferometer bandwidth is

$$\mathcal{N}_c \sim M^{-5/3} f_0^{-5/3}. \quad (7.185)$$

Using eq. (7.184) to eliminate r from eq. (7.183), and eq. (7.185) to eliminate M , we get

$$\frac{S}{N} \sim \frac{h_0}{(f_0 S_0)^{1/2}} \mathcal{N}_c^{1/2}, \quad (7.186)$$

which shows indeed that, in order of magnitude, the signal-to-noise ratio (in amplitude) is larger by a factor $\mathcal{N}_c^{1/2}$ than for a burst with a characteristic frequency f_0 (compare with eq. (7.107) with $\tau_g = 1/f_0$ and $f_{\max} = f_0$). Of course, a more precise estimate requires the real form of $S_n(f)$, as well as the exact computation of the integral in eq. (7.181). This shows explicitly how the matched filtering procedure allows us to dig deeply into the noise floor, as we discussed already on page 344. Consider in fact the situation in which, after tracking the signal by $\mathcal{N}_c \gg 1$ cycles, we finally get S/N of order one, so we begin to see the signal. According to eq. (7.186), this means that $h_0/(f_0 S_0)^{1/2}$ was of order $1/\mathcal{N}_c^{1/2}$. However, $h_0/(f_0 S_0)^{1/2}$ is the “instantaneous” value of the signal-to-noise ratio, i.e. the value of S/N over a single cycle.

⁶¹Recall however from page 359 that the signal can combine with the noise either in a constructive or in a destructive way, so the output ρ of the interferometer is a random variable whose average is S/N and which follows, in the presence of signal, a non-central χ^2 distribution with two degrees of freedom. Therefore, at any distance r , there is a probability of missed detection, and the fact that a source is at $r < d_{\text{sight}}$ does not mean that it will be certainly detected. Conversely, there is also a non-zero probability that the signal from a source at $r > d_{\text{sight}}$ combines with the noise so that its S/N raises above the threshold.

Therefore, the integrated signal-to-noise ratio provided by the matched filtering procedure can be of order one or larger, even when the *instantaneous* signal is deeply buried into the noise.

Finally, an important issue is the precision that can be obtained in the reconstruction of the source parameters. In particular the chirp mass M_c , that appears in the phase of the waveform, can be estimated very precisely, since the phase can be followed accurately for \mathcal{N}_c cycles. Thus, any mismatch ΔM_c between the true value of the source and the value used in our template will be amplified by a factor \mathcal{N}_c , and we could expect that

$$\frac{\Delta M_c}{M_c} \sim \frac{1}{\mathcal{N}_c}. \quad (7.187)$$

Given that at a ground-based interferometer \mathcal{N}_c can be of order $10^3 - 10^4$, see eq. (4.23), this would give a rather remarkable accuracy $\Delta M_c/M_c \sim 10^{-4} - 10^{-3}$. As for the reduced mass μ , it appears in the 1PN corrections to the phase, which are smaller by a factor $O(v^2/c^2)$ than the leading term, so it can be measured less precisely.⁶²

⁶²The precise computation of the errors on the parameters can be done using the explicit expression of the waveform to evaluate the Fisher information matrix defined in eq. (7.74), and then we can compute the errors on the parameters as in eq. (7.75). Using the waveform with the post-Newtonian corrections to the phase and assuming a detection with $S/N = 10$ one finds that, if one knew that the spins of the star are negligible, then M_c could indeed be measured with a precision of 0.01–0.1%, while the reduced mass μ , which enters in the post-Newtonian corrections, could be measured to 1%. However, one in general has no a priori information on the spins, and the measurements of masses and spins happen to be strongly correlated. This degrades the accuracy on the mass reconstruction, so one finally obtains $\Delta M_c/M_c \sim 0.1 - 1\%$ (which, however, is still a quite remarkable accuracy) and $\Delta\mu/\mu \sim 10 - 15\%$ for NS-NS and NS-BH binaries, or $\Delta\mu/\mu \sim 50\%$ for BH-BH binaries with typical BH masses of order $10M_\odot$. Observe that, the larger the mass of the stars, the smaller is the number of cycles in the detector bandwidth, since the coalescence takes place earlier, see eq. (4.39), so the precision in the reconstruction of the parameters is less good. See Cutler and Flanagan (1994) for details.

7.8 Stochastic backgrounds

In 1965 Penzias and Wilson discovered that the Universe is permeated by the Cosmic Microwave Background (CMB) electromagnetic radiation. This radiation is a relic of the early Universe, and the microwave photons that compose it decoupled from the primordial plasma about 3×10^5 years after the Big Bang, and since then they have been propagating essentially freely. This discovery, providing direct evidence for the Big Bang, was one of the most significant in the history of cosmology.

Since then, the CMB has been subject to deep investigations. We now know that its spectrum is a perfect black-body (in fact, the most perfect black-body spectrum existing in nature). This background is, to a first approximation, isotropic. The observation by the COBE satellite of temperature fluctuations over the sky, at the level $\Delta T/T \sim 10^{-5}$, has been one of the most important discoveries in cosmology in the last decades, and the detailed investigation of the multipole moments of these anisotropies by COBE and various other experiments, and particularly by WMAP, has opened up the field of precision cosmology.

There are good reasons to expect that the Universe is permeated also by a stochastic background of GWs generated in the early Universe. Furthermore, a stochastic background of GWs can also emerge from the incoherent superposition of a large number of astrophysical sources, too weak to be detected separately, and such that the number of sources that contribute to each frequency bin is much larger than one.

The mechanisms that can lead to the production of stochastic GW backgrounds in cosmology and in astrophysics will be examined in detail in Vol. 2. Here we discuss how to characterize such a background in general, and what are the optimal strategies for its detection.

7.8.1 Characterization of stochastic backgrounds

Using the plane wave expansion (1.58), we can write

$$h_{ij}(t, \mathbf{x}) = \sum_{A=+, \times} \int_{-\infty}^{\infty} df \int d^2 \hat{\mathbf{n}} \tilde{h}_A(f, \hat{\mathbf{n}}) e_{ij}^A(\hat{\mathbf{n}}) e^{-2\pi i f(t - \hat{\mathbf{n}} \cdot \mathbf{x}/c)}. \quad (7.188)$$

We work in the TT gauge, so $h_i^i = 0$ and $\partial^j h_{ij} = 0$. The tensors $e_{ij}^A(\hat{\mathbf{n}})$ are given in eq. (1.54). A stochastic background is a superposition of waves with all possible propagation directions $\hat{\mathbf{n}}$, therefore the indices i, j above take the values 1, 2, 3, contrary to the case of the GWs emitted from a single far source, where we could label the GW in the TT gauge as h_{ab} with a, b , taking the values 1, 2 and labeling the two directions in the transverse plane. A stochastic background is defined by the fact that the amplitudes $\tilde{h}_A(f, \hat{\mathbf{n}})$ are random variables, characterized statistically by their ensemble averages.⁶³

We will make the following assumptions on stochastic backgrounds of GWs.

- The background is stationary. This means that all correlators depend only on time differences, and not on the absolute values of time. So, for instance, the two-point correlator $\langle h_A(t)h_{A'}(t') \rangle$ can depend only on $t - t'$, and not separately on t and t' . In Fourier space, this means that $\langle \tilde{h}_A^*(f)\tilde{h}_{A'}(f') \rangle$ must be proportional to $\delta(f - f')$. This assumption is certainly justified. For a background created in cosmological epochs, the typical time-scale on which it can change substantially is of the order of the age of the Universe (for instance, its spectrum changes because it is redshifted). During the duration of the experiment, which is at most a few years, it is very difficult to imagine that the properties of the background could change appreciably.⁶⁴
- The background is Gaussian. This means that all N -point correlators are reduced to sum and products of the two-point correlator $\langle h_A(t)h_{A'}(t') \rangle$ (and of the vacuum expectation value $\langle h_A \rangle$ that however, as we have seen, can be set to zero). Gaussianity is rooted in the central limit theorem, that states that the sum of a large number of independent events produces a Gaussian stochastic process, whatever the probability distribution of the individual events. This assumption is therefore expected to hold to a very good accuracy for cosmological backgrounds. It would not hold for astrophysical backgrounds, if the number of sources that contribute is not that large, and we are on the verge of distinguishing the individual contributions. In this case, further information can be extracted from the higher-point correlators.
- The stochastic background is isotropic. Experience with CMB indicates that the early Universe was highly isotropic and, for the photons, temperature fluctuations across the sky are at the level $\Delta T/T \sim 10^{-5}$. It is reasonable to expect that a stochastic background of GWs of cosmological will also be in a first approximation

⁶³An ensemble average is the average over many copies of the system. Our system is in this case the Universe and we do not have many copies of it! Of course, the ergodic assumptions must be used here, and the ensemble average is replaced by a temporal average, compare with Note 3 on page 337.

⁶⁴Stationarity also implies that $\langle h_A(t) \rangle$ is a constant so, even if it were non-zero, it would just contribute to the vacuum energy density. As far as we are interested in GWs, that is in the time-dependent part, we can therefore set $\langle h_A \rangle = 0$.

isotropic. Of course, after a first detection of a GW background, it will be extremely interesting to investigate its anisotropies and therefore to give up this assumption. In particular, in a cosmological background we must expect a dipole term, dominated by the Earth motion in the rest frame of the CMB, while higher multipoles could give extremely interesting information on the early Universe.

We might have to give up completely the assumption of isotropy when we study stochastic backgrounds of astrophysical origin. In particular a background of galactic origin will not be isotropic, but rather it will be more intense when we look in the direction of the galactic plane, just as the electromagnetic background due to galactic sources gives its characteristic appearance to the Milky Way. We will in fact discuss in Vol. 2 an example of this type, the background created by galactic white dwarf binaries.

Waves coming from different directions should be uncorrelated, so $\langle \tilde{h}_A^*(f, \hat{\mathbf{n}}) \tilde{h}_{A'}(f', \hat{\mathbf{n}}') \rangle$ should be proportional to a Dirac delta over the two-sphere, defined as

$$\delta^2(\hat{\mathbf{n}}, \hat{\mathbf{n}}') = \delta(\phi - \phi')\delta(\cos \theta - \cos \theta'), \quad (7.189)$$

where (θ, ϕ) are the polar angles that define $\hat{\mathbf{n}}$. Isotropy implies that the proportionality constant must be independent of $\hat{\mathbf{n}}$.

- Finally, we assume that the background is unpolarized, as it is natural both in a cosmological context and if it is the result of the superposition of many different astrophysical sources. This means that $\langle \tilde{h}_A^*(f, \hat{\mathbf{n}}) \tilde{h}_{A'}(f', \hat{\mathbf{n}}') \rangle$ must be proportional to $\delta_{AA'}$ and the proportionality coefficient must be independent of the polarization index A .

Under these assumptions, a stochastic background of GWs is uniquely characterized by a single function $S_h(f)$, defined by

$$\langle \tilde{h}_A^*(f, \hat{\mathbf{n}}) \tilde{h}_{A'}(f', \hat{\mathbf{n}}') \rangle = \delta(f - f') \frac{\delta^2(\hat{\mathbf{n}}, \hat{\mathbf{n}}')}{4\pi} \delta_{AA'} \frac{1}{2} S_h(f). \quad (7.190)$$

The function $S_h(f)$ is called the spectral density of the stochastic background, in analogy with the spectral density of the noise defined in Section 7.1. Just as for the noise spectral density, we use the convention that $S_h(f)$ is single-sided. It has dimensions Hz^{-1} and satisfies $S_h(f) = S_h(-f)$. The factor $1/(4\pi)$ in eq. (7.190) is a choice of normalization such that

$$\int d^2\hat{\mathbf{n}} d^2\hat{\mathbf{n}}' \langle \tilde{h}_A^*(f, \hat{\mathbf{n}}) \tilde{h}_{A'}(f', \hat{\mathbf{n}}') \rangle = \delta(f - f') \delta_{AA'} \frac{1}{2} S_h(f). \quad (7.191)$$

where, as usual, $d^2\hat{\mathbf{n}} = d\cos \theta d\phi$. We see that the factor $1/2$ in the definition of $S_h(f)$ has been inserted so that $S_h(f)$ is normalized in the same way as the single-sided spectral density of the noise, see eq. (7.6).

Using eqs. (7.188) and (7.190), as well as $\sum_A e_{ij}^A e_{ij}^A = 4$, which follows from the normalization (1.55) of the polarization tensor e_{ij}^A , we get

$$\langle h_{ij}(t) h^{ij}(t) \rangle = 4 \int_0^\infty df S_h(f). \quad (7.192)$$

The sum over i, j is understood, and $h_{ij}(t) = h_{ij}(t, \mathbf{x} = 0)$. The spectral density of the signal, $S_h(f)$, is the quantity that allows us to perform a direct comparison with the noise in a detector, which is characterized by $S_n(f)$. However, to have a physical understanding it is much more convenient to think in terms of the energy density carried by the stochastic background. According to eq. (1.135), this is related to h_{ij} by

$$\rho_{\text{gw}} = \frac{c^2}{32\pi G} \langle \dot{h}_{ij} \dot{h}^{ij} \rangle. \quad (7.193)$$

In cosmology there is a very natural unit of energy density, that is, the energy density needed for closing the Universe. This critical energy density is

$$\rho_c = \frac{3c^2 H_0^2}{8\pi G}, \quad (7.194)$$

where H_0 is the present value of the Hubble expansion rate. As we mentioned on page 194, the value of H_0 is usually written as $H_0 = h_0 \times 100 \text{ km s}^{-1} \text{ Mpc}^{-1}$, where h_0 parametrizes the existing experimental uncertainty and is called the normalized Hubble expansion rate. The most recent determinations give $h_0 = 0.73(3)$. Numerically,

$$\rho_c \simeq 1.688 \times 10^{-8} h_0^2 \text{ erg cm}^{-3}. \quad (7.195)$$

Normalizing ρ_{gw} to ρ_c , the intensity of a stochastic background of gravitational waves can be characterized by the dimensionless quantity

$$\Omega_{\text{gw}} \equiv \frac{\rho_{\text{gw}}}{\rho_c}. \quad (7.196)$$

Using eqs. (7.192) and (7.193), the energy density can be written as an integral over $d \log f$ of some spectral density, that we denote by⁶⁵ $d\rho_{\text{gw}}/d \log f$,

$$\rho_{\text{gw}} \equiv \int_{f=0}^{f=\infty} d(\log f) \frac{d\rho_{\text{gw}}}{d \log f}. \quad (7.197)$$

We also define

$$\Omega_{\text{gw}}(f) \equiv \frac{1}{\rho_c} \frac{d\rho_{\text{gw}}}{d \log f},$$

(7.198)

so Ω_{gw} in eq. (7.196) is related to $\Omega_{\text{gw}}(f)$ by⁶⁶

$$\Omega_{\text{gw}} = \int_{f=0}^{f=\infty} d(\log f) \Omega_{\text{gw}}(f). \quad (7.199)$$

⁶⁵There is a slight abuse of notation here. Of course ρ_{gw} , on the left-hand side of eq. (7.197), is independent of the frequency, so its derivative with respect to f , or to $\log f$, vanishes. On the right-hand side, $d\rho_{\text{gw}}/d \log f$ is not the derivative of ρ_{gw} with respect to $\log f$, but just a notation for the spectral density of ρ_{gw} , which stresses that it is the energy density contained in a logarithmic interval of frequency.

⁶⁶Here again there is a slight ambiguity in the notation, because we use the same symbol Ω_{gw} for the normalized energy density, on the left-hand side of eq. (7.199), and for its spectral density, on the right-hand side. This notation is however standard in the GW literature, and we will conform to it.

The fact that we consider the energy per unit logarithmic interval of frequency, $d\rho_{\text{gw}}/d\log f$, rather than $d\rho_{\text{gw}}/df$, is useful because in this way $\Omega_{\text{gw}}(f)$ is dimensionless.

Even if the experimental error on the Hubble expansion rate is becoming smaller and smaller (just a few years ago values of h_0 between 0.4 and 1 were considered possible), still it is not very convenient to normalize ρ_{gw} to a quantity, ρ_c , which is uncertain: this uncertainty would appear in all the subsequent formulas, although it has nothing to do with the uncertainties on the GW background itself. Therefore, one rather characterizes the stochastic GW background with the quantity $h_0^2\Omega_{\text{gw}}(f)$, which is independent of h_0 .⁶⁷

We now compute the relation between $S_h(f)$ and $h_0^2\Omega_{\text{gw}}(f)$. As discussed in Section 1.4.3, the brackets in eq. (7.193) denote a time average. However (under the ergodic assumption, see Notes 3 and 63), this is just the ensemble average used above. We can then substitute the plane wave expansion (7.188) into eq. (7.193), and compute the ensemble average using eq. (7.190). The result is

$$\rho_{\text{gw}} = \frac{c^2}{8\pi G} \int_{f=0}^{f=\infty} d(\log f) f(2\pi f)^2 S_h(f). \quad (7.200)$$

Comparing with the definition (7.197) we get

$$\frac{d\rho_{\text{gw}}}{d\log f} = \frac{\pi c^2}{2G} f^3 S_h(f), \quad (7.201)$$

and

$$\Omega_{\text{gw}}(f) = \frac{4\pi^2}{3H_0^2} f^3 S_h(f). \quad (7.202)$$

Finally, it is interesting to express $h_0^2\Omega_{\text{gw}}(f)$ in terms of the number of gravitons per cell of the phase space, $n(\mathbf{x}, \mathbf{k})$. For an isotropic stochastic background $n(\mathbf{x}, \mathbf{k}) = n_f$ depends only on the frequency (which is related to the momentum \mathbf{k} by $|\mathbf{k}| = \hbar\omega/c = 2\pi\hbar f/c$), and not on the direction $\hat{\mathbf{k}}$. Then, writing $d^3k = |\mathbf{k}|^2 d|\mathbf{k}| d\Omega \rightarrow 4\pi(2\pi\hbar/c)^3 f^2 df$, and $df = f d\log f$, and considering that a graviton of frequency f carries an energy $\hbar\omega = \hbar(2\pi f)$, we have

$$\begin{aligned} \rho_{\text{gw}} &= 2 \int \frac{d^3k}{(2\pi\hbar)^3} \hbar(2\pi f) n_f \\ &= \frac{16\pi^2\hbar}{c^3} \int_0^\infty d(\log f) f^4 n_f, \end{aligned} \quad (7.203)$$

where the factor of 2 in front of the integral is due to the two helicity states of the graviton. Therefore

$$\frac{d\rho_{\text{gw}}}{d\log f} = \frac{16\pi^2\hbar}{c^3} n_f f^4, \quad (7.204)$$

and

$$h_0^2\Omega_{\text{gw}}(f) \simeq 3.6 \left(\frac{n_f}{10^{37}} \right) \left(\frac{f}{1\text{kHz}} \right)^4. \quad (7.205)$$

⁶⁷Unfortunately, we sometime use h_0 also to denote a GW amplitude. Since the reduced Hubble constant h_0 will only appear in the combination $h_0^2\Omega_{\text{gw}}$, no confusion is possible.

As we will see in Vol. 2, this equation is useful in particular when one computes the production of a stochastic background of GWs due to amplification of vacuum fluctuations, since this computation gives directly n_f .

7.8.2 SNR for single detectors

The comparison of eqs. (7.6) and (7.191) makes it clear that an isotropic stochastic background of GWs is seen in a detector as an additional source of noise. This poses an important conceptual problem in the identification of a stochastic GW background. In practice what will happen is that, after a careful modeling of the detector and of its noise sources, one would expect to have a certain value of the spectral density of the noise, $S_n(f)$. When the detector is turned on, one measures $\langle s^2(t) \rangle$, where as usual $s(t) = n(t) + h(t)$, with $n(t)$ the noise and $h(t)$ the response of the detector to a GW signal. If one observes that $\langle s^2(t) \rangle$ is larger than expected, the crucial problem is how to tell whether this is really due to a GW background or, more trivially, to some source of noise that has not been adequately accounted for when estimating $S_n(f)$. Similar problems were faced in the discovery of the cosmic microwave background; Penzias and Wilson found an excess noise in their antenna (a horn reflector that was meant for satellite communications) and worked hard for one year in order to exclude all possible sources of terrestrial and astrophysical noise, before writing a short paper with the modest title “A Measurement of Excess Antenna Temperature at 4080 Mc/s”, and concluding “*From a combination of the above, we compute the remaining unaccounted-for antenna temperature to be 3.5 ± 1.0 K at 4080 Mc/s*”.

To cope with this problem, it is clear that in the search for stochastic backgrounds of GWs with a single detector one must set at least a relatively high threshold on the signal-to-noise ratio; for instance, a signal-to-noise ratio $S/N = 5$ on the amplitude could be a typical choice (while lower values of S/N could be used for the only purpose of putting upper bounds). Further handles could come from an anisotropy of the stochastic GW background, if it is due to unresolved galactic sources, since this would produce a sidereal time modulation due to the motion of the detector. Another handle is the possibility that the dependence of the excess noise on the frequency is found to be in agreement with some theoretical prediction from a given cosmological or astrophysical mechanism.

To compute the minimum value of $h_0^2 \Omega_{\text{gw}}$ that can be measured at a given S/N , we observe that, if there is no signal, we have (see eq. (7.12))

$$\langle s^2(t) \rangle = \langle n^2(t) \rangle = \int_0^\infty df S_n(f), \quad (7.206)$$

while, if a stochastic GW background is present, there is also a contribution from $h(t)$. For each propagation direction $\hat{\mathbf{n}}$ we can write $h(t) = h_+ F_+ + h_\times F_\times$, and therefore, taking the ensemble average and

averaging also over $\hat{\mathbf{n}}$ and over the polarization angle ψ ,

$$\int \frac{d^2\hat{\mathbf{n}}}{4\pi} \frac{d\psi}{2\pi} \langle h^2 \rangle = \left(\int \frac{d^2\hat{\mathbf{n}}}{4\pi} \frac{d\psi}{2\pi} F_+^2 \right) \langle h_+^2 + h_\times^2 \rangle, \quad (7.207)$$

where we used the fact that the angular averages of F_+^2 and of F_\times^2 are equal, see eq. (7.35). For an isotropic background, the ensemble average $\langle h^2 \rangle$ that appears on the left-hand side of eq. (7.207) is independent of the angles $\hat{\mathbf{n}}$ and ϕ , so the angular average gives one. The term on the right-hand side of eq. (7.207), instead, can be written in terms of $S_h(f)$ using eq. (7.192) and observing that, for any given propagation direction, we have $h_{ij}h^{ij} = 2(h_+^2 + h_\times^2)$. Then

$$\langle h^2 \rangle = 2\langle F_+^2 \rangle \int_0^\infty df S_h(f), \quad (7.208)$$

where, with an abuse of notation, the brackets in $\langle h^2 \rangle$ denote the ensemble average while the brackets in $\langle F_+^2 \rangle$ denotes the average over $d^2\hat{\mathbf{n}}$ and $d\psi$. In eq. (7.37) we have defined the angular efficiency factor $F = \langle F_+^2 \rangle + \langle F_\times^2 \rangle = 2\langle F_+^2 \rangle$, whose value for various detectors are given in Table 7.1. In particular, $F = 2/5$ for interferometers and $F = 8/15$ for resonant bars. Then

$$\langle h^2(t) \rangle = F \int_0^\infty df S_h(f). \quad (7.209)$$

So, in the presence of signal,

$$\begin{aligned} \langle s^2(t) \rangle &= \langle n^2(t) \rangle + \langle h^2(t) \rangle \\ &= \int_0^\infty df [S_n(f) + FS_h(f)]. \end{aligned} \quad (7.210)$$

Therefore, if a stochastic background is present, one simply observes that $\langle s^2(t) \rangle$ is higher than the value expected from the noise, everywhere or just in some frequency range. More precisely, we can compare the output with the expected value of $S_n(f)$ in each frequency bin (with bins of size $\Delta f = 1/T$ after an observation time T). To take the binning into account, we replace

$$\int S_h(f) df \rightarrow \sum_i S_h(f_i) \Delta f, \quad (7.211)$$

and

$$\int S_n(f) df \rightarrow \sum_i S_n(f_i) \Delta f \quad (7.212)$$

The signal-to-noise ratio in each bin is therefore⁶⁸

$$\begin{aligned} \left(\frac{S}{N} \right)^2 &= F \frac{S_h(f_i) \Delta f}{S_n(f_i) \Delta f} \\ &= F \frac{S_h(f_i)}{S_n(f_i)}. \end{aligned} \quad (7.213)$$

⁶⁸Observe that here S/N is the signal-to-noise ratio with respect to the GW amplitude, just as we have defined it for bursts, coalescence and periodic signals. For stochastic backgrounds, what is actually measured is an energy density, and it make sense to introduce the signal-to-noise ratio with respect to the energy density, which is quadratic in the amplitude. If one prefers to reserve the notation S/N for the signal-to-noise ratio in energy, then on the left-hand side of eq. (7.213) one must write S/N rather than $(S/N)^2$.

Of course the integration time T , which enters through Δf , canceled in eq. (7.213). Increasing the integration time, we decrease the size of the bins and therefore the noise in each bin, but we equally decrease the signal present in each bin. Therefore, in a single detector, as far as the signal-to-noise ratio is concerned, there is no gain in integrating the signal in time. Either the signal stands out immediately as soon as we switch on the detector, or it will always remain below the noise. If however the signal stands out, integrating it for a longer time we get a more detailed resolution of its frequency dependence.

In conclusion, the minimum value of $S_h(f)$ measurable with a single detector having a noise spectral density $S_n(f)$, at a given level S/N of signal-to-noise ratio in amplitude, is

$$[S_h(f)]_{\min} = S_n(f) \frac{(S/N)^2}{F}, \quad (7.214)$$

and correspondingly the minimum detectable value of Ω_{gw} is

$$[\Omega_{\text{gw}}(f)]_{\min} = \frac{4\pi^2}{3H_0^2} f^3 S_n(f) \frac{(S/N)^2}{F}. \quad (7.215)$$

A very important feature of this expression is the factor f^3 . It tells us that, if one is able to reach a given level in $S_n(f)$ at low frequencies, it will be possible to reach a much better sensitivity in $\Omega_{\text{gw}}(f)$ compared to what can be obtained with a similar value of $S_n(f)$ at high frequencies. Of course, the experimental problems that one has to solve in order to reach a given value of $S_n(f)$ depend very strongly on the frequency f . However, at $f = 10^{-3}$ Hz, the space detector LISA aims at reaching a strain sensitivity $S_n^{1/2}(f) = 4 \times 10^{-21} \text{ Hz}^{-1/2}$, while a ground-based interferometer at $f = 10^2$ Hz has $S_n^{1/2}(f) = 4 \times 10^{-23} \text{ Hz}^{-1/2}$, as we will see in Chapter 9. Therefore, moving from $f = 10^2$ Hz to $f = 10^{-3}$ Hz, we lose only four orders in magnitude in $S_n(f)$, but we gain a factor $(10^2/10^{-3})^3 = 10^{15}$ thanks to f^3 . Therefore, it is much easier to reach a small level for $[\Omega_{\text{gw}}(f)]_{\min}$ at low f rather than at high f . The other important question is in what frequency range should we expect that cosmological or astrophysical mechanisms produce an interesting value for $\Omega_{\text{gw}}(f)$. As we will see in Vol. 2, there is a large variety of possible mechanisms, which can produce stochastic GW backgrounds everywhere from $f = 10^{-18}$ Hz up to $f = 10^9$ Hz. Their detection is therefore easier when they are large at low frequencies, since then comparatively high value of the noise spectral density $S_n(f)$ can be overcompensated by the factor f^3 , and becomes more and more difficult as we go to high frequencies. Numerically, with normalizations useful for LISA, eq. (7.215) gives

$$\begin{aligned} [h_0^2 \Omega_{\text{gw}}(f)]_{\min} &= 1.1 \times 10^{-12} \left(\frac{f}{1 \text{ mHz}} \right)^3 \left(\frac{S_n^{1/2}}{4 \times 10^{-21} \text{ Hz}^{-1/2}} \right)^2 \\ &\times \left(\frac{1/\sqrt{5}}{F} \right) \left(\frac{S/N}{5} \right)^2. \end{aligned} \quad (7.216)$$

Using normalization factors appropriate for ground-based interferometers, we rather have

$$\begin{aligned} [h_0^2 \Omega_{\text{gw}}(f)]_{\min} &= 0.12 \left(\frac{f}{100 \text{ Hz}} \right)^3 \left(\frac{S_n^{1/2}}{4 \times 10^{-23} \text{ Hz}^{-1/2}} \right)^2 \\ &\quad \times \left(\frac{2/5}{F} \right) \left(\frac{S/N}{5} \right)^2. \end{aligned} \quad (7.217)$$

In both cases we used a rather high value of the signal-to-noise ratio as a reference value, $S/N = 5$, according to the discussion above. The huge difference between the value $h_0^2 \Omega_{\text{gw}} \sim 10^{-12}$ in eq. (7.216) and the value $h_0^2 \Omega_{\text{gw}} \sim 0.1$ in eq. (7.217) is due to the fact that LISA can reach a value of S_n not far from that of ground-based interferometers, at a much lower frequency.

As we will see in Vol. 2, no cosmological or astrophysical background of GW is expected to exceed $h_0^2 \Omega_{\text{gw}}(f) \sim 10^{-5}$, independently of the frequency. Therefore eqs. (7.216) and (7.217) tell us that LISA has an extremely good sensitivity for stochastic backgrounds of GWs, while ground-based interferometers, used as single detectors, do not reach an interesting level for stochastic backgrounds. However, having at our disposal more than one ground-based detector (interferometers or bars) we can correlate their outputs, and the sensitivity improves dramatically, as we discuss in the next section.

7.8.3 Two-detector correlation

Optimal signal-to-noise ratio

With a single detector, it is impossible to adapt to stochastic backgrounds the matched filtering technique that we studied in Section 7.3. The reason is that, to perform the matched filtering, we need to know the form of the signal, but for stochastic backgrounds the GW signal $h(t)$ is an unpredictable randomly fluctuating quantity, just like the noise $n(t)$. However, if we have two detectors, we can use a modified form of matched filtering in which, rather than trying to match the output of a single detector to a predetermined signal $h(t)$, we match the output of one detector to the output of the other.

To implement this idea we proceed as follows. We write the output $s_k(t)$ of the k -th detector as $s_k(t) = h_k(t) + n_k(t)$, where $k = 1, 2$ labels the detector. Observe that the scalar output $h_k(t)$ depends in general on the detector, because different detectors can have a different location and/or a different orientation and therefore a different pattern function. We are interested in the situation in which the GW signal $h_k(t)$ is much smaller than the noise $n_k(t)$, which is the realistic situation for all ground-based detectors, as we have seen in the previous section. Multiplying both sides of eq. (7.188) by the detector tensor D^{ij} and

using eq. (7.21), we can write the GW signal h_k in the k -th detector as

$$h_k(t, \mathbf{x}_k) = \sum_{A=+, \times} \int_{-\infty}^{\infty} df \int d^2\hat{\mathbf{n}} \tilde{h}_A(f, \hat{\mathbf{n}}) e^{-2\pi if(t - \hat{\mathbf{n}} \cdot \mathbf{x}_k/c)} F_k^A(\hat{\mathbf{n}}), \quad (7.218)$$

where F_k^A are the pattern functions of the k -th detector and \mathbf{x}_k is its location. As always, the size of the detector is taken to be much smaller than λ , so we can neglect the spatial variation of the GW over the extension of the detector. Passing to the Fourier transform, we have

$$\tilde{h}_k(f) = \sum_{A=+, \times} \int d^2\hat{\mathbf{n}} \tilde{h}_A(f, \hat{\mathbf{n}}) e^{2\pi if\hat{\mathbf{n}} \cdot \mathbf{x}_k/c} F_k^A(\hat{\mathbf{n}}), \quad (7.219)$$

where we denote $\tilde{h}_k(f, \mathbf{x}_k)$ simply as $\tilde{h}_k(f)$. To correlate the outputs $s_1(t)$ and $s_2(t)$ of the two detectors we define

$$Y = \int_{-T/2}^{T/2} dt \int_{-T/2}^{T/2} dt' s_1(t) s_2(t') Q(t - t'), \quad (7.220)$$

where T is the total observation time (e.g. one year) and Q a real filter function, analogous to the function $K(t)$ in Section 7.3. Y is our signal, and we want to maximize its signal-to-noise ratio.

We limit ourselves to functions $Q(t - t')$ that fall rapidly to zero for large $|t - t'|$. Passing to the Fourier transforms, we get

$$Y = \int_{-\infty}^{+\infty} df df' df'' \delta_T(f - f'') \delta_T(f' - f'') \tilde{s}_1^*(f) \tilde{s}_2(f') \tilde{Q}(f''), \quad (7.221)$$

where

$$\begin{aligned} \delta_T(f) &\equiv \int_{-T/2}^{T/2} dt e^{i2\pi ft} \\ &= \frac{\sin(\pi f T)}{\pi f}, \end{aligned} \quad (7.222)$$

and becomes a delta function in the limit $fT \rightarrow \infty$. Even on a relatively short stretch of data with, say, $T = 10^3$ s, at $f = 10$ Hz we have $fT = 10^4$. Over the whole useful bandwidth of ground-based detectors we can therefore replace $\delta_T(f)$ by a Dirac delta, and eq. (7.220) becomes

$$Y \simeq \int_{-\infty}^{+\infty} df \tilde{s}_1^*(f) \tilde{s}_2(f) \tilde{Q}(f). \quad (7.223)$$

Recall that, in the signal-to-noise ratio S/N , S is defined as the ensemble average value of Y when the signal is present, while N is the rms value of Y when the signal is absent. Then, assuming that the noise in the two detectors are not correlated (and averaging also over the polarization angle ψ),

$$S = \int_{-\infty}^{+\infty} df \langle \tilde{h}_1^*(f) \tilde{h}_2(f) \rangle \tilde{Q}(f)$$

$$= \int_{-\infty}^{+\infty} df \sum_{A,A'} \int d^2\hat{\mathbf{n}} d^2\hat{\mathbf{n}}' \int \frac{d\psi}{2\pi} e^{-2\pi if(\hat{\mathbf{n}} \cdot \mathbf{x}_1 - \hat{\mathbf{n}}' \cdot \mathbf{x}_2)/c} \\ \times F_1^A(\hat{\mathbf{n}}; \psi) F_2^{A'}(\hat{\mathbf{n}}'; \psi) \langle \tilde{h}_A^*(f, \hat{\mathbf{n}}) \tilde{h}_{A'}(f, \hat{\mathbf{n}}') \rangle \tilde{Q}(f). \quad (7.224)$$

Using eq. (7.190), together with $\delta(0) = \int_{-T/2}^{T/2} dt = T$, this becomes

$$S = \frac{T}{2} \int_{-\infty}^{\infty} df S_h(f) \Gamma(f) \tilde{Q}(f), \quad (7.225)$$

where we have defined

$$\Gamma(f) \equiv \int \frac{d^2\hat{\mathbf{n}}}{4\pi} \int \frac{d\psi}{2\pi} \left[\sum_A F_1^A(\hat{\mathbf{n}}) F_2^A(\hat{\mathbf{n}}) \right] \exp \left\{ i2\pi f \hat{\mathbf{n}} \cdot \frac{\Delta \mathbf{x}}{c} \right\},$$

(7.226)

and $\Delta \mathbf{x} = \mathbf{x}_2 - \mathbf{x}_1$ is the separation between the two detectors. The function Γ is called the (unnormalized) *overlap reduction function*. It takes into account the fact that the two detectors can see a different gravitational signal, either because they are at different location or because they have a different angular sensitivity.

The difference in location is reflected in the exponential factor. In particular, if $2\pi f \Delta x / c \gg 1$, i.e. if the separation $\Delta x \gg \lambda$, this exponential is rapidly oscillating and suppresses strongly the correlation. This reflects the fact that, when $\Delta x \gg \lambda$, the two detectors are experiencing GW signals that are uncorrelated.

The different angular sensitivity of the two detectors is instead reflected in the term $\sum_A F_1^A(\hat{\mathbf{n}}) F_2^A(\hat{\mathbf{n}})$. It is also useful to introduce the quantity

$$F_{12} \equiv \int \frac{d^2\hat{\mathbf{n}}}{4\pi} \int \frac{d\psi}{2\pi} \sum_A F_1^A(\hat{\mathbf{n}}) F_2^A(\hat{\mathbf{n}}) \Big|_{\text{aligned}}, \quad (7.227)$$

where the subscript means that we must compute F_{12} taking the two detectors to be at the same location and oriented one relative to the other so that the quantity F_{12} is maximized.⁶⁹ Observe that, if the two detectors are of the same type, e.g. two interferometers or two cylindrical bars, F_{12} is the same as the constant F defined in eq. (7.37). The (normalized) overlap reduction function $\gamma(f)$ is defined as

$$\gamma(f) = \frac{\Gamma(f)}{F_{12}}. \quad (7.228)$$

For instance, for the correlation between two interferometers, $F_{12} = 2/5$. The factor F_{12} takes into account the reduction in sensitivity due to the pattern functions, already present in the case of one interferometer, and therefore $\gamma(f)$ separately takes into account the effect of the separation $\Delta \mathbf{x}$ between the interferometers, and of their relative orientation. With

⁶⁹For two detectors of the same type this means to orient them in the same way, so in a two-interferometer correlation the arms are taken to be along the x and y axes for both interferometers, and for a two-bar correlation the longitudinal axes of the bars are taken parallel to each other. For the correlation between a bar and an interferometer, we see from the form of the pattern functions given in Table 7.1 that the optimal correlation is obtained aligning the longitudinal axis of the bar with one of the arms of the interferometer.

this definition, $\gamma(f) = 1$ if the separation $\Delta x = 0$ and if the detectors are perfectly aligned. However, the use of $\Gamma(f)$ is more convenient when we want to write equations that hold independently of what detectors (interferometers, bars, or spheres) are used in the correlation.

We now find the optimal choice of the filter function $\tilde{Q}(f)$ that maximizes the signal-to-noise ratio. We need to compute

$$\begin{aligned} N^2 &= [\langle Y^2 \rangle - \langle Y \rangle^2]_{h=0} \\ &= \int_{-\infty}^{\infty} df df' \tilde{Q}(f) \tilde{Q}^*(f') \\ &\quad \times [\langle \tilde{n}_1^*(f) \tilde{n}_2(f) \tilde{n}_1(f') \tilde{n}_2^*(f') \rangle - \langle \tilde{n}_1^*(f) \tilde{n}_2(f) \rangle \langle \tilde{n}_2^*(f') \tilde{n}_1(f') \rangle] . \end{aligned} \quad (7.229)$$

If the noise in the two detectors are uncorrelated, the mixed correlator $\langle \tilde{n}_1^*(f) \tilde{n}_2(f) \rangle$ vanishes, so the second term in brackets is zero, while the first factorizes $\langle \tilde{n}_1^*(f) \tilde{n}_2(f) \tilde{n}_1(f') \tilde{n}_2^*(f') \rangle = \langle \tilde{n}_1^*(f) \tilde{n}_1(f') \rangle \langle \tilde{n}_2(f) \tilde{n}_2^*(f') \rangle$. Then we get

$$N^2 = \int_{-\infty}^{\infty} df df' \tilde{Q}(f) \tilde{Q}^*(f') \langle \tilde{n}_1^*(f) \tilde{n}_1(f') \rangle \langle \tilde{n}_2^*(f') \tilde{n}_2(f) \rangle . \quad (7.230)$$

Using

$$\langle \tilde{n}_k^*(f) \tilde{n}_k(f') \rangle = \delta(f - f') \frac{1}{2} S_{n,k}(f) , \quad (7.231)$$

where $S_{n,k}(f)$ is the noise spectral density of the k -th detector, and using $\delta(0) = T$, we finally get

$$N^2 = \frac{T}{4} \int_{-\infty}^{\infty} df |\tilde{Q}(f)|^2 S_n^2(f) , \quad (7.232)$$

where we have defined the combined noise spectral density

$$S_n(f) = [S_{n,1}(f) S_{n,2}(f)]^{1/2} . \quad (7.233)$$

Equations (7.225) and (7.232) show the same crucial feature that we already observed when we discussed the matched filtering for periodic signals: the signal S increase linearly with the observation time T , while the noise N increases only as $T^{1/2}$. Therefore, the signal-to-noise ratio increases with the observation time as $T^{1/2}$. Putting together eqs. (7.225) and (7.232) we have

$$\frac{S}{N} = T^{1/2} \frac{\int_{-\infty}^{\infty} df S_h(f) \Gamma(f) \tilde{Q}(f)}{\left[\int_{-\infty}^{\infty} df |\tilde{Q}(f)|^2 S_n^2(f) \right]^{1/2}} . \quad (7.234)$$

We can now find the filter function $\tilde{Q}(f)$ that maximizes S/N . The procedure is analogous to what we have already done between eqs. (7.45) and (7.51). For any two complex functions $A(f), B(f)$ we define the positive definite scalar product

$$(A, B) = \int_{-\infty}^{\infty} df A^*(f) B(f) S_n^2(f) . \quad (7.235)$$

Then eq. (7.234) can be rewritten as

$$\frac{S}{N} = T^{1/2} \frac{(\tilde{Q}, \Gamma S_h / S_n^2)}{(\tilde{Q}, \tilde{Q})^{1/2}}. \quad (7.236)$$

As we already discussed below eq. (7.47), this expression is maximized choosing

$$\tilde{Q}(f) = \text{const.} \frac{\Gamma(f) S_h(f)}{S_n^2(f)}. \quad (7.237)$$

It is important to observe that the optimal filter depends on the signal that we are looking for, since $S_h(f)$ enters eq. (7.237). Plugging eq. (7.237) into eq. (7.236) we find the optimal signal-to-noise ratio,

$$\frac{S}{N} = T^{1/2} \left(\frac{\Gamma S_h}{S_n^2}, \frac{\Gamma S_h}{S_n^2} \right)^{1/2}, \quad (7.238)$$

⁷⁰Observe that, for periodic signals and for bursts, as well as for a single-detector search of stochastic backgrounds, we defined the quantity S/N as linear in the GW, i.e. if $\tilde{h}(f) \rightarrow \lambda \tilde{h}(f)$, then $(S/N) \rightarrow \lambda(S/N)$, see eq. (7.51) and eq. (7.213). For searches of stochastic backgrounds with two-detector correlations, we have rather defined S/N as linear both in $h_1(t)$ and in $h_2(t)$ and therefore S/N scales overall quadratically in the GW amplitude. If we prefer to use a quantity that is linear in the GW amplitude we can define $\text{SNR} = (S/N)^{1/2}$, so SNR is proportional to $T^{1/4}$. Of course, it is a matter of conventions whether to use SNR or (S/N) .

or, writing explicitly the scalar product,⁷⁰

$$\frac{S}{N} = \left[2T \int_0^\infty df \Gamma^2(f) \frac{S_h^2(f)}{S_n^2(f)} \right]^{1/2}. \quad (7.239)$$

In particular, for a two-interferometer correlation, $\Gamma(f) = (2/5)\gamma(f)$ and

$$\left(\frac{S}{N} \right)_{\text{intf-intf}} = \left[\frac{8}{25} T \int_0^\infty df \gamma^2(f) \frac{S_h^2(f)}{S_n^2(f)} \right]^{1/2}. \quad (7.240)$$

For two cylindrical bars, instead, $\Gamma(f) = (8/15)\gamma(f)$, while for the correlation between an interferometer and a cylindrical bar, from the explicit expressions of the pattern functions in Table 7.1, we get again $\Gamma(f) = (2/5)\gamma(f)$.

Using eqs. (7.233) and (7.202) we can also rewrite eq. (7.239) as

$$\frac{S}{N} = \frac{3H_0^2}{4\pi^2} \left[2T \int_0^\infty df \Gamma^2(f) \frac{\Omega_{\text{gw}}^2(f)}{f^6 S_{n,1}(f) S_{n,2}(f)} \right]^{1/2}, \quad (7.241)$$

and in particular, for a two-interferometer correlation,

$$\left(\frac{S}{N} \right)_{\text{intf-intf}} = \frac{3H_0^2}{10\pi^2} \left[2T \int_0^\infty df \gamma^2(f) \frac{\Omega_{\text{gw}}^2(f)}{f^6 S_{n,1}(f) S_{n,2}(f)} \right]^{1/2}. \quad (7.242)$$

We can now compare the measurements of stochastic backgrounds performed with the two-detector correlation, to the measurement which uses a single detector, both from the point of view of sensitivity, and of the ability to discriminate true GWs from noise.

Comparison of two-detector and single-detector sensitivities

To compare the sensitivity of a two-detector correlation with the sensitivity of a single detector we assume that we have two identical detectors at a very close distance and with the same orientation, so that $\Gamma(f)$ becomes equal to the angular efficiency factor $F_{12} = F$. (This is the most favorable situation; however in practice, if the detectors are too close, there will be correlated noise.) To perform an order-of-magnitude estimate, we approximate eq. (7.239) as

$$\left(\frac{S}{N}\right)^2 \sim (2T\Delta f) F^2 \frac{S_h^2}{S_n^2}, \quad (7.243)$$

where Δf is the useful bandwidth of the detectors, centered around a frequency f , and S_n and S_h are typical values of $S_n(f)$ and $S_h(f)$, respectively, over this bandwidth. Then the minimum detectable value of S_h , at signal-to-noise level S/N , is

$$(S_h)_{\min} \sim \frac{S_n}{(2T\Delta f)^{1/2}} \frac{(S/N)}{F}, \quad (7.244)$$

and therefore

$$[\Omega_{\text{gw}}]_{\min} \sim \frac{4\pi^2}{3H_0^2} \frac{f^3 S_n}{(2T\Delta f)^{1/2}} \frac{(S/N)}{F}. \quad (7.245)$$

where f^3 is really a typical value of f^3 over the bandwidth. Comparing eq. (7.244) with eq. (7.214) we see that, correlating two detectors, we have gained a factor $(2T\Delta f)^{-1/2}$. Numerically,

$$\frac{1}{(2T\Delta f)^{1/2}} \simeq 1 \times 10^{-5} \left(\frac{150 \text{ Hz}}{\Delta f}\right)^{1/2} \left(\frac{1 \text{ yr}}{T}\right)^{1/2}. \quad (7.246)$$

Therefore, integrating for one year the output of two detectors with a bandwidth of 150 Hz, we can improve our sensitivity to S_h , and therefore to $h_0^2 \Omega_{\text{gw}}$, by approximately five orders of magnitudes, with respect to the sensitivity of a single detector.⁷¹ It is interesting to compare these results with the matched filtering procedure discussed in Section 7.3. In Section 7.3 we took advantage of the fact that we knew the form of the signal, in order to discriminate it from the noise. Here, instead, in a single detector both the signal and the noise have the same statistical properties, but we took advantage of the fact the signals in the two detectors are correlated, while the noise are decorrelated. In particular, the measure of the correlation between the signals in the two detectors is given by the overlap reduction function $\Gamma(f)$ of eq. (7.226), which shows that the signals are indeed well correlated if the separation between the detectors is much smaller than λ , and if the detectors are well oriented with respect to each other. Technically, the assumptions that the noise are uncorrelated entered in eq. (7.224), as well as when passing from eq. (7.229) to eq. (7.230), where we neglected the correlator $\langle \tilde{n}_1^*(f) \tilde{n}_2(f) \rangle$.

⁷¹The precise numbers, of course, can only be obtained once we have the form of $S_h(f)$ and of $S_n(f)$, carrying out the integral in eq. (7.239). Observe also that in eq. (7.214) appears $(S/N)^2$ while in eq. (7.244) appears (S/N) , but this is simply a consequence of the fact that, for the two-detector correlation, we have defined S/N as a quantity quadratic in the GW amplitude, while for a single detector we defined it to be linear in the GW amplitude. Once we choose our criterion for fixing the confidence level, e.g. a signal-to-noise ratio 1.7 in amplitude, the quantity that we are denoting by $(S/N)^2$ here and the quantity denoted by S/N in eq. (7.214) have the same numerical value.

Recall however that the optimal filter depends on the form of the signal. A stochastic background of cosmological origin, as we will see in Vol. 2, is not expected to show strong spectral features in the bandwidth $\Delta f \sim 1$ kHz of ground based interferometers, so it should be adequate a simple power-law parametrization,

$$h_0^2 \Omega_{\text{gw}}(f) = K f^\alpha \quad (7.247)$$

where K and α are two parameters, and α could be positive or negative. For each value of α we can construct the optimal filter (the overall constant in the filter is irrelevant, as we have seen, so different values of K give the same filter) and, given the noise spectral density $S_n(f)$, eq. (7.239) gives S/N as a function of K and α , and therefore tells us what region of this parameter space can be explored, at a given confidence level. For astrophysical backgrounds, more elaborated parametrizations of $h_0^2 \Omega_{\text{gw}}(f)$ might be necessary at broadband detectors.

Non-stationary noise

Until now, we have assumed that the noise in the detectors is stationary, and that it can be represented by a fixed function $S_n(f)$. However, such an assumption is not realistic, even more considering that we wish to use a very long observation time, of the order of months. Each detector has periods where it is more quiet and periods where, because of environmental or other disturbances, it is more noisy. Therefore the function $S_n(f)$ changes with time, and we must know how to combine periods in which the detectors had different noise. To study this issue we can subdivide the total observation time T into n intervals of length T_I , where $I = 1, \dots, m$ labels the interval of data, and with $T = \sum_{I=1}^m T_I$. We choose the T_I so that within each interval the noise of the two detectors can be considered stationary. To each of these intervals we can then apply eq. (7.239), so the value of the optimal signal-to-noise ratio from this interval is

$$\left(\frac{S}{N}\right)_I^2 = 2T_I \int_0^\infty df \Gamma^2(f) \frac{S_h^2(f)}{S_n^2(f; I)}. \quad (7.248)$$

Here $S_n(f; I)$ is the total noise spectral density during the I -th interval, $S_n^2(f; I) = S_{n,1}(f; I)S_{n,2}(f; I)$, where $S_{n,j}(f; I)$ is the noise spectral density of the j -th detector during the I -th interval. We now ask how we should combine the $(S/N)_I$ of the different intervals to form the total optimal signal-to-noise ratio. The correct answer can be guessed observing that the optimal $(S/N)_I^2$ is linear in T_I , see eq. (7.248) and, in the limit in which the noise is stationary over the whole observation time T , we must find that the total optimal signal-to-noise ratio S/N satisfies $(S/N)^2 \sim T = \sum_I T_I$. This fixes uniquely the relation between the total optimal signal-to-noise ratio S/N and the $(S/N)_I$,

$$\left(\frac{S}{N}\right)^2 = \sum_{I=1}^m \left(\frac{S}{N}\right)_I^2. \quad (7.249)$$

The same result can also be obtained more formally introducing the observable

$$Y_{\text{tot}} = \frac{\sum_I \lambda_I Y_I}{\sum_I \lambda_I} \quad (7.250)$$

(where it is understood that the sums run over $I = 1, \dots, m$) and choosing the variables $\lambda_I > 0$ so that the signal-to-noise ratio of Y_{tot} is maximized. From eq. (7.225), with T replaced by T_I , we see that the Y_I have a mean value

$$S_I \equiv \langle Y_I \rangle = \mu T_I, \quad (7.251)$$

where $\mu = \int_0^\infty df S_h(f) \Gamma(f) \tilde{Q}(f)$ is independent of I . For the noise, from eq. (7.232) we have

$$\begin{aligned} N_I^2 &= \frac{T_I}{4} \int_{-\infty}^{\infty} df |\tilde{Q}(f)|^2 S_n^2(f; I) \\ &\equiv T_I \sigma_I^2. \end{aligned} \quad (7.252)$$

The signal-to-noise ratio S/N of Y_{tot} is obtained by writing

$$S = \langle Y_{\text{tot}} \rangle = \mu \frac{\sum_I \lambda_I T_I}{\sum_I \lambda_I}, \quad (7.253)$$

and

$$\begin{aligned} N^2 &= [\langle Y_{\text{tot}}^2 \rangle - \langle Y_{\text{tot}} \rangle^2]_{\mu=0} \\ &= \frac{\sum_I \lambda_I^2 \sigma_I^2 T_I}{(\sum_I \lambda_I)^2}, \end{aligned} \quad (7.254)$$

where we assumed that noise in different intervals are uncorrelated, so $\langle Y_I Y_J \rangle = \delta_{IJ} N_I^2$. Therefore

$$\frac{S^2}{N^2} = \mu^2 \frac{(\sum_I \lambda_I T_I)^2}{\sum_I \lambda_I^2 \sigma_I^2 T_I}. \quad (7.255)$$

The maximization of this expression with respect to the λ_I can be performed very simply, introducing the positive definite scalar product between two vectors with real components a_I and b_I ,

$$(a, b) \equiv \sum_I a_I b_I \sigma_I^2 T_I. \quad (7.256)$$

Then

$$\frac{S}{N} = \mu \frac{(\lambda_I, \sigma_I^{-2})}{(\lambda_I, \lambda_I)^{1/2}}. \quad (7.257)$$

This expression is maximized if the vectors with components λ_I and σ_I^{-2} are parallel, so $\lambda_I = 1/\sigma_I^2$ (apart from an irrelevant overall constant). Physically, this means that more noisy periods are weighted less. Then the variable Y_{opt} , whose signal-to-noise ratio is optimal, is given by

$$Y_{\text{opt}} = \frac{\sum_I \sigma_I^{-2} Y_I}{\sum_I \sigma_I^{-2}} \quad (7.258)$$

and the value of the optimal S/N is given by

$$\left(\frac{S}{N}\right)^2 = \mu^2 (\sigma_I^{-2}, \sigma_I^{-2}) = \mu^2 \sum_I \frac{T_I}{\sigma_I^2}, \quad (7.259)$$

which, using eqs. (7.251) and (7.252), is equivalent to eq. (7.249), as expected. Equation (7.239) then becomes

$$\frac{S}{N} = \left[2 \int_0^\infty df \Gamma^2(f) S_h^2(f) \sum_{I=1}^m \frac{T_I}{S_n^2(f; I)} \right]^{1/2}. \quad (7.260)$$

This is equivalent to saying that, in eq. (7.239), we must make the replacement

$$\frac{T}{S_n^2(f)} \rightarrow \sum_{I=1}^m \frac{T_I}{S_n^2(f; I)}. \quad (7.261)$$

This way of composing the noise is very natural. It means that noisy periods contribute little to the total signal-to-noise ratio. If we perform the same order-of-magnitude estimate as in eq. (7.245), we conclude that

$$\frac{1}{[\Omega_{\text{gw}}(f)]_{\min}^2} = \sum_{I=1}^m \frac{1}{[\Omega_{\text{gw}}(f; I)]_{\min}^2}, \quad (7.262)$$

where $[\Omega_{\text{gw}}(f; I)]_{\min}$ is the minimum value of Ω_{gw} detectable using only the data in the I -th interval, and $[\Omega_{\text{gw}}(f)]_{\min}$ is the minimum value of Ω_{gw} detectable combining the n intervals.

How the background is actually measured

We can now give an example of an operative way of measuring the stochastic background. First of all, one divides the total observation time T into intervals of length T_I , such that within each interval the detector noise is stationary. This scale is chosen based on observations of the detector noise variation, and could typically be of order of one to a few minutes. Within each interval, the spectral density $S_n(f; I)$ can be considered constant in time, and is determined experimentally. We can now compute the filter function, using the measured value of $S_n(f; I)$ and assuming a given form for Ω_{gw} . For instance, $\Omega_{\text{gw}} = \text{const.}$ can be the simplest choice, or one can use the parametrization (7.247) and repeat the procedure for various values of α .

To have an experimental determination of $S_I = \langle Y_I \rangle$ and of $N_I = [\langle Y_I^2 \rangle - \langle Y_I \rangle^2]^{1/2}$ one further divides each interval into segments of length Δt , labeled by an index $J = 1, \dots, n$, and with $T_I = n\Delta t$ (with Δt much larger than the light travel time between the detectors, which for the two LIGO observatories is about 10 ms). The signal Y_{IJ} relative to the J -th segment of the I -th interval is computed using eq. (7.220), with the time integration running only over the J -th segment of the I -th interval.⁷² Observe that the filter function $Q(t - t')$ typically vanishes very fast for $|t - t'|$ larger than a few tens of ms, so in practice if t belongs to the

⁷²In practice, it can be more convenient to perform a FFT over the segment and use the frequency space expression (7.223).

J -th interval, the support of $Q(t - t')$ is entirely contained in the J -th interval.

From the set of Y_{IJ} at fixed I , one can construct the sample mean

$$S_I = \frac{1}{n} \sum_{J=1}^n Y_{IJ}, \quad (7.263)$$

and the sample variance

$$N_I^2 = \frac{1}{n-1} \sum_{J=1}^n (Y_{IJ} - S_I)^2, \quad (7.264)$$

of the I -th interval. We repeat this procedure for all intervals and, according to eq. (7.249), the total signal-to-noise ratio is

$$\left(\frac{S}{N}\right)^2 = \sum_{I=1}^m \left(\frac{S_I^2}{N_I^2}\right). \quad (7.265)$$

If this S/N exceeds a predetermined threshold value one can state that a stochastic background is detected, with a confidence level which depends on the threshold used.⁷³

⁷³A subtle point is that it can be shown that, if we wait long enough, i.e. if the total observation time is sufficiently large, any predetermined fixed threshold will be exceeded. In other words, in the limit $T \rightarrow \infty$ the false alarm probability is 100%! To have a finite false alarm probability even in the limit $T \rightarrow \infty$, the value of the threshold must increase with the number of intervals n faster than $\log \log n$.

Multiple-detector correlation

Another interesting question is what happens if we correlate the outputs of N detectors, with $N > 2$. For simplicity, we assume at first that we have N identical detectors, with the same noise spectral density $S_n(f)$, and all running simultaneously for a time T .

With N detectors we can form $N(N - 1)/2$ independent two-point correlators

$$Y_{ij} = \int_{-T/2}^{T/2} dt \int_{-T/2}^{T/2} dt' s_i(t) s_j(t') Q(t - t'), \quad (7.266)$$

with $i < j$. (If the detectors have different noise spectral densities, then also the filter function depends on i, j , and we write it $Q_{ij}(t - t')$.) Conceptually, for a stationary stochastic background, there is no difference between the situation in which $N(N - 1)/2$ identical pairs of detectors run for a time T , and the situation in which a single pair of detectors runs for a time $T_{\text{total}} = T \times N(N - 1)/2$. In the former case, sampling the output of the detectors at times t_k , with $k = 1, \dots, k_{\max}$, we get a set of values $Y_{ij}(t_k)$, for each of the $N(N - 1)/2$ pairs (i, j) . In the latter case we directly get a set of values $Y(t_k)$ for the single pair considered, with k taking values up to $k_{\max} \times N(N - 1)/2$. In both cases we must then compute the average of Y over all these values, so the result is the same and the difference is just a matter of notation. In conclusion, the signal-to-noise ratio with N identical detectors can be obtained from eq. (7.239) making the replacement

$$T \rightarrow \frac{N(N - 1)}{2} T. \quad (7.267)$$

If we denote by $[\Omega_{\text{gw}}]_{\min,N}$ the minimum value of Ω_{gw} measurable with N identical detectors and by $[\Omega_{\text{gw}}]_{\min,2}$ the minimum value of Ω_{gw} detectable with two detectors, then

$$[\Omega_{\text{gw}}]_{\min,N} = \left[\frac{2}{N(N-1)} \right]^{1/2} [\Omega_{\text{gw}}]_{\min,2}. \quad (7.268)$$

In the more realistic case in which the detectors have different noise spectral densities, or have different common time of operation, the situation is formally identical to the case of non-stationary noise discussed above, where the observations taken during a time T_{ij} by each pair of detectors (i, j) , with $i < j$, plays the role of the observations taken during the time intervals labeled by I in eqs. (7.260) to (7.262). Therefore, the signal-to-noise ratio is obtained from eq. (7.239) with the replacement

$$\frac{T}{S_n^2(f)} \rightarrow \sum_{i < j} \frac{T_{ij}}{S_n^2(f; \langle ij \rangle)}, \quad (7.269)$$

where T_{ij} is the common time of operation of the detectors i and j , and $S_n^2(f; \langle ij \rangle) = S_n(f; i)S_n(f; j)$ is the product of the spectral densities of the i -th and j -th detector. The order-of-magnitude estimate of the minimum detectable value of Ω_{gw} , eq. (7.262), becomes

$$\frac{1}{[\Omega_{\text{gw}}(f)]_{\min,N}^2} = \sum_{i < j} \frac{1}{[\Omega_{\text{gw}}(f; \langle ij \rangle)]_{\min}^2}. \quad (7.270)$$

When all detectors are equal and have the same common time of operation, $[\Omega_{\text{gw}}(f; \langle ij \rangle)]_{\min}$ becomes independent of the pair i, j considered, and is the quantity that we denoted by $[\Omega_{\text{gw}}]_{\min,2}$, so we recover eq. (7.268).

In a sense, this result is disappointing. We have seen in eq. (7.245) that, passing from a single detector to a two-detector correlation, we gain a factor $1/(2T\Delta f)^{1/2}$ in the minimum detectable value of Ω_{gw} . For $T = 1$ yr and $f = 100$ Hz, this means an improvement by a factor 10^5 in sensitivity. Passing from $N = 2$ to $N = 3$ detectors, instead, we see from eq. (7.268) that we gain only a further factor $\sqrt{3}$.

This is very different from the situation for bursts discussed in Section 7.5.3. In the case of bursts, the noise that compete with the signal consists of large, relatively rare fluctuations. At any given moment the probability that, in a single detector and within a given time window, say of order few tens of ms, a fluctuation with a signal-to-noise ratio above a large threshold takes place, is a small number $\epsilon \ll 1$. The probability that a second detector has a simultaneous independent fluctuation above this threshold, within the same window, is $O(\epsilon^2)$, the probability of a three-detector coincidence is $O(\epsilon^3)$, etc. Then, for bursts, the gain in statistical significance passing from a single detector to a two-detector coincidence is that same as the gain passing from a two-detector to a three-detector coincidence. The crucial point is that for bursts, after matched filtering, we are left with short events with a large value of S/N , which are rare.

In contrast, for stochastic backgrounds we are never confronted with rare events. At any given moment the GW stochastic signal is always much below the noise, and is never responsible for large fluctuations of the output. There are no rare events to be searched in coincidence, and the only advantage of using more detector pairs is that the total amount of data available increases, which means that we have a longer effective observation time.

The situation does not change substantially if, rather than two-point correlators, we consider M -point correlators, with M smaller than or equal the number of detectors N . For instance, with four detectors we can consider a four-point correlator $\langle s_1(f)s_2(f)s_3(f)s_4(f) \rangle$. Repeating the same steps as above, one finds again that the signal-to-noise ratio (always defined to be quadratic in the GW signal, in order to compare with the same quantity as in two-detector case) scales as \sqrt{T} .

On the other hand, an advantage of multiple-detector correlations is that it might be easier to suppress correlated environmental noise, especially if the various detectors are not close to each other.

Correlated noise and signal chopping

Equation (7.239) shows that a true GW signal has a signature that in principle could allow us to distinguish it from the noise: increasing the observation time, the signal-to-noise ratio in the presence of a real GW signal must increase as $T^{1/2}$.

Actually, this is a signature that only allows us to distinguish a stochastic GW background from uncorrelated noise in the two detectors. Unfortunately, any residual correlated noise would still mimic the behavior of a real GW signal. The problem is therefore how to make sure that correlated noise are negligible, and this can be a hard task, particularly for very long integration times. If two detectors are at the same site, or very close, their overlap reduction function is maximized, but we will certainly have correlated environmental noise. We have seen that the overlap reduction function suppresses the GW correlation if the detector separation is $\Delta x \gg \lambda$. For instance, at $f = 50$ Hz, $\lambda \simeq 1000$ km. Most environmental disturbances will decorrelate on a much shorter length-scale, so it is possible that two detectors at a suitable distance are still correlated as far as the GW background is concerned, but they have negligible correlated noise. However, beyond a given sensitivity level, seismic noise or propagating electromagnetic disturbances might still give important correlated noise, and this is a difficult issue that will have to be carefully studied experimentally.

An interesting option offered by the two-detector correlation is the possibility of *chopping* the signal. Chopping is a general term for measurements in which we switch our detector between the quantity that we want to measure and a reference quantity. It is a very powerful experimental technique, that exploits the fact that in many situations one can measure with a much better precision the variation of a quantity rather than the quantity itself because, taking the difference, many uncertain-

⁷⁴The classical example of this technique was the Dicke radiometer, which was developed by Dicke during World War II for application to microwave radars, and measured the radiation temperature of a radio source (i.e. the temperature of a black body having the same radio brightness). A direct measurement was difficult: the signal needed a large amplification, and fluctuations in the amplifier gain resulted in large errors. To overcome this difficulty, in the Dicke radiometer the receiver switches quickly between the source and a carefully calibrated black body, whose temperature was chosen to be of the order of the value expected for the source. To tell when these temperatures were equal was much easier than to obtain a direct determination of the source temperature. The same principle of comparing with a reference black body was used by the FIRAS spectrometer on board of the COBE satellite to measure the black-body spectrum of CMB. To measure the CMB anisotropies, i.e. the variation of the black-body temperature over the sky, the principle used by the DMR detector on COBE and by the subsequent high-precision experiments such as WMAP is to compare the temperatures between two points in the sky.

ties, e.g. calibration uncertainties, cancel out.⁷⁴ In particular, one can compare the measurement in a situation where the signal is expected, to the situation where a null answer should come out.

At first sight, it appears that a measurement of this type is impossible for a stochastic backgrounds of GWs, since the background is always there, and gravitational forces cannot be screened. It seems therefore impossible to compare the output of a detector when no stochastic GW background acts on it, with the output when the background is acting on it. Remarkably, this is no longer true when we consider a two-detector correlation. In fact, changing the relative orientation of the two detectors, the factor $\sum_A F_1^A(\hat{\mathbf{n}})F_2^A(\hat{\mathbf{n}})$ in eq. (7.226) changes, and it is therefore possible to modulate the signal. To illustrate this point, we compute F_{12} for a bar-interferometer correlation. Using Table 7.1 and eqs. (7.31) and (7.32) we see that, for ψ generic, the pattern functions of an interferometer are

$$\begin{aligned} F_+^{(\text{intf})}(\theta, \phi; , \psi) &= \frac{1}{2}(1 + \cos^2 \theta) \cos 2\phi \cos 2\psi - \cos \theta \sin 2\phi \sin 2\psi, \\ F_x^{(\text{intf})}(\theta, \phi; \psi) &= \frac{1}{2}(1 + \cos^2 \theta) \cos 2\phi \sin 2\psi + \cos \theta \sin 2\phi \cos 2\psi. \end{aligned} \quad (7.271)$$

The pattern functions of the bar for ψ generic can also be obtained from Table 7.1 and eqs. (7.31) and (7.32). We must however pay attention to the fact that in Table 7.1, the variable denoted by θ for resonant bars is the angle measured from its longitudinal axis, while for an interferometer with arms along the x and y axes, we denoted by θ the polar angle measured from the z axis, so these two angles are not the same unless the bar is vertical. If instead the bar lies in the x, y plane, at an angle α with the y axis, and we denote by θ the polar angles measured from the z axis, then the pattern functions of the bar become

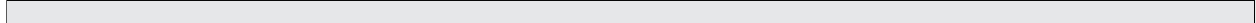
$$\begin{aligned} F_+^{(\text{bar})}(\theta, \phi; , \psi) &= [-\cos^2 \theta \cos^2(\phi - \alpha) + \sin^2(\phi - \alpha)] \cos 2\psi \\ &\quad + [\cos \theta \sin 2(\phi - \alpha)] \sin 2\psi \\ F_x^{(\text{bar})}(\theta, \phi; , \psi) &= [-\cos^2 \theta \cos^2(\phi - \alpha) + \sin^2(\phi - \alpha)] \sin 2\psi \\ &\quad - [\cos \theta \sin 2(\phi - \alpha)] \cos 2\psi. \end{aligned} \quad (7.272)$$

From this it follows that

$$\int \frac{d\hat{\mathbf{n}}}{4\pi} \frac{d\psi}{2\pi} \sum_A F_A^{(\text{bar})} F_A^{(\text{intf})} = -\frac{2}{5} \cos 2\alpha. \quad (7.273)$$

(The overall sign of F_{12} is irrelevant since $\Gamma(f)$ enters quadratically in the signal-to-noise ratio.) We see that the correlation is maximum when the bar is aligned with one of the interferometer arms (i.e. when $\alpha = 0$ or $\alpha = \pi/2$). In contrast, when $\alpha = \pi/4$ we have $F_{12} = 0$. Therefore in this configuration the signal obtained from the interferometer-bar correlation vanishes. Even if GWs cannot be screened, the “composite detector” whose output is the correlation between a bar and an interferometer can be set in the “off source” position! We can then compare the result

in this configuration with the result when the resonant bar is parallel to one of the interferometer arms, which is the position that maximizes the correlation. This chopping strategy has been used in the LIGO–ALLEGRO correlation. The ALLEGRO resonant bar (which has now terminated its activity) was located relatively close to the LIGO observatory in Livingston, and was mounted on a platform that allowed to rotate it easily. (After a rotation, data taking of good quality resumed in just half an hour.) The bar was therefore taken for a few months in the “off source” position, and then rotated to the “on source” position for a few more months.



Further reading

- For a textbook discussion of matched filtering and of detection of signals in noise see Wainstein and Zubakov (1962) and McDonough and Whalen (1995). For matched filtering and optimal signal-to-noise ratio for GW bursts see Thorne (1987), and Saulson (1994), Chapter 4. Statistical aspects of parameter estimation are discussed in Finn (1992) and in Cutler and Flanagan (1994), where the multiple detector case is also treated. For a review of data analysis for interferometric GW detector see Viceré (2000).
- Books on probability and statistics typically cover many shelves in any physics library, and recommendation are very much subjective. For an elementary but very practical introduction to statistics (tuned to the needs of particle physicists, but quite useful also in the GW context), see Lyons (1986). A concise and useful summary is given in the sections on probability and statistics of the Review of Particle Properties, in Yao *et al.* [Particle Data Group] (2006). A very nice discussion of Bayesian vs. frequentist method, in the context of particle physics, is given in Cousins (1995). A discussion of the frequentist vs. Bayesian approach in the GW context is given in appendix A of Cutler and Flanagan (1994).
- The analysis of bursts of unknown shape using band-pass filtering is discussed in Flanagan and Hughes (1998a, 1998b), in the context of the merging phase of black hole binaries. Time-frequency techniques are further discussed in Anderson and Balasubramanian (1999), Anderson, Brady, Creighton and Flanagan (2001) and Viceré (2002). An algorithm based on clusters of pixels in the time–frequency domain (termed TFCLUS-TERS) is presented in Sylvestre (2002). A book on the use of wavelets in physics is van den Berg (1999). Application of wavelets to the analysis of GW bursts can be found in Klimenko, Yakushin, Rakhmanov and Mitselmakher (2004) and Klimenko and Mitselmakher (2004) (the WaveBurst algorithm).
- Some sources, such as accreting neutron or quark stars, as well as neutron stars stressed by large interior magnetic fields (magnetars), could emit repeatedly small bursts of GWs, with very characteristic correlations, both in energy and in time, among the different bursts, typical of systems displaying self-organized criticality. These correlations could give a further handle in their data analysis. These “GW bursters” are discussed in Coccia, Dubath and Maggiore (2004) and Dubath, Foffa, Gasparini, Maggiore and Sturani (2005).
- The search strategy for GW bursts using the three LIGO interferometers is discussed in Abbott *et al.* [LSC] (2004b). The sensitivity of a network of interferometers for reconstructing the source position is studied in Gürsel and Tinto (1989). Searches for GW bursts using coincidences between up to five resonant bars are described in Astone *et al.* [IGEC] (2003a). Results with correlations among three bars, with improved sensitivities, are reported in Astone *et al.* [IGEC2] (2007).
- Introductory discussions of the search strategies for periodic signals can be found in Saulson (1994), Section 14.6 and Schutz (1991). More detailed analysis are given in Brady, Creighton, Cutler and

Schutz (1998) and in Brady and Creighton (2000). The application of the Hough transform to periodic GWs is discussed in Krishnan *et al.* (2004). A search for periodic GWs from a single specific source, using the LIGO and GEO detectors, is described in Abbott *et al.* [LSC] (2004a). Limits on 28 isolated pulsar using the LIGO S2 run are given in Abbott *et al.* [LSC] (2005b).

- The importance of post-Newtonian corrections for the data analysis of coalescing binaries is emphasized in Cutler *et al.* (1993). Detailed discussions of data analysis procedure and parameter extraction for coalescences is given in Cutler and Flanagan (1994), Poisson and Will (1995), Królak, Kokkotas and Schäfer (1995) and Flanagan and Hughes (1998a). For computations of the waveform with the PN formalism, see the Further Reading section in Chapter 5.
- Optimal template placement for inspiraling compact binaries is discussed in Owen (1996) and Owen

and Sathyaprakash (1999). A comparison of templates for binary inspiral is given in Damour, Iyer and Sathyaprakash (2001). A particularly useful family of templates for BH-BH inspiral have been proposed by Buonanno, Chen and Vallisneri (2003). A description of the LIGO search strategy for coalescences can be found in Abbott *et al.* [LSC] (2005a).

- The optimal SNR in a two-detector correlation and the overlap reduction function are discussed in Michelson (1987), Christensen (1992) and Flanagan (1993). A detailed discussion of signal processing strategies for stochastic backgrounds of GWs is given in Allen and Romano (1999). Signal chopping is discussed in Finn and Lazzarini (2001). Stochastic backgrounds of GWs are reviewed in Maggiore (2000). The search strategy of LIGO for stochastic backgrounds of GWs is discussed in Abbott *et al.* [LSC] (2004d) and (2005c).

Resonant-mass detectors

8

The history of experimental GW physics began with resonant-mass detectors. The pioneer was Joseph Weber who, in the 1960s, developed the concept and built the first resonant bars. In the course of the subsequent four decades, resonant-mass detectors operated by various groups have reached sensitivities better than Weber’s original bars by about four orders of magnitudes in energy. Still, we will see in this chapter that these sensitivities could allow the detection of only relatively strong signals in our Galaxy or at most in our immediate galactic neighborhood, which are expected to be rare. To gain access to sources at large extragalactic distances it is necessary to build large interferometers, which will be the subject of the next chapter.

The passage from resonant detectors to interferometers implies a jump from “small-scale” experiments, performed by groups which can be as small as half a dozen people, to “Big Science”, with collaborations of hundreds of people and financial costs which are higher by factors $O(10^2–10^3)$. As we will see in the next chapter, such a jump is justified by the formidable discovery potential of interferometers and especially advanced interferometers. We nevertheless begin our discussion of experiments with resonant-mass detectors, both because they still have the possibility of detecting rare or unexpected events, and also because their study is instructive in itself. Our emphasis will be on aspects that have an intrinsic conceptual interest, such as understanding how a GW interacts with a macroscopic piece of matter, and on how it is possible to detect vibrations of a macroscopic body which are incredibly small, with amplitude many orders of magnitude smaller than the size of a nucleus. We will see that, by themselves, resonant detectors are remarkable instruments; it is possible to measure vibrations in a two-ton object, such as a typical bar, which corresponds to just a few tens of phonons, and variations ΔL of their length L , with $\Delta L/L \sim 10^{-19}–10^{-18}$.

8.1 The interaction of GWs with an elastic body

8.1.1 The response to bursts

A typical bar is a cylinder of length $L \simeq 3$ m and radius $R \simeq 30$ cm, so in a first approximation we can treat its vibrations as one-dimensional. We orient the bar along the x axis, with the end-faces at $\pm L/2$, and we study the dynamics of a volume element dV of the bar originally located

8.1 The interaction of GWs with an elastic body	415
8.2 The read-out system	427
8.3 Noise sources	436
8.4 Resonant spheres	459

at a position x . In the proper detector frame introduced in Section 1.3.3, under the action of the GW this volume element will be displaced to a new position $x+u(t, x)$, with $u(t, x) \ll x$. In this section we consider the response to a GW burst of duration τ_g much smaller than the relaxation time of the bar. As we will see in more detail later, for a typical bar this relaxation time is of order 600 s, and the approximation $\tau_g \ll 600$ s is excellent for astrophysical bursts, which can have $\tau_g = O(1)$ ms. In this case we can neglect dissipative effects in the bar during the passage of the burst, and we know from elasticity theory¹ that the longitudinal elastic oscillations of the material are governed by a wave equation,

$$dm \left(\frac{\partial^2 u}{\partial t^2} - v_s^2 \frac{\partial^2 u}{\partial x^2} \right) = dF_x(t, x), \quad (8.1)$$

where dm is the mass of the volume dV considered, dF_x is the x component of the force exerted by the gravitational wave on the mass dm , and v_s is the speed of sound in the material, related to the Young modulus Y and to the density ρ by $v_s^2 = Y/\rho$.

Before proceeding with the formalism, we observe that eq. (8.1) is appropriate only if the effect of GWs on the bar can be approximated by a Newtonian force rather than by the full equations of general relativity. We saw in Chapter 1 that the effect of GWs on test masses can be approximated by a Newtonian force, and is expressed by the equation of the geodesic deviation (1.95), only if the spatial separation between test masses (and therefore, in our case, the size L of the bar) is much smaller than the typical scale of variation of the GWs, which in turn is equal to the reduced wavelength $\bar{\lambda}$ of the waves. Otherwise, the expansion performed in the derivation of the equation of the geodesic deviation breaks down, and a full general relativistic treatment becomes necessary. As we will see in this chapter, the fundamental mode of the bar resonates at the frequency $\omega_0 = \pi v_s/L$, and the bar is sensitive to GWs with frequencies of the order of its resonance frequency. Then, the relation between the length L of the bar and the reduced wavelength $\bar{\lambda}$ of the GW that it searches is $L/\bar{\lambda} \simeq \pi v_s/c$. Of course, in any available material $v_s \ll c$. For instance, in aluminum at low temperatures, $v_s \simeq 5.4$ km/s and $\pi v_s/c \simeq 6 \times 10^{-5}$. Therefore for resonant bars the approximation $L/\bar{\lambda} \ll 1$ is excellent and we can use the equation of the geodesic deviation to discuss their interaction with GWs.

Using eq. (1.95) we can write the Newtonian force in the proper detector frame in terms of the expression of h_{ij} in the TT frame,

$$dF_i = \frac{1}{2} \ddot{h}_{ij}^{TT} x^j dm, \quad (8.2)$$

with $x^j = (x + u, 0, 0)$. Since $u = O(h)$, to linear order in h we can simply set $x^j = (x, 0, 0)$ on the right-hand side of eq. (8.2). In this chapter the GW will always be expressed in the TT gauge and, to make the notation lighter, we omit the label TT from h_{ij} . Then we have $dF_x(t, z) = (1/2)x\ddot{h}_{xx} dm$, and eq. (8.1) becomes

$$\frac{\partial^2 u}{\partial t^2} - v_s^2 \frac{\partial^2 u}{\partial x^2} = \frac{1}{2} x \ddot{h}_{xx}. \quad (8.3)$$

¹See, e.g. Landau and Lifshitz, Vol. VII (1970), or Love (1944).

The appropriate boundary conditions are

$$\left. \left(\frac{\partial u}{\partial x} \right) \right|_{x=\pm L/2} = 0, \quad (8.4)$$

and express the fact that there is no flux of elastic energy flowing outside the bar. Equations (8.3) and (8.4) determine the elastic deformation of the bar produced by the GW. Again from elasticity theory we know that the energy stored in the elastic deformations is given by

$$E = \int dm \frac{1}{2} \left[\left(\frac{\partial u}{\partial t} \right)^2 + v_s^2 \left(\frac{\partial u}{\partial x} \right)^2 \right]. \quad (8.5)$$

The mode expansion compatible with the boundary conditions (8.4) is

$$u(t, x) = \sum_{n=0}^{\infty} \xi_n(t) \sin\left[\frac{\pi x}{L}(2n+1)\right] + \xi'_n(t) \cos\left[\frac{\pi x}{L}(2n+2)\right]. \quad (8.6)$$

Substituting into eq. (8.3) we get

$$\sum_{n=0}^{\infty} [\ddot{\xi}_n + \omega_n^2 \xi_n] \sin\left[\frac{\pi x}{L}(2n+1)\right] + [\ddot{\xi}'_n + \omega_n'^2 \xi'_n] \cos\left[\frac{\pi x}{L}(2n+2)\right] = \frac{1}{2} x \ddot{h}_{xx}, \quad (8.7)$$

with

$$\omega_n = \frac{\pi v_s}{L} (2n+1), \quad \omega_n' = \frac{\pi v_s}{L} (2n+2). \quad (8.8)$$

Using the orthogonality relations

$$\int_{-L/2}^{L/2} dx \sin\left[\frac{\pi x}{L}(2n+1)\right] \sin\left[\frac{\pi x}{L}(2m+1)\right] = \frac{L}{2} \delta_{n,m}, \quad (8.9)$$

$$\int_{-L/2}^{L/2} dx \sin\left[\frac{\pi x}{L}(2n+1)\right] \cos\left[\frac{\pi x}{L}(2m+2)\right] = 0, \quad (8.10)$$

we find from eq. (8.7)

$$\begin{aligned} \ddot{\xi}_n + \omega_n^2 \xi_n &= \frac{1}{L} \ddot{h}_{xx} \int_{-L/2}^{L/2} dx x \sin\left[\frac{\pi x}{L}(2n+1)\right] \\ &= \frac{(-1)^n}{(2n+1)^2} \frac{2L}{\pi^2} \ddot{h}_{xx}, \end{aligned} \quad (8.11)$$

while

$$\begin{aligned} \ddot{\xi}'_n + \omega_n'^2 \xi'_n &= \frac{1}{L} \ddot{h}_{xx} \int_{-L/2}^{L/2} dx x \cos\left[\frac{\pi x}{L}(2n+1)\right] \\ &= 0. \end{aligned} \quad (8.12)$$

The latter integral vanishes because the integrand is odd under $x \rightarrow -x$, and therefore the modes ξ'_n do not couple to GWs.² We now restrict to the fundamental mode ξ_n with $n = 0$, whose dynamics is governed by the equation

$$\ddot{\xi}_0 + \omega_0^2 \xi_0 = \frac{2L}{\pi^2} \ddot{h}_{xx}, \quad (8.13)$$

²Physically this can be understood recalling, from Section 1.3.1, that the equation of the geodesic deviation describes displacements from a fixed point $x = 0$. Therefore, by definition, the volume element located at the origin does not move. In the case of a bar this means that, as long as we are interested only in its response to GWs, we can further impose the boundary condition $\xi(x = 0, t) = 0$. The function $\sin[\pi x(2n+1)/L]$ satisfies it and therefore the modes $\xi_n(t)$ are allowed, while $\cos[\pi x(2n+2)/L]$ does not vanish at $x = 0$ and therefore $\xi'_n(t) = 0$. Of course, this result is specific to the form (8.2) of the force exerted by GWs. More specifically, it is a consequence of the spin-2 nature of the gravitational field, which is described by a traceless symmetric tensor with two indices h_{ij}^{TT} , so to obtain dF_i we are forced to saturate one index with x^j .

with

$$\omega_0 = \frac{\pi v_s}{L}. \quad (8.14)$$

To obtain the elastic energy of this mode we replace $u(t, x)$ in eq. (8.5) with $\xi_0(t) \sin(\pi x/L)$. For a uniform bar of mass M we have $dm = (M/L)dx$, and we can perform the integral over x , obtaining

$$E = \frac{M}{4} (\dot{\xi}_0^2 + \omega_0^2 \xi_0^2). \quad (8.15)$$

Equations (8.13) and (8.15) show that the fundamental mode of a thin cylindrical bar of mass M and length L is formally identical to a harmonic oscillator with frequency ω_0 and mass $m_0 = M/2$, driven by a force $F(t) = (2/\pi^2)m_0 L \ddot{h}_{xx}$. Comparing with eq. (8.3), we see that this is the force exerted by GWs on a oscillator with an effective mass³ m_0 and an effective length $l = (4/\pi^2)L$.

An oscillator of mass m_0 subject to an external impulsive force $F(t)$ absorbs from it an energy E_s (the label s stands for “signal”) given by⁴

$$E_s = \frac{1}{2m_0} \left| \int_{-\infty}^{\infty} dt F(t) e^{-i\omega_0 t} \right|^2. \quad (8.16)$$

The energy transferred to the fundamental mode of the bar by a GW burst is obtained using $F(t) = (2/\pi^2)m_0 L \ddot{h}_{xx}$ with $m_0 = M/2$, so

$$E_s = \frac{ML^2}{\pi^4} \left| \int_{-\infty}^{\infty} dt \ddot{h}_{xx}(t) e^{-i\omega_0 t} \right|^2. \quad (8.17)$$

By definition, a burst is described by a function $h(t)$ which goes to zero very fast at $t \rightarrow \pm\infty$. We can therefore integrate by part twice the above expression, and we get

$$\begin{aligned} E_s &= \frac{ML^2(2\pi f_0)^4}{\pi^4} \left| \int_{-\infty}^{\infty} dt h_{xx}(t) e^{-i2\pi f_0 t} \right|^2 \\ &= 16ML^2 f_0^4 |\tilde{h}_{xx}(f_0)|^2. \end{aligned} \quad (8.18)$$

Therefore the value of $|\tilde{h}_{xx}(f_0)|^2$ can be obtained measuring the energy E_s deposited in the bar,⁵

$$|\tilde{h}_{xx}(f_0)| = \frac{1}{4L f_0^2} \sqrt{\frac{E_s}{M}}. \quad (8.19)$$

It is interesting to see how an elastic bar, once excited by a GW, evolves in time. If we are interested in the long-time behavior of the signal, we must take into account that the energy E_s absorbed by the bar will be slowly dissipated by internal frictions. As we mentioned before, this dissipation takes place on a time-scale of about 600 s, which is much longer than the duration of a burst. Therefore, while the absorption of energy from a GW burst is extremely well described by eq. (8.13), to

³This value of the effective mass simply reflects the normalization of the normal modes. Here we have chosen $\sin[\pi x(2n+1)/L]$ as normal modes, which are normalized as in eq. (8.9). If we rather choose as normal modes $\Psi_n = \sqrt{2} \sin[\pi x(2n+1)/L]$ and we expand $u(x, t) = \sum_n a_n(t) \Psi_n(x)$, then $\xi_n(t) = \sqrt{2} a_n(t)$ and the effective mass of $a_n(t)$ is M rather than $M/2$. In Section 8.4, when we discuss resonant spheres, we will in fact adopt the latter normalization.

⁴See, e.g. Landau and Lifshitz, Vol. I (1976), eq. (22.12).

⁵Observe that this relation is completely independent of the shape of the burst, and E_s depends only on the Fourier component of the GW at the bar’s resonance frequency f_0 . This is a consequence of the fact that the duration of the burst τ_g is much smaller than the dissipation time so, as far as the absorption of energy from a burst is concerned, the resonance can be considered infinitely narrow.

study the subsequent time development of the signal we must generalize this equation to

$$\ddot{\xi}_0 + \gamma_0 \dot{\xi}_0 + \omega_0^2 \xi_0 = \frac{2L}{\pi^2} \ddot{h}_{xx}, \quad (8.20)$$

where γ_0 describes the effect of dissipation on the mode ξ_0 . A very important parameter is the *quality factor* of the bar (or, more precisely, of the mode ξ_0) Q_0 , defined by⁶

$$Q_0 = \frac{\omega_0}{\gamma_0}. \quad (8.21)$$

Experimentally, values of Q_0 of order 3×10^6 (and even up to 2×10^7) are obtained in bars at cryogenic temperatures, which corresponds, for $f_0 \sim 900$ Hz, to a relaxation time $1/\gamma_0 \sim 600$ s.

Equation (8.20) is easily solved going in Fourier space,

$$\tilde{\xi}_0(\omega) = T_0(\omega) \tilde{h}_{xx}(\omega), \quad (8.22)$$

where⁷

$$T_0(\omega) = \frac{2L}{\pi^2} \frac{\omega^2}{\omega^2 - \omega_0^2 + i\gamma_0\omega} \quad (8.23)$$

is called the transfer function for the mode ξ_0 . The form of $|T_0(\omega)|^2$ is shown in Fig. 8.1. We write $\omega^2 - \omega_0^2 + i\gamma_0\omega = (\omega - \bar{\omega}_+)(\omega - \bar{\omega}_-)$ with

$$\bar{\omega}_\pm = \pm \sqrt{\omega_0^2 - (\gamma_0/2)^2} - i\frac{\gamma_0}{2}. \quad (8.24)$$

In a typical bar γ_0 is smaller than ω_0 by a factor $Q_0 = O(10^6)$ so the second term in the square root is completely negligible and

$$\bar{\omega}_\pm \simeq \pm \omega_0 - i\frac{\gamma}{2}. \quad (8.25)$$

Then eq. (8.22) gives

$$\xi_0(t) = \frac{2L}{\pi^2} \int_{-\infty}^{\infty} \frac{d\omega}{2\pi} \frac{\omega^2 \tilde{h}_{xx}(\omega)}{(\omega - \bar{\omega}_+)(\omega - \bar{\omega}_-)} e^{-i\omega t}. \quad (8.26)$$

As an example, we consider the case of a Dirac delta perturbation,

$$h_{xx}(t) = h_0 \tau_g \delta(t). \quad (8.27)$$

As discussed below eq. (7.99), this can be taken as a crude description of a burst of amplitude h_0 and duration τ_g . For the Dirac delta perturbation, the Fourier transform $\tilde{h}_{xx}(\omega) = h_0 \tau_g$ is a constant and

$$\xi_0(t) = \frac{2L}{\pi^2} h_0 \tau_g \int_{-\infty}^{\infty} \frac{d\omega}{2\pi} \frac{\omega^2}{(\omega - \bar{\omega}_+)(\omega - \bar{\omega}_-)} e^{-i\omega t}. \quad (8.28)$$

For $t < 0$ we can close the contour in the upper half-plane and, since $\bar{\omega}_\pm$ both lies below the real axis, see eq. (8.24), we get zero, as required by causality. For $t > 0$ we close the contour in the lower half-plane, where we pick the contribution of the two poles at $\omega = \bar{\omega}_\pm$, and we get

$$\xi_0(t) \simeq -\frac{2L}{\pi^2} h_0 \omega_0 \tau_g e^{-\gamma_0 t/2} \sin \omega_0 t. \quad (8.29)$$

We therefore have damped oscillations, and we see that, even if the GW burst lasts only a few ms, the bar continues to ring for a very long time, of order 10 min.

⁶In later sections we will meet other quality factors, like that of the transducer, or the total mechanical quality factor of the bar-transducer system. To avoid confusion, we denote by Q_0 (rather than simply by Q , as usually done in the literature) the quality factor of the mode ξ_0 .

⁷The sign of the factor $i\gamma_0\omega$ depends on our conventions on the Fourier transform (see the Notation). Often in the literature the opposite convention on the Fourier transform is used, $F(t) = \int [d\omega/(2\pi)] \tilde{F}(\omega) e^{i\omega t}$, and then $T_0(\omega) = (2L/\pi^2) \omega^2 / (\omega^2 - \omega_0^2 - i\gamma_0\omega)$.

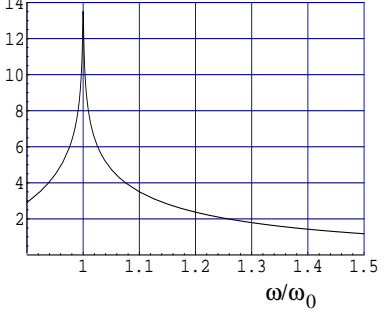


Fig. 8.1 The logarithm of the function $|(\pi^2/2L)T_0(\omega)|^2$, against ω/ω_0 , for $Q_0 = 10^3$.

8.1.2 The response to periodic signals

We have seen that the fundamental mode of a resonant bar has an intrinsic time-scale $\tau_0 = 1/\gamma_0 \sim 10$ min, which is the time on which it dissipates its elastic energy due to internal frictions. GW bursts have a typical duration of the order of the ms, and therefore dissipation effects are completely negligible as long as we are interested in the total energy absorbed from the GW. For this reason, we could compute the energy absorbed by the bar during a burst setting $\gamma_0 = 0$, and the basic equation (8.19) is independent of γ_0 .

For a periodic signal at the resonant frequency ω_0 the situation is different. Operatively, a periodic signal is just a wave-packet with frequencies around the resonant frequency ω_0 of the bar, sufficiently narrow in frequency space, so that its temporal duration is much longer than $1/\gamma_0 \simeq 10$ min. In the limiting case of an exactly monochromatic wave the temporal duration of the signal becomes infinite. If an ideal harmonic oscillator, with no losses, is driven by an exactly periodic force at its resonant frequency, its amplitude (and therefore the energy it absorbs) grows indefinitely. In a real harmonic oscillator there is a damping force proportional to $\gamma_0 \dot{\xi}_0$ which becomes larger and larger as $\dot{\xi}_0$ grows, until the losses become so large that they compensate for the energy absorbed by the external source. At this point a stationary regime is reached.

To study the response of the fundamental mode of the bar to periodic signals we must therefore use eq. (8.20). We consider a wave propagating along the z axis,

$$h_{xx}(t) = h_0 \operatorname{Re} [e^{-i\omega(t-z/c)}] , \quad (8.30)$$

where h_0 is a real constant and Re denotes the real part. The bar is located in the plane $z = 0$, so

$$\ddot{\xi}_0 + \gamma_0 \dot{\xi}_0 + \omega_0^2 \xi_0 = -\frac{2Lh_0\omega^2}{\pi^2} \operatorname{Re} [e^{-i\omega t}] , \quad (8.31)$$

and a particular solution of this inhomogeneous equation is

$$\begin{aligned} \xi_0(t) &= \frac{2Lh_0\omega^2}{\pi^2} \operatorname{Re} \left[\frac{e^{-i\omega t}}{\omega^2 - \omega_0^2 + i\gamma_0\omega} \right] \\ &= \frac{2Lh_0\omega^2}{\pi^2} \frac{(\omega^2 - \omega_0^2) \cos \omega t - \gamma_0\omega \sin \omega t}{(\omega^2 - \omega_0^2)^2 + \gamma_0^2\omega^2} . \end{aligned} \quad (8.32)$$

The energy of this solution is found from eq. (8.15). If $\omega = \omega_0$ it is time-independent, and is given by

$$\begin{aligned} E &= \frac{M}{4} (\dot{\xi}_0^2 + \omega_0^2 \xi_0^2) \\ &= \frac{1}{\pi^4} M L^2 h_0^2 \omega_0^2 Q_0^2 , \end{aligned} \quad (8.33)$$

where $Q_0 = \omega_0/\gamma_0$. This shows that eq. (8.32) describes an equilibrium state where the energy absorbed by the wave is compensated by the

losses due to friction. For an ideal oscillator, $Q_0 \rightarrow \infty$ and therefore $E \rightarrow \infty$. A bar which initially is not excited and which is then hit by a wave-packet centered around ω_0 , with a spread of frequencies $\Delta\omega \ll \omega_0$, reaches asymptotically this solution after a transient time of order $1/\gamma_0$. At $\omega = \omega_0$ eq. (8.32) becomes

$$\xi_0(t) = -\frac{2L}{\pi^2} \frac{h_0\omega_0}{\gamma_0} \sin \omega_0 t. \quad (8.34)$$

Comparing this with the situation in which the bar is hit by a Dirac delta excitation, eq. (8.29) we see that, first of all, there is no exponential decay $\exp\{-\gamma_0 t/2\}$, since the periodic wave continuously feeds energy into the bar, compensating for the internal losses. And, second, the overall amplitude is much larger since $\tau_g \sim 1$ ms is now replaced by $1/\gamma_0 \sim 600$ s. Physically this is clearly understood: a burst excites the bar only for the short time τ_g , while under a periodic perturbation the amplitude of the oscillation keeps increasing for a time $1/\gamma_0$, until the rate of losses due to dissipation become equal to the rate at which energy is feed in by the GW, and an equilibrium regime is established.

8.1.3 The absorption cross-section

Equation (8.32) in principle characterizes completely the response of a bar to a monochromatic wave. However, it is instructive to express this result in terms of the cross-section of the bar for GW absorption.⁸ The power absorbed by an oscillator with velocity $\dot{\xi}_0$ subject to a force $F(t)$ is $F(t)\dot{\xi}_0$. In our case, recalling that the effective mass of the mode $\dot{\xi}_0$ is $M/2$, the force is

$$\begin{aligned} F &= \frac{M}{2} \frac{2L}{\pi^2} \ddot{h}_{xx} \\ &= -\frac{MLh_0\omega^2}{\pi^2} \cos \omega t, \end{aligned} \quad (8.35)$$

and, using eq. (8.32),

$$F(t)\dot{\xi}_0 = 2M \left(\frac{Lh_0\omega^2}{\pi^2} \right)^2 \frac{\omega(\omega^2 - \omega_0^2) \sin \omega t \cos \omega t + \gamma_0\omega^2 \cos^2 \omega t}{(\omega^2 - \omega_0^2)^2 + \gamma_0^2\omega^2}. \quad (8.36)$$

Since the energy of the incoming waves is defined as an average over several cycles, we are more interested in the average power absorbed over a cycle,

$$\begin{aligned} \frac{dE_{\text{abs}}}{dt} &\equiv \langle F(t)\dot{\xi}_0 \rangle \\ &= \frac{ML^2h_0^2}{\pi^4} \frac{\gamma_0\omega^6}{(\omega^2 - \omega_0^2)^2 + \gamma_0^2\omega^2}. \end{aligned} \quad (8.37)$$

In particular, at the resonance frequency

$$\frac{dE_{\text{abs}}}{dt} = \frac{1}{\pi^4} ML^2 h_0^2 \omega_0^3 Q_0. \quad (8.38)$$

⁸We limit ourselves for the moment to a wave with pure + polarization, propagating in a direction perpendicular to the bar. See page 425 for the most general result.

Comparing with eq. (8.33) we see that at the resonant frequency (and once we have reached the stationary regime, where the solution for a bar initially at rest approaches (8.32)) $dE_{\text{abs}}/dt = \gamma_0 E$. Of course dE_{abs}/dt depends both on the properties of the bar and on the intensity of the incoming radiation. A quantity that characterizes uniquely the detector is the *absorption cross-section* $\sigma_{\text{abs}}(\omega)$, defined by

$$\frac{dE_{\text{abs}}}{dt} = \sigma_{\text{abs}}(\omega) \frac{dE_{\text{in}}}{dAdt}, \quad (8.39)$$

where ω is the frequency of the incoming monochromatic wave and E_{in} is the incoming energy, so $dE_{\text{in}}/dAdt$ is the energy arriving per unit time on a unit area, again averaged over a few cycles, as we always do for the energy of a wave. We consider a GW propagating along the z direction, with $h_+ = h_{xx} = h_0 \cos \omega t$ and $h_x = 0$. Then, using eq. (1.155),

$$\frac{dE_{\text{in}}}{dAdt} = \frac{c^3 h_0^2 \omega^2}{32\pi G}, \quad (8.40)$$

(where we used $\langle \cos^2 \omega t \rangle = 1/2$), and therefore

$$\sigma_{\text{abs}}(\omega) = \frac{32\gamma_0 GML^2}{\pi^3 c^3} \frac{\omega^4}{(\omega^2 - \omega_0^2)^2 + \gamma_0^2 \omega^2}. \quad (8.41)$$

At the resonance frequency we have⁹

$$\sigma_{\text{abs}}(\omega_0) = \frac{32GML^2\omega_0 Q_0}{\pi^3 c^3}. \quad (8.42)$$

The cross-section at resonance, however, is not really the best indicator of the detector sensitivity. Consider for instance a wave-packet whose Fourier modes $\tilde{h}(\omega)$ are approximately constant over a narrow interval $\omega_1 < \omega < \omega_2$ which includes the resonance frequency of the bar ω_0 . The response of a bar to this wave-packet is determined by the integral of the cross-section

$$\int_{\omega_1}^{\omega_2} \frac{d\omega}{2\pi} \sigma(\omega). \quad (8.43)$$

Since the cross-section is peaked around the resonance frequency ω_0 , to compute this integral we can approximate $\sigma(\omega)$ using

$$\frac{\omega^4}{(\omega - \omega_0)^2(\omega + \omega_0)^2 + \gamma_0^2 \omega^2} \simeq \frac{\omega_0^2}{4(\omega - \omega_0)^2 + \gamma_0^2}. \quad (8.44)$$

This approximation is the leading term in an expansion in $\gamma_0/\omega_0 = 1/Q_0$. Since $Q_0 \gg 1$, to a very good accuracy we have¹⁰

$$\int_{\omega_1}^{\omega_2} \frac{d\omega}{2\pi} \sigma(\omega) \simeq \frac{32\gamma_0 GML^2}{\pi^3 c^3} \int_{-\infty}^{\infty} \frac{d\omega}{2\pi} \frac{\omega_0^2}{4(\omega - \omega_0)^2 + \gamma_0^2}. \quad (8.45)$$

Then, to leading order in $1/Q_0$, we find

$$\begin{aligned} \Sigma_0 &\equiv \int_{-\infty}^{\infty} \frac{d\omega}{2\pi} \sigma_{\text{abs}}(\omega) \\ &= \frac{8GML^2\omega_0^2}{\pi^3 c^3}. \end{aligned} \quad (8.46)$$

⁹Numerically, setting $M = 2270$ kg, $L = 3$ m, $f_0 = 1$ kHz and $Q = 10^6$, we get $\sigma_{\text{abs}}(\omega_0) \simeq 3 \times 10^{-18}$ cm², which can be written as $\sigma_{\text{abs}}(\omega_0) = \pi r^2$, with $r \simeq 10^{-9}$ cm. It is amusing to see that, even at the resonance, the cross-section for absorption of GWs of a whole two-ton bar is of order of the cross-section of a hard sphere (i.e. a sphere that absorbs with unit probability everything that arrives within its radius r) with a typical atomic size. This reflects of course the weakness of the gravitational interaction.

¹⁰Observe that we extended the integral from $-\infty$ to $+\infty$. The error that we are introducing is negligible because the contribution to the integral from the region $|\omega - \omega_0| \gg \gamma_0$ is very small. For the same region, the detailed form of the incoming wave-packet is not important.

Using eq. (8.14) we can express ω_0 in terms of the speed of sound in the material, $\omega_0 = \pi v_s / L$, and then

$$\Sigma_0 = \frac{8}{\pi} \frac{GM}{c} \left(\frac{v_s}{c} \right)^2. \quad (8.47)$$

This shows that the result depends only on the mass M of the bar, and on the speed of sound in the material. Numerically, for an aluminum bar with mass $M = 2270$ kg, $\Sigma_0 \simeq 4.4 \times 10^{-21}$ cm² Hz.¹¹

Observe that the integrated cross-section is independent of Q_0 , because the peak value of $\sigma(\omega)$ is proportional to Q_0 , but such a large value is obtained only over a range $\Delta\omega \sim 1/Q_0$, so Q_0 cancels in $\int d\omega \sigma(\omega)$. More precisely, from the explicit expressions we see that the integrated cross-section is related to the cross-section at the peak by

$$\Sigma_0 = \frac{\gamma_0}{4} \sigma_{\text{abs}}(\omega_0). \quad (8.49)$$

Naively, one might then think that the value of Q_0 is not relevant for the performance of the detector. However, what really matters for detection is the ratio between the signal and the noise. In Section 8.3 we will discuss the possible sources of noise and we will appreciate the importance of having a large Q_0 .

We will see below that, despite the fact that a resonant bar is a macroscopic object, weighting more than two tons, one is able to detect bar's oscillations which are so small that a classical treatment is no longer adequate, and it is instead appropriate to describe them in terms of the number of phonons that are excited.¹² It is therefore instructive to verify that the cross-section (8.46) is recovered in a quantum treatment of the fundamental mode ξ_0 .

We have seen that the variable ξ_0 describes a harmonic oscillator of mass $m_0 = M/2$ and frequency ω_0 . According to the standard rules of quantum mechanics, we promote it to an operator and we write

$$\xi_0 = \left(\frac{\hbar}{M\omega_0} \right)^{1/2} (a + a^\dagger), \quad (8.50)$$

with a, a^\dagger the creation and annihilation operators, and $[a, a^\dagger] = 1$ (compare with eqs. (8.171) and (8.172) below). The free Hamiltonian of the quantum oscillator is given by the familiar expression $H_0 = \hbar\omega_0(a^\dagger a + 1/2)$ and acts on the harmonic oscillator states labeled by $|n\rangle$. In a quantum field theory interpretation, the state vector $|n\rangle$ describes a collection of n phonons, each one with frequency ω_0 . To compute the cross-section we study the interaction of this quantum harmonic oscillator with the classical external force given in eq. (8.35),¹³

$$F(t) = -(1/\pi^2)MLh_0\omega^2 \cos \omega t. \quad (8.51)$$

We define the interaction Hamiltonian from $F = -\partial H_{\text{int}}/\partial\xi_0$. In the quantum treatment the interaction Hamiltonian is then

$$H_{\text{int}} = \frac{1}{\pi^2} MLh_0\omega^2 \xi_0 \cos \omega t$$

¹¹Using eq. (8.11), it is straightforward to repeat the above computation for the n -th longitudinal mode ξ_n of the bar. Its resonance frequency is $\omega_n = (2n + 1)\omega_0$, and for the cross-section, integrated around ω_n , we get

$$\Sigma_n = \frac{1}{(2n + 1)^2} \Sigma_0. \quad (8.48)$$

Thus, the first excited mode of the bar which couples to GWs (ξ_n with $n = 1$) is at a frequency $f_1 = 3f_0$, and its integrated cross-section Σ_1 is smaller by a factor of 9 compared to the integrated cross-section Σ_0 of the fundamental mode.

¹²In particular, we will discuss in Sections 8.3.3 and 8.3.4 that the ultimate limitation of resonant bars, unless one uses quantum non-demolition techniques, is given by the so-called “standard quantum limit”, where we are detecting single-phonon transitions induced by the GW.

¹³Any detectable GW is exceedingly classical, so we only need to use a quantum description for the oscillator.

$$= \frac{1}{\pi^2} (MLh_0\omega^2 \cos \omega t) \left(\frac{\hbar}{M\omega_0} \right)^{1/2} (a + a^\dagger). \quad (8.52)$$

We assume that before the arrival of the GW the oscillator ξ_0 is in its ground state $|0\rangle$. To first order in perturbation theory, the interaction Hamiltonian (8.52) induces transitions to the state $|1\rangle$, with a transition amplitude

$$\begin{aligned} T_{0 \rightarrow 1} &= -\frac{i}{\hbar} \int_{-\infty}^{\infty} dt e^{-i\omega_0 t} \langle 1 | H_{\text{int}} | 0 \rangle \\ &= -i \frac{MLh_0\omega_0^2}{2\pi^2(\hbar M\omega_0)^{1/2}} 2\pi\delta(\omega - \omega_0), \end{aligned} \quad (8.53)$$

where we have taken $\omega_0 > 0$, $\omega > 0$. The probability that a transition takes place at any time is $|T_{0 \rightarrow 1}|^2$. We regularize the time interval restricting to $-T/2 < t < T/2$, and therefore the transition rate is

$$\lim_{T \rightarrow \infty} \frac{1}{T} |T_{0 \rightarrow 1}|^2 = \frac{ML^2 h_0^2 \omega_0^3}{2\pi^3 \hbar} \delta(\omega - \omega_0), \quad (8.54)$$

where we used the fact that, on a finite time interval $-T/2 < t < T/2$,

$$2\pi\delta(\omega) = \int_{-T/2}^{T/2} dt e^{i\omega T}, \quad (8.55)$$

and therefore $2\pi\delta(\omega = 0) = T$. In each transition is absorbed an energy $\hbar\omega_0$, therefore the energy absorbed per unit time is

$$\frac{dE_{\text{abs}}}{dt} = \frac{ML^2 h_0^2 \omega_0^4}{2\pi^3} \delta(\omega - \omega_0). \quad (8.56)$$

The incoming flux corresponding to the force $F(t)$ is given by eq. (8.40). Using eq. (8.39), we then obtain

$$\sigma_{\text{abs}} = \frac{32GML^2 f_0^2}{\pi c^3} \delta(f - f_0). \quad (8.57)$$

Of course, having neglected the decay width of the excited quantum state, the cross-section is a Dirac delta rather than a curve with the Breit–Wigner shape (8.41). To compare with the classical calculation, it is simpler to consider the integral of σ_{abs} around the resonance, and from eq. (8.57) we get

$$\int df \sigma_{\text{abs}} = \frac{32GML^2 f_0^2}{\pi c^3}, \quad (8.58)$$

in agreement with eq. (8.46). It is not difficult to check that the same result is obtained if the initial state of the oscillator is a generic state $|n\rangle$ rather than $|0\rangle$. (Observe that in this case the quantity relevant for the absorption of energy is $|T_{n \rightarrow n+1}|^2 - |T_{n \rightarrow n-1}|^2$).

Angular sensitivity and pattern functions

We have seen that the output of a resonant bar with its axis along the x direction is determined by the value of $h_{xx}(t)$. More generally, if we denote by $\hat{\mathbf{l}}$ the unit vector in the direction of the longitudinal axis of the bar, the scalar output is $h(t) = \hat{l}^i \hat{l}^j h_{ij}(t)$. Comparing with eq. (7.1) we see that the detector tensor of the bar is

$$D^{ij} = \hat{l}^i \hat{l}^j. \quad (8.59)$$

Since h_{ij} is traceless, we can equivalently choose to define D^{ij} in the traceless form $D^{ij} = \hat{l}^i \hat{l}^j - (1/3)\delta^{ij}$. We now compute the pattern functions, defined in Section 7.1, for a cylindrical bar. The geometry is illustrated in Fig. 8.2. We denote by $\hat{\mathbf{n}}$ the unit vector in the propagation direction of the GW, with polar angles (θ, ϕ) . We use as polar axis the longitudinal axis of the bar, so θ is the angle between $\hat{\mathbf{n}}$ and the x axis and, because of the cylindrical symmetry of the bar, we can take $\phi = 0$ without loss of generality. In Fig. 8.2, we have a reference frame (x, y, z) , where the bar is along x axis and the y axis is perpendicular to the plane of the page, in the downward direction. Since we have set $\phi = 0$, the source is in the (x, z) plane. We introduce a second reference frame (x', y', z') such that the propagation direction $\hat{\mathbf{n}}$ of the GW coincides with the z' axis, and the y' axis is parallel to the y axis. Therefore the plane defined by the (x, z) axis is the same as the plane defined by the (x', z') axes (and is the plane of the page). The (x, z) axes are obtained from the (x', z') axis performing a counterclockwise rotation by an angle $\alpha = (\pi/2) - \theta$ around the y axis. In the (x', y', z') frame the GW has the form

$$h'_{ij} = \begin{pmatrix} h_+ & h_\times & 0 \\ h_\times & -h_+ & 0 \\ 0 & 0 & 0 \end{pmatrix}_{ij}, \quad (8.60)$$

where $h_{+, \times}$ are defined with respect to the (x', y') axes. To find the form of this GW in the (x, y, z) frame, we must compute how this tensor transforms under the rotation that brings the (x', y', z') frame onto the (x, y, z) frame. This rotation is described by the matrix

$$\mathcal{R} = \begin{pmatrix} \cos \alpha & 0 & \sin \alpha \\ 0 & 1 & 0 \\ -\sin \alpha & 0 & \cos \alpha \end{pmatrix}, \quad (8.61)$$

with $\sin \alpha = \cos \theta$ and $\cos \alpha = \sin \theta$. The components of the tensor h_{ij} in the (x, y, z) frame are obtained from the components h'_{ij} in the (x', y', z') frame by $h_{ij} = \mathcal{R}_{ik}\mathcal{R}_{jl}h'_{kl}$. Then

$$\begin{aligned} h_{xx} &= \mathcal{R}_{1k}\mathcal{R}_{1l}h'_{kl} \\ &= h_+[(\mathcal{R}_{11})^2 - (\mathcal{R}_{12})^2] + 2h_\times\mathcal{R}_{11}\mathcal{R}_{12} \\ &= h_+ \sin^2 \theta. \end{aligned} \quad (8.62)$$

Then we find $F_+(\hat{\mathbf{n}}; \psi = 0) = \sin^2 \theta$ and $F_\times(\hat{\mathbf{n}}; \psi = 0) = 0$. The label $\psi = 0$ in $F_{+,\times}$ refers to the fact that these are the values of the pattern

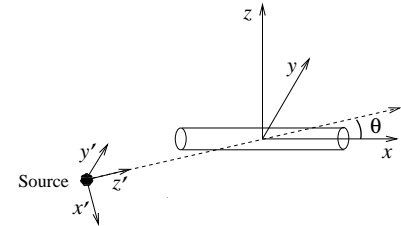


Fig. 8.2 The relation between the (x, y, z) and the (x', y', z') reference frames.

¹⁴In general, a useful choice of axes, i.e. a preferred value of ψ , could be suggested by the geometry of the source. For instance, if the source is a binary star in an elliptic orbit, with the plane of the orbit perpendicular to the z' axis, a preferential frame will be given by the two major axes of the ellipse, and in this frame the GW amplitudes h_+ and h_\times have a simpler form.

functions when the plus and cross polarizations are defined with respect to the (x', y') axes. More generally, we might wish to refer the plus and cross polarizations to another system of axes, obtained rotating the (x', y') axes by an angle ψ around the z' axis.¹⁴ We have already seen in eqs. (7.31) and (7.32) how F_+ and F_\times transform under such a rotation, and then we get

$$h_{xx} = F_+(\hat{\mathbf{n}}; \psi)h_+ + F_\times(\hat{\mathbf{n}}; \psi)h_\times, \quad (8.63)$$

with

$$F_+(\hat{\mathbf{n}}; \psi) = \sin^2 \theta \cos 2\psi, \quad F_\times(\hat{\mathbf{n}}; \psi) = \sin^2 \theta \sin 2\psi. \quad (8.64)$$

We see that the pattern functions have been determined by two factors: the geometry of the detector (which, in the case of resonant bars, is reflected in the fact that only the component h_{xx} enters, where x is the bar axis) and the transformation property of h_{ij} under rotations.

In general, we do not have experimental information on the polarization state of the wave, i.e. we do not know with respect to which axes the GW takes a given form. This could be the situation, for instance, when we search for GWs from a binary system of which we do not know the orientation of the orbit. In this case it can be useful to average $|\tilde{h}_{xx}(f)|^2$ over the angle ψ . We denote this average by $\langle \dots \rangle_\psi$. Using eqs. (8.63) and (8.64) and the fact that $\langle \cos^2 2\psi \rangle_\psi = \langle \sin^2 2\psi \rangle_\psi = 1/2$ while $\langle \sin 2\psi \cos 2\psi \rangle_\psi = 0$ we get

$$\langle |\tilde{h}_{xx}(f)|^2 \rangle_\psi = \frac{1}{2} \sin^4 \theta \left(|\tilde{h}_+(f)|^2 + |\tilde{h}_\times(f)|^2 \right). \quad (8.65)$$

In eq. (8.47) we found the bar cross-section for a wave arriving from optimal direction, $\theta = \pi/2$, and a purely + polarization with optimal angle $\psi = 0$. We can now compute the bar cross-section for waves with arbitrary arrival direction. In the incoming energy, eq. (8.40), h_0^2 is replaced by $|h_+|^2 + |h_\times|^2$ (in eq. (8.40) we limited ourselves to the case $h_+ = h_0$, $h_\times = 0$) while, if we average over the polarization, from eq. (8.65) we find that in the absorbed energy h_0^2 is replaced by $(1/2) \sin^4 \theta (|h_+|^2 + |h_\times|^2)$. Therefore the cross-section (8.47) is replaced by

$$\langle \Sigma_0(\theta) \rangle_\psi = \left(\frac{1}{2} \sin^4 \theta \right) \frac{8}{\pi} \frac{GM}{c} \left(\frac{v_s}{c} \right)^2. \quad (8.66)$$

The factor $\sin^4 \theta$ is the price that we pay when the wave arrives from a non-optimal direction, while the factor $1/2$ reflects the fact that we are averaging over ψ rather than taking the optimal value. For GWs coming from all directions, a conventional measure of the sensitivity can be given by the average of this cross-section over the solid angle. Since the average of $\sin^4 \theta$ over the solid angle is $8/15$, we find

$$\langle \Sigma_0(\theta) \rangle_{\psi, \theta} = \frac{32}{15\pi} \frac{GM}{c} \left(\frac{v_s}{c} \right)^2. \quad (8.67)$$

8.2 The read-out system: how to measure extremely small displacements

A resonant mass is a device that absorbs a very small fraction of the energy of the incoming GW and transforms it into mechanical oscillations. The next task is to detect these oscillations. It is here that most of the experimental ingenuity enters, and in fact the great improvements in the sensitivities of resonant bars from the times of Weber are due mostly to two factors: (1) The fact that bars have been cooled to cryogenic temperatures, as low as 0.1 K. (2) The continuous improvements in the read-out system.

To have a first idea of the difficulty of the problem, recall from eq. (8.29) that a GW burst with amplitude h_0 , typical frequency f_0 and duration $\tau_g \sim 1/f_0$ drives oscillations of the fundamental mode of the bar with an amplitude $\xi_0 \sim Lh_0$. From eqs. (7.109) and (7.112) we see that even a supernova explosion in our Galaxy, which is an event that takes place only a few times per century and, from numerical simulations, is expected to release 10^{-6} – 10^{-7} solar masses in GWs in a few milliseconds, would produce on Earth a GW with at most $h_0 \sim 10^{-20}$. More realistically, to have some chances of detection we might need to reach a value $h_0 \sim 10^{-21}$. This gives

$$\xi_0 \sim 3 \times 10^{-21} \text{ m} \quad (8.68)$$

for a bar with $L \simeq 3$ m. This is a factor 10^6 smaller than the size of a nucleus, so such a measure might seem hopeless. As we will see in this and in the next section, this is not so, at least at a sensitivity level of $\xi_0 \sim 10^{-19}$ – 10^{-18} m, where resonant bars already perform routinely measurements. There are two main issues to address here. First, how it is possible to detect, in absolute terms, such a small displacement. This will be the subject of this section. The second issue is how to make sure that the effect of GWs is not swamped by much larger noise, and will be discussed in the next section.

Before entering into technical aspects, however, it is important to realize that what we want to measure is indeed an extremely small displacement, but it is a coherent displacement of a macroscopic body, such as the end-face of the bar, or the mirror of an interferometer. If we wanted to detect a displacement such as that given in eq. (8.68) on a microscopic scale, this would be utterly impossible. At the atomic scale, the notion of position of the bar end-point is not even defined with that precision. However, our sensors really detect the displacement of a macroscopic portion of the bar face (or of the mirror of an interferometer), and in this case the individual fluctuations at the microscopic level average out, and we are only left with the coherent part of the motion. It is intuitively clear, and we will see it quantitatively in the next section, that for instance thermal noise cannot easily generate collective vibrations of a very heavy object. The other important clue is that we do not really want to measure the displacement $\xi_0(t)$, but just some of

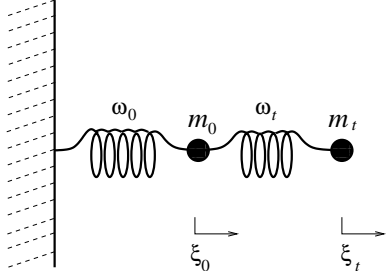


Fig. 8.3 The schematization of the bar-transducer system as a double oscillator.

¹⁵In the pioneering times of Weber the transducer was a piezoelectric, i.e. a material (a ceramic or a crystal) that, under mechanical compression, becomes polarized and generates an electric field. So a piezoelectric is really sensitive to the strain $\partial\xi/\partial x$. For the mode ξ_n the spatial dependence is $\sin[\frac{\pi x}{L}(2n+1)]$ and

$$\frac{\partial}{\partial x} \sin[\frac{\pi x}{L}(2n+1)] \sim \cos[\frac{\pi x}{L}(2n+1)]. \quad (8.69)$$

Therefore the strain is maximum near the center of the bar, and the piezoelectrics were glued on the bar surface, near the midpoint. Modern resonant bars operate at low (2–4 K) or ultra-low (0.1–0.5 K) temperatures, both to reduce the thermal noise and to allow for the use of superconducting devices like SQUIDs in the read-out. Piezoelectrics, instead, are not suitable for cryogenic detectors, since some of their properties degrade at low temperatures; in particular, they have high intrinsic losses and therefore they lower the Q factor of the system. Piezoelectrics have therefore been abandoned, and all recent resonant-mass detectors have used the resonant transducer scheme.

¹⁶This schematization neglects back-action forces, that will be treated in Section 8.3.3. It also neglects the effect of the electric oscillator that performs the transduction process, see Section 8.2.2.

its Fourier modes $\tilde{\xi}_0(f)$, in a frequency window where the effect of the GW is important. In this sense, eq. (8.68) is a bit misleading. The GWs that we are searching do indeed produce a displacement of this order in $\xi_0(t)$, but in Fourier space their contribution is localized in some frequency range, so we only have to fight against the Fourier modes of the noise in the same frequency range.

We now enter in the detail of how such a small displacement can be measured. In general, it is necessary to use a transducer, i.e. an object that transforms the displacement into an electric signal. A particularly convenient scheme is the *resonant transducer*. In a resonant transducer the displacement, before being converted into an electric signal, is amplified mechanically. This is obtained coupling the bar to an oscillator with a light mass. We will see in Section 8.2.2 how such a device is actually built, but for the moment we can simply schematize this system as a double oscillator, consisting of an oscillator with (effective) mass m_0 and frequency ω_0 coupled to an oscillator of (effective) mass m_t and frequency ω_t , as shown in Fig. 8.3. The first oscillator represents the fundamental mode of the bar, and we denote its displacement from the equilibrium position by $\xi_0(t)$. As we found in eq. (8.15), its effective mass m_0 is equal to $M/2$, where M is the mass of the bar. The second mass represents instead the transducer, and we denote its displacement from the equilibrium position by $\xi_t(t)$.¹⁵

8.2.1 The double oscillator

As a first step, we discuss the dynamics of the double oscillator. For the moment, we neglect dissipation effects. Then the system is described by the Lagrangian

$$L = \frac{1}{2}m_0\dot{\xi}_0^2 + \frac{1}{2}m_t\dot{\xi}_t^2 - V(\xi_0, \xi_t), \quad (8.70)$$

with

$$V(\xi_0, \xi_t) = \frac{1}{2}m_0\omega_0^2\xi_0^2 + \frac{1}{2}m_t\omega_t^2(\xi_t - \xi_0)^2. \quad (8.71)$$

Defining $\mu = m_t/m_0$, the equations of motion in the presence of external forces F_0 and F_t acting on ξ_0 and ξ_t , respectively, are¹⁶

$$\ddot{\xi}_0 + \omega_0^2\xi_0 + \mu\omega_t^2(\xi_0 - \xi_t) = \frac{F_0}{m_0}, \quad (8.72)$$

$$\ddot{\xi}_t + \omega_t^2(\xi_t - \xi_0) = \frac{F_t}{m_t}. \quad (8.73)$$

These equations are easily solved performing the Fourier transform and inverting the resulting 2×2 matrix. Consider in particular the response of the system to an impulsive force on the bar, like a GW burst, so that $F_0/m_0 = a_0\delta(t)$, while we set $F_t = 0$, since the direct effect of the GWs on the light mass is much smaller than the “kick” that it receives from the bar, when the latter is hit by a GW. Then we get

$$\tilde{\xi}_0(\omega) = a_0 \frac{-\omega^2 + \omega_t^2}{(\omega^2 - \omega_+^2)(\omega^2 - \omega_-^2)}, \quad (8.74)$$

$$\tilde{\xi}_t(\omega) = a_0 \frac{\omega_t^2}{(\omega^2 - \omega_+^2)(\omega^2 - \omega_-^2)}, \quad (8.75)$$

where ω_{\pm}^2 are the solutions of

$$\omega^4 - [\omega_0^2 + (1 + \mu)\omega_t^2]\omega^2 + \omega_0^2\omega_t^2 = 0. \quad (8.76)$$

We see that the bar-transducer system has two resonance frequencies ω_{\pm} . Formally, at $\omega = \omega_{\pm}$, eqs. (8.74) and (8.75) state that $\tilde{\xi}_0(\omega)$ and $\tilde{\xi}_t(\omega)$ diverge. Once we include the dissipation terms in the equations, as we will do below, ω_{\pm} get an imaginary part and $\tilde{\xi}_0(\omega)$ and $\tilde{\xi}_t(\omega)$ at the resonances are large but finite. From eqs. (8.74) and (8.75) we get

$$\xi_0(t) = a_0 \int_{-\infty}^{\infty} \frac{d\omega}{2\pi} \frac{-\omega^2 + \omega_t^2}{(\omega^2 - \omega_+^2)(\omega^2 - \omega_-^2)} e^{-i\omega t}, \quad (8.77)$$

$$\xi_t(t) = a_0 \int_{-\infty}^{\infty} \frac{d\omega}{2\pi} \frac{\omega_t^2}{(\omega^2 - \omega_+^2)(\omega^2 - \omega_-^2)} e^{-i\omega t}. \quad (8.78)$$

Actually, these integrals are well defined only after we give a prescription for displacing the four poles (at $\omega = \pm\omega_+$ and at $\omega = \pm\omega_-$) from the real axis. In principle, we can find explicitly the imaginary parts of the poles including the dissipation terms in the equations, as indeed we will do below. However, this is not really necessary here, since the position of the poles with respect to the real axis is fixed by causality: $\xi_0(t)$ and $\xi_t(t)$ must both be zero at $t < 0$, i.e. before the Dirac delta perturbation arrives. Since for $t < 0$ we must close the contour in the upper half-plane, all poles must be in the lower half-plane, so that for $t < 0$ none of them contributes, and we correctly get $\xi_0(t) = 0$ and $\xi_t(t) = 0$. As a consequence, for $t > 0$, when we close the contour in the lower half-plane, we pick the contribution from all the four poles, which are circled clockwise. (We already checked explicitly this pole structure in the simpler case of eq. (8.28), see eq. (8.24).) Then a straightforward application of Cauchy theorem gives, for $t > 0$,

$$\xi_0(t) = \frac{a_0}{\omega_+^2 - \omega_-^2} \left(\frac{\omega_+^2 - \omega_t^2}{\omega_+} \sin \omega_+ t + \frac{\omega_t^2 - \omega_-^2}{\omega_-} \sin \omega_- t \right), \quad (8.79)$$

$$\xi_t(t) = \frac{a_0 \omega_t^2}{\omega_+^2 - \omega_-^2} \left(-\frac{1}{\omega_+} \sin \omega_+ t + \frac{1}{\omega_-} \sin \omega_- t \right). \quad (8.80)$$

Therefore the solution is a superposition of modes $\xi_{\pm}(t)$ oscillating with frequencies ω_+ and ω_- . Of course, $\xi_{\pm}(t)$ are simply the normal modes of the system, and the same results could have been found diagonalizing the Lagrangian.

We now consider the limit $\mu \ll 1$. In this case the amplitude of $\xi_t(t)$ is maximized taking $\omega_t = \omega_0$, apart from corrections of higher order in μ . This choice defines the *resonant* transducer. Then eq. (8.76) gives

$$\omega_{\pm} \simeq \omega_0 \left(1 \pm \frac{\sqrt{\mu}}{2} + O(\mu) \right), \quad (8.81)$$

and the solutions (8.79) and (8.80) become

$$\xi_0(t) \simeq \frac{a_0}{2\omega_0} (\sin \omega_+ t + \sin \omega_- t) \quad (8.82)$$

$$\xi_t(t) \simeq \frac{a_0}{2\omega_0 \sqrt{\mu}} (-\sin \omega_+ t + \sin \omega_- t) . \quad (8.83)$$

Writing $\omega_{\pm} = \omega_0 \pm \omega_b$, with $\omega_b = (1/2)\omega_0\sqrt{\mu} \ll \omega_0$, the above equations can be rewritten as

$$\xi_0(t) \simeq \frac{a_0}{\omega_0} \sin \omega_0 t \cos \omega_b t , \quad (8.84)$$

$$\xi_t(t) \simeq -\frac{a_0}{\omega_0 \sqrt{\mu}} \cos \omega_0 t \sin \omega_b t , \quad (8.85)$$

so we have beatings between the two oscillators, and the energy flows periodically from the bar to the transducer and backward, with a frequency equal to the beat frequency ω_b , which is much smaller than ω_0 . The evolution of the system is shown in Fig. 8.4.

The maximum oscillation amplitude of the transducer, A_t , is larger than the maximum oscillation amplitude of the bar, A_0 , by a factor $1/\sqrt{\mu}$. This is the maximum value allowed by energy conservation, since it means that the elastic energy of the bar, $(1/2)m_0\omega_0^2 A_0^2$, periodically is completely transferred to the transducer, so at that moment A_t is given by $(1/2)m_t\omega_0^2 A_t^2 = (1/2)m_0\omega_0^2 A_0^2$, and $A_t/A_0 = 1/\sqrt{\mu}$. We therefore have a mechanical amplification of the bar oscillation. This result suggests to take μ as small as possible. However, as we will see in Section 8.3, if we take m_t too small, the thermal noise of the transducer becomes large, and this fixes an optimal value of μ . The optimal values of μ is typically of order $10^{-3}-10^{-4}$.

The conclusion is that, while the fundamental mode of the bar resonates at the frequency ω_0 , the system composed by the bar's mode ξ_0 and the resonant transducer, with $\mu \ll 1$, has two resonant frequencies ω_{\pm} , slightly displaced from ω_0 and given in eq. (8.81), and the oscillation amplitude of the transducer is larger than that of the bar's fundamental mode by a factor $1/\sqrt{\mu}$.

We now introduce dissipation in the system. Then eqs. (8.72) and (8.73) are replaced by

$$m_0[\ddot{\xi}_0 + \omega_0^2 \xi_0 + \mu \omega_t^2 (\xi_0 - \xi_t)] = F_0 + f_0^{\text{diss}} , \quad (8.86)$$

$$m_t[\ddot{\xi}_t + \omega_t^2 (\xi_t - \xi_0)] = F_t + f_t^{\text{diss}} , \quad (8.87)$$

where, as before, F_0, F_t are the external forces. The dissipative forces $f_0^{\text{diss}}, f_t^{\text{diss}}$ are given by

$$f_0^{\text{diss}} = -m_0 \gamma_0 \dot{\xi}_0 - m_t \gamma_t (\dot{\xi}_0 - \dot{\xi}_t) , \quad (8.88)$$

$$f_t^{\text{diss}} = -m_t \gamma_t (\dot{\xi}_t - \dot{\xi}_0) , \quad (8.89)$$

where γ_0 and γ_t are related to the quality factors of the bar and of the transducer by $Q_0 = \omega_0/\gamma_0$ and $Q_t = \omega_t/\gamma_t$, respectively. Limiting

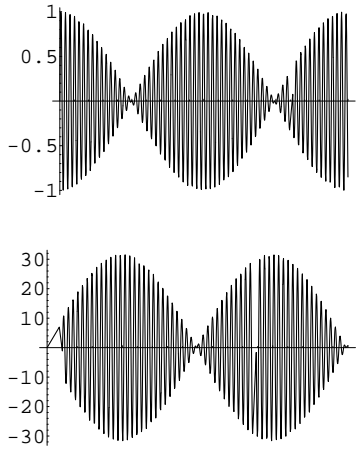


Fig. 8.4 The displacements of the bar, $\xi_0(t)$ (upper graph) and of the transducer, $\xi_t(t)$ (lower graph), both in units of a_0/ω_0 , for $\mu = 10^{-3}$, as a function of $\omega_0 t$. Observe the difference in vertical scale between the two figures.

ourselves for simplicity to the lowest non-trivial order in $\mu = m_t/m$, we introduce the modes $\xi_{\pm}(t)$ from

$$\xi_0 = \frac{1}{\sqrt{2}} (\xi_+ + \xi_-), \quad \xi_t = \frac{1}{\sqrt{2}\mu} (-\xi_+ + \xi_-). \quad (8.90)$$

In terms of $\xi_{\pm}(t)$ the equations of motion, with the inclusion of the dissipative terms, become

$$\ddot{\xi}_+ + \bar{\gamma} \dot{\xi}_+ + \frac{\gamma_0 - \gamma_t}{2} \dot{\xi}_- + \omega_+^2 \xi_+ = \frac{1}{\sqrt{2}} \left(\frac{F_0}{m_0} - \sqrt{\mu} \frac{F_t}{m_t} \right), \quad (8.91)$$

$$\ddot{\xi}_- + \bar{\gamma} \dot{\xi}_- + \frac{\gamma_0 - \gamma_t}{2} \dot{\xi}_+ + \omega_-^2 \xi_- = \frac{1}{\sqrt{2}} \left(\frac{F_0}{m_0} + \sqrt{\mu} \frac{F_t}{m_t} \right), \quad (8.92)$$

where $\omega_{\pm}^2 = \omega_0^2(1 \pm \sqrt{\mu})$ and $\bar{\gamma} = (\gamma_0 + \gamma_t)/2$. We see that these equations decouple only if $\gamma_0 = \gamma_t$ (and in this case, as well as in the absence of dissipation, $\xi_{\pm}(t)$ are the two normal modes of the system). Going in Fourier space, it is easy to find the solution for $\tilde{\xi}_{\pm}$ and therefore for $\tilde{\xi}_t$, which is¹⁷

$$\tilde{\xi}_t(\omega) = \frac{(\tilde{F}_0(\omega)/m_0)\omega_0^2 - (\tilde{F}_t(\omega)/m_t)(\omega^2 - \omega_0^2 + i\omega\gamma_0)}{(\omega^2 - \omega_+^2 + i\omega\bar{\gamma})(\omega^2 - \omega_-^2 + i\omega\bar{\gamma})}. \quad (8.93)$$

This general result will be useful in Section 8.3 when we study the different sources of noise acting on the bar and on the transducer. For the moment we are only interested in the response to a GW so we set, according to eq. (8.13) $\tilde{F}_0(\omega) = -(2L/\pi^2)m_0\omega^2\tilde{h}(\omega)$, and $\tilde{F}_t(\omega) = 0$. Then we find

$$\tilde{\xi}_t(\omega) = T_t(\omega)\tilde{h}(\omega), \quad (8.94)$$

where the transducer transfer function is

$$T_t(\omega) = -\frac{2L}{\pi^2} \frac{\omega_0^2\omega^2}{(\omega^2 - \omega_+^2 + i\omega\bar{\gamma})(\omega^2 - \omega_-^2 + i\omega\bar{\gamma})}. \quad (8.95)$$

The squared modulus of this transfer function is shown in Fig. 8.5 (solid line), together with the same quantity for a single oscillator (dashed line), given in eq. (8.23) and already shown in Fig. 8.1. Observe that, because of the small value of μ , the two peak values of the transducer transfer function are much larger than the peak value of a bar alone, having the same quality factor. In contrast, at $\omega \gg \omega_0$ $|T_t(\omega)|$ goes to zero as $1/\omega^2$, while $|T_0(\omega)|$ goes to a constant.

We see that dissipation is governed by $\bar{\gamma}$. We can then define the mechanical quality factor of the bar-transducer system by $\bar{\gamma} = \omega_0/Q_m$, i.e.

$$\frac{1}{Q_m} = \frac{1}{2} \left(\frac{1}{Q_0} + \frac{1}{Q_t} \right). \quad (8.96)$$

Typical values that have been reached in resonant bars are of order $Q_m \sim 10^6$.

¹⁷In the denominator we neglected a term that depends on $(\gamma_t - \gamma_0)^2\omega^2$ and, numerically, is totally negligible.

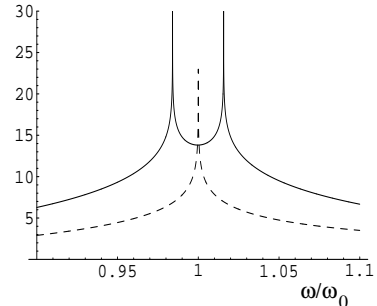


Fig. 8.5 $\text{Log}_{10}|(\pi^2/2L)T_t(\omega)|^2$ as a function of ω/ω_0 , for $\bar{Q} = \omega_0/\bar{\gamma} = 10^6$ and $\mu = 10^{-3}$ (solid line) and the same quantity for the bar alone, with $Q = 10^6$ (dashed line), plotted against ω/ω_0 .

8.2.2 Resonant transducers

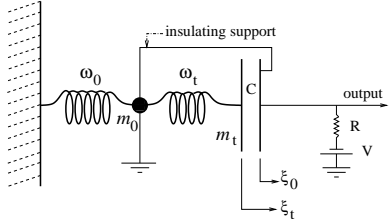


Fig. 8.6 A schematic representation of the capacitive transducer.

The double oscillator provides a mechanical amplification of the oscillation of the bar. The next step is to read the displacement of the light mass, transforming it into an electric signal. Various schemes have been devised by different experimental groups. The principle of all these transducers is to use the displacement of the small mass to modulate a stored electromagnetic field. In general terms, transducers can be distinguished between passive and active (also called parametric). Passive transducers modulate a d.c. field, while parametric transducers modulates an a.c. field generated by an external source.

In particular, in capacitive transducers a d.c. electric field is stored in the gap of a capacitor (values of the gap as small as $10 \mu\text{m}$ have been obtained). The light mass of the double oscillator is used as one of the plate of the capacitor, while the other plate is rigidly fixed with an electrically isolated support to the bar face so, in the same schematization used in the previous section for the double oscillator, the system is as shown in Fig. 8.6. In inductive transducers, instead, a persistent superconductive current is stored in a flat coil. The light mass of the double oscillator is now a superconductive ground plane, whose oscillations induce modulations of the inductance.¹⁸

The resulting electric signal is still very small and must be further amplified electronically. At cryogenic temperatures the best amplifier is invariably a SQUID. However, here we face a problem of mismatch between the large output impedance of the transducer, $1/(\omega C) \sim 10^5 \text{ ohm}$, and the small input impedance of the SQUID, $\omega L_{\text{SQ}} \sim 10^{-2} \text{ ohm}$. Optimal signal transfer is then obtained inserting a transformer between the transducer and the SQUID. As a result, we end up with a system of three oscillators, two mechanical (the oscillation ξ_0 of the bar and the oscillation ξ_t of the transducer) and one electric (the LC circuit formed by the transducer capacitance and the transformer inductance). These oscillators are coupled, and therefore the system is described by a generalization of eqs. (8.86) and (8.87) that includes the dynamics of the electric mode. The full system of equations is somewhat complicated. However, to get a qualitative understanding, we observe that the strength of the coupling between oscillators can be measured by the fraction of the energy that flows from one to the next. For the two mechanical oscillators we have seen that, taking $\mu \ll 1$ and tuning $\omega_t = \omega_0$, all the energy of the first oscillator (the bar) can be transferred periodically to the second (the transducer), with a beating frequency $\omega_b = \omega_0\sqrt{\mu}$. We want to characterize similarly the coupling between the transducer and the electric mode.

For this, we start by observing that the output of the electromechanical transducer is a potential V , which is a linear function of the transducer motion, so a displacement $\tilde{\xi}_t$ of the transducer generates a potential V given, in Fourier transform, by

$$\tilde{V}(\omega) = \alpha(\omega)\tilde{\xi}_t(\omega). \quad (8.97)$$

¹⁸Observe that, in these schemes, the quantity that is actually monitored is not ξ_t but $\xi_t - \xi_0$. The transfer function for $\xi_t - \xi_0$ is easily obtained repeating the steps that led to eq. (8.95). However, by construction the amplitude of ξ_t is much larger than the amplitude of ξ_0 , so $\xi_t(t) - \xi_0(t) \simeq \xi_t(t)$.

When $\alpha(\omega)$ is a constant, the potential $V(t)$ is linear in $\xi_t(t)$ while, if $\alpha(\omega) \sim i\omega$, the potential $V(t)$ is linear in $d\xi_t(t)/dt$. On the relatively small frequency range of interest for resonant bars, α can usually be approximated by its value at ω_0 , which means that we can write eq. (8.97) equivalently as $V(t) = \alpha \xi_t(t)$, or as

$$V(t) = Z_{21} \dot{\xi}_t(t), \quad (8.98)$$

with $Z_{21} = \alpha/(-i\omega_0)$. The electromagnetic energy $E_{\text{em}} = (1/2)CV^2$ of the capacitive transducer is then given by

$$E_{\text{em}} = \frac{1}{2} C \alpha^2 \xi_t^2. \quad (8.99)$$

The elastic energy of a transducer is¹⁹

$$E_{\text{elas}} = \frac{1}{2} m_t \omega_0^2 \xi_t^2. \quad (8.100)$$

The ratio of these energies, β , gives a measure of the transfer of energy from the bar to the electric mode,

$$\beta \equiv \frac{E_{\text{em}}}{E_{\text{elas}}} = \frac{C \alpha^2}{m_t \omega_0^2} = \frac{\alpha^2}{m_t \omega_0^3 |Z|}, \quad (8.101)$$

where $|Z| = 1/\omega_0 C$ is the impedance. Recalling the definition $Z_{21} = \alpha/(-i\omega_0)$ we can also write

$$\beta = \frac{|Z_{21}|^2}{m_t \omega_0 |Z|}. \quad (8.102)$$

Observe that β is inversely proportional to the mass of the transducer m_t . If, instead of using the resonant transducer scheme, one coupled directly the bar to the capacitor, β would rather be proportional to $1/m_0$, where m_0 is the effective bar mass, and the transfer of energy from the bar to the amplifier would be much less effective. Thus, we can see the resonant transducer as the solution to a problem of impedance matching: the mechanical output impedance of the bar is very high, compared to the mechanical impedance of the electric field in the capacitor, and the light mass in the resonant transducer scheme plays the role of a mechanical transformer for the bar elastic energy.

The best coupling between the mechanical modes and the electric mode is obtained setting $\omega_{\text{em}} = \omega_0$, in which case the two mechanical modes and the electric mode are all in resonance. Unfortunately, to obtain a high quality factor for an electric circuit is more difficult than for mechanical resonators. If we couple resonantly our double oscillator with a mechanical quality factor $Q_m \sim 10^6$ to an resonant electric circuit with a quality factor Q_{em} much lower than 10^6 , in the electro-mechanical system composed by the two mechanical oscillators and the electric circuit, dissipation would take place mostly when the energy is in the electric circuit. As we will discuss in Section 8.3.1, a high overall Q is however necessary in order to fight thermal noise. One solution, which has been

¹⁹More precisely, since the transducer is an extended object, the relation between E_{elas} and $\omega_0^2 \xi_t^2$ includes numerical factors of order one that depends on the geometry of the transducer, and m_t is an effective mass, defined so that eq. (8.100) holds, and which differ from the actual transducer mass by a factor of order one.

used by all detectors until recently, is to detune the electric mode, keeping its frequency f_{em} about 30% higher than the resonances of the two mechanical modes because, if the oscillators are detuned, only a fraction of the total energy $O(\beta)$ is transferred to the electric mode, where it is dissipated fast. The drawback of this solution is that the bandwidth of the detector increases with β , so a small β means a narrow bandwidth.²⁰

However, recently various groups have improved the quality factor of the electric resonator and brought it in resonance, or close to the mechanical modes. As a result, the bandwidth of the detectors has been greatly enhanced, and in particular for the AURIGA detector is now of order or larger than 100 Hz, see Fig. 8.17 below.

We have now transformed the bar displacement into an electromagnetic signal, and the final step of the transduction process is its amplification. At cryogenic temperatures, SQUIDs are by far the amplifiers with the lowest noise, so they are the natural choice for the final amplification chain in resonant detectors.²¹ In this way it has been possible to measure changes in energy corresponding to the absorption of $O(100)$ quanta of frequencies ω_0 , i.e. $\Delta E = N\hbar\omega_0$ with $N = O(100)$. This is quite remarkable, if we think that we are detecting vibrations corresponding to just about 100 phonons, in a two-ton object!

Alternative read-out systems have also been actively investigated. We briefly discuss two possibilities.

Parametric resonant transducers

These transducers make use of an external power source (the “pump” oscillator). The oscillation of the light mass in the double oscillator can be used to modulate a capacitance, just as in the capacitive transducer discussed above, but the capacitor is now part of a high-Q resonant circuit which, in turn, modulates the phase and amplitude of the reflected or transmitted signal. This produces sidebands at the frequencies $\omega_p \pm \omega_0$, where ω_p is the pump frequency, which can be at optical, microwaves or radio frequencies. Then the signal is demodulated using as reference the original pump signal. Contrary to passive devices, parametric transducers have an intrinsic power gain, due to the up-conversion of the signal to much higher frequencies. We can see passive transducers as objects in which the transduction process, i.e. the transformation of the mechanical oscillations into an electric signal, is completely separated by the amplification process, which is performed later by a SQUID. In parametric devices, instead, the transduction and at least part of the amplification are performed simultaneously. On the other hand, for parametric transducers, important limitations come from phase noise and stability problems in the pump. It is also necessary an excellent carrier suppression, otherwise the pump power reflected from the cavity overwhelms the signal in the sidebands.

An important difference between passive and parametric transducers is that in passive transducers the relation between the input and the output is linear, both in amplitude and in phase, while this is not the

²⁰We will see this formally in Section 8.3.2, see in particular Note 27. However, the reason can be understood physically observing that, if β is small, only a small part of the total energy flows from the mechanical modes to the electric mode, so the oscillation amplitude of the electric mode is small. To pick up a signal with a smaller oscillation amplitude we need a larger integration time, and a large integration time means a small bandwidth, $\Delta f \sim 1/\Delta t$. Furthermore, with a larger value of β , a smaller mechanical amplification is required, and the mass m_t of the resonant transducer can be made heavier. As we will see in Section 8.3.1, this reduces the transducer thermal noise, which is another fact that limits the bandwidth.

²¹Actually, both the AURIGA and MiniGRAIL groups developed double-stage SQUIDS, in which a dc SQUIDs senses the signal and its output is further amplified by a second stage SQUID.

case for a parametric transducer, because of the effect of the external pump field. We will see in Section 8.3.3 that, because of the role of the uncertainty principle in the measurement process, this difference has important implications for the ultimate sensitivity attainable with passive and with parametric transducers.

Dual detectors

The resonant transducer scheme has two advantages. The first is that it provides a much needed mechanical amplification of the signal. The second is that, since it amplifies only the mode to which it is tuned (normally the fundamental mode of the bar) it allows us to forget about all the higher modes of the bar. This means that we can neglect the thermal noise associated to all the higher modes ξ_n of the bar, and we can describe the bar-transducer system as a simple system with two degrees of freedom, ξ_0 and ξ_t .

On the other hand, when in the next section we discuss the various contributions to the noise, we will see that the resonant transducer also introduces an important limitation. In particular, because of its thermal noise the sensitivity of a resonant bar is restricted to a relatively narrow region Δf around its resonance frequency.

An alternative that has been recently proposed is the so-called *dual resonator*. In this scheme one has two nested objects, such as two concentric cylinders, or an outer hollow sphere and an inner concentric solid sphere. One can arrange the size and material so that the fundamental mode of the inner body f_{inner} is, say, around 3 kHz, while the fundamental mode of the outer body, f_{outer} is around 1 kHz. The idea is to measure the differential displacement between these two surfaces. The displacement could for instance be detected by an optical read-out made of a high-finesse Fabry-Perot cavity,²² resonant with an incident laser beam, as in Fig. 8.7. Since no resonant transducer is introduced, the useful bandwidth covers the whole interval $f \in [f_{\text{outer}}, f_{\text{inner}}]$ (in fact, in this region one can even show that the oscillation amplitude of the two nested bodies adds up, while some noise partially cancel).

The first problem that must be solved is to have sufficient power in the cavity and a sufficiently high finesse, in order to be able to reach the required sensitivity, taking into account that we have given up the amplification that was provided by the resonant transducer scheme. Cavities of this type are being developed, but still we are not yet at the required sensitivity level. Second, one should find a way to get rid of the contribution of all the higher modes. In the resonant transducer scheme one has a selective read-out based on frequency: only the mode with the same frequency as the resonant transducer is amplified. In the dual scheme, it has been proposed a geometrically based mode selection, which consists in sensing a large portion of the surface, so that the effect of higher modes averages out and, comparing the deformations on different parts of the body, one can enhance the contribution of deformations with a quadrupolar symmetry.

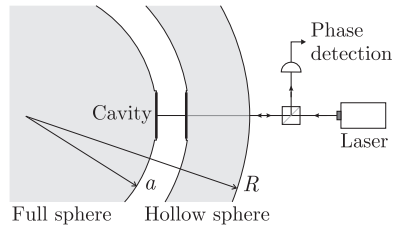


Fig. 8.7 Scheme for a possible read-out of a dual detector. The small gap between the two spheres is measured using a high-finesse single-ended cavity. Reprinted figure with permission, from Briant *et al.* *Phys. Rev. D* **67**, 102005 (2003). Copyright 2003 by the American Physical Society.

²²Fabry-Perot cavities will be discussed in detail when we come to interferometers, in Chapter 9.

8.3 Noise sources

In this section we examine the sources of noise that limit the performances of resonant bars. In particular, in Sections 8.3.1 and 8.3.2 we discuss the two types of noise that are more important in existing detectors, namely thermal noise and read-out noise, and we will see that their combination fixes the useful frequency bandwidth. We will then discuss other sources of noise, including some fundamental limitations imposed by quantum mechanics.

For each source of noise, we can characterize its effect in two complementary ways: (1) We can compute the minimum detectable energy that should be deposited in a bar by a short GW burst in order to overcome this noise, say at signal-to-noise ratio $S/N = 1$. (2) We can give its contribution to the noise spectral density. The former characterization is physically more intuitive, but it carries less detailed information, because it is a quantity integrated over the frequency bandwidth. The noise spectral density, on the other hand, carries the full spectral information. Below we will use both characterizations.

The noise spectral density has been defined in Section 7.1. To compute it, for resonant bars it is convenient to proceed as follows. First of all, we write as usual the output of the detector in the form $s(t) = h(t) + n(t)$, where $h(t)$ is the contribution due to GWs and $n(t)$ is the noise.²³ We have seen that, when GWs provide the only force acting on the bar, the corresponding displacement, that we denote here by $\xi^{(h)}$ is related to the GW by

$$\tilde{\xi}^{(h)}(\omega) = T(\omega)\tilde{h}(\omega), \quad (8.103)$$

where $T(\omega)$ is the transfer function. We can use this equation to study the displacement of a single oscillator like the bar fundamental mode ξ_0 , in which case the transfer function is the function $T_0(\omega)$ given in eq. (8.23), or we can use it to study the transducer displacement ξ_t , in which case the transfer function is given in eq. (8.95). The latter quantity is more relevant, since it is the motion of the transducer that is sensed, but it can also be useful to compare the situation with the resonant transducer with what happens if we have only the mode ξ_0 .²⁴ We denote generically by ξ the displacement in which we are interested, either ξ_0 or ξ_t , and it is understood that the corresponding transfer function is used.

The noise gives further contributions to the displacement,

$$\tilde{\xi}^{(n)}(\omega) = T(\omega)\tilde{n}(\omega). \quad (8.104)$$

Following the general definition of spectral density given in Section 7.1, the single-sided spectral density of a displacement, $S_\xi(\omega)$, is defined by

$$\langle \xi^2(t) \rangle = \int_0^\infty \frac{d\omega}{2\pi} S_\xi(\omega), \quad (8.105)$$

Using eq. (8.104) we see that the noise spectral density $S_n(\omega)$ is related to the spectral density of the displacement induced by that noise by

$$S_\xi^{\text{noise}}(\omega) = |T(\omega)|^2 S_n(\omega). \quad (8.106)$$

²³More precisely, $n(t)$ is the noise referred to the detector's input, see the discussion in Section 7.1.

²⁴Observe that the use of the transfer function of the bar-transducer system is still an oversimplification. We have seen that the electromagnetic transducer is really a three-mode system composed by the bar, transducer, and electric mode. If the electric mode is detuned, a two-mode description can be sufficient. Otherwise, the full transfer function of the three-mode system must be used for a detailed quantitative understanding. Thus, the analysis that we present below is really meant to obtain only a qualitative understanding of the effect of the principal noise in a resonant detector, and is not sufficient to reproduce accurately the details of the sensitivity curves.

Therefore, to compute the contribution to $S_n(\omega)$ due to a given noise source, say thermal noise, we can compute the spectral density of the displacement induced by this noise, and we then divide it by $|T(\omega)|^2$.²⁵

8.3.1 Thermal noise

Thermal (or Brownian) noise is due to the thermal kinetic energy of the atoms of the detector. Naively one might think that, in a bar at temperature T , the minimum detectable energy excitation should be $\Delta E_{\min} \simeq kT$, otherwise the excitation is drown into the thermal fluctuations. A key contribution by Weber was the realization that, in a mechanical oscillator with a high Q , the minimum detectable energy due to thermal noise is in fact much smaller. The physical intuition behind this result is that a high- Q oscillator dissipates very slowly; if we excite the oscillator, we know that it will return to its original state in a very long time. In particular, the fundamental mode of a bar has a relaxation time $\tau_0 = 1/\gamma_0 = Q_0/\omega_0$ of order 10 min, which means that it is extremely weakly coupled to the thermal bath constituted by all other bar's modes. Therefore we expect not only that the time needed to go from an excited state back to the ground state will be long but also, conversely, that the time needed to develop energy fluctuations of order kT in the fundamental mode will be of order τ_0 .

On the other hand we have seen that a GW burst, in a time τ_g corresponding to the burst duration, excites bar's oscillations with an amplitude $\xi_0 \sim hL$. Since τ_g is much smaller than the relaxation time τ_0 of the fundamental mode of the bar, we can expect that the energy fluctuations due to thermal noise in such a short time are much smaller than kT , and rather of order $kT(\tau_g/\tau_0)$. The idea is therefore that, if we sample the bar's state with a time resolution Δt , the minimum GW energy detectable against thermal noise should be

$$(\Delta E_{\min})_{\text{thermal}} \simeq kT \frac{\Delta t}{\tau_0}, \quad (8.107)$$

as long as $\Delta t \gtrsim \tau_g$ (of course, if Δt become smaller than the burst duration, we start to lose part of the signal). In practice this will be achieved using the matched filtering procedure of Section 7.3, with a filter functions, such as a Dirac delta, that discriminates a fast excitation from the slow thermal modes.

To confirm this physical intuition, we study the evolution of the bar's fundamental mode in the presence of thermal noise. In the previous sections we studied the evolution of ξ_0 using the equation for the damped oscillator,

$$\ddot{\xi}_0 + \omega_0^2 \xi_0 = -\gamma_0 \dot{\xi}_0. \quad (8.108)$$

If this were the complete description of the bar's dynamics, the time evolution of $\xi_0(t)$ would be fully deterministic. In principle, we could then simply subtract it, and attribute any deviation from the expected evolution to external causes like GWs. However, thermal noise enters in

²⁵Observe that $S_n(\omega)$ has dimensions Hz^{-1} , so the strain sensitivity $S_n^{1/2}(\omega)$ has dimensions $\text{Hz}^{-1/2}$, while $S_\xi(\omega)$ has dimensions m^2/Hz . The sensitivity of the bar is usually displayed plotting either $S_n(\omega)$ or $S_n^{1/2}(\omega)$. This is more useful than plotting $S_\xi(\omega)$ or $S_\xi^{1/2}(\omega)$, especially when we compare the sensitivity of different experiments like bars and interferometers. In fact, a bar and an interferometer with the same sensitivity to GWs, i.e. with the same $S_n(\omega)$, would have very different spectral density of the displacement, since for bars the length-scale that enters in the transfer function is the bar's length $L = 3 \text{ m}$, while for interferometers it is the pathlength of the light in the interferometer arms. As we will see, for ground based interferometers this is of the order 10^2 kms . Therefore, in different detectors, very different values of $S_\xi(\omega)$ can correspond to the same minimum value of $\tilde{h}(\omega)$ that can be measured.

the fact that it produces a stochastic force, responsible both for the dissipation term $-\gamma_0 \dot{\xi}_0$, and for fluctuations around it. To take fluctuations into account the above equation must be replaced by

$$m_0(\ddot{\xi}_0 + \omega_0^2 \xi_0) = F_{\text{stoc}} \quad (8.109)$$

with

$$\langle F_{\text{stoc}} \rangle = -m_0 \gamma_0 \dot{\xi}_0. \quad (8.110)$$

We write $F_{\text{stoc}} = -m_0 \gamma_0 \dot{\xi}_0 + F(t)$, where $F(t)$ is a stochastic force that describes the thermal fluctuations, known as the Nyquist force. By definition $\langle F(t) \rangle = 0$. Thermal noise fluctuations can be described by a stochastic Gaussian process, since they are the sum of many independent contributions, so the stochastic properties of $F(t)$ are uniquely defined by its average value that, as we have seen, is zero, and by its auto-correlation function $\langle F(t)F(t') \rangle$. At the microscopic level, $F(t)$ is due to atomic collisions, at a rate which can be, say, $O(10^{19})$ collisions per second. Therefore, on a macroscopic time-scale, the force at time t and at time t' are completely uncorrelated if $t \neq t'$, and we can write

$$\langle F(t)F(t') \rangle = A_0 \delta(t - t'). \quad (8.111)$$

We will see in a moment how to fix the constant A_0 . The dynamics of $\xi_0(t)$ is now governed by

$$\ddot{\xi}_0 + \gamma_0 \dot{\xi}_0 + \omega_0^2 \xi_0 = \frac{F(t)}{m_0}, \quad (8.112)$$

which has the solution

$$\xi_0(t) = \xi_0^{\text{hom}}(t) + \frac{1}{m_0} \int_{-\infty}^{\infty} dt' G(t - t') F(t'), \quad (8.113)$$

where $\xi_0^{\text{hom}}(t)$ is the general solution of the homogeneous equation and $G(t)$ is a Green's function, i.e. a solution of eq. (8.112) with $F(t)/m_0$ replaced by $\delta(t)$. The Green's function can be easily found performing the Fourier transform and repeating basically the same steps that lead to the integration of eq. (8.22),²⁶ and we get

$$G(t) = \frac{1}{\omega_0} \theta(t) e^{-\gamma_0 t/2} \sin \omega_0 t, \quad (8.114)$$

where $\theta(t)$ is the step function, $\theta(t) = 0$ for $t < 0$ and $\theta(t) = 1$ for $t > 0$. Therefore

$$\xi_0(t) = \xi_0^{\text{hom}}(t) + \frac{1}{m_0 \omega_0} \int_{-\infty}^t dt' e^{-\gamma_0(t-t')/2} \sin[\omega_0(t-t')] F(t'). \quad (8.115)$$

We assume for simplicity that $F(t)$ is switched on at $t = 0$, and that $\xi_0(0) = 0$ and $\dot{\xi}(0) = 0$. With these boundary conditions we get, for $t > 0$,

$$\xi_0(t) = \frac{1}{m_0 \omega_0} \int_0^t dt' e^{-\gamma_0(t-t')/2} \sin[\omega_0(t-t')] F(t'). \quad (8.116)$$

²⁶The Green's function is selected uniquely imposing the causality condition, i.e. requiring that the particular solution of the inhomogeneous equation, at time t , depends only on $F(t')$ at $t \leq t$.

Using eq. (8.111) and introducing $u = t - t'$ we then obtain

$$\begin{aligned}\langle \xi_0^2(t) \rangle &= \frac{A_0}{m_0^2 \omega_0^2} \int_0^t du e^{-\gamma_0 u} \sin^2 \omega_0 u \\ &\simeq \frac{A_0}{2m_0^2 \omega_0^2 \gamma_0} (1 - e^{-\gamma_0 t}),\end{aligned}\quad (8.117)$$

where in the last line we neglected terms which are small for $\gamma_0 \ll \omega_0$. The time evolution of the average kinetic plus potential energy of the mode ξ_0 due to thermal noise is therefore given by

$$\begin{aligned}\langle E(t) \rangle &= \frac{1}{2} m_0 \omega_0^2 \langle \xi_0^2 \rangle + \frac{1}{2} m_0 \langle \dot{\xi}_0^2 \rangle \\ &= m_0 \omega_0^2 \langle \xi_0^2 \rangle \\ &\simeq \frac{A_0}{2m_0 \gamma_0} (1 - e^{-\gamma_0 t}).\end{aligned}\quad (8.118)$$

In the limit $t \rightarrow \infty$, the system thermalizes and the equipartition of energy states that $\langle E_{\text{kin}}(t) \rangle \rightarrow (1/2)kT$ and $\langle E_{\text{pot}}(t) \rangle \rightarrow (1/2)kT$, so $\langle E(t) \rangle \rightarrow kT$. Comparison with eq. (8.118) fixes the value of A_0 ,

$$A_0 = 2kT m_0 \gamma_0,\quad (8.119)$$

and therefore

$$\langle E(t) \rangle = kT(1 - e^{-t/\tau_0}),\quad (8.120)$$

where $\tau_0 = 1/\gamma_0$. This shows that, while asymptotically $\langle E(t) \rangle \rightarrow kT$, equilibrium is reached only on a time-scale $t \gg \tau_0$. On a time-scale $\Delta t \ll \tau_0$, expanding the exponential in eq. (8.120) we rather get

$$\langle E(t = \Delta t) \rangle \simeq kT \frac{\Delta t}{\tau_0},\quad (8.121)$$

confirming the physical intuition that led to eq. (8.107). It is instructive to realize that the result (8.119) is a particular case of a very general theorem. According to the definition (7.15), which expresses in general the relation between the spectral density and the auto-correlation function of any quantity, the (single-sided) spectral density of the force $F(t)$, that we denote by $S_F(\omega)$, is related to the auto-correlation function of $F(t)$, $R_F(t' - t) \equiv \langle F(t')F(t) \rangle$, by

$$\langle F(t')F(t) \rangle = \frac{1}{2} \int_{-\infty}^{\infty} \frac{d\omega}{2\pi} S_F(\omega) e^{-i\omega(t' - t)}.\quad (8.122)$$

Comparison with eq. (8.111) shows that $S_F(\omega) = 2A_0$, so the spectral density is flat. Equation (8.119) can therefore be seen as a relation between the fluctuations due to the force F (represented by S_F) and the dissipation (represented by γ_0),

$$S_F = 4kT m_0 \gamma_0.\quad (8.123)$$

This result is a particular case of the *fluctuation-dissipation theorem*, which can be formulated as follows. Let $x(t)$ by a variable describing

a linear system (either mechanical or electrical) subject to an external force $F(t)$, and let $v(t) = \dot{x}(t)$ be the velocity. In Fourier space, we can always cast the equation of motion of a linear system in the general form

$$\tilde{F}(\omega) = Z(\omega)\tilde{v}(\omega). \quad (8.124)$$

This defines the impedance $Z(\omega)$. Its inverse, $Y(\omega) = Z^{-1}(\omega)$, is called the admittance. The fluctuation-dissipation theorem states that the (single-sided) power spectrum of the force responsible for thermal fluctuations, $S_F(\omega)$, is related to the real part of Z by

$$S_F(\omega) = 4kT \operatorname{Re} Z(\omega). \quad (8.125)$$

For the damped oscillator, eq. (8.112) gives

$$Z = -\frac{im_0}{\omega}(\omega^2 - \omega_0^2 + i\gamma_0\omega), \quad (8.126)$$

so $\operatorname{Re} Z = m_0\gamma_0$ and we recover eq. (8.123). The real part of Z in general is responsible for dissipation in the system, so eq. (8.125) relates fluctuations to dissipation.

We can now compute the spectral density of the noise due to thermal fluctuations, considering for the moment only the bar's mode ξ_0 . Below we will generalize to the bar-transducer system. Writing the velocity as $\tilde{v}(\omega) = -i\omega\xi_0(\omega)$, eq. (8.124) can be written as

$$\tilde{\xi}_0(\omega) = \frac{1}{-i\omega Z(\omega)} \tilde{F}(\omega), \quad (8.127)$$

and therefore

$$\begin{aligned} S_\xi^{\text{thermal}}(\omega) &= \frac{1}{\omega^2|Z(\omega)|^2} S_F(\omega) \\ &= \frac{4kT m \gamma_0}{\omega^2|Z(\omega)|^2}. \end{aligned} \quad (8.128)$$

From the explicit forms (8.126) and (8.23) we see that $Z(\omega)$ is related to the transfer function of the mode ξ_0 , $T_0(\omega)$, by

$$T_0(\omega) = \frac{2L}{\pi^2} \frac{m_0\omega}{iZ(\omega)}. \quad (8.129)$$

Therefore we can rewrite eq. (8.128) as

$$S_\xi^{\text{thermal}}(\omega) = \frac{4kT \gamma_0}{m_0 \omega^4} \left(\frac{\pi^2}{2L} \right)^2 |T_0(\omega)|^2. \quad (8.130)$$

The contribution to the noise spectral density due to the thermal noise is obtained using eq. (8.106). We see that $|T(\omega)|^2$ cancels, and we end up with

$$S_n^{\text{thermal}}(f) = \frac{\pi}{Q_0} \frac{kT}{Mv_s^2} \frac{f_0^3}{f^4}, \quad (8.131)$$

where we eliminated L using $\omega_0 = \pi v_s/L$, with v_s the speed of sound in the bar, we used $m_0 = M/2$, with M the total mass of the bar, $\gamma_0 = \omega_0/Q_0$, and we expressed everything in terms of $f = \omega/(2\pi)$. We can make the following comments.

- We have found that $S_\xi^{\text{thermal}}(\omega)$ is proportional to $|T_0(\omega)|^2$. Since however the contribution of thermal noise to $S_n(\omega)$ is obtained dividing $S_\xi^{\text{thermal}}(\omega)$ by $|T_0(\omega)|^2$, see eq. (8.106), the transfer function $T_0(\omega)$ cancels, and $S_n(f)$ shows no special feature around the resonance frequency f_0 ; rather, it has a smooth frequency dependence, $S_n(f) \sim f^{-4}$. This means that, if thermal noise were the only source of noise, resonant bars would be wide-band detectors, that is, their sensitivity would not be limited to a region close to f_0 . As we will see below, bars become narrow-band detectors only when we include the noise introduced by the read-out scheme.
- We understand the importance of a large quality factor, since we found $S_n^{\text{thermal}}(f) \sim 1/Q_0$. This is in agreement with eq. (8.107), since $\tau_0 = Q_0/\omega_0$, so $(\Delta E_{\min})_{\text{thermal}} \sim 1/Q_0$. Furthermore, we learn from eq. (8.131) that thermal noise can be fought lowering T (obviously), but also taking M and v_s as large as possible. The dependence $1/M$ expresses the physically obvious fact that thermal noise is not effective in generating a coherent motion of a massive object. We also see that $S_n^{\text{thermal}}(f)$ decreases at high frequencies, but this result will be modified when we include the transducer.

The computation of the noise spectral density performed above takes into account only the bar mode ξ_0 . We now consider the bar-transducer system, and we compute the effect of thermal noise on the transducer displacement. At first sight, eq. (8.131) can be alarming, because it suggests that, if the thermal noise of the bar is proportional to $1/M$, the thermal noise of the transducer should be proportional to $1/m_t$, and therefore it will be very large, since the transducer is very light. This would ruin completely the usefulness of the resonant transducer scheme. However, eq. (8.131) has been derived for a single oscillator, while here we have two coupled oscillators. We now show that it is indeed correct that, in the bar-transducer system, the thermal noise in the transducer is $S_n(f) \sim 1/m_t$, except in a narrow frequency range around the resonant frequency. This will provide a first (but, as it turns out, not the most important) reason that limits the bandwidth of resonant bar detectors.

To this end, we go back to eq. (8.93), which gives the transducer displacement $\xi_t(\omega)$, when we apply a force F_0 on the bar and a force F_t on the transducer. In terms of the transfer function given in eq. (8.95) we can write

$$\tilde{\xi}_t(\omega) = -\frac{\pi^2}{2L} \frac{T_t(\omega)}{\omega^2} \left[\frac{\tilde{F}_0(\omega)}{m_0} - \frac{\tilde{F}_t(\omega)}{m_t} \frac{\omega^2 - \omega_0^2 + i\omega\gamma_0}{\omega_0^2} \right]. \quad (8.132)$$

To compute the effect of thermal noise, we take as F_0 and F_t the Nyquist forces acting on the bar's fundamental mode and on the transducer,

respectively. From the fluctuation-dissipation theorem, in the form of eq. (8.123), we have

$$S_{F_0} = 4kT m_0 \gamma_0, \quad S_{F_t} = 4kT m_t \gamma_t. \quad (8.133)$$

Assuming that the Nyquist forces acting on the bar and on the transducer are uncorrelated we find, for the spectral density of the transducer displacement,

$$S_{\xi_t}(\omega) = \frac{\pi^4}{4L^2} \frac{|T_t(\omega)|^2}{\omega^4} 4kT \left[\frac{\gamma_0}{m_0} + \frac{\gamma_t}{m_t} \frac{(\omega^2 - \omega_0^2)^2 + \omega^2 \gamma_0^2}{\omega_0^4} \right]. \quad (8.134)$$

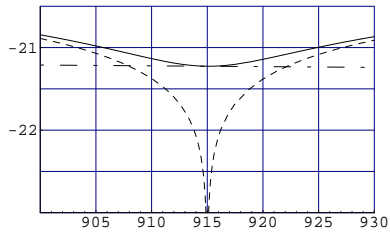


Fig. 8.8 $\log_{10}[S_n^{\text{thermal}}(f)]^{1/2}$, as a function of the frequency f (in Hz). Dashed line: transducer contribution. Dot-dashed: bar contribution. Solid line: total thermal noise. We use as numerical values $Q_0 = Q_t = 2 \times 10^6$, $T = 1$ K, $M = 2300$ kg, $L = 3$ m, $v_s = 5400$ m/s, $f_0 = 915$ Hz, $\mu = 2.4 \times 10^{-4}$.

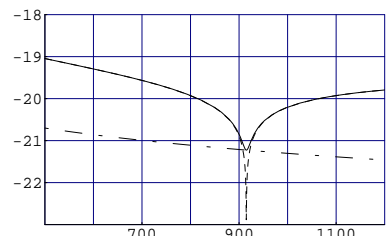


Fig. 8.9 The same as Fig. 8.8, on a larger frequency range.

As discussed above, the noise spectral density is obtained dividing by $|T_t(\omega)|^2$, so we get (using $L = \pi v_s / \omega_0$, $m_0 = M/2$, $\gamma_0 = \omega_0/Q_0$, $\gamma_t = \omega_0/Q_t$ and expressing the result in terms of $f = \omega/2\pi$)

$$S_n^{\text{thermal}}(f) = \pi \frac{kT}{Mv_s^2} \frac{f_0^3}{f^4} \left[\frac{1}{Q_0} + \frac{1}{\mu Q_t} \frac{(f^2 - f_0^2)^2 + (ff_0/Q_0)^2}{f_0^4} \right]. \quad (8.135)$$

The term $1/Q_0$ in the bracket is the thermal noise of the bar, see eq. (8.131). The second term is the transducer thermal noise, and we see that it is indeed proportional to $1/m_t$, so it is enhanced by a factor $1/\mu$ compared to the bar's noise. What saves the situation is the fact that $1/m_t$ is multiplied by a function of f which becomes very small at $f = f_0$,

$$S_n^{\text{thermal}}(f_0) = \pi \frac{kT}{Q_0} \frac{f_0^3}{Mv_s^2} \frac{1}{f^4} \left[1 + \frac{1}{\mu Q_t Q_0} \right]. \quad (8.136)$$

Numerically, for $Q_0 \sim Q_t \sim 10^6$ and $\mu = 10^{-4}$, we have $1/(\mu Q_t Q_0) \sim 10^{-8}$, so at $f = f_0$ the transducer thermal noise is completely negligible, and it remains smaller or of the same order of magnitude of the bar's thermal noise as long as $(f^2 - f_0^2)^2/f_0^4 \leq \mu(Q_t/Q_0)$, or, since $(Q_t/Q_0) = O(1)$, as long as $|f - f_0| \lesssim f_0 \sqrt{\mu}$.

We see that the term $(ff_0/Q)^2$ in eq. (8.135) gives a totally negligible contribution to $S_n^{\text{thermal}}(f)$ even when $f^2 - f_0^2 = 0$, so we can neglect it everywhere, and we can write more simply

$$S_n^{\text{thermal}}(f) = \pi \frac{kT}{Mv_s^2} \frac{f_0^3}{f^4} \left[\frac{1}{Q_0} + \frac{1}{\mu Q_t} \frac{(f^2 - f_0^2)^2}{f_0^4} \right]. \quad (8.137)$$

In Fig. 8.8 we plot the function $[S_n^{\text{thermal}}(f)]^{1/2}$, and the two separate contributions from the bar and the transducer. With the parameters given in the figure caption, at $f = f_0$ we get $[S_n^{\text{thermal}}(f_0)]^{1/2} \simeq 6 \times 10^{-22} \text{ Hz}^{-1/2}$. Observe that the thermal noise is minimum at f_0 , rather than at the normal mode frequencies f_\pm . Figure 8.9 shows the same quantities on a larger frequency window. Observe also that, at low f , $S_n^{\text{thermal}}(f)$ diverges as $1/f^4$, while at large f it goes to a constant.

8.3.2 Read-out noise and effective temperature

We now consider the other crucial source of noise in resonant detectors, that is, the noise introduced by the read-out scheme. We have seen that the output of a capacitive transducer is a potential, V , which is modulated by the displacement of the light mass, as in eq. (8.97), and further amplified electronically. Any amplifier has however an associated wideband noise, described by a spectral density of the output potential, S_V approximately constant in frequency, and with dimensions volts²/Hz. Since $V = \alpha\xi_t$, any fluctuation in the potential due to electronic noise results in an error in the measurement of ξ_t , which can be described by a spectral density of the displacement

$$S_{\xi_t}^{\text{ampl}} = \frac{1}{\alpha^2} S_V. \quad (8.138)$$

With good approximation α and S_V are independent of the frequency in the bandwidth of interest, so $S_{\xi_t}^{\text{ampl}}$ is approximately a white noise. Observe also that $S_{\xi_t}^{\text{ampl}}$ can be made smaller increasing α , that is, transferring more efficiently the energy from the mechanical oscillators to the amplifier.

As we did for thermal noise, we can characterize the amplifier noise either in terms of the energy that must be deposited by a GW burst in order to overcome it, or in terms of the noise spectral density. We consider first the energetic point of view. If, as in eq. (8.107), we use a sampling time Δt , the bandwidth is $\Delta f \simeq 1/\Delta t$. Then the fluctuations in ξ_t^2 due to amplifier noise in such a sampling time are given by

$$\langle \xi_t^2(t) \rangle = \int_{f_0 - \Delta f/2}^{f_0 + \Delta f/2} df S_{\xi_t}^{\text{ampl}} = S_{\xi_t}^{\text{ampl}} \Delta f. \quad (8.139)$$

The corresponding minimum value of the detectable energy is therefore given by

$$(\Delta E_{\min})_{\text{ampl}} = m_t \omega_0^2 \langle \xi_t^2(t) \rangle \simeq m_t \omega_0^2 S_{\xi_t}^{\text{ampl}} \frac{1}{\Delta t}. \quad (8.140)$$

We see that $(\Delta E_{\min})_{\text{ampl}}$ is proportional to $1/\Delta t$. This is due to the fact that, if the sampling time is small, the bandwidth is large and we are flooded with amplifier noise. On the contrary, we saw in eq. (8.107) that $(\Delta E_{\min})_{\text{thermal}}$ is proportional to Δt . Therefore, putting together the amplifier and thermal noise, we discover that there is an optimum value of the sampling time Δt and therefore of the bandwidth. We come back to this below

The other useful (and more detailed) characterization of amplifier noise is in terms of its noise spectral density, $S_n^{\text{ampl}}(f)$. According to the general definition (8.106), to get S_n^{ampl} we must divide the spectral density of the transducer displacement, $S_{\xi_t}^{\text{ampl}}$ by the squared modulus of the transducer transfer function $T_t(\omega)$, given in eq. (8.95). Recalling

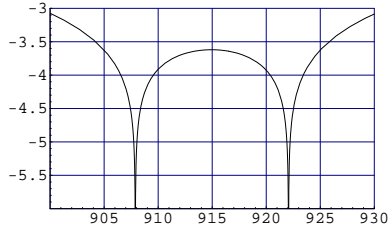


Fig. 8.10 $\log_{10}[S_n^{\text{ampl}}(f)/\mathcal{A}]^{1/2}$, as a function of the frequency, for $\mu = 2.4 \times 10^{-4}$ and $f_0 = 915$ Hz.

that $\bar{\gamma} = \omega_0/Q_m$, see eq. (8.96), we get

$$S_n^{\text{ampl}}(f) = \mathcal{A} \frac{[(f^2 - f_+^2)^2 + (ff_0/Q_m)^2][(f^2 - f_-^2)^2 + (ff_0/Q_m)^2]}{f^4 f_0^4}, \quad (8.141)$$

where

$$\mathcal{A} = \frac{\pi^4}{4L^2} S_{\xi_t}^{\text{ampl}}. \quad (8.142)$$

In Fig. 8.10 we show the dimensionless quantity $[S_n^{\text{ampl}}(f)/\mathcal{A}]^{1/2}$, for the same values of f_0 , μ , Q_0 and Q_t used above for thermal noise. The amplifier thermal noise is minimum at the two resonance frequencies f_{\pm} .

Thermal and amplifier noise are the two dominant contributions to the strain sensitivity in present detectors, so we can now put these two effects together and obtain a first understanding of the detector's sensitivities. We start from the energy considerations, that are less accurate (since the detailed frequency dependence is integrated over) but more intuitive. Combining eqs. (8.107) and (8.140) we see that the minimum detectable energy is

$$\Delta E_{\min} \sim kT \frac{\Delta t}{\tau} + m_t \omega_0^2 S_{\xi_t}^{\text{ampl}} \frac{1}{\Delta t}, \quad (8.143)$$

where Δt is the sampling time. We take τ to be the relaxation time of the full three modes system (mechanical plus electric), and we write $\tau = Q/\omega_0$, where Q is the overall quality factor of the system. Since the first term is proportional to Δt and the second to $1/\Delta t$, we can minimize ΔE_{\min} choosing an optimal value of Δt . This gives

$$\Delta f \simeq \frac{1}{(\Delta t)_{\text{opt}}} \sim \pi \frac{f_0}{Q} \Gamma^{-1/2}. \quad (8.144)$$

where

$$\Gamma = \frac{m_t \omega_0^3 S_{\xi_t}^{\text{ampl}}}{4QkT}, \quad (8.145)$$

In typical experimental situations, we can have $Q = O(10^6)$ and $\Gamma = O(10^{-8}-10^{-9})$. Therefore, at a frequency $f_0 \simeq 1$ kHz, we can have $\Delta f = O(10-100)$ Hz. An important point that we understand from this result (and which was fully realized only in the 1980s) is that the useful bandwidth of a resonant bar has nothing to do with the width of the peak of the resonance in the transfer function. In fact, the latter is $(\Delta f)_{\text{res}} = f_0/Q$ and, for typical values $Q \sim 10^6$ and $f_0 \sim 1$ kHz, it is extremely small, of order of 1 mHz. Instead the useful bandwidth, given in eq. (8.144), is many order of magnitude larger: it depends on Q only as $1/Q^{1/2}$ rather than as $1/Q$ (since $\Gamma \sim 1/Q$), and we see from eq. (8.145) that it can be made larger lowering the amplifier noise, so it really depends on the details of the read-out system.²⁷

When $\Delta t = (\Delta t)_{\text{opt}}$, the two terms on the right-hand side of eq. (8.143) become equal, and

$$\Delta E_{\min} \sim 2kT \frac{(\Delta t)_{\text{opt}}}{\tau}. \quad (8.146)$$

²⁷Observe also that $S_{\xi_t}^{\text{ampl}}$ is proportional to $1/\alpha^2$, see eq. (8.138), and therefore to $1/\beta^2$, see eq. (8.101). Therefore eq. (8.145) show that Γ is proportional to $1/\beta^2$ and, from eq. (8.144), Δf is proportional to β . Therefore the bandwidth can be enlarged increasing β , i.e. the coupling of the mechanical to the electric modes, compare with Note 20 on page 434.

Writing $(\Delta t)_{\text{opt}} \sim 1/\Delta f$ and $1/\tau_0 = \gamma_0 = \omega_0/Q$, we get

$$\Delta E_{\min} = kT_{\text{eff}}, \quad (8.147)$$

with an *effective temperature* T_{eff} given by

$$T_{\text{eff}} \sim \frac{4\pi}{Q} \frac{f_0}{\Delta f} T \simeq 4\Gamma^{1/2} T. \quad (8.148)$$

For a bar cooled at a thermodynamic temperature $T \simeq 2$ K, with $Q \simeq 1 \times 10^6$, $\Delta f \simeq 10$ Hz, $f_0 \simeq 900$ Hz, eq. (8.148) gives $T_{\text{eff}} \simeq 2$ mK. This result is quite interesting; it means that, even in a bar at the thermodynamical temperature of 2 K, we can detect bursts that deposited in it an energy E_s of just a few mK. The fact that, sampling the output at a fast rate, we can dig deeply into thermal noise, is of course just an example of the general concept of matched filtering that we discussed in Section 7.3.

To have a more detailed picture, we consider now the noise spectral density. The total noise spectral density is

$$S_n(f) = S_n^{\text{thermal}}(f) + S_n^{\text{ampl}}(f), \quad (8.149)$$

with $S_n^{\text{thermal}}(f)$ is the spectral density of thermal noise (bar plus transducer) given in eq. (8.137) and $S_n^{\text{ampl}}(f)$ is the spectral density of the amplifier noise given in eq. (8.141). The total strain sensitivity is $S_n^{1/2}(f)$. Explicitly, recalling that $\mu = m_t/m = 2m_t/M$, we have

$$S_n(f) = \frac{\pi kT}{Mv_s^2 f_0} \left\{ \frac{f_0^4}{f^4} \left[\frac{1}{Q_0} + \frac{1}{\mu Q_t} \frac{(f^2 - f_0^2)^2}{f_0^4} \right] + \frac{Q\Gamma}{\mu} \frac{[(f^2 - f_+^2)^2 + (ff_0/Q_m)^2][(f^2 - f_-^2)^2 + (ff_0/Q_m)^2]}{f^4 f_0^4} \right\}. \quad (8.150)$$

We recall that Q_0, Q_t are the quality factors of the fundamental mode of the bar ξ_0 and of the transducer ξ_t , respectively; Q_m is the total mechanical quality factor, see eq. (8.96) and Q , which enters in the definition (8.145) of Γ , is the total quality factor of the system.

We see that, for given values of the quality factors and of μ , the factor Γ determines the relative importance of thermal and read-out noise, and therefore controls the bandwidth Δf .

In Figs. 8.11–8.13 we plot the logarithm of the total strain sensitivity $[S_n(f)]^{1/2}$ (solid line) and the separate contribution from thermal noise of the bar and of the transducer $[S_n^{\text{thermal}}(f)]^{1/2}$ (dot-dashed line), and from the amplifier noise, $[S_n^{\text{ampl}}(f)]^{1/2}$ (dashed line). We use for definiteness the values $\mu = 2.4 \times 10^{-4}$, $Q_0 = Q_t = Q = 2 \times 10^6$, $T = 1$ K, $M = 2300$ kg, $v_s = 5400$ m/s, $f_0 = 915$ Hz, and we vary Γ , so we change the relative importance of amplifier and thermal noise.

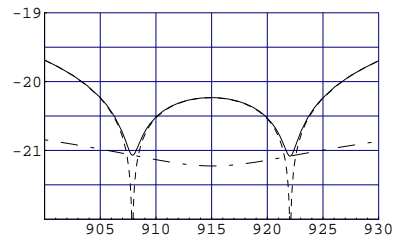


Fig. 8.11 $\log_{10}[S_n^{1/2}]$ as a function of the frequency, in Hz, taking $\Gamma = 10^{-7}$. The other parameters are given in the text. Dashed line: amplifier noise. Dot-dashed line: thermal noise (bar plus transducer). Solid line: total. Here the amplifier noise dominates, except very close to the resonances.

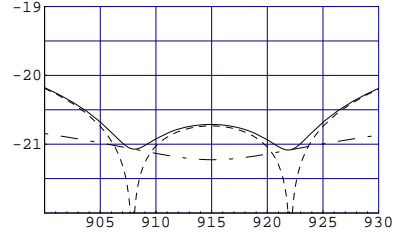


Fig. 8.12 The same as Fig. 8.11, but with $\Gamma = 10^{-8}$. Thermal and amplifier noise are comparable.

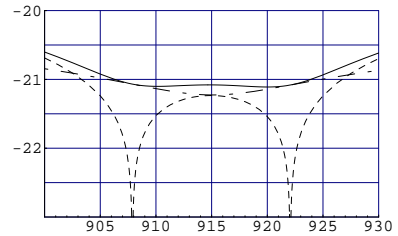


Fig. 8.13 The same as Fig. 8.11, but with $\Gamma = 10^{-9}$. Now thermal noise dominates (which means that one has chosen a transducer too light).

8.3.3 Back-action noise and the quantum limit

In this section we discuss another source of intrinsic noise, the *back-action* noise, that in present resonant detectors is small, but which can become important for the design of advanced detectors, and also has an intrinsic conceptual interest, because of its relation with fundamental limitations imposed by quantum mechanics.

When we studied the double oscillator, in Section 8.2.1, we introduced external forces acting on the oscillator ξ_0 (which represents the fundamental mode of the bar) and on the oscillator ξ_t , which represents the light mass, and we denoted these forces by F_0 and F_t respectively. We then wrote the equations of motion in the form (8.72)–(8.73). Furthermore, we had an elastic force acting *between* the bar and the light mass. Defining the spring constant $k = m_t \omega_t^2$, eqs. (8.72) and (8.73) can be rewritten as

$$m(\ddot{\xi}_0 + \omega_0^2 \xi_0) = +k(\xi_t - \xi_0) + F_0, \quad (8.151)$$

$$m_t \ddot{\xi}_t = -k(\xi_t - \xi_0) + F_t. \quad (8.152)$$

Of course, since the force $k(\xi_t - \xi_0)$ acts between the bar and the light mass, it enters with opposite signs in the equations for $\ddot{\xi}_0$ and for $\ddot{\xi}_t$.

As we saw in Section 8.2.2, this coupling between ξ_0 and ξ_t is a schematization of an extended device which consists of a capacitor, which in turn is part of an LC circuit, and is connected to an amplifier. This read-out has been designed so that the mechanical oscillations of the transducer are transformed into an electric signal. Unfortunately this process is reversible, and fluctuations in the electric circuit generate a force that actually shakes the transducer and the bar. Any noise in the electronic apparatus will then appear as a stochastic force F_{0t} acting *between* the bar and the light mass. This force is called the back-action exerted on the bar and on the light mass by the amplifier. More generally, it describes the effect of any fluctuation taking place between the bar and the transducer, e.g. fluctuations of the electric field in the capacitor. Then eqs. (8.151) and (8.151) must rather be written as

$$\begin{aligned} m(\ddot{\xi}_0 + \omega_0^2 \xi_0) &= +k(\xi_t - \xi_0) + F_{0t} + F_0, \\ m_t \ddot{\xi}_t &= -k(\xi_t - \xi_0) - F_{0t} + F_t, \end{aligned} \quad (8.153)$$

or, including also the dissipation terms as in eqs. (8.88) and (8.89),

$$\begin{aligned} m(\ddot{\xi}_0 + \omega_0^2 \xi_0) &= +k(\xi_t - \xi_0) + [F_{0t} + m_t \gamma_t (\dot{\xi}_t - \dot{\xi}_0)] + [F_0 - m \gamma_0 \dot{\xi}_0], \\ m_t \ddot{\xi}_t &= -k(\xi_t - \xi_0) - [F_{0t} + m_t \gamma_t (\dot{\xi}_t - \dot{\xi}_0)] + F_t. \end{aligned} \quad (8.154)$$

Having extracted explicitly these dissipation terms, now F_0 and F_{0t} are stochastic forces with zero mean, $\langle F_{0t} \rangle = \langle F_0 \rangle = 0$, characterized by their spectral densities S_{F_0} and $S_{F_{0t}}$. (Since we are studying the noise acting on the bar, we can assume that there is no GW contribution to F_0 ; otherwise, we can just extract the GW force and write it explicitly.) Then the spectral densities of eq. (8.133) must be replaced by

$$S_{F_0} \rightarrow S_{F_0} + S_{F_{0t}}, \quad S_{F_t} \rightarrow S_{F_t} + S_{F_{0t}}. \quad (8.155)$$

To evaluate S_{F_0t} we consider for instance the case of a voltage amplifier.²⁸ In a voltage amplifier the noise can be described by a voltage noise plus independent fluctuations in the current. We denote the single-sided spectral densities of the voltage and current noise by v_n^2 (measured in volts²/Hz) and i_n^2 (in amp²/Hz), respectively. The spectral density of the output voltage V is given by $S_V = v_n^2 + |Z|^2 i_n^2$, where Z is the impedance, and we neglected correlated noise between voltage and current. It is customary to define the noise temperature T_n of the amplifier by $2kT_n = v_n i_n$ (where the factor of 2 is due to the fact that we use single-side spectral densities), and the amplifier noise resistance $R_n = v_n / i_n$. Introducing further the dimensionless quantity $\lambda = R_n / |Z|$, known as the impedance match ratio, and using eq. (8.101), one gets

$$\begin{aligned} S_{\xi_t}^{\text{ampl}} &= \frac{1}{\alpha^2} (v_n^2 + |Z|^2 i_n^2) \\ &= \frac{2kT_n}{m_t \omega_0^3 \beta} \left(\lambda + \frac{1}{\lambda} \right). \end{aligned} \quad (8.156)$$

The back-action force due to current fluctuations can be computed in this case observing that the power dissipated in the electric circuit is $P = VI$. The contribution to V due to the displacement of the transducer is obtained from eq. (8.98), $V = Z_{21}\dot{\xi}_t$, so the corresponding power is $P = Z_{21}I\dot{\xi}_t$. This is the power generated by a force of modulus $Z_{21}I$ acting on a mechanical object with velocity $\dot{\xi}_t$. Therefore a current I in the circuit exerts on the transducer a force of modulus $F_{0t} = Z_{21}I$, and the spectral density of this back-action force is $S_{F_{0t}} = |Z_{21}|^2 i_n^2$, where i_n is the spectral density of the current. As we saw below eq. (8.98), $|Z_{21}| = \alpha/\omega_0$, so $S_{F_{0t}} = \alpha^2 i_n^2 / \omega_0^2$. In terms of T_n and λ , we have $i_n^2 = 2kT_n / \lambda |Z|$, and therefore

$$S_{F_t} + S_{F_{0t}} = 4kT m_t \gamma_t + 2kT_n \frac{\alpha^2}{\omega_0^2 \lambda |Z|}. \quad (8.157)$$

Expressing the result in terms of β , given in eq. (8.102), we find

$$S_{F_t} + S_{F_{0t}} = 4m_t \gamma_t \left(kT + kT_n \frac{\beta Q_t}{2\lambda} \right). \quad (8.158)$$

Therefore, at least in a first approximation,²⁹ the back action is formally equivalent to a shift of the transducer temperature

$$T \rightarrow T + \frac{\beta Q_t}{2\lambda} T_n.$$

(8.159)

For the amplifier noise we use eq. (8.156). Typically $\lambda \gg 1$ so, $S_{\xi_t}^{\text{ampl}} \simeq 2kT_n \lambda / m_t \omega_0^3 \beta$. Then, including the back-action, the minimum detectable energy (8.143) becomes

$$\Delta E_{\min} \sim \left(kT + \frac{\beta Q}{2\lambda} kT_n \right) \frac{\Delta t}{\tau} + \frac{2kT_n \lambda}{\beta \omega_0 \Delta t}. \quad (8.160)$$

²⁸This example is somewhat old-fashioned, since modern resonant detectors use SQUIDS rather than voltage amplifiers, but is the simplest setting for illustrating the general ideas.

²⁹A more detailed computation based on the full set of equations governing the coupled mechanical and electric modes show that the strain sensitivity of the back-reaction has a different form, as a function of the frequency, from that due to thermal noise.

This expression raises an interesting issue of principle because it shows that, even if one were able to cool the bar to a negligibly small value of the thermodynamic temperature T , still there would be a minimum value of the detectable energy, since even at $T = 0$ we have both a term proportional to Δt and a term proportional to $1/\Delta t$. Setting $T = 0$ in eq. (8.160) and writing $\tau = Q/\omega_0$, we have

$$\Delta E_{\min} \sim kT_n \left(\frac{\beta\omega_0}{2\lambda} \Delta t + \frac{2\lambda}{\beta\omega_0} \frac{1}{\Delta t} \right). \quad (8.161)$$

This is minimized choosing $(\Delta t)_{\text{opt}} = 2\lambda/(\beta\omega_0)$, and the corresponding minimum detectable value of the energy is

$$\Delta E_{\min} \sim 2kT_n. \quad (8.162)$$

Therefore, even if we cool the detector to T close to zero, an ultimate limitation is provided by the amplifier noise temperature. For a SQUID, $T_n \sim 10^{-3}$ mK, while the lowest effective temperatures that have been reached by bars at present are of the order of 0.3 mK, so this limit at present is not very important from a practical point of view.

Nevertheless, this observation brings us to a second interesting question, namely, what is the minimum value that can be obtained in principle for the amplifier noise temperature T_n ? As we will discuss in the next subsection (and as was shown by Heffner, already in 1962) any linear amplifier (e.g. an object that preserves a linear relation between the input and output values of the amplitude and the phase of the signal) working at a frequency ω_0 , as a consequence of the uncertainty principle, has a minimum noise temperature given by

$$kT_n \sim \hbar\omega_0. \quad (8.163)$$

We therefore discover that the ultimate limitation for a resonant bar operating with a linear amplifier is given by the uncertainty principle,

$$\Delta E_{\min} \gtrsim \hbar\omega_0.$$

(8.164)

This is known as the *standard quantum limit*. It states that the best we can do (with a linear amplifier) is to detect an acoustic oscillation of the fundamental mode of the bar which, at the quantum level, corresponds to a single phonon.

A measure of how far we are presently from the quantum limit is provided by

$$N_{\text{phonon}} = \frac{kT_{\text{eff}}}{\hbar\omega_0}. \quad (8.165)$$

For $T_{\text{eff}} \simeq 2$ mK and $f_0 = 900$ Hz, $N_{\text{phonon}} \simeq 5 \times 10^4$. Both the group that runs the EXPLORER and NAUTILUS detectors and the AURIGA group have attained $N_{\text{phonon}} \simeq 10^2$ so, for the moment, the quantum limit is not the main limitation in resonant bars, although we are getting closer to it. The detection of a single-phonon excitation in a two-ton bar

would be a remarkable technical achievement, and would correspond to an energy detection sensitivity at the level $\hbar\omega_0 \simeq 6 \times 10^{-31}$ J.

Further reflection shows that the quantum limit, in itself, cannot be an absolute limit. Quantum mechanics does not forbid arbitrarily precise measurements of energy, but only arbitrarily precise simultaneous measurements of conjugate variables. The origin of the problem is that a linear amplifier allows us to reconstruct both the amplitude and the phase of the motion of the oscillator ξ_t . However, for a harmonic oscillator, to know its amplitude and its phase is equivalent to knowing simultaneously the position and the momentum, and it is here that the Heisenberg principle comes into play. The quantum limit can therefore be evaded if we give up the information on the phase. We discuss the issue in more detail in the next subsection.

8.3.4 Quantum non-demolition measurements

Consider a generic harmonic oscillator, with mass m and frequency ω_0 , described classically by a coordinate $x(t)$. The solution of the equation of motion with the initial conditions $x(0) = x_0$ and $\dot{x}(0) = v_0$ is

$$x(t) = x_0 \cos \omega_0 t + \frac{v_0}{\omega_0} \sin \omega_0 t. \quad (8.166)$$

Let $v(t) = \dot{x}(t)$, and define X_1, X_2 as

$$X_1 = x(t) \cos \omega_0 t - \frac{v(t)}{\omega_0} \sin \omega_0 t, \quad (8.167)$$

$$X_2 = x(t) \sin \omega_0 t + \frac{v(t)}{\omega_0} \cos \omega_0 t. \quad (8.168)$$

Using eq. (8.166) and the corresponding expression for $v(t)$, we see that $X_1 = x_0$ and $X_2 = v_0/\omega_0$, so X_1, X_2 are conserved on the equations of motion, and eq. (8.166) can be rewritten as

$$x(t) = \text{Re} [(X_1 + iX_2)e^{-i\omega_0 t}]. \quad (8.169)$$

At the quantum level, we denote the operators by a caret, so \hat{x} and \hat{p} are the position and momentum operators, with $[\hat{x}, \hat{p}] = i\hbar$. As usual, the Hamiltonian of the harmonic oscillator is

$$\hat{H}_0 = \frac{\hat{p}^2}{2m} + \frac{1}{2}m\omega_0^2 \hat{x}^2 = \hbar\omega_0 \left(\hat{N} + \frac{1}{2} \right), \quad (8.170)$$

where $\hat{N} = \hat{a}^\dagger \hat{a}$, and

$$\hat{a} = \left(\frac{m\omega_0}{2\hbar} \right)^{1/2} \left(\hat{x} + i \frac{\hat{p}}{m\omega_0} \right), \quad (8.171)$$

$$\hat{a}^\dagger = \left(\frac{m\omega_0}{2\hbar} \right)^{1/2} \left(\hat{x} - i \frac{\hat{p}}{m\omega_0} \right). \quad (8.172)$$

In the Heisenberg picture we define the operators \hat{X}_1 and \hat{X}_2 as in eqs. (8.167) and (8.168),

$$\hat{X}_1(t) = \hat{x}(t) \cos \omega_0 t - \frac{\hat{p}(t)}{m\omega_0} \sin \omega_0 t, \quad (8.173)$$

$$\hat{X}_2(t) = \hat{x}(t) \sin \omega_0 t + \frac{\hat{p}(t)}{m\omega_0} \cos \omega_0 t. \quad (8.174)$$

Similarly to what happens classically, in the absence of external forces the Heisenberg operators $\hat{X}_1(t)$ and $\hat{X}_2(t)$ are conserved,

$$\frac{d\hat{X}_i}{dt} = \frac{\partial \hat{X}_i}{\partial t} - \frac{i}{\hbar} [\hat{X}_i, H_0] = 0. \quad (8.175)$$

This property selects \hat{X}_1 and \hat{X}_2 as particularly useful observables, since any change they experience must be due to external disturbances, such as GWs or other external forces. The interaction of the quantum harmonic oscillator with an external classical force $F(t)$ can be described by an interaction Hamiltonian $\hat{H}_{\text{int}} = -F(t)\hat{x}$. In the presence of $F(t)$, \hat{X}_1 and \hat{X}_2 are no longer conserved; rather

$$\frac{d\hat{X}_1}{dt} = -\frac{i}{\hbar} [\hat{X}_1, H_{\text{int}}] = -\frac{F(t)}{m\omega_0} \sin \omega_0 t, \quad (8.176)$$

$$\frac{d\hat{X}_2}{dt} = -\frac{i}{\hbar} [\hat{X}_2, H_{\text{int}}] = +\frac{F(t)}{m\omega_0} \cos \omega_0 t. \quad (8.177)$$

This integrates to

$$\hat{X}_1(t) = \hat{X}_1(t_0) - \frac{1}{m\omega_0} \int_{t_0}^t dt' F(t') \sin \omega_0 t', \quad (8.178)$$

and similarly for \hat{X}_2 . The important point is that, since $F(t)$ is a classical force, the second term on the right-hand side is a *c*-number rather than an operator. Suppose that at time t_0 we perform a measurement of the observable \hat{X}_1 on the oscillator. We will find some value X_1^0 , and the measurement leaves the oscillator in the corresponding eigenstate $|X_1^0\rangle$ of $\hat{X}_1(t_0)$. In the Heisenberg picture the state $|X_1^0\rangle$ does not evolve, while the operator $\hat{X}_1(t)$ evolves as in eq. (8.178). Then, since the second term on the right-hand side of eq. (8.178) is a *c*-number, for $t > t_0$ we have

$$\hat{X}_1(t)|X_1^0\rangle = X_1(t)|X_1^0\rangle, \quad (8.179)$$

with

$$X_1(t) = X_1^0 - \frac{1}{m\omega_0} \int_{t_0}^t dt' F(t') \sin \omega_0 t'. \quad (8.180)$$

So, at time $t > t_0$ the oscillator is still in an eigenstate of $\hat{X}_1(t)$, and a measurement of \hat{X}_1 at time t will give the above value, and will not affect the oscillator state (apart possibly for a phase, since states in the Fock space that differ by a phase correspond to the same physical state). In other words, when the classical force $F(t)$ is acting, after the

first measurement, all successive measurements of \hat{X}_1 leave unchanged the state of the oscillator, even if the result $X_1(t)$ of this measurement changes continuously in time, see eq. (8.180).

This is of course very different from what happens when we rather measure the position operator $\hat{x}(t)$ of the oscillator, since in this case each time we perform a measurement of $\hat{x}(t)$ we have a wavefunction reduction which forces the oscillator in an eigenstate of $\hat{x}(t)$, and the result obtained at $t = t_0$ does not fix uniquely the outcome of a successive measurement at $t > t_0$. It is clear that X_1 (or X_2) are the best quantities to be measured when quantum mechanics becomes important, since from a series of repeated measurements of it we can reconstruct deterministically the time-evolution of the external classical force $F(t)$. A measurement that leaves the state of the system unchanged, as the measurement of $\hat{X}_1(t)$ described above, is called a *quantum non-demolition* measurement.

Having established that \hat{X}_1 and \hat{X}_2 are the most useful observables for our purposes, we can discuss what the uncertainty principles has to tell about their measurement. From the definition, eq. (8.173), we see that

$$[X_1, X_2] = \frac{i\hbar}{m\omega_0}. \quad (8.181)$$

Therefore, on any state,

$$\Delta X_1 \Delta X_2 \geq \frac{1}{2} |\langle [X_1, X_2] \rangle| = \frac{\hbar}{2m\omega_0}. \quad (8.182)$$

Suppose that we measure X_1 and X_2 using an amplifier with a bandwidth $\Delta f \ll f_0$. This means that we sample the oscillator position over a time Δt much longer than the period of the oscillator. Therefore we are actually measuring the average value of X_1 and X_2 over a period, that we denote by \bar{X}_1 and \bar{X}_2 , respectively. If we use a linear amplifier, when the input is given by eq. (8.169), the output is of the form

$$y(t) = \text{Re} [A(\bar{X}_1 + i\bar{X}_2)e^{-i\omega_0 t}], \quad (8.183)$$

with A a constant amplification factor, in general complex. Since \bar{X}_1 and \bar{X}_2 are treated symmetrically in this expression, their errors are equal, $\Delta\bar{X}_1 = \Delta\bar{X}_2$. In this case eq. (8.182) gives

$$\Delta\bar{X}_1 = \Delta\bar{X}_2 \geq \left(\frac{\hbar}{2m\omega_0} \right)^{1/2}. \quad (8.184)$$

Recall from eq. (8.173) that (X_1, X_2) are obtained from $(x, p/m\omega_0)$ performing a rotation by an angle $\omega_0 t$. Then $\Delta\bar{X}_1 = \Delta\bar{X}_2$ implies also $\Delta x = \Delta p/m\omega_0$ which, together with $\Delta x \Delta p \geq \hbar/2$, means

$$\Delta x = \frac{\Delta p}{m\omega_0} \geq \left(\frac{\hbar}{2m\omega_0} \right)^{1/2}. \quad (8.185)$$

Therefore, if we monitor the fundamental mode of the bar with a linear amplifier, quantum mechanics sets a limit to the error Δx . Writing, as

usual, $m = M/2$, where M is the total mass of the bar, we have

$$(\Delta x)_{\min} \simeq 2.9 \times 10^{-19} \text{ cm} \left(\frac{2000 \text{ kg}}{M} \right)^{1/2} \left(\frac{1 \text{ kHz}}{f_0} \right)^{1/2}. \quad (8.186)$$

In terms of energy, writing

$$\hat{H}_0 = \frac{m\omega_0^2}{2} \left[\left(\frac{\hat{p}}{m\omega_0} \right)^2 + \hat{x}^2 \right], \quad (8.187)$$

we see from eq. (8.185) that, even if the oscillator is in its ground state, there is a minimum error on the energy

$$(\Delta E)_{\min} \simeq \frac{m\omega_0^2}{2} \left[\left(\frac{\Delta p}{m\omega_0} \right)^2 + (\Delta x)^2 \right] = \frac{1}{2} \hbar\omega_0. \quad (8.188)$$

More generally, if one takes as wavefunction a Gaussian both in X_1 and X_2 , centered on the expectation values $\langle \hat{X}_1 \rangle$ and $\langle \hat{X}_2 \rangle$, and with variances $\Delta X_1 = \Delta X_2 = (\hbar/2m\omega_0)^{1/2}$, one finds that the variance of the average number of quanta in this state is $\Delta N = (N + 1/4)^{1/2}$ and therefore

$$(\Delta E)_{\min} = \hbar\omega_0 \left(N + \frac{1}{4} \right)^{1/2}. \quad (8.189)$$

We have therefore understood how eq. (8.164) comes out: it is a consequence of the uncertainty principle *and* of the specific way of performing the measurement with a linear amplifier, which gives $\Delta X_1 = \Delta X_2$. Now, however, we can also understand how, at least in principle, such a limit can be evaded: from eq. (8.178) we see that measuring *either* X_1 *or* X_2 is sufficient to reconstruct the external force $F(t)$, which in our case means to measure the incoming GW. So, we need to perform a very precise measurement of, say, X_1 , giving up completely the information of X_2 . Strategies of this type are called back-action evasion measurements, since the back-action force on X_1 caused by the measurement process, which in general is responsible for the uncertainty principle, has been evaded, or rather has been concentrated uniquely on the conjugate variable X_2 .

More precisely, from eq. (8.180), we have

$$\frac{dX_1(t)}{dt} = -\frac{1}{m\omega_0} F(t) \sin \omega_0 t, \quad (8.190)$$

and from this we can accurately reconstruct $F(t)$, except when $\sin \omega_0 t$ is close to zero. However, when $F(t)$ is a classical force, we can also use a second transducer, on which we measure only $X_2(t)$, since this second transducer is affected by the same classical force $F(t)$. Then from this measurement we get

$$\frac{dX_2(t)}{dt} = \frac{1}{m\omega_0} F(t) \cos \omega_0 t, \quad (8.191)$$

and $F(t)$ can be completely reconstructed.

8.3.5 Experimental sensitivities

In this section we discuss the sensitivities of existing resonant detectors. Actually, the experimental situation is in continuous evolution; all detectors typically alternate data-taking periods with upgrades, old experiments terminate their activity, and new ones are sometime proposed. Thus, any discussion of the experimental situation is bound to become obsolete on a relatively short time-scale. We therefore discuss only very briefly the various detectors, referring the reader to the web pages of the various collaborations in the Further Reading section for updated information, and we rather discuss what results can be achieved with existing or foreseeable sensitivities.

Presently (2007) three resonant bars are in operation: AURIGA (Legnaro, near Padua), EXPLORER (CERN) and NAUTILUS (Frascati, near Rome), while a fourth bar, ALLEGRO (Baton Rouge, Louisiana), terminated operation during 2007. EXPLORER and NAUTILUS are operated by the same collaboration (ROG). We show in Fig. 8.14 a picture of NAUTILUS and in Fig. 8.15 a picture of AURIGA. In Fig. 8.16 we show a typical strain sensitivity curve of the EXPLORER and NAUTILUS detector, and in Fig. 8.17 a typical the strain sensitivity of AURIGA. We see that, thanks to the improvement in the read-out system discussed in Section 8.2.2, this strain sensitivity has a minimum value

$$S_n^{1/2} \simeq 1 \times 10^{-21} \text{ Hz}^{-1/2}, \quad (8.192)$$

and stays below $4 \times 10^{-21} \text{ Hz}^{-1/2}$ over a bandwidth of 100 Hz. We now discuss, using the results of Section 7.3, the sensitivity to bursts, periodic and stochastic signals that can be obtained with these strain sensitivities.

Sensitivity to bursts

Using eq. (7.96) at $S/N = 1$ (of course a higher threshold, typically of order 5–6, must be used), we can estimate that $|\tilde{h}(f_0)| \simeq [S_n/(4\Delta f)]^{1/2}$. Using an average reference value $S_n^{1/2} \sim 4 \times 10^{-21} \text{ Hz}^{-1/2}$ over a bandwidth $\Delta f \sim 100 \text{ Hz}$ gives the order-of magnitude estimate for the minimum detectable value of $\tilde{h}(f_0)$,

$$|\tilde{h}(f_0)| \sim 2 \times 10^{-22} \text{ Hz}^{-1}. \quad (8.193)$$

Assuming a sine-Gaussian waveform (7.103), centered on the resonance frequency f_0 of the detector and of duration τ_g , and using eq. (7.105), we get the minimum detectable value of the GW amplitude,

$$h_0 \sim 2 \times 10^{-19} \left(\frac{1 \text{ ms}}{\tau_g} \right), \quad (8.194)$$

or equivalently, using eq. (7.110), the minimum detectable value of h_{rss} ,

$$h_{\text{rss}} \sim 5 \times 10^{-21} \text{ Hz}^{-1/2} \left(\frac{1 \text{ ms}}{\tau_g} \right)^{1/2}. \quad (8.195)$$



Fig. 8.14 A picture of the NAUTILUS resonant bar and of the cryostat.



Fig. 8.15 A picture of the AURIGA resonant bar. The transducer is visible.

³⁰These are the values for NAUTILUS, but they are very close for the other bars.

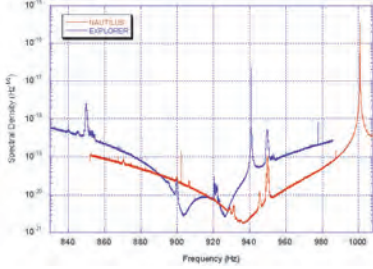


Fig. 8.16 The strain sensitivity $[S_n(f)]^{1/2}$ of EXPLORER (the curve with two minima) and NAUTILUS (the curve with one broad minimum) in 2004. The peaks around 940 and 1000 Hz, respectively, are reference signals sent to the detectors to monitor the SQUID gain.

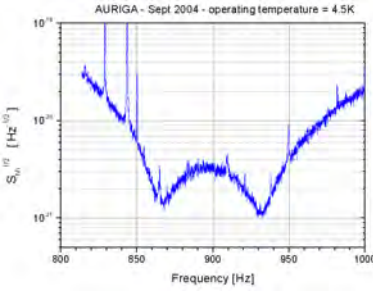


Fig. 8.17 The strain sensitivity $[S_n(f)]^{1/2}$ of AURIGA in 2004.

For resonant bars it is often useful to think directly in terms of the energy deposited by a burst in the detector. In this case, inserting the numerical values³⁰ $M = 2260$ kg, $L = 3$ m, $f_0 = 940$ Hz, and measuring E_s in milliKelvin, eq. (8.19) gives

$$\tilde{h}(f_0) \simeq 2.5 \times 10^{-22} \text{ Hz}^{-1} \left(\frac{E_s}{1 \text{ mK}} \right)^{1/2}, \quad (8.196)$$

and we see from eq. (8.193) that present resonant detectors can measure excitations that leave in a bar an energy $E_s \sim 1$ mK. Assuming again a sine-Gaussian waveform centered within the detector bandwidth, and using eqs. (7.104) and (7.110), we get $h_{\text{rss}}^2 = (2/\pi)^{1/2} |\tilde{h}(f_0)|^2 / \tau_g$. Inserting this into eq. (7.112) and using eq. (8.196) we find that a GW burst that deposited in a resonant bar an energy E_s should originate from a process that liberated in GWs the energy

$$\Delta E_{\text{rad}} \simeq 5 \times 10^{-5} M_\odot c^2 \left(\frac{E_s}{1 \text{ mK}} \right) \left(\frac{r}{8 \text{ kpc}} \right)^2 \left(\frac{1 \text{ ms}}{\tau_g} \right) \left(\frac{f_0}{1 \text{ kHz}} \right)^2. \quad (8.197)$$

The above equation tells us at what maximum distance a resonant bar can see a GW burst, given the minimum value of E_s that can be measured. For a GW burst that liberates an energy $10^{-2} M_\odot c^2$ (such as the merging phase of a NS-NS coalescence), with $f_0 = 1$ kHz and $\tau_g = 1$ ms, we get

$$r_{\text{max}} \sim O(100) \text{ kpc} \left(\frac{1 \text{ mK}}{E_{s,\text{min}}} \right)^{1/2}, \quad (8.198)$$

so we have access to galactic events and to our immediate galactic neighborhood. However, events liberating $10^{-2} M_\odot c^2$ are extremely rare on a galactic scale. Less energetic events will be more common, but of course we can see them only if they are even closer. From eq. (8.197), setting $E_{s,\text{min}} = 1$ mK, we see that for a phenomenon taking place at 80 pc (corresponding to the distance to the closest known neutron stars, while the closest estimated neutron star should be at 5–10 pc), we need a process that liberates $\Delta E_{\text{rad}} \simeq 5 \times 10^{-9} M_\odot c^2$.

Sensitivity to periodic signals

The minimum detectable amplitude of a periodic signal has been computed in eq. (7.164). For present resonant bars, we normalize the spectral sensitivity to the value given in eq. (8.192). Recall also that $\eta = (S/N) \mathcal{N}^{1/4} \langle F_+^2 \rangle^{-1/2}$, see eq. (7.165), is a factor that takes into account the desired level of S/N , the need to split the data into \mathcal{N} stack for computational feasibility, and the angular efficiency factor $\langle F_+^2 \rangle^{-1/2}$. For resonant bars $\langle F_+^2 \rangle^{-1/2} = (15/4)^{1/2} \simeq 2$, see Table 7.1. For a blind full sky search one could use stacks of length less than one hour, which is

about the maximum value for which the Doppler effect within a stack can be neglected, see eq. (7.140). This, for one year of data, gives $\mathcal{N} \sim 10^4$, so $\mathcal{N}^{1/4} \simeq 10$. Therefore, at $S/N = 1$, we have $\eta \simeq 20$.

Using this reference values for η , the minimum detectable amplitude of a periodic signal, eq. (7.164), can be rewritten as

$$h_{\min} = 4 \times 10^{-24} \left(\frac{\eta}{20} \right) \left(\frac{S_n^{1/2}(f_0)}{10^{-21} \text{ Hz}^{-1/2}} \right) \left(\frac{3 \times 10^7 \text{ s}}{T} \right)^{1/2}, \quad (8.199)$$

and, using eq. (7.166), the maximum distance at which we can see the signal from a spinning NS is

$$\begin{aligned} r \simeq 290 \text{ pc} & \left(\frac{20}{\eta} \right) \left(\frac{10^{-21} \text{ Hz}^{-1/2}}{S_n^{1/2}(f_0)} \right) \left(\frac{T}{3 \times 10^7 \text{ s}} \right)^{1/2} \\ & \times \left(\frac{\epsilon}{10^{-6}} \right) \left(\frac{I_{zz}}{10^{38} \text{ kg m}^2} \right) \left(\frac{f_0}{1 \text{ kHz}} \right)^2. \end{aligned} \quad (8.200)$$

However, if one is targeting a specific pulsar, the reference values for $S_n^{1/2}$ and η change. First of all, as discussed in Section 7.6, the need to divide the observation time into \mathcal{N} stacks with $\mathcal{N} \gg 1$ emerges only when we perform blind searches, in order to keep the computational burden within affordable limits. In a dedicated search to a single source there is no need for it, and the only limitation comes from the maximum consecutive time that a detector can run without interruptions due to maintenance. Taking $T_{\text{stack}} \sim 1 - 2$ week, in one year we get $\mathcal{N}^{1/4} \sim 2.5$ and therefore, at $S/N = 1$, we can take $\eta = 5$ as a more appropriate reference value.

Furthermore, if we know the frequency of the source, we can tune the frequency of the detector to this value.³¹ Once one of the resonance frequencies of the bar-transducer system has been tuned to the target source, we can give up the condition of having a bandwidth as large as possible, in favor of a better sensitivity at the resonance frequency. According to the discussion in Section 8.3, this means that we must reduce as much as possible the thermal noise, so that it goes below the amplifier noise, which is by itself very much suppressed at the resonance frequencies f_{\pm} . In this way, better peak sensitivity can indeed be obtained. For instance, AURIGA reached $S_n^{1/2} = 4 \times 10^{-22} \text{ Hz}^{-1/2}$ over a 2 Hz bandwidth, cooling the detector down to 0.24 K. Using these reference values for $S_n^{1/2}$ and η , eqs. (8.199) and (8.200) can be rewritten as

$$h_{\min} = 4 \times 10^{-25} \left(\frac{\eta}{5} \right) \left(\frac{S_n^{1/2}(f_0)}{4 \times 10^{-22} \text{ Hz}^{-1/2}} \right) \left(\frac{3 \times 10^7 \text{ s}}{T} \right)^{1/2}, \quad (8.201)$$

$$\begin{aligned} r \simeq 2.9 \text{ kpc} & \left(\frac{5}{\eta} \right) \left(\frac{4 \times 10^{-22} \text{ Hz}^{-1/2}}{S_n^{1/2}(f_0)} \right) \left(\frac{T}{3 \times 10^7 \text{ s}} \right)^{1/2} \\ & \times \left(\frac{\epsilon}{10^{-6}} \right) \left(\frac{I_{zz}}{10^{38} \text{ kg m}^2} \right) \left(\frac{f_0}{1 \text{ kHz}} \right)^2. \end{aligned} \quad (8.202)$$

³¹Within $O(50)$ Hz this can be done simply at the level of electronics, changing the electric field in the transducer, which results in a change in the normal modes of the three-modes system made by the two mechanical oscillator and the electric mode. Otherwise, if one has a specific target in mind, one could build a dedicated bar, choosing length and material so to have the appropriate resonance frequency.

Coalescences

This is the kind of source for which the difference between bars and interferometers is more important. A ground-based interferometer is a broad-band detector, that operates from a few tens of Hz to a few kHz. In this bandwidth, we saw in Sections 4.1 and 7.7.2 that we can follow the evolution of the waveform for a number of cycles $\mathcal{N}_c \sim 10^4$, which results in a gain of order $\mathcal{N}_c^{1/2} \sim 100$ in the maximum distance at which we can detect a coalescence. For resonant detectors this is not possible. First of all, for BH-BH binaries with typical BH masses $\sim 10M_\odot$, the coalescence takes place when $f_{\text{gw}} \sim 400$ Hz, see eq. (4.40), therefore the signal never enters in the bandwidth of resonant bars, which operate at the kHz.³² For NS-NS binaries the coalescence takes place at the kHz, but then the bars only see the final merging phase, which lasts a few milliseconds, rather than the long inspiral phase. Thus, for a bar, a NS-NS coalescence is just a burst, and there is no gain associated to the number of cycles \mathcal{N}_c .

³²To build a resonant detector with a lower resonance frequency one should increase its size and mass, with a corresponding increase in technical difficulties, particularly in the cryogeny, and in the financial costs.

Stochastic backgrounds

Performing the correlation between two resonant bars, both working in a relatively narrow bandwidth around a frequency f_0 , the expression of the signal-to-noise ratio for stochastic backgrounds, eq. (7.239), becomes

$$\frac{S}{N} \simeq (2T\Delta f)^{1/2} \Gamma(f_0) \frac{S_h(f_0)}{S_n(f_0)}, \quad (8.203)$$

and for two resonant bars $\Gamma(f) = (8/15)\gamma(f)$, see eqs. (7.228) and (7.37) and Table 7.1 Therefore the minimum detectable value of $S_h(f_0)$, using an optimistic value $S/N = 1$, is

$$S_h^{1/2}(f_0) \simeq 7 \times 10^{-24} \text{ Hz}^{-1/2} \left(\frac{25 \text{ Hz}}{\Delta f} \right)^{1/4} \left(\frac{1 \text{ yr}}{T} \right)^{1/4} \times \left(\frac{S_n^{1/2}(f_0)}{10^{-21} \text{ Hz}^{-1/2}} \right)^{1/2} \left(\frac{1}{\gamma(f_0)} \right)^{1/2}, \quad (8.204)$$

corresponding to

$$h_0^2 \Omega_{\text{gw}}(f_0) \simeq 6 \times 10^{-2} \left(\frac{f_0}{1 \text{ kHz}} \right)^3 \left(\frac{25 \text{ Hz}}{\Delta f} \right)^{1/2} \left(\frac{1 \text{ yr}}{T} \right)^{1/2} \times \left(\frac{S_n^{1/2}(f_0)}{10^{-21} \text{ Hz}^{-1/2}} \right)^2 \frac{1}{\gamma(f_0)}. \quad (8.205)$$

As we will discuss in Vol. 2, there are bounds on stochastic background of GWs of cosmological origin that forbid values of $h_0^2 \Omega_{\text{gw}}$ larger than $\sim 10^{-5}-10^{-6}$ at any frequency, and astrophysical backgrounds are also expected to be below this value. With these sensitivities, resonant bars do not seem therefore capable of detecting a stochastic background, and for this reason these searches have not been much pursued.

The sensitivity at the quantum limit

We have seen in the previous sections that present resonant bars are dominated by thermal and read-out noise. Thermal noise in principle can be lowered cooling further the bars and increasing the quality factors, while for the read-out noise we have seen that an intrinsic limitation, if we do not use quantum non-demolition techniques, is given by the quantum limit.

We first of all compute under what conditions the thermal noise can be reduced below the quantum limit. Combining eqs. (7.96) and (8.19) we get

$$S_n(f_0) \simeq 4\Delta f \frac{E_s}{16ML^2f_0^4}. \quad (8.206)$$

If the read-out noise allows us to detect a vibration corresponding to N phonons, $S_n^{\text{ampl}}(f_0)$ is obtained from eq. (8.206) setting $E_s = N\hbar\omega_0$. We express L in terms of the speed of sound, $L = \pi v_s/\omega_0$, and we obtain

$$S_n^{\text{ampl}}(f_0) \simeq \frac{2\pi}{Mv_s^2} \left(\frac{\Delta f}{f_0} \right) N\hbar. \quad (8.207)$$

As for thermal noise, eq. (8.137) gives

$$S_n^{\text{thermal}}(f_0) = \frac{\pi}{Q} \frac{kT}{Mv_s^2} \frac{1}{f_0}. \quad (8.208)$$

Requiring that $S_n^{\text{thermal}}(f_0) < S_n^{\text{ampl}}(f_0)$ we therefore get

$$Q > \frac{kT}{2N\hbar\Delta f}. \quad (8.209)$$

The quantum limit corresponds to $N = 1$, and we then find that, to bring thermal noise below the quantum limit, we need

$$Q > 6.6 \times 10^7 \left(\frac{T}{100 \text{ mK}} \right) \left(\frac{100 \text{ Hz}}{\Delta f} \right). \quad (8.210)$$

Therefore, for a detector cooled at $T = 20 \text{ mK}$ and with a bandwidth $\Delta f = 100 \text{ Hz}$, we need $Q > 10^7$. This is not an unrealistic target with present improvements in materials. Of course, beside being able to push thermal noise below the quantum limit, we must also be able to detect excitations with $N = O(1)$ in a two-ton bar. Presently, using double SQUIDs, one is able to reach $N = O(100)$, and further progress can be expected in the near future. It therefore appears that reaching the quantum limit, or at least getting close to it, is a challenging but not unrealistic target, and we can take the quantum limit as the estimate of the best sensitivity that resonant-mass detectors could achieve with improvements of existing technologies.³³

Numerically, taking $M = 2300 \text{ kg}$, $v_s = 5400 \text{ m/s}$, $\Delta f/f_0 \simeq 0.1$, and setting $N = 1$, eq. (8.207) gives

$$\left[S_n^{1/2}(f_0) \right]_{\text{quantum limit}} \sim 3 \times 10^{-23} \text{ Hz}^{-1/2}. \quad (8.211)$$

³³This is not necessarily the ultimate sensitivity of resonant detectors, since, as discussed in Section 8.3.4, in principle the quantum limit can be circumvented using quantum non-demolition techniques.

For periodic signals, the minimum GW amplitude that can be detected with such a strain sensitivity, when one searches for a specific target, can be read from eq. (8.201), and we see that it is

$$h_{\min} = 3 \times 10^{-26} \left(\frac{\eta}{5}\right) \left(\frac{3 \times 10^7 \text{ s}}{T}\right)^{1/2}, \quad (8.212)$$

corresponding to a maximum distance at which a spinning NS is visible

$$r \simeq 40 \text{ kpc} \left(\frac{5}{\eta}\right) \left(\frac{T}{3 \times 10^7 \text{ s}}\right)^{1/2} \left(\frac{\epsilon}{10^{-6}}\right) \left(\frac{I_{zz}}{10^{38} \text{ kg m}^2}\right) \left(\frac{f_0}{1 \text{ kHz}}\right)^2. \quad (8.213)$$

Concerning bursts, detecting a single quantum at $f_0 = 900$ Hz means to measure an energy $E_s = 4 \times 10^{-5}$ mK. From eq. (8.198) we see that, with this sensitivity, we can measure a burst which releases 10^{-2} solar masses, such as a NS-NS coalescence, up to about 15 Mpc, which is just the distance to the Virgo cluster. However, recalling that these estimates assumed $S/N = 1$ we see that, even at the quantum limit, we would not really have access to the Virgo cluster, but rather to distances of order a few Mpc. To explore larger distances with a resonant bar, it would be necessary to use quantum non-demolition techniques to circumvent the quantum limit, as discussed in Section 8.3.4.

In terms of the dimensionless GW amplitude h_0 for a burst with duration $\tau_g = 1$ ms, with the above sensitivity eq. (8.194) is replaced by $h_0 \sim 2 \times 10^{-21}$. The same result can be obtained, in a physically transparent way, simply applying the uncertainty principle to the harmonic oscillator ξ_0 that represents the bar's fundamental mode. From eq. (8.29) we see that the maximum amplitude ξ_0 of the bar oscillation is

$$\Delta\xi_0 = \frac{2L}{\pi^2} h_0 \omega_0 \tau_g. \quad (8.214)$$

On the other hand, for any harmonic oscillator of mass m , if we sense its motion without using quantum non-demolition techniques, we have $\Delta p = m\omega_0 \Delta x$, and then the uncertainty principle $\Delta x \Delta p \geq \hbar$ implies

$$\Delta x \geq \sqrt{\frac{\hbar}{m\omega_0}}. \quad (8.215)$$

Applying this to the oscillator described by ξ_0 , and recalling that its effective mass is $m = M/2$, where M is the mass of the bar, we get

$$\frac{2L}{\pi^2} h_0 \omega_0 \tau_g \geq \sqrt{\frac{2\hbar}{M\omega_0}} \quad (8.216)$$

and therefore, for a burst with duration τ_g such that $f_0 \tau_g \simeq 1$,

$$h_0 \geq \left(\frac{\pi}{2\sqrt{2}}\right) \frac{1}{L} \sqrt{\frac{\hbar}{M\omega_0}} \simeq \frac{1}{L} \sqrt{\frac{\hbar}{M\omega_0}}. \quad (8.217)$$

Taking $M = 2300$ kg and $L = 3$ m, this gives $h_0 \gtrsim 1 \times 10^{-21}$, in agreement with the previous estimate.

8.4 Resonant spheres

We conclude this chapter with a discussion of spherical resonant-mass detectors. From a conceptual point of view, this study reveals interesting features of the interaction of GWs with a macroscopic body. In particular we will see that, due to the spin-2 nature of the gravitational field, GWs couple only to some quadrupolar normal modes of the sphere and, more generally, a spin- s field couples only to some normal modes with angular dependence given by the spherical harmonics Y_{lm} with $l = s$. From the experimental point of view, we will see that resonant spheres can improve on resonant bars on at least three aspects. First, for a given resonance frequency, they are more massive, and therefore have a larger cross-section for absorption of GWs, and hence a better sensitivity. Second, a sphere has isotropic sensitivity and offers a full sky coverage, while all other detectors have blind directions. And third, using the information in the different quadrupolar modes of the sphere, it is possible to reconstruct the arrival direction and the polarization of a GW, something that cannot be done with a single bar or interferometer.

8.4.1 The interaction of a sphere with GWs

The three-dimensional equations of elasticity

In Section 8.1 we studied the response to GWs of a cylindrical bar, treating the problem as one-dimensional. To study a resonant sphere, instead, we need the full equations of elasticity in a three-dimensional body, which we recall in this section.³⁴ We first write the equations for a generic elastic body, and we will later specialize to a sphere.

We consider an infinitesimal volume element of the elastic body, located at the position \mathbf{x} . Under the action of an external force, like that exerted by a GW, it will be displaced to a new position $\mathbf{x} + \mathbf{u}(\mathbf{x}, t)$. Within elasticity theory the equation governing the dynamics of $\mathbf{u}(\mathbf{x}, t)$ is

$$\rho \frac{\partial^2 u_i}{\partial t^2} = \frac{\partial \sigma_{ij}}{\partial x^j} + f_i, \quad (8.218)$$

where \mathbf{f} is the force per unit volume acting on the elastic body, and σ_{ij} is called the stress tensor. Hooke's law states that, for homogeneous and isotropic media,

$$\sigma_{ij} = \lambda u_{kk} \delta_{ij} + 2\mu u_{ij}, \quad (8.219)$$

where $u_{lm} \equiv (1/2)(\partial_l u_m + \partial_m u_l)$ and λ and μ are known as the Lamé coefficients.³⁵ The equation of motion (8.218) then becomes

$$\rho \frac{\partial^2 \mathbf{u}}{\partial t^2} = (\lambda + \mu) \nabla(\nabla \cdot \mathbf{u}) + \mu \nabla^2 \mathbf{u} + \mathbf{f}. \quad (8.223)$$

The boundary condition (in the absence of external tractions on the surface of the body) is that, on the surface, $\sigma_{ij} \hat{n}_j = 0$, where $\hat{\mathbf{n}}$ is the unit normal to the surface of the elastic body. Using eq. (8.219) this can be rewritten as

$$\lambda(\nabla \cdot \mathbf{u}) \hat{n} + 2\mu(\hat{\mathbf{n}} \cdot \nabla) \mathbf{u} + \mu \hat{\mathbf{n}} \times (\nabla \times \mathbf{u}) = 0. \quad (8.224)$$

³⁴See, e.g. Landau and Lifshitz, Vol VII (1970) or Love (1944).

³⁵Alternatively one can use the combinations Y (Young modulus) and σ_P (Poisson ratio), related to the Lamé coefficients by

$$\mu = \frac{Y}{2(1 + \sigma_P)}, \quad (8.220)$$

$$\lambda = \frac{\sigma_P Y}{(1 - 2\sigma_P)(1 + \sigma_P)}, \quad (8.221)$$

so in particular

$$\sigma_P = \frac{\lambda}{2(\mu + \lambda)}. \quad (8.222)$$

Typical materials have $\lambda/(2\mu)$ close to one. For instance the alloy Al 5056 used in many resonant detectors at cryogenic temperatures has $\lambda \simeq 6.3 \times 10^{10} \text{ N/m}^2$ and $\mu \simeq 3.0 \times 10^{10} \text{ N/m}^2$, so $\lambda/(2\mu) = 1.05$. Observe that for $\lambda/(2\mu) = 1$ we have $\sigma_P = 1/3$.

To search for the normal modes we set the external force $\mathbf{f} = 0$ and we write

$$\mathbf{u}(\mathbf{x}, t) = \mathbf{u}(\mathbf{x}, \omega)e^{-i\omega t} + c.c., \quad (8.225)$$

so $\mathbf{u}(\mathbf{x}, \omega)$ satisfies

$$(\lambda + \mu)\nabla(\nabla \cdot \mathbf{u}) + \mu\nabla^2\mathbf{u} = -\rho\omega^2\mathbf{u}. \quad (8.226)$$

To solve eq. (8.226) we separate $\mathbf{u}(\mathbf{x}, \omega)$ into its longitudinal and transverse parts, $\mathbf{u} = \mathbf{u}_{\parallel} + \mathbf{u}_{\perp}$, defined by $\nabla \times \mathbf{u}_{\parallel} = 0$ and $\nabla \cdot \mathbf{u}_{\perp} = 0$. Substituting this into (8.226) (and taking once the divergence and once the curl of the resulting equation) we get the two equations

$$(\nabla^2 + q^2)\mathbf{u}_{\parallel}(\mathbf{x}, \omega) = 0, \quad (8.227)$$

$$(\nabla^2 + k^2)\mathbf{u}_{\perp}(\mathbf{x}, \omega) = 0, \quad (8.228)$$

where $q^2 = \rho\omega^2/(\lambda + 2\mu)$ and $k^2 = \rho\omega^2/\mu$. Observe that k and q are related by

$$\frac{q^2}{k^2} = \frac{\mu}{\lambda + 2\mu}. \quad (8.229)$$

Equations (8.227) and (8.228) show that $\mathbf{u}_{\parallel}(\mathbf{x}, t)$ and $\mathbf{u}_{\perp}(\mathbf{x}, t)$ describe waves propagating with velocities $v_{\parallel} = [(\lambda + 2\mu)/\rho]^{1/2}$ and $v_{\perp} = (\mu/\rho)^{1/2}$, respectively.³⁶ Writing $\mathbf{u}(\mathbf{x}, \omega)$ as a superposition of plane waves,

$$\mathbf{u}(\mathbf{x}, \omega) = \sum_{\mathbf{k}} \tilde{\mathbf{u}}(\mathbf{k}, \omega)e^{i\mathbf{k}\cdot\mathbf{x}}, \quad (8.230)$$

we see that for \mathbf{u}_{\parallel} we have $\mathbf{k} \times \tilde{\mathbf{u}}(\mathbf{k}, \omega) = 0$, so it describes a wave which displaces a volume element of the material along its propagation direction $\hat{\mathbf{k}}$, i.e. a longitudinal wave, and similarly \mathbf{u}_{\perp} displaces it in the transverse direction. Furthermore, the condition $\nabla \cdot \mathbf{u}_{\perp}$ means that transverse waves do not involve changes in volume, contrary to \mathbf{u}_{\parallel} which induces compressions and expansions of the volume element. We can construct the longitudinal and transverse solutions introducing two scalar functions $\chi(\mathbf{x}; q)$ and $\varphi(\mathbf{x}; k)$. We write the longitudinal part as

$$\mathbf{u}_{\parallel}(\mathbf{x}, \omega) = \nabla\chi(\mathbf{x}, q), \quad (8.231)$$

while, defining the operator $\mathbf{L} = -i\mathbf{r} \times \nabla$, we can form two independent transverse vectors, that we denote by $\mathbf{u}_t(\mathbf{x}, \omega)$ and $\mathbf{u}_{t'}(\mathbf{x}, \omega)$, respectively,

$$\mathbf{u}_t(\mathbf{x}, \omega) = i\nabla \times \mathbf{L}\varphi(\mathbf{x}, k) \quad \mathbf{u}_{t'}(\mathbf{x}, \omega) = i\mathbf{L}\varphi(\mathbf{x}, k). \quad (8.232)$$

Equations (8.227) and (8.228) become

$$(\nabla^2 + q^2)\chi(\mathbf{x}, q) = 0, \quad (\nabla^2 + k^2)\varphi(\mathbf{x}, k) = 0. \quad (8.233)$$

The most general solution for \mathbf{u} is therefore of the form

$$\begin{aligned} \mathbf{u}(\mathbf{x}, \omega) &= C_0\mathbf{u}_{\parallel}(\mathbf{x}, \omega) + C_1\mathbf{u}_t(\mathbf{x}, \omega) + C_2\mathbf{u}_{t'}(\mathbf{x}, \omega) \\ &= C_0\nabla\chi(\mathbf{x}, q) + iC_1\nabla \times \mathbf{L}\varphi(\mathbf{x}, k) + iC_2\mathbf{L}\varphi(\mathbf{x}, k), \end{aligned} \quad (8.234)$$

where χ and φ are solutions of eq. (8.233). We now impose the boundary condition (8.224). This quantizes the allowed values of k (and therefore of q , since q and k are related by eq. (8.229)) and, apart from an overall normalization factor, fixes the value of the constants C_0 , C_1 and C_2 . The solutions so obtained are the normal modes of the system, and we denote them by $\psi_N(\mathbf{x})$, where N labels collectively all the labels that are necessary to classify the normal modes. Since the normal modes form a complete set, the most general displacement $\mathbf{u}(\mathbf{x}, t)$ that satisfies the boundary conditions can be expanded as

$$\mathbf{u}(\mathbf{x}, t) = \sum_N \xi_N(t) \psi_N(\mathbf{x}). \quad (8.235)$$

For a thin cylindrical bar the problem is one-dimensional, and we found in Section 8.1.1 that there are two families of normal modes, given by $\psi_{n,1}(x) = \sin[\pi x(2n+1)/L]$ and $\psi_{n,2}(x) = \cos[\pi x(2n+2)/L]$, so in this case $N = \{n, \alpha\}$ with $\alpha = 1, 2$ a discrete label. We also found that the modes $\psi_{n,2}$ do not couple to GWs while the coupling of the modes $\psi_{n,1}$ to GWs can be summarized in terms of an effective mass of the mode and an effective external force. In the next subsections we discuss the analogous results for a sphere.

The normal modes of a sphere

We can now specify the above general formalism to a spherical elastic body of radius R . The solution of eq. (8.233) is

$$\chi(\mathbf{x}, q) = j_l(qr) Y_{lm}(\theta, \phi), \quad \varphi(\mathbf{x}, k) = j_l(kr) Y_{lm}(\theta, \phi), \quad (8.236)$$

where $j_l(z)$ is the spherical Bessel function. Inserting this into eq. (8.234) and imposing the boundary condition (8.224) we find two families of solutions, called toroidal and spheroidal modes. To write the result in a compact form, it is useful to define the functions

$$\beta_0(z) \equiv \frac{j_l(z)}{z^2}, \quad \beta_1(z) \equiv \frac{d}{dz} \left(\frac{j_l(z)}{z} \right), \quad \beta_2(z) \equiv \frac{d^2}{dz^2} j_l(z), \quad (8.237)$$

$$\beta_3(z) = \frac{1}{2} [\beta_2(z) + (l-1)(l+2)\beta_0(z)], \quad (8.238)$$

$$\beta_4(z) = \beta_2(z) - \frac{\lambda}{2\mu} z^2 \beta_0(z). \quad (8.239)$$

Then we have the following classification.

Spheroidal modes. These modes have $l \geq 0$. When $l \neq 0$, their allowed values of k are the solutions of the equation

$$\beta_3(kR)\beta_4(qR) - l(l+1)\beta_1(kR)\beta_1(qR) = 0, \quad (8.240)$$

where q and k are related by eq. (8.229). For each l this equation has an infinity of solutions, that we denote by k_{nl}^S , with $n = 1, 2, \dots$. Equa-

Table 8.1 The values of k_{nl}^S for $l = 0$ and $l = 2$ and $n = 1, \dots, 4$, taking $\lambda/(2\mu) = 1.05$, which corresponds to the alloy Al 5056. (In a real detector, these values change by $O(10\%)$ because of the effect of the suspension system.)

l	n	$(kR)^S$	l	n	$(kR)^S$
0	1	5.580	2	1	2.651
	2	12.394		2	5.111
	3	18.870		3	8.639
	4	24.286		4	11.100

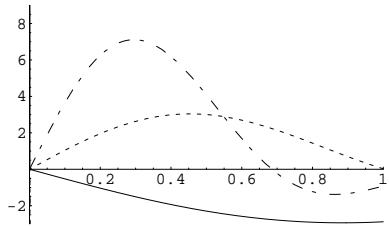


Fig. 8.18 The functions $a_{nl}(r)$, for $l = 2$ and $n = 1$ (solid line), $n = 2$ (dashed line), and $n = 3$ (dot-dashed), plotted against r/R , for $\lambda/(2\mu) = 1.05$. The functions $a_{nl}(r)$ are normalized according to eq. (8.246).

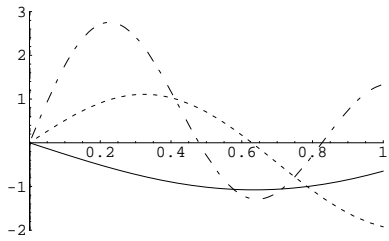


Fig. 8.19 The functions $b_{nl}(r)$, for $l = 2$ and $n = 1$ (solid line), $n = 2$ (dashed line), and $n = 3$ (dot-dashed), plotted against r/R , for $\lambda/(2\mu) = 1.05$. The functions b_{nl} are and normalized according to eq. (8.246).

tion (8.240) however does not depend on m , so there is a $(2l+1)$ -fold degeneracy. The corresponding frequencies are obtained from eq. (8.228),

$$\omega_{nl}^S = (\mu/\rho)^{1/2} k_{nl}^S. \quad (8.241)$$

The explicit form of the spheroidal modes with $l \neq 0$ is

$$\psi_{nlm}^S(r, \theta, \phi) = [a_{nl}(r)\hat{\mathbf{r}} + b_{nl}(r)R\boldsymbol{\nabla}] Y_{lm}(\theta, \phi), \quad (8.242)$$

where

$$a_{nl}(r) = c_{nl} \left[\alpha_{nl} \frac{dj_l(z)}{dz} \Big|_{z=q_{nl}^S r} - \beta_{nl} l(l+1) \frac{j_l(z)}{z} \Big|_{z=k_{nl}^S r} \right], \quad (8.243)$$

$$b_{nl}(r) = c_{nl} \frac{r}{R} \left[\alpha_{nl} \frac{j_l(z)}{z} \Big|_{z=q_{nl}^S r} - \beta_{nl} \left(\frac{j_l(z)}{z} + \frac{dj_l(z)}{dz} \right) \Big|_{z=k_{nl}^S r} \right].$$

The constants α_{nl} and β_{nl} are given by

$$\alpha_{nl} = \beta_3(k_{nl}^S R), \quad \beta_{nl} = \frac{q}{k} \beta_1(q_{nl}^S R). \quad (8.244)$$

The constants c_{nl} are normalization factors. We fix them requiring

$$\int_V d^3x \rho (\psi_{nlm}^S)^* \cdot \psi_{nlm}^S = M, \quad (8.245)$$

where M is the mass of the sphere and V its volume. If ρ is constant, as will typically be the case, the normalization condition becomes

$$\int_V d^3x (\psi_{nlm}^S)^* \cdot \psi_{nlm}^S = V. \quad (8.246)$$

We can also write eq. (8.242) in the equivalent form

$$\psi_{nlm}^S(r, \theta, \phi) = A_{nl}(r)Y_{lm}(\theta, \phi)\hat{\mathbf{r}} - B_{nl}(r)i\hat{\mathbf{r}} \times \mathbf{L}Y_{lm}(\theta, \phi), \quad (8.247)$$

where $A_{nl}(r) = a_{nl}(r)$ and $B_{nl}(r) = (R/r)b_{nl}(r)$. The functions $a_{nl}(r)$ and $b_{nl}(r)$ are plotted in Figs. 8.18 and 8.19.

For $l = 0$, instead, the allowed values of k are the solution of the equation

$$\beta_4(qR) = 0, \quad (8.248)$$

and the spheroidal modes are given by

$$\psi_{n00}^S(r, \theta, \phi) = a_{n0}(r)\hat{\mathbf{r}}, \quad a_{n0}(r) = c_{n0} \frac{dj_0}{dz} \Big|_{z=q_{n0}^S r}. \quad (8.249)$$

Therefore the spheroidal modes with $l = 0$ are purely radial. In Table 8.1 we give the value of k_{nl}^S for some of the lowest $l = 0$ and $l = 2$ spheroidal modes, computed numerically from eqs. (8.240) and (8.248), taking $\lambda/(2\mu) = 1.05$ (as we will see in the next subsection, the modes $l = 2$ are the most interesting, since they are the only ones coupled to GWs). Observe that the numerical values of k_{nl}^S depend on $\lambda/(2\mu)$.

Toroidal modes. These modes are purely transverse and exist only for $l \geq 1$. The eigenvalues k_{nl}^T are determined by the equation $\beta_1(kR) = 0$ and have the form

$$\psi_{nlm}^T(r, \theta, \phi) = c'_{nl} j_l(k_{nl}^T r) i \mathbf{LY}_{lm}, \quad (8.250)$$

with c'_{nl} the normalization constant. Observe that $i \mathbf{LY}_{lm} = \mathbf{r} \times \nabla Y_{lm}$ is orthogonal both to $Y_{lm} \hat{\mathbf{r}}$ and to ∇Y_{lm} , i.e. to the displacements due to the spheroidal modes. The values of k_{nl}^T for $l = 1, 2$ and $n = 1, \dots, 4$ are given in Table 8.2. They are independent of $\lambda/(2\mu)$, since they are determined only by the function $\beta_1(z)$, given in eq. (8.237).

The interaction of the normal modes with GWs

We next discuss how these normal modes interact with GWs. We start from the expansion of the displacement $\mathbf{u}(\mathbf{x}, t)$ in terms of normal modes, eq. (8.235), and we substitute it into eq. (8.223). Using the fact that, by definition, the normal modes $\psi_N(\mathbf{x})$ satisfy eq. (8.226) with $\omega = \omega_N$, we get

$$\rho \sum_{N'} (\ddot{\xi}_{N'} + \omega_{N'}^2 \xi_{N'}) \psi_{N'}(\mathbf{x}) = \mathbf{f}. \quad (8.251)$$

Here $N = \{nlm; \alpha\}$, where the label $\alpha = \{S, T\}$ denotes spheroidal and toroidal modes, respectively. To obtain an equation for ξ_N we take the scalar product of both sides by ψ_N^* and we integrate over d^3x . Since the normal modes are orthogonal, and normalized as in eq. (8.245), we get

$$\ddot{\xi}_N + \omega_N^2 \xi_N = \frac{1}{M} \int d^3x \mathbf{f} \cdot \psi_N^*. \quad (8.252)$$

Recall that \mathbf{f} is the force per unit volume. In the case of GWs, eq. (8.2) gives $f_i = (1/2) \ddot{h}_{ij}^{TT} x^j \rho$ and therefore (omitting for simplicity the label TT on h_{ij})

$$\ddot{\xi}_N + \gamma_N \dot{\xi}_N + \omega_N^2 \xi_N = \frac{1}{2V} \int_V d^3x (\psi_N^*)^i x^j, \quad (8.253)$$

where on the left-hand side we also added a term $\gamma_N \dot{\xi}_N$ to take into account the effect of dissipation. The above equation is completely general and holds in any geometry, with ψ_N equal to the normal modes appropriate for the geometry in question. Here we are interested in a resonant sphere, so we must compute the right-hand side for the toroidal and spheroidal modes. For the toroidal modes ψ_{nlm}^T , the integral vanishes for all l , and therefore they do not couple to GWs.³⁷ This is analogous to the fact that, in a cylindrical bar, the modes proportional to $\cos[\pi x(2n+2)/L]$ do not couple to GWs. They can therefore be used as a veto to distinguish spurious excitations due to noise from GWs.

We then turn our attention to the spheroidal modes. Writing them in the form (8.247) we have

$$\int d^3x (\psi_{nlm}^S)^* x_j = \int r dr d\Omega [A_{nl}(r) x_i x_j Y_{lm}^* + B_{nl}(r) i \epsilon_{ipq} x_p x_j L_q Y_{lm}^*]. \quad (8.255)$$

Table 8.2 The values of k_{nl}^T for $l = 1$ and $l = 2$, and $n = 1, \dots, 4$. They do not depend on $\lambda/(2\mu)$.

l	n	$(kR)^T$	l	n	$(kR)^T$
1	1	5.763	2	1	2.501
	2	9.095		2	7.136
	3	12.323		3	10.515
	4	15.515		4	13.772

³⁷The proof is straightforward. Inserting the explicit form (8.250) of the toroidal modes, we are left with an integral of the type

$$\int d^3x f(r) x_j (i L_i Y)^*,$$

where $f(r) = j_l(k_{nl}^T r)$, $Y \equiv Y_{lm}$ and $L_i = -i \epsilon_{ipq} x_p \partial_q$. We integrate ∂_q by parts, obtaining

$$\begin{aligned} & \int d^3x f(r) x_j \epsilon_{ipq} x_p \partial_q Y^* \\ &= \int d^2S \hat{x}_q f(r) x_j \epsilon_{ipq} x_p Y^* \\ &\quad - \epsilon_{ipq} \int d^3x Y^* x_p \partial_q [f(r) x_j], \end{aligned}$$

where d^2S is the surface element of the boundary, $\hat{x}_q = x_q/r$ is its normal, and we used $\epsilon_{ipq} \partial_q x_p = \epsilon_{ipq} \delta_{pq} = 0$. The first integral vanishes because $\epsilon_{ipq} x_p \hat{x}_q = 0$. In the second integral we use $\partial_q [f(r) x_j] = f'(r) \hat{x}_q x_j + f(r) \delta_{jq}$. The term $f'(r) \hat{x}_q x_j$ vanishes after contraction with $\epsilon_{ipq} x_p$, so we finally get

$$\begin{aligned} & \int d^3x f(r) x_j (i L_i Y)^* \\ &= \epsilon_{ijk} \int d^3x f(r) x_k Y^*. \quad (8.254) \end{aligned}$$

The result is therefore antisymmetric in (i, j) . In eq. (8.253) this quantity is contracted with h_{ij} , which is symmetric in (i, j) , so the right-hand side of eq. (8.253) vanishes.

It is easy to see that the angular integral is non-vanishing only if $l = 0$ or $l = 2$. In fact, the symmetric and traceless tensor $x_i x_j - (1/3)\delta_{ij}r^2$ is a pure spin-2 tensor and therefore, expanding it in spherical harmonics, it contains only the harmonics with $l = 2$, i.e.

$$x_i x_j = \frac{1}{3}\delta_{ij}r^2 + r^2 \sum_{m'=-2}^2 c_{ij}^{m'} Y_{2m'}, \quad (8.256)$$

where $c_{ij}^{m'}$ are coefficients, whose explicit form we do not need here (but we already found them in eq. (3.221)). Since the spherical harmonics are orthogonal, when we integrate the term proportional to $A_{nl}(r)$ over $d\Omega$ we find that $\delta_{ij}Y_{lm}^* \sim \delta_{ij}Y_{00}Y_{lm}^*$ gives a non-zero contribution only if $l = 0$, while $Y_{2m'}Y_{lm}^*$ gives a non-zero contribution only if $l = 2$. As for the term proportional to B_{nl} , recall from elementary quantum mechanics that the angular momentum operator L_p , acting on the spherical harmonics Y_{lm} , gives a combination of spherical harmonics with the same value of l . Therefore, $x_p x_j L_q Y_{lm}^*$ has a non-vanishing integral over the solid angle only if $l = 2$ (when $l = 0$ the term proportional to B_{nl} is absent from the spheroidal modes, see eq. (8.249)).

In general relativity h_{ij} is traceless and symmetric. Then, when in eq. (8.253) we perform the contraction with \ddot{h}_{ij} , the terms with $l = 0$ vanish since they are proportional to $A_{n0}(r)\delta_{ij}$. In conclusion, within the framework of general relativity, *GWs excite only the spheroidal modes with $l = 2$* .³⁸

We can now compute the right-hand side of eq. (8.253), restricting to $l = 2$. It is convenient to write h_{ij} in terms of its spherical components h_m , with $m = -2, \dots, 2$, introduced in Section 3.5.2. The h_m are defined as in eq. (3.222)

$$h_{ij}(t) = \sum_{m=-2}^2 h_m(t) \mathcal{Y}_{ij}^{2m}, \quad (8.257)$$

where the five tensors \mathcal{Y}_{ij}^{2m} , with $m = -2, \dots, 2$, are a basis in the space of the tensors traceless and symmetric with respect to the two indices (i, j) , and are given explicitly in eq. (3.218). We insert this into eq. (8.253) and we compute explicitly the integral when $l = 2$. The result is

$$\frac{1}{2V} \ddot{h}_{ij} \int d^3x (\psi_{n2m}^S)_i^j x_j = \frac{1}{2} R \chi_n \ddot{h}_m, \quad (8.258)$$

where the coefficients χ_n are given by

$$\chi_n = \frac{3}{4\pi} \int_0^1 du u^3 [A_{n2}(\kappa_{n2}u) + 3B_{n2}(\kappa_{n2}u)], \quad (8.259)$$

and $\kappa_{nl} \equiv k_{nl}^S R$ is independent of R (the values for $l = 2$ and $n = 1, \dots, 4$ are given in Table 8.1). The numerical values of χ_n for $n = 1, \dots, 4$ and $\lambda/(2\mu) = 1.05$ are given in Table 8.3. Therefore eq. (8.253) becomes

$$\ddot{\xi}_{nm} + \gamma_n \dot{\xi}_{nm} + \omega_n^2 \xi_{nm} = \frac{1}{2} R \chi_n \ddot{h}_m,$$

(8.260)

where, for notational simplicity, we denoted ξ_{n2m}^S simply as ξ_{nm} and ω_{n2}^S as ω_n . Equation (8.260) shows another remarkable feature of a resonant sphere: the modes ξ_{nm} are sensitive only to the component h_m of the GW with the same m . Therefore, from the five quadrupolar modes ξ_{nm} , at n given, we can reconstruct the full matrix $h_{ij}(\omega)$, at the frequency $\omega = \omega_n$. This is different from what happens in resonant bars and, as we will see, in interferometers, where there is only a single output, of the form $h_+F_+ + h_\times F_\times$, where $F_{+,\times}$ are functions that depend on the direction of the arrival of the GW (which is a priori unknown). The output of a sphere contains much more information, as we will see in detail in Section 8.4.2.

Comparing eq. (8.260) with eq. (8.3) we see that the quadrupolar modes ξ_{nm} of a sphere are formally equivalent to an oscillator with effective length $l_{\text{eff}} = R\chi_n$ while, from the normalization condition (8.245), it follows that the effective mass of the modes is equal to mass M of the sphere.³⁹ Comparing with the results obtained for the fundamental mode of the cylinder of mass M_{cyl} and length L , we see that all results that we obtained for the fundamental mode of a cylindrical bar can be immediately applied to the spheroidal modes with $l = 2$ and n generic of a sphere of mass M_{sph} , simply performing the replacements $(1/2)M_{\text{cyl}} \rightarrow M_{\text{sph}}$ and $(4/\pi^2)L \rightarrow \chi_n R$, and taking into account that the mode ξ_{nm} is driven by h_m rather than by h_{xx} .

We can then obtain the cross-section of the sphere for absorption of GWs, simply repeating the computations performed in Section 8.1.3. The result is

$$\Sigma_n = F_n \frac{GM}{c} \left(\frac{v_s}{c} \right)^2, \quad (8.261)$$

with

$$F_n = \frac{8\pi^2}{15} \frac{\chi_n^2}{1 + \sigma_P} (Rk_{n2}^S)^2. \quad (8.262)$$

The numerical values of χ_n and F_n for $n = 1, \dots, 4$ and $\lambda/(2\mu) = 1.05$ are given in Table 8.3. We see here another important advantage of a spherical resonant-mass detector, over a cylinder. A cylinder of length L and a sphere of radius R searching for GWs at the same frequency ω must have $L \simeq 2R$, as we see comparing eq. (8.14) with eq. (8.241) which, for a material such as aluminum, gives for $l = 2$ and $n = 1$ (the fundamental quadrupolar mode) $\omega \simeq 1.62v_s/R$. However, a sphere with diameter L is much more massive than a thin cylinder of length L of the same material, and therefore its cross-section for GW absorption is much higher. Furthermore, for the sphere the sensitivity is isotropic, while for the bar we assumed a wave coming from the optimal direction. Averaging over all possible directions the bar cross-section is further reduced by a factor 4/15, see eq. (8.67).

³⁹By definition of normal modes, the ξ_N are oscillators with frequencies ω_N , so the energy associated to ξ_N is proportional to $\dot{\xi}_N^2 + \omega_N^2\xi_N^2$. The overall coefficient is found observing that the kinetic energy of an oscillation $\mathbf{u}(\mathbf{x}, t) = \xi_N(t)\psi_N(\mathbf{x})$ is given by

$$\begin{aligned} & \frac{1}{2} \int dm |\dot{\mathbf{u}}|^2 \\ &= \frac{1}{2} \dot{\xi}_N^2 \int d^3x \rho(\mathbf{x}) |\psi_N|^2 \\ &= \frac{1}{2} M \dot{\xi}_N^2, \end{aligned}$$

where in the last line we used the normalization condition (8.245). Therefore the effective mass of the modes ξ_{nm} is equal to the mass M of the sphere.

Table 8.3 The values of χ_n and of F_n , for $n = 1, \dots, 4$, setting $\lambda/(2\mu) = 1.05$.

n	χ_n	F_n
1	-0.328	2.996
2	-0.105	1.141
3	0.020	0.116
4	0.007	0.026

8.4.2 Spheres as multi-mode detectors

One of the most interesting features of a spherical resonant mass is that it is a multi-mode detector. A resonant cylinder is a single-mode detector because, at each resonant frequency ω_n , there is only one longitudinal mode. The output of a resonant cylinder is therefore a single quantity, the component of h_{ij} along the bar axis, say h_{xx} . This is related to the components h_+ and h_\times of the GW and to the direction of arrival of the wave by $h_{xx} = h_+ F_+(\theta, \phi) + h_\times F_\times(\theta, \phi)$, where $F_{+, \times}(\theta, \phi)$ are the pattern functions of the bar. From this single output we cannot disentangle the information on the GW amplitude from that on the source direction. The same signal could be induced by a GW with a smaller amplitude but well oriented with respect to the bar, i.e. impinging transversally on it, or by a GW arriving from a less optimal direction, but with a higher amplitude. Even less can be said as to how this energy is shared between the two polarizations.

Therefore, if we detect a signal in a single cylindrical bar, in the absence of an optical counterpart the best one can do is to guess that the wave came from a more-or-less optimal direction and to guess that $h_+ \sim h_\times$, and under these assumptions one can estimate the energy flux carried by the wave. Almost nothing can be said about the source location, except that it cannot be too close to the bar's blind direction, which is its longitudinal axis. As we will see in later chapters, the situation is similar for a single interferometer, and to improve it substantially, with bars or interferometers, it is necessary to detect the signal simultaneously in different detectors.

A sphere is completely different from this point of view. At each resonance frequency ω_n , corresponding to an $l = 2$ spheroidal mode, it has five degenerate modes coupled to the GWs, and therefore a sphere has five independent outputs. As we have seen in eq. (8.260), each of the five modes ξ_{nm} (with n given and $m = -2, \dots, 2$) is driven only by the spherical component $\tilde{h}_m(\omega_n)$ of the GW which has the same value of m . Therefore, monitoring the five ξ_{nm} we obtain the five quantities $\tilde{h}_m(\omega_n)$ and, using eq. (8.257), we can reconstruct the full matrix \tilde{h}_{ij} at the resonance frequency or, more precisely, in a bandwidth centered around ω_n .

The full matrix \tilde{h}_{ij} contains all the information on the arrival direction and on the amplitude of the two polarizations. In particular, if the excitation of the detector is really due to a GW, rather than to noise, it must be possible to rotate the axes of our reference frame so that the new z axis coincides with the propagation direction of the wave. In other words, once we measure the quantities h_m and we construct h_{ij} as in eq. (8.257), it must exist a rotation \mathcal{R} such that

$$\mathcal{R}_{ik} \mathcal{R}_{jl} h_{kl} = \begin{pmatrix} h_+ & h_\times & 0 \\ h_\times & -h_+ & 0 \\ 0 & 0 & 0 \end{pmatrix}_{ij}. \quad (8.263)$$

Then the propagation direction $\hat{\mathbf{n}}$ of the GW is obtained applying this

rotation to the original z axis, i.e. $n_i = \mathcal{R}_{ij}\hat{z}_j = \mathcal{R}_{i3}$. Given the original matrix h_{ij} , the determination of the incoming direction (in the absence of noise) is therefore a straightforward algebraic problem, whose solution is

$$\tan \varphi \equiv n_y/n_x = \frac{h_{22}h_{13} - h_{12}h_{23}}{h_{12}h_{13} - h_{11}h_{23}}, \quad (8.264)$$

$$\tan \theta \equiv \frac{(n_x^2 + n_y^2)^{1/2}}{n_z} = \frac{h_{13}}{h_{12} \cos \varphi - h_{11} \sin \varphi}. \quad (8.265)$$

We have therefore reconstructed the arrival direction, up to a sign ambiguity: we cannot distinguish a wave coming from the direction $\hat{\mathbf{n}}$ from a wave coming from $-\hat{\mathbf{n}}$, since if (θ, φ) satisfy eqs. (8.264) and (8.265) then also $(\pi - \theta, \pi + \varphi)$ satisfy it. (This ambiguity could be fixed measuring the time delay between two detectors.) We have therefore determined the arrival direction and we can now read the two separate amplitudes h_+ and h_\times from eq. (8.263).⁴⁰

At this stage we have used five outputs to determine four quantities: the two amplitudes h_+, h_\times (or, equivalently, the amplitude $h = (h_+^2 + h_\times^2)^{1/2}$ and the polarization angle Ψ defined by $h = h_+ \cos 2\Psi + h_\times \sin 2\Psi$), and the two angles θ, ϕ that give the unit vector $\hat{\mathbf{n}}$. We still have one unused information. This is a veto that distinguishes GWs from spurious events due to noise. In fact, given five arbitrary numbers h_m , the matrix $\sum_m h_m \mathcal{Y}_{ij}^m$ is by definition traceless and symmetric, because the \mathcal{Y}_{ij}^m are traceless and symmetric, but this just means that, with an appropriate rotation, we can bring it to the form

$$\begin{pmatrix} a & d & 0 \\ d & b & 0 \\ 0 & 0 & c \end{pmatrix}_{ij}, \quad (8.266)$$

with $a + b + c = 0$. That is, we can choose two Euler angles associated to a rotation to set to zero the (1,3) and (2,3) elements of the matrix (and of course at this point we can also set $d = 0$ with a rotation around the new z axis). The fact that, after performing such a rotation, we automatically find $c = 0$ and therefore $a = -b$ is instead a specific property of GWs, due to their transverse nature. In conclusion, the five quadrupolar modes of the sphere allow us to determine the source direction $\hat{\mathbf{n}}$ (up to a sign ambiguity $\hat{\mathbf{n}} \rightarrow -\hat{\mathbf{n}}$), the two separate amplitudes h_+ and h_\times , and to have a veto that discriminates GWs from noise.

Other vetoes emerge naturally in a resonant sphere. For instance, from Tables 8.1 and 8.2 we see that the toroidal mode with $l = 2, n = 1$ is quite close, in frequency, to the spheroidal mode with $l = 2, n = 1$. Since the former is not coupled to GWs while the latter is the main mode that is monitored for GW detection, an excitation of the latter when the former is not excited would give further confidence on the GW origin of the signal.⁴¹

We have seen above that, in the ideal case in which the signal is given uniquely by the GWs, and the noise is negligible, a sphere is able to locate *exactly* the direction of the source, contrary to a single bar or

⁴⁰Of course, once we find a rotation that brings h_{ij} to the form (8.263), any further rotation around the new z axis still leaves h_{ij} in this form. This further rotation just amounts to a redefinition of the axes with respect to which the two polarizations are defined, and mixes h_+ and h_\times as in eq. (2.194). In particular, it can be chosen so that h_\times is set to zero and h_{ij} becomes diagonal, $h_{ij} = \text{diag}(h_+, -h_+, 0)$.

⁴¹Toroidal modes have no radial displacement, so to detect them we need transducers coupled to the transverse oscillations of the surface.



Fig. 8.20 The MiniGRAIL resonant sphere. A few resonant transducers are also visible.

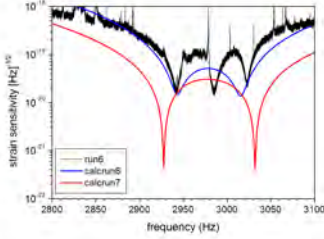


Fig. 8.21 The strain sensitivity of MiniGRAIL (as of Jan 2005) compared to the prediction of a simplified two-mode model, cooling the detector to a temperature $T = 5$ K. The lowest curve is the sensitivity expected cooling at $T = 80$ mK. The final goal is to reach $T = 20$ mK.

a single interferometer that, even in the ideal noiseless limit, have an angular resolution of order 4π . Of course, in a real situation noise is present, and the angular resolution of the sphere depends on the signal-to-noise ratio. We denote by θ_0 and ϕ_0 the actual angles which give the direction of propagation of the wave and by θ_c and ϕ_c the angles computed from the five outputs of a noisy resonant sphere. We introduce the notation $\Delta\theta = \theta_c - \theta_0$ and $\Delta\phi = \phi_c - \phi_0$. A useful indicator of the angular resolution is

$$\Delta\Omega \equiv \pi [(\Delta\theta)^2 + \sin^2 \theta_0 (\Delta\phi)^2], \quad (8.267)$$

which is the area of a circle on the unit sphere, centered on the actual source location, and with radius $\delta\hat{\mathbf{n}} = \hat{\mathbf{n}}_c - \hat{\mathbf{n}}_0$, where $\hat{\mathbf{n}}_0$ is the unit vector of the actual propagation direction of the GW and $\hat{\mathbf{n}}_c$ is the direction computed from the noisy outputs. Then it can be shown (Zhou and Michelson 1995, Stevenson 1997) that, if we denote by SNR the signal-to-noise ratio in energy, in the limit of large SNR the angular resolution is given by

$$(\Delta\theta)^2 = \sin^2 \theta_0 (\Delta\phi)^2 = \frac{1}{\text{SNR}}, \quad (8.268)$$

and therefore

$$\boxed{\Delta\Omega = \frac{2\pi}{\text{SNR}}}. \quad (8.269)$$

A spherical resonant mass detector, MiniGRAIL, has been developed at Leiden University, in the Netherlands, and is in its commissioning phase. It is a sphere of 68 cm of diameter and a mass $M \simeq 1.3$ ton, shown in Fig. 8.20. At 4 K its spheroidal quadrupolar modes are at $f \simeq 2980$ Hz. The material is an alloy CuAl6%, chosen because of its high quality factor ($Q \sim 10^7$ at low T), high sound velocity ($v_s \simeq 4100$ m/s) and a sufficient thermal conductivity, which already allowed to cool it below 100 mK. The ultimate goal is to operate it at a thermodynamical temperature $T \simeq 20$ mK. The expected bandwidth should be of order 230 Hz, and possibly higher. The quadrupole modes are monitored using various transducers, coupled to double-stage SQUID amplifiers. The optimal choice is to have six transducers in the so-called TIGA configuration, see the Further Reading section. The target is to reach a temperature $T = 20$ mK, and a strain sensitivity $S_h^{1/2}$ of order $10^{-22} - 10^{-23} \text{ Hz}^{-1/2}$. The present sensitivity is shown in Fig. 8.21.

Since its size is relatively small, MiniGRAIL explores high frequencies, in the 3 kHz region. As we will discuss in Vol. 2, this could still be an interesting region for astrophysical signals from compact objects.

Further reading

- A historical account of GW research can be found in Thorne (1987). For overviews of resonant bars see e.g. Thorne (1987), Coccia (1997), Ju, Blair and Zhao (2000) and Bassan (2002).
 - Computations of the sensitivity of resonant bars can be found in Pallottino and Pizzella (1981, 1984, 1991), Michelson and Taber (1981, 1984), and Price (1987). It is interesting to observe that the role of the amplifier noise was first pointed out by two distinguished theorists, Gibbons and Hawking (1971).
 - Resonant transducers have been proposed by Paik (1976). For detailed reviews on passive transducers see Richard and Folkner (1991). Parametric transducer are discussed in Veitch (1991) and in Ju, Blair and Zhao (2000). The dual scheme is proposed in Cerdonio *et al.* (2001) and Briant *et al.* (2003). See also the review Cerdonio (2003).
 - For back-action and the quantum limit in resonant bars see Giffard (1976). Quantum non-demolition measurements are discussed in detail in Caves, Thorne, Drever, Sandberg and Zimmermann (1980) and in Braginsky and Kalili (1992).
 - Analysis of the coincidences between the five resonant bars ALLEGRO, AURIGA, EXPLORER, NAUTILUS and NIOBE, and the relative upper limit on GW bursts, can be found in Allen *et al.* [IGEC] (2000) and Astone *et al.* [IGEC] (2003a). Searches for periodic GWs are reported in Astone *et al.* [ROG] (2002).
 - Descriptions of the detectors can be found in Astone *et al.* (1997b) for NAUTILUS, Astone *et al.* (2003b) for EXPLORER, Blair *et al.* (1995) for NIOBE, Mauceli *et al.* (1996) for ALLEGRO, M. Cerdonio *et al.* (1997) and J.-P. Zendri *et al.* (2002) for AURIGA.
- For information on the resonant bar experiments see the links:
- <http://sam.phys.lsu.edu>
<http://www.auriga.lng.infn.it>
<http://www.roma1.infn.it/rog/explorer>
<http://www.lng.infn.it/esperimenti/rog/nautilus>
- Coordination among the various GW experiments (both resonant masses and interferometers) is provided by the Gravitational Wave International Committee (GWIC), see the link <http://gwic.gravity.psu.edu>
 - The advantages of a resonant sphere in terms of cross-section and its multi-mode capability were already realized in the 1970s, see Forward (1971), Ashby and Dreitlein (1975) and Wagoner and Paik (1977). Detailed discussion of spherical detectors can be found in Zhou and Michelson (1995), Lobo (1995) and Coccia, Lobo and Ortega (1995). Hollow spheres are studied in Coccia, Fafone, Frossati, Lobo, and Ortega (1998) and Lobo (2002). The multi-frequency capability of the sphere and the possibility of reconstruction of the chirp mass and orbital parameters of a coalescing binary with a single sphere is discussed in Coccia and Fafone (1996) and Spallicci, Frossati and Krolak (1997). The response of a resonant sphere to GWs in extensions of general relativity is discussed in Bianchi, Coccia, Colacino, Fafone and Fucito (1996) and, for scalar fields, in Bianchi, Brunetti, Coccia, Fucito and Lobo (1998) and Maggiore and Nicolis (2000).
 - A particularly useful configuration of transducers for a spherical detector, the TIGA configuration, was proposed and investigated experimentally in Johnson and Merkowitz (1993) and Merkowitz and Johnson (1995, 1997). See also the PhD thesis of Merkowitz (1995). Another configuration requiring only five transducers, but with four of them sensitive to transverse displacements, is proposed in Zhou and Michelson (1995). Detailed discussion of sensitivity and optimal filtering in the presence of multiple transducers is given in Stevenson (1997).
 - For MiniGRAIL, see de Waard, Gottardi, van Houwelingen, Schumack, and Frossati (2003), and the PhD theses of de Waard (2003) and of Gottardi (2004). Updated information can be found at <http://www.minigrail.nl>. Another spherical resonant-mass under development is the “Mario Schembren” detector of the Brazilian GRAVITON project, see Aguiar (2004).

9

Interferometers

9.1 A simple Michelson interferometer	470
9.2 Interferometers with Fabry–Perot cavities	480
9.3 Toward a real GW interferometer	497
9.4 Noise sources	515
9.5 Existing and planned detectors	528

The idea of interferometric detection of GWs is in principle simple and elegant, and goes back to 1962, when it was first considered by two Russian theorists, M. Gertsenshtein and V. I. Pustovoit. Weber also considered it, and it was then pushed in the late 1960s by R. Forward, R. Weiss, R. Drever, and others. In practice, however, a large GW interferometer is an extremely complex instrument, with many degrees of freedom that must be kept under control with extraordinary accuracy. Thus, their development up to the present scale has required the building up of large collaborations, comparable in size to modern particle physics experiments, as well as more than 30 years of preparation. Following the general approach of this book, as outlined in the Preface, we will not discuss the interesting history of the development of this idea, referring the reader to the Further Reading section for reviews, and we will rather focus on the present understanding of these detectors. We will begin in Section 9.1 with the most naive setting, a simple Michelson interferometer, and we will then add up successive layers of complexity in Sections 9.2 and 9.3. Having defined the experimental set-up, we will be able to discuss the principal noise sources in Section 9.4. The existing detectors (LIGO, VIRGO, GEO600 and TAMA) are discussed in Section 9.5.1 while advanced ground-based detectors, as well as the space-borne alternative, are discussed in Section 9.5.2.

9.1 A simple Michelson interferometer

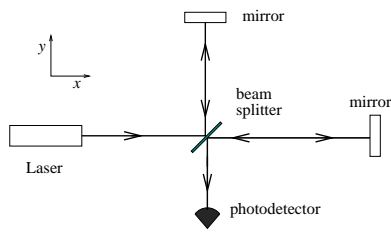


Fig. 9.1 The layout of a simple Michelson-type interferometer.

A Michelson interferometer, of the type used in the classical Michelson–Morley experiment in 1887 to show the non-existence of the ether, is an extraordinarily accurate instrument for measuring changes in the travel time of light in its arms. The simplest conceptual scheme (which is not exactly the one used historically by Michelson and Morley) is shown in Fig. 9.1. It consists of a monochromatic light source, which today is of course a laser, whose light is sent on a beam-splitter which separates the light, with equal probability amplitudes, into a beam traveling in one arm and a beam traveling in a second, orthogonal, arm. At the end of each arm we put totally reflecting mirrors. After traveling once back and forth, the two beams recombine at the beam-splitter, and part of the resulting beam goes to a photodetector, that measures its intensity (while a part goes back toward the laser). We denote by ω_L the frequency of the laser (the subscript L distinguishes it from the frequency ω_{gw} of the GWs that we want to detect), so $k_L = \omega_L/c$ and $\lambda_L = 2\pi/k_L$ are

the wavenumber and the wavelength of the laser light. It is convenient to use a complex notation for the electromagnetic field. Thus, a given spatial component of the electric field of the input laser light is written as

$$E_0 e^{-i\omega_L t + i\mathbf{k}_L \cdot \mathbf{x}}. \quad (9.1)$$

We denote by L_x and L_y the length of the two arms, where we have oriented the x and y axis as shown in Fig. 9.1. Consider a photon that arrives at the beam-splitter, coming from the laser, at some initial time t_0 .¹ The part of the electric field that goes into the x arm bounces on the mirror at a distance L_x and arrives back at the beam-splitter at a time $t = t_0 + 2L_x/c$, while the part that went through the y arm comes back at the beam-splitter at $t' = t_0 + 2L_y/c$. Thus, the beam that finally recombines at the beam-splitter at a given observation time t is the superposition of a beam that entered the beam-splitter at a time $t_0^{(x)} = t - 2L_x/c$, and then went through the x arm, and a beam that entered the beam-splitter at a *different* time $t_0^{(y)} = t - 2L_y/c$, and then went through the y arm. Setting the beam-splitter at $\mathbf{x} = 0$, the former beam has an initial phase $\exp\{-i\omega_L t_0^{(x)}\} = \exp\{-i\omega_L t + 2ik_L L_x\}$, and the latter $\exp\{-i\omega_L t_0^{(y)}\} = \exp\{-i\omega_L t + 2ik_L L_y\}$. The phase of the field is conserved during the free propagation, while the fields acquire overall factors from reflections and transmission at the mirrors.² So, the two electric fields that recombine at time t at the beam-splitter are given by

$$E_1 = -\frac{1}{2} E_0 e^{-i\omega_L t + 2ik_L L_x}. \quad (9.2)$$

and

$$E_2 = +\frac{1}{2} E_0 e^{-i\omega_L t + 2ik_L L_y}. \quad (9.3)$$

The total electric field is $E_{\text{out}} = E_1 + E_2$. Writing $2L_x = (L_x + L_y) + (L_x - L_y)$ and $2L_y = (L_x + L_y) - (L_x - L_y)$, we see that

$$E_{\text{out}} = -iE_0 e^{-i\omega_L t + ik_L(L_x + L_y)} \sin[k_L(L_y - L_x)], \quad (9.4)$$

and the power measured by the photodetector is proportional to

$$|E_{\text{out}}|^2 = E_0^2 \sin^2[k_L(L_y - L_x)]. \quad (9.5)$$

Therefore any variation in the length of a arm results in a corresponding variation of the power at the photodetector. We now discuss how to apply this general idea to GW detection. We saw in Section 1.3.3 that the interaction of a GW with a detector can be described in two different languages, i.e. either using the TT frame, or using the proper detector frame. It is quite instructive to understand the functioning of an interferometer in both ways, as we do in the next two subsections.

9.1.1 The interaction with GWs in the TT gauge

Recall from Section 1.3.3 that, in the TT gauge, the coordinates are marked by the position of freely falling objects so, even when a GW

¹Observe that, until we discuss shot noise, in Section 9.4.1, there is really no need to introduce photons, and the whole discussion could be done purely classically, replacing the word “photon” by “wave-packet”.

²As we will discuss in a more general setting in Section 9.2.1, the reflection off a 50–50 beam splitter can be modeled multiplying the amplitude of the incoming electric field by a factor $r = +1/\sqrt{2}$ for reflection from one side and $r = -1/\sqrt{2}$ for reflection from the other side, while the transmission multiplies it by $t = 1/\sqrt{2}$, and reflection at the perfectly reflecting mirrors at the end of each arm multiplies the amplitude by -1 . Thus, overall one beam acquires a factor $(1/\sqrt{2}) \times (-1) \times (1/\sqrt{2}) = -1/2$ and the other a factor $+1/2$.

is passing, the coordinates of freely falling masses by definition do not change. Of course, the mirrors of a ground-based interferometer are not freely falling; rather, the Earth's gravity is compensated by the suspensions. However, as we already discussed in Section 1.3.3, these forces are static, compared to the frequency of the GWs that we are searching and, as far as the motion in the horizontal plane is concerned, the mirrors can be taken to be in free fall, i.e. they follow the geodesics of the time-dependent part of the gravitational field.³

³Of course, there will also be some non-static forces, such as those due to suspension thermal noise or, more generally, to the coupling with the environment, which will provide the background noise, and that will be discussed in Section 9.4.

Thus, in the TT gauge description, the coordinates of the mirrors and of the beam-splitter are not affected by the passage of the wave. We define the origin of the coordinate system as the location of the beam-splitter, while the position of the mirror which terminates the x arm defines the point with coordinates $(L_x, 0)$, and the position of the other mirror defines the point with coordinates $(0, L_y)$, and this remains true also when a GW is present.

In the TT gauge description, the physical effect of the GW is manifested in the fact that it affects the propagation of light between these fixed points. We assume for the moment that the GW has only the plus polarization, and comes from the z direction.⁴ In the $z = 0$ plane of the interferometer we therefore have

$$h_+(t) = h_0 \cos \omega_{\text{gw}} t, \quad (9.6)$$

and the space-time interval in the TT frame is given by

$$ds^2 = -c^2 dt^2 + [1 + h_+(t)] dx^2 + [1 - h_+(t)] dy^2 + dz^2. \quad (9.7)$$

Photons travel along null geodesics, $ds^2 = 0$, so for the light in the x arm we have, to first order in h_0 ,

$$dx = \pm c dt \left[1 - \frac{1}{2} h_+(t) \right], \quad (9.8)$$

where the plus sign holds for the travel from the beam-splitter to the mirror and the minus sign for the return trip. Consider a photon that leaves the beam-splitter at a time t_0 . It reaches the mirror, at the fixed coordinate $x = L_x$, at a time t_1 obtained integrating eq. (9.8) with the plus sign,

$$L_x = c(t_1 - t_0) - \frac{c}{2} \int_{t_0}^{t_1} dt' h_+(t'). \quad (9.9)$$

Then the photon is reflected and reaches again the beam-splitter at a time t_2 obtained integrating eq. (9.8) with the minus sign, between $x = L_x$ and $x = 0$,

$$\int_{L_x}^0 dx = -c \int_{t_1}^{t_2} dt' \left[1 - \frac{1}{2} h_+(t') \right], \quad (9.10)$$

i.e.

$$L_x = c(t_2 - t_1) - \frac{c}{2} \int_{t_1}^{t_2} dt' h_+(t'). \quad (9.11)$$

Summing eqs. (9.9) and (9.11) we get

$$t_2 - t_0 = \frac{2L_x}{c} + \frac{1}{2} \int_{t_0}^{t_2} dt' h_+(t'). \quad (9.12)$$

For a given value of t_0 , the time of arrival t_2 after a round trip in the x arm is therefore $t_0 + 2L_x/c$, plus a correction of order h_0 . In the upper limit of the integral on the right-hand side we can replace t_2 by $t_0 + 2L_x/c$, since the integrand is already $O(h_0)$ and we are anyway neglecting terms $O(h_0^2)$, so we get

$$\begin{aligned} t_2 - t_0 &= \frac{2L_x}{c} + \frac{1}{2} \int_{t_0}^{t_0+2L_x/c} dt' h_0 \cos(\omega_{\text{gw}} t') \\ &= \frac{2L_x}{c} + \frac{h_0}{2\omega_{\text{gw}}} \{ \sin[\omega_{\text{gw}}(t_0 + 2L_x/c)] - \sin \omega_{\text{gw}} t_0 \}. \end{aligned} \quad (9.13)$$

Using the identity $\sin(\alpha + 2\beta) - \sin \alpha = 2 \sin \beta \cos(\alpha + \beta)$, we can rewrite this as

$$t_2 - t_0 = \frac{2L_x}{c} + \frac{h_0 L_x}{c} \frac{\sin(\omega_{\text{gw}} L_x/c)}{(\omega_{\text{gw}} L_x/c)} \cos[\omega_{\text{gw}}(t_0 + L_x/c)]. \quad (9.14)$$

Observe that the difference $t_2 - t_0$ is a function of the time t_0 at which the photon left the beam-splitter, because of the term $\cos[\omega_{\text{gw}}(t_0 + L_x/c)]$. Using eq. (9.6), we can also rewrite the above result as

$$t_2 - t_0 = \frac{2L_x}{c} + \frac{L_x}{c} h(t_0 + L_x/c) \frac{\sin(\omega_{\text{gw}} L_x/c)}{(\omega_{\text{gw}} L_x/c)}. \quad (9.15)$$

The quantity $t_0 + L_x/c$ which appears in the argument of $h(t)$ is, to zeroth order in h_0 , the value of time t_1 at which the photon touches the far mirror on the x arm. This result will be easily understood physically in the next subsection, thanks to the Newtonian intuition that we can use in the proper detector frame. The function

$$\text{sinc}\left(\frac{\omega_{\text{gw}} L}{c}\right) = \frac{\sin(\omega_{\text{gw}} L/c)}{(\omega_{\text{gw}} L/c)} \quad (9.16)$$

goes to one when $\omega_{\text{gw}} L/c \rightarrow 0$. Therefore, when the period of the GW is large compared to L_x/c , the shift Δt in the travel time $t_2 - t_0$, with respect to the unperturbed value $2L_x/c$, is simply $h(t_1)L_x/c$. If $\omega_{\text{gw}} L_x/c \gg 1$, Δt is suppressed. This is clearly understood physically: if $\omega_{\text{gw}} L_x/c \gg 1$, during the travel time of the photon $h(t)$ changes sign many times, so it contributes sometimes positively and sometimes negatively to Δt , and these contributions partially cancel out. A plot of the function $\text{sinc}(x)$ is shown in Fig. 9.2.

In the y arm the analysis is similar, but now the sign of $h(t)$ is reversed, as we see from eq. (9.7), so we now have

$$t_2 - t_0 = \frac{2L_y}{c} - \frac{L_y}{c} h(t_0 + L_y/c) \frac{\sin(\omega_{\text{gw}} L_y/c)}{(\omega_{\text{gw}} L_y/c)}. \quad (9.17)$$

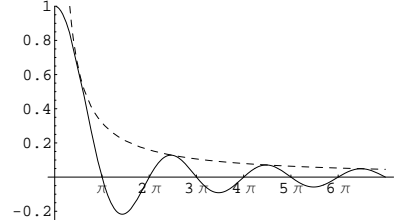


Fig. 9.2 The function $\text{sinc}(x) = (1/x) \sin x$ (solid line) and, for comparison, the function $1/x$ (dashed line).

In practice we will be interested in the light that comes out of the beam-splitter at a given value of the observation time t , so it is useful to rewrite these relations holding fixed the value of the time $t_2 \equiv t$ at which we observe the light that has recombined at the beam-splitter, and computing the corresponding value of t_0 . In order to come back at the beam-splitter at time t , the light that went through the x arm must have started its round-trip travel at a time $t_0^{(x)}$ obtained inverting eq. (9.15) to first order in h_0 , which means that $h(t_0 + L_x/c)$ is replaced by $h(t - 2L_x/c + L_x/c) = h(t - L_x/c)$, so

$$t_0^{(x)} = t - \frac{2L_x}{c} - \frac{L_x}{c} h(t - L_x/c) \operatorname{sinc}(\omega_{\text{gw}} L_x/c), \quad (9.18)$$

and similarly the light that went through the y arm, in order to arrive back at the beam-splitter at the same time t , must have started its round-trip travel at a different time $t_0^{(y)}$ given by

$$t_0^{(y)} = t - \frac{2L_y}{c} + \frac{L_y}{c} h(t - L_y/c) \operatorname{sinc}(\omega_{\text{gw}} L_y/c). \quad (9.19)$$

Again, we use the fact that the phase of the field is conserved during the free propagation. Setting the origin of the coordinate system at the beam-splitter, and writing the electric field of the light as in eq. (9.1), we see that the light that is at the beam splitter ($\mathbf{x} = 0$) at time $t_0^{(x)}$ has a phase $\exp\{-i\omega_L t_0^{(x)}\}$. The free propagation along the arm does not change this phase, while reflections and transmission at the mirrors give an overall factor $\pm 1/2$, see Note 2 on page 471, so⁵

$$\begin{aligned} E^{(x)}(t) &= -\frac{1}{2} E_0 e^{-i\omega_L t_0^{(x)}} \\ &= -\frac{1}{2} E_0 e^{-i\omega_L (t - 2L_x/c) + i\Delta\phi_x(t)}, \end{aligned} \quad (9.20)$$

where

$$\Delta\phi_x(t) = h_0 \frac{\omega_L L_x}{c} \operatorname{sinc}(\omega_{\text{gw}} L_x/c) \cos[\omega_{\text{gw}}(t - L_x/c)], \quad (9.21)$$

and similarly the field that went through the y arms, at time t has the form

$$\begin{aligned} E^{(y)}(t) &= +\frac{1}{2} E_0 e^{-i\omega_L t_0^{(y)}} \\ &= +\frac{1}{2} E_0 e^{-i\omega_L (t - 2L_y/c) + i\Delta\phi_y(t)}, \end{aligned} \quad (9.22)$$

where

$$\Delta\phi_y(t) = -h_0 \frac{\omega_L L_y}{c} \operatorname{sinc}(\omega_{\text{gw}} L_y/c) \cos[\omega_{\text{gw}}(t - L_y/c)]. \quad (9.23)$$

⁵The superscript (x) on $E^{(x)}(t)$ reminds us that this is the electric field of the light that went through the x -arm, and should not be confused with the x -component of the electric field vector. Here we are considering a given spatial component of the electric field.

⁶Except for a small asymmetry, the Schnupp asymmetry, that we will discuss in Section 9.3.2.

In general, L_x and L_y will be made as close as possible,⁶ in order to cancel many common noise in the two arms. Thus, in $\Delta\phi_x$ and $\Delta\phi_y$, which are already of order h_0 , we simply replace L_x and L_y by $L =$

$(L_x + L_y)/2$, while in the terms $t - 2L_x/c$ and $t - 2L_y/c$ we still take into account any small difference between L_x and L_y , writing $2L_x = 2L + (L_x - L_y)$ and $2L_y = 2L - (L_x - L_y)$. Then

$$E^{(x)}(t) = -\frac{1}{2}E_0 e^{-i\omega_L(t-2L/c)+i\phi_0+i\Delta\phi_x(t)}, \quad (9.24)$$

$$E^{(y)}(t) = +\frac{1}{2}E_0 e^{-i\omega_L(t-2L/c)-i\phi_0+i\Delta\phi_y(t)}, \quad (9.25)$$

where

$$\phi_0 = k_L(L_x - L_y), \quad (9.26)$$

$\Delta\phi_y = -\Delta\phi_x$, and

$$\begin{aligned} \Delta\phi_x(t) &= h_0 k_L L \operatorname{sinc}(\omega_{\text{gw}} L/c) \cos[\omega_{\text{gw}}(t - L/c)] \\ &\equiv |\Delta\phi_x| \cos(\omega_{\text{gw}} t + \alpha), \end{aligned} \quad (9.27)$$

with $\alpha = -\omega_{\text{gw}} L/c$ a phase. The total phase difference induced by GWs in the Michelson interferometer is

$$\Delta\phi_{\text{Mich}} \equiv \Delta\phi_x - \Delta\phi_y = 2\Delta\phi_x. \quad (9.28)$$

The total electric field at the output is

$$\begin{aligned} E_{\text{tot}}(t) &= E^{(x)}(t) + E^{(y)}(t) \\ &= -iE_0 e^{-i\omega_L(t-2L/c)} \sin[\phi_0 + \Delta\phi_x(t)]. \end{aligned} \quad (9.29)$$

The phase ϕ_0 is a parameter that the experimenter can adjust, choosing the best working point for the interferometer, as we will discuss in Section 9.3.2, while $\Delta\phi_x(t)$ contains the effect of the GW. In the limit $\omega_{\text{gw}} L/c \ll 1$, eq. (9.27) reduces to

$$\Delta\phi_x(t) \simeq h(t - L/c) k_L L. \quad (9.30)$$

Comparing with eq. (9.26) we see that, in this limit, the effect of the GW on the phase shift is formally equivalent to a change of $L_x - L_y$ given by

$$\frac{\Delta(L_x - L_y)}{L} \simeq h(t - L/c). \quad (9.31)$$

The total power $P \sim |E_{\text{tot}}|^2$ observed at the photodetector is modulated by the GW signal as

$$\begin{aligned} P &= P_0 \sin^2[\phi_0 + \Delta\phi_x(t)] \\ &= \frac{P_0}{2} \{1 - \cos[2\phi_0 + 2\Delta\phi_x(t)]\} \\ &= \frac{P_0}{2} \{1 - \cos[2\phi_0 + \Delta\phi_{\text{Mich}}(t)]\}. \end{aligned} \quad (9.32)$$

Clearly, we want to have $\Delta\phi_{\text{Mich}}$ as large as possible. For a GW of a given frequency ω_{gw} , we see from eq. (9.27) that the dependence on L is given by the factor $(\omega_L L/c) \operatorname{sinc}(\omega_{\text{gw}} L/c) = (\omega_L/\omega_{\text{gw}}) \sin(\omega_{\text{gw}} L/c)$.

Thus the optimal length of the arms is given by $\omega_{\text{gw}}L/c = \pi/2$, i.e. $L = \lambda_{\text{gw}}/4$. In terms of $f_{\text{gw}} = \omega_{\text{gw}}/(2\pi)$, this gives

$$L \simeq 750 \text{ km} \left(\frac{100 \text{ Hz}}{f_{\text{gw}}} \right). \quad (9.33)$$

For such a value of L , the time shift induced by the GW on the light has the same sign all along its round trip in a arm, so the effect adds up. For longer arms, the GW amplitude inverts its sign during the round trip, so past this moment it starts canceling the phase shift that the light already accumulated.⁷ Arms of hundreds of kms are impossible to obtain in a ground-based interferometer, for practical and financial reasons. We will see in Section 9.2 how to “fold” this optimal pathlength of the light into an interferometers of manageable size.

It is useful to realize that the effect of the GW on the laser light is to generate sidebands in the light propagating in each of the two arms. Using eq. (9.27), and making use of the fact that $\Delta\phi_x$ is linear in h_0 , we can expand $E^{(x)}(t)$ in eq. (9.24) to order h_0 as

$$\begin{aligned} E^{(x)}(t) &= -\frac{1}{2}E_0e^{-i\omega_L(t-2L/c)+i\phi_0}[1+i|\Delta\phi_x|\cos(\omega_{\text{gw}}t+\alpha)] \\ &= \frac{1}{2}E_0e^{i\beta}\left[e^{-i\omega_L t} + \frac{i}{2}|\Delta\phi_x|e^{i\alpha}e^{-i(\omega_L-\omega_{\text{gw}})t}\right. \\ &\quad \left.+ \frac{i}{2}|\Delta\phi_x|e^{-i\alpha}e^{-i(\omega_L+\omega_{\text{gw}})t}\right], \end{aligned} \quad (9.34)$$

with β an irrelevant constant phase. Thus, beside the original electromagnetic wave at a frequency ω_L (the “carrier”, in the language of radio engineering), we have two more electromagnetic waves, at the frequencies $\omega_L \pm \omega_{\text{gw}}$ (the “sidebands”). The modulus of the amplitude of the sidebands is $O(h_0)$ with respect to the carrier, and is given by $|\Delta\phi_x|/2$.

9.1.2 The interaction in the proper detector frame

It is instructive to compare the above results, obtained in the TT frame, with the description obtained using the language of the proper detector frame. Recall from Section 1.3.3 that the proper detector frame is the one implicitly used by the experimenter when he/she thinks about the apparatus. In particular, here coordinates are not marked by freely falling masses, as in the TT gauge, but rather are measured with a rigid ruler. We saw that in the proper detector frame the effect of the passage of a GW is a displacement of the test masses from their original position and, if these test masses are at a distance small compared to the reduced wavelength $\bar{\lambda}_{\text{gw}}$ of the GW, this displacement is determined by the equation of the geodesic deviation (1.95). At the same time, the space-time metric can be taken as flat, at least in a region of space small compared to the scale of variation of the gravitational wave, which is its reduced wavelength $\bar{\lambda}_{\text{gw}}$.⁸

⁸This is correct as far as the fast-varying part of the gravitational field is concerned, while the static gravitational field of the Earth is compensated by the mirror suspensions, and other effects related to the laboratory frame (Coriolis forces, etc.) are negligible because slowly varying, see the detailed discussion in Section 1.3.3.

Thus, the proper detector frame description has the advantage of being very intuitive, since in a first approximation we can use the language of flat space-time, and the interaction of the mirrors with GWs is described by the equation of the geodesic deviation, i.e. in terms of Newtonian forces, so we can use our Newtonian intuition. However it must be kept in mind that, contrary to the TT gauge description, which is exact, the proper-frame description is approximate, and is valid only if the test masses are at a distance small compared to the reduced wavelength λ_{gw} of the GW, see eq. (1.97). Since for a Michelson interferometer the distance between the beam-splitter and the end mirror of an arm is the arm-length L , the proper detector frame description assumes $L \ll \lambda_{\text{gw}}$, that is,

$$\frac{\omega_{\text{gw}} L}{c} \ll 1. \quad (9.35)$$

Thus, we cannot expect to recover the full TT gauge result (9.27), which is exact, but only its limit for small values of $\omega_{\text{gw}} L/c$.

We first perform the computation in the proper detector frame to lowest-order in $\omega_{\text{gw}} L/c$. In this limit the space-time metric is exactly flat, see eq. (1.86), while the effect of the GW on the test masses is given by the equation of the geodesic deviation, eq. (1.95). Thus, the situation is reversed compared to the TT gauge description. In the TT gauge, the position of the mirrors is not affected by GWs, while the propagation of light between the mirrors is affected. In the proper detector frame, the mirrors are affected by the GWs, while light propagation is not. We fix the origin of the coordinate system on the beam-splitter so, by definition, the beam-splitter does not move, and we consider as before a GW with only the plus polarization coming from the z direction, written as in eq. (9.6). The equation of the geodesic deviation for the mirror on the x arm, described by coordinates (ξ_x, ξ_y) , is then⁹

$$\ddot{\xi}_x = \frac{1}{2} \ddot{h}_+ \xi_x, \quad (9.36)$$

while $\xi_y(t)$ remains zero at all times if $\xi_y(0) = \dot{\xi}_y(0) = 0$. Equation (9.36) can be solved perturbatively in h_0 ; to zeroth order we have $\xi_x = L_x$, so to $O(h_0)$ we get $\ddot{\xi}_x = (1/2)\ddot{h}_+ L_x$, which has the solution

$$\xi_x(t) = L_x + \frac{h_0 L_x}{2} \cos \omega_{\text{gw}} t, \quad (9.37)$$

where we choose the integration constants so that the average value of ξ_x over one period of the GW is equal to L_x , and the average value of the velocity $\dot{\xi}_x$ vanishes.

Since space-time is flat, a photon that starts at the beam-splitter at time t_0 , moving along the positive x axis, follows the trajectory $x(t) = c(t - t_0)$, so it reaches the mirror at a time t_1 given by $c(t_1 - t_0) = \xi_x(t_1)$. This equation is easily solved for t_1 , perturbatively in h_0 . To zeroth order in h_0 we get the trivial result $t_1 = t_0 + (L_x/c)$. Inserting this into $\cos \omega_{\text{gw}} t$ in eq. (9.37) (which is already multiplied by h_0), we get

$$c(t_1 - t_0) = L_x + \frac{h_0 L_x}{2} \cos[\omega_{\text{gw}}(t_0 + L_x/c)]. \quad (9.38)$$

⁹The fact that here appears the form of $h_{\mu\nu}$ in the TT gauge, even if we are working in the proper detector frame, is a consequence of the fact that the right-hand side of eq. (9.36) is really $-c^2 R_{10j0} \xi^j$, see eq. (1.93). Recall from Section 1.1 that, in linearized theory, the Riemann tensor is invariant under coordinate transformations, so we are free to compute it in the frame that we wish, and in particular we can use the form of $h_{\mu\nu}$ in the TT gauge.

The round-trip time is twice as large, so the photon gets back at the beam-splitter at a time t_2 given by

$$t_2 - t_0 = \frac{2L_x}{c} + \frac{h_0 L_x}{c} \cos[\omega_{\text{gw}}(t_0 + L_x/c)]. \quad (9.39)$$

This coincide with the result that we got in the TT gauge, eq. (9.14), *except* that the function $\text{sinc}(\omega_{\text{gw}}L/c) = [\sin(\omega_{\text{gw}}L/c)]/[\omega_{\text{gw}}L/c]$ has been replaced by one, which is the lowest-order term of its Taylor expansion. This is as expected, since the proper-frame computation just performed is valid only to lowest order in $\omega_{\text{gw}}L/c$.

It is instructive to compute also the next term in the expansion in $\omega_{\text{gw}}L/c$ in the proper detector frame, and verify that we correctly recover the next term in the expansion of $\text{sinc}(\omega_{\text{gw}}L/c)$. In principle, we have two kinds of corrections. (1) Corrections to the equation of motion of the mirrors, since the geodesic equation that we have used is the first term in an expansion in $L/\lambda_{\text{gw}} = \omega_{\text{gw}}L/c$, as it is clear from the derivation leading from eq. (1.66) to eq. (1.71). (2) Correction to the propagation of the photons, since the space-time metric is no longer flat.

Actually, the former type of correction in our problem vanishes at next-to-leading order.¹⁰ The first correction to the photon propagation can be computed using the metric (1.87). For the propagation along a trajectory with $y = z = 0$ (and therefore with $dy = dz = 0$), recalling that the Riemann tensor is antisymmetric in the first and second pair of indices, eq. (1.87) reduces to

$$ds^2 = -c^2 dt^2 (1 + R_{0101}x^2) + dx^2. \quad (9.40)$$

We can compute the Riemann tensor using the form of $h_{\mu\nu}$ in the TT gauge (compare with Note 9) which gives, for a wave with only the plus polarization,

$$\begin{aligned} R_{0101} &= -\frac{1}{2c^2} \ddot{h}_+ \\ &= \frac{\omega_{\text{gw}}^2}{2c^2} h_0 \cos \omega_{\text{gw}} t, \end{aligned} \quad (9.41)$$

see eq. (1.94). Light propagation is obtained imposing $ds^2 = 0$ in eq. (9.40); then, to next-to-leading order, the position $x(t)$ of a photon propagating along the x arm is obtained integrating

$$dx = \pm c dt \left[1 + \frac{\omega_{\text{gw}}^2}{4c^2} x^2(t) h_0 \cos \omega_{\text{gw}} t \right], \quad (9.42)$$

while the motion of the mirrors is still given by eq. (9.37).

Consider a photon that leaves the beam-splitter at time t_0 and propagates along the positive x direction. To lowest order in h_0 we have the trivial result $x(t) = c(t - t_0)$. Inserting this into the right-hand side of eq. (9.42) we find the solution to order h_0 ,

$$x(t) = c(t - t_0) + h_0 \frac{c \omega_{\text{gw}}^2}{4} \int_{t_0}^t dt' (t' - t_0)^2 \cos \omega_{\text{gw}} t'. \quad (9.43)$$

¹⁰This can be shown by observing that the geodesic equation (1.66) for a mirror moving non-relativistically is simply $\ddot{\xi}^i = -\Gamma_{00}^i(\xi)$. Expanding it to second order in ξ , with $\Gamma_{00}^i(\xi = 0) = 0$, we get

$$\ddot{\xi}^i = -\xi^j \partial_j \Gamma_{00}^i - \frac{1}{2} \xi^j \xi^k \partial_k \partial_j \Gamma_{00}^i + O(\xi^3),$$

where the derivatives of Γ_{00}^i are computed at $\xi = 0$. The first term gives the equation of motion that we already used. For a mirror along the x arm $\xi^i = (\xi_x, 0, 0)$, so the second term is proportional to $\partial_1(\partial_1 \Gamma_{00}^1)$. A plane wave propagating along the z direction is function only of t and z , and so its Riemann tensor, as well as $(\partial_1 \Gamma_{00}^1)$, is independent of x , and $\partial_1(\partial_1 \Gamma_{00}^1)$ vanishes.

Writing

$$\begin{aligned}\cos \omega_{\text{gw}} t' &= \cos[\omega_{\text{gw}}(t' - t_0) + \omega_{\text{gw}} t_0] \\ &= \cos[\omega_{\text{gw}}(t' - t_0)] \cos \omega_{\text{gw}} t_0 - \sin[\omega_{\text{gw}}(t' - t_0)] \sin \omega_{\text{gw}} t_0,\end{aligned}\quad (9.44)$$

the integral over t' can be performed exactly. Consistently with the order to which we are working, we then expand the exact result to the first non-trivial order in $\omega_{\text{gw}}(t - t_0)$ (which, in the final result, will correspond to the first non-trivial order in $\omega_{\text{gw}}L/c$), and we get

$$x(t) \simeq c(t - t_0) + h_0 \frac{c \omega_{\text{gw}}^2}{12} (t - t_0)^3 \cos \omega_{\text{gw}} t_0. \quad (9.45)$$

The time t_1 at which the photon reaches the mirror is now obtained solving the equation $x(t_1) = \xi(t_1)$ iteratively in h_0 . This gives

$$c(t_1 - t_0) = L_x + \frac{h_0 L_x}{2} \cos[\omega_{\text{gw}}(t_0 + L_x/c)] - h_0 \frac{\omega_{\text{gw}}^2}{12c^2} L_x^3 \cos(\omega_{\text{gw}} t_0). \quad (9.46)$$

Observe that (writing $\epsilon \equiv \omega_{\text{gw}} L_x/c$)

$$\begin{aligned}\cos[\omega_{\text{gw}}(t_0 + L_x/c)] &= \cos(\omega_{\text{gw}} t_0) \cos \epsilon - \sin(\omega_{\text{gw}} t_0) \sin \epsilon \\ &= [1 + O(\epsilon^2)] \cos(\omega_{\text{gw}} t_0) + O(\epsilon) \sin(\omega_{\text{gw}} t_0),\end{aligned}\quad (9.47)$$

so in the last term of eq. (9.46), which is already a factor $(\omega_{\text{gw}} L_x/c)^2$ smaller than the second term, we can replace $\cos(\omega_{\text{gw}} t_0)$ by $\cos[\omega_{\text{gw}}(t_0 + L_x/c)]$, since the difference is of higher order in $\omega_{\text{gw}} L_x/c$. Then we finally get

$$c(t_1 - t_0) = L_x + \frac{h_0 L_x}{2} \cos[\omega_{\text{gw}}(t_0 + L_x/c)] \left[1 - \frac{1}{6} \left(\frac{\omega_{\text{gw}} L_x}{c} \right)^2 \right]. \quad (9.48)$$

Writing similarly the equations for the round trip we find that, to this order in $\omega_{\text{gw}} L_x/c$, the round-trip travel $t_2 - t_0$ is twice $t_1 - t_0$. In the last bracket we recognize the first two terms of the expansion

$$\frac{\sin x}{x} = 1 - \frac{x^2}{6} + O(x^4). \quad (9.49)$$

We have therefore verified that the analysis in the proper detector frame correctly reproduces the leading and the next-to-leading terms of the TT gauge result given in eq. (9.15). It is also clear from this discussion that, while the description in the detector proper frame is more intuitive, since it allows us to think in terms of Newtonian forces acting on the mirrors, and of light propagating (in a first approximation) in the flat space-time of Newtonian physics, still the TT gauge description is much more powerful, since it allows us to get the exact closed form of the dependence on $\omega_{\text{gw}} L_x/c$. In the detector proper frame the computation of still higher-order corrections becomes more and more involved and, without the hindsight from the TT gauge analysis, it would be difficult to imagine that the whole series resums to such a simple closed form.

9.2 Interferometers with Fabry–Perot cavities

We have seen in eq. (9.33) that, to measure GWs with frequencies of order of a few hundreds Hz, the optimal choice would be an arm-length L of several hundreds kms. For Earth-based interferometers this is in practice impossible (consider, among other things, that the arms of the interferometers must be enclosed in a very high vacuum system, as we will see in the Section 9.4). Taking into account technological and financial constraints, LIGO has arms of length $L = 4$ km and VIRGO of 3 km, while GEO600 has $L = 600$ m and TAMA has $L = 300$ m. The idea is therefore to “fold” the optical path of light, making it bounce back and forth many times in each arm, before recombining the two beams. A solution that was first considered is the so-called “delay line”. In this case, in each arm the light beam goes back and forth between two mirrors along trajectories that do not superimpose, and which make different spots on the mirrors. However, to reach an effective path length of order 750 km out of arms of order 3–4 km we need $O(100)$ bounces. In the delay line scheme, this leads to unpractically large mirrors.¹¹ Thus, the solution which has been adopted in LIGO and VIRGO is that of transforming each arm into a Fabry–Perot cavity. In the next subsection we will discuss the principles of operation of a Fabry–Perot (FP) cavity, and in Section 9.2.2 we will discuss its interaction with a GW, and we will see how it improves on the simple Michelson scheme.

¹¹Furthermore, this scheme turns out to be quite sensitive to the problem that some part of the light is scattered inside the interferometer off the nominal path, and this light interferes with the main beam.

9.2.1 Electromagnetic fields in a FP cavity

Reflection and transmission coefficients

First of all we recall from elementary electromagnetism that, at the interface between two media with different index of refraction, the relation between the incoming field E_{in} , the reflected field E_{refl} and the transmitted field E_t can be written as

$$E_{\text{refl}} = rE_{\text{in}}, \quad E_t = tE_{\text{in}}, \quad (9.50)$$

where r and t are called the reflection and transmission coefficients, respectively, and are in general complex numbers. We consider for the moment the transmission and reflection across a sharp boundary. At a sharp boundary there is no physical mechanism that can produce a phase shift, so in this limit r and t are real. More precisely, (r, t) are the reflection and transmission coefficients when E_{in} comes from the first medium, say the denser (from the left in Fig. 9.3). Similarly, we denote by r' and t' the reflection and transmission coefficients when E_{in} comes from the second medium, i.e. from the right in Fig. 9.4. Between these coefficients hold useful relations. In particular, since the energy associated to the electric field is proportional to $|E|^2$, and on a sharp boundary there are no losses and r, t are real, energy conservation

Fig. 9.3 The situation in which the incoming field comes from the denser medium.

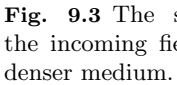
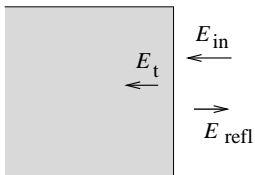


Fig. 9.4 The situation in which the incoming field comes from the rarer medium.



requires

$$r^2 + t^2 = 1, \quad (9.51)$$

and $r'^2 + t'^2 = 1$.¹² Between (r, t) and (r', t') we have so-called reciprocity relations, which can be obtained as follows. Consider the arrangement shown in Fig. 9.5, in which the incoming electric field arrives from the left, and there is a gap of width d of a less dense medium between two layers of the more dense medium. We denote by E_{cav} and E'_{cav} , respectively, the right-moving and left-moving electric fields in the gap, close to the first interface. Then, by definition of reflection and transmission coefficients, at the first interface we have the two relations

$$E_{\text{cav}} = t E_{\text{in}} + r' E'_{\text{cav}}, \quad (9.52)$$

$$E_{\text{refl}} = r E_{\text{in}} + t' E'_{\text{cav}}. \quad (9.53)$$

We now take the limit $d \rightarrow 0$. In this case E_{cav} and E'_{cav} are also the right and left-moving fields, respectively, at the second interface. Thus, we also have the relations

$$E_t = t' E_{\text{cav}}, \quad (9.54)$$

$$E'_{\text{cav}} = r' E_{\text{cav}}. \quad (9.55)$$

On the other hand, if $d \rightarrow 0$, there is no gap, and we must have

$$E_t = E_{\text{in}}, \quad (9.56)$$

$$E_{\text{refl}} = 0. \quad (9.57)$$

Combining the six relations (9.52)–(9.57) we find the two conditions

$$r' = -r, \quad (9.58)$$

$$tt' - rr' = 1. \quad (9.59)$$

Inserting eqs. (9.58) and (9.51) into eq. (9.59) we get $t' = t$. In conclusion, we have

$$\boxed{r' = -r, \quad t' = t.} \quad (9.60)$$

For a perfectly reflecting mirror, reflection from the less dense to the more dense medium is associated to a factor $r' = -1$, while from the denser to the less dense medium we have $r = 1$.

Reflected, transmitted and interior field in a FP cavity

We can now apply the above results to the study of a Fabry–Perot cavity. A Fabry–Perot cavity consists of two parallel mirrors, that for the time being we assume plane and of infinite transverse extent. We consider a component E_{in} of the incoming electric field. Part of the incoming field is reflected and partly transmitted, see Fig. 9.6. The

¹²More precisely, the energy density is actually proportional to $\mathbf{E} \cdot \mathbf{D}$, where \mathbf{D} is the displacement vector. If we define the coefficients r, t in terms of \mathbf{E} , we should then write $r^2 + t^2(n_1/n_2) = 1$. We can however simply reabsorb n into the definition of \mathbf{E} to keep the equations in simpler forms such as eq. (9.51). In any case, the issue is irrelevant for a situation such as that shown in Fig. 9.6, where we are interested in the fields in the vacuum, on both sides of the mirror.

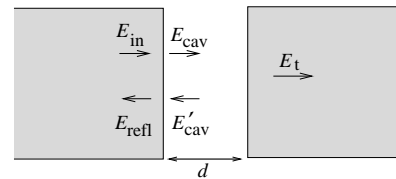


Fig. 9.5 A gap of a less dense medium between two layers of denser media.

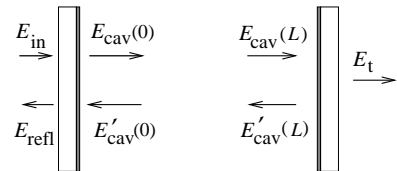


Fig. 9.6 A schematic Fabry–Perot cavity.

transmitted field $E_{\text{cav}}(0)$ propagates to the far mirror, where it is partly reflected and partly transmitted. The reflected part goes back to the first mirror, where again it is partly reflected and partly transmitted, and so on. The total reflected, interior and transmitted fields are therefore determined by the superposition of many beams, corresponding to the multiple bounces.

The light from the laser comes from the left in Fig. 9.6. The mirrors are set with their high-reflectivity coating on the interior of the cavity. Before reaching the high-reflectivity coating, light enters from the left face of the mirror and passes through the substrate, so in general it acquires a further complex phase shift, both from the substrate and from the coating, and can also suffer losses. A beam which enters the cavity and, after a number of round-trips, is reflected back, traverses once more this substrate, acquiring a further phase. The important point, however, is that these phase shifts are the same for all beams, independently of the number of bounces made inside the FP cavity, so they just give an overall phase factor, independent of the length L of the cavity, to the reflected (and transmitted) fields. This phase factor is compensated by the experimenter, moving the position of the mirrors until the interference pattern of the interferometer is on the desired working point (the dark fringe, as we will see), so we can simply forget about them.¹³ We can therefore simply model the two mirrors of the FP cavity stating that, for the first mirror, we have real reflection and transmission coefficients r_1 and t_1 when the incoming field propagates from the interior of the mirror toward the cavity, and $r'_1 = -r_1$ and $t'_1 = t_1$ when it is going from the cavity toward the mirror. We then take into account the losses in the mirror writing

$$r_1^2 + t_1^2 = 1 - p_1, \quad (9.61)$$

where p_1 (typically of order of a few parts per million) represents the losses in the first mirror. We similarly introduce coefficients (r_2, t_2) and $(r'_2 = -r_2, t'_2 = t_2)$ for the second mirror, with $r_2^2 + t_2^2 = 1 - p_2$, so again a field that propagates from the cavity toward the mirror and is reflected back gets a factor $-r_2$.

Other modelizations of the mirrors are possible. In particular, one could treat the reflection and transmission from the two sides of the mirror symmetrically so that, if a field A is coming from the left, the reflected field is $A_R = z_R A$ and the transmitted field is $A_T = z_T A$, where z_R and z_T are the reflection and transmission coefficients, which now a priori can be complex because of the finite thickness of the mirror, and which satisfy $|z_R|^2 + |z_T|^2 = 1 - p$. Similarly, if a field B is coming from the right, the reflected field is $B_R = z_R B$ and the transmitted field is $B_T = z_T B$, with the same z_R, z_T . In the presence of both a field A coming from the left and a field B coming from the right, as in Fig. 9.7, we have

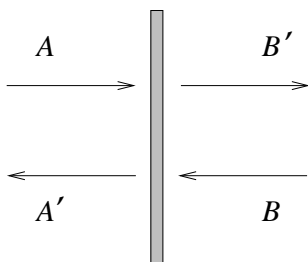


Fig. 9.7 A symmetric mirror, with a field A coming from the left and a field B incoming from the right.

$$A' = z_R A + z_T B \quad (9.62)$$

$$B' = z_T A + z_R B. \quad (9.63)$$

Requiring the energy balance $|A'|^2 + |B'|^2 = (1-p)(|A|^2 + |B|^2)$, we get the condition $\text{Re}(z_R z_T^*) = 0$. A possible solution is $z_R = ir$, $z_T = t$, where r and t are real and satisfy $r^2 + t^2 = 1 - p$.

These different modelizations of the mirrors of a cavity of length L can however be compensated by a constant shift ΔL of some fraction of wavelength. For instance, with the modelization $r' = -r$, we will find below that a Fabry–Perot cavity resonates at $2k_L L = 2\pi n$, with n integer. Repeating the computation for $z_R = ir$, equal for both sides, one would rather find resonances at $2k_L L = 2\pi(n + 1/2)$. In practice, the experimenter tunes the position of the mirrors until he/she finds a resonance, and all that matters is the behavior around resonance, which is the same in the two cases, so the modelization chosen for the mirrors becomes irrelevant. Similarly, using $z_R = ir$ and $z_T = t$, instead of eq. (9.5) one would find $|E_{\text{out}}|^2 = E_0^2 \cos^2[k_L(L_y - L_x)]$, but again the experimenter simply adjusts the lengths L_x and L_y until he/she finds the desired working point, such as the dark fringe. For definiteness, we will always use the modelization leading to eq. (9.60).

We can now compute the reflected and transmitted fields, and the field inside the cavity, as follows. We choose the coordinates so that the left mirror is at $x = 0$ and the right mirror at $x = L$. From the laser we send light with an electric field of the form $E_0 \exp\{-i\omega_L t + ik_L x\}$. Let $t = t_0$ be the value of time at which a given wave-packet reaches the mirror, at $x = 0$. Thus, the corresponding electric field is simply

$$E_0 e^{-i\omega_L t_0}. \quad (9.64)$$

Part of this beam will be immediately reflected back from the mirror, with amplitude $+r_1$, giving rise to a reflected beam with field

$$E_{\text{refl}}^{(0)} = r_1 E_0 e^{-i\omega_L t_0}. \quad (9.65)$$

This field will interfere with a beam that was sent toward the mirror *earlier*, which entered the cavity, was reflected back at the second mirror, and then was transmitted from the first mirror, see Fig. 9.8. In order to arrive back at the first mirror at the same time t_0 , it must have entered the cavity at time $t_0 - 2L/c$. So, its initial amplitude when it entered the mirror for the first time, arriving from the laser, was $E_0 e^{-i\omega_L(t_0 - 2L/c)}$, that is $E_0 e^{-i\omega_L t_0} e^{2ik_L L}$. After transmission from the first mirror it gets a factor t_1 , reflection at the second mirror gives a factor $-r_2$ and finally transmission from the first mirror gives again t_1 . Thus, at time t_0 the total reflected field gets also a contribution

$$E_{\text{refl}}^{(1)} = [-t_1^2 r_2 e^{2ik_L L}] E_0 e^{-i\omega_L t_0}. \quad (9.66)$$

This beam has a relative amplitude $-r_2 t_1^2 e^{2ik_L L}$ compared to the incoming laser field given in eq. (9.64).¹⁴ Then, we have the field that entered the cavity at time $t_0 - 4L/c$, and went twice back and forth in the cavity. It comes out at time t_0 with an amplitude

$$E_{\text{refl}}^{(2)} = [-r_1 r_2^2 t_1^2 e^{4ik_L L}] E_0 e^{-i\omega_L t_0}. \quad (9.67)$$

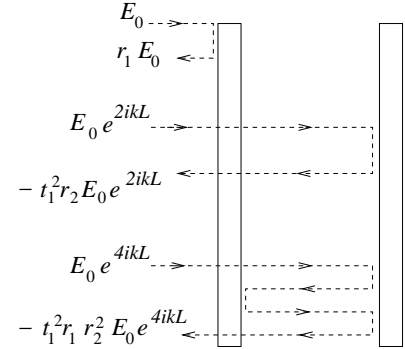


Fig. 9.8 The building up of the reflected field from the interference of the directly reflected beams and of beams that entered the cavity at earlier times and made a number of bounces inside the cavity. For clarity, the various path have been drawn as if they were spatially separated.

¹⁴This result is often colloquially explained stating that the field has acquired a phase $e^{2ik_L L}$ from the free propagation, and the factors $-r_2 t_1^2$ from its various transmissions and reflection. This is misleading. Of course, a wave does not acquire any phase factor from its free propagation. Photons in free space propagate along a trajectory $x(t) = x_0 + c(t - t_0)$, so $x(t) - ct = x_0 - ct_0$ is a constant, and the phase factor $k_L x - \omega_L t = k_L(x - ct)$ is also constant along the free propagation. In flat space-time, multiplicative factors and phases are acquired by the amplitude only when there is interaction with matter, i.e. at reflection and transmission from the mirrors, and in our case this gives the factor $-r_2 t_1^2$. The factor $e^{2ik_L L}$ relative to eq. (9.64) is there because the beam that we are considering entered the cavity *earlier*, at a time $t_0 - 2L/c$, and spent a time $2L/c$ going back and forth in the cavity. Thus, this second beam already had from the start a phase different by a factor $e^{2ik_L L}$, compared to the field (9.64) that arrives at time t_0 directly from the laser.

More generally, the field that entered the cavity at time $t_0 - n(2L/c)$ and performed n round trips comes out at time t_0 with an amplitude

$$E_{\text{refl}}^{(n)} = [-r_1^{n-1} r_2^n t_1^2 e^{2n i k_L L}] E_0 e^{-i \omega_L t_0}. \quad (9.68)$$

The total reflected field is therefore given by

$$\begin{aligned} E_{\text{refl}} &= E_0 e^{-i \omega_L t_0} \left[r_1 - t_1^2 \sum_{n=1}^{\infty} r_1^{n-1} r_2^n e^{2n i k_L L} \right] \\ &= E_0 e^{-i \omega_L t_0} \left[r_1 - t_1^2 r_2 e^{2 i k_L L} \sum_{m=0}^{\infty} (r_1 r_2 e^{2 i k_L L})^m \right] \\ &= E_0 e^{-i \omega_L t_0} \left[r_1 - t_1^2 r_2 \frac{e^{2 i k_L L}}{1 - r_1 r_2 e^{2 i k_L L}} \right], \end{aligned} \quad (9.69)$$

or, using $t_1^2 = 1 - p_1 - r_1^2$,

$$E_{\text{refl}} = E_0 e^{-i \omega_L t_0} \frac{r_1 - r_2 (1 - p_1) e^{2 i k_L L}}{1 - r_1 r_2 e^{2 i k_L L}}.$$

(9.70)

The transmitted field is computed similarly,

$$\begin{aligned} E_t &= E_0 e^{-i \omega_L t_0} t_1 t_2 \sum_{n=0}^{\infty} (r_1 r_2)^n e^{i k_L L (2n+1)} \\ &= E_0 e^{-i \omega_L t_0} \frac{t_1 t_2 e^{i k_L L}}{1 - r_1 r_2 e^{2 i k_L L}}. \end{aligned} \quad (9.71)$$

The field inside the cavity, at the left mirror ($x = 0$), again at time t_0 , is

$$\begin{aligned} E_{\text{cav}}(0) &= E_0 e^{-i \omega_L t_0} t_1 \sum_{n=0}^{\infty} (r_1 r_2)^n e^{2n i k_L L} \\ &= E_0 e^{-i \omega_L t_0} \frac{t_1}{1 - r_1 r_2 e^{2 i k_L L}}, \end{aligned} \quad (9.72)$$

and for the field inside the cavity, at the other mirror, at time t_0 , we have $E_{\text{cav}}(L) = e^{i k_L L} E_{\text{cav}}(0)$. The same results can be obtained also in the following way, which is maybe less vivid physically, but will be easier to generalize to the situation in which GWs are present. We consider the total reflected, transmitted and cavity fields as shown in Fig. 9.6. Then, just as in eqs. (9.52) and (9.53), using $r'_1 = -r_1$ and $t'_1 = t_1$, at the first mirror we have

$$E_{\text{cav}}(0) = t_1 E_{\text{in}} - r_1 E'_{\text{cav}}(0), \quad (9.73)$$

$$E_{\text{refl}} = r_1 E_{\text{in}} + t_1 E'_{\text{cav}}(0). \quad (9.74)$$

Similarly, at the second mirror we have

$$E_t = t_2 E_{\text{cav}}(L), \quad (9.75)$$

$$E'_{\text{cav}}(L) = -r_2 E_{\text{cav}}(L). \quad (9.76)$$

Finally, since the solution inside the cavity is given by plane waves, the field $E_{\text{cav}}(t, x)$, which represent a right-moving wave, is proportional to $\exp\{-i(\omega_L t - k_L x)\}$, while $E'_{\text{cav}}(t, x)$, which represent a left-moving wave, is proportional to $\exp\{-i(\omega_L t + k_L x)\}$. Thus the cavity fields at $x = L$ and at $x = 0$, at equal value of time, are related by

$$E_{\text{cav}}(L) = e^{ik_L L} E_{\text{cav}}(0), \quad (9.77)$$

$$E'_{\text{cav}}(L) = e^{-ik_L L} E'_{\text{cav}}(0). \quad (9.78)$$

Then we have six equations, eqs. (9.73)–(9.78), that we can solve for the six quantities E_{refl} , E_t , $E_{\text{cav}}(0)$, $E_{\text{cav}}(L)$, $E'_{\text{cav}}(0)$, $E'_{\text{cav}}(L)$, in terms of $E_{\text{in}} = E_0 e^{-i\omega_L t}$. With straightforward algebra we get back the solution found above. For instance, combining eqs. (9.76), (9.77) and (9.78) we get

$$E'_{\text{cav}}(0) = -r_2 e^{2ik_L L} E_{\text{cav}}(0). \quad (9.79)$$

Substituting this into eq. (9.73) we get

$$E_{\text{cav}}(0) = t_1 E_{\text{in}} + r_1 r_2 e^{2ik_L L} E_{\text{cav}}(0), \quad (9.80)$$

from which the solution (9.72) for $E_{\text{cav}}(0)$ follows, and similarly we get E_{refl} and E_t .

Resonant FP cavities

We see that the reflected, transmitted and interior fields are all proportional to the factor $1/[1 - r_1 r_2 e^{2ik_L L}]$. When $2k_L L = 2\pi n$, with $n = 0, \pm 1, \pm 2, \dots$, this factor becomes $1/(1 - r_1 r_2)$ and, if the reflection coefficients r_1 and r_2 are close to one, this is large. We therefore have a set of resonances. Physically this means that, for $2k_L L = 2\pi n$, the various beams that bounce back and forth interfere constructively, so the field inside the cavity raises to a very large value. Correspondingly, the transmitted field also gets large. As for the reflected field, for assessing its strength we must also take into account the dependence on $k_L L$ of the numerator, which describes the interference between the field that is reflected after having entered the cavity and made one or more round trips, and the field that is immediately reflected. We first consider the power $P_t \sim |E_t|^2$ of the transmitted field (or, equivalently, of the interior field, E_{cav} , since $|E_t|$ and $|E_{\text{cav}}|$ differ just by a constant factor t_2). From eq. (9.71),

$$|E_t|^2 = E_0^2 \frac{t_1^2 t_2^2}{1 + (r_1 r_2)^2 - 2r_1 r_2 \cos 2k_L L}. \quad (9.81)$$

This is plotted, as a function of $2k_L L$, in Fig. 9.9. Writing $k_L = \omega_L/c$, the distance between the maxima is

$$\Delta\omega_L = \frac{\pi c}{L}. \quad (9.82)$$

This is called the *free spectral range* of the cavity. Expanding the denominator in eq. (9.81) to quadratic order around a resonance, we find

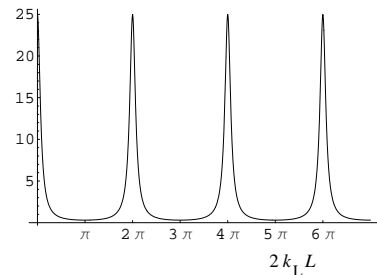


Fig. 9.9 $|E_t|^2$, in units of $(E_0 t_1 t_2)^2$, as a function of $2k_L L$, for $r_1 r_2 = 0.8$.

that the full width of the peaks at half maximum is

$$\delta\omega_L = \frac{c}{L} \frac{1 - r_1 r_2}{\sqrt{r_1 r_2}}. \quad (9.83)$$

The *finesse* \mathcal{F} of the cavity is defined as the ratio of the free spectral range to the full width at half maximum, $\mathcal{F} \equiv \Delta\omega_L/\delta\omega_L$, so

$$\mathcal{F} = \frac{\pi\sqrt{r_1 r_2}}{1 - r_1 r_2}. \quad (9.84)$$

To understand the physical meaning of these results it is useful to compute the *storage time*, i.e. the average time spent by a photon inside the cavity. For simplicity we take $r_2 = 1$, so each photon has an amplitude probability $A(n)$ of making n round trips, and finally comes out from the first mirror. Recall that the number density of photons is proportional to the modulus squared of the electric field, so the factors $-r_1$ and $-r_2$ acquired at the reflections from the mirrors are the quantum-mechanical probability amplitudes, while their squared modulus is a probability. Thus, the amplitude for performing n round-trips and then coming out from the first mirror is given by $A(n) = t_1^2(-1)^n(-r_1)^{n-1} = \text{constant} \times r_1^n$, since each reflection at the far mirror has a probability amplitude -1 and at the first mirror $(-r_1)$. Thus, if a photon enters the cavity, the probability that it comes out after n round-trips is

$$p(n) = \frac{r_1^{2n}}{\sum_{n=1}^{\infty} r_1^{2n}}, \quad (9.85)$$

where the denominator normalizes the total probability to one. The average number of round-trips is therefore

$$\sum_{n=1}^{\infty} n p(n) = \frac{1}{1 - r_1^2}. \quad (9.86)$$

Since each round-trip lasts for a time $2L/c$, the storage time of the cavity, i.e. the average time spent inside by a photon, is

$$\tau_s = \frac{2L}{c} \frac{1}{1 - r_1^2}. \quad (9.87)$$

If r_1 is close to one we can write $1 - r_1^2 = (1 - r_1)(1 + r_1) \simeq 2(1 - r_1)$, and we can express the storage time in terms of the finesse, as

$$\tau_s \simeq \frac{L}{c} \frac{\mathcal{F}}{\pi}. \quad (9.88)$$

We see that, in the limit of high finesse, light is trapped in the FP cavity for a long time. If we illuminate the cavity and then we suddenly shut off the laser at $t = 0$, light will still continue to come out from the cavity for a long time. According to eq. (9.85), the intensity of the light coming out after n round trips is proportional to $r_1^{2n} = \exp\{n \log r_1^2\}$. For r_1 close to one, $\log r_1^2 = \log[1 - (1 - r_1^2)] \simeq -(1 - r_1^2)$. Therefore the

intensity of light decreases with n as $\exp\{-n(1 - r_1^2)\}$. Since the light that performs n round trips comes out at time $t = (2L/c)n$, for r_1 close to one and $r_2 = 1$ the intensity of the reflected light decreases with time as $\exp\{-t(c/2L)(1 - r_1^2)\} = \exp\{-t/\tau_s\}$, with τ_s given in eq. (9.87), confirming the interpretation of τ_s as a storage time.

We consider now the reflected field. We write $E_{\text{refl}} = |E_{\text{refl}}|e^{-i\omega_L t} e^{i\phi}$, and we find from eq. (9.70) that the phase ϕ can be written as $\phi = \phi_1 - \phi_2$, where

$$\tan \phi_1 = -\frac{r_2(1 - p_1) \sin(2k_L L)}{r_1 - r_2(1 - p_1) \cos(2k_L L)}, \quad (9.89)$$

$$\tan \phi_2 = -\frac{r_1 r_2 \sin(2k_L L)}{1 - r_1 r_2 \cos(2k_L L)}. \quad (9.90)$$

A plot of ϕ as a function of $2k_L L$ is shown in Fig. 9.10. Two aspects of this graph are interesting. First, away from the resonances (which, as we have seen, are at $2k_L L = 2\pi n$), ϕ is almost flat as a function of $2k_L L$, and is basically equal to zero (mod 2π). So, here the phase of the reflected light is insensitive to changes in the length L of the cavity or of the frequency of the laser light. However, close to the resonances this dependence suddenly becomes very sharp. Writing $2k_L L = 2\pi n + \epsilon$ and expanding for small ϵ , eqs. (9.89) and (9.90) give (setting for simplicity $r_2 = 1$ and $p_1 = 0$ and neglecting $O(\epsilon^2)$) $\partial\phi/\partial\epsilon = (1 + r_1)/(1 - r_1)$ or, taking r_1 close to one,

$$\frac{\partial\phi}{\partial\epsilon} \simeq \frac{2\mathcal{F}}{\pi}. \quad (9.91)$$

We can compare this with the result (9.2) for one arm of a simple Michelson interferometer which, in the present notation, reads $\phi = \epsilon$. When r_1 is close to one, the sensitivity of a FP cavity to changes in $2k_L L$ is enhanced by the large factor $(2/\pi)\mathcal{F}$, compared to the arm of a Michelson interferometer.

The result for generic values of r_1, r_2 (but still such that $\mathcal{F} \gg 1$) can be conveniently written observing that, for large \mathcal{F} , eq. (9.84) can be inverted to give

$$r_1 r_2 = 1 - \frac{\pi}{\mathcal{F}} + O\left(\frac{\pi^2}{\mathcal{F}^2}\right). \quad (9.92)$$

We define p from

$$(1 - p_1)r_2^2 = (1 - p), \quad (9.93)$$

and we introduce the *coupling rate* σ ,

$$\sigma = \frac{p\mathcal{F}}{\pi}. \quad (9.94)$$

From the condition $r_1^2 = 1 - p_1^2 - t_1^2 < 1 - p_1$ it follows that $r_1^2 r_2^2 < 1 - p$ and for small p (typical values in VIRGO and LIGO are $p \sim 2 \times 10^{-5}$)

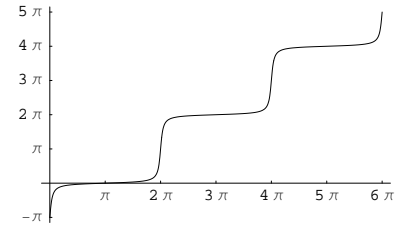


Fig. 9.10 The phase ϕ of the reflected field, as a function of $2k_L L$, setting $r_1 = 0.9$, $r_2 = 1$, $p_1 = 0$. We have defined ϕ so that it is a continuous function of $2k_L L$, rather than reporting it always to the interval $[0, 2\pi]$.

we have $r_1 r_2 < 1 - (p/2)$. Using eq. (9.92) we then obtain

$$1 - \frac{\pi}{\mathcal{F}} < 1 - \frac{p}{2}, \quad (9.95)$$

which, in terms of σ , gives $\sigma < 2$. Since of course $\sigma > 0$, we have

$$0 < \sigma < 2. \quad (9.96)$$

Writing $2k_L L = 2\pi n + \epsilon$ and expanding for small ϵ , eqs. (9.89) and (9.90) become $\tan \phi_1 = (\mathcal{F}\epsilon/\pi)/(1 - \sigma)$ and $\tan \phi_2 = -\mathcal{F}\epsilon/\pi$, so $\phi_2 = -\pi + \arctan(\mathcal{F}\epsilon/\pi)$. For $\phi = \phi_1 - \phi_2$ we get

$$\phi = \pi + \arctan \left[\frac{\mathcal{F}\epsilon}{\pi} \frac{1}{1 - \sigma} \right] + \arctan \left[\frac{\mathcal{F}\epsilon}{\pi} \right]. \quad (9.97)$$

When $\sigma > 1$ this is rewritten more conveniently as

$$\phi = \arctan \left[\frac{\mathcal{F}\epsilon}{\pi} \frac{1}{\sigma - 1} \right] + \arctan \left[\frac{\mathcal{F}\epsilon}{\pi} \right]. \quad (9.98)$$

Observe from eq. (9.70) that, at the resonances, the reflected electric field is

$$E_{\text{refl}} = E_0 e^{-i\omega_L t_0} \frac{r_1 - r_2(1 - p_1)}{1 - r_1 r_2}. \quad (9.99)$$

In particular, if $r_1 = r_2(1 - p_1)$, at resonance there is no reflected light from the cavity. Physically, what happens is that the light that is immediately reflected back interferes destructively with the light that is reflected after one or more round trips in the cavity.¹⁵ This situation is called the *optimal (or critical) cavity coupling*. Of course, it is optimal from the point of view of the transmitted field since, except for the losses, all incident light finally leaks out from the second mirror. For the arms of a GW interferometer, we will see that we are interested in the reflected signal and therefore we do not want this situation. If $r_1 > r_2(1 - p_1)$ the cavity is undercoupled, while for $r_1 < r_2(1 - p_1)$ the cavity is overcoupled. In terms of the coupling rate, using the definition (9.94) and neglecting $O(\pi^2/\mathcal{F}^2)$ in eq. (9.92), we have

$$\frac{r_1 - r_2(1 - p_1)}{1 - r_1 r_2} = \frac{\sigma - 1}{r_2}, \quad (9.100)$$

so optimal coupling corresponds to $\sigma = 1$, while for $0 < \sigma < 1$ the cavity is overcoupled, and for $1 < \sigma < 2$ the cavity is undercoupled. Observe that Fig. 9.10 refers to an overcoupled cavity. For undercoupled cavities, instead, the region where the phase of the reflected field is very sensitive to changes in $2k_L L$ becomes smaller and smaller, and disappears completely when $\sigma \rightarrow 2$. A comparison of ϕ , as a function of ϵ , for $\sigma < 1$ and for $\sigma > 1$ is shown in Fig. 9.11. Clearly, the sensitivity to a change of $2k_L L$ is higher for an overcoupled cavity. For the arms of VIRGO and LIGO, the losses are such that $p \sim 2 \times 10^{-5}$ and the finesse is $\mathcal{F} \simeq 50$ for VIRGO and $\mathcal{F} \simeq 200$ for LIGO, so we have $\sigma \sim 3 \times 10^{-4}$ for VIRGO and $\sigma \sim 10^{-3}$ for LIGO. Therefore these cavities are well overcoupled.

¹⁵This at first sight can be surprising. If for instance $r_1 = 0.99$, almost all the incoming light is reflected back immediately and is not so intuitive that the total reflected field can be zero. What happens is that the small amount of light that enters the cavity eventually builds up a sufficiently strong interior cavity field, and the part of it that finally leaks back from the first mirror has a large enough amplitude, and the appropriate phase, to cancel the promptly reflected field.

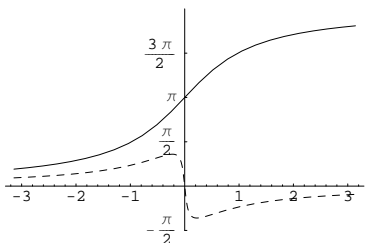


Fig. 9.11 The phase ϕ of the reflected field, as a function of $\epsilon = 2k_L L - 2\pi n$, for an overcoupled cavity with $\sigma = 0.05$ (solid line) and for an undercoupled cavity with $\sigma = 1.05$ (dashed line).

9.2.2 Interaction of a FP cavity with GWs

We have seen that the effective storage time of light, which in the arm of a Michelson interferometer is $2L/c$, becomes $(L/c)\mathcal{F}/\pi$ in a Fabry–Perot cavity, i.e. is enhanced by a factor $\mathcal{F}/(2\pi)$, and the sensitivity to a phase shift is enhanced by a factor $(2/\pi)\mathcal{F}$. Since we finally measure a phase shift, we can expect that the same response to GWs of a Michelson interferometer with arm-length of hundreds of kms, as would be optimal for GWs with frequency $f_{\text{gw}} = O(10^2)$ Hz, should be obtained replacing the arms by Fabry–Perot cavities with a length of a few kms, and a finesse $\mathcal{F} = O(10^2)$. Thus, our next approximation toward a realistic GW interferometer is as in Fig. 9.12. In this section we study the response of a FP interferometer to GWs, and we will see that the above expectation is indeed correct.

We want to compute how the reflected field of a FP cavity is affected by an incoming GW. We consider a FP cavity oriented along the x axis and a GW with only the plus polarization propagating along z , as in eq. (9.6). We begin with a description in the proper detector frame. As we saw in Section 9.1.2, in this frame we can easily obtain the result to lowest order in $\omega_{\text{gw}}L/c$ by making use of the fact that, even in the presence of GWs, light propagates along the geodesics of flat space-time, while the mirrors are shaken by a force exerted by GWs, so that their motion is given in eq. (9.37). Therefore the length L of the cavity changes as

$$\Delta L_x(t) = \frac{Lh_0}{2} \cos \omega_{\text{gw}} t. \quad (9.101)$$

This induces a change $\Delta\phi_x$ in the phase ϕ_x of the field reflected from the cavity along the x arm, which is obtained from eq. (9.91), i.e. from $\Delta\phi_x = (2\mathcal{F}/\pi)\epsilon$, setting $\epsilon = 2k_L\Delta L$,

$$\begin{aligned} \Delta\phi_x &\simeq \frac{4\mathcal{F}}{\pi} k_L \Delta L \\ &= \frac{2\mathcal{F}}{\pi} k_L L h_0 \cos \omega_{\text{gw}} t. \end{aligned} \quad (9.102)$$

The phase shift of a FP cavity along the y arm is obtained reversing the sign of h_0 (see eq. (9.7)), so the total phase shift in the Fabry–Perot interferometer of Fig. 9.12 is $\Delta\phi_{\text{FP}} = \Delta\phi_x - \Delta\phi_y = 2\Delta\phi_x$. We write $\Delta\phi_{\text{FP}}(t) = |\Delta\phi_{\text{FP}}| \cos \omega_{\text{gw}} t$, so

$$|\Delta\phi_{\text{FP}}| = \frac{4\mathcal{F}}{\pi} k_L L h_0. \quad (9.103)$$

This is the change of phase that would be induced in a Michelson interferometer with arm-length $(2/\pi)\mathcal{F}L$. Similar to what happens in a Michelson interferometer, we expect that, when the storage time τ_s given in eq. (9.88) becomes comparable to the period of the GW, the sensitivity degrades because we are summing over contributions with both positive and negative sign, so the above result is really the lowest order in an expansion in $\omega_{\text{gw}}\tau_s$. To compute the result for $\omega_{\text{gw}}\tau_s$ generic, we

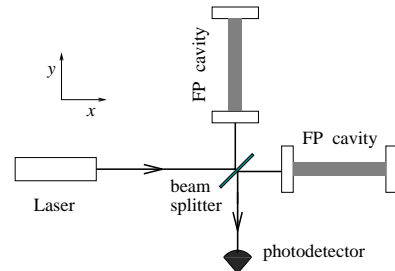


Fig. 9.12 The layout of an interferometer with Fabry–Perot cavities.

already know from our discussion in Section 9.1.2 that we cannot work in the proper detector frame, and we must rather switch to a TT gauge description.

First, it is useful to observe that, for a FP cavity, we can repeat without any modification the derivation done in eq. (9.34) for an arm of a Michelson interferometer, and we again conclude that, if a GW induces a phase shift $\Delta\phi_x(t) = |\Delta\phi_x| \cos \omega_{\text{gw}} t$ in the field reflected from a cavity along the x axis, this produces in the reflected field sidebands with frequencies $\omega_L \pm \omega_{\text{gw}}$ and an amplitude, relative to the carrier, whose modulus is $|\Delta\phi_x|/2$ in each sideband. Thus, to compute the phase shift $|\Delta\phi_x|$ of the reflected field, to all order in $\omega_{\text{gw}}\tau_s$, we can compute in the TT gauge the amplitude of the sidebands of the reflected field. This can be done generalizing the computation of pages 483–485 as follows.

Consider the electric field coming on the first mirror of the cavity from the laser, as in Fig. 9.8. This incoming field is monochromatic, and oscillates as $e^{-i\omega_L t}$. When it enters the cavity and bounces once back and forth, besides acquiring the usual transmission and reflection coefficients, when a GW is present it also acquires a phase modulation, so that when it comes back to the first mirror it consists of the carrier at frequency ω_L plus the two sidebands at $\omega_L \pm \omega_{\text{gw}}$. These three monochromatic fields are partly reflected, with the usual coefficient $-r_1$, and can make one more round trip in the cavity, and so on. So, we need to know how a generic field with carrier plus sidebands is modified by a round trip. We therefore consider a right-moving electromagnetic field which, at the left mirror, has the time-dependence

$$A(t) = A_0 e^{-i\omega_L t} + \frac{1}{2} h_0 A_1 e^{-i(\omega_L - \omega_{\text{gw}})t} + \frac{1}{2} h_0 A_2 e^{-i(\omega_L + \omega_{\text{gw}})t}, \quad (9.104)$$

while we denote by $B(t)$ the right-moving field at the end of the round trip,

$$B(t) = B_0 e^{-i\omega_L t} + \frac{1}{2} h_0 B_1 e^{-i(\omega_L - \omega_{\text{gw}})t} + \frac{1}{2} h_0 B_2 e^{-i(\omega_L + \omega_{\text{gw}})t}. \quad (9.105)$$

If we denote by t the time at which the field terminates its round-trip, the time t_0 at which it started is given by (compare with eq. (9.18))

$$t_0 = t - \frac{2L}{c} - \frac{L}{c} h_0 \cos[\omega_{\text{gw}}(t - L/c)] \operatorname{sinc}(\omega_{\text{gw}}L/c). \quad (9.106)$$

Since during free propagation the phase is unchanged, we must have (apart from the reflection coefficients at the mirrors that we will add separately) $B(t) = A(t_0)$,¹⁶ that is

$$B(t) = A_0 e^{-i\omega_L t_0} + \frac{1}{2} h_0 A_1 e^{-i(\omega_L - \omega_{\text{gw}})t_0} + \frac{1}{2} h_0 A_2 e^{-i(\omega_L + \omega_{\text{gw}})t_0}. \quad (9.107)$$

Using eq. (9.106) and developing to first order in h_0 ,

$$e^{-i\omega_L t_0} = e^{-i\omega_L(t - 2L/c)} \quad (9.108)$$

$$\begin{aligned} &+ \frac{1}{2} h_0 i k_L L \operatorname{sinc}(\omega_{\text{gw}}L/c) e^{i(2\omega_L - \omega_{\text{gw}})L/c} e^{-i(\omega_L - \omega_{\text{gw}})t} \\ &+ \frac{1}{2} h_0 i k_L L \operatorname{sinc}(\omega_{\text{gw}}L/c) e^{i(2\omega_L + \omega_{\text{gw}})L/c} e^{-i(\omega_L + \omega_{\text{gw}})t}. \end{aligned}$$

¹⁶Recall that the superposition of carrier and sidebands given in eqs. (9.104) and (9.105) derives from the expansion of a phase factor, see eqs. (9.24) and (9.34).

Again to order h_0 , we can simply replace the terms $h_0 e^{-i(\omega_L \pm \omega_{gw})t_0}$ in eq. (9.107) by $h_0 e^{-i(\omega_L \pm \omega_{gw})(t - 2L/c)}$. Collecting terms with the same time dependence in eq. (9.107) and comparing with eq. (9.105) we get a matrix relation $B_i = X_{ij} A_j$ (with $i = 0, 1, 2$), where

$$\mathbf{X} = \begin{pmatrix} X_{00} & 0 & 0 \\ X_{10} & X_{11} & 0 \\ X_{20} & 0 & X_{22} \end{pmatrix}. \quad (9.109)$$

The diagonal elements describe the free propagation of the carrier and of the sidebands, while the X_{10} and X_{20} term describe the fact that a round-trip of the carrier produces further contributions to the sidebands. Using eq. (9.108), the explicit expression of the matrix elements is

$$\begin{aligned} X_{00} &= e^{2i\omega_L L/c}, \\ X_{11} &= e^{2i(\omega_L - \omega_{gw})L/c}, \\ X_{22} &= e^{2i(\omega_L + \omega_{gw})L/c}. \\ X_{10} &= ik_L L \operatorname{sinc}(\omega_{gw}L/c) e^{i(2\omega_L - \omega_{gw})L/c}, \\ X_{20} &= ik_L L \operatorname{sinc}(\omega_{gw}L/c) e^{i(2\omega_L + \omega_{gw})L/c}. \end{aligned} \quad (9.110)$$

For a Fabry–Perot cavity along the y axis the same expressions hold, inverting the sign of h_0 (see eq. (9.7)) or, equivalently, inverting the sign of X_{10} and of X_{20} .

This result allows us to generalize eq. (9.80) to the case when GWs are present, simply replacing the factors $e^{2ik_L L}$ with the matrix \mathbf{X} . Thus, we can write the fields $\mathcal{B} = (B_0, B_1, B_2)$ inside the cavity, at $x = 0$, in matrix form as

$$\mathcal{B} = t_1 \mathcal{A}_{\text{in}} + r_1 r_2 \mathbf{X} \mathcal{B}, \quad (9.111)$$

where $\mathcal{A}_{\text{in}} = (E_0, 0, 0)$. The solution is

$$\mathcal{B} = (\mathbf{1} - r_1 r_2 \mathbf{X})^{-1} t_1 \mathcal{A}_{\text{in}}. \quad (9.112)$$

This is the right-moving field at the first mirror (the equivalent of what we denoted by $E_{\text{cav}}(0)$ in the absence of GWs, see Fig. 9.6). The left-moving field ($E'_{\text{cav}}(0)$ in Fig. 9.6) in the absence of GWs is obtained from $E_{\text{cav}}(0)$ using eq. (9.79). In the presence of GWs, we have seen that the factor $e^{2ik_L L}$ is replaced by the matrix \mathbf{X} , acting on the vector space of the amplitude of the carrier and of the sidebands, so the left-moving field is now

$$\mathcal{B}' = -r_2 \mathbf{X} \mathcal{B}, \quad (9.113)$$

and the total reflected field, which includes also the promptly reflected part, is given by

$$\begin{aligned} \mathcal{A}_{\text{refl}} &= r_1 \mathcal{A}_{\text{in}} - t_1 r_2 \mathbf{X} \mathcal{B} \\ &= [r_1 - r_2(1 - p_1)\mathbf{X}] (\mathbf{1} - r_1 r_2 \mathbf{X})^{-1} \mathcal{A}_{\text{in}}, \end{aligned} \quad (9.114)$$

which replaces eq. (9.70). Setting $\mathcal{A}_{\text{in}} = (1, 0, 0)$, we can now compute $\mathcal{A}_{\text{refl}} \equiv (\mathcal{A}_0, \mathcal{A}_1, \mathcal{A}_2)$. According to eq. (9.34), and taking into account

the factor $h_0/2$ in the definition (9.104), the phase shift $|\Delta\phi_x|$ in a single Fabry–Perot cavity along the x axis, is given by

$$\frac{1}{2}|\Delta\phi_x| = \frac{1}{2}h_0 \left| \frac{\mathcal{A}_1}{\mathcal{A}_0} \right|. \quad (9.115)$$

We are interested in particular in the situation when the FP cavity is locked on resonance, so $e^{2ik_L L} = 1$. In this case, with straightforward matrix algebra (easily performed with the help of any symbolic manipulation program) we get

$$\frac{\mathcal{A}_1}{\mathcal{A}_0} = X_{10} e^{2i\omega_{\text{gw}} L/c} \frac{r_2(1-p) - r_1^2 r_2}{(e^{2i\omega_{\text{gw}} L/c} - r_1 r_2)[r_2(1-p) - r_1]}, \quad (9.116)$$

so

$$\begin{aligned} |\Delta\phi_x| &= h_0 k_L L \text{sinc}(\omega_{\text{gw}} L/c) \frac{r_2(1-r_1^2-p)}{[r_2(1-p)-r_1]} \frac{1}{|e^{2i\omega_{\text{gw}} L/c} - r_1 r_2|} \\ &= h_0 k_L L \text{sinc}(\omega_{\text{gw}} L/c) \frac{r_2(1-r_1^2-p)}{[r_2(1-p)-r_1]} \\ &\quad \times \frac{1}{[1+(r_1 r_2)^2 - 2r_1 r_2 \cos(2\omega_{\text{gw}} L/c)]^{1/2}}. \end{aligned} \quad (9.117)$$

If we set $p = 0$ and $r_2 = 1$ (e.g. the present value for VIRGO is $r_2 \simeq 0.99995$) and we take r_1 close to one, the first fraction becomes simply $1+r_1 \simeq 2$. So, we write

$$\frac{r_2(1-r_1^2-p)}{[r_2(1-p)-r_1]} = 2[1+\epsilon(r_1, r_2, p)], \quad (9.118)$$

where, in the typical experimental situation, $\epsilon(r_1, r_2, p) \ll 1$. Then

$$|\Delta\phi_x| = h_0 2k_L L [1+\epsilon(r_1, r_2, p)] \frac{\text{sinc}(\omega_{\text{gw}} L/c)}{[1+(r_1 r_2)^2 - 2r_1 r_2 \cos(2\omega_{\text{gw}} L/c)]^{1/2}}. \quad (9.119)$$

The dependence on $\omega_{\text{gw}} L/c$ can be simplified observing that we want to have $\mathcal{F}L/c$ comparable to the wavelength of the GW, so $\mathcal{F}\omega_{\text{gw}} L/c = O(1)$. However, we achieve this by using a large value of \mathcal{F} , so $\omega_{\text{gw}} L/c$ is much smaller than one in the region where the interferometer operates. For instance, if $f_{\text{gw}} = 100$ Hz and $L = 4$ km, $\omega_{\text{gw}} L/c \sim 10^{-2}$. We can therefore replace $\text{sinc}(\omega_{\text{gw}} L/c) \simeq 1$ in the numerator, and we expand $\cos(2\omega_{\text{gw}} L/c)$ in the denominator. Then we get

$$\begin{aligned} |\Delta\phi_x| &\simeq h_0 2k_L L \frac{1+\epsilon(r_1, r_2, p)}{1-r_1 r_2} \frac{1}{[1+\frac{r_1 r_2}{(1-r_1 r_2)^2} (2\omega_{\text{gw}} L/c)^2]^{1/2}} \\ &\simeq h_0 2k_L L \frac{\mathcal{F}}{\pi} \frac{1}{[1+(4\pi f_{\text{gw}} \tau_s)^2]^{1/2}}, \end{aligned} \quad (9.120)$$

where, in the last line, we wrote the result in terms of the finesse \mathcal{F} , given in eq. (9.84), and of the storage time τ_s of the cavity, given in eq. (9.87), and we neglected in the numerator terms that are small when

$r_2, r_1 \rightarrow 1$. The phase shift of a FP cavity along the y arm is obtained changing the sign of h_0 , so $\Delta\phi_y = -\Delta\phi_x$, and the difference between them is $\Delta\phi_{\text{FP}} = \Delta\phi_x - \Delta\phi_y = 2\Delta\phi_x$.

We rewrite the result introducing the so-called *pole frequency*,

$$f_p \equiv \frac{1}{4\pi\tau_s}, \quad (9.121)$$

or, from eq. (9.88),

$$f_p \simeq \frac{c}{4\mathcal{F}L}. \quad (9.122)$$

For initial LIGO, $L = 4$ km and $\mathcal{F} \simeq 200$ this gives $f_p \simeq 90$ Hz. For VIRGO, $L = 3$ km and $\mathcal{F} \simeq 50$, so $f_p \simeq 500$ Hz. The phase shift in a Fabry–Perot interferometer can then be written as

$$|\Delta\phi_{\text{FP}}| \simeq h_0 \frac{4\mathcal{F}}{\pi} k_L L \frac{1}{\sqrt{1 + (f_{\text{gw}}/f_p)^2}}. \quad (9.123)$$

For $f_{\text{gw}} \ll f_p$ we recover the result found in the proper detector frame, eq. (9.103), as expected.¹⁷ At $f_{\text{gw}} \gg f_p$, eq. (9.123) shows that the sensitivity degrades linearly with f_{gw} . This formula holds as long as $\omega_{\text{gw}}L/c \ll 1$, i.e

$$\begin{aligned} f_{\text{gw}} &\ll \frac{c}{2\pi L} \\ &\simeq 12 \text{ kHz} \left(\frac{4 \text{ km}}{L} \right). \end{aligned} \quad (9.124)$$

Above this frequency the factor $\text{sinc}(\omega_{\text{gw}}L/c)$ in eq. (9.119) can no longer be approximated by one, and cuts the response further, reflecting the fact that in each round-trip the GW changes sign.

In Fig. 9.13 we show the function $1/[1 + (f_{\text{gw}}/f_p)^2]^{1/2}$, and we compare it with the function $|\text{sinc}(f/f_p)|$, which is the corresponding quantity for a Michelson interferometer whose length $L_{\text{Mich}} = (2/\pi)\mathcal{F}L$ is chosen so that, in the limit $f_{\text{gw}} \rightarrow 0$, its response function is the same as a FP cavity of length L and finesse \mathcal{F} .

It is useful to write eq. (9.123) in the form

$$|\Delta\phi_{\text{FP}}| = h_0 T_{\text{FP}}(f), \quad (9.125)$$

where (writing $k_L = 2\pi/\lambda_L$)

$$T_{\text{FP}}(f) \simeq \frac{8\mathcal{F}L}{\lambda_L} \frac{1}{\sqrt{1 + (f_{\text{gw}}/f_p)^2}}, \quad (9.126)$$

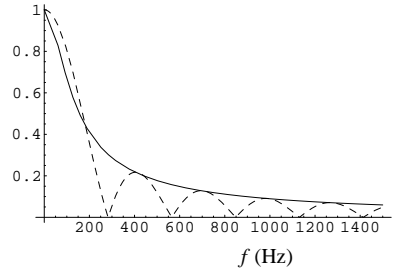


Fig. 9.13 A plot of the function $[1 + (f/f_p)^2]^{-1/2}$, (solid line), compared to the function $|\text{sinc}(f/f_p)|$ (dashed line). We have taken $f_p = 90$ Hz.

¹⁷Recall that eq. (9.91), and therefore eq. (9.103), were obtained in the limit $r_2 = 1$, $p = 0$ and r_1 close to one. If we keep r_1 generic, still setting $r_2 = 1$ and $p = 0$, in eq. (9.91) the overall factor of 2 is replaced by $1 + r_1$, and the same result is obtained from eq. (9.117).

9.2.3 Angular sensitivity and pattern functions

Until now we have restricted ourselves to a GW with plus polarization, propagating along the z axis. We now compute the response of an interferometer to GWs with arbitrary direction and polarization. As discussed in Section 7.2, this is encoded in the pattern functions $F_+(\theta, \phi)$ and $F_\times(\theta, \phi)$. We first consider the limit $\omega_{\text{gw}}L/c \ll 1$. In this case we can use the proper detector frame, so the motion of the mirrors is governed by the geodesic equation,

$$\ddot{\xi}^i = \frac{1}{2}\ddot{h}_{ij}\xi^j. \quad (9.127)$$

For the mirror located at $\xi^j = (L, 0, 0)$, we are interested in its displacement along the x direction, which is given by

$$\ddot{\xi}_x = \frac{1}{2}\ddot{h}_{xx}L. \quad (9.128)$$

This equation governs the change in the length of the x -arm of a Michelson interferometer, as well as the change in the length of a FP cavity lying along the x axis. For the mirror located at $\xi^j = (0, L, 0)$, we are rather interested in its displacement along the y direction, which is given by

$$\ddot{\xi}_y = \frac{1}{2}\ddot{h}_{yy}L. \quad (9.129)$$

The relative phase shift between the x and y arms is therefore driven by $(1/2)(\ddot{h}_{xx} - \ddot{h}_{yy})$. When the wave comes from the z direction we have $h_{xx} = h_+$ and $h_{yy} = -h_+$, so $(1/2)(h_{xx} - h_{yy}) = h_+$, but in the most general situation we must replace h_+ by $(1/2)(h_{xx} - h_{yy})$ in the computations of the phase shift in a Michelson or in a FP interferometer performed in the previous sections. In other words, the detector tensor (defined in eq. (7.1)) for an interferometer with arms along the \hat{x} and \hat{y} directions is

$$D_{ij} = \frac{1}{2}(\hat{x}_i\hat{x}_j - \hat{y}_i\hat{y}_j). \quad (9.130)$$

We compute h_{xx} and h_{yy} in terms of h_+, h_\times for a wave coming from arbitrary direction. The computation is similar to that performed for resonant bars on page 425. The geometry is illustrated in Fig. 9.14: we have a frame (x, y, z) such that the arms of the interferometer are along the x and y axes. We introduce a second reference frame (x', y', z') such that the propagation direction of the GW coincides with the z' axis. With respect to the (x, y, z) frame, the z' axis has polar angles θ and ϕ , defined as in the figure.¹⁸

The polarizations h_+ and h_\times are defined with respect to the (x', y') axes, so in the (x', y', z') frame the GW has the form

$$h'_{ij} = \begin{pmatrix} h_+ & h_\times & 0 \\ h_\times & -h_+ & 0 \\ 0 & 0 & 0 \end{pmatrix}_{ij}. \quad (9.131)$$

¹⁸When comparing with the calculation for resonant bars on page 425, observe that here we define θ as the angle from the z axis, rather than from the x axis.

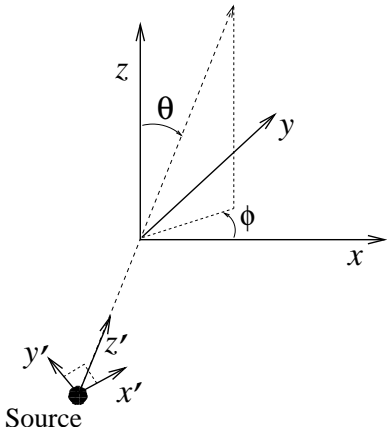


Fig. 9.14 The geometry used in the computation of the pattern functions. The arms of the interferometer are along the x and y axes.

The rotation that brings the (x', y', z') frame onto the (x, y, z) frame is given by a rotation by an angle θ around the y axis followed by a rotation by an angle ϕ around the z axis, i.e.

$$\mathcal{R} = \begin{pmatrix} \cos \phi & \sin \phi & 0 \\ -\sin \phi & \cos \phi & 0 \\ 0 & 0 & 1 \end{pmatrix} \begin{pmatrix} \cos \theta & 0 & \sin \theta \\ 0 & 1 & 0 \\ -\sin \theta & 0 & \cos \theta \end{pmatrix}. \quad (9.132)$$

The GW in the (x, y, z) frame is then given by the transformation law of a tensor with two indices, $h_{ij} = \mathcal{R}_{ik}\mathcal{R}_{jl}h'_{kl}$. From this we obtain

$$h_{xx} = h_+(\cos^2 \theta \cos^2 \phi - \sin^2 \phi) + 2h_\times \cos \theta \sin \phi \cos \phi, \quad (9.133)$$

$$h_{yy} = h_+(\cos^2 \theta \sin^2 \phi - \cos^2 \phi) - 2h_\times \cos \theta \sin \phi \cos \phi, \quad (9.134)$$

so

$$\frac{1}{2}(h_{xx} - h_{yy}) = \frac{1}{2}h_+(1 + \cos^2 \theta) \cos 2\phi + h_\times \cos \theta \sin 2\phi, \quad (9.135)$$

and therefore

$$F_+(\theta, \phi) = \frac{1}{2}(1 + \cos^2 \theta) \cos 2\phi,$$

$$F_\times(\theta, \phi) = \cos \theta \sin 2\phi.$$

(9.136)

We see that GW interferometers have blind directions. For instance, for a GW with plus polarization, the direction with $\phi = \pi/4$ is blind, since $F_+ = 0$. This is due to the fact that this wave produces the same displacement in the x and in the y arm, so the differential phase shift vanishes. If we change the definition of the axes with respect to which the polarizations h_+ and h_\times are defined, rotating them by an angle ϕ in the (x', y') plane, the pattern functions transform as in eq. (7.30).

Equation (9.136) has been obtained in the limit $\omega_{\text{gw}}L/c \ll 1$. To compute the pattern functions for $\omega_{\text{gw}}L/c$ generic we must perform the computation in the TT gauge, so we should repeat the computation leading to eq. (9.15) for a GW coming from arbitrary direction. Consider the arm of a simple Michelson interferometers, with the beam splitter at $x = 0$ and the far mirror at $x = L_x$ (or a FP cavity with mirrors at $x = 0$ and $x = L_x$). Then eq. (9.9) is replaced by

$$L_x = c(t_1 - t_0) - \frac{c}{2} \int_{t_0}^{t_1} dt' h_{xx}(t', \mathbf{x}). \quad (9.137)$$

If we denote by $\hat{\mathbf{n}}$ the propagation direction of the GW, we have $h_{xx}(t) = h_{xx} \cos[\omega_{\text{gw}}(t - \hat{\mathbf{n}} \cdot \mathbf{x}/c)]$, and we must evaluate \mathbf{x} on the trajectory $\mathbf{x}(t)$ of the photon, so along the x arm we have

$$h_{xx}(t) = h_{xx} \cos \left[\omega_{\text{gw}} \left(t - \frac{n_x x(t)}{c} \right) \right], \quad (9.138)$$

which replaces eq. (9.6). To lowest order in h_{xx} the trajectory of a photon is just the unperturbed one, so inside the cosine we can set $x(t) = c(t - t_0)$, while $\hat{\mathbf{n}}$ can be written in terms of the angles θ, ϕ as $\hat{\mathbf{n}} = (\sin \theta \cos \phi, \sin \theta \sin \phi, \cos \theta)$. Therefore, beside the dependence on (θ, ϕ) in h_{xx} and h_{yy} , that we already computed in eqs. (9.133) and (9.134), there is also an angular dependence through the term n_x in eq. (9.138), and a similar term n_y for the y arm. In particular, eq. (9.137) becomes

$$L_x = c(t_1 - t_0) - \frac{c}{2} h_{xx} \int_{t_0}^{t_1} dt' \times \cos [(1 - \sin \theta \cos \phi) \omega_{\text{gw}} t' + \omega_{\text{gw}} t_0 \sin \theta \cos \phi]. \quad (9.139)$$

The return trip can be treated similarly, with the unperturbed photon trajectory given now by $x(t) = L - c(t - t_1)$, so eq. (9.11) is replaced by

$$L_x = c(t_2 - t_1) - \frac{c}{2} h_{xx} \int_{t_1}^{t_2} dt' \times \cos [(1 + \sin \theta \cos \phi) \omega_{\text{gw}} t' - \omega_{\text{gw}} (t_1 + L/c) \sin \theta \cos \phi]. \quad (9.140)$$

Summing the two equations we get

$$t_2 = t_0 + \frac{2L_x}{c} + \frac{1}{2} h_{xx} \int_{t_0}^{t_0+L_x/c} dt' \cos[\omega_- t' + \phi_0] + \frac{1}{2} h_{xx} \int_{t_0+L_x/c}^{t_0+2L_x/c} dt' \cos[\omega_+ t' - \phi_2], \quad (9.141)$$

where we introduced the short-hand notation

$$\omega_{\pm} = \omega_{\text{gw}} (1 \pm \sin \theta \cos \phi), \quad (9.142)$$

$$\phi_0 = \omega_{\text{gw}} t_0 \sin \theta \cos \phi, \quad (9.143)$$

$$\phi_2 = \omega_{\text{gw}} t_2 \sin \theta \cos \phi, \quad (9.144)$$

and in the limits of the integral, as well as in ϕ_2 , we can use $t_1 = t_0 + L_x/c$ and $t_2 = t_0 + 2L_x/c$. For the y arm we have similar expressions, with L_y replacing L_x and $n_y = \sin \theta \sin \phi$ replacing $n_x = \sin \theta \cos \phi$.

It is now in principle straightforward to perform the integrals and compute how $t_2 - t_0$ depends on the propagation direction of the GW. Carrying out the integrals, however, we see that all terms which depend on θ, ϕ are multiplied by the factor $\omega_{\text{gw}} L_x/c$. For instance, θ and ϕ enter in terms such as

$$\text{sinc} \left[\frac{\omega_{\text{gw}} L_x}{2c} (1 \pm \sin \theta \cos \phi) \right]. \quad (9.145)$$

For a FP interferometer we saw that $\omega_{\text{gw}} L_x/c$ is small, typically $O(10^{-2})$ in LIGO and VIRGO, and therefore the function sinc in eq. (9.145) is essentially unity, and its dependence on θ and ϕ is negligible, at least as long as the condition (9.124) is satisfied. Then, we can neglect the dependence on the GW direction in the travel time $t_2 - t_0$ and the only angular dependence comes from h_{xx} and h_{yy} , as computed in eqs. (9.133) and (9.134), so for the pattern function we can use, to a very good approximation, the expressions given in eq. (9.136).

9.3 Toward a real GW interferometer

In this section we discuss a number of issues that are more technical, but are important for understanding how a real interferometer works.

9.3.1 Diffraction and Gaussian beams

Until now we have considered idealized FP cavities with mirrors of infinite transverse extent, so we could neglect any dependence of the electric field on the transverse coordinates. For a cavity along the x axis, we have then treated the interior electric field as a plane wave, with a dependence on x, t of the form $\exp\{-i\omega_L(t \pm x/c)\}$, and no dependence on the transverse coordinates $\mathbf{x}_\perp = (y, z)$. Of course, in practice the mirrors have a finite extent, and the beam has a profile in the transverse direction.

A beam of finite transverse extent is subject to diffraction. If, at some point in space, a photon of wavelength λ_L (and therefore longitudinal momentum $p = \hbar/\lambda_L$) is localized within a transverse width $\Delta\mathbf{x}_\perp = a$, by the Heisenberg principle it has an uncertainty on the transverse momentum $\Delta p_\perp \sim \hbar/a$, so the beam will widen, filling a cone of angle $\Delta\theta = \Delta p_\perp/p \sim \lambda_L/a$. After traveling a longitudinal distance x the beam has become larger, in the transverse direction, by $x\Delta\theta \sim x\lambda_L/a$. As long as $x\lambda_L/a \ll a$ we are in the regime of *Fresnel diffraction*, and the broadening of the beam is negligible. When $x\lambda_L/a \gg a$, or, in terms of $k_L = 1/\lambda_L$,

$$x \gg k_L a^2, \quad (9.146)$$

we are in the regime of *Fraunhofer diffraction*, and the beam has become much broader than its original size. For interferometers such as LIGO and VIRGO, the wavelength of the laser is typically

$$\lambda_L \simeq 1 \mu m. \quad (9.147)$$

The border between these regimes is at $a = (x\lambda)^{1/2}$ which, for $x = 4$ km and $\lambda_L = 1 \mu m$, gives $a \simeq 2.5$ cm. This means that, for a laser beam whose initial width is smaller than 2.5 cm, the broadening of the beam becomes important already after a single one-way trip through the cavity. Furthermore for cavities with a finesse $O(100)$, as we need for GW detection, the beam is supposed to perform $O(100)$ round trips and, if the mirrors were flat, at each one-way trip the beam would widen further, as illustrated in Fig. 9.15, and would be finally dispersed on a region of transverse size larger than the mirrors.

Thus, it is clear that diffraction effects are important, and the naive scheme of a narrow beam (as typically obtained from a laser) bouncing between two flat mirrors cannot work. As a first step, we must understand in more detail the propagation of a beam of finite transverse extent over large distances. The tool that we need is the *paraxial propagator*, that we introduce in the next subsection.

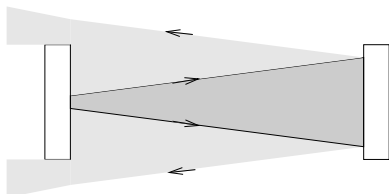


Fig. 9.15 The widening of a beam due to diffraction as it bounces between two flat mirrors.

The paraxial propagator

A given spatial component of the electric field, propagating in the vacuum, obeys the equation

$$\left[-\frac{1}{c^2} \frac{\partial^2}{\partial t^2} + \nabla^2 \right] E(t, \mathbf{x}) = 0. \quad (9.148)$$

We take a single monochromatic component, which we write in complex notation as $E(t, \mathbf{x}) = E(\mathbf{x})e^{-i\omega_L t}$, so $E(\mathbf{x})$ satisfies

$$[\nabla^2 + k_L^2] E(\mathbf{x}) = 0. \quad (9.149)$$

We want to compute the propagation across a long distance in the x direction, so x is the longitudinal coordinate and $\mathbf{x}_\perp = (y, z)$ are the transverse coordinate, and we search for solutions of the form

$$E(\mathbf{x}) = \mathcal{E}(x; y, z) e^{ik_L x}, \quad (9.150)$$

where $\mathcal{E}(x; y, z)$ is a slowly varying function of x , in the sense that

$$|\partial_x \mathcal{E}| \ll k_L |\mathcal{E}|. \quad (9.151)$$

Therefore $E(t, \mathbf{x}) = \mathcal{E}(x; y, z) \exp\{-i\omega_L t + ik_L x\}$ is in a first approximation a plane wave, with a slower dependence on x , which manifests itself only on scales $x \gg \lambda_L$. Plugging the ansatz (9.150) into eq. (9.149) we get

$$\nabla_\perp^2 \mathcal{E} + 2ik_L \partial_x \mathcal{E} + \partial_x^2 \mathcal{E} = 0, \quad (9.152)$$

where $\nabla_\perp^2 = \partial_y^2 + \partial_z^2$. Because of the condition (9.151), we can neglect $\partial_x^2 \mathcal{E}$ with respect to $k_L \partial_x \mathcal{E}$, so in this approximation we write

$$\nabla_\perp^2 \mathcal{E} + 2ik_L \partial_x \mathcal{E} = 0. \quad (9.153)$$

We now perform the Fourier transform with respect to the transverse variables,

$$\mathcal{E}(x; y, z) = \int \frac{dp_y}{2\pi} \frac{dp_z}{2\pi} \tilde{\mathcal{E}}(x; p_y, p_z) e^{ip_y y + ip_z z}. \quad (9.154)$$

In terms of $\tilde{\mathcal{E}}(x; p_y, p_z)$, eq. (9.153) reads

$$-(p_y^2 + p_z^2) \tilde{\mathcal{E}}(x; p_y, p_z) + 2ik_L \partial_x \tilde{\mathcal{E}}(x; p_y, p_z) = 0. \quad (9.155)$$

The x dependence can be integrated, and we get

$$\tilde{\mathcal{E}}(x; p_y, p_z) = \tilde{\mathcal{E}}(x = 0; p_y, p_z) \exp \left\{ -i \frac{p_y^2 + p_z^2}{2k_L} x \right\}. \quad (9.156)$$

Then eq. (9.154) becomes

$$\mathcal{E}(x; y, z) = \int \frac{dp_y}{2\pi} \frac{dp_z}{2\pi} \tilde{\mathcal{E}}(x = 0; p_y, p_z) e^{ip_y y + ip_z z - i \frac{p_y^2 + p_z^2}{2k_L} x}$$

$$\begin{aligned}
&= \int \frac{dp_y}{2\pi} \frac{dp_z}{2\pi} \left[\int dy' dz' \tilde{\mathcal{E}}(x=0; y', z') e^{-ip_y y' + ip_z z'} \right] \\
&\quad \times e^{ip_y y + ip_z z - i \frac{p_y^2 + p_z^2}{2k_L} x} \\
&= \int dy' dz' \tilde{\mathcal{E}}(x=0; y', z') \\
&\quad \times \int \frac{dp_y}{2\pi} \frac{dp_z}{2\pi} e^{ip_y(y-y') + ip_z(z-z') - i \frac{p_y^2 + p_z^2}{2k_L} x}. \tag{9.157}
\end{aligned}$$

The integrals over dp_y and dp_z are Fresnel integrals, that we already met in eq. (4.365), so we finally get

$$\mathcal{E}(x; y, z) = \int dy' dz' G(x; y - y', z - z') \tilde{\mathcal{E}}(x=0; y', z'), \tag{9.158}$$

where

$$G(x; y - y', z - z') = \frac{-ik_L}{2\pi x} \exp \left\{ i \frac{k_L}{2x} [(y - y')^2 + (z - z')^2] \right\} \tag{9.159}$$

is called the paraxial propagator. Equations (9.158) and (9.159) allow us to compute the field at x generic, once we have its value on a transverse surface $x = 0$.

Fraunhofer diffraction

As a first application, we consider a plane wave of infinite transverse extent that arrives on an aperture S on a plane opaque screen and we compute the image on another screen at a large distance x , and at transverse coordinates (y, z) , see Fig. 9.16. Then, at $x = 0$, we have $\tilde{\mathcal{E}}(x = 0; y', z') = \tilde{\mathcal{E}}_0$ if (y', z') are inside the aperture S , and zero otherwise, so

$$\begin{aligned}
E(x, y, z) &= \frac{-ik_L}{2\pi x} \tilde{\mathcal{E}}_0 e^{ik_L x} \int_S dy' dz' \exp \left\{ i \frac{k_L}{2x} [(y - y')^2 + (z - z')^2] \right\} \\
&= \frac{-ik_L}{2\pi x} \tilde{\mathcal{E}}_0 \exp \left\{ ik_L \left[x + \frac{y^2 + z^2}{2x} \right] \right\} \\
&\quad \times \int_S dy' dz' \exp \left\{ -i \frac{k_L}{x} (yy' + zz') + i \frac{k_L}{x} (y'^2 + z'^2) \right\}. \tag{9.160}
\end{aligned}$$

Fraunhofer diffraction is defined by the condition (9.146), where a is the size of the aperture. In this limit, we can neglect the term $k_L(y'^2 + z'^2)/x$ in the exponential. Furthermore we observe that, if $y^2 + z^2 \ll x^2$, the term $x + (y^2 + z^2)/2x$ in the first exponential is just the first-order

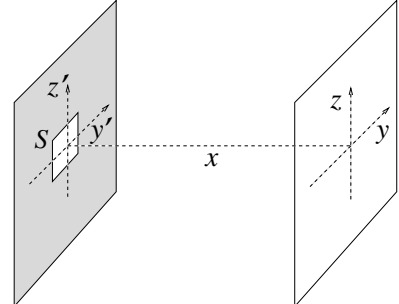


Fig. 9.16 An aperture S on a opaque screen. The plane of the opaque screen is parametrized by coordinates (y', z') . The image is observed on a screen at a distance x , parametrized by coordinates (y, z) .

expansion of the distance $r = (x^2 + y^2 + z^2)^{1/2}$ from the observation point to the center of the aperture, since

$$(x^2 + y^2 + z^2)^{1/2} = x \left(1 + \frac{y^2 + z^2}{x^2} \right)^{1/2} \simeq x \left(1 + \frac{y^2 + z^2}{2x^2} \right). \quad (9.161)$$

Similarly, to lowest order we can replace $1/x$ with $1/r$ in eq. (9.160). Then we get the well-known formula for the Fraunhofer diffraction by an aperture,

$$E(x, y, z) = \frac{-i\tilde{\mathcal{E}}_0 k_L}{2\pi} \frac{e^{ik_L r}}{r} \int_S dy' dz' e^{-ik_L(y'y' + zz')/r}. \quad (9.162)$$

Consider for example a circular aperture of radius a . In this case the integral can be performed exactly in terms of the Bessel function J_1 . Writing $y = \rho \cos \varphi$, $z = \rho \sin \varphi$, and similarly $y' = \rho' \cos \varphi'$, $z' = \rho' \sin \varphi'$, we get

$$\begin{aligned} \int_S dy' dz' e^{-ik_L(y'y' + zz')/r} &= \int_0^a \rho' d\rho' \int_0^{2\pi} d\varphi' e^{-i(k_L/r)\rho\rho' \cos(\varphi-\varphi')} \\ &= 2\pi \int_0^a \rho' d\rho' J_0(k_L \rho \rho' / r) \\ &= \frac{2\pi a r}{k_L \rho} J_1(k_L \rho a / r). \end{aligned} \quad (9.163)$$

Writing $\rho/r = \sin \theta$ and recalling that $\lim_{u \rightarrow 0} J_1(u)/u = 1/2$, we see that the intensity of light, which is proportional to the squared modulus of the electric field, is distributed in the scattering angle θ as¹⁹

$$I(\theta) = I(0) \left[\frac{2J_1(k_L a \sin \theta)}{k_L a \sin \theta} \right]^2, \quad (9.164)$$

A plot of the function $2J_1(x)/x$ is shown in Fig. 9.17. $I(\theta)$ has its first zero at $k_L a \sin \theta \simeq 3.8$. Taking this as an estimate of the angular width $\Delta\theta$ of the beam we get (for $\lambda \ll a$) $\Delta\theta \simeq 3.8\lambda/a$, which is consistent with the uncertainty principle bound, but does not saturate it.

Propagation of Gaussian beams

Consider now a beam that, at $x = 0$, has a Gaussian profile in the transverse direction,

$$\mathcal{E}(x = 0; y, z) = \mathcal{E}_0 e^{-(y^2 + z^2)/w_0^2}. \quad (9.165)$$

Its profile at x generic can be computed by inserting this initial value into eqs. (9.158) and (9.159). The resulting integrals can be computed exactly, without resorting to the Fraunhofer approximation, using

$$\int_{-\infty}^{\infty} e^{-(1+ia^2)y^2} = \frac{\sqrt{\pi}}{(1+a^2)^{1/4}} \exp \left\{ -\frac{i}{2} \arctan a \right\}, \quad (9.166)$$

¹⁹This result was first derived by Airy in the 19th century, and this intensity distribution is known as the Airy pattern.

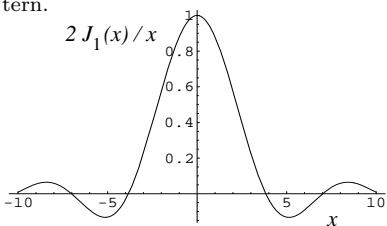


Fig. 9.17 The function $2J_1(x)/x$.

where a is a real constant. The result, written in terms of $E(x, y, z) = e^{ik_L x} \mathcal{E}(x; y, z)$, is

$$\boxed{E(x, y, z) = \frac{\mathcal{E}_0}{\sqrt{1 + x^2/b^2}} e^{-(y^2+z^2)/w^2(x)} \times \exp \left\{ ik_L \left[x + \frac{y^2+z^2}{2R(x)} \right] - i \arctan(x/b) \right\}, \quad (9.167)}$$

where the *Rayleigh range* b is defined by

$$b = \frac{1}{2} k_L w_0^2, \quad (9.168)$$

the width $w(x)$ is given by

$$w(x) = w_0 \sqrt{1 + x^2/b^2}, \quad (9.169)$$

and the curvature radius $R(x)$ is

$$R(x) = x + \frac{b^2}{x}. \quad (9.170)$$

This shows that a beam which at $x = 0$ has a Gaussian profile, remains Gaussian at all x , with a x -dependent width given by eq. (9.169). Observe that, since w_0 is the initial transverse size, b given in eq. (9.168) is the parameter that separates the Fresnel regime (at $x \ll b$) from the Fraunhofer regime (at $x \gg b$), compare with eq. (9.146). In agreement with the discussion above eq. (9.146), at $|x| \ll b$ we find that there is no appreciable widening of the beam, while at $|x| \gg b$ the width increases linearly, $w(x) \simeq w_0|x|/b$, as demanded by the uncertainty principle. Using the definition (9.168) of the Rayleigh range b , we get

$$w(x) \simeq \frac{|x|\lambda_L}{\pi w_0}, \quad (|x| \gg b). \quad (9.171)$$

Actually Gaussian beams saturate the uncertainty principle, i.e. they have the minimum possible spreading.

The term $\arctan(x/b)$ in eq. (9.167) is called the Gouy phase, and is an extra phase factor compared to the plane wave propagation. The surfaces of constant phase are obtained requiring that

$$k_L \left[x + \frac{y^2+z^2}{2R(x)} \right] - \arctan(x/b)$$

be constant. For a typical GW interferometer, with $\lambda_L = 1 \mu\text{m}$ and w_0 of order of a few cm, b is of order of several hundred meters. Thus, if we want to compute the surfaces of constant phase in a region close to a point on the optical axis, i.e. in a region with coordinates $(x = x_0 + \delta x, y = \delta y, z = \delta z)$, with $\delta x, \delta y, \delta z$ of the order of a few cm, we can

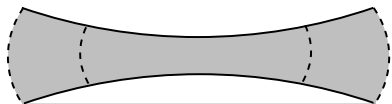


Fig. 9.18 A surface of constant intensity of the Gaussian beam (solid line) and surfaces of constant phase (dashed lines).

neglect the variation of $R(x)$ and of the Gouy phase, so at a given x_0 we simply have the condition

$$\delta x + \frac{\delta y^2 + \delta z^2}{2R(x_0)} = \text{constant}. \quad (9.172)$$

²⁰The solution (9.167) holds also at $x < 0$; in this case both the term $k_L x$ and $R(x)$ in the exponential change sign, and the radius of curvature is as shown in the figure.

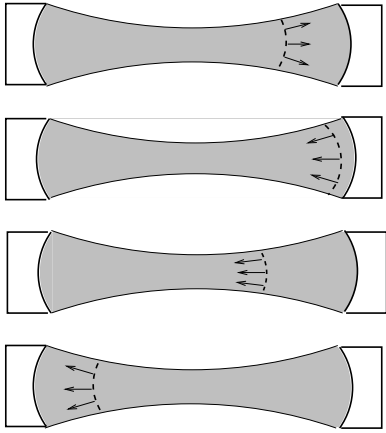


Fig. 9.19 A wavefront (dashed lines) that propagates toward a spherical mirror is reflected back and focused toward the waist. After passing the waist it expands again toward the other mirror.

This equation describes a portion of spherical surface with radius $R(x_0)$, as we can check immediately by expanding the equation $x^2 + y^2 + z^2 = R^2$ around $x = R + \delta x, y = \delta y, z = \delta z$. Therefore the wavefronts of a Gaussian beam are spherical to an excellent approximation (as long as the transverse distances are much smaller than $b = O(10^2)$ m), and $R(x)$ is their curvature radius. The shape of the beam is therefore as shown in Fig. 9.18.²⁰ The characteristic length w_0 , which determines the transverse size at $x = 0$, is called the *waist* of the beam.

When the beam bounces many times between two mirrors, we want to avoid that at each trip it widens further, as in Fig. 9.15. This can be obtained shaping the mirrors so that their surfaces match exactly surfaces of constant phase of the beam. For Gaussian beams we have seen that the wavefronts are spherical, so we must use spherical mirrors. When the expanding wavefront of a Gaussian beam reaches a spherical mirror located at a position x_0 and with radius of curvature $R(x_0)$, its direction of propagation is reversed, and the beam is focused back and converges toward the waist at $x = 0$, before re-expanding again for $x < 0$. If we have another spherical mirror at $x = -x_0$ the beam bounces back and forth between them, and at each reflection its wavefronts are forced to converge back toward the waist, as shown in Fig. 9.19, so the beam does not increment its transverse size at each bounce.

Gaussian beams have two advantages over other shapes. First, they have the minimum spreading compatible with the uncertainty principle. Second, their wavefronts are spherical, and mirrors with a spherical shape are easy to manufacture. For these reasons, they are the choice used in present GW interferometers. Thus, we can replace the scheme given in Fig. 9.12 with the more realistic scheme of Fig. 9.20. Alternatively, rather than using two spherical mirrors with the waist in the middle of the cavity, we can put a flat mirror in the position of the waist and, at a distance L , a spherical mirror with curvature radius $R = L + b^2/L$. Presently, the former option is used in LIGO and the latter in VIRGO. With the waist of the beam chosen in the middle of the cavity, the value of $w(x)$ at the position of the mirrors $x = \pm L/2$ is given by

$$w^2(\pm L/2) = w_0^2 + \frac{\chi_L^2 L^2}{w_0^2}. \quad (9.173)$$

In order to be able to use mirrors of manageable size, we want to have $w(\pm L/2)$ small. Minimizing eq. (9.173) with respect to w_0 we find the optimal value of the waist,

$$w_0^{\text{optimal}} = (\chi_L L)^{1/2}. \quad (9.174)$$

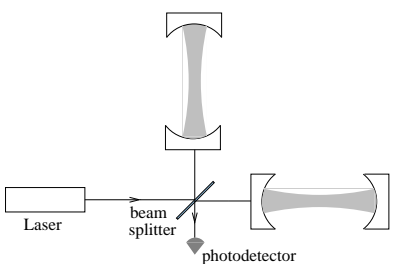


Fig. 9.20 The scheme of an interferometer with Fabry-Perot cavities, with Gaussian beams and spherical mirrors.

For arms of length $L = 4$ km and a wavelength of the laser light $\lambda_L \simeq 1.0 \mu\text{m}$ this gives $w_0 \simeq 2.5$ cm, to which corresponds a value $w(L/2) = (2\bar{\chi}_L L)^{1/2} \simeq 3.6$ cm. A suitable mirror radius for such a beam can therefore be $O(10)$ cm.²¹ Observe that, since the waist w_0 is much larger than the wavelength $\bar{\chi}_L$, the paraxial approximation that we have used is well justified.

The Gaussian beams that we have considered are by definition solutions of the paraxial evolution equation (9.153), since we obtained them evolving an initial condition on the surface $x = 0$ with the paraxial propagator. Of course, we can also verify this by direct substitution in the equation. Actually, the Gaussian beam is just one of many possible solutions. As can be checked by direct substitution into eq. (9.153), there is a complete orthonormal set of solutions called the *Hermite–Gauss modes*, given by

$$\begin{aligned} u_{mn}(x, y, z) &= \frac{c_{mn}}{\sqrt{1+x^2/b^2}} e^{-(y^2+z^2)/w^2(x)} H_m \left(\frac{y\sqrt{2}}{w(x)} \right) H_n \left(\frac{z\sqrt{2}}{w(x)} \right) \\ &\times \exp \left\{ ik_L \left[x + \frac{y^2+z^2}{2R(x)} \right] - i(m+n+1) \arctan(x/b) \right\}, \end{aligned} \quad (9.175)$$

where c_{mn} are normalization constants and $H_n(\xi)$ are the Hermite polynomials, defined by

$$H_n(\xi) = e^{\xi^2} \left(-\frac{d}{d\xi} \right)^n e^{-\xi^2}. \quad (9.176)$$

In particular, $H_0(\xi) = 1$, $H_1(\xi) = 2\xi$, and $H_2(\xi) = 4\xi^2 - 2$. For these modes, both the electric and magnetic fields are transverse to the propagation direction, just as plane wave in free space, so they are also denoted as TEM_{mn} modes. Comparing with eq. (9.167) we see that the Gaussian beam is just the mode TEM_{00} . In Figs. 9.21–9.23 we show the intensity $|u_{mn}|^2$ of the modes TEM_{00} , TEM_{01} and TEM_{11} . Alternatively, one can use as a basis the so-called Laguerre–Gauss modes LG_{mn} , which are written in terms of Laguerre polynomials. The fundamental mode LG_{00} is again the Gaussian beam.

Since the Gouy phase for the mode TEM_{mn} is $(m+n+1) \arctan(x/b)$, see eq. (9.175), the resonance condition in a FP cavity depends on (m, n) . The laser emits predominantly in the TEM_{00} mode, with a contamination typically less than 10% from higher modes (mostly TEM_{01} and TEM_{10}). To eliminate these residual higher modes, which would not be resonant and would just produce noise, before sending it to the beam splitter the laser beam is sent into a Fabry–Perot cavity operated in transmission, called the *mode-cleaner*. Since the Gouy phase for the mode TEM_{mn} depends on (m, n) , we can choose the length of the mode cleaner so that only the $(0, 0)$ mode is in resonance and is efficiently transmitted.

²¹A small spot allows us to keep down the mirror size. However, it also results in large intensity gradients, in region of high intensity of the electromagnetic field, inducing thermal deformations of the mirrors that must be compensated. An alternative possibility, that has been studied for advanced interferometers, is the use of so-called “mesa beams”, i.e. beams with a flat profile, which average more effectively over these thermoelastic fluctuations, see Bondarescu and Thorne (2006).

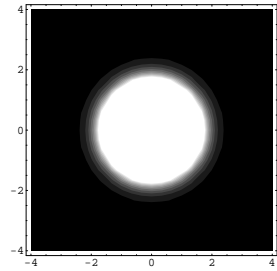


Fig. 9.21 The intensity of the mode TEM_{00} as a function of the transverse variables (y, z) , at a given x . (in units such that $w(x) = \sqrt{2}$).

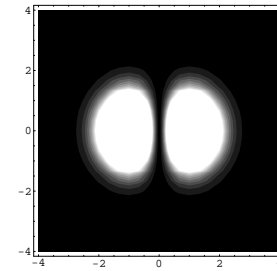


Fig. 9.22 The same as Fig. 9.21, for the mode TEM_{01} .

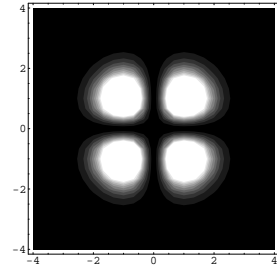


Fig. 9.23 The same as Fig. 9.21, for the mode TEM_{11} .

9.3.2 Detection at the dark fringe

Michelson interferometer

We have seen that the passage of a GW in an interferometer, whether of the simple Michelson type or with Fabry–Perot cavities in the arms, produces a phase shift $\Delta\phi_{\text{gw}}(t)$. We now ask how to extract this phase from the output of the detector. The issue, as we will discuss in this section, is quite non-trivial. The origin of the problem can be seen as follows. We consider first for simplicity a Michelson interferometer. We saw in eq. (9.32) that the power at its output is given by $P(\phi) = P_0 \sin^2 \phi$ where $\phi = \phi_0 + \Delta\phi_{\text{gw}}(t)$, and ϕ_0 is a phase that can be adjusted at will by the experimenter. A plot of $P(\phi)/P_0$ is shown in Fig. 9.24. Naively, one might think from this figure that the best working point for the interferometer is at $\phi_0 = \pi/4$, since there the derivative $\partial P/\partial\phi_0$ is maximum, and the sensitivity to a small displacement $\phi_0 \rightarrow \phi_0 + \Delta\phi_{\text{gw}}(t)$ due to the passage of a GW is highest. Unfortunately, such a strategy would be doomed to failure. In fact, at this working point we are also very sensitive to fluctuations in the power P_0 of the laser. Since all that we measure is the power $P = P_0 \sin^2 \phi$ at the photodetector, it is impossible to tell whether a given variation in the measured power is due a variation $\phi_0 \rightarrow \phi_0 + \Delta\phi_{\text{gw}}(t)$ induced by the passage of a GW, or to a variation $P_0 \rightarrow P_0 + \Delta P_0(t)$ due to a fluctuation in the laser power. In particular, a GW with frequency $f_{\text{gw}} = O(10^2–10^3)$ Hz induces variations in the power P with a frequency $f = 2f_{\text{gw}}$, which therefore must be compared with the power fluctuations of the laser in the same frequency range. With present lasers, the latter turns out to be much larger than the signal that we expect from GWs.

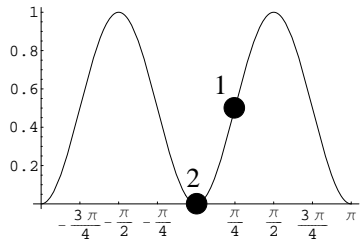


Fig. 9.24 The power $P(\phi)/P_0$. The naive working point is marked as 1, and the dark fringe as 2.

From a more general point of view, whenever we are looking for very small effects a sound experimental strategy is to build a *null instrument*, that is an instrument that, when the signal is absent, records a zero output. This makes the instrument insensitive to calibration uncertainties that would otherwise overwhelm the tiny signal that we are searching. A prototype of a null instrument is the Dicke radiometer that we discussed in Note 74 on page 412. At the naive operation point marked as 1 in Fig. 9.24, the interferometer is not a null instrument. Even in the absence of a GW, the photodetector measures a large power. In this state, small variations in the power due to GWs should be read against this large DC contribution, and would be overwhelmed by its fluctuations.

This suggests that the best working point should be the dark fringe, marked as the point 2 in Fig. 9.24. There the output in the absence of GWs is zero, and we are insensitive to fluctuations in the laser power. Unfortunately, at the dark fringe not only $P = 0$, but even $\partial P/\partial\phi = 0$. Since $\Delta\phi_{\text{gw}} = O(h)$, this means that at the dark fringe the change in the output power induced by GWs is $\Delta P = O(h^2)$. Given that we expect GWs with amplitude h at most $O(10^{-21})$, an effect quadratic in h is of course invisible. So, apparently the choice is between operation points where the response of the interferometer is linear in h , but we have a large DC contribution whose fluctuations overwhelm the signal, and an

operation point where we have no DC contribution, but no sensitivity to GWs either.

There is however a very elegant way out of this dilemma. The idea is to apply a *phase modulation* to the input laser light.²² This can be obtained by passing the incident beam through a Pockels cell, which is a crystal or a block of dielectric material whose index of refraction depends on an applied electric field, $E_{\text{appl}} = |E_{\text{appl}}| \cos \Omega_{\text{mod}} t$. The speed of the response that can be obtained with appropriate materials is quite high, and the index of refraction oscillates with the frequency $f_{\text{mod}} = \Omega_{\text{mod}}/(2\pi)$, for values of f_{mod} up to tens of MHz. Passing through a material with a time-varying index of refraction, the laser beam acquires a time-varying phase, so the beam which reaches the beam-splitter has the form

$$E_{\text{in}} = E_0 e^{-i(\omega_L t + \Gamma \sin \Omega_{\text{mod}} t)}, \quad (9.177)$$

where Γ is called the modulation index, or the modulation depth. This expression can be expanded in Fourier modes as

$$E_{\text{in}} = E_0 [J_0(\Gamma) e^{-i\omega_L t} + J_1(\Gamma) e^{-i(\omega_L + \Omega_{\text{mod}})t} - J_1(\Gamma) e^{-i(\omega_L - \Omega_{\text{mod}})t} + \dots], \quad (9.178)$$

where J_n are Bessel functions and the dots denote terms with frequencies $\omega_L \pm n\Omega_{\text{mod}}$, with $n = 2, 3, \dots$. For $\Gamma \ll 1$ this expression can be simplified using $J_0(\Gamma) \simeq 1 - (\Gamma^2/4)$ and $J_1(\Gamma) \simeq \Gamma/2$. (In the limit $\Gamma \ll 1$ this expansion is obtained more simply expanding directly eq. (9.177) in powers of Γ). Therefore, the effect of the phase modulation is to generate sidebands.²³ For small Γ , higher sidebands are suppressed by higher powers of Γ , so we will limit ourselves to the carrier, which has frequency ω_L and wavenumber $k_L = \omega_L/c$, and to the first two sidebands, with frequencies

$$\omega_{\pm} = \omega_L \pm \Omega_{\text{mod}}, \quad (9.179)$$

and wavenumbers

$$k_{\pm} = \frac{\omega_{\pm}}{c} = 2\pi \left(\frac{1}{\lambda_L} \pm \frac{1}{\lambda_{\text{mod}}} \right). \quad (9.180)$$

Consider now what happens to the carrier and to the sidebands in a Michelson interferometer with arms of length L_x and L_y . For the carrier the incoming electric field has amplitude $E_0 J_0(\Gamma)$ so, from the discussion in Section 9.1, the electric field at the output of the interferometer is

$$(E_{\text{out}})_c = \frac{1}{2} (r_1 e^{2ik_L L_x} - r_2 e^{2ik_L L_y}) E_0 J_0(\Gamma) e^{-i\omega_L t}, \quad (9.181)$$

where r_1, r_2 are the reflectivities of the two end-mirrors. Taking perfectly reflecting mirrors, $r_1 = r_2 = -1$, we have

$$\begin{aligned} (E_{\text{out}})_c &= -i E_0 J_0(\Gamma) e^{-i\omega_L t + ik_L(L_x + L_y)} \sin[k_L(L_x - L_y)] \quad (9.182) \\ &= -i E_0 J_0(\Gamma) e^{-i\omega_L t + ik_L(L_x + L_y)} \sin \left[2\pi \frac{L_x - L_y}{\lambda_L} \right], \end{aligned}$$

²²Another possible solution would be to control so well the laser fluctuations, that a detection scheme of the type discussed above becomes possible (typically at a working point which is slightly displaced from the dark fringe). This solution is under investigation for Advanced LIGO.

²³For $\lambda_L = 1 \mu\text{m}$ we have $\omega_L/(2\pi) \simeq 300 \text{ THz}$, while typically $\Omega_{\text{mod}}/(2\pi) \simeq 30 \text{ MHz}$, so $\Omega_{\text{mod}} \ll \omega_L$.

compare with eq. (9.4). For the sidebands the calculation is the same, but of course now k_L is replaced by k_{\pm} and ω_L by ω_{\pm} , and the amplitude of the incident field is $\pm J_1(\Gamma)E_0$. Thus, writing $L_x - L_y = \Delta L$, the electric field of the sidebands at the output is

$$\begin{aligned}(E_{\text{out}})_{\pm} &= \mp iE_0J_1(\Gamma)e^{-i\omega_{\pm}t+ik_{\pm}(L_x+L_y)}\sin(k_{\pm}\Delta L) \\ &= \mp iE_0J_1(\Gamma)e^{-i\omega_{\pm}t+ik_{\pm}(L_x+L_y)}\sin\left[2\pi\left(\frac{\Delta L}{\lambda_L} \pm \frac{\Delta L}{\lambda_{\text{mod}}}\right)\right].\end{aligned}\quad (9.183)$$

Now comes the crucial point. If we take $L_x = L_y$, both the carrier and the sidebands are on the dark fringe, $(E_{\text{out}})_c = (E_{\text{out}})_{\pm} = 0$. However, instead of choosing $L_x = L_y$, we can set $L_x - L_y$ equal to an integer number of laser wavelengths, i.e. $\Delta L = n\lambda_L$. Then, as far as the carrier is concerned, we are still on the dark fringe, while the sidebands are no longer on the dark fringe. Rather,

$$(E_{\text{out}})_{\pm} = -iE_0J_1(\Gamma)e^{-i\omega_{\pm}t+ik_{\pm}(L_x+L_y)}\sin(2\pi\Delta L/\lambda_{\text{mod}}).\quad (9.184)$$

This choice of asymmetric arms is called the *Schnupp asymmetry*. Consider now what happens when a GW arrives, taking for simplicity a plus polarization with optimal direction, and $\omega_{\text{gw}}L/c \ll 1$. Then eq. (9.31) gives $L_x \rightarrow L_x + hL_x/2$ and $L_y \rightarrow L_y - hL_y/2$, so

$$(L_x - L_y) \rightarrow (L_x - L_y) + Lh(t),\quad (9.185)$$

where $L = (L_x + L_y)/2$ and, to lowest order in $\omega_{\text{gw}}L/c$, we could replace $h(t - L_x/c)$ and $h(t - L_y/c)$ by $h(t)$. Then we see from eq. (9.182) that the electric field of the carrier is shifted from the value $(E_{\text{out}})_c = 0$ on the dark fringe to the value

$$(E_{\text{out}})_c = -iE_0J_0(\Gamma)e^{-i\omega_L t+2ik_L L}k_L Lh(t).\quad (9.186)$$

This is linear in h and, if this were the total electric field, the power $|(E_{\text{out}})_c|^2$ would be quadratic in h , as we saw above. However, now we also have the field of the sidebands, and the total electric field is

$$(E_{\text{out}})_{\text{tot}} = (E_{\text{out}})_c + (E_{\text{out}})_+ + (E_{\text{out}})_-.\quad (9.187)$$

From eq. (9.184), in the absence of GW we have

$$\begin{aligned}(E_{\text{out}})_+ + (E_{\text{out}})_- &= -2iE_0J_1(\Gamma)e^{-i\omega_L t+2ik_L L} \\ &\quad \times \sin(2\pi\Delta L/\lambda_{\text{mod}})\cos(\Omega_{\text{mod}}t - \alpha),\end{aligned}\quad (9.188)$$

where $\alpha = 4\pi L/\lambda_{\text{mod}}$ is a phase. In the presence of GWs this is modified by the fact that $\Delta L \rightarrow [1 + O(h)]\Delta L$. However, here we can neglect the term $O(h)$ because, as we will see below, it is the term $O(1)$ that combines with the carrier, giving a term proportional to h in $|(E_{\text{out}})_{\text{tot}}|^2$ that will encode the GW signal.²⁴ Thus, the total electric field at the output, in the presence of GWs, is

$$\begin{aligned}(E_{\text{out}})_{\text{tot}} &= -iE_0e^{-i\omega_L t+2ik_L L}[J_0(\Gamma)k_L Lh(t) \\ &\quad + 2J_1(\Gamma)\sin(2\pi\Delta L/\lambda_{\text{mod}})\cos(\Omega_{\text{mod}}t - \alpha)].\end{aligned}\quad (9.189)$$

²⁴Furthermore, the term $O(h)$ is multiplied here by ΔL , and $\Delta L \ll L$.

When we compute $|(E_{\text{out}})_{\text{tot}}|^2$ we therefore have three terms. (1) The squared modulus of the first term, which is $O(h^2)$, and therefore unobservable. (2) The squared modulus of the second, which is independent of h , and proportional to

$$\cos^2(\Omega_{\text{mod}}t - \alpha) = \frac{1}{2}[1 + \cos(2\Omega_{\text{mod}}t - 2\alpha)]. \quad (9.190)$$

Therefore it is the sum of a DC term and a term which oscillates with a frequency $2\Omega_{\text{mod}}$. (3) Finally we have the mixed term, i.e. the beatings between the carrier and the sidebands, which is

$$4E_0^2 J_0(\Gamma) J_1(\Gamma) k_L L h(t) \sin(2\pi\Delta L/\lambda_{\text{mod}}) \cos(\Omega_{\text{mod}}t - \alpha). \quad (9.191)$$

This term is linear in h and oscillates with a frequency Ω_{mod} .²⁵ Therefore in the output we have a term linear in h , even if the carrier is on the dark fringe. This term can be extracted from the total output $|(E_{\text{out}})_{\text{tot}}|^2$ using a mixer, which is a non-linear device which takes at its input two voltages, and produces an output voltage proportional to the product of the two input voltages. Then, we can multiply the voltage produced by $|(E_{\text{out}})_{\text{tot}}|^2$ in the photodetector by a voltage $V_{\text{osc}} \cos(\Omega_{\text{mod}}t - \alpha)$. The time-averaged output of the mixer selects the part of $|(E_{\text{out}})_{\text{tot}}|^2$ which oscillates as $\cos(\Omega_{\text{mod}}t - \alpha)$, while the DC part and the part oscillating as $\cos(2\Omega_{\text{mod}}t - 2\alpha)$ average to zero. The result (9.191) can be optimized choosing $\Delta L/\lambda_{\text{mod}} = m + 1/4$, with m any integer.

In this way we have an output which is linear in h , and is insensitive to the power fluctuations of the carrier, which is on the dark fringe. In principle, we are still sensitive to power fluctuations of the laser because the sidebands are not on the dark fringe. However, apart from the fact that the electric field of the sidebands is smaller since it is $O(\Gamma)$, the crucial point is that now the signal has been encoded in a term which oscillates as $\cos(\Omega_{\text{mod}}t - \alpha)$, so it must no longer compete with the fluctuations of the laser at a frequency f_{gw} of the GWs that we are searching, but rather with the fluctuations of the laser at a frequency f_{mod} which is much higher, typically 30 MHz. The power fluctuations of the laser is an example of a $1/f$ noise (see page 339), and at high frequencies it is small. In conclusion, we have achieved two results with this technique: (1) We are using the interferometer as a null instrument, since when $h = 0$ the output of the mixer, i.e. the term in the output power oscillating as $\cos(\Omega_{\text{mod}}t - \alpha)$, vanishes. (2) The signal is linear in the GW amplitude and is encoded into a high-frequency term, so that it must now compete with much smaller $1/f$ noise.

Interferometers with Fabry–Perot cavities

We now discuss how to apply this technique to an interferometer with Fabry–Perot cavities in the arms. In this case we consider two FP cavities both with the same length L , and the Schnupp asymmetry consists in the fact that the distances of their respective input mirrors (i.e. the mirror first encountered by the beam) from the beam-splitter are l_x and l_y respectively, with $l_x \neq l_y$.

²⁵More precisely, since $h(t)$ is proportional to $\cos \omega_{\text{gw}} t$, it oscillates at frequencies $\Omega_{\text{mod}} \pm \omega_{\text{gw}}$. Since $f_{\text{mod}} = O(10)$ MHz and $f_{\text{gw}} < O(1)$ kHz, $\omega_{\text{gw}} \ll \Omega_{\text{mod}}$.

The field at the output of the photodetector can be computed using eq. (9.70), which states that, as far as the reflected field is concerned, for light with wavenumber k a FP cavity is equivalent to a mirror with a reflectivity

$$\mathcal{R}(k) = \frac{r_1 - r_2(1 - p_1)e^{2ikL}}{1 - r_1r_2e^{2ikL}}. \quad (9.192)$$

Again we modulate the laser light with a Pockels cell, so the light incident on the beam-splitter is composed of a carrier at the laser frequency ω_L and two sidebands at $\omega_L \pm \Omega_{\text{mod}}$. We choose the cavity length L so that the carrier is resonant. The modulation frequency $f_{\text{mod}} = \Omega_{\text{mod}}/2\pi$ is much larger than the width of the resonances of the FP cavities. For instance, for $L = 4$ km and $\mathcal{F} = 200$, eqs. (9.82) and (9.83) give a width at half maximum $\delta f = O(200)$ Hz, while the modulation frequency is in the MHz region. Therefore, the modulation frequency Ω_{mod} can be chosen so that the sidebands are not resonant, and fall roughly in between resonant peaks. From eqs. (9.99) and (9.100) we see that, for an overcoupled cavity, setting $r_2 = 1$, at the resonance $\mathcal{R} = -(1 - \sigma)$, so the phase $\phi \equiv \arg(\mathcal{R})$ is equal to π . In contrast, for a generic value of $2kL$ far from the resonance (using $r_2 = 1$ and $\sigma \ll 1$), eq. (9.192) gives $\mathcal{R} = 1 + O(\sigma^2)$, so in particular $\arg(\mathcal{R}) = 0 \pmod{2\pi}$, as we see also from Fig. 9.11. Thus, as far as the reflected field is concerned, a FP cavity is equivalent to a mirror with a reflectivity \mathcal{R} which is different for the carrier and for the sidebands,

$$\mathcal{R}(k) \simeq \begin{cases} -(1 - \sigma) & \text{(if } k = k_L) \\ +1 & \text{(if } k \text{ is not close to } k_L) \end{cases} \quad (9.193)$$

The total electric field at the photodetector is the superposition of the field that propagates in the x arm for a length l_x , and is then reflected by the Fabry–Perot cavity with a reflection coefficient \mathcal{R}_x , and of the field that propagates in the y arm for a length l_y , and is then reflected by the Fabry–Perot cavity, with a reflection coefficient \mathcal{R}_y . In the absence of GWs we have $\mathcal{R}_x = \mathcal{R}_y = \mathcal{R}$, with the appropriate value of \mathcal{R} depending on whether we consider the carrier or the sidebands. Then, as in eq. (9.181), the field at the output is

$$\begin{aligned} E_{\text{out}} &= \frac{1}{2}(\mathcal{R}_x e^{2ikl_x} - \mathcal{R}_y e^{2ikl_y}) E_{\text{in}} e^{-i\omega t} \\ &= i\mathcal{R} E_{\text{in}} e^{-i\omega t + 2ikl} \sin(k\Delta l), \end{aligned} \quad (9.194)$$

where $2l = l_x + l_y$, $\Delta l = l_x - l_y$, and (k, ω) are equal to (k_L, ω_L) for the carrier and to (k_{\pm}, ω_{\pm}) for the sidebands. Thus, for the carrier we have

$$(E_{\text{out}})_c = -i(1 - \sigma) E_0 J_0(\Gamma) e^{-i\omega_L t + 2ik_L l} \sin(2\pi\Delta l/\lambda_L), \quad (9.195)$$

and for the sidebands

$$(E_{\text{out}})_{\pm} = \pm i E_0 J_1(\Gamma) e^{-i\omega_{\pm} t + 2ik_{\pm} l} \sin\left[2\pi\left(\frac{\Delta l}{\lambda_L} \pm \frac{\Delta l}{\lambda_{\text{mod}}}\right)\right]. \quad (9.196)$$

Just as we did for the Michelson interferometer, we choose as working point the dark fringe of the carrier, that is we choose l_x and l_y so that

the Schnupp asymmetry Δl is equal to an integer times λ_L , and also $\Delta l/\lambda_{\text{mod}} = m + 1/4$ for some integer m , so that $\sin(2\pi\Delta l/\lambda_{\text{mod}}) = 1$. Thus, in the absence of GWs, $(E_{\text{out}})_c = 0$ while

$$(E_{\text{out}})_+ + (E_{\text{out}})_- = 2iE_0J_1(\Gamma)e^{-i\omega_L t + 2ik_L l} \cos(\Omega_{\text{mod}}t - \alpha), \quad (9.197)$$

with $\alpha = 4\pi l/\lambda_{\text{mod}}$. Consider now what happens in the presence of a GW, as usual with optimal orientation and $\omega_{\text{gw}}L/c \ll 1$. The effect of the GW is to change the reflectivities \mathcal{R}_x and \mathcal{R}_y of the Fabry–Perot cavities. Consider first the carrier. The passage of the GW induces a phase shift $\Delta\phi_x$ in the reflected field given in eq. (9.102), so we get (for $\sigma \ll 1$)

$$\mathcal{R}_x(k_L) = -(1 - \sigma)e^{i\Delta\phi_x}, \quad (9.198)$$

with

$$\Delta\phi_x = \frac{2\mathcal{F}}{\pi} k_L L h(t). \quad (9.199)$$

For the cavity along the y arm we have an opposite phase shift, $\Delta\phi_y = -\Delta\phi_x$, so $\mathcal{R}_y(k_L) = -(1 - \sigma)e^{-i\Delta\phi_x}$. Then eq. (9.194) gives

$$\begin{aligned} (E_{\text{out}})_c &= -\frac{1}{2}(1 - \sigma)(e^{i\Delta\phi_x} e^{2ik_L l_x} - e^{-i\Delta\phi_x} e^{2ik_L l_y}) E_{\text{in}} e^{-i\omega_L t} \\ &= -i(1 - \sigma)E_0 J_0(\Gamma) e^{-i\omega_L t + 2ik_L l} \sin\left[2\pi\frac{\Delta l}{\lambda_L} + \Delta\phi_x\right]. \end{aligned} \quad (9.200)$$

On the dark fringe $\Delta l/\lambda_L = n$ and $\sin\left[2\pi\frac{\Delta l}{\lambda_L} + \Delta\phi_x\right] = \sin(\Delta\phi_x) \simeq \Delta\phi_x$. Thus, in the presence of a GW the electric field of the carrier at the photodetector shifts from the value $(E_{\text{out}})_c = 0$ to the value

$$(E_{\text{out}})_c = -i(1 - \sigma)E_0 J_0(\Gamma) e^{-i\omega_L t + 2ik_L l} \frac{2\mathcal{F}}{\pi} k_L L h(t). \quad (9.201)$$

As we already saw for the Michelson interferometer, the modification of the electric field of the sidebands due to the GWs is negligible, since it gives a corrections $1 + O(h)$, but it is the term $O(1)$ which, beating against the term $O(h)$ in the carrier, gives a term linear in h in the output. In conclusion, we can write the total (carrier plus sidebands) electric field at the output as

$$\begin{aligned} (E_{\text{out}})_{\text{tot}} &= -2iE_0 e^{-i\omega_L t + 2ik_L l} \\ &\times \left[(1 - \sigma)J_0(\Gamma)\frac{\mathcal{F}}{\pi} k_L L h(t) - J_1(\Gamma) \cos(\Omega_{\text{mod}}t - \alpha) \right]. \end{aligned} \quad (9.202)$$

The situation is now the same that we already discussed for a Michelson interferometer: taking the modulus squared, the term which oscillates as $\cos(\Omega_{\text{mod}}t - \alpha)$ is linear in h and is demodulated with a mixer. We therefore have an output that is linear in $h(t)$ even if the carrier is on the dark fringe, and is encoded in a term which oscillates at the frequency Ω_{mod} , so $1/f$ noise such as laser power fluctuations are small. This procedure is a special case of the Pound–Drever–Hall locking, see Section 9.3.4.

9.3.3 Basic optical layout

We can now complete the description of a realistic GW interferometer. One further improvement with respect to the scheme that we have discussed is the *power recycling*. The basic observation is that, since we have chosen as working point the dark fringe for the carrier, in the absence of GWs no light at all emerges from the beam-splitter in the direction of the photodetector, at the carrier frequency. This means that all the light at frequency ω_L that circulates in the arms is eventually reflected by the beam-splitter back toward the laser and, in this sense, is wasted. When we discuss the noise sources in the next section, and in particular the shot noise, we will see that we want to have the highest possible laser intensity circulating in the arms. However, the power of a continuous (and very stable) laser is currently limited to $O(10)$ watts, which could become $O(100)$ W in the near future. To increase the power circulating in the interferometer, the idea is to “recycle” the light that comes back toward the laser, placing a mirror (the power-recycling mirror) that reflects the light back toward the beam-splitter. As far as the light reflected toward the laser is concerned, we can model the whole interferometer as an equivalent mirror, with a reflectivity that accounts for the total reflected field. The addition of the power-recycling mirror between the laser and the beam-splitter creates a new Fabry–Perot cavity, made of the power-recycling mirror and the “equivalent interferometer mirror”. If this cavity is arranged so that it is resonant for the input laser light, the total intensity of the light that circulates in the interferometer is enhanced. Indeed, in this way a gain of $O(100)$ can be obtained (the maximum gain that can be reached is inversely proportional to the losses inside the interferometer), so the power circulating between the power-recycling mirror and the beam splitter raises to about 1 kW. Inside the Fabry–Perot cavities in the arms, this power increases further because it is resonant, and in initial LIGO and VIRGO it reaches a value of order 15 kW.

A second feature of a real interferometer is an output mode cleaner. Even if the initial beam has been accurately prepared in the TEM_{00} mode thanks to the input mode cleaner, various imperfections in the mirrors, as well as misalignments, regenerate higher modes inside the interferometer. These higher modes are not on the dark fringe, and therefore simply produce a noise that lowers the contrast at the output. The output mode cleaner, placed between the beam-splitter and the photodetectors, filters out these higher modes, enhancing the contrast and therefore the sensitivity.

Putting together all these elements, we arrive at the optical layout shown in Fig. 9.25 where, for definiteness, we have used the parameters of VIRGO. The laser, a continuous Nd:Yag with wavelength $\lambda_L = 1.064 \mu\text{m}$, provides 20 W of power. The laser beam passes through an electro-optic modulator, i.e. a Pockels cell, which generates sidebands at $\Omega_{\text{mod}}/(2\pi) = 6.2 \text{ MHz}$. The beam is then passed through the input mode cleaner. This is a long cavity with very high finesse, and a trian-

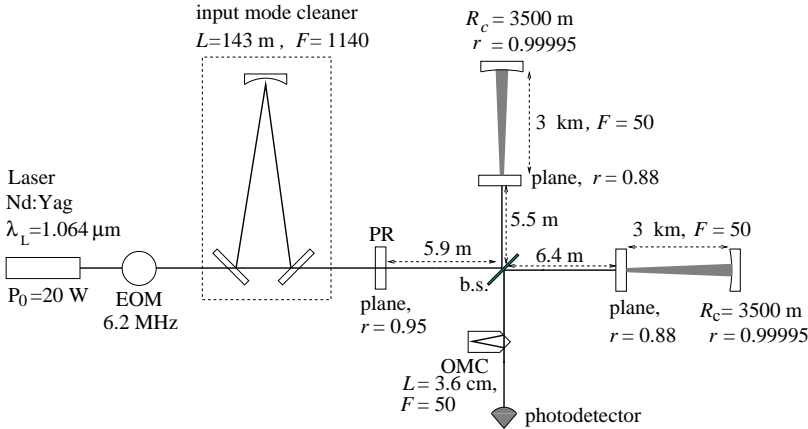


Fig. 9.25 The basic layout of a GW interferometer. EOM = Electro-optic modulator (Pockels cell); PR = power recycling mirror; OMC = output mode cleaner; b.s. = beam splitter. The curvature radius R_c and reflectivity r of the various mirrors are indicated. For definiteness, we used the values for the initial VIRGO interferometer.

gular shape that forbids reflection back toward the laser. The beam that comes out of the input mode cleaner is very nearly a TEM_{00} mode, both in the carrier and in the sidebands. It is transmitted through the power recycling mirror and enters the interferometer. The Schnupp asymmetry is realized choosing $l_x \simeq 6.4$ m and $l_y \simeq 5.5$ m for the distances between the beam splitter and the input mirrors of the two Fabry-Perot cavities. After going back and forth in the Fabry-Perot cavities, with a length of 3 km and a finesse $F = 50$, the beams are recombined on the beam-splitter. Since we work on the dark fringe, at the beam-splitter the carrier is entirely reflected back toward the laser, and then finds the power-recycling mirror, that sends it back to the interferometer. When the carrier is displaced from the dark fringe, for instance because of the passage of a GW, the beating between the carrier and the sidebands goes toward the photodetector. It first passes through the output mode cleaner, a single crystal of 3.6 cm, where again makes a triangular path, and then goes to an array of photodetectors, and it is finally demodulated and detected.²⁶

9.3.4 Controls and locking

This section is slightly technical, but is meant to give at least a flavor of the problems that must be overcome to turn the beautiful theoretical idea of a GW interferometer into a working instrument.

The scheme that we have discussed above reaches its high sensitivity because the laser light is resonant in the Fabry-Perot cavities. On resonance, a FP cavity is extremely sensitive to changes in its length L , but as soon as we move away from the resonance, it becomes “dead”, and the phase of the reflected field loses essentially any dependence on

²⁶Figure 9.25 is still somewhat simplified. For instance, there are also lenses that are used to match the laser beam into the mode cleaner. A Faraday isolator is used to protect the laser from back-tracking light from the interferometer. A mode-matching telescope is used to blow the input laser beam, which has an initial transverse size of just a few millimeters, to the waist appropriate for the Fabry-Perot cavities which, as we have seen, is rather of order 2–3 cm. Further mirrors are used to pick up signals that are needed for control purposes.

L , see Fig. 9.10. This means that the mirrors of the FP cavity must be held still, and in the right position, so that $k_L L = \pi n$ for some integer n . To estimate the precision needed we observe from eq. (9.81) that the half-width of the resonance peak, as a function of L at fixed k_L , is reached if L shifts from the value that fulfills the resonance condition to a value $L + \delta L$, with

$$\delta L = \frac{\lambda_L}{4\mathcal{F}}. \quad (9.203)$$

(Compare with eqs. (9.83) and (9.84), where we computed the full width at half maximum in ω_L , at fixed L .) With a finesse $\mathcal{F} = O(200)$ this means that we need to keep the length L of the Fabry-Perot cavities fixed, within a precision better than $\delta L \sim 10^{-3}\lambda_L$. Similarly, the power-recycling technique that we have discussed allows us to gain a factor $O(100)$ in laser power, but again the power-recycling mirror must be located in a precise position, in order to satisfy the resonance condition in the power-recycling cavity, i.e. in the cavity made by the power-recycling mirror and the equivalent interferometer mirror. Again, this must hold to a precision much smaller than λ_L . Finally, our detection scheme requires that the interferometer be on the dark fringe, again within a small fraction of wavelength. Typically, a value $\delta L \sim (10^{-6}-10^{-4})\lambda_L$ is required for good performances. With $\lambda_L = 1\mu\text{m}$, this means that the relative position of the mirrors must be kept fixed, at a distance L of order a few kms, within a precision

$$\delta L \sim (10^{-12}-10^{-10})\text{ m}, \quad (9.204)$$

which is less than the size of an atom! Last but not least, all these lengths are measured with respect to λ_L , so we also need a laser whose frequency is stabilized to great precision. At first sight, the idea of controlling the length of a 4-km cavity down to an accuracy of 10^{-10} m might seem preposterous. Indeed, it is here that a large part of the complexity of GW interferometers resides. However, by now this is routinely achieved in the large GW interferometers, and it is quite interesting to understand how this is possible.

First of all, one could make the possibly naive remark that a mirror does not have a smooth surface down to 10^{-10} m, since at this level we resolve the individual atoms, and even more so at 10^{-12} m; thus, one might object that the notion of the length L of the cavity is not even well defined down to these scales. However, we must keep in mind that the laser beam at the mirror locations has a transverse size of a few centimeters. This means that what the laser beams actually senses is the position of the surface of the mirror, *averaged over a macroscopic scale*, of order a few cms. Thus, the individual atomic fluctuations cancel out, at least to a first approximation²⁷ and, in this averaged sense, the notion of the length L of the cavity *is* well defined, even down to such small scales. This is a simple but fundamental point to keep in mind to understand the statement that interferometers (or, as we saw in Chapter 8, resonant bars) are finally able to detect displacements which are much smaller than the size of a nucleus.

²⁷Of course, any imperfection in the mirrors will create noise, such as scattered light in the interferometer, so their micro-roughness cannot exceed too much the figure $O(10^{-10})$ m found above. The mirrors of LIGO and VIRGO are polished so that their rms micro-roughness is about 0.5\AA , that is 50 times larger than 10^{-10} m.

Another simple but important conceptual point is that, actually, we do not need to know the value of the length L of a FP cavity down to a precision 10^{-10} m. All that we need, in order to have a FP cavity which works properly, is that it is on one of its resonances, i.e. $2k_L L = 2\pi n$, or $L = \lambda_L n/2$, for some integer n . Since $2L/\lambda_L = O(10^{10})$, the corresponding value of n is very large, but we do not need to know it. All that we want is that the FP cavity be on some resonance, corresponding to some unspecified value of n , and does not move away from it by more than $\delta L \sim 10^{-4}\lambda_L$. Once the two FP cavities in the arms are resonant, we must arrange their relative position so that the interferometer is on some dark fringe. Again, we do not need to know on which one.

So, what we need is to “trap”, or lock, each FP cavity in some of its resonances, and to lock the interferometer on some dark fringe. The general strategy is the one common to all *feedback control systems*. In general terms, this consists of a sensor and an actuator. The sensor detects the value of the quantity of interest and produces an error signal, which measures the difference between the actual and the desired value. The actuator then provides a feedback, which corrects the error, driving the observed value closer to the desired one.

For a FP cavity, the error signal is obtained using the Pound–Drever–Hall locking scheme. This is a widely used technique, originally invented for stabilizing the wavelength of a laser, using as a reference the length L of a Fabry–Perot cavity. Suppose that we have a FP cavity whose length is fixed, to a sufficiently good precision. The wavelength of any laser has in general fluctuations, and if we want to stabilize it a simple idea is to shine it on a FP cavity of the appropriate length L , chosen so that the desired value of λ_L is resonant, and look at the transmitted light. As shown in Fig. 9.9, we have a series of narrow peaks as a function of λ_L . If the wavelength of the laser has a slight mismatch with respect to the resonant value, we are just slightly displaced from the peak, so the transmitted intensity is lower. We could then use this as an error signal, and correct for this error with a feedback mechanism. This scheme however has two drawbacks. First, from the fact that the power decreases we cannot tell in which direction the wavelength fluctuated, and therefore we do not know the sign of the correction to be applied. Second, we cannot disentangle wavelength fluctuations from intrinsic power fluctuations of the laser.

The solution is to use modulated light, so the electric field entering the FP cavity has the form (9.178), with the carrier at the resonant frequency. Upon reflection, taking $\sigma \ll 1$, we see from eq. (9.193) that the carrier takes a minus sign while the sidebands get a plus sign. Using the fact that $J_0(-\Gamma) = J_0(\Gamma)$ and $J_1(-\Gamma) = -J_1(\Gamma)$, we see that this still has the form of modulated light, with modulation index $-\Gamma$. Thus the reflected power is simply $|E_0|^2$, i.e. it contains a DC term and no term at the modulation frequency Ω_{mod} . In this sense, we have a null instrument: the signal that we use, which is the part oscillating as Ω_{mod} , vanishes in the absence of perturbations. Suppose now that a fluctuation changes the wavelength λ_L of the laser, with respect to the length L

of the cavity. The carrier, which is on resonance, is very sensitive to this perturbation, while the sidebands, which are far from resonance, are completely insensitive, see Fig. 9.10. Thus the reflected field of the carrier is multiplied by a factor $\exp\{i\Delta\phi\}$, while the sidebands are unchanged. In the power $|E_{\text{refl}}|^2$, the beating between the carrier and the sidebands now produces a term oscillating at a frequency Ω_{mod} and linear in $\Delta\phi$, which can be demodulated with a mixer. This is a way to obtain an error signal which, at least close to the resonance, is linear in the deviation $\Delta\phi$. We can therefore use it to lock the laser wavelength to the length L of the cavity.

If we assume for a moment that the laser frequency is already sufficiently stable (we will come back below to this point) and the cavity is not rigid, as in a GW interferometer, we can turn the argument around, using λ_L as our standard of length, and lock the cavity length L to the wavelength λ_L of the laser. We now realize that the detection scheme on the dark fringe that we discussed in Section 9.3.2 is nothing but a variant of this Pound–Drever–Hall locking scheme. In the original Pound–Drever–Hall method the need for a signal linear in $\Delta\phi$ arises because we want to know the sign of $\Delta\phi$ in order to correct for it in the proper direction, while in the detection scheme for GWs it arises first of all from the fact that the shift $\Delta\phi$ is $O(h)$, and a quantity $O(h^2)$ would be undetectably small. Observe that, even if the interferometer is always on the dark fringe, the information on the value of h can then be read from the fact that we know the feedback that we had to apply to keep it there.

For the control of the interferometer, one generally collects all the beams that come out from it (including the little light that comes out in transmission from the end-mirrors of the arms) and uses all the information contained in this modulated light to perform a Pound–Drever–Hall locking of the three FP cavities of the interferometer (the two arms and the power-recycling cavity). Actually, if we had a laser sufficiently stable in frequency, we could use as GW detector a single arm with a FP cavity, and the sensitivity of the detector would degrade only by a factor of two (given that, for optimal orientation, the contribution of the GWs in the two arms is summed up). However, lasers of the required stability do not exist. So, the above procedure can be seen as locking first the laser to the length of the FP cavity in one arm, and then using the laser wavelength so stabilized, to lock the second arm cavity to it, so we are really measuring the displacement in one arm in units of the length of the other arm. More precisely, we lock the laser to the common mode, where the two arms move symmetrically, and we detect GWs in the differential mode, where the two arms move anti-symmetrically.

The Pound–Drever–Hall locking ensures that all the FP cavities are operating on resonance. Then, we must ensure that the two beams combine at the output of the interferometer so that they are on the dark fringe. This is done using as error signal the one generated by the Schnupp asymmetry. We discussed it on page 506, considering the phase shift $\Delta\phi$ induced by a GW, but the same argument can be repeated for

the phase shift induced by the noise. Again, using modulated light and asymmetric arm lengths, we get a signal linear in $\Delta\phi$ at the frequency Ω_{mod} , that we can use as error signal. This technique is called Schnupp locking.

Experimentally, once the interferometer is at its working point, it is not so difficult to keep it there for very long time. The most difficult part is the so-called lock acquisition, i.e. bringing the instrument from the free state down to a controlled state. In the absence of controls, the mirrors are typically swinging with an amplitude of a few microns, therefore a factor $O(10^4)$ larger than what we can tolerate, and have typical speeds of a few microns per second, so they are sweeping across many resonances. Thus the control system must be fast enough to “grab” a mirror when it passes close to a resonance, and keep it there, using magnetic actuators. Moreover, we have stringent conditions on the alignment of the mirrors; for instance the input mirrors of the Fabry–Perot cavities must be aligned within $\delta\theta < O(10^{-8})$ rad. Such efficient control systems have by now been developed by the collaborations running the large GW interferometers, and locking and correct alignment are by now obtained quite routinely.

9.4 Noise sources

Having defined the experimental setup, we can now investigate the sensitivity that can be obtained. The sensitivity at which a GW interferometer must aim, to have good chances of detection, is extremely ambitious. We saw in Chapter 7 that the GW amplitude that can be detected depends crucially on the kind of signal (burst, periodic, coalescence or stochastic) that we are searching. As a first benchmark, we can consider a burst that releases in GWs an energy of 10^{-2} solar masses, taking place in the Virgo cluster of galaxies. As we saw on page 365, this gives a GW amplitude on Earth of just $h_0 \sim 10^{-21}$. As we have seen in this chapter, the corresponding displacement of the mirror of the interferometer is $\Delta L = (1/2)h_0L$ (for $\omega_{\text{gw}}L/c \ll 1$), so for $L = 4$ km, we have

$$\Delta L \sim 2 \times 10^{-18} \text{ m}, \quad (9.205)$$

which is smaller than the size of a nucleus by a factor 10^3 ! Impressive as it might be, this figure is however somewhat misleading because, as we have repeatedly emphasized, we must not forget that this is a coherent displacement of all the atoms of a macroscopic body such as a mirror. A better figure is given by the corresponding phase shift, which for a simple Michelson interferometer is $\Delta\phi_{\text{Mich}} = (4\pi/\lambda_L) h_0 L$, see eqs. (9.27) and (9.28). Setting $\lambda_L = 1 \mu\text{m}$ gives $\Delta\phi_{\text{Mich}} \sim 5 \times 10^{-11}$ rad. We have seen however that for an interferometer with Fabry–Perot cavities we gain a factor $2\mathcal{F}/\pi$ in $\Delta\phi$, see eq. (9.102). For $\mathcal{F} = 200$ this is a factor $\simeq 130$, which means that we aim at measuring a phase shift

$$\Delta\phi_{\text{FP}} \sim 10^{-8} \text{ rad}. \quad (9.206)$$

In the following subsections we examine the dominant noise sources, to see what sensitivity can be reached. The sensitivity is conveniently expressed in terms of the strain sensitivity $S_n^{1/2}(f)$, with dimensions $\text{Hz}^{-1/2}$. From its value we can then obtain the sensitivity to all type of signals, such as bursts, periodic signals, etc., as discussed in Chapter 7.

9.4.1 Shot noise

The first source of noise that we consider is the shot noise of the laser. This originates from the fact that the laser light comes in discrete quanta, the photons. Let N_γ be the number of photons that arrives on the photodetector in an observation time T . Then the average power measured at the photodetector during this observation time is

$$P = \frac{1}{T} N_\gamma \hbar \omega_L. \quad (9.207)$$

When we measure the average output power, we are actually counting the number of photons that arrived in a time T . Whenever we count a number of *discrete* independent events the set of outcomes follows the Poisson distribution,

$$p(N; \bar{N}) = \frac{1}{N!} \bar{N}^N e^{-\bar{N}}, \quad (9.208)$$

where \bar{N} is the average value of N . Since this is the probability distribution when we count a number of independent events, it is also known as the *counting statistics*. For large N the Poisson distribution becomes a Gaussian, with standard deviation equal to $\sqrt{\bar{N}}$. Therefore, the fluctuation in the number of photons is given by

$$\Delta N_\gamma = \sqrt{N_\gamma}. \quad (9.209)$$

It is worth stressing that this is a fundamental limitation due to the corpuscular nature of light. This produces a fluctuation in the observed power given by

$$\begin{aligned} (\Delta P)_{\text{shot}} &= \frac{1}{T} N_\gamma^{1/2} \hbar \omega_L \\ &= \left(\frac{\hbar \omega_L}{T} P \right)^{1/2}, \end{aligned} \quad (9.210)$$

where in the second line we eliminated $N_\gamma^{1/2}$ using eq. (9.207). We want to compare this result with the power fluctuations induced by a GW.

To make the setting simpler, we first consider a Michelson interferometer, with no Fabry–Perot cavities in the arms. We neglect the modulation of the laser light and for the moment we work at a generic point ϕ_0 . Then, according to eq. (9.32), in the absence of GWs the output power P is related to the input power P_0 by $P = P_0 \sin^2 \phi_0$, so eq. (9.210) becomes

$$(\Delta P)_{\text{shot}} = \left(\frac{\hbar \omega_L}{T} P_0 \right)^{1/2} |\sin \phi_0|. \quad (9.211)$$

On the other hand, again from eq. (9.32), the variation in power due to a GW is

$$(\Delta P)_{\text{GW}} = \frac{P_0}{2} |\sin 2\phi_0| (\Delta\phi)_{\text{Mich}}. \quad (9.212)$$

We consider a periodic GW with frequency f , with only the plus polarization and coming from optimal orientation, and at first we take for simplicity $2\pi f L/c \ll 1$. According to eqs. (9.21) and (9.28), the amplitude of the phase shift $\Delta\phi_{\text{Mich}}$ is then

$$|\Delta\phi_{\text{Mich}}| = \frac{4\pi L}{\lambda_L} h_0, \quad (9.213)$$

so the power fluctuations induced by this GW have an amplitude

$$(\Delta P)_{\text{GW}} = \frac{P_0}{2} |\sin 2\phi_0| \frac{4\pi L}{\lambda_L} h_0. \quad (9.214)$$

The signal-to-noise ratio (defined, as in Chapter 7 to be linear in the amplitude h_0 of the GW, when the only source of noise is the shot noise, is then

$$\begin{aligned} \frac{S}{N} &= \frac{(\Delta P)_{\text{GW}}}{(\Delta P)_{\text{shot}}} \\ &= \left(\frac{P_0 T}{\hbar \omega_L} \right)^{1/2} \frac{4\pi L}{\lambda_L} h_0 |\cos \phi_0|. \end{aligned} \quad (9.215)$$

For definiteness, we compute the shot noise at the naive working point where $\cos \phi_0 = 1/\sqrt{2}$ (the point 1 in Fig. 9.24),²⁸ so

$$\frac{S}{N} = \left(\frac{P_0 T}{2\hbar \omega_L} \right)^{1/2} \frac{4\pi L}{\lambda_L} h_0. \quad (9.216)$$

On the other hand, we see from eq. (7.129) that, for a periodic GW of frequency f , coming from optimal direction and observed for a time T , the signal-to-noise ratio is written in terms of the strain sensitivity $S_n^{1/2}(f)$ as

$$\frac{S}{N} = \left[\frac{T}{S_n(f)} \right]^{1/2} h_0. \quad (9.217)$$

Comparing eqs. (9.216) and (9.217) we see that $T^{1/2}$ and h_0 cancel, and we get the strain sensitivity due to the shot noise,

$$S_n^{1/2}(f) \Big|_{\text{shot}} = \frac{\lambda_L}{4\pi L} \left(\frac{2\hbar \omega_L}{P_0} \right)^{1/2}. \quad (9.218)$$

For an interferometer with Fabry–Perot cavities, the result can be obtained replacing $|\Delta\phi_{\text{Mich}}|$ in eq. (9.213) by $|\Delta\phi_{\text{FP}}|$. For an interferometer with power recycling, the input laser power P_0 in eq. (9.220) must be replaced with the power circulating in the recycling cavity, so $P_0 \rightarrow CP_0$, where C is the factor gained with power recycling (typically $C = O(50–100)$ with present detectors, so that $CP_0 = O(1)$ kW). We

²⁸Actually, eq. (9.215) is maximized when $\phi_0 = 0$, i.e. on the dark fringe. Thus, even in the absence of phase modulation, the dark fringe would be the optimal working point, if the only noise were the shot noise. However, this comes out because both the GW signal and the shot noise vanish at the dark fringe, with a finite ratio which optimizes S/N . Since there are other noise, such as test mass movements, that do not vanish at the dark fringe, in the absence of phase modulation the dark fringe is not an acceptable working point.

also take into account the efficiency of the photodetector, which reduces the effective power used to extract electrons at the photodiode by a factor η (a typical value can be $\eta = 0.93$), so $P_0 \rightarrow \eta P_0$.

Furthermore, we do not want to limit ourselves to the static limit, but we take into account the dependence on the GW frequency. Thus we use eq. (9.123) for $|\Delta\phi_{\text{FP}}|$, and eq. (9.217) is replaced by

$$\frac{S}{N} = \left(\frac{\eta CP_0 T}{2\hbar\omega_L} \right)^{1/2} \frac{8\mathcal{F}L}{\lambda_L} h_0 \frac{1}{\sqrt{1 + (f/f_p)^2}}, \quad (9.219)$$

and (writing $\omega_L = 2\pi c/\lambda_L$) eq. (9.218) becomes

$$S_n^{1/2}(f) \Big|_{\text{shot}} = \frac{1}{8\mathcal{F}L} \left(\frac{4\pi\hbar\lambda_L c}{\eta P_{\text{bs}}} \right)^{1/2} \sqrt{1 + (f/f_p)^2}, \quad (9.220)$$

where $P_{\text{bs}} \equiv CP_0$ is the power on the beam-splitter after recycling.

An instructive way to rephrase the above computation is as follows. According to eq. (9.32), the variation in the output power of a Michelson interferometer induced by a GW, choosing as working point $\phi_0 = \pi/4$, is $\Delta P = P_0 \Delta\phi_{\text{Mich}}/2$. Since all we measure is the power at the photodetector, the power fluctuation eq. (9.210) has the same effect as a phase shift $\Delta\phi_{\text{Mich}}$ induced by a GW, with

$$\frac{1}{2}P_0 \Delta\phi_{\text{Mich}} = \frac{1}{T} N_\gamma^{1/2} \hbar\omega_L. \quad (9.221)$$

On the other hand, at $\phi_0 = \pi/4$, we have $P = P_0/2$, so $P_0 = 2P = 2N_\gamma \hbar\omega_L/T$, which, inserted in eq. (9.221), gives

$$\Delta\phi_{\text{Mich}} = \frac{1}{\sqrt{N_\gamma}}. \quad (9.222)$$

This is the rms value of the equivalent phase shift. To compute its spectral density $S_{\Delta\phi}(f)$ we proceed as follows. Let $A(t)$ be any random variable, such that

$$\langle A(t)A(t') \rangle = A_0 \delta(t - t'). \quad (9.223)$$

This is the case of shot noise, since there is no correlation between the fluctuations of photon number at different times. As we saw in eq. (7.16), the (single-sided) spectral density $S_A(f)$ of any quantity A is in general defined from

$$\langle A(t)A(t') \rangle = \frac{1}{2} \int_{-\infty}^{\infty} df S_A(f) e^{-i2\pi f(t-t')}. \quad (9.224)$$

When eq. (9.223) holds, we see that $S_A(f)$ is independent of f , and has the value $S_A = 2A_0$ (as we already saw below eq. (8.122)). On the other hand, setting $t = t'$ in eq. (9.223), we get $\langle A^2(t) \rangle = A_0 \delta(0) =$

$(1/2)S_A\delta(0)$. If we do not have an instantaneous resolution in time, but rather we perform a coarse graining over an observation time T , the Dirac delta must be replaced by its regularized version (with unit area), defined by $\delta(t) = 1/T$ if $-T/2 < t < T/2$ and $\delta(t) = 0$ if $|t| > T/2$, so $\delta(0) = 1/T$. Therefore

$$\langle A^2(t) \rangle = \frac{1}{2T}S_A. \quad (9.225)$$

Thus the strain sensitivity $S_A^{1/2}$ can be obtained from the rms value of A , $\langle A^2(t) \rangle^{1/2}$, multiplying it by $(2T)^{1/2}$. In particular the spectral density of the phase shift, $S_{\Delta\phi}$, is given by

$$\begin{aligned} S_{\Delta\phi}^{1/2} &= \sqrt{\frac{2T}{N_\gamma}} \\ &= \sqrt{\frac{2\hbar\omega_L}{P}}. \end{aligned} \quad (9.226)$$

To pass from the spectral density of $\Delta\phi$ to the spectral density of the noise $n(t)$, which is the quantity to be compared with the GW signal $h(t)$, we use eq. (9.125), i.e. we divide by the transfer function (9.126). (In the language explained at the beginning of Chapter 7, dividing by the transfer function we are referring the noise to the input of the detector). This gives back eq. (9.220).

Observe that $S_n^{1/2}(f)|_{\text{shot}}$ is flat up to the pole frequency, and then raises linearly in f . This is due to the fact that the shot noise in itself is independent of the frequency, while the transfer function, i.e. the sensitivity of a FP interferometer to GWs, degrades linearly with f beyond f_p . Inserting the numerical values we get

$$\begin{aligned} S_n^{1/2}(f)|_{\text{shot}} &\simeq 1.5 \times 10^{-23} \text{ Hz}^{-1/2} \left(\frac{50}{\mathcal{F}} \right) \left(\frac{3 \text{ km}}{L} \right) \left(\frac{1 \text{ kW}}{P_{\text{bs}}} \right)^{1/2} \\ &\times \sqrt{1 + (f/f_p)^2}, \end{aligned} \quad (9.227)$$

where we set $\lambda_L = 1 \mu\text{m}$, and we used reference values appropriate for the initial VIRGO. Recall that (at the initial detector stage) for VIRGO $f_p \simeq 500 \text{ Hz}$ and for LIGO $f_p \simeq 90 \text{ Hz}$.²⁹

²⁹ Our discussion is simplified, since we have not taken into account the effect of the phase modulation of the laser light. Numerically, this gives a strain sensitivity higher by approximately a factor of $(3/2)^{1/2}$ compared to the one obtained in eq. (9.220), see the Further Reading section.

9.4.2 Radiation pressure

Equation (9.220) indicates that, to beat the shot noise, we should increase the power P_{bs} , either increasing the input laser power or increasing the recycling factor C . However, a beam of photons that impinges on a mirror and is reflected back exerts a pressure on the mirror itself. If this radiation pressure were constant, it could simply be compensated by the mechanism that holds the mirrors in place. However, since the number of photons arriving on the mirror fluctuates as in eq. (9.209), the radiation pressure fluctuates, too, and generates a stochastic force that shakes the mirrors. We see from eq. (9.210) that this stochastic force

grows as $\sqrt{P_{\text{bs}}}$ while, from eq. (9.220), shot noise decreases as $1/\sqrt{P_{\text{bs}}}$. If, in order to beat the shot noise, we increase the power P_{bs} , beyond a certain limiting value the fluctuations in the radiation pressure will become important, and will dominate over the shot noise.

To compute the strain sensitivity due to radiation pressure we proceed as follows. Consider a laser beam with power P that impinges perpendicularly on a mirror. At reflection each photon changes its momentum from $+|\mathbf{p}|$ to $-|\mathbf{p}|$, so it transfers a momentum $2|\mathbf{p}|$ to the mirror. Since the photon energy is $E_\gamma = |\mathbf{p}|/c$, the force that a beam of power P exerts on the mirror is $F = 2P/c$. The rms fluctuations of the force in a time T are therefore related to the power fluctuations by $\Delta F = 2\Delta P/c$. Using eq. (9.210),

$$\Delta F = 2 \sqrt{\frac{\hbar\omega_L P}{c^2 T}}. \quad (9.228)$$

The fluctuation in the number of photons is independent of the frequency, so the spectral density of the force, $S_F(f)$, must be flat in frequency and, using eq. (9.225), is given by

$$S_F^{1/2} = 2 \sqrt{\frac{2\hbar\omega_L P}{c^2}}. \quad (9.229)$$

This stochastic force F acts on a mirror that, in the horizontal plane, is otherwise free, so we have $F = M\ddot{x}$, where M is the mass of the mirror and x its coordinate. In Fourier space, this means $\tilde{F}(f) = -M(2\pi f)^2 \tilde{x}$, so the spectral density of the displacement of the mirror is³⁰

$$S_x^{1/2}(f) = \frac{2}{M(2\pi f)^2} \sqrt{\frac{2\hbar\omega_L P}{c^2}}. \quad (9.230)$$

Consider now what happens in an interferometer. We consider first a simple Michelson interferometer, taking the beam-splitter much heavier than the end-mirrors (so we can neglect its recoil). When a photon arrives on the beam-splitter, it is scattered randomly into one or the other arm. As a result, in each arm the distribution of photons is a Poissonian. The important point is that the distributions in the two arms are *anti-correlated*. One more photon into one arm means one less in the other. In the differential mode of the interferometer the contributions due to radiation pressure in the two arms therefore add up, so the radiation pressure in an interferometer is obtained multiplying eq. (9.230) by a factor of two (while correlated fluctuations in the two arms, such as intrinsic laser power fluctuations, cancel out).³¹

To express the result in terms of the equivalent noise spectral density, we must divide by the transfer function that relates ΔL to the GW amplitude h . For a simple Michelson interferometer, at $f \ll f_p$ we have $\Delta L = hL$, so the transfer function is simply L , and the strain sensitivity $S_n^{1/2}(f)$ due to radiation pressure is

$$S_n^{1/2}(f) \Big|_{\text{rad pres}} = \frac{4}{ML(2\pi f)^2} \sqrt{\frac{2\hbar\omega_L P}{c^2}}. \quad (9.231)$$

³⁰More accurately, when a suspended mirror oscillates there is a restoring force due to gravity, so it should be really treated as a harmonic oscillator, with resonance frequency ω_0 and dissipation coefficient γ (defined as in eq. (8.20)). Then the factor $(2\pi f)^2 = \omega^2$ in the denominator of eq. (9.230) must be replaced by $|\omega^2 - \omega_0^2 + i\gamma\omega_0|$, compare with eq. (8.23). However, the resonance frequency ω_0 and the dissipation coefficient γ are smaller than the frequency ω at which we are interested, and in a first approximation can be neglected.

³¹Another way to describe the same phenomenon is in terms of vacuum fluctuations of the electromagnetic field entering the interferometer from the output port, see Caves (1980, 1981).

Consider next an interferometer with Fabry–Perot cavities. In this case the result depends on the finesse \mathcal{F} of the arm cavities. Physically, this dependence can be understood observing that, in a FP cavity with finesse \mathcal{F} , light is performing on average $\mathcal{N} = 2\mathcal{F}/\pi$ bounces. Then each photon hits the mirrors $O(\mathcal{N})$ times, so the rms value ΔL of the length of the cavity is $O(\mathcal{N})$ times larger than the value when the light make only one bounce. Furthermore, when the cavity is at resonance, a given value of ΔL produces a phase shift in the reflected light larger by a factor $T_{\text{FP}}(f) = O(\mathcal{N})$, compared to the one-bounce case. Overall, the total effect on the phase shift induced by the radiation pressure is therefore $O(\mathcal{N}^2)$. However, to compare with the effect of a GW (i.e. to refer the noise to the detector input, in the language of Chapter 7) we must divide by the transfer function of an interferometer with Fabry–Perot cavities, which is again $T_{\text{FP}}(f)$, and we are left with a single factor $O(\mathcal{N})$.

In other words, a given displacement $\Delta \tilde{x}(f)$ of a mirror due to radiation pressure results in a phase shift $\Delta\phi_{\text{FP}}(f)$ which is much larger than for the single-bounces case, since now the transfer function is $T_{\text{FP}}(f)$, given in eq. (9.126), which is proportional to \mathcal{F} or, equivalently, to the number of bounces. However, in order to refer the noise to the detector input, we must divide by the same transfer function, so the two effects cancel. The fact that each photon performs $O(\mathcal{N})$ bounces results in the fact that the power inside the cavity is larger by a factor $O(\mathcal{N})$ than the power P_{bs} at the beam-splitter. Indeed, from eq. (9.72), at resonance the power inside the cavity is

$$P_{\text{cav}} = P_{\text{bs}} \frac{t_1^2}{(1 - r_1 r_2)^2}. \quad (9.232)$$

Setting for simplicity $r_2 = 1$ and $t_1^2 = 1 - r_1^2 - p_1 \simeq 1 - r_1^2$, this gives $P_{\text{cav}} = P_{\text{bs}}(1 + r_1)/(1 - r_1)$ which, for r_1 close to one, can be written as

$$P_{\text{cav}} \simeq P_{\text{bs}} \frac{2\mathcal{F}}{\pi}. \quad (9.233)$$

Therefore a fluctuation ΔP_{bs} of the light arriving on the input mirror induces a fluctuation of the field inside the cavity $\Delta P_{\text{cav}} \simeq \Delta P_{\text{bs}}(2\mathcal{F}/\pi)$. Actually, if the mirror vibrates at a frequency f , the cavity is displaced off resonance, and the power inside the cavity is reduced by a factor $[1 + (f/f_p)^2]$, as we see from eq. (9.81), together with the definitions (9.84) and (9.122). As a result (writing $\omega_L = 2\pi c/\lambda_L$ in eq. (9.231))

$$S_n^{1/2}(f) \Big|_{\text{rad}} = \frac{16\sqrt{2}\mathcal{F}}{ML(2\pi f)^2} \sqrt{\frac{\hbar}{2\pi}} \frac{P_{\text{bs}}}{\lambda_L c} \frac{1}{\sqrt{1 + (f/f_p)^2}}. \quad (9.234)$$

This result answers a question that might have been asked when we realized that the response to GWs of an interferometer with Fabry–Perot cavities, with arm-length L and finesse \mathcal{F} , is equivalent to that

of a simple Michelson interferometer with arm-length $(2/\pi)\mathcal{F}L$. Given that very high finesse cavities are not difficult to build (e.g. the mode cleaner has a finesse $O(10^3)$) why bother to construct a km-sized arm, with all the financial and technical problems that this implies (e.g. the very high vacuum in such a long arm, see below)? We could think that it is sufficient to build a table-top interferometer with a sufficiently large finesse.

The answer is that the response of the detector to GWs, encoded in the transfer function (9.126), is only one side of the issue. What really matters is the signal-to-noise ratio, and we must also ask how the various noise scale with \mathcal{N} and L . For instance, shot noise is independent of \mathcal{N} . When divided by the transfer function, which is $O(\mathcal{N})$, the signal-to-noise ratio therefore scales as $1/\mathcal{N} = O(1/\mathcal{F})$. To beat down such a noise we could in principle keep L small, as long as we use a cavity with a sufficiently high finesse. However, we have seen that radiation pressure noise rather scales as \mathcal{N}^2 , so after dividing by the transfer function we have a dependence proportional to \mathcal{N} , i.e. to \mathcal{F} . In this case a very large finesse would be harmful. Below, we will see that displacement noise, such as mirror thermal noise, scale as \mathcal{N} , so after dividing by the transfer function we get a the signal-to-noise ratio which is independent of \mathcal{F} (but still proportional to $1/L$), so in this case a high finesse does not help to beat it down, and we need a large arm-length L . So, in general we still want to keep L as large as possible, compatibly with technological and financial constraints.

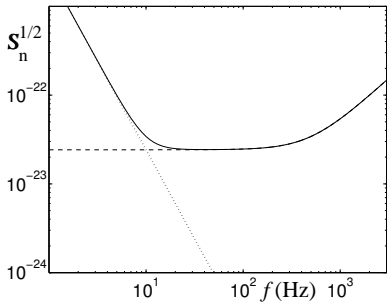


Fig. 9.26 The strain sensitivity $S_n^{1/2}(f)$ (in units $\text{Hz}^{-1/2}$) due to shot noise (dashed), to radiation pressure (dotted) and the total optical read-out noise (solid line). For definiteness, we have used numerical values of the various parameters typical of the initial VIRGO interferometer.

³²We already met a similar situation for resonant bars in Sections 8.3.3 and 8.3.4, where we found that, without quantum non-demolition techniques, the best one can do is to detect vibrations in the bar corresponding to $O(1)$ phonon. We have seen that present bar sensitivities are not that far from this limit.

9.4.3 The standard quantum limit

Consider now the combined effect of shot noise and radiation pressure, that we denote as *optical read-out noise*. Its spectral density is

$$S_n(f)|_{\text{opt}} = S_n(f)|_{\text{shot}} + S_n(f)|_{\text{rad}} . \quad (9.235)$$

A plot of this expression, and of the separate shot noise and radiation pressure contributions, is shown in Fig. 9.26. The shot noise contribution is proportional to $P_{\text{bs}}^{-1/2}$ while the radiation pressure to $P_{\text{bs}}^{1/2}$. We see here the uncertainty principle in action. The situation is conceptually similar to the Heisenberg microscope. We are using photons to measure the position of an object. The photons impart non-deterministically a recoil to the object, here in the form of fluctuations of the radiation pressure, and this recoil disturbs the measure that we are performing. It is amazing that a quantum effect due to the uncertainty principle can be important in the measurement of the position of a macroscopic body, like the mirror of an interferometer, which typically weights $O(20)$ kg. However, for GW detection we need such an extreme accuracy in the determination of the mirror position that, as we will see in this section, the uncertainty principle can indeed become important.³²

Using the explicit expressions and defining

$$f_0 = \frac{8\mathcal{F}}{2\pi} \sqrt{\frac{P_{\text{bs}}}{\pi\lambda_L c M}} , \quad (9.236)$$

eq. (9.235) can be written as

$$S_n^{1/2}(f)|_{\text{opt}} = \frac{1}{L\pi f_0} \sqrt{\frac{\hbar}{M}} \left[\left(1 + \frac{f^2}{f_p^2} \right) + \frac{f_0^4}{f^4} \frac{1}{1 + f^2/f_p^2} \right]^{1/2}. \quad (9.237)$$

For a given value of f we can minimize $S_n^{1/2}(f)|_{\text{opt}}$ with respect to f_0 . (In particular, f_0 is varied changing the power P_{bs} , so this amounts to finding the optimal value of P_{bs} .) The optimal value of f_0 is the one for which the shot noise and radiation pressure contributions are equal, and is given by

$$1 + \frac{f^2}{f_p^2} = \frac{f_0^2}{f^2}. \quad (9.238)$$

The corresponding optimal value of $S_n^{1/2}(f)$ defines the *standard quantum limit* (SQL),

$$S_{\text{SQL}}^{1/2}(f) = \frac{1}{2\pi f L} \sqrt{\frac{8\hbar}{M}}. \quad (9.239)$$

It should be stressed that $S_{\text{SQL}}(f)$, even if written as a function of f , cannot be interpreted as the minimum noise spectral density that can be reached with this type of optical read-out. In fact, the value of f_0 , i.e. of the laser power, has been optimized keeping fixed the value of f . It therefore represents the minimum value of the spectral density which can be obtained (as long as only optical read-out noise is concerned) at that value of f . Once we have chosen the power so to optimize the sensitivity at a given frequency f , at all other values of the frequency we are not in the optimal situation, and the strain sensitivity is higher than the standard quantum limit. So, eq. (9.239) rather gives the envelope of the minima of the family of functions $S_n^{1/2}(f; f_0)|_{\text{opt}}$, parametrized by f_0 , as shown in Fig. 9.27. (For this reason, it is called a “pseudo-spectral density”.)

It is useful to define the dimensionless quantity

$$\mathcal{K}(f) \equiv \frac{8\omega_L P_{\text{bs}}}{ML^2} \frac{1}{\omega^2(\omega_p^2 + \omega^2)}, \quad (9.240)$$

where $\omega_p = 2\pi f_p$ and $\omega = 2\pi f$. Then eq. (9.237) can be rewritten as³³

$$S_n(f)|_{\text{opt}} = \frac{1}{2} S_{\text{SQL}}(f) \left[\frac{1}{\mathcal{K}(f)} + \mathcal{K}(f) \right]. \quad (9.241)$$

We have seen that the existence of the limiting value $S_{\text{SQL}}(f)$ is a manifestation of the Heisenberg uncertainty principle. However the uncertainty principle does not put a limit on the accuracy of measurements of position, but only on the accuracy of simultaneous measurements of conjugate variables, and it is possible to go beyond the standard quantum

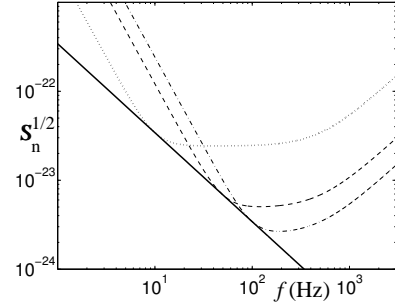


Fig. 9.27 The optical read-out strain sensitivity $S_n^{1/2}(f)|_{\text{opt}}$ (in units $\text{Hz}^{-1/2}$) for $f_0 = 10$ Hz (dotted line), $f_0 = 50$ Hz (dashed line) and $f_0 = 100$ Hz (dot-dashed line), compared to the SQL pseudo-spectral density (solid line). The other parameters are $L = 3$ km, $M = 20.3$ kg, $f_p = 500$ Hz.

³³This result can also be obtained with an elegant formalism, in which radiation pressure and shot noise are related to the quantum vacuum fluctuations entering the interferometer from the output port, see Kimble, Levin, Matsko, Thorne and Vyatchanin (2000). The quantity that we denote by ω_p corresponds to γ in this reference. More precisely, $\gamma = ct_1^2/(4L)$, where t_1 is the transmissivity of the first mirror. In our computation we have assumed negligible losses, so $t_1^2 = 1 - r_1^2$, and r_1, r_2 close to one, so $\gamma \simeq \pi c/(2L\mathcal{F})$. Observe also that we have set to one the efficiency η of the photodiode and we have neglected the effect of light modulation. For instance, in the present configuration of VIRGO, this results in the replacement $1/\mathcal{K}(f) \rightarrow 3/[2\eta\mathcal{K}(f)]$ in the first term of eq. (9.241). Different modulation schemes can give rise to different numerical factor for this shot noise term.

limit using quantum non-demolition (QND) techniques. The general principles of QND measurements have already been presented in Section 8.3.4. We refer the reader to the Further Reading section for the application of these techniques to GW interferometers. These techniques can become important for advanced interferometers.

9.4.4 Displacement noise

The optical read-out noise discussed above is intrinsic to the way that we use to detect the displacement of the test masses induced by GWs, using a laser beam that bounces between them. Of course, the test masses also move because of many other effects that have nothing to do with GWs. We generically denote all these other effects as “displacement noise”, and we characterize them with a strain spectral density of the displacement $S_x^{1/2}(f)$, that we denote simply as $x(f)$.

Recall that the effect of a GW on the length L of a FP cavity is to change it by the amount $\Delta L = hL$ (as long as $\omega_{\text{gw}}L/c \ll 1$, i.e. as long as eq. (9.124) holds). Thus, if the length of the cavity changes by an amount Δx because of one of these displacement noise, the corresponding equivalent GW amplitude is $\Delta x/L$. So, to refer the noise at the detector input (i.e. to compute the equivalent GW that would induce the same phase shift), we must divide the strain sensitivity of the displacement by the arm-length L . The finesse of the cavity, or equivalently the number of bounces \mathcal{N} performed by the laser beam inside the FP cavity, does not enter here. This can also be understood in terms of the phase shift $\Delta\phi_{\text{FP}}$, observing that the phase shift induced by a GW and that induced by the displacement noise of a mirror are both multiplied by the number of bounces of the light inside the cavity, so when we refer the noise to the detector input the factor \mathcal{N} cancels.

The computation of these displacement noise depends on many technical issues such as properties of materials, details of the suspension mechanisms, etc. and a complete discussion is beyond the scope of this book. We limit ourselves to mentioning the most important displacement noise below. Graphs showing their separate effect on the strain sensitivity are shown in Section 9.5 below, in Fig. 9.31 for VIRGO and in Fig. 9.32 for LIGO.

³⁴This background originates mostly from atmospheric cyclonic systems over the oceans. Energy is transferred from the atmosphere to the ocean, and then to the ocean floor. From there it is transmitted through the crust for long distances, $O(10^3)$ km, mostly in the form of surface waves. Its amplitude presents a peak corresponding to the period of the ocean waves (12 s) and another one at twice this frequency, and decreases as a power law at higher frequencies. Near the coast, there is also a contribution from sea waves breaking on the shore.

Seismic and Newtonian noise

The Earth’s ground is in continual motion, with amplitudes of order a few microns. In the region 1–10 Hz this is mostly due to human activity such as local traffic, trains, etc. as well as to local phenomena such as winds. Furthermore, there is a micro-seismic background, which affects a GW interferometer mostly in the form of surface waves that shake the suspension mechanisms and, finally, the mirrors.³⁴ Its strain sensitivity has in general the form

$$x(f) \simeq A \left(\frac{1 \text{ Hz}}{f^\nu} \right) \text{ m Hz}^{-1/2}, \quad (9.242)$$

where (above about 1 Hz) the index $\nu \simeq 2$ while, at a typical quiet location, A can be of order 10^{-7} . Dividing $x(f)$ by the length $L = 3\text{--}4$ km, we are left with a noise strain sensitivity at least 10 orders of magnitude larger than the values at which we are aiming. The seismic noise must therefore be attenuated by a huge factor. This is in general obtained with a set of pendulums in cascade.³⁵ A single pendulum with resonance frequency f_0 , at frequencies $f \gg f_0$ attenuates the strain sensitivity $x(f)$ by a factor f_0^2/f^2 , and a multistage filter made by N stages provides an attenuation factor $(f_0^2/f^2)^N$. Therefore one must choose f_0 much smaller than the GW frequency of interest. In practice, this means that the seismic noise can be reduced below a level interesting for GW detection only at frequencies above, say, 10 Hz. This is the main reason while a ground-based interferometer cannot search for GWs below the ~ 10 Hz region.

Newtonian noise, also known as “gravity gradient noise”, is due to the Newtonian gravitational forces of objects that are moving, which results in a time-varying gravitational force.³⁶ The most important Newtonian effect is induced by micro-seismic noise, which produce mass density fluctuations and therefore a fluctuation of the gravitational field of the Earth, which couples directly to the test masses of the interferometer. One can get a feeling for the extreme sensitivity of a GW interferometer, when one realizes that even the changing gravitational attraction due to atmospheric turbulence gives a non-negligible contribution to the Newtonian noise below $O(1)$ Hz.

While the seismic noise can be attenuated arbitrarily (at least in principle, if one were able to build an arbitrarily good attenuator), the Newtonian noise cannot be eliminated, since the gravitational force cannot be screened. In present GW interferometers the Newtonian noise is not the dominant effect (below a few Hz it is overwhelmed by the seismic noise and above a few Hz by the pendulum thermal noise, see Fig. 9.31). However, even if one were able to push further down the seismic and thermal noise, which in principle can be done with technological improvements, still one would remain with the Newtonian noise which, for a ground-based detector, would anyway provide the ultimate limitation at low frequencies (although some noise reduction might be possible monitoring it with a complex network of accelerometers, and then subtracting it).

Thermal noise

Thermal noise induce vibrations both in the mirrors and in the suspensions. As discussed in Section 8.3.1, its effect can be computed using the fluctuation–dissipation theorem. We saw that, for a linear system subject to a force F , we can always write the equation of motion in the form

$$\tilde{F}(\omega) = -i\omega Z(\omega)\tilde{x}(\omega), \quad (9.243)$$

where $Z(\omega)$ is called the impedance. The fluctuation–dissipation theorem gives the spectral density of the force responsible for thermal fluc-

³⁵Such an attenuation system is in itself a remarkable technological achievement. In particular, the VIRGO superattenuator, made of 8 m tall towers, is the most performing device of this kind ever built. The construction of these towers also present non-trivial problems in material science. To get a feeling for the kind of issues involved, consider that the slippage of two grains of steel under stress releases an energy sufficient to shake the mirror at the level of 10^{-12} m, about a million times larger than the expected GW signal.

³⁶Obviously, these are quasi-static gravitational fields in the near region of their sources, and are distinct from GWs, that are time-varying gravitational fields in the far region of their sources.

tuations, $S_F(\omega)$, in terms of the real part of Z , see eq. (8.125). The displacement spectral density is then given by eq. (8.128), that we write as

$$x(\omega) = \frac{1}{\omega|Z(\omega)|} [4kT \operatorname{Re} Z(\omega)]^{1/2}. \quad (9.244)$$

Therefore, $x(\omega)$ is known once we have $Z(\omega)$. This has the great advantage that we do not need to have a detailed microscopic model of the dissipation mechanism. For a simple damped harmonic oscillator, $Z(\omega)$ is given by eq. (8.126). For a more complex extended object, the impedance associated to a normal mode with frequency ω_0 can be modeled more generally as

$$Z = -\frac{im}{\omega} [\omega^2 - \omega_0^2 + i\omega^2\phi(\omega)], \quad (9.245)$$

where the dimensionless function $\phi(\omega)$ is called the loss angle. The most important thermal noise are the following.

Suspension thermal noise. Any vibration induced in the suspension of the test masses results in a displacement noise. In particular, we have

- Pendulum thermal fluctuations. These are thermal fluctuations that induce a swinging motion in the suspensions, and therefore a horizontal displacement of the mirrors. In the present detectors this noise is the dominant one between a few Hz and $O(50)$ Hz, see Fig. 9.31.
- Vertical thermal fluctuations. Thermal noise induce also a vertical motion of the suspensions. In a GW interferometer, we are only interested in the horizontal distance between the mirrors. However, because of the curvature of the Earth, the direction of the vertical at the two mirror locations, which are separated by a distance $L = 3\text{--}4$ km, is not the same. This results in a vertical–horizontal coupling of the order of the angle $\theta = L/(2R_{\oplus}) \simeq 2 \times 10^{-4}$.
- Violin modes. These are vibrations that can be described in terms of fluctuations of the normal modes of the wire. They are responsible for the set of spikes between 300 Hz and a few kHz in Fig. 9.31. The width of these resonances is however very narrow, so they affect the sensitivity only in very small intervals of frequencies.

Test-mass thermal noise. These are thermal fluctuations within the test masses themselves. We can distinguish the following effects.

- Brownian motion of the mirrors. The atoms of a mirror at temperature T have a Brownian motion due to their kinetic energy, which gives rise to mirror thermal noise. Just as with the violin modes, its effect can be computed performing a normal-mode decomposition. This is presently the dominant noise between a few tens and a few hundred Hz, see Fig. 9.31.

- Thermo-elastic fluctuations. These are due to the fact that, in a finite volume V , the temperature fluctuates, with a variance $(\delta T)^2 = k_B T^2 / (\rho C_V V)$, where C_V is the specific heat and ρ the density of the material. These temperature fluctuations generate displacement noise through the expansion of the material. Thermo-elastic fluctuations take place both in the mirror bulk and in the mirror coatings.
- Thermo-refractive fluctuations. The refraction index of the coatings is a function of the temperature. Thus, the same temperature fluctuations responsible for the thermo-elastic noise also induce fluctuations in the refraction index of the mirrors.

Of course, thermal noise is proportional to the dissipations present in the system, which depend strongly on the material used, and therefore there is an ongoing search for materials with optimal properties.

Other noise

Beside read-out and displacement noise, other noise are relevant, and keeping them under control require advanced technologies. We mention some of them, to give a feeling for the complexity of a GW interferometer.

- The laser beam must travel in a ultra-high vacuum pipe, in order to keep the noise induced by fluctuations in the index of refraction below the design sensitivity. For the initial interferometers the pressure must be lower than 10^{-7} mbar while, for advanced interferometers, it must be lower than 10^{-9} mbar.³⁷ Furthermore, the residual gas must be free of condensable organic molecules (hydrocarbons), in order to keep the optical surfaces clean. It is estimated that a hydrocarbon partial pressure of 10^{-13} mbar is required if one wants to avoid the cumulative deposition of one monolayer of molecules on the optical elements in 4 years.
- To limit diffuse light scattering in the interferometer, the mirrors are polished to a rms micro-roughness of about 0.5\AA , over a diameter of order 20 cm, and have losses of order a few parts per million.³⁸
- Fluctuations of the laser in power and in frequency must be kept under control to great accuracy.
- Other important concerns are so-called technical noise, often related to the servo loops that keep the many degrees of freedom of an interferometer under control.
- Seismic noise can be reinjected in the detector because the enclosure walls couple to the mirror magnets both directly, because of diamagnetism, and through eddy currents.
- The suspension wires undergo creep, i.e. sudden grain-boundaries slipping, which at this sensitivity level are so frequent that they finally constitute a Gaussian noise.

³⁷These vacuum tubes have a diameter of about 1.2 m in order to contain the diffraction-limited laser beam, and a 3- or 4-km length, resulting in a total high-vacuum volume of about 9000 m³. For comparison, this is much larger than the vacuum volume of the LEP particle accelerator, where the ring is almost 27 kms in length, but the transverse section of the vacuum pipe was an ellipse with semiaxes of about 6 cm and 3 cm, respectively.

³⁸Nevertheless, the remaining diffused light still generates important noise because it can interact with the pipe walls, thereby getting modulated by its seismic noise, and then it can be re-diffused back in the beam by reflection on a mirror. Even if only a few parts per million of the circulating light is diffused, an unacceptably high noise results. For this reason, in each of the 3 km arms of VIRGO have been mounted about 100 circular rings, obtained from a conical surface, that trap and absorb most of the residual diffused light.

- Non-Gaussian noise is also present. For instance, the release of residual gas pockets from the tube walls can generate sudden bursts.

So, many subtle effects can become important at the sensitivity level at which a GW interferometer aims. In spite of the apparent simplicity of the original idea, a GW interferometer is clearly a very complex instrument.

9.5 Existing and planned detectors

9.5.1 Initial interferometers

At time of writing (2007) there are various collaborations running GW interferometers. In the US, the LIGO collaboration runs two interferometers with arms of 4 km, one in Hanford (Washington State) and one in Livingstone (Louisiana). The two detectors have been placed at a large distance (the light travel time between them is about 10 ms), so that their noise should be uncorrelated, and are used to search for coincidences. In the Hanford site there is also a second smaller interferometer, with 2 km arms, in the same vacuum system. While of course there will be correlated noise between the shorter and the longer interferometer, still the presence of the smaller interferometer gives a further handle that helps discriminating real signals from spurious noise, making use of the fact that many common noise in the two detectors are independent of L , while the effect of the GW scales with L . A view of the Hanford detector is shown in Fig. 9.28. The scientists collaborating to the project are members of the LIGO Scientific Community (LSC).

The VIRGO interferometer, located near Pisa, Italy, is a collaboration between Italy and France, and has arms of 3 km. A view of the detector is shown in Fig. 9.29.

Beside these large GW interferometers, there are two smaller ones: GEO600, with arms of 600 m, is located near Hannover and is a German-British collaboration. GEO600 works in close collaboration with LIGO, and its members are also members of the LSC. TAMA is located in Tokyo, and has arms of 300 m. These smaller detectors are useful also for developing techniques that will be used by LIGO and VIRGO in their advanced stage.

In Fig. 9.30 we show a simplified model of the strain sensitivity of these detectors, in their initial stage. The best sensitivities are reached by the two detectors with longer arms, LIGO and VIRGO. In the low-frequency regime, the dominant noise is the seismic. For LIGO and GEO this results in a “seismic wall” below about 30–40 Hz. VIRGO has developed an advanced super-attenuator, so its target sensitivity is better at low frequencies. In the intermediate region the dominant noise is the mirror thermal noise. In this region GEO600 compensates the smaller arm length using fused silica suspensions, an advanced technique that reduces suspension thermal noise, and that will be adopted in advanced



Fig. 9.28 A view of the LIGO detector in Hanford, Washington State. (Courtesy of the LIGO collaboration.)



Fig. 9.29 A view of the VIRGO interferometer in Cascina, near Pisa. (Courtesy of the VIRGO collaboration.)

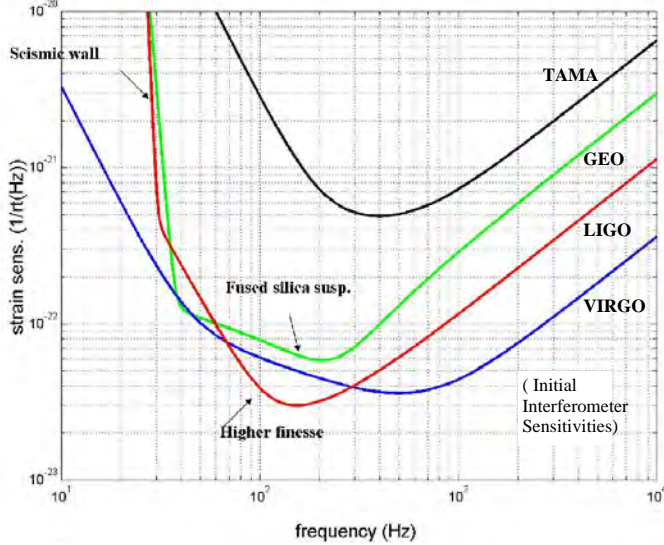


Fig. 9.30 A simplified model of the strain sensitivities of the initial interferometers.

interferometers. Then, shot noise takes over and becomes the limiting noise at high frequencies. In this regime, the difference between the sensitivities of LIGO and VIRGO is due to the fact that LIGO has longer arms (4 km instead of 3 km for VIRGO) and a higher finesse ($\mathcal{F} = 200$ for LIGO and $\mathcal{F} = 50$ for VIRGO). On the one hand this means that, at $f \ll f_{\text{pole}}$, the shot noise of LIGO is smaller than that of VIRGO, see eq. (9.220), which helps to give a better sensitivity in the 100 Hz region. On the other hand, we see from eq. (9.88) that the pole frequency of LIGO is smaller, $f_p \simeq 90$ Hz for LIGO and $f_p \simeq 500$ Hz for VIRGO. This means that in LIGO the shot noise curve begins to raise linearly earlier, so it finally get higher than in VIRGO.

A more accurate plot of the sensitivity, including the separate contributions from the various noise sources, is shown in Fig. 9.31 for VIRGO, while actual data from LIGO are shown in Fig. 9.32, and in Fig. 9.33 for GEO.³⁹

Once we have the strain sensitivity, the signal-to-noise ratio of GW interferometers for different type of signals (coalescences, bursts, periodic signals and stochastic backgrounds) can be computed using the results of Chapter 7, similarly to what we did in Section 8.3.5 for resonant bars.

For a broadband GW detector such as an interferometer, a useful measure of the sensitivity is given in terms of the sight distance to coalescing binaries, that we introduced in Section 7.7.2. Inserting in eq. (7.182) the strain sensitivity of the initial LIGO and VIRGO one finds that, for a NS-NS binary, with NS masses $m_1 = m_2 = 1.4M_\odot$, initial interferometers have a range

$$d_{\text{NS-NS}} = O(20) \text{ Mpc}, \quad (9.246)$$

³⁹At time of writing (2007) initial LIGO has reached its target sensitivity and is completing a long science run, termed S5, with one year of coincident data between its detectors. As shown in Fig. 9.32, the noise budget is very well understood, and reproduces precisely the theoretical curves. VIRGO is presently close to reaching its target sensitivity, and is starting its first science runs. VIRGO and the LSC have signed an agreement for joint data taking and data exchange. The sensitivity of GW interferometers will probably be in rapid evolution in the near future, with various improvements and upgrades leading from the initial detectors to advanced interferometers.

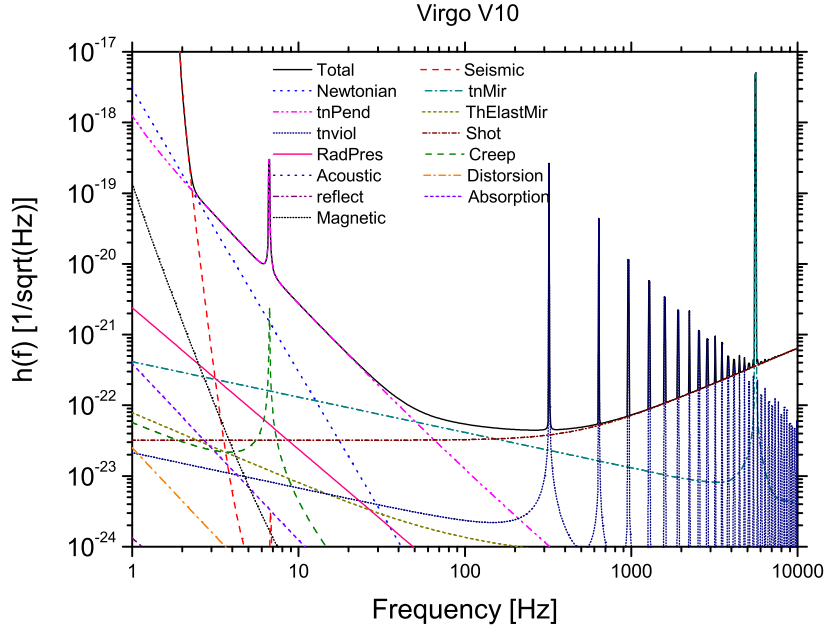


Fig. 9.31 The predicted strain sensitivity $S_n^{1/2}(f)$ (here denoted $h(f)$) of the initial VIRGO detector, and the various noise contributions. (Courtesy of the VIRGO collaboration.)

which barely includes the Virgo cluster of galaxies. For BH-BH binaries, assuming a black-hole mass of $10M_\odot$, as suggested by the observation of typical stellar-mass galactic black holes, gives a sight distance at initial interferometers

$$d_{\text{BH-BH}} = O(100) \text{ Mpc}. \quad (9.247)$$

Estimates of the rate are uncertain and will be discussed in detail in Vol. 2, where we will see that, if our theoretical understanding of the formation and evolution of compact binaries is correct, at these distances the chances of a detection are small, with $O(10^{-4})$ – $O(10^{-1})$ events per year for BH-BH coalescences, and $O(10^{-3})$ – $O(10^{-2})$ for NS-NS binaries. We will see however in Section 9.5.2 that these rates improves drastically for advanced interferometer.

For burst searches, the sensitivity of a broadband detector depends strongly on where, in frequency, the burst is peaked, and on its temporal duration. Assuming for definiteness a flat spectrum over the frequency bandwidth, a burst that radiates an energy $10^{-6}M_\odot c^2$ in GWs would be visible, at SNR = 8 and assuming optimal orientation, up to $O(10)$ kpc.

For spinning pulsars, the sight distance is obtained from eq. (7.166) as a function of the ellipticity ϵ and of its frequency f_0 .

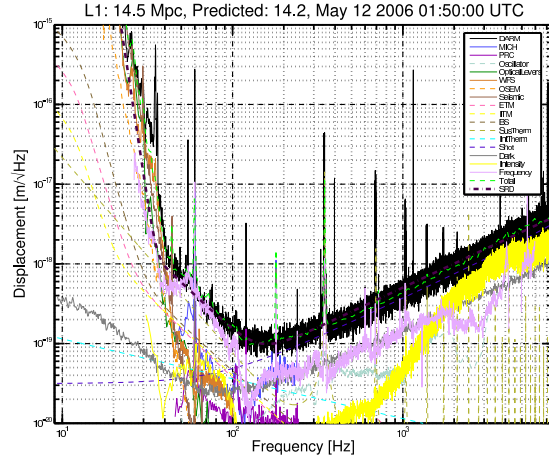


Fig. 9.32 The strain sensitivity, in $\text{m}/\sqrt{\text{Hz}}$, of the LIGO detector in Livingston. The strain sensitivity in $\text{Hz}^{-1/2}$ is obtained dividing by the arm length $L = 4000$ m. The noise budget is very well understood. (Courtesy of the LIGO collaboration.)

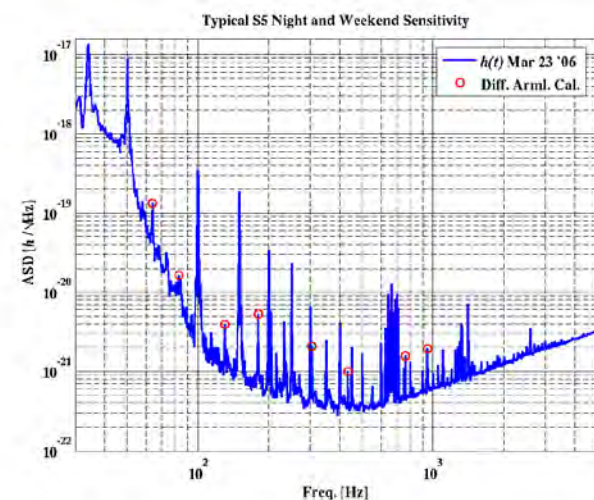


Fig. 9.33 The strain sensitivity, in $1/\sqrt{\text{Hz}}$, of the GEO detector during the S5 run. (Courtesy of the GEO collaboration.)

9.5.2 Advanced interferometers

Ground-based detectors

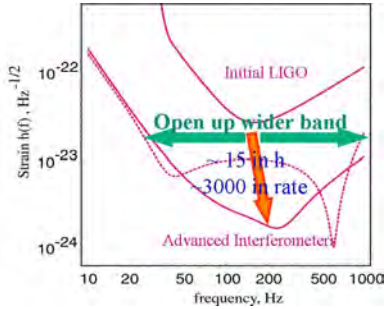


Fig. 9.34 The planned sensitivity of Advanced LIGO compared to initial LIGO. A wideband and a narrow-band configuration are shown. (Courtesy of the LIGO collaboration.)

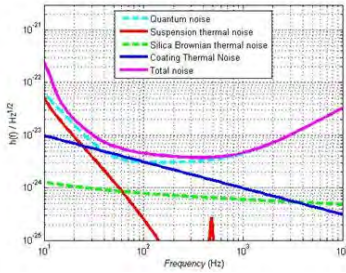


Fig. 9.35 The main noise contributions in a possible Advanced LIGO configuration. (Courtesy of the LIGO collaboration.)

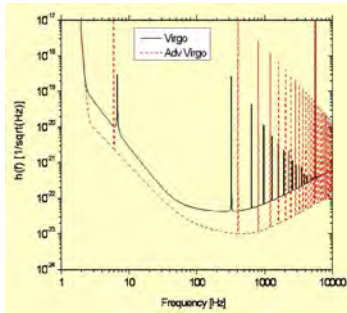


Fig. 9.36 A possible sensitivity curve of Advanced Virgo, compared to the initial Virgo. (Courtesy of the VIRGO collaboration.)

For the LIGO and VIRGO interferometers there is a well-defined plan for upgrades which should lead, in a few years, to second-generation detectors with much better sensitivities, Advanced LIGO (to which will contribute also GEO600 and the Australian consortium ACIGA) and Advanced VIRGO. GEO600 should evolve into a tunable narrow-band detector in the high-frequency region (GEO-HF), and in a facility for testing technologies for future interferometers. A cryogenic detector, LCGT, is under study in Japan, and there are plans for an interferometer in Australia, AIGO. Examples of planned sensitivities are shown in Figs. 9.34–9.36.

While a number of details might still change, the baseline for the main improvements that are planned is the following.

- An increase in the input laser power from the present value of order 10–20 W up to 100–200 W. After power recycling, this would lead to a laser power in the Fabry–Perot arm cavities of order 1 MW. This has the effect of reducing the shot noise, improving the sensitivity in the high-frequency region. Such a huge power will however induce thermal lensing in the test mass optics, due to absorption in the substrate and coatings, and compensation effects will be added.
- As discussed in Section 9.4.2, the increased laser power will produce a larger radiation pressure noise, up to the point that this becomes a dominant noise at low frequency. This is compensated increasing the mirror masses, up to about 40 kg.
- LIGO will introduce much better seismic isolation, improving the sensitivity at low frequencies and bringing the “seismic wall” from 40 Hz down to about 10 Hz. VIRGO already has a seismic isolation appropriate for an advanced interferometer.
- The test-mass suspensions, presently made of steel wires, will be replaced by silica (which has lower losses), fused to the mirror with silicate bonding to create a single monolithic object, thereby reducing suspension thermal noise. This technique has already been developed in GEO600. Further improvement can be obtained shaping the suspension fibers in the form of a ribbon. The resulting suspension thermal noise will be lower than the radiation pressure noise (in broad-band observation mode, see below), and comparable to the Newtonian background at 10 Hz.
- New mirror coatings, with lower thermal noise and lower losses (e.g. thanks to the insertion of dopants) are investigated.

The basic optical configuration is still a power-recycled interferometer with Fabry–Perot cavities in the arms. To this configuration is added *signal recycling*. This consists of adding a new mirror, the signal-recycling mirror, at the output port of the interferometer, i.e. between the beam-splitter and the photodetectors in Fig. 9.25. As in our discussion of the

power recycling cavity, the addition of this mirror creates a new cavity, the signal-recycling cavity, composed by the “effective interferometer mirror” and the signal-recycling mirror.

Recall from Section 9.2.2 that a GW of frequency ω_{gw} generates in the interferometer sidebands at $\omega_L \pm \omega_{\text{gw}}$. If the signal-recycling cavity is tuned in resonance with a sideband corresponding to some given value of ω_{gw} , the sensitivity of the interferometer for this GW frequency is enhanced, at the cost of the bandwidth. This enhancement depends on the finesse of the signal-recycling cavity. If the signal-recycling cavity is tuned to anti-resonance, the sidebands are extracted and the bandwidth of the detector is increased, with respect to the case where no signal-recycling cavity is present. This technique is known as *resonant sideband extraction*. As a result, with tiny adjustments of the position of the signal-recycling mirror, of order of fractions of λ_L , we can either tune the interferometer to some specific source or increase the bandwidth. These two options are illustrated in Fig. 9.34. The signal-recycling technique is already implemented in GEO600, although without Fabry–Perot cavities in the arms.

Thanks to these and to other improvements, an advanced interferometer in wideband mode will be limited, over a bandwidth from about 10 Hz to a few kHz, mostly by the optical read-out noise, as we see from Fig. 9.35, and therefore by the quantum limit. In the signal-recycling configuration it is however possible to perform quantum non-demolition measurements, hence going beyond the standard quantum limit, with a simple modification of the input–output optics, see Fig. 9.37 and the papers by Buonanno and Chen in the Further Reading section.

With the strain sensitivity of an advanced interferometer, the perspective for detection and for opening the field of GW astrophysics are quite good. A detailed discussion of the sources and their strength will be the subject of Vol. 2. Here we observe that the sight distance to NS-NS binaries becomes

$$d_{\text{NS-NS}} = O(300) \text{ Mpc}. \quad (9.248)$$

At this distance, the expected rate is between $O(10)$ per year and $O(100)$ per year. For BH-BH with masses $10M_\odot$, the sight distance becomes

$$d_{\text{BH-BH}} = O(1.5) \text{ Gpc}, \quad (9.249)$$

and expected rates are between one signal per year and $O(500)$ per year.⁴⁰ For BH-NS binaries,

$$d_{\text{BH-NS}} = O(750) \text{ Mpc}, \quad (9.250)$$

with an expected rate between one signal per year and $O(30)$ per year.

Looking further ahead, there are ideas for “third generation” interferometers. Among the features that are being considered, is the possibility of building an underground detector. As discussed in Section 9.4.4 (compare with Note 34 on page 524) the micro-seismic noise is mostly propagated through surface waves, so underground it is sensibly reduced, which also results in a reduction of the Newtonian noise induced by the

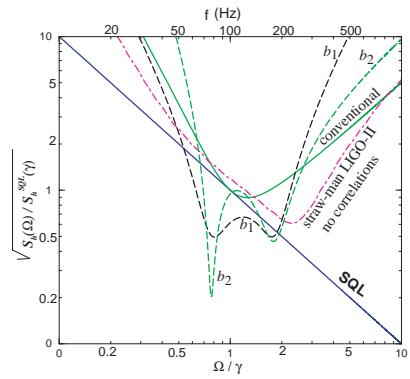


Fig. 9.37 Plot of $\sqrt{S_n(\Omega)/S_n^{\text{SQL}}(\gamma)}$ (where $\Omega = 2\pi f$ and $\gamma = 2\pi f_{\text{pole}}$) as a function of Ω/γ , for different optical configurations. Reprinted with permission from Buonanno and Chen, *Class. Quantum Grav.* **18** L95 (2001b).

⁴⁰A major source of theoretical uncertainty is related to the fact that the potential progenitors of a BH-BH system can go through a phase of common envelope evolution, that can lead to the merging of the progenitor stars rather than to the formation of a BH-BH binary. See Belczynski, Taam, Kalogera, Rasio and Bulik (2006) for a discussion of these rates and of their theoretical uncertainties.

micro-seismic motion. Another third-generation feature could be the use of cryogeny. A Japanese collaboration, building on the experience gained with TAMA, has proposed the realization of the LCGT detector, made of two independent underground interferometers in the same vacuum system, with 3 kms arms and cryogenic mirrors, cooled at 20 K, to be located at Kamioka, an old mine transformed in an underground physics laboratory. This site is about 1000 m below the top of a mountain, and provides a very stable seismic and temperature environment. A prototype, CLIO, has already been installed and is under development.

Interferometers in space

The region below about 10 Hz is unaccessible to ground-based interferometers, because of the wall due to seismic and Newtonian noise. Still, we will see in Vol. 2 that the mHz region is potentially very rich in GW sources, including particularly fascinating objects such as supermassive black holes. The only way to detect them is to go in space, where the seismic noise is absent. One such project is LISA. The LISA mission is a collaboration between the European Space Agency (ESA) and NASA. The concept of the LISA mission is quite impressive. It consists of three spacecrafts, separated by 5 million kms, in a equilateral triangle configuration, orbiting the Sun. The center of the triangle should be at a distance of about 50 million kms (i.e. about 20° degrees along the orbit) behind the Earth. The size of the arms is chosen to optimize the sensitivity for GWs in the 10 mHz region, and in general LISA would be sensitive to GW frequencies in the range 0.1 mHz–0.1 Hz.

For a detailed description of the mission concept we refer the reader to the Further Reading section. Here we briefly mention some aspects of this remarkable experiment.

- Inside each spacecraft there will be two test masses (one for each arm), freely floating. The spacecraft is kept centered on the test masses using a *drag free* technique, in which the position of the masses is sensed, and the spacecraft adjusts its position with respect to them, using micro-thrusters. The thrusts necessary to maintain drag-free operation are extremely small, less than $100 \mu\text{N}$, and the required recoil is obtained emitting in space just a handful of fast ions. This compensates for external influences such as solar winds, micro-meteorites, etc. that in the long term would sensibly alter the nominal position of the spacecraft. The LISA Pathfinder is a ESA mission to demonstrate the drag-free control technique at the required accuracy.
- The free masses exchange among them laser signals. Over a distance of 5 million kms, reflection is impossible because of power losses due to diffraction; after a travel of 5 million kms, the laser beam is spread over a surface of radius 20 kms. So LISA uses a laser transponding scheme in which the incoming laser light is sensed, and another laser is phase-locked to it and sends back another beam.

- LISA has unequal arms, with arm-lengths known to ± 20 m from the measurement of the round-trip time. Then, contrary to what happens in a Michelson interferometer with equal arms, laser frequency fluctuations do not cancel out when taking the difference between two arms. For this reason, the LISA concept uses time-delay interferometry, in which the outputs of the two arms are recombined with a time delay that takes care of the arm difference. In the process, laser frequency noise is canceled (while the signal from GWs with frequencies in the mHz region is unaffected).
- After minimizing spurious forces on test masses, the other most important issue is the need to keep the temperature distribution in the spacecraft as constant as possible, since the mass displacements due local temperature fluctuations would induce changes in the Newtonian gravitational forces on the test mass, as well as accelerations of the test masses due to thermal radiation pressure.

Clearly, LISA would be an extremely impressive instrument and its scientific achievements could be truly spectacular.

A number of other space missions are currently discussed, such as DECIGO, a Japanese space project with arm-lengths shorter than LISA, to bridge the gap between LISA and the ground-based detectors; and ASTROD, a Chinese space project with arm-lengths longer than LISA which, among other relativity experiments, would extend the search for GWs to lower frequencies. Follows-up to the LISA mission, such as the Big-Bang Observer (BBO), are also being investigated.

Further reading

- For a lively discussion of the history of gravitational-wave research, as well as the development of GW interferometers, see the popular book Thorne (1994). See also the review Thorne (1987).
- A textbook devoted to the interferometric detection of GWs is Saulson (1994). For reviews, see also Giazotto (1989), Drever (1991), and Ju, Blair and Zhao (2000). A large bibliography on GW interferometers can be found in the review by Rowan and Hough (2000).
- A detailed discussion of the optics of GW interferometers is the “VIRGO Physics Book, Optics and related Topic”, available at <http://wwwcascina.virgo.infn.it/vpb/>. The effect of scattered light in interferometers is discussed in Vinet, Vission and Braccini (1996) and Vinet *et al.* (1997). Mesa beams are proposed in Bondarescu and Thorne (2006).
- Computations of the sensitivities to GWs of Fabry–Perot cavities in various configurations can be found in Vinet, Meers, Man and Brillet (1988) and Meers (1988, 1989).
- A pedagogical discussion of lock-in detection is given in Black and Gutenkunst (2003). A nice discussion of null instrument is given in Saulson (1994), Chapter 10. For a discussion of Pound–Drever–Hall locking see Saulson (1994), Section 12.5, and Black (2001). A discussion of the global control of the VIRGO detector can be found in Arnoud *et al.* (2005). For resonant sideband extraction see Mizuno *et al.* (1993).
- Shot noise in modulated interferometers is discussed in Niebauer, Schilling, Danzmann, Rüdiger and Winkler (1991) and Bondu (2003). Radiation pressure is discussed in Edelstein, Hough, Pugh and Martin (1978) and Caves (1980, 1981).

- For quantum non-demolition measurements see Caves, Thorne, Drever, Sandberg and Zimmermann (1980) and Braginsky and Kalili (1992). For application to advanced interferometers see Kimble, Levin, Matsko, Thorne and Vyatchanin (2000) and Buonanno and Chen (2001a, 2001b, 2002). For a review of quantum noise in GW interferometers see Corbitt and Mavalvala (2004).
 - The effect of seismic noise in GW interferometers is discussed in Saulson (1994), Chapter 8. Newtonian noise are studied in Saulson (1984) and Beccaria *et al.* (1998). Our discussion of thermal noise followed the internal VIRGO note Flaminio *et al.* (2005), where calculations of the various thermal noise are performed in detail. Thermo-elastic noise is discussed in Braginsky and Vyatchanin (2003).
 - Updated information on the existing GW inter-
- ferometers, as well as technical documents, PhD theses, etc. can be found at
<http://www.ligo.caltech.edu/> (LIGO)
<http://www.cascina.virgo.infn.it/> (VIRGO)
<http://www.geo600.uni-hannover.de/> (GEO600)
<http://tamago.mtk.nao.ac.jp/> (TAMA)
- A detailed description of the LISA mission can be found in the LISA Pre-Phase A Report (1998). See also the reviews Bender (2001), Danzmann and Rüdiger (2003), and the web site <http://lisa.jpl.nasa.gov>.
 - For lack of space, we have not discussed experiments searching for GWs using the Doppler tracking of spacecraft. For a recent review, see Armstrong (2006).

Bibliography

- Abbott, B. *et al.* [LIGO Science Community, LSC] (2004a). *Phys. Rev. D* **69**, 082004.
- Abbott, B. *et al.* [LSC] (2004b). *Phys. Rev. D* **69**, 102001.
- Abbott, B. *et al.* [LSC] (2004c). *Phys. Rev. D* **69**, 122001.
- Abbott, B. *et al.* [LSC] (2004d). *Phys. Rev. D* **69**, 122004.
- Abbott B. *et al.* [LSC] (2005a). *Phys. Rev. D* **72**, 082001.
- Abbott, B. *et al.* [LSC] (2005b). *Phys. Rev. Lett.* **94**, 181103.
- Abbott, B. *et al.* [LSC] (2005c). *Phys. Rev. Lett.* **95**, 221101.
- Abramowitz, M. and I. A. Stegun (1972). *Handbook of Mathematical Functions*, Dover, New York.
- Aguiar, O. D. *et al.* (2004). *Class. Quant. Grav.* **21**, S457.
- Allen, Z. A. *et al.* [IGEC] (2000). *Phys. Rev. Lett.* **85**, 5046 .
- Allen, B. and J. D. Romano (1999). *Phys. Rev. D* **59**, 102001.
- Anderson, W. G. and R. Balasubramanian (1999). *Phys. Rev. D* **60**, 102001.
- Anderson, W. G., P. R. Brady, J. D. E. Creighton and E. E. Flanagan (2001). *Phys. Rev. D* **63**, 042003.
- de Andrade, V. C., L. Blanchet and G. Faye (2001). *Class. Quant. Grav.* **18**, 753.
- Apostolatos, T. A., C. Cutler, G. J. Sussman and K. S. Thorne (1994). *Phys. Rev. D* **49**, 6274.
- Arnaud, N. *et al.* (2005). *Nucl. Instr. Meth. A* **550**, 467.
- Arnowitt, R., S. Deser and C. W. Misner (1961). *Phys. Rev.* **121**, 1556.
- Arkani-Hamed, N., H. Georgi and M. D. Schwartz (2003). *Ann. Phys.* **305**, 96.
- Arkani-Hamed, N., H. C. Cheng, M. A. Luty and S. Mukohyama (2004). *JHEP* **0405**, 074.
- Armstrong, J. W. (2006). *Living Rev. Relativity* **9**, 1. Online article <http://www.livingreviews.org/lrr-2006-1>.
- Arun, K. G., L. Blanchet, B. R. Iyer and M. S. Qusailah (2004). *Class. Quant. Grav.* **21**, 3771. [Erratum-*ibid.* **22**, (2005) 3115].
- Ashby, N. and J. Dreitlein (1975). *Phys. Rev. D* **12**, 336.
- Astone, P., *et al.* [ROG] (1997b). *Astroparticle Phys.* **7**, 231.
- Astone, P., *et al.* [ROG] (2002). *Phys. Rev. D* **65**, 022001.
- Astone, P., *et al.* [IGEC] (2003a). *Phys. Rev. D* **68**, 022001
- Astone, P., *et al.* [IGEC-2] (2007). arXiv:0705.0688[gr-qc].
- Astone, P., *et al.* [ROG] (2003b). *Phys. Rev. Lett.* **91**, 111101.
- Backer, D. C. and R. W. Hellings (1986). *Ann. Rev. Astron. Astrophys.*

- 24**, 537.
- Bardeen, J. M. and W. H. Press (1973). *J. Math. Phys.* **14**, 7.
- Bassan, M. (2002). In *Proceeding of the 15th International Conference on General Relativity and Gravitation*, M. Francaviglia ed., World Scientific, Singapore.
- Beccaria, M. *et al.* (1998). *Class. Quant. Grav.* **15**, 3339.
- Belczynski, K., R. E. Taam, V. Kalogera, F. A. Rasio and T. Bulik (2006). arXiv:astro-ph/0612032.
- Bender, P. L. (2001). In *Gravitational Waves*, I. Ciufolini *et al.* eds, IoP Publishing, Bristol.
- van den Berg, J. C. ed. (1999). *Wavelets in Physics*. Cambridge University Press, Cambridge.
- Bertotti, B. and A. M. Anile (1973). *Astron. Astrophys.* **28**, 429.
- Bianchi, M., E. Coccia, C. N. Colacino, V. Fafone and F. Fucito (1996). *Class. Quant. Grav.* **13**, 2865.
- Bianchi, M., M. Brunetti, E. Coccia, F. Fucito, and J. A. Lobo (1998). *Phys. Rev. D* **57**, 4525.
- Binney, J. and M. Merrifield (1998). *Galactic Astronomy*. Princeton University Press, Princeton.
- Binney, J. and S. Tremaine (1994). *Galactic Dynamics*. Princeton University Press, Princeton.
- Black E. D. (2001). *Am. J. Phys.* **69**, 79.
- Black E. D. and R. N. Gutenkunst (2003). *Am. J. Phys.* **71**, 365.
- Blair, D., *et al.* (1995). *Phys. Rev. Lett.* **74**, 1908.
- Blanford, R. D. and S. A. Teukolsky (1976). *Astrophys. J.* **205**, 580.
- Blanchet, L. (1987). *Proc. Roy. Soc. Lond. A* **409**, 383.
- Blanchet, L. (1993). *Phys. Rev. D* **47**, 4392.
- Blanchet, L. (1995). *Phys. Rev. D* **51**, 2559.
- Blanchet, L. (1996). *Phys. Rev. D* **54**, 1417.
- Blanchet, L. (1997). *Phys. Rev. D* **55**, 714.
- Blanchet, L. (1998a). *Class. Quant. Grav.* **15**, 89.
- Blanchet, L. (1998b). *Class. Quant. Grav.* **15**, 113.
- Blanchet, L. (1998c). *Class. Quant. Grav.* **15**, 1971.
- Blanchet, L. (2006). *Living Rev. Relativity* **9**, 4. Online article <http://www.livingreviews.org/lrr-2006-4>.
- Blanchet, L. and T. Damour (1986). *Phil. Trans. R. Soc. London* **A320**, 379.
- Blanchet, L. and T. Damour (1988). *Phys. Rev. D* **37**, 1410.
- Blanchet, L. and T. Damour (1989). *Ann. Inst. H. Poincaré* **50**, 377.
- Blanchet, L. and G. Schäfer (1989). *Mon. Not. R. Astron. Soc.* **239**, 845.
- Blanchet, L. and T. Damour (1992). *Phys. Rev. D* **46**, 4304.
- Blanchet, L. and G. Schäfer (1993). *Class. Quant. Grav.* **10**, 2699.
- Blanchet, L., T. Damour and B. R. Iyer (1995). *Phys. Rev. D* **51**, 5360. [Erratum-*ibid. D* **54**, (1996) 1860].
- Blanchet, L. and B. S. Sathyaprakash (1995). *Phys. Rev. Lett.* **74**, 1067.
- Blanchet, L., B. R. Iyer, C. M. Will and A. G. Wiseman (1996). *Class. Quant. Grav.* **13**, 575.

- Blanchet, L., G. Faye and B. Ponsot (1998). *Phys. Rev. D* **58**, 124002.
- Blanchet, L. and G. Faye (2001). *Phys. Rev. D* **63**, 062005.
- Blanchet, L., B. R. Iyer and B. Joguet (2002). *Phys. Rev. D* **65**, 064005. [Erratum-*ibid. D* **71**, 129903 (2005)]
- Blanchet, L., G. Faye, B. R. Iyer and B. Joguet (2002). *Phys. Rev. D* **65**, 061501. [Erratum-*ibid. D* **71**, 129902 (2005)].
- Blanchet L. and B. R. Iyer (2003). *Class. Quant. Grav.* **20**, 755.
- Blanchet, L., T. Damour and G. Esposito-Farèse (2004). *Phys. Rev. D* **69**, 124007.
- Blanchet, L., T. Damour, G. Esposito-Farèse and B. R. Iyer (2004). *Phys. Rev. Lett.* **93**, 091101.
- Blanchet, L., T. Damour, G. Esposito-Farèse and B. R. Iyer (2005). *Phys. Rev. D* **71**, 124004.
- Blanchet, L., G. Faye, and S. Nissanke (2005). *Phys. Rev. D* **72**, 044024.
- Blanchet, L., A. Buonanno and G. Faye (2006). *Phys. Rev. D* **74**, 104034.
- Bonazzola, S. and E. Gourgoulhon (1996). *Astron. Astrophys.* **312**, 675.
- Bondarescu, M. and K. S. Thorne (2006). *Phys. Rev. D* **74**, 082003.
- Bondi, H., M. G. J. van der Burg and A. K. W. Metzner (1962). *Proc. Roy. Soc. London A* **269**, 21.
- Bondu, F. (2003). VIRGO internal note VIR-NOT-OCA-1390-243, unpublished.
- Bontz R.J. and M.P. Haugan (1981). *Astrophysics and Space Science* **78**, 199.
- Boulware, D. G. and S. Deser (1972). *Phys. Rev. D* **6**, 3368.
- Brady, P. R., T. Creighton, C. Cutler and B. F. Schutz (1998). *Phys. Rev. D* **57**, 2101.
- Brady, P. R. and T. Creighton (2000). *Phys. Rev. D* **61**, 082001.
- Braginsky, V. B. and L. P. Grishchuk (1986). *Sov. Phys. JETP* **62**, 427.
- Braginsky, V. B. and K. S. Thorne (1987). *Nature* **327**, 123.
- Braginsky, V. B. and F. Ya. Kalili (1992). *Quantum Measurement*. Cambridge University Press, Cambridge.
- Braginsky, V. B. and S. P. Vyatchanin (2003). *Phys. Lett. A* **312**, 244.
- Briant, T., et al. (2003). *Phys. Rev. D* **67**, 102005.
- Bruhat, Y. (1962). In *Gravitation: An Introduction to Current Research*, L. Witten ed., Wiley, New York.
- Buonanno, A. and Y. B. Chen (2001a). *Phys. Rev. D* **64**, 042006.
- Buonanno, A. and Y. B. Chen (2001b). *Class. Quant. Grav.* **18**, L95.
- Buonanno, A. and Y. B. Chen (2002). *Phys. Rev. D* **65**, 042001.
- Buonanno, A., Y. B. Chen and M. Vallisneri, (2003). *Phys. Rev. D* **67**, 024016.
- Burgay, M. et al. (2003). *Nature*, **426**, 531.
- Burke, W. L. (1971). *J. Math. Phys.* **12**, 401.
- Caves, C. M. (1980). *Phys. Rev. Lett.* **45**, 75.
- Caves, C. M. (1981). *Phys. Rev. D* **23**, 1693.
- Caves, C. M., K. S. Thorne, R. W. P. Drever, V. D. Sandberg, and M. Zimmermann (1980). *Rev. Mod. Phys.* **52**, 341.
- Cerdonio, M. et al. [AURIGA] (1997). *Class. Quant. Grav.* **14**, 1491.

- Cerdonio, M., L. Conti, J. A. Lobo, A. Ortolan and J. P. Zendri (2001). *Phys. Rev. Lett.* **87**, 031101.
- Cerdonio, M. (2003). *Class. Quant. Grav.* **20**, S23.
- Chandrasekhar, S. (1969). *Ellipsoidal Figures of Equilibrium*. Yale University Press, New Haven.
- Chandrasekhar, S. and F. P. Esposito (1970). *Astrophys. J.* **160**, 153.
- Christensen, N. (1992). *Phys. Rev. D* **46**, 5250.
- Christodoulou, D. (1991). *Phys. Rev. Lett.* **67**, 1486.
- Christodoulou, D. and S. Klainerman (1993). *The global nonlinear stability of the Minkowski space*. Princeton University Press, Princeton.
- Clark, J.P.A. and D. M. Eardley (1977). *Astrophys. J.* **215**, 315.
- Coccia, E. (1997). In *Proceeding of the 14th International Conference on General Relativity and Gravitation*, M. Francaviglia ed., World Scientific, Singapore.
- Coccia, E., J. A. Lobo, and J. A. Ortega (1995). *Phys. Rev. D* **52**, 3735.
- Coccia, E. and V. Fafone (1996). *Phys. Lett. A* **213**, 16.
- Coccia, E., V. Fafone, G. Frossati, J. A. Lobo and J. A. Ortega (1998). *Phys. Rev. D* **57**, 2051.
- Coccia, E., F. Dubath and M. Maggiore (2004). *Phys. Rev. D* **70**, 084010.
- Corbitt, T. and N. Mavalvala (2004). *J. Opt. B* **6**, S675.
- Cousins, R. D. (1995). *Am. J. Phys.* **63**, 398.
- Creminelli, P., A. Nicolis, M. Papucci and E. Trincherini (2005). *JHEP* **0509**, 003.
- Cutler, C. et al. (1993). *Phys. Rev. Lett.* **70**, 2984.
- Cutler, C. and E. E. Flanagan (1994). *Phys. Rev. D* **49**, 2658.
- Cutler, C. and D. I. Jones (2001). *Phys. Rev. D* **63**, 024002.
- van Dam, H. and M. Veltman (1970). *Nucl. Phys. B* **22**, 397.
- Damour, T. (1983a). *Phys. Rev. Lett.* **51**, 1019.
- Damour, T. (1983b). In *Gravitational Radiation*, N. Deruelle and T. Piran eds., Les Houches 1982, North-Holland, Amsterdam.
- Damour, T. (1986). In *Proceedings of the 4th Marcel Grossmann Meeting on General Relativity* ed R. Ruffini, North-Holland, Amsterdam.
- Damour, T. (1987). In *300 Years of Gravitation*, S. Hawking and W. Israel eds., Cambridge University Press, Cambridge.
- Damour, T. and N. Deruelle (1981). *Phys. Lett. A* **87**, 81.
- Damour, T. and N. Deruelle (1985). *Ann. Inst. H. Poincaré* **43**, 107.
- Damour, T. and N. Deruelle (1986). *Ann. Inst. H. Poincaré* **44**, 263.
- Damour, T. and G. Schäfer (1988). *Nuovo Cimento B*, **101**, 127.
- Damour, T. and B. R. Iyer (1991a). *Phys. Rev. D* **43**, 3259.
- Damour, T. and B. R. Iyer (1991b). *Ann. Inst. H. Poincaré* **54**, 115.
- Damour, T. and J. H. Taylor (1991). *Astrophys. J.* **366**, 501.
- Damour, T. and J. H. Taylor (1992). *Phys. Rev. D* **45**, 1840.
- Damour, T., P. Jaranowski and G. Schäfer (2000). *Phys. Rev. D* **62**, 021501. [Erratum-ibid. *D* **63**, (2001) 029903].
- Damour, T., P. Jaranowski and G. Schäfer (2001a). *Phys. Rev. D* **63**, 044021. [Erratum-ibid. *D* **66**, (2002) 029901].
- Damour, T., P. Jaranowski and G. Schäfer (2001b). *Phys. Lett.* **513**,

147.

- Damour, T., B. R. Iyer and B. S. Sathyaprakash (2001). *Phys. Rev. D* **63**, 044023. [Erratum-ibid. *D* **72** (2005) 029902].
- Damour, T., I. I. Kogan and A. Papazoglou (2003). *Phys. Rev. D* **67**, 064009.
- Damour, T., A. Gopakumar and B. R. Iyer (2004). *Phys. Rev. D* **70**, 064028.
- Danzmann, K. and A. Rüdiger (2003). *Class. Quant. Grav.* **20**, S1.
- Davies, M. R., R. Ruffini, W. H. Press and R.H. Price (1971). *Phys. Rev. Lett.* **27**, 1466.
- Davies, M. R., R. Ruffini and J. Tiomno (1972). *Phys. Rev. D* **5**, 2932.
- Deffayet, C., G. R. Dvali, G. Gabadadze and A. I. Vainshtein (2002). *Phys. Rev. D* **65**, 044026.
- Detweiler, S. L. and E. Szedenits (1979). *Astrophys. J.* **231**, 211.
- Deser, S. (1970). *Gen. Relativ. Gravit.* **1**, 9.
- DeWitt, B. S. (1967). *Phys. Rev.* **162**, 1239.
- Drever, R. W. P. (1991). In *The Detection of Gravitational Waves*, D. G. Blair ed., Cambridge University Press, Cambridge.
- Dubath, F., S. Foffa, M. A. Gasparini, M. Maggiore and R. Sturani (2005). *Phys. Rev. D* **71**, 124003.
- Dubovski, S.L., P. G. Tinyakov and I. I. Tkachev (2005). *Phys. Rev. Lett.* **94**, 181102.
- Edelstein, W. A., J. Hough, J. R. Pugh and W. Martin (1978). *J. Phys. E* **11**, 710.
- Ehlers, J., A. Rosenblum, J. N. Goldberg and P. Havas (1976). *Astrophys. J.* **208**, L77.
- Einstein, A., L. Infeld and B. Hoffmann (1938). *Ann. Math.* **39**, 65.
- Epstein, R. (1977). *Astrophys. J.* **216**, 92.
- Epstein, R. (1979). *Astrophys. J.* **231**, 644.
- Epstein, R. and R. V. Wagoner (1975). *Astrophys. J.* **197**, 717.
- Faye, G., L. Blanchet and A. Buonanno (2006). *Phys. Rev. D* **74**, 104033.
- Feldman G. J. and R. D. Cousins (1998). *Phys. Rev. D* **57**, 3873.
- Feynman, R. P., F. B. Morinigo, and W. G. Wagner (1995). *Feynman Lectures on Gravitation*, Addison-Wesley, Reading, MA.
- Finn, L. S. (1992). *Phys. Rev. D* **46**, 5236.
- Finn, L. S. and D. F. Chernoff (1993). *Phys. Rev. D* **47**, 2198.
- Finn, L. S. and A. Lazzarini (2001). *Phys. Rev. D* **64**, 082002.
- Finn, L. S. and P. J. Sutton (2002). *Phys. Rev. D* **65**, 044022.
- Flaminio, R. *et al.* (2005). Internal VIRGO note VIR-NOT-DIR-1390-304, unpublished.
- Flanagan, E. E. (1993). *Phys. Rev. D* **48**, 2389.
- Flanagan, E. E. and S. A. Hughes (1998a). *Phys. Rev. D* **57**, 4535.
- Flanagan, E. E. and S. A. Hughes (1998b). *Phys. Rev. D* **57**, 4566.
- Forward, R. (1971). *Gen. Relativ. Gravit.* **2**, 149.
- Giazotto, A. (1989). *Phys. Rept.* **182**, 365.
- Gottardi, L. (2004). *Transducers and low-noise two-stage SQUID amplifiers for the spherical gravitational wave antenna MiniGrail*. PhD

- thesis, Leiden University, Leiden, The Netherlands.
- Gibbons, G. W. and S. W. Hawking (1971). *Phys. Rev. D* **4**, 219.
- Giffard, R. P. (1976). *Phys. Rev. D* **14**, 2478.
- Goldhaber, A. S. and Nieto, M. M. (1974). *Phys. Rev. D* **9**, 1119.
- Goldberger, W. D. and I. Z. Rothstein (2006). *Phys. Rev. D* **73**, 104029.
- Gopakumar, A., B. R. Iyer and S. Iyer (1997). *Phys. Rev. D* **55**, 6030.
- Gopakumar, A. and B. R. Iyer (2002). *Phys. Rev. D* **65**, 084011.
- Gradshteyn I. S. and Ryzhik, I. M. (1980). *Table of Integrals, Series and Products*. Academic Press, London.
- Grisaru, M. T., P. van Nieuwenhuizen, and C. C. Wu (1975). *Phys. Rev. D* **12**, 397.
- Gupta S. N. (1954). *Phys. Rev.* **96**, 1683.
- Gürsel, Y. and M. Tinto (1989). *Phys. Rev. D* **40**, 3884.
- Hamermesh, M. (1962). *Group Theory*. Addison-Wesley, Redwood.
- Hartle, J. B. (2003). *Gravity. An Introduction to Einstein's General Relativity*. Addison Wesley, San Francisco.
- Haugan, M. P. (1985). *Astrophys. J.* **296**, 1.
- Haugan, M. P., S. L. Shapiro, and I. Wasserman (1982). *Astrophys. J.* **257**, 283.
- Hulse, R. A. (1994) *Rev. Mod. Phys.* **66**, 699.
- Hulse, R. A. and J. H. Taylor (1975). *Astrophys. J.* **195**, L51.
- Isaacson, R. A. (1968a). *Phys. Rev.* **166**, 1263.
- Isaacson, R. A. (1968b). *Phys. Rev.* **166**, 1272.
- Iwasaki, Y. (1970). *Phys. Rev. D* **2**, 2255.
- Iyer, B. R. and C. M. Will (1993). *Phys. Rev. Lett.* **70**, 113.
- Iyer, B. R. and C. M. Will (1995). *Phys. Rev. D* **52**, 6882.
- Itoh, Y. (2004). *Phys. Rev. D* **69**, 064018.
- Itoh, Y., Futamase, T. and Asada, H. (2000). *Phys. Rev. D* **62**, 064002.
- Itoh, Y., Futamase, T. and Asada, H. (2001). *Phys. Rev. D* **63**, 064038.
- Itoh, Y. and Futamase, T. (2003). *Phys. Rev. D* **68**, 121501(R).
- Jackson, J. D. (1975). *Classical Electrodynamics*. Wiley, Chichester.
- Jackson, J. D. and L. B. Okun (2001). *Rev. Mod. Phys.* **73**, 663.
- Jaranowski, P. and G. Schäfer (1998). *Phys. Rev. D* **57**, 7274. [Erratum-*ibid. D* **63** (2001) 029902].
- Jaranowski, P. and G. Schäfer (1999). *Phys. Rev. D* **60**, 124003.
- Jaranowski, P. and G. Schäfer (2000). *Ann. Phys.* **9**, 378.
- Johnson, W. W. and S. M. Merkowitz (1993). *Phys. Rev. Lett.* **70**, 2367.
- Johnson, W. W. and S. M. Merkowitz (1997). *Phys. Rev. D* **56**, 7513.
- Ju, L., D. G. Blair and C. Zhao (2000). *Rep. Prog. Phys.* **63**, 1317.
- Kennefick, D. (1994). *Phys. Rev. D* **50**, 3587.
- Kennefick, D. (1997). arXiv:gr-qc/9704002.
- Kennefick, D. (2007). *Traveling at the Speed of Thought*. Princeton University Press, Princeton.
- Kidder, L. E. (1995). *Phys. Rev. D* **52**, 821.
- Kidder, L. E., C. M. Willand and A. G. Wiseman (1993). *Phys. Rev. D* **47**, R4183.
- Klimenko, S., I. Yakushin, M. Rakhmanov and G. Mitselmakher (2004).

- Class. Quant. Grav.* **21**, S1685.
- Klimenko, S. and G. Mitselmakher (2004). *Class. Quant. Grav.* **21**, S1819.
- Kimble, H. J., Y. Levin, A. B. Matsko, K. S. Thorne and S. P. Vyatchanin (2002). *Phys. Rev. D* **65**, 022002.
- Konigsdorffer, C., G. Faye and G. Schäfer (2003). *Phys. Rev. D* **68**, 044004.
- Kolb, E. W. and M. S. Turner (1990). *The Early Universe*, Addison Wesley, Reading, MA.
- Kraichnan, R. H. (1955). *Phys. Rev.* **98**, 1118; *ibid.* **101**, 482.
- Kramer, M. *et al.*, (2005). "Testing GR with the Double pulsar: Recent Results", astro-ph/0503386.
- Kramer, M. *et al.*, (2006). "Tests of general relativity from timing the double pulsar" astro-ph/0609417.
- Krishnan, B. *et al.* (2004). *Phys. Rev. D* **70**, 082001.
- Królak, A., K. D. Kokkotas and G. Schäfer (1995). *Phys. Rev. D* **52**, 2089.
- Landau, L. D. and E. M. Lifshitz (1976). *Course of Theoretical Physics*, Vol. I: *Mechanics*. Pergamon Press, Oxford.
- Landau, L. D. and E. M. Lifshitz (1979). *Course of Theoretical Physics*, Vol. II: *The Classical Theory of Fields*. Pergamon Press, Oxford.
- Landau, L.D. and E. M. Lifshitz (1982). *Course of Theoretical Physics*, Vol. IV (by V.B. Berestetskij, E. M. Lifshitz and L. P. Pitaevskij): *Quantum Electrodynamics*. Pergamon Press, Oxford.
- Landau, L. D. and E. M. Lifshitz (1970). *Course of Theoretical Physics*, Vol. VII: *Theory of Elasticity*. Pergamon Press, Oxford.
- Larson, S. L. and W. A. Hiscock (2000). *Phys. Rev. D* **61**, 104008.
- LISA: Pre-Phase A Report*, MPQ 208, Max-Planck-Institute für Quantenoptik, Garching, Germany.
- Lobo, J. A. (1995). *Phys. Rev. D* **52**, 591.
- Lobo, J. A. (2002). *Class. Quant. Grav.* **19**, 2029.
- Lorimer, D. R. (2005). Living Rev. Relativity **8**, 7. Online article <http://www.livingreviews.org/lrr-2005-7>.
- Love, A. E. H. (1944). *A Treatise on the Mathematical Theory of Elasticity*. Dover, New York.
- Lyne, A. G. *et al.* (2004). *Science*, **303**, 1153.
- Lyne, A. G. and F. Graham-Smith (2005). *Pulsar Astronomy*, 3rd edition, Cambridge University Press, Cambridge.
- Lyons, L. (1986). *Statistics for Nuclear and Particle Physicists*, Cambridge University Press, Cambridge.
- McDonough, R. N. and A. D. Whalen (1995). *Detection of Signals in Noise*, 2nd edition. Academic Press, San Diego.
- Maggiore, M. (2000). *Phys. Rept.* **331**, 283.
- Maggiore, M. (2005). *A Modern Introduction to Quantum Field Theory*. Oxford University Press, Oxford.
- Maggiore, M. and A. Nicolis, (2000). *Phys. Rev. D* **62**, 024004.
- Mauceli, E., *et al.* [ALLEGRO] (1996). *Phys. Rev. D* **54**, 1264.
- Meers, B. J. (1988). *Phys. Rev. D* **38**, 2317.

- Meers, B. J. (1989). *Phys. Lett. A* **142**, 465.
- Merkowitz, S. (1995). *Truncated icosahedral gravitational wave antenna*, PhD Thesis, Louisiana State University, available online at <http://sam.phys.lsu.edu>.
- Merkowitz, S. M. and W. W. Johnson (1995). *Phys. Rev. D* **51**, 2546.
- Michelson, P. F. (1987). *Mon. Not. R. Astron. Soc.* **227**, 933.
- Michelson, P. F. and R. C. Taber (1981). *J. Appl. Phys.* **52**, 4313.
- Michelson, P. F. and R. C. Taber (1984). *Phys. Rev. D* **29**, 2149.
- Misner, C. W., K. S. Thorne and J. A. Wheeler (1973). *Gravitation*, Freeman, New York.
- Mizuno, J. et al. (1993). *Phys. Lett. A* **175**, 273.
- Newman, E. T. and R. Penrose (1968). *Proc. Roy. Soc. London A*, **305**, 175.
- Ni, W.-T. and M. Zimmermann (1978). *Phys. Rev. D* **17**, 1473.
- Niebauer, T.M., R. Schilling, K. Danzmann, A. Rüdiger and W. Winkler (1991). *Phys. Rev. A* **43**, 5022.
- van Nieuwenhuizen, P. (1973). *Phys. Rev. D* **7**, 2300.
- Nissanke, S. and L. Blanchet (2005). *Class. Quant. Grav.* **22**, 1007.
- Ogievetsky, V. I. and I. V. Polubarinov (1965). *Ann. Phys.* **35**, 167.
- Ohanian, H. C. and R. Ruffini (1994). *Gravitation and Spacetime*. Norton, New York.
- Owen, B. J. (1996). *Phys. Rev. D* **53**, 6749.
- Owen, B. J. and B. S. Sathyaprakash (1999). *Phys. Rev. D* **60**, 022002.
- Padmanabhan, T. (2004). arXiv:gr-qc/0409089.
- Paik, H. J. (1976). *J. Appl. Phys.* **47**, 1168.
- Pallottino, G. V. and G. Pizzella (1981). *Nuovo Cim. C* **4**, 237.
- Pallottino, G. V. and G. Pizzella (1984). *Nuovo Cim. C* **7**, 155.
- Pallottino, G. V. and G. Pizzella (1991). In *The Detection of Gravitational Waves*, D. G. Blair ed., Cambridge University Press, Cambridge.
- Pati, M. E. and C. M. Will (2000). *Phys. Rev. D* **62**, 124015.
- Pati, M. E. and C. M. Will (2002). *Phys. Rev. D* **65**, 104008.
- Penrose, R. (1963). *Phys. Rev. Lett.* **10**, 66.
- Penrose, R. (1965). *Proc. Roy. Soc. London A* **284**, 159.
- Peters, P. C. (1964). *Phys. Rev.* **136**, B1224.
- Peters, P. C. and J. Mathews (1963). *Phys. Rev.* **131**, 435.
- Pirani, F. A. E. (1964). In *Lectures on General Relativity*, A. Trautman et al. eds., Prentice-Hall, Englewood Cliffs.
- Poisson, E. (1993). *Phys. Rev. D* **47**, 1497.
- Poisson, E. (1999). arXiv:gr-qc/9912045.
- Poisson, E. and C. M. Will (1995). *Phys. Rev. D* **49**, 848.
- Poujade, O. and L. Blanchet (2002). *Phys. Rev. D* **65**, 124020.
- Price, J. C. (1987). *Phys. Rev. D* **36**, 3555.
- Rendall, A. D. (1992). *Proc. Roy. Soc. London A* **438**, 341.
- Richard J.-P. and W. M. Folkner (1991). In *The Detection of Gravitational Waves*, D. G. Blair ed., Cambridge University Press, Cambridge.
- Rowan, S. and J. Hough, (2000). *Living Rev. Rel.* **3**, 3. Online article

- <http://www.livingreviews.org/lrr-2000-3>.
- Rubakov, V., arXiv:hep-th/0407104.
- Sachs, R. K. (1961). *Proc. Roy. Soc. London A* **264**, 309.
- Sachs, R. K. (1962). *Proc. Roy. Soc. London A* **270**, 103.
- Sasaki, M. (1994). *Prog. Theor. Phys.* **92**, 17.
- Saulson, P. R. (1984). *Phys. Rev. D* **30**, 732.
- Saulson, P. R. (1994). *Fundamentals of Interferometric Gravitational Wave Detectors*, World Scientific, Singapore.
- Schutz, B. F. (1986). *Nature*, **323**, 310.
- Schutz, B. F. (1991). In *The Detection of Gravitational Waves*, D. G. Blair ed., Cambridge University Press, Cambridge.
- Schutz, B. F. and F. Ricci (2001). In *Gravitational Waves*, I. Ciufolini *et al.* eds, IoP Publishing, Bristol.
- Shapiro, S.L. and S.A. Teukolsky (1983). *Black Holes, White Dwarfs and Neutron Stars*, Wiley, New York.
- Smarr, L. (1979). In *Sources of Gravitational Radiation*, ed. L. Smarr. Cambridge University Press, Cambridge.
- Spallicci, A., G. Frossati and A. Królak (1997) *Class. Quant. Grav.* **14**, 577.
- Stairs, I. H. (2003). *Living Rev. Relativity* **6**, 5. Online article <http://www.livingreviews.org/lrr-2003-5>.
- Stairs, I. H., S. E. Thorsett, J. H. Taylor and A. Wolszczan (2002). *Astrophys. J.* **581**, 501.
- Stevenson, T. R. (1997). *Phys. Rev. D* **56**, 564.
- Straumann, N. (2004). *General Relativity. With Applications to Astrophysics*. Springer, Berlin.
- Tagoshi, H. and M. Sasaki (1994). *Prog. Theor. Phys.* **92**, 745.
- Tagoshi, H., A. Ohashi and B. J. Owen (2001). *Phys. Rev. D* **63**, 044006.
- Tanaga, T., H. Tagoshi and M. Sasaki (1996). *Prog. Theor. Phys.* **96**, 1087.
- Taylor, J. H. (1994). *Rev. Mod. Phys.* **66**, 711.
- Taylor, J. H., L. A. Fowler and P. M. McCulloch (1979). *Nature* **277**, 437.
- Taylor, J. H. and J. M. Weisberg (1982). *Astrophys. J.* **253**, 908.
- Taylor, J. H. and J. M. Weisberg (1989). *Astrophys. J.* **345**, 434.
- Thorne, K. S. (1980). *Rev. Mod. Phys.* **52**, 299.
- Thorne, K. S. (1983). In *Gravitational Radiation*, N. Deruelle and T. Piran eds., Les Houches 1982, North-Holland, Amsterdam.
- Thorne, K. S. (1987). In *300 Years of Gravitation*, S. Hawking and W. Israel eds., Cambridge University Press, Cambridge.
- Thorne, K. S. (1992). *Phys. Rev. D* **45**, 520.
- Thorne, K. S. (1994). *Black Holes and Time Warps: Einstein's Outrageous Legacy*, Norton, New York.
- Thorne, K. S. and Y. Gürsel (1983). *Mon. Not. R. Astron. Soc.* **205**, 809.
- Vainshtein, A. I. (1972). *Phys Lett. B* **39**, 393.
- Van Den Broeck, C. (2005). *Class. Quant. Grav.* **22**, 1825.

- Veitch P. J. (1991). In *The Detection of Gravitational Waves*, D. G. Blair ed., Cambridge University Press, Cambridge.
- Veltman, M. J. G. (1976). *Quantum Theory of Gravitation*, in *Methods in Field Theory*, Les Houches 1975, R. Balian and J. Zinn-Justin eds., North-Holland, Amsterdam.
- Viceré, A. (2000). In *Experimental Physics of Gravitational Waves*, Urbino 1999 Summer School, M. Barone *et al.* eds., World Scientific, Singapore.
- Viceré, A. (2002). *Phys. Rev. D* **66**, 062002.
- Vinet, J.-Y., B. Meers, C. N. Man and A. Brillet (1988). *Phys. Rev. D* **38**, 433.
- Vinet, J.-Y., V. Brisson and S. Braccini (1996). *Phys. Rev. D* **54**, 1276.
- Vinet, J.-Y. *et al.* (1997). *Phys. Rev. D* **56**, 6085.
- de Waard, A. (2003). *MiniGrail. The first spherical gravitational wave antenna*. PhD thesis, Leiden University, Leiden, The Netherlands.
- de Waard, A., L. Gottardi, J. van Houwelingen, A. Schumack and G. Frossati (2003). *Class. Quant. Grav.* **20**, S143.
- Wagoner, R. V. (1979). *Phys. Rev. D* **19**, 2897.
- Wagoner, R. V. and C. M. Will (1976). *Astrophys. J.* **210**, 764.
- Wagoner, R. V. and H. J. Paik (1977). In *Experimental Gravitation, Proceedings of the Pavia International Symposium*, Accademia Naz. dei Lincei, Roma.
- Wainstein, L. A. and V. D. Zubakov (1965). *Extraction of Signals from Noise*, Dover Publications, New York.
- Walker, M. and C. Will (1980a). *Phys. Rev. Lett.* **45**, 1741.
- Walker, M. and C. Will (1980b). *Astrophys. J.* **242**, L129.
- Watson, (1966). *A Treatise on the Theory of Bessel Functions*, Cambridge University Press, Cambridge.
- Weinberg, S. (1972). *Gravitation and Cosmology*. Wiley, New York.
- Weisberg, J. M. and J. H. Taylor, (2002). In Proceedings of “Binary Pulsars”, Chania, Crete 2002, APS Conference Series, M. Bailes, D. J. Nice and S.E. Thorsett eds., astro-ph/0211217.
- Weisberg, J. M. and J. H. Taylor, (2004). In Proceedings of “Aspen Winter Conference on Astrophysics: Binary Radio Pulsars”, ASP Conference Series, F. A. Rasio and I. H. Stairs eds., astro-ph/0407149.
- Will, C. M. (1984). *Ann. Phys.* **155**, 133.
- Will, C. M. (1993). *Theory and Experiment in Gravitational Physics*, Revised edition, Cambridge University Press, Cambridge.
- Will, C. M. (1998). *Phys. Rev. D* **57**, 2061.
- Will, C. M. (2005). *Phys. Rev. D* **71**, 084027.
- Will, C. M. (2006). *Living Rev. Relativity* **9**, 3. Online article <http://www.livingreviews.org/lrr-2006-3>.
- Wiseman, A. G. (1992). *Phys. Rev. D* **46**, 1517.
- Wiseman, A. G. (1993). *Phys. Rev. D* **48**, 4757.
- Wiseman, A. G. and C. M. Will (1991). *Phys. Rev. D* **44**, R2945.
- Wiseman, A. G. and C. M. Will (1996). *Phys. Rev. D* **54**, 4813.
- Wolszczan, A. (1991). *Nature*, **350**, 688.

- Yao, W.-M. *et al.* [Particle Data Group] (2006). *J. Phys. G* **33**, 1. Online version at <http://pdg.lbl.gov/>
- Zakharov, V. I. (1970). *JETP Lett.* **12**, 312.
- Zeldovich, Ya. B. and A. G. Polnarev (1974). *Sov. Astron.* **18**, 17.
- Zendri, J.-P., *et al.* [AURIGA] (2002). *Class. Quant. Grav.* **19**, 1925.
- Zhou, C. Z. and P. F. Michelson (1995). *Phys. Rev. D* **51**, 2517.
- Zimmermann, M. (1980). *Phys. Rev. D* **20**, 351.
- Zimmermann, M. and E. Szedenits (1979). *Phys. Rev. D* **21**, 891.

Index

- ACIGA, 532
Active gravitational-mass density, 138, 244
Admittance, 440
AIGO, 532
Airy pattern, 500
ALLEGRO, 413, 453, 469
Amplifier noise, 443–444
Amplifier noise temperature, 447
Angular momentum of GWs, 58–65
ASTROD, 535
AURIGA, 434, 453, 469
strain sensitivity, 454
Auto-correlation function, 338

Back-action evasion, 452
Back-action noise, 446–452
Back-reaction of GWs, 116–121, 275–279
Bayes' theorem, 347
Bayesian statistics, 346–350
BBO, 535
Bessel function J_n
integral representation, 233
Bias, 352
Binary systems, 167–199
at cosmological distances, 190–199
chirp amplitude, 169–176
cycles spent in the detector bandwidth, 171
energy spectrum of GWs, 175
Keplerian orbits, 176
mass function, 328
Newtonian waveform, 168, 172–174
PN corrections, 289–299
PN waveform, 296–299
radiated angular momentum, 184–186
radiated power, 169, 179
time to coalescence, 171, 188
Bondi-type coordinates, 266
Burke-Thorne potential, 119, 279

Bursts
bar's sensitivity, 453–454
interferometer's sensitivity, 530
matched filtering, 361–365

Central limit theorem, 393
Chirp amplitude, 169–176
post-Newtonian, 289–299
Chirp mass, 198
accuracy of reconstruction, 392
Chopping technique, 411
Christodoulou memory, 274, 300
Circular polarization, of GWs, 159
CLIO, 534
COBE, 392
Comoving coordinates, 190
Confidence level, 348
Conformal time, 195
Counting statistics, 516
Coupling rate, 487
Covariant derivative along a curve, 14
Cross-section
resonant bars, 422, 426
resonant spheres, 465
Current quadrupole, 125–131, 164

d'Alembertian
in curved space, 195
inversion, 257
Dark fringe, 504
De Donder gauge, 6, 242, 250
Deceleration parameter, 193, 194
DECIGO, 535
Detector tensor, 336
bars, 425
interferometers, 494
Dicke radiometer, 412, 504
Diffeomorphisms, 4
Diffraction, 497–503
Dipole radiation
absent for GWs, 112
DIRE, 279–281
Dispersion measure, 312
Displacement noise, 524
Doppler tracking of spacecrafts, 536

- Drag free control, 534
- Drever, R., 470
- Dual detectors, 435
- Eccentric anomaly, 177, 315
- Eccentricity, 176
- Effacement of the internal structure
 - in Einstein gravity, 286–289
 - in Newtonian gravity, 282–286
- Eikonal approximation, 42
- Eikonal equation, 43
- Einstein action, 4
 - linearized theory, 59, 72
- Einstein angle, 45
- Einstein equations, xvii, 4
 - coarse-graining, 34
 - relaxed, 250–252
- Einstein parameter, 316
- Einstein tensor, 251
- Einstein–Infeld–Hoffmann Lagrangian, 246
- Ellipticity, of rotating body, 203
- Energy density of GWs, 36
- Energy filter, 370
- Energy flux, 37–39
- Energy localization, 57–58, 61
- Energy–momentum tensor
 - electromagnetism, 56–58
 - GWs, 32–39, 58–61
 - improved, 57
 - matter, xvii, 4
 - point-like particle, 121, 245
- Equivalence principle, 15
 - and radiation from accelerated masses, 120–121
- Estimator, 352
- Euler angles, 204
- Euler equations for rigid body, 205
- Event (definition), 337
- Excess power statistic, 365, 367
- EXPLORER, 445, 453, 469
 - strain sensitivity, 454
- Fabry–Perot cavity, 480–488
 - finesse, 486
 - free spectral range, 485
 - interaction with GWs, 489–493
 - optimal coupling, 488
 - storage time, 486
- False alarm probability, 359
- Feedback control systems, 513
- Feldman and Cousins construction, 349
- Fermi normal coordinates, 17
- Fisher information matrix, 356
- Fluctuation–dissipation theorem, 439
- Forward, R., 470
- Four-velocity, 14
- Fourier transform
 - conventions, xvii
 - discrete, 366
 - windowed, 368
- Fraunhofer diffraction, 497, 499–500
- Freely falling frames, 15–17
- Frequentist coverage, 348
- Frequentist statistics, 346–350
- Fresnel diffraction, 497
- Friedmann–Robertson–Walker cosmology, 190–194
- Gabor transform, 368
- GEO600, 480, 528–530
- Geodesic deviation, 13–15, 23
- Geodesic equation, 13–15
- Geometric optics in curved space, 42–47
- Gertsenshtein, M., 470
- Gothic metric, 250
- Gouy phase, 501
- Graviphoton, 90
- Graviscalar, 90
- Gravitational wave absorption, 46
- Gravitational wave production
 - mass in circular orbit, 158–160, 167–189
 - mass in Keplerian elliptic orbit, 176–189
 - mass in parabolic orbit, 180–181
 - non-relativistic sources, 105–155
 - octupole, 161–162
 - oscillating mass, 156–158
 - post-Newtonian sources, 236–299
 - quadrupole, 109–121, 156–160
 - relativistic sources, 102–105
- Gravitational wave propagation, 40–46
 - geometric optics, 42
- Graviton, 70–95
 - angular momentum states, 98–99

- bounds on the mass, 82
- helicity, 98–99
- massive, 81–95
- non-linear couplings, 74–79
- propagator, 74
- spin, 66–70
- GRAVITON project, 469
- Gravity
 - as a field theory, 66–95
 - linearized, 53–65
 - non-renormalizable, 79
- Green’s function, retarded, 102, 257
- GW bursters, 413
- GWIC, 469
- Gyroscopes and freely falling frame, 16
- $h_{3/\text{yr}}$, 375
- Hadamard regularization, 300
- Harmonic coordinates, 242
- Harmonic gauge, 6, 242
- Hereditary terms, in the PN expansion, 267–275
- Hermite-Gauss modes, 503
- Hilbert gauge, 6
- Hooke’s law, 459
- Hough transform, 385–386
- Hubble expansion rate, 193, 194, 395
- Hulse–Taylor binary pulsar, 83, 188, 189, 302–305, 323–326
- Impedance, 440, 525
- Impedance match ratio, 447
- Inertia tensor, of rigid body, 200
- Innermost Stable Circular Orbit (ISCO), 174
- Interferometers, 470–536
 - advanced, 532–535
 - dark fringe, 504–509
 - delay line, 480
 - detector tensor, 494
 - displacement noise, 524–530
 - Fabry–Perot, 480–488
 - Gaussian beams, 497–503
 - locking, 511–515
 - Michelson, 470–479
 - noise, 515–530
 - optical read-out noise, 522
 - pattern functions, 496
 - thermal noise, 525–528
- Irreducible representations of $SO(N)$, 163
- Kepler equation, 177
- Keplerian orbits, 176
 - anomalous eccentricity, 315
 - Fourier decomposition, 181–183, 233
 - Post-Newtonian corrections, 317–320
- Lamé coefficients, 459
 - aluminum, 459
- Lambda tensor, 9–10
 - angular integration, 113
- Landau–Lifshitz energy–momentum pseudotensor, 250
- Laplace effect, 275
- Laplacian
 - in spherical coordinates, 132
- LCGT, 532, 534
- LIGO, 413, 528–530
 - advanced, 532–534
 - arms, 480
 - finesse, 488
 - laser wavelength, 497
 - mirror losses, 487
 - pole frequency, 493
 - waist, 502
- Likelihood, 352–356
- Likelihood function, 347
- Linear momentum losses, 40, 130, 139
- Linearization
 - Christoffel symbol, 17, 48
 - Riemann tensor, 5, 48
- Linearized theory
 - action, 70–81
 - energy–momentum conservation, 7
 - equations of motion, 6
 - symmetries, 4
- LISA, 534–535
- LISA Pathfinder, 534
- Local inertial frames, 15
- Lock acquisition, 515
- Locking, 511–515
- Lorentz gauge, 6
- Lorentz transformations, 5
- Loss angle, 526
- Luminosity, 113
- Luminosity distance, 192
- Mass momenta
 - definition, 107
- Matched asymptotic expansion, 249

- Matched filtering, 343–413
 - bursts, 361–365
 - coalescences, 387–392
 - parameters estimation, 350–356
 - periodic signals, 371–386
 - stochastic backgrounds, 392–413
- Maximum likelihood estimation, 352–356
- Memory effect
 - linear, 300
 - non-linear, 274
- Mesa beams, 503
- Michelson interferometer, 470–479
- Microlensing, 45
- MiniGRAIL, 434, 468
 - strain sensitivity, 468
- Mode cleaner
 - input, 503
 - output, 510
- Modulation index, 377, 505
- Momentum flux, 39
- Momentum radiated by GWs, 130
- Monopole radiation
 - absent for GWs, 112
- Multi-index notation, 134
- Multipolar post-Minkowskian (MPM) expansion, 256
- Multipole moments, 139–155
 - algorithmic, 256
 - current quadrupole, 125–131
 - mass octupole, 125–131
 - mass quadrupole, 109–125
 - radiative, 266
- NAUTILUS, 445, 453, 469
 - strain sensitivity, 454
- Near zone, 238
- Newtonian limit, 240–241
- Newtonian noise, 525
- Neyman construction, 348
- Neyman-Pearson criterium, 354
- NIOBE, 469
- Noether’s theorem, 53–58
- Noise
 - $1/f$, 339, 507
 - amplifier, 443–444
 - non-stationary, 406
 - thermal, 437–442
 - white, 339
- Non-central chi-squared density, 361
- Null instrument, 504
- Nyquist force, 438
- Ω_{gw} , 395
- Octupole radiation, 125–131, 161–162
- Overlap reduction function, 402
- Paraxial propagator, 498–503
- Pattern functions, 339–342
 - bars, 342, 425–426
 - interferometers, 342, 494–496
 - sphere, 342
- Pauli–Fierz action, 70–81
- Pauli–Fierz mass term, 87
- Penzias, A., 392
- Periodic signals
 - bar’s sensitivity, 454–455
 - interferometer’s sensitivity, 530
 - matched filtering, 371–386
- Photon
 - absence of dipole radiation, 112
 - angular momentum states, 98–99
 - massive, 84–86
- Piezoelectric transducers, 428
- Planck mass, 80
- Pockels cell, 505
- Poincaré group, representations, 70–71, 96–97
- Poincaré transformations, 5
- Poisson distribution, 371, 516
- Poisson integral, 247
- Poisson ratio, 459
 - of Al5056, 459
- Polarization tensors, 12
- Post-Minkowskian expansion, 253–259
- Post-Newtonian expansion, 237–249
 - 1PN, 242–245
 - for coalescing binaries, 289–299
 - hereditary terms, 267–275
 - limit of validity, 247–249, 265–266
 - multipolar, 260
 - tail integral, 267–275
- Posterior probability, 347
- Pound–Drever–Hall locking, 509, 513–515
- Power recycling, 510
- Power spectrum, single-sided, 338
- Precession of rigid bodies, 204–205

- Prior probability, 347
 Proca Lagrangian, 84
 Proper detector frame, 19–26
 Proper distance, 13
 Proper time, 13
 PSR B1534+12, 83, 329–331
 PSR B1913+16, *see* Hulse–Taylor binary pulsar
 PSR J0737–3039 (double pulsar), 326–329
 Pulsars
 braking index, 204, 380
 coherent searches, 382
 dispersion in the interstellar medium, 311–312
 glitches, 313, 380
 hierarchical searches, 384
 incoherent searches, 383
 magnetosphere, 305
 spindown age, 380
 Pure-spin $s = 2$ tensor spherical harmonics, 148
 Pure-spin vector harmonics, 147
 Pustovoit, V. I., 470
 Quadrupole formula controversy, 277, 299
 Quadrupole moment, 109, 113
 spherical components, 141
 Quadrupole radiation, 109–121
 radiated angular momentum, 114–116
 radiated power, 113, 142
 Quality factor, 419
 Quantum limit, 448
 bars, 446–452
 interferometers, 522–524
 Quantum non-demolition, 449–452
 Radiation pressure, 519–522
 Radiation reaction, 275–279
 Radiative coordinates, 266
 Rayleigh distribution, 360
 Rayleigh range, 501
 Reciprocity relations, 481
 Recoil, due to GW backreaction, 279
 Redshift of gravitons, 45
 in FRW cosmology, 191
 Reflection coefficient, 480
 Relaxed Einstein equations, 250–252
 Renormalization group
 and definition of GWs, 34
 Resonant bars
 absorption cross-section, 421–423
 bandwidth, 444
 detector tensor, 425
 effective temperature, 444–445
 higher modes, 423
 mode expansion, 417
 noise spectral density, 436–437, 440, 441, 443, 445
 pattern functions, 425
 quantum limit, 446–452, 457–458
 response to bursts, 415–419
 response to periodic GWs, 420–423
 transfer function, 419, 431
 Resonant sideband extraction, 533
 Resonant spheres, 459–468
 cross-section, 465
 normal modes, 461–463
 Resonant transducers, 427–435
 Restricted PN approximation, 297
 Riemann normal coordinates, 16
 Riemann tensor, xvii
 linearized, 5
 Rigid bodies, kinematics, 200–201
 Rigid ruler, 19
 Roemer time delay, 306–307
 ROG collaboration, 453
 Root-sum-square (rss) amplitude, 364
 Sagnac effect, 20
 Schnupp asymmetry, 506, 507
 Schnupp locking, 515
 Seismic noise, 524
 Shapiro time delay, 308–310
 range and shape, 321
 Shifting algorithm, 371
 Shklovsky effect, 322
 Short-wave expansion, 26–47
 Shot noise, 516–519
 Sidebands, 476, 505
 Sight distance to coalescing binaries, 391, 529, 533
 Signal recycling, 532–533
 Signal-to-noise ratio
 bursts, 361–365
 coalescences, 390
 definition, 344

- optimal, 345
- periodic signals, 371–386
- Sine-Gaussian waveform, 363
- Singular perturbation theory, 248
- Spectral density
 - bars, 436–437, 440, 441, 443, 445
 - single-sided, 338
- Speed of GWs, 7, 273
- Speed of sound
 - aluminum, 416
 - CuAl, 468
- Spherical components of tensors, 140–144
- Spherical harmonics
 - l generic, 142
 - $l = 2$, 140
 - addition theorem, 133
- Spheroidal modes, 461, 463
- Spin-2 tensor harmonics, 148–151
- Spindown parameters, 313
- Spinor spherical harmonics, 145
- SQUID, 434
- Standard candles, 194
- Standard quantum limit, 448, 522–524
- STF projection, 134
- STF tensors, 133
- Stochastic backgrounds, 392–413
 - chopping, 411
 - multiple-detector correlation, 409
 - single detectors, 397–400
 - two-detector correlation, 400–409
- Strain amplitude, 337
- Strain sensitivity, 338
- Tail integral, 274
- TAMA300, 480, 528–530
- Templates, 351
 - for coalescing binaries, 387
 - orthogonal, 389
- Tensor spherical harmonics, 144–151
- TFCLUSTERS algorithm, 369, 413
- Thermal compensation, 532
- Thermal noise
 - bars, 437–442
 - interferometers, 525–528
- Thermo-elastic noise, 527
- Tidal radius, 220
- Time-frequency analysis, 365
- Transducers
 - active, 432
 - capacitive, 432
 - for resonant bars, 427–435
 - magnetic, 432
 - parametric, 432
 - piezoelectric, 428
- Transfer function, 336
 - bar, 419
 - bar-transducer, 431
 - interferometer with Fabry–Perot cavities, 493
- Transmission coefficient, 480
- True anomaly, 178
- TT frame, 17–19
- TT gauge, 7–12
 - projection onto, 9
- Units $\hbar = c = 1$, 66
- Vainshtein radius, 92–95
- van Dam-Veltman-Zakharov (vDVZ) discontinuity, 90
- Vector spherical harmonics, 145–148
- VIRGO, 528–530
 - advanced, 532–534
 - arms, 480
 - finesse, 488
 - laser wavelength, 497
 - mirror losses, 487
 - optical layout, 510
 - pole frequency, 493
 - waist, 502
- WaveBurst algorithm, 413
- Wavelets, 368
- Weber, J., 415, 470
- Wiener filter, 345
- Wiener–Khinchin relation, 339
- Wilson, R., 392
- Wobble radiation, 205–211
- \mathcal{V}_{ij}^{2m} , basis for $l = 2$ traceless symmetric tensors, 140, 143
- Young diagrams, 163
- Young modulus, 416, 459
- Yukawa potential, 68